Related titles

Durability and Reliability of Medical Polymers
(ISBN 978-1-84569-929-1)

Natural Based Polymers for Biomedical Applications
(ISBN 978-1-84569-264-3)

Degradation Rate of Bioresorbable Materials
(ISBN 978-1-84569-329-9)

Woodhead Publishing Series in Biomaterials: Number 108

Advances in Polyurethane Biomaterials

Edited by

Stuart L. Cooper
Jianjun Guan

Notices
Knowledge and best practice in this field are constantly changing. As new research and experience broaden our understanding, changes in research methods, professional practices, or medical treatment may become necessary.

Practitioners and researchers must always rely on their own experience and knowledge in evaluating and using any information, methods, compounds, or experiments described herein. In using such information or methods they should be mindful of their own safety and the safety of others, including parties for whom they have a professional responsibility.

To the fullest extent of the law, neither the Publisher nor the authors, contributors, or editors, assume any liability for any injury and/or damage to persons or property as a matter of products liability, negligence or otherwise, or from any use or operation of any methods, products, instructions, or ideas contained in the material herein.

For information on all Woodhead Publishing publications
visit our website at http://store.elsevier.com/

Working together
to grow libraries in
developing countries

www.elsevier.com • www.bookaid.org

List of contributors

G.A. Abraham Research Institute for Materials Science and Technology, INTEMA (UNMdP-CONICET), Mar del Plata, Argentina

A. Basu Faculty of Medicine, School of Pharmacy, The Hebrew University of Jerusalem, Jerusalem, Israel; Birla Institute of Technology, Ranchi, Jharkhand, India

K.G. Battiston Institute of Biomaterials and Biomedical Engineering, University of Toronto, Toronto, ON, Canada

A. Biswas School of Material Science and Technology, Indian Institute of Technology (BHU), Varanasi, Uttar Pradesh, India

M. Boffito Politecnico di Torino, Torino, Italy

E.J. Brisbois University of Michigan Medical Center, Ann Arbor, MI, USA

P.C. Caracciolo Research Institute for Materials Science and Technology, INTEMA (UNMdP-CONICET), Mar del Plata, Argentina (*email:* pcaracciolo@fi.mdp.edu.ar)

S. Chung Northeastern University, Boston, MA, USA

G. Ciardelli Politecnico di Torino, Torino, Italy (*email:* gianluca.ciardelli@polito.it)

J. Clauser Department of Cardiovascular Engineering, Institute of Applied Medical Engineering, RWTH Aachen University, Pauwelsstraße 20, Aachen, Germany (*email:* clauser@ame.rwth-aachen.de)

E.M. Cosgriff-Hernandez Texas A&M University, TX, USA (*email:* cosgriff.hernandez@bme.tamu.edu)

A.J. Domb Faculty of Medicine, School of Pharmacy, The Hebrew University of Jerusalem, Jerusalem, Israel (*email:* avid@ekmd.huji.ac.il)

S. Doppalapudi National Institute of Pharmaceutical Education & Research, Hyderabad, Telangana, India

S. Farah Faculty of Medicine, School of Pharmacy, The Hebrew University of Jerusalem, Jerusalem, Israel

S. Fernando School of Medicine, Vanderbilt University Medical Center, Nashville, TN, USA

I. Francolini Sapienza Univeristy of Rome, Piazzale Aldo Moro, Rome, Italy (*email:* iolanda.francolini@uniroma1.it)

M.J. García-Celma University of Barcelona, Barcelona, Spain; Institute of Advanced Chemistry of Catalonia (IQAC-CSIC) and Networking Research Center on Bioengineering, Biomaterials and Nanomedicine, CIBER-BBN, Barcelona, Spain (*email:* mjgarcia@ub.edu)

K. Gester Department of Cardiovascular Engineering, Institute of Applied Medical Engineering, RWTH Aachen University, Pauwelsstraße 20, Aachen, Germany

M.J. Goudie University of Georgia, Athens, GA, USA

J.E. Greenwood Skin Engineering Laboratory, Hanson Institute, Adelaide, South Australia; Royal Adelaide Hospital, Adelaide, South Australia (*email:* john. greenwood@sa.gov.au)

J. Guan The Ohio State University, Columbus, OH, USA (*email:* guan.21@osu.edu)

S.A. Guelcher Department of Biomedical Engineering, Vanderbilt University, Nashville, TN, USA; Department of Chemical and Biomolecular Engineering, Vanderbilt University, Nashville, TN, USA (*email:* scott.guelcher@vanderbilt. edu)

J. Guo Department of Biomedical Engineering, Materials Research Institute, The Pennsylvania State University, University Park, PA, USA; The Huck Institutes of the Life Sciences, The Pennsylvania State University, University Park, PA, USA

H. Handa University of Georgia, Athens, GA, USA (*email:* hhanda@uga.edu)

S.M. Hasan Department of Biomedical Engineering, Texas A&M University, College Station, TX, USA

Y. Hong University of Texas at Arlington, Arlington, TX, USA; Joint Biomedical Engineering Program, University of Texas Southwestern Medical Center, Dallas, TX, USA (*email:* yihong@uta.edu)

S.-H. Hsu Institute of Polymer Science and Engineering, National Taiwan University, Taiwan, Republic of China (*email:* shhsu@ntu.edu.tw)

J. Hu Department of Biomedical Engineering, Materials Research Institute, The Pennsylvania State University, University Park, PA, USA; The Huck Institutes of the Life Sciences, The Pennsylvania State University, University Park, PA, USA

K.-C. Hung Institute of Polymer Science and Engineering, National Taiwan University, Taiwan, Republic of China

Y. Inoue The University of Tokyo, Tokyo, Japan

K. Ishihara The University of Tokyo, Tokyo, Japan (*email:* ishihara@mpc.t.u-tokyo.ac.jp)

W. Khan National Institute of Pharmaceutical Education & Research, Hyderabad, Telangana, India

G.B. Kim Department of Biomedical Engineering, Materials Research Institute, The Pennsylvania State University, University Park, PA, USA; The Huck Institutes of the Life Sciences, The Pennsylvania State University, University Park, PA, USA

K.R. Kunduru Faculty of Medicine, School of Pharmacy, The Hebrew University of Jerusalem, Jerusalem, Israel

R.S. Labow University of Ottawa, Ottawa, ON, Canada

T.L. Landsman Department of Biomedical Engineering, Texas A&M University, College Station, TX, USA

C. Liu Aleo BME, Inc., Innovation Boulevard, State College, PA, USA

X.Y. Liu Department of Materials Science and Engineering, Jinan University, Guangzhou, China

Y. Liu The University of Tokyo, Tokyo, Japan

P. Maiti School of Material Science and Technology, Indian Institute of Technology (BHU), Varanasi, Uttar Pradesh, India (*email:* pmaiti.mst@itbhu.ac.in)

D.J. Maitland Department of Biomedical Engineering, Texas A&M University, College Station, TX, USA (*email:* djmaitland@tamu.edu)

L.A. Matheson University of Ottawa, Ottawa, ON, Canada

C. Mattu Politecnico di Torino, Torino, Italy

J.E. McBane Children's Hospital of Eastern Ontario Research Institute, Ottawa, ON, Canada

M. McEnery Department of Biomedical Engineering, Vanderbilt University, Nashville, TN, USA

P. Melgar-Lesmes University of Barcelona, Barcelona, Spain

F. Montini-Ballarin Research Institute for Materials Science and Technology, INTEMA (UNMdP-CONICET), Mar del Plata, Argentina

G. Morral-Ruíz University of Barcelona, Barcelona, Spain

Y.Q. Niu Department of Materials Science and Engineering, Jinan University, Guangzhou, China

J. Pant University of Georgia, Athens, GA, USA

D.K. Patel School of Material Science and Technology, Indian Institute of Technology (BHU), Varanasi, Uttar Pradesh, India

J. Paul Santerre Institute of Biomaterials and Biomedical Engineering, University of Toronto, Toronto, ON, Canada; Faculty of Dentistry, University of Toronto, Toronto, ON, Canada (*email:* paul.santerre@dentistry.utoronto.ca)

A. Piozzi Sapienza Univeristy of Rome, Piazzale Aldo Moro, Rome, Italy

S. Sartori Politecnico di Torino, Torino, Italy

D. Shan Department of Biomedical Engineering, Materials Research Institute, The Pennsylvania State University, University Park, PA, USA; The Huck Institutes of the Life Sciences, The Pennsylvania State University, University Park, PA, USA

C.A. Siedlecki Department of Surgery, Biomedical Engineering Institute, The Pennsylvania State University, College of Medicine, Hershey, PA, USA; Department of Biomedical Engineering, The Pennsylvania State University, College of Medicine, Hershey, PA, USA (*email:* csiedlecki@psu.edu)

C. Solans Institute of Advanced Chemistry of Catalonia (IQAC-CSIC) and Networking Research Center on Bioengineering, Biomaterials and Nanomedicine, CIBER-BBN, Barcelona, Spain

S.J. Sonntag Department of Cardiovascular Engineering, Institute of Applied Medical Engineering, RWTH Aachen University, Pauwelsstraße 20, Aachen, Germany

U. Steinseifer Department of Cardiovascular Engineering, Institute of Applied Medical Engineering, RWTH Aachen University, Pauwelsstraße 20, Aachen, Germany

R.S. Thompson Department of Biomedical Engineering, Texas A&M University, College Station, TX, USA

T.J. Touchet Texas A&M University, TX, USA

C.-S. Tseng National Central University, Taiwan, Republic of China

M.J.D. Wagstaff Royal Adelaide Hospital, Adelaide, South Australia

T.J. Webster Northeastern University, Boston, MA, USA; Center of Excellence for Advanced Materials Research, King Abdulaziz University, Jeddah, Saudi Arabia (*email:* th.webster@neu.edu)

A.C. Weems Department of Biomedical Engineering, Texas A&M University, College Station, TX, USA

T.S. Wilson Physical and Life Sciences Directorate, Lawrence Livermore National Laboratory, Livermore, CA, USA

K.T. Xu Department of Materials Science and Engineering, Jinan University, Guangzhou, China (*email:* kaitianxu@yahoo.com)

L.-C. Xu Department of Surgery, Biomedical Engineering Institute, The Pennsylvania State University, College of Medicine, Hershey, PA, USA

Y. Xu The Ohio State University, Columbus, OH, USA

J. Yang Department of Biomedical Engineering, Materials Research Institute, The Pennsylvania State University, University Park, PA, USA; The Huck Institutes of the Life Sciences, The Pennsylvania State University, University Park, PA, USA (*email:* jxy30@psu.edu)

H. Zhang Lubrizol Advanced Materials Inc., Brecksville, OH, USA (*email:* asterphoenix@gmail.com)

X. Zhang Institute of Biomaterials and Biomedical Engineering, University of Toronto, Toronto, ON, Canada

Y.H. Zhu Department of Materials Science and Engineering, Jinan University, Guangzhou, China

Woodhead Publishing Series in Biomaterials

Preface

Polyurethane elastomers were first considered as potential biomaterials by John Boretos at the US National Institutes of Health in the 1960s and have found medical applications ever since. Polyurethanes generally have outstanding physical properties including high strength and stiffness, excellent flexibility and fatigue resistance, abrasion resistance, and reasonably good biocompatibility. This has led to their use in applications such as catheters, blood pumps, artificial heart components, and wound dressings. That is not to say that there are still unanswered questions in areas such as biostability and long-term biocompatibility and in the potential toxicity of aromatic diisocyanates used in many formulations. Over the years there have been numerous publications and book chapters devoted to polyurethanes as biomaterials, but as the field advances, particularly in the area of applications in tissue engineering and regenerative medicine, new venues for describing the state of the art in the field are needed. To meet at least part of the need to provide a summary of recent research in polyurethane biomaterials we have compiled 22 chapters on the topic of *Advances in Polyurethane Biomaterials* from authors making outstanding contributions to the field.

Advances in Polyurethane Biomaterials is organized in three sections. The first section contains 9 chapters on the chemistry, processing, and applications of polyurethane biomaterials. The second and third parts have chapters grouped around polyurethanes for vascular applications and polyurethanes for tissue-engineering applications. The authors have combined solid reviews as well as state of the art summaries of recent advances on their topics. Each contribution also contains copious and timely references on the topics covered. The editors thank the authors for their enthusiastic response to participate in this project and hope that readers of this volume will find value in the assembled material.

S. L. Cooper and J. Guan
September 2015
Ohio State University
Columbus, Ohio

Hierarchal structure–property relationships of segmented polyurethanes

1

*T.J. Touchet, E.M. Cosgriff-Hernandez**
Texas A&M University, TX, USA
*Corresponding author: cosgriff.hernandez@bme.tamu.edu

1.1   Introduction

The use of polyurethanes in medical devices has been well documented since 1965 [1–7]. More recently, efforts have focused on the design of biodegradable formulations for use in tissue-engineered scaffolds and other resorbable implants. Biodegradable polyurethanes have a unique set of design requirements that include the use of biocompatible components, tissue-like mechanical properties, bioactivity, and an appropriate degradation rate. To accommodate these design criteria, the traditional polyurethane structure is often modified to incorporate degradable linkages or cell-responsive moieties. The impact of these modifications on the resulting properties is affected by a number of factors including phase mixing, soft segment chemistry, hard segment chemistry, hard segment content, and molecular weight [8–12]. To enable rational design for these applications, an in-depth understanding of the effects that structure has on the properties is necessary. Characterization of polyurethane structure–property relationships has historically been focused on biostable formulations [4,9,13–17]. This chapter will provide an overview of the effect of polyurethane structure on physical properties with an emphasis on biodegradable polyurethane elastomers.

1.2   Structure of segmented polyurethanes

1.2.1   Polyurethane reactions

Polyurethane reactions fall into the category of step growth or condensation polymerization. In this process, bifunctional monomers react in a stepwise manner to produce long chains of the reacting monomers [18]. Step growth and polycondensation polymerizations typically expel a small molecule such as water or CO_2; however, there is no by-product in the segmented polyurethane synthesis. Segmented polyurethanes comprise a low Tg soft segment that is commonly a low molecular weight macrodiol ranging from 400 to 6000 kg/mol and a glassy or semicrystalline hard segment of diisocyanate and chain extender. In a typical segmented polyurethane synthesis, the macrodiol is reacted with an excess of isocyanate to form a prepolymer. The prepolymer is then reacted with a chain extender to build molecular weight and form a linear

One-shot method

Polyol

Isocyanate → Mix/polymerization → Polyurethane

Chain extender

Prepolymer method

Polyol

Isocyanate → Prepolymer → Mix/polymerization → Polyurethane

Chain extender
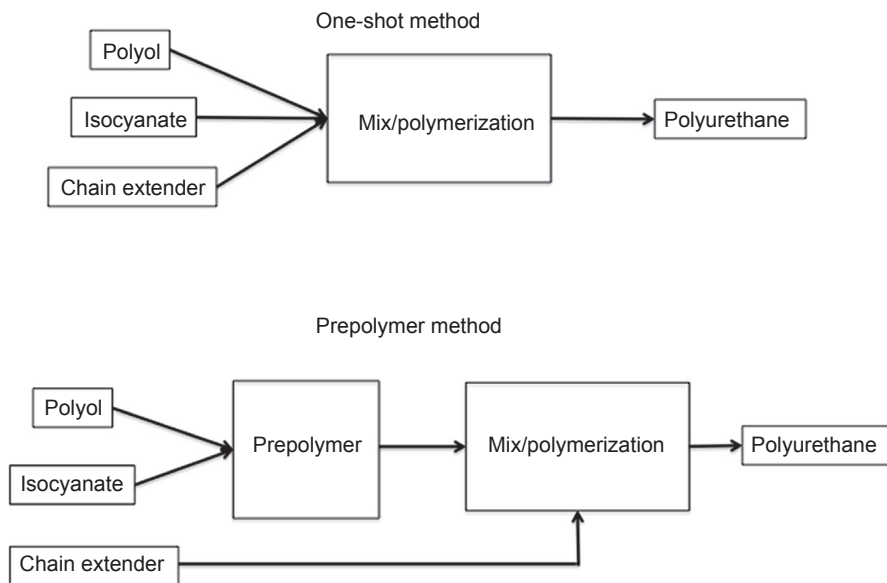
Figure 1.1 Polyurethane polymerization based on the one-shot method and prepolymer method.

block copolymer with alternating blocks of hard segment and soft segment. In contrast to the one-shot method in which the isocyanate, polyol, and chain extender are all reacted at once, the prepolymer method yields more ordered structure and control of properties [18]. Figure 1.1 provides a schematic comparing the polyurethane reaction using the one shot-method and the prepolymer method.

The central reactions of polyurethane synthesis are the formation of the carbamate or urethane linkage that occurs when an isocyanate reacts with an alcohol and the urea linkage that occurs when an isocyanate reacts with an amine. Isocyanates are a unique functional group that has several resonant structures and allows for the reaction with both nucleophiles and electrophiles [6,7,18]. Isocyanates react readily with primary alcohol functional groups but will also react with both secondary and tertiary alcohols at slower rates. The reaction kinetics can be influenced by factors such as steric hindrance that can slow down the reaction or proximity of electron-withdrawing groups that increase the rate of reaction [6,7]. The nitrogen of the urethane can also undergo a secondary reaction with excess isocyanate to form allophanates. Urea linkages can undergo similar reactions with excess isocyanate to form biurets [6,7,18]. These reactions provide thermally labile crosslinks and provide additional structural diversity in polyurethane design (Figure 1.2).

1.2.2 Segmented polyurethane elastomers

Elastomers are a class of polymers that can be repeatedly strained and then return to the approximate original length on release of the load. Traditional elastomers such as rubber are able to achieve this elastic behavior by having a low glass transition temperature and a small number of chemical crosslinks that form a permanent network
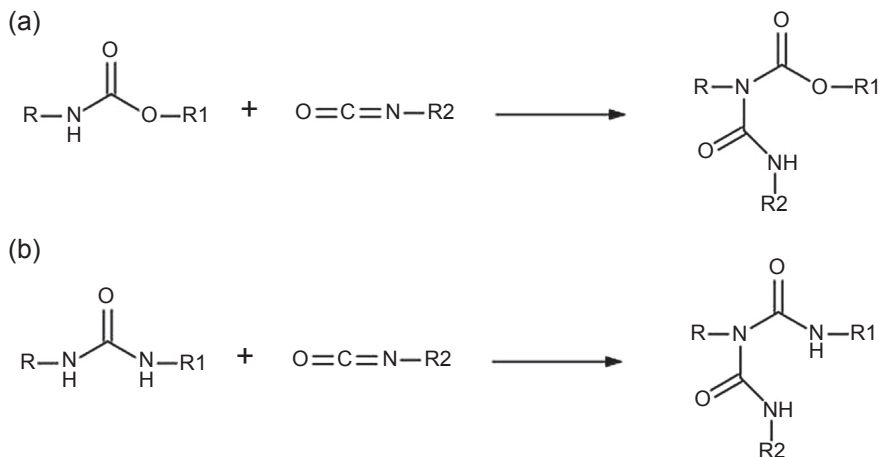
Figure 1.2 Reaction of urethane linkage with isocyanate to produce allophanate (a); reaction of urea linkage with isocyanate to produce biuret (b).

for high recovery. Similar to rubber, thermoplastic polyurethane elastomers have soft segments with low glass transition temperatures but are reinforced with ordered hard domains that serve as rigid fillers and pseudo-net points. These physical crosslinks and the hydrogen bonds that stabilize them are thermally reversible, which permits thermal processing. The high elastic recovery and fatigue resistance of thermoplastic polyurethanes have generated significant interest in the field of tissue engineering, particularly in applications where mechanical properties are key design criteria [5,19–24].

1.3 Soft segment chemistry

Typical polyols used in resorbable polyurethanes include polyesters, polyethers, polycarbonates, and combinations of these polyols in the form of diblocks and triblocks [6,25,26]. In general, polyols have low glass transition temperatures that are in the rubbery regime at physiological temperatures. The length and type of polyol used can play a large role in the resulting physical properties, ranging from long polyols that produce low-modulus polyurethane elastomers to short and/or multifunctional polyols that result in rigid polyurethanes [27,28]. The reaction rate of the alcohol group allows for the reaction with isocyanate to occur under relatively mild conditions with primary alcohols reacting orders of magnitude faster than secondary or tertiary alcohols [18].

1.3.1 Polyester soft segments

Polyesters are hydrolytically labile and offer excellent mechanical properties compared to the other commonly used polyols for biomedical applications. Table 1.1 provides a list of common polyester diol structures used in resorbable polyurethanes. Although polyester urethanes were generally considered unsuitable for biostable

Table 1.1 **List of common polyester diol structures used in resorbable polyurethanes**

Chemical name	Structure
Poly(ε-caprolactone) (PCL) diol	
Poly(D,L-lactide) (PDLLA) diol	
Poly(glycolide) (PGA) diol	
Poly(ethylene adipate) diol	

devices, they are the most common choice for biodegradable applications [13,29–34]. One of the most studied polyester soft segments is polycaprolactone (PCL). Although PCL undergoes ester hydrolysis, its hydrophobicity and crystallinity allow for a slower reaction rate compared to other polyesters. Polyglycolide, polylatide, and polygyl-colide-co-lactide have also been investigated. Polyglycolide has the fastest degradation rate while polylactide displayed the highest tensile properties of the three [35]. With the exception of very low molecular weight diols, polyester polyols form semic-rystalline soft segment domains that can strongly influence both mechanical properties and degradation rate.

1.3.2 Polyether soft segments

In biodegradable polyurethanes, polyethers are often used to add flexibility or hydro-philicity to the polyurethane. Polyethers are more hydrolytically stable than polyes-ters and can be used in combination with polyesters to tailor the degradation rate [1,34]. Polyether urethanes typically have lower moduli than polyester urethanes and are often selected when high flexibility and extensibility are needed. Table 1.2 provides a list of common polyether polyol structures used in resorbable polyurethanes. Com-mon polyether polyols include poly(tetramethylene) glycol (PTMO), poly(propylene oxide) (PPO), and poly(ethylene) glycol (PEG). PTMO has been widely used in bio-medical polyurethanes due to its low swelling and excellent mechanical properties [18]. In contrast, PEG has been a popular choice in tissue engineering applications to increase hydrophilicity and increase the degradation rate of the polyurethane. PPO is used less often in biomedical applications because it generally leads to reduced mechanical properties but allows for a softer grade material [18]. Although

Table 1.2 List of common polyether diol structures used in resorbable polyurethanes

Chemical name	Structure
Poly(ethylene oxide) (PEO)	
Poly(propylene oxide) (PPO)	
Poly(tetramethylene oxide) (PTMO)	
Poly(hexamethylene oxide) (PHMO)	

Table 1.3 List of common triblock diol structures used in resorbable polyurethanes

Chemical name	Structure
PCL-*b*-PEO-*b*-PCL diol	
PCL-*b*-PPO-*b*-PCL diol	
PCL-*b*-PTMO-*b*-PCL diol	

polyethers are considered stable in terms of hydrolysis, they are susceptible to oxidation mediated by adherent inflammatory cells [1,3,13,29,34,36–44].

1.3.3   Triblock soft segments

An emerging class of soft segments that has found a niche in biodegradable polyurethanes is block copolymers in an A–B–A structure that are variations of the commonly used polyols. Table 1.3 provides a list of common triblock structures used in resorbable

polyurethanes. The versatility of the triblock structure can offer better control over morphology, hydrophilicity, mechanical properties, and degradation behavior of the resulting polyurethane. PCL–PEG–PCL is the most frequently used for soft tissue applications and provides flexibility in addition to an increased degradation rate compared to PCL. Similar to PCL–PEG–PCL, other triblocks that follow the ester–ether–ester structure such as PCL–PTMO–PCL and PLA–PEG–PLA are used for the same function but develop different properties [45,46]. Peptide-based triblocks have also been used in an attempt to control degradation by using an enzyme-specific sequence in between PEG to make a PEG–PEP–PEG triblock [47]. More recent advances have been aimed at incorporating peptides to induce bioactivity into the soft segment [48].

1.4   Hard segment chemistry

The hard segment of polyurethanes typically consists of a low molecular weight isocyanate and a low molecular weight diol or diamine as the chain extender. In contrast to the soft segment, the hard segment typically has a high glass transition temperature and is semicrystalline or highly ordered. The selection of the isocyanate and chain extender strongly influences the physical properties of the resulting polyurethane.

1.4.1   Isocyanates

The two main classes of isocyanates used to generate biomedical polyurethanes are aromatic and aliphatic. Table 1.4 provides a list of commonly used isocyanates in resorbable polyurethanes. Aromatic isocyanates are the most commonly used in biomedical polyurethanes, specifically methylene diisocyanate (MDI), and yield the highest tensile properties with high melting temperatures. Toluene diisocyanate (TDI) is often used in polyurethanes in various industries but concerns over the potential degradation product toluene diamine has curbed its use in the biomedical field [46,54,62–65]. MDI has the distinct advantages of low cost, high reactivity, and ability to crystallize [7,18]. Although aromatic polyurethanes possess excellent mechanical properties, there is still some debate as to whether or not the degradation by-products of aromatic isocyanates produce carcinogenic diamines in large enough quantities to cause adverse effects *in vivo*. More recently, there has been development of biodegradable aromatic diisocyanates. These compounds, developed by Bezwada Biomedical, incorporate labile ester linkages allowing the diisocyanate to degrade into nontoxic by-products while achieving properties comparable to those of traditional aromatic diisocyanates. Aliphatic diisocyanates are more often used in degradable polyurethanes to circumvent any potential toxicity concerns. Typically, aliphatic polyurethanes do not match the mechanical properties of their aromatic counterparts. The most commonly used aliphatic diisocyanates include 1,4-butane diisocyanate, 1,6-hexamethylene diisocyanate [14,17], and lysine diisocyanates. Lysine diisocyanate has gained popularity in recent years due to the assumption that its lysine-based chemistry will yield safe carboxylic by-products [32,49–51]. Butane diisocyanate is also considered to have biocompatible degradation products, as the hydrolyzed product, putrescine, is naturally occurring in the body [52,53].
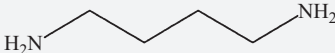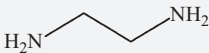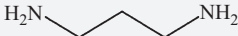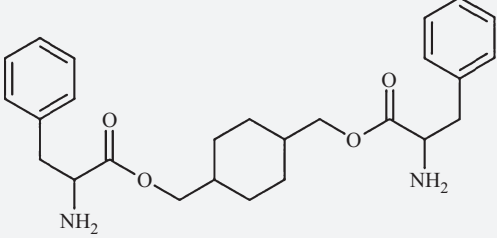
Table 1.4 **List of common diisocyanate structures used in resorbable polyurethanes**

Chemical name	Structure
1,4-Diisocyanatobutane (BDI)	
1,6-Diisocyanatohexane (HDI)	
Lysine methyl ester diisocyanate (LDI)	
Dicyclohexylmethane diisocyanate (H12MDI)	
Glycolide–ethylene glycol–glycolide isocyanate (Bezwada, LLC)	
Methylene diphenyl diisocyanate (MDI)	

1.4.2   Chain extenders

Chain extenders are low molecular weight diols or diamines that react with diisocyanates to build polyurethane molecular weight and increase the block length of the hard segment. Much like the diisocyanates, chain extenders can be either aliphatic or aromatic. Table 1.5 provides a list of commonly used chain extenders in resorbable polyurethanes. Chain extenders made from diols such as ethylene glycol, butane diol, and propylene gylcol result in a urethane linkage [16,54–56]. The use of diamine chain extenders results in a urea linkage that results in bidentate hydrogen bonding. Diamine chain extenders are associated with increased modulus and tensile strength and with decreased elongation, as compared to their diol counterparts [57]. Ethylene diamine, putrescine, and diaminopropane have been used extensively in biomedical applications. One method of generating degradable hard segments is to incorporate degradable chain extenders based on diesters or amino acids that can be either diol or diamine terminated. Several groups have previously developed diol and diamine chain extenders based on amino acids that have been shown to increase the mechanical properties over more conventional chain extenders while introducing degradable ester linkages [12,58,59].

Table 1.5 **List of common chain extender structures used in resorbable polyurethanes**

Chemical name	Structure
1,4-Butane diol	
1,4-Butanediamine (putrescine)	
Ethylene diamine (ED)	
Diaminopropane (DAP)	
Cyclohexane diphenylalanine	

1.5 Microphase separation

It has been well established by Cooper and Tobolsky that the unique properties of polyurethanes are strongly linked to its two-phase morphology [21]. Characterization of microphase separation is performed using a variety of techniques including dynamic mechanical thermal analysis (DMTA), Fourier transform infrared spectroscopy (FTIR), small-angle X-ray scattering (SAXS), and atomic force microscopy. Consideration of both the thermodynamic driving forces and the kinetics is needed to elucidate microstructure formation in polyurethanes [60–66].

1.5.1 Thermodynamics

Thermodynamics is the principle driving factor of microphase separation that is predicted well by the Gibbs free energy of mixing $\Delta G_m = \Delta H_m - T\Delta S_m$. Where ΔG_m is the free energy of mixing, ΔH_m is the enthalpy of mixing and ΔS_m is the entropy of mixing. In the event of a positive ΔG_m, the thermodynamic incompatibility of the two phases drives phase separation [67,68]. Macrophase separation is prevented by molecular restrictions imposed by covalent bonds that link the incompatible segments but microdomains are formed [62]. In general, hard segment blocks are considered to be highly polar when compared to the relatively nonpolar soft segment. This difference in polarity leads to a positive heat of mixing and results in a thermodynamic incompatibility between the two segments. The hard domains are then stabilized by hydrogen

bonding between the urethane and the urea linkages. There has been extensive investigation into predicting the microphase separation and its behavior in polyurethane systems [9,62,63,67,68].

1.5.2 Structural morphology

The thermodynamic incompatibility between the hard and the soft segments drives microphase separation into semicrystalline hard domains and amorphous, rubbery soft segment domains. As such, the degree of phase separation is dependent on hard and soft segment chemistries. Phase separation is also influenced by the processing history and improves with increased mobility of the soft segment [69–72]. Morphology models of polyurethanes have been developed to describe the heterogeneity at the domain and higher level. The organization of this morphology is often characterized by the use of DMTA, FTIR, and most commonly SAXS. FTIR is often used to identify key chemical relationships that translate to morphological changes such as hydrogen bonding of urethane linkages [58,73,74]. SAXS is the most quantitative of the techniques and allows for quantitative analysis of domain size and spacing [28,75]. At low hard segment content, discrete hard domains are dispersed in the amorphous soft segment matrix (Figure 1.3). These hard domains act as physical net points and rigid filler. Increasing hard segment content results in increased hard domain interconnectivity and a transition from discrete to continuous hard domains [28]. Larger scale, spherulitic-like organization of the lamellar hard domains is also possible in polyurethanes with increased phase separation [76]. These hard segment domains are
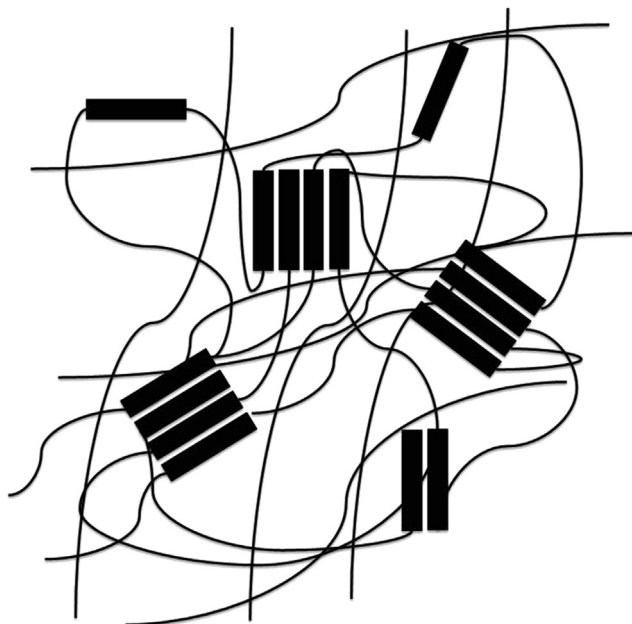
Figure 1.3 Schematic of polyurethane microphase morphology.

dynamic and can be broken and reformed into more favorable and cohesive conformations under heat and stress through the process of annealing [28,77–79].

1.5.3   Kinetics

The kinetics of microphase separation has been the subject of increasing research in recent years. The process of phase separation of the polyurethane following thermal treatment is time dependent. Raising the temperature breaks hydrogen bonds between hard segments and induces phase mixing of the polyurethane. Lowering the temperature permits phase separation and microdomain formation. Given that this macromolecular process is subject to kinetic and viscous effects, a finite amount of time is required to generate a change in morphology [80]. Techniques such as FTIR, differential scanning calorimetry (DSC), and X-ray scattering have been used to monitor microphase morphology formation and the impact of processing variables on domain size [28,43,44,74,81]. For example, X-ray scattering studies were used to demonstrate that changes in temperature led to changes in the domain spacing of polyester urethanes [82]. Chu et al. reported that phase separation kinetics are in part controlled by molecular mobility in polyether urethanes. Specifically, the hard segment had the greatest effect on the relaxation times [61].

1.6   Compositional effects on mechanical properties

Mechanical properties are a key design feature for any biomaterial. A property mismatch can lead to early device failure due to insufficient mechanical properties or undesired tissue responses due to stress shielding. Biodegradable polyurethane mechanical properties can be tailored by altering the soft segment chemistry, hard segment chemistry, soft segment molecular weight, hard segment content, and degree of crystallinity [6]. All of these factors influence variables such as modulus, elongation, tensile strength, and compressive strength [18,19,32,33,55,81,83–86]. A major component in modulating mechanical properties is the degree of chain mobility. Chain mobility can be affected by molecular flexibility, degree of crystallinity, and crosslinking [18,33,84]. Polyurethane structure–property relationships can be generally divided into soft segment and hard segment effects.

1.6.1   Effect of the soft segment

Key soft segment variables that influence mechanical properties include polyol molecular weight, chemistry, and crystallinity. There has been extensive investigation into the effect of soft segment molecular weight changes in the absence of any other structural change. Ma et al. [33] demonstrated these effects using a library of biodegradable polyurethanes with the same hard segment chemistry and content. An increase in the soft segment molecular weight was correlated with a decrease in the initial modulus. In addition, Gisselfalt and Helgee [27] reported that increasing the soft segment length

Table 1.6 **Effect of polycaprolactone soft segment molecular weight on the modulus of a resorbable polyurethane [12]**

Molecular weight (kDa)	Modulus (MPa)	Ultimate tensile strength (MPa)	Ultimate elongation (%)
530	6.6	12.5	618
1250	20.2	28	580
2000	81.9	30.8	676

led to increased phase separation. This resulted in a decrease in increased soft segment mobility as evidenced by lower glass transition temperatures and a corollary reduction in modulus. Both of these studies aligned with the mechanical theory of rubber elasticity where there is an inverse relationship between the average length between crosslinks (hard domain) and modulus. Ma et al. [33] also reported that a large chain length also led to a decrease in permanent deformation due to a reduction in hard domain reorganization. Conversely, semicrystalline PCL displays an opposite effect as molecular weight is increased [12]. As the molecular weight of the PCL soft segment is increased, the degree of crystallinity increases. This increase in crystallinity leads to elastomeric polyurethanes with increased modulus and tensile strength. Table 1.6 illustrates the effect of soft segment molecular weight on modulus in biodegradable polyurethanes [9,12,59,85,87,88].

Soft segment chemistry can also have a large impact on the polyurethane mechanical properties. In the use of biodegradable polyurethanes, polyesters are commonly selected based on the hydrolytically labile linkage that allows for degradation. These polyurethanes also possess excellent mechanical properties that are largely attributed to the ability of the polyol to crystallize or its ability to undergo strain-induced crystallization [89,90]. Although soft segment crystallinity increases modulus and ultimate tensile strength, elongation and percentage recovery are often reduced substantially [12,33,48]. Elongation and, more importantly, high recovery are required to mimic native tissue function [29]. As discussed earlier, the crystallinity of the soft segment can decrease the elongation, recovery, and degradation rate [33]. To address the limitations in using semicrystalline polyesters, triblocks in a polyester–polyether–polyester structure such as PCL–PEG–PCL have been investigated. By using two different types of polyols, a combination of mechanical properties can be achieved [48,91]. Incorporation of PEG can be used to increase the degradation due to its hydrophilicity while PCL can provide mechanical properties due to its semicrystalline morphology. Guan et al. tested biodegradable poly(ester urethane urea)s with varying PEG/PCL contents in the soft segment. As the molecular weight of PEG was increased, there was a decrease in tensile strength with minimal effect on elongation [48]. In general, the modulation of mechanical properties strongly correlates with the degree of soft segment crystallinity with higher tensile strength and reduced flexibility associated with increased crystallinity. Work by Gunatillake et al. showed that variations in the polyether choice such as PTMO, poly(hexamethylene oxide) (PHMO), and PEG displayed changes in tensile properties,

with PTMO and PHMO displaying higher properties than PEG soft segments. Similar to the polyester–polyether triblock, there have been studies into the effects of using a polyester–polycarbonate triblock and random copolymers. Ma et al. [33] demonstrated that using copolymers of aliphatic polycarbonates and polyesters as the soft segment resulted in polyurethanes with high tensile strength, low modulus, and high recovery.

1.6.2 Effect of hard segment

Much like the soft segment, mechanical properties such as tensile strength and modulus are influenced by hard segment content and chemistry [18]. The relative amounts of hard and soft segment can have a profound effect on the mechanical properties of polyurethanes. This relationship is based on the role of hard domains as rigid fillers that reinforce the amorphous soft segment matrix and as pseudo-net points or physical crosslinks. It follows that an increase in crosslinking would result in an increase in modulus and tensile strength as illustrated in Figure 1.4.

Studies by Klinedinst et al. have shown that increases in the hard segment content increased the size of the hard domains and increased phase separation. As the hard domain size increased they noted increases in both the modulus and the tensile strength. The increase in hard segment content also led to an increase in permanent set [56]. In addition to hard segment content, hard segment chemistry can also impact mechanical properties [9,74,92]. Aromatic isocyanates such as MDI and TDI possess superior mechanical properties; however, their use in biodegradable applications is limited due to toxicity concerns [14,17,93]. Dempsey et al. reported the effect of a novel aromatic degradable diisocyanate based on glycolic acid developed by Bezwada Biomedical. When compared to polyester urethanes made with aliphatic hard segments, this novel degradable polyurethane displayed a higher modulus and ultimate tensile strength [93]. A large fraction of biodegradable polyurethane research has focused on the use of linear aliphatic diisocyanates [16,26,35,49,52,53,55]. It has been established that diisocyanates such dicyclohexylmethane diisocyanate (H_{12}MDI),
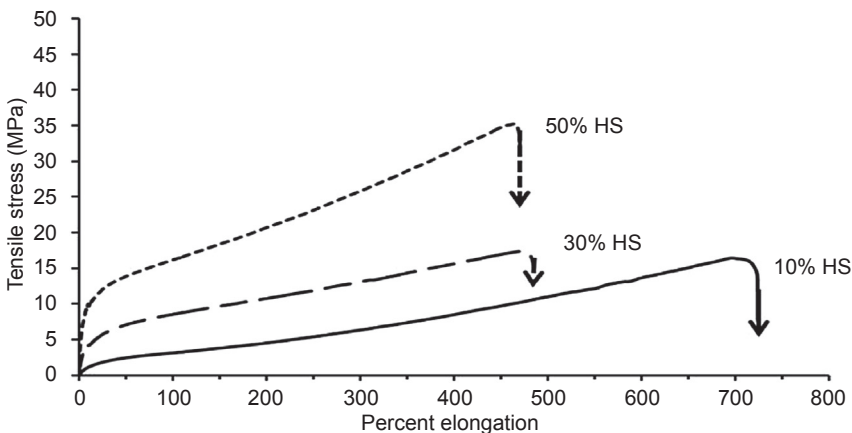
Figure 1.4 Effect of hard segment content on mechanical properties.

1,6-diisocyanatohexane (HDI), and 1,4-diisocyanatobutane (BDI) exhibit higher mechanical properties due to symmetry when compared to asymmetrical diisocyanates that inhibit crystallization [14,17,94–96]. One such asymmetrical diisocyanate that has gained popularity is lysine methyl ester diisocyanate (LDI), which is used because of its amino acid-based structure. In terms of mechanical properties, LDI has been shown to have reduced tensile properties compared to current aliphatic diisocyanates such as BDI and HDI. This decrease in mechanical properties was attributed to reduced registry and the associated loss of hard segment cohesion [32,49–51,96].

1.7 Compositional effects on degradation rate

1.7.1 Effect of soft segment

The effect of soft segment chemistry on degradation rate is related to the concentration of labile groups, hydrophilicity, and crystallinity. The chemical composition of soft segments influences the degree of water diffusion into the polymer. As such, hydrophilicity has been shown to have a strong effect on the degradation rates of polyesters [97]. Several studies have examined the effect of polyurethane hydrophilicity on degradation rate by altering the balance of hydrophilic and/or hydrophobic components of the soft segment [12,46,98–101]. Cohn et al. demonstrated that by increasing the PEG length or decreasing the PCL length, the rate of degradation was increased. It should be noted that the degree of crystallinity was also decreased [46]. Further studies showed similar trends by varying the molar ratios of PEG and PPO [12,33,48,102,103]. In a study by Gorna and Gogolewski, a triblock based on PluronicF-68 and PCL was investigated with similar effects on the rate of degradation [99]. The crystalline morphology of the polyurethane structure can also affect the degradation rate by decreasing the diffusion rate of water through the polyurethane and restricting access of water to the polymer chains in crystalline domains. It follows that an increase in crystallinity reduces the rate of hydrolytic degradation. Indeed, Skarja and Woodhouse reported that polyurethanes with amorphous soft segments displayed an increased rate of hydrolysis while an increase in crystallinity decreased the degradation rate [12,101].

Another route for modulating the degradation rates is to incorporate nondegradable moieties into the soft segment. A secondary effect is that copolymerization or blending in these nondegradable moieties also disrupts the polymer crystallinity. In a study by Hong et al., a polycarbonate diol was mixed with PCL diol at different ratios to investigate the effect on degradation. They found that introducing the polycarbonate diol in increasing amounts slowed the degradation rate [103]. Ma et al. [33] demonstrated that a decrease in soft segment crystallinity, even with nondegradable groups such as carbonates, resulted in an increase in the degradation rate over the semicrystalline polyester.

1.7.2 Effect of hard segment

Several studies have been conducted on biostable polyurethanes to elucidate the effects of hard segment chemistry on polyurethane degradation rate. Tang et al. [104,105] observed the effects of hard segment chemistry and hard segment content

on the enzymatic degradation of polycarbonate urethanes (PCU). The study on hard segment chemistry specifically looked at differences in polycarbonate–polyurethanes synthesized from HDI, MDI, and H_{12}MDI. Although it was also found that PCU with both MDI and HMDI were found to degrade similarly initially, later time points indicated increased degradation of HMDI-based polyurethanes [104]. Similar degradation patterns were observed by Kim and Kim [106] in poly(ester urethane)s synthesized with the same isocyanates. Tang and colleagues concluded that the increased cohesion of the MDI-based hard domains made it more resistant to degradation [104]. It is reasonable to assume that the same principle can be applied to resorbable polyurethanes.

Additional labile sites have been introduced into the hard segment to increase the degradation rate through the use of a biodegradable chain extender. Tatai et al. reported an increased rate of hard segment hydrolytic degradation with the use of an ester-based chain extender that was made by end capping ethylene glycol with lactic acid. Their results indicated that the hard segment rate of degradation was higher than that of the PCL soft segment and the control polyurethane [107]. Similarly, Skarja and Woodhouse tested the degradation of several polyurethanes that contained an amino acid-derived chain extender. Compared to control polyester urethanes, this amino acid-based chain extender increased the degradation rate when treated with enzymatic media but showed no significant difference in buffer. From these results, they suggested that amino acid ester chain extenders were susceptible to enzymatic attack.

Along with the effects that chemical structures have on degradation, the weight fraction of hard segment also influences rate. Tang et al. [108] looked at the effect of hard segment content on the degradation and reported that as the hard segment content increased, the enzymatic degradation rate was reduced. Similar results were obtained by Lendlein and Langer on polyester urethanes that ranged from zero to 83% hard segment content [109]. In summary, the hard segment content does influence enzymatic degradation rate as much as hard segment chemistry [12].

1.8   Summary and future perspectives

Significant effort has been focused on the development of resorbable polyurethanes for applications in a variety of biomedical applications including tissue engineering scaffolds, controlled release applications, wound dressings, abdominal wall reconstruction, and many others. In this chapter, key structure–property relationships of biodegradable polyurethanes were presented. In addition to the traditional hard segment and soft segment effects on mechanical properties, the compositional effects on degradation rate were also discussed. Design of biodegradable polyurethane devices depends on balancing mechanical property requirements and the desired degradation rate. These properties are often coupled in biodegradable polyurethane formulations and this makes it difficult to tune degradation rate independent of target mechanical properties. Furthermore, biodegradable formulations lack the breadth of properties available in the more established biostable polyurethanes. Current research is focused on both of these key areas: decoupling mechanical properties from degradation rate and expanding the properties available. Overall, the highly tunable mechanical and

physicochemical properties of biodegradable polyurethanes make them promising candidates in the rapidly growing resorbable device market.

References

[1] Anderson J, et al. Recent advances in biomedical polyurethane biostaility and biodegradation. Polym Int 1998;46(3):163–71.

[2] Bezwada R. From biostable to biodegradable polymers for biomedical applications. PMSE Prepr 2009;101:1044–5.

[3] Boretos JW, Pierce WS. Segmented polyurethane: a polyether polymer. An initial evalution for biomedical applications. J Biomed Mater Res 1968;2(1):121–30.

[4] Gogolewski S. Selected topics in biomedical polyurethanes: a review. Colloid Polym Sci 1989;267(9):757–85.

[5] Gunatillake PA, et al. Designing biostable polyurethane elastomers for biomedical implants. Aust J Chem 2003;56(6):545–57.

[6] Lamba NMK, Woodhouse KA, Cooper SL. Polyurethanes in biomedical applications. Boca Raton, FL: CRC Press LLC; 1998. p. 277.

[7] Vermette P, et al. Biomedical applications of polyurethanes, vol. 6. Georgetown, TX: Landes Bioscience; 2001.

[8] Gogolewski S, et al. Structure-property relations and cytotoxicity of isosorbide-based biodegradable polyurethane scaffolds for tissue repair and regeneration. J Biomed Mater Res 2008;85A:456–65.

[9] Klinedinst DB, et al. Structure-property behavior of new segmented polyurethanes and polyureas without use of chain extenders. Rubber Chem Technol 2005;78(5):737–53.

[10] Sarkar D, Yang J-C, Lopina S. Structure-property relationship of L-tyrosine-based polyurethanes for biomaterial applications. J Appl Polym Sci 2008;108(4):2345–55.

[11] Sheth J, et al. A comparative study of the structure-property behavior of highly branched segmented poly(urethane urea) copolymers and their linear analogs. Polymer 2005;46:10180–90.

[12] Skarja GA, Woodhouse KA. Structure-property relationships of degradable polyurethane elastomers containing an amino acid-based chain extender. J Appl Polym Sci 2000;75(12):1522–34.

[13] Abouzahr S, Wilkes GL. Structure property studies of polyester–and polyether–based MDI–BD segmented polyurethanes: effect of one–vs two–stage polymerization conditions. J Appl Polym Sci 1984;29(9):2695–711.

[14] Hourston DJ, et al. Structure–property study of polyurethane anionomers based on various polyols and diisocyanates. J Appl Polym Sci 1997;66(10):2035–44.

[15] Blackwell J, Nagarajan M, Hoitink T. Structure of polyurethane elastomers: effect of chain extender length on the structure of MDI/diol hard segments. Polymer 1982;23(7):950–6.

[16] Speckhard T, et al. Properties of polyisobutylene polyurethane block copolymers: 3. Hard segments based on 4, 4′-dicyclohexylmethane diisocyanate (H_{12}MDI) and butane diol. Polymer 1985;26(1):70–8.

[17] Fernández d'Arlas B, et al. Microdomain composition and properties differences of biodegradable polyurethanes based on MDI and HDI. Polym Eng Sci 2008;48(3):519–29.

[18] Szycher M. Szycher's Handbook of polyurethanes. 2nd ed. Boca Raton, FL: Taylor & Francis; 2012.

[19] Ahn TO, et al. Thermal and mechanical properties of thermoplastic polyurethane elastomers from different polymerization methods. Polym Int 1993;31(4):329–33.

[20] Blackwell J, Gardner KH. Structure of the hard segments in polyurethane elastomers. Polymer 1979;20(1):13–7.
[21] Cooper SL, Tobolsky AV. Properties of linear elastomeric polyurethanes. J Appl Polym Sci 1966;10(12):1837–44.
[22] Kanyanta V, Ivankovic A. Mechanical characterisation of polyurethane elastomer for biomedical applications. J Mech Behav Biomed Mater 2010;3(1):51–62.
[23] Koevoets RA, et al. Molecular recognition in a thermoplastic elastomer. J Am Chem Soc 2005;127(9):2999–3003.
[24] Król P, Pilch–Pitera B. Phase structure and thermal stability of crosslinked polyurethane elastomers based on well-defined prepolymers. J Appl Polym Sci 2007;104(3):1464–74.
[25] Guelcher SA. Biodegradable polyurethanes: synthesis and applications in regenerative medicine. Tissue Eng Part B Rev 2008;14(1):3–17.
[26] Hafeman A, Davidson J, Guelcher S. Effects of polyol, isocyanate, and additives on poly(ester urethane)urea scaffolds: material and in vivo histological properties. PMSE Prepr 2007;97:546.
[27] Gisselfalt K, Helgee B. Effect of soft segment length and chain extender structure on phase separation and morphology in poly(urethane urea)s. Macromol Mater Eng 2003;288(3):265–71.
[28] Martin DJ, et al. The effect of average soft segment length on morphology and properties of a series of polyurethane elastomers. II. SAXS–DSC annealing study. J Appl Polym Sci 1997;64(4):803–17.
[29] Bakker D, et al. Biocompatibility of a polyether urethane, polypropylene oxide, and a polyether polyester copolymer. A qualitative and quantitative study of three alloplastic tympanic membrane materials in the rat middle ear. J Biomed Mater Res 1990;24(4):489–515.
[30] Brown D, Lowry R, Smith L. Hydrolytic degradation of polyester polyurethanes containing carbodiimides. Macromolecules 1982;15(2):453–8.
[31] Driffield M, Bradley EL, Castle L. A method of test for residual isophorone diisocyanate trimer in new polyester-polyurethane coatings on light metal packaging using liquid chromatography with tandem mass spectrometric detection. J Chromatogr A 2007;1141(1):61–6.
[32] Guelcher S, et al. Synthesis, in vitro degradation, and mechanical properties of two-component poly(ester urethane)urea scaffolds: effects of water and polyol composition. Tissue Eng 2007;13(9):2321–33.
[33] Ma Z, et al. Biodegradable polyurethane ureas with variable polyester or polycarbonate soft segments: effects of crystallinity, molecular weight, and composition on mechanical properties. Biomacromolecules 2011;12(9):3265–74.
[34] Stokes K, McVenes R. Polyurethane elastomer biostability. J Biomater Appl 1995; 9(4):321–54.
[35] Wang Y, et al. Degradation studies on segmented polyurethanes prepared with poly (D, L-lactic acid) diol, hexamethylene diisocyanate and different chain extenders. Polym Degrad Stab 2011;96(9):1687–94.
[36] Chen JH, et al. Studies on segmented polyetherurethane for biomedical application: effects of composition and hard-segment content on biocompatibility. J Biomed Mater Res 1998;41(4):633–48.
[37] Lin S, et al. Segmental orientation studies of polyether polyurethane block copolymers with different hard segment lengths and distributions. Colloid Polym Sci 1985;263(2):128–40.
[38] Miller J, et al. Properties of polyether-polyurethane block copolymers: effects of hard segment length distribution. Macromolecules 1985;18:32–44.

[39] Paik Sung C, Smith T, Sung N. Properties of segmented polyether poly(urethaneureas) based of 2, 4-toluene diisocyanate. 2. Infrared and mechanical studies. Macromolecules 1980;13(1):117–21.

[40] Santerre J, Labow R. The effect of hard segment size on the hydrolytic stability of polyether-urea-urethanes when exposed to cholesterol esterase. J Biomed Mater Res 1997;36(2):223–32.

[41] Wang CB, Cooper SL. Morphology and properties of segmented polyether polyurethaneureas. Macromolecules 1983;16(5):775–86.

[42] Yilgör E, et al. Comparison of hydrogen bonding in polydimethylsiloxane and polyether based urethane and urea copolymers. Polymer 2000;41(3):849–57.

[43] Yilgör E, Yurtsever E, Yilgör I. Hydrogen bonding and polyurethane morphology. II. Spectroscopic, thermal and crystallization behavior of polyether blends with 1, 3-dimethylurea and a model urethane compound. Polymer 2002;43(24):6561–8.

[44] Yilgor I, et al. Time-dependent morphology development in segmented polyether-urea copolymers based on aromatic diisocyanates. J Polym Sci Part B Polym Phys 2009;47(5):471–83.

[45] Rueda-Larraz L, et al. Synthesis and microstructure–mechanical property relationships of segmented polyurethanes based on a PCL–PTHF–PCL block copolymer as soft segment. Eur Polym J 2009;45(7):2096–109.

[46] Cohn D, et al. Biodegradable poly(ethylene oxide)/poly(e-caprolactone) multiblock copolymers. J Biomed Mater Res 2002;59(2):273–81.

[47] Benhardt H, et al. Synthesis of collagenase–sensitive polyureas for ligament tissue engineering. Macromol Biosci 2011;11(8):1020–30.

[48] Guan J, Wagner WR. Synthesis, characterization and cytocompatibility of polyurethan-eurea elastomers with designed elastase sensitivity. Biomacromolecules 2005;6(5):2833–42.

[49] Abraham G, Marcos-Fernandez A, San Roman J. Bioresorbable poly(ester-ether urethane)s from L-lysine diisocyanate and triblock copolymers with different hydrophilic character. J Biomed Mater Res Part A 2006;76A(4):729–36.

[50] Guelcher SA, et al. Synthesis and in vitro biocompatibility of injectable polyurethane foam scaffolds. Tissue Eng 2006;12(5):1247–59.

[51] Wiggins J, Storey R. Synthesis and characterization of L-lysine-based poly(ester urethane) networks. Polym Prepr 1992;33(2):516–7.

[52] Spaans C, et al. High molecular weight polyurethanes and a polyurethane urea based on 1, 4-butanediisocyanate. Polym Bull 1998;41(2):131–8.

[53] Zuidema J, et al. In vitro degradation of a biodegradable polyurethane foam, based on 1,4-butanediisocyanate: a three-year study at physiological and elevated temperature. J Biomed Mater Res Part A 2009;90A(3):920–30.

[54] Chen TK, Shieh TS, Chui JY. Studies on the first DSC endotherm of polyurethane hard segment based on 4,4′-diphenylmethane diisocyanate and 1,4-butanediol. Macromolecules 1998;31(4):1312–20.

[55] Hirt TD, Neuenshwander P, Suter UW. Synthesis of degradable, biocompatible, and tough block-copolyesterurethanes. Macromol Chem Phys 1996;197:4253–68.

[56] Klinedinst DB, et al. The effect of varying soft and hard segment length on the structure–property relationships of segmented polyurethanes based on a linear symmetric diisocyanate, 1,4-butanediol and PTMO soft segments. Polymer 2012;53(23):5358–66.

[57] Ramesh S, Rajalingam P, Radhakrishnan G. Chain–extended polyurethanes—synthesis and characterization. Polym Int 1991;25(4):253–6.

[58] Garrett JT, et al. Phase separation of diamine chain-extended poly(urethane) copolymers: FTIR spectroscopy and phase transitions. Polymer 2003;44(9):2711–9.

[59] Gisselfalt K, Edeberg B, Flodin P. Synthesis and properties of degradable poly(urethane urea)s to be used for ligament reconstructions. Biomacromolecules 2002;3:951–8.

[60] Bassi M, Tonelli C, Di Meo A. Glass transition behavior of a microphase segregated polyurethane based on PFPE and IPDI. A calorimetric study. Macromolecules 2003;36(21):8015–23.

[61] Chu B, et al. Microphase separation kinetics in segmented polyurethanes: effects of soft segment length and structure. Macromolecules 1992;25(21):5724–9.

[62] Garrett J, Runt J, Lin J. Microphase separation of segmented poly(urethane urea) block copolymers. Macromolecules 2000;33(17):6353–9.

[63] He Y, Zhang X, Runt J. The role of diisocyanate structure on microphase separation of solution polymerized polyureas. Polymer 2014;55(3):906–13.

[64] Nakamae K, Nishino T, Asaoka S. Microphase separation and surface properties of segmented polyurethane—Effect of hard segment content. Int J Adhes Adhes 1996;16(4):233–9.

[65] Pongkitwitoon S, et al. Temperature dependent microphase mixing of model polyurethanes with different intersegment compatibilities. Polymer 2009;50(26):6305–11.

[66] Wagener K, Matayabas Jr J. Quantitative determination of microphase separation: effect of hard-segment length. Macromolecules 1992;25(21):5591–6.

[67] Hansen CM. The universality of the solubility parameter. Ind Eng Chem Prod Res Dev 1969;8(1):2–11.

[68] Hansen CM. 50 Years with solubility parameters—past and future. Prog Org Coat 2004;51(1):77–84.

[69] Lee SY, Lee JS, Kim BK. Preparation and properties of water-borne polyurethanes. Polym Int 1997;42(1):67–76.

[70] Chang A, et al. Morphological study of the structure developed during the polymerization of a series of segmented polyurethanes. Polymer 1982;23(7):1060–8.

[71] Zha L, Wu M, Yang J. Hydrogen bonding and morphological structure of segmented polyurethanes based on hydroquinone–bis (β–hydroxyethy) ether as a chain extender. J Appl Polym Sci 1999;73(14):2895–902.

[72] O'Sickey MJ, Lawrey BD, Wilkes GL. Structure–property relationships of poly(urethane urea)s with ultra–low monol content poly(propylene glycol) soft segments. I. Influence of soft segment molecular weight and hard segment content. J Appl Polym Sci 2002;84(2):229–43.

[73] Senich G, MacKnight W. Fourier transform infrared thermal analysis of a segmented polyurethane. Macromolecules 1979;13:106–10.

[74] Yilgor I, et al. FTIR investigation of the influence of diisocyanate symmetry on the morphology development in model segmented polyurethanes. Polymer 2006;47(11):4105–14.

[75] Musselman S, et al. Domain structure and interphase dimensions in poly(urethaneurea) elastomers using DSC and SAXS. J Polym Sci Part B Polym Phys 1999;37(18):2586–600.

[76] Fridman I, Thomas E. Morphology of crystalline polyurethane hard segment domains and spherulites. Polymer 1980;21(4):388–92.

[77] Bonart R. Macromol Sci D Phys 1968;B2(1):115–38.

[78] Hu W, Koberstein J. The effect of thermal annealing on the thermal properties and molecular weight of a segmented polyurethane copolymer. J Polym Sci Part B Polym Phys 1994;32(3):437–46.

[79] Saiani A, et al. Origin of multiple melting endotherms in a high hard block content polyurethane: effect of annealing temperature. Macromolecules 2007;40(20):7252–62.

[80] Lelah MD, Cooper SL. Polyurethanes in medicine. Boca Raton, FL: CRC press; 1986.

[81] Mi H-Y, et al. Morphology, mechanical properties, and mineralization of rigid thermo-plastic polyurethane/hydroxyapatite scaffolds for bone tissue applications: effects of fabrication approaches and hydroxyapatite size. J Mater Sci 2014;49(5):2324–37.

[82] Wilkes CE, Yusek CS. Investigation of domain structure in urethan elastomers by X-ray and thermal methods. J Macromol Sci Part B Phys 1973;7(1):157–75.

[83] Wilkes GL, Wildnauer R. Kinetic behavior of the thermal and mechanical properties of segmented urethanes. J Appl Phys 1975;46(10):4148–52.

[84] Grujicic M, et al. Multi-length scale modeling and analysis of microstructure evolution and mechanical properties in polyurea. J Mater Sci 2011;46(6):1767–79.

[85] Madhavan K, Reddy BSR. Synthesis and characterization of poly(dimethylsiloxane-urethane) elastomers: effect of hard segments of polyurethane on morphological and mechanical properties. J Polym Sci Part A Polym Chem 2006;44(9):2980–9.

[86] Wisse E, et al. Unusual tuning of mechanical properties of thermoplastic elastomers using supramolecular fillers. Macromolecules 2006;39(21):7425–32.

[87] Das S, et al. Structure–property relationships and melt rheology of segmented, non-chain extended polyureas: effect of soft segment molecular weight. Polymer 2007; 48(1):290–301.

[88] Yilgor I, et al. Influence of soft segment molecular weight on the mechanical hysteresis and set behavior of silicone-urea copolymers with low hard segment contents. Polymer 2011;52(2):266–74.

[89] Morbitzer L, Hespe H. Correlations between chemical structure, stress−induced crystallization, and deformation behavior of polyurethane elastomers. J Appl Polym Sci 1972;16(10):2697–708.

[90] Yeh F, et al. In-situ studies of structure development during deformation of a segmented poly(urethane-urea) elastomer. Macromolecules 2003;36(6):1940–54.

[91] Santerre J, et al. Understanding the biodegradation of polyurethanes: from classical implants to tissue engineering materials. Biomaterials 2005;26(35):7457–70.

[92] Sheth JP, et al. Role of chain symmetry and hydrogen bonding in segmented copolymers with monodisperse hard segments. Polymer 2005;46(18):7317–22.

[93] Dempsey DK, et al. Characterization of a resorbable poly(ester urethane) with biodegradable hard segments. J Biomater Sci Polym Ed 2014;25(6):535–54.

[94] Chan-Chan L, et al. Degradation studies on segmented polyurethanes prepared with HMDI, PCL and different chain extenders. Acta Biomater 2010;6:2035–44.

[95] Seefried C, Koleske J, Critchfield F. Thermoplastic urethane elastomers. III. Effects of variations in isocyanate structure. J Appl Polym Sci 1975;19(12):3185–91.

[96] De Groot J, et al. New biomedical polyurethane ureas with high tear strengths. Polym Bull 1997;38(2):211–8.

[97] Sawhney A, Hubbell J. Rapidly degraded terpolymers of dl-lactide, glycolide, and e-caprolactone with increased hydrophilicity by copolymerization with polyethers. J Biomed Mater Res 1990;24(10):1397–411.

[98] Fromstein J, Woodhouse K. Elastomeric biodegradable polyurethane blends for soft tissue applications. J Biomater Sci Polym Ed 2002;13(4):391–406.

[99] Gorna K, Gogolewski S. In vitro degradation of novel medical biodegradable aliphatic polyurethanes based on e-caprolactone and Pluronics with various hydrophilics. Polym Degrad Stab 2002;75:113–22.

[100] Guan J, et al. Synthesis, characterization, and cytocompatibility of elastomeric, biodegradable poly(ester-urethane)ureas based on poly(caprolactone) and putrescine. J Biomed Mater Res 2002;61(3):493–503.

[101] Skarja G, Woodhouse K. Synthesis and characterization of degradable polyurethane elastomers containing an amino acid-based chain extender. J Biomater Sci Polym Ed 1998;9(3):271–95.

[102] Wang F, et al. Synthesis, characterization and surface modification of low moduli poly(ether carbonate urethane)ureas for soft tissue engineering. Acta Biomater 2009;5(8):2901–12.

[103] Hong Y, et al. Tailoring the degradation kinetics of poly(ester carbonate urethane)urea thermoplastic elastomers for tissue engineering scaffolds. Biomaterials 2010;31(15):4249–58.

[104] Tang Y, Labow R, Santerre J. Enzyme-induced biodegradation of polycarbonate-polyurethanes: dependence on hard-segment chemistry. J Biomed Mater Res 2001;57(4):597–611.

[105] Tang Y, Labow R, Santerre J. Enzyme-induced biodegradation of polycarbonate-polyurethanes: dependence on hard-segment concentration. J Biomed Mater Res 2001;57:516–28.

[106] Kim Y, Kim S. Effect of chemical structure on the biodegradation of polyurethanes under composting conditions. Polym Degrad Stab 1998;62:343–52.

[107] Tatai L, et al. Thermoplastic biodegradable polyurethanes: the effect of chain extender structure on properties and in vitro degradation. Biomaterials 2007;28:5407–17.

[108] Tang Y, et al. Influence of surface morphology and chemistry on the enzyme catalyzed biodegradation of polycarbonate-urethanes. J Biomater Sci Polym Ed 2002;13(4):463–83.

[109] Lendlein A, Langer R. Biodegradable, elastic shape-memory polymers for potential biomedical applications. Science 2002;296(5573):1673–6.

Surface characterization techniques for polyurethane biomaterials

2

*H. Zhang**
Lubrizol Advanced Materials Inc., Brecksville, OH, USA
*Corresponding author: asterphoenix@gmail.com

> Disclaimer: Mention of trade names or commercial products in this chapter is solely for the purpose of providing specific information and does not imply endorsement by Lubrizol Corp.

Polyurethane is probably the most versatile thermoplastic elastomer with many great properties. Commercial products made from polyurethanes include artificial hearts, catheters, feeding tubes, surgical drains, intraaortic balloon pumps, dialysis devices, nonallergenic gloves, medical garments, hospital bedding, wound dressings, and more. In typical applications, polyurethane surfaces have to interact with various body fluids, tissues, or organs. Thus the surface properties of polyurethane biomaterials are the key factors in determining the performance of finished products. Deficiencies in surface properties are the leading cause of implant failure such as surface erosion, immune response, chronic inflammation, thrombi formation, and bacterial infection. For this reason, a tremendous amount of research has been focused on surface modification of polyurethane biomaterials to improve their lubricity, hydrophilicity/hydrophobicity, hemocompatability, antithromobogenicity, and antimicrobial activity. Thus, it is equally important that proper surface characterization techniques are applied during such research. The scope of this chapter is to provide a brief introduction to nine popular surface characterization techniques and also offer several examples to show how each technique may be applied. Some characterization techniques such as atomic force microscopy and attenuated total reflectance infrared spectroscopy (ATR–FTIR) are not covered in this chapter. If more detailed information is needed, multiple reviews are available for further reading [1–7].

2.1   Friction measurement

Using medical devices such as catheters, angioplasty balloons, pacemaker leads, and cardiovascular stents usually involves insertion of such devices into urinal tracts or blood vessels. During insertion, high surface lubricity of the devices helps to facilitate the insertion process and reduce insertion-associated tissue damage, which benefits both the patient and the surgeon. Early approaches to decrease insertion friction involve using lubricants such as olive oil and silicon oil, or low friction materials like polyethylene. Due to the superior mechanical properties, polyurethane is extensively used in catheters/balloons and it is desirable to improve the lubricity of polyurethane materials.
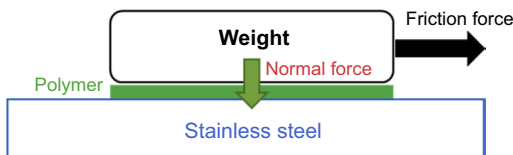
Figure 2.1 COF measurement demonstration.

In modern theory of friction, 90% of the total friction is believed to come from interatomic adhesion between two surfaces [8]. If the interatomic adhesion is weakened, the friction force could be reduced. If water, the most abundant fluid in the body, easily wets the polymer surface and creates a thin layer between two surfaces to eliminate solid/solid contact, the friction force could be significantly reduced. Therefore, a general approach of friction reduction is to increase the surface hydrophilicity of polyurethane by coating or by surface chemical modification [9–22].

2.1.1   Coefficient of friction measurement

Coefficient of friction (COF) is a dimensionless number that is defined as the ratio between friction force and normal force (Eqn (2.1)). Materials with COF smaller than 0.1 are considered lubricous materials. COF depends on the nature of the materials and surface roughness. Usually, ASTM D1894-14 is the most widely used method for COF measurement. This method involves a polymer sheet or film with a fixed weight on top. The polymer sample is dragged along a stainless steel sheet under dry or wet conditions and friction force is thus measured by a forcemeter (Figure 2.1). The normal force in this test is equal to the gravity force of the weight.

$$COF = F_{friction}/F_{normal} \qquad\qquad (2.1)$$

Gu et al. [23] used ozone to pretreat a Pellethane® surface and later functionalized the surface with polyacrylic acid. The surface hydrophilicity of Pellethane® thermoplastic polyurethane ("TPU") is significantly improved by showing a much lower water contact angle (CA; 25° vs 92° of pure Pellethane® TPU, for CA test, please see Section 2.2) The COF of the modified surface was as low as 0.1.

A modified COF measurement method for testing finished catheters was reported by Kazmierska [24]. The tribology device is shown in Figure 2.2. A motor winds the strand and pulls the catheter against a weighted surface in a water bath. The friction force is measured by a forcemeter and the normal force is the difference of gravity force of the weight subtracted by the buoyancy force.

2.1.2   Trackability measurement

When a medical prosthesis such as a catheter, guide wire, angioplasty balloon, or stent is inserted to a blood vessel, external force is needed to advance the prosthesis into the right position. Ideally, the force used should be as low as possible to minimize surgeons'
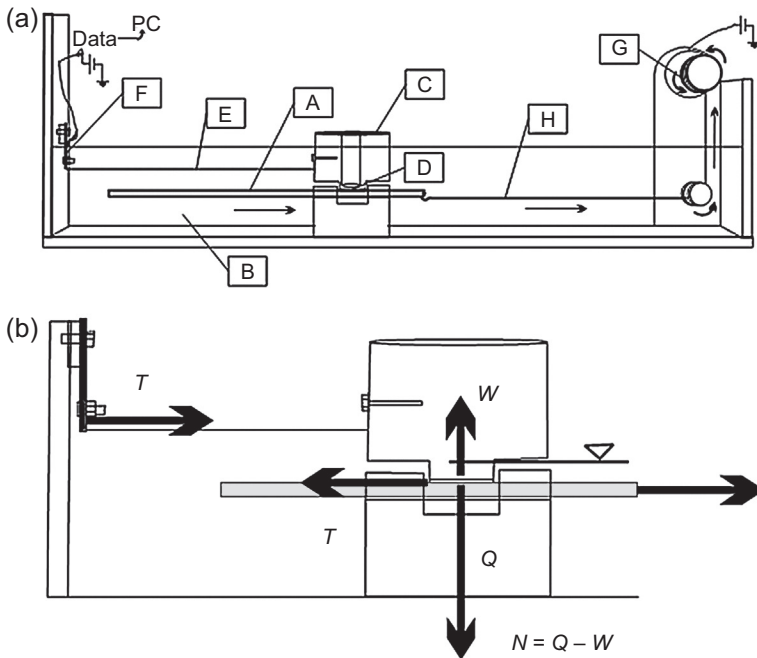
Figure 2.2 Modified COF device for a catheter. (a) A, tested catheter; B, a vessel filled with distilled water; C, polymer element pressing down the catheter, rigidly connected, via rod E, with forcemeter F; D, an exchangeable counterface; G, DC motor coiling the strand H; (b) I = N/T; T, friction force; N, normal force, which is the difference of a force of gravity Q and a buoyancy W.
Reprinted with permission from Ref. [24].

work and damage to the blood vessel. COF measurement is a simple method to test raw materials. In order to simulate the insertion of a finished product in a tortuous pathway [25], ANSI/AAMI/ISO 25539 has been used as a test protocol (Figure 2.3). A polytetrafluoroethylene (PTFE) tube is commonly used to simulate a blood vessel and is placed in a temperature-controlled water bath. The test sample (guide wire/catheter) is inserted into the PTFE tube by a proximal roller assembly. The pushing force versus advancement distance is measured and plotted to show the trackability of the sample.

2.2 Contact angle

When a drop of liquid is sitting on a flat, horizontal solid surface, the CA is defined as the angle formed by the intersection of the liquid–solid interface and liquid–gas interface. Thomas Young first proposed to treat the CA of a liquid on a surface as the mechanical equilibrium of surface tension of three interfaces: solid–gas, solid–liquid, and liquid–gas (Figure 2.4). Since the liquid droplet is in mechanical equilibrium, the CA θ is determined from these surface tensions using Young's equation (Eqn (2.2)).
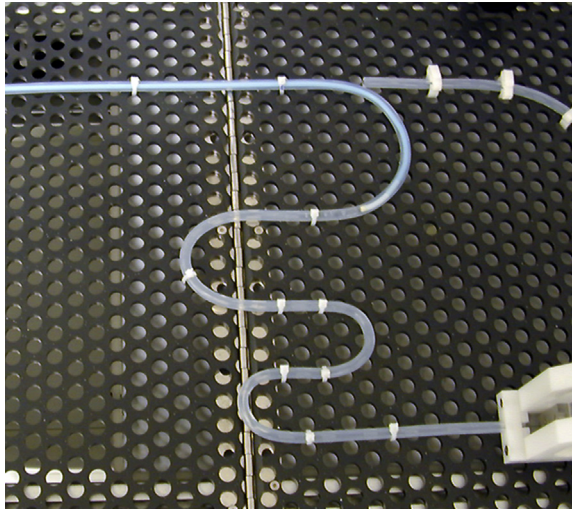
Figure 2.3 Trackability test.
Credited from Machine Solution Inc.
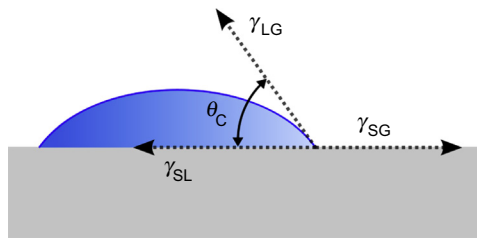
Figure 2.4 A static liquid droplet showing all three surface tensions (γ_{SG}, γ_{SL}, and γ_{LG} represent the surface tension of solid–gas, solid–liquid, and liquid–gas, respectively).

A CA less than 90° suggests that wetting of the surface is favorable; a CA greater than 90° means that the liquid prefers to minimize the contact with the surface.

$$\gamma_{SG} = \gamma_{SL} + \gamma_{LG} \cos \theta \tag{2.2}$$

CA measurement is a facile, easy to apply technique that produces surface wetting and/or surface tension information. For polyurethane biomaterials, the commonly used liquid in this test is water. The CA gives us important information about the polyurethane, such as hydrophilicity/hydrophobicity, surface tension, and surface reorganization kinetics [26–29].

Although CA seems like a very easy measurement, care must be taken during CA measurements since many factors can interfere with CA results: The water must be as pure as possible since impurity such as surfactants will drastically change the interfacial tension of water; the polymer surface must be thoroughly cleaned and should not have any extractable low molecular weight (MW) contaminants, such as unreacted monomers or wax or additives.
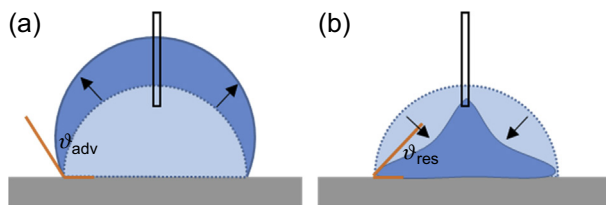
Figure 2.5 Demonstration of dynamic sessile drop method (a) add water for θ_{adv}; (b) withdraw water for θ_{rec}.

There are two categories of CAs: static and dynamic. Each category has several test methods/instruments. Some of these methods will be discussed in the following section.

2.2.1 Static sessile drop

A typical static sessile drop is created by a microsyringe with an automated plunger to place a tiny drop of water on the polymer surface. Ideally, the polymer sample should be in a humidity chamber to minimize the water evaporation that would change the shape, and thus the CA of the droplet. The shape of the droplet is captured by a camera and CA is measured by an image analysis software [30].

2.2.2 Dynamic contact angle

Polyurethane is a segmented polymer with both a hard segment (diisocyanate/chain extender crystalline region) and a soft segment (polyols amorphous region). Essentially, all polymers with nonhomogeneous surfaces will reorganize, to a certain extent, to expose their hydrophilic segment toward the polymer/water interface when contacting water [31–39]. Such nonhomogeneity can only be fully evaluated with the dynamic CA method. In the dynamic CA method, information of both advancing CA (θ_{adv}) and receding CA (θ_{rec}) is obtained. The advancing CA, θ_{adv}, is sensitive to the hydrophobic surface component because θ_{adv} is measured when water tries to wet the surface. During this process, the hydrophobic parts of the polymer try to prevent the wetting process. On the contrary, the receding CA, θ_{rec}, is sensitive to the hydrophilic surface component since the water is trying to dewet the surface and the hydrophilic region will try to keep the water from dewetting [40].

2.2.2.1 Dynamic sessile drop

Dynamic sessile drop is very similar to the static sessile method. A small drop of water is carefully added on top of the polymer surface by a microsyringe with a very thin needle. The needle is kept inside of the water droplet after the droplet is settled. A computer program controls the syringe to add a very small quantity of water to the existing droplet to gradually expand the size of the droplet while the contact area between water and polymer is kept the same. Just when this contact area starts to expand, a CA is recorded. The CA obtained during this process is θ_{adv} since water tends to advance to wet the surface (Figure 2.5(a)). After θ_{adv} is recorded, a reverse process is carried out to
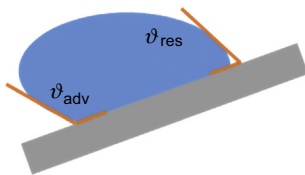
Figure 2.6 Tilting stage method to obtain dynamic CA.

slowly decrease the size of droplet by withdrawing water from the droplet. Such process will generate θ_{rec}, which is obtained right when the contact area shrinks (Figure 2.5(b)).

A modified sessile drop method does not involve addition and subtraction of water. Instead, water droplet is added on a tilting stage. The stage is tilted by an automated program and water drop will deform into an asymmetric shape (Figure 2.6). While the stage is tilting, the image of water drop is captured by software right before it rolls down the polymer surface. Both θ_{adv} and θ_{rec} are measured at this point (Figure 2.6).

Tremendous efforts have been put into surface modification of polyurethane biomaterials to promote cell adhesion [41] and/or depress platelet adhesion [42,43], biofilm formation [44], or protein adsorption [45]. CA is the quickest indirect evidence of confirming these surface modifications. Cooper et al. [41] prepared a series of polyurethanes with surfaces functionalized with three hexapeptides to improve cell adhesion. The polar peptides on the surface increase the hydrophilicity and thus decreased CAs were observed. Again, CA is only an indirect proof of a successful surface modification since there are many factors that contribute to a change in CA. Many other surface characterization techniques must be combined to obtain a full picture of the surface properties of polyurethane biomaterials.

2.2.2.2 Wilhelmy plate

The Wilhelmy plate method is named after the German chemist Ludwig Wilhelmy. It is an indirect method for CA measurement that can be applied to samples in plate, rod, or fiber shape. The experimental setup is shown in Figure 2.7. The sample is attached to the arm of a precision balance. A programmed stage moves up a temperature-controlled water bath so that the sample becomes immersed in water. The stage moves down and then the sample leaves the water. The force applied on the arm is recorded together with the information of the stage positon. The CA is calculated using Eqn (2.3). F is the pulling force and measured by the balance (weight of sample is automatically deducted at the beginning of experiment), L is the wetting length, which is equal to two times the width of the sample, $\gamma_{water/air}$ is the water surface interfacial tension with air at given temperature, θ is the CA, d is the immersed depth of sample (recorded by stage positon), $\Delta\rho$ is the density difference between water and sample, and g is the acceleration of gravity. The Wilhelmy plate machine plots F/L versus d and $\cos\theta$ can be extrapolated at $d=0$. When the sample enters the water, the F/L versus d plot gives θ_{adv}; when sample leaves the water, the F/L versus d plot gives θ_{rec}.

$$\frac{F}{L} = \gamma_{water/air} \cos\theta - d\Delta\rho g$$

(2.3)
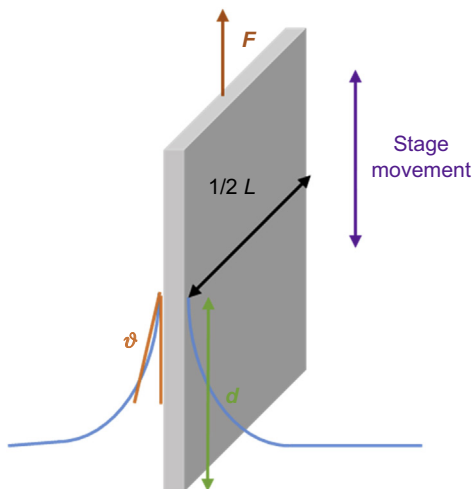
Figure 2.7 Demonstration of Wilhelmy plate method.
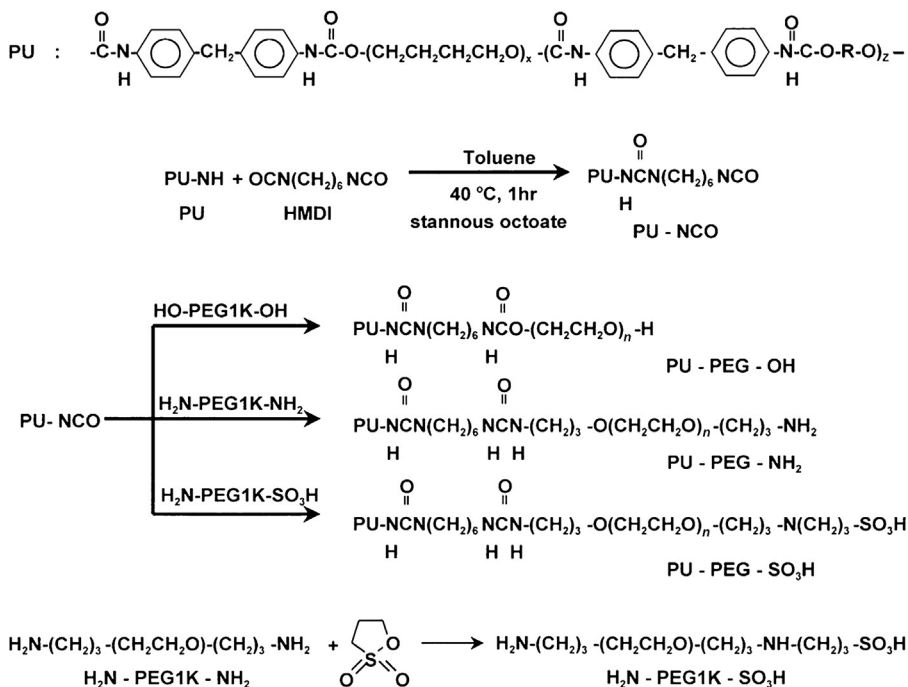
Figure 2.8 Synthetic procedure for PEG modification of PU surfaces.
Reprinted with permission from Ref. [44].

Park et al. [44] modified a Pellethane® surface with poly(ethylene glycol) (MW) = 1000, PEG1k carrying terminal hydroxyl, amino, and sulfonate groups, respectively, to reduce bacterial adhesion (Figure 2.8). After modification, the authors measured the dynamic CA before and after hydration using the Wilhelmy plate method.

Because the polymer surface reorients the hydrophilic groups toward polymer/water interfaces, modified polyurethanes show much lower CA after hydration (Table 2.1). PU–PEG 1K–OH, PU–PEG 1K–NH$_2$, and PU–PEG 1K–SO$_3$H show complete wetting (undetectable θ_{rec}) after hydration, suggesting a superhydrophilic nature of the modified surfaces. The hydrophilic surface modifications greatly reduced *Escherichia coli* adhesion.

2.3   X-ray photoelectron spectroscopy

X-ray photoelectron spectroscopy (XPS), also referred to as electron spectroscopy for chemical analysis, is a surface characterization technique based on the photoelectron effect. XPS surveys the electron binding energy spectrum of a sample surface resulting in a plot of binding energy versus total electron count. Since the binding energy of electrons of different elements is different, XPS can be used to identify the different elements present on the surface and the composition ratio of each element. In theory, XPS can detect all elements. However, H and He are barely detected in practical situations [46].

Chemical bonding or chemical state plays an important role in the binding energy of the electron orbital and thus gives rise to observable energy shifts in the kinetic energy of the photoelectron. These binding energy shifts can be used to extract information of a chemical nature (such as atomic oxidation state/chemical bonding) at the sample surface. The data are readily available on the National Institute of Standards and Technology Website (http://srdata.nist.gov/xps/Default.aspx).

XPS uses the photoelectronic effect to obtain binding energy information (Eqn (2.4)). When the ample surface is irradiated by X-rays, the X-rays knock out outer electrons on the surface. This process is an energy conservation process so the photonic

Table 2.1 Dynamic contact angles of PEG-modified Pellethane® surfaces

Materials	Dry		Hydration	
	θ_{adv}	θ_{rec}	θ_{adv}	θ_{rec}
PU (Pellethane®)	93.0±3.0	46.5±4.0	87.6±4.1	39.5±4.7
PU–PPG 1K–OH	78.8±3.0	42.1±5.1	83.6±2.0	41.9±5.6
PU–PEG 1K–OH	44.6±2.5	30.2±0.7	43.9±1.6	Wetting
PU–PEG 1K–NH$_2$	37.0±2.8	24.8±5.4	28.3±3.0	Wetting
PU–PEG 1K–SO$_3$H	33.8±1.2	25.2±6.9	25.6±2.5	Wetting

energy of X-ray E_{photon} (varies with X-ray source: Al Kα X-rays, $E_{photon} = 1486.7\,eV$ and Mg Kα X-rays, $E_{photon} = 1253.6\,eV$) is equal to the sum of $E_{kinetic}$ (kinetic energy of electrons escaped from samples, which can be determined by an energy analyzer) and $E_{binding}$ (binding energy of outer electrons). $E_{binding}$ can be calculated by subtracting $E_{kinetic}$ from E_{photon}.

$$E_{photon} = E_{binding} + E_{kinetic} \qquad (2.4)$$

Because the emitted photoelectrons are strongly attenuated when passing through the sample material itself, only photoelectrons of the top 0–10 nm of the sample can escape from the sample itself and become analyzed. Therefore, XPS is a characterization technique that provides the information of the very topmost layer of the material. For the same reason, XPS requires high vacuum or ultrahigh vacuum so that the energy of photoelectrons can be preserved during the process between leaving the sample and entering the energy analyzer of XPS instrument.

To increase the hemocompatability and reduce platelet adhesion to TPUs, different approaches have been employed such as coating, surface grafting, and blending with surface modification additives. XPS is a crucial technique for confirming the surface chemical composition of these modifications. For example, Ishihara et al. synthesized a series of methacrylate copolymers with a phosphoryl choline moiety. These polymers were coated on a Pellethane® film to reduce platelet adhesion on blood contact [47]. XPS indicated the chemical composition before and after the coating process. Both carbon and oxygen peaks barely change because the PMBBU (Figures 2.9 and 2.10) polymer has carbon and oxygen bonds similar to those of the substrate Pellethane® TPU. Nitrogen of urethane bonds appears (401 eV) in samples both before and after coating. However, after coating, another nitrogen peak appears at approximately 403 eV, indicating quaternary nitrogen from the phosphoryl choline moiety. Other evidence of the phosphoryl choline moiety at the surface is the appearance of the phosphorus peak at 135 eV.

Zwitterionic groups such as phosphoryl choline and sulfonyl betaine can form a hydrated layer to prevent protein adsorption [48–51]. Li and coworkers used urethane chemistry to synthesize a series of oligomeric polyurethanes with terminal
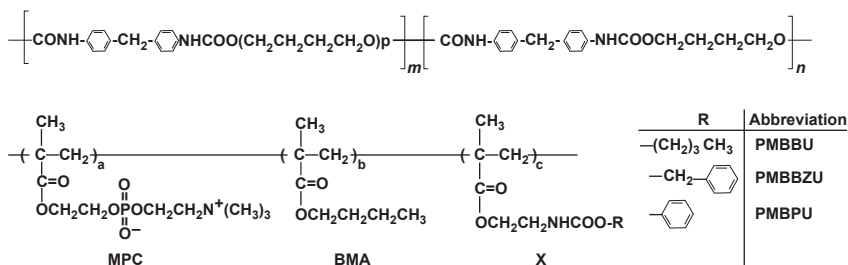
Figure 2.9 Chemical structure of Pellethane® TPU and coating polymers. Reprinted with permission from Ref. [47].
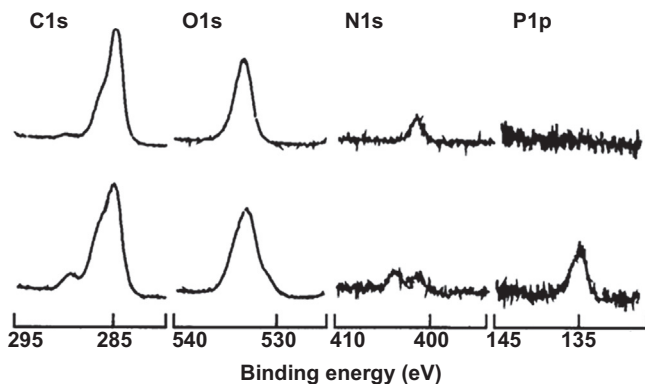
Figure 2.10 XPS comparison before (top) and after (bottom) coating with MPC polymers.
Reprinted with permission from Ref. [47].
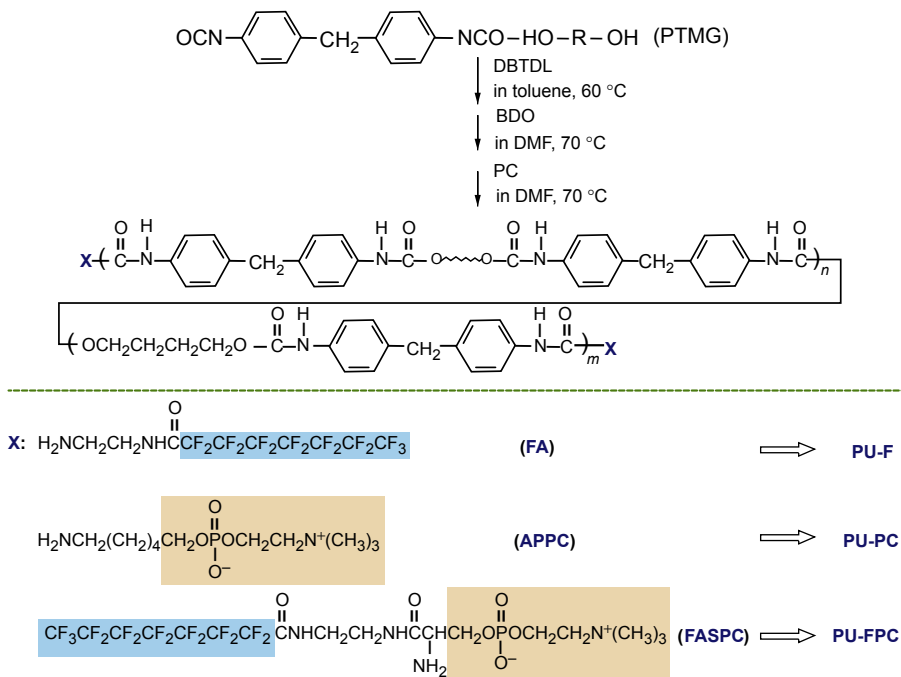
Figure 2.11 Synthesis route of oligomeric polyurethane with terminal phosphorous choline groups.
Reprinted with permission from Ref. [52].

phosphoryl choline groups to reduce protein adsorption on polyurethane surfaces (Figure 2.11) [52,53]. The key to preventing protein adsorption is to have phosphorous choline groups at the polymer surface. To achieve this goal, PU–FPC is synthesized by putting fluorocarbon and phosphorous choline groups together because fluorine has a much lower surface energy and has a great tendency to concentrate at

the polymer/air interface. As a result, PU–FPC shows much higher fluorine content at the surface than in the bulk TPU (Table 2.2). PU–FPC shows 2.5 times higher phosphorous contents than its bulk phosphorous content because fluorinated terminal groups "drag" phosphoryl choline groups to the surface when fluorine concentrates at the surface (Table 2.2).

Polyethylene glycol (PEG) is another well-known molecule used to reduce protein adsorption and/or platelet adhesion. Surface enrichment of a triblock oligomeric PEG containing additive from a polyurethane matrix was reported [54,55]. The authors used PEG as the active groups to suppress protein and platelet adhesion. The authors first synthesized a methylene diphenyl diisocyanate (MDI)–poly (tetramethylene oxide) (PTMO) 1000 prepolymer with a MW of approximately 4750 (PU4750), and then this prepolymer was terminally functionalized with mono amino-polyethylene oxide (PEO) with different MW (PEO550, 2000, or 5000, Table 2.3). This triblock copolymer was mixed with a polyurethane (MDI/ PTMO 1000/ethylene diamine (ED)) at different ratios in dimethylformamide (DMF) and cast into polymer films. The surface compositions of these films were evaluated by XPS.

The authors used high-resolution XPS to fully deconvolute the C1s spectra into C—C, C—O, NHCOO (urethane carbonyl), and NHCONH (urea carbonyl). On the surface of matrix PU, the majority of carbon were from the carbons in the C—C bond (Figure 2.12(a)). The fresh polymer blend with 20% copolymer 2 in the PU showed more carbon from the C—O ether bond (note that all the ether bonds are from the PEO groups) (Figure 2.12(b)). It was noted that after a prolonged aging process, predominant carbons were those from C—O ether bonds, suggesting that the surface was covered by copolymer 2.

The degree of surface enrichment of PEO groups depends on not only the aging time but also the MW of the triblock copolymer. When the low MW copolymer 1 was blended with matrix PU, the surface of the blended polymer film had the same ether carbon content as that of copolymer 2 after just 3 days of aging

Table 2.2 XPS composition comparison of regular TPU versus different oligomeric polyurethanes

Sample	Element contents on the surface[a] (at%)					Element contents in the bulk[b] (wt%)	
	C	O	N	P	F	P	F
PU	76.27	21.90	1.83	0	0	–	–
PU–F	48.81	7.65	4.79	0	38.75	0	7.67±0.26
PU–PC	77.48	19.73	2.50	0.29	0	0.28±0.02	0
PU–FPC	51.94	12.07	6.16	0.53	29.30	0.19±0.06	1.02±0.01

"–" not detected.
[a]Values detected by XPS.
[b]Values detected by element determination.
Reprinted with permission from Ref. [52].

Table 2.3 **Triblock polyurethane composition**

Properties of copolymers					
	Expected structure	PEO content (expected, wt%)	Expected M_n	Measured M_n	M_w/M_n
Copolymer 1	PEO550–PU4750–PEO550	19	5850	6200	1.2
Copolymer 2	PEO2000–PU4750–PEO2000	46	8750	8600	1.1
Copolymer 3	PEO5000–PU4750–PEO5000	68	14,750	11,800	1.1

Reprinted with permission from Ref. [54]].
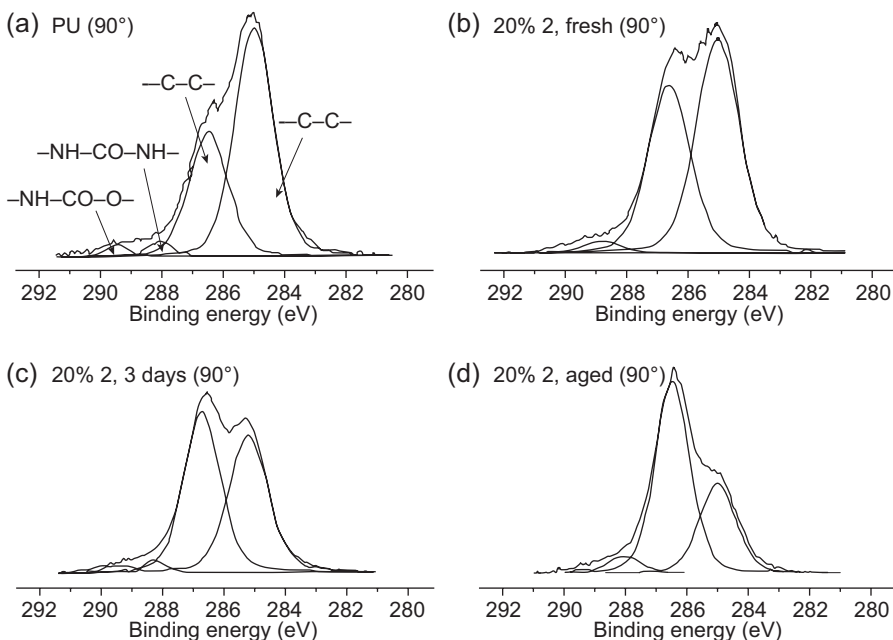
Figure 2.12 C1s spectra at a takeoff angle of 90°. (a) Matrix PU, (b) 20% copolymer 2 with 80% matrix PU fresh film, (c) 20% copolymer 2 with 80% matrix PU aged for 3 days, (d) 20% copolymer 2 with 80% matrix PU fully aged.
Reprinted with permission from Ref. [54].

(Figure 2.13). However, it took 20 days for polymer blend using higher MW copolymer 2 and 3 to achieve a complete enrichment (Figure 2.13).

Another important property researchers strive to give to polyurethane biomaterials is antimicrobial activity. Wynne et al. [56] used self-concentrating amphiphilic quaternary ammonium antimicrobials to modify polyurethane surfaces (Figure 2.14). These small molecule antimicrobials showed good antimicrobial activity in minimum inhibition concentration (MIC) tests. These antimicrobials were later solvent-mixed with matrix PU at 1% and cast into films. These antimicrobials also demonstrated surface enrichment as XPS spectra showed that the observed quaternary nitrogen was much higher than the calculated nitrogen value, assuming that these antimicrobials were evenly distributed (3f showed the highest surface enrichment, up to 19 times higher than the calculated value). Such self-enriched quaternary surfaces showed up to 7 log reduction of surface bacteria (Table 2.4).
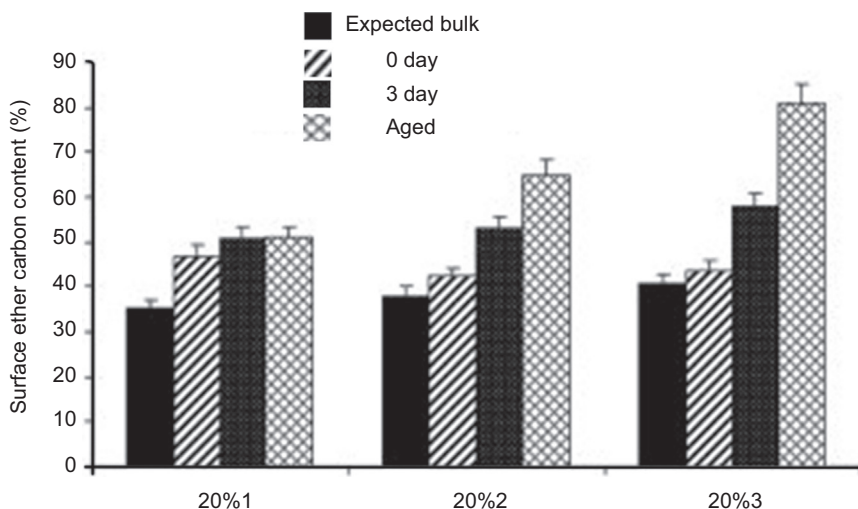
Figure 2.13 Surface ether carbon (C—O—C) content of 20% blends after different aging time in air. (Theoretical ether carbon contents of pure copolymer 1, 2, and 3 are 50.8%, 65.3%, and 78.4% of total C1s spectra.)
Reprinted with permission from Ref. [54].
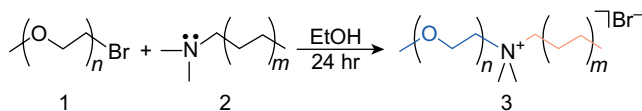
Figure 2.14 Synthesis of surface enriching antimicrobials.
Reprinted with permission from Ref. [56].

Table 2.4 **Antimicrobial activity and XPS results**

Entry	Product	*m*	*n*	Yield (%)	MIC[a] (mmol/L)		Log kill[b]		XPS[cd]	
					Staphylococcus aureus (G+)	*Escherichia coli* (G−)	*Staphylococcus aureus* (G+)	*Escherichia coli* (G−)	*% N* obsd	*% N* calcd
1	**3a**	2	1	83	9.3	9.3	5	3	0.1	0.05
2	**3b**	2	2	82	16.0	8.0	6	3	0.3	0.05
3	**3c**	2	3	96	14.0	7.0	3	1	0.1	0.05
4	**3d**	2	4	53	6.2	6.2	3	1	0.1	0.04
5	**3e**	3	1	79	0.7	2.0	7	6	0.5	0.05
6	**3f**	3	2	87	0.9	7.3	7	7	0.9	0.05
7	**3g**	3	3	94	1.3	6.5	5	4	0.3	0.04
8	**3h**	3	4	85	1.9	3.0	4	4	0.2	0.04

[a]Minimum inhibitory concentration.
[b]Log reduction starting with 107 CFU/cm^2 on a coating of hydrothane containing 1% biocide.
[c]% N obsd is the weight percent of biocidal nitrogen in the surface, excluding hydrogen, as observed by XPS.
[d]% N calcd is the calculated number expected if the additive were evenly distributed throughout the coating, with no surface concentration.
Reprinted with permission from Ref. [56]].

2.4 Secondary ion mass spectrometry

Secondary ion mass spectrometry (SIMS) is a mass spectrometry characterization technique sensitive to surface composition (sampling depth less than 1 μm) and it works in a manner similar to that of XPS. For XPS, the sample is irradiated by X-rays whereas for SIMS, the sample surface is bombarded with a focused, pulsed primary ion beam that is either positively or negatively charged. For XPS the detector picks up the kinetic energy of escaped electrons, but for SIMS escaped secondary ions are captured and separated based on m/z (mass/charge ratio) of the fragments. Fragments with different m/z are used to identify molecules on the surfaces. SIMS can also be operated in a mode where etching on the surface takes place, allowing one to obtain a composition versus depth profile.

SIMS can be a complementary survey tool in addition to XPS and it can be used to differentiate samples with similar XPS spectra. SIMS has a much lower limit of detection (LOD) (ppb level) compared to XPS (0.1%). SIMS can also provide more detail on chemical structure, but comparable quantitative information is only available via XPS [57,58].

Ratner et al. [59] have done detailed SIMS and XPS studies on aromatic polyurethanes with different soft segments. In this paper, polyethylene glycol (PEG)/Methylene diphenyl diisocyanate (MDI)/ethylene diamine (ED), PTMO/MDI/ED, and polypropylene glycol (PPG)/MDI/ED polyurethanes were synthesized. Using SIMS, the three different polyurethanes were easily discriminated by their soft segments. PEG/MDI/ED polyurethane showed strong ion cluster of $m/z = 45$, which matched with $[(CH_2CH_2O)_nH]^+$ ($n = 1$), and less strong signals of $m/z = 89$, 133, and 177 ($n = 2,3,4$) were also found. In PTMO/MDI/ED polyurethane, the strongest signal $m/z = 55$ came from both $C_3H_3O^+$ and $C_4H_7^+$, and a peak of 73 Da is also found at lower intensity, which matches with the repeating unit of polytetramethylene oxide (PTMO) $[(CH_2CH_2CH_2CH_2O)_nH]^+$ ($n = 1$). In PPG/MDI/ED polyurethane, 59 Da is the most abundant peak in all soft segment fragments, which matches with $[(CH_3CHCH_2O)_nH]^+$ ($n = 1$), the repeating unit of PPG polyol. Such differentiation among different polyurethanes would be more challenging if only an XPS survey was used since the bonding information and elemental composition are barely conclusive in polyurethane identification.

SIMS can also be used to investigate polyurethane surface contamination caused by antioxidants, wax, or other processing agents. Ratner et al. [60,61] used SIMS to investigate lot-to-lot variation of Biomer® polyurethane. Particularly, one lot of Biomer® had both antioxidant 4,4′-butylidene-bis-(t-butyl-m-cresol) (BBBC) and UV stabilizer poly(diisopropylaminoethyl methacrylate) (DPA-EMA) while the other lot only had BBBC. FTIR showed almost identical spectra on both polyurethanes. XPS did show different spectra on two lots of polyurethanes but failed to reveal the identity of the chemicals on the surface. In the SIMS study, Biomer® with both BBBC and DPA-EMA showed that its surface is predominately covered by DPA-EMA without signals from PTMO or MDI (Figure 2.15). On the contrary, Biomer® with only BBBC showed secondary ion signals from PTMO, MDI, and BBBC (Figure 2.16).

Researchers have also used SIMS to investigate the protein adsorption on different materials [57,62–64]. Castner et al. [65,66] compared surface protein adsorption
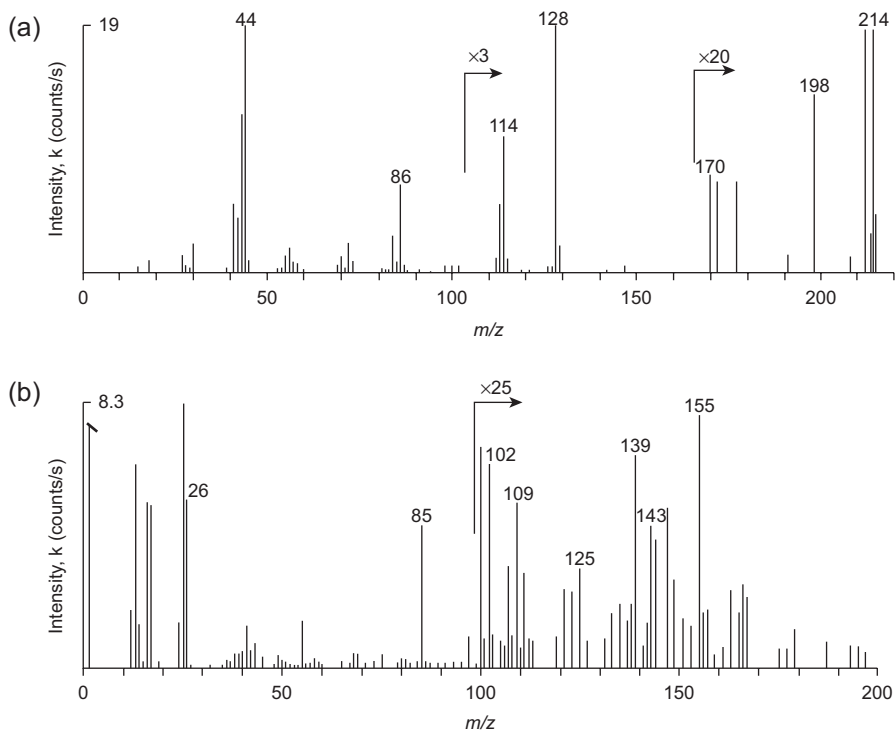
Figure 2.15 SIMS of Biomer® with both BBBC and DPA-EMA. (a) The positive ion SIMS spectrum for lot BSUA contains peaks for the DPA-EMA additive. Characteristic ions for PTMG ($m/z = 55$) and MDI ($m/z = 106$ and 132) are absent. (b) The negative ion SIMS spectrum contains methacrylate backbone peaks and peaks for the diisopropyl amino ethyl side chain ($m/z = 85, 97, 109, 125, 139$, and 155).
Reprinted with permission from Ref. [60].

quantification by time-of-flight (TOF) SIMS survey with ^{125}I radiolabeled protein counting. (See Section 2.6.2 for more information.) TOF–SIMS survey is known to be a qualitative method rather than quantitative method due to limitations of sensitivity and matrix complexity. The authors did a computation regression program to calculate protein adsorption based on intensity of several specific peaks in the TOF–SIMS spectrum. The authors found that TOF–SIMS results matched well with the ^{125}I radiolabeling method in BSA/γ-globulin (IgG) and BSA/fibrinogen (Fg) binary protein binding. However, a larger discrepancy was observed between the ^{125}I radiolabeling and TOF–SIMS measurements in IgG/Fg.

2.5 Scanning electron microscopy

Scanning electron microscopy (SEM) uses a focused electron beam to survey a surface of interest. The working principle of SEM is very similar to that of optical microscopy but with an approximately 250 times higher resolution. The electrons
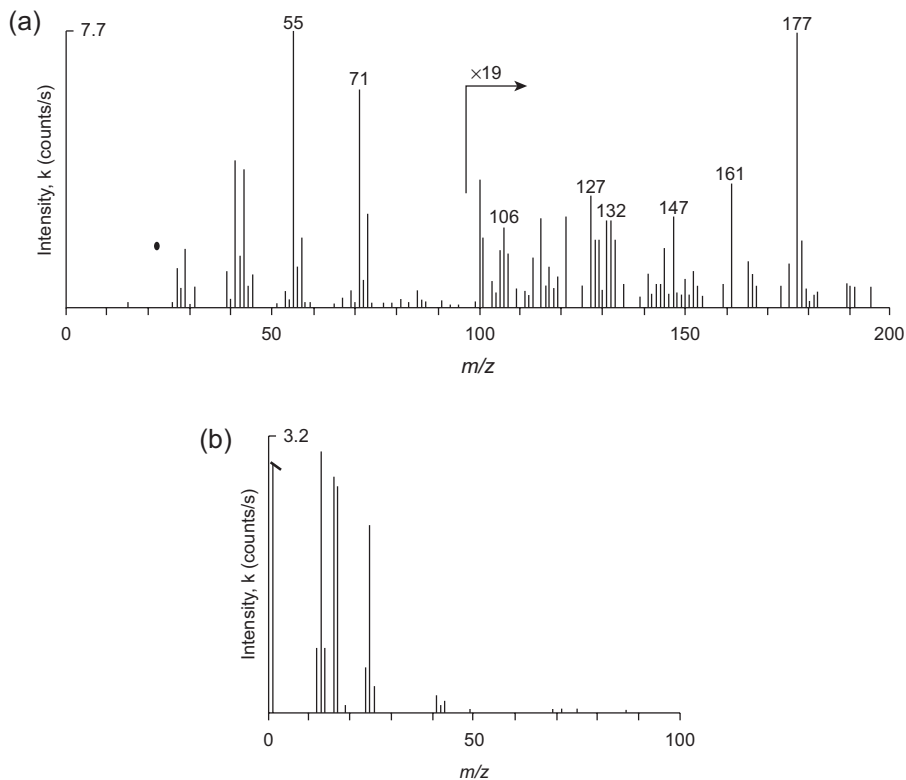
Figure 2.16 SIMS of Biomer® with only BBBC. (a) The positive ion SIMS spectrum contains peaks characteristic of PTMG ($m/z=55$), MDI ($m/z=106$ and 132), and BBBC ($m/z=177$). (b) The negative ion SIMS spectrum for lot BSP shows only a few low m/z fragments. Reprinted with permission from Ref. [60].

are generated by either thermionic guns or field emission guns and are then focused by a series of electromagnetic "lenses." When electron beams hit the sample surface, the sample emits X-rays and three kinds of electrons: primary backscattered electrons, secondary electrons, and Auger electrons. In SEM, only primary backscattered electrons and secondary electrons are collected and are used to generate images of the sample. Just like XPS, a high vacuum environment is required to allow free passage of electron beams. However, recent developments in environmental SEM allow samples to be analyzed under low vacuum in high humidity. The SEM technique is a very versatile but semiquantitative technique in polyurethane materials to visualize protein adsorption [67], bacteria adhesion [68–70], platelet binding [71–78], and degradation [79–83].

Brash et al. [84] modified a Tecothane™ surface with PEGylated lysine, which binds plasminogen to reduce platelet adhesion. The general surface modification involved first to introduce reactive isocyanate groups into Tecothane™ TPU by soaking Tecothane™ TPU in MDI toluene solution. PEGs (MW 300 and 1000) were further immobilized on this reactive surface. The PEGylated Tecothane™ surface was

then activated by a typical coupling reaction with BOC-protected lysine. Finally, the BOC-protecting group was removed by trifluoroacetic acid. The terminal NH_2 on lysine preferentially captures plasminogen when exposed to blood. Plasminogen can be later converted into plasmin. Plasmin is believed to lyse fibrin, which binds platelets and participates in blood clotting. By rapidly lysing fibrin, the polyurethane surface could avoid platelet activation and adhesion. A reduction in platelet adhesion was visualized by SEM. As Figure 2.17 indicates, unmodified Tecothane™ TPU showed significant platelet adhesion (Figure 2.17(a)) whereas modified Tecothane™ surfaces (Figure 2.17(b–d)) showed little platelet adhesion.

Sun et al. [85] developed an antimicrobial modification of Estane® film with N-halamine groups on the surface. The authors introduced reactive isocyanate groups into Estane® film by reacting hexamethylene diisocyanate (HDI) with the existing urethane bonds in polyurethane. The grafted isocyanate groups then reacted with 5,5-dimethylhydantoin (DMH) and DMH groups were finally converted to N-halamine groups by chlorination with a bleach solution (Figure 2.18). The N-halamine group is well known to release low concentrations of Cl^+ to kill bacteria on contact [86]. Both contact kill and zone of inhibition (ZOI) test (see Section 2.8) showed positive biocidal activity. SEM images of biofilm formation were compared before and after
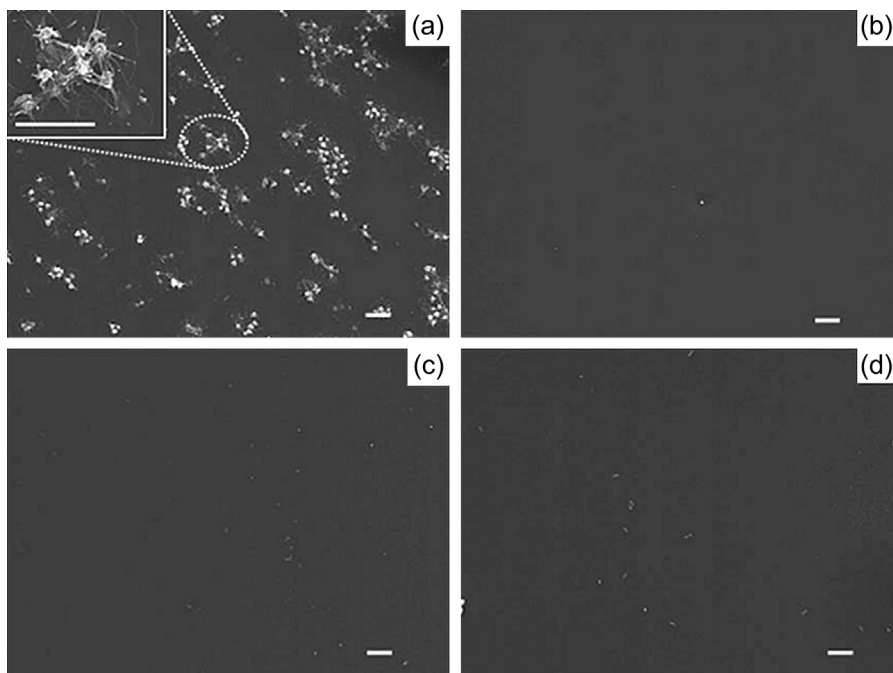
Figure 2.17 SEM images of platelet adhesion after 15 min of exposure to whole blood at $300 s^{-1}$ on (a) unmodified Tecothane™ TPU, (b) Tecothane™–PEG300, (c) Tecothane™–PEG300–Lys(BOC protected), and (d) Tecothane™–PEG300–Lys. Scale bars = 10 μm. Reprinted with permission from Ref. [84].
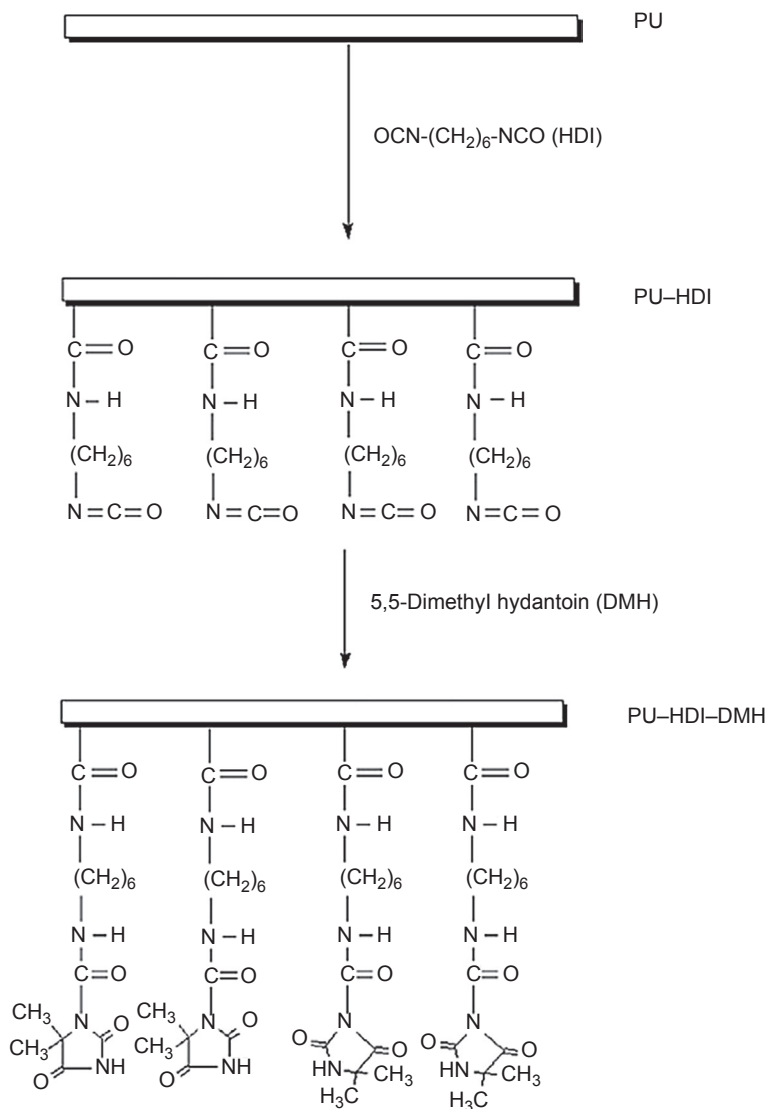
Figure 2.18 Surface modification of polyurethane with DMH group. DMH group is finally chlorinated with bleach to warrant antimicrobial activity.
Reprinted with permission from Ref. [85].

polyurethane surface modification. Widespread bacteria colonies cover the polymer surface on the original Estane® polymer (Figure 2.19(a), (c), and (e)). Significant biofilm reduction was confirmed by SEM after surface modification (Figure 2.19(b), (d), and (f)).

Polyurethane degradation is a common issue for polyurethane-based medical implants. The degradation mechanisms vary depending on the type of polyurethane used and their environment. For example, polyester polyurethane undergoes hydrolytic
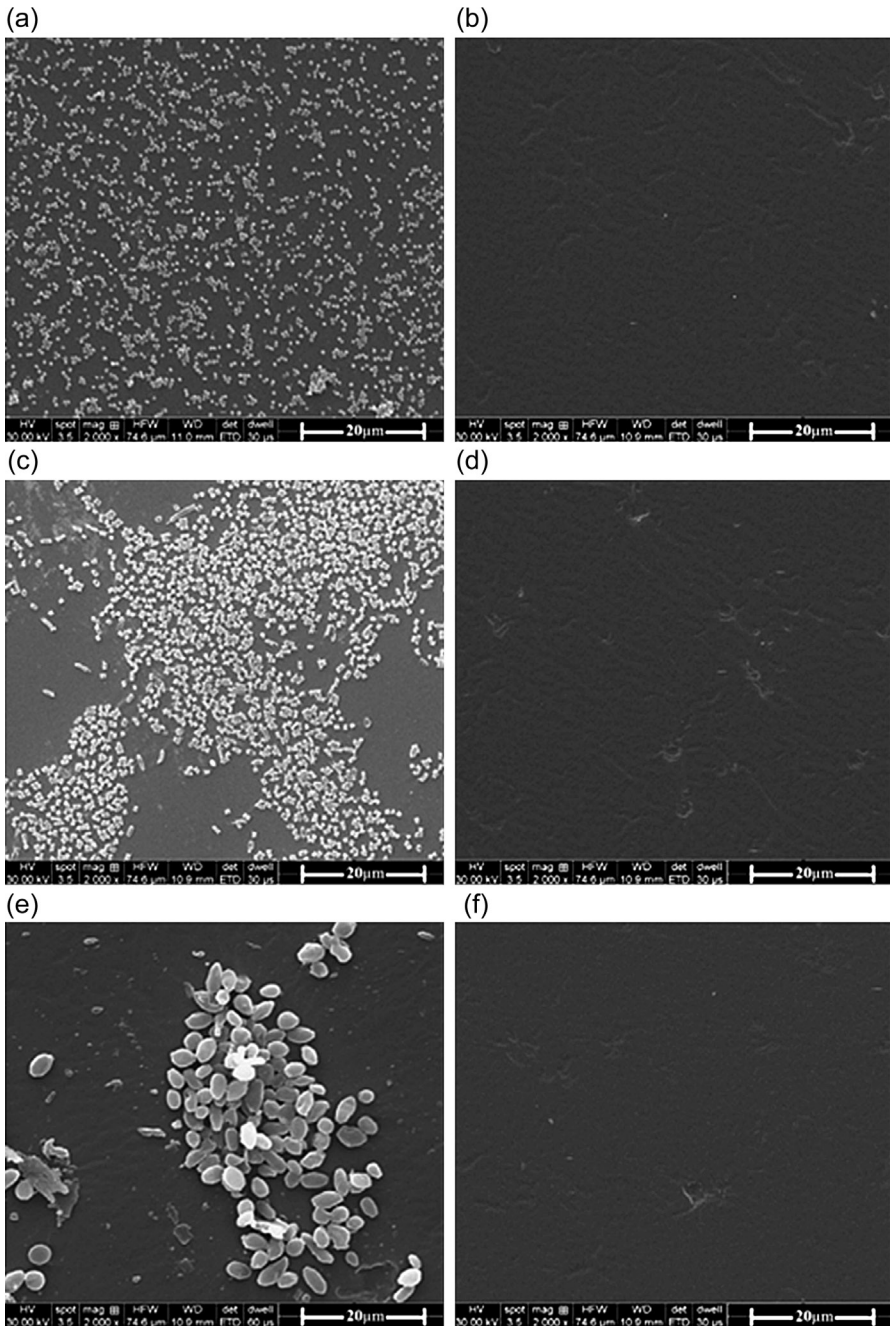
Figure 2.19 Antibiofilm formation performance of (a) the original PU film against *Staphylococcus aureus*, (b) the chlorinated PU–HDI–DMH film against *S. aureus*, (c) the original PU film against *Escherichia coli*, (d) the chlorinated PU–HDI–DMH film against *E. coli*, (e) the original PU film against *Candida albicans*, and (f) the chlorinated PU–HDI–DMH film against *Candida albicans*.
Reprinted with permission from Ref. [85].

degradation due to the ester bond hydrolysis. Polyether polyurethane is more resistant to hydrolytic degradation but subject to oxidative attack and crack formation and propagation under stress, usually referred to as environmental stress cracking (ESC) [87]. There are other kinds: Polyurethane surfaces can also be attacked by reactive oxidative radicals excreted from attached macrophage cells, when an implanted device induces a chronic inflammatory response [79,88,89]. Polyurethane pacemaker leads suffer from metal ion-induced oxidation during service [90–93].

Martin et al. [80] investigated and compared ESC of Pellethane® 80A with 50D. Previous efforts to retard ESC involved the use of poly(dimethylsiloxane) (PDMS) as coating materials or as a surface-modifying agents [94,95] because polysiloxane can reduce macrophage and giant cell coverage. However, polyurethanes with such a modification still exhibited ESC when they were stretched to higher elongation. To further improve the biostability of a polyurethane with lower hardness, the authors utilized bishydroxyethoxypropyl PDMS as the polyol, replacing the polytetramethylene glycol (PTMG) polyol, to synthesize soft polyurethanes. It was found that higher durometer harder Pellethane® 50D showed better stability than 80A (softer) after a 3 month ovine implantation (Figure 2.20(a) and (b)). Pellethane® 80A showed significant cracks compared with PDMS polyurethane tested at 150% elongation rate (Figure 2.20(a) and (c)).
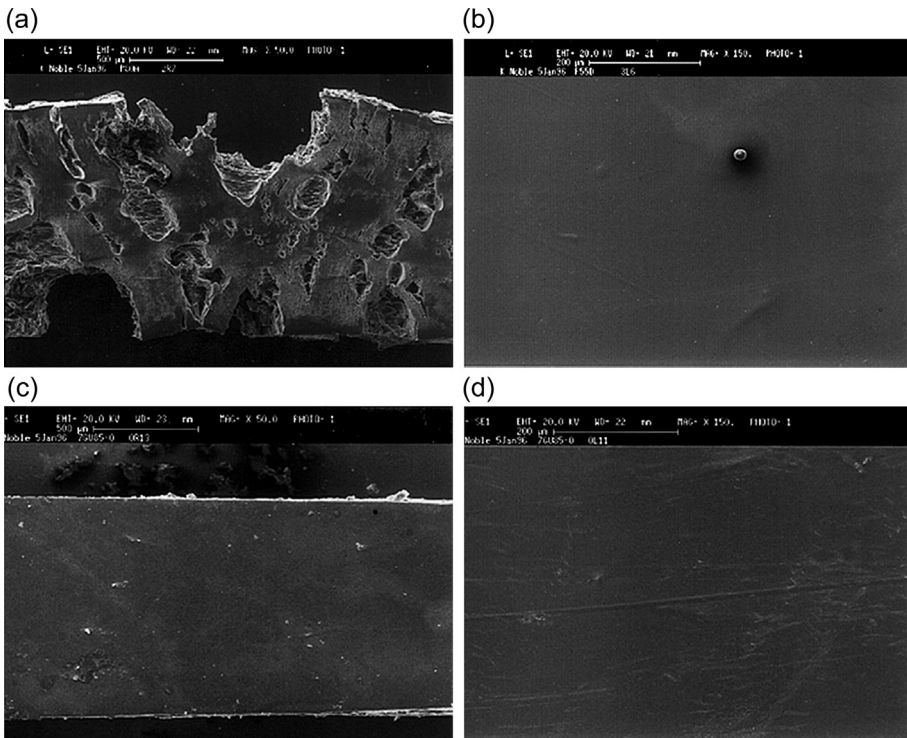
Figure 2.20 SEM images of polyurethane samples after 3 month implantation. (a) Pellethane® 80A; (b) Pellethane® 55D; (c) polyurethane made of PDMS polyol (×50 magnification); (d) polyurethane made of PDMS polyol (×150 magnification).
Reprinted with permission from Ref. [80].

2.6 Protein adsorption test

When a medical device is in contact with body fluid such as blood, the first thing that occurs on the surface is protein adsorption [96–98]. Proteins in solution trying to minimize the total surface energy is the thermodynamic driving force of protein adsorption on solid surfaces. In blood contact protein adsorption is believed to be the initial event in thrombus formation [99–101], calcification [102–104], and biofilm attachment [105–107], which leads to the failure of implanted devices. Therefore, protein-reducing surface modifications of polyurethane biomaterials have been applied to improve the service life of implants. Previous studies of protein adsorption have focused on adsorption of albumin, IgG, and Fg, which are the predominant three proteins in blood plasma. Surface protein adsorption can be quantitated by several methods such as quartz crystal microbalance (QCM) [108–112], surface plasmon resonance (SPR) [113–118], and iodonization radiolabeling [78,119–125].

2.6.1 *Quartz crystal microbalance*

The QCM method utilizes the piezoelectric property of quartz crystals to measure extremely low mass changes per unit area. When an alternating electric current is applied to the quartz crystal, the quartz crystal produces an acoustic oscillation. Such oscillation frequency is partially dependent on the thickness of the crystal. If biomolecules such as proteins adsorb on the crystal and thus increase the crystal thickness, the instrument will pick up the frequency change and the mass of adsorption can be calculated by Sauerbrey's equation (Eqn (2.5)), where Δf is frequency change; f_0, resonate frequency; Δm, mass change; A, area between electrode; ρ, density of quartz; μ, shear modulus of quartz).

$$\Delta f = -\frac{2f_0^2}{A\sqrt{\rho\mu}}\Delta m$$

$$(2.5)$$

Zhang et al. [108] used chain transfer free radical polymerization to synthesize a polyol with a pendant dimethylamine group. The polyol further reacted with MDI and 1,4-butane diol to produce a novel polyurethane material. The pendant dimethylamine group was further betainized to yield polyurethane with a pendant sulfobetaine group (Figure 2.21). Sulfobetaine belongs to a large group of zwitterionic functional groups with superhydrophilicity and protein adsorption resistance. By covalently incorporating sulfobetaine groups into a polyurethane backbone, the protein adsorption can be greatly reduced. QCM was used in this research to investigate the protein adsorption reduction. Figure 2.22 shows frequency shift (Δf) and energy dissipation shift (ΔD). With the QCM, whenever there is a mass change on the quartz chip, the instrument will detect frequency shift and energy dissipation shift. A decreased frequency usually suggests a mass increase on the chip, meaning protein adsorption. zPDEM–PU32 and zPDEM–PU42 showed little frequency change, which suggested minimal Fg adsorption due to high sulfobetaine density on the polymer chain. zPDEM–PU19 showed
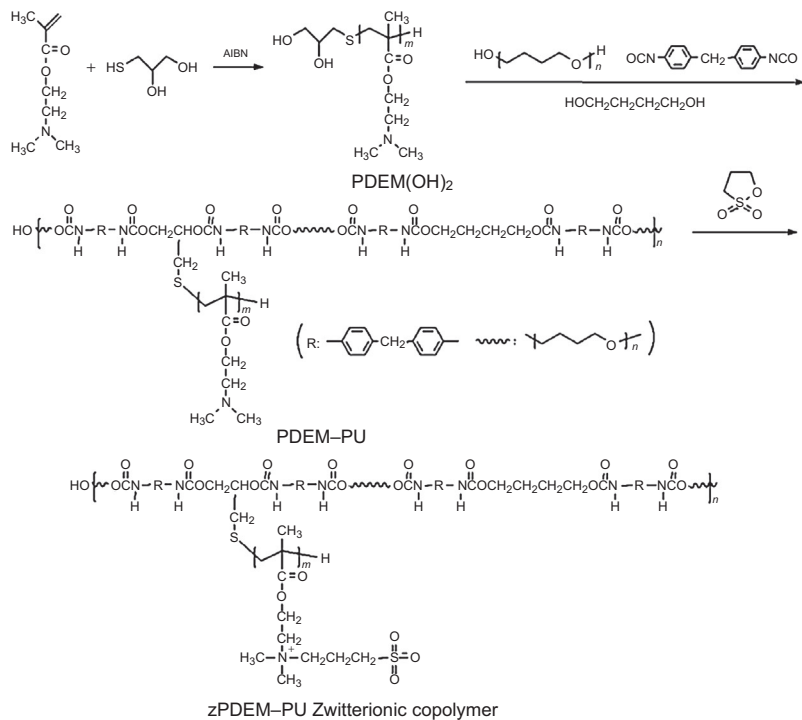
Sample	MDI/PTMG/PDEM(OH)$_2$ / 1,4-BD [a]
PU0	6/1/0/5
PDEM–PU19	6/1/0.4/4.6
PDEM–PU32	6/1/0.8/4.2
PDEM–PU42	6/1/1.2/3.8
zPDEM–PU19	[b]
zPDEM–PU32	[b]
zPDEM–PU42	[b]

Figure 2.21 Synthesis and composition of the polyurethane with sulfobetaine pendant groups. (a) Feeding ratio of monomers; (b) ZPDEM is synthesized by betainization of corresponding PDEM polymer.
Reprinted with permission and modified from Ref. [108].
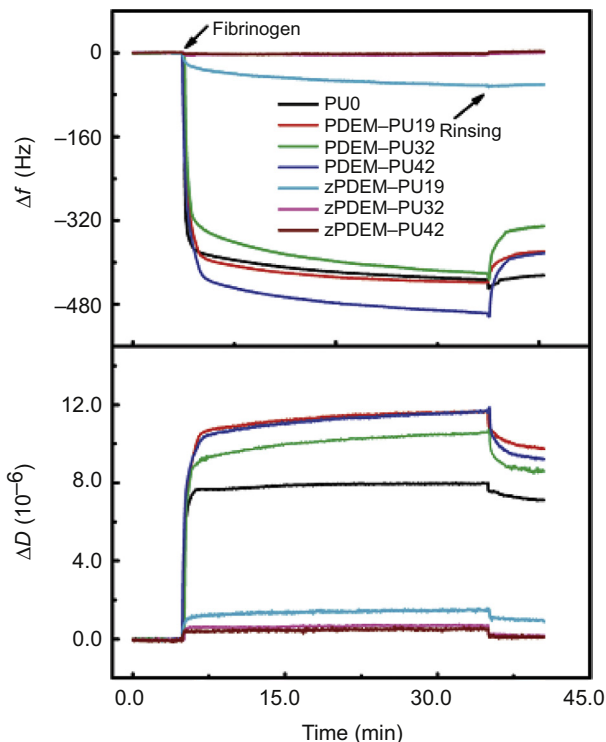
Figure 2.22 Time dependence of frequency shift (Δf) and dissipation shift (ΔD) for the adsorption of fibrinogen on a polymeric surfaces at 25 °C.
Reprinted with permission from Ref. [108].

some Fg adsorption but not as much as the control polymer by showing medium frequency change. ΔD will increase if the thickness of the protein adsorption layer increases. Again, zPDEM–PU32 and zPDEM–PU42 barely showed any increase of the baseline, implying significant protein adsorption reduction compared with control polymers.

2.6.2 Iodination radiolabeling

When proteins adsorb onto a polymer surface, one method of quantifying the amount of protein adsorption is radiolabeling. The most widely used radiolabeling technique is iodination. Iodine isotope was chosen as the radiolabeling agent instead of ^{14}C because ^{125}I is a γ emitter that requires a much simpler instrument for detection. Another reason is that iodine isotope has much shorter half-life (60 days); thus it is much less hazardous [126]. Iodination radiolabeling is a gold standard for protein adsorption because of its extreme high sensitivity (ng/cm^2) and because it is a well-established method with various commercial labeling products available.

The mechanism of iodination radiolabeling involves reactive iodine, generated by enzymatic or chemical oxidation of isotopic sodium iodide, reacting as an
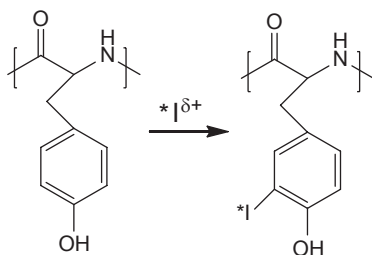
Figure 2.23 Iodination on tyrosyl group.

electrophilic agent with tyrosyl groups on the protein (Figure 2.23). Oxidation agents commonly used are chloramine-T [127,128], *N*-chlorobenzenesulfonamide sodium salt [129,130], iodine monochloride [131,132], Bolton and Hunter agent [127,133], lactoperoxidase [134,135], and iodogen [136].

A brief iodination protocol is summarized here: protein solution is mixed with Na^{125}I solution and the oxidation agent. After the iodination reaction is complete, the radiolabeled protein is recovered by passing through a desalting column to remove any unreacted iodide. The integrity of radiolabeled protein is checked via gel electrophoresis for MW weight comparison before and after radiolabeling. The radiolabeled protein is then mixed with unlabeled protein at a certain dilution factor. Afterward, polymer samples are incubated with such mixed protein solution. After gently washing off loosely adsorbed protein, radioactivity is counted by a γ-counter and then converted to radiolabeled protein mass. The final protein adsorption is calculated by multiplying radiolabeled protein mass with dilution factor (if radiolabeled protein is diluted 10 times with unlabeled protein, the actual protein adsorption is 10 times the radiolabeled protein mass data from the γ-counter). Compared with the QCM method, which requires polymer to be solvent cast on a chip, radiolabeling gives more realistic adsorption information on real devices.

Brash et al. [137] studied heparin-modified polyurethane surfaces to inhibit Fg adsorption while promoting antithrombin adhesion (Figure 2.24). Heparin is the most widely used thrombin inhibitor via both systematic administration and surface modification. The mechanism of such inhibition is well established. Heparin can preferentially bind to antithrombin. Antithrombin, which undergoes a conformational change, will bind and inhibit thrombin. After the antithrombin/thrombin complex (ATH) is formed, heparin is released and another binding cycle with antithrombin begins [138]. Brash created isocyanate groups on a Tecothane™ surface via allophanate bond formation between MDI and urethane hydrogen. The free isocyanate could further react with PEO. Additionally the ATHs can be grafted onto polyurethane by this method.

Brash studied Fg and antithrombin radiolabeled using ^{125}I and ^{131}I, respectively, so that adsorption of both proteins could be measured in the mixture. After functionalization with ATH, the polyurethane surface (PEO–OH–ATH and PEO–COOH–ATH) preferentially binds with antithrombin rather than Fg, suggesting the strong heparin surface binding activity (Figure 2.25). By labeling both Fg and antithrombin with different iodine isotopes, the authors obtained competitive adsorption information on the same heparin-modified surface.
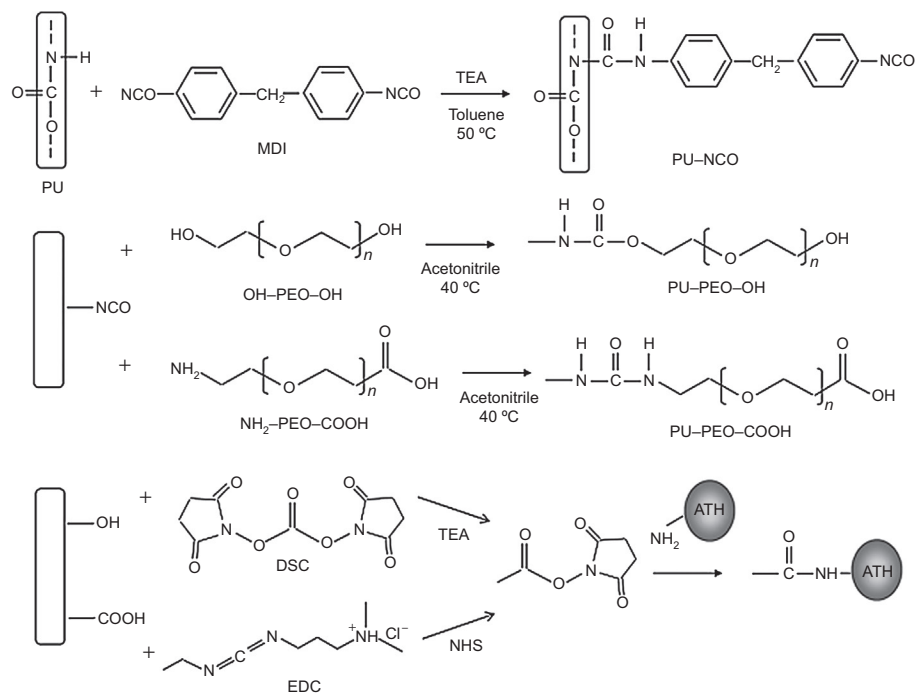
Figure 2.24 Tecothane™ surface modifications using conventional polyethylene oxide (PEO), hetero-bifunctional PEO.
Reprinted with permission from Ref. [137].
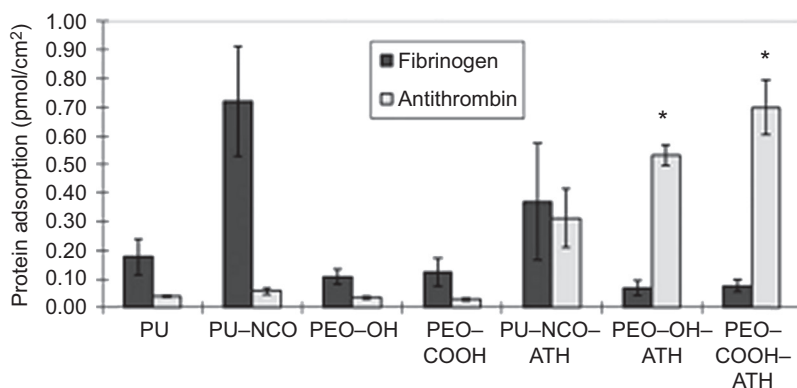
Figure 2.25 Fibrinogen and antithrombin (AT) adsorption from plasma (2 h). PEO MW = 1000 Da. Data are means ± SD, $n = 4$. *AT adsorption on PEO–OH–ATH and PEO–COOH–ATH is significantly greater than that on all other surfaces ($P < 0.05$). Reprinted with permission from Ref. [137].

2.7 Hemocompatability measurement

Polyurethane medical devices such as central venous catheters (CVCs) [139–141] and hemodialysis devices [142–144] require good hemocompatibility [145]. In Section 2.6, we know that when a device is implanted in the human body protein adsorption occurs in just a few seconds. In contact with blood, the protein layer interacts with platelets, which leads to thrombus formation and eventually to device failure. There are several tests available to evaluate hemocompatibility. Visualization by SEM is one semiquantitative method, which is covered in Section 2.5. More accurate quantitative methods are described below.

2.7.1 In vitro *platelet adhesion*

2.7.1.1 *Radioactive isotope labeling*

The general protocol of this test is described as follows (detailed procedure can be found in Ref. [58]): First, fresh venous blood is collected and mixed with anticoagulant, during which great care must be taken to avoid traumatic venipuncture and excess negative pressure to prevent activation of platelets. The blood is centrifuged to obtain platelet-rich plasma (PRP) and the pH of PRP is adjusted to 6.5–6.7 with acid–citrate–dextrose. This PRP is further centrifuged until a platelet "button" is formed and the platelet-poor plasma (PPP) is collected. The platelet is then resuspended in PPP to yield an appropriate concentration. A proper amount of radio labeling agent is added to such suspension to label the platelets. This suspension is incubated for a certain time. More PPP is added to the suspension followed by centrifugation to remove excess radioactive agent. This procedure is repeated several times. The labeled platelets are resuspended again in PPP. The labeled platelets are incubated with polyurethane samples for a certain time and samples are rinsed with saline solution to remove unattached platelets. The attached platelets are fixed by glutaraldehyde. Finally, the radioactive intensity is measured by a γ-counter and platelet adhesion calculated.

2.7.1.2 *Lactate dehydrogenase assay*

To avoid radioactive materials, other tests on platelet adhesion have been developed. The lactate dehydrogenase (LDH) assay was first developed by Schnaar et al. [146]. It was later adopted and modified for evaluation of platelet adhesion on polymeric films [147] and microplates [148]. This platelet adhesion procedure is similar to the radioactive labeling method in that a PRP suspension is incubated on polyurethane surfaces. After removal of the unattached platelets by saline rinsing, the attached platelets are subjected to complete lysis to release LDH by adding Triton-X surfactant solution. The lysed solution is further incubated with LDH substrate nicotinamide adenine dinucleotide (NADH). NADH is oxidized into NAD^+ by LDH. The final NAD^+ solution is measured by a microplate reader at 490 nm with a reference wavelength at 620 nm. The optical density at 490 nm is linear with the platelets cell number within calibration curve range [149,150]. Therefore, by measuring the concentration of NAD^+, the number of absorbed platelets can be calculated.

2.7.1.3   Acid phosphatase assay

The acid phosphatase (ACP) method, developed by Bellavite et al. [151], is based on acid phosphatase platelet activity. Acid phosphatase is a stable enzyme present in platelets. This method is similar to the LDH method. It uses regular PRP and the same Triton-X to completely lyse attached platelets. But in this test, a different enzyme (acid phosphatase) is measured. On addition of *p*-nitrophenyl phosphate substrate, acid phosphatase converts the substrate into *p*-nitrophenol, which can be easily measured by a photospectrometer at a wavelength of 405 nm. Side-by-side comparison of both DCH and ACP assays suggests that the ACP assay is better than the LDH assay in terms of reproducibility [152].

2.7.2   Scanning electron microscopy

SEM imaging of platelets attached to polyurethane surfaces is a semiquantitative method (see Section 2.5).

2.7.3   In vitro *blood loop method*

A standard blood loop test (*in vitro*) uses whole blood instead of PRP to test the hemocompatability of polyurethane materials. Blood used in this test can be bovine, porcine, or human. Although human blood seems to be best for this test, bovine blood is the most popular. The reason is that when multiple devices are compared at a high blood flow rate, it usually requires a relatively large quantity of blood. Five hundred milliliters of blood is usually considered as the maximum amount that can be drawn from one human donor each time. Blood from different donors must be pooled together for this test, which increases the cost and inconvenience. However, 5–10 L of bovine blood could be collected from one donor [153]. Once the blood is collected, anticoagulant is added to prevent blood clotting in blood bags or tubing. The typical anticoagulant is heparin. Heparin can enhance antithrombin's activity to eliminate thrombus and prolong the test period. Another important characteristic of heparin is that it can prevent blood clotting [154,155]. Blood is circulated in a loop with a chamber in which medical devices such as catheters and stents can be placed inside. There are three different loop configurations (Figure 2.26): (1) A Chandler loop uses a closed tubing loop partially filled with a plug of air. The whole loop is vertically rotated in such way that the test device is continuously exposed to the blood–air interface while maintaining the air plug on top. (2) A roller pump loop uses a roller pump to circulate blood within a pulsatile fashion inside the tubing instead of rotating the whole loop. (3) A hemobile loop uses a special ball valve to allow unidirectional blood flow. The test sample cylinder comes in contact with blood when the loop is rotated back and forth. When the loop is rotated in one direction and the ball valve is open, the test sample experiences pulsatile blood flow. Rotating the loop in the opposite direction makes the valve close and the test sample experiences static flow [156]. After a given period of testing, the thrombus formation on the device can be checked by visual inspection (qualitative) or γ-counter if using radiolabeled blood (quantitative, see Section 2.7.1.1).
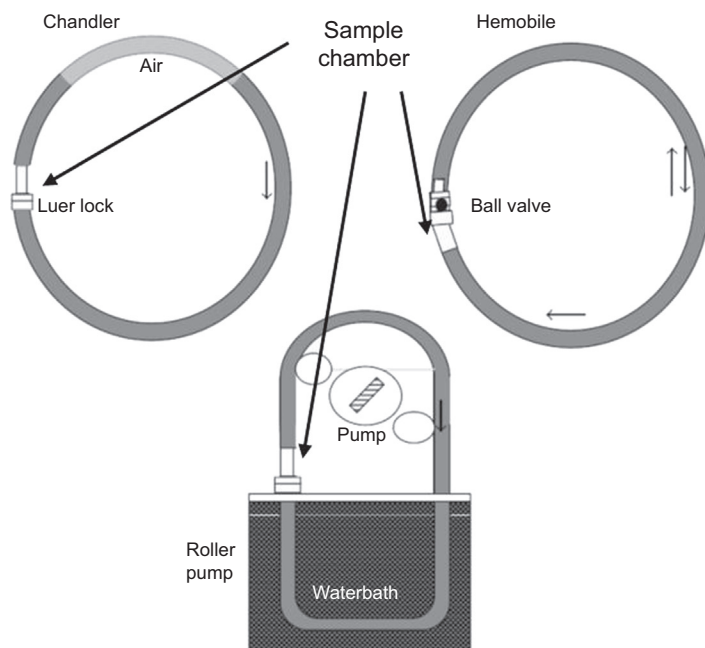
Figure 2.26 Schematic presentation of *in vitro* blood loop test: Chandler, hemobile, and roller pump.
Reprinted with permission from Ref. [156].

2.7.4 Ex vivo *shunt blood loop*

The shunt loop test is an animal test method for hemocompatability, which has characteristics of both *in vitro* and *in vivo* blood exposure. The animal model chosen in this test is usually sheep, swine, or canine. A typical experimental setup is shown in Figure 2.27. A shunt is placed between the femoral artery of the animal. Radiolabeled proteins and platelets are deposited on the test surfaces and quantified using a γ-counter. A PVC conduit with test sample and flow meter completes the external blood loop. Emboli induced by the test sample can be detected in an *ex vivo* shunt using a light-scattering emboli detector (LSED). By collecting the scattered light, LSED can detect tiny emboli. The light scattered by red blood cells and emboli are different and can be both picked up by LSED (Figure 2.28) [157–159]. The amount and size of emboli induced by polyurethane samples can be recorded as a measure of blood compatibility.

2.8 Antimicrobial efficacy test

Medical devices such as catheters, implants, and prosthetics are continuously challenged in bacterial environments. For example, CVC's total number of days of insertion for all patients is estimated to be 15 million in intensive care unit in the United States every year [161]. One potential risk of CVC utilization is catheter-related bloodstream
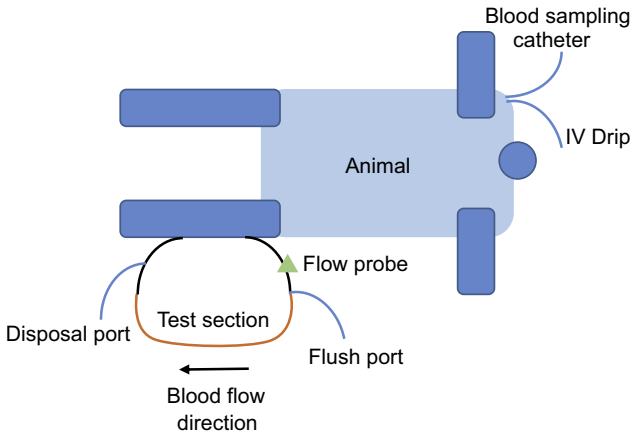
Figure 2.27 Schematic of *ex vivo* shunt animal experiment.
Reprinted with permission from Ref. [160].
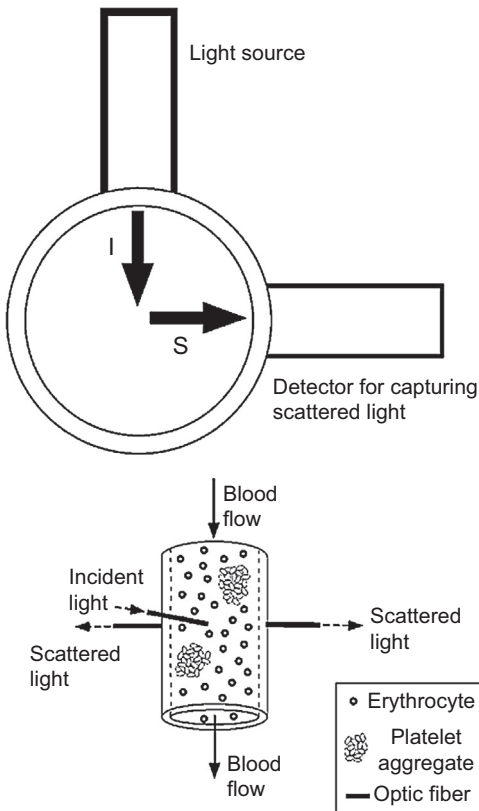
Figure 2.28 Schematic of the basic configuration of the LSMD.
Reprinted with permission from Ref. [159].

infection, which increases hospital cost and length of hospital stay [162–165]. Another example is catheter-associated urinary tract infection that has been reported to involve over five million cases leading to 13,000 deaths annually in the United States [166–168]. As a result, catheters with antimicrobial activity are highly desirable. In the case of polyurethane catheters, antimicrobial agents such as silver and antibiotics can be designed to elute from the polyurethane matrix. Polyurethanes can also be surface modified/coated with antimicrobial active groups/agents. Finally, antimicrobial groups can be permanently attached to the polymer backbone. The efficacy of each approach requires a different antimicrobial assessment.

2.8.1 Zone of inhibition

The ZOI test, also widely known as the Kirby–Bauer disk diffusion test, is a fast *in vitro* but semiquantitative test [169]. The original purpose of this test was to replace the MIC test for small molecule antibiotic efficacy [169]. Soon, this method was adopted and modified to evaluate antimicrobial efficacy of silver and polymeric devices with eluting antimicrobial agents [170]. Commonly used eluting antimicrobial agents are zinc salt/particles [171–173], silver salt/particles [173–177], and chlorhexidine [178,179]. These antimicrobial agents can be compounded/blended into polyurethanes or coated/adsorbed on polyurethanes.

A standard test protocol is described as follows: bacteria strains of interest are first incubated in a nutritious broth to reach the plateau phase. An aliquot of bacteria solution is streaked onto nutritious agar plates, polymer samples are placed on top of agar, and then the whole agar plate is incubated. If there is antibiotic eluting from the polymer matrix and present at a specific area in the agar, colony formation will be inhibited around the sample, and the ZOI can be visually observed and measured (Figure 2.29). Finally, actual ZOI is measured by subtracting the diameter of the sample disk from the diameter of total ZOI. The ZOI is a benchmark for the antimicrobial efficacy. Ross et al. [180] reported a modified ZOI test with much shortened incubation time (6.5h compared to 12–16h) by spraying cell stains on the agar plates. In this method, the ZOI remained unstained while the live bacteria show a certain color depending on the cell dye.

Kaplan et al. [181] reported using the synergy of both Dispersin B and cefamandole nafate (CEF) to improve antimicrobial activity of Pellethane® TPU. Surface absorbed with Dispersin B showed moderate bacterial reduction. In addition, Dispersin B has a great affinity with Pellethane® soft segment and thus works as a priming agent for further surface absorption of CEF. Treated Pellethane® TPU shows a 4mm ZOI. Spangler et al. [178] used porous polyurethane foam to absorb chlorhexidine gluconate, which imparts the polyurethane with antimicrobial activity as confirmed by ZOI test.

2.8.2 Contact kill

The ZOI test is designed for polymers with eluting antimicrobial kill mechanisms. However, when antimicrobial groups are covalently bonded to polymer chains, or antimicrobial agents are permanently trapped in polyurethane, the ZOI test is no longer suitable and will yield false negative results (no bacterial kill shown).
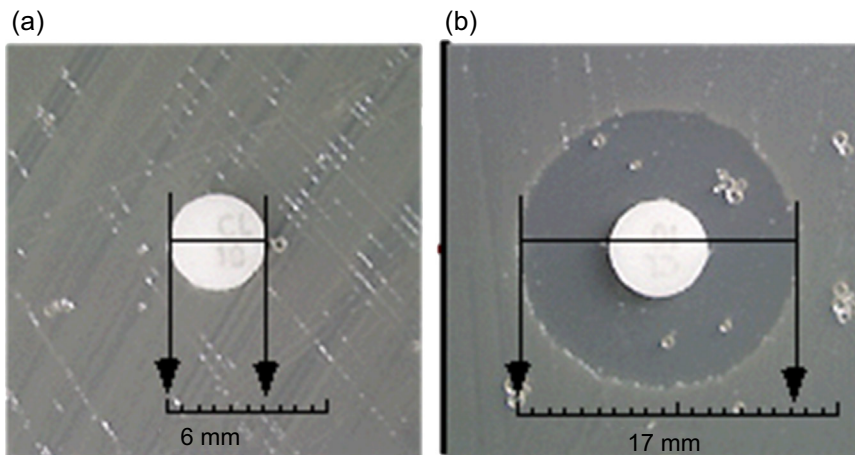
Figure 2.29 Typical ZOI test result: (a) No leachable antimicrobial shows no ZOI. (b) Leachable antimicrobial shows clear ZOI. ZOI can be measured by a caliper to give semiquantitative antimicrobial efficacy information.
Figure credited from Center of Disease Control and Prevention.

JIS Z2108 and ISO 22196 are two industry suggested protocols for nonporous polymer materials (ISO 20743 for textile materials) with noneluting antimicrobial agents. The general procedure is described as follows: the bacteria is incubated in a liquid broth and diluted to a stock solution of concentration between 2.5×10^5 and 10×10^5 cell/mL. (This stock solution must be used within 2 h after preparation to avoid significant concentration changes.) Then 0.4 mL of stock solution is carefully added onto a flat sample surface (minimum 50×50 mm) in a petri dish. The polymer test film (40×40 mm) is gently pressed onto the sample surface to ensure good contact between inoculated stock solution and sample surface. The entire sample is further incubated in a petri dish for at least 24 h. After incubation, the sample surface is carefully rinsed with broth to recover any live bacteria. The broth with live bacteria is spread and inoculated on an agar plate. The number of live bacteria is later counted. Results are reported as percentage reduction compared to negative control surface. However, it is advised that an eluting antimicrobial will also yield the same but false positive results in a contact kill experiment. Therefore, a negative ZOI result (lack of ZOI) is needed to confirm that there is no leaching of a bound antimicrobial agent.

Cooper et al. [182] have synthesized a series of polyurethanes with *N,N*-bis(2-hydroxyethyl)isonicotinamide (BIN) as chain extender. The stoichiometry of PTMO/MDI/BIN was varied to make polyurethanes with different contents of pyridine groups. The pyridine groups were further quaternized with 1-iodooctane, 1-iodooctadecane, and 1,1,1,2,2,3,3,4,4,5,5,6,6,7,7,8,8-heptadecafluoro-iododecane, respectively, to yield polyurethane C8, C18, and CF with quaternary pyridium pendant groups, respectively (Figure 2.30). A slightly different antimicrobial protocol was used in this paper. The bacteria inoculate solution is spread on the polyurethane-coated glass slides. After the polyurethane coating was challenged with bacteria, the number of live bacteria was
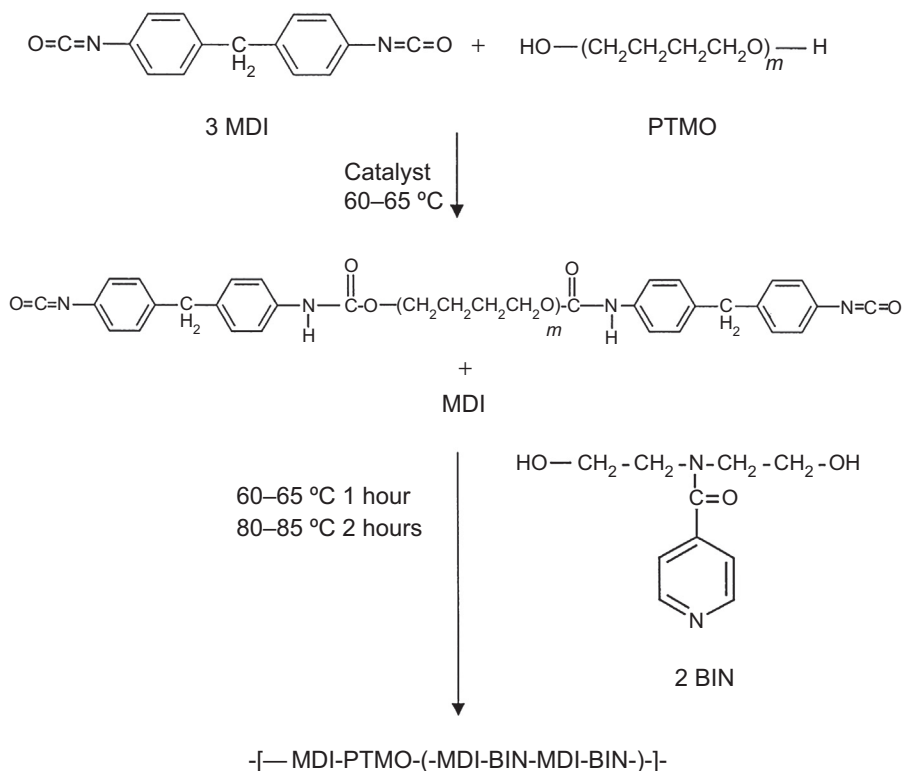
Figure 2.30 Typical reaction sequence for polyurethane synthesis. The PUs synthesized were 1 : 2 : 1 (molar ratio) PTMO/MDI/BIN, 1 : 3 : 2 PTMO/MDI/BIN, and 1 : 4 : 3 PTMO/MDI/BIN. Reprinted with permission from Ref. [182].

measured by a fluorescent probe under a confocal microscope. All three polyurethane films showed antimicrobial activity against *Staphylococcus aureus* (Figure 2.31) without showing any ZOI, suggesting a true surface kill mechanism. Among all three polymers, polyurethanes with longer alkyl groups on the pyridium nitrogens (C18 polyurethane) had the highest antimicrobial efficacy (95% bacterial reduction).

Wynne et al. [183,184] utilized a similar strategy to synthesize nonleaching antimicrobial polyurethane additives. They used quaternary ammonium containing polyols (soft segment) to synthesize different polyurethane additives (Figure 2.32). The PEO groups in P[(ME2Ox)(C6)] 0.86:0.14–PU and P[(ME2Ox)(C12)] 0.86:0.14–PU and trifluoromethyl groups in P[(3FOx)(C6)] 0.89:0.11–PU and P[(3FOx)(C12)] 0.89:0.11–PU of these additives have the tendency to concentrate at the interface between air and polyurethane due to their lower surface energy. Therefore, these antimicrobial additives can be blended with base polyurethane (nonantimicrobial) but still produce antimicrobial surfaces since the additives will self-concentrate on the base polyurethane surface. Contact kill results suggested that both P[(ME2Ox)(C18)] 0.86:0.14–PU and P[(3FOx) (C18)] 0.89:0.11–PU show 100% biocidal efficacy (Table 2.5).
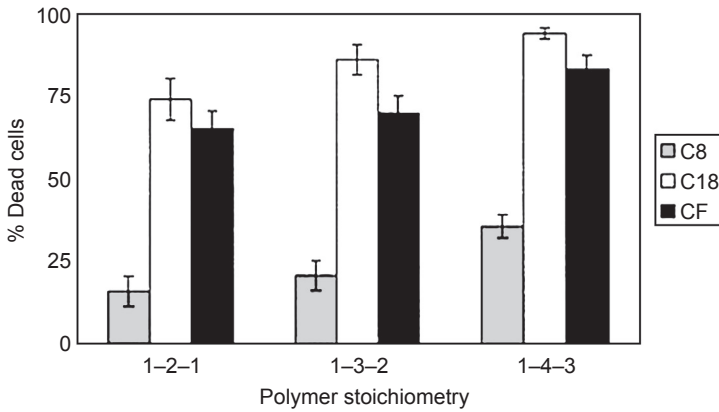
Figure 2.31 Viability of *Staphylococcus aureus* after 30 min contact with quaternized polyurethanes.
Reprinted with permission from Ref. [182].

HMDI-BD (30%), where HMDI = 4,4′-(methylene bis(p-cyclohexyl isocyanate)) and BD = 1,4-butane diol, HMDI-BD block is 30 wt% of PU composition
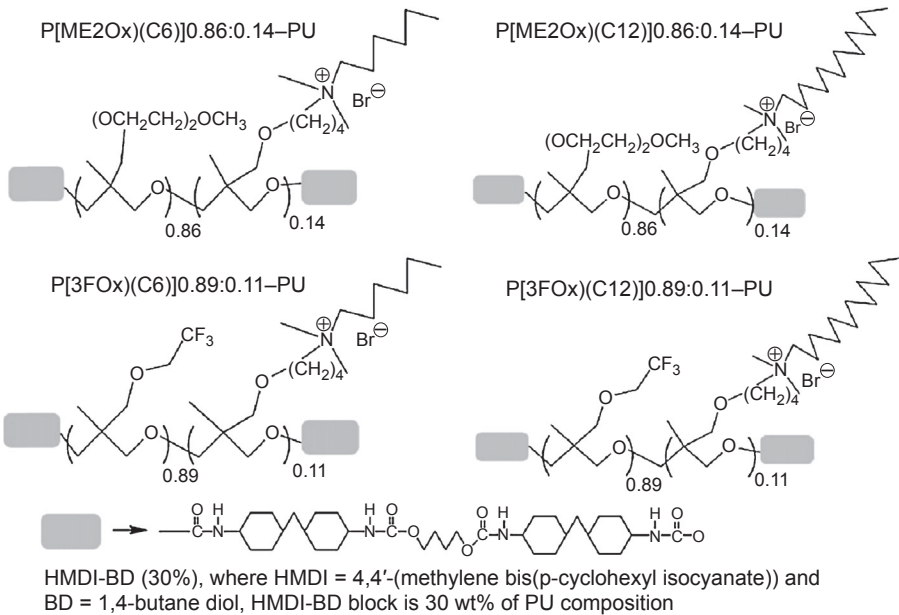
Figure 2.32 Polyurethane additives with alkyl ammonium-functionalized soft blocks.
Reprinted with permission from Ref. [184].

2.9 Antibiofilm efficacy

Biofilm is defined as a bacteria community attached to a solid surface. Biofilm formation is a natural defense mechanism of bacteria to survive under harsh environments. The sequential formation of biofilm is schematically described in Figure 2.33. First,

Table 2.5 **Results from aerosol spray testing for coatings prepared from 2% additives (column 1) and 98% H$_{12}$MDI/BD(50)– PTMO(1000)**

2 wt% PSM designation	Escherichia coli (G−)		Pseudomonas aeruginosa (G−)		Staphylococcus aureus (G+)	
	Kill (%)	Log red	Kill (%)	Log red	Kill (%)	Log red
P[(ME2Ox)(C6)]0.86:0.14–PU	61.1	0.41	59.0	0.39	65.0	0.46
P[(ME2Ox)(C12)]0.86:0.14–PU	100.0	4.30	100.0	4.28	98.7	1.90
P[(3FOx)(C6)]0.89:0.11–PU	97.7	1.65	98.5	1.83	98.7	1.88
P[(3FOx)(C12)]0.89:0.11–PU	100.0	4.38	100.0	4.33	100.0	3.57
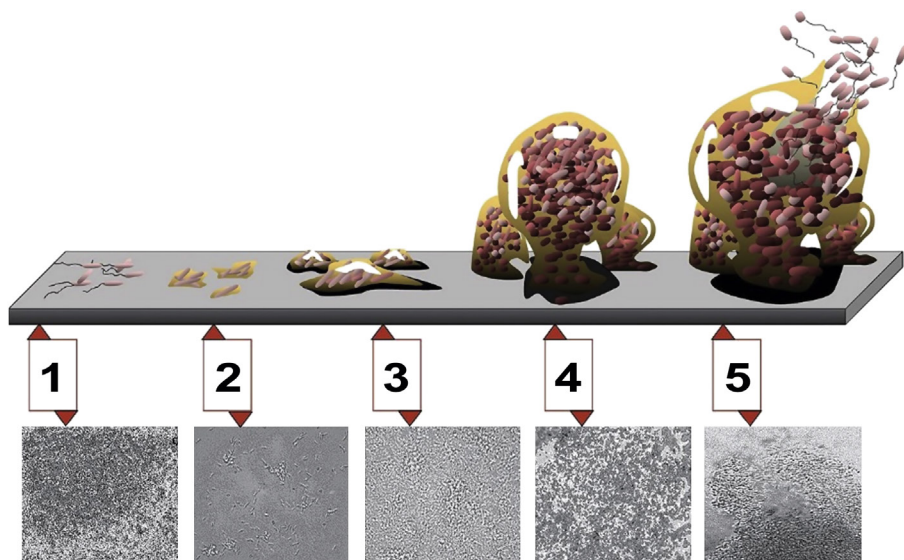
Figure 2.33 Schematic demonstration of biofilm in all stages.

planktonic bacteria cells make initial attachment to a biological or nonbiological surface. Once the bacteria have colonized on the surface, they send out signal proteins to call in more bacteria to colonize at the same site. More and more bacteria start to accumulate on the surface, which excrete polysaccharide extracellulose matrix (ECM) to form a slimy and robust film-like biofilm. After the biofilm matures, it can dissemble to release bacteria into the nearby fluid, which can spread and produce new

biofilms elsewhere. The eradication of a biofilm is extremely difficult since systematic antibiotics can barely penetrate protective ECM. In addition, most bacteria in biofilm are in their dormant state with little metabolic activity. Since most antibiotics focus on inhibiting bacterial metabolistic pathways, dormant bacteria are hardly affected. The presence of biofilms can be found almost anywhere, from food processing facilities to implanted medical devices. Biofilm formation on medical devices, caused by insufficient sterilization during operation or late infection from the bacteria circulating in body fluid, is a major reason for device failure [185–187]. Therefore, surface modification of biomaterials and polyurethane in particular to impart biofilm resistance is of great interest.

It is important to note that antimicrobial and biofilm resistance are two different characteristics though some materials show both properties at the same time. Antimicrobial materials do not automatically prevent biofilm formation and vice versa. Antimicrobial surfaces could kill bacteria on contact but if dead bacteria cell debris blocks the active biocidal surface, biofilm formation could eventually occur. For example, quaternary ammonium polymers can effectively kill bacteria but when the surface is fouled with dead bacteria debris, biofilm formation is inevitable [188]. Materials with antibiofilm properties will repel the bacterial adhesion very effectively but may not kill the bacteria when they do colonize the surface. PEG surfaces are well known to repel bacteria adhesion. However, PEG surfaces show little antimicrobial activity. Quantitative antibiofilm efficacy tests can be divided into two categories: static (minimum biofilm eradication concentration assay, MBEC) and dynamic (flow cell assay). In addition, SEM is a semiquantitative assay, which is discussed in Section 2.5.

2.9.1   Minimum biofilm eradication concentration assay

The MBEC assay was first developed as a high-throughput test method for antibiotics' efficacy to eradicate mature biofilms [189,190]. This test involves a specially designed "peg" microplate lid with small polystyrene cones that fit into microplate wells (Figure 2.34(b)). Bacteria-inoculated solutions fill the wells of a microplate and the microplate is covered with this peg lid that allows bacteria to form biofilm on the peg surface after incubation (Figure 2.34(a)). Antibiotic solutions are diluted to different concentrations in a new microplate. The peg lid with mature biofilm grown on it is then moved to the new microplate with antibiotic solutions. After incubation, the remaining bacteria on the peg surface are recovered by sonication with buffer saline and live bacteria are counted on agar plates. Bacterial log reduction versus antibiotic concentration can be further plotted (Figure 2.35).

The MBEC assay described is designed for antibiotics rather than polyurethane materials. Therefore, Russell et al. [191] modified this method to evaluate acrylate–urethane coating's performance. Salicylic acid was first conjugated with an acrylate group to form a polymerizable monomer. This monomer was then copolymerized with urethane acrylate via UV free radical polymerization (Figure 2.36). The peg cones on
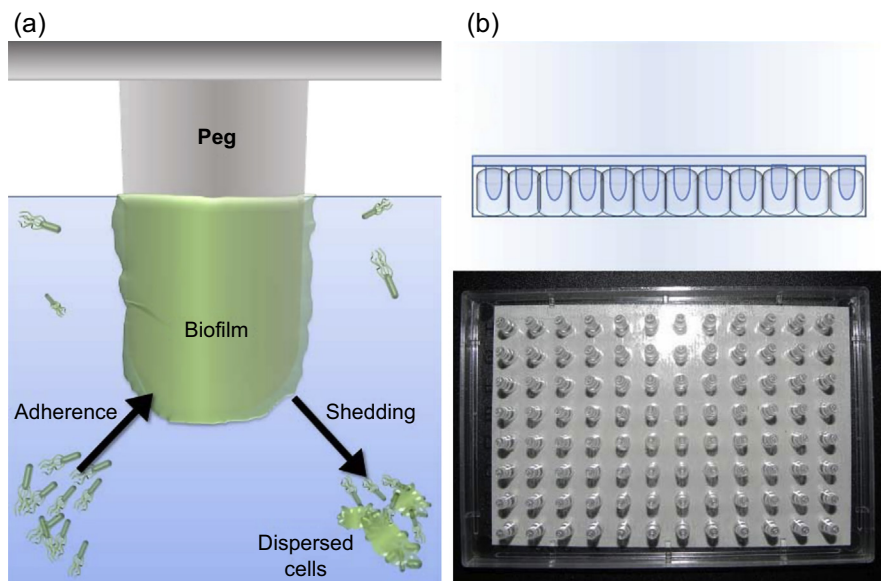
Figure 2.34 MBEC assay. (a) Biofilms form on the polystyrene pegs of the MBEC device when planktonic bacteria adsorb to the surface. These bacteria become irreversibly attached and grow to form mature biofilms. Biofilms are encased in "slime," which is sometimes visible to the naked eye. Planktonic cells are also shed from the surface of biofilms, which serves as the inoculum for CA determinations. (b) The peg lid has 96 identical plastic pegs. This lid fits into a trough with channels designed to guide an inoculum across the surface of the pegs. The peg lid fits into a standard 96-well microplate as well, which is used to set up serial dilutions of antimicrobials.
Credited from http://www.innovotech.ca/.

the lid are dip-coated with salicylic acid-releasing polymer. Such coated cones were challenged with bioluminescent *Pseudomonas aeruginosa* and *E. coli*. The luminescence of peg lids was measured every day and plotted as reduction compared with negative control (Figure 2.37). Some formulations of the coating polymer showed 50–60% reduction of biofilm formation.

2.9.2   Scanning electron microscopy

See Section 2.5 for more information on SEM.

2.9.3   Flow cell assay

A typical flow cell assay involves a flow cell chamber, a microscope (white light or fluorescent), a peristaltic pump, and connection tubings. The basic construct of a flow cell is shown in Figure 2.38. The flow chamber is sandwiched between two optical clear plates (glass or plastic). Based on test specification, the flow chamber
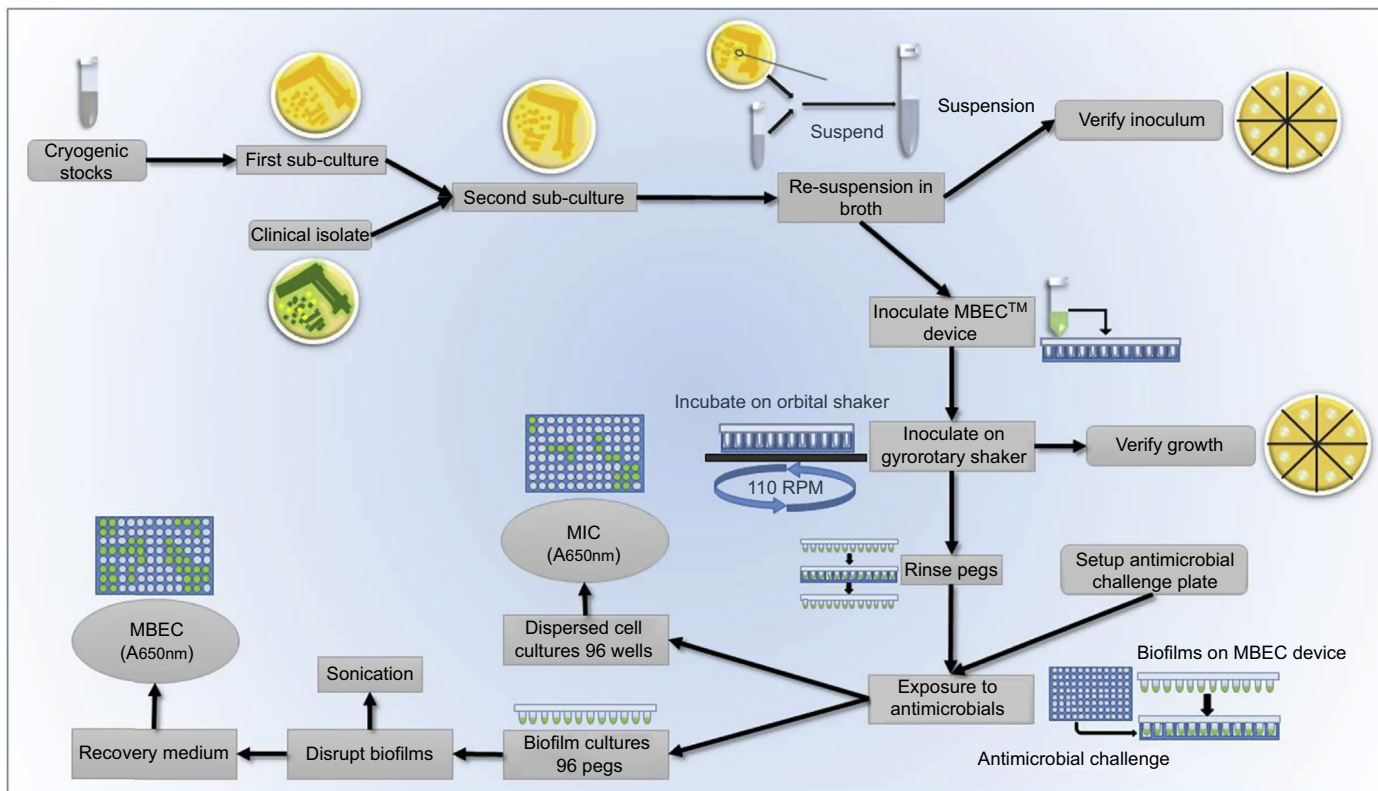
Figure 2.35 Flow chart of MBEC protocol.
Credited from http://www.innovotech.ca/.
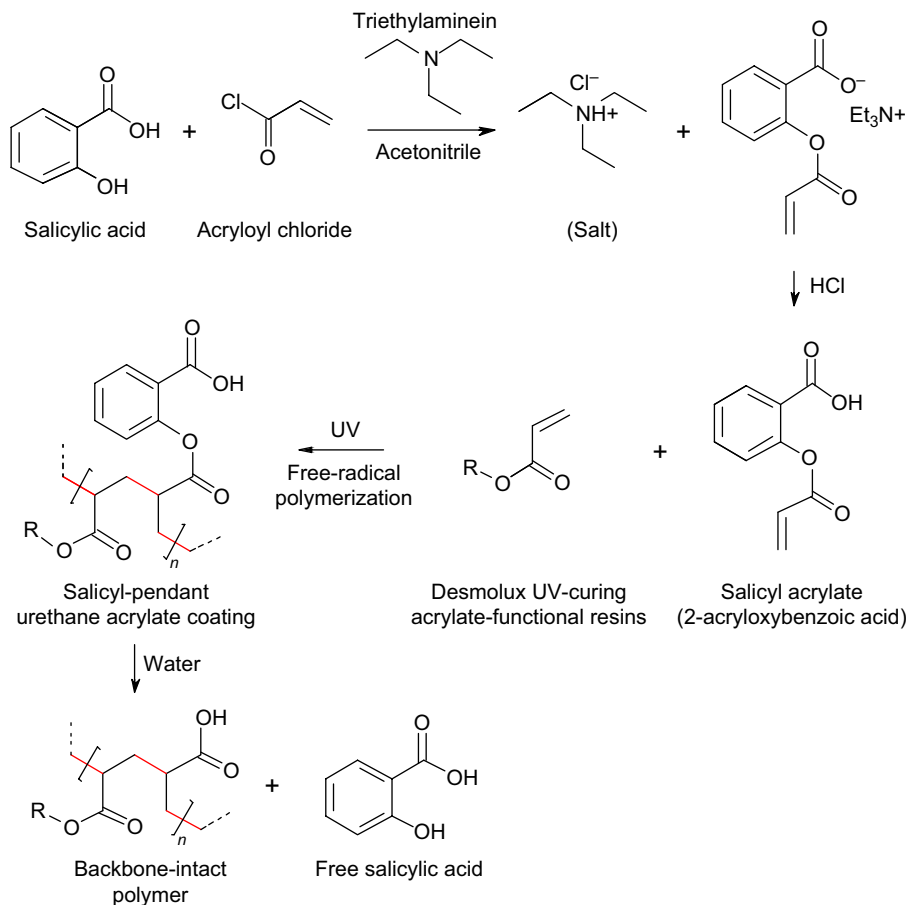
Figure 2.36 Synthetic route of acrylate–urethane coating polymer with hydrolyzable ester bonds for salicylic acid release.
Reprinted with permission from Ref. [191].

has one (single channel) or multiple (multichannel) inlet/s and outlet/s that can test one or multiple samples. The peristaltic pump draws fresh inoculated bacteria solution into the flow cell and the bacteria solution is further collected in a biohazard waste container. Test polymer samples are placed in sample wells inside of the flow chamber and polymer samples are challenged with continuous flow of bacteria solution. Biofilm formation on polymer samples can be visualized by a white light microscope or quantified by a fluorescent microscope after staining with fluorescence dye.

Russell et al. [191] (for detailed information, see Section 2.9.1) tested salicylic acid releasing urethane–acrylate-coated polymer coupon against *P. aeruginosa* biofilm using this flow cell method. The biofilm was then stained with propidium iodide. A control polymer coupon showed much higher fluorescence intensity due
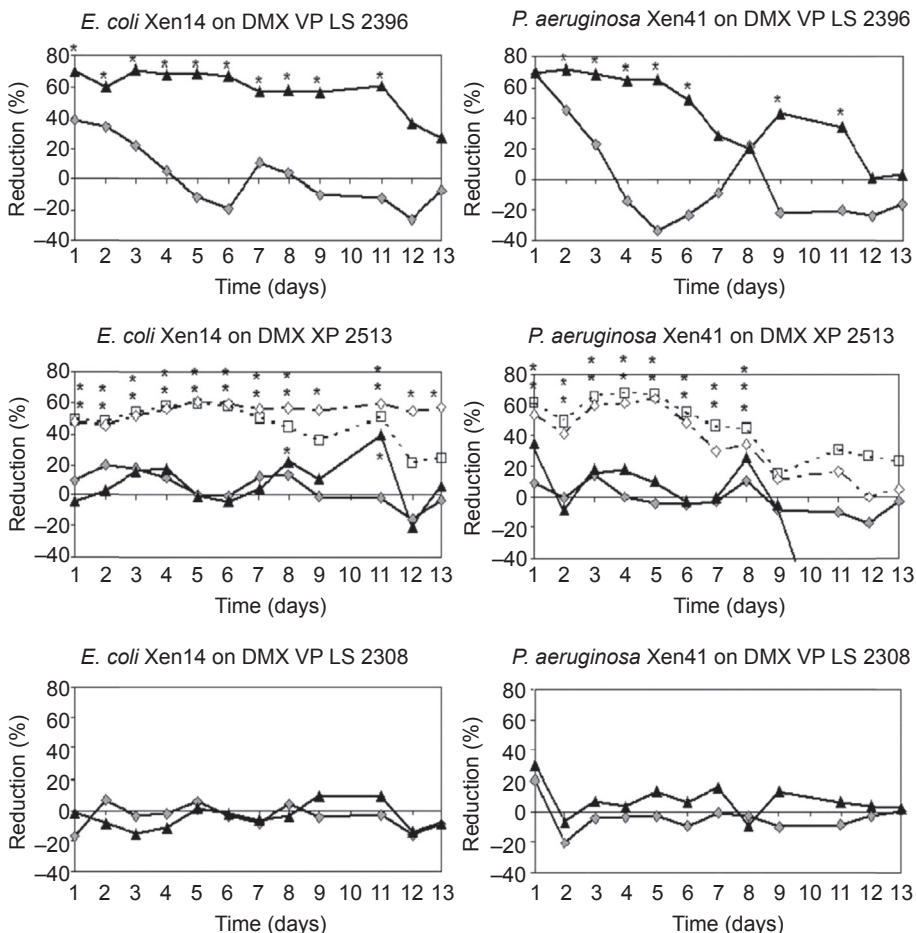
Figure 2.37 Percentage reduction of biofilm compared to control resins of *Escherichia coli* Xen14 (left column) and *Pseudomonas aeruginosa* Xen41 (right column) caused by the Desmolux (DMX) resins containing backbone-reacted salicylic acrylate (SAcr), 11% (solid diamond) or 33% (solid triangles), or admixed salicylic acid, 8% (open square) or 24% (open diamond). Statistically significant (*P*<0.05) reductions are indicated by a ''*'' above the symbol.
Reprinted with permission from Ref. [191].

to heavy biofilm accumulation. The coated samples, however, showed lower fluorescence intensity because the polymer coating greatly inhibited biofilm formation (Figure 2.39).

The surface properties of polyurethane biomaterials are so important that they cannot be overemphasized and there have been many innovative ways to tailor polyurethanes interfaces. In this chapter, we discussed some important but not all surface
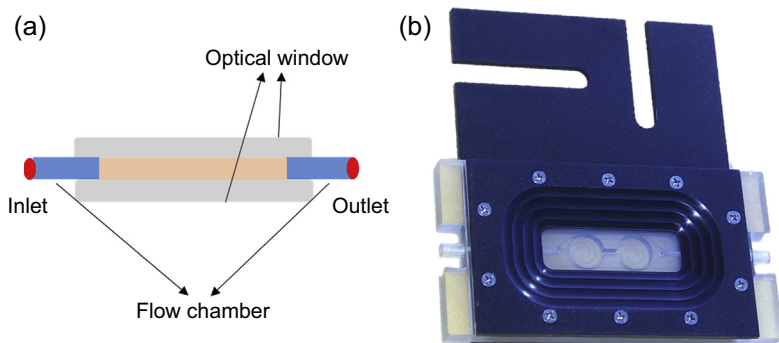
Figure 2.38 Construct of a flow cell: (a) side intersection view; (b) commercial product from BioSurface Technologies Corporation.
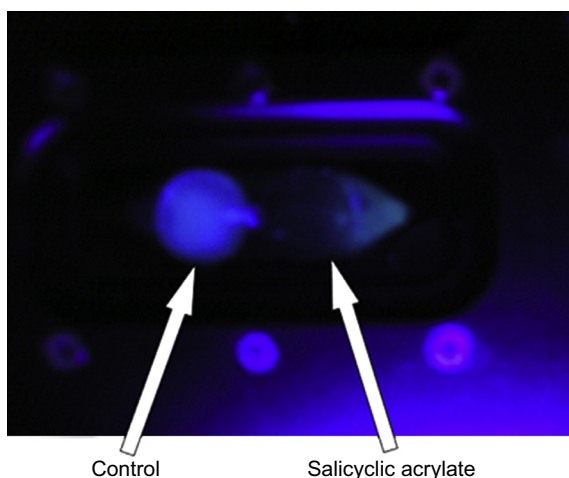
Figure 2.39 Fluorescence image of the flow cell after 5 days of *Pseudomonas aeruginosa* biofilm growth, showing the arrangement of the two coated coupons oriented in series in the flow cell. Extensive biofilm growth is evident on the control sample (Desmolux VP LS 2396/0% SAcr) but minimal growth on the downstream salicylic acid-releasing sample (Desmolux VP LS 2396/35 wt% SAcr). The flow was from left to right. Note the biofilm growth evident at the outlet port directly downstream of the sample coupon. The blue color from the screws and the metal top plate in the upper panel was due to reflected light. Reprinted with permission from Ref. [191].

characterization techniques. Because the interactions of polyurethanes with the biological environment are very complicated issues, it usually requires the combination of multiple characterization techniques from simple CA measurements to more complicated radiolabeling techniques. Advancement of new characterization techniques can better guide the polyurethane research and supply a new generation of polyurethane biomaterials with improved properties.

Acknowledgments

References

[1] Ratner B. Surface characterization of biomaterials by electron spectroscopy for chemical analysis. Ann Biomed Eng 1983;11:313–36.

[2] Ratner BD. Surface modification of polymers: chemical, biological and surface analytical challenges. Biosens Bioelectron 1995;10:797–804.

[3] Wang Y-X, Robertson J, Spillman Jr W, Claus R. Effects of the chemical structure and the surface properties of polymeric biomaterials on their biocompatibility. Pharm Res 2004;21:1362–73.

[4] Kannan RY, Salacinski HJ, Vara DS, Odlyha M, Seifalian AM. Review paper: principles and applications of surface analytical techniques at the vascular interface. J Biomater Appl 2006;21:5–32.

[5] Lamba NM, Woodhouse KA, Cooper SL. Polyurethanes in biomedical applications. CRC Press; 1997. ISBN 13 No: 978-0849345173.

[6] Ma Z, Mao Z, Gao C. Surface modification and property analysis of biomedical polymers used for tissue engineering. Colloids Surf B Biointerfaces 2007;60:137–57.

[7] Belu AM, Graham DJ, Castner DG. Time-of-flight secondary ion mass spectrometry: techniques and applications for the characterization of biomaterial surfaces. Biomaterials 2003;24:3635–53.

[8] Rubenstein CA. General theory of the surface friction of solids. Proc Phys Soc Sect B 1956;69:921.

[9] Jimenez O, Moll F. Highly lubricious hydrophilic coating utilizing dendrimers. U.S. Patent No. 20030135195 A1; 2003.

[10] Gould FE, Kliment CK, Seems GE. Articles having low friction surfaces and production thereof. U.S. Patent No. 4810543 A; 1989.

[11] Creasy WS, Lorenz DH, LaCasse RG, Malagreca SA. Hydrophilic polymer blend. U.S. Patent No. 4642267 A; 1987.

[12] Hunter WL. Medical implants with a combination of compounds. U.S. Patent No. 20100074934 A1; 2010.

[13] Hudgin DE, Blair EA. Hydrophilic or hydrogel carrier systems such as coatings, body implants and other articles. U.S. Patent No. 20030135195; 1976.

[14] Kocak N. Introducer sheath assembly. U.S. Patent No. 4705511 A; 1987.

[15] Wright JG, Mcdaid E. Medical device treated with a hydrophilic polymer composition. U.S. Patent No. 4487808 A; 1996.

[16] Lambert HR. Medical article having a hydrophilic coating. U.S. Patent No. 4487808 A; 1984.

[17] Lambert HR. Preparation of hydrophilic coating. U.S. Patent No. 4585666 A; 1986.

[18] Lambert HR. Hydrophilic coating. U.S. Patent No. 4666437 A; 1987.

[19] Kangas S. Lubricious coating. U.S. Patent No. 20050054774 A1; 2005.

[20] Larsson NE. Medical article with a lubricious coating. European Patent No. 0799623 A2; 1997.

[21] Elton RK. Flexible lubricious organic coatings. U.S. Patent No. 5179174 A; 1993.

[22] Yoshito Ikada YU. Lubricating polymer surfaces. CRC Press; 1993. ISBN 13 No: 9781566760133.

[23] Zhou X, Zhang T, Jiang X, Gu N. The surface modification of medical polyurethane to improve the hydrophilicity and lubricity: the effect of pretreatment. J Appl Polym Sci 2010;116:1284–90.

[24] Kazmierska K, Szwast M, Ciach T. Determination of urethral catheter surface lubricity. J Mater Sci Mater Med 2008;19:2301–6.

[25] Scheuermann C. Mastering endovascular techniques: a guide to excellence. In: Lanzer P, editor. J Vasc Interv Radiol. Lippincott Williams & Wilkins (2006); 2008;19:1263.

[26] Evans SD, Sharma R, Ulman A. Contact angle stability: reorganization of monolayer surfaces? Langmuir 1991;7:156–61.

[27] Wu D, Ming W, van Benthem RATM, de With G. Superhydrophobic fluorinated polyurethane films. J Adhes Sci Technol 2008;22:1869–81.

[28] Sullivan DE. Surface tension and contact angle of a liquid–solid interface. J Chem Phys 1981;74:2604–15.

[29] Johnson RE, Dettre RH. Contact angle hysteresis. III. Study of an idealized heterogeneous surface. J Phys Chem 1964;68:1744–50.

[30] Yuan Y, Lee TR. Contact angle and wetting properties. In: Bracco G, Holst B, editors. Surface science techniques. Springer Berlin Heidelberg; 2013. p. 3–34.

[31] Holly FJ, Refojo MF. Wettability of hydrogels I. Poly(2-hydroxyethyl methacrylate). J Biomed Mater Res 1975;9:315–26.

[32] Ruckenstein E, Lee SH. Estimation of the equilibrium surface free energy components of restructuring solid surfaces. J Colloid Interface Sci 1987;120:153–61.

[33] Lee SH, Ruckenstein E. Surface restructuring of polymers. J Colloid Interface Sci 1987;120:529–36.

[34] Lee SH, Ruckenstein E. Stability of polymeric surfaces subjected to ultraviolet irradiation. J Colloid Interface Sci 1987;117:172–8.

[35] Mason R, Jalbert CA, O'Rourke Muisener PAV, Koberstein JT, Elman JF, Long TE, et al. Surface energy and surface composition of end-fluorinated polystyrene. Adv Colloid Interface Sci 2001;94:1–19.

[36] Jalbert CJ, Koberstein JT, Balaji R, Bhatia Q, Salvati L, Yilgor I. Surface depletion of end groups in amine-terminated poly(dimethylsiloxane). Macromolecules 1994;27:2409–13.

[37] Jerome R, Teyssie P, Pireaux JJ, Verbist JJ. Surface analysis of polymers end-capped with metal carboxylates using X-ray photoelectron spectroscopy. Appl Surf Sci 1986; 27:93–105.

[38] Elman JF, Johs BD, Long TE, Koberstein JT. A neutron reflectivity investigation of surface and interface segregation of polymer functional end groups. Macromolecules 1994;27:5341–9.

[39] Jalbert C, Koberstein JT, Hariharan A, Kumar SK. End group effects on surface properties of polymers: semiempirical calculations and comparison to experimental surface tensions for α,ω-functional poly(dimethylsiloxanes). Macromolecules 1997;30:4481–90.

[40] Dettre RH, Johnson RE. Contact angle hysteresis. IV. Contact angle measurements on heterogeneous surfaces. J Phys Chem 1965;69:1507–15.

[41] Lin H-B, García-Echeverría C, Asakura S, Sun W, Mosher DF, Cooper SL. Endothelial cell adhesion on polyurethanes containing covalently attached RGD-peptides. Biomaterials 1992;13:905–14.

[42] Park JH, Park KD, Bae YH. PDMS-based polyurethanes with MPEG grafts: synthesis, characterization and platelet adhesion study. Biomaterials 1999;20:943–53.

[43] Silver JH, Myers CW, Lim F, Cooper SL. Effect of polyol molecular weight on the physical properties and haemocompatibility of polyurethanes containing polyethylene oxide macroglycols. Biomaterials 1994;15:695–704.

[44] Park KD, Kim YS, Han DK, Kim YH, Lee EHB, Suh H, et al. Bacterial adhesion on PEG modified polyurethane surfaces. Biomaterials 1998;19:851–9.

[45] Fujimoto K, Tadokoro H, Ueda Y, Ikada Y. Polyurethane surface modification by graft polymerization of acrylamide for reduced protein adsorption and platelet adhesion. Biomaterials 1993;14:442–8.

[46] Stojilovic N. Why can't we see hydrogen in X-ray photoelectron spectroscopy? J Chem Educ 2012;89:1331–2.

[47] Ishihara K, Hanyuda H, Nakabayashi N. Synthesis of phospholipid polymers having a urethane bond in the side chain as coating material on segmented polyurethane and their platelet adhesion-resistant properties. Biomaterials 1995;16:873–9.

[48] Zhou J, Yuan J, Zang X, Shen J, Lin S. Platelet adhesion and protein adsorption on silicone rubber surface by ozone-induced grafted polymerization with carboxybetaine monomer. Colloids Surf B Biointerfaces 2005;41:55–62.

[49] Sun Q, Su Y, Ma X, Wang Y, Jiang Z. Improved antifouling property of zwitterionic ultrafiltration membrane composed of acrylonitrile and sulfobetaine copolymer. J Membr Sci 2006;285:299–305.

[50] Hu Y, Yang G, Liang B, Fang L, Ma G, Zhu Q, et al. The fabrication of superlow protein absorption zwitterionic coating by electrochemically mediated atom transfer radical polymerization and its application. Acta Biomater 2015;13:142–9.

[51] Yuan Y-Y, Mao C-Q, Du X-J, Du J-Z, Wang F, Wang J. Surface charge switchable nanoparticles based on zwitterionic polymer for enhanced drug delivery to tumor. Adv Mater 2012;24:5476–80.

[52] Tan D, Li Z, Yao X, Xiang C, Tan H, Fu Q. The influence of fluorocarbon chain and phosphorylcholine on the improvement of hemocompatibility: a comparative study in polyurethanes. J Mater Chem B 2014;2:1344–53.

[53] Li J, Zhang Y, Yang J, Tan H, Li J, Fu Q. Synthesis and surface properties of polyurethane end-capped with hybrid hydrocarbon/fluorocarbon double-chain phospholipid. J Biomed Mater Res A 2013;101A:1362–72.

[54] Tan J, Brash JL. Nonfouling biomaterials based on polyethylene oxide-containing amphiphilic triblock copolymers as surface modifying additives: synthesis and characterization of copolymers and surface properties of copolymer–polyurethane blends. J Appl Polym Sci 2008;108:1617–28.

[55] Tan J, McClung WG, Brash JL. Non-fouling biomaterials based on blends of polyethylene oxide copolymers and polyurethane: simultaneous measurement of platelet adhesion and fibrinogen adsorption from flowing whole blood. J Biomater Sci Polym Ed 2012;24:497–506.

[56] Harney MB, Pant RR, Fulmer PA, Wynne JH. Surface self-concentrating amphiphilic quaternary ammonium biocides as coating additives. ACS Appl Mater Interfaces 2008;1:39–41.

[57] Goddard JM, Hotchkiss JH. Polymer surface modification for the attachment of bioactive compounds. Prog Polym Sci 2007;32:698–725.

[58] Ratner BD, Tyler BJ, Chilkoti A. Analysis of biomedical polymer surfaces: polyurethanes and plasma-deposited thin films. Clin Mater 1993;13:71–84.

[59] Hearn MJ, Ratner BD, Briggs D. SIMS and XPS studies of polyurethane surfaces. 1. Preliminary studies. Macromolecules 1988;21:2950–9.

[60] Tyler BJ, Ratner BD, Castner DG, Briggs D. Variations between Biomer™ lots. I. Significant differences in the surface chemistry of two lots of a commercial poly(ether urethane). J Biomed Mater Res 1992;26:273–89.

[61] Tyler BJ, Ratner BD. Variations between biomer lots. 2: The effect of differences between lots on in vitro enzymatic and oxidative degradation of a commercial polyurethane. J Biomed Mater Res 1993;27:327–34.

[62] Schilke KF, McGuire J. Detection of nisin and fibrinogen adsorption on poly(ethylene oxide) coated polyurethane surfaces by time-of-flight secondary ion mass spectrometry (TOF-SIMS). J Colloid Interface Sci 2011;358:14–24.

[63] Wang D-A, Ji J, Sun Y-H, Shen J-C, Feng L-X, Elisseeff JH. In situ immobilization of proteins and RGD peptide on polyurethane surfaces via poly(ethylene oxide) coupling polymers for human endothelial cell growth. Biomacromolecules 2002;3:1286–95.

[64] Chen Z, Ward R, Tian Y, Malizia F, Gracias DH, Shen YR, et al. Interaction of fibrinogen with surfaces of end-group-modified polyurethanes: a surface-specific sum-frequency-generation vibrational spectroscopy study. J Biomed Mater Res 2002;62:254–64.

[65] Wagner MS, Shen M, Horbett TA, Castner DG. Quantitative analysis of binary adsorbed protein films by time of flight secondary ion mass spectrometry. J Biomed Mater Res A 2003;64A:1–11.

[66] Wagner MS, Horbett TA, Castner DG. Characterization of the structure of binary and ternary adsorbed protein films using electron spectroscopy for chemical analysis, time-of-flight secondary ion mass spectrometry, and radiolabeling. Langmuir 2003;19:1708–15.

[67] Marchant RE, Anderson JM, Phua K, Hiltner A. In vivo biocompatibility studies. II. Biomer: preliminary cell adhesion and surface characterization studies. J Biomed Mater Res 1984;18:309–15.

[68] Park JH, Cho YW, Kwon IC, Jeong SY, Bae YH. Assessment of PEO/PTMO multiblock copolymer/segmented polyurethane blends as coating materials for urinary catheters: in vitro bacterial adhesion and encrustation behavior. Biomaterials 2002; 23:3991–4000.

[69] Yao C, Li X, Neoh KG, Shi Z, Kang ET. Surface modification and antibacterial activity of electrospun polyurethane fibrous membranes with quaternary ammonium moieties. J Membr Sci 2008;320:259–67.

[70] Ruggeri V, Francolini I, Donelli G, Piozzi A. Synthesis, characterization, and in vitro activity of antibiotic releasing polyurethanes to prevent bacterial resistance. J Biomed Mater Res A 2007;81A:287–98.

[71] Korematsu A, Takemoto Y, Nakaya T, Inoue H. Synthesis, characterization and platelet adhesion of segmented polyurethanes grafted phospholipid analogous vinyl monomer on surface. Biomaterials 2002;23:263–71.

[72] Poussard L, Burel F, Couvercelle JP, Merhi Y, Tabrizian M, Bunel C. Hemocompatibilty of new ionic polyurethanes: influence of carboxylic group insertion modes. Biomaterials 2004;25:3473–83.

[73] Aksoy EA, Hasirci V, Hasirci N, Motta A, Fedel M, Migliaresi C. Plasma protein adsorption and platelet adhesion on heparin-immobilized polyurethane films. J Bioact Compat Polym 2008;23:505–19.

[74] Vaudaux PE, François P, Proctor RA, McDevitt D, Foster TJ, Albrecht RM, et al. Use of adhesion-defective mutants of *Staphylococcus aureus* to define the role of specific plasma proteins in promoting bacterial adhesion to canine arteriovenous shunts. Infect Immun 1995;63:585–90.

[75] Poussard L, Burel F, Couvercelle JP, Lesouhaitier O, Merhi Y, Tabrizian M, et al. In vitro thrombogenicity investigation of new water-dispersible polyurethane anionomers bearing carboxylate groups. J Biomater Sci Polym Ed 2005;16:335–51.

[76] Yuan Y, Zhang J, Ai F, Yuan J, Zhou J, Shen J, et al. Surface modification of SPEU films by ozone induced graft copolymerization to improve hemocompatibility. Colloids Surf B Biointerfaces 2003;29:247–56.

[77] Zhang F, Kang ET, Neoh KG, Wang P, Tan KL. Reactive coupling of poly(ethylene glycol) on electroactive polyaniline films for reduction in protein adsorption and platelet adhesion. Biomaterials 2002;23:787–95.

[78] Jahangir AR, McClung WG, Cornelius RM, McCloskey CB, Brash JL, Santerre JP. Fluorinated surface-modifying macromolecules: modulating adhesive protein and platelet interactions on a polyether-urethane. J Biomed Mater Res 2002;60:135–47.

[79] Zhao Q, Topham N, Anderson JM, Hiltner A, Lodoen G, Payet CR. Foreign-body giant cells and polyurethane biostability: in vivo correlation of cell adhesion and surface cracking. J Biomed Mater Res 1991;25:177–83.

[80] Martin DJ, Poole Warren LA, Gunatillake PA, McCarthy SJ, Meijs GF, Schindhelm K. Polydimethylsiloxane/polyether-mixed macrodiol-based polyurethane elastomers: biostability. Biomaterials 2000;21:1021–9.

[81] Takahara A, Coury AJ, Hergenrother RW, Cooper SL. Effect of soft segment chemistry on the biostability of segmented polyurethanes. I. In vitro oxidation. J Biomed Mater Res 1991;25:341–56.

[82] Stokes K, McVenes R, Anderson JM. Polyurethane elastomer biostability. J Biomater Appl 1995;9:321–54.

[83] Santerre JP, Woodhouse K, Laroche G, Labow RS. Understanding the biodegradation of polyurethanes: from classical implants to tissue engineering materials. Biomaterials 2005;26:7457–70.

[84] Li D, Chen H, Glenn McClung W, Brash JL. Lysine-PEG-modified polyurethane as a fibrinolytic surface: effect of PEG chain length on protein interactions, platelet interactions and clot lysis. Acta Biomater 2009;5:1864–71.

[85] Sun X, Cao Z, Porteous N, Sun Y. An N-halamine-based rechargeable antimicrobial and biofilm controlling polyurethane. Acta Biomater 2012;8:1498–506.

[86] Liang J, Chen Y, Barnes K, Wu R, Worley SD, Huang TS. N-halamine/quat siloxane copolymers for use in biocidal coatings. Biomaterials 2006;27:2495–501.

[87] Szycher M, Reed AM, Siciliano AA. In vivo testing of a biostable polyurethane. J Biomater Appl 1991;6:110–30.

[88] Ward R, Anderson J, McVenes R, Stokes K. In vivo biostability of polysiloxane polyether polyurethanes: resistance to biologic oxidation and stress cracking. J Biomed Mater Res A 2006;77A:580–9.

[89] Zhao Q, Agger MP, Fitzpatrick M, Anderson JM, Hiltner A, Stokes K, et al. Cellular interactions with biomaterials: in vivo cracking of pre-stressed Pellethane 2363-80A. J Biomed Mater Res 1990;24:621–37.

[90] Amiel A, Lehmann G, Touchard G, Boutaud P, Herpin D, Demange J. Immunity mechanisms involved in the degradation of polyurethane leads. In: Steinbach K, editor. Cardiac pacing. Steinkopff; 1983. p. 311–5.

[91] Wiggins MJ, Wilkoff B, Anderson JM, Hiltner A. Biodegradation of polyether polyurethane inner insulation in bipolar pacemaker leads. J Biomed Mater Res 2001;58:302–7.

[92] Stokes K. Polyurethane pacemaker leads. In: Becker K, Whyte J, editors. Clinical evaluation of medical devices. Humana Press; 2006. p. 285–304. http://dx.doi.org/10.1007/978-1-59745-004-1_17.

[93] Chawla AS, Blais P, Hinberg I, Johnson D. Degradation of explanted polyurethane cardiac pacing leads and of polyurethane. Biomater Artif Cells Artif Organs 1988;16:785–800.

[94] Capone CD. Biostability of a non-ether polyurethane. J Biomater Appl 1992;7:108–29.

[95] Mathur AB, Collier TO, Kao WJ, Wiggins M, Schubert MA, Hiltner A, et al. In vivo biocompatibility and biostability of modified polyurethanes. J Biomed Mater Res 1997;36:246–57.

[96] Thomas AH, John LB. Proteins at interfaces II. American Chemical Society; 1995. p. 1–23.

[97] Macritchie F. Proteins at interfaces. In: Anfinsen CB, John TE, Frederic MR, editors. Advances in protein chemistry. Academic Press; 1978. p. 283–326. http://dx.doi.org/10.1016/S0065-3233(08)60577-X.

[98] Norde W, Lyklema J. Why proteins prefer interfaces. J Biomater Sci Polym Ed 1991;2:183–202.

[99] Gifford R, Kehoe JJ, Barnes SL, Kornilayev BA, Alterman MA, Wilson GS. Protein interactions with subcutaneously implanted biosensors. Biomaterials 2006;27:2587–98.

[100] Hu W-J, Eaton JW, Ugarova TP, Tang L. Molecular basis of biomaterial-mediated foreign body reactions. Blood 2001;98(4):1231–8.

[101] Tang L, Wu Y, Timmons RB. Fibrinogen adsorption and host tissue responses to plasma functionalized surfaces. J Biomed Mater Res 1998;42:156–63.

[102] Ferrans VJ, Boyce SW, Billingham ME, Jones M, Ishihara T, Roberts WC. Calcific deposits in porcine bioprostheses: structure and pathogenesis. Am J Cardiol 1980;46:721–34.

[103] Sevastianov VI. Biocompatible biomaterials: current status and future perspectives. Trends Biomater Artif Organs 2002;15:20–30.

[104] Lian JB, Levy RJ, Bernhard W, Szycher M. LVAD minerization and γ-carboxyglutamic acid containing proteins in normal and pathologically mineralized tissues. ASAIO J 1981;27:683–9.

[105] Pavithra D, Mukesh D. Biofilm formation, bacterial adhesion and host response on polymeric implants—issues and prevention. Biomed Mater 2008;3:034003.

[106] Teughels W, Van Assche N, Sliepen I, Quirynen M. Effect of material characteristics and/or surface topography on biofilm development. Clin Oral Implants Res 2006;17:68–81.

[107] Sun D, Accavitti MA, Bryers JD. Inhibition of biofilm formation by monoclonal antibodies against *Staphylococcus epidermidis* RP62A accumulation-associated protein. Clin Diagn Lab Immunol 2005;12:93–100.

[108] Ma C, Zhou H, Wu B, Zhang G. Preparation of polyurethane with zwitterionic side chains and their protein resistance. ACS Appl Mater Interfaces 2011;3:455–61.

[109] Michel R, Pasche S, Textor M, Castner DG. Influence of peg architecture on protein adsorption and conformation. Langmuir 2005;21:12327–32.

[110] Saito N, Matsuda T. Protein adsorption on self-assembled monolayers with water-soluble non-ionic oligomers using quartz-crystal microbalance. Mater Sci Eng C 1998;6:261–6.

[111] Zhou G, Ma C, Zhang G. Synthesis of polyurethane-*g*-poly(ethylene glycol) copolymers by macroiniferter and their protein resistance. Polym Chem 2011;2:1409–14.

[112] Chen H, Yuan L, Song W, Wu Z, Li D. Biocompatible polymer materials: role of protein–surface interactions. Prog Polym Sci 2008;33:1059–87.

[113] Green RJ, Frazier RA, Shakesheff KM, Davies MC, Roberts CJ, Tendler SJB. Surface plasmon resonance analysis of dynamic biological interactions with biomaterials. Biomaterials 2000;21:1823–35.

[114] Vogler EA. Protein adsorption in three dimensions. Biomaterials 2012;33:1201–37.

[115] Lü XY, Huang Y, Qian WP, Tang ZM, Lu ZH. An effective method for quantitative evaluation of proteins adsorbed on biomaterial surfaces. J Biomed Mater Res A 2003;66A:722–7.

[116] Yang S-H, Lee Y-SJ, Lin F-H, Yang J-M, Chen K-S. Chitosan/poly(vinyl alcohol) blending hydrogel coating improves the surface characteristics of segmented polyurethane urethral catheters. J Biomed Mater Res B Appl Biomater 2007;83B:304–13.

[117] Chang Y, Chen S, Zhang Z, Jiang S. Highly protein-resistant coatings from well-defined diblock copolymers containing sulfobetaines. Langmuir 2006;22:2222–6.

[118] Chang Y, Shu S-H, Shih Y-J, Chu C-W, Ruaan R-C, Chen W-Y. Hemocompatible mixed-charge copolymer brushes of pseudozwitterionic surfaces resistant to nonspecific plasma protein fouling. Langmuir 2010;26:3522–30.

[119] Jahangir R, McCloskey CB, Mc Clung WG, Labow RS, Brash JL, Santerre JP. The influence of protein adsorption and surface modifying macromolecules on the hydrolytic degradation of a poly(ether–urethane) by cholesterol esterase. Biomaterials 2003;24:121–30.

[120] Alibeik S, Rizkalla AS, Mequanint K. The effect of thiolation on the mechanical and protein adsorption properties of polyurethanes. Eur Polym J 2007;43:1415–27.

[121] Fabrizius-Homan DJ, Cooper SL. Competitive adsorption of vitronection with albumin, fibrinogen, and fibronectin on polymeric biomaterials. J Biomed Mater Res 1991; 25:953–71.

[122] Du YJ, Brash JL, McClung G, Berry LR, Klement P, Chan AKC. Protein adsorption on polyurethane catheters modified with a novel antithrombin-heparin covalent complex. J Biomed Mater Res A 2007;80A:216–25.

[123] Underwood PA, Steele JG. Practical limitations of estimation of protein adsorption to polymer surfaces. J Immunol Methods 1991;142:83–94.

[124] Xu Y, Dong A, Zhao Y, Zhang T, Jiang Z, Wang S, et al. Synthesis, characterization and biomedical properties of UV-cured polyurethane acrylates containing a phosphorylcholine structure. J Biomater Sci Polym Ed 2012;23:2089–104.

[125] McMillan R, Meeks B, Bensebaa F, Deslandes Y, Sheardown H. Cell adhesion peptide modification of gold-coated polyurethanes for vascular endothelial cell adhesion. J Biomed Mater Res 2001;54:272–83.

[126] Seevers RH, Counsell RE. Radioiodination techniques for small organic molecules. Chem Rev 1982;82:575–90.

[127] Hunter WM, Greenwood FC. Preparation of iodine-131 labelled human growth hormone of high specific activity. Nature 1962;194:495–6.

[128] Bailey G. The chloramine t method for radiolabeling protein. In: Walker J, editor. The protein protocols handbook. Humana Press; 2002. p. 963–5. http://dx.doi.org/10.1385/1-59259-169-8:963.

[129] Markwell MAK. A new solid-state reagent to iodinate proteins: I. Conditions for the efficient labeling of antiserum. Anal Biochem 1982;125:427–32.

[130] Radioimmunoassay (RIA). Encyclopedia of genetics, genomics, proteomics and informatics. Netherlands: Springer; 2008. p. 1629.

[131] Chen H, Zhang Z, Chen Y, Brook MA, Sheardown H. Protein repellant silicone surfaces by covalent immobilization of poly(ethylene oxide). Biomaterials 2005;26:2391–9.

[132] Wagner MS, Horbett TA, Castner DG. Characterizing multicomponent adsorbed protein films using electron spectroscopy for chemical analysis, time-of-flight secondary ion mass spectrometry, and radiolabeling: capabilities and limitations. Biomaterials 2003;24:1897–908.

[133] Bailey G. The Bolton and Hunter method for radiolabeling protein. In: Walker J, editor. The protein protocols handbook. Humana Press; 2002. p. 969–70.

[134] Loeb MR, Smith DH. Lactoperoxidase and Iodo-Gen-catalyzed iodination labels inner and outer membrane proteins of *Haemophilus influenzae*. J Bacteriol 1983;155:443–6.

[135] Bailey G. The lactoperoxidase method for radiolabeling protein. In: Walker J, editor. The protein protocols handbook. Humana Press; 2002. p. 967–8.

[136] Bailey G. The iodogen method for radiolabeling protein. In: Walker J, editor. The protein protocols handbook. Humana Press; 1996. p. 673–4. http://dx.doi.org/10.1007/978-1-60327-259-9_115.

[137] Sask KN, Berry LR, Chan AKC, Brash JL. Polyurethane modified with an antithrombin-heparin complex via polyethylene oxide linker/spacers: influence of PEO molecular weight and PEO-ATH bond on catalytic and direct anticoagulant functions. J Biomed Mater Res A 2012;100A:2821–8.

[138] Jin L, Abrahams JP, Skinner R, Petitou M, Pike RN, Carrell RW. The anticoagulant activation of antithrombin by heparin. Proc Natl Acad Sci 1997;94:14683–8.

[139] McGee DC, Gould MK. Preventing complications of central venous catheterization. N Engl J Med 2003;348:1123–33.

[140] Bozzetti F, Mariani L, Bertinet DB, Chiavenna G, Crose N, De Cicco M, et al. Central venous catheter complications in 447 patients on home parenteral nutrition: an analysis of over 100.000 catheter days. Clin Nutr 2002;21:475–85.

[141] Massicotte MP, Dix D, Monagle P, Adams M, Andrew M. Central venous catheter related thrombosis in children: analysis of the Canadian Registry of Venous Thrombo-embolic Complications. J Pediatr 1998;133:770–6.

[142] Erlenkötter A, Endres P, Nederlof B, Hornig C, Vienken J. Score model for the evaluation of dialysis membrane hemocompatibility. Artif Organs 2008;32:962–9.

[143] Ma L, Su B, Cheng C, Yin Z, Qin H, Zhao J, et al. Toward highly blood compatible hemodialysis membranes via blending with heparin-mimicking polyurethane: study in vitro and in vivo. J Membr Sci 2014;470:90–101.

[144] Li L, Cheng C, Xiang T, Tang M, Zhao W, Sun S, et al. Modification of polyethersulfone hemodialysis membrane by blending citric acid grafted polyurethane and its anticoagulant activity. J Membr Sci 2012;405–406:261–74.

[145] Burke A, Hasirci N. Polyurethanes in biomedical applications. In: Hasirci N, Hasirci V, editors. Biomaterials. US: Springer; 2004. p. 83–101.

[146] Schnaar RL, Weigel PH, Kuhlenschmidt MS, Lee YC, Roseman S. Adhesion of chicken hepatocytes to polyacrylamide gels derivatized with N-acetylglucosamine. J Biol Chem 1978;253:7940–51.

[147] Tamada Y, Ikada Y. Cell attachment to various polymer surfaces. In: Chiellini E, Giusti P, Migliaresi C, Nicolais L, editors. Polymers in medicine II. US: Springer; 1986. p. 101–15.

[148] Tamada Y, Ikada Y. Cell adhesion to plasma-treated polymer surfaces. Polymer 1993;34:2208–12.

[149] Vaníčková M, Suttnar J, Dyr JE. The adhesion of blood platelets on fibrinogen surface: comparison of two biochemical microplate assays. Platelets 2006;17:470–6.

[150] Jen CJ. Direct observation of platelet adhesion to fibrinogen- and fibrin-coated surfaces. Am J Physiol 1991;261:1457–63.

[151] Bellavite P, Andrioli G, Guzzo P, Arigliano P, Chirumbolo S, Manzato F, et al. A colorimetric method for the measurement of platelet adhesion in microtiter plates. Anal Biochem 1994;216:444–50.

[152] Xia N, May CJ, McArthur SL, Castner DG. Time-of-Flight secondary ion mass spectrometry analysis of conformational changes in adsorbed protein films. Langmuir 2002;18:4090–7.

[153] Sukavaneshvar S. Assessment and management of vascular implant thrombogenecity. In: Thrombus and Stroke. p. 57–78.

[154] McNeely T, Griffith M. The anticoagulant mechanism of action of heparin in contact-activated plasma: inhibition of factor X activation. Blood 1985;65:1226–31.

[155] Hirsh J, Warkentin TE, Shaughnessy SG, Anand SS, Halperin JL, Raschke R, et al. Heparin and low-molecular-weight heparin mechanisms of action, pharmacokinetics, dosing, monitoring, efficacy, and safety. Chest 2001;119:64S–94S.

[156] van Oeveren W, Tielliu IF, de Hart J. Comparison of modified chandler, roller pump, and ball valve circulation models for in vitro testing in high blood flow conditions: application in thrombogenicity testing of different materials for vascular applications. Int J Biomater 2012;2012:7.

[157] Reynoids LO, Mohammad SF, Soien KA, Pantalos GM, Burns GL, Otstn DB. Light scattering detection of microemboli in an extracorporeal LVAD bovine model. ASAIO J 1990;36:M518–21.

[158] Goodman PD, Hall MW, Sukavaneshvar S, Solen KA. In vitro model for studying the effects of hemodynamics on device induced thromboembolism in human blood. ASAIO J 2000;46:576–8.

[159] Solen K, Sukavaneshvar S, Zheng Y, Hanrahan B, Hall M, Goodman P, et al. Light-scattering instrument to detect thromboemboli in blood. BIOMEDO 2003;8:70–9.

[160] Lelah MD, Lambrecht LK, Cooper SL. A canine ex vivo series shunt for evaluating thrombus deposition on polymer surfaces. J Biomed Mater Res 1984;18:475–96.

[161] Mermel LA. Prevention of intravascular catheter-related infections. Ann Intern Med 2000;132:391–402.

[162] Dimick JB, Pelz RK, Consunji R, Swoboda SM, Hendrix CW, Lipsett PA. Increased resource use associated with catheter-related bloodstream infection in the surgical intensive care unit. Arch Surg 2001;136:229–34.

[163] Rello J, Ochagavia A, Sabanes E, Roque M. Evaluation of outcome of intravenous catheter-related infections in critically ill patients. Am J Respir Crit Care Med 2000;162:1027–30.

[164] DiGiovine B, Chenoweth C, Watts C, Higgins M. The attributable mortality and costs of primary nosocomial bloodstream infections in the intensive care unit. Am J Respir Crit Care Med 1999;160:976–81.

[165] Blot SI, Depuydt P, Annemans L, Benoit D, Hoste E, De Waele JJ, et al. Clinical and economic outcomes in critically ill patients with nosocomial catheter-related bloodstream infections. Clin Infect Dis 2005;41:1591–8.

[166] Kunin CM. Catheter-associated urinary tract infections: a syllogism compounded by a questionable dichotomy. Clin Infect Dis 2009;48:1189–90.

[167] Saint S. Clinical and economic consequences of nosocomial catheter-related bacteriuria. Am J Infect Control 2000;28:68–75.

[168] Klevens RM, Edwards JR, Richards CL, Horan TC, Gaynes RP, Pollock DA, et al. Estimating health care-associated infections and deaths in US hospitals, 2002. Public Health Rep 2007;122:160.

[169] Bauer AW, Perry DM, Kirby WM. Single-disk antibiotic-sensitivity testing of *Staphylococci*: an analysis of technique and results. AMA Arch Intern Med 1959;104:208–16.

[170] Zhang H, Wu M, Sen A. Silver nanoparticle antimicrobials and related materials. In: Cioffi N, Rai M, editors. Nano-antimicrobials. Springer Berlin Heidelberg; 2012. p. 3–45.

[171] Liu X, Lin T, Gao Y, Xu Z, Huang C, Yao G, et al. Antimicrobial electrospun nanofibers of cellulose acetate and polyester urethane composite for wound dressing. J Biomed Mater Res B Appl Biomater 2012;100B:1556–65.

[172] Jesline A, John N, Narayanan PM, Vani C, Murugan S. Antimicrobial activity of zinc and titanium dioxide nanoparticles against biofilm-producing methicillin-resistant *Staphylococcus aureus*. Appl Nanosci 2015;5:157–62.

[173] Karandikar BM, Gibbins BL. Antimicrobial polyurethane foam and process to make the same. U.S. Patents No. 20120322903 A1; 2012.

[174] Sheikh F, Barakat NM, Kanjwal M, Chaudhari A, Jung I-H, Lee J, et al. Electrospun anti-microbial polyurethane nanofibers containing silver nanoparticles for biotechnological applications. Macromol Res 2009;17:688–96.

[175] Guggenbichler JP, Böswald M, Lugauer S, Krall T. A new technology of microdispersed silver in polyurethane induces antimicrobial activity in central venous catheters. Infection 1999;27:S16–23.

[176] Francolini I, Ruggeri V, Martinelli A, D'Ilario L, Piozzi A. Novel metal-polyure-thane complexes with enhanced antimicrobial activity. Macromol Rapid Commun 2006;27:233–7.

[177] Timofeeva L, Kleshcheva N. Antimicrobial polymers: mechanism of action, factors of activity, and applications. Appl Microbiol Biotechnol 2011;89:475–92.

[178] Bhende S, Spangler D. In vitro assessment of chlorhexidine gluconate–impregnated polyurethane foam antimicrobial dressing using zone of inhibition assays. Infect Control Hosp Epidemiol 2004;25:664–7.

[179] Fong N, Simmons A, Poole-Warren LA. Antibacterial polyurethane nanocomposites using chlorhexidine diacetate as an organic modifier. Acta Biomater 2010;6:2554–61.

[180] Boyle VJ, Fancher ME, Ross RW. Rapid, modified Kirby–Bauer susceptibility test with single, high-concentration antimicrobial disks. Antimicrob Agents Chemother 1973; 3:418–24.

[181] Donelli G, Francolini I, Romoli D, Guaglianone E, Piozzi A, Ragunath C, et al. Synergis-tic activity of dispersin B and cefamandole nafate in inhibition of staphylococcal biofilm growth on polyurethanes. Antimicrob Agents Chemother 2007;51:2733–40.

[182] Grapski JA, Cooper SL. Synthesis and characterization of non-leaching biocidal polyure-thanes. Biomaterials 2001;22:2239–46.

[183] Wynne JH, Fulmer PA, McCluskey DM, Mackey NM, Buchanan JP. Synthesis and development of a multifunctional self-decontaminating polyurethane coating. ACS Appl Mater Interfaces 2011;3:2005–11.

[184] Kurt P, Wood L, Ohman DE, Wynne KJ. Highly effective contact antimicrobial surfaces via polymer surface modifiers. Langmuir 2007;23:4719–23.

[185] Donlan RM. Biofilms and device-associated infections. Emerg Infect Dis 2001;7:277–81.

[186] Donlan RM. Biofilm formation: a clinically relevant microbiological process. Clin Infect Dis 2001;33:1387–92.

[187] Khardori N, Yassien M. Biofilms in device-related infections. J Ind Microbiol 1995; 15:141–7.

[188] Sambhy V, MacBride MM, Peterson BR, Sen A. Silver bromide nanoparticle/polymer composites: dual action tunable antimicrobial materials. J Am Chem Soc 2006; 128:9798–808.

[189] Ceri H, Olson ME, Stremick C, Read RR, Morck D, Buret A. The Calgary biofilm device: new technology for rapid determination of antibiotic susceptibilities of bacterial biofilms. J Clin Microbiol 1999;37:1771–6.

[190] LaPlante KL, Mermel LA. In vitro activity of daptomycin and vancomycin lock solutions on staphylococcal biofilms in a central venous catheter model. Nephrol Dial Transplant 2007;22:2239–46.

[191] Nowatzki PJ, Koepsel RR, Stoodley P, Min K, Harper A, Murata H, et al. Salicylic acid-releasing polyurethane acrylate polymers as anti-biofilm urological catheter coat-ings. Acta Biomater 2012;8:1869–80.

Design of biodegradable polyurethanes and the interactions of the polymers and their degradation by-products within *in vitro* and *in vivo* environments

3

X. Zhang[1], K.G. Battiston[1], J.E. McBane[2], L.A. Matheson[3], R.S. Labow[3], J. Paul Santerre[1,4,]*

[1]Institute of Biomaterials and Biomedical Engineering, University of Toronto, Toronto, ON, Canada; [2]Children's Hospital of Eastern Ontario Research Institute, Ottawa, ON, Canada; [3]University of Ottawa, Ottawa, ON, Canada; [4]Faculty of Dentistry, University of Toronto, Toronto, ON, Canada

*Corresponding author: paul.santerre@dentistry.utoronto.ca

3.1 Fundamentals of polyurethane degradation

From before and on out to 2015 polyurethanes (PUs) have been used extensively in numerous biomedical applications. Their lasting popularity has been a direct result of their segmented block copolymeric chemistry, which provides a wide range of versatility in terms of tailoring physical properties, biocompatibility, and degradation rates. The literature cites many examples of early PU devices showing signs of degradation (i.e., valves [1], vascular prostheses [2], and PU-coated silicone breast implants [3–5]), leading many research groups to question the safety of PU devices and to continue the quest for more biocompatible PUs without compromising their desirable physical properties.

3.1.1 Polyurethane chemistry influences stability

It is important to recognize that the chemical composition and the resulting surface domain organization of PU materials will ultimately affect degradation [6]. Classical PUs are formulated with a desired stoichiometry from all three major components: (1) an aliphatic or aromatic diisocyanate (DI), (2) a long chain oligomeric diol (soft segment), and (3) a low molecular weight chain extender [7]. In PU-based materials, a microphase segregation process leads to the formation of regions enriched in either hard or soft segments, directly impacting the dimensional stability of the elastomer [8].

3.1.2 Polyurethane bulk degradation

Although original PUs used in biomedical applications were widely accepted as flexible, durable, and relatively biocompatible, they have also been singled out as being

problematic in terms of their long-term stability *in vivo*. Polyether PUs were generally recognized as hydrolytically stable at neutral and basic pH and had been extensively evaluated for use in long-term implantable devices [9,10]. It was not until Pellethane® was used in marketed devices, such as pacemaker lead insulators, that several oxidation failure mechanisms were discovered to affect the polyether soft segment [11]. A synergistic effect of chemical degradation and physical damage was proposed since the brittle surface layer is more susceptible to cracking under repeated strains (i.e., physiological movement of tissues, limbs, or fluids). In addition, polyether PU devices containing metal parts, such as pacemaker leads, have been subject to metal ion oxidation because of redox reactions and catalysis with corrosion products in combination with H_2O_2 released by cells on the surface during the foreign body response (FBR) [12,13].

Early on, Stokes et al. put forth a description of a failure mechanism affecting polyether PUs under strain, termed environmental stress cracking (ESC) [14]. This description implicated factors from the *in vivo* environment: oxidative processes, residual stress, ether content in the soft segment, and the presence of cells associated with the FBR, as well as an unknown biological element. Many subsequent studies embraced the ESC theory and built on it, to understand the molecular mechanisms associated with cleavage of the polymer chains. Anderson's group focused on the oxidative mechanism of ESC and was the first to use inflammatory cells to study the biodegradation of PUs [15].

3.1.3   Hydrolytic degradation

Other groups focused on the nature of the biodegradation products and investigated the hydrolytic pathway of PU chain cleavage. A number of reports described the generation of potentially carcinogenic aromatic diamines from polyester urethanes (PEUs) that had been used in the Meme breast implant [16,17].

Subsequent reports proposed that hydrolytic enzymes associated with monocyte-derived macrophage (MDM) activity are as important as oxidation in the degradation of PUs. Santerre and coworkers demonstrated that cholesterol esterase (CE) preferably degraded ester linkages immediately adjacent to the hard segment rather than catalyzing the hydrolysis of the urethane linkage in the hard segment to generate toluenediamine [18]. The group went on to identify oligomeric degradation products from the polymer to gain a greater understanding of the polymer's breakdown by CE [19]. Through a series of experiments with radiolabeled DIs and the degradative enzyme CE [20–26], it was determined that biodegradation showed a strong dependence on hard segment chemistry and molecular weight. Stable H-bonded microdomains in the hard segment are thought to create a protective structure for cleavage points favored by the enzyme. *In vivo* experiments also confirmed an association between polymers with increased hard segment content and improved biostability (i.e., methylene diphenyl diisocyanate (MDI)-based polycarbonate PUs reported for Corethane® materials) [27,28]. However, the role of hydrolytic enzymes in the FBR and *in vivo* biodegradation had not been fully defined in those early studies.

3.1.4   Molecular mechanisms at the cell–material interface

In most cases, the actual chronic tissue interface is layered as follows: the biomaterial surface, adsorbed protein, MDMs and/or foreign body giant cells, a fibrotic capsule

composed primarily of collagen-containing phagocytic cells and fibroblasts, and then subsequently the native tissue [29]. It is not surprising that white blood cells have emerged as the predominant cell type coordinating the biodegradation process. The temporal variation in the acute and chronic inflammatory response describes polymorphonuclear neutrophils (PMNs) appearing within minutes, but not lasting more than 48 h [15,30]. Adherent PMNs, a source of initial reactive oxygen species (ROS), have been shown to be differentially activated based on material chemistry [31–33]. For this reason, PMNs have been linked to biodegradation; however, it is unclear what the extent of their involvement is given their short life span at the cell–material interface. A comparison of PMNs versus MDMs for their destructive potential toward a radiolabeled PEU determined that there was 25 times more radiolabel release elicited by MDMs [25].

3.1.5 *Environmental biodegradation*

A model of environmental biodegradation has been described in such a way that the central interaction between the cells and the materials is a cyclic process that influences two critical end points that have significant clinical impact: degradation of the biomaterial and chronic inflammation [7]. The model shows how an external perturbation, such as mechanical strain, metal ions, or other factors, influences the material morphology by redefining the interactions between the polymer chains. The external perturbation disrupts the PU surface microenvironment, which dictates the type, amount, and conformation of protein adsorbed onto the material surface. Taken together all of these factors influence the response of the cells, in turn altering the inflammatory process feeding back to the material.

3.2 Design of new degradable polyurethanes inspired by biodegradation mechanisms

The study of PU degradation mechanisms has motivated the development of novel degradable PU materials from 2005 to 2015, particularly in the area of tissue engineering (TE) applications. Specifically, chemical linkages that are susceptible to oxidative, hydrolytic, or enzymatic degradation have been incorporated into the segmented block copolymeric structure of new PU materials to achieve desirable degradation processes.

3.2.1 *Degradable polyurethanes designed with hydrolytically susceptible soft segments*

Guan et al. have developed poly(ester urethane) urea (PEUU) and poly(ether ester urethane) urea (PEEUU) [34], both designed to be degraded by cleavage of their soft segment bonds. The PEEUU used polyethylene glycol (PEG) in a copolymer with polycaprolactone (PCL)–PEG–PCL soft segment rather than pure PCL, as in PEUU [34]. The addition of PEG into the soft segment of PEEUU contributed to increased

hydrophilicity and a faster hydrolytic degradation rate of the polymer when compared to PEUU. Despite the slight difference in hydrophilicity and change in degradation behavior for the two materials, both PEUU and PEEUU scaffolds demonstrated desirable mechanical properties (tensile strength and breaking strains) comparable to those of the canine thoracic aorta [34]. Two other interesting examples consisting of poly(ether carbonate urethane) ureas (PETCUUs) were developed by Wang and coworkers [35]. While both PETCUUs were synthesized with butanediisocyanate (BDI) and putrescine as in the PEUU and PEEUU materials discussed above, one of the PETCUUs contained a triblock copolymer of poly(trimethylene carbonate)–poly(ethylene oxide)–poly(trimethylene carbonate) (PTMC–PEO–PTMC) as the soft segment, while the other one included a pentablock copolymer PTMC–PEO–PPO–PEO–PTMC (PPO, polypropylene oxide) as the soft segment [35]. PTMC was chosen for its low modulus and relative hydrophobicity [35,36], which helped maintain the mechanical integrity of the polymer for an extended period of time. The PEO (highly hydrophilic) or PEO–PPO–PEO (moderately hydrophilic) provided the ability to change the rate of degradation and cell adhesion behavior [37–40]. These polymers demonstrated comparable cell compatibility, as smooth muscle cells (SMCs) cultured in an 8-week study with both PETCUUs showed similar morphology and viability [35]. Cell adhesion could be further enhanced with the incorporation of an Arg–Gly–Asp–Ser (RGDS) surface modification [35].

3.2.2 Degradable polyurethanes developed with blended soft segments

Given the need for degradable scaffolds to enable new tissue regeneration, to allow for timely scaffold decomposition, and to achieve mechanical criteria, a series of novel degradable PUs were developed with blended soft segments. For example, the partial replacement of the polyester units with polycarbonate elements in the soft segment has resulted in polymers (PECUU) with degradation properties in between those of the PEUU described above and a poly(carbonate urethane) urea (PCUU) [41]. Polyester hydrolysis can induce acidic by-product release [42], which further catalyzes the degradation process, where the weak acidic by-products can be quickly converted into alcohol in the decomposition process of polycarbonate [42]. Following a similar logic, Niu and colleagues generated a novel PU by coupling PCL with PEG for its soft segment [43]. Degradation of the PU material occurred over 20 weeks *in vivo*, with no significant elevation of pH in the local tissue [43]. Scaffolds made with this polymer also provided excellent mechanical support and important structural cues that facilitated better nerve regeneration in a rat nerve injury model [43]. Moreover, to better modulate the degradation kinetics of the materials, PUs with different soft segments were mixed together to generate novel composite PUs. In one study, PEG– hexamethylene diisocyanate (HDI)–desamino tyrosine tyrosyl hexyl ester (DTH) and PCL–HDI–DTH (both containing the same hard segment, HDI, and chain extender, DTH, but PEG versus PCL as respective soft segments) were blended at different ratios by electrospinning [44]. While the incorporation of HDI and the amino acid-based DTH were selected to improve the biocompatibility of the polymers [44], the biodegradability of

the materials depended on PCL and PEG (with PCL being more hydrophobic than PEG). It was observed that a higher ratio of PEG–HDI–DTH to PCL–HDI–DTH resulted in faster degradation of the composite polymer [44]. As well, electrospun scaffolds were shown to decompose faster than films made with the same material chemistry [44].

3.2.3   Degradable polyurethanes with varying chain extenders

Wagner et al. substituted the chain extender putrescine in PEUU, discussed above, with the enzymatically sensitive diamine peptide–Ala–Ala–Lys [45], aiming to develop an elastase-sensitive PU. Elastase-sensitive PU scaffolds with oriented pores supported muscle-derived stem cell growth [45], suggesting its potential use in TE applications.

Furthermore, elastomeric PUs with flexible degradability were prepared with PCL, HDI, and varying chain extenders [46,47]. Specifically, three new PUs, PU-S, PU-M, and PU-F, with bioactive isosorbidediol (1,4:3,6-dianhydro-D-sorbitol) (ISO), bis(2-mercaptoethyl) ether, and ISO combined with 3,7,11-trimethyl-2,6,10-dodecatrien-1-diaminobutane amide (TDD), respectively, used as chain extenders were synthesized [46,47]. These chain extenders acted as labile units and introduced different levels of polymer chain mobility into the polymeric materials [46].

Another attractive PEUU that showed controlled degradability based on its unique arginine-containing chain extender was reported by He et al. [48]. More specifically, HDI was reacted with the hydroxyl group in glycerol α-monoallyl ether (GAE) to form a prepolymer, which was then chain extended with L-Arg hydrochloride alkylenediester (Arg-x-Cl) via a urea bond to produce the PEUU [48]. The degradation rate of this arginine-derived PEUU could be adjusted by varying the proportion of Arg-x-Cl in the polymer, since Arg-x-Cl bears hydrolytically susceptible ester bonds [49]. In addition, the arginine-containing PEUU could elicit desirable cellular responses because the cationic arginine moiety not only plays a role in nitrogen metabolism and production of nitrogen oxide (NO) but also regulates the inflammatory response *in vivo* [50–56].

3.2.4   Degradable polyurethanes generated from novel chemistries

Degradable PUs synthesized with novel chemistries have demonstrated other attractive characteristics such as injectability, exclusive stimuli sensitivity, and anti-inflammatory properties. A novel injectable PU consisting of a flowable lysine triisocyanate (LTI)–PEG prepolymer and a polyester triol was prepared by Adolph and colleagues [57]. The polymer was designed to be degraded through hydrolysis of ester bonds (polyester triol) and oxidation initiated by peroxidase expressed by MDMs interacting with the biomaterial *in vivo* [58]. The study showed that the injection of the PU resulted in wound healing rather than fibrosis in rat excisional wounds after 7 days [57].

Since production of ROS is a common biological response in cell–material interactions on biomaterial implantation [59], PUs designed to degrade by a ROS-dependent mechanism could be more advantageous in TE applications. Martin and coworkers have fabricated a series of poly(thioketal) urethanes (PTKU) that could be exclusively

degraded by cell-generated ROS [59]. Briefly, poly(thioketal) (PTK) (synthesized with 2-mercaptoethyl ether (MEE), acetone, and 1,4-butanedithiol) was reacted with hard segment HDI trimer (HDIt) to yield PTKU [59]. It was found that PTKU degradation in the oxidative environment promoted the release of hydroxyl radicals, which acted as a positive feedback to further attack the thioketal bond and decompose the compound into its original monomers [59]. Additionally, ether oxidation also contributed to the overall degradation of the polymer [59]. The mechanism of degradation for PTKU was verified by assessing the response of the material to ROS released from activated murine-derived RAW267.4 macrophages and oxidative medium after 10 days *in vitro*. However, the material remained nonreactive to hydrolysis in phosphate-buffered saline (PBS) for 25 weeks [59]. PTKU demonstrated greater cell infiltration for subcutaneous wounds in a rat model when compared to standard PEU control [59].

Work by Santerre et al. has conceived degradable polar hydrophobic ionic (D-PHI) PUs, which possess excellent anti-inflammatory characteristics [60,61]. The novel D-PHI PU was synthesized from a lysine-based polycarbonate divinyl oligomer (DVO, which consists of a poly(hexamethylene carbonate) diol (PCN) soft segment and lysine diisocyanate (LDI)/2-hydroxyethyl methacrylate (HEMA) hard segments) and anionic/hydrophobic acrylate monomers (methacrylic acid (MAA) and methyl methacrylate (MMA)) [60]. PCN was chosen as the soft segment not only because it provides high tensile strength while being biodegradable but also because it yields relatively low proinflammatory degradation products such as carbon dioxide and alcohols [7,62]. The traditional hard segment is substituted by HEMA, which was incorporated into the material to confer cross-linking functionality to the DVO. The vinyl groups generated reactivity with MAA and MMA via the terminal ends of the oligomeric polycarbonate chain and thus enhanced the mechanical strength of the material [60]. Additionally, MMA and MAA were introduced to induce procell adhesion and cell–material interactions, because they generated hydrophobic and anionic function integrated with the nonionic polar nature via the polycarbonate [63]. D-PHI displayed a more controlled degradation rate *in vivo* as compared to PLGA, and maintained its physical structure [64]. In addition, D-PHI promoted a wound-healing phenotype of monocytes with and without protein coating [65,66] and demonstrated good compatibility with vascular SMCs (VSMCs) [67], endothelial cells (ECs) [68], and human gingival fibroblasts (HGFs) [68].

These novel chemistries have been strongly considered for use in TE applications and as such they have been optimized for multiple design features both in terms of the chemistry and the processing of the materials. A list of key factors affecting PU performance in orthopedic, cardiovascular, and connective TE is provided in Table 3.1.

3.3   *In vivo* testing of polyurethanes from 2005 to 2015

In vivo testing in animal models is essential for implanted biomaterial devices (e.g., scaffolds) to determine biodegradation, mechanical compatibility, FBR, and biocompatibility of the material with host tissue or device function.

Table 3.1 Factors affecting degradable PU performance in tissue engineering applications

Parameter	Notes	References
Orthopedic		
Processing	Some applications require the polymer to be injectable and cured *in situ*.	[69]
Elasticity	Sufficient elasticity required to ensure intimate contact with bone when used to fill a defect.	[70]
Mechanical strength	Compressive modulus >1 GPa, compressive strength around 100 MPa. For highly porous polymers, this may be achieved with an appropriate filler material.	[69,71,72]
Degradation	Some studies have suggested >18 months, depending on rate of new bone growth. Nontoxic degradation by-products.	[70]
Hydrophilicity	Reduced hydrophilicity has been proposed as a means to reduce degradation rate, allowing more time for new bone to form. However, more hydrophilic materials have shown greater calcium deposition than hydrophobic PUs in some cases.	[70,73]
Porosity	Porosity can influence the rate of PU degradation and the ability of cells to infiltrate the scaffold.	[70,71]
Osteoconductivity	Must promote new bone formation at a rate that outpaces PU degradation. This can be enhanced through inclusion of calcium-complexing agents and drugs (e.g., lovastatin) in some cases.	[70,74]
Cardiovascular		
Mechanical properties	Materials must be suturable, elasticity depending on the application, and have sufficient modulus without being too stiff (e.g., cardiac tissue has modulus of 10–50 kPa, tensile strength of 3–15 kPa, and strain of 22–90%).	[75,76]
Degradation	Slower degrading materials have performed better than faster degrading PUs. Nontoxic degradation by-products.	[76]
Porosity	Porosity must be sufficient to allow tissue infiltration, not compromise rate of degradation, and promote cell attachment and growth.	[60,77,78]
Nonactivating chemistries	For blood contacting PUs, chemistries that reduce platelet and white blood cell activation are essential.	[61,65,79,80]
Connective tissue		
Mechanical properties	PUs should have mechanical properties that mimic those of native tissue (compliance, modulus, strain).	[81,82]
Degradation	Appropriate degradation rate to support new tissue formation. Nontoxic degradation by-products that could also activate cells to promote positive remodeling outcomes.	[57,58,83]
Porosity	Must allow for new tissue ingrowth.	[84,85]
New tissue formation	Inclusion of bioactive agents, such as ECM components (e.g., ECM digest) can promote tissue infiltration.	[82,86,87]
Nonactivating chemistries	In addition to white blood cell interactions, new PUs should prevent fibroblast to myofibroblast differentiation to support healthy tissue regeneration instead of scarring.	[57]

3.3.1 In vivo *testing of polyurethanes to assess biodegradation and the foreign body response*

Preliminary *in vivo* biodegradation and the FBR are often assessed by subcutaneously implanting a PU disk (porous or nonporous). While the cage implant model has often been used to study biodegradation and the FBR because of the advantage of allowing removal of the PU, surrounding cells/tissues and exudates [88–90], it presents a significant perturbation to the implant site. A cageless subcutaneous implant allows for direct contact with host cells and in the case of porous scaffolds leads to cell infiltration, reflecting more of what would be seen in TE applications [64,91]. Recent studies have shown that D-PHI lost only 20% of its original mass after 100 days of implantation in a rat model, suggesting a relatively slow and controlled degradation rate [64]. In a mouse system, it was found that 14 day D-PHI explants showed good cell infiltration and matrix deposition as well as a pro-wound healing cytokine profile (compared to 1-day explants) [91]. Both studies favored D-PHI as a good scaffold for TE as it allowed for tissue ingrowth while maintaining structural support.

Using a 14-day subcutaneous implant, Da Silva et al. compared aqueous anionic PU dispersions (PUD) (with PCL and PEG soft segment and isophorone diisocyanate (IPDI) and hydrazine (HZ) hard segment) with or without montmorillonite clay nanoparticles (NPs) [92]. The number of cells infiltrating the PUD scaffolds decreased from day 1 to day 14 but did not significantly change between formulations, suggesting that by day 14 the FBR had been resolved [92]. Dey et al. compared a cross-linked urethane-doped polyester (CUPE) scaffold to a poly-L-lactic acid (PLLA) scaffold in a subcutaneous rat model system. It was found that after 1 week, the CUPE scaffold had a thinner fibrous capsule when compared to the PLLA scaffold, suggesting a more modest FBR [93].

3.3.2 In vivo *wound healing assays*

Dermal TE using PU scaffolds/membranes requires the precise reconstitution of the skin bilayer. In an ovine full thickness wound model, which tested a PU (biodegradable temporizing matrix; BTM-2) [94], the Integra™ dermal regeneration template was compared to BTM-2. It was found that by 29 days all wound sites had healed comparably [94].

Hafeman et al. recently compared two PEUs prepared from LTI versus HDIt for use in skin TE, looking at the *in vivo* degradation of the two PEUs in a full excision model [58]. Both PUs showed limited inflammation; however, the LTI scaffold degraded significantly faster than the HDIt scaffold at 28 days, suggesting that it may be better for skin TE [58] as this rate is aligned with the desired design specifications.

3.3.3 In vivo *polyurethane soft tissue engineering*

Soft tissue TE scaffolds are temporary templates that are gradually degraded and replaced by the host's own cells and tissue. New methods in *in vivo* imaging provide an

attractive strategy for determining structural and mechanical changes in PU scaffolds without explanting or sacrificing the animal. This allows for longer term monitoring of the scaffold's compatibility and host tissue integration. Park et al. used multimodality imaging to compare degradation rates of PEUU scaffolds versus polydiaxanone scaffolds [95]. They found that mechanical and histological assessments of explants correlated well with ultrasound shear wave imaging and photoacoustic imaging data [95].

Cardiac biomaterials for TE have been a major PU research area for years. Many PU trileaflet heart valves have been developed, but most of these have failed due to calcification and stiffening. More recently, Thomas and Jayabalan developed a calcification-resistant high flex life polyurethane urea (HFL18-PU) for use as a trileaflet valve [96]. The long-term *in vivo* biodurability testing (subcutaneous implant in rabbit) showed little FBR with an absence of PMNs and MDMs after 3 months, and by 6 months there was no change in weight, color, or surface pitting and minimal changes in mechanical properties, suggesting that the implant was not degraded [96]. Stachelek et al. evaluated a cholesterol-modified PU as a valve cusp that can promote EC adhesion [97]. They found that bovine blood outgrowth ECs (BOECs) could adhere to the PU valve cusps and that the BOEC-seeded valves implanted in an ovine model system appeared translucent with no abnormalities when compared to the unseeded valves, which appeared opaque with visible thrombi [97].

Similar to dermal patches for TE, cardiac patches to repair cardiac tissue can also be made of PUs. Fujimoto et al. used a PEUU scaffold to replace a surgical defect in the right ventricular outflow tract of a rat heart [98]. After 12 weeks, the PEUU scaffold showed host tissue ingrowth, which was not apparent in a comparison to expanded polytetrafluoroethylene patches [98].

3.3.4 In vivo *polyurethane bone tissue engineering*

PUs designed for bone replacement applications need to be subjected to weight-bearing *in vivo* studies. For instance, Dumas et al. used a rabbit weight-bearing unicortical plug defect model system to evaluate an allograft bone that uses a 2-component biodegradable PU as a binder [72]. Within 6 weeks there was extensive cellular infiltration into the graft and new bone formation [72].

Adhikari et al. developed a biodegradable injectable PU for orthopedic applications [99]. The group chose to evaluate both the preformed PU and the *in vivo* injected PU to determine degradation and biocompatibility using an ovine model [99]. The preformed and injected PUs were well tolerated by the sheep and both showed evidence of new bone growth and controlled polymer degradation after 6-month implantation [99].

Other biodegradable PUs for bone TE have incorporated drugs to enhance wound healing and bone regeneration and prevent bacterial contamination. For example, a group prepared a biodegradable PU with lovastatin to promote BMP-2 expression to stimulate bone formation [74]. A rat plug defect *in vivo* model was used where a 3 mm defect was created in the femur and the biomaterial was formed into a 3×5 mm cylinder implanted into the defect. The femurs were then explanted at 2 and 4 weeks for X-ray microtomography evaluation [74]. By 4 weeks, there were

increases in bone regeneration using the lovastatin/PU, which was not seen at the 2-week time point [74].

3.4   Coculture using degradable polyurethanes from 2005 to 2015

Bone and soft tissues are complex multicellular structures requiring oxygen, nutrients, and cell signaling cues to allow cells to form functional tissues. The oxygen diffusion limit of 150 μm [100] limits the size of *in vitro* TE constructs without vascularization. Often coculture is employed to promote prevascularization of the TE graft (reviewed in [101]).

3.4.1   Polyurethane coculture systems for liver tissue engineering

Salerno et al. cocultured human hepatocytes with human umbilical vein ECs (HUVECs) on a polyetheretherketone PU membrane to promote vascularization of an *in vitro* engineered liver tissue [102]. There was improved hepatocyte function and the formation of luminal structures occurred within 3 days of coculture on the PU versus hepatocyte-only samples [102]. Another study demonstrated that coculturing bone marrow-derived mesenchymal stromal cells with hepatocytes greatly reduced the secretion of stress enzymes by the hepatocytes and that the cells attached better to nanofiber PU versus unstructured PU [103].

3.4.2   Polyurethanes coculture systems for cardiac tissue engineering

Surprisingly, the use of cocultures with degradable PUs in cardiac TE systems has been limited when vascular grafts are excluded from the research. A study by Parrag et al. used murine-derived embryonic stem cells (mESCs) and mouse embryonic fibroblasts (MEFs) to TE cardiomyocyte-derived tissues. mESCs are pluripotent cells that require proper cues to differentiate into specific cell types. In the study, Parrag et al. showed that both the coculture of mESCs with MEFs and the use of aligned microfibrous PU scaffolds provided the cues necessary to induce mESC differentiation to a functioning cardiomyocyte phenotype [104].

   More recently, the Santerre lab used the coculture of primary cells with monocytes/MDMs to promote a wound-healing milieu to encourage cell attachment, infiltration, and proliferation on D-PHI PU films and scaffolds for TE vascular graft applications [67,91,105–107]. In the context of blood vessel TE, it was found that by coculturing monocytes with ECs on D-PHI films that the ECs attached better and spread out more while displaying more EC functional markers than EC monocultures (CD31) [91]. VSMCs benefited from coculture with monocytes on both film and porous scaffold forms of D-PHI [67,106,107]. On porous scaffolds, the monocyte coculture helped VSMCs migrate within the pores and increased deposition of extracellular matrix (ECM) proteins [107]. A recent study found that monocyte-conditioned medium could also promote VSMC attachment to

D-PHI, while allowing VSMC differentiation marker expression [106]. This suggests that it is the cytokines and signaling cues released from the monocyte (i.e., paracrine effects) rather than cell–cell contact alone that contribute to a desirable VSMC phenotype [106].

3.4.3 Polyurethane coculture system for dermal and other soft tissue engineering

Dermal TE grafts meet a critical need for nonhealing wounds and burn repair. For dermal TE, a vascularized bilayer of fibroblasts and keratinocytes is the ultimate goal. Li et al., using Novo Sorb™ PU variant BTM-2, showed that keratinocytes could form a monolayer over the BTM-2 scaffold preseeded with dermal fibroblasts [94]. In a 2014 follow-up paper, the Greenwood group described their coculture system (fibroblasts then keratinocytes) on BTM as a cultured composite skin, suggesting that the BTM-2 construct may be moving closer to the clinic [108].

Gingival atrophy, where the root is exposed leading to tooth sensitivities and caries, is a prevalent disorder that requires better graft options [109]. The Santerre group recently published that a D-PHI PU is compatible with HGFs cultured in a medium-perfused bioreactor [110]. The coculture of HUVECs with HGFs was subsequently tested to see if HUVECs could vascularize the PU scaffolds. HUVEC clusters could be seen at the end of the 28-day test and the cocultures had modulated cytokine activities depending on the ratio of HUVEC:HGF [105].

3.4.4 Polyurethane coculture systems for bone tissue engineering

Bone has been one of the largest research areas for PUs and coculture systems (coculture strategies in bone TE, reviewed by Janardhanan et al. [111]). Duttenhoefer et al. coseeded human endothelial progenitor cells (EPCs) with mesenchymal stem cells (MSCs) onto a porous bioresorbable elastomeric PU scaffold containing NPs of hydroxylapatite (HA) to induce vascularization and encourage osteogenic differentiation [112]. The presence of EPCs promoted more tubular structures per mm^2 and greater EC marker-expressing tubular structures [112]. In another study, Hofmann et al. showed that coculturing human osteoblasts with HUVECs promoted vascularization of a degradable PU scaffold and stable cell differentiation after more than 14 days in culture [113]. Together, these studies suggest that coculture is beneficial for promoting cell attachment, desirable cell phenotypes, and tissue vascularization in the context of bone TE.

3.5 Degradable polyurethanes cultured with stem cells for tissue engineering applications

Since mature cells usually have limited expansion abilities *in vitro* [114], stem cells have become a promising substitute for mature cells in tissue repair and regeneration when assessed with a variety of PUs and stem cell culture systems.

3.5.1   *Biodegradable polycaprolactone-containing polyurethanes seeded with stem cells*

Stem cell interactions with PCL-containing PEU or PEUU scaffolds (degraded via hydrolysis) have been studied for TE applications, and in particular using immunomodulating and multipotent MSCs [115–117]. Zahedmanesh and colleagues have seeded MSCs on 3D fibrin–PU composite scaffolds, with the PU synthesized from HDI, PCL, and ISO, and incorporation of a fibrin gel [118]. A 10% triaxial compression of the scaffold matrix combined with interfacial shear promoted chondrogenesis of MSCs, as indicated by their elevated expression of collagen and proteoglycans after 14 days in culture (in the presence of TGF-β-dexamethasone) [119]. In addition, the importance of mechanical stimulation in modulating the behavior of MSCs has been reported by Liu et al., who cultured MSCs on degradable PU scaffolds (generated using PCL/ʟ-lactide, 1,4-butanediol (BDO), and BDI) [120]. Moreover, Laschke et al. reported culturing adipose-derived stem cells (ASCs) either as 3D spheroids or single cells on PEU scaffolds (which has the same chemistry as the PU used in Zahedmanesh's study) combined with HA [121]. ASC spheroids were shown to encourage significantly more new vasculature formation than single ASCs (40% vs. 20%). The results corresponded well to the findings in Kuo's study, where it was reported that human MSC aggregates proliferated more and showed greater osteogenesis/chondrogenesis potential than single cells on PU after 7 days in culture [122]. The investigators then carried out a study to determine if the differentiation of ASCs on HA–PEU before implantation would affect their angiogenic capacity [123]. They found that osteogenic preconditioning of ASCs significantly impaired their ability to generate new microvessel networks [123]. In addition, dedifferentiation of preconditioned ASCs was evident with a reduction in mineralized matrix after 14 days in a mouse implant model [123]. Since the structure of electrospun fibrous scaffolds can be controlled to resemble natural ECM by adjusting the processing parameters [124], Gugerell and coworkers have incorporated ASCs into two PCL-containing electrospun PUs. Both remained degradable by hydrolysis (with ester bonds more susceptible than urethane and urea linkages) [125]. The two PU polymers were poly(ε-caprolactone-courethane-co-urea) (PCLUU) and poly [(ʟ-lactide-co-ε-caprolactone)-co-(ʟ-lysine ethyl ester diisocyanate)-block-oligo(ethylene glycol)-urethane] (PLLEGU), with PLLEGU showing more degradability (34.3%) than PCLUU (2.4%) after 44 weeks in PBS [125]. ASCs were shown to be able to adhere, proliferate, and differentiate into adipocytes on both scaffolds (with lipid droplet formation after 21 days). However, they exhibited a more physiological morphology on PCLUU (more spread) than on PLLEGU (elongated) [125].

3.5.2   *Commercial degradable polyurethanes used in stem cell culture*

Commercial PUs have also been studied for use with stem cell culture. For instance, electrospun commercial PU (Desmopan® 9370A) scaffolds were fabricated with

high porosity (84%) and an average fiber diameter of 360 nm [126]. Human ESCs were cultured on PU scaffolds in neuronal proliferation (1–17 days) and differentiation medium (18–47 days), and the results indicated successful transformation of the ESCs to dopaminergic tyrosine hydroxylase-positive neurons [126]. More importantly, ESCs seeded on PU scaffolds showed expression of neuronal markers (MAP2ab, β-tubulin III), neurite outgrowth, and formation of cell–cell/cell–PU fiber connections [126]. On the other hand, the reference culture (without the PU fiber, but with the same proliferation/differentiation medium) promoted differentiation along the astrocyte lineage [126]. Therefore, the electrospun commercial PU could provide topographical cues to guide ESCs and allow them to differentiate into neuronal cells [126].

3.5.3 Injectable degradable polyurethanes cultured with stem cells

Injectable PU gels, containing a hydrophilic PEG segment and hydrophobic poly (serinol hexamethylene urethane), have been developed by Ritfeld et al. for seeding with MSCs [127]. In this specific design, the PU gel could act as a scavenger for ROS via its urethane groups and thus protect MSCs from oxidation-mediated cell death *in vivo* [127].

3.6 Degradable polyurethanes used in drug delivery systems

PU-based drug delivery systems can be manipulated to have site-specific release (via cell targeting designs) and controllable drug release kinetics [128].

3.6.1 Degradable polyurethane-based growth factor delivery systems

Growth factors have been covalently coupled to PUs (such as PEU and PEUU) such that the materials are degraded mainly via hydrolysis of the soft segment (cleavage of ester bonds). It is believed that biologics anchored to PUs can be released following Fick's diffusion kinetics, breakdown of the polymers, or a combination of both. For example, Guan et al. loaded basic fibroblast growth factor (bFGF) with the addition of heparin and bovine serum albumin to stabilize bFGF [129,130]. A biphasic release behavior with an initial fast release followed by a slow release over 4 weeks was observed in PEUU/bFGF scaffolds without heparin. However, with the incorporation of heparin into the material, drug release in the burst phase was increased within the first 24 h [129]. Similarly, insulin-like growth factor-1 and hepatocyte growth factor were introduced into the same PEUU by Wagner's group [131]. Proteins in this case showed complex multiphasic release profiles, influenced

by the rates of degradation and the different protein/polymer interactions of the different segments of the block copolymers [131]. Li and coworkers have coupled platelet-derived growth factor (PDGF) to a polyester triol-based PU [132]. The PDGF–PU system yielded a two-stage release profile as seen in Guan's study. Most importantly, the Guan, Wagner, and Li studies all showed sustained bioactivity of the released growth factors [129,131,132].

3.6.2   Commercial degradable polyurethane-based anti-inflammatory/anticancer drug delivery systems

Anti-inflammatory/anticancer drugs have been incorporated into and delivered with IPDI-based PUs or commercially available PUs. Moura et al. reported on mixing the anti-inflammatory dexamethasone acetate (ACT) with PU (prepared with hard segments, IPDI and HZ; soft segments, PCL and PEG) [133]. ACT was seen to be continuously released from the PU matrix following an approximately linear relationship over 120 days, indicating drug release mechanisms that implicated both polymer degradation (hydrolysis of ester linkages in PCL) and Fickian diffusion [133]. Babanejad and coworkers designed highly soluble carboxylated PU (CPU) NPs by substituting HZ in the PU used by Pinto et al. (2012) with dimethylol propionic acid (DMPA) and BDO [134]. The anticancer drug raloxifene hydrochloride (R-HCl) was complexed with CPU by interactions of cationic amino groups from R-HCl with the anionic CPU [134]. The results suggested Fickian diffusion release kinetics from the NPs, with a sustained drug release up to $24.19 \pm 4.35\%$ after 4 weeks *in vitro* [134].

3.6.3   Degradable polyurethane-based gene delivery systems

Nonviral transfection vectors are providing a promising alternative to viral vectors due to their ease of production and low immunogenicity. Cationic amine groups can effectively bind DNA with strong electrostatic force and therefore have been coupled to PUs via hydrolytically degradable ester or urethane bonds [135]. Positively charged polymers also have a pH buffering effect, which would assist the escape of vectors and increase the efficiency of transfection [136–139]. One example of an amine-containing PU was synthesized with LDI, PEG, and 2-diethylaminoethylamine (DEAE) via an aminolysis reaction [140]. Cationic amino groups in the PU established strong interactions with DNA molecules, which allowed condensation of DNA into nanoscale structures for endocytosis. As well, the cationic groups protected the NPs from nuclease degradation [140]. Tseng and Tang also developed a similar poly(amino ester glycol urethane)–PAEGU based gene carrier, with the hard segment being BDI rather than LDI [135]. PAEGU DNA carrier was determined to be an efficient and safe tool, with a high transfection rate (35% transfection) and cell viability (90%) when cultured with human fibroblasts for 24 h [135].

3.6.4   *Stimuli-sensitive polyurethane drug delivery systems*

Intelligent stimuli-sensitive PUs designed from 2005 to 2015 are emerging as promising tools for targeted drug delivery. One example is the pH-sensitive biodegradable PCLH–PUs developed by Zhou et al. for targeted antitumor drug release [141]. Briefly, the pH-responsive PU was synthesized with soft segments PCL and pH-sensitive PCL-hydrazone–PEG-hydrazone–PCL macrodiol (PCLH); hard segments LDI, BDO, and L-lysine derivative tripeptide (LDT); and end-capped with hydrazone-linked methoxyl-PEG (*m*-PEG-Hyd) [141]. In PCLH–PU, *m*-PEG-Hyd was introduced to shield the polymeric micelles from plasma proteins or phagocytotic cells in blood circulation [142], and could be cleaved in the low pH environment of tumor tissue, enabling efficient internalization of micelles by cancer cells. Song and colleagues also developed tumor-cleavable PUs by reacting PCL and LDI with an L-cysteine-derived diamine chain extender bearing a redox-responsive disulfide bond, clickable alkynyl groups (Cys-PA), and a detachable pH-sensitive methoxyl-PEG unit [143]. The hydrophobic core of the micelles was formed mainly by PCL to entrap water-repelling biologics (doxorubicin (DOX)) [143]. What made this latter multisensitive drug carrier unique was that a model targeting ligand, folic acid (FA), was conjugated to the alkyne groups on the PU via facile click chemistry, which improved the drug efficacy toward HeLa cells (FA-receptor positive) after 4 h *in vitro* [143]. With a similar design logic, He and coworkers have incorporated reduction-sensitive bis(2-hydroxyl ethyl) disulfide (DHDS) into their polymers to generate paclitaxel (PTX)-coupled PU (PTX–PU) micelles, for on-demand drug delivery [144]. The rate of drug release (via polymer disintegration) was designed to be modulated by the redox-sensitive disulfide content DHDS in the material [144]. *In vitro* studies showed effective uptake of drug micelles within 1 h by tumor cells [144].

3.7   Physical forms and processing of degradable polyurethanes

Many fabrication methods exist for processing degradable PUs, whose final forms affect their degradability [145].

3.7.1   *Porous polyurethane scaffolds*

Many biomedical applications require PUs to be in the form of 3D constructs. For TE in particular, a porous scaffold architecture is necessary to permit cell and tissue ingrowth as well as to allow for integration with the host. Different porosity values, pore sizes, and pore interconnectivities are required for different TE applications. The method of solvent casting and particle leaching is popular for fabricating PU scaffolds due to its ease of use and versatility. In this method, the PU is dissolved in an appropriate solvent and cast into a porogen-filled mold. The most commonly used porogens are salts and sugar, but polymer particles and paraffin can also be

used [146]. Scaffold geometry can easily be manipulated by the design of templates made of solvent-compatible materials that are fabricated in the required shape. Care must be taken with this approach to ensure that residual solvent is removed to avoid cytotoxicity.

A degradable PU fabricated from a prepolymer of PCN:LDI:HEMA (1:2:2) and cross-linked in the presence of MMA and MAA has been processed into porous scaffolds (80–90% porosity, 100–400 μm macropores, 1–5 μm micropores) using the aforementioned porogen leaching technique [68,78]. In this system, NaHCO$_3$ provides a macroporous structure, while PEG (M$_n$ 600) supports the formation of micropores in the scaffold walls to facilitate nutrient diffusion. For this PU, the pre-polymer (PCN:LDI:HEMA) is dissolved in the MMA and MAA monomer mixture, while the microporogen increases the salt-loading capacity, obviating the need for a solvent.

Another scaffold fabrication technique is thermally induced phase separation (TIPS) [34,46,84,147–149]. TIPS involves decreasing the temperature of a polymer solution to obtain a polymer-rich and polymer-poor phase. Following phase separation, the solvent is removed using one of a number of methods (freeze drying, evaporation) resulting in the formation of pores in the polymer structure. TIPS can also be combined with the use of porogens to increase void fraction, have better control over pore size, or improve pore interconnectivity.

Studies with degradable PUs have investigated the parameters involved in the TIPS process on the final scaffold properties achieved. Using a PU synthesized from HDI, PCL, and ISO, the use of dimethyl sulfoxide (DMSO) or *N*-methylpyrrolidone (NMP) as solvents resulted in scaffolds with a nonporous polymer layer that excluded non-solvent from the bulk of the scaffold (DMSO) or a dense, irregular pore structure (NMP). The latter had low pore interconnectivity, as demonstrated by a high porosity but low water permeability [46]. Dimethylformamide (DMF), however, resulted in larger, open, and interconnected pores. The use of a cosolvent with DMF, which leads to the formation of micropores in the walls of macropores due to liquid-induced phase separation, also influenced the scaffold properties, with tetrahydrofuran (THF) producing larger pores and greater pore interconnectivity than ethanol or isopropanol. While investigating the use of other processing parameters with TIPS using a PU (BDI, PCL, and putrescine) dissolved in DMSO, it was shown that pore size increased with an increase in quenching temperature (0 > −20 > −80 °C) and that porosity was higher when using a lower PU concentration (5% > 10% PU in DMSO) [84]. The freezing phase of TIPS can further be modified using a temperature gradient to achieve oriented pore structures [150].

3.7.2   Electrospun polyurethane scaffolds

Detailed descriptions of the theory and setup with electrospinning systems can be found in reviews by Pham et al., Bhardwaj et al., and Rutledge et al. [151–153]. A generic setup consists of a PU solution held in a syringe connected to a syringe pump, a high voltage source, and a collector [151]. The high voltage source is used to induce charge into the polymer solution, which is attracted toward the collector of opposite

polarity. As the polymer solution travels from the needle tip of the syringe to the collector, the solvent evaporates, resulting in the deposition of polymer micro- or nanoscale fibers.

Degradable PUs based on HDI, PCL, and chain extenders of either 2-aminoethanol (PEUU) or a diesterdiphenol derivative of tyrosine (PEU) were electrospun using different electrospinning parameters, and provided a case study for the importance of both polymer type and electrospinning parameters on the final formed scaffold [154]. Below certain concentrations (<30 wt% in dimethylacetamide (DMAc) and <20% in DMAc/acetone 60/40), electrospinning of these PUs results in only beads, while elevating the concentration results in a polymer solution too viscous to electrospin [154]. In contrast, the use of 1,1,1,3,3,3-hexafluoroisopropanol (HFIP) as the electrospinning solvent generates uniform fibers with no beading at concentrations greater than 20%. HFIP is considered a good solvent for the electrospinning of highly hydrogen bonded polymers, such as PUs, as the hydroxyl group interacts with hydrophilic hard segment domains through hydrogen bonding, while fluorine is able to interact with the hydrophobic soft segments, allowing for a well-dispersed polymer solution with reduced chain entanglements. The appropriateness of the solvent was also dependent on the polymer type, since the PEU, but not PEUU which experiences greater hydrogen bonding, could be reliably electrospun with 50:50 DMF:THF [154].

Modifications to the traditional electrospinning setup have also been reported to further customize PU scaffolds. Hybrid scaffolds have been achieved using a dual-syringe system where simultaneous electrospinning of PLGA and a PEUU is used to produce a scaffold with one polymer providing mechanical stability, and the other antibiotic release [155]. Wet electrospinning has also been reported, wherein during the electrospinning of a PEUU (based on PCL, BDI, and putrescine) cell culture medium was electrosprayed, resulting in the incorporation of biological factors that improved the ability of the formed scaffold to support cellular infiltration [83]. Reactive electrospinning, achieved by placing a UV source above the mandrel, can be used with PU formulations that are UV sensitive, such as Pellethane® modified with reactive pentenoyl groups [156]. Electrospinning can also perturb the surface distribution of chemical functional groups. While fluorinated components of PUs are typically reported to demonstrate significant surface segregation [157]. In the latter work Blit and colleagues introduced cell adhesive chemistries onto the surface of a degradable polycarbonate urethane via fluorinated surface carrier oligomers. However, others have reported that the electrospinning process results in perfluoropolyether components of a PU to aggregate in the electrospinning solution, which results in a minimized surface fluorine content due to the fluorinated segments being frozen in the fiber core during the rapid evaporation of solvent that occurs during electrospinning [158], thereby influencing the potential for surface degradation by chemically changing the surface.

Another modification involves removing the potentially cytotoxic solvent from the electrospinning equation in a process called melt electrospinning [159]. This process involves tight control of temperature, and for the case of a PU based on BDI, PCL, 1,4-butanediamine (BDA), and BDO involved temperatures of 220–240°C [160].

While thermal degradation of PUs is generally not considered an issue for biomedical applications due to the range of temperatures expected, when processing degradable polymers at high temperatures thermal degradation can occur, which can release toxic degradation by-products into the body, depending on the hard and soft segment components of the PU. In a study by Karchin et al. [160], degradable PUs made of PCL:LDI:BDA (1:2:1) underwent degradation, yielding weak and oxidized fibers following melt electrospinning, while a PU of PCL:BDI:BDO (1:4:3) could successfully be electrospun with good quality fibers.

3.7.3   Polyurethane nanoparticles

Several methods have been reported for the synthesis of PU NPs. Using a soft segment of PCL diol with either PLLA diol or polyethylene butylene adipate (PEBA) diol, hard segment of IPDI and DMPA, as well as triethylamine (TEA) and ethylenediamine (EDA), NPs of <50 nm diameter were fabricated using a waterborne procedure [161]. In this method, the soft segment components and IPDI are first reacted to form a prepolymer, after which DMPA is added with 0.27% methyl ethyl ketone. To neutralize the carboxylic acid groups of DMPA, TEA is added, followed by end-capping of the polymer with EDA in water under vigorous stirring to form the NPs (final stoichiometric ratio of IPDI:oligodiols: DMPA:EDA:TEA of 3.52:1.1:1.52:1).

The use of oil/water (O/W) emulsions has also been employed to fabricate PU NPs [162–165]. In this method, the diisocyanate (IPDI) is first dissolved in an oil/surfactant mixture (90/10, saturated medium chain triglyceride/polysorbate 80 [polyoxyethylene 20-sorbitan monooleate]). Addition of the aqueous phase with PEG 400 (diamine or diol) to the O/S mixture in dropwise fashion (to obtain 90% aqueous component) occurs under mechanical stirring to obtain nanoemulsions, followed by heating to 70 °C to allow polymerization and achieve PU or PU urea NPs, which can be isolated by ultracentrifugation [165]. This method works by having IPDI present in the core of oil nanodroplets in the O/W nanoemulsion, which react with the diols or diamines at the surface of the oil droplet, resulting in the formation of the NPs with a size distribution from 40 to 100 nm.

Core–shell PU NPs can also be prepared by appropriate choice of isocyanate [166]. Blocked amphiphilic prepolymers were prepared by Cheong et al., where the hydrophobic block is composed of IPDI–polytetramethylene adipate polyol (PTMA) and the hydrophilic block is MDI–DMPA. The resulting polymer is added dropwise to water under stirring, resulting in a core–shell structure with the hydrophobic IPDI–PTMA in the core and hydrophilic MDI–DMPA in the shell (80–100 nm diameter) [166].

3.7.4   Effect of processing parameters on polyurethane biodegradation characteristics

While the chemistry of the PU itself is of critical importance in determining the biodegradability of the PU, the final form it takes can also alter its degradation

characteristics. Increasing the porosity of the scaffolds enhances cellular and tissue infiltration, but the greater surface area associated with the porous form may also increase the rate of degradation [167]. For some polymer scaffolds, the degradation rate has been shown to increase slowly with increases in porosity up until 80%, after which a sharp increase in degradation rate is seen [167]. Likewise, PCL nanofibers demonstrated an increase in degradation with decreasing electrospun fiber diameter due to the associated increase in surface area. Furthermore, the process of electrospinning resulted in reduced surface hydrophilicity of PCL nanofibers, thereby generating decreased water uptake and thus reduced degradation versus other processing techniques. This emphasizes the importance of processing parameters on surface chemistry that can ultimately influence degradation properties [168].

Nanocomposites involve the inclusion of NPs into otherwise familiarly processed PUs, which can be in the form of films or electrospun or porous scaffolds. In addition to providing bioactivity to the PU material [169–173], inclusion of NPs in the polymer matrix can also alter the degradation characteristics. Nanocomposites involving the inclusion of a polyhedral oligomeric silsesquioxane (POSS) integrated within a poly(carbonate–urea) urethane (POSS–PCU) resulted in shielding of the soft segment from oxidative and hydrolytic degradation [174]. The inclusion of POSS in a poly(caprolactone/carbonate) urethane urea also allowed for a more controlled degradation rate, specifically demonstrating the ability to protect the mechanical properties of the polymer under hydrolytic degradation [175]. Gold and silver NPs have also been incorporated into PU materials to alter degradation kinetics. The inclusion of gold NPs (30.2–113 ppm) in a polyether-type waterborne PU was shown to increase the biostability of the PU by acting as a free radical scavenger [176].
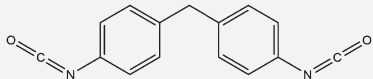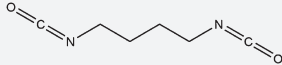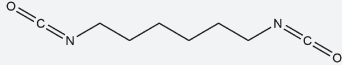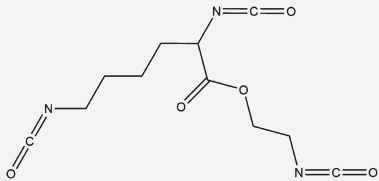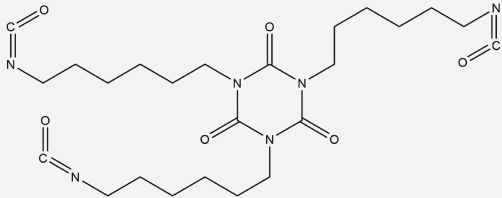
3.8   Monomers and oligomers used in degradable polyurethanes
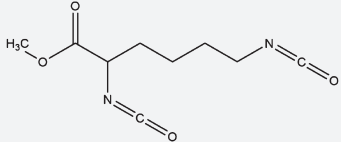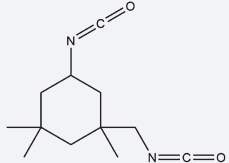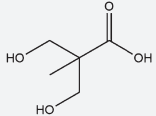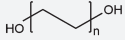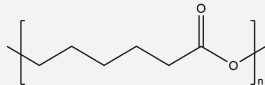
The monomers and oligomers used in the design of degradable PUs are summarized in Table 3.2.

3.9   Summary

Block copolymeric/degradable PUs provide significant advantages over classical degradable polyesters because of their chemical diversity, which yields uniquely compatible materials with respect to the biological responses to implants, and provides the field with a versatile range of physical properties when compared to other classes of biomaterials. Their attributes will enable many practical solutions to medical devices that are currently not afforded by other contemporary biomaterials. Hopefully this review will inspire the exploration of new PU chemistries with respect to biological interactions.
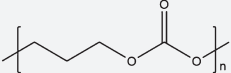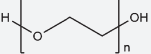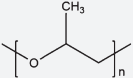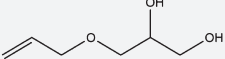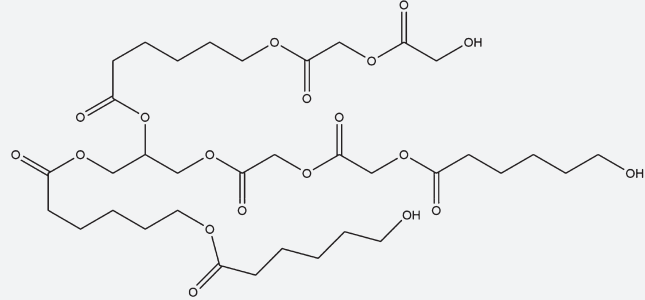
Table 3.2 **Monomers and oligomers used in degradable PUs**
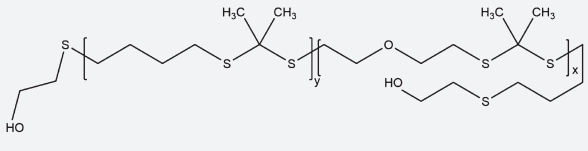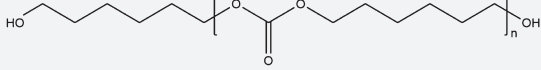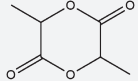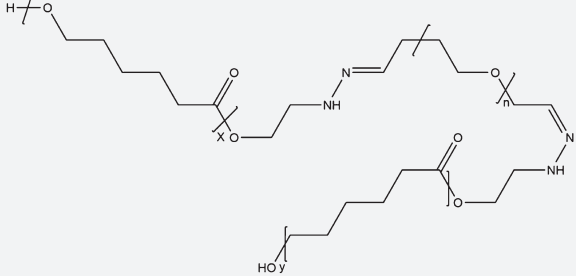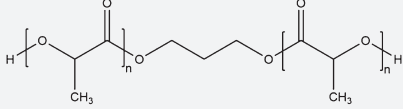
Monomer	Chemical structure	Comment	References
Polyisocyanate			
MDI		• Toxic aromatic diamine degradation products	[27,28,166]
BDI		• Yields putrescine following degradation, a polyamine essential for cell growth	[35,82,84,120,135,160]
HDI		• Diamines released on degradation are toxic to human liver and kidney, though less toxic than aromatic diamines from MDI or TDI	[44,46–48,118,154]
LTI		• Hydrolytic, esterolytic, and oxidative degradation • Nontoxic degradation by-product (lysine)	[57,58]
HDIt		• Hydrolytic, esterolytic, and oxidative degradation • Slower *in vivo* degradation than LTI-based PUs • Degradation releases cyanuric acid	[58,59]

LDI		• Nontoxic degradation by-product (lysine) • Methyl ester provides steric hindrance of hydrolysis sites	[60,125,140,141,143,160]
IPDI		• Lower toxicity than aromatic diisocyanates • Reduced hydrolytic degradation vs. HDI-based PUs due to asymmetrical structure	[92,133,161,165,166]
DMPA		• Hydrophilic, and thus expected to increase susceptibility to hydrolytic degradation	[134,161,166]
Soft segment			
PEG		• Most susceptible to oxidative degradation • Can increase PU hydrophilicity, thus increasing hydrolytic degradation	[34,43,44,57,92,125, 133,135,140,165]
PCL		• Most susceptible to hydrolytic degradation • Slow degrading, but faster than just hydrolysis due to autocatalytic bulk degradation from lower pH due to acidic degradation by-products	[34,43,44,46,47, 82,84,92,115–118, 120,125,133,143, 154,160,161,168,174]

Continued
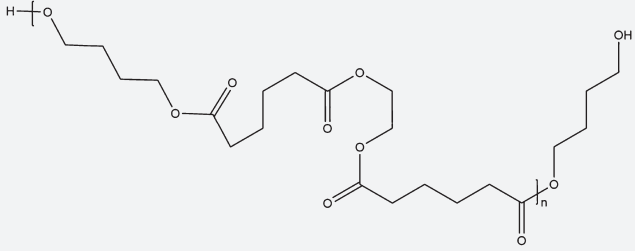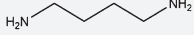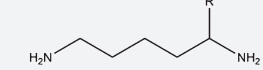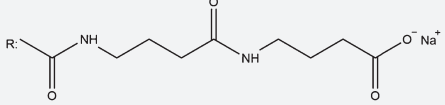
Table 3.2 Continued
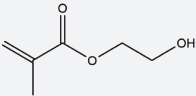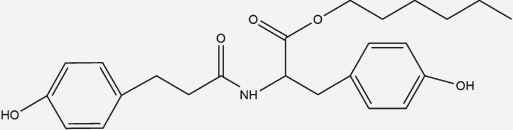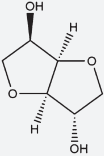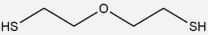
Monomer	Chemical structure	Comment	References
PTMC		• Has been shown to undergo surface degradation, which may allow for maintenance of mechanical properties for prolonged periods • Slow degradation rate	[35]
PEO		• Can be used to accelerate hydrolytic degradation due to high hydrophilicity	[35]
PPO		• Less hydrophilic than PEO, thus maintains slower hydrolysis rate	[35]
GAE		• High GAE content results in higher cross-link density, reducing enzymatic biodegradation rate	[48]
Polyester triol		• Composition of the polyester triol (ε-caprolactone, glycolide, lactide) can be modified to tailor degradation rate	[57,132]

PTK diol		• Stable under aqueous conditions, but selectively degraded through cell-generated ROS	[59]
PCN		• More resistant to oxidative degradation than PEU, but can be designed to be prone to hydrolytic degradation	[60]
L-Lactide		• Releases acidic degradation by-products • Most susceptible to hydrolytic degradation	[120,125]
PCLH macrodiol		• Confers pH sensitivity • Increases susceptibility to hydrolytic degradation • Undergoes bulk degradation • Hydrolysis rate inversely correlated to pH	[141]
PLLA diol		• Most susceptible to hydrolytic degradation • Acidic degradation by-products	[161]

Continued
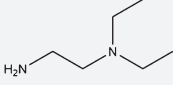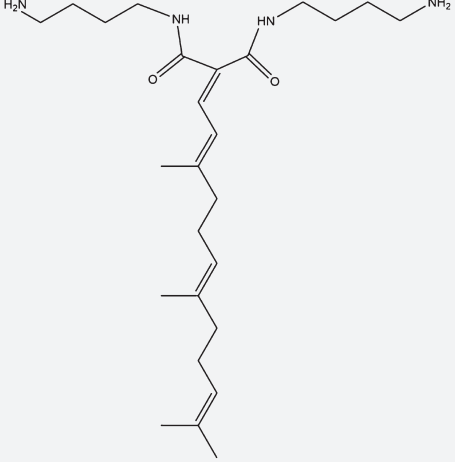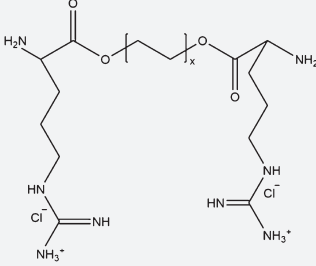
Table 3.2 **Continued**

Monomer	Chemical structure	Comment	References
PEBA diol		• Hydrophobic, and thus reduces susceptibility to hydrolytic degradation	[161]
Chain extender			
Putrescine (BDA)		• Important mediator of cell growth and differentiation when released on degradation	[35,82,84,160]
HZ			[92,133]
LDT		• Can be used to bind targeting molecules to PU	[141]
BDO			[120,134,141,160]

HEMA		• Confers cross-linking functionality to prepolymer • Increases susceptibility to hydrolytic degradation	[60]
DTH		• Nontoxic, noncarcino-genic peptide degradation by-products	[44]
ISO		• Provides enhanced biological activity, due to release of active agents on degradation that act as vasodilators and promote bone formation	[46,47,118]
Bis(2-mercaptoethyl) ether (MEE)		• Provides stability in aqueous medium, but susceptibility to oxidative degradation from cell-generated ROS • Limited *in vitro* cytotoxicity • Minimal host inflammatory response • Thiourea more susceptible to hydrolysis than urethane	[46,47,59]

Continued

Table 3.2 **Continued**

Monomer	Chemical structure	Comment	References
DEAE			[135,140]
TDD		• Potential to increase cell viability and morphology	[46,47]
Arg-x-Cl		• Increased susceptibility to hydrolytic and enzymatic degradation due to presence of alkylene diester content	[48]
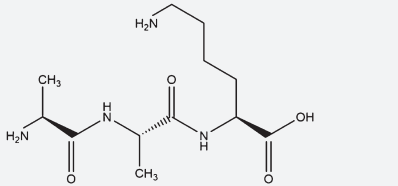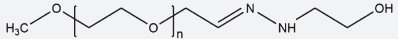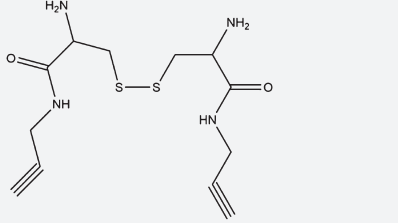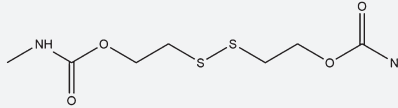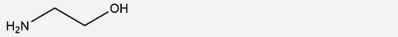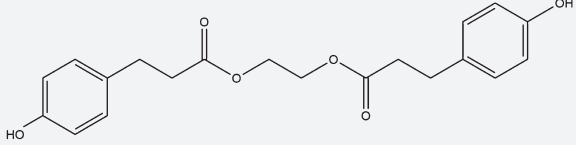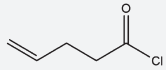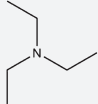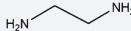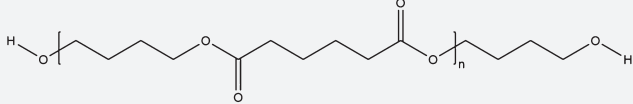
Diamine peptide– Ala–Ala–Lys		• Introduces sensitivity to degradation mediated by elastase	[45]
m-PEG-Hyd		• Hydrazine bonds provide pH-sensitive degradation to target tumor environments (>degradation at low pH)	[141,143]
Cys-PA		• Redox-sensitive disulfide bond, allows for triggered release of payloads due to intracellular glutathione • Nontoxic amino acid (cysteine) by-product	[143]
DHDS		• Disulfide bond allows for synthesis of reduction-sensitive PUs	[144]
2-Amino ethanol		• Introduces both urea and urethane bonds, which have different sensitivities to hydrolytic degradation (urea > urethane)	[154]

Continued

Table 3.2 **Continued**

Monomer	Chemical structure	Comment	References
Diester diphenol derivative of tyrosine		• Nontoxic amino acid tyrosine released on degradation	[154]
4-Pentenoyl chloride		• UV-mediated cross-linking • Increased cross-linking expected to decrease degradation rate	[156]
TEA			[161]
EDA			[161]
PTMA		• Provides hydrophobic character to PU • Introduces hydrolyzable ester linkages	[166]
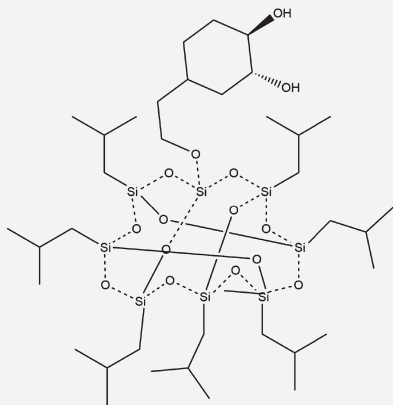
Other			
POSS		• Shields soft segment of polyurethanes from oxidation and hydrolysis	[174]
MAA		• Increasing MAA content increases polymer swelling, which may yield greater hydrolytic sensitivity	[60]
MMA			[60]
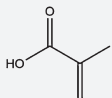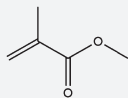
References

[1] Mackay TG, Bernacca GM, Fisher AC, Hindle CS, Wheatley DJ. In vitro function and durability assessment of a novel polyurethane heart valve prosthesis. Artif Organs September 1996;20(9):1017–25.

[2] Paynter RW, Askill IN, Glick SH, Guidoin R. The hydrolytic stability of mitrathane (a polyurethane urea)–an x-ray photoelectron spectroscopy study. J Biomed Mater Res August 1988;22(8):687–98.

[3] Wagner H, Beller FK, Pfautsch M. Electron and light microscopy examination of capsules around breast implants. Plast Reconstr Surg July 1977;60(1):49–55.

[4] Bucky LP, Ehrlich HP, Sohoni S, May Jr JW. The capsule quality of saline-filled smooth silicone, textured silicone, and polyurethane implants in rabbits: a long-term study. Plast Reconstr Surg May 1994;93(6):1123–31. Discussion 1132–3.

[5] Slade CL, Peterson HD. Disappearance of the polyurethane cover of the Ashley Natural Y prosthesis. Plast Reconstr Surg September 1982;70(3):379–83.

[6] Bonart RJ. X-ray investigations concerning the physical structure of cross-linking in segmented urethane elastomers. J Macromol Sci Phys 1968;B2:115–38.

[7] Santerre JP, Woodhouse K, Laroche G, Labow RS. Understanding the biodegradation of polyurethanes: from classical implants to tissue engineering materials. Biomaterials December 2005;26(35):7457–70.

[8] Wen J, Somorjai G, Lim F, Ward R. XPS study of surface composition of a segmented polyurethane block copolymer modified by PDMS end groups and its blends with phenoxy. Macromolecules 1997;30:7206.

[9] Boretos JW. Tissue pathology and physical stability of a polyether elastomer on three-year implantation. J Biomed Mater Res September 1972;6(5):473–6.

[10] Stokes K, Cobian K. Polyether polyurethanes for implantable pacemaker leads. Biomaterials October 1982;3(4):225–31.

[11] Stokes KB. Polyether polyurethanes: biostable or not? J Biomater Appl October 1988;3(2):228–59.

[12] Ward R, Anderson J, McVenes R, Stokes K. In vivo biostability of shore 55D polyether polyurethanes with and without fluoropolymer surface modifying endgroups. J Biomed Mater Res A December 15, 2006;79(4):836–45.

[13] Wiggins MJ, Wilkoff B, Anderson JM, Hiltner A. Biodegradation of polyether polyurethane inner insulation in bipolar pacemaker leads. J Biomed Mater Res May 1, 2001;58(3):302–7.

[14] Stokes K, McVenes R, Anderson JM. Polyurethane elastomer biostability. J Biomater Appl April 1995;9(4):321–54.

[15] Marchant RE, Miller KM, Anderson JM. In vivo biocompatibility studies. V. In vivo leukocyte interactions with biomer. J Biomed Mater Res November–December 1984;18(9):1169–90.

[16] Cardy RH. Carcinogenicity and chronic toxicity of 2,4-toluenediamine in F344 rats. J Natl Cancer Inst April 1979;62(4):1107–16.

[17] Schoental R. Carcinogenic and chronic effects of 4,4'-diaminodiphenylmethane, an epoxyresin hardener. Nature September 14, 1968;219(5159):1162–3.

[18] Wang GB, Labow RS, Santerre JP. Biodegradation of a poly(ester)urea-urethane by cholesterol esterase: isolation and identification of principal biodegradation products. J Biomed Mater Res September 5, 1997;36(3):407–17.

[19] Wang GB, Labow RS, Santerre JP. Probing the surface chemistry of a hydrated segmented polyurethane and a comparison with its dry surface chemical structure. Macromolecules 2000;33:7321.

[20] Santerre JP, Labow RS. The effect of hard segment size on the hydrolytic stability of polyether-urea-urethanes when exposed to cholesterol esterase. J Biomed Mater Res August 1997;36(2):223–32.

[21] Labow RS, Meek E, Santerre JP. The biodegradation of poly(urethane)s by the estero-lytic activity of serine proteases and oxidative enzyme systems. J Biomater Sci Polym Ed 1999;10(7):699–713.

[22] Tang YW, Labow RS, Santerre JP. Enzyme-induced biodegradation of polycarbonate-polyurethanes: dependence on hard-segment chemistry. J Biomed Mater Res December 15, 2001;57(4):597–611.

[23] Tang YW, Labow RS, Santerre JP. Enzyme-induced biodegradation of polycarbon-ate polyurethanes: dependence on hard-segment concentration. J Biomed Mater Res September 15, 2001;56(4):516–28.

[24] Labow RS, Meek E, Santerre JP. Hydrolytic degradation of poly(carbonate)-urethanes by monocyte-derived macrophages. Biomaterials November 2001;22(22):3025–33.

[25] Labow RS, Meek E, Santerre JP. Model systems to assess the destructive potential of human neutrophils and monocyte-derived macrophages during the acute and chronic phases of inflammation. J Biomed Mater Res February 2001;54(2):189–97.

[26] Labow RS, Meek E, Matheson LA, Santerre JP. Human macrophage-mediated bio-degradation of polyurethanes: assessment of candidate enzyme activities. Biomaterials October 2002;23(19):3969–75.

[27] Pinchuk L, Martin Jr JB, Esquivel MC, MacGregor DC. The use of silicone/polyurethane graft polymers as a means of eliminating surface cracking of polyurethane prostheses. J Biomater Appl October 1988;3(2):260–96.

[28] Pande GS. Thermoplastic polyurethanes as insulating materials for long-life cardiac pac-ing leads. Pacing Clin Electrophysiol September 1983;6(5 Pt 1):858–67.

[29] Anderson JM. Inflammatory response to implants. ASAIO Trans April–June 1988;34(2):101–7.

[30] Anderson JM. Mechanisms of inflammation and infection with implanted devices. Cardiovasc Pathol 1993;2(3 Suppl.):33–41.

[31] Sutherland K, Mahoney II JR, Coury AJ, Eaton JW. Degradation of biomaterials by phagocyte-derived oxidants. J Clin Invest November 1993;92(5):2360–7.

[32] Hunt JA, Flanagan BF, McLaughlin PJ, Strickland I, Williams DF. Effect of biomaterial surface charge on the inflammatory response: evaluation of cellular infiltration and TNF alpha production. J Biomed Mater Res May 1996;31(1):139–44.

[33] Falck P. Characterization of human neutrophils adherent to organic polymers. Biomaterials January 1995;16(1):61–6.

[34] Guan J, Fujimoto KL, Sacks MS, Wagner WR. Preparation and characterization of highly porous, biodegradable polyurethane scaffolds for soft tissue applications. Biomaterials June 2005;26(18):3961–71.

[35] Wang F, Li Z, Lannutti JL, Wagner WR, Guan J. Synthesis, characterization and surface modification of low moduli poly(ether carbonate urethane)ureas for soft tissue engineer-ing. Acta Biomater October 2009;5(8):2901–12.

[36] Zhu K, Hendren R, Jensen K, Pitt C. Synthesis, properties, and biodegradation of poly(1,3-trimethylene carbonate). Macromolecules 1991;24(8):1736–40.

[37] Pego AP, Van Luyn MJ, Brouwer LA, van Wachem PB, Poot AA, Grijpma DW, et al. In vivo behavior of poly(1,3-trimethylene carbonate) and copolymers of 1,3-trimethylene carbonate with D,L-lactide or epsilon-caprolactone: degradation and tissue response. J Biomed Mater Res A December 1, 2003;67(3):1044–54.

[38] Storey R, Hickey T. Degradable polyurethane networks based on d,l-lactide, glycolide, ε-caprolactone, and trimethylene carbonate homopolyester and copolyester triols. Polymer 1994;35(4):830–8.

[39] Asplund JO, Bowden T, Mathisen T, Hilborn J. Synthesis of highly elastic biodegradable poly(urethane urea). Biomacromolecules March 2007;8(3):905–11.

[40] Asplund B, Aulin C, Bowden T, Eriksson N, Mathisen T, Bjursten LM, et al. In vitro degradation and in vivo biocompatibility study of a new linear poly(urethane urea). J Biomed Mater Res B Appl Biomater July 2008;86(1):45–55.

[41] Hong Y, Guan J, Fujimoto KL, Hashizume R, Pelinescu AL, Wagner WR. Tailoring the degradation kinetics of poly(ester carbonate urethane)urea thermoplastic elastomers for tissue engineering scaffolds. Biomaterials May 2010;31(15):4249–58.

[42] Kuran W, Sobczak M, Listos T, Debek C, Florjanczyk Z. New route to oligocarbonate diols suitable for the synthesis of polyurethane elastomers. Polymer 2000;41(24):8531–41.

[43] Niu Y, Chen KC, He T, Yu W, Huang S, Xu K. Scaffolds from block polyurethanes based on poly(varepsilon-caprolactone) (PCL) and poly(ethylene glycol) (PEG) for peripheral nerve regeneration. Biomaterials May 2014;35(14):4266–77.

[44] Spagnuolo M, Liu L. Fabrication and degradation of electrospun scaffolds from l-tyrosine-based polyurethane blends for tissue engineering applications. ISRN Nanotechnol 2012;2012:1–11.

[45] Guan J, Fujimoto KL, Wagner WR. Elastase-sensitive elastomeric scaffolds with variable anisotropy for soft tissue engineering. Pharm Res October 2008;25(10):2400–12.

[46] Gorna K, Gogolewski S. Biodegradable porous polyurethane scaffolds for tissue repair and regeneration. J Biomed Mater Res A October 2006;79(1):128–38.

[47] Laschke MW, Strohe A, Scheuer C, Eglin D, Verrier S, Alini M, et al. In vivo biocompatibility and vascularization of biodegradable porous polyurethane scaffolds for tissue engineering. Acta Biomater July 2009;5(6):1991–2001.

[48] He M, Chu C. A new family of functional biodegradable arginine-based polyester urea urethanes: synthesis, chracterization and biodegradation. Polymer 2013;54(16):4112–25.

[49] Huang S, Bansleben D, Knox J. Biodegradable polymers: chymotrypsin degradation of a low molecular weight poly(ester-urea) containing phenylalanine. J Appl Polym Sci 1979;23(2):429–37.

[50] Wu J, Chu CC. Block copolymer of poly(ester amide) and polyesters: synthesis, characterization, and in vitro cellular response. Acta Biomater December 2012;8(12):4314–23.

[51] Wu J, Wu D, Mutschler M, Chu C. Cationic hybrid hydrogels from amino-acid-based poly(ester amide): fabrication, characterization, and biological properties. Adv Funct Mater 2012;22(18):3815–23.

[52] Wu J, Yamanouchi D, Liu B, Chu C. Biodegradable arginine-based poly(ether ester amide)s as a non-viral DNA delivery vector and their structure–function study. J Mater Chem 2012;22(36):18983–91.

[53] Yamanouchi D, Wu J, Lazar AN, Kent KC, Chu CC, Liu B. Biodegradable arginine-based poly(ester-amide)s as non-viral gene delivery reagents. Biomaterials August 2008;29(22):3269–77.

[54] Wu J, Chu C. Water insoluble cationic poly(ester amide)s: synthesis, characterization and applications. J Mater Chem B 2013;1(3):353–60.

[55] Wu J, Mutschler MA, Chu CC. Synthesis and characterization of ionic charged water soluble arginine-based poly(ester amide). J Mater Sci Mater Med March 2011;22(3):469–79.

[56] Song H, Chu C. Synthesis and characterization of a new family of cationic amino acid-based poly(ester amide)s and their biological properties. J Appl Polym Sci 2012;124(5):3840–53.

[57] Adolph EJ, Hafeman AE, Davidson JM, Nanney LB, Guelcher SA. Injectable polyurethane composite scaffolds delay wound contraction and support cellular infiltration and remodeling in rat excisional wounds. J Biomed Mater Res A February 2012;100(2):450–61.

[58] Hafeman AE, Zienkiewicz KJ, Zachman AL, Sung HJ, Nanney LB, Davidson JM, et al. Characterization of the degradation mechanisms of lysine-derived aliphatic poly(ester urethane) scaffolds. Biomaterials January 2011;32(2):419–29.

[59] Martin JR, Gupta MK, Page JM, Yu F, Davidson JM, Guelcher SA, et al. A porous tissue engineering scaffold selectively degraded by cell-generated reactive oxygen species. Biomaterials April 2014;35(12):3766–76.

[60] Sharifpoor S, Labow RS, Santerre JP. Synthesis and characterization of degradable polar hydrophobic ionic polyurethane scaffolds for vascular tissue engineering applications. Biomacromolecules October 12, 2009;10(10):2729–39.

[61] McBane JE, Matheson LA, Sharifpoor S, Santerre JP, Labow RS. Effect of polyurethane chemistry and protein coating on monocyte differentiation towards a wound healing phenotype macrophage. Biomaterials October 2009;30(29):5497–504.

[62] Pinchuk L. A review of the biostability and carcinogenicity of polyurethanes in medicine and the new generation of 'biostable' polyurethanes. J Biomater Sci Polym Ed 1994;6(3):225–67.

[63] van Wachem PB, Beugeling T, Feijen J, Bantjes A, Detmers JP, van Aken WG. Interaction of cultured human endothelial cells with polymeric surfaces of different wettabilities. Biomaterials November 1985;6(6):403–8.

[64] McBane JE, Sharifpoor S, Cai K, Labow RS, Santerre JP. Biodegradation and in vivo biocompatibility of a degradable, polar/hydrophobic/ionic polyurethane for tissue engineering applications. Biomaterials September 2011;32(26):6034–44.

[65] McBane JE, Ebadi D, Sharifpoor S, Labow RS, Santerre JP. Differentiation of monocytes on a degradable, polar, hydrophobic, ionic polyurethane: two-dimensional films vs. three-dimensional scaffolds. Acta Biomater January 2011;7(1):115–22.

[66] Battiston KG, Labow RS, Santerre JP. Protein binding mediation of biomaterial-dependent monocyte activation on a degradable polar hydrophobic ionic polyurethane. Biomaterials November 2012;33(33):8316–28.

[67] McBane JE, Battiston KG, Wadhwani A, Sharifpoor S, Labow RS, Santerre JP. The effect of degradable polymer surfaces on co-cultures of monocytes and smooth muscle cells. Biomaterials May 2011;32(14):3584–95.

[68] Cheung JW, Rose EE, Paul Santerre J. Perfused culture of gingival fibroblasts in a degradable/polar/hydrophobic/ionic polyurethane (D-PHI) scaffold leads to enhanced proliferation and metabolic activity. Acta Biomater June 2013;9(6):6867–75.

[69] Guelcher SA, Srinivasan A, Dumas JE, Didier JE, McBride S, Hollinger JO. Synthesis, mechanical properties, biocompatibility, and biodegradation of polyurethane networks from lysine polyisocyanates. Biomaterials April 2008;29(12):1762–75.

[70] Gogolewski S, Gorna K, Turner A. Regeneration of bicortical defects in the iliac crest of estrogen-deficient sheep, using new biodegradable polyurethane bone graft substitutes. J Biomed Mater Res Part A June 15, 2006;77A(4):802–10.

[71] Dumas JE, Zienkiewicz K, Tanner SA, Prieto EM, Bhattacharyya S, Guelcher SA. Synthesis and characterization of an injectable allograft bone/polymer composite bone void filler with tunable mechanical properties. Tissue Eng Part A August 2010;16(8):2505–18.

[72] Dumas JE, Davis T, Holt GE, Yoshii T, Perrien DS, Nyman JS, et al. Synthesis, characterization, and remodeling of weight-bearing allograft bone/polyurethane composites in the rabbit. Acta Biomater July 2010;6(7):2394–406.

[73] Gogolewski S, Gorna K. Biodegradable polyurethane cancellous bone graft substitutes in the treatment of iliac crest defects. J Biomed Mater Res Part A January 2007;80A(1):94–101.

[74] Yoshii T, Hafeman AE, Nyman JS, Esparza JM, Shinomiya K, Spengler DM, et al. A sustained release of lovastatin from biodegradable, elastomeric polyurethane scaffolds for enhanced bone regeneration. Tissue Eng Part A July 2010;16(7):2369–79.

[75] Boffito M, Sartori S, Ciardelli G. Polymeric scaffolds for cardiac tissue engineering: requirements and fabrication technologies. Polym Int January 2014;63(1):2–11.

[76] Hashizume R, Hong Y, Takanari K, Fujimoto KL, Tobita K, Wagner WR. The effect of polymer degradation time on functional outcomes of temporary elastic patch support in ischemic cardiomyopathy. Biomaterials October 2013;34(30):7353–63.

[77] Jiang X, Yu F, Wang Z, Li J, Tan H, Ding M, et al. Fabrication and characterization of waterborne biodegradable polyurethanes 3-dimensional porous scaffolds for vascular tissue engineering. J Biomater Sci Polym Ed 2010;21(12):1637–52.

[78] Sharifpoor S, Simmons CA, Labow RS, Santerre JP. A study of vascular smooth muscle cell function under cyclic mechanical loading in a polyurethane scaffold with optimized porosity. Acta Biomater November 2010;6(11):4218–28.

[79] Ye S, Hong Y, Sakaguchi H, Shankarraman V, Luketich SK, D'Amore A, et al. Non-thrombogenic, biodegradable elastomeric polyurethanes with variable sulfobetaine content. Acs Appl Mater Interfaces December 24, 2014;6(24):22796–806.

[80] Ou W, Qiu H, Chen Z, Xu K. Biodegradable block poly(ester-urethane)s based on poly (3-hydroxybutyrate-co-4-hydroxybutyrate) copolymers. Biomaterials April 2011;32(12):3178–88.

[81] Yu J, Takanari K, Hong Y, Lee KW, Amoroso NJ, Wang Y, et al. Non-invasive characterization of polyurethane-based tissue constructs in a rat abdominal repair model using high frequency ultrasound elasticity imaging. Biomaterials April 2013;34(11):2701–9.

[82] Hashizume R, Fujimoto KL, Hong Y, Amoroso NJ, Tobita K, Miki T, et al. Morphological and mechanical characteristics of the reconstructed rat abdominal wall following use of a wet electrospun biodegradable polyurethane elastomer scaffold. Biomaterials April 2010;31(12):3253–65.

[83] Sicari BM, Dziki JL, Siu BF, Medberry CJ, Dearth CL, Badylak SF. The promotion of a constructive macrophage phenotype by solubilized extracellular matrix. Biomaterials October 2014;35(30):8605–12.

[84] Guan J, Stankus J, Wagner W. Development of composite porous scaffolds based on collagen and biodegradable poly(ester urethane)urea. Cell Transpl 2006;15:S17–27.

[85] Kumbar SG, James R, Nukavarapu SP, Laurencin CT. Electrospun nanofiber scaffolds: engineering soft tissues. Biomed Mater September 2008;3(3):034002.

[86] Hong Y, Takanari K, Amoroso NJ, Hashizume R, Brennan-Pierce EP, Freund JM, et al. An elastomeric patch electrospun from a blended solution of dermal extracellular matrix and biodegradable polyurethane for rat abdominal wall repair. Tissue Eng Part C Methods February 2012;18(2):122–32.

[87] Hong Y, Huber A, Takanari K, Amoroso NJ, Hashizume R, Badylak SF, et al. Mechanical properties and in vivo behavior of a biodegradable synthetic polymer microfiber-extracellular matrix hydrogel biohybrid scaffold. Biomaterials May 2011;32(13):3387–94.

[88] Rodriguez A, Macewan SR, Meyerson H, Kirk JT, Anderson JM. The foreign body reaction in T-cell-deficient mice. J Biomed Mater Res A July 2009;90(1):106–13.

[89] Rodriguez A, Voskerician G, Meyerson H, MacEwan SR, Anderson JM. T cell subset distributions following primary and secondary implantation at subcutaneous biomaterial implant sites. J Biomed Mater Res A May 2008;85(2):556–65.

[90] Christenson EM, Anderson JM, Hiltner A. Antioxidant inhibition of poly(carbonate urethane) in vivo biodegradation. J Biomed Mater Res A March 1, 2006;76(3):480–90.

[91] McDonald SM, Matheson LA, McBane JE, Kuraitis D, Suuronen E, Santerre JP, et al. Use of monocyte/endothelial cell co-cultures (in vitro) and a subcutaneous implant mouse model (in vivo) to evaluate a degradable polar hydrophobic ionic polyurethane. J Cell Biochem December 2011;112(12):3762–72.

[92] Da Silva GR, Ayres E, Orefice RL, Moura SA, Cara DC, Cunha Ada Jr S. Controlled release of dexamethasone acetate from biodegradable and biocompatible polyurethane and polyurethane nanocomposite. J Drug Target June 2009;17(5):374–83.

[93] Dey J, Xu H, Shen J, Thevenot P, Gondi SR, Nguyen KT, et al. Development of biodegradable crosslinked urethane-doped polyester elastomers. Biomaterials December 2008;29(35):4637–49.

[94] Li A, Dearman BL, Crompton KE, Moore TG, Greenwood JE. Evaluation of a novel biodegradable polymer for the generation of a dermal matrix. J Burn Care Res July–August 2009;30(4):717–28.

[95] Park DW, Ye SH, Jiang HB, Dutta D, Nonaka K, Wagner WR, et al. In vivo monitoring of structural and mechanical changes of tissue scaffolds by multi-modality imaging. Biomaterials September 2014;35(27):7851–9.

[96] Thomas V, Jayabalan M. A new generation of high flex life polyurethane urea for polymer heart valve–studies on in vivo biocompatibility and biodurability. J Biomed Mater Res A April 2009;89(1):192–205.

[97] Stachelek SJ, Alferiev I, Connolly JM, Sacks M, Hebbel RP, Bianco R, et al. Cholesterol-modified polyurethane valve cusps demonstrate blood outgrowth endothelial cell adhesion post-seeding in vitro and in vivo. Ann Thorac Surg January 2006;81(1):47–55.

[98] Fujimoto KL, Guan J, Oshima H, Sakai T, Wagner WR. In vivo evaluation of a porous, elastic, biodegradable patch for reconstructive cardiac procedures. Ann Thorac Surg February 2007;83(2):648–54.

[99] Adhikari R, Gunatillake PA, Griffiths I, Tatai L, Wickramaratna M, Houshyar S, et al. Biodegradable injectable polyurethanes: synthesis and evaluation for orthopaedic applications. Biomaterials October 2008;29(28):3762–70.

[100] Awwad HK, Naggar M El, Mocktar N, Barsoum M. Intercapillary distance measurement as an indicator of hypoxia in carcinoma of the cervix uteri. Int J Radiat Oncol Biol Phys August 1986;12(8):1329–33.

[101] Kirkpatrick CJ, Fuchs S, Unger RE. Co-culture systems for vascularization–learning from nature. Adv Drug Deliv Rev April 30, 2011;63(4–5):291–9.

[102] Salerno S, Campana C, Morelli S, Drioli E, De Bartolo L. Human hepatocytes and endothelial cells in organotypic membrane systems. Biomaterials December 2011;32(34):8848–59.

[103] Marekova D, Lesny P, Jendelova P, Michalek J, Kostecka P, Pradny M, et al. Hepatocyte growth on polycapronolactone and 2-hydroxyethylmethacrylate nanofiber sheets enhanced by bone marrow-derived mesenchymal stromal cells. Hepatogastroenterology July–August 2013;60(125):1156–63.

[104] Parrag IC, Zandstra PW, Woodhouse KA. Fiber alignment and coculture with fibroblasts improves the differentiated phenotype of murine embryonic stem cell-derived cardiomyocytes for cardiac tissue engineering. Biotechnol Bioeng March 2012;109(3): 813–22.

[105] Cheung JW, Jain D, McCulloch C, Santerre P. Pro-angiogenic character of endothelial cells and gingival fibroblasts co-cultures in perfused degradable polyurethane (D-PHI) scaffolds. Tissue Eng Part A May, 2015;21(9–10):1587–99. http://dx.doi.org/10.1089/ten.TEA.2014.0548. Epub 2015 Mar 10.

[106] Battiston KG, Ouyang B, Labow RS, Simmons CA, Santerre JP. Monocyte/macrophage cytokine activity regulates vascular smooth muscle cell function within a degradable polyurethane scaffold. Acta Biomater March 2014;10(3):1146–55.

[107] McBane JE, Cai K, Labow RS, Santerre JP. Co-culturing monocytes with smooth muscle cells improves cell distribution within a degradable polyurethane scaffold and reduces inflammatory cytokines. Acta Biomater February 2012;8(2):488–501.

[108] Dearman BL, Li A, Greenwood JE. Optimization of a polyurethane dermal matrix and experience with a polymer-based cultured composite skin. J Burn Care Res September–October 2014;35(5):437–48.

[109] Kassab MM, Cohen RE. The etiology and prevalence of gingival recession. J Am Dent Assoc February 2003;134(2):220–5.

[110] Cheung JW, McCulloch CA, Santerre JP. Establishing a gingival fibroblast phenotype in a perfused degradable polyurethane scaffold: mediation by TGF-beta1, FGF-2, beta1-integrin, and focal adhesion kinase. Biomaterials December 2014;35(38):10025–32.

[111] Janardhanan S, Wang MO, Fisher JP. Coculture strategies in bone tissue engineering: the impact of culture conditions on pluripotent stem cell populations. Tissue Eng Part B Rev August 2012;18(4):312–21.

[112] Duttenhoefer F, Lara de Freitas R, Meury T, Loibl M, Benneker LM, Richards RG, et al. 3D scaffolds co-seeded with human endothelial progenitor and mesenchymal stem cells: evidence of prevascularisation within 7 days. Eur Cell Mater August 29, 2013;26:49–64. discussion 64–5.

[113] Hofmann A, Ritz U, Verrier S, Eglin D, Alini M, Fuchs S, et al. The effect of human osteoblasts on proliferation and neo-vessel formation of human umbilical vein endothelial cells in a long-term 3D co-culture on polyurethane scaffolds. Biomaterials November 2008;29(31):4217–26.

[114] Wang C, Cen L, Yin S, Liu Q, Liu W, Cao Y, et al. A small diameter elastic blood vessel wall prepared under pulsatile conditions from polyglycolic acid mesh and smooth muscle cells differentiated from adipose-derived stem cells. Biomaterials February 2010;31(4):621–30.

[115] Phinney DG, Prockop DJ. Concise review: mesenchymal stem/multipotent stromal cells: the state of transdifferentiation and modes of tissue repair–current views. Stem Cells November 2007;25(11):2896–902.

[116] Pittenger MF, Martin BJ. Mesenchymal stem cells and their potential as cardiac therapeutics. Circ Res July 9, 2004;95(1):9–20.

[117] Cho SW, Lim SH, Kim IK, Hong YS, Kim SS, Yoo KJ, et al. Small-diameter blood vessels engineered with bone marrow-derived cells. Ann Surg March 2005;241(3):506–15.

[118] Li Z, Kupcsik L, Yao SJ, Alini M, Stoddart MJ. Mechanical load modulates chondrogenesis of human mesenchymal stem cells through the TGF-beta pathway. J Cell Mol Med June 2010;14(6A):1338–46.

[119] Zahedmanesh H, Stoddart M, Lezuo P, Forkmann C, Wimmmer MA, Alini M, et al. Deciphering mechanical regulation of chondrogenesis in fibrin-polyurethane composite scaffolds enriched with human mesenchymal stem cells: a dual computational and experimental approach. Tissue Eng Part A April 2014;20(7–8):1197–212.

[120] Liu C, Abedian R, Meister R, Haasper C, Hurschler C, Krettek C, et al. Influence of perfusion and compression on the proliferation and differentiation of bone mesenchymal stromal cells seeded on polyurethane scaffolds. Biomaterials February 2012;33(4):1052–64.

[121] Laschke MW, Schank TE, Scheuer C, Kleer S, Schuler S, Metzger W, et al. Three-dimensional spheroids of adipose-derived mesenchymal stem cells are potent initiators of blood vessel formation in porous polyurethane scaffolds. Acta Biomater June 2013;9(6): 6876–84.

[122] Kuo YC, Hung SC, Hsu SH. The effect of elastic biodegradable polyurethane electrospun nanofibers on the differentiation of mesenchymal stem cells. Colloids Surf B Biointerfaces October 1, 2014;122:414–22.

[123] Laschke MW, Schank TE, Scheuer C, Kleer S, Shadmanov T, Eglin D, et al. In vitro osteogenic differentiation of adipose-derived mesenchymal stem cell spheroids impairs their in vivo vascularization capacity inside implanted porous polyurethane scaffolds. Acta Biomater October 2014;10(10):4226–35.

[124] Kral JG, Crandall DL. Development of a human adipocyte synthetic polymer scaffold. Plast Reconstr Surg November 1999;104(6):1732–8.

[125] Gugerell A, Kober J, Laube T, Walter T, Nurnberger S, Gronniger E, et al. Electrospun poly(ester-urethane)- and poly(ester-urethane-urea) fleeces as promising tissue engineering scaffolds for adipose-derived stem cells. PLoS One March 4, 2014;9(3):e90676.

[126] Carlberg B, Axell MZ, Nannmark U, Liu J, Kuhn HG. Electrospun polyurethane scaffolds for proliferation and neuronal differentiation of human embryonic stem cells. Biomed Mater August 2009;4(4). 045004–6041/4/4/045004. Epub 2009 Jun 30.

[127] Ritfeld GJ, Rauck BM, Novosat TL, Park D, Patel P, Roos RA, et al. The effect of a polyurethane-based reverse thermal gel on bone marrow stromal cell transplant survival and spinal cord repair. Biomaterials February 2014;35(6):1924–31.

[128] Crisante F, Francolini I, Bellusci M, Martinelli A, D'Ilario L, Piozzi A. Antibiotic delivery polyurethanes containing albumin and polyallylamine nanoparticles. Eur J Pharm Sci March 2, 2009;36(4–5):555–64.

[129] Guan J, Stankus JJ, Wagner WR. Biodegradable elastomeric scaffolds with basic fibroblast growth factor release. J Control Release July 16, 2007;120(1–2):70–8.

[130] Gospodarowicz D, Cheng J. Heparin protects basic and acidic FGF from inactivation. J Cell Physiol September 1986;128(3):475–84.

[131] Nelson DM, Baraniak PR, Ma Z, Guan J, Mason NS, Wagner WR. Controlled release of IGF-1 and HGF from a biodegradable polyurethane scaffold. Pharm Res June 2011;28(6):1282–93.

[132] Li B, Davidson JM, Guelcher SA. The effect of the local delivery of platelet-derived growth factor from reactive two-component polyurethane scaffolds on the healing in rat skin excisional wounds. Biomaterials July 2009;30(20):3486–94.

[133] Moura SA, Lima LD, Andrade SP, Da Silva-Cunha Jr A, Orefice RL, Ayres E, et al. Local drug delivery system: inhibition of inflammatory angiogenesis in a murine sponge model by dexamethasone-loaded polyurethane implants. J Pharm Sci July 2011;100(7):2886–95.

[134] Babanejad N, Nikjeh M, Amini M, Dorkoosh F. A nanoparticulate raloxifene delivery system based on biodegradable carboxylated polyurethane: design, optimization, characterization, and in vitro evaluation. J Appl Polym Sci 2014;131(1).

[135] Tseng SJ, Tang SC. Synthesis and characterization of the novel transfection reagent poly(amino ester glycol urethane). Biomacromolecules January 2007;8(1):50–8.

[136] Behr J. The proton sponge: a trick to enter cells the viruses did not exploit. Chim Chim 1997;51:34–6.

[137] Belguise-Valladier P, Behr JP. Nonviral gene delivery: towards artificial viruses. Cytotechnology May 2001;35(3):197–201.

[138] Forrest ML, Meister GE, Koerber JT, Pack DW. Partial acetylation of polyethylenimine enhances in vitro gene delivery. Pharm Res February 2004;21(2):365–71.

[139] Sonawane ND, Szoka Jr FC, Verkman AS. Chloride accumulation and swelling in endosomes enhances DNA transfer by polyamine-DNA polyplexes. J Biol Chem November 7, 2003;278(45):44826–31.

[140] Shau MD, Tseng SJ, Yang TF, Cherng JY, Chin WK. Effect of molecular weight on the transfection efficiency of novel polyurethane as a biodegradable gene vector. J Biomed Mater Res A June 15, 2006;77(4):736–46.

[141] Zhou L, Liang D, He X, Li J, Tan H, Li J, et al. The degradation and biocompatibility of pH-sensitive biodegradable polyurethanes for intracellular multifunctional antitumor drug delivery. Biomaterials March 2012;33(9):2734–45.

[142] Gref R, Luck M, Quellec P, Marchand M, Dellacherie E, Harnisch S, et al. 'Stealth' corona-core nanoparticles surface modified by polyethylene glycol (PEG): influences of the corona (PEG chain length and surface density) and of the core composition on phagocytic uptake and plasma protein adsorption. Colloids Surf B Biointerfaces October 1, 2000;18(3–4):301–13.

[143] Song N, Ding M, Pan Z, Li J, Zhou L, Tan H, et al. Construction of targeting-clickable and tumor-cleavable polyurethane nanomicelles for multifunctional intracellular drug delivery. Biomacromolecules December 9, 2013;14(12):4407–19.

[144] He X, Ding M, Li J, Tan H, Fu Q, Li L. Biodegradable multiblock polyurethane micelles with tunable reduction-sensitivity for on-demand intracellular drug delivery. RSC Adv 2014;4(47):24736–46.

[145] Janik H, Marzec M. A review: fabrication of porous polyurethane scaffolds. Mater Sci Eng C Mater Biol Appl March 2015;1(48):586–91.

[146] Sussman EM, Halpin MC, Muster J, Moon RT, Ratner BD. Porous implants modulate healing and induce shifts in local macrophage polarization in the foreign body reaction. Ann Biomed Eng July 2014;42(7):1508–16.

[147] van Minnen B, van Leeuwen MBM, Kors G, Zuidema J, van Kooten TG, Bos RRM. In vivo resorption of a biodegradable polyurethane foam, based on 1.4-butanediisocyanate: a three-year subcutaneous implantation study. J Biomed Mater Res Part A June 15, 2008;85A(4):972–82.

[148] Gogolewski S, Gorna K, Zaczynska E, Czary A. Structure-property relations and cytotoxicity of isosorbide-based biodegradable polyurethane scaffolds for tissue repair and regeneration. J Biomed Mater Res Part A May 2008;85A(2):456–65.

[149] Asefnejad A, Khorasani MT, Behnamghader A, Farsadzadeh B, Bonakdar S. Manufacturing of biodegradable polyurethane scaffolds based on polycaprolactone using a phase separation method: physical properties and in vitro assay. Int J Nanomed 2011;6:2375–84.

[150] Silvestri A, Sartori S, Boffito M, Mattu C, Di Rienzo AM, Boccafoschi F, et al. Biomimetic myocardial patches fabricated with poly(epsilon-caprolactone) and polyethylene glycol-based polyurethanes. J Biomed Mater Res Part B Appl Biomater July 2014;102(5):1002–13.

[151] Pham Q, Sharma U, Mikos A. Electrospinning of polymeric nanofibers for tissue engineering applications: a review. Tissue Eng May 2006;12(5):1197–211.

[152] Bhardwaj N, Kundu SC. Electrospinning: a fascinating fiber fabrication technique. Biotechnol Adv May–June 2010;28(3):325–47.

[153] Rutledge GC, Fridrikh SV. Formation of fibers by electrospinning. Adv Drug Deliv Rev December 10, 2007;59(14):1384–91.

[154] Caracciolo PC, Thomas V, Vohra YK, Buffa F, Abraham GA. Electrospinning of novel biodegradable poly(ester urethane)s and poly(ester urethane urea)s for soft tissue-engineering applications. J Mater Sci Mater Med October 2009;20(10):2129–37.

[155] Hong Y, Fujimoto K, Hashizume R, Guan J, Stankus JJ, Tobita K, et al. Generating elastic, biodegradable polyurethane/poly(lactide-co-glycolide) fibrous sheets with controlled antibiotic release via two-stream electrospinning. Biomacromolecules April 2008;9(4):1200–7.

[156] Theron JP, Knoetze JH, Sanderson RD, Hunter R, Mequanint K, Franz T, et al. Modification, crosslinking and reactive electrospinning of a thermoplastic medical polyurethane for vascular graft applications. Acta Biomater July 2010;6(7):2434–47.

[157] Blit PH, Battiston KG, Woodhouse KA, Santerre JP. Surface immobilization of elastin-like polypeptides using fluorinated surface modifying additives. J Biomed Mater Res Part A March 15, 2011;96A(4):648–62.

[158] Wu W, Yuan G, He A, Han CC. Surface depletion of the fluorine content of electrospun fibers of fluorinated polyurethane. Langmuir March 3, 2009;25(5):3178–83.

[159] Hutmacher DW, Dalton PD. Melt electrospinning. Chem Asian J January 3, 2011;6(1):44–56.

[160] Karchin A, Simonovsky FI, Ratner BD, Sanders JE. Melt electrospinning of biodegradable polyurethane scaffolds. Acta Biomater September 2011;7(9):3277–84.

[161] Ou C, Su C, Jeng U, Hsu S. Characterization of biodegradable polyurethane nanoparticles and thermally induced self-assembly in water dispersion. Acs Appl Mater Interfaces April 23, 2014;6(8):5685–94.

[162] Melgar-Lesmes P, Morral-Ruiz G, Solans C, Jose Garcia-Celma M. Quantifying the bioadhesive properties of surface-modified polyurethane-urea nanoparticles in the vascular network. Colloids Surf B Biointerfaces June 1, 2014;118:280–8.

[163] Morral-Ruiz G, Melgar-Lesmes P, Luisa Garcia M, Solans C, Jose Garcia-Celma M. Polyurethane and polyurea nanoparticles based on polyoxyethylene castor oil derivative surfactant suitable for endovascular applications. Int J Pharm January 30, 2014;461(1–2):1–13.

[164] Morral-Ruiz G, Melgar-Lesmes P, Solans C, Garcia-Celma MJ. Multifunctional polyurethane-urea nanoparticles to target and arrest inflamed vascular environment: a potential tool for cancer therapy and diagnosis. J Control Release October 28, 2013;171(2):163–71.

[165] Morral-Ruiz G, Solans C, Luisa Garcia M, Jose Garcia-Celma M. Formation of pegylated polyurethane and lysine-coated polyurea nanoparticles obtained from O/W nano-emulsions. Langmuir April 17, 2012;28(15):6256–64.

[166] Cheong I, Kim J. Synthesis of core-shell polyurethane-urea nanoparticles containing 4,4'-methylenedi-p-phenyl diisocyanate and isophorone diisocyanate by self-assembled neutralization emulsification. Chem Commun 2004;21:2484–5.

[167] Zhang Q, Jiang Y, Zhang Y, Ye Z, Tan W, Lang M. Effect of porosity on long-term degradation of poly (epsilon-caprolactone) scaffolds and their cellular response. Polym Degrad Stab January 2013;98(1):209–18.

[168] Bolgen N, Menceloglu Y, Acatay K, Vargel I, Piskin E. In vitro and in vivo degradation of non-woven materials made of poly(epsilon-caprolactone) nanofibers prepared by electrospinning under different conditions. J Biomater Sci Polym Ed 2005;16(12):1537–55.

[169] Hung H, Yang Y, Lin Y, Lin S, Kao W, Hsieh H, et al. Regulation of human endothelial progenitor cell maturation by polyurethane nanocomposites. Biomaterials August 2014;35(25):6810–21.

[170] Moon H, Lee Y, Han J, Byun Y. A novel formulation for controlled release of heparin-DOCA conjugate dispersed as nanoparticles in polyurethane film. Biomaterials February 2001;22(3):281–9.

[171] Saralegi A, Fernandes SCM, Alonso-Varona A, Palomares T, Foster EJ, Weder C, et al. Shape-memory bionanocomposites based on chitin nanocrystals and thermoplastic polyurethane with a highly crystalline soft segment. Biomacromolecules December 2013;14(12):4475–82.

[172] Fong N, Simmons A, Poole-Warren LA. Antibacterial polyurethane nanocomposites using chlorhexidine diacetate as an organic modifier. Acta Biomater July 2010;6(7):2554–61.

[173] Rocha de Oliveira AA, de Carvalho SM, Leite MDF, Orefice RL, Pereira MDM. Development of biodegradable polyurethane and bioactive glass nanoparticles scaffolds for bone tissue engineering applications. J Biomed Mater Res Part B Appl Biomater July 2012;100B(5):1387–96.

[174] Kannan R, Salacinski H, Odlyha M, Butler P, Seifalian A. The degradative resistance of polyhedral oligomeric silsesquioxane nanocore integrated polyurethanes: an in vitro study. Biomaterials March 2006;27(9):1971–9.

[175] Raghunath J, Georgiou G, Armitage D, Nazhat SN, Sales KM, Butler PE, et al. Degradation studies on biodegradable nanocomposite based on polycaprolactone/polycarbonate (80:20) polyhedral oligomeric silsesquioxane. J Biomed Mater Res Part A December 1, 2009;91A(3):834–44.

[176] Chou C, Hsu S, Wang P. Biostability and biocompatibility of poly(ether) urethane containing gold or silver nanoparticles in a porcine model. J Biomed Mater Res Part A March 1, 2008;84A(3):785–94.

Novel applications of urethane/urea chemistry in the field of biomaterials

4

G.B. Kim, J. Guo, J. Hu, D. Shan, J. Yang*
Department of Biomedical Engineering, Materials Research Institute, The Pennsylvania State University, University Park, PA, USA; The Huck Institutes of the Life Sciences, The Pennsylvania State University, University Park, PA, USA
*Corresponding author: jxy30@psu.edu

4.1 Introduction

Urethane/urea chemistry refers to both isocyanate-based and nonisocyanate-based reactions that form urethane (—HNCOO—) or urea (—HNCONH—) bonds. The reactions between isocyanate groups and hydroxyl (to form urethane bonds, Figure 4.1(a)) or amino (to form urea bonds, Figure 4.1(d)) groups [1–3] are the most commonly found. Nonisocyanate-based urethane reactions include the reactions between cyclic carbonates or activated carbonate/carbamate/chloroformate derivative groups and amine groups (Figure 4.1(b) and (c)) [4–6]. The latter were often used as coupling reactions between hydroxyl and amino groups [5,7–9]. The polyaddition reaction between polyisocyanates and polyols is often used to make polyurethanes (PUs) [1–3], the generic term which represents the most versatile family of synthetic polymers containing repeating urethane (—HNCOO—) linkages in the polymer chains. Polyols used for PUs can be small molecules or macromolecules, biodegradable polyesters or nondegradable polyethers, or other polymers with two or more terminal or pendent hydroxyl groups [1–3].

Segments of polyisocyanates can be aliphatic or aromatic, di-, tri-, or multifunctional, pure carbon chains or containing some biodegradable ester bonds [1–3,10]. A variety of polyols and polyisocyanates make PUs a class of polymers that can display thermoplastic, elastomeric, and thermoset behavior depending on their chemical and morphological characteristics [2]. The unsurpassed physical and chemical properties, along with their biocompatibility, have led to their use in a wide range of biomedical applications, including external applications as catheters, padding and bedding [1,3,11,12], cardiovascular applications [1,3,11,13–16], nerve guides [1,3,11,14,17], bone tissue engineered substrates [14,18], artificial organs [12], tissue replacement and augmentation, breast implantation, and wound dressings and adhesives [11,19,20].

Traditional and most commonly used PUs are linear multiblock polymers made by the polyaddition reaction between diols and diisocyanates. Diols can be polyesters, polyethers, other polymers with two terminal hydroxyl groups, or small molecular diols and their mixtures. Diisocyanates can be aliphatic, such as 1,6-hexamethylene diisocyanate (HDI) and isophorone diisocyanate (IPDI), or aromatic, such as toluene diisocyanate [2]. Using different types of diols and diisocyanates, various thermoplastic, elastic, or thermoset
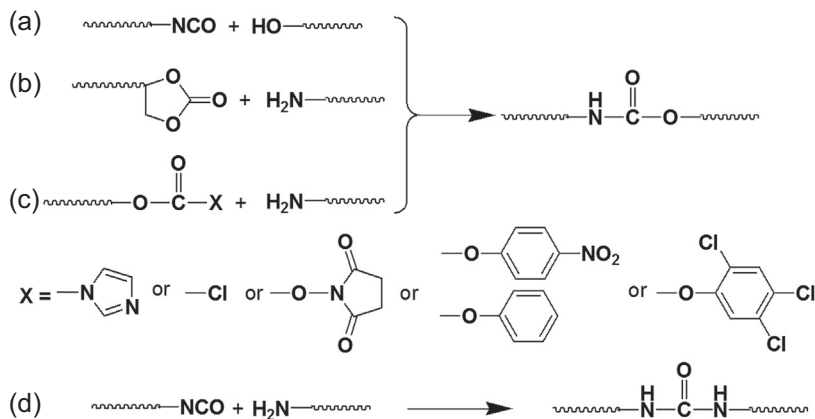
Figure 4.1 Representative urethane/urea chemistry reactions: (a) between isocyanate and hydroxyl groups (to form a urethane bond); (b) between a cyclic carbonate; activated carbonate, carbamate, or chloroformate derivative group and amino group (c); between isocyanate and amino groups (to form a urea bond) (d).

PUs have been developed and thoroughly investigated for various industrial and biomedical applications [1–3]. By alternately connecting soft and hard segments together through urethane bonds, assorted PUs, such as poly(ε-caprolactone) (PCL) containing block PUs [21], polylactide (PLA)-based PUs [22], and poly(ε-caprolactone-co-lactide acid) (PCLA)-based PUs [23], were prepared with useful shape-memory properties.

Since the synthesis and applications of traditional biodegradable PUs have been thoroughly reviewed by many other researchers, we will particularly analyze the biomedical applications of urethane/urea chemistry from a different view in this chapter. We will focus on the development of novel PUs, such as citrate-based urethane-doped polyesters, including cross-linked urethane-doped polyester elastomers (CUPE) [13,16], clickable CUPE (CUPE-click) [24], urethane-doped biodegradable photoluminescent polymers (UBPLPs) [15], photo-cross-linkable CUPE [25], and biodegradable citrate-based waterborne PUs and their clickable counterparts. In addition, their applications in cardiovascular and orthopedic applications, nerve regeneration, and drug delivery will be reviewed. We will also expand our discussion to nonisocyanate-based urethane reactions and nontraditional applications of isocyanate- and nonisocyanate-based urethane/urea chemistry in polymer synthesis, surface functionalization, polymer grafting, polymer cross-linking, peptide, protein, and deoxyribonucleic acid (DNA) bioconjugations.

4.2 Citrate-based urethane-doped polyesters

Different from traditional PUs designed for long-term implantation applications, PUs used for soft tissue engineering (e.g., cardiac, bone tissue, and neural engineering) and drug delivery should be able to decompose to nontoxic degradation products *in vivo*. One of the most common methods to synthesize biodegradable PUs is to incorporate biodegradable polyester macrodiol soft segments that hydrolyze *in vitro* and *in vivo*, such as PLA, poly(lactide-co-glycolide) (PLGA), and PCL.

Polyester is a group of polymers that contain the ester functional group in their chain. Esters are chemical compounds derived from a carboxylic acid and a hydroxyl compound, usually an alcohol. Most esters are considered biocompatible since they are endogenous to the human metabolism and able to break down to natural metabolic products by simple hydrolysis. Elastomers composed of aliphatic polyester chains cross-linked with each other by ester bonds, such as poly(diol citrates) and poly(glycerol sebacate) (PGS), have received much attention because they are soft, elastic, and biocompatible [26,27]. Yang et al. synthesized the first citrate-based biodegradable elastomer (CABE), poly(diol citrates), in 2004 using a convenient and cost-effective polycondensation reaction [26,28].

A key feature of CABEs is that citric acid serves as a robust multifunctional monomer in prepolymer formation through a simple polycondensation reaction while preserving pendant functionality for postpolymerization to produce a cross-linked polyester network with degradable ester bonds [29]. Citric acid is a nontoxic metabolic product of the Krebs cycle and has been used in Food and Drug Administration (FDA)-approved products or devices. Citric acid prevents blood clotting so it can function as an anticoagulant for blood specimens. In biomaterials, citric acid is mainly used to participate in the ester cross-link formation, but also enhances hemocompatibility, balances the hydrophobicity of the polymer network, and provides hydrogen bonding and additional binding sites for bioconjugation to confer an additional functionality such as optical properties. The pendant functionality gives the CABEs their unique degradation, mechanical, and optical properties over existing biomaterials.

However, traditional polyester elastomers lack mechanical compatibility with surrounding living tissues and the strategy for increasing cross-link density to improve their mechanical properties often makes them lose their flexibility. Although these polyester elastomer scaffolds have been proposed for tissue engineering of nerve tissues [30–32] and small diameter blood vessels [33], they are weak and unsuitable for engineering tissues such as ligaments, which require high tensile strength and load bearing ability. For example, the human anterior cruciate ligament has an ultimate tensile strength of at least 38 MPa [34], which is much higher than that of poly(diol citrates) (up to 11.15 ± 2.62 MPa). Sufficient mechanical strength is also desired for an ideal tissue-engineering scaffold especially during surgical handling following initial cell seeding. Maintaining proper mechanical strength becomes even harder when using elastomers for porous scaffolds. Polymers used for tissue engineering tend to lose a significant amount of mechanical strength when fabricated into porous scaffolds. For example, poly(diol citrate) underwent a significant loss in peak stress from 2.93 ± 0.09 MPa (film) to 0.3 ± 0.1 (scaffold) on pore introduction [33].

Thus, recent effort in biodegradable elastomer designs has focused primarily on developing a soft, strong, and completely elastic (100% recovery from deformation) material with balanced, tunable biodegradability and mechanical properties. For a decade, multifunctional CABEs with tunable mechanical and degradation properties for tissue engineering, drug delivery, bioimaging, and other applications have been developed [17]. The resulting materials have shown a wide range of mechanical properties, degradation profiles, and surface energies, which are all important in controlling the biological response to an implant. Recently, a new class of biodegradable elastomers, cross-linked urethane-doped polyesters (CUPEs), has been developed by doping urethane bonds in the poly(diol citrate) polyester

network [16]. CUPEs fuse the advantages of a fully elastic cross-linked polyester network with the high strength of linear PUs so they are soft and elastic with improved mechanical strength, which make them highly suitable for soft tissue-engineering applications. Briefly, the rationale behind CUPE synthesis was: (1) cross-linking confers excellent elasticity of CUPEs; (2) ester bonds confer degradability of CUPEs, all the cross-links of the polymer's network consist of ester bonds to ensure a degradable cross-linked polymer network; (3) introduction of urethane bonds into the polyester chains between ester cross-links enhances the hydrogen bonding within the polyester network, thus significantly improving the mechanical strength of the CUPE network. The first CUPE prepolymers were synthesized in two steps similar to previously published methods as shown in Figure 4.2 [16]. The first step involves the synthesis of a POC (poly(1,8-octanediol citrate)) prepolymer, which is chain-extended by 1,6-hexamethylene diisocyanate (HDI) in the second PU synthesis step. Briefly, a POC prepolymer was first synthesized by reacting a 1:1.1 monomer ratio of citric acid to 1,8-octanediol [35].

The purified POC prepolymer was then lyophilized for the next step of chain extension. In the second step, chain extension was achieved by dissolving pre-POC in 1,4-dioxane (3 wt%) and allowing it to react with HDI using stannous octoate as a catalyst (0.1 wt%). The reaction was terminated on the disappearance of the isocyanate peak located at $2267\,cm^{-1}$, which was determined by Fourier transform infrared (FT-IR) analysis. HDI was chosen here as a chain extender as it has previously been used in the synthesis of various biodegradable PUs [36–41]. To obtain cross-linked CUPE, the material was postpolymerized in an oven at $80\,°C$ for predetermined durations (0.5, 1, 2, 3 days). Free carboxylic acids and hydroxyl groups available on CUPEs allow for further biofunctionalization.

Subsequently, the physical and biological properties of CUPE both *in vitro* and *in vivo* [16] have been examined. The tensile strength of CUPE was as high as $41.07 \pm 6.85\,MPa$ while still maintaining over 200% elongation at break [16]. The initial modulus ranged from 4.14 ± 1.71 to $38.35 \pm 4.5\,MPa$. It is important to note that a simple chemical modification to the previous polyester network, poly(diol citrate) resulted in over a 10-fold increase in mechanical strength [42]. Mechanical properties are known to be involved with different material and process parameters such as the (1) choice of diol, (2) choice of isocyanate and its molar ratio used during synthesis, and (3) postpolymerization conditions. Consequently, these parameters can be used to modulate the material properties of CUPEs, which ultimately affect their biological performance *in vitro* and *in vivo*.

Higher tensile strength of CUPE was obtained by increasing the amount of isocyanate, polymerization time, or temperature used during the synthesis. Various CUPE prepolymers were synthesized using different molar feeding ratios of the pre-POC:HDI (1:0.6, 1:0.9, 1:1.2 M ratio) to evaluate the influence of HDI on CUPEs. The properties of CUPE polymers can also be controlled by varying the diol content. Various diols can be used to control the material performance and create a family of elastomers with their diols varied in their methylene content. Dey et al. conducted a detailed investigation on the development of CUPE polymers synthesized using diols with 4, 6, 8, 10, or 12 methylene units in an attempt to elucidate the influence of the diol component on the physical properties of the resulting material and assessing
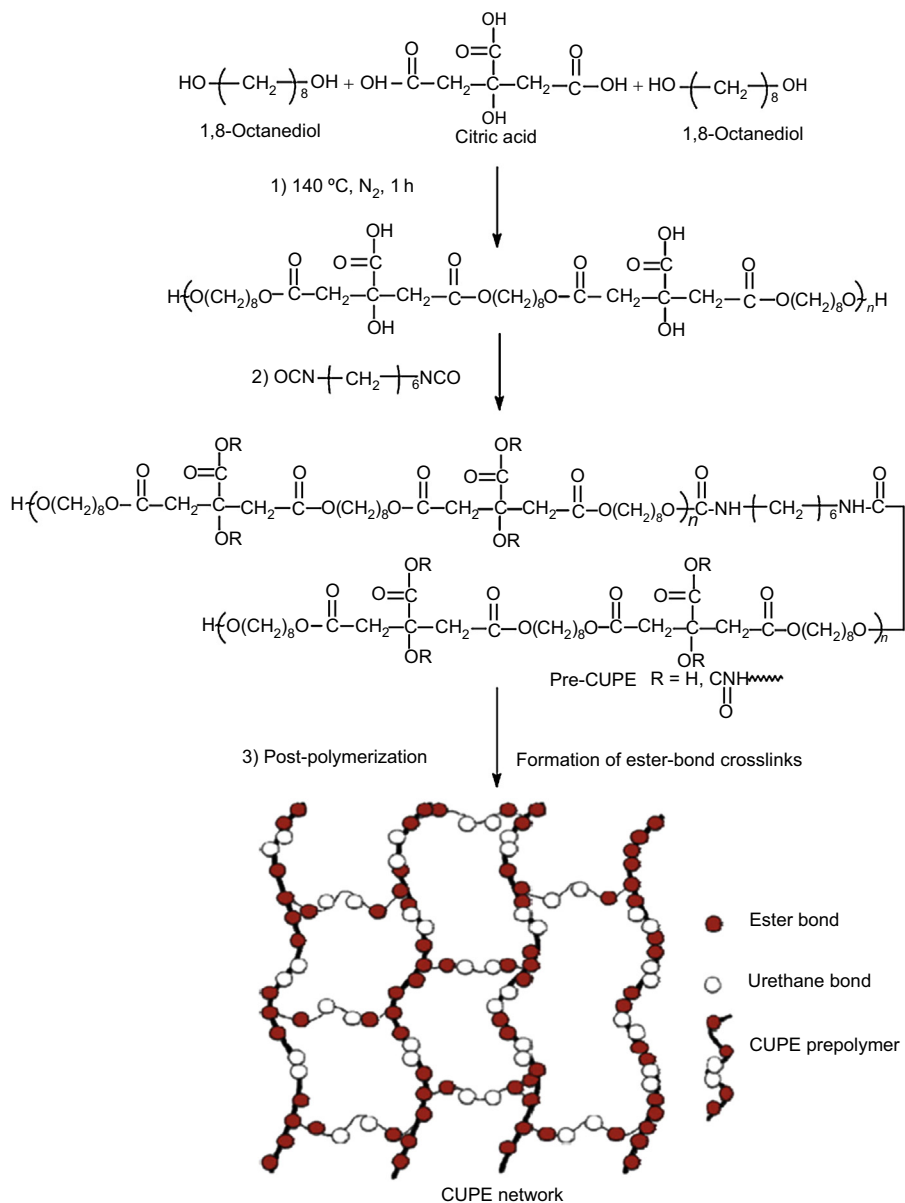
Figure 4.2 Schematic representative of cross-linked urethane-doped polyester (CUPE) synthesis.
Reprinted with permission from Ref. [16]. Copyright © 2008, Elsevier Ltd.

their long-term biological performance *in vivo* [43]. They prepared CUPE polymers using diols with different numbers of carbon atoms, while maintaining the constant ratio 1:1.2 of the soft segment prepolymer/diisocyanate. Along with the diol content, polymerization times were varied from 1 to 4 days. It was found that increasing the diol length leads to a lower cross-linking density, higher hydrophobicity, higher tensile strength and elasticity, and slower polymer degradation.

Initial contact angles of the CUPE prepolymer films were affected by the diol used during the synthesis. Incorporating polyethylene glycol (PEG) into the diol segment of the polymer chain increased the hydrophilicity, thus reducing the initial contact angle. CUPE films made with 1,8-octanediol were more hydrophobic with an average contact angle of $94.20 \pm 2.87°$. Meanwhile, HDI played a negligible role in affecting the initial contact angles of CUPE films. It is likely due to the fact that the urethane-bonded segment formed a small portion of the polyester chain and did not significantly influence the wettability of the material.

By controlling the temperature and time of postpolymerization, the elastomer's mechanical properties and degradation rate can be tuned to fit a wide range of tissue-engineering applications. An increase in postpolymerization temperature and time resulted in a network with increased mechanical properties due to the increased cross-linking density. The introduction of CUPEs presents new avenues to meet the versatile requirements for tissue engineering and other biomedical applications.

CUPEs demonstrated good *in vitro* and *in vivo* biocompatibility. Hemocompatibility studies indicated that CUPE adhered and activated a lower number of platelets compared to poly(L-lactic acid) (PLLA) [16]. In addition to biocompatibility, CUPEs facilitate processing of the materials into highly porous structures compared to other poly(diol citrates); the higher molecular weights and nonsticky nature of the CUPE prepolymers allow the use of fabrication techniques such as thermally induced phase separation (TIPS) technique and electrospinning. Soft and elastic CUPE three-dimensional porous sheets (150 μm thick) fabricated from a simple TIPS allowed for even seeding, growth, and distribution of 3T3 fibroblasts. Good mechanical properties, processibility, and biocompatibility make CUPE materials well suited for soft tissue-engineering applications.

4.2.1 Photo-cross-linkable citrate-based urethane-doped polyesters

Photo-cross-linkable biomaterials can be of interest in biomedical applications (i.e., as they may allow *in situ* polymerization directly in or on tissues). They may provide advantages including localized drug delivery for site-specific action, ease of application, and a reduction in the dosage amount. A citrate-based photo-cross-linked biodegradable elastomer was developed, poly(octamethylene maleate citrate) (POMC), derived from the previously reported POC material [44]. POMC preserves pendant hydroxyl and carboxylic functionalities even after cross-linking, keeping both available for potential conjugation of biologically active molecules.

POMC films promoted the adhesion and proliferation of human aortic smooth muscle cells and NIH-3T3 fibroblast cell lines and demonstrated minimal inflammatory response when subcutaneously implanted in Sprague–Dawley rats. The success in

designing POMC prompted the development of another novel photo-cross-linkable urethane-doped polyester elastomer (CUPOMC) by reacting POMC prepolymers with HDI followed by thermo- or photopolymerization [25].

The synthesis of CUPOMCs was carried out in the following three steps (Figure 4.3). The monomers, citric acid and 1,8-octanediol, and maleic acid underwent
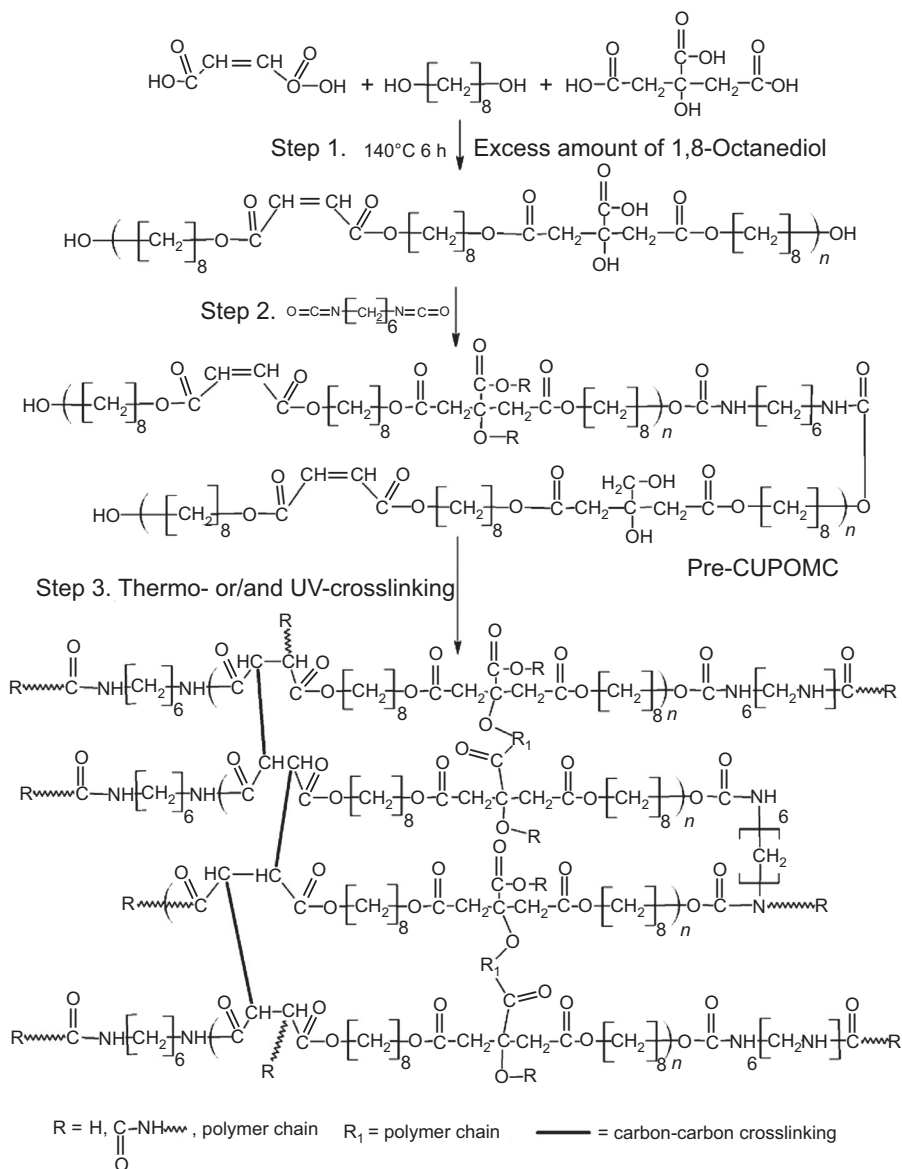
Figure 4.3 Schematic diagram for the synthesis of CUPOMC.
Reprinted with permission from Ref. [25]. Copyright © 2011, ICI Global.
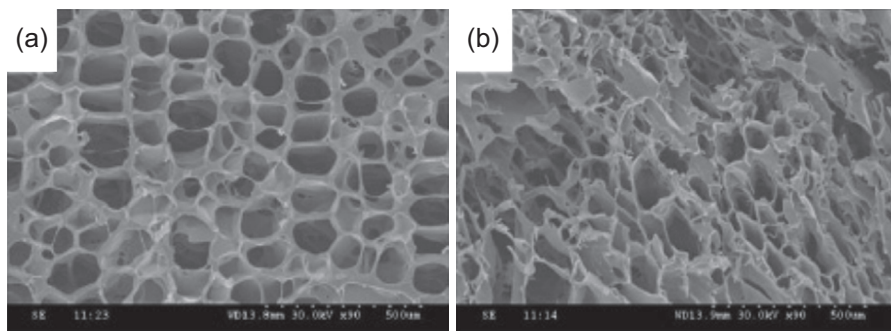
Figure 4.4 SEM images of (a) the surface and (b) cross-section of a CUPOMC-0.2–0.8–1.1–1.0 scaffold thermally cross-linked at 80 °C for 1 day. Reprinted with permission from Ref. [25]. Copyright © 2011, ICI Global.

polycondensation to yield hydroxyl group capped pre-POMC in step 1. In step 2, 1,6-hexamethylene diisocyanate (HDI) was used to extend the pre-POMC chain. In step 3, pre-CUPOMC was thermo- and/or UV-cross-linked to obtain the CUPOMC network. Similar to CUPEs, mechanical properties of the CUPOMCs can be tuned by varying the molar ratios of pre-POMC monomers and the prepolymer:HDI ratios. The mechanical strength and elongation at break of the CUPOMCs range from 0.73 ± 0.12 to 10.91 ± 0.64 MPa and from $72.91 \pm 9.09\%$ to $300.41 \pm 21.99\%$, respectively.

The results suggest that doping urethane bonds in photo-cross-linkable POMCs to make CUPOMCs did not compromise the elasticity, thus making CUPOMCs a candidate for soft tissue engineering. CUPOMCs can be cross-linked into a three-dimensional network via either polycondensation or UV polymerization. Using thermal polymerization, a highly interconnected porous CUPOMC structure was built (Figure 4.4). Tensile tests on the pre-CUPOMC scaffolds confirmed the elastic property of the material (Young's modulus, 0.09 ± 0.01 MPa; elongation at break, $192.44 \pm 24.76\%$).

4.2.2 Urethane-doped biodegradable photoluminescent polymers

CABEs have demonstrated excellent biocompatibility *in vivo* animal studies [16–18,43]. Although it is recognized that the scaffold degradation rate should match the rate of new tissue formation [45], biomaterial designs to control the *in vivo* scaffold degradation rate remain empirical due to the lack of *in vivo* quantitative validation. Histological analysis is commonly used for probing such processes, but it is an end-point measurement and requires sacrifice of an animal for each time point [46]. It is imperative to find an *in situ* real-time method to facilitate tracking or monitoring tissue regeneration and scaffold degradation processes without sacrificing animals. This issue has been rarely addressed previously.

To meet this unmet need in regenerative tissue engineering, a breakthrough was recently made in developing soft and elastic biodegradable photoluminescent polymers (BPLPs) with tunable and *in vivo* detectable fluorescence with emission from

blue to near infrared (up to 725 nm) that can function as a noninvasive, real-time imaging probe to monitor the scaffold degradation and tissue infiltration/formation by measuring the fluorescence decay over time *in vivo* [15,47,48]. It is notable that BPLPs' tunable fluorescence emission results by the use of different natural amino acid residues. For example, BPLP-serine (BPLP-Ser) emits strong red fluorescence.

Although BPLPs are attractive materials for tissue engineering and drug delivery, the tensile strength of BPLPs is 6.5 ± 0.8 MPa, which is not sufficient for certain tissue-engineering applications (e.g., vasculature grafts). To address the above challenges, UBPLPs were synthesized [15]. As shown in Figure 4.5(a), BPLPs were first synthesized via condensation polymerization of 1.0:1.1:0.2 monomer ratios of citric acid, 1,8-octanediol, and L-cysteine, respectively. Next, the BPLP prepolymer (3 w/v% in 1,4-dioxane) was chain-extended at 55 °C with HDI to obtain UBPLP using stannous octoate as a catalyst. The reaction was terminated on the disappearance of the isocyanate peak located at $2267 \, cm^{-1}$, determined by FT-IR analysis. The resulting UBPLP was cross-linked in an oven maintained at 80 °C for predetermined periods to obtain cross-linked urethane-doped BPLP or CUBPLP.

Mechanical properties of UBPLPs were manipulated by (1) postpolymerization conditions, (2) feeding ratio of diisocyanates, and (3) choice of amino acids. A dramatic improvement was made by doping with urethane bonds (tensile strength, 49.41 ± 6.17 MPa; elongation at break, $456.60 \pm 62.49\%$) from the previously reported mechanical strength of cross-linked BPLP (tensile strengths, 6.50 ± 0.80 MPa; elongation, $240 \pm 36\%$) [47]. UBPLPs synthesized with different amino acids retained their fluorescent properties. This confirms that the fluorophores of BPLPs remained intact during the synthesis of UBPLPs, although the chain extension of BPLPs caused some loss of fluorescence intensity after urethane bond doping, due to the increased average number of fluorophores per polymer chain. Degradation properties can also be modulated by varying the feeding ratios of diisocyanate to prepolymers and the choice of amino acids.

The potential of using UBPLPs as an organic dye-free theranostic system has been evaluated. Using a nanoprecipitation technique, UBPLP-Ser 1.2 was able to form nanoparticles in PBS (Figure 4.5(b)). Nanoparticles have a spherical shape with an average diameter of 103 nm. The cytocompatibility of UBPLP nanoparticles was also found to be significantly higher than quantum dots at all dilutions and comparable to PLGA nanoparticles at 2, 10, and 50X dilutions. Tubular triphasic scaffolds made of CUBPLP-Cys and CUBPLP-Ser 1.2 were subcutaneously implanted in the back of black mice for *in vivo* fluorescence imaging (Figure 4.5(d)). Fluorescence was detected with a concentration of the UBPLP-Ser 1.2 at 5 mg/mL (Figure 4.5(e)). UBPLPs present new avenues for noninvasive and real-time assays to advance the fields of tissue engineering and drug delivery.

4.2.3 Click chemistry to enhance citrate-based urethane-doped polyesters

Click chemistry represents a rapid, selective, and high-yielding bioorthogonal reaction that is also capable of immobilizing materials on cell surfaces [49,50]. To further expand click chemistry-based elastomers, Guo et al. introduced click chemistry into
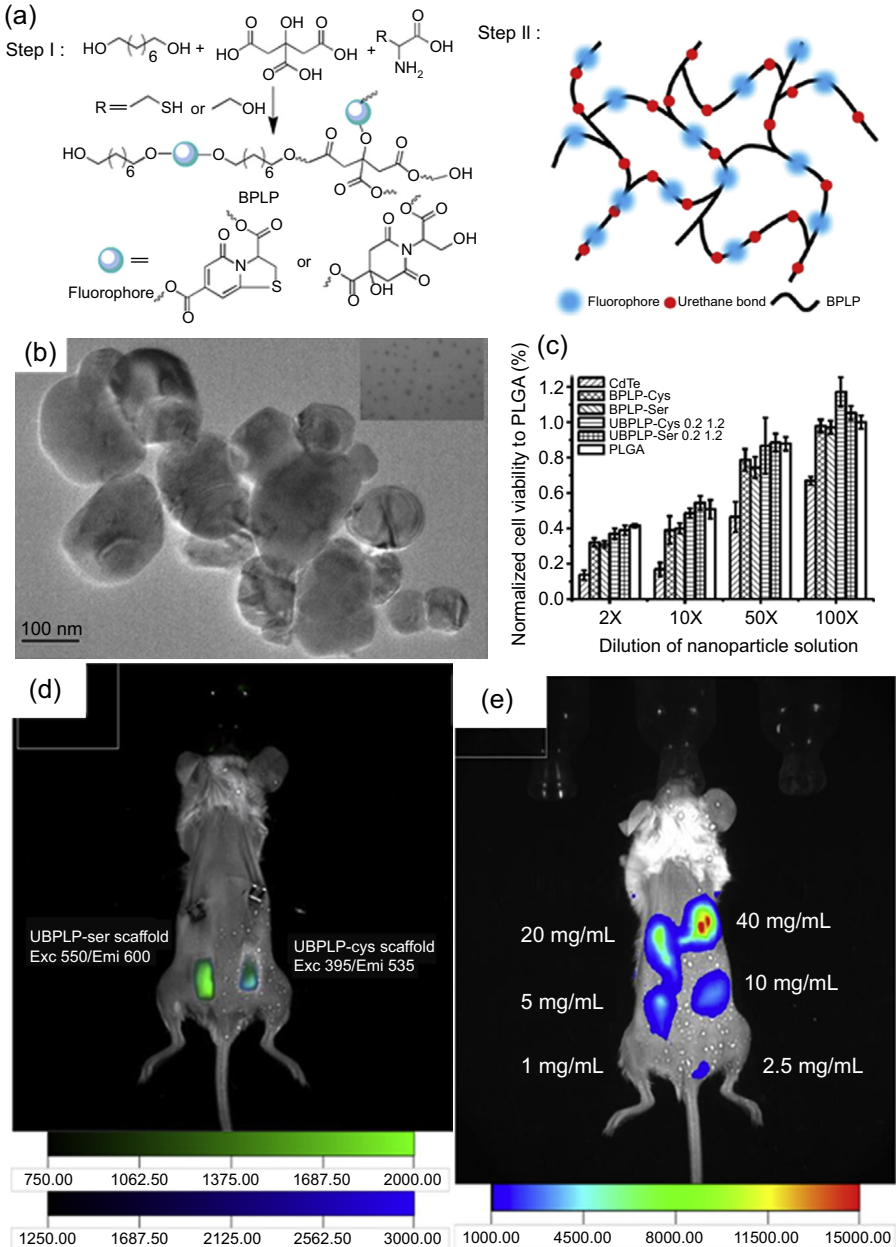
Figure 4.5 (a) Synthesis of UBPLP polymers; (b) TEM images of UBPLP-Ser 1.2 nanoparticles. Inset image was captured under higher magnification showing evenly dispersed nanoparticles; (c) cytotoxicity evaluation of BPLP and UBPLP nanoparticle solutions at different dilutions. PLGA nanoparticles as a control; (d) combined fluorescence images of CUBPLP-Cys and CUBPLP-Ser triphasic scaffolds implanted in a black mouse; (e) *in vivo* fluorescence images of UBPLP-Ser nanoparticles at various concentrations injected subcutaneously in the back of a black mouse.

Reprinted with permission from Ref. [15]. Copyright © 2013, Elsevier Ltd.

CABEs as a strategy to both improve mechanical properties and enable facile surface site-specific bioconjugation [24].

Azide and alkyne groups were introduced to POC prepolymers to synthesize pre-POC-N$_3$ and pre-POC-Al, respectively (Figure 4.6(a)). Pre-POC-N$_3$ and pre-POC-Al were cross-linked via a thermal synchronous binary (TSB) cross-linking mechanism to make POC-clicks (Figure 4.6(b)). In the TSB cross-linking, thermal click reaction between azide groups and alkyne groups and esterification between –COOH and –OH groups took place simultaneously to form TSB cross-linked POC-click polymers. The introduction of click chemistry into POCs improved their mechanical properties significantly. For example, the wet mechanical strength of POC-click was stronger than that of CUPE [16].

Cross-linked urethane-doped polyester clickable prepolymer (UPE-click) was synthesized by chain-extending pre-POC-click macromolecules (pre-POC-N$_3$ and pre-POC-Al) with HDI as a chain extender using the weight ratio 1:0.22 of pre-POC-click:HDI followed by TSB cross-linking. The TSB cross-linked polymer (CUPE-click) showed significantly enhanced mechanical strength compared to normal CUPE. As shown in Figure 4.6(c) and (d), click chemistry also fortified the mechanical strength of CUPE and CBPLP materials after chemical modification with azide and alkyne groups and TSB cross-linking.

The residual azide groups on the surface of click materials can be sites for convenient and efficient bioconjugation. As an example, collagen mimetic peptide p15 was conjugated onto the surface of POC-click-3 films by strain-promoted azide–alkyne cycloaddition (SPAAC) and the viability and proliferation of human umbilical vein endothelial cells (HUVECs) on POC-click-3-p15 films were investigated. Based on the methylthiazolyldiphenyl-tetrazolium bromide (MTT) results, HUVEC proliferation on POC-click-3-p15 films was much faster than that on untreated POC-click-3 films. The HUVEC cell density on POC-click-3 films was nearly twice that of the control POC-click-3 films. The results suggest that the same SPAAC method can be utilized for conjugating CUPE-click materials with such biomolecules for various biomedical applications.

The triazole rings formed by click reactions were recently found to possess antimicrobial properties. The large dipole moment of triazole modulates N-2 and N-3 nitrogen atoms present in the triazole ring as good H-bond acceptors [51]. The hydrogen-bonded triazole acts as a biologically active site that protects the material from bacterial and fungal attacks. The antimicrobial property of triazoles is expected to make CUPE-click more promising for future applications in tissue engineering.

4.2.4   Applications

4.2.4.1   Vascular grafts

To demonstrate the feasibility of using CUPEs as a tissue engineered vascular graft (TENG), Dey et al. developed biphasic CUPE scaffolds prepared as previously reported [33]. The nonporous phase was created by dip coating a glass rod (outer diameter 3 mm) in a 3 w/w% CUPE0.9 in 1,4-dioxane. The prepolymer coated glass rods were air-dried and cross-linked for 12 h in an oven at 80 °C. The porous phase
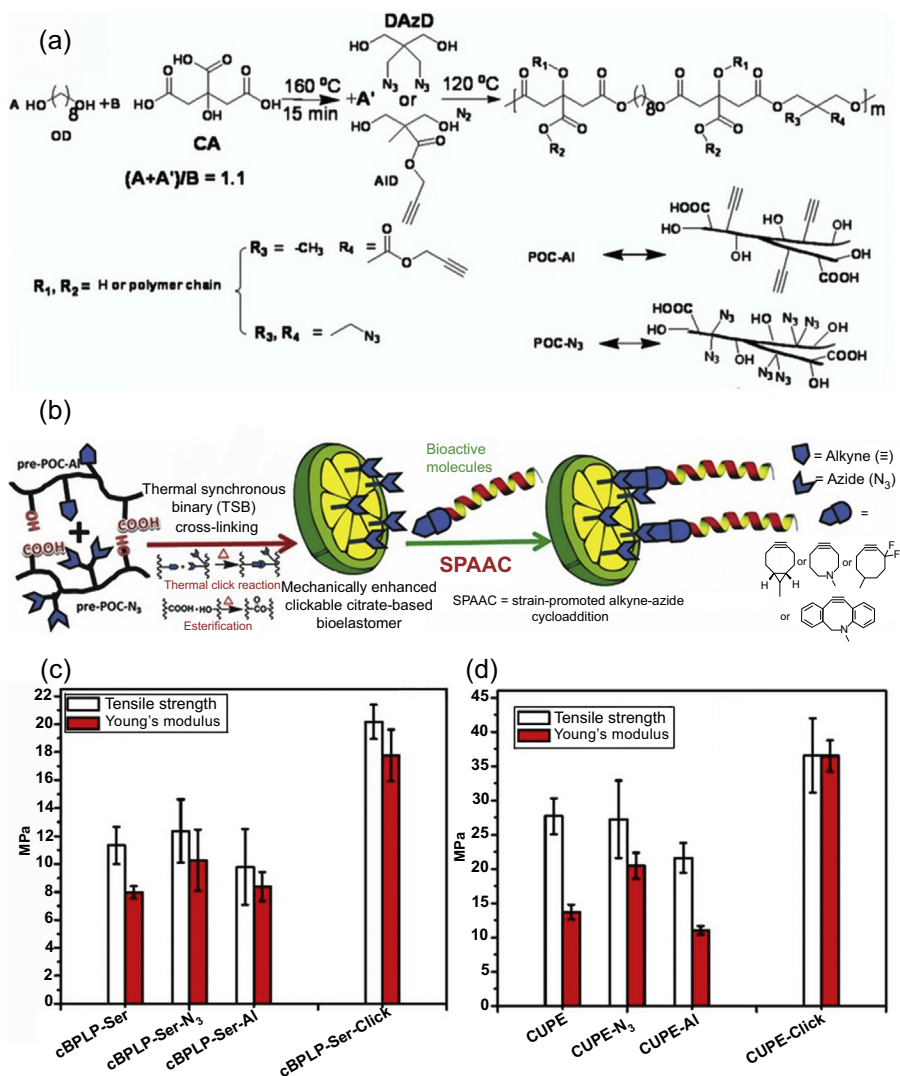
Figure 4.6 (a) Synthesis of functional POC prepolymers: POC-N$_3$ and POC-Al; (b) cartoon illustration of a new class of citrate-based biodegradable clickable elastomers (CABEs) with greatly improved mechanical strength and easily clickable surface for biofunctionalization; (c) mechanical properties of cBPLP-Ser, cBPLP-Ser-N$_3$, cBPLP-Ser-Al, and cBPLP-click (cBPLP-Ser-N$_3$, Al) polymers; (d) mechanical properties of CUPE, CUPE-N$_3$, CUPE-Al, and CUPE-click (CUPE-N$_3$, Al) polymers. The polymers used in (c) and (d) were cross-linked at 100 °C for 3 days.
Reprinted with permission from Ref. [24]. Copyright © 2014, Wiley-VCH Verlag GmbH & Co. KGaA, Weinheim.

consists of a 3 w/w% solution of CUPE0.9 in 1,4-dioxane mixed with salt particles (150–250 μm) in a 1:9 ratio by weight. The biphasic scaffolds were prepared by (1) casting the slurry into tubular poly(tetrafluorethylene) molds (inner diameter 6 mm), or by (2) inserting the partially polymerized nonporous phase, consisting of the glass rod with the prepolymer coats, concentrically into the mold. Purely porous salt-leached scaffolds were used as controls.

The prepared CUPE material was evaluated for its mechanical properties (tensile strength, burst pressure, and suture retention) and hemocompatibility as a potential blood-contacting vascular graft material. The tensile strength of CUPE biphasic scaffolds (5.02 ± 0.70 MPa) was greater than that of native vessels (1.43 ± 0.60 MPa). CUPE scaffolds showed tunable burst pressure between 1500 and 2600 mm Hg and their suture retention values were 2.45 ± 0.23 N. CUPE scaffolds exhibited mechanical properties similar to those of native veins and arteries. Hemocompatibility of CUPE *in vitro* was evaluated by assessing blood clotting characteristics, leukocyte activation, inflammatory cytokine release, and red blood cell hemolysis. The results showed that CUPE is less prone to thrombosis and inflammation, compared to PLLA. CUPE also behaved similarly to PLLA in terms of leukocyte activation. Suitable mechanical properties combined with a reduced tendency to cause thrombosis make CUPE a promising material for implantation in *in vivo* vascular tissue-engineering applications.

4.2.4.2   Bone tissue engineering applications

In the field of bone tissue engineering, it is highly desirable to design mechanically strong and osteoconductive scaffold materials for orthopedic applications. A class of citrate-based polymer blends (CBPBs) with hydroxyapatite (HA) (CBPBHAs) was developed for bone regeneration [18]. Citrate makes up about 5 wt% of the organic component in bone, and is responsible for regulating and stabilizing apatite nanocrystals. Additionally, a study has shown that citrate has an innate ability to induce the HA formation in simulated body fluid (SBF) [52]. It was hypothesized that the mechanically strong CUPE material increased the strength of the resulting material to meet the load-bearing requirements of orthopedic devices. In addition, the introduction of an optimal percentage of carboxyl-rich POC into the CUPE network helps the polymer/HA interactions to better mimic the inorganic composition of bone.

For these reasons, HA was used in CSPBs to better replicate the natural bone citrate and inorganic mineral content to produce a more biomimetic material and to enhance bone formation (Figure 4.7(a)).

CBPBHA composites were fabricated in three steps. First, a mixture of CUPE and POC prepolymers was prepared by dissolving POC prepolymer in 1,4-dioxane and mixing with various weight ratios of CUPE prepolymer to form a homogeneous CSPB. In the second step, various CBPBs were mixed with 65 wt% HA and stirred in Teflon dishes, which were prewarmed to 50 °C to help solvent evaporation, until a homogeneous mixture was formed. Following solvent evaporation, the mixture was inserted into machined cylindrical metal molds and compressed into rod-shaped samples. In the final step, the resulting cylindrical composites were postpolymerized for

1 day to form a cross-linked CBPBHA-X composite (where X denotes the weight ratio of CUPE in CBPB).

The CBPBHA composite material possesses a compressive strength of 116.23 ± 5.37 MPa, comparable to human cortical bone (100–230 MPa). *In vitro* mineralization of CBPBHA composites was assessed in SBF. CBPBHA exhibited a rapid mineralization in SBF and showed promising osteoconductivity results (Figure 4.7(b)). As shown in Figure 4.7(c) and (d), it also increased osterix gene (obstoeblast-specific transcription factor required for osteoblast differentiation and bone formation) and alkaline phosphatase (an early osteoblast differentiation gene marker for bone formation) gene expression in C2C12 (a typical pluripotent mesenchymal cell line) cells. The role of soluble citrate was also investigated to show that exogenous
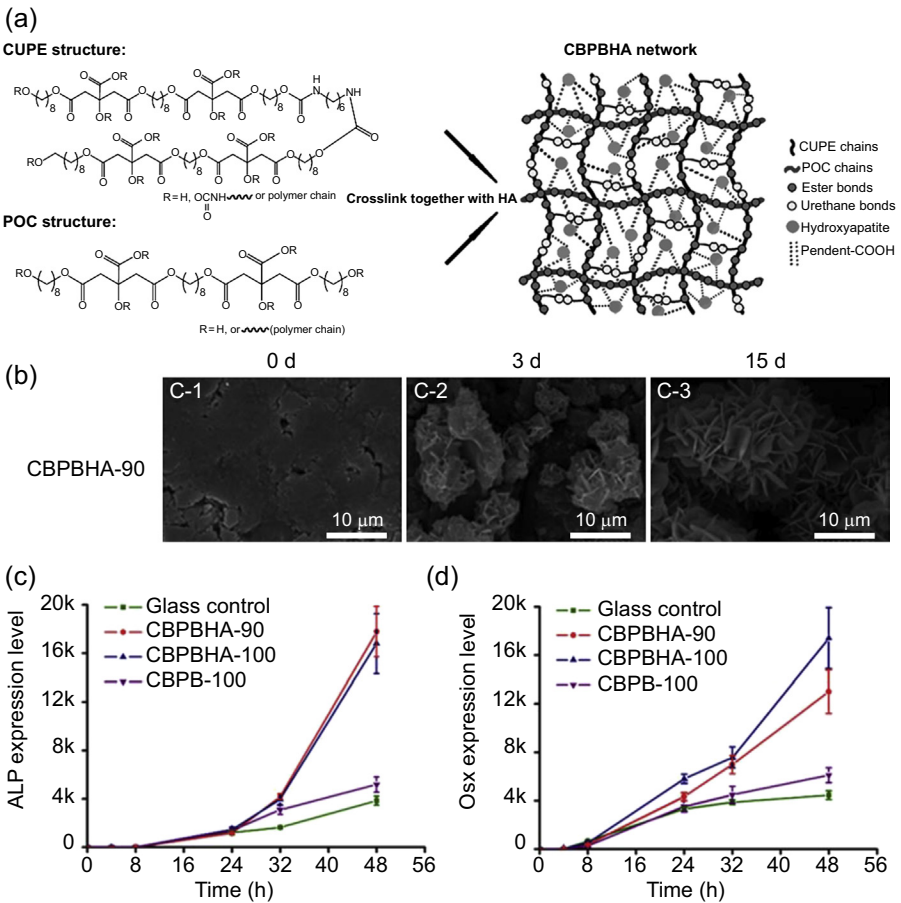
Figure 4.7 (a) Schematics of CBPBHA composites; (b) representative SEM images of CBPBHA-90 composites mineralized in 4X simulated body fluid (SBF) at 0, 3, and 15 days; (c) alkaline phosphatase (ALP); and (d) osterix (Osx) gene expression of C2C12 cells cultured on CBPB and CBPBHA films.

citrate supplemented into cell media improved the *in vitro* phenotype progression of MG-63 (a *Homo sapien* bone osteosarcoma) osteoblasts. CBPBHA composites induced minimal fibrous tissue encapsulation and were well integrated with the surrounding tissues after 6 weeks of implantation in a rabbit lateral femoral condyle defect model. This study highlighted the role of citrate molecules that had previously been overlooked.

4.2.4.3 Nerve applications

To demonstrate the applicability of using our soft, elastic, and biodegradable CUPE for nerve tissue engineering, TENGs for peripheral nerve regeneration were designed [17]. Porous, suturable, and multichanneled CUPE TENGs were fabricated using microengineering approaches and particulate leaching (Figure 4.8). Elastic CUPE TENGs showed an ultimate peak stress of 1.38 ± 0.22 MPa and a corresponding elongation at break of $122.76 \pm 42.71\%$, which were comparable to those of native nerve tissue. Our CUPE TENGs were successfully implanted to repair a 1 cm sciatic nerve defect. They showed comparable performance with nerve autografts and outperformed
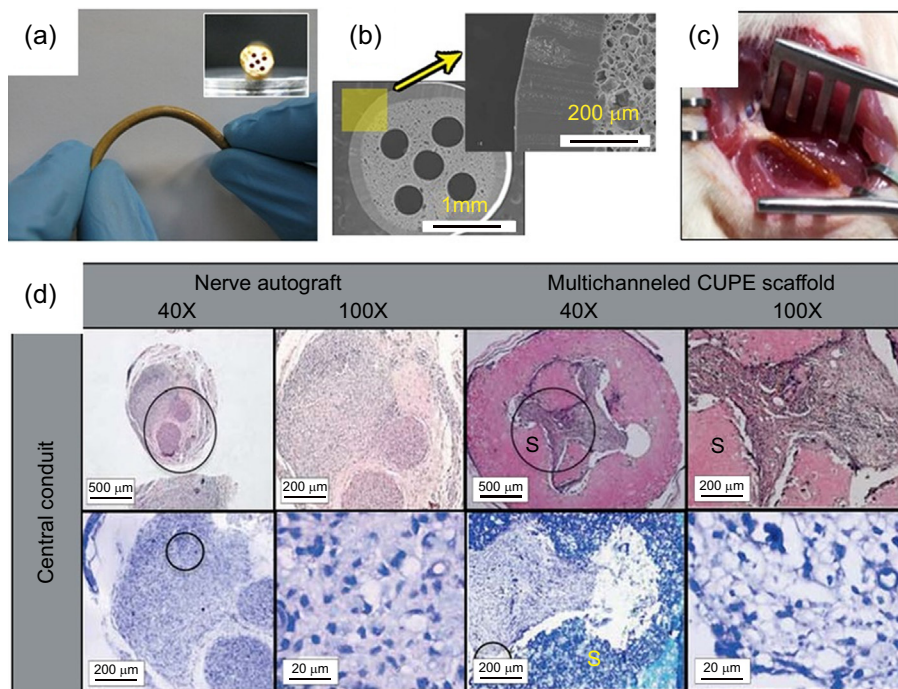
Figure 4.8 (a) Multidirectional bend without kinks to show soft and elastic nature of CUPE materials; (b) scanning electron microscope images of porous and elastic multichannel CUPE TENG with five channels; (c) surgical image of a rat with the implantation of CUPE scaffold; (d) microscopic images of a semithin cross-sections of tissue explants stained with H&E (top row) and toluidine blue (bottom row).
Reprinted with permission from Ref. [17] Copyright ©2014, Wiley Periodicals, Inc.

PCL hollow tubes in terms of fiber population and densities 8 weeks after their implantation. The elastic and biomimetic CUPE TENGs could serve as off-the-shelf nerve conduits for peripheral nerve regeneration.

4.3   Waterborne polyurethane biomaterials

4.3.1   *Waterborne polyurethane technology*

Traditional solvent-based PUs have long established the standard for high performance systems. However, due to high levels of volatile organic compounds (VOCs) in solvent-based PUs, serious concerns have emerged about environmental and application safety in the use of typical solvent-based PUs [53]. Waterborne PU technology uses water as the primary dispersion solvent. The resultant waterborne PU materials have many advantages: (1) zero or very low levels of VOCs (environmentally friendly), (2) absence of isocyanate residues (nontoxic), and (3) good applicability, versatility, and a wide range of superior properties, such as abrasion resistance, impact strength, and low temperature flexibility. As such, waterborne PUs have rapidly become important materials used in diverse applications [54].

An aqueous waterborne PU dispersion is a binary colloid system in which PU particles range in size from 0.01 to 5.0 μm [55]. The effective method for making PU dispersible in water is to introduce ionic and/or nonionic hydrophilic moieties into its backbone structure. The most important and practical type of waterborne PU is the anionic type. This type of waterborne PU possesses pendant ionized carboxylic acid groups [56]. Anionic waterborne PUs with carboxylic acid groups can be synthesized by a four-step process, which is schematically presented in Figure 4.9.

In the first step, macromonomer diisocyanate is prepared by reacting excess diisocyanate with a long-chain polyol and/or low-molecular-weight glycol. Then, carboxylic acid-containing macromonomer diisocyanate is prepared through the hydrophilization of macromonomer diisocyanate in a second step, where bis-hydroxycarboxylic acid, such as dimethylolpropionic acid (DMPA), is incorporated into the backbone of macromonomer diisocyanate. The next step involves the neutralization of carboxylic acid with tertiary amine. Finally, the anionic PU prepolymer is vigorously sheared and stirred in water with diamine. Chain extension in water causes the residual isocyanate groups to transform into urea linkages resulting in an anionic PU that is stably dispersed in water.

4.3.2   *Design and synthesis of waterborne polyurethane biomaterials*

Most conventional waterborne PUs derived from petroleum resources are not biorenewable or biodegradable. The most common method to obtain biorenewable and/or biodegradable waterborne PU is to incorporate bio-based and/or biodegradable components into a waterborne PU backbone during polymer synthesis.
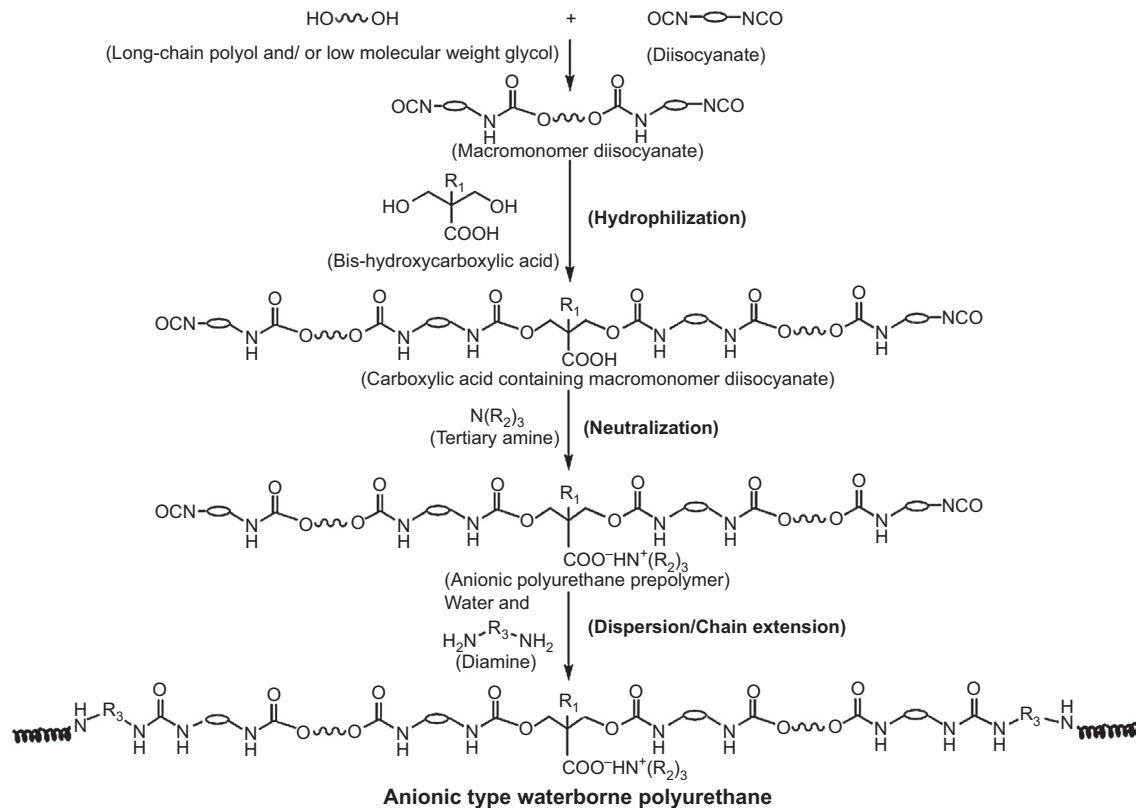
Figure 4.9 Representative schematic synthesis process of carboxylic acid-type anionic waterborne polyurethane.

4.3.2.1 Introduction of bio-based materials into waterborne polyurethanes

Vegetable oils are widely used bio-based renewable resources due to their low toxicity, inherent biodegradability, ready availability, and relatively low price. As such, a great deal of effort has been made to develop waterborne PUs from vegetable oils [57,58]. Castor oil, which has inherent hydroxyl groups in its structure, was the first vegetable oil directly used in the synthesis of waterborne PUs. Other vegetable oils, such as sunflower, corn, palm, rapeseed, soybean, and linseed oils, must be modified into polyols for synthesizing waterborne PUs [59,60].

Vegetable oil-based polyols are long-chain polyols that offer promise in producing biorenewable waterborne PUs. Castor oil-based waterborne PUs show good mechanical properties in terms of both tensile strength (9.3 ± 1.5 MPa) and elongation at break ($520 \pm 20\%$). Thus they have been used to modify plasticized starch to prepare novel biodegradable materials with high performance [60]. Waterborne PUs containing 50–60 wt% of biorenewable components have been prepared using methoxylated soybean oil polyols (MSOLs) with hydroxyl functionality ranging from 2.4 to 4.0 by Lu and Larock. Particle sizes of the resultant waterborne PUs range from 12 to 130 nm. An increase in the hydroxyl functionality of the MSOL significantly improved the cross-link density of the waterborne PUs and resulted in biorenewable PUs ranging from elastomeric polymers to ductile plastics [61]. A challenge in the synthesis of vegetable oil-based, environmentally friendly waterborne PU is the high cross-linking of the PU prepolymers caused by high hydroxyl functionality of the vegetable oil-based polyols. Vegetable oils are also susceptible to hydrolytic breakdown due to the three ester bonds in their structure. Vegetable oil-based waterborne PU bonds may degrade when exposed to excessive humidity, releasing amines and carbon dioxide and they are also susceptible to microorganism attack [62].

Chain extenders can also be substituted with bio-based components in the synthesis of waterborne PUs. For example, chitosan, a derivative of abundant naturally occurring polysaccharides that has active amino groups, can be used to chain-extend waterborne PUs in water. Chitosan possesses unique biological properties such as nontoxicity, biocompatibility, anticoagulant properties, and biodegradability. Waterborne PU films synthesized with chitosan as a chain extender exhibited excellent mechanical and anticoagulating properties, as well as antibacterial and antifungal activities [63].

Gelatin from cold fish skin also can be introduced into waterborne PUs by covalent bonding, to reinforce and render biodegradability. Lee et al. chemically modified gelatin with vinyltrimethoxysilane and incorporated the modified gelatin into waterborne PU with terminal hydroxyl ethyl acrylate groups by UV polymerization. The waterborne PU showed excellent mechanical properties and water-resistant properties along with significantly enhanced biodegradability both in trypsin solution and in soil [64].

4.3.2.2 Introduction of biodegradable polyesters into waterborne polyurethanes

To render waterborne PUs biodegradable, researchers have attempted to incorporate biodegradable polymeric materials into the backbones of waterborne PUs. The biodegradable polymeric materials can be long-chain polyols, chain extenders, or

diisocyanates. Among biodegradable long-chain polyols, PCL diols, PLA diols, poly(lactic acid-caprolactone) (PLCL) diols, and PLGA diols are often used for the synthesis of biodegradable waterborne PUs. However, it is reported that satisfactory mechanical properties (e.g., elongation higher than 25%) are not obtainable by merely reacting a single PLA diol as a long-chain polyol component [65]. Biodegradable long-chain polyols and conventional polyether/polyester polyols are often synergistically used in the synthesis of waterborne PUs to adjust the biodegradability and the film-forming properties of waterborne PUs [66].

Recently, a breakthrough on the development of biodegradable photoluminescent prepolymers (BPLPs as described in Figure 4.10(a)) with superior inherent photoluminescence and photostability has been made [47]. BPLP–cysteine, a hydroxyl-terminated aliphatic polyol, is fully biodegradable and biocompatible. It can be used as a long-chain polyol to produce biodegradable BPLP-based waterborne polyurethane (BPLP-WPU as in Figure 4.10(b)). The emission spectra of the obtained BPLP-WPU excited at different wavelengths of 335, 365, 380, 425, 455, and 485 nm are shown in Figure 4.10(c), which demonstrates the versatile and strong photoluminescence of BPLP-WPU. Nanomicelles of BPLP-WPU are distributed evenly in water with the average size of 20–30 nm as shown in Figure 4.10(d). The resulting photoluminescent waterborne polyurethane can be used as noninvasive bioimaging elastomeric films and porous scaffolds in tissue engineering, as well as amphiphilic fluorescent nanomicelles for theranostic drug delivery.

Many amino acid derivatives can be used as chain extenders for the synthesis of PUs in bulk or in organic solvents. Among natural amino acids, water soluble L-lysine, which contains two active amino groups and one carboxyl group, is a good extender candidate for waterborne PUs [36]. Low-molecular-weight L-lysine can be incorporated as a biodegradable component to help the degradation of high-molecular-weight waterborne PUs. Waterborne PUs made from isophorone diisocyanate (IPDI), DMPA, and PCL were prepared and chain-extended in water using L-lysine by Chen et al. [67]. Results demonstrated that the prepared waterborne PU films exhibited excellent mechanical properties, good anticoagulating characteristics, desirable water swellability, and hydrolysis properties. Jiang et al. have successfully prepared nontoxic waterborne biodegradable PU by using IPDI, 1,4-butanediol (BDO), and L-lysine as hard segments, and PEG and PCL as soft segments with a molar feed ratio of IPDI/PCL/PEG/BDO/L-lysine = 3/0.75/0.25/0.85/0.85. Three-dimensional interconnected porous scaffolds fabricated with the waterborne PU showed better adhesion and proliferation of endothelial cells and can be utilized in soft tissue engineering [68].

To achieve biodegradability and nontoxicity, there has been intensive research on replacing common isocyanates with amino acid diisocyanates in the development of waterborne PUs [69]. L-Lysine diisocyanate and L-lysine ethyl ester diisocyanate have gained attention because lysine is nontoxic, less prone to inflammation, and easy to connect with bioactive molecules. Lysine ethyl ester diisocyanate was prepared with an improved method that avoids the use of gaseous phosgene, elevated temperature, and strongly acidic conditions as described by Nowick et al. [70]. L-Lysine diisocyanate and PCL diol were used as main components to prepare nontoxic and
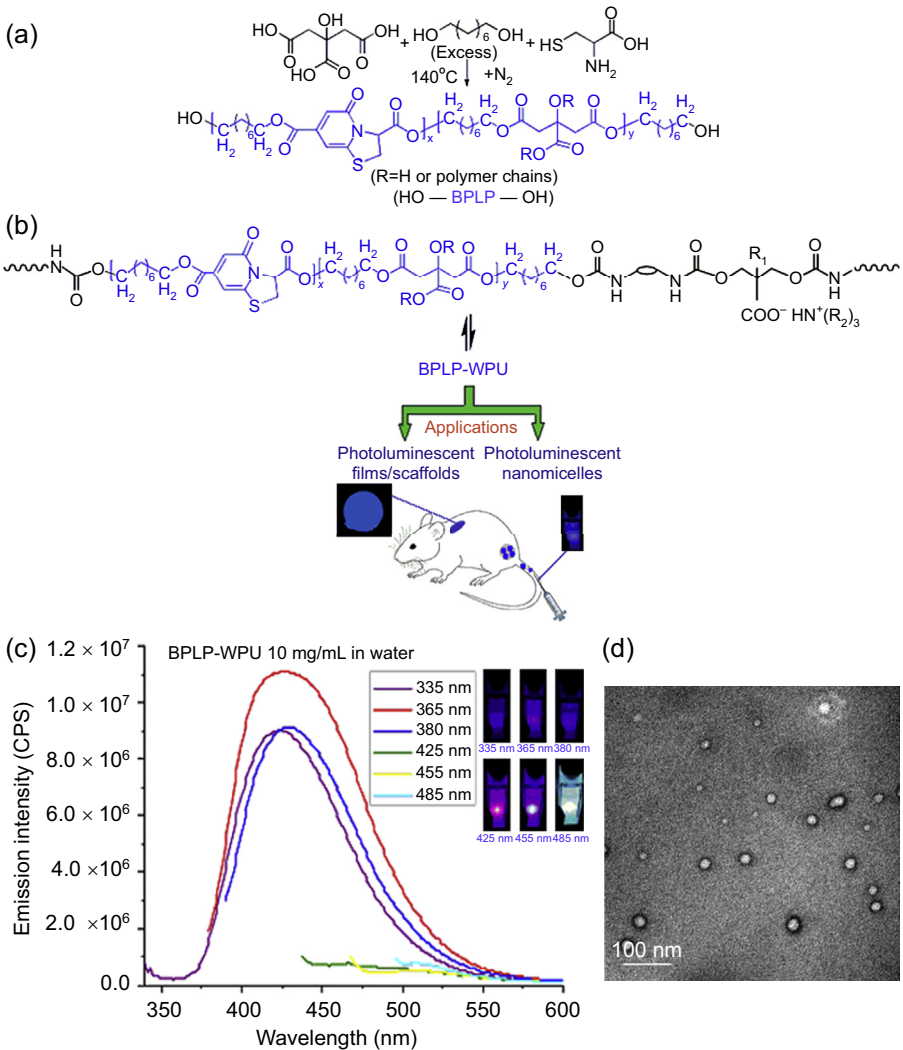
Figure 4.10 Synthesis and properties of BPLP and biodegradable BPLP-based biodegradable waterborne polyurethane (BPLP-WPU). (a) Synthesis of BPLP. (b) Structure and application of BPLP-WPU. (c) Emission spectra of BPLP-WPU excited at wavelengths of 335, 365, 380, 425, 455, and 485 nm. (d) Particle size distribution of BPLP-WPU dispersed in water.

biodegradable waterborne PUs. The materials showed tensile strength up to 46.5 MPa and 42% hydrolytic degradation after 80 days [71].

In conclusion, waterborne PU biomaterials have the advantages of low viscosity at high molecular weight, nontoxicity, and good applicability over conventional PU biomaterials. Driven by the continuous reduction in costs and the control of VOC emissions, the development of waterborne PUs as biomaterials has significantly increased.

4.3.3 Applications of waterborne polyurethane biomaterials

Much effort has been made to improve the biocompatibility and biodegradability of waterborne PUs, thus making them suitable for a wide range of medical applications. For example, waterborne PUs have great potential in the field of tissue engineering. Xu et al. studied the response of bladder smooth muscle cells (BSMCs) on biodegradable waterborne PUs. BSMCs showed better attachment, proliferation, and α-actin distribution behavior on waterborne PU membranes than on PLGA membranes [72]. Waterborne PUs have also been developed as nanoparticles for drug delivery. Biodegradable waterborne PU nanocomposites containing clay nanoparticles have been used to deliver dexamethasone acetate for the treatment of ocular diseases [73]. Researchers also prepared bioactive waterborne PU nanomicelles for breast cancer treatment. The nanomicelles successfully caused apoptosis of human breast cancer MCF-7 cells [74]. In addition, waterborne PUs could be used in wound healing [75] and antibacterial materials [76]. Hsu et al. have developed biodegradable elastomeric nanoparticles that could self-assemble into hydrogels, microspheres, nanofibers, sponges, and films, all of which have great value in biomedical applications [77].

4.4 Functionalization of polyurethanes and novel applications of urethane/urea chemistry

The properties of biodegradable PUs (e.g., hydrophobicity/hydrophilicity, biocompatibility, biodegradability, and conjugation with proteins, drugs, or biological agents) can be tailored by the introduction of different functional groups for various biomedical applications. Urethane/urea reactions (isocyanate-based and nonisocyanate-based reactions) can be used to impart specific functionalities to polymers or biomaterials. The reactions between polyisocyanates and polymers/proteins that contain abundant hydroxyl or amino groups have also been applied as a room temperature cross-linking method to fabricate tissue-engineering scaffolds or 3D printed patterns. In the following sections, applications of urethane/urea chemistry in biomaterials will be discussed in detail.

4.4.1 Functionalization of polyurethanes

4.4.1.1 An overview of functionalization methods for polyurethanes

The introduction of functionalities into PUs can be made before, during, or after polymerization. Traditional linear PUs are made by the polyaddition reactions between diols and diisocyanates. One route to obtain functional PUs is to use monofunctional compounds (alcohol or isocyanate, b1, b2, and c1 in Figure 4.11(a)), but they lead to a limited number of terminal functionalities and reduced molecular weight [78]. Although there are some examples of introducing specific functionalities using functional diisocyanates, such as diisocyanates derived from L-lysine (e.g., L-lysine methyl
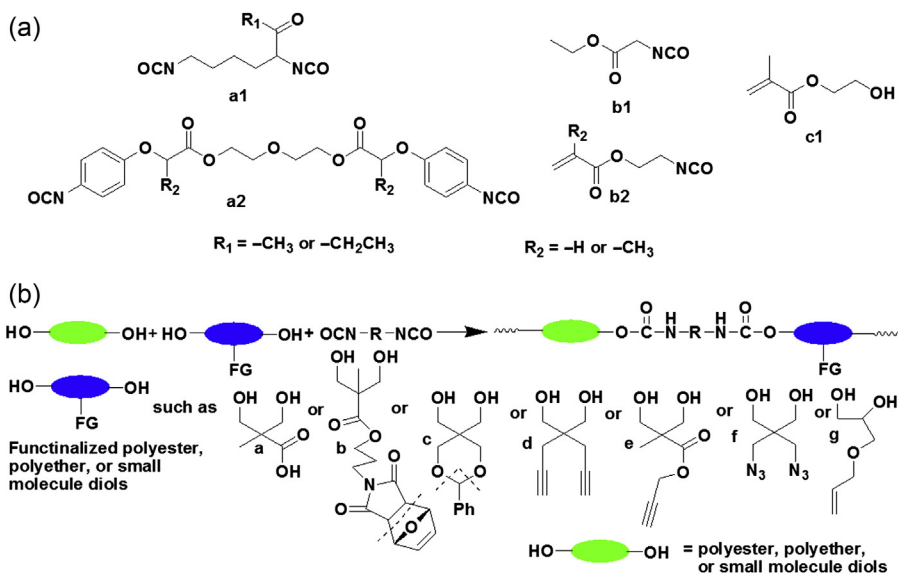
Figure 4.11 (a) Examples of functional diisocyanates (a1, a2), functional monoisocyanates (b1, b2), and monofunctional alcohol (c1) used for polyurethane functionalization before, concurrent, or post polymerization; (b) introduction of functional groups into polyurethane through functional diols.

ester diisocyanate [LDI], a1 in Figure 4.11(a)) [79], or biodegradable diisocyanates (a2 in Figure 4.11(a)) [10], the sources of functional diisocyanates are limited and their synthesis processes are inconvenient. By controlling the feed ratios of diols and diisocyanates, desired terminated groups, such as isocyanates, can be obtained and can be used for functionalizing PUs through postmodification [78]. Side ester groups introduced by either LDI or ethyl isocyanatoacetate (b1 in Figure 4.11(a)) [79,80] can be further modified through aminolysis by amino group-containing compounds, such as *N,N*-dimethylenediamine [79] or poly(ethyleneimine) [80], to obtain cationic polymers. The cationic polymers can then be used for gene delivery. All of the functionalization methods noted above are limited by a complex reaction process or limited raw material sources. In contrast, the incorporation of functionalities into PUs through the addition of functional diols is convenient and straightforward (Figure 4.11(b)).

4.4.1.2 Introduction of functional groups into polyurethanes using functional diols

The introduction of hydrophilic carboxyl groups by the addition of 2,2-bis(hydroxymethyl) propionic acid (DMPA, a in Figure 4.11(b)) followed by salt formation of carboxyl groups with amines, such as triethylamine, is frequently applied as a functionalization method, to obtain waterborne PUs [81]. Du Prez and colleagues developed maleimide-functionalized PUs by adding furan-protected maleimide-containing diols (FMD, b in Figure 4.11(b)) followed by simple heating at 100 °C under

vacuum overnight. Maleimide-functionalized PUs can be further used to conduct thiol–maleimide reactions without the use of UV light or any toxic catalyst [82]. Biodegradable PUs with pendant hydroxyl groups were synthesized by Yang et al. by the introduction of benzal pentaerythritol (BPO, c in Figure 4.11(b)) into PUs followed by de-protection [83]. The pendant hydroxyl groups were used for reaction with 4-azido-benzoic acid to obtain PUs functionalized with photoactive phenyl azide groups. The PUs had the ability to immobilize proteins under UV light [84]. Clickable functional groups can also be directly introduced into PUs by the addition of click functional diols, such as 2,2-bis(prop-2-yl) propane-1,3-diol (DPPD, d in Figure 4.11(b)) [85–87], propargyl 2,2-bis(hydroxymethyl)propionate (e in Figure 4.11(b)), 2,2-bis(azi-domethyl)propane-1,3-diol (f in Figure 4.11 (b)), and click functionality containing macromolecular diols [87]. Pendant vinyl groups can be obtained by the addition of double bond-containing diols such as 3-allyloxy-1,2-propanediol [87]. By adding dihydroxy-terminated poly(2-(dimethylamino)-ethyl methacrylate) (PDEM(OH)$_2$), Zhang et al. developed protein-resistant PUs containing zwitterionic side chains [88].

Overall, the incorporation of functionalities through the addition of functional diols is convenient and straightforward, especially when the desired functional groups have no obvious side reactions with isocyanate groups such as carboxyl, azide, alkyne, and vinyl groups [80–88]. The introduction of functional groups that can react with isocyanate groups, such as hydroxyl or amino groups, requires these functional groups be protected before PU formation and de-protected afterward [83].

4.4.2   Urethane/urea chemistry as a functionalization method

4.4.2.1   Introduction of functional groups into OH- or NH$_2$-containing polymers using functionalized monoisocyanates

As noted above, the addition of monofunctional isocyanates/alcohols in the polyaddition process of diols and diisocyanates is a way of obtaining terminally functionalized PUs [78]. The urethane/urea reactions between monofunctional isocyanates and hydroxyl or amino groups on polymers can also serve as a functionalization route for OH- or NH$_2$-containing polymers (Figure 4.12(a)). Among monofunctional isocyanates, ester group-containing monoisocyanate, which can be further modified by aminolysis post polymerization [80], and vinyl group functional isocyanates, such as 2-isocyanatoethyl (meth)acrylate and allyl isocyanate, are the most commonly used (Figure 4.12(a)). 2-Isocyanatoethyl methacrylate (IEM) has been used to react with the terminal OH– groups of star shaped PCL [89] or amino groups of silk protein [90,91] to obtain photo/free radical cross-linkable PCL or silk protein for gelation, precise patterning, dynamic topographical control, or microfabrication. IEM has also been used to introduce vinyl groups onto cellulose [92], or perfluoropolyether polyol macromonomer, creating a polymer with low surface energy [93]. Through the modification of 1,1,1-tri-[4-(methacryloxyethyl-aminocarbonyloxy)-phenyl]ethane with IEM, urethane-based trimethacrylate monomer has been also developed and used as a dentin adhesive [94].
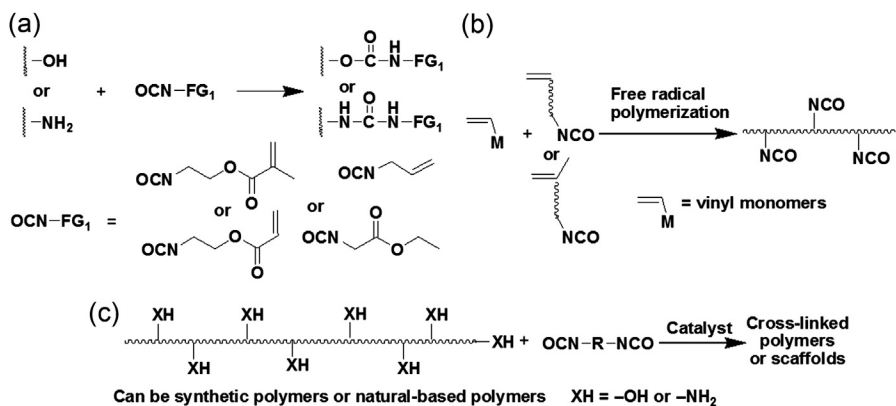
Figure 4.12 Application of urethane/urea chemistry in polymer functionalization and cross-linking: (a) introduction of functional groups using functionalized monoisocyanates; (b) introduction of isocyanates as functional groups; (c) application of urethane/urea reaction as a cross-linking method.

4.4.2.2   Introduction of isocyanates as functional groups

Vinyl group-functional isocyanates, such as IEM, can be polymerized through free radical polymerization with other vinyl monomers to give polymers with pendant isocyanate groups (Figure 4.12(b)). Polymers with pendant isocyanate groups have been used as tissue adhesives [95]. The pendant isocyanate groups can also be used to react with thiol/amino group-containing compounds for polymer surface functionalization [96].

4.4.2.3   Urethane/urea chemistry as a cross-linking method

As noted above, monofunctional isocyanates can be used to introduce functionalities onto OH- or NH_2-containing polymers. Similarly, compounds with two or more isocyanate groups can be used as cross-linkers for OH- or NH_2-containing polymers (Figure 4.12(c)). The application of PUs with preserved isocyanates as tissue adhesives is based on the cross-linking reaction between isocyanate and amino groups that are from tissue proteins or produced by water hydrolysis of isocyanate groups [19,20]. By employing the urethane reaction between 1,6-hexamethylene diisocyanate (HDI) and the pendant hydroxyl groups on PGS, Pereira et al. developed a highly tunable biocompatible biodegradable elastomer, poly(glycerol sebacate urethane), which can be cross-linked under melt conditions through solvent-based or solvent-free methods [97]. Similarly, by simply employing LDI as a cross-linker for gelatin, Neffe et al. were able to create open porous three-dimensional architecture hydrogels that can induce bone regeneration in just one step [98]. By reacting 1,2,3-triazole-rich hyperbranched polyether polyols with diisocyanate, moist-curable antimicrobial hyperbranched PU–urea coatings were developed by Kantheti et al. [51]. A DNA–lipid organogel cross-linked by IPDI has been developed by Yao et al. and reported to possess shape-memory properties [99].

4.4.2.4   Nonisocyanate-based urethane reactions and the application of urethane-forming hydroxyl–amino coupling reactions

In addition to the most intensively researched urethane reactions between isocyanate and hydroxyl groups (Figure 4.1(a)) that form urethane bonds, there are also nonisocyanate urethane reactions, such as the reactions between cyclic carbonate or activated carbonate/carbamate/chloroformate derivative groups and amine groups (Figure 4.1(b) and (c)) [4–6].

The ring-opening polymerization of cyclic carbonates with polyfunctional amines forms poly(hydroxyl-urethanes). The most traditional syntheses of cyclic carbonates use phosgene chemistry, which involves environmental hazard issues [100].

Another approach with cyclic carbonates is the transesterification of diols with dicarbonates [101]. The development of a green chemistry approach has eliminated the use of phosgene in cyclic carbonate syntheses. Among them, catalytic conversion of epoxides with carbon dioxide into cyclic carbonates is the most promising (Figure 4.13(a)) [4,102–104]. This chemistry opens the development of isocyanate-free bio-based green PUs from natural-based compounds, such as vegetable oils (including castor oil) [103–105]. Poly(hydroxyl-urethanes), as one type of nonisocyanate polyurethane, contain side hydroxyl groups that bring hydrophilicity and can be used as functionalities (Figure 4.13(b)). Furthermore, they do not have labile allophanate
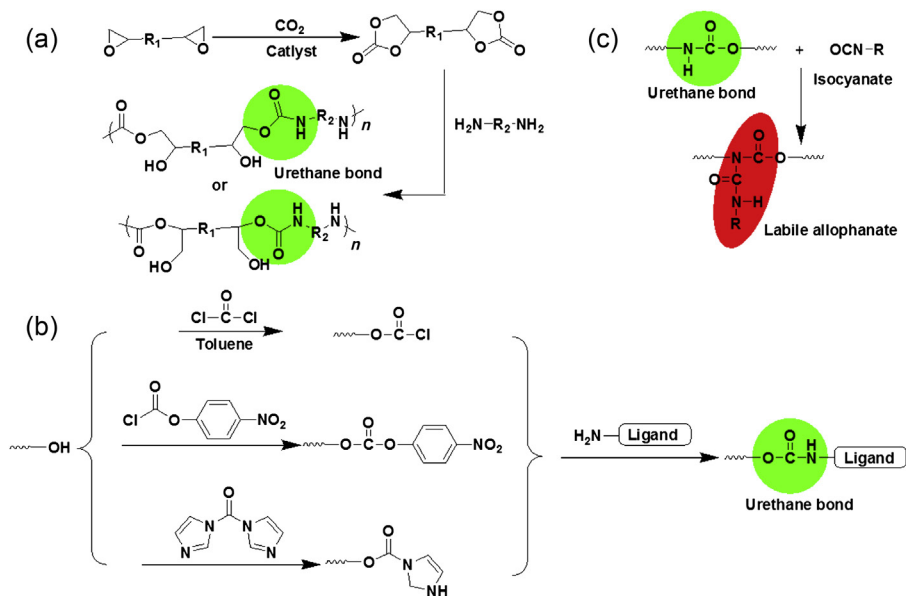
Figure 4.13 Nonisocyanate urethane reactions: (a) example of the formation of cyclic carbonate and the reaction with polyamines servers as a new polyurethane synthesis route; (b) representative coupling reactions between hydroxyl group and amino group that form a urethane bond; (c) the reaction between urethane bond and isocyanate group results in labile allophanate groups, which make traditional isocyanate-based polyurethanes less chemical resistant.

groups, side reaction products between urethane and isocyanate that make conventional isocyanate-based PU less chemical resistant (Figure 4.13(c)) [4].

Activated carbonate, carbamate, or chloroformate derivative groups, including (imidazolylcarbony1)oxyl (IC) derivative, carbonate derivatives of 2,4,5-trichlorophenyl and *p*-nitrophenyl, succinimidyl carbonate, and chloroformate derivative (Figure 4.1(c)), can react with amino groups under mild conditions to form urethane bonds that are very stable under physiological conditions and show little breakdown in various buffers of pH 2–11 [6]. Thus these reactions have been extensively used as the coupling reactions between hydroxyl and amino groups (Figure 4.13(c)) and applied in protein-selective modification on amino groups, drug or protein bioconjugation, and polymer modification [5–9,104]. An example of the application of urethane bond forming hydroxyl–amino group coupling reactions in drug conjugation is described below. By activating the side hydroxyl groups on biodegradable amphiphatic mPEG-b-P(LA-co-DHP) polymer with 4-nitrophenyl chloroformate (NPC), Hu et al. conjugated the amino group containing the anticancer drug doxorubicin (Dox) onto the polymer by a direct hydroxyl–amino coupling reaction with the formation of a stable urethane bond. In the same work, the acid-liable hydrazine linkage between the polymer and the Dox was also formed by reacting the NPC-activated polymer with hydrazine monohydrate followed by the reaction between the hydrazine and the ketone group on Dox [9]. The drug release profiles of these two different polymer–drug conjugate micelles were investigated [9]. Urethane bonds formed from hydroxyl–amino group coupling reactions have also been widely used in polymer modification or functionalization. By the reaction between NPC-modified PEG diols and tyramine, followed by the grafting of monotyramine-terminated NPC-activated PEG diol onto gelatin or chitosan, Park et al. [7] and Tran et al. [8] synthesized tyramine-modified gelatin or chitosan. They could be cross-linked enzymatically into bioadhesive hydrogels and used for tissue regeneration or wound healing. By modifying monohydroxyl PCL with carbonyldiimidazole, Yu el al. synthesized IC terminal PCL. It was grafted onto chitosan and formed into an amphiphilic biodegradable polymer that can be used to form micelles [5]. By activating terminal hydroxyl groups with phosgene, Wang et al. synthesized a chloroformate terminated PEO–PPO–PEO block copolymer and reacted it with propargylamine to obtain alkyne group-functionalized PEO–PPO–PEO block copolymer [106].

4.5   Conclusions and outlook

Urethane/urea chemistry has evolved and transformed to offer convenient and effective tools for the modification of biomaterials, providing them with desirable properties for biomedical applications. The efforts described above have produced an array of multifunctional urethane/urea chemistry-based biomaterials to meet the specific requirements of each application. A collection of citric acid-based PUs has been developed with tunable mechanical, degradation, photoluminescent, and biomedical properties. The CABE platform technology enables easy modulation of their unique properties by simply altering the ratios of diols, prepolymers, and other additive(s) and

the polymerization conditions. With this expandable list of CABEs, the development of more robust, elastic, soft, and biocompatible materials for biomedical applications is possible. Additionally, novel urethane/urea chemistry with isocyanate-based and nonisocyanate-based approaches was discussed in this chapter to provide insights on their potential for designing novel biomaterials. The versatility of urethane/urea chemistry in modern biomaterial designs that have been described has an impact on a broad range of applications, especially in the field of biomedical engineering.

Acknowledgments

References

[1] Q.Z. Chen, S.L. Liang, G.A. Thouas, Elastomeric biomaterials for tissue engineering, Prog. Polym. Sci. 38 (March–April 2013) 584–671.

[2] H.W. Engels, H.G. Pirkl, R. Albers, R.W. Albach, J. Krause, A. Hoffmann, et al., Polyurethanes: versatile materials and sustainable problem solvers for today's challenges, Angew. Chem. Int. Ed. 52 (September 2, 2013) 9422–9441.

[3] Q.Y. Liu, L. Jiang, R. Shi, L.Q. Zhang, Synthesis, preparation, in vitro degradation, and application of novel degradable bioelastomers – a review, Prog. Polym. Sci. 37 (May 2012) 715–765.

[4] M. Fleischer, H. Blattmann, R. Mulhaupt, Glycerol-, pentaerythritol- and trimethylol-propane-based polyurethanes and their cellulose carbonate composites prepared via the non-isocyanate route with catalytic carbon dioxide fixation, Green Chem. 15 (2013) 934–942.

[5] H.J. Yu, W.S. Wang, X.S. Chen, C. Deng, X.B. Jing, Synthesis and characterization of the biodegradable polycaprolactone-graft-chitosan amphiphilic copolymers, Biopolymers 83 (October 15, 2006) 233–242.

[6] S. Zalipsky, Functionalized poly(ethylene glycol) for preparation of biologically relevant conjugates, Bioconjug. Chem. 6 (March–April 1995) 150–165.

[7] K.M. Park, K.S. Ko, Y.K. Joung, H. Shin, K.D. Park, In situ cross-linkable gelatin-poly(ethylene glycol)-tyramine hydrogel via enzyme-mediated reaction for tissue regenerative medicine, J. Mater. Chem. 21 (2011) 13180–13187.

[8] N.Q. Tran, Y.K. Joung, E. Lih, K.D. Park, In situ forming and rutin-releasing chitosan hydrogels as injectable dressings for dermal wound healing, Biomacromolecules 12 (August 2011) 2872–2880.

[9] X.L. Hu, S. Liu, Y.B. Huang, X.S. Chen, X.B. Jing, Biodegradable block copolymer-doxorubicin conjugates via different linkages: preparation, characterization, and in vitro evaluation, Biomacromolecules 11 (August 2010) 2094–2102.

[10] R.S. Bezwada, S.P. Nukavarapu, D.L. Dorcemus, N. Srivasthava, R.J. Armentano, Novel absorbable polyurethane biomaterials and scaffolds for tissue engineering, MRS Proc. 1621 (2014) 93–99.

[11] P. Alves, P. Ferreira, M.H. Gil, Biomedical Polyurethane-Based Materials, in: Polyurethane: Properties, Structure and Applications, Nova Publishers, New York, 2012. ISBN: 978-1-61942-453-1.

[12] R.J. Zdrahala, I.J. Zdrahala, Biomedical applications of polyurethanes: a review of past promises, present realities, and a vibrant future, J. Biomater. Appl. 14 (July 1999) 67–90.

[13] J. Dey, H. Xu, K.T. Nguyen, J.A. Yang, Crosslinked urethane doped polyester biphasic scaffolds: potential for in vivo vascular tissue engineering, J. Biomed. Mater. Res. Part A 95A (November 2010) 361–370.

[14] J.S. Guo, D.Y. Nguyen, R.T. Tran, Z.W. Xie, X.C. Bai, J. Yang, Design strategies and applications of citrate-based biodegradable elastomeric polymers, in: Natural and Synthetic Biomedical Polymers, 2014, pp. 259–285.

[15] Y. Zhang, R.T. Tran, I.S. Qattan, Y.T. Tsai, L.P. Tang, C. Liu, et al., Fluorescence imaging enabled urethane-doped citrate-based biodegradable elastomers, Biomaterials 34 (May 2013) 4048–4056.

[16] J. Dey, H. Xu, J.H. Shen, P. Thevenot, S.R. Gondi, K.T. Nguyen, et al., Development of biodegradable crosslinked urethane-doped polyester elastomers, Biomaterials 29 (December 2008) 4637–4649.

[17] R.T. Tran, W.M. Choy, H. Cao, I. Qattan, J.C. Chiao, W.Y. Ip, et al., Fabrication and characterization of biomimetic multichanneled crosslinked-urethane-doped polyester tissue engineered nerve guides, J. Biomed. Mater. Res. A 102 (August 2014) 2793–2804.

[18] R.T. Tran, L. Wang, C. Zhang, M.J. Huang, W.J. Tang, C. Zhang, et al., Synthesis and characterization of biomimetic citrate-based biodegradable composites, J. Biomed. Mater. Res. Part A 102 (August 2014) 2521–2532.

[19] P. Ferreira, R. Pereira, J.F.J. Coelho, A.F.M. Silva, M.H. Gil, Modification of the biopolymer castor oil with free isocyanate groups to be applied as bioadhesive, Int. J. Biol. Macromol. 40 (January 30, 2007) 144–152.

[20] M. Mehdizadeh, J. Yang, Design strategies and applications of tissue bioadhesives, Macromol. Biosci. 13 (March 2013) 271–288.

[21] P. Ping, W.S. Wang, X.S. Chen, X.B. Jing, Poly(ε-caprolactone) polyurethane and its shape-memory property, Biomacromolecules 6 (March–April 2005) 587–592.

[22] W.S. Wang, P. Ping, X.S. Chen, X.B. Jing, Polylactide-based polyurethane and its shape-memory behavior, Eur. Polym. J. 42 (June 2006) 1240–1249.

[23] W.S. Wang, P. Ping, H.J. Yu, X.S. Chen, X.B. Jing, Synthesis and characterization of a novel biodegradable, thermoplastic polyurethane elastomer, J. Polym. Sci. A Polym. Chem. 44 (October 1, 2006) 5505–5512.

[24] J. Guo, Z. Xie, R.T. Tran, D. Xie, D. Jin, X. Bai, et al., Click chemistry plays a dual role in biodegradable polymer design, Adv. Mater. 26 (March 26, 2014) 1906–1911.

[25] Y. Zhang, R.T. Tran, D. Gyawali, J. Yang, Development of photocrosslinkable urethane-doped polyester elastomers for soft tissue engineering, Int. J. Biomater. Res. Eng. 1 (January 2011) 18–31.

[26] J. Yang, A.R. Webb, G.A. Ameer, Novel citric acid-based biodegradable elastomers for tissue engineering, Adv. Mater. 16 (6) (2004) 511–516.

[27] D. Motlagh, J. Yang, K.Y. Lui, A.R. Webb, G.A. Ameer, Hernocompatibility evaluation of poly(glycerol-sebacate) in vitro for vascular tissue engineering, Biomaterials 27 (August 2006) 4315–4324.

[28] J. Yang, D. Motlagh, A.R. Webb, G.A. Ameer, Novel biphasic elastomeric scaffold for small-diameter blood vessel tissue engineering, Tissue Eng. 11 (11–12) (2005) 1876–1886.

[29] R.T. Tran, Y. Zhang, D. Gyawali, J. Yang, Recent developments on citric acid derived biodegradable elastomers, Recent Pat. Biomed. Eng. 2 (2009) 216–227.

[30] M. Schappacher, T. Fabre, A.F. Mingotaud, A. Soum, Study of a (trimethylenecarbonate-co-ε-caprolactone) polymer part 1: preparation of a new nerve guide through controlled random copolymerization using rare earth catalysts, Biomaterials 22 (November 2001) 2849–2855.

[31] A.P. Pego, C.L. Vleggeert-Lankamp, M. Deenen, E.A. Lakke, D.W. Grijpma, A.A. Poot, et al., Adhesion and growth of human Schwann cells on trimethylene carbonate (co)polymers, J. Biomed. Mater. Res. A 67 (December 1, 2003) 876–885.

[32] C.A. Sundback, J.Y. Shyu, Y.D. Wang, W.C. Faquin, R.S. Langer, J.P. Vacanti, et al., Biocompatibility analysis of poly(glycerol sebacate) as a nerve guide material, Biomaterials 26 (September 2005) 5454–5464.

[33] J. Yang, D. Motlagh, A.R. Webb, G.A. Ameer, Novel biphasic elastomeric scaffold for small-diameter blood vessel tissue engineering, Tissue Eng. 11 (November–December 2005) 1876–1886.

[34] F.R. Noyes, E.S. Grood, The strength of the anterior cruciate ligament in humans and Rhesus monkeys, J. Bone Joint Surg. Am. 58 (December 1976) 1074–1082.

[35] J. Yang, A.R. Webb, S.J. Pickerill, G. Hageman, G.A. Ameer, Synthesis and evaluation of poly(diol citrate) biodegradable elastomers, Biomaterials 27 (March 2006) 1889–1898.

[36] G.A. Skarja, K.A. Woodhouse, Synthesis and characterization of degradable polyurethane elastomers containing an amino acid-based chain extender, J. Biomater. Sci. Polym. Ed. 9 (1998) 271–295.

[37] J. Kylma, J.V. Seppala, Synthesis and characterization of a biodegradable thermoplastic poly(ester-urethane) elastomer, Macromolecules 30 (May 19, 1997) 2876–2882.

[38] L. Tatai, T.G. Moore, R. Adhikari, F. Malherbe, R. Jayasekara, I. Griffiths, et al., Thermoplastic biodegradable polyurethanes: the effect of chain extender structure on properties and in-vitro degradation, Biomaterials 28 (December 2007) 5407–5417.

[39] C.R. Lee, S. Grad, K. Gorna, S. Gogolewski, A. Goessl, M. Alini, Fibrin-polyurethane composites for articular cartilage tissue engineering: a preliminary analysis, Tissue Eng. 11 (September 2005) 1562–1573.

[40] S. Grad, L. Kupcsik, K. Gorna, S. Gogolewski, M. Alini, The use of biodegradable polyurethane scaffolds for cartilage tissue engineering: potential and limitations, Biomaterials 24 (December 2003) 5163–5171.

[41] S.L. Chia, K. Gorna, S. Gogolewski, M. Alini, Biodegradable elastomeric polyurethane membranes as chondrocyte carriers for cartilage repair, Tissue Eng. 12 (July 2006) 1945–1953.

[42] J. Yang, J. Dey, in: Bio-polymer and Scaffold-Sheet Method for Tissue Engineering, Google Patents, 2009.

[43] J. Dey, R.T. Tran, J.H. Shen, L.P. Tang, J. Yang, Development and long-term in vivo evaluation of a biodegradable urethane-doped polyester elastomer, Macromol. Mater. Eng. 296 (December 12, 2011) 1149–1157.

[44] D. Gyawali, R.T. Tran, K.J. Guleserian, L.P. Tang, J.A. Yang, Citric-acid-derived photo-cross-linked biodegradable elastomers, J. Biomater. Sci. Polym. Ed. 21 (2010) 1761–1782.

[45] S.H. Kim, J.H. Lee, H. Hyun, Y. Ashitate, G. Park, K. Robichaud, et al., Near-infrared fluorescence imaging for noninvasive trafficking of scaffold degradation, Sci. Rep. 3 (2013) 1198.

[46] K.M. Bratlie, T.T. Dang, S. Lyle, M. Nahrendorf, R. Weissleder, R. Langer, et al., Rapid biocompatibility analysis of materials via in vivo fluorescence imaging of mouse models, PLoS One 5 (2010) e10032.

[47] J. Yang, Y. Zhang, S. Gautam, L. Liu, J. Dey, W. Chen, et al., Development of aliphatic biodegradable photoluminescent polymers, Proc. Natl. Acad. Sci. U.S.A. 106 (June 23, 2009) 10086–10091.

[48] Z. Xie, Y. Zhang, L. Liu, H. Weng, R.P. Mason, L. Tang, et al., Development of intrinsically photoluminescent and photostable polylactones, Adv. Mater. 26 (26) (March 26, 2014) 4491–4496.

[49] M.D. Best, Click chemistry and bioorthogonal reactions: unprecedented selectivity in the labeling of biological molecules, Biochemistry 48 (July 21, 2009) 6571–6584.

[50] C.S. McKay, M.G. Finn, Click chemistry in complex mixtures: bioorthogonal bioconjugation, Chem. Biol. 21 (September 18, 2014) 1075–1101.

[51] S. Kantheti, R. Narayan, K.V.S.N. Raju, Click chemistry engineered hyperbranched polyurethane-urea for functional coating applications, Ind. Eng. Chem. Res. 53 (May 21, 2014) 8357–8365.

[52] S.H. Rhee, J. Tanaka, Effect of citric acid on the nucleation of hydroxyapatite in a simulated body fluid, Biomaterials 20 (November 1999) 2155–2160.

[53] S. Gogoi, N. Karak, Biobased biodegradable waterborne hyperbranched polyurethane as an ecofriendly sustainable material, ACS Sustain. Chem. Eng. 2 (2014) 2730–2738.

[54] F.M.B. Coutinho, M.C. Delpech, Waterborne anionic polyurethanes and poly (urethane-urea)s- influence of the chain extender on mechanical and adhesive properties, Polym. Test. 19 (2000) 939–952.

[55] B.K. Kim, Aqueous polyurethane dispersions, Colloid Polym. Sci. 274 (1996) 599–611.

[56] M.G. Lu, J.Y. Lee, M.J. Shim, S.W. Kim, Synthesis and properties of anionic aqueous polyurethane dispersions, J. Appl. Polym. Sci. 86 (2002) 3461–3465.

[57] M.A.R. Meier, J.O. Metzger, U.S. Schubert, Plant oil renewable resources as green alternatives in polymer science, Chem. Soc. Rev. 36 (2007) 1788.

[58] T. Gurunathan, S. Mohanty, S.K. Nayak, Effect of reactive organoclay on physicochemical properties of vegetable oil-based waterborne polyurethane nanocomposites, RSC Adv. 5 (2015) 11524–11533.

[59] Y. Xia, R.C. Larock, Vegetable oil-based polymeric materials: synthesis, properties, and applications, Green Chem. 12 (2010) 1893.

[60] I. Vroman, L. Tighzert, Biodegradable polymers, Materials 2 (2009) 307–344.

[61] Y. Lu, R.C. Larock, Soybean-oil-based waterborne polyurethane dispersions: effects of polyol functionality and hard segment content on properties, Biomacromolecules 9 (2008) 3332–3340.

[62] N.M.K. Lamba, K.A. Woodhouse, S.L. Cooper, Polyurethanes in Biomedical Applications, CRC Press, New York, 1998, pp. 205–241.

[63] D. Xu, Z. Meng, M. Han, K. Xi, X. Jia, X. Yu, et al., Novel blood-compatible waterborne polyurethane using chitosan as an extender, J. Appl. Polym. Sci. 109 (2008) 240–246.

[64] T.J. Lee, S.H. Kwon, B.K. Kim, Biodegradable sol-gel coatings of waterborne polyurethane/gelatin chemical hybrids, Prog. Org. Coat. 77 (2014) 1111–1116.

[65] W. Wang, P. Ping, X. Chen, X. Jing, Shape memory effect of poly(L-lactide)- based polyurethanes with different hard segments, Polym. Int. 56 (2007) 840–846.

[66] S.A. Dai, C.-W. Chen, Y.-S. Chen, S.-H. Hsu, Biodegradable and biocompatible waterborne polyurethane, Patent US 20120108742 (October 25, 2011).

[67] H. Chen, X. Jiang, L. He, T. Zhang, M. Xu, X. Yu, Novel biocompatible waterborne polyurethane using L-lysine as an extender, J. Appl. Polym. Sci. 84 (2002) 2474–2480.

[68] X. Jiang, F. Yu, Z. Wang, J. Li, H. Tan, M. Ding, et al., Fabrication and characterization of waterborne biodegradable polyurethanes 3-dimensional porous scaffolds for vascular tissue engineering, J. Biomater. Sci. Polym. Ed. 21 (2010) 1637–1652.

[69] D. Cohn, A.H. Salomon, Designing biodegradable multiblock PCL/PLA thermoplastic elastomers, Biomaterials 26 (May 2005) 2297–2305.

[70] J.S. Nowick, N.A. Powell, T.M. Nguyen, G. Noronha, An improved method for the synthesis of enantiomerically pure amino acid ester isocyanates, J. Org. Chem. 57 (1992) 7364–7366.

[71] F. Liang, B. Qin, Y. Yang, M. Jia, Study on the synthesis and properties of biodegradable waterborne polyurethane, Adv. Mater. Res. 554-556 (2012) 130–135.

[72] F. Xu, Y. Wang, X. Jiang, H. Tan, H. Li, K.J. Wang, Effects of different biomaterials: comparing the bladder smooth muscle cells on waterborne polyurethane or poly-lactic-co-glycolic acid membranes, Kaohsiung J. Med. Sci. 28 (January 2012) 10–15.

[73] G.R. da Silva, A. da Silva-Cunha, F. Behar-Cohen, E. Ayres, R.L. Oréfice, Biodegradable polyurethane nanocomposites containing dexamethasone for ocular route, Mater. Sci. Eng. C 31 (2011) 414–422.

[74] A.Y. Khosroushahi, H. Naderi-Manesh, H. Yeganeh, J. Barar, Y. Omidi, Novel water-soluble polyurethane nanomicelles for cancer chemotherapy: physicochemical characterization and cellular activities, J. Nanobiotechnol. 10 (2012) 2.

[75] H.J. Yoo, H.D. Kim, Synthesis and properties of waterborne polyurethane hydrogels for wound healing dressings, J. Biomed. Mater. Res. B Appl. Biomater. 85 (May 2008) 326–333.

[76] S.H. Hsu, H.J. Tseng, Y.C. Lin, The biocompatibility and antibacterial properties of waterborne polyurethane-silver nanocomposites, Biomaterials 31 (September 2010) 6796–6808.

[77] S.-H. Hsu, K.-C. Hung, Y.-Y. Lin, C.-H. Su, H.-Y. Yeh, U.S. Jeng, et al., Water-based synthesis and processing of novel biodegradable elastomers for medical applications, J. Mater. Chem. B 2 (2014) 5083.

[78] Y.H. Lin, K.H. Liao, N.K. Chou, S.S. Wang, S.H. Chu, K.H. Hsieh, UV-curable low-surface-energy fluorinated poly(urethane-acrylate)s for biomedical applications, Eur. Polym. J. 44 (September 2008) 2927–2937.

[79] T.F. Yang, W. Chin, J. Cherng, M. Shau, Synthesis of novel biodegradable cationic polymer: N,N-diethylethylenediamine polyurethane as a gene carrier, Biomacromolecules 5 (September–October 2004) 1926–1932.

[80] X.Y. Liu, W.Y. Ho, W.J. Hung, M.D. Shau, The characteristics and transfection efficiency of cationic poly (ester-co-urethane) – short chain PEI conjugates self-assembled with DNA, Biomaterials 30 (December 2009) 6665–6673.

[81] S.A. Madbouly, J.U. Otaigbe, A.K. Nanda, D.A. Wicks, Rheological behavior of aqueous polyurethane dispersions: effects of solid content, degree of neutralization, chain extension, and temperature, Macromolecules 38 (May 3, 2005) 4014–4023.

[82] L. Billiet, O. Gok, A.P. Dove, A. Sanyal, L.T.T. Nguyen, F.E. Du Prez, Metal-free functionalization of linear polyurethanes by thiol-maleimide coupling reactions, Macromolecules 44 (October 25, 2011) 7874–7878.

[83] L.X. Yang, J.Z. Wei, L.S. Yan, Y.B. Huang, X.B. Jing, Synthesis of OH-group-containing, biodegradable polyurethane and protein fixation on its surface, Biomacromolecules 12 (June 2011) 2032–2038.

[84] D. Fournier, F. Du Prez, "Click" chemistry as a promising tool for side-chain functionalization of polyurethanes, Macromolecules 41 (July 8, 2008) 4622–4630.

[85] C. Ott, C.D. Easton, T.R. Gengenbach, S.L. McArthur, P.A. Gunatillake, Applying "click" chemistry to polyurethanes: a straightforward approach for glycopolymer synthesis, Polym. Chem. 2 (2011) 2782–2784.

[86] L. Billiet, D. Fournier, F. Du Prez, Step-growth polymerization and 'click' chemistry: the oldest polymers rejuvenated, Polymer 50 (July 31, 2009) 3877–3886.

[87] M. Basko, M. Bednarek, L. Billiet, P. Kubisa, E. Goethals, F. Du Prez, Combining cationic ring-opening polymerization and click chemistry for the design of functionalized polyurethanes, J. Polym. Sci. Part A Polym. Chem. 49 (April 1, 2011) 1597–1604.

[88] C.F. Ma, H. Zhou, B. Wu, G.Z. Zhang, Preparation of polyurethane with zwitterionic side chains and their protein resistance, ACS Appl. Mater. Interfaces 3 (February 2011) 455–461.

[89] D.M. Le, K. Kulangara, A.F. Adler, K.W. Leong, V.S. Ashby, Dynamic topographical control of mesenchymal stem cells by culture on responsive poly(ε-caprolactone) surfaces, Adv. Mater. 23 (August 2, 2011) 3278–3283.

[90] N.E. Kurland, T. Dey, S.C. Kundu, V.K. Yadavalli, Precise patterning of silk microstructures using photolithography, Adv. Mater. 25 (November 20, 2013) 6207–6212.

[91] N.E. Kurland, T. Dey, C.Z. Wang, S.C. Kundu, V.K. Yadavalli, Silk protein lithography as a route to fabricate sericin microarchitectures, Adv. Mater. 26 (July 9, 2014) 4431–4437.

[92] K.S. Halake, S.Y. Choi, S.M. Hong, S.Y. Seo, J. Lee, Regioselective substitution of 2-isocyanatoethylmethacrylate onto cellulose, J. Appl. Polym. Sci. 128 (May 5, 2013) 2056–2062.

[93] Z.K. Hu, L.M. Pitet, M.A. Hillmyer, J.M. DeSimone, High modulus, low surface energy, photochemically cured materials from liquid precursors, Macromolecules 43 (December 28, 2010) 10397–10405.

[94] J.G. Park, Q. Ye, E.M. Topp, P. Spencer, Enzyme-catalyzed hydrolysis of dentin adhesives containing a new urethane-based trimethacrylate monomer, J. Biomed. Mater. Res. Part B Appl. Biomater. 91B (November 2009) 562–571.

[95] G.M. Brauer, C.H. Lee, Oligomers with pendant isocyanate groups as tissue adhesives. 2. Adhesion to bone and other tissues, J. Biomed. Mater. Res. 23 (July 1989) 753–763.

[96] R.M. Hensarling, S.B. Rahane, A.P. LeBlanc, B.J. Sparks, E.M. White, J. Locklin, et al., Thiol-isocyanate "click" reactions: rapid development of functional polymeric surfaces, Polym. Chem. 2 (2011) 88–90.

[97] M.J.N. Pereira, B. Ouyang, C.A. Sundback, N. Lang, I. Friehs, S. Mureli, et al., A highly tunable biocompatible and multifunctional biodegradable elastomer, Adv. Mater. 25 (February 25, 2013) 1209–1215.

[98] A.T. Neffe, B.F. Pierce, G. Tronci, N. Ma, E. Pittermann, T. Gebauer, et al., One step creation of multifunctional 3D architectured hydrogels inducing bone regeneration, Adv. Mater. 27 (10) (January 20, 2015) 1738–1744.

[99] W.G. Liu, J.R. Zhang, K.D. Yao, DNA/lipid complex organogel with shape-memory behavior, J. Appl. Polym. Sci. 86 (October 3, 2002) 259–263.

[100] S.A. Barker, H.C. Tun, S.H. Doss, C.J. Gray, J.F. Kennedy, Preparation of cellulose carbonate, Carbohydr. Res. 17 (1971) 471–474.

[101] K.M. Tomczyk, P.A. Gunka, P.G. Parzuchowski, J. Zachara, G. Rokicki, Intramolecular etherification of five-membered cyclic carbonates bearing hydroxyalkyl groups, Green Chem. 14 (2012) 1749–1758.

[102] J.H. Clements, Reactive applications of cyclic alkylene carbonates, Ind. Eng. Chem. Res. 42 (February 19, 2003) 663–674.

[103] H. Blattmann, M. Fleischer, M. Bahr, R. Mulhaupt, Isocyanate- and phosgene-free routes to polyfunctional cyclic carbonates and green polyurethanes by fixation of carbon dioxide, Macromol. Rapid Commun. 35 (July 2014) 1238–1254.

[104] B. Nohra, L. Candy, J.F. Blanco, C. Guerin, Y. Raoul, Z. Mouloungui, From petrochemical polyurethanes to biobased polyhydroxyurethanes, Macromolecules 46 (May 28, 2013) 3771–3792.

[105] C. Carre, L. Bonnet, L. Averous, Original biobased nonisocyanate polyurethanes: solvent- and catalyst-free synthesis, thermal properties and rheological behaviour, RSC Adv. 4 (2014) 54018–54025.

[106] W.J. Wang, T. Li, T. Yu, F.M. Zhu, Synthesis of multiblock copolymers by coupling reaction based on self-assembly and click chemistry, Macromolecules 41 (December 23, 2008) 9750–9754.

3D printing of polyurethane biomaterials

5

K.-C. Hung[1], C.-S. Tseng[2], S.-H. Hsu[1,*]
[1]Institute of Polymer Science and Engineering, National Taiwan University, Taiwan, Republic of China; [2]National Central University, Taiwan, Republic of China
*Corresponding author: shhsu@ntu.edu.tw

5.1 Polyurethane as a candidate material for 3D printing

5.1.1 History and general terminology

Polyurethanes (PUs) are a family of condensation polymers that include the urethane (–NHCOO–) group in the chemical structure (Figure 5.1). The history of PUs started in 1937 when Dr Otto Bayer of Bayer Germany invented the diisocyanate polyaddition process. The early applications of PUs were mainly on soft foams and nonsegmented semicrystalline fibers. The lack of rubber materials during WWII has led to the intensive development of PU elastomers. In 1950, Bayer launched the first PU elastomer product, Vulkollan rubbers. Since then, PU elastomers have been used extensively, particular in medical, textile, automobile, and architecture industries [1–3].

PU is obtained from the reaction of diisocyanate, oligodiol (i.e., macrodiol or polyol), and a chain extender (diol or diamine). PU thus is considered a multiblock polymer. Isocyanates employed in PU synthesis can be either aromatic or aliphatic. Aromatic isocyanates have higher reactivity than aliphatic isocyanates and generally develop better mechanical properties than aliphatic isocyanate-based PUs [4]. Some of the common aromatic isocyanates are 2,4-toluene diisocyanate (TDI), 4,4-diphenylmethane diisocyanate (MDI), and 1,5-naphthalene diisocyanate (Figure 5.2) [5–7]. Aromatic isocyanate-based PUs have lower light stability, leading to a yellowish color after light exposure. Aromatic isocyanate-based PUs are also considered to have higher toxicity due to their potential to form aromatic amines after degradation. Aliphatic isocyanate-based PUs have better light stability and lower toxicity [8,9]. Major aliphatic isocyanates are 1,6-hexamethylene diisocyanate (HDI), 4,4-dicyclohexylmethane diisocyanate, and
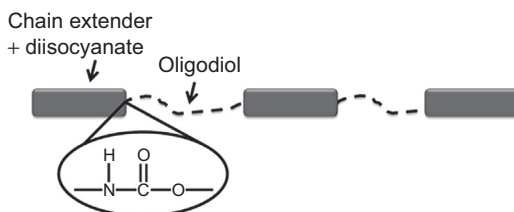
Figure 5.1 Structure of linear PUs.

Isocyanates

◆ Aromatic

2,4-toluene
diisocyanate (TDI)

4,4-diphenylmethane
diisocyanate (MDI)

1,5-naphthalene
diisocyanate (NDI)

◆ Aliphatic

1,6-hexamethylene
diisocyanate (HDI)

4,4-dicyclohexylmethane
diisocyanate (H$_{12}$MDI)

Isophorone
diisocyanate (IPDI)
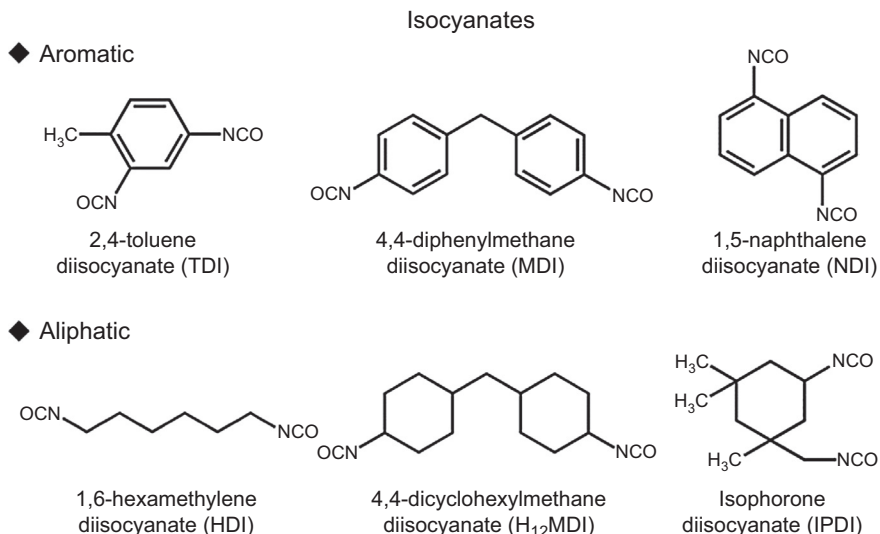
Figure 5.2 Chemical structure of common isocyanates.

isophorone diisocyanate (IPDI) (Figure 5.2) [10,11]. Oligodiols used in PU synthesis are normally between 1000 and 5000 Da. They can be categorized as polyether, polyester, or polycarbonate based. Polyether-based PU [poly(ether urethane)] has flexibility and hydrolytic resistance as well as better low-temperature properties. A disadvantage is its lower oxidative and thermal stability [12,13]. Common polyethers are polyethylene glycol (PEG) and poly(tetramethylene ether) glycol (Figure 5.3) [14,15]. Polyester-based PU [poly(ester urethane)] has greater mechanical strength and heat resistance, while it is susceptible to hydrolytic degradation [16,17]. Common polyesters are poly(ethylene adipate) diol and poly(butylene adipate) diol (Figure 5.3) [18,19]. Polycarbonate-based PU [poly(carbonate urethane)] is more biodurable than the other two types of PUs with good mechanical properties, heat stability, and hydrolytic resistance [20,21]. Even so, polycarbonate-based PUs can still undergo enzymatic hydrolysis and oxidative degradation by inflammatory cells in long-term *in vivo* applications [22,23]. Chain extenders are low molecular weight diols or diamines. The molecular weight is normally below 400 Da. The structure of a chain extender normally contributes to hydrogen bonding and enhances the mechanical properties of the product by increasing the molecular weight of PUs during synthesis [24,25].

Segmented PUs are composed of soft and hard segments. The soft segment comprises oligodiol, which has a relatively low glass transition temperature (T$_g$). The hard segment is built from the isocyanate and the chain extender [26]. The two segments have different polarities and free energy, which lead to the incompatibility between the segments termed microphase separation (Figure 5.4) [27]. The aggregated hard segments (dispersed phase) form hydrogen bonds and can be viewed as physical crosslinks [28]. The microphase separation equips PUs with elasticity. The degree of microphase separation has significant impact on the mechanical properties, thermal stability, water vapor permeability, and hydrolytic resistance of PUs [4,29,30]. The degree of

Oligodiols

◆ Polyether

Polyethylene glycol
(PEG)

Poly(tetramethylene ether)
glycol (PTMEG or PTMO)

◆ Polyester

Poly(ethylene adipate)
diol (PEA diol)

Poly(butylene adipate)
diol (PBA diol)
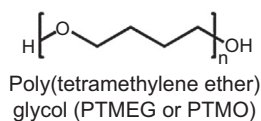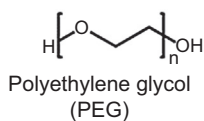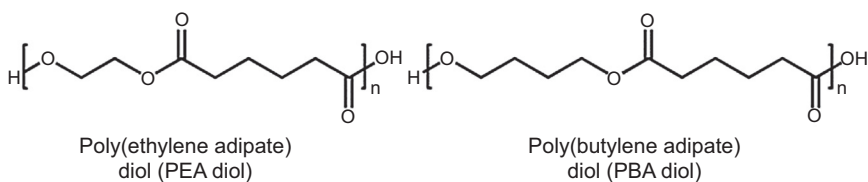
◆ Polycarbonate
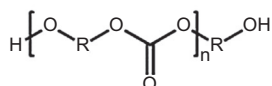
Figure 5.3 Chemical structure of common oligodiols.

Hard segment
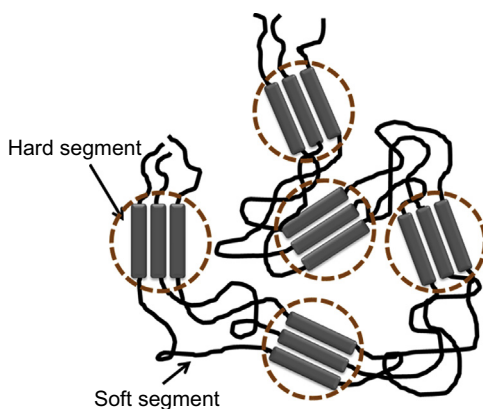
Soft segment

Figure 5.4 Microphase-separated structure of PUs.

microphase separation can be adjusted by selecting hard/soft segments with proper chemistry, molecular weight, and tendency to form hydrogen bonding [31,32]. The degree of microphase separation can be analyzed by differential scanning calorimetry, dynamic mechanical analysis, small angle X-ray scattering, small angle neutron scattering, electron microscopy, and atomic force microscopy (AFM) [27,29,33]. AFM can obtain the information of microphase separation on the surface (rather than in the bulk), which can be particularly important for biomedical applications.

5.1.2 Synthesis of polyurethanes

PU synthesis is based on the nucleophilic reaction of –NCO groups with electrophilic agents such as alcohols, amines, or water. PUs can be synthesized by one-stage or two-stage polymerization. The synthetic scheme of PUs is illustrated in Figure 5.5. In one-stage polymerization, isocyanates, oligodiols, and chain extenders are mixed to react simultaneously. In two-stage polymerization, oligodiols and isocyanates first react to form a prepolymer before further chain extension. The two-stage polymerization requires a longer reaction time, but the product has a more uniform structure, which is advantageous for achieving microphase separation and better properties [34].

PUs can be thermoset or thermoplastic. Thermoset PUs can be prepared by choosing multifunctional group chain extenders such as trimethylolpropane and glycerol [35,36]. Thermosetting PU elastomers can maintain their physical properties to somewhat higher temperatures. They can also be prepared by adding crosslinking
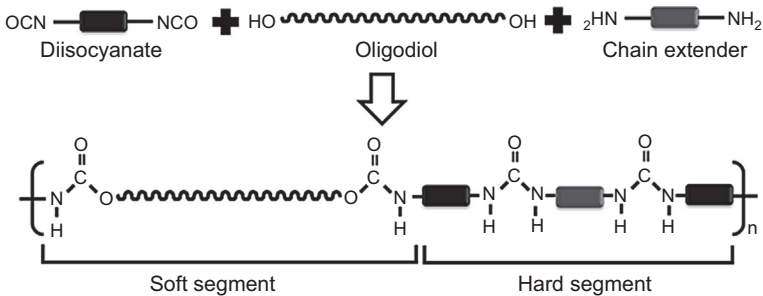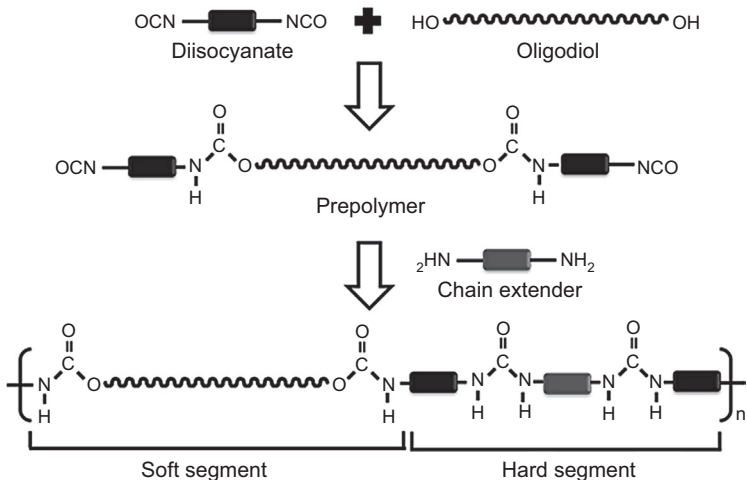
Figure 5.5 Synthetic methods of PUs.

agents such as adding isocyanates in excess, which react at high temperatures with the –NHCOO– groups to form allophanate linkages, to create a network structure [37,38]. PUs and other polymers can form interpenetrating polymer networks (IPN). IPN is an interpenetrating network structure that forms when polymers of different molecular weights and compositions are fully mixed and penetrate each other. The advantageous properties of different polymers can be combined without bulk phase separation [39]. For example, PU/epoxy resins can have the toughness of epoxy resins [40] and PU/acrylate IPN can possess high tensile strength and the weather resistance of acrylates [41,42]. Thermoplastic PUs (TPUs) are linear block polymers that can be processed by heating via extrusion molding, injection molding, blow molding, and compression molding [43–45]. They can also be dissolved in polar solvents for solution processing such as solvent casting and fiber spinning. The elasticity of PU is attributed to the hydrogen bonding between hard segments and microphase separation of soft and hard segments, with hard segments acting as physical crosslinking points [28,46].

During PU synthesis, the molecular weight and the viscosity increase sharply; therefore, solvents can be added to achieve better mixing. This type of PU is called solvent-borne PU. Highly polar organic solvents are often used such as dimethylacetamide, dimethylformamide, and dimethyl sulfoxide (DMSO) [47–49]. However, when solvent-borne PU is manufactured for further applications, the volatile organic solvents might diffuse into the air, raising environmental concerns. Furthermore, highly polar solvents are more difficult to remove and might remain in the final product [50,51]. The more eco-friendly waterborne PU has received recent attention [52]. By incorporating hydrophilic groups into the chemical structure, PU can be dispersed in water, turning into an emulsion, which thus becomes less viscous [53,54]. Waterborne PU can be classified into nonionic, anionic, and cationic according to the incorporated hydrophilic groups. Nonionic PU employs hydrophilic polyethers such as PEG or polypropylene glycol in the backbone [32]. In contrast, cationic PUs use tertiary amines [55] and anionic PUs use sulfonate, carboxyl, and phosphate to assist them to be dispersed in aqueous solutions [56]. Waterborne PUs may have lower tensile strength and water resistance because their chain extenders are less reactive after dispersion than they are in the case of solvent-borne PUs, and PUs with lower molecular weights are often formed [57,58].

To improve the mechanical properties of waterborne PUs, highly reactive or hydrogen bond-forming monomers can be used and, under proper reaction conditions, microphase separation to a greater extent can be attained [59,60]. For example, IPDI with relatively higher reactivity and the ability to form hydrogen bonding may be selected. We have recently shown that by changing the carbon/oxygen (C/O) ratio of biodegradable soft segments, waterborne PUs of excellent mechanical properties and tunable degradation rate could be obtained [61]. Due to the low viscosity, the conventional waterborne PUs may not be suitable for further manufacturing, limiting their use to adhesives and surface coatings [62,63]. By taking advantage of the nanoscale dispersion of waterborne PU particles ("nanoelastomer") and their self-assembly, we demonstrated that waterborne PUs may become a versatile biomedical polymer platform. They can encapsulate anticancer drugs and

superparamagnetic nanoparticles and be applied in the field of cancer theranostics [64]. Additionally, the waterborne PU nanoparticles may be subjected to further processing and easily transformed into microspheres, temperature-sensitive gels, electrospun fibers, elastic foams, and three-dimensional (3D)-printed scaffolds [61,65–68].

5.1.3   Biomedical polyurethanes

Biomaterials intended for biomedical applications should have good biocompatibility and appropriate physical properties. PUs in general have been demonstrated to have good biocompatibility and hemocompatibility [69]. In addition, since PU is easily processed and the mechanical properties can be easily tuned by modifications in chemical structure, it has been widely used in tubings, dressings, blood-contacting devices, etc. [28,32].

The first generation of biomedical PUs was mainly poly(ester urethane)s, which have good tensile strength, wear resistance, and low immune response after short-term implantation, thus finding use in conduits for blood pumps and in breast implants [70]. However, polyester-based PU is unstable under high temperature, and hydrolysis may occur, leading to a loss of mechanical properties [71]. Polyester-based PU may be prone to attack by hydrolytic enzymes for long-term applications [72]. Early poly(ester urethane)s mostly incorporated aromatic diisocyanate hard segments for improved mechanical properties [73]. Poly(ether urethane)s were developed for their excellent hydrolytic resistance as well as excellent elasticity [23] and have been used in neurologic leads and cardiac leads since the 1970s and have challenged silicone rubber for pacemaker insulation [70]. Commercially available products included Biomer® of Ethicon and Pellethane® of Upjohn. Nevertheless, in the late 1980s it was found that poly(ether urethane) suffered from stress cracking after being placed in the human body for long periods of time [74]. Macrophages or foreign body giant cells that attached to the PU could release peroxides that prompted free radical attack [75,76], causing PUs to degrade in particular near areas of stress concentration, leading to fracture in the long term [76,77]. Metal ions from the pacemaker coil also catalyzed oxidative degradation. Polyether-based PUs can also be attacked by enzymes [78]. Surface modification by fluoropolymers [79], introducing polysiloxane to replace part of polyether as soft segments [80], or adding gold, silver nanoparticles [81,82], or nanosilica [83–85] to form nanocomposites can improve PU biocompatibility and biostability.

Polycarbonate-based PUs and polyolefin-based PUs are third-generation biomedical PUs or biodurable PUs, which have even better hydrolytic resistance and oxidative stability both *in vivo* and *in vitro* compared to poly(ether urethane) [21,86]. They also possess excellent mechanical properties [87]. They are available in the market as Carbothane® of Thermedics and Chronoflex™ of PolyMedica [88]. Although poly(carbonate urethane) (PCU) has excellent biostability, it can degrade by the attack of free radicals [89,90]. Methods have been applied to improve the biostability of PCUs, such as enhancing the hydrogen bonding of hard segments [91]. The microphase separation may affect their biocompatibility and biostability of PCUs [92] and can be adjusted

by the structure and molecular weight of the oligodiol [93], the ratio of oligodiol to isocyanate [94], or by adding nanoparticles [95].

5.1.4 Biodegradable polyurethanes

In the earlier development of biomedical polymers much attention was focused on conceiving PUs of high biostability. Immune responses, however, could still occur for long-term applications [22,23]. Opposite to this strategy, biodegradable PUs were designed to provide short-term support in the human body and to degrade into small molecules excreted from the body without having to be taken out by surgery [96]. Biodegradable PUs can be synthesized by introducing biodegradable content into the backbone. The general method is to incorporate natural biodegradable materials, including starch and cellulose into soft segments [97,98], or choosing synthetic bio-degradable oligodiols such as polylactides, polycaprolactones, and polyhydroxyal-kanoates [61,99,100]. A poly(lactide-co-caprolactone)-based PU was developed and implanted into the subcutaneous tissues of rats for 26 weeks and New Zealand white rabbits for two and a half years. Despite the fact that in the first week macrophages and foreign body giant cells attached to the surface of the material, they tended to decrease in number as the degradation continued [101].

The degradation products of biodegradable PUs might be biologically toxic; therefore, care is required in selecting the monomers. PUs that contain aromatic isocyanates may release aromatic diamines after degradation, which are toxic to the human body [74]. Aliphatic isocyanates have been proven to have degradation prod-ucts of low toxicity by *in vitro* and *in vivo* studies [102,103]. The commonly used isocyanates in the synthesis of biodegradable PUs include IPDI, HDI, and lysine-di-isocyanate [22,61,101]. Concerning chain extenders, there is current research to introduce biological peptides such as Arg–Gly–Asp–Ser (RGDS) [104] or amino acid-based chain extenders (phenylalanine-based [105] or L-cystine-based [106]) into hard segments of PU.

The main degradation mechanism of biodegradable PU is hydrolysis, in which the ester of soft segments and the urethane of hard segments hydrolyze [107]. Hydro-lytic reactions can be classified into two types, enzyme-catalyzed hydrolysis and non-enzyme-catalyzed hydrolysis [108,109]. In the enzyme-catalyzed hydrolysis, as the name implies, the hydrolysis is catalyzed by a specific kind of enzyme, while non-enzyme-catalyzed hydrolysis occurs by contact with body fluid or water. The former one has a faster degradation rate in general [2]. Furthermore, since hard segments in PU reside in hard microdomains and are less accessible, soft segments often degrade faster than hard segments [25]. The degradation rate of PUs can be easily adjusted through selecting the appropriate monomers when synthesizing the materials, includ-ing changing the chemical structures of soft segments [61] and hard segments [25], and the molecular weight [110], crystallinity [111], hydrogen bonding [112], and hydrophobicity of monomers [113]. The degradation rate of PU thus can vary over a broad range. Additionally, the extent of microphase separation between hard seg-ments and soft segments may affect the permeability of water or the attachment of enzymes [114], consequently having an influence on the degradation rate. Our recent
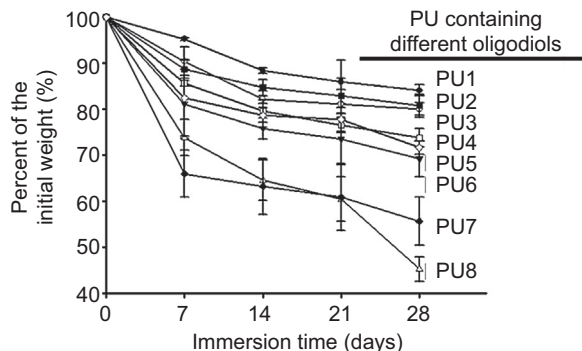
Figure 5.6 Tunable degradation rates for a series of biodegradable waterborne PUs immersed in 50 °C phosphate-buffered saline.
Adapted from [61]. They differed only in soft segment (oligodiol) compositions: PU1 employed 100% PCL diol; PU2, PU4, and PU7 employed 80%/20%, 60%/40%, and 40%/60% of PCL diol/poly (L-lactic acid) diol, respectively; PU3, PU6, and PU8 employed 80%/20%, 60%/40%, and 40%/60% PCL diol/polyethylene butylene adipate diol, respectively; PU5 employed 80%/20% PCL diol/poly(D,L-lactic acid) diol. All oligodiols had a molecular weight of 2000. The isocyanate employed in the series of PUs was IPDI.

work showed that biodegradable waterborne PU consisting of PCL diol and a second oligodiol may have different degradation rates depending on the composition, as shown in Figure 5.6. The degradation rate of PU increased with the molar ratio of the second oligodiol, which was probably associated with the greater hydrophilicity. The main mechanism has been suggested to be nonenzyme-catalyzed hydrolysis [61].

Biodegradable PUs can be processed into various products such as freeze-dried foams [67], electrospun fibers [115], and 3D-printed scaffolds [68], by the use of solvent or heat. In the case of thermal processing, the moisture must be removed to avoid heat-induced hydrolysis [72]. Biodegradable PU has been used as scaffolds for the repair of bones, cartilages, and blood vessels [68,116,117], demonstrating the potential in a wide range of medical applications.

5.2 Applications of polyurethanes in 3D printing

3D printing technology (additive manufacturing) is a process in which objects are formed layer by layer on an operating platform through computer-aided design and manufacturing. Due to the fast and precise manufacturing process, and the fact that the products can be customized, 3D printing technology is very suitable for applications in the biomedical field where individual differences abound [118]. 3D printing technology can be classified into various manufacturing processes including stereolithography (SLA), selective laser sintering (SLS), power bed and inkjet head 3D printing (PIP), fused deposition manufacturing (FDM), and liquid frozen deposition manufacturing (LFDM) (Figure 5.7) [119,120]. In SLA, monomers are mixed with photoinitiators, and then free radical polymerization occurs under exposure to light. Moreover, the structure

Stereolithography (SLA)

Scanner system

Laser source

Laser beam

Scaffolds

Photopolymer

Movable platform

Moves in z-axis

Selective laser sintering (SLS)

Scanner system

Laser source

Laser beam

Scaffolds

Roller

Power bed

Movable platform

Moves in z-axis

Power bed and inkjet head 3D printing (PIP)

Liquid adhesive supply

Inject head

Scaffolds

Roller

Power bed

Movable platform

Moves in z-axis

Fused deposition manufacturing (FDM)

Plastic filament

Liquefier

Moves in x-y-z

Extrusion nozzle

Scaffolds

Platform

Liquid frozen deposition manufacturing (LFDM)

Storage tank of polymer solution

Moves in x-y-z

Extrusion nozzle

Scaffolds

Low-temperature chamber
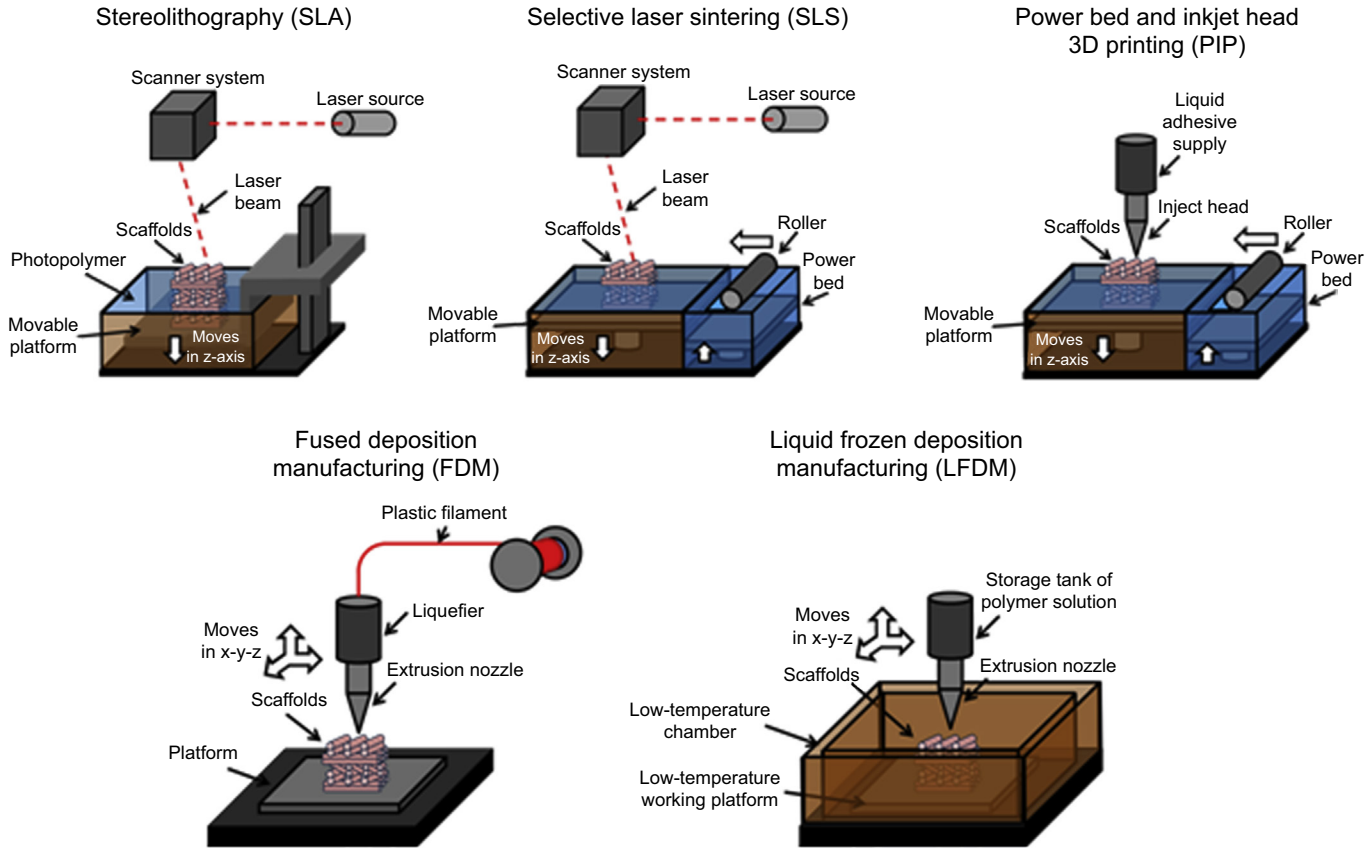
Low-temperature working platform

Figure 5.7 Schematics of 3D-printing systems classified by the processing techniques.

of the products is formed along the path on which the light is introduced. However, this method requires toxic photoinitiators that are retained in the final products and cannot be completely removed. Consequently, the method is unfavorable for manufacturing biomedical products that may be implanted [121]. On the other hand, in SLS and PIP, the objects are formed from polymer powder sintered under high temperature generated by laser light and from polymer powder clustering together via adhesives, respectively. These two methods require powder beds on which a huge amount of material is stored, often leading to wasted material [122]. In FDM and LFDM, polymers are melted by heat and are dissolved in solvents, respectively, and deposited layer by layer to form the objects. By choosing the proper temperature and solvents, objects can be manufactured from a broad range of materials [120].

According to a market estimation in 2013 [123], the total value of the global market of 3D-printing materials is currently 400 million dollars (as of May 2014), which is a 29% increase from 2011. Photo-polymers account for 50% of 3D-printed material and thermoplastic polymers account for 40%. PU has excellent elasticity, and the mechanical properties can be tuned by changing its chemical structure. When combined with the customized 3D printing, different PU materials can be selected and adjusted based on which part of the body it is applied to manufacture multifunctional and sophisticated products. In addition, since PU has been widely used in a variety of fields such as the transportation, furniture, construction, and biomedical products industries, the fast and precise process of PU manufacturing in combination with 3D printing technology has potential in each field [28].

TPU becomes molten at high temperature. The excellent processability allows PU to be fabricated by various 3D-printing procedures. Vasquez et al. chose SLS to 3D print TPU, and studied the effect of sintering energy input and laser scanning rate on the merging of TPU powder and the resultant mechanical properties. It was found that as temperature rose, the extent to which the PU powder merged increased, enhancing the mechanical properties. Increasing the laser scanning rate had the same influence on the mechanical properties of the final product [124]. In SLS the polymer powder is processed under high temperature. Some studies have pointed out that the high-temperature process may reduce the molecular weight of TPU, resulting in a decrease of tensile strength [125,126].

TPU materials for 3D printing, including such products as Bayer's Desmosint® TPU 92A-1 and BASF's Elastollan® for SLS, have been developed. For FDM, there are Bayer's Desmopan® and Falshforge's TPU wires. The TPU products fabricated from the above materials by 3D printing have demonstrated high elasticity and tear strength.

5.3 Applications of biodegradable polyurethanes in 3D printing

Biodegradable polyesters are commonly incorporated as soft segments during the synthesis of biodegradable PUs. However, pyrohydrolysis of these biodegradable polyesters tend to occur at high temperature, which leads to a decrease in tensile

strength and release of acidic components [127]. Therefore, FDM and SLS are not suitable for 3D printing of biodegradable PUs. In recent years, most of the studies turned to the other methods to successfully print objects. Pfister et al. adopted adhesive ZP11 (mixture of cellulose and starch) to 3D print biodegradable PU [128]. Unfortunately, the adhesive was water-soluble and the mechanical properties of the final products could not be maintained. To overcome this shortcoming, isocyanate was added to the adhesive ZP11 to react with PU. While some success was achieved in increasing the water-resistance and tensile strength, the final products were shown to swell when implanted [128].

Kröber et al. prepared two types of ink for 3D printing consisting of IPDI/catalyst and oligodiol/trifunctional polyol, respectively, to be applied in reactive inkjet printing. After these two types of ink were squeezed out and mixed on the operating platform, they solidified very quickly [129]. Müller et al. started from this concept to develop the ink for 3D printing composed of oligodiol, MDI, and trifunctional polyol. By changing the relative ratios of each component of the ink while the object was printed, the mechanical properties at various sites could be adjusted accordingly [130]. In addition, to prevent the catalyst from being extracted by body fluids after the product was implanted into the human body and at the same time maintain the reaction rate, highly reactive aromatic isocyanates were employed.

Kim et al. applied commercially available acrylated PU resin in SLA 3D printing, in which inorganic substances were added to increase the viscosity of the resin to a degree that it could be squeezed out before the light-induced polymerization. This method also required toxic photoinitiators to bring about the reaction [131]. Tartarisco et al. mixed commercially available liquid PU Polytek 74-20 with crosslinking agents, and pushed the materials through a nozzle to print objects. By changing the pressure and the rate at which the nozzle moved, the linewidth of the products could be tuned. Nevertheless, the unreacted crosslinking agents used made it unfavorable for use as implants [132]. Given that the above-noted methods may not be suitable for use in biomedical applications, current research efforts are focusing on applying the LFDM process for the printing of objects.

Xu et al. dissolved biodegradable PU in 1,4-dioxane and deposited it on the low-temperature operating platform to make vascular stents. After solvent removal, the vascular stents showed biodegradability and excellent mechanical properties [133]. Yan et al. also dissolved biodegradable PU in 1,4-dioxane, which was further mixed with heparin solution. They printed vascular stents on a low-temperature operating platform and obtained biodegradable venular stents with elasticity and anticoagulation properties [117]. In other literature, a double nozzle was employed to print double-layer nerve conduits from ink consisting of PU/1,4-dioxane or type I collagen/ acetic acid. Among the printed conduits, those with type I collagen as the internal layer and PU as the external layer were able to promote nerve repair [134,135]. In all the above LFDM methods for printing 3D biodegradable PU scaffolds, toxic organic solvents were still used to dissolve the PU material. This is the main disadvantage of LFDM. Besides, PU must be dissolved in a solvent that can be freeze-dried, for example, 1,4-dioxane and acetic acid. The choices of chemical compositions for the PUs are thus limited.

5.4 Low-temperature printing process of waterborne biodegradable polyurethanes

As noted, for 3D-printed PU scaffolds made by LFDM, the materials are often dissolved in the toxic organic solvents before manufacturing begins. Thus there may be residual solvent in the final product. These raise concerns for possible harmful effects when these materials are used as implants. Adopting waterborne biodegradable PUs can solve the above problems; however, the viscosity of waterborne PU is too low to be 3D printed directly. Zhang et al. sprayed anionic waterborne biodegradable PU into an acidic solution via a 3D-printing nozzle to change the dissociation degree of anions on the chains of PU, causing it to precipitate. However, the squeezed-out liquid in the method had such a low viscosity that it spread out on making contact with the platform, and could not be stacked layer after layer. Therefore, this method only resulted in two-dimensional final products [136].

A recent effort has successfully fabricated waterborne biodegradable PU scaffolds by 3D printing. First, an emulsion of waterborne biodegradable PU (soft segment 40% PCL diol and 60% polyethylene butylene adipate diol) was synthesized as a nanoparticle dispersion [61]. Before printing, polyethylene oxide (PEO) was added as a viscosity enhancer. By changing the amount of PEO, it was found that the viscosity of 3D-printing ink had a decisive influence on printing PUs by the LFDM platform. As shown in Figure 5.8, PU/PEO ink of various formulations had different viscosities, and as the PEO content increased, the viscosity increased. On the other hand, as displayed in Figure 5.9, when the viscosity of 3D-printing ink became too high to be able to pass continuously through the nozzle, serious deficiencies in the final products emerged. When the viscosity was too low, the ink was unable to solidify into a fixed shape on the platform, causing the product to collapse. The scaffolds were successfully fabricated
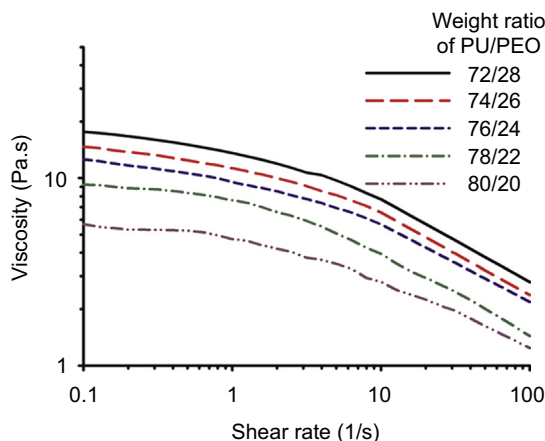

Figure 5.8 The viscosity of waterborne biodegradable PU dispersion mixed with PEO in the shear rate range between 0.1 and $100\,s^{-1}$, measured by a rheometer.
Adapted from [68]. Copyright 2014 Wiley-VCH Verlag GmbH & Co. KGaA.

only when the rheological properties of the PU-printing ink were optimal (i.e., PU/PEO 76/24). The as-prepared 3D-printed scaffolds were tested to prove that in addition to having biodegradability and excellent compliance (elasticity) (Figure 5.10), they also had good cytocompatibility. Cells may be easily seeded to the water-based 3D-printed scaffolds without any prewetting. Therefore, sophisticated 3D products made in this way are more suitable for applications in the biomedical field than those from the other biodegradable polyesters or those made by the other printing methods [68].

There are other advantages for the low-temperature printing process of waterborne PUs. Since for most of the manufacturing process of 3D printing, organic solvents and heating are required, it is difficult to include bioactive factors such as growth factors or hydrophilic drugs/antibiotics [137]. For waterborne 3D printing, the medium was water. It is thus convenient to encapsulate bioactive factors in the products for customized tissue engineering. The potential for such applications is worthy of further investigation.

Weight ratio of PU/PEO

72/28   74/26   76/24   78/22   80/20
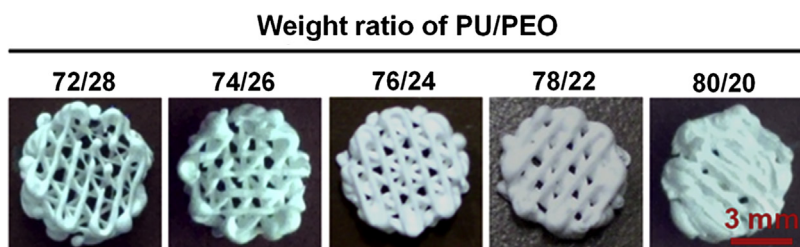
Figure 5.9 The appearance of the 3D-printed scaffolds from waterborne biodegradable PU dispersion mixed with PEO in various ratios.
Adapted from [68]. Copyright 2014 Wiley-VCH Verlag GmbH & Co. KGaA.
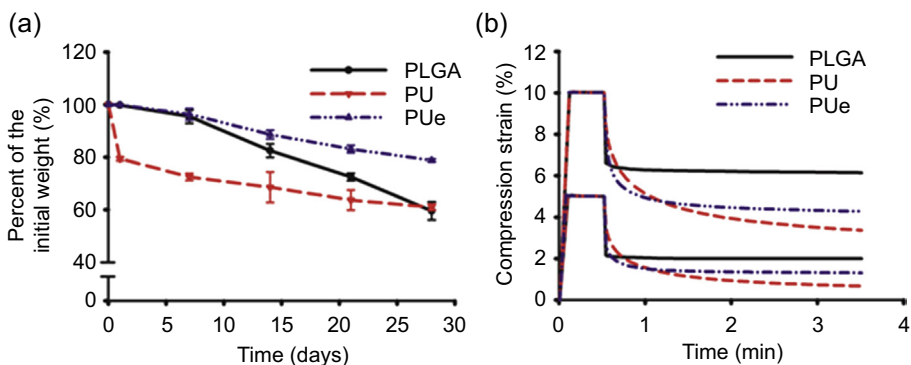
Figure 5.10 (a) The degradation profiles of 3D-printed scaffolds made of PLGA, PU, and PUe (PEO extracted first) scaffolds in 37 °C phosphate-buffered saline. (b) The dimensional recovery of 3D-printed PLGA, PU, and PUe scaffolds on removal of 5% and 10% strain. PU was synthesized from a waterborne process. The soft segment was 40% PCL diol and 60% polyethylene butylene adipate diol. PLGA was 3D-printed from 1,4-dioxane solution. PUe was prepared by immersing the PU 3D-printed scaffolds in water at 25 °C for 3 days to remove PEO. Adapted from [68]. Copyright 2014 Wiley-VCH Verlag GmbH & Co. KGaA.

At present, there is still room for improving the ink formula and manufacturing processes for biological applications of the water-based 3D printing of biodegradable PUs. The viscosity enhancer should have high viscosity and at the same time be biodegradable. Moreover, the low-temperature platform for solidification is not applicable for cell encapsulation. To avoid a liquid freezing process, waterborne PU serving as cell-containing hydrogel for 3D printing has been mixed with DMSO to dissolve PU for encapsulating cells [138,139]. However, since the cells may die from being in contact with DMSO for long periods of time, this method may not be favorable for making cell-containing scaffolds [140]. Finally, modification of the PU chemical structure can create a stimulus responsive material leading to temperature-responsive or pH-sensitive systems [66,141]. The combination of smart PU materials and 3D printing can bring significant advances to bio-3D printing for customized biomaterial applications.

5.5　Conclusion

With the progress in PU synthesis and understanding of the microphase separation and degradation mechanism, PU has become a polymer with many advantages. PUs can be designed to have various biodegradation rates by using mixed oligodiols as soft segments and by other strategies. TPU can be 3D-printed at high temperature from polymer melts or from low-temperature polymer solutions or dispersions. In particular, water-based PU dispersions can be 3D-printed into elastic, highly compliant scaffolds. Biodegradable waterborne PUs have high potential for development into novel 3D-bioprinting ink for customized tissue or organ printing.

References

[1] Engels HW, Pirkl HG, Albers R, Albach RW, Krause J, Hoffmann A, et al. Polyurethanes: versatile materials and sustainable problem solvers for today's challenges. Angew Chem Int Ed 2013;52(36):9422–41.

[2] Howard GT. Biodegradation of polyurethane: a review. Int Biodeterior Biodegrad 2002;49(4):245–52.

[3] Seymour RB, Kauffman GB. Polyurethanes: a class of modern versatile materials. J Chem Educ 1992;69(11):909–10.

[4] Chattopadhyay DK, Raju KVSN. Structural engineering of polyurethane coatings for high performance applications. Prog Polym Sci 2007;32(3):352–418.

[5] Savelyev Y, Veselov V, Markovskaya L, Savelyeva O, Akhranovich E, Galatenko N, et al. Preparation and characterization of new biologically active polyurethane foams. Mater Sci Eng C 2014;45:127–35.

[6] Ding YS, Register RA, Yang C, Cooper SL. Synthesis and characterization of sulphonated polyurethane ionomers based on toluene diisocyanate. Polymer 1989;30(7):1204–12.

[7] Wilson LD, Mohamed MH, Headley JV. Surface area and pore structure properties of urethane-based copolymers containing β-cyclodextrin. J Colloid Interface Sci 2011;357(1):215–22.

[8] Brauman SK, Mayorga GD, Heller J. Light stability and discoloration of segmented polyether urethanes. Ann Biomed Eng 1981;9(1):45–58.

[9] Lindberg HK, Korpi A, Santonen T, Säkkinen K, Järvelä M, Tornaeus J, et al. Micronuclei, hemoglobin adducts and respiratory tract irritation in mice after inhalation of toluene diisocyanate (TDI) and 4,4'-methylenediphenyl diisocyanate (MDI). Mutat Res 2011;723(1):1–10.

[10] Bruin P, Meeuwsen EA, van Andel MV, Worst JG, Pennings AJ. Autoclavable highly cross-linked polyurethane networks in ophthalmology. Biomaterials 1993;14(14):1089–97.

[11] Gurunathan T, Mohanty S, Nayak SK. Isocyanate terminated castor oil-based polyurethane prepolymer: synthesis and characterization. Prog Org Coat 2015;80:39–48.

[12] Rychlý J, Lattuati-Derieux A, Lavédrine B, Matisová-Rychlá L, Malíková M, Csomorová K, et al. Assessing the progress of degradation in polyurethanes by chemiluminescence and thermal analysis. II. flexible polyether- and polyester-type polyurethane foams. Polym Degrad Stab 2011;96(4):462–9.

[13] Yilgör E, Burgaz E, Yurtsever E, Yilgör İ. Comparison of hydrogen bonding in polydimethylsiloxane and polyether based urethane and urea copolymers. Polymer 2000;41(3):849–57.

[14] Silver JH, Marchant JW, Cooper SL. Effect of polyol type on the physical properties and thrombogenicity of sulfonate-containing polyurethanes. J Biomed Mater Res 1993;27(11):1443–57.

[15] Ma H, Darmawan ET, Zhang M, Zhang L, Bryers JD. Development of a poly(ether urethane) system for the controlled release of two novel anti-biofilm agents based on gallium or zinc and its efficacy to prevent bacterial biofilm formation. J Control Release 2013;172(3):1035–44.

[16] Thompson DG, Osborn JC, Kober EM, Schoonover JR. Effects of hydrolysis-induced molecular weight changes on the phase separation of a polyester polyurethane. Polym Degrad Stab 2006;91(12):3360–70.

[17] Awasthi S, Agarwal D. Preparation and characterisation of polyurethane coatings based on polyester polyol. Pigment Resin Technol 2010;39(4):208–13.

[18] Oprea S. Structure and properties of cross-linked polyurethane copolymers. Adv Polym Technol 2009;28(3):165–72.

[19] Frensdorff HK. Block-frequency distribution of copolymers. Macromolecules 1971;4(4):369–75.

[20] Špírková M, Pavličević J, Strachota A, Poreba R, Bera O, Kaprálková L, et al. Novel polycarbonate-based polyurethane elastomers: composition–property relationship. Eur Polym J 2011;47(5):959–72.

[21] Tanzi MC, Mantovani D, Petrini P, Guidoin R, Laroche G. Chemical stability of polyether urethanes versus polycarbonate urethanes. J Biomed Mater Res 1997;36(4):550–9.

[22] Hafeman AE, Zienkiewicz KJ, Zachman AL, Sung HJ, Nanney LB, Davidson JM, et al. Characterization of the degradation mechanisms of lysine-derived aliphatic poly(ester urethane) scaffolds. Biomaterials 2011;32(2):419–29.

[23] Anderson JM, Rodriguez A, Chang DT. Foreign body reaction to biomaterials. Semin Immunol 2008;20(2):86–100.

[24] Chan-Chan LH, Vargas-Coronado RF, Cervantes-Uc JM, Cauich-Rodríguez JV, Rath R, Phelps EA, et al. Platelet adhesion and human umbilical vein endothelial cell cytocompatibility of biodegradable segmented polyurethanes prepared with 4,4'-methylene bis(cyclohexyl isocyanate), poly(caprolactone) diol and butanediol or dithioerythritol as chain extenders. J Biomater Appl 2013;28(2):270–7.

[25] Tatai L, Moore TG, Adhikari R, Malherbe F, Jayasekara R, Griffiths I, et al. Thermoplastic biodegradable polyurethanes: the effect of chain extender structure on properties and in-vitro degradation. Biomaterials 2007;28(36):5407–17.

[26] Liu Q, Jiang L, Shi R, Zhang L. Synthesis, preparation, in vitro degradation, and application of novel degradable bioelastomers-a review. Prog Polym Sci 2012;37(5):715–65.

[27] Cooper SL, Tobolsky AV. Properties of linear elastomeric polyurethanes. J Appl Polym Sci 1966;10(12):1837–44.

[28] Chen Q, Liang S, Thouas GA. Elastomeric biomaterials for tissue engineering. Prog Polym Sci 2013;38(3–4):584–671.

[29] Yang CZ, Li C, Cooper SL. Synthesis and characterization of polydimethylsiloxane polyurea-urethanes and related zwitterionomers. J Polym Sci Part B Polym Phys 1991;29(1):75–86.

[30] Rueda L, Fernandez d'Arlas B, Corcuera MA, Eceiza A. Biostability of polyurethanes. Study from the viewpoint of microphase separated structure. Polym Degrad Stab 2014;108:195–200.

[31] Tawa T, Ito S. The role of hard segments of aqueous polyurethane- urea dispersion in determining the colloidal characteristics and physical properties. Polym J 2006;38(7):686–93.

[32] Lan PN, Corneillie S, Schacht E, Davies M, Shard A. Synthesis and characterization of segmented polyurethanes based on amphiphilic polyether diols. Biomaterials 1996;17(23):2273–80.

[33] Taylor JE, Laity PR, Wong SS, Norris K, Khunkamchoo P, Cable M, et al. Examination of hard segment and soft segment phase separation in polyurethane medical materials by electron microscopy techniques. Microsc Microanal 2006;12(2):151–5.

[34] Penczek P, Frisch KC, Szczepaniak B, Rudnik E. Synthesis and properties of liquid crystalline polyurethanes. J Polym Sci Part A Polym Chem 1993;31(2):1211–20.

[35] He Y, Zhang X, Zhang X, Huang H, Chang J, Chen H. Structural investigations of toluene diisocyanate (TDI) and trimethylolpropane (TMP)-based polyurethane prepolymer. J Ind Eng Chem 2012;18(5):1620–7.

[36] Li Z, Li J. Control of hyperbranched structure of polycaprolactone/poly(ethylene glycol) polyurethane block copolymers by glycerol and their hydrogels for potential cell delivery. J Phys Chem B 2013;117(47):14763–74.

[37] Pilch-Pitera B. Polyurethane powder coatings crosslinked with allophanate structures containing polyisocyanates. J Appl Polym Sci 2010;116(6):3613–20.

[38] Jung IK, Bae JW, Choi WS, Choi JH, Park KD. Surface graft polymerization of poly(ethylene glycol) methacrylate onto polyurethane via thiol-ene reaction: preparation and characterizations. J Biomater Sci Polym Ed 2009;20(10):1473–82.

[39] Dragan ES. Design and applications of interpenetrating polymer network hydrogels. A review. Chem Eng J 2014;243:572–90.

[40] Chen S, Wang Q, Wang T. Hydroxy-terminated liquid nitrile rubber modified castor oil based polyurethane/epoxy IPN composites: damping, thermal and mechanical properties. Polym Test 2011;30(7):726–31.

[41] Chai SL, Jin MM, Tan HM. Comparative study between core-shell and interpenetrating network structure polyurethane/polyacrylate composite emulsions. Eur Polym J 2008;44(10):3306–13.

[42] Akay M, Rollins SN. Polyurethane-poly(methyl methacrylate) interpenetrating polymer networks. Polymer 1993;34(9):1865–73.

[43] Wang X, Luo X, Wang X. Study on blends of thermoplastic polyurethane and aliphatic polyester: morphology, rheology, and properties as moisture vapor permeable films. Polym Test 2005;24(1):18–24.

[44] Vlad S, Oprea S. Evaluation of rheological behaviour of some thermoplastic polyurethane solutions. Eur Polym J 2001;37(12):2461–4.

[45] Hou Q, Grijpma DW, Feijen J. Porous polymeric structures for tissue engineering prepared by a coagulation, compression moulding and salt leaching technique. Biomaterials 2003;24(11):1937–47.

[46] Qi HJ, Boyce MC. Stress-strain behavior of thermoplastic polyurethanes. Mech Mater 2005;37:817–39.

[47] Guan J, Fujimoto KL, Sacks MS, Wagner WR. Preparation and characterization of highly porous, biodegradable polyurethane scaffolds for soft tissue applications. Biomaterials 2005;26(18):3961–71.

[48] More AS, Lebarbé T, Maisonneuve L, Gadenne B, Alfos C, Cramail H. Novel fatty acid based di-isocyanates towards the synthesis of thermoplastic polyurethanes. Eur Polym J 2013;49(4):823–33.

[49] Tan H, Li J, Luo J, Xie X, Zhong Y, Fu Q. Synthesis and properties of novel segmented polyurethanes containing alkyl phosphatidylcholine side groups. Eur Polym J 2005;41(8):1893–900.

[50] Ley DA, Fiori DE, Quinn RJ. Optimization of acrylic polyols for low VOC two-component water reducible polyurethane coatings using tertiary isocyanate crosslinkers. Prog Org Coat 1999;35(1–4):109–16.

[51] Chang K, Lu C, Lin MR. Treatment of volatile organic compounds from polyurethane and epoxy manufacture by a trickle-bed air biofilter. J Biosci Bioeng 2001;92(2):126–30.

[52] Lei L, Zhong L, Lin X, Li Y, Xia Z. Synthesis and characterization of waterborne polyurethane dispersions with different chain extenders for potential application in waterborne ink. Chem Eng J 2014;253:518–25.

[53] Ding M, Li J, Tan H, Fu Q. Self-assembly of biodegradable polyurethanes for controlled delivery applications. Soft Matter 2012;8:5414–28.

[54] Król P. Synthesis methods, chemical structures and phase structures of linear polyurethanes. Properties and applications of linear polyurethanes in polyurethane elastomers, copolymers and ionomers. Prog Mater Sci 2007;52(6):915–1015.

[55] Lu Y, Larock RC. Soybean oil-based, aqueous cationic polyurethane dispersions: synthesis and properties. Prog Org Coat 2010;69(1):31–7.

[56] Jaudouin O, Robin JJ, Lopez-Cuesta JM, Perrin D, Imbert C. Ionomer-based polyurethanes: a comparative study of properties and applications. Polym Int 2012;61(4):495–510.

[57] Hou L, Ding Y, Zhang Z, Sun Z, Shan Z. Synergistic effect of anionic and nonionic monomers on the synthesis of high solid content waterborne polyurethane. Colloids Surf A Physicochem Eng Aspects 2015;467:46–56.

[58] Yen MS, Tsai PY, Hong PD. The solution properties and membrane properties of polydimethylsiloxane waterborne polyurethane blended with the waterborne polyurethanes of various kinds of soft segments. Colloids Surf A Physicochem Eng Aspects 2006;279(1–3):1–9.

[59] Rahman MM, Kim HD. Synthesis and characterization of waterborne polyurethane adhesives containing different amount of ionic groups (I). J Appl Polym Sci 2006;102(6):5684–91.

[60] Park SH, Chung ID, Hartwig A, Kim BK. Hydrolytic stability and physical properties of waterborne polyurethane based on hydrolytically stable polyol. Colloids Surf A Physicochem Eng Aspects 2007;305(1–3):126–31.

[61] Hsu SH, Hung KC, Lin YY, Su CH, Yeh HY, Jeng US, et al. Water-based synthesis and processing of novel biodegradable elastomers for medical applications. J Mater Chem B 2014;2:5083–92.

[62] Scrinzi E, Rossi S, Deflorian F, Zanella C. Evaluation of aesthetic durability of water-borne polyurethane coatings applied on wood for interior applications. Prog Org Coat 2011;72(1–2):81–7.

[63] Bhargava S, Kubota M, Lewis RD, Advani SG, Prasad AK, Deitzel JM. Ultraviolet, water, and thermal aging studies of a waterborne polyurethane elastomer-based high reflectivity coating. Prog Org Coat 2015;79:75–82.

[64] Chen YP, Hsu SH. Preparation and characterization of novel water-based biodegradable polyurethane nanoparticles encapsulating superparamagnetic iron oxide and hydrophobic drugs. J Mater Chem B 2014;2:3391–401.

[65] Lin CY, Hsu SH. Fabrication of biodegradable polyurethane microspheres by a facile and green process. J Biomed Mater Res Part B Appl Biomater 2014. [online] Available at: http://onlinelibrary.wiley.com/doi/10.1002/jbm.b.33266/pdf. [accessed 03.08.14].

[66] Ou CW, Su CH, Jeng US, Hsu SH. Characterization of biodegradable polyurethane nanoparticles and thermally induced self-assembly in water dispersion. ACS Appl Mater Interfaces 2014;6(8):5685–94.

[67] Tsai MC, Hung KC, Hung SC, Hsu SH. Evaluation of biodegradable elastic scaffolds made of anionic polyurethane for cartilage tissue engineering. Colloids Surf B Biointerfaces 2015;125:34–44.

[68] Hung KC, Tseng CS, Hsu SH. Synthesis and 3D printing of biodegradable polyurethane elastomer by a water-based process for cartilage tissue engineering applications. Adv Healthc Mater 2014;3(10):1578–87.

[69] Ulery BD, Nair LS, Laurencin CT. Biomedical applications of biodegradable polymers. J Polym Sci Part B Polym Phys 2011;49(12):832–64.

[70] Stokes K, McVenes R. Polyurethane elastomer biostability. J Biomater Appl 1995;9(4):321–54.

[71] Schoen FJ, Harasaki H, Kim KM, Anderson HC, Levy RJ. Biomaterial-associated calcification: pathology, mechanisms, and strategies for prevention. J Biomed Mater Res 1988;22(A1 Suppl.):11–36.

[72] Amin P, Wille J, Shah K, Kydonieus A. Analysis of the extractive and hydrolytic behavior of microthane poly(ester-urethane) foam by high pressure liquid chromatography. J Biomed Mater Res 1993;27(5):655–66.

[73] Batich C, Williams J, King R. Toxic hydrolysis product from a biodegradable foam implant. J Biomed Mater Res 1989;23(A3 Suppl.):311–9.

[74] Wiggins MJ, Wilkoff B, Anderson JM, Hiltner A. Biodegradation of polyether polyurethane inner insulation in bipolar pacemaker leads. J Biomed Mater Res 2001;58(3):302–7.

[75] Schubert M, Wiggins M, Hiltner A, Anderson J. Role of oxygen in biodegradation of poly(ether urethane urea) elastomers. J Biomed Mater Res 1997;34(4):519–30.

[76] Zhao Q, Topham N, Anderson J, Hiltner A, Lodoen G, Payet C. Foreign-body giant cells and polyurethane biostability: In vivo correlation of cell adhesion and surface cracking. J Biomed Mater Res 1991;25(2):177–83.

[77] Zhao QH, McNally AK, Rubin KR, Renier M, Wu Y, Rose-Caprara V, et al. Human plasma alpha2-macroglobulin promotes in vitro oxidative stress cracking of Pellethane 2363-80A: in vivo and in vitro correlations. J Biomed Mater Res 1993;27(3):379–88.

[78] Takahara A, Hergenrother RW, Coury AJ, Cooper SL. Effect of soft segment chemistry on the biostability of segmented polyurethanes. II. In vitro hydrolytic degradation and lipid sorption. J Biomed Mater Res 1992;26(6):801–18.

[79] Ward B, Anderson J, McVenes R, Stokes K. In vivo biostability of polyether polyurethanes with fluoropolymer surface modifying endgroups: resistance to biologic oxidation and stress cracking. J Biomed Mater Res Part A 2006;79A(4):827–35.

[80] Ward R, Anderson J, McVenes R, Stokes K. In vivo biostability of polysiloxane polyether polyurethanes: resistance to biologic oxidation and stress cracking. J Biomed Mater Res Part A 2006;77A(3):580–9.

[81] Chou CW, Hsu SH, Wang PH. Biostability and biocompatibility of poly(ether)urethane containing gold or silver nanoparticles in a porcine model. J Biomed Mater Res Part A 2008;84A(3):785–94.

[82] Hsu SH, Chou CW. Enhanced biostability of polyurethane containing gold nanoparticles. Polym Degrad Stab 2004;85(1):675–80.

[83] Wang MC, Lin JJ, Tseng HJ, Hsu SH. Characterization, antimicrobial activities, and biocompatibility of organically modified clays and their nanocomposites with polyurethane. ACS Appl Mater Interfaces 2012;4(1):338–50.

[84] Tseng HJ, Lin JJ, Ho TT, Tseng SM, Hsu SH. The biocompatibility and antimicrobial activity of nanocomposites from polyurethane and nano silicate platelets. J Biomed Mater Res Part A 2011;99A(2):192–202.

[85] Lin JJ, Lin WC, Li SD, Lin CY, Hsu SH. Evaluation of the antibacterial activity and biocompatibility for silver nanoparticles immobilized on nano silicate platelets. ACS Appl Mater Interfaces 2013;5(2):433–43.

[86] Fare S, Petrini P, Motta A, Cigada A, Tanzi M. Synergistic effects of oxidative environments and mechanical stress on in vitro stability of poly(ether urethanes) and poly(carbonate urethanes). J Biomed Mater Res 1999;45(1):62–74.

[87] Kojio K, Furukawa M, Nonaka Y, Nakamura S. Control of mechanical properties of thermoplastic polyurethane elastomers by restriction of crystallization of soft segment. Materials 2010;3(12):5097–110.

[88] Yang M, Zang Z, Hahn C, Laroche G, King MW, Guidoin R. Totally implantable artificial hearts and left ventricular assist devices: selected impermeable polycarbonate urethane to manufacture ventricles. J Biomed Mater Res 1999;48(1):13–23.

[89] McBane JE, Santerre JP, Labow RS. The interaction between hydrolytic and oxidative pathways in macrophage-mediated polyurethane degradation. J Biomed Mater Res Part A 2007;82A(4):984–94.

[90] Labow RS, Meek E, Matheson LA, Santerre JP. Human macrophage-mediated biodegradation of polyurethanes: assessment of candidate enzyme activities. Biomaterials 2002;23(19):3969–75.

[91] Tang YW, Labow RS, Santerre JP. Enzyme-induced biodegradation of polycarbonate polyurethanes: dependence on hard-segment concentration. J Biomed Mater Res 2001;56(4):516–28.

[92] Hsu SH, Kao YC, Lin ZC. Enhanced biocompatibility in biostable poly(carbonate)urethane. Macromol Biosci 2004;4(4):464–70.

[93] Hsu SH, Lin ZC. Biocompatibility and biostability of a series of poly(carbonate) urethanes. Colloids Surf B Biointerfaces 2004;36(1):1–12.

[94] Hsu SH, Kao YC. Biocompatibility of poly(carbonate urethane)s with various degrees of nanophase separation. Macromol Biosci 2005;5(3):246–53.

[95] Chi TY, Yeh HY, Lin JJ, Jeng US, Hsu SH. Amphiphilic silver-delaminated clay nanohybrids and their composites with polyurethane: physico-chemical and biological evaluations. J Mater Chem B 2013;1:2178–89.

[96] Guelcher SA. Biodegradable polyurethanes: synthesis and applications in regenerative medicine. Tissue Eng Part B 2008;14(1):3–17.

 [97] Ge J, Zhong W, Guo Z, Li W, Sakai K. Biodegradable polyurethane materials from bark and starch. I. Highly resilient foams. J Appl Polym Sci 2000;77(12):2575–80.

 [98] Wang JW. Cellulose-based biodegradable cushioning packaging material. Appl Mech Mater 2013;446-447:1570–3.

 [99] Loh XJ, Tan YX, Li Z, Teo LS, Goh SH, Li J. Biodegradable thermogelling poly(ester urethane)s consisting of poly(lactic acid)–thermodynamics of micellization and hydrolytic degradation. Biomaterials 2008;29(14):2164–72.

[100] Ou W, Qiu H, Chen Z, Xu K. Biodegradable block poly(ester-urethane)s based on poly(3-hydroxybutyrate-co-4-hydroxybutyrate) copolymers. Biomaterials 2011;32(12):3178–88.

[101] van Minnen B, Leeuwen MBMV, Kors G, Zuidema J, van Kooten TG, Bos RRM. In vivo resorption of a biodegradable polyurethane foam, based on 1,4-butanediisocyanate: a three-year subcutaneous implantation study. J Biomed Mater Res Part A 2008;85A(4):972–82.

[102] Gorna K, Gogolewski S. Biodegradable polyurethanes for implants. II. In vitro degradation and calcification of materials from poly(epsilon-caprolactone)-poly(ethylene oxide) diols and various chain extenders. J Biomed Mater Res 2002;60(4):592–606.

[103] Gogolewski S, Gorna K. Biodegradable polyurethane cancellous bone graft substitutes in the treatment of iliac crest defects. J Biomed Mater Res Part A 2007;80A(1):94–101.

[104] Guan J, Wagner WR. Synthesis, characterization, and cytocompatibility of polyurethaneurea elastomers with designed elastase sensitivity. Biomacromolecules 2005;6(5):2833–42.

[105] Parrag IC, Woodhouse KA. Development of biodegradable polyurethane scaffolds using amino acid and dipeptide-based chain extenders for soft tissue engineering. J Biomater Sci Polym Ed 2010;21(6):843–62.

[106] Wang J, Zheng Z, Chen L, Tu X, Wang X. Glutathione-responsive biodegradable poly(urea-urethane)s containing L-cystine-based chain extender. J Biomater Sci Polym Ed 2013;24(7):831–48.

[107] Pierre TS, Chiellini E. Biodegradability of synthetic polymers used for medical and pharmaceutical applications: Part 1-principles of hydrolysis mechanisms. J Bioact Compat Polym 1986;1(4):467–97.

[108] Guo Q, Lu Z, Zhang Yi, Li S, Yang J. In vivo study on the histocompatibility and degradation behavior of biodegradable poly(trimethylene carbonate-co-D,L-lactide). Acta Biochim Biophys Sinica 2011;43(6):433–40.

[109] Christenson EM, Patel S, Anderson JM, Hiltner A. Enzymatic degradation of poly(ether urethane) and poly(carbonate urethane) by cholesterol esterase. Biomaterials 2006;27(21):3920–6.

[110] Khan F, Valere S, Fuhrmann S, Arrighi V, Bradley M. Synthesis and cellular compatibility of multi-block biodegradable poly(3-caprolactone)-based polyurethanes. J Mater Chem B 2013;1:2590–600.

[111] Kavlock KD, Whang K, Guelcher SA, Goldstein AS. Degradable segmented polyurethane elastomers for bone tissue engineering: effect of polycaprolactone content. J Biomater Sci Polym Ed 2013;24(1):77–93.

[112] Christenson EM, Anderson JM, Hiltner A. Biodegradation mechanisms of polyurethane elastomers. Corros Eng Sci Technol 2007;42(4):312–23.

[113] Skarja GA, Woodhouse KA. Synthesis and characterization of degradable polyurethane elastomers containing and amino acid-based chain extender. J Biomater Sci Polym Ed 1998;9(3):271–95.

[114] Huang SL, Chao MS, Ruaan RC, Lai JY. Microphase separated structure and protein adsorption of polyurethanes with butadiene soft segment. Eur Polym J 2000;36(2):285–94.

[115] Kuo YC, Hung SC, Hsu SH. The effect of elastic biodegradable polyurethane electrospun nanofibers on the differentiation of mesenchymal stem cells. Colloids Surf B Biointerfaces 2014;122:414–22.

[116] Moon SH, Baek SO, Jung SN, Seo BF, Lee DC, Kwon H. Efficacy of biodegradable synthetic polyurethane foam for packing nasal bone fractures. J Craniofacial Surg 2012;23(6):1848–50.

[117] Yan Y, Wang XH, Yin D, Zhang R. A new polyurethane/heparin vascular graft for small-caliber vein repair. J Bioact Compat Polym 2007;22(3):323–41.

[118] Bartolo P, Kruth JP, Silva J, Levy G, Malshe A, Rajurkar K, et al. Biomedical production of implants by additive electro-chemical and physical processes. CIRP Ann Manuf Technol 2012;61(2):635–55.

[119] Billiet T, Vandenhaute M, Schelfhout J, Vlierberghe SV, Dubruel P. A review of trends and limitations in hydrogel-rapid prototyping for tissue engineering. Biomaterials 2012;33(26):6020–41.

[120] Hollister SJ. Porous scaffold design for tissue engineering. Nat Mater 2005;4(7):518–24.

[121] Gauvin R, Chen YC, Lee JW, Soman P, Zorlutuna P, Nichol JW, et al. Microfabrication of complex porous tissue engineering scaffolds using 3D projection stereolithography. Biomaterials 2012;33(15):3824–34.

[122] Yeong WY, Chua CK, Leong KF, Chandrasekaran M. Rapid prototyping in tissue engineering: challenges and potential. Trends Biotechnol 2004;22(12):643–52.

[123] Wohlers Associates, Inc. Wohlers report 2013 reveals continued growth in 3D printing and additive manufacturing, Colorado; 2013.

[124] Vasquez GM, Majewski CE, Haworth B, Hopkinson N. A targeted material selection process for polymers in laser sintering. Addit Manuf 2014;1:127–38.

[125] Plummer K, Vasquez M, Majewski C, Hopkinson N. Study into the recyclability of a thermoplastic polyurethane powder for use in laser sintering. Proc Inst Mech Eng Part B J Eng Manuf 2012. [online] Available at: http://pib.sagepub.com/content/early/2012/03/30/0954405412440066.full.pdf. [accessed 27.01.12].

[126] Ziegelmeier S, Wölleckea F, Tucka CJ, Goodridgea RD, Haguea RJM. Aging behavior of thermoplastic elastomers in the laser sintering process. J Mater Res 2014;29(17):1841–51.

[127] Yen HJ, Hsu SH, Tseng CS, Huang JP, Tsai CL. Fabrication of precision scaffolds using liquid-frozen deposition manufacturing for cartilage tissue engineering. Tissue Eng Part A 2009;15(5):965–75.

[128] Pfister A, Landers R, Laib A, Hübner U, Schmelzeisen R, Mülhaupt R. Biofunctional rapid prototyping for tissue-engineering applications: 3D bioplotting versus 3D printing. J Polym Sci Part A Polym Chem 2004;42(3):624–38.

[129] Kröber P, Delaney JT, Perelaer J, Schubert US. Reactive inkjet printing of polyurethanes. J Mater Chem 2009;19:5234–8.

[130] Müller M, Huynh QU, Uhlmann E, Wagner MH. Study of inkjet printing as additive manufacturing process for gradient polyurethane material. Prod Eng Res Dev 2014;8(1–2):25–32.

[131] Kim SG, Chu WS, Jung WK, Ahn SH. Evaluation of mechanical and electrical properties of nanocomposite parts fabricated by nanocomposite deposition system (NCDS). J Mater Process Technol 2007;187-188:331–4.

[132] Tartarisco G, Gallone G, Carpi F, Vozzi G. Polyurethane unimorph bender microfabricated with pressure assisted microsyringe (PAM) for biomedical applications. Mater Sci Eng C 2009;29(6):1835–41.

[133] Xu W, Wang X, Yan Y, Zhang R. Rapid prototyping of polyurethane for the creation of vascular systems. J Bioact Compat Polym 2008;23(2):103–14.

[134] Cui T, Yan Y, Zhang R, Liu L, Xu W, Wang X. Rapid prototyping of a double-layer polyurethane-collagen conduit for peripheral nerve regeneration. Tissue Eng Part C 2009;15(1):1–9.

[135] Wang X, Cui T, Yan Y, Zhang R. Peroneal nerve regeneration using a unique bilayer polyurethane-collagen guide conduit. J Bioact Compat Polym 2009;24(2):109–27.

[136] Zhang C, Wen X, Vyavahare N, Boland T. Synthesis and characterization of biodegradable elastomeric polyurethane scaffolds fabricated by the inkjet technique. Biomaterials 2008;29(28):3781–91.

[137] Sohier J, Moroni L, van Blitterswijk C, de Groot K, Bezemer JM. Critical factors in the design of growth factor releasing scaffolds for cartilage tissue engineering. Expert Opin Drug Deliv 2008;5(5):543–66.

[138] Huang Y, He K, Wang X. Rapid prototyping of a hybrid hierarchical polyurethane-cell/hydrogel construct for regenerative medicine. Mater Sci Eng C 2013;33(6):3220–9.

[139] Wang X, He K, Zhang W. Optimizing the fabrication processes for manufacturing a hybrid hierarchical polyurethane-cell/hydrogel construct. J Bioact Compat Polym 2013;28(4):303–19.

[140] Wang HY, Lun ZR, Lu SS. Cryopreservation of umbilical cord blood-derived mesenchymal stem cells without dimethyl sulfoxide. CryoLetters 2011;32(1):81–8.

[141] Sartori S, Chiono V, Tonda-Turo C, Mattu C, Gianluca C. Biomimetic polyurethanes in nano and regenerative medicine. J Mater Chem B 2014;2:5128–44.

Nanoparticle-induced phenomena in polyurethanes

6

D.K. Patel, A. Biswas, P. Maiti*
School of Material Science and Technology, Indian Institute of Technology (BHU),
Varanasi, Uttar Pradesh, India
*Corresponding author: pmaiti.mst@itbhu.ac.in

6.1 Introduction

Polyurethanes (PUs), versatile polymeric materials, are used extensively in biomedical applications due to their excellent biocompatibility, processability, and exceptional mechanical flexibility [1,2]. PUs are widely used as adhesives, coatings, construction materials, synthetic leathers, flame retardants, and wound dressings. PUs can be tailored in terms of their mechanical properties, oxygen permeability, barrier properties, and drug transport for a variety of biomedical applications [3–8]. PUs are usually synthesized using three components, for example, diols, diisocyanates, and chain extenders, and their properties can be modified either by changing the composition and nature of the diols, diisocyanates, and chain extenders or by incorporation of fillers in the polymer matrix [9]. Segmented PUs consist of hard and soft segment units that determine the mechanical properties of the polymer. Both relatively biostable and biodegradable PUs are used in different forms in artificial organs and medical devices [10]. Biodegradable PUs are used in drug delivery systems and implant materials for tissue repair [11].

Polymers with different forms of fillers such as carbon black, fullerenes, carbon nanotubes (CNTs), graphene, layered silicates (nanoclay), layered double hydroxides (LDHs), different metals, and ceramics are extensively used to modify the properties of pure polymers [12–17]. There are several metals and their oxides such as Ag, Au, TiO_2, Fe_3O_4, and ZnO that are frequently used to improve the properties of polymers. Since silver exhibits antibacterial properties, its nanoparticles embedded in polymers are utilized in various medical applications including wound dressings, artificial skin, bone tissue engineering, and urinary catheters [18–20]. Nanoparticles having superparamagnetic properties have received much attention as composites because they do not retain their magnetization properties in the absence of a magnetic field. This nanoparticle feature is very useful in magnetic resonance imaging and targeted drug delivery [21–24]. Fe_3O_4 is a superparamagnetic nanoparticle widely used in polymer composites due to its large surface area, biocompatibility, and nontoxic nature with good magnetic properties [25]. CNTs have also been used in composites due to their high electrical, thermal, and mechanical properties [26]. Inorganic materials having nanometer dimensions show very interesting physical and chemical properties, leading to development of new materials for various applications [27]. Montmorillonite (MMT), which is the major ingredient of bentonite, is commonly used for the

preparation of polymer composites for enhancement of properties. In MMT, two tetrahedrally coordinated silicon atoms are joined to an edge-shared octahedral sheet of magnesium or aluminum hydroxide. Cationic species present in the lattice structure are replaceable by other cations, for example, Al^{3+} can be replaced by divalent species such as Fe^{2+} or Mg^{2+} and Mg^{2+} or even by monovalent Li^{1+}, leading to generation of a negative charge in the lattice that is counterbalanced by the positive ions present in the interlayer spacing. Due to the presence of weak van der Waals forces acting within the matrix, these materials can easily be dispersed and provide high surface areas available for interaction during synthesis. Another advantage of these nanoparticles is their easy surface modification through ion exchange, which can enhance their polymer compatibility. Considerable enhancements in the thermal stability [28–30], barrier properties [31–33], mechanical strength [34–36], elastic properties [37,38], biodegradation, and high energy shielding [39,40] were observed in nanocomposites using nanoclay as the filler [41]. Tuning of the morphology and mechanical properties of the polymer and its nanocomposites in the presence of nanoclay was also reported [9,42]. Nanoparticle-induced self-assembly in PUs has several benefits such as improvement in mechanical properties, thermal stability, and decrease of the rate of enzymatic degradation [43]. LDH and anionic clay have received much attention in the field of nanocomposites due to their anion exchange capabilities, catalysis, and delivery of drugs as well as biological molecules such as DNA and enzymes [44]. LDH has a brucite-like structure and the replacement of divalent cations by trivalent ones results in excess charges that are counterbalanced by anions located between two layers [45]. Enhancement in mechanical properties and thermal stability were observed in those polymer nanocomposites in which exfoliated/disordered LDH was used as filler material [46]. Recently, the use of carbon materials as a filler has received tremendous attention in the composite field due to their exceptional properties. Different forms of carbon allotropes are used and depending on their structure are termed as fullerenes (0-D), CNT and nanoribbons (1-D), graphene (2-D), and graphite (3-D). Fullerenes can be formed through wrapping of graphene sheets, which leads to the formation of CNT. Stacking of graphene sheets is responsible for the formation of the graphite allotrope of carbon [47]. Graphene, a single layer of sp^2 hybridized carbon atoms arranged in a hexagonal lattice, is the fundamental structural unit of all kinds of carbon allotropes [48]. The chemical modifications of graphene are comparatively simple and important properties such as mechanical, thermal, electronic, and optical can be varied [49–52]. This allows graphene to have a wide range of applications in the field of energy technology [53,54], sensors [55], nanoelectronics [56], composites [57–60], and biomaterials [61]. Zeolites, another inorganic material, are frequently used in nanocomposites and in catalysis. Zeolites are also used in various applications due to their mechanical and thermal stability [62]. Zeolites are aluminosilicate minerals containing micropores in their structure. Since aluminosilicates have a negatively charged oxygen framework, this excess charge is balanced by the positively charged cations. Zeolites can be utilized for the preparation of antibacterial polymer nanocomposites. By tuning the Si/Al ratio as well as ion exchange properties of zeolites, one can tune the properties of composites material for a variety of purposes [63]. Classification of nanoparticles with different dimensions are shown in Scheme 6.1.
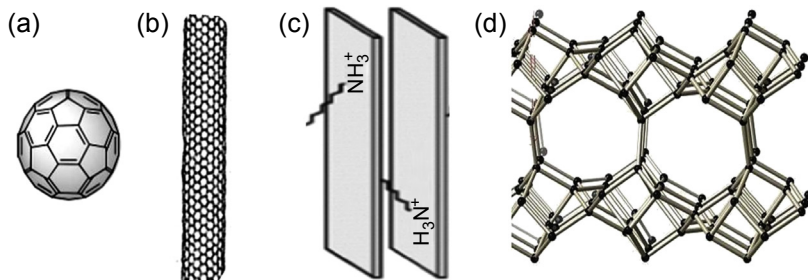
Scheme 6.1 Various types of nanoparticles. (a) 0D, fullerene; (b) 1D, carbon nanotube; (c) 2D, clay; and (d) 3D, zeolite [64–67].

6.2 Preparation of composites

There are different ways to prepare polymer composites and their advantages or drawbacks are as follows:

6.2.1 Solution casting technique

This is a common technique for the preparation of polymer composites. In the first step, dispersion of filler is achieved in appropriate solvent through mechanical stirring or sonication, followed by dissolution of the polymer in the same solvent. The dispersed fillers are then mixed with polymer solution either at room temperature or at higher temperature depending on the solubility of the polymer. Composite films are obtained either by precipitation or by casting the solution/mixture.

6.2.2 Melt blending process

This process of composite preparation is achieved using equipment such as an extruder [68] that has the ability to generate high shear force at elevated temperatures. The filler is added to the molten polymer and is sheared at a high rate. The advantage of this technique is that there is no solvent required. The drawbacks of this process are that a fine dispersion may not be achieved and that only limited filler concentrations can be used [69]. In addition the polymer chain may degrade under high shear conditions at high temperatures.

6.2.3 In Situ techniques

This is an efficient technique for the preparation of composites, allowing uniform dispersion of the filler to take place. Fillers are dispersed in monomer, possibly in the presence of solvent followed by the addition of the curing agents, hardener, or chain extender for polymerization at an appropriate temperature. One of the major advantages of this technique is that homogeneous dispersion of filler occurs in polymer matrix leading to significant improvement of most properties.

6.2.4   Latex method

Latex is a colloidal dispersion of polymer in an aqueous solvent. This method is more suitable for those polymers that can be prepared via emulsion polymerization or those that have the ability to form emulsion. It consists of an aqueous dispersion/stabilization of filler using a surfactant followed by the addition of the dispersed filler into the polymer latex. Nanocomposites can be obtained after freeze-drying the above mixture followed by melt processing. The latex method has several advantages including no requirement for organic solvent, reliability, ease of processing, and improved dispersion of the filler in the viscous polymer matrix [70].

6.3   Morphology

The presence of filler alters the morphology of the polymer matrix in various ways. Composite morphologies are highly influenced by the preparation method and extent and chemical nature of the filler used. Transmission electron microscopy (TEM), scanning electron microscopy (SEM) , atomic force microscopy (AFM), and optical microscopes are usually used to characterize the morphology. Dispersion of gold nanoparticles (0-D) in PU matrix is presented in Figure 6.1(a). At a low concentration, the distribution is homogeneous whereas it aggregates at a higher concentration (>65 ppm). The surface morphology observed through SEM shows a globular pattern in an Ag nanoparticle (AgNP) dispersed in a PU composite (Figure 6.1(a′)) while an AFM phase topography of the gold nanoparticles composite is given in Figure 6.1(a″). Roughness of the pure PU and its composites is in the range of 2.0–2.8 nm, indicating moderately flat surfaces. Hsu et al. and Cho were observed the formation of a lamellar structure through the hard segment of PU, which tends toward a micelle shape with increase of the hard segment content in PU [71,72]. Homogeneous dispersion of CNTs (1-D nanoparticles) in a PU matrix through *in situ* polymerization is shown in Figure 6.1(b) [73]. Uniform dispersion of filler through the *in situ* method provides a high surface area to interact better with polymer matrix and control the mechanical properties of the composite [74]. Better dispersion is also observed in the SEM and AFM images of the PU–CNT composites [75,76] (Figure 6.1(b′) and (b″)). The distribution of nanoclay (2-D nanoparticles) in a PU matrix and its effect on surface morphology are shown in Figure 6.1(c, c′, c″). Homogeneous dispersion is clearly observed as the composite was prepared *in situ* by dispersing nanoclay in polyol followed by polymerization with diol and diisocyanate. The surface morphology of the nanocomposite was also affected by the time of incorporation of the clay during the polymerization process. Pure PU exhibits a flake-like structure whereas the nanocomposites show a grainy morphology, which does not occur when the nanoclays are incorporated at an early stage of polymerization [9]. The banded pattern in the AFM image is evident in nanoclay PU composites with the band size becoming narrower in the composite than in pure PU. The SEM image of a PU–zeolite composite reveals the well-dispersed zeolite in the PU matrix (Figure 6.1(d)). The asymmetric structure of membrane consists of top skin, substructure, and bottom skin. Some aggregation of zeolite is observed in dense bottom skin. A study of the cross-section of the membrane reveals that the incorporation of zeolite is
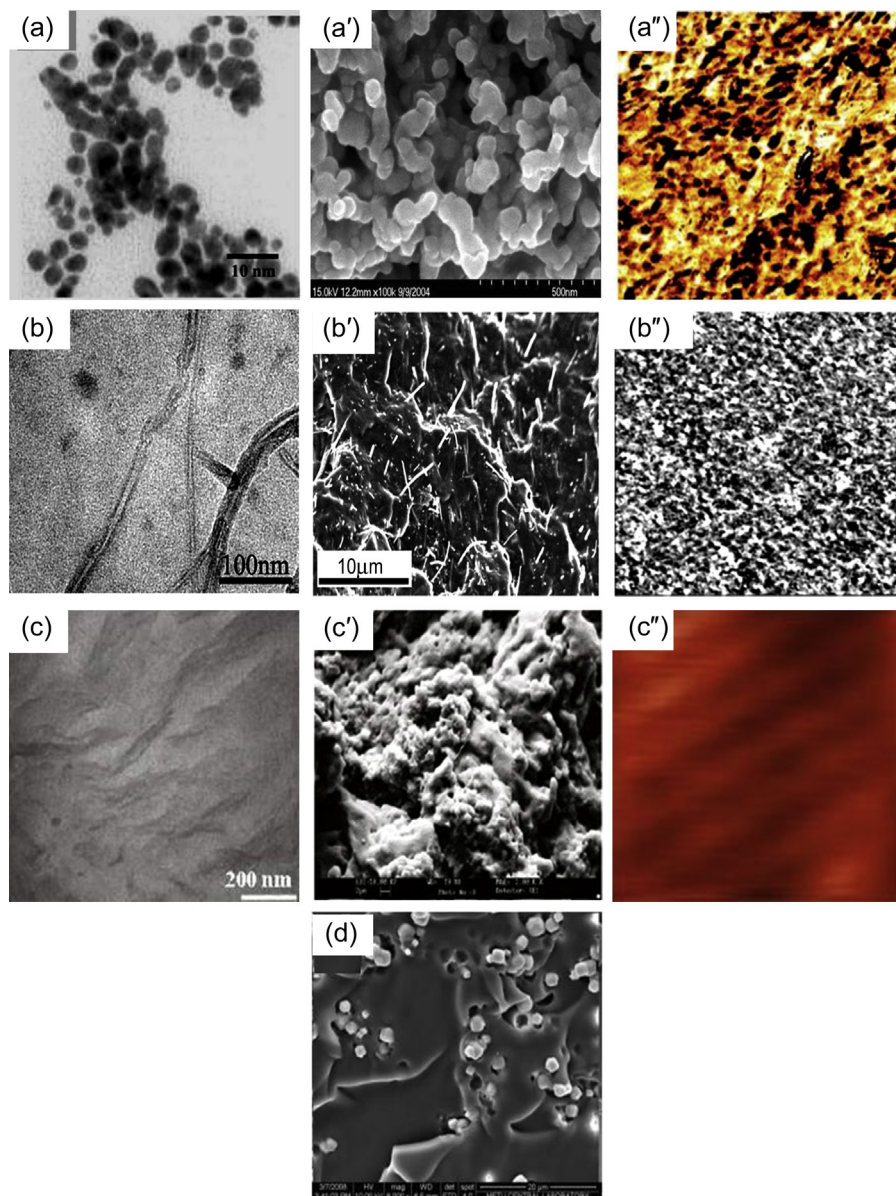
Figure 6.1 Morphology of polyurethane with various types of nanoparticles. (a) TEM micrograph of PU–Au nanocomposites containing 43.5 ppm gold particles [71], (a′) SEM image of PU–Ag fiber [72], (a″) AFM phase containing 17.4 ppm gold in PU matrix [71]; (b) TEM image of PU–CNT nanocomposites [73], (b′) SEM micrograph of PU–CNT nanocomposites containing 10 wt% CNT in matrix [75], (b″) AFM image of PU–MWCNTs [76]; (c)TEM image of PU–nanoclay, (c′) SEM micrograph of PU–nanoclay, and (c″) AFM image of PU–nanoclay [9]; and (d) SEM micrograph of PU–zeolite nanocomposites [78].

uniform only in the top skin (active layer) and in the substructure of the membrane. The pore size also decreases in the composite compared to the pure PU [77,78].

6.4　Structure

The incorporation of various nanoparticles in a PU matrix produces structural changes that are summarized here. X-ray diffraction (XRD) shows that the aromatic-based PU matrix is amorphous while the nano-TiO$_2$ (0-D filler) reveals its diffraction peaks (Figure 6.2(a)) [79]. The addition of CNT into a PU matrix disrupts the microphase morphology [80] (Figure 6.2(b)). Considerable enhancement of nanoclay interlayer spacing occurs when the clay is added to diol. Subsequent addition of diisocyanate and polymerization increase the spacing further as polymerization takes place, which displaces the silicate layers making an exfoliated structure [9] (Figure 6.2(c)). XRD patterns of PU–LDH nanocomposites exhibit the exfoliated nature at lower concentration of LDH while an intercalated nature is seen at higher LDH (2-D nanofiller) content [44]. PU having zeolite in its matrix shows a sharp peak at $2\theta = 37°$ and the intensity as well as position of this peak is affected by the content of the zeolite (Figure 6.2(d)) [81] due to the change in the

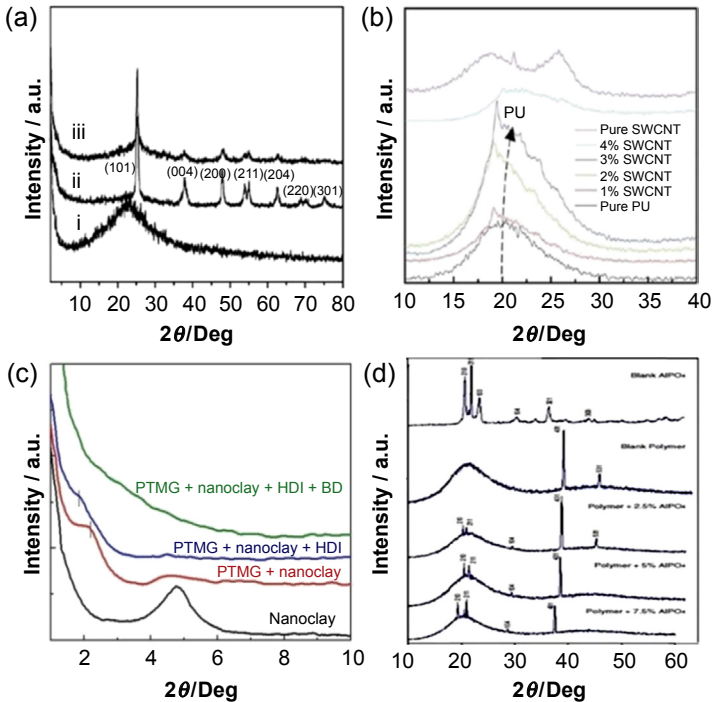**Figure 6.2** XRD patterns of PU and its nanocomposites with different types of nanoparticles: (a–i) pure PU, (a–ii) pure nano-TiO$_2$, and (a–iii) PU–nano-TiO$_2$ composite [79], (b) PU–CNT composites [80], (c) PU–clay nanocomposites [9], and (d) PU–AlPO$_4$-5 zeolite composites [81].

microcrystalline structure of the composites. For all types of filler, as expected, the intensity of the filler peak increases with increase of the content of filler in the composites.

6.5 Nanoparticle-induced self-assembly

Self-assembly plays an important role in enhancing the physical and mechanical properties of polymers. Nanoclay-induced self-assembly in aliphatic PUs via *in situ* polymerization has been observed [9]. Layer by layer self-assembly in aliphatic PU was observed through XRD, small-angle neutron scattering (SANS), AFM, and polarizing optical microscopy (POM). The appearance of a peak at ~5.8° (d-spacing ~1.6 nm) in XRD measurement suggests the formation of molecular layers in the PU nanocomposite (Figure 6.3(a)). Further, a shoulder/peak in SANS measurement with characteristic value ($\Lambda_c \sim 12$–14 nm) indicates the presence of a nanostructure in PU/nanocomposites (Figure 6.3(b)). The lower value of the characteristic length in nanocomposite (12 nm) compared to pure PU (14 nm) indicates nanoclay-induced self-assembly where a lesser number of molecular sheets is required for greater assembly
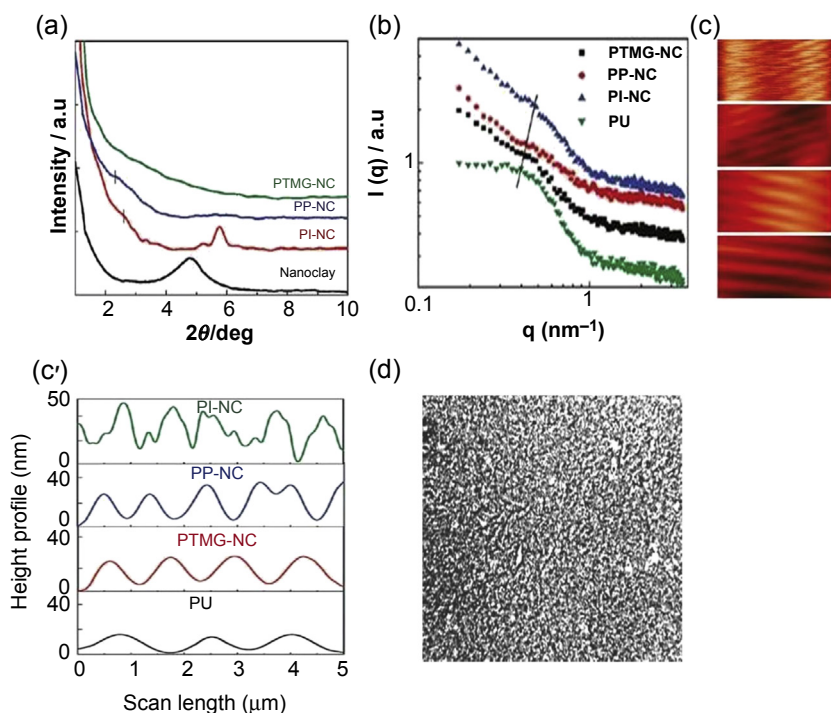

Figure 6.3 (a) X-ray diffraction patterns of organically modified Closite-30B nanoclay and nanocomposites, (b) small-angle neutron scattering patterns; I(q) versus q (wave vector) plot of indicated PU and nanocomposites, (c, c′) AFM image of PU and its nanocomposites with height profile, and (d) POM image PU–nanoclay composite [9].

through hydrogen bonding. The domain structure observed in AFM topographs suggests a larger assembly (lateral dimension of ~0.5 μm) (Figure 6.3(c)). A greater number of peaks as well as intensity of the height profile in the nanocomposite compared to pure PU appears in AFM topographs. This suggests the formation of a more consolidated structure in the nanocomposites. Larger structures in the nanocomposites were observed in the PU using optical microscopy (Figure 6.3(d)). The driving force for this self-assembly is the extensive hydrogen bonding between the urethane moieties in the polymer chains with the clay nanocrystals. Tuning of the surface morphology and properties due to the influence of clay through self-assembly was also revealed in aliphatic PUs having various chain extenders [42].

6.6   Mechanical behavior

The mechanical properties of composites depend on the amount, aspect ratio, surface area, orientation, interaction, and dispersion of the filler in polymer matrix [82]. Deka et al. synthesized PU nanocomposites with different weight percentages of Ag particles and measured the mechanical properties (tensile strength, bending, hardness (Shore A), and impact resistance). Tensile strength, hardness, and impact resistance increase with increasing weight percentage of nanoparticles while the elongation at break and bending remains the same compared to pure PU. The enhancement in mechanical properties was due to homogeneously dispersed Ag nanoparticles (AgNPs) with larger surface areas, which can interact with the matrix and facilitate easy transfer of stress to the fillers (Figure 6.4(a)) [83]. Mechanical properties of the composites can also be tuned by using different sizes of nanoparticles. Larger particles in the matrix result in lower stiffness and higher elongation at break compared to the composites with smaller particles, which show increased stiffness and lower elongation at break. Most differences in properties of the composites arise due to the interaction between filler and matrix polymer [84]. CNT with its high surface area and aspect ratio has a tensile strength of 50–200 GPa and Young's modulus of 1.2 TPa, which make it attractive for enhancing the mechanical properties of polymer matrices [68]. Figure 6.4(b) shows stress–strain curves of CNT-based PU composites as a function of CNT content [85]. The improvement of mechanical properties is due to the good dispersion of CNT that facilitates the load transfer between the polymer matrix and the CNTs. PU composites formed by using multiwall CNTs (MWNTs) and single wall CNTs (SWNTs) have shown different mechanical properties. MWNTs exhibit greater improvement in modulus whereas SWNT-based composites show improvement in tensile strength and elongation at break compared to the pure PU [86]. Considerable improvement in mechanical properties of PU/LDH composites is also reported. These improved properties are mainly due to the interaction of hydroxyl groups of LDH and the polar urethane linkages along with the high aspect ratio and orientation of LDH, which help the load transfer process during measurement (Figure 6.4(c)) [87]. PU/clay nanocomposites prepared through the *in situ* polymerization technique exhibit enhanced mechanical properties in terms of modulus and toughness. Orientation of the two-dimensional nanoclay toward the applied force field is responsible for the toughness enhancement in nanohybrids [88]. Incorporation
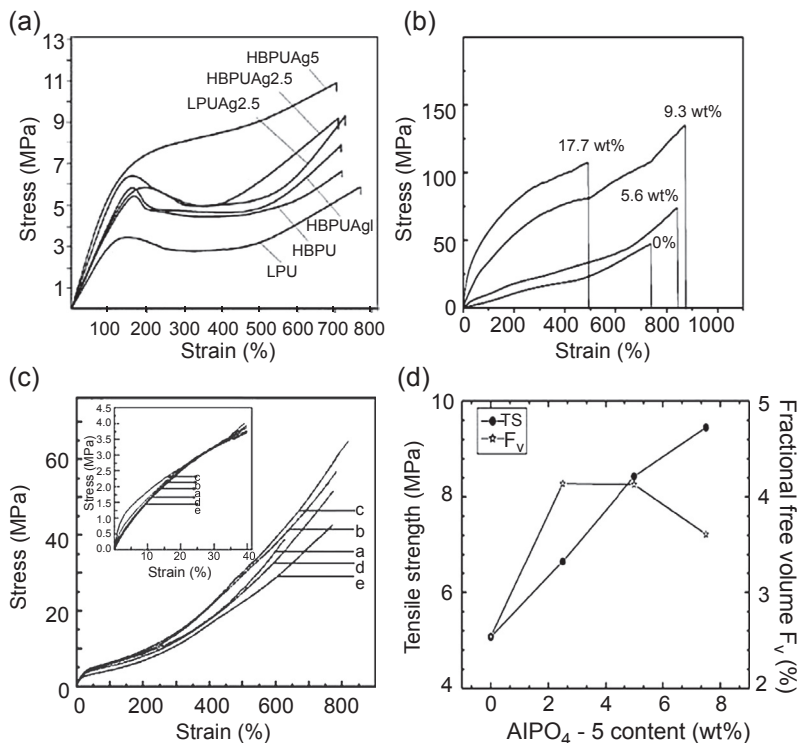
Figure 6.4 Mechanical behavior of polyurethane composites with various types of nanoparticles: (a) PU and its nanocomposites containing silver particles [83], (b) PU and its nanocomposites with CNTs [85], (c) PU–LDH nanocomposite (in which a, b, c, d, and e represent the pure PU, 1, 3, 5, and 8 wt% of LDH in matrix) [87], and (d) PU–zeolite composites [81].

of 2 wt% of graphene in PU matrix during the polymerization process increases tensile strength and elongation at break in PU/graphene composites presumably due to homogeneous dispersion of graphene in the PU matrix. TEM measurements suggest good interfacial interaction between the polymer chain and the graphene sheets [13]. Several workers report a decrease of mechanical properties of CNT PU nanocomposites due to poor dispersion of the CNTs and the preparation method (*ex situ* polymerization) [89,90]. The improvement in mechanical properties of TDI-based PUs after the addition of zeolites (*in situ* process) has been investigated by Kumar et al., comparing surface hardness, tensile strength, and modulus. Surface hardness of the composites increased slightly with the addition of zeolite $AlPO_4$-5. Considerable improvements in tensile strength and modulus were observed with increasing $AlPO_4$-5 content, which indicates good interfacial adhesion between the PU and the zeolite filler [81] (Figure 6.4(d)).

A general observation is that composites having smaller nanoparticles in a PU matrix exhibit higher storage modulus compared to larger particles. The larger surface area also causes a shifting of the damping factor ($\tan \delta$) peak toward higher temperatures compared to the pure PU [84] (Figure 6.5(a) and (b)). Incorporation of CNTs in a PU matrix leads
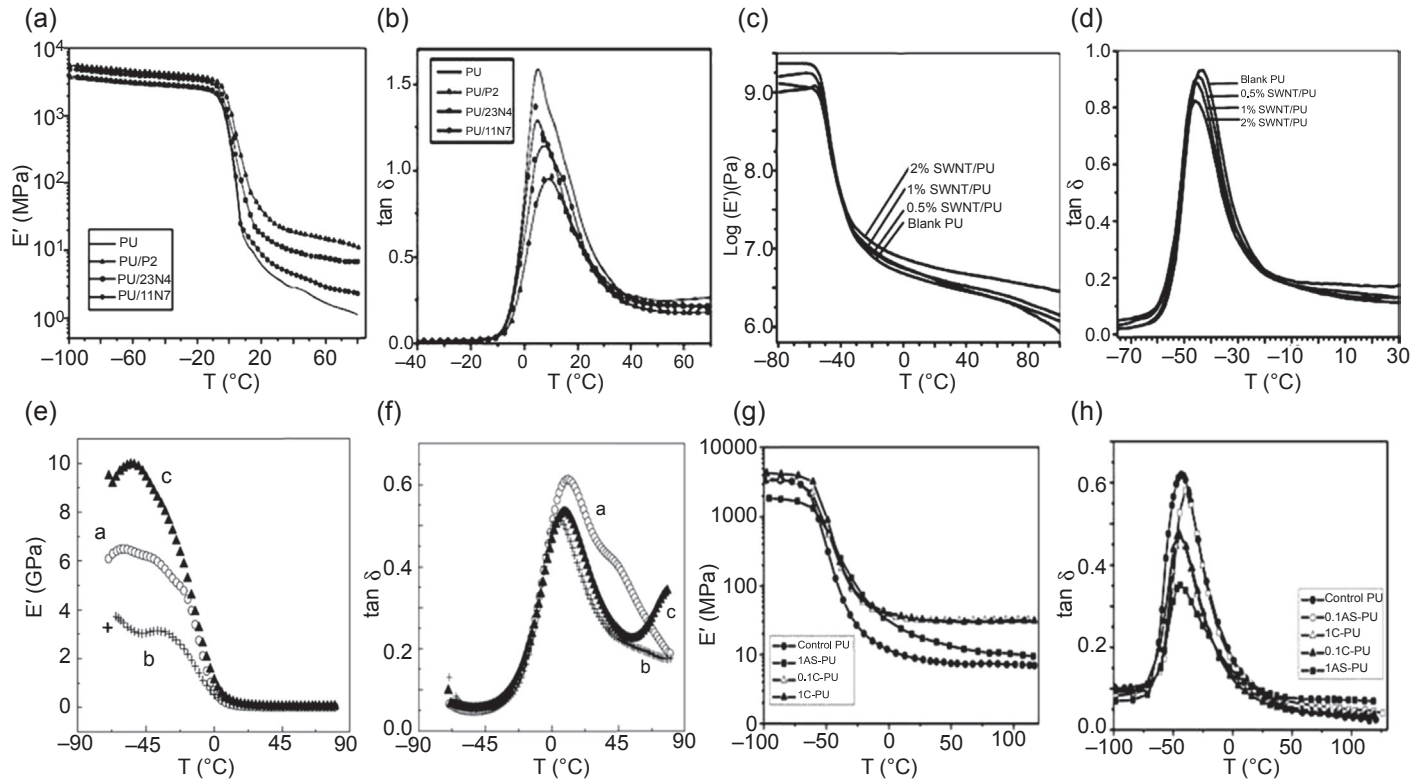
Figure 6.5 Dynamic mechanical behavior of polyurethane nanocomposite in the presence of various types of nanoparticles. (a and b) Storage modulus and damping factor in the presence of alumina [84], (c and d) storage modulus and damping factor in the presence of CNTs [86], (e and f) storage modulus and damping factor in the presence of clay [91], and (g and h) storage modulus and damping factor in the presence of zeolite, respectively [92].

to the enhancement in storage modulus at room temperature as well as a slight decrease in tan δ and glass transition temperature likely due to an increase in microphase separation creating slightly purer soft segment microdomains [86] (Figure 6.5(c) and (d)). The storage modulus and tan δ of nanoclay-based PU composites are presented in Figure 6.5(e) and (f). Different types of clay exhibit different behavior toward the storage modulus and damping behavior. Nanoclay with aromatic organic modification exhibits a higher storage modulus compared to the composites made of nanoclay modified with aliphatic ammonium salt. The peak position of tan δ curves of the composites shifted toward the lower temperature region and becomes narrower than that of the pure PU [91]. Composites of zeolite exhibit a different behavior of storage modulus in the glassy region. The calcined zeolite filler exhibits a higher storage modulus compared to freshly synthesized zeolite composites in the glassy region due to the increase in the density of material resulting from the loss of porosity after calcination. The addition of small amounts of as-prepared β-zeolite in the PU matrix shifts the damping peak toward higher temperatures due to restriction on the mobility of the polymer chains. However, as the content of filler increased, the peak shifts toward the lower temperature, a phenomenon not observed with the calcined zeolite [92] (Figure 6.5(g) and (h)).

The rheological behavior of PU-grafted SWCNT in terms of viscosity versus shear rate at 80 °C is presented in Figure 6.6(a). Grafted PU composites exhibit higher viscosity compared to the pure diol as well as the diol/SWCNT composites. The lowest shearing thinning exponent observed in grafted composites indicates better dispersion in polycaprolactone (PCL) diol [93]. The rheological behavior in terms of modulus and complex viscosity versus frequency of PU clay nanocomposites was studied by Mishra et al. [9]. Nanoclay-based composites exhibit higher storage modulus (G') and complex viscosity (η^*) compared to unfilled PU due to the presence of the nanoparticles. In the melt phase, the modulus drops abruptly at a certain frequency due to a disruption of the network structure. This disruptive frequency shifts toward higher frequency in the nanocomposites [9] (Figure 6.6(b) and (c)). Further increase of frequency enhances the storage modulus and complex viscosity.
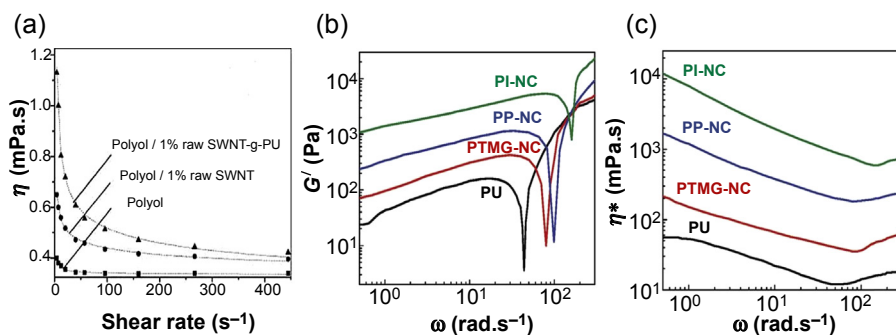

Figure 6.6 Rheological behavior of polyurethane and its nanocomposites in the presence of nanoparticles. (a) The viscosity at 80 °C versus shear rate for blank PCL diol and PCL diol/SWNT dispersions, (b) storage modulus, (c) complex viscosity of pure PU and its nanocomposites as a function of frequency at $T_{ref} = T_m + 20$ °C.

6.7 Thermal behavior

The thermal properties of a given composite are influenced, for example, by quality of dispersion, interaction with the polymer matrix, and filler content as well as the aspect ratio. Enhancement in the thermal stability was observed in composites by the addition of nano-TiO_2 in a PU matrix. The thermal degradation temperature increases from 347 to 365 °C in 1 wt% TiO_2 composites [94]. Composites having different particle dimensions exhibit a range of thermal stability [84] (Figure 6.7(a)). The addition of CNTs also affects the thermal stability of the composites. PU/CNT composites exhibit a two-step degradation process [95]. The addition of minute quantities of MWCNTs during the polymerization process of PU considerably enhances the thermal stability [96]. Figure 6.7(b) shows the thermogravimetric analysis (TGA) curves of PU/CNT
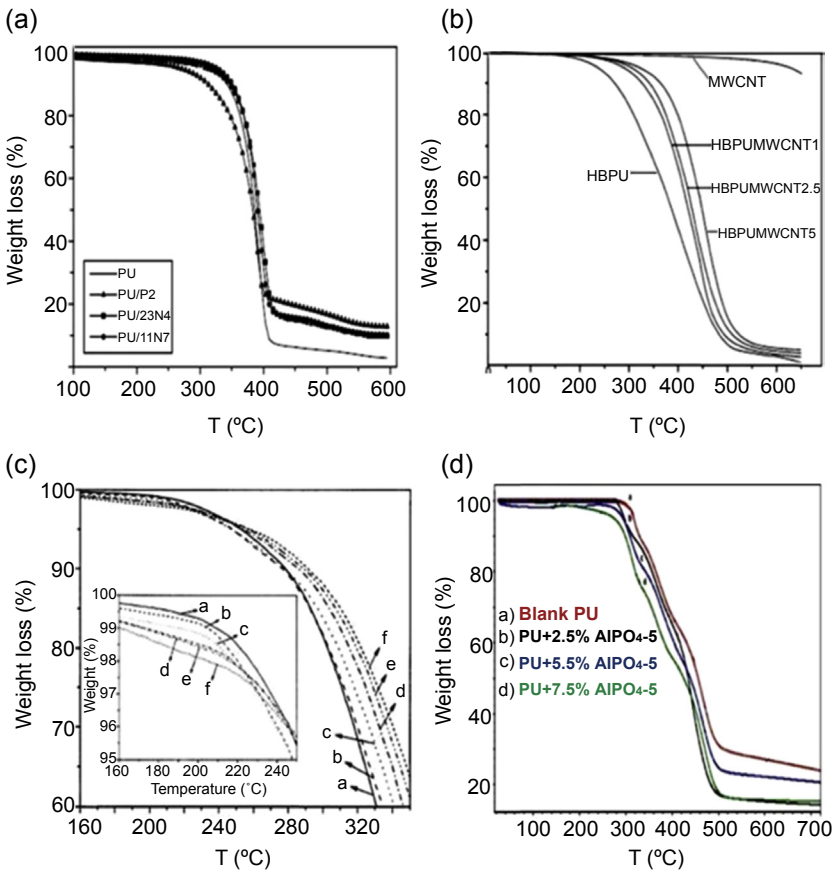

Figure 6.7 TGA curves of polyurethane and its nanocomposites in the presence of different types of nanoparticles. (a) In the presence of alumina powder [84], (b) in the presence of CNTs [96], (c) in the presence of clay (here a, b, c, d, e, and f represent 0, 1, 2, 3, 4, and 5 wt% of clay in PU matrix) [14], and (d) in the presence of zeolite [81].

composites. Incorporation of 1 wt% of MWCNTs in the PU matrix enhances the thermal degradation from 215 to 275 °C and the degradation temperature further increases with the increasing amounts of MWCNT in the PU matrix [97]. A comparison of the thermal stability of PU/CNT composites reveals that more stable dispersions result in better thermal stability [98]. LDH as a filler in PU matrix also enhances the thermal stability of the composites. Degradation patterns of the LDH composites were very similar to those of pure PU [44]. Similarly, composites of organically modified nanoclay–PU composites show better thermal stability than pure PU and the stability was further increased with nanoclay content due to the thermally insulating behavior of the nanoclay (Figure 6.7(c)) [14]. Different types of nanoclays exhibit a range of thermal stability. Nanocomposites having aromatic amine-modified clay exhibit better thermal stability than quaternary alkyl ammonium salt-containing nanocomposites [91]. Composites having graphene or modified graphene as filler exhibit better thermal stability than pure PU due to the tortuous path created by two-dimensional graphene sheets, which prevent the elimination of the volatile products along with the formation of char [99]. Incorporation of 2 wt% of graphene in PU matrix during the polymerization (*in situ*) leads to the improvement in thermal stability of 40 °C compared to the pure PU [13]. TGA of pure PU and its composites with zeolite 13X shows the effect of zeolite on thermal stability. The degradation temperature increases with increase of the zeolite content in composite, indicating good heat resistance and heat transfer properties of the zeolite filler (Figure 6.7(d)) [81,100]. CNTs exhibit thermal conductivity ~3000 W/m/K at room temperature and this property has been utilized to prepare thermally conductive composites [101]. Xia and Song observed a significant improvement of thermal conductivity of 21% and 42% for composites containing 1% of MWCTs and SWNTs, respectively [86]. Further increases of CNT reduce the thermal conductivity due to the large interfacial thermal resistance between the CNTs and the polymer matrix [102]. Similar results were also obtained in the case of MWNT/water-based PU composites prepared through the latex method [103].

Differential scanning calorimetry (DSC) thermograms of PU–Au nanocomposites are presented in Figure 6.8(a). Nanocomposites having 6.5×10^{-2} wt% gold particles in the matrix do not show an endothermic soft segment melting peak while composites with less than the amount of Au particles show a sharp melting endotherm. The disappearance of the peak at a higher content of Au particles is possibly due to gold–polyol interactions, which inhibit crystallization [104]. SWCNTs do not alter the glass transition temperature of composites of PCL-based PUs while the nanofiller strongly influences the melting behavior of the soft and hard segments. The melting temperatures of the soft and hard segments decrease slightly with increasing amounts of SWCNT (Figure 6.8(b)) [80]. In contrast the melting temperature of the soft segment increases in PU–nanoclay composites prepared through *in situ* polymerization where the nanoclay was incorporated before prepolymer formation. Interestingly a decrease in melting temperature is noted for the hard segment compared to the pure PU, indicating a strong interaction between the nanoclay and the hard segment of the aliphatic-based PU (Figure 6.8(c)). This suggests that the organically modified nanoclay disrupts the urethane interactions of the polymer chain, which causes a decrease in the melting temperature [9].
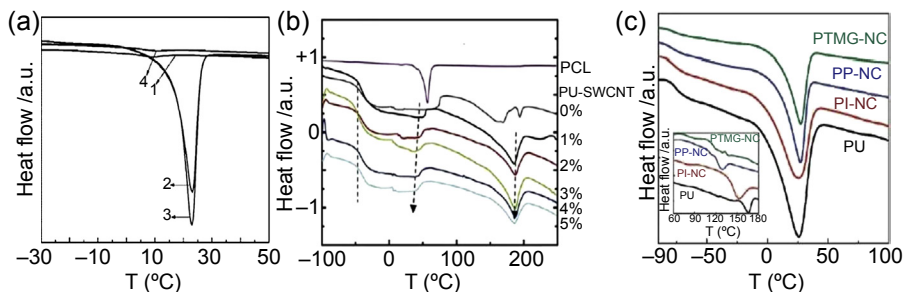
Figure 6.8 DSC curves of polyurethane and its nanocomposites in the presence of different types of nanoparticles. (a) PU–Au nanocomposites, 1 for pure PU, 2, 3, and 4 indicate 1.74, 4.35, and 6.5×10^{-2} wt% of Au nanoparticles [104], (b) PU–CNT composites [80], and (c) PU-nanoclay composites [9].

6.8 Flame retardancy

PUs can be used as coating materials for the improvement of flame retardant properties [105,106]. Initially, halogen and phosphorous-based materials were used in these applications [107]. Layer by layer nanocoating is an important process that can enhance the flame retardant activity of highly flammable materials like nylon [108], PET fabric [109], polycarbonate [110], and cotton [111,112]. PU coating with cationic boehmite and anionic vermiculite filler material exhibits considerable improvement in flame retardant activity. PU melts and ignites when a hand-held butane torch is focused on the uncoated PU sample for 10 s while a coated clay-filled PU is not influenced by the torch and retains its original shape [113]. Incorporation of a few percent of clay in a PU matrix enhances its the thermal stability and flame retardant properties due to the formation of a protecting clay layer on the polymer surface [114]. Patel and Patel have used different types of diisocyanate for the preparation of PU nanoclay composites and compared the flame retardant properties in terms of limiting oxygen index value. Nanocomposites show better flame retardant properties compared to the pure PU [115].

6.9 Antimicrobial activity

Nanoparticles, especially silver ions (Ag^+), are frequently used for their antibacterial activity. Ag^+ ions prevent the replication of the microbial DNA, which in turn suppress the expression of the ribosomal protein as well as the enzymes for ATP hydrolysis [116]. Liu et al. have prepared composites of MDI and H_{12}MDI-based PU using small, medium, and large sizes of silver nanoparticles to study the effect of nanoparticles size on bacterial activity (*Escherichia coli* and *Staphylococcus aureus*). The smaller size silver nanoparticles in composites show better response in comparison to the composites with larger particles [117]. PU composites using nanoscale silicate platelets (NSP) and AgNPs in different ratios also exhibit strong antibacterial activity. Figure 6.9 shows the bactericidal LIVE/DEAD analysis of the growth of *S. aureus* (after exposure for 12 h), indicating
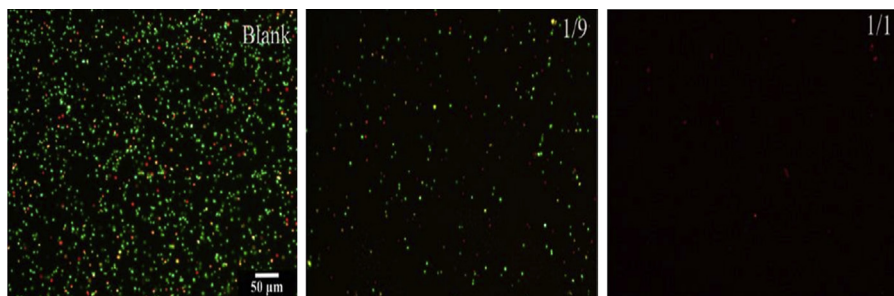
Figure 6.9 Bactericidal LIVE/DEAD analysis. Growth of *Staphylococcus aureus* (after 12 h exposure) on AgNP/NSP-PU-coated stainless steel. Greens are viable cells and reds are nonviable cells, where 1/1 and 1/9 are the ratios of AgNP/NSP in PU composites [118].

full inhibition for the composition of AgNP:NSP of 1:1 in a PU composite [118]. Zvekić et al. performed antimicrobial tests against bacteria and fungi (pour plate method) with nano-ZnO-containing PU varnishes. The colonies of *Pseudomonas aeruginosa* and *Saccharomyces cerevisiae* are not observed in the ZnO-containing varnishes in comparison to pure PU varnishes. Further, PU composites with 0.4 and 0.7 wt% ZnO inhibit growth of *S. aureus* by more than 85% and 95%, respectively [119].

6.10   Biomedical application of nanocomposites

6.10.1   Drug delivery

Controlled drug release and its application in the biomedical arena have received much attention from 1995 to 2015. Materials used as a vehicle for drug delivery should be safe, biocompatible, and nontoxic in nature and must not be the basis of an excess immune response. Other criteria such as suitable mechanical strength, easy processing/manufacturing, and a highly porous structure also must be met [120]. Large surface area along with the presence of different functionalities on the surface of CNTs provides an advantage for the loading of different kinds of drugs. Release of drug from polymer composites depends on several factors such as interactions between the drug and the polymer matrix, pH, and temperature of the medium [121]. Prolonged efficient drug release can also achieve a minimization of side effects [122]. Figure 6.10 shows the drug release profile of gentamicin sulfate in PU composites containing different types of nanoparticles. Albumin nanoparticle composites release drug at a faster rate in comparison to pure PU [123]. Similarly, CNT-based hyperbranched PU composites also exhibit slower release compared to pure PU and the release rate decreases with increasing amounts of CNTs in the matrix [124]. Two-dimensional nanoclay also sustained the release rate of drugs by controlling the diffusion mechanism through a tortuous path caused by the fine dispersion of the nanoclay in the PU matrix [42,125]. In summary, nanoparticles play an important role in drug release either by enhancing the interaction between the drug and the nanoparticles or by creating a tortuous diffusion path. Nanoparticles also appear to suppress the burst release of the drug from the PU.
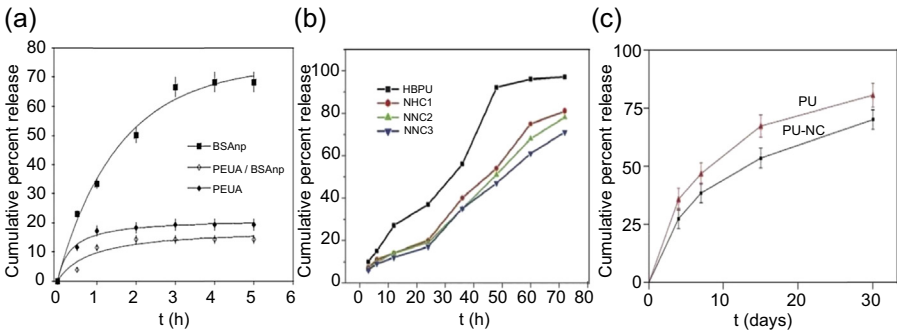
Figure 6.10 Sustained drug release profile of polyurethane composites with different types of nanoparticles. (a) In the presence of albumin nanoparticles [123], (b) in CNTs [124], the number indicates the percentage of CNT, and (c) in the presence of clay [125].
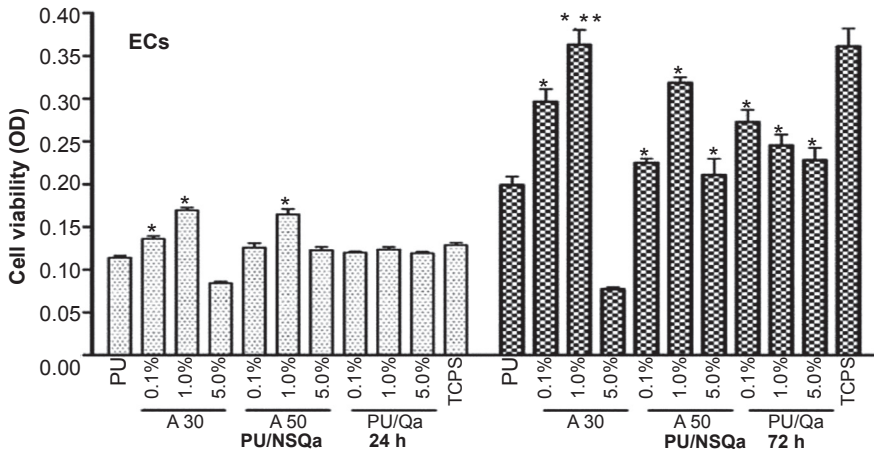

Figure 6.11 The viability of ECs grown on the surface of PU/NSQa (nanosilicate platelet exchange with cationic surfactant; A30 and A50; surfactant and reduced surfactant, respectively) and PU/Qa nanocomposites at 1 and 3 days. * indicates $P < 0.05$, significantly greater than pure PU and ** indicates $P < 0.05$, significantly greater than all other samples [129].

6.10.2　Tissue engineering

PUs have received considerable attention for engineering applications [126]. These include the construction of different types of structures for blood vessels, skin repair, and nerve reconstruction as well as bone growth [127]. Cell adhesion and proliferation on these structures are considered to be important in addition to their biocompatibility [128]. Different types of organically modified nanoclay have been used to prepare composites of PU for biological applications. Cell viability on composites was shown to be better than the PU matrix after 3 days of incubation [129] (Figure 6.11). Mishra et al. have also reported on the biocompatible nature of the PU/clay nanohybrid films in terms of cell viability, adhesion, and proliferation [9]. Recently, organically modified graphene has been used in tissue-engineering applications [130].

6.10.3 Implant materials

There are several polymers such as collagen, silicone rubber, and poly(tetrafluoro-ethylene) as well as PUs that are available for implant applications [131–133]. The basic requirement for implant material is that material should be mechanically strong to serve as a substrate for cell attachment and proliferation and be easily removable/bioadsorbable after the newly generated tissue restored the natural function [134]. Kannan et al. prepared PU (polycarbonate as soft segment) nanocomposites using polyhedral oligomeric silsesquioxanes (POSS) as the filler and used them as a biostable and biocompatible material [135]. POSS is responsible for the better resistance against oxidative and hydrolytic degradation for the PU–POSS composite [136]. The nanocomposite is nontoxic and has good thrombo-resistance and is also resistant toward degradation *in vivo*. *In vivo* experiments demonstrate minimal inflammation, capsule formation, and no degradation after 36 months of postimplantation in a sheep model compared to control [137]. Another *in vivo* study involving a vascular graft indicates good surface properties, superior biostability, and biocompatibility of the nanocomposite compared to the unfilled polymer [138]. Hence, a PU–POSS nanocomposite is an excellent material for tissue implants such as vascular grafts and heart valves. Khan et al. have prepared biocellulose nanoparticle-based composites (PU–BC) that have strong potential as bone tissue implants in terms of biodegradation, mechanical strength, porosity, and three-dimensional structure [139]. In summary, PU nanoparticles have potential in the biomedical arena for controlled drug delivery, tissue engineering, and implants and are a very active area of research.

6.11 Conclusions

Composites prepared using different types of nanoparticles can show superior properties compared to pure PU and have a wide range of applications in structural and biomedical fields. The surface morphology of nanocomposites is affected by the nature and amount of the nanoparticles embedded in polymer matrix. Different shapes and sizes of the nanoparticles play a significant role in enhancement of the mechanical, rheological, thermal, and fire retardant properties of the PU nanocomposites. Considerable improvements in antibacterial properties have been reported using nanocomposites compared to pure PU. Incorporation of the different kinds of nanoparticles in PU matrix alters the biocompatible nature of the composites, suggesting that PU composites may have use in biomaterial applications.

Acknowledgments

References

[1] Lan PN, Corneillie S, Schacht E, Davies M, Shard A. Synthesis and characterization of segmented polyurethanes based on amphiphilic polyester diols. Biomaterials December 1996;17(23):2273–80.

[2] Guan J, Fujimoto KL, Sacks MS, Wanger WR. Preparation and characterization of highly porous, biodegradable polyurethane scaffolds for soft tissue applications. Biomaterials June 2005;26(18):3961–71.

[3] Lee SH, Cyriac A, Jeon JY, Lee BY. Preparation of thermoplastic polyurethanes using in situ generated poly (propylene carbonate)-diols. Polym Chem March 2012;3(3):1215.

[4] Cyriac A, Lee SH, Lee BY, et al. Preparation of flame retarding poly (propylene carbonates). Green Chem October 2011;13(13):3469–75.

[5] Xu H, Chang J, Chen Y, Fan H, Shi B. Asymmetric polyurethane membrane with inflammation-responsive antibacterial activity for potential wound dressing application. J Mater Sci October 2013;48(19):6625–39.

[6] Camposa E, Cordeiroa R, Santosb AC, Gil MH, et al. Design and characterization of bi-soft segmented polyurethane microparticles for biomedical application. Colloids Surf B Biointerfaces July 2011;88:477–82.

[7] Molak ID, Lekka M, Kurzydlowski KJ. Surface properties of polyurethane composites for biomedical applications. Appl Surf Sci April 2013;270:553–60.

[8] Choi Y, Nirmala R, Lee JY, Rahman M, Hong ST, Kim HY. Antibacterial ciprofloxacin HCl incorporated polyurethane composite nanofibers via electrospinning for biomedical applications. Ceram Int July 2013;39(5):4937–44.

[9] Mishra A, Purkayastha BPD, Roy JK, Aswal VK, Maiti P. Tunable properties of self-assembled polyurethane using two–dimensional nanoparticles: potential nano-biohybrid. Macromolecules November 2010;43:9928–36.

[10] Zdrahala RJ, Zdrahala IJ. Biomedical applications of polyurethanes: a review of past promises, present realities, and a vibrant future. J Biomater Appl July 1999;14(1):67–90.

[11] Sun X, Gao H, Wu G, Wang Y, Fan Y, Ma J. Biodegradable and temperature-responsive polyurethane for adriamycin delivery. Int J Pharm June 2011;412:52–8.

[12] Li F, Qi L, Yang J, Xu M, Luo X, Ma D. Polyurethane/conducting carbon black composites: structure, electric conductivity, strain recovery behavior, and their relationships. J Appl Polym Sci January 2000;75:68–77.

[13] Wang X, Hu Y, Song L, Yang H, Xing W, Lu H. *In situ* polymerization of graphene nanosheets and polyurethane with enhanced mechanical and thermal properties. J Mater Chem February 2011;21:4222–7.

[14] Lee HT, Lin LH. Waterborne polyurethane/clay nanocomposites: novel effect of the clay and its interlayer ions on the morphology and physical and electrical properties. Macromolecules August 2006;39(18):6133–41.

[15] Wang Q, O'Hare D. Recent advances in the synthesis and application of layered double hydroxide (LDH) nanosheets. Chem Rev March 2012;112(7):4124–55.

[16] Bigg DM. Mechanical, thermal, and electrical properties of metal fiber-filled polymer composites. Polym Eng Sci December 1979;19(16):1188–92.

[17] Arbatti M, Shan X, Cheng ZY. Ceramic–polymer composites with high dielectric constant. Adv Mater May 2007;19(10):1369–72.

[18] Saint S, Elmore JG, Koepsell TD, et al. The efficacy of silver alloy-coated urinary catheters in preventing urinary tract infection: a meta-analysis. Am J Med September 1998;05:236–41.

[19] Bishop JB, Phillips LG, Mustoe TA. A prospective randomized evaluator-blinded trial of two potential wound healing agents for the treatment of venous stasis ulcers. J Vasc Surg August 1992;16:251–7.

[20] Morones JR, Elechiguerra JL, Camacho A, et al. The bactericidal effect of silver nanoparticles. Nanotechnology August 2005;16:2346–53.

[21] Sitharaman B, Kissell KR, Rusakova I, et al. Superparamagnetic gadonanotubes are high-performance MRI contrast agents. Chem Commun July 2005;31:3915–7.

[22] Cho HS, Dong ZY, Gu HC, et al. Fluorescent, superparamagnetic nanospheres for drug storage, targeting, and imaging: a multifunctional nanocarrier system for cancer diagnosis and treatment. ACS Nano September 2010;4:5398–404.

[23] Zhao Y, Lu Y, Lin LN, et al. Synthesis of superparamagnetic $CaCO_3$ mesocrystals for multistage delivery in cancer therapy. Small November 2010;6:2436–42.

[24] Huang YJ, Liu MZ, Gong QY, et al. A novel magnetic triple-responsive composite semi-IPN hydrogels for targeted and controlled drug delivery. Eur Polym J October 2012;48:1734–44.

[25] Gupta AK, Gupta M. Synthesis and surface engineering of iron oxide nanoparticles for biomedical applications. Biomaterials June 2005;26:3995–4021.

[26] Baughman RH, Zakhidov AA, Heer WAD. Carbon nanotubes-the route toward applications. Science August 2002;297:787–92.

[27] Schubert U. Polymers reinforced by covalently bonded inorganic clusters. Chem Mater June 2001;13:3487–94.

[28] Gorrasi G, Tortora M, Vittoria V. Synthesis and physical properties of layered silicates/polyurethane nanocomposites. J Polym Sci Part B Polym Phys July 2005;43:2454–67.

[29] Devaux E, Rochery M, Bourbigot S. Polyurethane/clay and polyurethane/POSS nanocomposites as flame retarded coating for polyester and cotton fabrics. Fire Mater December 2002;26:149–54.

[30] Solarski S, Benali S, Rochery M, Devaux E, Alexandre M, Monteverde F, et al. Synthesis of a polyurethane/clay nanocomposite used as coating: interactions between the counterions of clay and the isocyanate and incidence on the nanocomposite structure. J Appl Polym Sci November 2005;95:238–44.

[31] Xu R, Manias E, Snyder AJ. New biomedical poly(urethane urea)- layered silicate nanocomposites. Macromolecules December 2001;34:337–9.

[32] Osman MA, Mittal V, Morbidelli M, Suter UW. Polyurethane adhesive nanocomposites as gas permeation barrier. Macromolecules December 2003;36:9851–8.

[33] Jana KK, Charan C, Shahi VK, Mitra K, Ray B, Rana D, et al. Functionalized poly(vinylidene fluoride) nanohybrid for superior fuel cell membrane. J Membr Sci February 2015;481:124–36.

[34] Beloqui BJ, Garcia JCF, Martinez JMM, et al. Rheological properties of thermoplastic polyurethane adhesive solutions containing fumed silicas of different surface areas. Int J Adhes Adhes August 1999;19:321–8.

[35] Yao KJ, Song M, Hourston DJ, Luo DZ. Polymer/layered clay nanocomposites: 2 polyurethane nanocomposites. Polymer November 2002;43:1017–20.

[36] Ma J, Zhang S, Qi Z. Synthesis and characterization of elastomeric polyurethane/clay nanocomposites. J Appl Polym Sci August 2001;82:1444–8.

[37] Chen TK, Tien YI, Wei KH. Synthesis and characterization of novel segmented polyurethane/clay nanocomposite via poly(ε-caprolactone)/clay. J Polym Sci Part A Polym Chem July 1999;37:2225–33.

[38] Petrovic ZS, Javni I, Waddon A, Banhegyi G. Structure and properties of polyurethane–silica nanocomposites. J Appl Polym Sci April 2000;76:133–51.

[39] Singh NK, Singh SK, Dash D, Purkayastha BPD, Roy JK, Maiti P. Nanostructure controlled anti-cancer drug delivery using poly(3-caprolactone) based nanohybrids. J Mater Chem 2012;22:17853–63.

[40] Tiwari VK, Kulriya PK, Avasthi DK, Maiti P. Radiation-resistant behavior of poly-(vinylidene fluoride)/layered silicate nanocomposites. ACS Appl Mater Interfaces December 2009;1(2):311–8.

[41] Discher BM, Won YY, Ede DS, Hammer DA, et al. Polymersomes: tough vesicles made from diblock copolymers. Science May 1999;284:1143–6.

[42] Mishra A, Purkayastha BPD, Roy JK, Aswal VK, Maiti P. Nanoparticle controlled self-assembly in varying chain extended polyurethanes as potential nanobiomaterials. J Phys Chem C December 2012;116:2260–70.

[43] Choy JH, Kwak SY, Park JS, Portier J. Intercalative nanohybrids of nucleoside monophosphates and DNA in layered metal hydroxide. J Am Chem Soc May 1999;121:1399–400.

[44] Guo S, Zhang C, Peng H, Wang W, Liu T. Structural characterization, thermal and mechanical properties of polyurethane/CoAl layered double hydroxide nanocomposites prepared via in situ polymerization. Compos Sci Technol February 2011;71:791–6.

[45] Chen W, Qu B. LLDPE/ZnAl LDH-exfoliated nanocomposites: effects of nanolayers on thermal and mechanical properties. J Mater Chem May 2004;14:1705–10.

[46] Kim H, Abdala AA, Macosko CW. Graphene/polymer nanocomposites. Macromolecules July 2010;43:6515–30.

[47] Terrones M, Olga Martín O, Cabanelas JC, Baselga J. Interphases in graphene polymer-based nanocomposites: achievements and challenges. Adv Mater September 2011;23:5302–10.

[48] Novoselov KS, Geim AK, Morozov SV, et al. Electric field effect in atomically thin carbon films. Science October 2004;306:666–9.

[49] Zhang K, Zhang LL, Zhao XS, et al. Graphene-polyaniline nanofiber composites as supercapacitor electrodes. Chem Mater January 2010;22:1392–401.

[50] Balandin AA, Ghosh S, Bao WZ, et al. Superior thermal conductivity of single-layer graphene. Nano Lett February 2008;8:902–7.

[51] Latil S, Henrard L. Charge carriers in few-layer graphene films. Phys Rev Lett July 2006;97:036803–6.

[52] Stoller MD, Park S, Zhu YW, et al. Graphene-based ultracapacitors. Nano Lett September 2008;8:3498–502.

[53] Wang L, Lee K, Sun YY, et al. Graphene oxide as an ideal substrate for hydrogen storage. ACS Nano September 2009;3:2995–3000.

[54] Lu CH, Yang HH, Zhu CL, et al. A graphene platform for sensing biomolecules. Angew Chem Int Ed May 2009;121:4879–81.

[55] Xuan Y, Wu YQ, Shen T, et al. Atomic-layer-deposited nanostructures for graphene-based nanoelectronics. Appl Phys Lett January 2008;92:013101–3.

[56] Yang XM, Tu YF, Li L, et al. Well-dispersed chitosan/graphene oxide nanocomposites. ACS Appl Mater Interfaces June 2010;2:1707–13.

[57] Bai H, Li C, Wang XL, et al. A pH-sensitive graphene oxide composite hydrogel. Chem Commun March 2010;46:2376–8.

[58] Sun ST, Wu PY. A one-step strategy for thermal- and pH-responsive graphene oxide interpenetrating polymer hydrogel networks. J Mater Chem February 2011;21:4095–7.

[59] Fang F, Long J, Zhao WF, et al. pH-Responsive chitosan-mediated graphene dispersions. Langmuir October 2010;26:16771–4.

[60] Liu Z, Robinson JT, Sun XM, et al. PEGylated nanographene oxide for delivery of water-insoluble cancer drugs. J Am Chem Soc July 2008;130:10876–7.

[61] Jia M, Peinemann KV, Behling RD. preparation and characterization of thin film zeolite–pdms composite membranes. J Membr Sci October 1992;73:119–28.

[62] Berry MB, Libby BE, Rose K, Haas KH, Thompson RW. Incorporation of zeolites into composite matrices. Microporous Mesoporous Mater 2000;39:205–17.

[63] Aksoy EA, Akata B, Bac N, Hasirci N. Preparation and characterization of zeolite beta–polyurethane composite membranes. J Appl Polym Sci June 2007;104(5):3378–87.

[64] Giacalone F, Martin N. Fullerene polymers: synthesis and properties. Chem Rev December 2006;106:5136–90.

[65] Bianco A, Kostarelos K, Partidos CD, Prato M. Biomedical applications of functionalised carbon nanotubes. Chem Commun February 2005;5:571–7.

[66] Ouros ACD, Souzab MOD, Pastore HO. Metallocene supported on inorganic solid supports: an unfinished history. J Braz Chem Soc 2014;25(12):2164–85.

[67] Wang YX, Gies H, Marler B. Synthesis and crystal structure of zeolite RUB-41 obtained as calcination product of a layered precursor: a systematic approach to a new synthesis route. Chem Mater December 2005;17:43–9.

[68] Ma PC, Siddiqui NA, Marom G, Kim JK. Dispersion and functionalization of carbon nanotubes for polymer-based nanocomposites: a review. Composites Part A October 2010;41(10):1345–67.

[69] Moniruzzaman M, Winey KI. Polymer nanocomposites containing carbon nanotubes. Macromolecules July 2006;39:5194–205.

[70] Grossiord N, Loos J, Regev O, Koning CE. Toolbox for dispersing carbon nanotubes into polymers to get conductive nanocomposites. Chem Mater January 2006;18(5):1089–99.

[71] Hsu SH, Tang CM, Tseng HJ. Gold nanoparticles induce surface morphological transformation in polyurethane and affect the cellular response. Biomacromolecules December 2008;9(1):241–8.

[72] Cho JW, So JH. Polyurethane–silver fibers prepared by infiltration and reduction of silver nitrate. Mater Lett February 2006;60:2653–6.

[73] Xiong J, Zheng Z, Qin X, Li M, Li H, Wang X. The thermal and mechanical properties of a polyurethane/multi-walled carbon nanotube composite. Carbon May 2006;44:2701–7.

[74] Liu LQ, Wagner HD. Rubbery and glassy epoxy resins reinforced with carbon nanotubes. Compos Sci Technol September 2005;65:1861–8.

[75] Koerner H, Liu W, Alexander M, Mirau P, Vaia RA, et al. Deformation–morphology correlations in electrically conductive carbon nanotube—thermoplastic polyurethane nanocomposites. Polym J March 2005;46:4405–20.

[76] Yoo HJ, Jung YC, Sahoo NG, Cho JW. Polyurethane-carbon nanotube nanocomposites prepared by in-situ polymerization with electroactive shape memory. J Macromol Sci Part B Phys August 2006;45:441–51.

[77] Ciobanu G, Carja G, Ciobanu O. Structure of mixed matrix membranes made with SAPO-5 zeolite in polyurethane matrix. Microporous Mesoporous Mater February 2008;115:61–6.

[78] Kamisoglu K, Aksoy EA, Akata B, Hasirci N, Bac N. Preparation and characterization of anti-bacterial zeolite–polyurethane composites. J Appl Polym Sci September 2008;110:2854–61.

[79] Chen J, Zhou Y, Nan Q, Sun Y, Ye X, Wang Z. Synthesis, characterization and infrared emissivity study of polyurethane/TiO_2 nanocomposites. Appl Surf Sci May 2007;253:9154–8.

[80] Lee HF, Yu HH. Study of electroactive shape memory polyurethane–carbon nanotube hybrids. Soft Matter February 2011;7:3801–7.

[81] Kumar BVS, Siddaramaiah, Shayan MB, Byrappa K, et al. Effect of zeolite particulate filler on the properties of polyurethane composites. J Polym Res May 2010;17:135–42.

[82] Kim JK, Mai Y. Engineered interfaces in fiber reinforced composites. Oxford: Elsevier; 1998. p. 1–100.

[83] Deka H, Karak N, Kalita RD, Buragohain AK. Bio-based thermostable, biodegradable and biocompatible hyperbranched polyurethane/Ag nanocomposites with antimicrobial activity. Polym Degrad Stab June 2010;95:1509–17.

[84] Gatos KG, Alcazar JGM, Psarras GC, Thomann R, Kocsis JK. Polyurethane latex/water dispersible boehmite alumina nanocomposites: thermal, mechanical and dielectric properties. Compos Sci Technol September 2007;67:157–67.

[85] Chen W, Tao X, Liu Y. Carbon nanotube-reinforced polyurethane composite fibers. Compos Sci Technol March 2006;66:3029–34.

[86] Xia H, Song M. Preparation and characterization of polyurethane–carbon nanotube composites. Soft Matter October 2005;1:386–94.

[87] Kotal M, Kuila T, Srivastava SK, Bhowmick AK. Synthesis and characterization of polyurethane/Mg-Al layered double hydroxide nanocomposites. J Appl Polym Sci July 2009;114:2691–9.

[88] Shah D, Maiti P, Gunn E, Schmidt DF, Jiang DD, Batt CA, et al. Dramatic enhancements in toughness of polyvinylidene fluoride nanocomposites via nanoclay-directed crystal structure and morphology. Adv Mater August 2004;16:1173–7.

[89] Ma PC, Tang BZ, Kim JK. Effect of CNT decoration with silver nanoparticles on electrical conductivity of CNT–polymer composites. Carbon September 2008;46(11):1497–505.

[90] Ma PC, Liu MY, Kim JK, Tang BZ, et al. Enhanced electrical conductivity of nanocomposites containing hybrid fillers of carbon nanotubes and carbon black. ACS Appl Mater Interfaces May 2009;1(5):1090–6.

[91] Xiong J, Liu Y, Yang X, Wang X. Thermal and mechanical properties of polyurethane/montmorillonite nanocomposites based on a novel reactive modifier. Polym Degrad Stab December 2004;86(3):549–55.

[92] Aksoy EA, Akata B, Bac N, Hasirc N. Preparation and characterization of zeolite beta–polyurethane composite membranes. J Appl Polym Sci March 2007;104:3378–87.

[93] Xia H, Song M. Preparation and characterisation of polyurethane grafted single-walled carbon nanotubes and derived polyurethane nanocomposites. J Mater Chem March 2006; 16:1843–51.

[94] Saha MC, Kabir MdE, Jeelani S. Enhancement in thermal and mechanical properties of polyurethane foam infused with nanoparticles. Mater Sci Eng A April 2008;479:213–22.

[95] Rana S, Karak N, Cho JW, Kim YH. Enhanced dispersion of carbon nanotubes in hyperbranched polyurethane and properties of nanocomposites. Nanotechnology November 2008;19:495707 (8 pp.).

[96] Deka H, Karak N, Kalita RD, Buragohain AK. Biocompatible hyperbranched polyurethane/multi-walled carbon nanotube composites as shape memory materials. Carbon February 2010;4(8):2013–22.

[97] Jin SH, Park YB, Yoon KH. Rheological and mechanical properties of surface modified multi-walled carbon nanotube-filled PET composite. Compos Sci Technol December 2007;67:3434–41.

[98] Jana RN, Cho JW. Thermal stability and molecular interaction of polyurethane nanocomposites prepared by in situ polymerization with functionalized multiwalled carbon nanotubes. J Appl Polym Sci June 2008;108:2857–64.

[99] Cao Y, Feng J, Wu P. Preparation of organically dispersible graphene nanosheet powders through a lyophilization method and their poly(lactic acid) composites. Carbon June 2010;48:3834–9.

[100] Lv Z, Zhang L, Yang Y, Bi X. Preparation and properties of polyurethane/zeolite 13X composites. Mater Des June 2011;32:3624–8.

[101] Smalla JP, Shib L, Kima P. Mesoscopic thermal and thermoelectric measurements of individual carbon nanotubes. Solid State Commun 2003;127(2):181–6.

[102] Huxtable ST, Cahill DG, Shenogin S, Keblinski P, et al. Interfacial heat flow in carbon nanotube suspensions. Nat Mater October 2003;2:731–4.

[103] Cai D, Song M. Latex technology as a simple route to improve the thermal conductivity of a carbon nanotube/polymer composite. Carbon September 2008;46:2107–12.

[104] Hsu SH, Chou CW, Tseng SM. Enhanced thermal and mechanical properties in polyurethane/Au nanocomposites. Macromol Mater Eng December 2004;289:1096–101.

[105] Morgan AB. Flame retarded polymer layered silicate nanocomposites: a review of commercial and open literature systems. Polym Adv Technol April 2006;17(4):206–17.

[106] Zhu SW, Shi WF. Synthesis and photopolymerization of hyperbranched polyurethane acrylates applied to UV curable flame retardant coatings. Polym Int March 2002;51(3):223–7.

[107] Yuan CY, Chen SY, Tsai CH, Chiu YS, Chen-yang YW. Thermally stable and flame-retardant aromatic phosphate and cyclotriphosphazene-containing polyurethanes: synthesis and properties. Polym Adv Technol May 2005;16(5):393–9.

[108] Apaydin K, Laachachi A, Ball V, Jimenez M, Ruch D, et al. Polyallylamine–montmorillonite as super flame retardant coating assemblies by layer-by layer deposition on polyamide. Polym Degrad Stab November 2013;98:627–34.

[109] Carosio F, Laufer G, Alongi J, Camino G, Grunlan JC. Layer-by-layer assembly of silica-based flame retardant thin film on PET fabric. Polym Degrad Stab May 2011;96:745–50.

[110] Carosio F, Blasio AD, Alongi J, Malucelli G. Layer by layer nanoarchitectures for the surface protection of polycarbonate. Eur Polym J February 2013;49(2):397–404.

[111] Li YC, Mannen S, Morgan AB, Chang S, Yang YH, Condon B, et al. Intumescent all-polymer multilayer nanocoating capable of extinguishing flame on fabric. Adv Mater September 2011;23(34):3926–31.

[112] Huang G, Yang J, Gao J, Wang X. Thin films of intumescent flame retardant-polyacrylamide and exfoliated graphene oxide fabricated via layer-by-layer assembly for improving flame retardant properties of cotton fabric. Ind Eng Chem Res September 2012;51:12355–66.

[113] Patra D, Vangal P, Cain AA, Cho C, Regev O, Grunlan JC. Inorganic nanoparticle thin film that suppresses flammability of polyurethane with only a single electrostatically-assembled bilayer. ACS Appl Mater Interfaces September 2014;6:16903–8.

[114] Wang ZY, Han EH, Ke W. Fire-resistant effect of nanoclay on intumescent nanocomposite coatings. J Appl Polym Sci February 2007;103(3):1681–9.

[115] Patel RH, Patel KS. Synthesis of flame retardant polyester-urethanes and their applications in nanoclay composites and coatings. Polym Int March 2014;63(3):529–36.

[116] Shah MdSAS, Nag M, Kalagara T, Singh S, Manorama SV. Silver on PEG-PU-TiO_2 polymer nanocomposite films: an excellent system for antibacterial applications. Chem Mater March 2008;20:2455–60.

[117] Liu HL, Dai SA, Fu KY, et al. Antibacterial properties of silver nanoparticles in three different sizes and their nanocomposites with a new waterborne polyurethane. Int J Nanomedicine November 2010;2010:1017–28.

[118] Huang YH, Chen MHH, Lee BH, Hsieh KH, Chang CH, et al. Evenly distributed thin-film Ag coating on stainless plate by tricomponent Ag/silicate/PU with antimicrobial and biocompatible properties. ACS Appl Mater Interfaces October 2014;6:20324–33.

[119] Zvekic D, Srdic VV, Karaman MA, Matavulj MN. Antimicrobial properties of ZnO nanoparticles incorporated in polyurethane varnish. Process Appl Ceram 2011;5(1):41–5.

[120] Papkov MS, Agashi K, Olaye A, Shakesheff K, Domb AJ. Polymer carriers for drug delivery in tissue engineering. Adv Drug Deliv Rev May 2007;59:187–206.

[121] Rosenbauer EM, Wagner M, Musyanovych A, Landfester K. Controlled release from polyurethane nanocapsules via pH- UV-light- or temperature-induced stimuli. Macromolecules May 2010;43:5083–93.

[122] Cho K, Wang X, Nie S, Chen ZG, Shin DM. Therapeutic nanoparticles for drug delivery in cancer. Clin Cancer Res March 2008;14(5):1310–6.

[123] Martinelli A, D'Ilario L, Francolini I, Piozzi A. Water state effect on drug release from an antibiotic loaded polyurethane matrix containing albumin nanoparticles. Int J Pharm January 2011;407:197–206.

[124] Das B, Chattopadhyay P, Upadhyay A, Gupta K, Mandalc M, Karak N. Biophysico-chemical interfacial attributes of Fe$_3$O$_4$ decorated MWCNT nanohybrid/bio-based hyperbranched polyurethane nanocomposite: an antibacterial wound healing material with controlled drug release potential. New J Chem May 2014;38:4300–11.

[125] Pinto FCH, Cunha AS, Pianetti GA, Ayres E, Orefice RL, Silva GRD. Montmorillonite clay-based polyurethane nanocomposite as local triamcinolone acetonide delivery system. J Nano Mat 2011;2011. 11 pp.

[126] Langer R, Vacanti JP. Tissue engineering. Science May 1993;260(5110):920–6.

[127] Wang X, Lin P, Yao Q, Chen C. Development of small-diameter vascular grafts. World J Surg March 2007;31:682–9.

[128] Sharifpoor S, Labow RS, Santerre JP. Synthesis and characterization of degradable polar hydrophobic ionic polyurethane scaffolds for vascular tissue engineering applications. Biomacromolecules October 2009;10:2729–39.

[129] Wang MC, Lin JJ, Tseng HJ, Hsu SH. Characterization antimicrobial activities and biocompatibility of organically modified clays and their nanocomposites with polyurethane. ACS Appl Mater Interfaces November 2012;4:338–50.

[130] Shen H, Zhang L, Liu M, Zhang Z. Biomedical applications of graphene. Theranostics March 2012;2(3):283–94.

[131] Chetta GE, Lloyd JR. The design, fabrication and evaluation of a tri-leaflet prosthetic heart valve. J Biomech Eng June 1980;102:34–41.

[132] Imamura E, Kaye MP. Function of expended–polytetrafluoroethylene laminated tri-leaflet heart valve in animals. Mayo Clin Proc December 1977;52:770–5.

[133] Nistal F, García MV, Arbe E, Fernández D, Artiñano E, Mazorra F, et al. In vivo experimental assessment of polytetraflouroethylene tri-leaflet heart valve prosthesis. J Thorac Cardiovasc Surg June 1990;99:1047–81.

[134] Dias RCM, Goes AM, Serakides R, Ayres E, Orefice RL. Porous biodegradable polyurethane nanocomposites : preparation, characterization and biocompatibility tests. Mat Res June 2010;13(2):211–8.

[135] Kannan RY, Salacinski HJ, De Groot J, Clatworthy I, Seifalian AM, et al. The antithrombogenic potential of a polyhedral oligomeric silsesquioxane (POSS) nanocomposite. Biomacromolecules January 2006;7(1):215–23.

[136] Kannan RY, Salacinski HJ, Odlyha M, Butler PE, Seifalian AM. The degradative resistance of polyhedral oligomeric silsesquioxane nanocore integrated polyurethanes: an in vitro study. Biomaterials March 2006;27(9):1971–9.

[137] Kannan RY, Salacinski HJ, Ghanavi JE, Narula A, Seifalian AM, et al. Silsesquioxane nanocomposites as tissue implants. Plast Reconstr Surg May 2007;119(6):1653–62.

[138] Sarkar S, Burriesci G, Wojcik A, Aresti N, Hamilton G, Seifalian AM. Manufacture of small calibre quadruple lamina vascular bypass grafts using a novel automated extrusion-phase-inversion method and nanocomposite polymer. J Biomech April 2009;42(6):722–30.

[139] Khan F, Dahman Y. A novel approach for the utilization of biocellulose nanofibres in polyurethane nanocomposites for potential applications in bone tissue implants. Des Monomers Polym April 2012;15(1):1–29.

Polyurethane nanoparticles, a new tool for biomedical applications?

7

G. Morral-Ruíz[1], P. Melgar-Lesmes[1], C. Solans[2], M.J. García-Celma[1,2,]*
[1]University of Barcelona, Barcelona, Spain; [2]Institute of Advanced Chemistry of Catalonia (IQAC-CSIC) and Networking Research Center on Bioengineering, Biomaterials and Nanomedicine, CIBER-BBN, Barcelona, Spain
*Corresponding author: mjgarcia@ub.edu

7.1 Introduction

In recent decades, polymeric nanoparticles have emerged as a powerful platform to be used in biomedical applications, particularly for therapeutic delivery,[1] medical imaging,[2] and simultaneous drug delivery and diagnosis.[3,4] Nanoparticles, traditionally defined as solid colloidal materials built from macromolecular or molecular assemblies with a diameter in the range of 1–500 nm,[5] exhibit unique key features such as high kinetic stability, wide structural variety, rigid morphology, capacity to incorporate different hydrophilic or hydrophobic drugs, and multiple possibilities for functionalization.[6] All these properties make nanomaterials promising therapeutic tools for synthesizing nanosystems with desirable biophysicochemical properties to target specific organs, tissues, or cells. In this regard, the main challenges in the design of polymeric nanoparticles as targeted therapeutic systems are in the engineering of nanostructured materials with desired size, specific shape, and surface to accomplish a drug-controlled release at the target site, minimizing adverse immune response.[7] Therefore the right choice of polymer and the preparation method are critical aspects since they will determine the final properties of the colloidal system. Among the wide array of polymers typically used to prepare nanoparticles, polyurethanes have received growing interest owing to their synthetic versatility, excellent mechanical properties, and good biocompatibility.[8] Moreover, it has been demonstrated that these materials undergo gradual biodegradation in the human body.[9,10] Polyurethanes represent one of the most versatile materials employed for biomedical applications and have been extensively used in clinic as prosthetic heart valves, catheters, blood pumps, and wound dressings.[11] These materials are classically synthesized from the polycondensation or polyaddition reaction of diisocyanates and diols/polyols or diamines, leading to the formation of polyurethane or polyurea polymers, respectively.[12] As a result of this process, polymers with carbamate bonds (—NH—CO—) in their main chains are obtained. In this chapter, we review the main synthesis processes used to prepare polyurethane nanoparticles with special emphasis on the preparation of polyurethane from nano-emulsions. In this regard, the simple preparation of polyurethanes and their high tailoring enable the incorporation of targeting ligands, cell-penetrating molecules, and stimuli-responsive linkages into the polymer structure.[13] These properties allow the design of

multifunctional nanoassemblies that are potential candidates as nanovectors for smart drug delivery. The potential use of polyurethane nanoparticles as drug targeted delivery systems, diagnostic and theranostic tools is described here with special interest in targeting cancer cells.

7.2   Synthesis of polyurethane nanoparticles

Polyurethane and polyurea polymers are typically obtained from the nucleophilic attack of hydroxyl or amine groups of polyols or polyamines on carbonyl groups of diisocyanate monomer to form carbamate or urea bonds.[14] Although this reaction is often described as occurring between two monomers, diisocyanates can also react with synthetic preformed polymers such as poly ε-caprolactone or polysaccharides to achieve more biocompatible and biodegradable polymers.[15,16] Taking advantage of the high reactivity of diisocyanate monomers with multiple molecules, a great variety of tailored structures can be engineered.[17,18] This fact offers important advantages in biomedical applications in the design of functionalized systems able to specifically recognize target organs, tissues, or cells. Polyurethane nanoparticles are usually obtained from polyaddition or polycondensation reactions.[19] When the polymerization reaction takes place at the interface between two nonmiscible liquids, the process is known as interfacial polyaddition or interfacial polycondensation. Considering that these reactions always yield polymers with reactive functional groups, additional molecules that are not involved in the step-growth polymerization can be incorporated to obtain functionalized structures.[19] The formation of polyurethane particles of different sizes by interfacial polyaddition has been described in different media such as microemulsions,[20] emulsions,[21] nano-emulsions,[18,22–27] and suspensions.[28] However, it should be noted that in an emulsion system a mixture of micelles and monomer droplets coexists in the polymerization medium, which could lead to the formation of nanoparticles with a bimodal size distribution.[19] Moreover in microemulsions, as a consequence of the high concentration of surfactant, the initiation of polymerization could not be obtained in all microdroplets simultaneously and therefore small nanoparticles and empty micelles could be produced.[29] Nano-emulsions exhibit interesting properties and can be used as a template to prepare polyurethane nanoparticles.[6] These systems are discussed in detail in Section 7.2.1. Furthermore, apart from these methods, polyurethane nanoparticles based on preformed polymers have also been obtained by the nanoprecipitation/solvent evaporation[30] or emulsion/solvent techniques.[31,32]

7.2.1   Polyurethane nanoparticles from nano-emulsions

Nano-emulsions constitute an attractive alternative for preparing polyurethane nanoparticles because of their small droplet size and, consequently, very large surface area and high kinetic stability.[6,26] Nano-emulsions are a class of emulsions with a uniform and extremely small droplet size, usually ranging between 20 and 200 nm.[33] They can be classified as oil-in-water (O/W) or water-in-oil (W/O) nano-emulsions if the internal phase is constituted by oil or aqueous droplets dispersed in aqueous or oily external phase, respectively. Therefore both hydrophobic and hydrophilic

materials can be incorporated into the droplets depending on the nature of the internal phase. Considering the internal structure of nano-emulsions polymers can be synthesized either in the dispersed phase or at the interface of the droplets by a polymerization reaction between functional monomers or with preformed polymers.[19] Since nano-emulsions are thermodynamically unstable systems, energy input is required for their formation. Thus, nano-emulsions can be obtained by high-energy emulsification methods using external energy input provided from mechanical devices or by low-energy emulsification methods that take advantage of the chemical potential stored into the components of the system.[33] Taking into account that drugs or biologically active substances can potentially be affected by the emulsification process, the preparation method of nano-emulsion should be chosen according to therapeutic goals and the administration route of the nanovector.[6]

The formation of polymeric nanoparticles from nano-emulsions with a particle size and narrow size distribution suitable for biomedical purposes has been extensively reported.[34–36] In this regard, nanodroplets used as template have been prepared generally by high-energy emulsification methods.[22–25,37,38] Enough energy should be supplied in the shortest possible time with the most homogeneous flow to obtain nano-emulsions with the smallest sizes.[39] Mechanical devices such as high-shear stirring, high-pressure homogenizers and ultrasounds generators are often employed to produce monomer nanodroplets with diameters below 500 nm.[23–25] These nano-emulsions act as "nanoreactors" leading to the formation of nanoparticles ideally in a 1:1 copying process. Thus, nano-emulsions consisting of diisocyanate monomer and hydrophobic diol droplets dispersed in an external aqueous phase and stabilized by the anionic surfactant sodium dodecyl sulfate (SDS) have been widely described as templates useful for obtaining polyurethane nanoparticles with particle diameters in the range of 200–400 nm.[22,23,25,38] These nanoparticles can be obtained by a one-pot method through the direct polyaddition reaction of monomers in the nano-emulsion system[22] or by two-step procedures.[40] These latter consist of incorporating previously prepared reactive prepolymers in the dispersed phase to react with diols in nano-emulsion medium in the presence of crosslinker and catalyst.[40] Although other cationic and nonionic surfactants were also used in these studies, the most stable nano-emulsions seemed to be achieved with SDS as surfactant. Furthermore, isophorone diisocyanate (IPDI) was chosen as the preferred monomer due to its low reactivity with diol. However the formation of colloidal systems based on polyurethanes with other aliphatic diisocyanates such as hexamethylene diisocyanate and lysine diisocyanate has also been reported.[41–43] Polyurethane nanoparticles have also been successfully synthesized using a natural triol, castor oil instead of synthetic diols, and employing nonionic surfactants.[24] The polyaddition reaction to obtain polyurethane nanocapsules has been also carried out using hydroxypropyl-β-cyclodextrin and low molecular weight chitosan as reagents.[16] To avoid premature reaction between isocyanate and hydroxyl groups before the nano-emulsion formation, the temperature must be controlled during the emulsification process. The polymerization reaction between diisocyanate and diol is accelerated by increasing the temperature of the system above 40 °C, leading to the nanoparticle formation in a second step. Some studies required the use of chemical catalysts to initiate the polymerization process.[25,37] Moreover, hybrid polymeric nanoparticles based on polystyrene or poly(butyl acrylate) and polyurethane have

been also synthesized by combining a polyaddition process with radical polymerization in a one-pot procedure using O/W nano-emulsions.[37] Nanocapsules can also be obtained by an interfacial polycondensation mechanism in nano-emulsion medium. Thereby, the large surface area generated during the emulsification process allows multiple reactions at the interface, leading to the formation of a thin film around the nanodroplets and core–shell and capsular morphologies.[19] Polyurethane nanocapsules with oily core and mean particle around 200 nm prepared by interfacial polymerization have also been reported.[23] The design consists of preparing nano-emulsions containing one of the monomers solubilized inside the droplets and then adding the other functional monomer dissolved in a small fraction of external phase to the system. Hexadecane is typically used as costabilizer to provide stability against Ostwald ripening. Polymerization takes place at the interface of the two immiscible phases to achieve nanoparticles. Moreover, hollow nanocapsules with a hydrophilic liquid core obtained by interfacial polycondensation or cross-linking reactions from W/O nano-emulsions have been also engineered.[41] The functionalization of these polyurethane nanocapsules by carboxymethylation or by physical adsorption of a cationic polyelectrolyte to enhance their bioaccessibility has been also reported.[44] Table 7.1 summarizes synthesis aspects of different polyurethane nanoparticles and the particle sizes obtained.

Even though high-energy emulsification methods described above have been well proven and repeatable it has been reported that nano-emulsions with even smaller and more uniform droplet sizes can be obtained by using low-energy methods.[33,45] Taking advantage of the physicochemical properties of the system, nano-emulsions are produced almost spontaneously. Formation of nano-emulsions by low-energy emulsification methods includes the phase inversion temperature (PIT) method, which consists of cooling or heating speedily the system, keeping the composition constant[46]; and the phase inversion composition (PIC) method, in which phase transitions take place by modifying the composition at constant temperature.[47] Although the formation of polyurethane nanoparticles from polymerization in nano-emulsions obtained by a low-energy method offers important advantages compared with high-energy methods, this polymerization route has barely been exploited (see Table 7.1). Polyurethane and polyether urethane nanoparticles with mean particle diameter in the range of 150–50 nm have been synthesized by combining an interfacial polycondensation process with spontaneous emulsification.[48] Acetone was used as water miscible solvent and nanoparticles were formed by nanoprecipitation followed by solvent evaporation. The formation of polyurethane and polyurea nanoparticles without organic solvent has also been successfully reported.[18,26,27] These compositions consist of O/W nano-emulsions with IPDI incorporated prepared by the PIC emulsification method in aqueous solution/ nonionic surfactant/saturated medium chain triglyceride systems and using biocompatible components.[18,26,27] Pegylated polyurethane and lysine-coated polyurea nanoparticles with small particle sizes (below 80 nm) were obtained by polymerization at the droplet interface after increasing the temperature of the system above 60 °C. These studies showed that nonionic surfactants Polysorbate 80 and Kolliphor® ELP were involved in the polymerization process, thus obtaining a polymeric matrix built by copolymers derived from reaction between the diisocyanate and the hydroxyl groups of both the nonionic surfactant and the highly hydrophilic components. These systems exhibit

Table 7.1 **Synthesis aspects of polyurethane and polyurea nanoparticles obtained from O/W nano-emulsions**

Nature of nanoparticle	Emulsification method	Nature of nano-emulsion	Monomers	Surfactants	Polymerization and emulsification parameters	Particle size (nm)	References
Polyurethane	High-energy (ultrasonication)	O/W	IPDI/1,12-dodecanediol IPDI/bisphenol A IPDI/neopentyl glycol	SDS	Influence of diol monomer	200 nm	Tiarks et al.[22]
Polyurethane	High-energy (ultrasonication)	O/W	IPDI 1,6-hexanediol	SDS Pluronic® F127 Pluronic® F68	Influence of volume ratio Influence of ultrasound power Influence of surfactant	170–190	Gaudin and Sintes-Zydowicz[38]
Polyurethane Pegylated polyurethane	High-energy (high-shear stirring)	O/W	IPDI/castor oil IPDI/PEG 400/castor oil	SDS Tween 80 Pluronic® F 68	Concentration of reactants Nature of stabilizers Shear speed	200–400	Zanetti-Ramos et al.[24]
Polyurethane nanocapsules	High-energy (ultrasonication)	O/W	IPDI/1,6-hexanediol	SDS Cationic Nonionic	Influence of surfactant	200	Torini et al.[23]
Polyurethane nanocapsules	High energy (high-shear stirring and high-pressure homogenizers)	O/W	IPDI/propanetriol catalyst	SDS Disponil® FES77 Lutensol® AT50	Influence of surfactant Influence of disperse phase	170–320	Johnsen and Schmid[25]

Table 7.1 **Continued**

Nature of nanoparticle	Emulsification method	Nature of nano-emulsion	Monomers	Surfactants	Polymerization and emulsification parameters	Particle size (nm)	References
Polyurethane Polyurea Polythiourea Cross-linked starch Cross-linked dextran	High-energy (ultrasonication)	W/O	IPDI Toluene diisocyanate hexamethylene diisocyanate 1,6-Hexanediol Diethylenetriamine Glycerol Starch Dextran 1,4-Diaminohexane	Block opolymer emulsifier poly-[(butylene-coethylene)-b-(ethylene oxide)]	Nature of reactive monomers and continuous phase	200–500	Crespy et al.[41]
Polyurethane Pegylated polyurethane Polyurea	Low-energy (PIC)	O/W	IPDI/Polysorbate 80 IPDI/Kolliphor® ELP IPDI/Polyethylene glycol IPDI/L-lysine	Polysorbate 80 Kolliphor® ELP	Influence of temperature Influence of monomer concentration Influence of oil/surfactant weight ratio	25–90	Morral-Ruíz et al.[18,26,27]

stealth properties and showed good biocompatibility after being tested by hemolysis and cell viability assays.

Multifunctional biotinylated and streptavidin-coated polyurethane–urea nanoparticles have also been engineered from O/W nano-emulsions.[4,49] In these studies, biotin or streptavidin reacts with diisocyanate at the droplet interface and are successfully attached to the nanoparticle polymeric matrices. These nanoparticles exhibit diameters around 110–140 nm (biotin nanoparticles) and 70–74 nm (streptavidin nanoparticles). In addition, streptavidin-coated polyurethane–urea nanoparticles were functionalized with biotin anti-VCAM-1 and anti-ICAM-1 antibodies for specific targeting. Both nanoparticulate systems showed no cytotoxicity in healthy endothelial cells and therefore good biocompatibility properties. Figure 7.1 shows a schema of the synthesis of different polyurethane nanoparticles obtained from O/W nano-emulsions by interfacial polymerization and images obtained by transmission electron microscopy.

The formation of polyurethane nanoparticles from inverse nano-emulsions (W/O) has also been achieved. Interfacial polyaddition in inverse nano-emulsion is of special interest since this allows the encapsulation of hydrophilic active materials such as proteins or nucleic acids. Thus, taking advantage of the high reactivity of tolylene 2,4-diisocyanate with water molecules, polyurea lipid nanocapsules with aqueous cores obtained from W/O nano-emulsions and prepared by PIT method were designed.[50] Polymer synthesis occurs by *in situ* interfacial polymerization after nano-emulsion formation. Volatile oils employed as the continuous phase were removed by evaporation and the nanocapsules were redispersed in water. These nanocapsules could be potentially used for encapsulation of both hydrophilic and lipophilic molecules simultaneously.

7.3   Polyurethane nanoparticles as drug delivery systems

The development of new strategies for the delivery of drugs and biologically active substances is an important challenge in the biomedical field. The use of therapeutic molecules is often limited due to their low bioavailability and solubility, low permeability across barriers, and short biological half-life in the organism.[35] The encapsulation of these molecules in nanocarriers offers important advantages in terms of pharmacokinetics and pharmacodynamics. Colloidal systems have been extensively used for several years to encapsulate and target different drugs.[51,52] Between diverse developed nanocarriers, polymeric nanoparticles have been demonstrated as useful tools for drug delivery.[1,53] These systems protect the drug against *in vivo* degradation, thus improving its bioavailability, allow a longer term therapeutic effect through the slow drug release from the polymeric matrix, and control the suitable biodistribution of the drug according to the properties of the nanoparticulate system.[54] The design of polymeric nanoparticles for drug release should be addressed to achieve specific targeting to enhance the therapeutic efficacy of the drug while minimizing its toxicity. *In vitro* and *in vivo* tests are useful for evaluating the efficacy of the nanovector compared to the administration of the drug in solution. Taking into account that one commonly used administration route is intravenous apart from oral and intratumoral, the biocompatibility and bioadhesion properties of the nanoparticles in contact with blood or soft tissues should be assessed.[55]
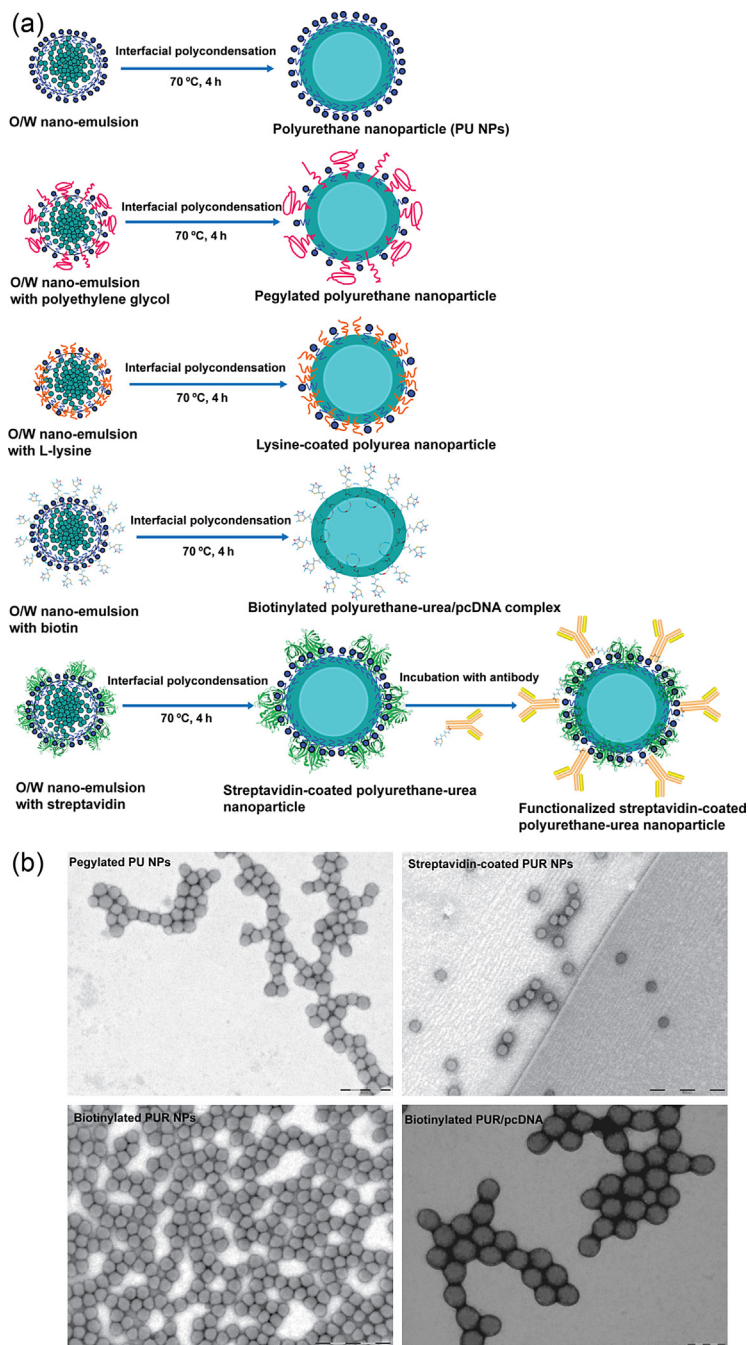
Figure 7.1 Formation of different polyurethane nanoparticles (naked polyurethane, pegylated polyurethane, lysine-coated polyurea, biotinylated polyurethane–urea/pc DNA complex, and functionalized streptavidin-coated polyurethane–urea nanoparticles) obtained by interfacial polycondensation from O/W nano-emulsions (a) and transmission electron micrographs of polyurethane nanoparticles after being negatively stained with 1% v/v uranyl acetate (b).

Moreover, intravenous administration implies that the nanocarrier should remain in the blood stream long enough to reach the target cell, organ, or tissue. Therefore nanoparticles should exhibit stealth properties for not being quickly recognized and removed by the action of the reticuloendothelial system.[56] In this regard, two strategies are usually employed[56]: one is to increase the hydrophilicity of the colloidal system with molecules such as polyethylene glycol, a second is to achieve nanoparticles with small particle size (under 100 nm). Furthermore, the choice of polymer to prepare nanoparticles should also be governed by the biodegradability of the polymer after the drug has been released. Regarding the synthesis of polyurethane nanoparticles, the use of aliphatic diisocyanate instead of aromatic diisocyanate is preferred for *in vivo* applications. Polyurethanes derived from the reaction between lysine–diisocyanate and polyesters such as poly(ε-caprolactone) or poly lactic acid/glycolic acid as soft segments are emerging as potential therapeutic systems with good biocompatibility and release properties.[31,57–59] Nanovectors based on polyurethane have been used to entrap multiple molecules and therapeutic agents for imaging, gene therapy, or drug delivery.[4,49,58,60–62] In this section we report some that have demonstrated high entrapment efficiency, therapeutic effect, good release profiles, and low cytotoxicity *in vitro* or *in vivo*.

Rosenbauer and coworkers[63] designed polyurea nanocapsules from aminofunctionalized surfactant, Lubrizol U, which can react with diisocyanate, thus being incorporated to the polymeric interfacial layer forming a more compact and impermeable capsule shell. These nanoparticles were used to encapsulate a hydrophilic fluorescent dye, fluorescein, with an entrapment efficiency around 85–95%. Cell uptake studies showed that nanoparticles were successfully internalized into HeLa cells. Similar studies demonstrated that functionalization by carboxymethylation or amino-functionalization, resulted in an increase of uptake by HeLa cells.[44] These researchers also developed nanocapsules with aqueous cores and polymeric shells containing azo bonds to achieve selective release of encapsulated material by stimuli such as temperature, UV light, or pH change.[64] The release of encapsulated sulforhodamine SR101 as a model molecule was also studied.[64] Furthermore, dsDNA was successfully encapsulated in starch cross-linked polyurea nanocapsules.[65] These nanocapsules were used as nanoreactors to amplify dsDNA through polymerase chain reactions. Similar nanocarrier platforms based on hydroxyethyl starch and polyurea functionalized with polyethylene glycol, which were able to encapsulate hydrophilic molecules, have been also reported.[66] These nanoparticles exhibited stealth properties in *in vitro* and *in vivo* studies.

Hydrophilic contrast agents such as Magnevist®, Gadovist®, and Multihance® for magnetic resonance imaging have been encapsulated in polyurethane, polyurea, and cross-linked dextran polyurea nanocapsules.[67,68] These systems exhibited good biocompatibility, efficient water exchange through different polymeric shells, high payload, and high stability in biological media.

The encapsulation of anti-inflammatory drugs in nanovectors in polyurethanes has been also reported.[69,70] A nonsteroidal anti-inflammatory drug, ketoprofen, has been successfully incorporated in pegylated polyurethane and lys-coated polyurea nanoparticles with high entrapment efficiency of 89–95%. *In vitro* release studies were performed achieving 80% of released free drug from the polymeric matrix after 6 h.[69] Dexamethasone, a glucocorticoid with anti-inflammatory properties, has been loaded

in nanocapsules consisting of a cross-linked hydroxyethylated glucose–polyurea polymer.[70] These systems showed a targeted delivery through the suppression of the inflammatory response in nonparenchymal murine liver cells, such as Kupffer cells.

CBO-P11, a specific inhibitor of vascular endothelial growth factor and other angiogenic pathways, was efficiently incorporated in multifunctional anti-VCAM-1 and anti-ICAM-1 polyurethane–urea nanoparticles.[49] These systems showed a significant and selective blockade of the proliferation only in inflamed endothelial cells and no cytotoxic effect was observed in healthy cells. Moreover, *in vivo* studies in CD1 mice demonstrated that these nanoparticles reach the target site after intravenous administration.

Polymeric polyurethane micelles and nanoparticles have also been shown to be good nanovehicles for transport and delivery of different anticancer drugs. Wang et al.[43] developed temperature- and pH-responsive polyurethane nanoparticles based on hexamethylene diisocyanate to encapsulate doxorubicin. These polyurethanes were not cytotoxic. Nanoparticles were effectively uptaken by Huh-7 cells. The release of doxorubicin occurred by pH- and temperature-stimulated variations. Similarly, targeting-clickable and tumor-cleavable polyurethane nanomicelles obtained from biodegradable poly(ε-caprolactone) and L-lysine ethyl ester diisocyanate showed a high loading capacity for doxorubicin, stimuli responsiveness, and good cytocompatibility.[71] Moreover, the functionalization with folic acid enhanced cellular uptake and improved drug efficacy in HeLa cancer cells. Biodegradable and temperature-responsive polyurethane nanoparticles consisting of polyethylene glycol and L-lysine ester diisocyanate loaded with Adriamycin® have also been reported.[72] Phenoxodiol and sunitinib malate were successfully incorporated into biotinylated polyurethane–urea nanoparticles.[4] *In vitro* studies in cells revealed that drugs loaded into these nanoparticles reduced the cell viability of hepatoma cells but not human endothelial cells, thereby exhibiting high specificity for tumor cells. Moreover a plasmid DNA encoding green fluorescent protein was also incorporated into these nanoparticles. Transfection of the reporter gene by fluorescent detection was only evidenced in cancer cells and no fluorescent signal attributed to GFP was observed in healthy endothelial cells. Furthermore, these studies demonstrated that biotinylated nanoparticles were only incorporated and accumulated in the perinuclear and nuclear area of tumor cells. This privileged subcellular localization in cancer cells makes these nanosystems good candidates for targeted gene therapy in cancer. Aspects related to targeting cancer cells are discussed in Section 7.3.1.

7.3.1 Polyurethane nanoparticles targeting cancer cells

Many different strategies and delivery systems have been evaluated for cell-selective drug targeting to tumors over the years. For that purpose, investigators have used liposomes, lipoplexes, albumin nanospheres, micelles, nano-emulsions polymers, and nanoparticles with antibodies, among others.[73] Significant progress has been made in this area of research both at the preclinical and at the clinical level, and some promising nanomedicines such as Abraxane®, Doxil®, DaunoXome®, Oncaspar®, and DepoCyt® have been approved for clinical use.

The high number of studies in the field of pathophysiological behavior of cancer cells and their milieu during past decades has improved the prospect of drug targeting to tumors. We know that cancer cells interplay with the immune system and with blood vessels to boost their uncontrolled growth. Indeed, many cancers arise from sites of infection, chronic irritation, and inflammation.[74–76] As a tumor proliferates, it rapidly outgrows its blood supply, and regions of hypoxia arise, thus stimulating angiogenesis.[77] In turn, along with the formation of blood vessels, tumors also recruit immune and inflammatory cells by means of the stimulation of the synthesis of cellular adhesion molecules in the vascular endothelium. Unfortunately, since tumors promote a tolerant microenvironment and the activation of an array of immunosuppressive mechanisms,[78] immune cells are not effective at fighting cancer cells. Quite the contrary, immune and inflammatory cells amplify the inflammatory reaction through the formation of new blood vessels, stimulate tumor cell growth, and induce tumor cells to migrate out of the tumor and enter vessels.[79] It is therefore now becoming clear that this vascular tumor microenvironment, which is largely orchestrated by inflammatory cells, is an indispensable participant in the neoplastic process, fostering proliferation, survival, and migration.[74] Moreover, one of the molecular events linking inflammation and cancer is an increase in cellular adhesion molecules that are expressed on the luminal surface of endothelium on inflammation. These adhesion molecules, such as VCAM-1 and ICAM-1, are shared by some cancer cells and have the ability to contribute to metastasis. Thus, an elevation of adhesion molecules in chronic inflammation may be a risk factor for metastasis.[80] In this regard, functionalizing polyurethane nanoparticles with streptavidin has been reported as a good strategy for targeting inflamed vessels in mice, taking advantage of the spontaneous binding of biotinylated antibodies to these multifunctional nanoplatforms.[49] The therapeutic strategy consisted of targeting polyurethane nanoparticles with anti-VCAM-1 or ICAM-1 antibodies and loading them with an antiangiogenic drug to arrest the blood supply.[49] Similarly, other investigators are focusing on targeting polyurethane nanocapsules to suppress the inflammatory response of phagocytic cells, by delivering anti-inflammatory drugs such as dexamethasone.[70] Another feature of tumor tissue that has been exploited to design nanomedicines is the acidic environment where cancer cells grow. The pH value of the bloodstream is approximately 7.4, while the existing tumoral pH and that of endocytic compartments of the cells generally ranges from 4 to 6. This difference in pH value makes pH-triggered drug release possible. Thus, the use of pH-sensitive biodegradable polyurethane nanoparticles and also mesoporous materials as delivery carriers with anticancer drug controlled release has been tested *in vitro* and *in vivo*, with promising outcomes.[43,81]

Advances in the understanding of the changes that healthy cells undergo when transforming into cancer cells are allowing improvements in the design of nanomedicines. However, the specific targeting of nanoparticles to only cancer cells and delivering chemotherapy without affecting healthy cells remain a challenge. Recent reports designing antibody-coated polyurethane nanoparticles or mutiblock polyurethanes have shown the efficacy of targeting a cell surface receptor that is overexpressed in many cancer cells, epidermal growth factor receptor.[31,82] However this receptor is ubiquitous[83] and that means that nontumor binding may occur when applied in

patients with cancer. For this reason, molecularly and targeted therapeutics with a time-delayed release of drug may more preferentially kill cancer cells and improve the balance between the efficacy and the toxicity of systemic anticancer therapy. In this regard, pegylation of polyurethane nanoparticles has shown a sustained-release profile of the anticancer drug doxorubicin due to the chemical structure and interactions with the polymeric shell.[30] Cancer cells also display an array of common traits that allow their permanent growth and spreading, such as angiogenesis promotion, release of matrix-degrading enzymes, and high expression of carriers for nutrients.[84] Among nutrient carriers, biotin and folic acid transporters have been found to be highly active and overexpressed in cancer cells.[85–87] Namely, biotin participates in cell signaling, gene expression, and chromatin structure in cell proliferation.[88] Cells accumulate biotin through both the sodium-dependent multivitamin transporter and the monocarboxylate transporter 1. These transporters, along with other biotin-binding proteins, drive biotin to compartments involved in metabolism, cell growth, and division. The activity of certain factors in cell signaling pathways, such as biotinyl-AMP, Sp1 and Sp3, nuclear factor-κB, and receptor tyrosine kinases is dependent on biotin supply.[88] Surface coating of polyurethane nanoparticles with biotin has been shown to be an effective strategy to selectively target and deliver drugs or plasmids into hepatocellular carcinoma cells with minimal binding to endothelial cells.[4] Similarly polyurethane micelles and nanoparticles coating folic acid to their surface have been demonstrated to have an enhanced cellular uptake and improved drug efficacy toward HeLa and HepG2 cancer cells *in vitro*.[61,71]

Nanotechnology-based therapeutics have exhibited clear benefits when compared with unmodified drugs, including improved half-lives, retention, targeting efficiency, and lower patient side effects. However, the problems to overcome are difficult. This field has led to the identification of several important pitfalls in tumor-targeted drug delivery:

1. Overestimation of the enhanced permeability and retention effect by which particles with a very small size (typically liposomes, nanoparticles, and macromolecular drugs) should be accumulated into the tumor microenvironment due to the unique anatomy of tumor vessels. This postulate must be tested for every polymeric composition because it is dependent not only on size but also on chemical and surface properties.
2. Reduced tumor and tissue penetration of nanomedicines.
3. Misinterpretation of the potential usefulness of active drug targeting.
4. Confusing formulation design, based on materials that are too complex and not broadly applicable in biomedicine.
5. Insufficient incorporation of effective drugs for a therapeutic effect clinically relevant in combination regimens.
6. Insufficient studies focusing on the highest medical needs in cancer, that is, treating metastasis, and not just solid tumors.
7. Inadequate integration of noninvasive imaging techniques and theranostics, which might be used to personalize nanomedicine-based therapeutic interventions.
8. Lack of appropriate animal models to reproduce the pathophysiology more similar to the clinical situation.

These perceptions strongly suggest that besides investigating ever more different polyurethane combinations for cancer, forthcoming efforts should also be addressed

to understanding the unique pathophysiology of every tumor and the interaction of cancer cell–material. With this conceptual integration, polyurethane carriers modified for drug targeting to tumors should help to overcome these shortcomings and help in clinical practice.

7.4 Polyurethane nanoparticles as diagnosis tools

Advances in imaging technology for medical diagnosis have revolutionized almost every aspect of medicine. Computed tomography (CT) and angiography scans, magnetic resonance imaging (MRIs), positron emission tomography (PET) scans, other techniques, and combinations of them have had a huge impact on the diagnosis and treatment of disease from 1995 to 2015. Some years ago, an angiography (an examination of the blood vessels) could only be done by inserting a catheter into an artery. In the procedure, contrast material (a substance that makes it easier to see tissue in an X-ray) is injected through the catheter. Then an X-ray image is taken to look for blockages, internal bleeding, etc. Catheter angiography can take up to several hours. It often requires sedatives and sometimes a night in the hospital. It also has risks, like a small chance of blood clots or bleeding. The newest CT scans are a completely noninvasive way to obtain the same information as an invasive catheter angiography. In CT angiography, the contrast material is injected into the arm and the arteries in the lungs, kidneys, brain, and legs can be examined. The entire process takes just 10–25 min. CT angiography has not completely replaced the old technique as traditional angiography is still commonly used to evaluate heart arteries for blockages.[89] Imaging tests have also replaced exploratory surgery. With CT, MRI scans, and ultrasound the surgical approach has improved substantially. PET has become increasingly important in recent years, particularly since it was combined with CT scanning in one device. Unlike many other imaging technologies, PET scans are not designed to analyze images of organs or tissue. Instead, PET images biological functions, such as blood flow or glucose metabolism. The fusion of PET and CT allows simultaneous determination of both the metabolic information of PET and the anatomic detail of CT. More detailed imaging is allowing increased resolution of the data while providing early and more accurate diagnoses. In many cases, it might even lead to more successful treatment.[90]

Different imaging agents for MRI, PET/SPECT, and fluorescent markers can be attached to the surface of polyurethane nanoparticles for targeting specific cells or tissues. The rationale of nanoimaging is to facilitate imaging by selectively targeting the injured or diseased area in contrast to unspecific current contrast agents. This strategy is designed to gain information about the extension of a diseased cell type or tissue (like in cancer), study kinetics, trafficking pathway, or therapeutic efficacy. A first approach in the field from a group of investigators was the use of polyurethane nanocapsules containing the hydrophilic commercial contrast agents Magnevist® and Gadovist®.[68] These investigations demonstrated that polyurethane matrices can preserve the porosity necessary for the exchange of water molecules through the capsule wall to ensure T1

relaxation of the contrast compound and be useful for MRI. The use of the miniemulsion technique produces small stable droplets; subsequent polymerization of these droplets leads to particles or capsules, which ideally keep their size.[91] Further investigations demonstrated that polyurethane nanocapsules are stable in human blood plasma without altering the effectiveness of the loaded contrast agent.[67] A different approach to transform bare polyurethane nanoparticles in real biosensors has been the noncovalent functionalization with multiwall carbon nanotubes loaded with hemoglobin.[92] This way, immobilized hemoglobin could maintain its native conformation and bioactivity and also exhibit an excellent electrochemical behavior to be detected by different techniques.

More recently, new approaches trend to multifunctional or targeted polyurethane nanoplatforms with different imaging agents. Multifunctional polyurethanes bearing cell-penetrating gemini quaternary ammonium-pendant groups in the side chain and redox-responsive disulfide linkages throughout the backbone, have been developed for potential MRI and drug delivery.[60] These nanocarriers are loaded with superparamagnetic iron oxide nanoparticles demonstrating excellent MRI contrast enhancement for both efficient intracellular delivery of anticancer drugs and real-time monitoring of therapeutic effect. Other investigators take advantage of the magnetic properties of metallic agents such as Fe_3O_4 to design nanoparticles based on a paraffin core and polyurea shell with the expectation that organic polyurea shells would offer structural flexibility and convenient processing, while the inorganic Fe_3O_4 would provide enhanced thermal conductivity and additional magnetic properties for imaging as well as thermal therapy.[93]

The functionalization of polyurethane nanoparticles to target fluorophores to specific cells has been focused on basic science since there are no devices designed for detecting low levels of cell-selective fluorescence in clinics currently. In this context, polyurethane nanoparticles from nano-emulsions have been described; these encapsulate pH independent fluorescent dyes or coating streptavidin fluorophores and have the potential to attach peptides or biotinylated agents (such as antibodies or receptors) to selectively target and detect cancer cells.[4,44] A convenient functionalization of the aqueous core of polyurethane nanoparticles with different imaging agents appears as a suitable strategy for improving the efficiency of current diagnostic imaging agents.

7.5   Polyurethane nanoparticles as theranostic tools

Simultaneous targeted drug therapy and imaging for diagnostics (theranostics) is still a current challenge in nanoscience. There have been increasing approaches in diverse nanoscale platforms from 2005 to 2015 to develop multifunctional medical nanocarriers for targeted delivery, fast diagnosis, and efficient therapy.[73,94,95] Particularly, in the field of nanomedicine, it is crucial that biocompatible nanocarriers are well designed to achieve a selective and efficient treatment and tagging of specific diseased cells, thus delivering drugs and coating imaging agents to aid in the recognition of targeted tissue during diagnosis. Among the numerous developed colloidal systems, nanoparticles based on polyurethane–urea matrices offer new possibilities to covalently bind bioactive molecules on the surface. This makes the functionalization of polyurethane–urea nanoparticles an interesting approach for obtaining new tools for theranostics. In this context, surface coating of polyurethane–urea nanoparticles with streptavidin

represents a multifunctional strategy to bind either specific biotinylated antibodies or imaging agents for therapy or diagnostics.[49] Surface coating of polyurethane–urea nanoparticles with biotin has been demonstrated also to be useful for biomedical diagnostics or specific drug delivery on cancer cells by means of delivering antiproliferative drugs plus a plasmid encoding for a fluorophore (GFP).[4] Therefore polyurethane nanoparticles can also transport and transfect nucleic acids, allowing the improvement of current transfection methods. Actually these plasmid DNA-biotinylated nanoparticles had higher transfection into hepatocellular carcinoma cells than healthy endothelial cells in comparison to DNA linked to the commercial FuGENE®6.[4] This means that both the therapy and the diagnostic potential properties of biotinylated nanoparticles are selective for human hepatoma cells and are not expected to have toxic effects on vasculature or false positives in the labeling of tumor tissue. Taken together, surface-modified polyurethane nanoparticles can be good carriers for targeting drugs and imaging agents and also bridge the gap between the promise of gene therapy and the clinical applications. The design, uptake, and multitargeting of typical pegylated polyurethane–urea nanoparticles for theranostics are shown in Figure 7.2.
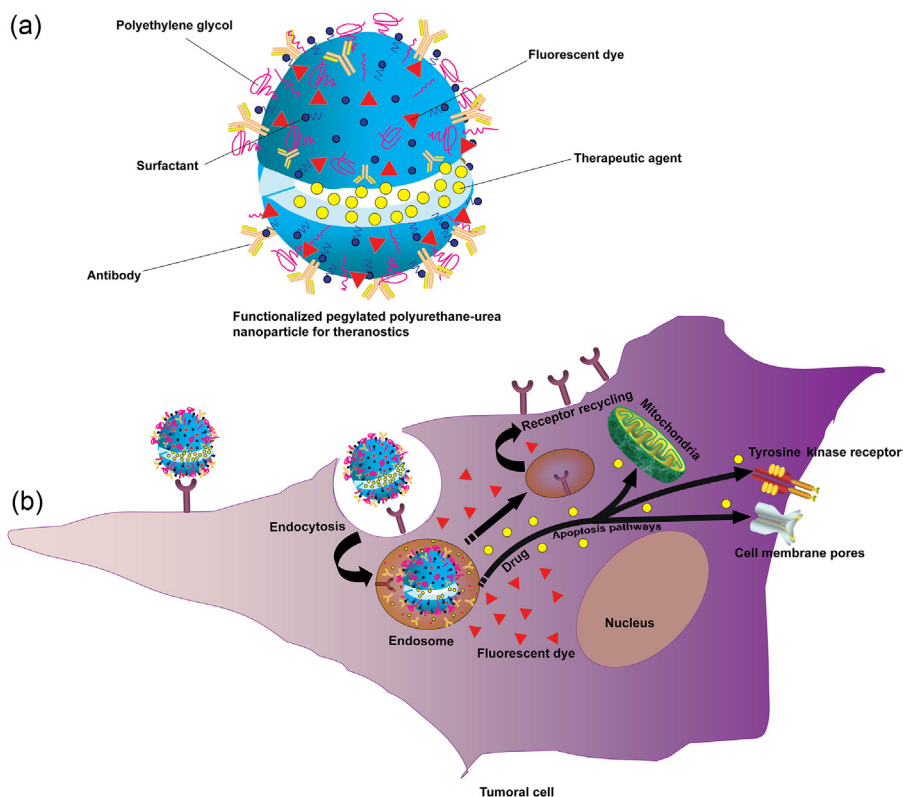
Figure 7.2 Design, uptake, and multitargeting of pegylated polyurethane–urea nanoparticles for theranostics. (a) Design of theranostic platform of polyurethane–urea and (b) theoretical mechanism of targeting and uptake of functionalized pegylated polyurethane–urea nanoparticles loading a therapeutic agent and fluorescent dye on tumor cells.

Maximal surgical resection of a tumor improves the survival of patients.[96] However success in surgery still relies on the surgeon's ability to delimit the presence of residual tumor tissue at the time of surgery. Neoplastic tissue limits are virtually indistinguishable from normal tissue, thus pointing to a clear need for improving tumor delineation during surgery. Some investigations suggest that DNA/nanoparticle hybrids are promising machinery for gene therapy and diagnostics in cancer.[97,98] These hybrids show clear advantages in relation to the use of fluorescein or other imaging agents coated to nanoparticles since it is very difficult to implement feasible tumor imaging techniques that simultaneously offer sufficient specificity and sensitivity. Nanotechnology offers a tremendous potential for medical diagnostics and novel therapeutic modalities. The combination of nanoscale materials with multitarget antitumor drugs and a reporter gene encoded by DNA can lead to the development of multifunctional medical nanoplatforms for simultaneous targeted delivery and diagnosis as well as better monitoring of the therapeutic process. Nanoscale carriers for multitarget drugs and nucleic acids require positively charged surfaces with the consequent increase of toxicity on healthy cells. In contrast, polyurethane nanoparticles do not require a positively charged surface to bond DNA, thus allowing minimal cytotoxicity. Overall polyurethane nanoparticles could provide new perspectives to overcome the current limitations of therapy and diagnostics by means of state-of-the-art nanostructure tools and also encourage the researchers to improve the promising field of gene therapy.

Theranostic nanoparticle usage, which combines both therapeutic and diagnostic capabilities in one dose, has promise to push the biomedical field toward personalized medicine. Different theranostic strategies developed for the diagnosis and treatment of disease, such as nucleic acid delivery, hyperthermia (photothermal ablation), photodynamic, chemo, and radiotherapy are combined with one or more imaging functionalities for both *in vitro* and *in vivo* studies.[99] Different imaging probes, such as MRI contrast agents, nuclear imaging agents (PET/SPECT agents), and fluorescent markers (organic dyes and inorganic quantum dots), can be shell-decorating therapeutic agents or polymeric vehicles to facilitate their imaging to gain information about the kinetics, trafficking pathway, or therapeutic efficacy. To date there are not many studies using polyurethane nanoparticles as vehicles for the wide array of commercial diagnostic contrast agents useful in clinics. Further study is required to allow the design of polyurethane particles to be easily detectable by equipment available in any medical center.

7.6   Future trends

Significant advances have been made in the design, formation, and characterization of polyurethane nanoparticles. Different approaches have been employed to synthesize polyurethane nanoparticles as carriers of imaging agents, as drugs, or as copolymers to form different versatile matrices. The chemical reactivity and properties of these polymers make them suitable to bind peptides, nucleic acids, antibodies,

and other biomolecules to obtain functionalized nanoparticles for an array of medical applications. Further work is still required to develop new methods to obtain nanoparticle matrices with tuned porosity and degradability for sustained controlled drug release. In the future, the goal is to obtain smart multifunctional nanoparticles to target specific cells for the release of drugs or imaging agents controllable and triggered by external signals (such as infrared light, ultrasound, and magnetic force) or the local environment. Moreover, polyurethane nanoparticles will have improved drug solubility, oral bioavailability, targeting ability, lower dosage with the same effects, better side-effect profile, more convenient dosage forms, and the ability to cross biological barriers. Overall, the development of polyurethane nanoparticles from 2005 to 2015 has boosted the use of polyurethanes as suitable materials for biomedical applications. Future advances should see these nanostructured material systems applied in the clinic in such applications as drug delivery, gene transfection, and tumor imaging.

References

1. Kumari A, Yadav SK, Yadav SC. Biodegradable polymeric nanoparticles based drug delivery systems. *Colloids Surf B Biointerfaces* 2010;**75**:1–18.
2. Weissleder R. Molecular imaging in cancer. *Science* 2006;**312**:1168–71.
3. Jia F, Liu X, Li L, Mallapragada S, Narasimhan B, Wan Q. Multifunctional nanoparticles for targeted delivery of immune activating and cancer therapeutic agents. *J Control Release* 2013;**172**(3):1020–34.
4. Morral-Ruíz G, Melgar-Lesmes P, López-Vicente A, Solans C, García-Celma MJ. Biotinylated polyurethane-urea nanoparticles for targeted theranostic in human hepatocellular carcinoma. *Nano Res* 2015;**8**(5):1729–45.
5. Kreuter J. In: Singh Nawla H, editor. *Encyclopedia of nanoscience and nano- technology*, vol. 7. Stevenson Ranch (USA): American Scientifics Publishers; 2004. p. 161.
6. Anton N, Benoit JP, Saulnier P. Design and production of nanoparticles formulated from nano-emulsion templates – a review. *J Control Release* 2008;**128**:185–99.
7. Park S, Kang S, Veach AJ, Vedvyas Y, Zarnegar R, Kim J-Y, et al. Self-assembled nanoplatform for targeted delivery of chemotherapy agents via affinity-regulated molecular interactions. *Biomaterials* 2010;**31**:7766–75.
8. Nair LS, Laurencin CT. Biodegradable polymers as biomaterials. *Prog Polym Sci* 2007;**32**:762–98.
9. Chandra R, Rustgi R. *Biodegrad Polym* 1998;**23**:1273–335.
10. Santerre JP, Woodhouse K, Laroche G, Labow RS. Understanding the biodegradation of polyurethanes: from classical implants to tissue engineering materials. *Biomaterial* 2005;**26**:7457–70.
11. Vermette P, Griesser HJ, Laroche G, Guidoin R. *Biomedical applications of polyurethanes*. 6th ed. Austin (TX): Landes Bioscience; 2001.
12. Ionescu M. Polyols and basic chemistry of polyurethanes. In: Ionescu M, editor. *Chemistry and technology of polyols for polyurethanes*. Shawbury, Shrewsbury (Shropshire, UK): Rapra Technology; 2005. p. 1–15.
13. Ding M, Li J, Tan H, Fu Q. Self-assembly of biodegradable polyurethanes for controlled delivery applications. *Soft Mater* 2012;**8**:5414–28.

14. Cherng JY, Hou TY, Shih MF, Talsma H, Hennink WE. Polyurethane-based drug delivery systems. *Int J Pharm* 2013;**450**:145–62.

15. Li GY, Li DD, Niu YQ, Chen KC, Xu KT. Alternating block polyurethanes based on PCL and PEG as potential nerve regeneration materials. *J Biomed Mater Res A* 2014;**102**:685–97.

16. Du Y-Z, Xu J-G, Wang L, Yuan H, Hu F-Q. Preparation and characteristics of hydroxy-propyl-β-cyclodextrin polymeric nanocapsules loading nimodipine. *Eur Polym J* 2009;**45**:1397–402.

17. Landfester K, Musyanovych A, Mailänder V. From polymeric particles to multifunctional nanocapsules for biomedical applications using the miniemulsion process. *J Polym Sci Part A Polym Chem* 2010;**48**:493–515.

18. Morral-Ruíz G, Melgar-Lesmes P, García ML, Solans C, García-Celma MJ. Polyurethane and polyurea nanoparticles based on polyoxyethylene castor oil derivative surfactant suit-able for endovascular applications. *Int J Pharm* 2014;**461**(1–2):1–13.

19. Crespy D, Landfester K. Miniemulsion polymerization as a versatile tool for the synthesis of functionalized polymers. *Beilstein J Org Chem* 2010;**6**:1132–48.

20. Texter J, Ziemer P. Polyurethanes via microemulsion polymerization. *Macromolecules* 2004;**37**:5841–3.

21. Zhu Q, Wang Y, Zhou M, Mao Ch, Huang X, Bao J, et al. Preparation of anionic polyurethane nanoparticles and blood compatible behaviors. *J Nanosc Nanotech* 2012;**12**(5):4051–6.

22. Tiarks F, Landfester K, Antonietti M. One-step preparation of polyurethane dispersions by miniemulsion polyaddition. *J Polym Sci Part A Polym Chem* 2001;**39**:2520–4.

23. Torini L, Argillier JF, Zydowicz N. Interfacial polycondensation encapsulation in miniemul-sion. *Macromolecules* 2005;**38**:3225–36.

24. Zanetti-Ramos BG, Lemos- Senna E, Soldi V, Borsali R, Cloutet E, Cramail H. Poly-urethane nanoparticles from a natural polyol via miniemulsion technique. *Polymer* 2006;**47**:8080–7.

25. Johnsen H, Schmid RB. Preparation of polyurethane nanocapsules by miniemulsion polyaddition. *J Microencapsul* 2007;**24**(8):731–42.

26. Morral-Ruíz G, Solans C, García ML, García-Celma MJ. Formation of pegylated poly-urethane and lysine-coated polyurea nanoparticles obtained from O/W nano-emulsions. *Langmuir* 2012;**28**(15):6256–64.

27. Morral-Ruíz G, Melgar-Lesmes P, García ML, Solans C, García-Celma MJ. Design of biocompatible surface-modified polyurethane and polyurea nanoparticles. *Polymer* 2012;**53**(26):6072–80.

28. Jabbari E, Khakpour M. Morphology of and release behaviour from porous polyurethane microspheres. *Biomaterials* 2000;**21**:2073–89.

29. Antonietti M, Landfester K. Polyreactions in miniemulsions. *Prog Polym Sci* 2002;**27**: 689–757.

30. Dessy A, Piras AM, Alderighi M, Sandreschi S, Chiellini F. Doxorubicin loaded polyure-thanes nanoparticles. *Nano Biomed Eng* 2012;**4**(2):83–8.

31. Mattu C, Pabari RM, Boffito M, Sartori S, Ciardelli G, Ramtoola Z. Comparative evalua-tion of novel biodegradable nanoparticles for the drug targeting to breast cancer cells. *Eur J Pharm Biopharm* 2013;**85**:463–72.

32. Naeem M, Kim W, Cao J, Jung Y, Yoo J-W. Enzyme/pH dual sensitive polymeric nanopar-ticles for targeted drug delivery to the inflamed colon. *Colloids Surf B Biointerfaces* 2014;**123**:271–8.

33. Solans C, Izquierdo P, Nolla J, Azemar N, Garcia-Celma MJ. Nano-emulsions. *Curr Opin Colloid Interf Sci* 2005;**10**:102–10.

34. Mora-Huertas CE, Fessi H, Elaissari A. Polymer-based nanocapsules for drug delivery. *Int J Pharm* 2010;**385**:113–42.

35. Vrignauld S, Benoit JP, Saulnier P. Strategies for the nanoencapsulation of hydrophilic molecules in polymer-based nanoparticles. *Biomaterials* 2011;**32**:8593–604.

36. Pridgen EM, Alexis F, Farokhzad OC. Polymeric nanoparticle drug delivery technologies for oral delivery applications. *Expert Opin Drug Deliv* 2015;**12**:1–15.

37. Barrère M, Landfester K. High molecular weight polyurethane and polymer hybrid particles in aqueous miniemulsion. *Macromolecules* 2003;**36**:5119–25.

38. Gaudin F, Sintes-Zydowicz N. Core–shell biocompatible polyurethane nanocapsules obtained by interfacial step polymerisation in miniemulsion. *Colloids Surf A Physicochem Eng Aspects* 2008;**33**:133–42.

39. Walstra P. Emulsion stability. In: Becher P, editor. *Encyclopedia of emulsion technology*. New York: Marcel Dekker; 1996. p. 1–62.

40. Li C-Y, Chiu W-Y, Don T-MJ. Preparation of polyurethane dispersions by miniemulsion polymerization. *Polym Sci, Part A Polym Chem* 2005;**43**:4870–81.

41. Crespy D, Stark M, Hoffmann-Richter C, Landfester K. Polymeric nanoreactors for hydrophilic reagents synthesized by interfacial polycondensation on miniemulsion droplets. *Macromolecules* 2007;**40**:3122–35.

42. Yu L, Zhou L, Ding M, Li J, Tan H, Fu Q, et al. Synthesis and characterization of novel biodegradable folate conjugated polyurethanes. *J Colloid Interface Sci* 2011;**358**:376–83.

43. Wang A, Gao H, Sun Y, Sun YL, Yang YW, Wu G, et al. Temperature- and pH-responsive nanoparticles of biocompatible polyurethanes for doxorubicin delivery. *Int J Pharm* 2013;**441**:30–9.

44. Paiphansiri U, Dausend J, Musyanovych A, Mailänder V, Landfester K. Fluorescent polyurethane nanocapsules prepared via inverse miniemulsion: surface functionalization for use as biocarriers. *Macromol Biosci* 2009;**9**:575–84.

45. Galindo-Alvarez J, Boyd D, Marchal P, Tribet C, Perrin P, Marie-Bégue E, et al. Miniemulsion polymerization templates: a systematic comparison between low energy emulsification (near-PIT) and ultra-sound emulsification methods. *Colloids Surf A Physicochem Eng Asp* 2011;**374**:134–41.

46. Izquierdo P, Esquena J, Tadros TF, Dederen JC, Feng J, Garcia-Celma MJ, et al. Phase behaviour and nano-emulsion formation by the phase inversion temperature method. *Langmuir* 2004;**20**:6594–8.

47. Solè I, Pey CM, Maestro A, González C, Porras M, Solans C, et al. Nano-emulsions prepared by the phase inversion composition method: preparation variables and scale up. *J Colloid Interface Sci* 2010;**344**:417–23.

48. Bouchemal K, Briançon S, Perrier E, Fessi H, Bonnet I, Zydowick N. Synthesis and characterization of polyurethane and poly (ether urethane) nanocapsules using a new technique of interfacial polycondensation combined to spontaneous emulsification. *Int J Pharm* 2004;**269**:89–100.

49. Morral-Ruíz G, Melgar-Lesmes P, Solans C, García-Celma MJ. Multifunctional polyurethane–urea nanoparticles to target and arrest inflamed vascular environment: a potential tool for cancer therapy and diagnosis. *J Control Release* 2013;**171**(2):163–71.

50. Anton N, Saulnier P, Gaillard C, Porcher E, Vrignaud S, Benoit JP. Aqueous-core lipid nanocapsules for encapsulating fragile hydrophilic and/or lipophilic molecules. *Langmuir* 2009;**25**:11413–9.

51. Peer D, Karp JM, Hong S, Farokhzad OC, Margalit R, Langer R. Nanocarriers as an emerging platform for cancer therapy. *Nat Nanotechnol* 2007;**2**:751–60.

52. Beija M, Salvayre R, Lauth-de Viguerie N, Marty JD. Colloidal systems for drug delivery: from design to therapy. *Trends Biotechnol* 2012;**30**:485–96.

53. Parveen S, Misra R, Sahoo SK. Nanoparticles: a boon to drug delivery, therapeutics, diagnostics and imaging. *Nanomed Nanotechnol* 2012;**8**:147–66.

54. Ishihara T, Mizushima T. Techniques for efficient entrapment of pharmaceuticals in biodegradable solid micro/nanoparticles. *Expert Opin Drug Deliv* 2010;**7**:565–75.

55. Melgar-Lesmes P, Morral-Ruíz G, Solans C, García-Celma MJ. Quantifying the bioadhesive properties of surface-modified polyurethane-urea nanoparticles in the vascular network. *Colloids Surf B Biointerfaces* 2014;**118**:280–8.

56. Beck-Broichsitter M, Nicolas J, Couvreur P. Design attributes of long-circulating polymeric drug delivery vehicles. *Eur J Pharm Biopharm* 2015. http://dx.doi.org/10.1016/j.ejpb.2015.03.033.

57. Zhang Y, Zhuo R-X. Synthesis and in vitro drug release behavior of amphiphilic triblock copolymer nanoparticles based on poly (ethylene glycol) and polycaprolactone. *Biomaterials* 2005;**26**:6736–42.

58. Zhou L, Liang D, He X, Li J, Tan H, Li J, et al. The degradation and biocompatibility of pH-sensitive biodegradable polyurethanes for intracellular multifunctional antitumor drug delivery. *Biomaterials* 2012;**33**:2734–45.

59. Ou ChW, Su Ch H, Jeng US, Hsu ShH. Characterization of biodegradable polyurethane nanoparticles and thermally induced self-assembly in water dispersion. *Appl Mater Interfaces* 2014;**6**:5685–94.

60. Ding M, Zeng X, He X, Li J, Tan H, Fu Q. Cell internalizable and intracellularly degradable cationic polyurethane micelles as a potential platform for efficient imaging and drug delivery. *Biomacromolecules* 2014;**15**:2896–906.

61. Piras AM, Sandreschi S, Malliappan SP, Dash M, Bartoli C, Dinucci D, et al. Surface decorated poly(ester-ether-urethane)s nanoparticles: a versatile approach towards clinical translation. *Int J Pharm* 2014;**475**:523–35.

62. Cass P, Knower W, Hinton T, Shi Sh, Grusche F, Tizard M, et al. Synthesis and evaluation of degradable polyurea block copolymersas siRNA delivery agents. *Acta Biomater* 2013;**9**:8299–307.

63. Rosenbauer EM, Landfester K, Musyanovych A. Surface-active monomer as a stabilizer for polyurea nanocapsules synthesized via interfacial polyaddition in inverse miniemulsion. *Langmuir* 2009;**25**(20):12084–91.

64. Rosenbauer EM, Wagner M, Musyanovych A, Landfester K. Controlled release from polyurethane nanocapsules via pH-, UV-light- or temperature-induced stimuli. *Macromolecules* 2010;**43**:5083–93.

65. Baier G, Musyanovich A, Dass M, Theisinger S, Landfester K. Cross-linked starch capsules containing dsDNA prepared in inverse miniemulsion as "nanoreactors" for polymerase chain reaction. *Biomacromolecules* 2010;**11**:960–8.

66. Kang B, Okwieka P, Schöttler S, Seifert O, Kontermann RE, Pfizenmaier K, et al. Tailoring the stealth properties of biocompatible polysaccharide nanocontainers. *Biomaterials* 2015;**49**:125–34.

67. Sharma S, Paiphansiri U, Hombach V, Mailänder V, Zimmermann O, Landfester K, et al. Characterization of MRI contrast agent-loaded polymeric nanocapsules as versatile vehicle for targeted imaging. *Contrast Media Mol Imaging* 2010;**5**:59–69.

68. Jagielski N, Sharma S, Hombach V, Mailänder V, Rasche V, Landfester K. Nanocapsules synthesized by miniemulsion technique for application as new contrast agent materials. *Macromol Chem Phys* 2007;**208**:2229–41.

69. Morral-Ruíz G. Estudi de la formació de nanopartícules polimèriques obtingudes a partir de nano-emulsions de fase externa aquosa i associació d'antiinflamatoris no esteroïdals [Doctoral thesis]. University of Barcelona; 2011.

70. Fichter M, Baier G, Dedters M, Pretsch L, Pietrzak-Nguyen A, Landfester K, et al. Nano-capsules generated out of a polymeric dexamethasone shell suppress the inflammatory response of liver macrophages. *Nanomedicine* 2013;**9**:1223–34.

71. Song N, Ding M, Pan Zh, Li J, Zhou L, Tan H, et al. Construction of targeting-clickable and tumor-cleavable polyurethane nanomicelles for multifunctional intracellular drug delivery. *Biomacromolecules* 2013;**14**:4407–19.

72. Sun X, Gao H, Wu G, Wang Y, Fan Y, Ma J. Biodegradable and temperature-responsive polyurethanes for adriamycin delivery. *Int J Pharm* 2011;**412**:52–8.

73. Lammers T, Kiessling F, Hennink WE, Storm G. Drug targeting to tumors: principles, pitfalls and (pre-) clinical progress. *J Control Release* 2012;**161**:175–87.

74. Coussens ML, Web Z. Inflammation and cancer. *Nature* 2002;**420**:860–7.

75. Pitroda SP, Zhou T, Sweis RF, Filippo M, Labay E, Beckett MA, et al. Tumor endo-thelial inflammation predicts clinical outcome in diverse human cancers. *PLoS One* 2012;**7**(10):e46104.

76. Riehl A, Németh J, Angel P, Hess J. The receptor RAGE: bridging inflammation and can-cer. *Cell Commun Signal* 2009;**7**:12.

77. Weis SM, Cheresh DA. Tumor angiogenesis: molecular pathways and therapeutic targets. *Nat Med* 2011;**17**:1359–70.

78. Rabinovich GA, Gabrilovich D, Sotomayor EM. Immunosuppressive strategies that are mediated by tumor cells. *Annu Rev Immunol* 2007;**25**:267–96.

79. Grivennikov SI, Greten FR, Karin M. Immunity, inflammation, and cancer. *Cell* 2010;**140**:883–99.

80. Kobayashi H, Lin PC. Angiogenesis links chronic inflammation with cancer. *Methods Mol Biol* 2009;**511**:185–91.

81. Bae Y, Jang WD, Nishiyama N, Fukushima S, Kataoka K. Multifunctional polymeric micelles with folate-mediated cancer cell targeting and pH-triggered drug releasing proper-ties for active intracellular drug delivery. *Mol Biosyst* 2005;**1**:242–50.

82. Ding M, Song N, He X, Li J, Zhou L, Tan H, et al. Toward the next-generation nano-medicines: design of multifunctional multiblock polyurethanes for effective cancer treat-ment. *ACS Nano* 2013;**7**:1918–28.

83. Adamson ED. EGF receptor activities in mammalian development. *Mol Reprod Dev* 1990;**27**:16–22.

84. Blanpain C. Tracing the cellular origin of cancer. *Nat Cell Biol* 2013;**15**:126–34.

85. Vadlapudi AD, Vadlapatla RK, Pal D, Mitra AK. Biotin uptake by T47D breast cancer cells: functional and molecular evidence of sodium-dependent multivitamin transporter (SMVT). *Int J Pharm* 2013;**441**:535–43.

86. Soininen SK, Lehtolainen-Dalkilic P, Karppinen T, Puustinen T, Dragneva G, Kaikkonen MU, et al. Targeted delivery via avidin fusion protein: intracellular fate of biotinylated doxorubicin derivative and cellular uptake kinetics and biodistribution of biotinylated lipo-somes. *Eur J Pharm Sci* 2012;**47**:848–56.

87. Ross JF, Chaudhuri PK, Ratnam M. Differential regulation of folate receptor isoforms in normal and malignant tissues in vivo and in established cell lines. Physiologic and clinical implications. *Cancer* 1994;**73**:2432–43.

88. Zempleni J. Uptake, localization, and noncarboxylase roles of biotin. *Annu Rev Nutr* 2005;**25**:175–96.

89. Rubin GD, Leipsic J, Joseph Schoepf U, Fleischmann D, Napel S. CT angiography after 20 years: a transformation in cardiovascular disease characterization continues to advance. *Radiology* 2014;**271**:633–52.

90. Boss A, Weiger M, Wiesinger F. Future image acquisition trends for PET/MRI. *Semin Nucl Med* 2015;**45**:201–11.

91. Landfester K, Willert M, Antonietti M. Preparation of polymer particles in nonaqueous direct and inverse miniemulsions. *Macromolecules* 2000;**33**:2370–6.

92. Zhao W, Zhang G, Jiang L, Lu T, Huang X, Shen J. Novel polyurethane ionomer nanoparticles displayed a good biosensor effection. *Colloids Surf B Biointerfaces* 2011;**88**:78–84.

93. Park S, Lee Y, Kim YS, Lee HM, Kim JH, Cheong IW, et al. Magnetic nanoparticle-embedded PCM nanocapsules based on paraffin core and polyurea shell. *Colloids Surf A Physicochem Eng Aspects* 2014;**450**:46–51.

94. Wang S, Kim G, Lee YE, Hah HJ, Ethirajan M, Pandey RK, et al. Multifunctional biodegradable polyacrylamide nanocarriers for cancer theranostics—a "see and treat" strategy. *ACS Nano* 2012;**6**:6843–51.

95. Le Droumaguet B, Nicolas J, Brambilla D, Mura S, Maksimenko A, De Kimpe L, et al. Versatile and efficient targeting using a single nanoparticulate platform: application to cancer and Alzheimer's disease. *ACS Nano* 2012;**6**:5866–79.

96. Forner A, Llovet JM, Bruix J. Hepatocellular carcinoma. *Lancet* 2012;**379**:1245–55.

97. Lu CH, Willner B, Willner I. DNA nanotechnology: from sensing and DNA machines to drug-delivery systems. *ACS Nano* 2013;**7**:8320–32.

98. Singh M, Ariatti M. Targeted gene delivery into HepG2 cells using complexes containing DNA, cationized asialoorosomucoid and activated cationic liposomes. *J Control Release* 2003;**92**:383–94.

99. Kelkar SS, Reineke TM. Theranostics: combining imaging and therapy. *Bioconjugate Chem* 2011;**22**:1879–903.

Polyurethanes for controlled drug delivery

8

A. Basu[1,2], S. Farah[1], K.R. Kunduru[1], S. Doppalapudi[3], W. Khan[3], A.J. Domb[1,]*

[1]Faculty of Medicine, School of Pharmacy, The Hebrew University of Jerusalem, Jerusalem, Israel; [2]Birla Institute of Technology, Ranchi, Jharkhand, India; [3]National Institute of Pharmaceutical Education & Research, Hyderabad, Telangana, India
*Corresponding author: avid@ekmd.huji.ac.il

8.1 Introduction

Polyurethanes (PUs) are found everywhere: the chair we sit on, the comfortable bed we sleep on, every nook and corner of our house, the car we drive, the refrigerator and air conditioner that comfort us, and many other day-to-day objects. PUs can also be used for drug delivery and may be fabricated as bioinert, biodegradable, stimulus-responsive, shape-memory, conjugated, self-assembled, rigid, flexible, and porous systems.

PUs were discovered as far back as 1947 by Otto Bayer [1]. A great variety of PUs can be synthesized based on the different substituents. The reactions are also straightforward, and they can be synthesized in large scales for industrial purposes. Chemically PUs are carbamates having an —NHCOO— backbone. PUs are synthesized by reaction between diisocyanates (DIs) and polyols in the presence of a suitable catalyst (Figure 8.1(a)). The physical property of PUs may be controlled by choosing the type of polyols or isocyanates.

PUs are unique type of polymers that may be thermoplastic, elastomeric, and thermosetting. PUs may be compact or foamed. They are extremely adaptable and sustainable problem solvers for the challenges that our society is facing, imposing special demands on materials [2]. Engels et al. comprehensively reviewed different applications of PUs. According to them, the secret to the success of PU chemistry is the reactivity of the isocyanate groups toward all types of nucleophiles plus the great variability of the polyols and polyisocyanates (Figure 8.1(b)), resulting in a combinatorial diversity of possible polymers. PUs have demonstrated their versatility and adaptability to new challenges for over 75 years, and they have many more to offer.

PUs have also been used in biomedical devices as they are biocompatible with significant control over mechanical strength and flexibility [3–7]. PUs can be rendered either biodegradable or bioinert by controlling the building blocks and their final chemical structure. Biodegradable PUs are mainly employed in drug delivery systems. PUs can be designed to be responsive [8–11] and also to carry positive charges [12]. These properties may be tuned according to the need by controlling the architecture of PUs. They are normally synthesized by step polymerization of DIs and
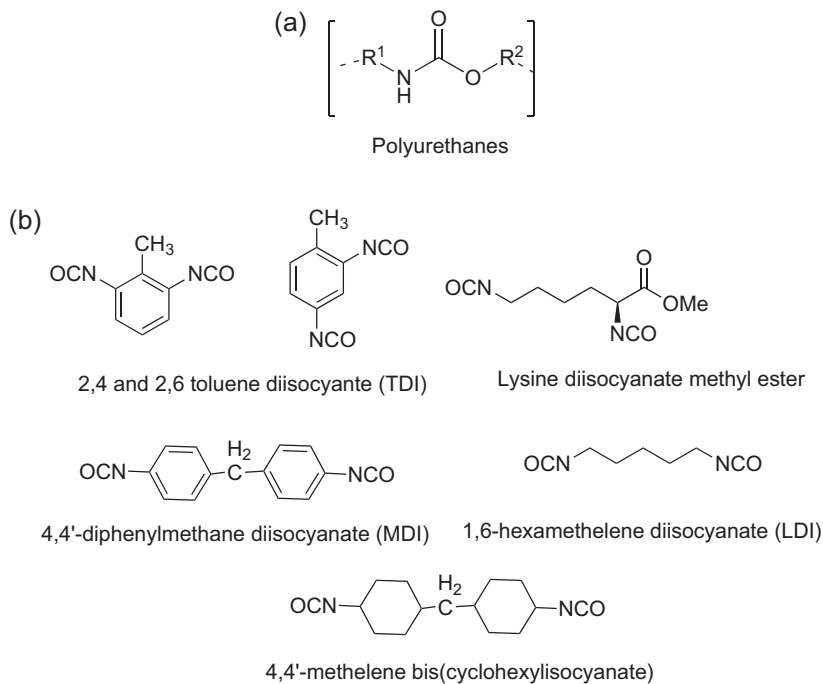
Figure 8.1 (a) Typical structure of polyurethane. (b) Commonly used isocyanates as building blocks for the synthesis of polyurethane.

diols/polyols [13]. Difunctional isocyanates and diols result in linear polymers whereas cross-linked PUs are synthesized using tri- (or higher) functional monomers. DIs can also react with bisamines to give polyureas.

Practically, for better control, PUs are synthesized using three different components: DIs (aliphatic or aromatic), polyols (mostly diols or triols), and chain extenders (diols or diamines).

Aromatic DIs are more reactive than aliphatic ones. PUs made from aliphatic DIs are more resistant to ultraviolet irradiation, while aromatic DI-based PUs can undergo photodegradation [14]. The structures of the DIs, polyols, and chain extenders play key roles in the final polymer properties [15].

Polyols are mostly dihydroxyl-terminated macroglycols of polyethers, polyesters, and polycarbonates (Figure 8.2). Relatively low molecular weight polyols such as pentaerythritol or N-BOC-serinol are also used for the synthesis of PUs. The polyol block plays an important role in the physicochemical and mechanical properties of the PUs.

Polyester-based PUs are more sensitive to hydrolytic cleavage than polyether-based PUs. However, the introduction of bulky alkyl side groups into a hydroxyl-terminated polyester (e.g., poly(2,4-diethyl-1,5-pentamethyleneadipate) yields PUs that are more hydrolytically stable with regard to hydrolysis [16]. Polyethylene oxide-based PUs exhibit water sensitivity due to their hydrophilicity and the water-absorbing capacity
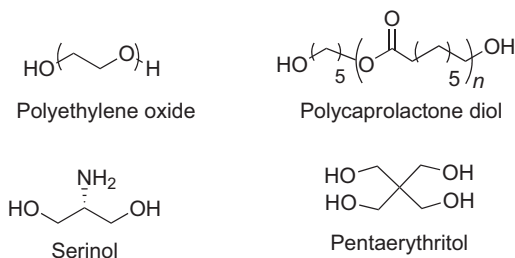
Figure 8.2 Commonly used polyols for the synthesis of polyurethanes.
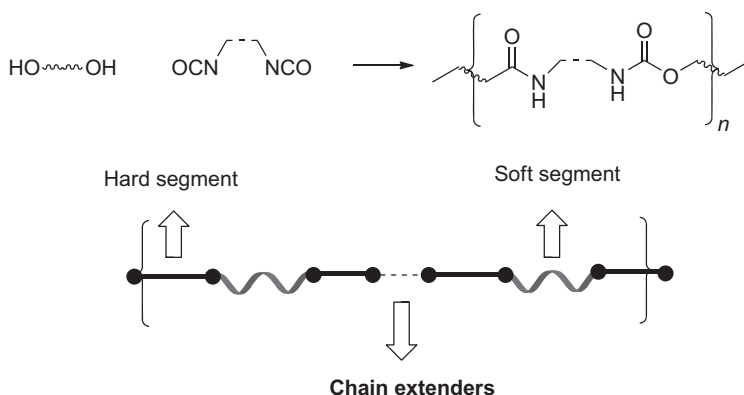
Figure 8.3 General structural architecture of polyurethanes.

of the ethylene oxide units. PUs based on the more hydrophobic polypropylene oxide, on the other hand, are less water sensitive [13].

Serinol, the serine derivative with two —OH groups, is suitable for reacting with DI [17]. The mechanical properties of PUs synthesized from only isocyanates and polyols are poor. Chain extenders render PU's microphase separation between the two thermodynamically incompatible segments *i.e.,* hard segments (composed of —NH—COO— and the chain extender) and the soft segments (the polyols part). The hard domains impart mechanical strength, and soft domains flexibility (Figure 8.3) [18–20]. Chain extenders are normally low molecular weight bisamines or diols such as 1,4-butanediol (BDO), 1,3-propanediol (PDO), ethylene diamine, and putrescine.

8.2   Chemistry of polyurethanes

PUs are synthesized by the reaction between isocyanates (commonly DIs) and diols (or polyols), which results in the formation of carbamates. Depending on the diols or isocyanates used the mechanical/physical properties of the resulting polymers can be controlled. The most commonly used isocyanates are the aromatic DIs, toluene diisocyanate (TDI) and 4,4'-diphenylmethane diisocyanate (MDI).

Chain extenders ($f = 2$) and cross-linkers ($f = 3$ or greater) are low molecular weight hydroxyl- and amine-terminated compounds that play an important role in the polymer morphology of PU fibers, elastomers, adhesives, and certain integral skin and microcellular foams. The elastomeric properties of these materials are due to phase separation of the hard and soft copolymer segments. The urethane hard segment domains serve as cross-linkers (through hydrogen bonding) between the amorphous polyether (or polyester) soft segment domains. This phase separation occurs because the mainly nonpolar, low melting soft segments are incompatible with the polar, high melting hard segments. The soft segments, which are formed from high molecular weight polyols, are mobile and are normally present in coiled form. The hard segments formed from the isocyanate and chain extenders are stiff and immobile. Because the hard segments are covalently coupled to the soft segments, they inhibit plastic flow of the polymer chains, thus imparting elastomeric properties (Figure 8.3).

8.3   Use in drug delivery

PUs can be differentiated into bioinert PUs and biodegradable PUs, among which the former is used in medical devices and applied as artificial organs. The latter is used in tissue engineering and as drug delivery carriers. The unique chemistry and flexible processing of these segmented polymers to produce the urethane materials with widely differing properties such as thermoplastic elastomers and flexible or rigid foams make them versatile materials. For instance, they are applicable as either permanent medical implants or biodegradable tissue scaffolds [21–23]. The applications of PUs in delivery of therapeutic moieties are listed in Table 8.1.

The chemistry of PUs can be tuned to render the polymer pH- and thermoresponsive. PU-based stimuli-responsive drug delivery systems are widely explored. For example, incorporation of pH-sensitive groups such as carboxyl and amino provides pH sensitivity to the polymer. PUs based on primarily DIs will provide temperature sensitivity. DI-dominated-based PUs have been reported to encapsulate doxorubicin (DOX) successfully, and uptaken by Huh-7 cells [29,34,39]. The surfaces of PU systems can be modified by attachment of targeting ligands such as monoclonal antibodies, which render recognition, binding, and internalization capacity for the system. For example, polyclonal IgG-loaded PU hydrogel coatings reduced the bacterial adhesion and can be applicable for biomaterial-centered infection [13,40]. PUs sensitive to pH can also be synthesized by using caprolactone derivatives in soft segment, and L-lysine DI in hard segment, which are proved to be safe and effective biodegradable carriers for intracellular antitumor drug delivery [41] (Figure 8.4).

Methods used for preparing of poly(ester urethane)–urea scaffolds are electrospinning, solvent casting/salt leaching, phase inversion, laser excimer, and thermally induced phase separation. Electrospun poly(ester urethane)–ureas are elastomeric and the synthesis method allows control of fiber diameter, porosity, and degradation rate. All these properties aid in the development of soft tissue scaffolds. However, electrospinning produces fibers with unacceptably small pore sizes. Thermally induced phase

Table 8.1 **Applications of polyurethanes in delivery of drugs and macromolecules**

S. No.	Delivery system	Drug incorporated	Remarks	References
1	Polyurethane film-based stent covering	Gemcitabine	Applied for local drug delivery in case of unresistable pancreatic or biliary malignant tumors Initial burst release was enhanced with increased loading whereas total amount released was higher with lower loading	[24]
2	Azo-containing polyurethane-coated drug pellets	Model drugs (hydrophilic in nature)	Double-coated drug pellets which are undercoated with (carboxymethyl)(ethyl)-cellulose and overcoated with the azo polymer Colon-specific delivery Effective prevention of the drug leakage was observed with PU	[25]
3	Polyurethane intravaginal rings	Dapivirine and tenofovir	Suitable delivery system for the sustained delivery of drugs with contrasting hydrophilicity Tenofovir showed sustained release whereas dapivirine exhibited linear release over time	[26]
4	Polyurethane matrices	Cefamandole nafate	Carboxylated polyurethane/antibiotic-loaded albumin nanoparticles composite Exhibited controlled drug release Prolonged antimicrobial activity from 4 to 9 days	[27]
5	Nanostructured polyure-thane matrix	Cefamandole nafate	Bovine serum albumin or polyallylamine nanoparticles loaded with antibiotic incorporated in a polyurethane matrix Prolonged antimicrobial activity up to 9 days.	[28]
6	Temperature- and pH-responsive PU-based nanoparticles	Doxorubicin	Hexamethylene diisocyanate (HDI) and 4,4′-diphenylmeth-ane diisocyanate (MDI)-based PUs showed temperature- and pH-responsive properties Efficient encapsulation into polyurethane nanoparticles and uptaken by Huh-7 cells HDI-based PUs were nontoxic	[29]

Table 8.1 Continued

S. No.	Delivery system	Drug incorporated	Remarks	References
7	Polyurethane foams	DB-67 and doxorubicin	Covalent incorporation of anticancer compounds DB-67 and doxorubicin into polyurethane foam Rates were dependent on temperature and chemical structure of the drug Differential release of covalently bound drugs	[30]
8	Polyurethane gels	Model dye (crystal violet)	Gels were prepared from polyether PUs Drug release from segmented polymer was based on partition of the drug in the heterogeneous matrix and the interaction between the drug and the hard segments whereas it depends on diffusion of drug through delivery system in case of PU gel.	[31]
9	Polyurethane scaffolds	Platelet-derived growth factor (PDGF)	Biphasic release of PDGF was observed PU/PDGF scaffolds accelerated wound healing when implanted in rat skin excisional wounds Formation of new granulation tissue as early as day 3 Opened the opportunities for the development of novel injectable therapeutics	[32]
10	Polyurethane nanoparticles	Adriamycin®	Temperature-sensitive polymers were synthesized based on poly(ethylene glycol) (PEG) and L-lysine ester diisocyanate (LDI) Showed about 25% encapsulation efficiency Release of drug was dependent on transition temperature of LDI-PEG600	[33]
11	Polyurethane films	Chlorhexidine diacetate	Release of the drug was dependent on the drug loading and the structure of the system Exhibited persistent antibacterial activity against *Staphylococcus species* Applicable in dental and clinical setup	[34]

12	Thermoplastic polyurethane matrix	Metoprolol tartrate	High drug loading up to 65% is possible On drug release, total porosity of the matrix increased gradually Oral administration of PUs did not show any adverse effects on GIT	[35]
13	Polyurethane scaffolds	Recombinant human bone morphogenetic protein (rhBMP)	Initial burst release followed by sustained release was observed Enhanced new bone formation was shown by BMP-loaded PU scaffolds	[36]
14	Polyurethane tablets	Diprophylline	High drug loading was possible with PU matrices Influence of drug release modifiers such as dicarboxylic acids on drug release was observed Succinic and maleic acid had the highest drug release-modifying capacity	[37]
15	Polyurethane pressure-sensitive adhesives	Thiamazole diclofenac sodium ibuprofen	Excellent stabilization of the model drugs without any skin irritation for PEG-based PU pressure-sensitive adhesives Drug release was dependent on the loading and solubility of the drug	[8]
16	Polyurethane bearing model drug	Ibuprofen	Ibuprofen was introduced into the polymeric backbone via ester linkages Drug release was based on degradation of ester linkages Tunable drug release can be achieved with this new macromolecular design	[38]
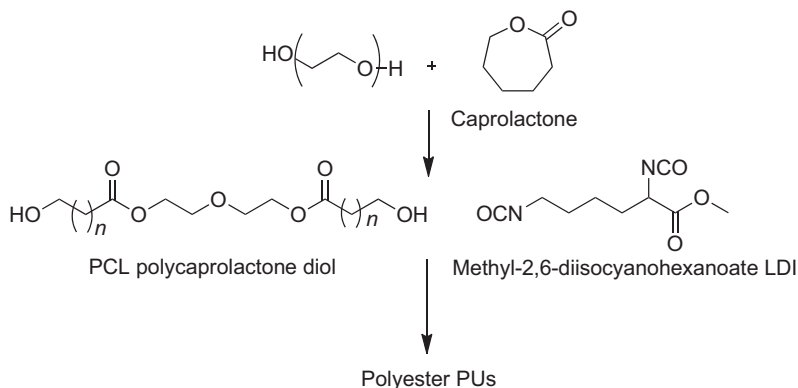
Figure 8.4 Polyester urethane commonly employed for biomedical applications and drug delivery. The polymer is synthesized from biocompatible fragment PEGs, polycaprolactone diols, and lysine diisocyanate.

separation seems to be the more popular method of scaffold construction, as pore size and structure can be controlled [42–44].

PU–esters are mainly employed as biodegradable drug delivery vehicles. These systems were generally fabricated as nanohybrids, implants, or other suitable dosage forms. The release may be modulated by controlling the chemistry of the polymer. The ratio of ester:urethane is intrinsic for controlling the rate of hydrolysis. Ester bonds of these polymers undergo a faster, but controlled hydrolysis. Later the urethane bonds degrade, resulting in smaller fragments, eliminated rapidly from the system (Figure 8.5).

Drug release from nonbiodegradable PU matrices will be via a diffusion mechanism, where the rate of release will be dependent on the thickness and permeability of the polymer matrix and solubility of the drug in the polymer matrix. The release profile from biodegradable PU matrices will be dependent on the composition, swelling, degradation rate, and initial drug loading [13,26,45]. The proportions of DI and diol play a crucial role in the synthesis of biodegradable PUs. Aliphatic DI yields less toxic diamine (degradation product of PUs) than aromatic DI [46,47].

8.3.1 Biocompatibility and biodegradability of polyurethanes

Coexistence of foreign materials inside the human tissue depends on the biocompatibility of the material. An ideal biocompatible material should not elicit inflammatory reactions [48]. Depending on the structure of PUs, they can be either biocompatible or biodegradable.

It has been observed that PUs synthesized from aliphatic isocyanates are reported as more biocompatible than aromatic isocyanate-based PUs [49–54]. Therefore, PUs based on aliphatic isocyanates are preferred over aromatics for *in vivo* applications [55]. Aromatic-based PUs degrade to yield aromatic amines, which may be carcinogenic, and therefore avoided for biological applications. The strategy for avoiding toxicity arising from such degradation product is to use naturally occurring substrates

Drug release modulated through ester:carbamate ratio
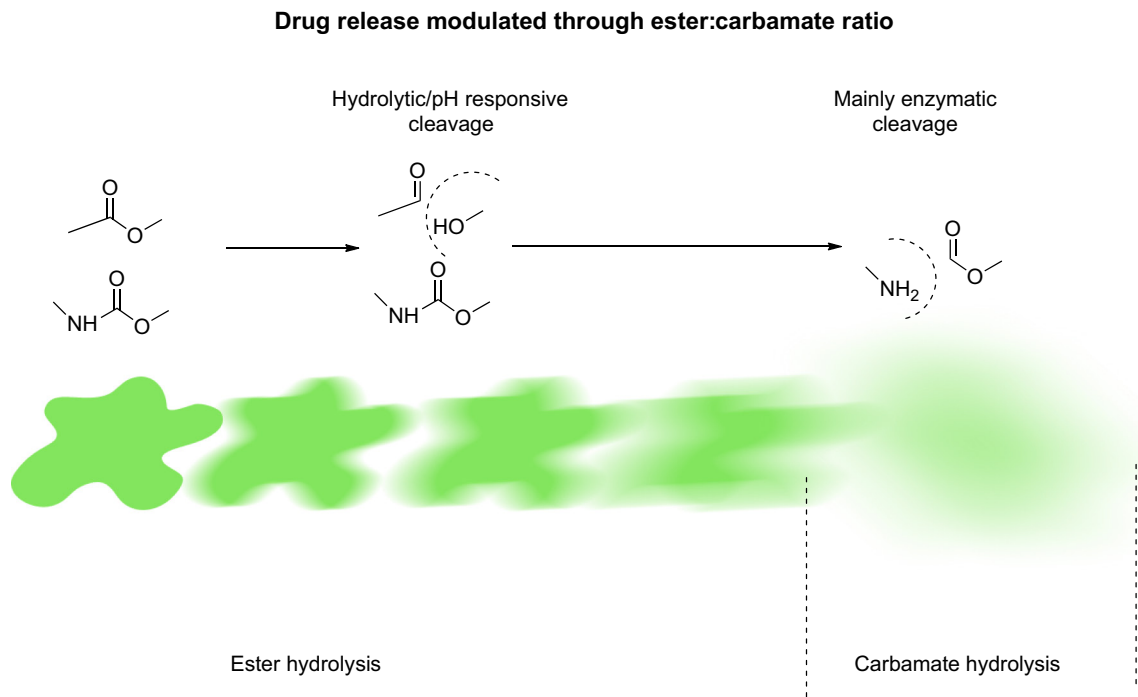
Figure 8.5 Drug release mechanism from polyurethane carriers. PU–ester carriers undergo relatively faster burst ester hydrolysis followed by slow carbamate cleavage. The release may be controlled by tuning the ester:carbamate ratio.

as backbone. Lysine DI is an example, it will degrade to yield a naturally occur-
ring amino acid lysine [56]. Another commonly used biocompatible PU is based on
poly(ε-caprolactone) diol and the degraded product is biocompatible and biodegrad-
able [57]. These materials have already been applied in tissue and bone engineering
[58]. Biocompatible cross-linked porous polyester urethanes based on ethyl lysine DI,
pentaerythritol, and lactic acid/glycolic acid were reported. Despite releasing higher
amount of amines, no adverse inflammatory responses were observed [59].

PUs undergo biodegradation mainly by hydrolytic cleavage of the carbamate
bonds. The hard segments in PUs may also undergo oxidative degradation. The kinet-
ics of the hydrolysis significantly depend on the PU structure [60]. Ester-based PUs
undergo enzymatic (e.g., cholesterol esterase, carboxyl esterase, lipase) hydrolysis
and the cleavage results in the formation of α-hydroxy acids [61].

Urethane bonds are also amide mimetics, so they can be hydrolyzed by enzymes
such as human neutrophil elastase and pancreatic elastase [62]. PUs containing ester
linkages degrade faster compared to those with ether linkages. The degradation of
poly(ester urethane urea) by porcine pancreatic elastase was 10 times faster than that
of poly(ether urethane urea).

The hard segment of PUs, urea linkages may be degraded by proteolytic enzymes
such as papain or urease [49,63]. Another way of degradation of PUs is through oxi-
dative degradation by hydrogen peroxide generated by enzyme myeloperoxidase to
generate respective amines and carbon dioxide [13]. PUs can be decomposed *in vivo*
through hydrogen peroxide (oxidative degradation), generated by the macrophages.

Zhou et al. described the synthesis of pH-sensitive biodegradable PUs. They
used a novel pH-sensitive macrodiol containing acid-cleavable hydrazone linkers,
poly(ε-caprolactone)–hydrazone–poly(ethylene glycol)–hydrazone–poly(ε-caprolactone)
diol (PCL–Hyd–PEG–Hyd–PCL). The macrodiol was used with L-lysine ethyl ester
diisocyanate (LDI) and L-lysine-derived tripeptide as chain extender [47]. These PUs
could self-assemble into micelles in aqueous solutions. Later, the same research group
synthesized pH-sensitive polymers using 1,4-butanediol as chain extenders and sug-
gested its use as antitumor drug carriers [41].

Highly pH-sensitive polymer was synthesized by introducing pyridine rings into
the backbone of PU. The mechanism of pH responsiveness was found to be the for-
mation of hydrogen bonding interactions between the N atom of the pyridine ring
and the H—N of urethane in neutral or alkaline environments, disrupted under acidic
conditions due to the protonation of the pyridine ring [64] (Figure 8.6).

8.3.2 *Polyurethane-based shape-memory polymers*

Materials that show a shape-memory effect can be deformed into a temporary shape
and afterwards they can recover their original shape on exposure to an external stim-
ulus [65,66]. Shape-memory polymers (SMPs) are stimuli-responsive "smart" poly-
mers that have dual shape, which responds to application of an external stimulus. SMP
is conventionally processed to receive its permanent shape. Afterward, the polymer
is deformed and the intended temporary shape is fixed [67,68]. This process is called
programming. These polymers basically consist of two phases, fixed points or frozen
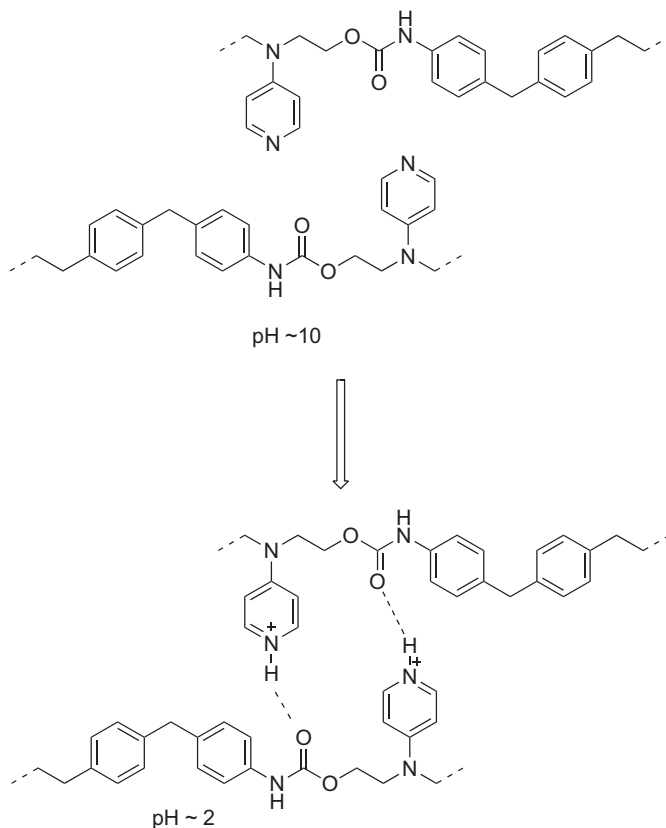
Figure 8.6 Highly sensitive pH-responsive PU, synthesized by incorporating pyridine to the backbone of the polymer.

phase and reversible flexible phase. In PUs (Figure 8.7) the soft segment domains form the reversible phase, with their crystalline melting temperature being the shape recovery temperature and hard segments of PUs become the fixed points or frozen phases [69].

Segmented PUs are basically block copolymers of soft segments and hard segments. Soft segments are polyols of typical molecular weight 1000–2000, whereas hard segments are built from DIs and extenders. Depending on the types and compositions of soft and hard segments and preparation procedures the structure–property relationships of PUs are extremely diverse and easily controlled. Hence, the shape-recovery temperature can be set at any temperature between –30 °C and 70 °C, allowing a broad range of applications. They can be molded using conventional processing techniques including extrusion, injection, and blow molding which allow versatility of shaping.

PUs have wide applications in tissue and bone engineering. SMPs can be inserted to the anatomical site by making a minimal incision. The devices may be provided

Random orientation   Orientation after external stimulus
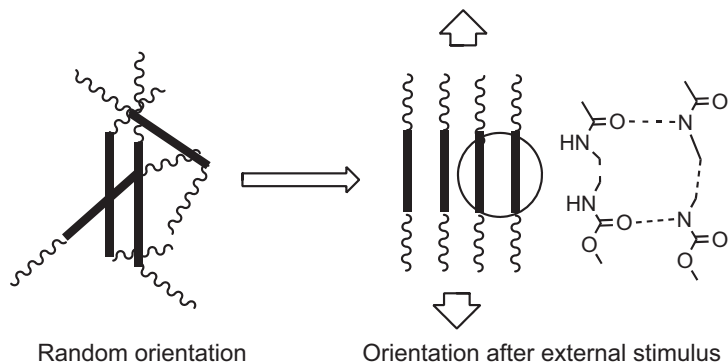
Figure 8.7 The structural architecture of PUs makes them ideal candidates for stimulus-responsive and shape-memory polymers.

appropriate stimulus so they regain their original shape. Such PU-based biodegradable foams aimed at bone and tissue-engineering applications and were reported [70–72].

Shape-recovery procedures in SMP are extremely important. Most SMPs used receive an external stimulus in the form of heat or light. Another practically feasible way is solvent-induced shape recovery. Kalita et al. reported PUs based on PDI and TDI with solvent-induced shape-responsive properties [73]. Recently, Thakur et al. reported PU SMP nanocomposites based on castor oil and their shape is recoverable by sunlight [74].

Recently Langer and Lendlein reported a PU-based shape-memory suture [75]. The smart surgical suture is tied loosely, and after exposure to physiological stress and pH it tightens the knot automatically. These sutures are biodegradable.

8.3.3   Polyurethane-based nanoparticle system

PUs are often used as nanomaterial carriers, but PU-based nanoparticles have also been reported. Most of the nanoparticles have been synthesized by miniemulsion techniques [76]. Miniemulsions are stable aqueous dispersions of oil droplets, which are prepared by high shear of a system containing oil, water, surfactant, and a hydrophobe.

PU nanoparticles have also been synthesized using several techniques such as suspension–polycondensation [77], interfacial polycondensation and concomitant emulsification [78], suspension polyaddition [79], and dispersion in organic solvent using supercritical carbon dioxide [80,81]. The preparation of PU nanoparticles via miniemulsion techniques was also reported.

Mishra et al. reported PU-based nanoparticle systems. They synthesized PUs by using aliphatic chain extenders of varying chain lengths. They also prepared nanohybrids of PUs by dispersing them in 2D nanoclay. They observed enhancement in toughness with increase in aliphatic chain length. Finally, they demonstrated controlled biodegradable PUs and their nanohybrids [82].

Wang et al. reported a series of temperature- and pH-responsive PUs based on hexamethylene diisocyanate (HDI) and 4,4′-diphenylmethane diisocyanate (MDI).
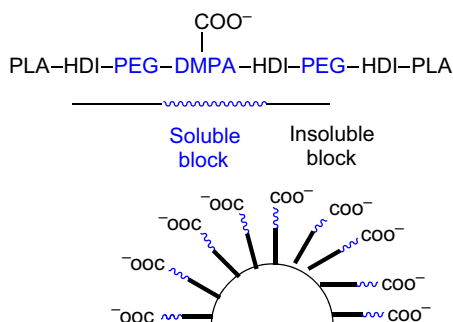
Figure 8.8 An example of self-assembled micelles formed by PU-based nanoparticle systems.

They used these PU-based nanoparticles for DOX encapsulation. The results indicated efficient encapsulation into PU nanoparticles and uptake by Huh-7 cells. The loaded DOX molecules could also be released on pH and temperature changes, responsively [29].

Polyurethane-based nano/microparticulate systems: The biocompatibility of PUs made them ideal for the development of nanosystems for local delivery of drugs. Amphiphilic poly(lactic acid, PLA)–polyurethane containing carboxylic acid groups was prepared by polycondensation reaction and used as a biodegradable carrier. The synthesized PU was used for preparing polymeric micelles loaded with gliclazide (Figure 8.8). The release rate of drug was dependent on pH and carboxylic groups of the micellar system [83]. PUs can be employed as stimuli-responsive drug delivery systems that can be used for targeted and controlled drug delivery. DI and diol-based PUs possess temperature and pH sensitivity, which release the drug according to temperature and pH changes. As the pathological site of tumors is acidic in nature and responds to pH changes, such stimuli-responsive carriers can be applied as potential antitumor agents.

DOX was successfully encapsulated in the stimuli-responsive PU-fabricated nanoparticles and the drug was released according to the changes in stimulus [29]. Double-coated pellets, undercoated with carboxymethyl cellulose and overcoated with PU containing azo groups in the main chain, were loaded with hydrophilic drugs and the release profile was analyzed. Release profile was dependent on the molecular weight, the composition of the overcoated PU, and the hydrophilicity of the loaded drugs [25]. PU–urea-based nanoparticles were developed and streptavidin a targeting ligand has been incorporated into nanoparticle matrix, which showed specificity in binding with biotinylated antibodies. This multifunctional PU-based nanoparticles can be explored in the area of cancer diagnostics and targeted drug delivery to the tumor vasculature [84].

Superparamagnetic iron oxide nanoparticles (SPIO NPs) are widely used in magnetic resonance imaging and magnetic hyperthermia. PUs having self-assembly behavior of biodegradable polyurethane nanoparticles (PU NPs) were reported. These nanoparticles can encapsulate SPIO NPs (SPIO–PU NPs) or hydrophobic drugs (drug–PU NPs). Hydrophobic drugs were entrapped in PU NPs effectively and showed a sustained release profile. On heating, the release of drug was accelerated [85].

8.3.3.1   Polyurethane-based nanofibers, nanovehicles, and devices carrying nanomaterials

Nanofibers have applications in medicine, including artificial organ components, tissue engineering, implant material, drug delivery, and wound dressings [86]. PUs consisting of soft and hard segments are easier to manipulate and they give better control over shape. Most of the PU-based nanofibers are made through an electrospinning method [87–90]. Composite materials synthesized from PU-based nanofibers have been used for tissue and skin engineering [91] and in vascular grafts [92]. Nifedipine loaded thermo-responsive nanofibers were reported by Lin et al. The nanofibers reported therein exhibited reversible hydrophilicity and hydrophobicity by a change of the temperature. They also exhibited significant mechanical properties and control over the drug release [93].

PU/nanoclay nanocomposite nanofibrous webs prepared by electrospinning were reported. Chlorhexidine acetate was loaded in the prepared clay and was then incorporated into PU nanofibers. The nanofibers were evaluated for moisture vapor transmission, porosity, contact angle, and antibacterial activity, important for topical drug delivery application [94]. Verreck et al. described the preparation of nanofibers by electrospinning of itraconazole and ketanserin in a non-biodegradable matrix. It improved the transdermal delivery of these poorly soluble drugs. It was shown that these two drugs exist in the amorphous state in the PU nanofibers [95].

Redox-responsive nanovehicles containing disulfide bonds have been reported. Biodegradable multiblock PUs bearing varied amounts of disulfide linkages were synthesized. The reducible PUs exhibited appropriate phase behavior and self-assembly properties. It was also found that the redox-sensitive PU micelles could rapidly enter tumor cells and can transport the encapsulated paclitaxel effectively (Figure 8.9). The inhibition effects were controlled by adjusting the disulfide content in the polymeric backbone [96].

A similar dual redox and pH-responsive delivery system was reported (Figure 8.10). Disulfide cross-linked PU micelles that respond to pH change and intracellular reducing agents were prepared. The micelles were prepared by cross-linking of PEG–PU multiblock copolymers containing tertiary amino and cyclic disulfide moieties. Around the tumor environment, the nanovehicle swelled and decomposed under a weakly acidic environment. Further, the intracellular reducing agent glutathione (GSH) cleaved the disulfide cross-linking bonds. The DOX-loaded nanoparticles suppressed the initial burst release at pH 7.4. It was found that the intracellular DOX release was accelerated by an acidic environment or enhanced intracellular GSH concentration [97].

8.3.4   Polyurethane-based membrane systems

PU controlled release films were developed for chlorhexidine diacetate (CDA), an antiseptic used widely for skin and mucosal infections, dentistry, etc. In conventional formulations of this drug, the uncontrolled release of the loaded moiety lead to teeth discoloration, bitter taste, and patient discomfort. These concerns were overcome by
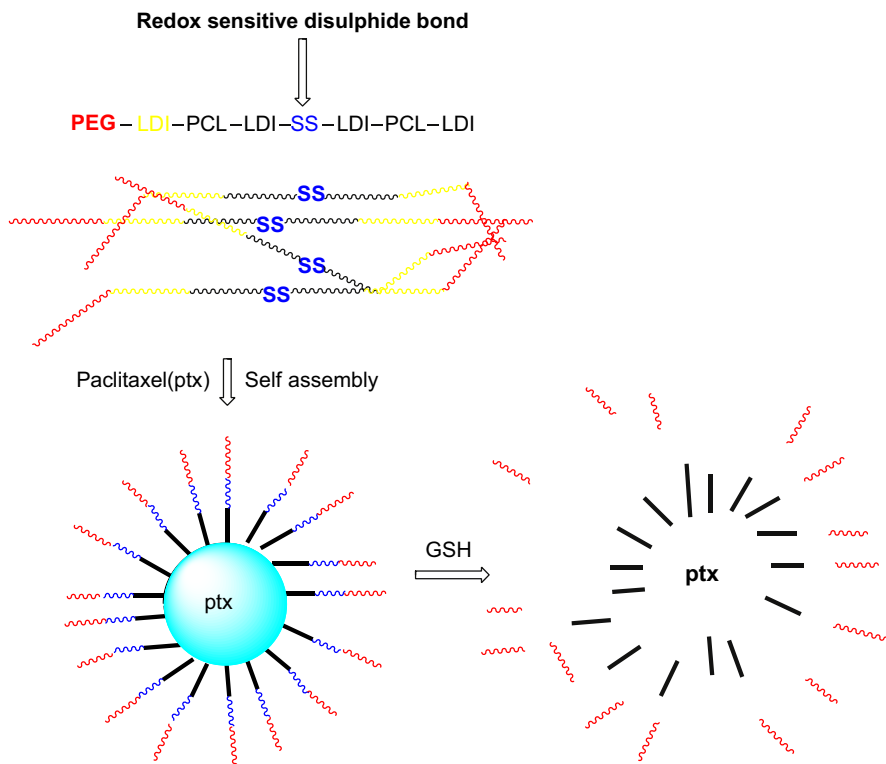
Figure 8.9 Example of redox-responsive PU, used to deliver paclitaxel to tumor cells.
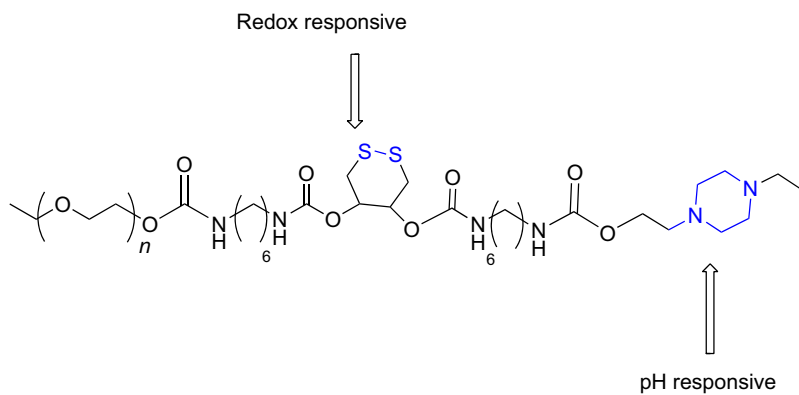
Figure 8.10 Redox and pH stimulus-based nanovehicles based on PU were reported. Doxorubicin was used as the anticancer drug triggered to be released near the tumor environment by acidic pH and GSH.

controlled release PU films of CDA. Release of the drug was dependent on the drug loading and structure of the system. The CDA-loaded PU films exhibited persistent antibacterial activity up to 35 days [34]. Bioactive PU foams were explored by incorporating bioactive compounds into the polymer chain by chemical or physical bonding. For instance, functional compounds such as quinoxaline and acetanilide derivatives were bonded to the polymer chain and PU foams were developed by using suitable foaming agents and foam stabilizers. Testing against Gram-positive and Gram-negative bacteria proved the antimicrobial efficacy of PU foams and they were shown to be non-toxic and adhesive in nature [98].

8.3.5   Polyurethane-based matrix systems

PUs can also be employed in the development of matrix systems for higher drug loading and for controlled release of the drugs. Thermoplastic polyurethanes (TPUs), which are inert, non ionic, water-insoluble polymers, were investigated as matrix excipients for developing oral sustained release formulations for metoprolol tartarate, diprophylline, and theophylline. Higher drug loading up to 65% and controlled drug release were possible in the case of metoprolol whereas diprophylline required drug release modifiers such as Tween 80 or PEG 4000. Also *Simulator of the Human Intestinal Microbial Ecosystem* (SHIME) study showed that the oral administration of TPUs did not affect the GI system [35].

PU gels were prepared using a prepolymer hydroxyl-terminated poly-(oxytetramethylene) and hydroxyl-terminated poly(oxyethylene)-b-poly(oxytetramethylene)-b-poly(oxyethylene) (HT-ETE), among which the latter one possesses the hydrophilic segment in the chain. This hydrophilic nature renders more swelling property and larger release rate of crystal violet (model dye employed to test the release) from the gel prepared from HT-ETE. The release profile from gel was dependent on the diffusion and movement of drug through the delivery system [31]. Incorporation of albumin nanoparticles into the carboxylated PU matrix system was explored for improvement in drug absorption due to greater surface/volume ratio and enhancement in drug release rates. Cefamandole nafate was loaded into the above nanostructured composite system from which long-term release of drug was observed [27]. Iodine, a strong disinfectant, was loaded into PU matrix, which was investigated as coating material for hospital equipment during the manufacture process. This strategy was found to be a good alternative for decontamination of medical equipment that is exposed to patient- contaminated fluids. It is also reported similar PU-based iodine releasing system that may attenuate human immunodeficiency virus. This system may be used for decontamination and disposal of medical devices [99]. A general depiction for grafting the halides on PU matrix is shown in (Figure 8.11).

Our group recently reported iodinated polyurethane (IPU) sponges. The IPU sponges were coated with ethylene vinyl acetate (EVA), to release iodine in a controlled rate for water decontamination combined with active carbon cartridge, which adsorbs the iodine residues after the microbial inactivation. Controlled and stable iodine release was observed with the EVA-coated IPU sponges and was effective in deactivating the bacteria and virus present in the contaminated water (Figure 8.12). Thus, these iodinated
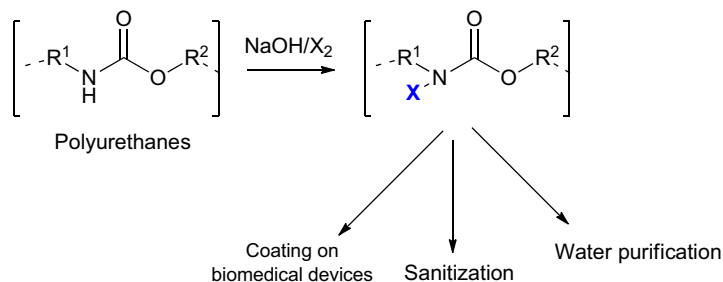
Figure 8.11 Application of halogen (-X) grafted PUs that are hydrolyzed to their nascent form and may be used for antimicrobial purposes.
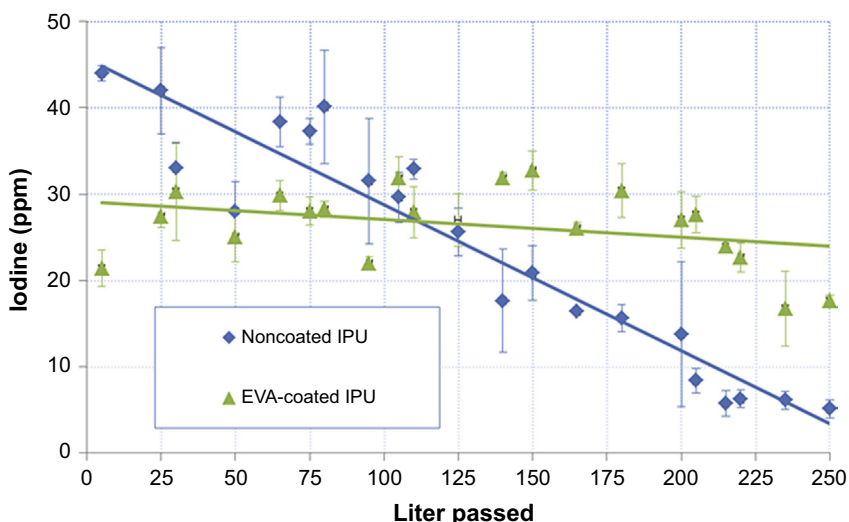
Figure 8.12 Iodine release profiles of noncoated IPU and EVA-coated IPU. The iodine release achieved by water flow through the IPU sponges, using 25 L tap water per day with five doses, each dose with 30 min break and flow rate of 6–8 min/1 L up to 250 L. Adapted from Ref. [100].

PU systems could be used in water purification to provide safe drinking water. These sponges may find applications as disinfectants in medicine [100].

Our group also developed rapamycin (RM)-eluting stents using electrospun PU vascular grafts that could effectively suppress local smooth muscle cell proliferation. We observed that the release kinetics was characteristic of a Fickian diffusion for at least 77 days *in vitro*. RM–PU fibers generated via powder blending showed the highest encapsulation efficiency.

Recently, our group, in collaboration with Peter I. Lelkes' group, developed RM-eluting mats/grafts using electrospun PU vascular grafts that could effectively suppress local smooth muscle cell proliferation. In this study, we employed blend electrospinning to incorporate RM into electrospun PU fibers at various dosages into PU fibrous mats/grafts using three distinct blending methods (Figure 8.13). The
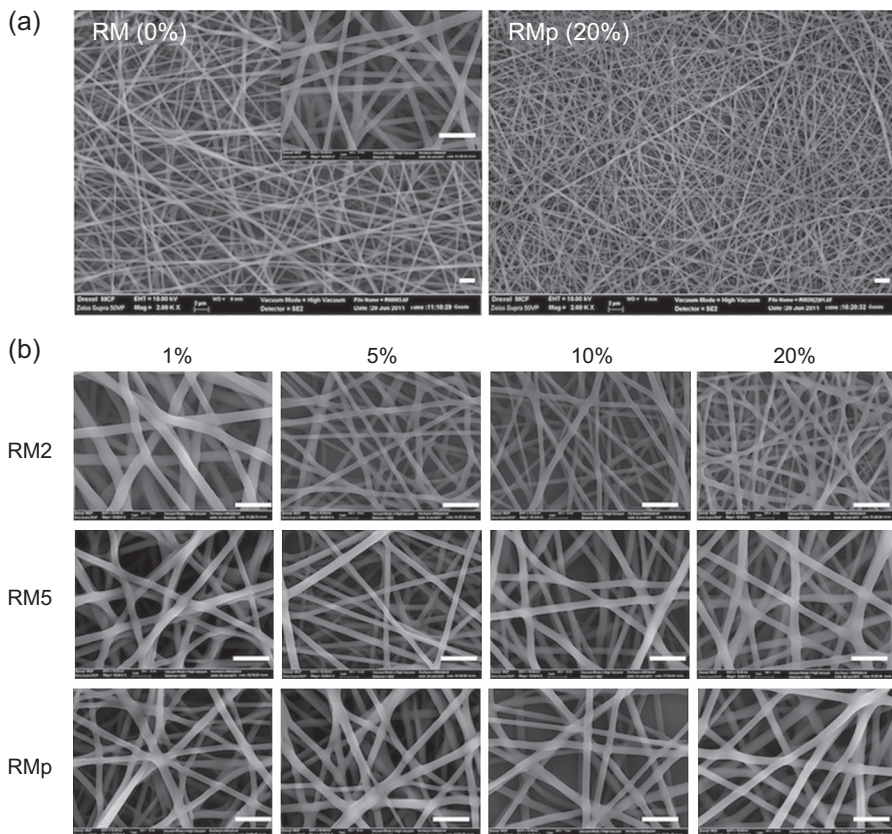
Figure 8.13 SEM images of electrospun rapamycin–PU fibers at a relative RM/SPU ratio (w/w) of 0, 1, 5, 10, or 20% via three different blending methods. Scale bar: 2 μm. Adapted from Ref. [101].

RM-eluting PU fibrous mats and grafts were then assessed in terms of their fiber morphology, fiber size, mechanical properties, and drug release profiles, as well as their ability to inhibit SMC proliferation *in vitro*.

The RM release study from electrospun RM–SPU mats/grafts prepared via the powder method and with different RM contents was initially carried out over a period of 49 days. All samples exhibited a small initial burst release (<10% of the theoretical total drug loading) within the first 3 days followed by an extended slow release till day 49. It was found that the amount of RM released at each time point was generally dependent on the amount of RM loading, but the release kinetics was not affected by the amount of RM (Figure 8.14). Grafts containing 20% RM released the maximum drug over the entire period examined. Moreover, the correlations between release profiles and PU fiber diameters were studied also at 20% RM with different fiber diameters via the three blending methods, and examined RM release profiles *in vitro* for up to 77 days (Figure 8.15). All samples exhibited a burst release for the first week followed by a sustained
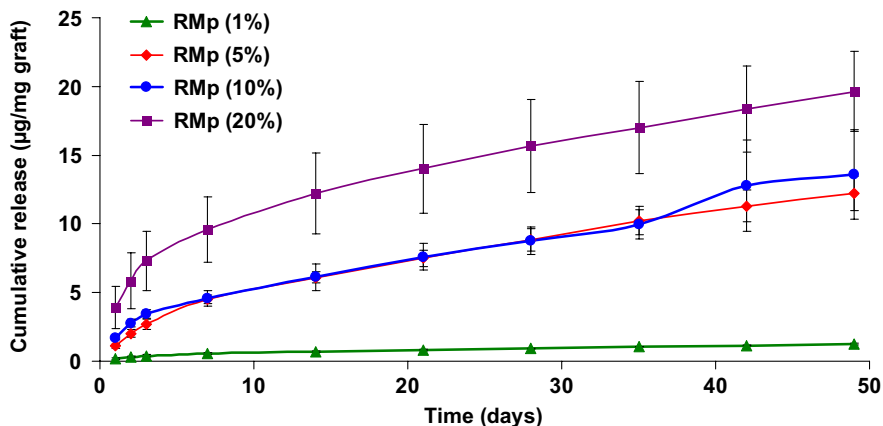
Figure 8.14 *In vitro* drug release profiles of electrospun RMp (1%), RMp (5%), RMp (10%), and RMp (20%) fibrous grafts. Each data point represents mean ± SD of three samples. Adapted from Ref. [101].
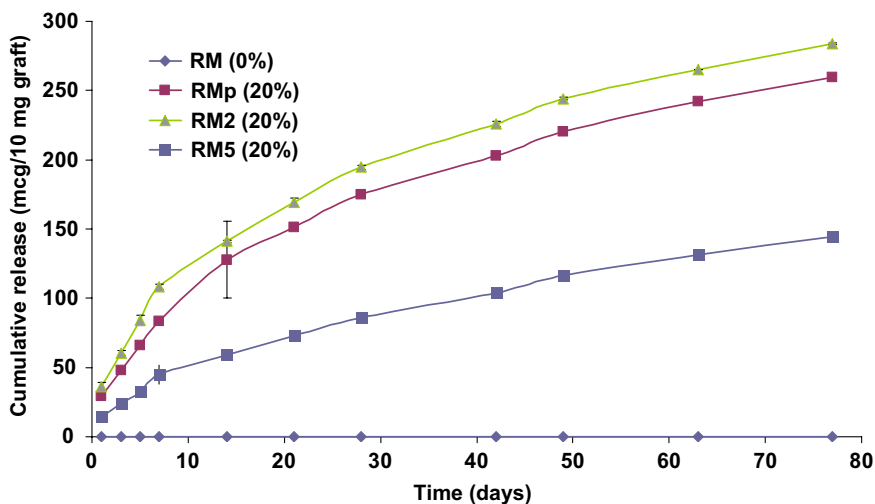
Figure 8.15 *In vitro* drug release profiles of grafts prepared using three distinct blending methods with fibers RM2 (20%), RM5 (20%), or RMp (20%) over 77 days period. Each data point represents mean ± SD of three samples. Adapted from Ref. [101].

release till day 77. Similar release kinetics was found for all fibers (Figure 8.16). However, the amount of RM release at each time point was different, suggesting that our data are consistent with the reported fact that the smaller the fiber, the faster the drug release. This suggested that the release of RM from all samples till day 77 was controlled by Fickian diffusion, a kinetics that has been widely reported for drug-laden electrospun fibers. These grafts maintained bioactive even after 77 days *in vitro* release.
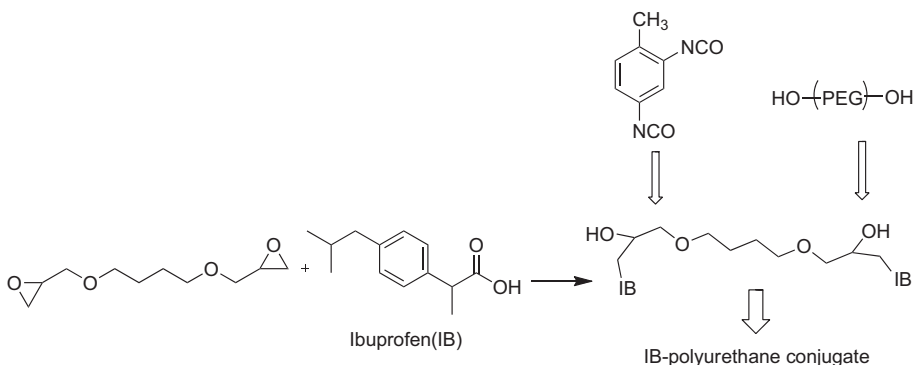
Figure 8.16 An example of covalently bound drug molecule (carboxylic acid functional group). Ibuprofen conjugated to PU synthesized from TDI and PEG, without using chain extenders.

Therefore, electrospun RM-containing PU fibers can serve as effective drug carriers for the local suppression of cell proliferation and could be used as RM-eluting scaffolds for vascular grafts [101,102].

In another study we traced the release of paclitaxel (ptx) from three different types of PU, degradable (two types) and nondegradable graft-preloaded ptx by soaking grafts in ptx solution. The release was traced in PBS for 2 months. The release data showed continuous release profiles from the three types and controlled release during the study period, whereas the three PU grafts showed almost identical release profiles for the first 3 weeks followed by faster release from degraded grafts, resulting in a larger amount of ptx released (data not shown). These results reflect the potential use of PU implants as carriers for controlled drug release for localized therapy and prolonged release systems.

8.3.6 Polyurethanes in macromolecular delivery

Segmented PUs are widely applicable as biomedical devices due to their excellent bio- and hemo-compatibility. A heparin release system based on PU and silk fibroin composite was reported. The release rate of heparin from this system depends on the thickness of the PU–fibroin film, PU–fibroin proportions, and initial loading of the heparin. *In vitro* coagulation tests showed that the antithrombogenicity of heparin can be maintained for long time and the film has good blood compatibility [103]. Osteoinductive molecules, such as recombinant human bone morphogenetic protein (rhBMP-2), were incorporated into biodegradable PU scaffolds and the effect of the scaffold was investigated by implanting it in the rat femoral plug model. For this purpose, rhBMP-2 was encapsulated into PLGA microspheres of different sizes and then embedded into PU scaffold. The results showed that microsphere encapsulation reduced the burst release of protein unlike the lyophilized powder loaded into scaffold. The new bone formation was higher in the PU/rhBMP-2 group than PU/PLGA–rhBMP-2 treatment groups. The above study concluded that a burst release during

initial stages as well as sustained release for up to 3 weeks is crucial for development of new bone tissue [36].

Insulin-like growth factor-1 and hepatocyte growth factor were incorporated into scaffolds prepared from poly(ester urethane)urea. The bioactivity of the growth factors was retained during the early period of drug delivery, which was confirmed by cellular assays. The complex release profile was replaced by single phase release when the degradation of scaffold was accelerated by lipase enzyme. PUs are flexible for processing, scaffold formation, and drug loading, making them appropriate for soft tissue applications [104]. Yet another growth factor, platelet-derived growth factor (PDGF) was incorporated into PU scaffolds, which exhibited a biphasic release profile, that is, initial burst followed by a period of sustained release for up to 21 days. PU/PDGF scaffolds resulted in the development of new granular tissue on the third day when they were implanted in rat skin wounds. The capacity to incorporate bioactive moieties into segmented PUs opens up new opportunities for the development of novel injectable therapeutics [32].

8.3.7 *Drug molecules covalently bound to polyurethanes*

Drugs covalently linked to PU have also been reported. Isocyanates are active functional groups through which hydroxyl- or amino-based drugs can be easily conjugated. Ascorbic acid, glycerol, and LDI-based PUs were synthesized, where the hydroxyl groups of ascorbic acid react with the isocyanates to form the urethane linkages. The release of ascorbic acid is therefore dependent on the cleavage of urethane linkages [105]. Silatecan (DB67) an anticancer topoisomerase inhibitor was also reported to be conjugated with LDI glycerol-based PUs. DB67 being a hydrophobic drug was not significantly released even after 65 days [106]. Similarly, DOX was also reported to be conjugated through urethane and urea linkages [30]. Carboxylic acid-based drugs may also be conjugated (Figure 8.16); an example is ibuprofen conjugated through epoxy(butanedioldiglycidyl ether). The resulting hydroxyl groups were then further reacted with isocyanates to form PU [38].

Azo-cleavage by colonic bacteria inspired the synthesis of amino salicylic acid-based PU system (Figure 8.17). The amino salicylate was diazotized and then self-coupled; the free phenolic groups were then utilized to synthesize PUs with hexane diisocyanate [107].

Folic acid-conjugated PUs were reported, using LDI, PEG diol, and PEG amine as chain extender [108].

A sugar active targeting system for the platinum (IV) prodrug of clinically relevant oxaliplatin (OxaPt(II)) was reported. Biocompatible PUs containing free pair-wised pendant amino groups (PU) were synthesized and then lactobionic acid (LA) was grafted to the PU as a targeting moiety. Thereafter, the prodrug, OxaPt(IV) was introduced into the PU–LA conjugates resulting in the formation of PU platinum (IV) conjugates (PU–LA/Pt) with targeting LA groups [109].

Conjugates of camptothecin were prepared. The polymeric matrixes were obtained by the ring-opening polymerization of ε-caprolactone, glycolide, *rac*-lactide, or trimethylene carbonate. The synthesized polymers were coupled with various
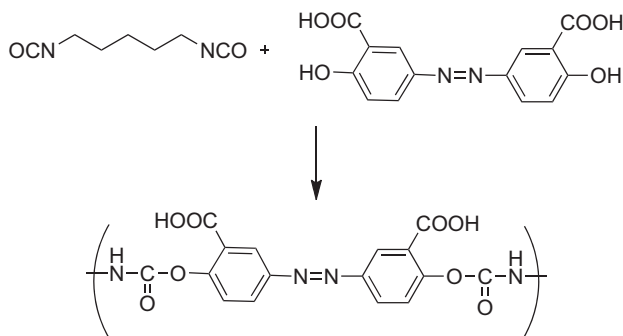
Figure 8.17 Diazotized para amino salicylic acid conjugated to HDI meant for releasing the drug in the colon, by specific cleavage of the diazo linkage by gut bacteria.
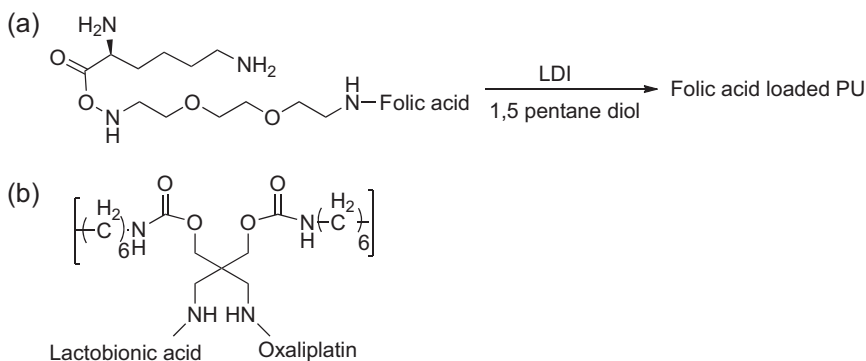
Figure 8.18 (a) An example of folic acid conjugated with PU, using LDI, and 1,5-pentane diol based PU–urea system. (b) PU-conjugated anticancer drug (oxaplatin) delivery to specific lactose receptor, overexpressed in cancer cells. Lactobionic acid (targeting moiety).

molecules like folic acid and anti-cancer agents like camptothecin to yield the final PUs based drug delivery systems [110] (Figure 8.18).

Poly(amino urethane) (PAU)-conjugated bovine serum albumin (BSA) hydrogels were reported. The synthesis included preparation of PAUs, acrylation of the synthesized PAUs, and conjugation of PAUs to BSA. The conjugate exhibited pH- and temperature-induced sol–gel phase transitions, facilitating the DOX-loaded conjugate solution to form gels under physiological conditions (Figure 8.19) [111].

8.4   Conclusion and future directions

In this chapter, the recent progress of PUs in drug delivery is reviewed. PUs are a successful class of polymers that have appropriate biocompatibility and biodegradability when it comes to biomedical applications. The chemistry of PUs gives us the opportunity to widen the possible combinations to fine-tune the final polymer with
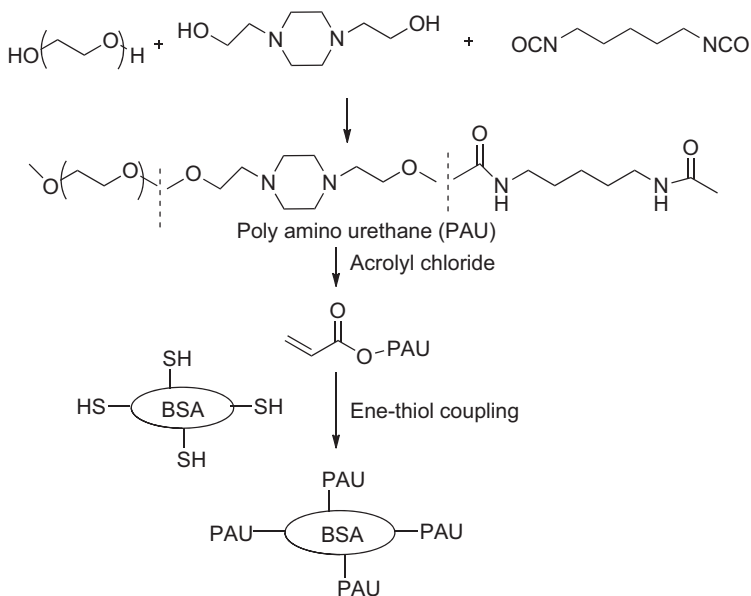
Figure 8.19 An example of BSA–PU-based hydrogel. BSA is conjugated to PU through ene–thiol coupling.

precise control. It was observed that mechanical, thermal, viscoelastic, optical, electrical, degradation, compatibility, shape, etc. might be precisely controlled by tuning the chemistry of PUs. The vast combinatorial options of combining the DIs, polyols, and chain extenders make PUs the material of choice for today. PUs are polymers of choice for biomedical applications when it comes to shape memory, stimulus responsiveness, and grafts. Their versatility and adaptability have been demonstrated for over 75 years now, and these are far from exhausted.

Abbreviations

BDO 1,4-Butandiol
BSA Bovine serum albumin
CDA Chlorhexidine diacetate
DIs Diisocyanates
DOX Doxorubicin
EVA Ethylene vinyl acetate
GSH Glutathione
HDI Hexamethylene diisocyanate
HT-ETE Hydroxyl-terminated poly(oxyethylene)-b-poly(oxytetramethylene)-b-poly-(oxyethylene)
HT-PT Hydroxyl-terminated poly(oxytetramethylene)
IPU Iodinated polyurethane
LDI L-Lysine ester diisocyanate

MDI 4,4'-Diphenylmethane diisocyanate
NPs Nanoparticles
OxaPt(II) Oxaliplatin
PAU Poly(amino urethane)
PCL Polycaprolactone diol
PCL–Hyd–PEG–Hyd–PCL Poly(ε-caprolactone)–hydrazone–poly(ethylene glycol)–hydrazone–poly(ε-caprolactone) diol
PDGF Platelet-derived growth factor
PDI Pentamethylene diisocyanate
PDO 1,3-Propanediol
PEG Poly(ethylene glycol)
ptx Paclitaxel
PUs Polyurethanes
rhBMP-2 Recombinant human bone morphogenetic protein
SHIME Simulator of the Human Intestinal Microbial Ecosystem
SMP Shape-memory polymers
SPIO NPs Superparamagnetic iron oxide nanoparticles
TDI Toluene diisocyanate
TPUs Thermoplastic polyurethanes

References

[1] O. Bayer, Das di-isocyanate-polyadditionsverfahren (polyurethane), Angew. Chem. Int. Ed. 59 (1947) 257–272.

[2] H.W. Engels, H.G. Pirkl, R. Albers, R.W. Albach, J. Krause, A. Hoffmann, H. Casselmann, J. Dormish, Polyurethanes: versatile materials and sustainable problem solvers for today's challenges, Angew. Chem. Int. Ed. 52 (2013) 9422–9441.

[3] S. Guelcher, A. Srinivasan, A. Hafeman, K. Gallagher, J. Doctor, S. Khetan, S. McBride, J. Hollinger, Synthesis, *in vitro* degradation, and mechanical properties of two-component poly(ester urethane) urea scaffolds: effects of water and polyol composition, Tissue Eng. 13 (2007) 2321–2333.

[4] S.A. Guelcher, A. Srinivasan, J.E. Dumas, J.E. Didier, S. McBride, J.O. Hollinger, Synthesis, mechanical properties, biocompatibility, and biodegradation of polyurethane networks from lysine polyisocyanates, Biomaterials 29 (2008) 1762–1775.

[5] R.J. Zdrahala, I.J. Zdrahala, Biomedical applications of polyurethanes: a review of past promises, present realities, and a vibrant future, J. Biomater. Appl. 14 (1999) 67–90.

[6] X. He, Z. Zhai, Y. Wang, G. Wu, Z. Zheng, Q. Wang, Y. Liu, New method for coupling collagen on biodegradable polyurethane for biomedical application, J. Appl. Polym. Sci. 126 (2012) E354–E361.

[7] M. Ding, J. Li, H. Tan, Q. Fu, Self-assembly of biodegradable polyurethanes for controlled delivery applications, Soft Matter 8 (2012) 5414–5428.

[8] X. Chen, W. Liu, Y. Zhao, L. Jiang, H. Xu, X. Yang, Preparation and characterization of PEG-modified polyurethane pressure-sensitive adhesives for transdermal drug delivery, Drug Dev. Ind. Pharm. 35 (2009) 704–711.

[9] X.J. Loh, K.B.C. Sng, J. Li, Synthesis and water-swelling of thermo-responsive poly(ester urethane)s containing poly(ε-caprolactone), poly(ethylene glycol) and poly(propylene glycol), Biomaterials 29 (2008) 3185–3194.

[10] C. Park, S. Cho, B. Kim, Synthesis and properties of thermosensitive polyurethane-b-poly(N-isopropyl acrylamide), React. Funct. Polym. 66 (2006) 585–591.

[11] T. Travinskaya, Y.V. Savelyev, Aqueous polyurethane–alginate compositions: peculiarities of behavior and performance, Eur. Polym. J. 42 (2006) 388–394.

[12] W. Wang, Y. Guo, J.U. Otaigbe, Synthesis and characterization of novel biodegradable and biocompatible poly(ester-urethane) thin films prepared by homogeneous solution polymerization, Polymer 49 (2008) 4393–4398.

[13] J.Y. Cherng, T.Y. Hou, M.F. Shih, H. Talsma, W.E. Hennink, Polyurethane-based drug delivery systems, Int. J. Pharm. 450 (2013) 145–162.

[14] L. Irusta, M. Fernandez-Berridi, Aromatic poly(ester–urethanes): effect of the polyol molecular weight on the photochemical behaviour, Polymer 41 (2000) 3297–3302.

[15] E. Ibarboure, A. Baron, E. Papon, J. Rodriguez-Hernandez, Self-assembly of graft polyurethanes having both crystallizable poly(ε-caprolactone) blocks and soft poly(n-butyl acrylate) segments, Thin Solid Films 517 (2009) 3281–3286.

[16] B.S. Kim, B.K. Kim, Enhancement of hydrolytic stability and adhesion of waterborne polyurethanes, J. Appl. Polym. Sci. 97 (2005) 1961–1969.

[17] D. Park, W. Wu, Y. Wang, A functionalizable reverse thermal gel based on a polyurethane/PEG block copolymer, Biomaterials 32 (2011) 777–786.

[18] P. Ping, W. Wang, X. Chen, X. Jing, The influence of hard-segments on two-phase structure and shape memory properties of PCL-based segmented polyurethanes, J. Polym. Sci. B Polym. Phys. 45 (2007) 557–570.

[19] P. Caracciolo, F. Buffa, G. Abraham, Effect of the hard segment chemistry and structure on the thermal and mechanical properties of novel biomedical segmented poly(esterurethanes), J. Mater. Sci. Mater. Med. 20 (2009) 145–155.

[20] Q. Cao, S. Chen, J. Hu, P. Liu, Study on the liquefied-MDI-based shape memory polyurethanes, J. Appl. Polym. Sci. 106 (2007) 993–1000.

[21] P. Vermette, H.J. Griesser, G. Laroche, R. Guidoin, Biomedical Applications of Polyurethanes, Landes Bioscience, Georgetown, TX, 2001.

[22] K.R.S. John, The use of polyurethane materials in the surgery of the spine: a review, Spine J. 14 (2014) 3038–3047.

[23] F.J. Davis, G.R. Mitchell, Polyurethane based materials with applications in medical devices, in: Bio-materials and Prototyping Applications in Medicine, Springer, NY, 2008, pp. 27–48.

[24] M.S. Shin, J.Y. Hong, S. Park, Gemcitabine release behavior of polyurethane matrixes designed for local anti-cancer drug delivery via stent, J. Drug Deliv. Sci. Technol. 22 (2012) 301–306.

[25] T. Yamaoka, Y. Makita, H. Sasatani, S.-I. Kim, Y. Kimura, Linear type azo-containing polyurethane as drug-coating material for colon-specific delivery: its properties, degradation behavior, and utilization for drug formulation, J. Controlled Release 66 (2000) 187–197.

[26] T.J. Johnson, K.M. Gupta, J. Fabian, T.H. Albright, P.F. Kiser, Segmented polyurethane intravaginal rings for the sustained combined delivery of antiretroviral agents dapivirine and tenofovir, Eur. J. Pharm. Sci. 39 (2010) 203–212.

[27] A. Martinelli, L. D'Ilario, I. Francolini, A. Piozzi, Water state effect on drug release from an antibiotic loaded polyurethane matrix containing albumin nanoparticles, Int. J. Pharm. 407 (2011) 197–206.

[28] F. Crisante, I. Francolini, M. Bellusci, A. Martinelli, L. D'Ilario, A. Piozzi, Antibiotic delivery polyurethanes containing albumin and polyallylamine nanoparticles, Eur. J. Pharm. Sci. 36 (2009) 555–564.

[29] A. Wang, H. Gao, Y. Sun, Y-l. Sun, Y.-W. Yang, G. Wu, Y. Wang, Y. Fan, J. Ma, Temperature-and pH-responsive nanoparticles of biocompatible polyurethanes for doxorubicin delivery, Int. J. Pharm. 441 (2013) 30–39.

[30] W.N. Sivak, J. Zhang, S. Petoud, E.J. Beckman, Simultaneous drug release at different rates from biodegradable polyurethane foams, Acta Biomater. 5 (2009) 2398–2408.

[31] S. Kohjiya, Y. Ikeda, S. Takesako, S. Yamashita, Drug release behavior from polyurethane gel, React. Polym. 15 (1991) 165–175.

[32] B. Li, J.M. Davidson, S.A. Guelcher, The effect of the local delivery of platelet-derived growth factor from reactive two-component polyurethane scaffolds on the healing in rat skin excisional wounds, Biomaterials 30 (2009) 3486–3494.

[33] X. Sun, H. Gao, G. Wu, Y. Wang, Y. Fan, J. Ma, Biodegradable and temperature-responsive polyurethanes for adriamycin delivery, Int. J. Pharm. 412 (2011) 52–58.

[34] T.T.N. Huynh, K. Padois, F. Sonvico, A. Rossi, F. Zani, F. Pirot, J. Doury, F. Falson, Characterization of a polyurethane-based controlled release system for local delivery of chlorhexidine diacetate, Eur. J. Pharm. Biopharm. 74 (2010) 255–264.

[35] B. Claeys, A. Vervaeck, X.K. Hillewaere, S. Possemiers, L. Hansen, T. De Beer, J.P. Remon, C. Vervaet, Thermoplastic polyurethanes for the manufacturing of highly dosed oral sustained release matrices via hot melt extrusion and injection molding, Eur. J. Pharm. Biopharm. 90 (2015) 44–52 .

[36] B. Li, T. Yoshii, A.E. Hafeman, J.S. Nyman, J.C. Wenke, S.A. Guelcher, The effects of rhBMP-2 released from biodegradable polyurethane/microsphere composite scaffolds on new bone formation in rat femora, Biomaterials 30 (2009) 6768–6779.

[37] B. Claeys, S. De Bruyn, L. Hansen, T. De Beer, J.P. Remon, C. Vervaet, Release characteristics of polyurethane tablets containing dicarboxylic acids as release modifiers–a case study with diprophylline, Int. J. Pharm. 477 (2014) 244–250.

[38] S. Ghosh, S.M. Mandal, Novel ibuprofen-based polyurethane: a new approach for drug delivery, J. Macro. Sci. A 45 (2008) 445–448.

[39] M. Ding, J. Li, X. Fu, J. Zhou, H. Tan, Q. Gu, Q. Fu, Synthesis, degradation, and cytotoxicity of multiblock poly(ε-caprolactone urethane)s containing gemini quaternary ammonium cationic groups, Biomacromolecules 10 (2009) 2857–2865.

[40] I.A. Rojas, J.B. Slunt, D.W. Grainger, Polyurethane coatings release bioactive antibodies to reduce bacterial adhesion, J. Controlled Release 63 (2000) 175–189.

[41] L. Zhou, D. Liang, X. He, J. Li, H. Tan, J. Li, Q. Fu, Q. Gu, The degradation and biocompatibility of pH-sensitive biodegradable polyurethanes for intracellular multifunctional antitumor drug delivery, Biomaterials 33 (2012) 2734–2745.

[42] M.A. Pattison, T.J. Webster, K.M. Haberstroh, Select bladder smooth muscle cell functions were enhanced on three-dimensional, nano-structured poly(ether urethane) scaffolds, J. Biomater. Sci. Polym. Ed. 17 (2006) 1317–1332.

[43] J. Guan, K.L. Fujimoto, M.S. Sacks, W.R. Wagner, Preparation and characterization of highly porous, biodegradable polyurethane scaffolds for soft tissue applications, Biomaterials 26 (2005) 3961–3971.

[44] M. Sokolsky-Papkov, K. Agashi, A. Olaye, K. Shakesheff, A.J. Domb, Polymer carriers for drug delivery in tissue engineering, Adv. Drug Deliv. Rev. 59 (2007) 187–206.

[45] L. Yu, L. Zhou, M. Ding, J. Li, H. Tan, Q. Fu, X. He, Synthesis and characterization of novel biodegradable folate conjugated polyurethanes, J. Colloid Interface Sci. 358 (2011) 376–383.

[46] S. Doppalapudi, A. Jain, W. Khan, A.J. Domb, Biodegradable polymers—an overview, Polym. Adv. Technol. 25 (2014) 427–435.

[47] L. Zhou, L. Yu, M. Ding, J. Li, H. Tan, Z. Wang, Q. Fu, Synthesis and characterization of pH-sensitive biodegradable polyurethane for potential drug delivery applications, Macromolecules 44 (2011) 857–864.

[48] D.F. Williams, On the mechanisms of biocompatibility, Biomaterials 29 (2008) 2941–2953.

[49] R. Marchant, Q. Zhao, J. Anderson, A. Hiltner, Degradation of a poly(ether urethane urea) elastomer: infra-red and XPS studies, Polymer 28 (1987) 2032–2039.

[50] M. Szycher, V.L. Poirier, D.J. Dempsey, Development of an aliphatic biomedical-grade polyurethane elastomer, J. Elastom. Plast. 15 (1983) 81–95.

[51] L. Pinchuk, A review of the biostability and carcinogenicity of polyurethanes in medicine and the new generation of 'biostable' polyurethanes, J. Biomater. Sci. Polym. Ed. 6 (1995) 225–267.

[52] Y. Tang, R. Labow, J. Santerre, Isolation of methylene dianiline and aqueous-soluble biodegradation products from polycarbonate-polyurethanes, Biomaterials 24 (2003) 2805–2819.

[53] J. Guan, W.R. Wagner, Synthesis, characterization and cytocompatibility of polyurethaneurea elastomers with designed elastase sensitivity, Biomacromolecules 6 (2005) 2833–2842.

[54] S. Gogolewski, K. Gorna, Biodegradable polyurethane cancellous bone graft substitutes in the treatment of iliac crest defects, J. Biomed. Mater. Res. A 80 (2007) 94–101.

[55] H. Til, H. Falke, M. Prinsen, M. Willems, Acute and subacute toxicity of tyramine, spermidine, spermine, putrescine and cadaverine in rats, Food Chem. Toxicol. 35 (1997) 337–348.

[56] T.T. Reddy, A. Kano, A. Maruyama, A. Takahara, Synthesis, characterization and drug release of biocompatible/biodegradable non-toxic poly(urethane urea)s based on poly(ε-caprolactone)s and lysine-based diisocyanate, J. Biomater. Sci. Polym. Ed. 21 (2010) 1483–1502.

[57] B. Bogdanov, V. Toncheva, E. Schacht, L. Finelli, B. Sarti, M. Scandola, Physical properties of poly(ester-urethanes) prepared from different molar mass polycaprolactone-diols, Polymer 40 (1999) 3171–3182.

[58] M. Bil, J. Ryszkowska, J. Roether, O. Bretcanu, A. Boccaccini, Bioactivity of polyurethane-based scaffolds coated with Bioglass®, Biomed. Mater. 2 (2007) 93.

[59] R. Adhikari, P.A. Gunatillake, I. Griffiths, L. Tatai, M. Wickramaratna, S. Houshyar, T. Moore, R. Mayadunne, J. Field, M. McGee, Biodegradable injectable polyurethanes: synthesis and evaluation for orthopaedic applications, Biomaterials 29 (2008) 3762–3770.

[60] R.F. Storey, T.P. Hickey, Degradable polyurethane networks based on D,L-lactide, glycolide, ε-caprolactone, and trimethylene carbonate homopolyester and copolyester triols, Polymer 35 (1994) 830–838.

[61] A.E. Hafeman, K.J. Zienkiewicz, A.L. Zachman, H.-J. Sung, L.B. Nanney, J.M. Davidson, S.A. Guelcher, Characterization of the degradation mechanisms of lysine-derived aliphatic poly(ester urethane) scaffolds, Biomaterials 32 (2011) 419–429.

[62] R.S. Labow, D.J. Erfle, J.P. Santerre, Elastase-induced hydrolysis of synthetic solid substrates: poly(ester-urea-urethane) and poly(ether-urea-urethane), Biomaterials 17 (1996) 2381–2388.

[63] S. Phua, E. Castillo, J. Anderson, A. Hiltner, Biodegradation of a polyurethane *in vitro*, J. Biomed. Mater. Res. 21 (1987) 231–246.

[64] H. Chen, Y. Li, Y. Liu, T. Gong, L. Wang, S. Zhou, Highly pH-sensitive polyurethane exhibiting shape memory and drug release, Polym. Chem. 5 (2014) 5168–5174.

[65] A. Lendlein, H. Jiang, O. Jünger, R. Langer, Light-induced shape-memory polymers, Nature 434 (2005) 879–882.

[66] W. Huang, B. Yang, Y. Zhao, Z. Ding, Thermo-moisture responsive polyurethane shape-memory polymer and composites: a review, J. Mater. Chem. 20 (2010) 3367–3381.

[67] A. Lendlein, S. Kelch, Shape-memory polymers, Angew. Chem. Int. Ed. 41 (2002) 2034–2057.

[68] M. Behl, A. Lendlein, Shape-memory polymers, Mater. Today 10 (2007) 20–28.

[69] B.K. Kim, S.Y. Lee, M. Xu, Polyurethanes having shape memory effects, Polymer 37 (1996) 5781–5793.

[70] P. Singhal, J.N. Rodriguez, W. Small, S. Eagleston, J. Van de Water, D.J. Maitland, T.S. Wilson, Ultra low density and highly crosslinked biocompatible shape memory polyurethane foams, J. Polym. Sci. B Polym. Phys. 50 (2012) 724–737.

[71] P. Singhal, W. Small, E. Cosgriff-Hernandez, D.J. Maitland, T.S. Wilson, Low density biodegradable shape memory polyurethane foams for embolic biomedical applications, Acta Biomater. 10 (2014) 67–76.

[72] A. Lendlein, R. Langer, Biodegradable, elastic shape-memory polymers for potential biomedical applications, Science 296 (2002) 1673–1676.

[73] H. Kalita, M. Mandal, N. Karak, Biodegradable solvent-induced shape-memory hyperbranched polyurethane, J. Polym. Res. 19 (2012) 1–8.

[74] S. Thakur, S. Barua, N. Karak, Self-healable castor oil based tough smart hyperbranched polyurethane nanocomposite with antimicrobial attributes, RSC Adv. 5 (2015) 2167–2176.

[75] A. Lendlein, R.S. Langer, Biodegradable Shape Memory Polymeric Sutures, US Patent, 2014.

[76] B.G. Zanetti-Ramos, E. Lemos-Senna, V. Soldi, R. Borsali, E. Cloutet, H. Cramail, Polyurethane nanoparticles from a natural polyol via miniemulsion technique, Polymer 47 (2006) 8080–8087.

[77] E. Jabbari, M. Khakpour, Morphology of and release behavior from porous polyurethane microspheres, Biomaterials 21 (2000) 2073–2079.

[78] K. Bouchemal, S. Briançon, E. Perrier, H. Fessi, I. Bonnet, N. Zydowicz, Synthesis and characterization of polyurethane and poly(ether urethane) nanocapsules using a new technique of interfacial polycondensation combined to spontaneous emulsification, Int. J. Pharm. 269 (2004) 89–100.

[79] B. Zanetti-Ramos, V. Soldi, E. Lemos-Senna, R. Borsali, Use of natural monomer in the synthesis of nano- and microparticles of polyurethane by suspension-polyaddition technique, Macromol. Symp. 229 (2005) 234–245.

[80] P. Chambon, E. Cloutet, H. Cramail, T. Tassaing, M. Besnard, Synthesis of core-shell polyurethane–polydimethylsiloxane particles in cyclohexane and in supercritical carbon dioxide used as dispersant media: a comparative investigation, Polymer 46 (2005) 1057–1066.

[81] P. Chambon, E. Cloutet, H. Cramail, Synthesis of core-shell polyurethane–poly(dimethylsiloxane) particles in supercritical carbon dioxide, Macromolecules 37 (2004) 5856–5859.

[82] A. Mishra, S.K. Singh, D. Dash, V.K. Aswal, B. Maiti, M. Misra, P. Maiti, Self-assembled aliphatic chain extended polyurethane nanobiohybrids: emerging hemocompatible biomaterials for sustained drug delivery, Acta Biomater. 10 (2014) 2133–2146.

[83] J. Zhang, M. Wu, J. Yang, Q. Wu, Z. Jin, Anionic poly(lactic acid)-polyurethane micelles as potential biodegradable drug delivery carriers, Colloids Surf. Physicochem. Eng. Aspects 337 (2009) 200–204.

[84] G. Morral-Ruiz, P. Melgar-Lesmes, C. Solans, M. García-Celma, Multifunctional polyurethane–urea nanoparticles to target and arrest inflamed vascular environment: a potential tool for cancer therapy and diagnosis, J. Controlled Release 171 (2013) 163–171.

[85] Y.-P. Chen, S.-H. Hsu, Preparation and characterization of novel water-based biodegradable polyurethane nanoparticles encapsulating superparamagnetic iron oxide and hydrophobic drugs, J. Mater. Chem. B 2 (2014) 3391–3401.

[86] R. Sridhar, R. Lakshminarayanan, K. Madhaiyan, V.A. Barathi, K.H.C. Lim, S. Ramakrishna, Electrosprayed nanoparticles and electrospun nanofibers based on natural materials: applications in tissue regeneration, drug delivery and pharmaceuticals, Chem. Soc. Rev. 44 (2015) 790–814.

[87] H. Zhuo, J. Hu, S. Chen, L. Yeung, Preparation of polyurethane nanofibers by electrospinning, J. Appl. Polym. Sci. 109 (2008) 406–411.

[88] F.A. Sheikh, M.A. Kanjwal, S. Saran, W.-J. Chung, H. Kim, Polyurethane nanofibers containing copper nanoparticles as future materials, Appl. Surf. Sci. 257 (2011) 3020–3026.

[89] F. Sheikh, N.M. Barakat, M. Kanjwal, A. Chaudhari, I.-H. Jung, J. Lee, H. Kim, Electrospun antimicrobial polyurethane nanofibers containing silver nanoparticles for biotechnological applications, Macromol. Res. 17 (2009) 688–696.

[90] H.J. Jeon, J.S. Kim, T.G. Kim, J.H. Kim, W.-R. Yu, J.H. Youk, Preparation of poly(ε-caprolactone)-based polyurethane nanofibers containing silver nanoparticles, Appl. Surf. Sci. 254 (2008) 5886–5890.

[91] A.R. Unnithan, P.B.T. Pichiah, G. Gnanasekaran, K. Seenivasan, N.A.M. Barakat, Y.-S. Cha, C.-H. Jung, A. Shanmugam, H.Y. Kim, Emu oil-based electrospun nanofibrous scaffolds for wound skin tissue engineering, Colloids Surf. Physicochem. Eng. Aspects 415 (2012) 454–460.

[92] C. Wong, X. Liu, Z. Xu, T. Lin, X. Wang, Elastin and collagen enhances electrospun aligned polyurethane as scaffolds for vascular graft, J. Mater. Sci. Mater. Med. 24 (2013) 1865–1874.

[93] X. Lin, D. Tang, S. Gu, H. Du, E. Jiang, Electrospun poly(N-isopropylacrylamide)/poly (caprolactone)-based polyurethane nanofibers as drug carriers and temperature-controlled release, New J. Chem. 37 (2013) 2433–2439.

[94] K. Saha, B.S. Butola, M. Joshi, Drug-loaded polyurethane/clay nanocomposite nanofibers for topical drug-delivery application, J. Appl. Polym. Sci. 131 (2014).

[95] G. Verreck, I. Chun, J. Rosenblatt, J. Peeters, A.V. Dijck, J. Mensch, M. Noppe, M.E. Brewster, Incorporation of drugs in an amorphous state into electrospun nanofibers composed of a water-insoluble, nonbiodegradable polymer, J. Controlled Release 92 (2003) 349–360.

[96] X. He, M. Ding, J. Li, H. Tan, Q. Fu, L. Li, Biodegradable multiblock polyurethane micelles with tunable reduction-sensitivity for on-demand intracellular drug delivery, RSC Adv. 4 (2014) 24736–24746.

[97] S. Yu, C. He, Q. Lv, H. Sun, X. Chen, pH and reduction dual responsive cross-linked polyurethane micelles as an intracellular drug delivery system, RSC Adv. 4 (2014) 63070–63078.

[98] Y. Savelyev, V. Veselov, L. Markovskaya, O. Savelyeva, E. Akhranovich, N. Galatenko, L. Robota, T. Travinskaya, Preparation and characterization of new biologically active polyurethane foams, Mater. Sci. Eng. C 45 (2014) 127–135.

[99] A.H. Shikani, M. St Clair, A. Domb, Polymer-iodine inactivation of the human immunodeficiency virus, J. Am. Coll. Surg. 183 (1996) 195–200.

[100] O. Aviv, N. Laout, S. Ratner, O. Harik, K.R. Kunduru, A.J. Domb, Controlled iodine release from polyurethane sponges for water decontamination, J. Controlled Release 172 (2013) 634–640.

[101] J. Han, S. Farah, A. Domb, P. Lelkes, Electrospun rapamycin-eluting polyurethane fibers for vascular grafts, Pharm. Res. 30 (2013) 1735–1748.

[102] J. Han, S. Farah, A.J. Domb, P.I. Lelkes, Sustained release of rapamycin from electrospun polyurethane vascular grafts, Cardiovasc. Pathol. 22 (2013) e52.

[103] X.-Y. Liu, C.-C. Zhang, W.-L. Xu, C.-X. Ouyang, Controlled release of heparin from blended polyurethane and silk fibroin film, Mater. Lett. 63 (2009) 263–265.

[104] D.M. Nelson, P.R. Baraniak, Z. Ma, J. Guan, N.S. Mason, W.R. Wagner, Controlled release of IGF-1 and HGF from a biodegradable polyurethane scaffold, Pharm. Res. 28 (2011) 1282–1293.

[105] J.-Y. Zhang, B.A. Doll, E.J. Beckman, J.O. Hollinger, Three-dimensional biocompatible ascorbic acid-containing scaffold for bone tissue engineering, Tissue Eng. 9 (2003) 1143–1157.

[106] W.N. Sivak, I.F. Pollack, S. Petoud, W.C. Zamboni, J. Zhang, E.J. Beckman, LDI–glycerol polyurethane implants exhibit controlled release of DB-67 and anti-tumor activity *in vitro* against malignant gliomas, Acta Biomater. 4 (2008) 852–862.

[107] S. Davaran, M.R. Rashidi, J. Hanaee, A. Khani, M. Mahkam, M. Hashemi, Synthesis and degradation characteristics of polyurethanes containing azo derivatives of 5-amino salicylic acid, J. Bioact. Compat. Polym. 21 (2006) 315–326.

[108] Z. Pan, L. Yu, N. Song, L. Zhou, J. Li, M. Ding, H. Tan, Q. Fu, Synthesis and characterization of biodegradable polyurethanes with folate side chains conjugated to hard segments, Polym. Chem. 5 (2014) 2901–2910.

[109] L. Yang, H. Xiao, L. Yan, R. Wang, Y. Huang, Z. Xie, X. Jing, Lactose targeting oxaliplatin prodrug loaded micelles for more effective chemotherapy of hepatocellular carcinoma, J. Mater. Chem. B 2 (2014) 2097–2106.

[110] M. Sobczak, E. Oledzka, M. Kwietniewska, G. Nałęcz-Jawecki, W. Kołodziejski, Promising macromolecular conjugates of camptothecin – the synthesis, characterization and *in vitro* studies, J. Macromol. Sci. A 51 (2014) 254–262.

[111] K. Manokruang, J.S. Lym, D.S. Lee, Injectable hydrogels based on poly(amino urethane) conjugated bovine serum albumin, Mater. Lett. 124 (2014) 105–109.

Antibacterial polyurethanes

9

L.-C. Xu[1], C.A. Siedlecki[1,2,]*

[1]Department of Surgery, Biomedical Engineering Institute, The Pennsylvania State University, College of Medicine, Hershey, PA, USA; [2]Department of Biomedical Engineering, The Pennsylvania State University, College of Medicine, Hershey, PA, USA
*Corresponding author: csiedlecki@psu.edu

9.1   Introduction

Health care-associated infections affect 5% of patients hospitalized in the United States every year and lead to nearly 100,000 infection-related deaths, resulting in up to $4.5 billion cost in health care annually.[1,2] The majority of these infections are associated with the use of indwelling medical devices such as intravascular catheters, mechanical heart valves, urinary catheters, and orthopedic implants.[3–5] The mortality rates of using these devices are significantly high. For example, the mortality rates approach 30% for infection associated with prosthetic valve endocarditis and 40% for infections associated with an aortic graft.[6] Due to the broad range of mechanical properties, fatigue resistance and relatively good hemocompatibility, polyurethanes are the most widely employed materials for the manufacturing of vascular catheters, and also have been widely used to prepare other medical devices including wound dressings, artificial organs, and drug controlled delivery devices.[7–9] However, polyurethanes seem to perform only moderately well in bacterial adhesion studies compared to other polymers,[10] and are susceptible to bacterial colonization and have a higher risk of infection.[11] Antibacterial or antibiotic polyurethanes are among the most intensive ongoing research areas in an effort to increase their ability to withstand infection.

The difficulty in treatment of biomaterial-associated infection is primarily related to biofilm formation on the surface. A biofilm is a complex consortium of surface adherent bacteria that becomes embedded in a polysaccharide matrix, and is generally proposed as a four-stage model for formation: adherence, accumulation, maturation, and dispersal.[12] When exposed to biological fluid, the surfaces of biomaterials are rapidly adsorbed with a layer of "conditioning film," which is composed of macromolecules such as proteins, carbohydrates, and lipids. This film mediates the interactions between bacterial cells and material surface through the van der Waals forces, electrostatic interactions, hydrophobic interactions, acid–base bonds, etc., as well as ligand–receptor interactions. Once the bacteria adhere to the material surface, bacteria multiply, accumulate in multilayered cell clusters, and produce a slime forming the biofilm matrix (Figure 9.1). When a mature biofilm has been established, conventional therapies based on systemic antibiotics are not efficacious because biofilms as a barrier protect bacteria from microbicidal systems and antimicrobial agents.[13–16] As a result, surgical removal and replacement of the implanted devices are often the only treatment to eradicate the infection.[17]
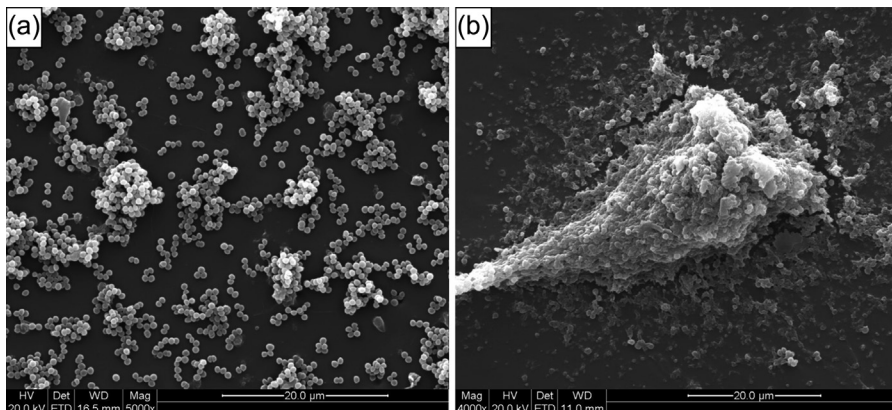
Figure 9.1 Representative SEM images of (a) bacterial adhesion on polyurethane surface after exposure to *Staphylococcus epidermidis* RP62A strain culture for 1 h and (b) biofilm formation after exposure of 24 h.

Various approaches have been proposed and developed to limit or prevent microbial colonization and biofilm formation on biomaterials and medical devices. Excellent reviews on infection-resistant biomaterials and technologies for infection-resistant surfaces can be found in recent publications.[18–21] As anti-infective biomaterials have progressively become a primary strategy for preventing medical device-associated infections, it is not at all surprising that a very broad variety of concepts and approaches have been developed to achieve the necessary antibacterial properties of materials. These approaches include antiadhesive strategies to prevent surface adhesion or production of bacterial adhesins, dissolution of already established biofilms, targeting of the biofilm matrix for degradation, and interference with biofilm regulation.[22] The rationale for approaches to develop antibacterial polyurethanes generally focuses on designing an antibacterial surface through incorporation or coating with antibiotic agents or surface modification. These surfaces have the ability to repel or resist the initial attachment of bacteria either by exhibiting an antibiofouling affect or by inactivating any cells coming into contact with the surface, causing cell death and therefore exhibiting a bactericidal effect. Therefore, the antibacterial polyurethanes can be broadly categorized into antiadhesive (antibiofouling) polyurethanes and bactericidal polyurethanes or polyurethanes exhibiting both antiadhesive and bactericidal characteristics.

9.2   Antiadhesive polyurethanes

Bacterial adhesion is the critical step in the pathogenesis of biomaterial-associated infection and is critically influenced by numerous variables including surface properties of biomaterials, the nature of the environment, and the bacterial cell surface. In addition, adsorbed proteins play an important role in bacteria–surface interactions.[23] One strategy for the development of antibacterial polyurethanes has focused on

modifying surface physicochemical properties to minimize the interactions between bacterial cells and surfaces or adsorbed proteins by chemical or physical treatments. Ostuni et al.[24] proposed that nonfouling polymers should be hydrophilic, electrically neutral, and possess hydrogen-bond acceptors. Therefore, one chemical treatment is to graft polymerized monomers or covalently couple hydrophilic polymer molecules, for example, polyethylene glycol (PEG),[25] onto the substrate surface forming a brush-like layer that shields the surface to repel protein adsorption and cell interactions.[26] Physical–topographical treatments modify biomaterial surface topography at the micro- and nanoscales to minimize the interactions of cells and surfaces and thereby reduce the bacterial adhesion.[27] With the development of nanotechnology the important roles of surface nanotopography and architecture in bacterial adhesion and biofilm formation have been recognized and attracted more interest to the biomaterial society.[28,29] Tethered antibiofouling brushes or topography modifications are advantageous in offering long-lasting effects and minimizing environmental problems associated with the leaching of antibiotic agents that cause the antibiotic resistance of bacteria.[30]

9.2.1 Polyethylene glycol-modified polyurethanes

PEG or polyethylene oxide (PEO) has gained wide recognition as a biomaterial because of its high efficiency in resisting protein adsorption, weak immunogenicity, and good compatibility with living cells. Due to lack of mechanical properties, PEG or PEO materials are generally attached to the surface of a material possessing suitable mechanical properties, such as a polyurethane. Both *in vitro* and *in vivo* experiments have shown that PEG-grafted surfaces have great potential for clinical applications in medical devices and implants.[31,32] PEG-grafted polyurethanes have been shown to be effective for prevention of bacterial adhesion and subsequent infection,[25] and also have exhibited significant reduction of platelet adhesion[33,34] and heparin-like anticoagulant activity.[35]

Grafting PEG onto polyurethane surfaces is generally performed by a two-step reaction that covalently binds PEG onto the urethane group through an allophanate linkage (Figure 9.2).[36] Hexamethylene diisocyanate (HMDI) is added to react with urethane bonds at the surface in the first step to functionalize the surface with isocyanate groups, and then the free isocyanate groups are utilized to bind PEG onto surfaces. The catalyst, such as trimethylamine,[36,37] di-*n*-butyl tin dilaurate,[25,38,39] stannous octoate,[40] and stannous 2-ethylhexanoate,[41] is necessary in allophanate reactions under lower reaction temperatures in the range of 40–60 °C where diisocyanate is used for activating the polyurethane surface, otherwise formation of allophanates from urethane and isocyanate groups generally does not occur below 100 °C. Such a reaction is relatively slow and easily controlled. After 60 min a maximum number of free NCO groups can be obtained and react with functional groups (e.g., —OH, —NH$_2$, —SO$_3$) in PEG in the second step to graft the polymer onto the surface and obtain the different surface chemistries.[25,36,39] Grafting PEG onto a polyurethane surface can also be performed by other techniques. Desai et al.[42] used the surface physical interpenetrating networks technique to incorporate PEO and other water-soluble polymers into the surfaces of polyurethane and found PEO with a molecular weight of 18,500 g/mol having an optimal chain length to reduce protein adsorption and prevent protein-mediated biological
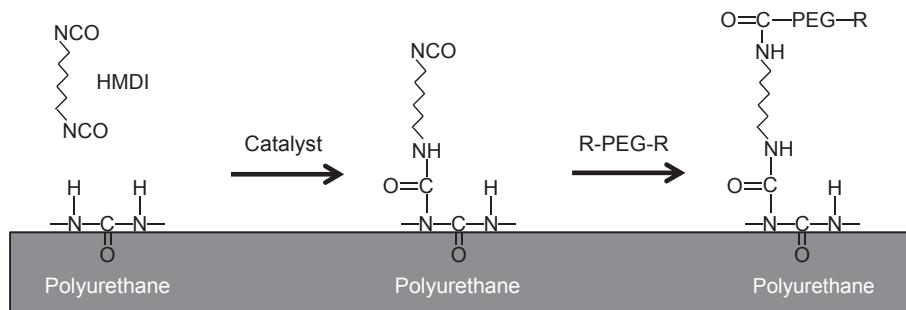
Figure 9.2 Two-step reaction scheme for grafting PEG to the polyurethane surface (R: —OH, —NH$_2$, —SO$_3$, etc.).
Ref. 36.

interactions. Orban et al.[43] reported a simple synthesis of PEG-grafted polyurethanes with the PEG grafts emanating from a secondary amine incorporated into the backbone of the polyurethane, and *N*-Boc-diethanolamine was used as chain extender. PEGs with different molecular weights were grafted onto the Boc-deprotected polyurethanes via chloroformate and the obtained grafted polymers exhibited very little platelet adhesion, although no data were reported about bacterial adhesion inhibition. The other type of PEG or PEO-modified polyurethane can be obtained by blending. Park et al.[44] prepared PEO-based multiblock copolymer/segmented polyurethane blends as coating materials for urinary catheters. To prepare this coating material, a copolymer containing hydrophilic PEO and hydrophobic poly(polytetramethylene oxide) (PTMO) was first created by a polycondensation reaction in the presence of HMDI, and then the copolymer was blended with segmented polyurethane solution for coating on the urinary catheters. The copolymer additive increased the swellability of coating and adsorbed a significant amount of water. The bacterial adhesion study showed that there was an 85% decrease in adhesion of *Staphylococcus epidermidis* for blends compared to bare polyurethane.

Inhibition of bacterial adhesion on PEG-modified polyurethane surfaces is related to chain density, chain length, and functional groups of PEG.[25,34] Grafting PEG onto a polyurethane surface forms a layer of polymer brush with a tightly bound water layer and acts as a physical barrier that hinders the adhesion of protein, platelet, and bacteria.[45,46] The steric repulsion, water barrier, osmotic repulsion, and excluded-volume effects are the most probable explanations for the antiadhesive effects of polymer brushes. With the excellent mechanical properties and biocompatibility, PEG-modified polyurethane is expected to be useful as coating, molding, and blending materials for artificial organs and medical devices.

9.2.2 Surface topography-modified polyurethanes

The surface topography of a material influences biological responses including protein adsorption, cell behaviors, blood-contacting interactions, and bacterial adhesion and has been utilized to design biomaterial and device surfaces for improved biocompatibility.[28,29,47] Surface topography has been explored to create antifouling surfaces

(antiadhesion of protein, platelet, and bacteria) without the need to change the bulk properties of the material or the surface chemistry. Ideas for development of nontoxic and fouling-resistant materials by surface topography have been inspired from nature, such as shark skin, lotus leaf, and the inner surface of blood vessels.[48–53] Reddy et al.[54] reported that the Sharklet micropatterned silicone surfaces inhibited bacterial colonization and migration of uropathogenic *Escherichia coli* in catheter-associated urinary tract infection. A similar microtopography was designed on poly(dimethyl siloxane) (PDMS) elastomer to disrupt the formation of biofilm and it was found that there was no biofilm colonization of *Staphylococcus aureus* until at 21 days while the smooth surface exhibited early-stage biofilms colonies at 7 days and mature biofilms at 14 days.[55] More evidence has shown that spatially organized topographic patterned surfaces represent a promising approach for controlling/inhibiting bacterial adhesion and biofilm formation, thereby reducing the risk of biomaterial-associated infection.[56]

The antifouling properties of topographical polyurethanes were rarely reported until recently. Zheng et al.[57] engineered a lotus leaf-like polyurethane/Pluronic® F-127 surface via replica molding using a natural lotus leaf as the template. The antifouling studies showed that protein adsorption on the PU/Pluronic® surface without topographic modification was significantly lower than that on the PU surface, and adsorption was further reduced when lotus leaf-like topography was constructed on the PU/Pluronic® surface. Yao et al.[58] studied the bacterial adhesion on nanostructured polyurethanes by HNO_3 treatment and found that the colonization of *S. epidermidis* density decreased by 5 times, *E. coli* density decreased by 6 times, and *Proteus mirabilis* density decreased by 8 times compared to conventional polyurethane. The significant increase in nanoscale roughness and hydrophobicity was regarded as contributing to the observed decrease of bacterial responses. We developed a submicrometer textured surface on polyurethane biomaterials and showed significant decreases in adhesion of *S. epidermidis* and *S. aureus* to textured polyurethanes as well as the inhibition of biofilm formation under shear and static conditions.[59] These similar textured polyurethane surfaces have also been shown to have the ability to reduce platelet adhesion, which is a critical step for thrombus formation on blood-contacting devices.[60–62] Therefore, the *in vitro* successes of textured polyurethanes are of great interest for the potential clinical use in combating health care-infections without addition of antibiotics and thrombosis.

Surface structural topography is created by either depositing material on a surface or etching away part of a surface. The techniques for patterning have been reviewed elsewhere.[63] Figure 9.3 illustrates an example of a soft lithography two-stage replication molding technique for fabrication of textured polyurethane surfaces. A silicon wafer master with desired texture may be fabricated either by etching the pattern in to the silicon wafer[64] or by patterning a photosensitive polymer on the silicon surface.[65–67] A "negative" of this pattern is molded in silicone (e.g., PDMS) and the original pattern can be transferred through a second molding step. To obtain the highest replication efficiency and quality of surface topography, a polyurethane replica can be prepared by spin casting diluted polyurethane solution onto a silicone mold in one thin layer first. After curing under vacuum, the additional thicker polyurethane layers are added until the desired film thickness is reached. Figure 9.4 shows the
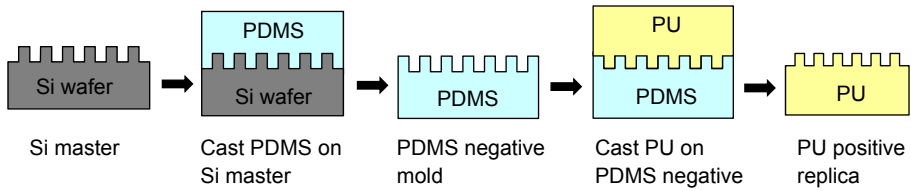
Figure 9.3 Soft lithography two-stage replication molding process for fabrication of textured polyurethane (PDMS, poly(dimethylsiloxane); PU, polyurethane).
Ref. 63.
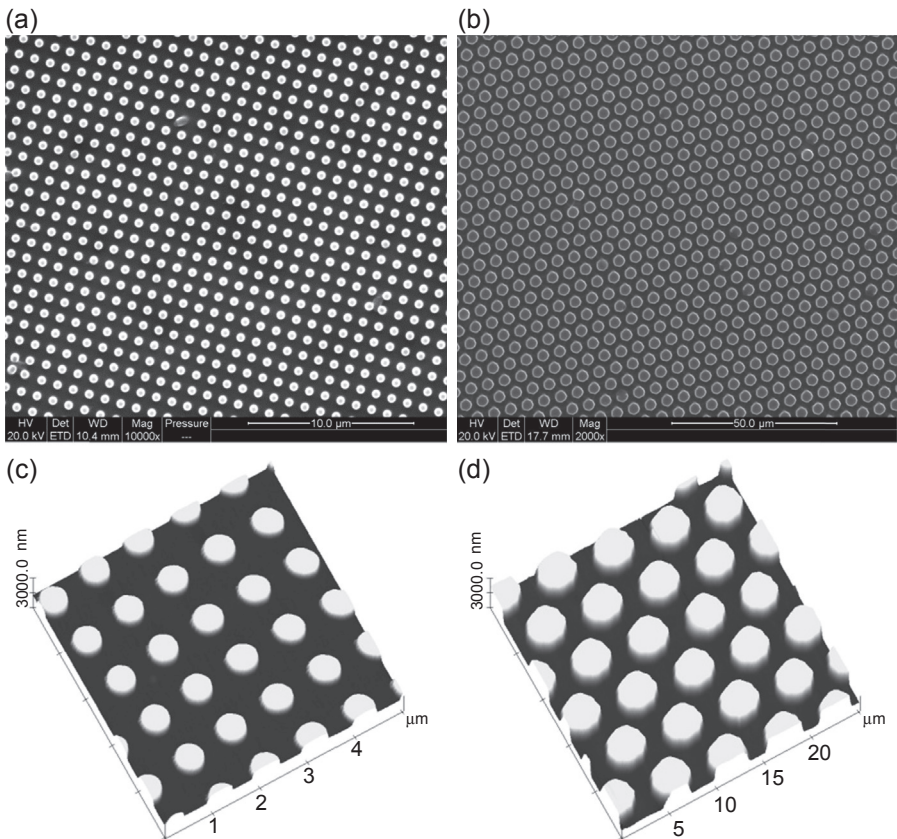
Figure 9.4 Representative (a and b) SEM images and (c and d) 3-D AFM images of textured polyurethanes, (a and c) 500/500 nm and (b and d) 4.0/1.5 μm. AFM scan size, (c) $5 \times 5\,\mu m^2$ and (d) 4.0/1.5 μm; size, $25 \times 25\,\mu m^2$; z scale, 1500 nm.
Ref. 69.

scanning electron microscopy (SEM) and atomic force microscopy (AFM) topography images of a textured polyurethane with the pillars having diameter/separation of 500/500 nm and 4.0/1.5 μm. With the soft lithography two-stage replication molding method, a pillar yield of more than 99.8% on polyurethane surfaces can be obtained.[59]

The fractions of total top surface area of pillars are 25.2% of the nominal surface area for 500/500 nm pattern and 51.6% for 4.0/1.5 μm pattern. Since the submicrometer patterned surface has low accessible surface contact area and is less energetically favorable for bacterial interactions, bacterial adhesion is inhibited; however, the bacterial adhesion on a micropatterned surface (e.g., 4.0/1.5 μm) is more dependent on surface wettability (see below).

The nanotopographical surface may induce surface energy differences. One important phenomenon of a topographical surface is the change of wettability described by the Wenzel and Cassie–Baxter wetting model.[68] Inherently, hydrophobic materials become more hydrophobic due to the entrapped air between the surface structures while hydrophilic materials become more wettable due to increased contact area of the liquid with surface.[29] For example, the water contact angle of the original Biospan MS/0.4 polyurethane is around 92°, and increases up to 140° after patterned with pillars of dimension of 500/500 nm; however, the polyurethane surface becomes wettable with a water contact angle of 35° if treated with air plasma, and the surface is more wettable with a contact angle of 28° or lower for the textured polyurethane surface after treatment with air plasma.[69]

The antibiofouling effect of antibacterial surfaces by topography is related to the changes in surface energy and surface architecture. Hydrophobic surface topography increases the surface hydrophobicity, resulting in a "slippery" surface. Epstein et al.[70] reported that the superhydrophobic microstructure arrays on a silicon wafer (termed as slippery liquid-infused porous surfaces) can prevent 99.6% of *Pseudomonas aeruginosa, S. aureus*, and *E. coli* biofilm attachment under flow conditions. Our study of bacteria adhesion on hydrophobic polyurethane surfaces shows that surface texturing can inhibit bacterial adhesion up to 90% for *S. epidermidis* in phosphate buffered saline (PBS) solution under shear, where the antiadhesive property depends on surface features, flow conditions, and microorganisms.[59] To understand the effect of surface geometry and surface wettability on bacterial adhesion as well as the underlying mechanism, the bacterial adhesions of *S. epidermidis* to smooth and textured polyurethane surfaces (both hydrophobic and hydrophilic) across a low shear stress range (0–13.2 dyn/cm^2) were further studied and are shown in Figure 9.5.[69] Here the hydrophilic polyurethane surfaces were obtained by glow discharge air plasma treatment. Results showed that all the textured hydrophobic surfaces have significant reductions in adhesion of *S. epidermidis* in PBS or 25% platelet poor plasma (PPP) solutions under shear as compared to smooth surfaces, regardless of the sizes of patterns. However, bacterial adhesion on hydrophilic surfaces is largely dependent on the size of patterns. The submicrometer patterned surfaces reduced bacterial adhesion, while the micrometer patterned surfaces led to increased bacterial adhesion. The data suggest that increased surface hydrophobicity and decreased availability of contact area contribute to a reduction in bacterial adhesion to hydrophobic textured surfaces, while the availability of contact area is the primary determinant factor for bacterial adhesion on hydrophilic textured surfaces.[69] In addition the flow condition may influence bacterial adhesion. More bacteria or clusters were found on micrometer sizes of patterned polyurethane surfaces under static conditions whereas less bacterial adhesion was colonized on submicrometer patterned surfaces (Figure 9.6).
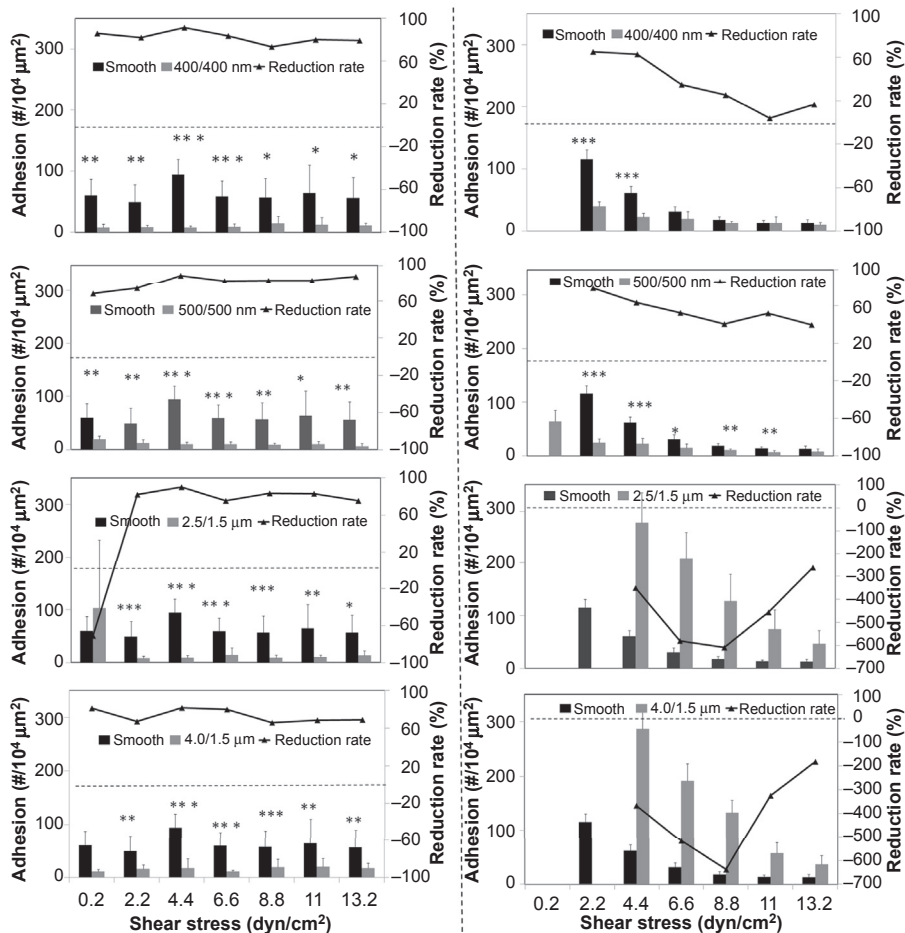
Figure 9.5 Bacterial adhesion on (left) hydrophobic and (right) hydrophilic polyurethane surfaces in PBS for 1 h. Each graph is shown as adhesion on a textured surface compared with that on a smooth surface (column, bacterial adhesion; marker + line, bacterial reduction rate). Columns missing in figure are due to bacterial aggregates on hydrophilic surfaces. Ref. 69.

The design parameters of topographical features including shape, size, height (depth), and separation distance are important for controlling biofouling. Whitehead et al.[27] studied the bacterial adhesion on titanium pattered surfaces with pits of different sizes and depths and found that the lowest number of bacteria was observed on the 500 nm diameter pits whereas it increased with pit size for other patterned surfaces. Biomimetic studies have shown that surface structures are most effective in the range of 50–90% of the size of settling organisms.[71] The stiffness of nanostructured features may influence bacterial adhesion and biofilm formation. Epstein et al.[72] studied high-aspect-ratio surface nanostructure arrays and found that the softness of hair-like
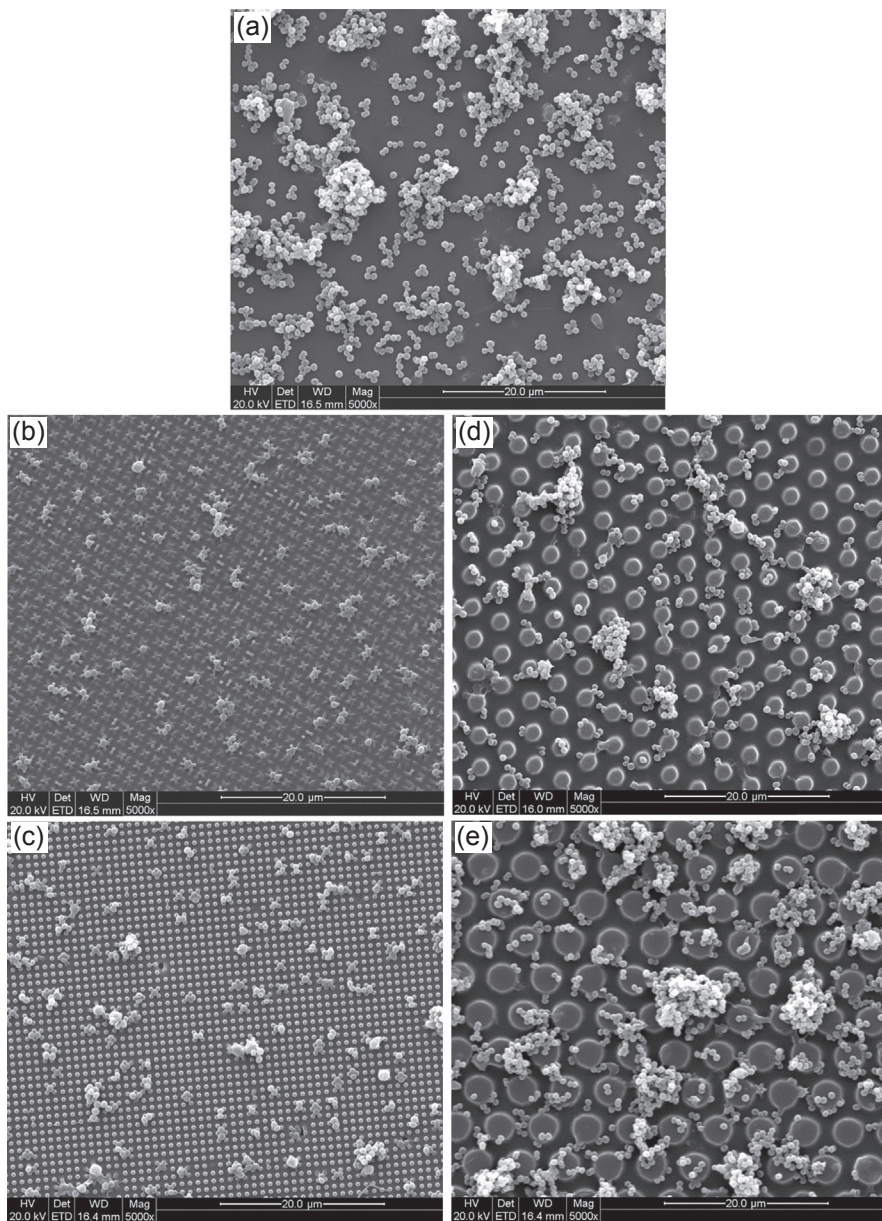
Figure 9.6 SEM images of bacterial adhesion on hydrophobic (a) smooth and textured PUU surfaces: (b) 400/400 nm, (c) 500/500 nm, (d) 2.5/1.5 μm, and (e) 4.0/1.5 μm, in PBS under static conditions (bar = 20 μm).
Ref. 69.

nanoarrays was increased beyond a threshold value and biofilm growth could be inhibited compared to a flat control surface. In our experiments the pillars of 400/400 nm on a submicrometer patterned polyurethane surface were sometimes found to be collapsed (Figure 9.6(b)), but lower bacterial adhesion was still observed. Apparently the parameters of topographical features for antibacterial polyurethane biomaterials should be exploited and optimized through *in vitro* and *in vivo* experiments.

9.2.3 Synergetic antibiofouling by combination of chemical and physical treatments

Physical approaches to biomaterial design provide a new concept and strategy in designing a new generation of implanted medical devices with truly biocompatible materials.[28,73] As the primary materials used in a variety of blood-contacting medical devices, polyurethane biomaterials, including those with surface topographical design, have numerous potential applications in the production of biomedical devices with improved hemocompatibility. However, defects on the surface during fabrication are unavoidable; for example, the defect with missed pillars in the transition of patterns from Si master to polyurethane replica and the seam (one kind of defect) during fabrication of cannulas or other clinical devices with shapes from flat textured polyurethane films may lead to colonization of bacteria on these areas. New designs and fabrication for minimizing defects may be necessary. An alternative approach is to combine the chemical modification (e.g., grafting PEG) to the topography approach so that the textured surfaces including the areas with defects are antiadhesive of bacteria. We developed a new antibiofouling polyurethane surface bearing modification of topography and chemical modification with PEG grafting. The bacterial adhesion study showed that the adhesion was significantly reduced by the surface with combined treatment, compared to the surface with single treatment. The adhesion reduction rates reached to 92.8% and 97.3% on PEG-400/400 nm and PEG-500/500 nm surfaces, respectively, compared to smooth surfaces without PEG treatment in PBS buffer (Figure 9.7(a)),
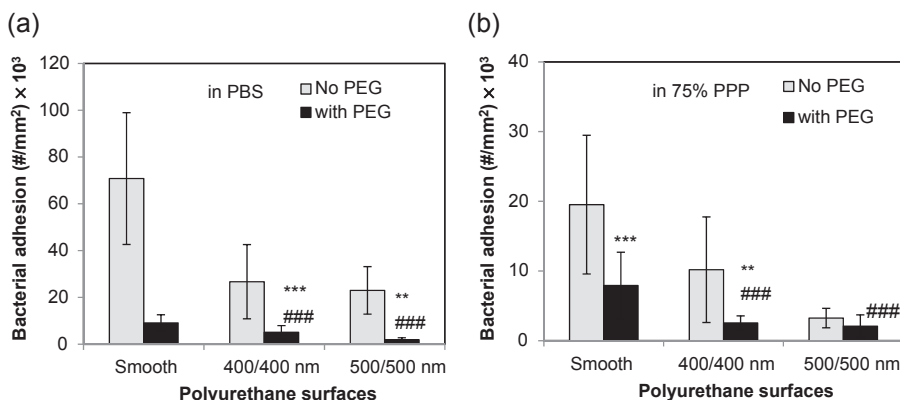
Figure 9.7 *Staphylococcus epidermidis* adhesion on textured polyurethane surfaces in (a) PBS and (b) 75% PPP for 1 h under static conditions. (Statistical symbols: ∗, compared to same polyurethane without PEG modification; #, compared to PEG smooth polyurethane.)

and the adhesion reduction rates were 87.0% and 89.3% in 75% PPP solution (Figure 9.7(b)). The large reduction in bacterial adhesion is probably due to the synergetic effects of chemical and physical modifications on interactions of bacteria–material.

9.2.4   Other approaches to antiadhesive polyurethanes

As described in the previous discussion, chemicophysical properties exhibited by the biomaterial surfaces determine the kinetics of bacterial adhesion. Efforts to design an antibiofouling surface have been focused on modifying the material bulk or surface properties to be hydrophilic and electrically neutral and possess hydrogen-bond acceptors.[24] Polyurethane biomaterials consist of hard and soft segments, in which hard domains are embedded in a soft domain matrix forming a microphase separation structure.[74] Notwithstanding the presence of soft domains that are hydrophilic, polyurethanes, if not properly functionalized, are not able to effectively resist bacterial adhesion. The functionalization of hard or soft domains in polyurethanes has been proposed to improve the surface wettability and the ability to control microbial infection. Francolin et al.[75] synthesized new polyurethanes having a common hard domain but a variety of soft domains made of different macrodiols: polypropylene oxide (PPO), polycaprolactide (PCL), and poly-L-lactide (PLA). The variation of soft domains caused a marked variation of polymers in thermal, viscoelastic, and swelling properties, as well as antifouling ability. The PCL- and PLA-containing polyurethanes possessed good antifouling properties due to the polymer bulk hydrophilicity and surface wettability. Similar works were also reported earlier by Corneillie et al.[76] who synthesized polyurethane with PEG, PPO, and PTMO as the different soft phases and bacterial adhesion was found to be significantly reduced. Francolin et al.[77] also reported the synthesis of heparin mimetic segmented polyurethanes in which sulfate or sulfamate groups, known to be responsible for the biological activity of heparin, were introduced into the side chain of a carboxylated polyurethane. The synthesized polymers possessed a higher hard/soft phase segregation and a greater hydrophilicity than the pristine polymer. The polymers were able to not only significantly delay the activated partial thromboplastin time but also prevent the adhesion of a strain of *S. epidermidis*. Thus, the features of these polymers represent an intrinsic ability to counteract bacterial adhesion and biofilm formation without any specific surface functionalization or incorporation with antimicrobial agents to release.

Immobilization of nonfouling polymers on biomaterial surfaces is particularly interesting since it avoids the use of drugs. Besides PEG, other polymers have also been explored. Polysaccharides are abundant in natural organic bodies and have been identified as nontoxic, biodegradable, and biocompatible materials. Polysaccharides and their derivatives have been immobilized onto the surfaces of polymeric biomaterials to improve their surface properties and biocompatibility. Using polysaccharides has a twofold advantage, that is, local control of the coagulation process and reducing bacterial adhesion. For example, heparin is a naturally occurring polysaccharide with negatively charged sulfate and aminosulfate groups and is often used as an anticoagulant to control blood clotting. It has been extensively investigated as a surface modifier for improving blood compatibility of polyurethane biomaterials.[78,79] Furthermore, heparin is also proven to be an effective surface modifier in prevention of catheter-related

bloodstream infections.[80] De Nardo et al.[81] synthesized a novel heparin-bound polycarbonate–urethane and the polymer surfaces were shown to decrease the colonization of *S. epidermidis* and *S. aureus*. As an alternative grafting technique, polysaccharide polymers can also be deposited on polyurethane surfaces via layer-by-layer assembly technique. Wang et al.[82] prepared polyurethanes modified by bioactive polysaccharide-based polyelectrolyte multilayers consisting of two polysaccharide-based polyelectrolytes, polyanionic lentinan sulfate and polycationic chitosan, alternatively deposited. These polysaccharide-based multilayers can not only improve hemocompatibility and cytocompatibility of the modified materials but also confer antibacterial bioactivity to the modified materials, for example, against *P. aeruginosa* at a reduction of 58% compared to unmodified polyurethane.

9.3   Bactericidal polyurethanes

The bactericidal biomaterial is bioactive and capable of inactivating bacterial cells and causing cell death when bacteria come into contact with the surface.[20] A general strategy for antibacterial polyurethane by the bactericidal effect is incorporation of a biocide into the bulk or at the surface. The scope of biocides is broad and includes quaternary ammonium compounds, antibiotics, phenols, iodine, and metal salts of silver and tin.[83] Bactericidal polyurethanes may be broadly categorized into intrinsically bioactive antimicrobial polyurethanes and bioactive antibiotic-coated polyurethanes by distribution of biocides in polymers. The former is the bulk material that exerts an antibacterial action and the latter is developed to achieve the desirable antibacterial properties at the biomaterial interface without compromising the quality of bulk material characteristics.[19] Using the mode of antimicrobial activity, the biocidal polymers may also be categorized into contact biocidal and biocide release-killing polyurethanes. Such biocidal modes can also be combined in a polymer, resulting in a synergistic effect on antibacterial activity.[84]

9.3.1   Contact biocidal polyurethanes

Many approaches have been used for incorporation of biocides to bulk polymeric materials. One method is the direct addition of biocide to the polymer material. This approach is economical, but the biocide is leachable and the rate of release may be a problem, resulting in overrelease at short times and underrelease at longer times, limiting the efficacy of the materials. Particularly, when the leaching antibacterial agent is exhausted, the ability of materials to retard bacteria is important.[83] Thus, nonleaching biocidal surfaces that kill bacterial on contact have been designed. The additional advantage of a contact biocidal surface is that it is effective against airborne bacteria even in the absence of a liquid medium while the biocide release-based strategy is only useful in aqueous solutions containing bacteria.[85]

9.3.1.1   Quaternary ammonium salt-containing polyurethanes

A nonleaching biocidal polyurethane was developed through covalent bonding of biocides to bulk polymer, often on the chain extender. Cooper reported the synthesis

of a series of functionalized polyurethanes containing different ionic groups based on Pellethane® including sulfonated Pellethane® phosphonated Pellethane® quaternized amine polyurethane, and a zwitterionic phosphonated polyurethane.[86] A bacterial adhesion study was conducted with exposure to radiolabeled *S. aureus* for 1 h and the results showed that the phosphonated polymers exhibited much lower amounts of bacterial adhesion while the quaternized amine polyurethane exhibited a greater amount of bacterial adhesion compared to unmodified Pellethane®. However, the radiolabeling technique may not support the long-term trend of bacterial colonization. In their latter experiments polymers were exposed to *S. aureus* culture for 24 h and the results showed that quaternized amine polyurethanes and the zwitterionic phosphonated polyurethane exhibited bactericidal abilities while Pellethane®, sulfonated Pellethane®, and phosphonated Pellethane® did not show potential as infection-resistant materials.[87] In fact, quaternary ammonium compounds have been well known as potent antimicrobials,[88,89] and they have been incorporated into polyurethanes as nonleaching infection-resistant biomaterials.[90–93] Park et al.[94] synthesized a polyurethane containing *N,N*-dodecyl,methyl-polyethylenimine (a polymeric quaternary ammonium compound) and the polymer surface was able to kill airborne Gram-positive *S. aureus* and Gram-negative *E. coli* bacteria, and also inactivate the enveloped influenza virus.

Quaternary ammonium salts are cationic disinfectants and kill bacteria by interaction with the constituents of the cell envelope: interaction with the negative charges of the cell wall, destabilization, weakening of the cytoplasmic membrane, causing a loss of cytoplasmic constituents and the death of the cell.[92] Sauvet et al.[91] reported on a polyurethane prepared by reaction of hydroxytelechelic polybutadienes carrying covalently bound quaternary ammonium salts with an aliphatic triisocyanate and that this polyurethane coating exhibited high biocidal activity against Gram-positive and Gram-negative bacteria, with 6–8 orders of magnitude in bacteria decay after 1 h of contact. However, a small decrease of activity (the magnitude order in bacteria decay was dropped to about 3.2) was noted within a few days due to the leaching of nonbonded quaternary ammonium salts or the splitting of a weak bond. Later the researchers developed a new class of insoluble polyurethanes based on polysiloxanes bearing pendant primary alcohol and quaternary ammonium groups in the same chain. The hydroxyl groups allow the polysiloxane to be incorporated in polyurethane films and the quaternary ammonium salts impart biocidal properties to the coating. These new polymers presented a high biocidal power that remained remarkably constant after 1 month of immersion in water.[92]

Bakhshi et al.[95,96] developed a synthetic approach for preparing bactericidal polyurethane coatings from soybean oil as a low cost, widely available, and renewable resource-based raw material. In this polymer, both quaternary ammonium salts and reactive hydroxyl groups were functionalized on to the backbone of soybean oil-based polyols, and then the polyols were reacted with different diisocyanate monomers to prepare polyurethane coatings. Since all active quaternary ammonium groups were covalently attached to the polymers there is no possibility for release of active groups from the polymers. No zone of inhibition around the specimens was observed. These materials showed excellent biocompatibility and very promising antibacterial properties against both Gram-positive and Gram-negative bacteria with bacterial reduction in the range of 83–100%.

The quaternized polyurethanes can be further incorporated with other functional groups such as pyridine. Cooper et al.[97] synthesized a series of nonleaching biocidal polyurethanes bearing incorporated pyridine moieties in the chain extender, followed by quaternization. In these materials, *N,N*-bis(2-hydroxyethyl)isonicotinamide (BIN) was used as the chain extender and the pyridine ring in BIN was quaternized with a variety of alkyl halides to form cationic polyurethanes. Such quaternized polymers possessed good mechanical properties in the dry state and displayed long-term stability in an aqueous environment with only small changes in sample mass after 2 years of immersion in water. Furthermore, similarly synthesized polyurethanes showed that the pyridinium moieties in the polyurethane were chemically cross-linked using short-chain divalent quaternizing agents, and the cross-linked polyurethane networks exhibited improved thermal stability.[98] The pyridine quaternized materials had good bactericidal activity against *S. aureus* and *E. coli,* and the percentage of dead cells on a surface was dependent on the alkyl halide used for quaternization, the concentration of quaternized moieties in the polyurethane, the Gram-type of the microorganism, and the contact time of the organism with the surface.[97]

9.3.1.2   N-*Halamine-containing polyurethanes*

Another important group of biocidal polymers is *N*-halamine polymers.[99] This type of polymer is prepared by introducing a heterocyclic ring containing amino, amide, or imide groups into the polymer structure followed by halogenation to the corresponding *N*-halamines, which confers on the polymer its biological activity.[100] The biocidal activity of the polymer is modulated by halogen stability, and the stability and antibacterial activity are opposite; that is, the stability follows an order of imide<amide<amine *N*-halamine,[101] and their antibacterial activities have an inverse trend, imide>amide>amine *N*-halamine.[102] This stability and biocidal activity trend provide guidance for the selection of an ideal biocidal material depending on the purpose.

The biocidal property of *N*-halamine polymers is mostly due to the direct transfer of the oxidative state of halide atoms in chloramine or bromamine groups to the cell wall of the microorganism, but a dissociation of Cl^+ or Br^+ into water followed by diffusion to the microorganism will also take place.[100] The *N*-halamine can have inorganic groups (e.g., phosphate, sulfate) or organic groups (e.g., alkyl and carbonyl groups). Among organic substituents, hydantoin (imidazolidine-2,4-dione) and dimethylhydantoin are basic moieties of *N*-halamine polymers (e.g., polyurethanes). Ahmed et al.[103] synthesized a novel *N*-halamine polyurethane by copolymerizing a heterocyclic ring-based monomer with either tolylene-2,6-diisocyanate or toluene-2,4-diisocyanate followed with different halogenations and found that the iodinated polymer showed greater biocidal power than chlorinated and brominated polymers. No bacterial growth was recorded in the presence of any of the halogenated polymers. Furthermore, the experimental results showed that the mode of action of these polymers was dual and proceeds both through release of halogen species into the medium and through bacteria–polymer contact.

Wynne et al.[83] synthesized a polyurethane with soft blocks containing semifluorinated ($-CH_2OCH_2CF_3$) and 5,5-dimethylhydantoin pendant groups as a biocidal

polymeric surface modifier (PSM), and this polyurethane was used as an additive (2% or less) for conventional model polyurethanes. The 2 wt% PSM-modified polyure-thane was activated with hypochlorite to generate a biocidal NCl function and was contact biocidal against both Gram-positive (*S. aureus*) and Gram-negative *(P. aeruginosa and E. coli)* bacteria. Effective biocidal activity can be conferred on a substrate polymer by as little as 1.6 wt% PSM, and *P. aeruginosa* can be completely killed in 15 min. However, the preparation of these hydantoin-containing PSMs includes a slow and incomplete reaction on the polymer for introducing hydantion. Wynne developed a more practical preparative method for incorporating hydantoin in a telechelic. A new oxetane monomer 5,5-dimethyl-3-(2-((3-methyloxetan-3-yl)methoxy)ethyl)-imidazolidine-2,4-dione (Hy4Ox) was synthesized.[104] This hydantoin–oxetane mono-mer is stable to cationic ring-opening polymerization. Copolymerization of Hy4Ox with another new monomer, 3-methyl-3-methoxymethyloxetane, provided a series of hydroxyl-terminated poly(2,2-substituted-1,3-propanediol) co-telechelics with low T_g for polyurethane synthesis. The new monomers and telechelics had promise in optimizing the effectiveness of biocidal polyurethane PSMs.[105]

The unique property of *N*-halamine biocidal polymers is that after many appli-cations they can be regenerated by simply reacting with Cl^+ or Br^+ donor com-pounds such as hypochlorite, sodium hypobromite, trichloroisocyanuric acid, or sodium dichlorocyanurate.[106,107] Worley et al.[108] reported on a group of *N*-halamine monomers, in which the chemical structures of these *N*-halamine compounds had electron-donating alkyl groups substituted on the heterocyclic rings adjacent to the oxidative NCl or NBr moieties. This structure prohibits significant release of "free halogen" into aqueous solutions and is stable for long term in aqueous solutions and in dry storage. The coating can be chlorinated with a source of free chlorine such as bleach to render it biocidal and the biocidal activity can be regenerated by further exposure to free chlorine. Sun et al.[109] reported a polyurethane sur-face covalently linked with an *N*-halamine precursor, 5,5-dimethylhydantoin, and 1,6-hexamethylene diisocyanate as the coupling agent. This new *N*-halamine-based polyurethane provided potent antimicrobial effects against *S. aureus* (Gram-positive bacterium), *E. coli* (Gram-negative bacterium), methicillin-resistant *S. aureus*, van-comycin-resistant *Enterococcus faecium*, and *Candida albicans* (fungus), and suc-cessfully prevented bacterial and fungal biofilm formation. The antimicrobial and biofilm-controlling effects by *N*-halamine-based polymers were stable for longer than 6 months under normal storage in open air; furthermore, the polymers could be recharged by another chlorination treatment. After 10 cycles of quenching–recharg-ing processes the chlorine contents in the polymers were almost unchanged (98.6%) and biocidal activity remained at the logarithm reduction rate of 4. The Kirby–Bauer test showed that the antimicrobial function was partly provided by the positively charged chlorines generated from the disassociation of the newly formed *N*-hala-mine structures, and the content of active chlorine in water was about 0.2 ppm, much lower than the allowed concentration by US Environmental Protection Agency (up to 4 ppm active chlorine as disinfection residues).[109] The low toxicity, ability for regeneration, and the promising biocidal activity have made *N*-halamine polymers or coatings widely used in many fields including medical facilities, food prepara-tion, and water disinfection.

9.3.1.3   Chitosan-containing polyurethanes

Chitosan, poly-(b-1/4)-2-amino-2-deoxy-ᴅ-glucopyranose, is a linear cationic poly-saccharide produced from chitin by partial deacetylation. Due to its unique biological characteristics, including high biodegradability, biocompatibility, nontoxicity, and antimicrobial properties, chitosan is widely used as an antimicrobial agent either alone or blended with other natural polymers in the food, pharmaceutical, textile, agriculture, water treatment, and cosmetics industries.[110] Since chitosan has a wide spectrum of activity and high killing rate against Gram-positive and Gram-negative bacteria,[111] chitosan and its derivatives have also been applied to polyurethane surfaces with antibacterial properties. Different mechanisms of antibacterial action of chitosan have been proposed, but the exact mechanism is still unknown. One explanation on the mechanism of antibacterial action of chitosan can be given as the strong interaction between positively charged chitosan molecules and negatively charged microbial cell membranes causing the leakage of proteinaceous and other intracellular constituents out of the cell membrane.[110,112]

Antibacterial activity of chitosan can be applied on polyurethane surfaces in different ways. Chitosan can be tethered on polyurethane surfaces by covalent immobilization. Kara et al.[113] synthesized polyurethane by a condensation reaction of toluene diisocyanate and polypropylene ethylene glycol, and the polyurethane film surfaces were modified with different concentrations of chitosan. The modified polyurethane surfaces were more hydrophilic and rough and had strong antibacterial activity against *S. aureus* and *P. aeruginosa*. Chitosan can be blended with other polymers as the coating applied onto polyurethane surfaces. Yang et al.[114] reported on a four-step surface modification method to create a thin lubricious layer of chitosan/poly(vinyl alcohol) hydrogel on the polyurethane catheter. Modification steps included oxidation of the polyurethane surface, functionalities modification, carbodiimide reaction and coupling, and hydrogel cross-linking. The coated polyurethane catheter surface possessed significantly better antibacterial effects against *S. aureus, P. aeruginosa,* and *E. coli*. Chitosan can act as an adsorbent to anionic antimicrobial drugs, and then slowly release the drugs to achieve antimicrobial and biofilm-controlling effects for weeks.[115] In a chitosan-based rechargeable system chitosan was first immobilized on methacrylic acid-grafted polyurethane surfaces, and then strongly bound anionic antibiotics (e.g., rifampin) and slowly released the drugs. The extraordinary advantage of this system is that the released drugs could be recharged to further extend antimicrobial duration. In the recharging process, rifampin could be replaced with other classes of antibiotics such as ciprofloxacin to achieve sustained and rechargeable drug release, providing a great potential application of a new system in controlling device-related biofilm formation.[116]

9.3.2   Biocide-releasing polyurethanes

Contact biocidal biomaterial surfaces kill bacteria on contact as the bactericidal agents are not released and are active following direct interaction with the bacterial cells.[117] Acting through direct contact with bacteria, however, these bioactive surfaces can

potentially be masked and inactivated when surfaces are coated with a film, for example, proteins, in physiological fluids. An effective alternative approach for reducing bacterial adhesion is actively releasing antibacterial agents from bulk or surface coating. Such products containing drugs within a medical device represent an emerging new trend in implantable therapeutics. The surface of these medical devices has been designed to release an initial flux of antibacterial agents during the critical short term after implantation (several hours) to inhibit the initial adhesion of bacteria, and biocides are continuously released beyond this short-term period to inhibit/kill bacteria over a longer time period (weeks to months).[118] The primary advantage of delivering antibiotics directly at the site of implantation is that a high local dose can be administered without exceeding the systemic toxicity level of the drug, and enhanced efficacy can be achieved at the implantation site.[119] The design of biocide-releasing polyurethanes can rely on different strategies: incorporating antibacterial agents into bulk materials, tethering the antibiotics on the surface by adsorbing or covalently bonding, polymer coating releasing metal ions (e.g., silver), and polymer coating releasing nitric oxide, all long known as powerful bactericidal molecules.

9.3.2.1   Antibiotic-releasing polyurethanes

Delivering the antibiotic in a controlled manner at the implant is perhaps the most direct approach for improving the efficacy of conventional antibiotics against implant-related infection.[118] The effectiveness of the antibiotic-releasing system is dependent on the release rate and manner of antibiotic, which are affected by the matrix where the antibiotic is loaded. Biocompatible polyurethane devices or polymer coatings that actively release antibiotics have been the first class of local antibiotic delivery systems. Two main strategies for incorporating antibiotics onto polyurethanes have been employed: (1) drug-coating/bonded systems, immobilizing antibiotics to the polyurethane surface via electrostatical charge or covalent bonds; (2) drug impregnation incorporating antimicrobials into the polymer bulk material directly.[120–122]

Antimicrobial-coated/bonded polyurethanes are generally adsorbed with antibiotics by swelling and diffusion[123,124] or via polymer–antibiotic interactions through hydrophilic interaction between noncharged polar groups or by ionic bonds.[125] For example, β-lactam antibiotics (e.g., cefamandole nafate) were bound to a functionalized polyurethane catheter device surface, and the polymer–antibiotic system was able to inhibit bacterial growth up to 7 days.[126] The adsorption amount and the kinetic release of antibiotics depend on the type of the surface–antibiotic interaction. In particular, matrix hydrophilicity, formation of strong ionic bonds, and the existence of spacer between the antibiotic and the matrix bonding site all play important roles in antibiotic adsorption and release. Marconi et al.[125] prepared sulfated ($—O—SO_3H$) polyurethane films for catheter application and two antibiotics, cefamandole and vancomycin, were adsorbed. Greater amounts of antibiotics were observed to be adsorbed on these matrixes due to the particularly strong ionic or hydrophilic bonds formed between polymer and antibiotics. When exhausted, the polymers can be submitted to a second adsorption process to recover the superior antibacterial activity.

Coating/bonding the surface of catheters with antibiotics can be problematic due to the rapid elution of the drug from the surface of the catheter.[127] An alternative approach for incorporating antibiotics to polymers is to have the antibiotic directly added in the polyurethane solution, and impregnated in the bulk of polyurethane biomaterials prior to fabrication. This strategy has allowed incorporation of various antimicrobials to a variety of medical devices with different shapes (e.g., central venous catheters and urinary catheters),[119] antibacterial polyurethane coating,[128] and polyurethane nanocomposites.[129,130] Biodegradable polyurethanes have been investigated as supportive scaffolds for tissue regeneration and new bone formation. The impregnation of antibiotics in these polyurethane scaffolds offers a comparable or better infection control than the traditional nonbiodegradable antibiotic-laden poly(methylmethacrylate) beads. Due to their biodegradable system, polyurethane scaffolds do not require the extra surgical removal step in clinical use.[131,132] With the development of nanotechnology, polyurethanes impregnated with antibiotics can be fabricated to nanofibrous constructs that can be used for wound-dressing materials. Unnithan et al.[133] prepared an antibacterial scaffold by electrospinning of a solution composed of polyurethane, dextran, and ciprofloxacin hydrochloride drug. These nanofiber mats had good biocompatibility and good bactericidal activity against both Gram-positive and Gram-negative bacteria. Sabitha and Rajiv[134] also prepared similar electrospun polyurethane scaffolds incorporated with ampicillin for wound healing and infection control, and the fibers exhibited a good zone of inhibition against Gram-positive *S. aureus* and Gram-negative *Klebsiella pneumoniae*. Analysis showed that weak interactions enable the antibiotic ampicillin sodium salt to migrate to the surface of the fibers, resulting in an initial rapid release of ampicillin on application to a wound and eliminating colonizing bacteria before they proliferate.

The homogeneous distribution of antibiotics in biocidal-releasing polymers dictates the sustained and prolonged release over time and the efficacy of antibiotics in inhibition of bacterial adhesion. Schierholz et al.[135] prepared a series of polyurethanes incorporating different antibiotics (ciprofloxacin, gentamycin, fosfomycin, flucloxacillin) by solvent casting and measured the drug release profile, bacterial colonization, and surface morphological features. They found that the physicochemical similarity of the polymeric material and the antibiotics was important for the homogeneity of polymer–antibiotic combinations. The hydrophilic drug, for example, ciprofloxacin hydrochloride, incorporated into hydrophobic polymers showed a fast initial release rate followed by substantially lower levels of release at extended periods. Conversely, a drug having similar hydrophobicity of polymer, for example, gentamicin and flucloxacillin, was characterized by a more continuous release type of behavior and demonstrated near 100% adhesion inhibition of *S. epidermidis* after 72 h in PBS.[135]

Impregnated polymers with antimicrobials often suffer low drug delivery. Using a pore former is an efficient way to increase release of antibiotics through polymers.[136,137] Pore formers are generally biologically inactive and water-soluble compounds able to form channels inside the polymeric matrix through which the drug can flow more easily. Kwok et al.[138] compared the efficiency of PEG and bovine serum albumin (BSA) as pore former agents in ciprofloxacin-loaded polyurethanes and found that the release of ciprofloxacin was substantially higher in PEG-containing

polymer than BSA-containing polymer. Ciprofloxacin release increased with the load of PEG by creating more interconnected channels to facilitate the process of migration of ciprofloxacin through the void volumes. However, the release behavior of drug in antibiotic-releasing polymer systems is often a high initial burst followed by a greatly reduced long-term rate of release. To achieve more sustained release, as well as zero-order release kinetics, researchers explored a release-controlling coating overlayer and applied it on ciprofloxacin- and PEG-loaded polyurethane, where this additional layer served as a rate-limiting barrier for drug diffusion, thereby reducing the initial burst of antibiotic released and achieving a constant, sustained release of ciprofloxacin for a long period.[139]

Impregnation of antibiotics in polymer can be reached via physical entrapping of drugs into the polymer matrix, and also through polymer–antibiotic interactions. Introduction of functional groups in a polyurethane to establish specific chemical interactions with the antimicrobial molecules can increase the ability of polymers to adsorb antibiotics, thereby obtaining a greater antibiotic matrix affinity and a more controlled drug release.[140] This provides the possibility of keeping an efficacious drug concentration during the entire period of device implantation to prevent biofilm formation. To reduce and control the risk of emergence of drug-resistant strains, multiple antibiotics having different mechanisms of actions can be loaded onto functionalized polyurethanes. Ruggeri et al.[141] developed polyurethanes with different functional groups on the side chains and two antibiotics, cefamandole nafate and rifampin, were loaded. PEG was used as the pore former in the polymer bulk. The controlled release of drug can last a long time (e.g., 23 days); furthermore, the presence of two antibiotics exerted a synergistic effect on bacterial growth and controlled the emergence of antibiotic resistance of bacteria.

9.3.2.2 Silver- and metal-containing polyurethanes

Metal- and silver ion-containing polyurethanes

Metal-containing polymers represent a broad classification of polymers having inorganic salt groups attached to the polymer chain and improvement of some typically desired functional properties such as mechanical, hydrophilic, conductive, or antibacterial. Metal-containing polyurethanes have been synthesized via ionic diols containing metal salts as starting materials, and the metal is firmly incorporated in the backbone of the polymer chain.[142] One group of metal-containing polyurethanes was synthesized by the polyaddition reaction of HMDI or toluene 2,4-diisocyanate with 1:1 mixtures of divalent metal salts of mono(hydroxypentyl)phthalate (Ca^{2+}, Cd^{2+}, Pb^{2+}, Zn^{2+}). All these metal-containing polyurethanes exhibited antibacterial activity.[143,144] In fact, the antimicrobial activity of silver, as well as copper and other metal ions, has been well known for centuries. It is very advantageous that silver is the element with the highest toxicity for microorganisms, followed by $Hg > Cu > Cd > Cr > Pb > Co > Au > Zn > Fe > Mn > Mo > Sn$, as silver has the least toxicity for animal cells.[145] Recently developed novel antibiofilm agents, gallium (Ga) or zinc (Zn) complexed with protoporphyrin IX or mesoprotoporphyrin IX, show efficacy as metal complexes in negating suspended bacterial growth and biofilm formation.[146] Poly(ether urethane) (PEU)

polymer films were fabricated for the controlled sustained release of the Ga or Zn complexes using PEG as an incorporated pore-forming agent. These chelated gallium or zinc complexes act as iron siderophore analogs, supplanting the natural iron uptake of most bacteria, and the drug-loaded polyurethane films exhibited *in vitro* ≥90% reduction of *S. epidermidis* and *P. aeruginosa* bacteria in both suspended and biofilm cultures versus the negative control PEU films releasing nothing.

Being relatively nontoxic to human cells, silver possesses extraordinary antibacterial properties for a broad spectrum of bacterial strains that are found in industrial processes as well as in the human body.[147] The silver ions released from silver-containing surfaces interact with sulfhydryl groups or thiol groups (—SH) on the membranes of bacteria, causing disruption of their permeability and thereby leading to microbial cell death. It is known that silver ions react with the negatively charged nitrogen, oxygen, or sulfur atoms present in the bacteria as phosphate, amino, carboxyl, and thiol groups in the cellular proteins and DNA, inducing hydroxyl radical formation and causing damage of the cellular DNA, thereby inhibiting bacterial replication.[148,149] Silver ions were also reported to block the respiratory chain of microorganisms reversibly in low concentrations and irreversibly in higher concentrations.[145] Because of the mechanism by which silver acts as a biocidal agent, the likelihood of bacteria becoming resistant to silver-based antibiotics is believed to be low.[147] In addition, the minimum concentration of silver ions that is capable of rendering an antimicrobial efficacy can be as low as 0.1 ppb.[150] These characteristics make silver-releasing materials a potential strategy for reducing bacterial activity on a wide range of medical devices.

The antimicrobial property of silver in polymer is related to its form and amount, and the rate that silver is released. As an antimicrobial agent, silver is mainly present in antibacterial polyurethanes in the form of ions or nanoparticles. Silver ion is highly reactive and it binds to tissue proteins and brings structural changes in the bacterial cell wall and nuclear membrane, leading to cell distortion and death.[149] Silver ions can be incorporated into the polyurethane hard segment or soft segment by altering the chemical structure of the diisocyanate, the diol, the soft segment, or the chain extender. Roohpour et al.[151] synthesized a silver-containing polyether–polyurethane via two reaction steps in which polytetramethylene oxide (PTMO) and methylene diphenyl diisocyanate (MDI) were first polymerized and the polymer was then chain-extended with butanediol followed by end capping with silver lactate or silver sulfadiazine. The synthesis was carried out in highly polar solvents (e.g., dimethylformamide and dimethyl sulfoxide) to enhance the solubility of silver salts and the molar ratio of salt and polymer was controlled to avoid cross-linking. The obtained silver-incorporated polyurethane does not have any significant change in mechanical properties but confers significant antibacterial activity. Acharya et al.[152] reported a synthesis of low molecular weight polyurethane incorporated with —SO$_2$ or —COOH functional groups, which were used for metal complexation with silver ions. It was found that the carboxylic acid group imparted a higher degree of hydrophilicity to the polymer surface than the sulfone group and represented a better bactericidal group with complexation of silver ions. Francolini et al.[153] compared the thermal, mechanical, and biological properties of polyurethanes containing Ag(I), Cu(II), Zn(II), Al(III), and Fe(III). Except for the Al-containing polymer, all

the other polymer aniomoners showed satisfactory antimicrobial properties, and the best antibacterial effect was obtained with the silver ion-containing polymer. To enhance the antimicrobial effect and to minimize the emergence of antibiotic resistance, ciprofloxacin was also adsorbed onto the above-noted ionomers. The metal ion-containing polymers loaded with ciprofloxacin possess different mechanisms of antibacterial actions, and a synergistic effect of the antibiotic and silver ions on bacterial growth inhibition was able to inhibit bacterial growth for at least 25 days.

Silver nanoparticle-containing polyurethanes

The use of silver ions as antimicrobial agents is limited due to the solubility of silver ions in biological and environmental media containing Cl^-. The most common form of silver in polyurethanes is nanoparticles. Silver nanoparticles are clusters of silver atoms that range in diameter from 1 to 100 nm, and are attracting interest as antibacterial and antimicrobial agents for applications in medicine.[154,155] Silver nanoparticles dispersed in polymers are much more stable than silver ions in polymer, and often show greater antimicrobial properties compared to other salts due to their extremely large surface area-to-volume ratios. Most importantly, silver nanoparticles and polymer form nanocomposites that largely decrease the cytotoxicity of nanoparticles, but still release ions exhibiting excellent antibacterial activity. The mechanism of antibacterial activity by nanosilver has not been fully elucidated; however, it is well accepted that silver in aqueous solution releases silver ions that are biologically active to bacteria. Nanoparticles can attach to the cell membrane and react with sulfur-containing proteins in the membrane. Nanosilver can also penetrate inside the bacteria and react with phosphorus-containing compounds like DNA. The nanoparticles preferably attack the respiratory chain and cell division, leading to cell death.[149]

Nanotechnology and modern chemistry have been used to establish a variety of well-characterized methods for silver nanoparticle synthesis.[154] The most common preparation method for silver nanoparticles for application in polyurethanes is the reduction of silver salts (e.g., silver nitrate, silver acetate) *ex situ* or *in situ* either using a reducing agent (e.g., sodium borohydride)[156] or using photoreduction via UV light.[157] Since nanoparticles tend to form agglomerates they need to be stabilized. A promising method is the *ex situ* generation of silver nanoparticles in a liquid phase with polymer or surfactants as stabilizing agents. Triebel et al.[158] developed an *ex situ* preparation method for the synthesis of nanoparticles in an invertible polyester. The particles were surrounded by a polyester cage that prevents agglomeration, and the particles were incorporated into polyurethanes with even distribution. The results showed that the composite with the *ex situ* silver nanoparticles exhibits better antimicrobial properties with a higher silver ion release (~two orders of magnitude) than the release from a composite with *in situ* silver nanoparticles obtained by a thermal reduction of silver acetate during melt mixing.

Chemical reduction is the most frequently applied method for the preparation of silver nanoparticles as stable, colloidal dispersions in water or organic solvents. However, a number of alternative "green" chemistry synthesis routes have been reported.[159,160] Inspired by mussel adhesive proteins, a novel functional polyurethane based on hydrolyzable tannins that contain a number of catechol groups was

recently synthesized. The catechol groups could reduce Ag^+ to form Ag^0 for preparing polyurethane/silver nanoparticle composites.[161] Mtimet et al.[162] reported a green synthesis process of silver nanoparticles by microwave irradiation of a silver nitrate aqueous solution in the presence of PEG 2000 without other chemicals. The synthesized Ag nanoparticles bonded to the hydroxyl groups at the chain ends of PEG, which was incorporated into a polyurethane backbone, allowing a good distribution of the metal particles inside the final nanocomposite without aggregation. These silver nanoparticles exhibited biocidal properties against *P. aeruginosa* and *Enterococuss faecalis* in liquid suspension and on the polyurethane surfaces. Some polyurethane anionomers can also reduce silver ions to silver nanoparticles without additional reducing and stabilizing agents. For example, a carboxylate anionic waterborne polyurethane containing *N*-methyl-2-pyrrolidone and trimethylamine can reduce the silver ions by the amine group, and also coordinate silver ions and stabilize silver nanoparticles through carboxylate and nitrogen in the urethane group. The polyurethane–Ag nanocomposites could release silver ions and reduce the bacterial activity 99.99% for *E. coli* and 53.97% for *S. aureus*.[163] Melinte et al.[164] reported a similar synthesis method for obtaining silver–polymer composite materials from a series of polyurethane acrylates, where the carboxyl groups and amino groups were totally/partially ionized, and silver nitrate was *in situ* reduced through an electron transfer reaction. The polymers obtained were uniformly distributed with Ag particles in a polyurethane acrylate film without agglomeration. Such green, one-step synthetic procedures of silver nanoparticles when the polymer acts simultaneously as a reductant and matrix may be recognized as the most sophisticated approaches with a high application potential, especially when a biocompatible polymer is used.[160]

The antibacterial activity of silver nanoparticles is influenced by intrinsic silver nanoparticle features such as size, concentration, chemistry, crystallinity, and capping agents.[155] Silver nanoparticles comprise nano-sized structures formed of silver atoms that are metallically bonded together. The silver ion release from a matrix increases with decreasing diameter of the silver particles only. It was reported that silver ion release at a distinct concentration could be enhanced if nanoparticles instead of microparticles were used because of the much larger specific surface area of the nanoparticles.[165] However, nanoparticles of smaller sizes increase the toxicity to human cells because smaller nanoparticles have the same dimensions as biological molecules (e.g., DNA and proteins, ~2 nm) and may directly interact to damage DNA, denature proteins and enzymes, and produce free radicals.[154] Liu et al.[166] compared the antibacterial activity and cytotoxicity of silver nanoparticles with three different sizes (i.e., 3–4, 5–7, and 10–40 nm) and different concentrations in waterborne polyurethane. The results showed that the nanocomposites with 60 ppm of medium size (5 nm) silver nanoparticles had the best antibacterial activity and biocompatibility. The good dispersion of nanoparticles and delicate nanostructure of polyurethane nanocomposite were believed to contribute to their good biological activity.

Significant progress has been made toward the silver/polyurethane nanomaterials exhibiting broad spectrum biocidal activity toward bacteria, fungi, viruses, and algae. This motivates its wide use in a large number of biomedical and environmental applications. However, the possible impact on the environment and its potential toxicity to

organisms including humans are of concern.[167] Optimization of silver nanoparticle features including size, concentration, shape, and chemistry to the biocompatibility and antibacterial activity still needs *in vivo* and *in vitro* studies.

9.3.2.3   Nitric oxide-releasing polyurethanes

Nitric oxide (NO), a diatomic free radical, naturally produced in the body by endothelial cells, is well known as an antithrombogenic mediator and its continuous release from the surface of endothelial cells effectively prevents the adhesion/activation of platelets on normal blood vessel walls.[168] Hence, materials that release or generate NO locally at the surface to inhibit thrombus formation have been developed with great potential applications in blood-contacting medical devices with improved biocompatibility.[169,170]

Nitric oxide also plays an important role in the immune response as an antimicrobial agent and host defense against pathogenic bacteria. As a free radical, nitric oxide can cross the membranes to enter the microbial cell readily and kill the microbe by directly nitrosating DNA, proteins, and lipids or by combining with reactive oxygen species (e.g., superoxide, peroxide) and oxidizing the same targets.[171,172] Nitric oxide has been identified as a key mediator of biofilm dispersal and provides an unprecedented opportunity for developing novel treatments to induce biofilm dispersal and improved treatment for chronic infection.[173] Nitric oxide is very reactive and has a short lifetime in the order of seconds in the body. Once it enters the body it quickly finds a target. The rapid reduction of microbial loads reduces the pressure for the evolution and spreading of variant bacteria and limits the possibility of promoting nitric oxide-resistant strains.

NO-releasing biomaterials have been developed for antibacterial applications including polymeric materials,[174,175] xerogel,[176,177] sol gel,[178,179] and silica nanoparticles.[180] Two different classes of NO donors, diazeniumdiolates and nitrosothiols, are commonly used. The diazeniumdiolates, also called as NONOates, are synthesized by reaction of amines with NO gas to form relatively stable compounds that spontaneously release NO on contact with bodily fluids.

The *S*-nitrosothiols are generally formed by reaction of nitrous acid with the parent thiol and are reported to require copper-mediated decomposition, reaction with ascorbate, or cleavage by light to release NO.[181] NO donors are incorporated into materials either by blending discrete NO donors within polymeric films or covalently attached to polymer backbones and/or to the inorganic polymeric filler particles that are often employed to enhance the strength of biomedical polymers (e.g., fumed silica or titanium dioxide).[169]

A variety of strategies for synthesizing NO-releasing polyurethanes by diazeniumdiolates NO donors have been reported. Jun et al.[182] synthesized a diazeniumdiolate peptide using standard fluorenylmethoxycarbonyl chemistry from a lysine-containing peptide by reaction with NO, in which the amine groups in lysine residues were converted to diazeniumdiolates and the hydroxyl groups in serine residues are allowed to incorporate the peptide into a polyurethane chain. A polyurethane polymer was obtained by reacting MDI and PTMO and then a combination of BD (1,4-butanediol) and

diazeniumdiolate peptide was added as the chain extender. The obtained polyurethane showed two-phase kinetics of NO release: an initial burst within 48h and a much slower sustained release over 2 months. The platelet adhesion to this NO-releasing polyurethane was dramatically decreased compared to control polyurethane. Reynolds et al.[183] reported two novel strategies for synthesizing stable nitric oxide-releasing polyurethanes with covalently attached diazeniumdiolate groups onto secondary amines in a polymer chain. The first approach was to attach diazeniumdiolate groups to secondary amino nitrogen of alkane diamines inserted within the diol chain extender of a polyurethane material, and the second strategy involved ω-haloalkylating the urethane nitrogens and then displacing the halide from the resulting polymer with a nucleophilic polyamine to form a polyurethane with pendant amino groups suitable for diazeniumdiolation. Both were successful in preparing NO-releasing polyurethanes. The flux of molecular NO from the polyurethane by the former strategy reached levels as high as 19 pmol/cm^2/s with a total recovery of 21 nmol of NO/mg of polyurethane on immersion in physiological buffer, and the released NO flux was at 14 pmol/cm^2/s and a total recovery of 17 nmol/mg from the polyurethanes synthesized by the secondary strategy. Polyurethane films containing polyethyleneimine can also be directly exposed to NO gas to form diazeniumdiolate *in situ* under pressure of 5 atm and in Ar gas environment.[184] The NO release capacity increased with increasing polydimethylsiloxane content in the soft segment of the polyurethane, and the NO releasing rates were maintained above the value of quiescent endothelial cells (0.83 pmol/cm^2/s) for 5–10 days.

NO-releasing polyurethane can also be synthesized from alternative NO donors, *S*-nitrosothiols, which are endogenous compounds involved in NO storage and transport in blood. Coneski and Schoenfisch[185] synthesized a polyurethane incorporating active *S*-nitrosothiol functionalities into hard and soft segment domains using thiol group protection and postpolymerization modification, respectively, and the polyurethanes were capable of releasing NO up to 0.20 μmol/cm^2. The total NO release and release kinetics were affected by the nitrosothiol position in hard and soft segment domains of the polyurethanes. Thiol modification on soft segments was the most promising avenue for NO donor incorporation due to the retention of surface restructuring and microphase separation, and high thiol to nitrosothiol conversion efficiencies related to the solution accessibility of the thiols. The decomposition of *S*-nitrosothiols can be facilitated by copper (II) complex to release NO. Therefore, NO-releasing polyurethanes from *S*-nitrosothiols are often tethered with a copper (II) complex such as copper (II)–cyclen moieties.[186,187] Puiu et al.[188] modified Pellethane® and Tecophilic® polyurethanes via covalently linked cyclen/Cu(II) moieties onto structural polymer backbones. Both derivatized polyurethanes were found to produce NO at levels at or above those of endothelial cells. The promising behaviors in prevention of platelet adhesion and blood coagulation make NO-generating polyurethane materials that are able to be used in a wide variety of long-term biomedical applications such as a coating material for catheters, vascular grafts, and other blood-contacting devices.

Since most uses of NO-releasing polyurethanes are still concentrated on the purpose of resistance to thrombosis, reports of NO-releasing polyurethanes for antibacterial application are few. Seabra et al.[174] reported on the synthesis of NO-releasing polyester for

the coating of a polyurethane intravascular catheter. The catheter coated with polymers was shown to release NO in PBS solution at 37 °C at a rate of 4.6 nmol/cm^2/h in the first 6 h and 0.8 nmol/cm^2/h over the next 12 h, and exerted a potent dose- and time-dependent antimicrobial activity against *S. aureus* and *P. aeruginosa* strains. Heilman et al.[189] synthesized a light-sensitive polyurethane-based composite material entrapped with silica xerogel particles and embedded with the photoactive NO donor manganese nitrosyls. This biocompatible material can readily release NO when exposed to visible light. The polymer film is durable and maintains its NO-releasing capacity for over 3 months of storage and exhibits antibiotic effects against a broad spectrum of bacteria including methicillin-resistant *S. aureus*, *Acinetobacter baumannii*, *P. aureginosa*, and *E. coli*. It is feasible to use these polymer films for the treatment of infected wounds.

9.4 Other strategies of antibacterial polyurethanes and future perspectives

Over the past decades, a number of strategies and products of antibacterial polyurethanes have been developed. In general, antibacterial polyurethanes and surfaces can be broadly classified as antiadhesive polymers and biocidal polymers based on the mechanisms of controlling bacterial adhesion and biofilm formation. However, such classifications might be limited since the polymer surfaces often involve multiple mechanisms of antiadhesion.[190] For example, antibacterial polyurethane surfaces are often modified to be hydrophilic and capable of repelling bacterial cells, and also to inactivate/kill cells that do come into contact with the surface through the release of antibiotics. Such multifunctional antibacterial surfaces greatly increase the antibacterial activity of materials and extend the efficacy of anti-infection properties and increase the biocompatibility. For future developments of antimicrobial polyurethane surfaces, it may be desirable to combine different working mechanisms and to optimize "release-on-demand" systems.

The strategies behind the antibacterial polyurethanes described above are either to reduce the adhesion of bacteria to the surface or to inactivate and destroy them. However, the development of antibacterial technology is not limited to the current strategies. Progress in the knowledge of the molecular mechanisms implicated in the physiology of biofilm formation of bacterial species has recently made new opportunities available to counteract the establishment of bacteria on biomaterial surfaces. These new approaches include enzyme treatment, targeting quorum-sensing, small molecules, and immunotherapy for biofilm treatment.[19,191] A newly purified β-*N*-acetylglucosaminidase, named dispersin B, is an enzyme produced by the Gram-negative periodontal pathogen *Actinobacillus actinomycetemcomitans* that was able to degrade the polysaccharide-based matrix biofilm produced by staphylococci and exhibited broad spectrum activity.[192] As an antibiofilm agent, it was bound to functionalized polyurethane matrices and found to exert hydrolytic activity against the exopolysaccharide matrix produced by staphylococcal strains, demonstrating a highly effective tool for preventing bacterial colonization of medical devices.[193]

The success of dispersin B at clearing established biofilms and preventing formation of these structures *in vitro* suggests that the enzyme could be a promising new treatment for staphylococcal infections on polyurethane-based medical devices.

Bacteria rely on chemical communication or quorum sensing to coordinate activities necessary for their survival in colonies. For example, staphylococci regulate biofilm formation and dispersal using the *agr* quorum-sensing system.[194] Their dependence on quorum sensing has made these signaling systems within bacteria an attractive target for the design of new therapeutic agents.[195] Nowatzki et al.[196] synthesized an ultraviolet-cured polyurethane acrylate polymer composed of salicyl acrylate, which hydrolyzed on exposure to aqueous conditions and released salicylic acid while leaving the polymer backbone intact. The controlled release of salicylic acid from polyurethane films exhibited significant inhibition of biofilm formation. The mechanism of salicylic acid to inhibit biofilm formation is not well understood; however, one proposed explanation is that salicylic acid might interfere with bacterial quorum-sensing signals since salicylic acid acts as a signal molecule involved in systemic acquired resistance against pathogens and suppresses the expression of genes associated with the quorum-sensing autoinducer.[196]

The future of implant surfaces lies in the design and development of a surface that interacts in a specific way to promote the desired processes and to minimize detrimental side effects.[28] Because of the increasing concern on the bacterial resistance to traditional antibiotics, strategies that do not lead to antibiotic resistance strains will be more attractive to scientists and clinicians. The studies of surface topographical modification have demonstrated their important applications for control of the initial bacterial adhesion and future colonization events without causing antibiotic resistances. Furthermore, a combination of the correct topography and surface chemistry may minimize the effects of defects during fabrication, and may be the most successful strategy for controlling the biological responses including bacterial adhesion, protein adsorption, and platelet adhesion as well as blood coagulation. Future work will further characterize such topographies and chemical modifications on a variety of polyurethanes, allowing us to select the features of biocompatibility and specific tissue responses required for the implants.[28]

Small molecules, such as nitric oxide and salicylic acid, have exhibited strong antimicrobial effects and have shown the ability to readily disperse biofilms. An important advantage of these small molecules is that bacteria often do not develop resistance to them. In addition, they are often more biocompatible and also resistant to thrombosis, for example, nitric oxide. It seems that small molecule treatment of bacterial infections with controlled delivery of suitable doses of small molecule (e.g., nitric oxide) is a very desirable goal. Development of nitric oxide- or other small molecule-releasing polyurethanes will provide promising approaches to antibiotic therapies with improved biocompatibility.

Because of the significant impact of biomaterial-induced infections and the loss of efficacy of antibiotic-based conventional therapies, it is imperative that new strategies against bacterial adhesion and biofilm formation on biomaterial surfaces are found. Antibacterial or anti-infection polyurethane biomaterials have been rapidly developed, similar to the most current infection-resistant biomaterial technologies, and their potential in

in vitro or in preclinical models has been recognized; however, the clinical experimental phase is weak. Multicenter clinical trials and appropriately designed and well-structured international registers are needed to obtain reliable comparative data for the development of anti-infection technologies and antibacterial biomaterials.[19,20] Knowledge of the medical devices and their clinical applications will guide future strategies, appropriately and specifically directing the design and selection of anti-infective biomaterials.

Acknowledgment

References

1. Liang SY, Marschall J. Update on emerging infections: news from the Centers for Disease Control and Prevention. Vital signs: central line-associated blood stream infections–United States, 2001, 2008, and 2009. *Ann Emerg Med* 2011;**58**:447–51.
2. Reed D, Kemmerly SA. Infection control and prevention: a review of hospital-acquired infections and the economic implications. *Ochsner J* 2009;**9**:27–31.
3. Donlan RM. Biofilms and device-associated infections. *Emerg Infect Dis* 2001;**7**:277–81.
4. Francolini I, Donelli G. Prevention and control of biofilm-based medical-device-related infections. *FEMS Immunol Med Microbiol* 2010;**59**:227–38. http://dx.doi.org/10.1111/j.1574-695X.2010.00665.x.
5. Zhang L, Gowardman J, Rickard CM. Impact of microbial attachment on intravascular catheter-related infections. *Int J Antimicrob Agents* 2011;**38**:9–15. http://dx.doi.org/10.1016/j.ijantimicag.2011.01.020.
6. Saginur R, StDenis M, Ferris W, Aaron SD, Chan F, Lee C, et al. Multiple combination bactericidal testing of staphylococcal biofilms from implant-associated infections. *Antimicrob Agents Chemother* 2006;**50**:55–61. http://dx.doi.org/10.1128/aac.50.1.55-61.2006.
7. Zdrahala RJ, Zdrahala IJ. Biomedical applications of polyurethanes: a review of past promises, present realities, and a vibrant future. *J Biomater Appl* 1999;**14**:67–90.
8. Xue L, Greisler HP. Biomaterials in the development and future of vascular grafts. *J Vasc Surg* 2003;**37**:472–80.
9. Wang W, Wang C. In: Paulo Davim J, editor. *The design and manufacture of medical devices*. Woodhead Publishing; Cambridge, UK. 2012. p. 115–51.
10. Lopez-Lopez G, Pascual A, Perea EJ. Effect of plastic catheter material on bacterial adherence and viability. *J Med Microbiol* 1991;**34**:349–53. http://dx.doi.org/10.1099/00222615-34-6-349.
11. Maya ID, Weatherspoon J, Young CJ, Barker J, Allon M. Increased risk of infection associated with polyurethane dialysis grafts. *Semin Dial* 2007;**20**:616–20. http://dx.doi.org/10.1111/j.1525-139X.2007.00372.x.
12. Xu L-C, Siedlecki CA. In: Hutmacher DW, Chrzanowski W, editors. *Biointerfaces: where material meets biology*. The Royal Society of Chemistry; 2015. p. 365–98.
13. Donlan RM. Role of biofilms in antimicrobial resistance. *ASAIO J* 2000;**46**:S47–52. http://dx.doi.org/10.1097/00002480-200011000-00037.

14. Stewart PS. Mechanisms of antibiotic resistance in bacterial biofilms. *Int J Med Microbiol* 2002;**292**:107–13.
15. Høiby N, Bjarnsholt T, Givskov M, Molin S, Ciofu O. Antibiotic resistance of bacterial biofilms. *Int J Antimicrob Agents* 2010;**35**:322–32. http://dx.doi.org/10.1016/j.ijantimicag.2009.12.011.
16. Ma H, Bryers JD. Non-invasive determination of conjugative transfer of plasmids bearing antibiotic-resistance genes in biofilm-bound bacteria: effects of substrate loading and antibiotic selection. *Appl Microbiol Biotechnol* 2013;**97**:317–28. http://dx.doi.org/10.1007/s00253-012-4179-9.
17. Klevens RM, Edwards JR, Richards CL, Horan TC, Gaynes RP, Pollock DA, et al. Estimating health care-associated infections and deaths in US hospitals, 2002. *Public Health Rep* 2007;**122**:160–6.
18. Delaviz Y, Santerra JP, Cvitkovitch DG. In: Cooper IR, Barnes L, editors. *Biomaterials and medical device associated infections*. Woodhead Publishing; Cambridge, UK. 2015. p. 223–54.
19. Campoccia D, Montanaro L, Arciola CR. A review of the biomaterials technologies for infection-resistant surfaces. *Biomaterials* 2013;**34**:8533–54. http://dx.doi.org/10.1016/j.biomaterials.2013.07.089.
20. Campoccia D, Montanaro L, Arciola CR. A review of the clinical implications of anti-infective biomaterials and infection-resistant surfaces. *Biomaterials* 2013;**34**:8018–29. http://dx.doi.org/10.1016/j.biomaterials.2013.07.048.
21. Hasan J, Crawford RJ, Ivanova EP. Antibacterial surfaces: the quest for a new generation of biomaterials. *Trends Biotechnol* 2013;**31**(5). http://dx.doi.org/10.1016/j.tibtech.2013.01.017.
22. Hogan S, Stevens NT, Humphreys H, O'Gara JP, O'Neill E. Current and future approaches to the prevention and treatment of staphylococcal medical device-related infections. *Curr Pharm Des* 2015;**21**:100–13.
23. Xu LC, Siedlecki CA. Effects of plasma proteins on *Staphylococcus epidermidis* RP62A adhesion and interaction with platelets on polyurethane biomaterial surfaces. *J Biomater Nanobiotechnol* 2012;**3**:487–98. http://dx.doi.org/10.4236/jbnb.2012.324050.
24. Ostuni E, Chapman RG, Holmlin RE, Takayama S, Whitesides GM. A survey of structure–property relationships of surfaces that resist the adsorption of protein. *Langmuir* 2001;**17**:5605–20. http://dx.doi.org/10.1021/la010384m.
25. Park KD, Kim YS, Han DK, Kim YH, Lee EHB, Suh H, et al. Bacterial adhesion on PEG modified polyurethane surfaces. *Biomaterials* 1998;**19**:851–9.
26. Uyama Y, Kato K, Ikada Y. Grafting/characterization techniques/kinetic modeling. In: Galina H, Ikada Y, Kato K, Kitamaru R, Lechowicz J, Uyama Y, et al., editors. *Advances in polymer science*, vol. 137. Springer Berlin Heidelberg; 1998. p. 1–39. [Chapter 1].
27. Whitehead KA, Colligon J, Verran J. Retention of microbial cells in substratum surface features of micrometer and sub-micrometer dimensions. *Colloids Surf B Biointerfaces* 2005;**41**:129–38. http://dx.doi.org/10.1016/j.colsurfb.2004.11.010.
28. Harvey AG, Hill EW, Bayat A. Designing implant surface topography for improved biocompatibility. *Expert Rev Med Devices* 2013;**10**:257–67. http://dx.doi.org/10.1586/erd.12.82.
29. Luong-Van E, Rodriguez I, Low HY, Elmouelhi N, Lowenhaupt B, Natarajan S, et al. Review: micro- and nanostructured surface engineering for biomedical applications. *J Mater Res* 2013;**28**:165–74. http://dx.doi.org/10.1557/jmr.2012.398.
30. Neoh KG, Shi ZL, Kang ET. In: Moriarty TF, Zaat SAJ, Busscher HJ, editors. *Biomaterials associated infection*. Springer New York; 2013. p. 405–32. [Chapter 16].
31. Alibeik S, Zhu S, Brash JL. Surface modification with PEG and hirudin for protein resistance and thrombin neutralization in blood contact. *Colloids Surf B Biointerfaces* 2010;**81**:389–96.

32. Nagaoka S, Nakao A. Clinical application of antithrombogenic hydrogel with long poly(ethylene oxide) chains. *Biomaterials* 1990;**11**:119–21. http://dx.doi.org/10.1016/0142-9612(90)90126-B.

33. Park JH, Park KD, Bae YH. PDMS-based polyurethanes with MPEG grafts: synthesis, characterization and platelet adhesion study. *Biomaterials* 1999;**20**:943–53. http://dx.doi.org/10.1016/S0142-9612(98)00250-6.

34. Han DK, Park KD, Kim YH. Sulfonated poly(ethylene oxide)-grafted polyurethane copolymer for biomedical applications. *J Biomater Sci Polym Ed* 1998;**9**:163–74.

35. Han DK, Lee NY, Park KD, Kim YH, Ik Cho H, Min BG. Heparin-like anticoagulant activity of sulphonated poly(ethylene oxide) and sulphonated poly(ethylene oxide)-grafted polyurethane. *Biomaterials* 1995;**16**:467–71. http://dx.doi.org/10.1016/0142-9612(95)98819-Z.

36. Freij–Larsson C, Wesslén B. Grafting of polyurethane surfaces with poly(ethylene glycol). *J Appl Polym Sci* 1993;**50**:345–52. http://dx.doi.org/10.1002/app.1993.070500215.

37. Chen H, Hu XY, Zhang YX, Li D, Wu ZK, Zhang T. Effect of chain density and conformation on protein adsorption at PEG-grafted polyurethane surfaces. *Colloids Surf B Biointerfaces* 2008;**61**:237–43. http://dx.doi.org/10.1016/j.colsurfb.2007.08.012.

38. Park KD, Okano T, Nojiri C, Kim SW. Heparin immobilization onto segmented polyurethaneurea surfaces—effect of hydrophilic spacers. *J Biomed Mater Res* 1988;**22**:977–92. http://dx.doi.org/10.1002/jbm.820221103.

39. Stern T, Penhasi A, Cohn D. Derivatization of a new poly(ether urethane amide) containing chemically active sites. *Biomaterials* 1995;**16**:17–23.

40. Han DK, Park KD, Ahn KD, Jeong SY, Kim YH. Preparation and surface characterization of PEO-grafted and heparin-immobilized polyurethanes. *J Biomed Mater Res* 1989;**23**:87–104.

41. Archambault JG, Brash JL. Protein repellent polyurethane-urea surfaces by chemical grafting of hydroxyl-terminated poly(ethylene oxide): effects of protein size and charge. *Colloids Surf B Biointerfaces* 2004;**33**:111–20. http://dx.doi.org/10.1016/j.colsurfb.2003.09.004.

42. Desai NP, Hubbell JA. Solution technique to incorporate polyethylene oxide and other water-soluble polymers into surfaces of polymeric biomaterials. *Biomaterials* 1991;**12**:144–53.

43. Orban JM, Chapman TM, Wagner WR, Jankowski R. Easily grafted polyurethanes with reactive main chain functional groups. Synthesis, characterization, and antithrombogenicity of poly(ethylene glycol)-grafted poly(urethanes). *J Polym Sci A Polym Chem* 1999;**37**:3441–8. http://dx.doi.org/10.1002/(sici)1099-0518(19990901)37:17<3441::aid-pola1>3.0.co;2-y.

44. Park JH, Cho YW, Kwon IC, Jeong SY, Bae YH. Assessment of PEO/PTMO multiblock copolymer/segmented polyurethane blends as coating materials for urinary catheters: in vitro bacterial adhesion and encrustation behavior. *Biomaterials* 2002;**23**:3991–4000.

45. Ayres N. Polymer brushes: applications in biomaterials and nanotechnology. *Polym Chem* 2010;**1**:769–77. http://dx.doi.org/10.1039/b9py00246d.

46. Jin J, Jiang W, Yin J, Ji X, Stagnaro P. Plasma proteins adsorption mechanism on polyethylene-grafted poly(ethylene glycol) surface by quartz crystal microbalance with dissipation. *Langmuir* 2013;**29**:6624–33. http://dx.doi.org/10.1021/la4017239.

47. Mitragotri S, Lahann J. Physical approaches to biomaterial design. *Nat Mater* 2009;**8**:15–23. http://dx.doi.org/10.1038/nmat2344.

48. Scardino AJ, Hudleston D, Peng Z, Paul NA, de Nys R. Biomimetic characterisation of key surface parameters for the development of fouling resistant materials. *Biofouling* 2009;**25**:83–93. http://dx.doi.org/10.1080/08927010802538480.

49. Scardino AJ, Zhang H, Cookson DJ, Lamb RN, de Nys R. The role of nano-roughness in antifouling. *Biofouling* 2009;**25**:757–67. http://dx.doi.org/10.1080/08927010903165936.

50. Barthlott W, Neinhuis C. Purity of the sacred lotus, or escape from contamination in biological surfaces. *Planta* 1997;**202**:1–8. http://dx.doi.org/10.1007/s004250050096.

51. Bhushan B, Jung YC. Natural and biomimetic artificial surfaces for superhydrophobicity, self-cleaning, low adhesion, and drag reduction. *Prog Mater Sci* 2011;**56**. http://dx.doi.org/10.1016/j.pmatsci.2010.04.003. 1-108.

52. Mao Y, Sun Q, Wang X, Ouyang Q, Han L, Jiang L, et al. In vivo nanomechanical imaging of blood-vessel tissues directly in living mammals using atomic force microscopy. *Appl Phys Lett* 2009;**95**. 013704-013703.

53. Weng Y, Chen J, Tu Q, Li Q, Maitz MF, Huang N. Biomimetic modification of metallic cardiovascular biomaterials: from function mimicking to endothelialization in vivo. *Interface Focus* 2012;**2**(3). http://dx.doi.org/10.1098/rsfs.2011.0126.

54. Reddy ST, Chung KK, McDaniel CJ, Darouiche RO, Landman J, Brennan AB. Micropatterned surfaces for reducing the risk of catheter-associated urinary tract infection: an in vitro study on the effect of sharklet micropatterned surfaces to inhibit bacterial colonization and migration of uropathogenic *Escherichia coli*. *J Endourol* 2011;**25**:1547–52. http://dx.doi.org/10.1089/end.2010.0611.

55. Chung KK, Schumacher JF, Sampson EM, Burne RA, Antonelli PJ, Brennan AB. Impact of engineered surface microtopography on biofilm formation of *Staphylococcus aureus*. *Biointerphases* 2007;**2**:89–94. http://dx.doi.org/10.1116/1.2751405.

56. Perera-Costa D, Bruque JM, González-Martín ML, Gómez-García AC, Vadillo-Rodríguez V. Studying the influence of surface topography on bacterial adhesion using spatially organized microtopographic surface patterns. *Langmuir* 2014;**30**:4633–41. http://dx.doi.org/10.1021/la5001057.

57. Zheng J, Song W, Huang H, Chen H. Protein adsorption and cell adhesion on polyurethane/Pluronic® surface with lotus leaf-like topography. *Colloids Surf B Biointerfaces* 2010;**77**:234–9. http://dx.doi.org/10.1016/j.colsurfb.2010.01.032.

58. Yao C, Webster TJ, Hedrick M. Decreased bacteria density on nanostructured polyurethane. *J Biomed Mater Res A* 2014;**102**:1823–8. http://dx.doi.org/10.1002/jbm.a.34856.

59. Xu L-C, Siedlecki CA. Submicron-textured biomaterial surface reduces staphylococcal bacterial adhesion and biofilm formation. *Acta Biomater* 2012;**8**:72–81. http://dx.doi.org/10.1016/j.actbio.2011.08.009.

60. Milner KR, Siedlecki CA, Snyder AJ. Development of novel submicron textured polyether(urethane urea) for decreasing platelet adhesion. *ASAIO J* 2005;**51**:578–84. http://dx.doi.org/10.1097/01.mat.0000171594.44974.89.

61. Milner KR, Snyder AJ, Siedlecki CA. Sub-micron texturing for reducing platelet adhesion to polyurethane biomaterials. *J Biomed Mater Res A* 2006;**76A**:561–70.

62. Clauser J, Gester K, Roggenkamp J, Mager I, Maas J, Jansen SV, et al. Micro-structuring of polycarbonate-urethane surfaces in order to reduce platelet activation and adhesion. *J Biomater Sci Polym Ed* 2014;**25**:504–18. http://dx.doi.org/10.1080/09205063.2013.879561.

63. Anselme K, Davidson P, Popa AM, Giazzon M, Liley M, Ploux L. The interaction of cells and bacteria with surfaces structured at the nanometre scale. *Acta Biomater* 2010;**6**: 3824–46. http://dx.doi.org/10.1016/j.actbio.2010.04.001.

64. Kapur R, Spargo BJ, Chen MS, Calvert JM, Rudolph AS. Fabrication and selective surface modification of 3-dimensionally textured biomedical polymers from etched silicon substrates. *J Biomed Mater Res* 1996;**33**:205–16.

65. Ng JMK, Gitlin I, Stroock AD, Whitesides GM. Components for integrated poly(dimethylsiloxane) microfluidic systems. *Electrophoresis* 2002;**23**:3461–73.

66. Kumar A, Biebuyck HA, Whitesides GM. Patterning self-assembled monolayers – applications in materials science. *Langmuir* 1994;**10**:1498–511.

67. Delamarche E, Schmid H, Michel B, Biebuyck H. Stability of molded polydimethylsiloxane microstructures. *Adv Mater* 1997;**9**:741–6.

68. Dong L, Nypelö T, Österberg M, Laine J, Alava M. Modifying the wettability of surfaces by nanoparticles: experiments and modeling using the Wenzel law. *Langmuir* 2010;**26**:14563–6. http://dx.doi.org/10.1021/la101934t.

69. Xu LC, Siedlecki CA. *Staphylococcus epidermidis* adhesion on hydrophobic and hydrophilic textured biomaterial surfaces. *Biomed Mater* 2014;**9**:035003.

70. Epstein AK, Wong T-S, Belisle RA, Boggs EM, Aizenberg J. Liquid-infused structured surfaces with exceptional anti-biofouling performance. *Proc Natl Acad Sci USA* 2012;**109**:13182–7. http://dx.doi.org/10.1073/pnas.1201973109.

71. Scardino AJ, de Nys R. Mini review: biomimetic models and bioinspired surfaces for fouling control. *Biofouling* 2011;**27**:73–86. http://dx.doi.org/10.1080/08927014.2010.536837.

72. Epstein AK, Hochbaum AI, Kim P, Aizenberg J. Control of bacterial biofilm growth on surfaces by nanostructural mechanics and geometry. *Nanotechnology* 2011;**22**:494007.

73. Chong DST, Lindsey B, Dalby MJ, Gadegaard N, Seifalian AM, Hamilton G. Luminal surface engineering, 'micro and nanopatterning': potential for self endothelialising vascular grafts? *Eur J Vasc Endovasc Surg* 2014;**47**:566–76. http://dx.doi.org/10.1016/j.ejvs.2014.02.007.

74. Xu LC, Soman P, Runt J, Siedlecki CA. Characterization of surface microphase structures of poly(urethane urea) biomaterials by nanoscale indentation with AFM. *J Biomater Sci Polym Ed* 2007;**18**:353–68.

75. Francolini I, Donelli G, Vuotto C, Baroncini FA, Stoodley P, Taresco V, et al. Antifouling polyurethanes to fight device-related staphylococcal infections: synthesis, characterization, and antibiofilm efficacy. *Pathog Dis* 2014;**70**:401–7. http://dx.doi.org/10.1111/2049-632x.12155.

76. Corneillie S, Lan PN, Schacht E, Davies M, Shard A, Green R, et al. Polyethylene glycol-containing polyurethanes for biomedical applications. *Polym Int* 1998;**46**:251–9. http://dx.doi.org/10.1002/(sici)1097-0126(199807)46:3<251::aid-pi6>3.0.co;2-z.

77. Francolini I, Crisante F, Martinelli A, D'Ilario L, Piozzi A. Synthesis of biomimetic segmented polyurethanes as antifouling biomaterials. *Acta Biomater* 2012;**8**:549–58. http://dx.doi.org/10.1016/j.actbio.2011.10.024.

78. Du YJ, Brash JL, McClung G, Berry LR, Klement P, Chan AKC. Protein adsorption on polyurethane catheters modified with a novel antithrombin-heparin covalent complex. *J Biomed Mater Res A* 2007;**80A**:216–25. http://dx.doi.org/10.1002/jbm.a.30977.

79. Aksoy EA, Hasirci V, Hasirci N, Motta A, Fedel M, Migliaresi C. Plasma protein adsorption and platelet adhesion on heparin-immobilized polyurethane films. *J Bioact Compat Polym* 2008;**23**:505–19. http://dx.doi.org/10.1177/0883911508097422.

80. Abdelkefi A, Achour W, Ben Othman T, Ladeb S, Torjman L, Lakhal A, et al. Use of heparin-coated central venous lines to prevent catheter-related bloodstream infection. *J Support Oncol* 2007;**5**:273–8.

81. De Nardo L, Fare S, Di Matteo V, Cipolla E, Saino E, Visai L, et al. New heparinizable modified poly(carbonate urethane) surfaces diminishing bacterial colonization. *J Mater Sci Mater Med* 2007;**18**:2109–15. http://dx.doi.org/10.1007/s10856-007-3083-9. ISSN: 0957-4530.

82. Wang Y, Hong Q, Chen Y, Lian X, Xiong Y. Surface properties of polyurethanes modified by bioactive polysaccharide-based polyelectrolyte multilayers. *Colloids Surf B Biointerfaces* 2012;**100**:77–83. http://dx.doi.org/10.1016/j.colsurfb.2012.05.030.

83. Makal U, Wood L, Ohman DE, Wynne KJ. Polyurethane biocidal polymeric surface modifiers. *Biomaterials* 2006;**27**:1316–26. http://dx.doi.org/10.1016/j.biomaterials.2005.08.038.

84. Li Z, Lee D, Sheng X, Cohen RE, Rubner MF. Two-level antibacterial coating with both release-killing and contact-killing capabilities. *Langmuir* 2006;**22**:9820–3. http://dx.doi.org/10.1021/la0622166.

85. Tiller JC, Liao C-J, Lewis K, Klibanov AM. Designing surfaces that kill bacteria on contact. *Proc Natl Acad Sci USA* 2001;**98**:5981–5. http://dx.doi.org/10.1073/pnas.111143098.

86. Flemming RG, Proctor RA, Cooper SL. Bacterial adhesion to functionalized polyurethanes. *J Biomater Sci Polym Ed* 1999;**10**:679–97.

87. Flemming RG, Capelli CC, Cooper SL, Proctor RA. Bacterial colonization of functionalized polyurethanes. *Biomaterials* 2000;**21**:273–81.

88. Ancelin ML, Vial HJ. Quaternary ammonium compounds efficiently inhibit *Plasmodium falciparum* growth in vitro by impairment of choline transport. *Antimicrob Agents Chemother* 1986;**29**:814–20. http://dx.doi.org/10.1128/aac.29.5.814.

89. Lindstedt M, Allenmark S, Thompson RA, Edebo L. Antimicrobial activity of betaine esters, quaternary ammonium amphiphiles which spontaneously hydrolyze into nontoxic components. *Antimicrob Agents Chemother* 1990;**34**:1949–54. http://dx.doi.org/10.1128/aac.34.10.1949.

90. Yagci MB, Bolca S, Heuts JPA, Ming W, de With G. Antimicrobial polyurethane coatings based on ionic liquid quaternary ammonium compounds. *Prog Org Coat* 2011;**72**:343–7. http://dx.doi.org/10.1016/j.porgcoat.2011.05.006.

91. Nurdin N, Helary G, Sauvet G. Biocidal polymers active by contact. II. Biological evaluation of polyurethane coatings with pendant quaternary ammonium salts. *J Appl Polym Sci* 1993;**50**:663–70. http://dx.doi.org/10.1002/app.1993.070500411.

92. Hazziza-Laskar J, Helary G, Sauvet G. Biocidal polymers active by contact. IV. Polyurethanes based on polysiloxanes with pendant primary alcohols and quaternary ammonium groups. *J Appl Polym Sci* 1995;**58**:77–84. http://dx.doi.org/10.1002/app.1995.070580108.

93. Wang HH, Lin MS. Biocidal polyurethane and its antibacterial properties. *J Polym Res Taiwan* 1998;**5**:177–86. http://dx.doi.org/10.1007/s10965-006-0054-7.

94. Park D, Larson A, Klibanov A, Wang Y. Antiviral and antibacterial polyurethanes of various modalities. *Appl Biochem Biotechnol* 2013;**169**:1134–46. http://dx.doi.org/10.1007/s12010-012-9999-7.

95. Bakhshi H, Yeganeh H, Mehdipour-Ataei S. Synthesis and evaluation of antibacterial polyurethane coatings made from soybean oil functionalized with dimethylphenylammonium iodide and hydroxyl groups. *J Biomed Mater Res A* 2013;**101A**:1599–611. http://dx.doi.org/10.1002/jbm.a.34461.

96. Bakhshi H, Yeganeh H, Mehdipour-Ataei S, Shokrgozar MA, Yari A, Saeedi-Eslami SN. Synthesis and characterization of antibacterial polyurethane coatings from quaternary ammonium salts functionalized soybean oil based polyols. *Mater Sci Eng C* 2013;**33**:153–64. http://dx.doi.org/10.1016/j.msec.2012.08.023.

97. Grapski JA, Cooper SL. Synthesis and characterization of non-leaching biocidal polyurethanes. *Biomaterials* 2001;**22**:2239–46. http://dx.doi.org/10.1016/S0142-9612(00)00412-9.

98. Sriram V, Radhakrishnan G. Novel short-chain crosslinked cationomeric polyurethanes. *Polym Bull* 2005;**55**:165–72. http://dx.doi.org/10.1007/s00289-005-0425-y.

99. Eknoian MW, Worley SD. New *N*-halamine biocidal polymers. *J Bioact Compat Polym* 1998;**13**:303–14. http://dx.doi.org/10.1177/088391159801300405.

100. Hui F, Debiemme-Chouvy C. Antimicrobial *N*-halamine polymers and coatings: a review of their synthesis, characterization, and applications. *Biomacromolecules* 2013;**14**:585–601. http://dx.doi.org/10.1021/bm301980q.

101. Qian L, Sun G. Durable and regenerable antimicrobial textiles: synthesis and applications of 3-methylol-2,2,5,5-tetramethyl-imidazolidin-4-one (MTMIO). *J Appl Polym Sci* 2003;**89**:2418–25. http://dx.doi.org/10.1002/app.12405.

102. Worley SD, Williams DE. Halamine water disinfectants. *Crit Rev Environ Control* 1988;**18**:133–75.

103. Ahmed AE-SI, Hay JN, Bushell ME, Wardell JN, Cavalli G. Biocidal polymers (II): determination of biological activity of novel *N*-halamine biocidal polymers and evaluation for use in water filters. *React Funct Polym* 2008;**68**:1448–58. http://dx.doi.org/10.1016/j.reactfunctpolym.2008.06.021.

104. Grunzinger SJ, Wynne KJ. Polyurethanes from novel 1,3-propyleneoxide co-telechelics having pendant hydantoin and methoxymethyl groups. *Polymer* 2006;**47**:4230–7. http://dx.doi.org/10.1016/j.polymer.2006.03.082.

105. Grunzinger SJ, Kurt P, Brunson KM, Wood L, Ohman DE, Wynne KJ. Biocidal activity of hydantoin-containing polyurethane polymeric surface modifiers. *Polymer* 2007;**48**: 4653–62. http://dx.doi.org/10.1016/j.polymer.2007.06.010.

106. Sun XB, Cao ZB, Porteous N, Sun YY. Amine, melamine, and amide *N*-halamines as antimicrobial additives for polymers. *Ind Eng Chem Res* 2010;**49**:11206–13. http://dx.doi.org/10.1021/ie101519u.

107. Bisquera WSFC. Regenerable antimicrobial polyurethane coating based on N-hydroxymethylated hydantoin. *Philipp J Sci* 2011;**140**:207–19.

108. Worley SD, Li F, Wu R, Kim J, Wei CI, Williams JF, et al. A novel *N*-halamine monomer for preparing biocidal polyurethane coatings. *Surf Coat Int B Coat Trans* 2003;**86**:273–7. http://dx.doi.org/10.1007/bf02699499.

109. Sun XB, Cao ZB, Porteous N, Sun YY. An *N*-halamine-based rechargeable antimicrobial and biofilm controlling polyurethane. *Acta Biomater* 2012;**8**:1498–506. http://dx.doi.org/10.1016/j.actbio.2011.12.027.

110. Kong M, Chen XG, Xing K, Park HJ. Antimicrobial properties of chitosan and mode of action: a state of the art review. *Int J Food Microbiol* 2010;**144**:51–63. http://dx.doi.org/10.1016/j.ijfoodmicro.2010.09.012.

111. Nigmatullin R, Konovalova V, Pobigay G. Development of antimicrobial membranes via the surface tethering of chitosan. *J Appl Polym Sci* 2009;**111**:1697–705. http://dx.doi.org/10.1002/app.29135.

112. Zheng L-Y, Zhu J-F. Study on antimicrobial activity of chitosan with different molecular weights. *Carbohydr Polym* 2003;**54**:527–30. http://dx.doi.org/10.1016/ j.carbpol.2003.07.009.

113. Kara F, Aksoy EA, Yuksekdag Z, Hasirci N, Aksoy S. Synthesis and surface modification of polyurethanes with chitosan for antibacterial properties. *Carbohydr Polym* 2014;**112**:39–47. http://dx.doi.org/10.1016/j.carbpol.2014.05.019.

114. Yang S-H, Lee Y-SJ, Lin F-H, Yang J-M, Chen K-S. Chitosan/poly(vinyl alcohol) blending hydrogel coating improves the surface characteristics of segmented polyurethane urethral catheters. *J Biomed Mater Res B Appl Biomater* 2007;**83B**:304–13. http://dx.doi.org/10.1002/jbm.b.30796.

115. Cao Z, Sun Y. Chitosan-based rechargeable long-term antimicrobial and biofilm-controlling systems. *J Biomed Mater Res A* 2009;**89**:960–7.

116. Lv W, Luo J, Deng Y, Sun Y. Biomaterials immobilized with chitosan for rechargeable antimicrobial drug delivery. *J Biomed Mater Res A* 2013;**101A**:447–55. http://dx.doi.org/10.1002/jbm.a.34350.

117. Williams JF, Worley SD. Infection-resistant nonleachable materials for urologic devices. *J Endourol* 2000;**14**:395–400.

118. Hetrick EM, Schoenfisch MH. Reducing implant-related infections: active release strategies. *Chem Soc Rev* 2006;**35**:780–9.
119. Wu P, Grainger DW. Drug/device combinations for local drug therapies and infection prophylaxis. *Biomaterials* 2006;**27**:2450–67. http://dx.doi.org/10.1016/j.biomaterials.2005.11.031.
120. Golomb G, Shpigelman A. Prevention of bacterial colonization on polyurethane in vitro by incorporated antibacterial agent. *J Biomed Mater Res* 1991;**25**:937–52. http://dx.doi.org/10.1002/jbm.820250803.
121. Bach A, Bohrer H, Motsch J, Martin E, Geiss HK, Sonntag HG. Prevention of bacterial colonization of intravenous catheters by antiseptic impregnation of polyurethane polymers. *J Antimicrob Chemother* 1994;**33**:969–78.
122. Jansen B, Schareina S, Treitz U, Peters G, Schumacher-Perdreau F, Pulverer G. In: Gebelein CG, Dunn RL, editors. *Progress in biomedical polymers*. US: Springer; 1990. p. 347–54. [Chapter 34].
123. Arora N, Ali A, Sen S, Jana NK, Basak P. Synthesis and characterization of polyether urethane coatings for preventing implant infection. *Compos Interfaces* 2013;**21**:51–8. http://dx.doi.org/10.1080/15685543.2013.831276.
124. Basak P, Adhikari B, Banerjee I, Maiti TK. Sustained release of antibiotic from polyurethane coated implant materials. *J Mater Sci Mater Med* 2009;**20**:213–21. http://dx.doi.org/10.1007/s10856-008-3521-3.
125. Marconi W, Francolini I, Piozzi A, Rosa RD. Antibiotic releasing urethane polymers for prevention of catheter related infections. *J Bioact Compat Polym* 2001;**16**:393–407. http://dx.doi.org/10.1106/g5eb-ll73-k59a-7ybf.
126. Donelli G, Francolini I, Piozzi A, Di Rosa R, Marconi W. New polymer-antibiotic systems to inhibit bacterial biofilm formation: a suitable approach to prevent central venous catheter-associated infections. *J Chemother* 2002;**14**:501–7.
127. Pai MP, Pendland SL, Danziger LH. Antimicrobial-coated/bonded and -impregnated intravascular catheters. *Ann Pharmacother* 2001;**35**:1255–63.
128. Akbarian M, Olya ME, Ataeefard M, Mahdavian M. The influence of nanosilver on thermal and antibacterial properties of a waterborne polyurethane coating. *Prog Org Coat* 2012;**75**:344–8. http://dx.doi.org/10.1016/j.porgcoat.2012.07.017.
129. Fong N, Poole-Warren LA, Simmons A. Development of sustained-release antibacterial urinary biomaterials through using an antimicrobial as an organic modifier in polyurethane nanocomposites. *J Biomed Mater Res B Appl Biomater* 2013;**101B**:310–9. http://dx.doi.org/10.1002/jbm.b.32841.
130. Fong N, Simmons A, Poole-Warren LA. Antibacterial polyurethane nanocomposites using chlorhexidine diacetate as an organic modifier. *Acta Biomater* 2010;**6**:2554–61. http://dx.doi.org/10.1016/j.actbio.2010.01.005.
131. Hafeman AE, Zienkiewicz KJ, Carney E, Litzner B, Stratton C, Wenke JC, et al. Local delivery of tobramycin from injectable biodegradable polyurethane scaffolds. *J Biomater Sci Polym Ed* 2010;**21**:95–112.
132. Li B, Brown KV, Wenke JC, Guelcher SA. Sustained release of vancomycin from polyurethane scaffolds inhibits infection of bone wounds in a rat femoral segmental defect model. *J Control Release* 2010;**145**:221–30. http://dx.doi.org/10.1016/j.jconrel.2010.04.002.
133. Unnithan AR, Barakat NAM, Tirupathi Pichiah PB, Gnanasekaran G, Nirmala R, Cha Y-S, et al. Wound-dressing materials with antibacterial activity from electrospun polyurethane–dextran nanofiber mats containing ciprofloxacin HCl. *Carbohydr Polym* 2012;**90**:1786–93. http://dx.doi.org/10.1016/j.carbpol.2012.07.071.

134. Sabitha M, Rajiv S. Preparation and characterization of ampicillin-incorporated elec-trospun polyurethane scaffolds for wound healing and infection control. *Polym Eng Sci* 2015;**55**:(3):541–48. http://dx.doi.org/10.1002/pen.23917. n/a-n/a.

135. Schierholz JM, Steinhauser H, Rump AFE, Berkels R, Pulverer G. Controlled release of antibiotics from biomedical polyurethanes: morphological and structural features. *Bioma-terials* 1997;**18**:839–44. http://dx.doi.org/10.1016/S0142-9612(96)00199-8.

136. Kim J-E, Kim S-R, Lee S-H, Lee C-H, Kim D-D. The effect of pore formers on the con-trolled release of cefadroxil from a polyurethane matrix. *Int J Pharm* 2000;**201**:29–36. http://dx.doi.org/10.1016/S0378-5173(00)00388-4.

137. Meier MM, Kanis LA, Soldi V. Characterization and drug-permeation profiles of micro-porous and dense cellulose acetate membranes: influence of plasticizer and pore forming agent. *Int J Pharm* 2004;**278**:99–110. http://dx.doi.org/10.1016/j.ijpharm.2004.03.005.

138. Kwok CS, Wan C, Hendricks S, Bryers JD, Horbett TA, Ratner BD. Design of infec-tion-resistant antibiotic-releasing polymers: I. Fabrication and formulation. *J Control Release* 1999;**62**:289–99. http://dx.doi.org/10.1016/S0168-3659(99)00106-6.

139. Kwok CS, Horbett TA, Ratner BD. Design of infection-resistant antibiotic-releasing polymers: II. Controlled release of antibiotics through a plasma-deposited thin film barrier. *J Control Release* 1999;**62**:301–11. http://dx.doi.org/10.1016/S0168-3659(99)00105-4.

140. Piozzi A, Francolini I, Occhiaperti L, Di Rosa R, Ruggeri V, Donelli G. Polyurethanes loaded with antibiotics: influence of polymer-antibiotic interactions on in vitro activity against *Staphylococcus epidermidis*. *J Chemother* 2004;**16**:446–52.

141. Ruggeri V, Francolini I, Donelli G, Piozzi A. Synthesis, characterization, and in vitro activity of antibiotic releasing polyurethanes to prevent bacterial resistance. *J Biomed Mater Res A* 2007;**81A**:287–98. http://dx.doi.org/10.1002/jbm.a.30984.

142. Jayakumar R, Nanjundan S, Prabaharan M. Metal-containing polyurethanes, poly(urethane–urea)s and poly(urethane–ether)s: a review. *React Funct Polym* 2006;**66**:299–314. http://dx.doi.org/10.1016/j.reactfunctpolym.2004.12.008.

143. Jayakumar R, Lee YS, Nanjundan S. Studies on metal-containing copolyurethanes. *React Funct Polym* 2003;**55**:267–76. http://dx.doi.org/10.1016/S1381-5148(03)00017-8.

144. Jayakumar R, Rajkumar M, Nagendran R, Nanjundan S. Synthesis and characteriza-tion of metal-containing polyurethanes with antibacterial activity. *J Appl Polym Sci* 2002;**85**:1194–206. http://dx.doi.org/10.1002/app.10694.

145. Guggenbichler JP, Böswald M, Lugauer S, Krall T. A new technology of microdispersed silver in polyurethane induces antimicrobial activity in central venous catheters. *Infection* 1999;**27**:S16–23. http://dx.doi.org/10.1007/bf02561612.

146. Ma HY, Darmawan ET, Zhang M, Zhang L, Bryers JD. Development of a poly(ether urethane) system for the controlled release of two novel anti-biofilm agents based on gallium or zinc and its efficacy to prevent bacterial biofilm formation. *J Control Release* 2013;**172**:1035–44. http://dx.doi.org/10.1016/j.jconrel.2013.10.005.

147. Clement JL, Jarrett PS. Antibacterial silver. *Met Based Drugs* 1994;**1**:467–82.

148. Gordon O, Vig Slenters T, Brunetto PS, Villaruz AE, Sturdevant DE, Otto M, et al. Silver coordination polymers for prevention of implant infection: thiol interaction, impact on respiratory chain enzymes, and hydroxyl radical induction. *Antimicrob Agents Chemother* 2010;**54**:4208–18.

149. Rai M, Yadav A, Gade A. Silver nanoparticles as a new generation of antimicrobials. *Biotechnol Adv* 2009;**27**:76–83. http://dx.doi.org/10.1016/j.biotechadv.2008.09.002.

150. Kumar R, Münstedt H. Silver ion release from antimicrobial polyamide/silver composites. *Biomaterials* 2005;**26**:2081–8. http://dx.doi.org/10.1016/j.biomaterials.2004.05.030.

151. Roohpour N, Moshaverinia A, Wasikiewicz JM, Paul D, Wilks M, Millar M, et al. Development of bacterially resistant polyurethane for coating medical devices. *Biomed Mater* 2012;**7**. http://dx.doi.org/10.1088/1748-6041/7/1/015007.

152. Acharya V, Ratna Prabha C, Narayanamurthy C. Synthesis of metal incorporated low molecular weight polyurethanes from novel aromatic diols, their characterization and bactericidal properties. *Biomaterials* 2004;**25**:4555–62. http://dx.doi.org/10.1016/j.biomaterials.2003.11.044.

153. Francolini I, D'Ilario L, Guaglianone E, Donelli G, Martinelli A, Piozzi A. Polyurethane anionomers containing metal ions with antimicrobial properties: thermal, mechanical and biological characterization. *Acta Biomater* 2010;**6**:3482–90. http://dx.doi.org/10.1016/j.actbio.2010.03.042.

154. Chaloupka K, Malam Y, Seifalian AM. Nanosilver as a new generation of nanoproduct in biomedical applications. *Trends Biotechnol* 2010;**28**:580–8. http://dx.doi.org/10.1016/j.tibtech.2010.07.006.

155. Marambio-Jones C, Hoek EV. A review of the antibacterial effects of silver nanomaterials and potential implications for human health and the environment. *J Nanopart Res* 2010;**12**:1531–51. http://dx.doi.org/10.1007/s11051-010-9900-y.

156. Wu C-I, Huang J-W, Wen Y-L, Wen S-B, Shen Y-H, Yeh M-Y. Preparation of antibacterial waterborne polyurethane/silver nanocomposite. *J Chin Chem Soc* 2009;**56**:1231–5. http://dx.doi.org/10.1002/jccs.200900177.

157. Saez S, Fasciani C, Stamplecoskie K, Gagnon LBP, Mah T-F, Marin ML, et al. Photochemical synthesis of biocompatible and antibacterial silver nanoparticles embedded within polyurethane polymers. *Photochem Photobiol Sci* 2015;**14**(4). http://dx.doi.org/10.1039/c4pp00404c. in publishing.

158. Triebel C, Vasylyev S, Damm C, Stara H, Ozpnar C, Hausmann S, et al. Polyurethane/silver-nanocomposites with enhanced silver ion release using multifunctional invertible polyesters. *J Mater Chem* 2011;**21**:4377–83. http://dx.doi.org/10.1039/c0jm03487h.

159. Sharma VK, Yngard RA, Lin Y. Silver nanoparticles: green synthesis and their antimicrobial activities. *Adv Colloid Interface Sci* 2009;**145**:83–96. http://dx.doi.org/10.1016/j.cis.2008.09.002.

160. Dallas P, Sharma VK, Zboril R. Silver polymeric nanocomposites as advanced antimicrobial agents: classification, synthetic paths, applications, and perspectives. *Adv Colloid Interface Sci* 2011;**166**:119–35. http://dx.doi.org/10.1016/j.cis.2011.05.008.

161. Chen J, Peng Y, Zheng Z, Sun P, Wang X. Silver-releasing and antibacterial activities of polyphenol-based polyurethanes. *J Appl Polym Sci* 2015;**132**:41349. http://dx.doi.org/10.1002/app.41349. n/a-n/a.

162. Mtimet I, Lecamp L, Kebir N, Burel F, Jouenne T. Green synthesis process of a polyurethane-silver nanocomposite having biocide surfaces. *Polym J* 2012;**44**:1230–7.

163. Wattanodorn Y, Jenkan R, Atorngitjawat P, Wirasate S. Antibacterial anionic waterborne polyurethanes/Ag nanocomposites with enhanced mechanical properties. *Polym Test* 2014;**40**:163–9. http://dx.doi.org/10.1016/j.polymertesting.2014.09.004.

164. Melinte V, Buruiana T, Moraru I, Buruiana E. Silver–polymer composite materials with antibacterial properties. *Dig J Nanomater Bios* 2011;**6**:213–23.

165. Damm C, Münstedt H, Rösch A. The antimicrobial efficacy of polyamide 6/silver-nano- and microcomposites. *Mater Chem Phys* 2008;**108**:61–6. http://dx.doi.org/10.1016/j.matchemphys.2007.09.002.

166. Liu H-L, Dai SA, Fu K-Y, Hsu S-H. Antibacterial properties of silver nanoparticles in three different sizes and their nanocomposites with a new waterborne polyurethane. *Int J Nanomed* 2010;**5**:1017–28. http://dx.doi.org/10.2147/ijn.s14572.

167. Taylor E, Webster TJ. Reducing infections through nanotechnology and nanoparticles. *Int J Nanomed* 2011;**6**:1463–73. http://dx.doi.org/10.2147/ijn.s22021.

168. Radomski MW, Palmer RMJ, Moncada S. The role of nitric oxide and cGMP in platelet adhesion to vascular endothelium. *Biochem Biophys Res Commun* 1987;**148**:1482–9. http://dx.doi.org/10.1016/S0006-291X(87)80299-1.

169. Frost MC, Reynolds MM, Meyerhoff ME. Polymers incorporating nitric oxide releasing/generating substances for improved biocompatibility of blood-contacting medical devices. *Biomaterials* 2005;**26**:1685–93. http://dx.doi.org/10.1016/j.biomaterials.2004.06.006.

170. Reynolds MM, Frost MC, Meyerhoff ME. Nitric oxide-releasing hydrophobic polymers: preparation, characterization, and potential biomedical applications. *Free Radic Biol Med* 2004;**37**:926–36. http://dx.doi.org/10.1016/j.freeradbiomed.2004.06.019.

171. Fang FC. Perspectives series: host/pathogen interactions. Mechanisms of nitric oxide-related antimicrobial activity. *J Clin Invest* 1997;**99**:2818–25.

172. Jones ML, Ganopolsky JG, Labbé A, Wahl C, Prakash S. Antimicrobial properties of nitric oxide and its application in antimicrobial formulations and medical devices. *Appl Microbiol Biotechnol* 2010;**88**:401–7.

173. Barraud N, Kelso MJ, Rice SA, Kjelleberg S. Nitric oxide: a key mediator of biofilm dispersal with applications in infectious diseases. *Curr Pharm Des* 2015;**21**:31–42.

174. Seabra AB, Martins D, Simoes M, da Silva R, Brocchi M, de Oliveira MG. Antibacterial nitric oxide-releasing polyester for the coating of blood-contacting artificial materials. *Artif Organs* 2010;**34**:E204–14. http://dx.doi.org/10.1111/j.1525-1594.2010.00998.x.

175. Park J, Kim J, Singha K, Han D-K, Park H, Kim WJ. Nitric oxide integrated polyethylenimine-based tri-block copolymer for efficient antibacterial activity. *Biomaterials* 2013;**34**:8766–75. http://dx.doi.org/10.1016/j.biomaterials.2013.07.064.

176. Hetrick EM, Schoenfisch MH. Antibacterial nitric oxide-releasing xerogels: cell viability and parallel plate flow cell adhesion studies. *Biomaterials* 2007;**28**:1948–56. http://dx.doi.org/10.1016/j.biomaterials.2007.01.006.

177. Privett BJ, Nutz ST, Schoenfisch MH. Efficacy of surface-generated nitric oxide against *Candida albicans* adhesion and biofilm formation. *Biofouling* 2010;**26**:973–83. http://dx.doi.org/10.1080/08927014.2010.534552.

178. Shin JH, Marxer SM, Schoenfisch MH. Nitric oxide-releasing sol−gel particle/polyurethane glucose biosensors. *Anal Chem* 2004;**76**:4543–9. http://dx.doi.org/10.1021/ac049776z.

179. Marxer SM, Rothrock AR, Nablo BJ, Robbins ME, Schoenfisch MH. Preparation of nitric oxide (NO)-releasing sol−gels for biomaterial applications. *Chem Mater* 2003;**15**:4193–9. http://dx.doi.org/10.1021/cm034347n.

180. Hetrick EM, Shin JH, Stasko NA, Johnson CB, Wespe DA, Holmuhamedov E, et al. Bactericidal efficacy of nitric oxide-releasing silica nanoparticles. *ACS Nano* 2008;**2**:235–46. http://dx.doi.org/10.1021/nn700191f.

181. Varu VN, Tsihlis ND, Kibbe MR. Basic science review: nitric oxide–releasing prosthetic materials. *Vasc Endovasc Surg* 2009;**43**:121–31.

182. Jun H-W, Taite LJ, West JL. Nitric oxide-producing polyurethanes. *Biomacromolecules* 2005;**6**:838–44. http://dx.doi.org/10.1021/bm049419y.

183. Reynolds MM, Hrabie JA, Oh BK, Politis JK, Citro ML, Keefer LK, et al. Nitric oxide releasing polyurethanes with covalently linked diazeniumdiolated secondary amines. *Biomacromolecules* 2006;**7**:987–94. http://dx.doi.org/10.1021/bm060028o.

184. Nguyen EB, Zilla P, Bezuidenhout D. Nitric oxide release from polydimethylsiloxane-based polyurethanes. *J Appl Biomater Funct Mater* 2014;**12**:172–82. http://dx.doi.org/10.5301/jabfm.5000192.

185. Coneski PN, Schoenfisch MH. Synthesis of nitric oxide-releasing polyurethanes with *S*-nitrosothiol-containing hard and soft segments. *Polym Chem* 2011;**2**:906–13. http://dx.doi.org/10.1039/c0py00269k.

186. Hwang S, Meyerhoff ME. Polyurethane with tethered copper(II)-cyclen complex: preparation, characterization and catalytic generation of nitric oxide from *S*-nitrosothiols. *Biomaterials* 2008;**29**:2443–52. http://dx.doi.org/10.1016/j.biomaterials.2008.02.004.

187. Liu K, Meyerhoff ME. Preparation and characterization of an improved Cu^{2+}-cyclen polyurethane material that catalyzes generation of nitric oxide from *S*-nitrosothiols. *J Mater Chem* 2012;**22**:18784–7. http://dx.doi.org/10.1039/c2jm32726k.

188. Puiu SC, Zhou ZR, White CC, Neubauer LJ, Zhang ZF, Lange LE, et al. Metal ion-mediated nitric oxide generation from polyurethanes via covalently linked copper(II)-cyclen moieties. *J Biomed Mater Res B Appl Biomater* 2009;**91B**:203–12. http://dx.doi.org/10.1002/jbm.b.31391.

189. Heilman BJ, Halpenny GM, Mascharak PK. Synthesis, characterization, and light-controlled antibiotic application of a composite material derived from polyurethane and silica xerogel with embedded photoactive manganese nitrosyl. *J Biomed Mater Res B Appl Biomater* 2011;**99B**:328–37. http://dx.doi.org/10.1002/jbm.b.31904.

190. Siedenbiedel F, Tiller JC. Antimicrobial polymers in solution and on surfaces: overview and functional principles. *Polymers* 2012;**4**:46–71.

191. Kiedrowski MR, Horswill AR. New approaches for treating staphylococcal biofilm infections. *Ann NY Acad Sci* 2011;**1241**:104–21. http://dx.doi.org/10.1111/j.1749-6632.2011.06281.x.

192. Kaplan JB, Ragunath C, Velliyagounder K, Fine DH, Ramasubbu N. Enzymatic detachment of *Staphylococcus epidermidis* biofilms. *Antimicrob Agents Chemother* 2004;**48**:2633–6. http://dx.doi.org/10.1128/aac.48.7.2633-2636.2004.

193. Donelli G, Francolini I, Romoli D, Guaglianone E, Piozzi A, Ragunath C, et al. Synergistic activity of dispersin B and cefamandole nafate in inhibition of staphylococcal biofilm growth on polyurethanes. *Antimicrob Agents Chemother* 2007;**51**:2733–40. http://dx.doi.org/10.1128/aac.01249-06.

194. Novick RP, Geisinger E. Quorum sensing in staphylococci. *Annu Rev Genet* 2008;**42**:541–64. http://dx.doi.org/10.1146/annurev.genet.42.110807.091640.

195. Kociolek MG. Quorum-sensing inhibitors and biofilms. *Anti-Infect Agents Med Chem* 2009;**8**:315–26. http://dx.doi.org/10.2174/187152109789760117.

196. Nowatzki PJ, Koepsel RR, Stoodley P, Min K, Harper A, Murata H, et al. Salicylic acid-releasing polyurethane acrylate polymers as anti-biofilm urological catheter coatings. *Acta Biomater* 2012;**8**:1869–80.

Regulating blood cell adhesion via surface modification of polyurethanes

J. Clauser*, K. Gester, U. Steinseifer, S.J. Sonntag
Department of Cardiovascular Engineering, Institute of Applied Medical Engineering,
RWTH Aachen University, Pauwelsstraße 20, Aachen, Germany
*Corresponding author: clauser@ame.rwth-aachen.de

10.1 Introduction

In the development of blood-contacting medical devices the biocompatibility and especially the hemocompatibility are still major challenges. Biocompatibility is defined by Williams as "the ability of a material to perform an appropriate host response in a specific application" [1]. Hemocompatibility as a subcategory of biocompatibility describes all blood–material interactions such as inflammation, platelet activation, and coagulation [2]. A material surface that lacks hemocompatibility can lead to thrombus formation, causing material failure, emboli, or in the worst case the patient's death [3,4]. But as the need for implants, organ-assist devices, and other blood-carrying systems such as artificial heart valves, total artificial hearts, lung-assist devices, blood bags and tubing systems is increasing, new and especially improved medical devices are required. Currently, patients with such devices undergo an anticoagulation therapy, which regulates the risk of thromboembolic events but at the same time raises the severe risk of bleeding [2,5]. Therefore, the improvement of all blood-contacting medical devices regarding hemocompatibility is inevitable for better medical care and higher quality of life for patients.

For achieving this aim, many different approaches are focusing on the modification of polymer surfaces in general and on polyurethane (PU) surfaces in particular. PUs are widely used for biomedical applications as they offer good mechanical properties and a better biocompatibility than other polymers [6–9]. Nevertheless, there is still a huge potential for improving the hemocompatibility of PUs. The modifications of PU surfaces can be roughly divided into chemical and physical methods. The chemical techniques include all modifications of the material's chemistry as, for example, organic and inorganic coatings, biofunctionalization, and biomimetic modification whereas all physical techniques alter only the surface properties and leave the chemistry constant [10,11]. Numerous research groups have tried to improve hemocompatibility physically by implementing surface structures in the micro- and nanometer range using diverse manufacturing methods. Various test setups, test fluids, and analysis methods for different hemocompatibility key factors such as platelet aggregation, platelet adhesion, and clotting times have been used [12–14]. A prominent example is the structured pump housing of the "Heart Mate I" (Thoratec Corp., USA),

a left ventricular-assist device, which was implanted in the early 1990s [15]. Microspheres in the range of 50 μm–75 μm were employed to trigger an encapsulation of the foreign surface with a neointima. But uncontrollable tissue ingrowth especially in the small parts of the device led to thrombotic events and the retraction of the structured pump housing [2,15,16]. This illustrates that surface structuring is a powerful tool for influencing blood cell adhesion, but is still far from being understood and needs to be intensively investigated in the future.

The following sections focus on both the chemical and the physical modification of PUs, summarize the different approaches, and highlight similarities as well as differences. Therefore, a short overview regarding blood–material interactions and the impact on medical devices is given first, followed by an explanation of surface–liquid interactions.

10.2   Blood–material interactions

The coagulation process is divided into the primary hemostasis, also known as cellular coagulation, and the secondary hemostasis, named plasmatic coagulation. The physiological primary hemostasis is initiated as a consequence of tissue injuries directly within the first few minutes (approximately 1–3 min) [17]. At first, the vasoconstriction narrows the blood vessels prior to the injury to reduce the blood flow and therewith the blood loss. Meanwhile, the collagen released by the injured endothelium triggers the platelet adhesion, which is followed by platelet aggregation caused by the von Willebrand Factor (vWF) [17–21]. In the physiological sequence, plasmatic coagulation follows, which leads to the final thrombus formation. This pathway is divided into two different processes as well: the extrinsic and the intrinsic path (see Figure 10.1).

The extrinsic path is a direct consequence of the endothelium injury and is thus initiated by the so-called tissue factor (Factor III). This is followed by the activation of other coagulation factors, such as Factor VII and Factor IX, which are additionally triggered and intensified by calcium (Ca^{2+}), leading to the activation of Factor X. The activated Factor X (Xa), Ca^{2+}, and phospholipids transform prothrombin to thrombin, which initiates the synthesis of fibrinogen to fibrin, amplifies the activation of Factors V, VIII, XI, and XII and furthermore triggers platelet activation and aggregation. Finally, fibrin strengthens the clot of the activated and adhered platelets.

The intrinsic pathway is triggered by protein adsorption on negatively charged surfaces, namely High Molecular Weight Kininogen (HMWK, Factor XIV) in the first instance. Receptors on the platelet membrane recognize the protein adsorption and bind on them, leading to platelet activation and further protein and coagulation factor release, namely Factors XII, XI, and IX. This results in the activation of Factor X as well, leading to thrombin generation and fibrin syntheses. At this point, both the extrinsic and the intrinsic pathways result in a joint final path. Within the physiological case, coagulation is followed by fibrinolysis, the degradation of fibrin, and thus the degradation of the whole thrombus [17,20,22,23].

With regard to the pathological thrombosis, three initiating key factors emerged during the nineteenth and twentieth centuries, nowadays known as the "Virchow triad" (see Figure 10.2). These are abnormalities concerning blood flow, blood constituents, and the blood-contacting surface [24–26].

Extrinsic pathway

Endothelium injury, collagen release

Intrinsic pathway

Protein adsorption on negatively charged surfaces
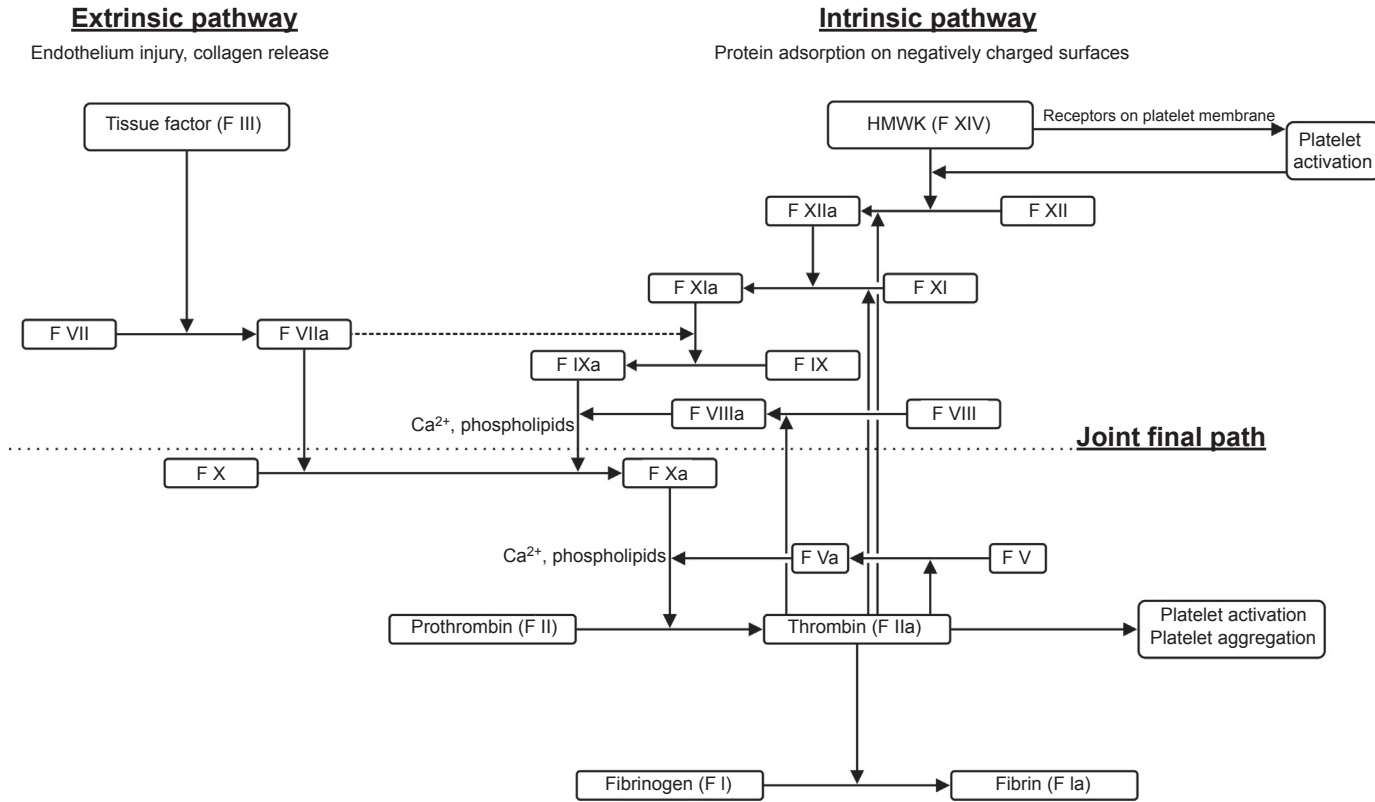
Figure 10.1 Scheme of the plasmatic coagulation cascade.

Abnormalities in the blood flow are possibly areas where the flow converges to zero, which leads to a stagnation of the blood, resulting in platelet activation and clot formation. The same outcome is caused by high shear stresses, namely above 10 Pa, or turbulence in the blood flow [27–31]. During the development of new medical devices these flow-related issues can be analyzed and predicted in advance by means of computational fluid dynamics and fluid structure interaction simulations or particle image velocimetry [32–36]. Virchow's second point is related to an unphysiological hypercoagulability due to illnesses such as hypertension, hemophilia, atrial fibrillation, or coronary artery disease. These risk factors should be treated by modern medicine [31,37,38]. The last point addresses the blood-contacting surface. Normally, blood is only in contact with the endothelium, which is the inner layer of all blood-carrying vessels and organs in the body [23]. But as soon as a foreign material is in contact with the blood stream, a foreign body reaction might be initiated. Triggered by the protein adsorption on the artificial surface, the intrinsic path of the coagulation cascade is activated, finally leading to clot formation on the foreign material [17,18,20,39]. In contrast to the physiological sequence, the pathway does not result in fibrinolysis and clot degradation as long as the foreign material remains in the blood stream and causes a subsequent activation of the coagulation cascade. This bears the severe risk of thromboembolic events possibly leading to implant failure or even the patient's death. This makes the improvement and modification of medically used material surfaces highly desirable [2,40,41].
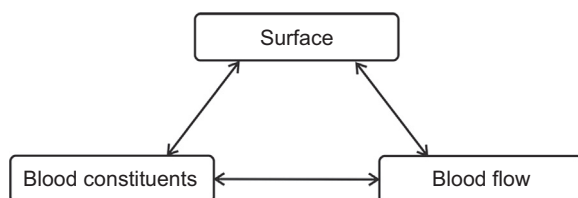
Figure 10.2 Virchow's triad.

10.3 Surface–liquid interactions

The wetting behavior of a liquid at a solid–gas interface is described by the water contact angle θ and can be divided into four different classes (see Figure 10.3) [42].

According to the Young's equation the contact angle can be calculated using the surface tension of the solid (γ_s), the liquid phase (γ_l), and the solid–liquid interfacial energy (γ_{sl}) [43]:

$$\cos \theta_Y = \frac{\gamma_s - \gamma_{sl}}{\gamma_l}$$

The majority of chemical PU modification approaches are aimed at establishing hydrophilic surfaces repelling nonspecific protein adsorption [6,44,45]. The

$\theta < 10°$: Superhydrophilic
$10° < \theta < 90°$: Hydrophilic
$90° < \theta < 150°$: Hydrophobic
$150° < \theta$: Superhydrophobic
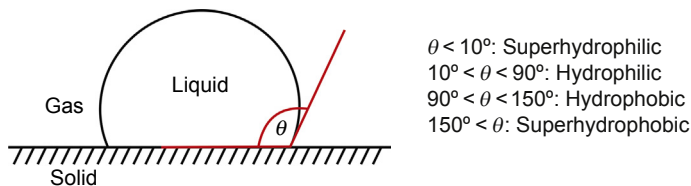
Figure 10.3 Four classes of contact angles.

alternative physical modifications are mostly focused on increasing the hydrophobicity to prevent platelet activation and adhesion on the surfaces [46–50]. If a surface has hydrophilic properties a liquid droplet spreads at the solid interface, wetting a large surface fraction. In contrast, for the hydrophobic case, the droplet remains in its original shape, which leads to a very small contact area at the surface. Both phenomena can be found in nature, especially in flora and fauna. For example, low contact angles are established on the surfaces of Bromeliaceae (e.g., pineapples) or epiphytic growing orchids for the most efficient water and nutrient uptake. Carnivorous plants also have such hydrophilic surfaces for a better insect capturing [42]. A high contact angle can be found on shark skin, reducing the water resistance during movement. The most prominent example for superhydrophobicity in nature is the so-called lotus effect, the self-cleaning and water repelling properties that are achieved by a two-scale surface structure on the lotus leaves (see Figure 10.4). This special structure consists of randomly arranged burling in the range of several micrometers, which are overlaid with a nanometer-scaled hair structure [42,43,51,52].
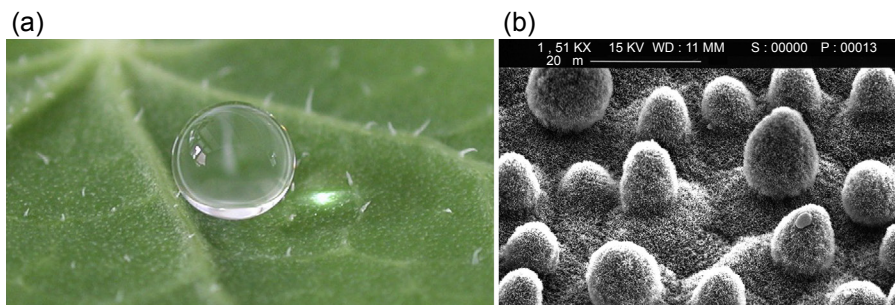
Figure 10.4 (a) Water droplet rolling off the lotus leaf *(reprinted by permission from Macmillan Publishers Ltd. Ref. [53], Copyright © 2003)*. (b) SEM picture of the double-scale structure of the lotus leaf *(reprinted from Ref. [54], with kind permission from Springer Science and Business Media)*.

For this special case of such a rough hydrophobic surface, two different wetting scenarios are reported. One is the homogeneous wetting state, which is described by the Wenzel equation and follows the assumption that all cavities between the rough topography come in contact with the liquid. The other is the heterogeneous wetting

(a)

$$\cos \theta_W = r * \cos \theta_Y$$

r: roughness ratio

(b)

$$\cos \theta_{CB} = r * \cos \theta_Y + f - 1$$

r: roughness ratio of wet area

f: fraction of wet area
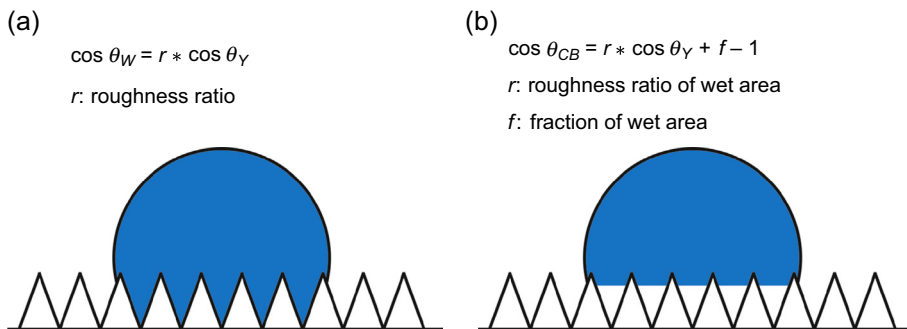
Figure 10.5 (a) Homogeneous wetting according to Wenzel; (b) heterogeneous wetting according to Cassie–Baxter [52].

state, which is described by the Cassie–Baxter equation and is based on air trapping between the liquid and the roughness (see Figure 10.5) [51,52,55].

Which wetting state applies on which surface depends on the free energy of the whole system. Nature always aims to reach the state of the lowest energy. Thus, either homogeneous or heterogeneous wetting fulfills the state of the lowest energy for each individual surface. Some research groups reported that a decrease of the roughness ratio r leads to a switch from Wenzel to Cassie–Baxter mode. The threshold was reported to be 1.7 or even lower. In this wetting scenario, the contact area between liquid and solid is significantly reduced as only the tips of the surface structure are touched by the liquid [51,52,55,56].

All these biomimetic approaches can be transferred to biomedical applications. Using hydrophilic surfaces in contact with blood is aimed at establishing a hydrate layer on the foreign surface, which serves as a barrier for blood protein adsorption. Minimizing or even avoiding any kind of protein adsorption on the surface tremendously inhibits the activation of the intrinsic coagulation pathway and thus the foreign body reaction [2,7,46]. In contrast, superhydrophobic surfaces aim at repelling aqueous-based liquids, including blood and its components as well as proteins enclosed in liquid droplets. As a consequence, neither platelets nor proteins can adsorb on the surface leading to coagulation and clotting on the biomaterial. Additionally, in the case of heterogeneous wetting of the surface the contact area between foreign material and blood is heavily reduced, which further reduces the contact-induced activation of coagulation [46,48,51,52].

10.4   Chemical surface modification

Improving the hemocompatibility of medically used materials via chemical modification techniques means altering the surface of the bulk material by, for example, polymerization, ligand binding, or coating. This is aimed at the development of either a bioinert or a bioactive material [6,8,10,11].

10.4.1 Bioinert polyurethanes

Bioinert materials are materials that do not release any substances that are, for example, toxic or inflammatory and do not trigger a material–tissue interaction. In the case of a blood-contacting foreign material this means that the blood components do not recognize the artificial surface as artificial and thus do not initiate a foreign body reaction [41,57].

For establishing such a bioinert PU surface, the most common technique is the incorporation of poly(ethylene glycol) (PEG) or poly(ethylene glycol) methacrylate (PEGMA). Both materials are known to be hydrophilic and hemocompatible as they avoid protein adsorption due to the formation of a hydrate layer between the material surface and the surrounding medium [6,58]. Furthermore, the hydrophilic properties lead to better endothelial cell (EC) attachment and proliferation in cell culture as it is needed for tissue engineering scaffolds [7,8]. Several research groups investigated the effect of grafting PEG or PEGMA onto PU surfaces, varying the graft ratio and/or molecular weight. Although they used different fabrication processes (e.g., electrospinning, UV polymerization, multistep grafting) and different experimental setups the results were all similar [6–8,58]: The higher the portion of PEG or PEGMA, the lower the contact angle and thus the platelet adhesion. The same relation was found for increasing the molecular weight of PEGMA. The best results according to platelet adhesion in static experiments with platelet-rich plasma (PRP) were achieved with a minimum ratio of PU/PEG and PU/PEGMA. In the case of PU/PEGMA a ratio of 70/30 wt% and a PEGMA molecular weight of 800 g/mol resulted in a greatly decreased amount of adherent platelets, resulting in minimal platelet adhesion on the modified PUs after 4 h incubation (see Figure 10.6). A prolonged activated partial thromboplastin time (aPTT) supports the assumption that PEG or PEGMA respectively leads to a suppression of the intrinsic coagulation cascade by avoiding the protein adsorption on the modified PU surfaces [6–8,58]. As protein adsorption triggers the intrinsic pathway of the coagulation cascade, its suppression leads to a highly hemocompatible foreign surface. These materials performed best in cell attachment and proliferation trials as well, using human umbilical vein endothelial cells (HUVECs) and a cultivation period of up to 14 days. Thus, PEG-modified PUs can also be used for tissue engineering scaffolds [7,8].

Grafting PEG on PU materials is used not only as a modification of the PU surface but also as a priming layer for further coating. By copolymerization of tetrahydroxyl-terminated poly(butadiene-co-acrylonitrile onto PEG-pretreated PU, Luo et al. established a new scaffold material that showed a prolonged prothrombin time (PT) as well as aPTT in static experiments carried out with human PRP [59]. The same experiments revealed less platelet adhesion after incubation for 1 h and 12 h. The adherent platelets showed reduced shape change and pseudopodia formation [59]. Other examples of polymer coatings for PU are the modification with fluorocarbon oligomers, which are highly protein repellent and hemocompatible [60–62] or other hydrophilicity-increasing polymers (e.g., polyethersulfone or poly-(2-hydroxyethyl methacrylate)) [63,64].

Besides polymer coating, the grafting of either zwitterions or betaines has been used for establishing protein-resistant PU surfaces as well. Both molecules have an equal number
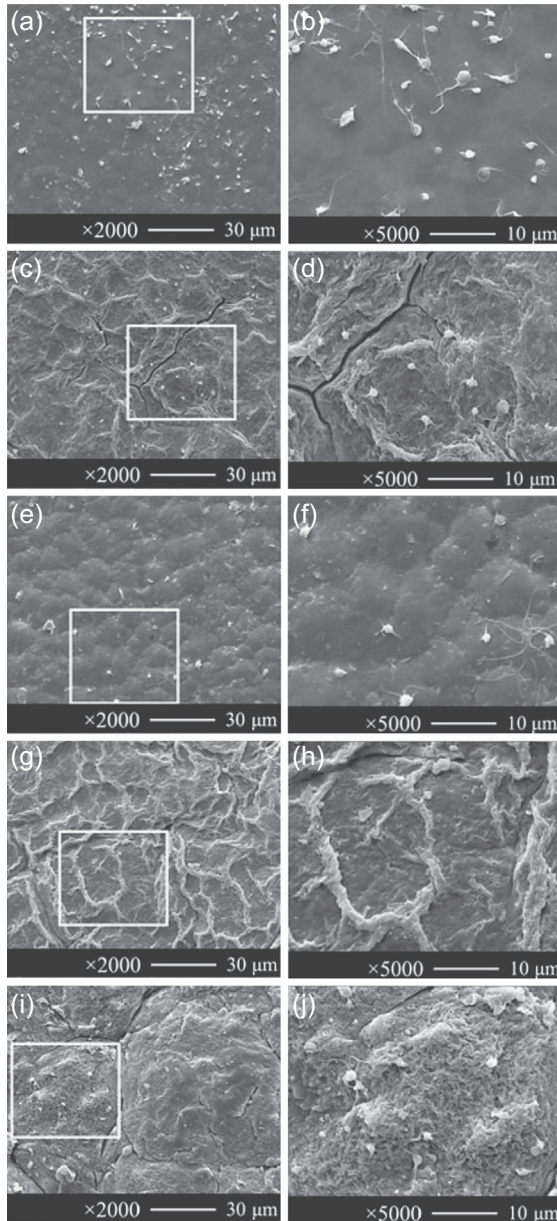
Figure 10.6 SEM pictures after PCU platelet adhesion tests, from left to right: plain PCU, 400 g/mol, 600 g/mol, 800 g/mol, and 1000 g/mol PEGMA.
Reprinted from Ref. [6], with kind permission from Springer Science and Business Media.

of positive and negative charged groups and have a biomembrane-like surface resulting in a high resistance to protein adsorption and platelet adhesion [45,61,65,66]. Phosphorylcholine (PC) is a prominent example for a zwitterionic phospholipid that has been used for PU coating. Several studies revealed that grafting PC results in very low contact angles down to 20° on PU surfaces, accompanied by several other indicators for better hemocompatibility such as reduced fibrinogen adsorption, less platelet adhesion and shape change, and prolonged aPTT and plasma recalcification time (PRT) as well as less P-selectin expression after shear exposure [45,61,65]. All these data indicate improved hemocompatibility due to PU surface modification. Additionally, the grafting of sulfobetaine onto PU surfaces leads to a higher hydrophilicity and thus to longer aPTT and thrombin time (TT), another hint for a suppressed activation of the coagulation cascade [66].

Another method for inhibiting a foreign body reaction between blood and artificial PU surfaces is the application of metal coating. This type of surface modification is already well established for other types of materials such as metals and ceramics. Common coatings are titanium oxide (TiO_x), titanium nitride (TiN), zirconium oxide, or diamond-like carbon (DLC), which are frequently used for VADs, stents, or guidewires [11,67–70]. To apply such coatings to polymeric surfaces several types of laser deposition are used, for example, pulsed laser deposition, plasma-activated chemical vapor deposition, or pulsed laser ablation in liquid [71–73]. These techniques allow the coating of pure and modified titanium (Ti) (e.g., TiN, TiO_x) as well as pure and doped DLC (e.g., doped with silicon (Si), titanium, nitride (N)). Depending on the content of the particular material the results all show reduced platelet activation and aggregation investigated under both static and dynamic conditions. The latter was performed in a cone-and-plate analyzer at a shear rate of $1800 \, s^{-1}$ for 5 min and revealed the best results for TiN and DLC–TiN coatings [72]. Additional cell culture experiments showed an improved EC growth with a confluent cell layer after 7 days successfully preventing platelet adhesion on titanium carboxonitride-modified (Ti(C, N, O)) PU surfaces [71].

A completely different approach was followed by Jia et al. who established fluorinated thermoplastic PUs via a two-step bulk polymerization aiming not at hydrophilic but at hydrophobic surfaces [74]. With an increasing content of fluorine the water contact angle increased, reaching ranges even above 100°. *In vitro* experiments with PRP revealed a decreasing number of adherent platelets and a lower degree of spreading. With a fluorine content of 6 wt% the platelet adhesion could even be as good as completely suppressed [74].

These contradictory approaches and results give a first hint that research is still far from having found "the one and only" surface modification technique for improving PU surfaces and establishing a perfectly hemocompatible biomaterial. A summary of modification techniques aiming at bioinert PU surfaces is shown in Table 10.1.

10.4.2   Bioactive polyurethanes

In contrast to bioinert materials, which are designed to prevent any interaction with the surrounding medium, bioactive materials come in contact with the environment as they trigger a specific material–tissue interaction such as EC proliferation or release drugs such as anticoagulation or anti-inflammatory agents [1,11,75].

Table 10.1 **Chemical modifications for bioinert surfaces**

Modification	Technique	Variation	Target	Testing conditions	Test medium	Result	
PEGMA on PU	UV polymerization	PEGMA molecular weight (400 g/mol–1000 g/mol)	Platelet adhesion	Static, *in vitro*	Rabbit PRP	Higher molecular weight=more hydrophilic; least adhesion with 800 g/mol	[6]
PEGMA on PU	Electrospinning	PU–PEGMA concentration	Cell proliferation	Static cell culture	HUVEC	The more PEGMA the more hydrophilic; best cell proliferation on PU–PEGMA 70/30	[7]
PEG on PU	Electrospinning	PU–PEG concentration	Platelet adhesion; cell proliferation	Static, *in vitro*; static cell culture	Rabbit PRP; HUVEC	Amount of adherent platelets decreases with PEG amount	[8]
PEGMA on PU	Three-step grafting	–	Platelet adhesion; cell proliferation	Static, *in vitro*; static cell culture	Rabbit PRP; HUVEC	Less platelets and better HUVEC proliferation on PU–PEGMA	[58]
THRPBA on PU	Copolymerization	–	Platelet adhesion, coagulation times	Static, *in vitro*	Human PRP	Less platelets on modified PU, prolonged PT and aPTT	[59]
Fluorocarbon oligomers on PU	Grafting	–	Platelet adhesion	Static, *in vitro*	Human PRP	Less adhesion, no aggregation or shape change	[60]
Fluorocarbon and/or phosphorylcholine on PU	Material mixing	Combination of materials	Platelet adhesion; fibrinogen adsorption	Static, *in vitro*	Human PRP; human fibrinogen	Phosphorylcholine most effective against fibrinogen; fluorocarbon more effective against platelets; combination of moth modifications best	[61]

Fluorocarbon into PU	Bulk modification	Chemical compositions	Platelet adhesion	Static, *in vitro*	Rabbit PRP	Less adhesion and spreading on fluorocarbon PU	[62]
Polyethersulfone on PU	Blending	Polyethersulfone concentration	Platelet adhesion; protein adsorption	Static, *in vitro*	Porcine PRP; protein solution	Less fibrinogen and platelet adhesion of modified PU	[63]
PHEMA on PU	Grafting	–	Platelet adhesion	Static, *in vitro*	Human PRP	Lower contact angle and less platelets with less spreading	[64]
Phosphorylcholine on PU	Three-step grafting	Portion of PC	Platelet adhesion, coagulation times	Static, *in vitro*	Rabbit PRP	Reduced adhesion and shape change; 5 % PC showed longer aPTT	[45]
Phosphorylcholine	Dip-coating	–	Fibrinogen and platelet adsorption, coagulation time	Static, *in vitro*	Human PPP and PRP	Contact angle decreased with PC, accordingly less platelets and longer PRT	[65]
			Platelet adhesion, P-selectin expression	Dynamic, *in vitro*	Human whole blood	No platelet adhesion, less P-selectin expression on modified surfaces	
Sulfobetaine on PU	Grafting	–	Coagulation times	Static, *in vitro*	Human blood	Lower contact angle, prolonged aPTT and TT	[66]
Ti, TiN, TiO and DLC modified PU	Pulsed laser deposition	Combination of materials	Platelet adhesion and activation, GPIIb/IIIa	Dynamic, *in vitro*	Human blood	Overall best results on DLC–TiN and TiN	[72]
Ti (C, N, O) on PU	Plasma-activated chemical vapor deposition	–	Cell proliferation	Static and dynamic cell culture	Endothelial cells	Confluent EC layer preventing platelet adhesion, resistant against shear stress	[71]
Fluorinated PU	Two-step Bulk polymerization	Fluorine content	Platelet adhesion and activation	Static, *in vitro*	Human PRP	Increasing content of fluorine = increasing contact angle, decreasing platelet adhesion and shape change	[74]

The field of tissue engineering typically is aimed at encapsulating the foreign material into a layer of native ECs and thus prohibiting a foreign body reaction. Therefore, the PU must be pretreated with some kind of biological or chemical substance allowing cell growth on the PU surface. One possibility is the incorporation of ligands that bind to integrins [76,77]. These are cell receptors that exist in the EC membrane. They bind specifically to molecules, which trigger a cell response like death, differentiation, or attachment, depending on the type of molecule. Those integrins can be separated out of peptide sequences and are, for example, RGD or REDV, both residing in fibronectin. Fibronectin is present in the native endothelium in its insoluble state and regulates cell migration and angiogenesis [76,78–81]. Binding of such ligands can be achieved by introducing several adhesive agents (e.g., carboxyl, hydroxyl, amino, or silane groups), which mediate the peptide binding. As a result, HUVEC cultivation revealed good adhesion with proper cell morphology [76,77].

Another cell type used for enhancing endothelialization of PU scaffolds are fibroblasts [82]. Fibroblasts have a repair function in the endothelium and thus can be bound to ECs [17]. A PU–fibroblast scaffold was seeded with ECs and compared to an autologous homograft, which was treated in the same manner. *In vitro* investigations revealed a confluent and vital EC layer on the tissue engineered PU scaffolds, combined with a decrease of inflammatory cells compared to the homograft [82].

Another chemical approach utilizes gold (Au) or platinum (Pt) nanoparticles or Ti-consisting coatings for triggering the EC adhesion [73,83,84]. Various experiments showed the potential of such coatings, as modified PUs revealed a confluent layer of ECs with proper morphology after both static and dynamic cultivation [73,83]. Additionally, *in vivo* experiments showed an enhanced CD31 expression from PU–Au nanocomposites, which is a key to promoting endothelialization. Furthermore, modified PU catheters had less collagen fibrosis and more newly formed vascular tissue in their surroundings, indicating a high repair potential of the tissue triggered by ECs (see Figure 10.7) [84].

To mimic the native endothelium, nitric oxide (NO) is a suitable substance to be included into a PU coating. One of the key functions of endothelium involves the NO release, as it inhibits thrombus formation and regulates vascular cell proliferation and migration. Therefore, it is often used for thromboresistant coatings on various materials [11,85–87]. Taite et al. combined both effects of NO release and integrin binding on a PU surface with a PEG adhesive layer [85]. As a ligand they used the laminin-derived sequence YIGSR, which is known to improve cell attachment and spreading. Besides static platelet adhesion trials, which proved the NO coating to be antithrombogenic, they investigated the proliferation of ECs as well as smooth muscle cells. The excessive growth of smooth muscle cells is a complication observed especially in small diameter grafts (<6 mm), triggered by platelet adhesion and aggregation and finally leading to the occlusion and thus the failure of the grafts. PU modified with YIGSR and NO at the same time revealed good EC adhesion and proliferation whereas no smooth muscle cell growth was observed [85].
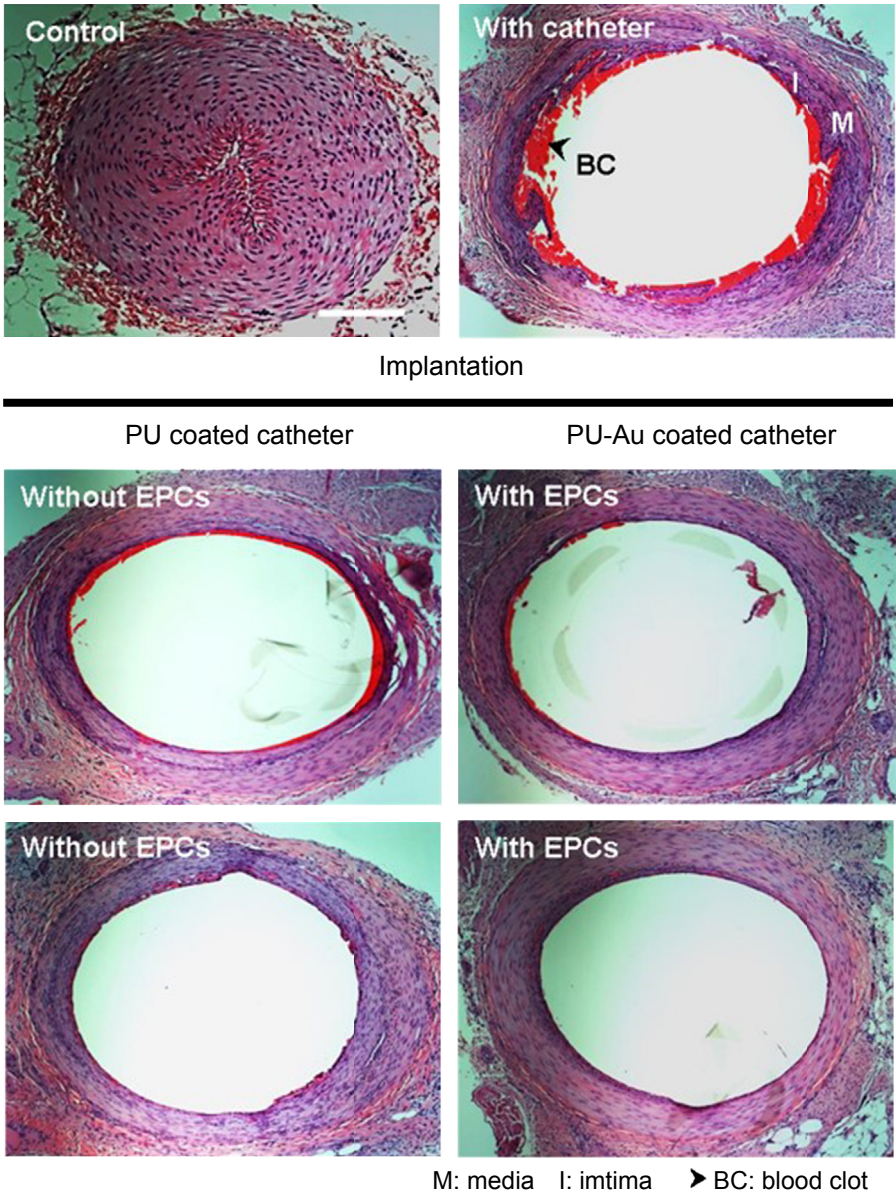
Figure 10.7 Results from the *in vivo* study; catheters with and without bare and Au-modified PU coating.
Reprinted from Ref. [84], Copyright © 2014, with permission from Elsevier.

Embedding antithrombogenicity agents into a PU coating is aimed at suppressing the coagulation cascade by interrupting at a key point. Heparin is a popular anticoagulation agent as it binds specifically via active pentasaccharides to antithrombin (AT), a plasma protein that is originally present in the blood circuit and acts as a natural coagulation antagonist. AT interrupts the coagulation cascade at several points, the most important ones are the inhibition of Factor Xa and thrombin (Section 10.2). If AT is bound to heparin, it undergoes a conformational change that leads to thrombin binding, resulting in the thrombin–antithrombin complex (TAT). This complex dissociates from the heparin, thus allowing new binding of AT and inhibition of thrombin [17,88]. This kind of anticoagulation effect in biomaterials has been achieved by heparin-loaded PU microspheres that can be included in biomaterial coatings [89]. The microspheres manufactured by Tong et al. showed a heparin release of 52 % over a period of 6 days, indicating an anticoagulation activity for more than one week [89]. Furthermore, aPTT, TT, and PT measurements with rabbit blood showed prolonged coagulation times. Additional analyses for complement activation (C3a) and platelet activation (CD62P and CD42) revealed no significant differences compared to control plasma and cytotoxicity testing showed no untoward results [89]. Similar outcomes were observed by Yan et al. who investigated PU-based grafts that were dip-coated with heparin in a 12 month rabbit model *in vivo* [90]. As control, a graft without the heparin coating was implanted as well. Due to the grafts' small diameter of 1.2 mm, the occlusion rate was the main criteria for a successful coating. After 12 months, the heparin-coated PU graft showed no occlusion and thus 100 % patency whereas the bare PU graft had only 83 %. The heparin coating showed a noninflammatory reaction combined with a decrease in smooth muscle cell growth, which also contributes to the lack of occlusion. Furthermore, a uniform coverage of ECs was observed [90].

Although heparin as an anticoagulation coating is widely used, there are some other approaches in trying to avoid its use as it bears some negative aspects. The efficacy of heparin is dependent on the amount of active pentasaccharide sequences as they are the binding site for AT. According to Du et al., commercially available heparin-coated PU catheters exhibited only one-third of active pentasaccharides, thus significantly reducing the anticoagulation effect [91]. In addition to the intended AT binding, there is the possibility of other proteins binding to inactive, negatively charged heparin chains. This scenario is similar to the protein adsorption on a foreign surface and thus may trigger an increased coagulation [92]. Therefore, a different method directly includes AT into a heparin coating (ATH), ensuring effective AT binding and at the same time preventing nonspecific protein adsorption [88,91–93]. *In vitro* experiments revealed good specificity of ATH bound to PU surfaces via a PEG–OH intermediate layer as AT binding was superior to fibrinogen attachment when both proteins were present simultaneously. Comparing different PEG intermediate layers proved that PEG–OH had an amplifying effect on AT binding [88]. Experiments with ECs showed good cell proliferation on ATH-immobilized PU films resulting in a homogenous distributed and a well spread cell layer. Thus, ATH modification to heparinized surfaces

seems to improve the specific anticoagulation effect and at the same time to promote endothelialization [88,93].

Similar results were achieved in *in vivo* rabbit experiments by Du et al. [91,92]. PU catheters either uncoated, heparin-coated, or ATH-coated were inserted into the jugular veins of different animals. Blood was drawn through the catheter into a syringe, held for 2 min, and slowly released again. The experiment was stopped either when releasing the blood was not possible anymore due to clotting or after 4 h. Only the ATH-treated catheters reached the final experiment duration as there was no clotting after 4 h whereas the uncoated catheters clotted after 78 min and the heparin-coated even after 56 min. Further *in vitro* tests showed a lower binding of fibrinogen and its products on the ATH-modified PU surfaces in comparison to good AT adsorption. An anti-FXa assay proved the coating's functionality as there was a high anti-FXa activity measured [91,92].

To avoid all heparin- and AT-related complications, there is also the alternative of incorporating other anticoagulants into PU coatings. One possibility is argatroban, as this is a direct thrombin inhibitor and thus is not dependent on AT binding. Additionally, argatroban is suitable for patients who suffer heparin-induced thrombocytopenia (HIT). Major et al. combined an argatroban coating with a nitric oxide-releasing coating to amplify the anticoagulation and antiplatelet activation effects [94]. A 4 h extracorporeal circulation experiment in rabbits revealed reduced thrombus formation as well as low platelet activation compared to uncoated and only argatroban-coated PU surfaces [94].

Another approach of coating PU surfaces with a physiological substance is the use of hyaluronic acid. Hyaluronic acid is part of the extracellular matrix and, among other functionalities, prevents thrombus formation and triggers angiogenesis. Accordingly, a PU surface modification with hyaluronic acid revealed a decrease in platelet adhesion and protein adsorption and at the same time exhibited better EC growth and proliferation. ECs grew well on hyaluronic acid-modified samples resulting in a viable EC layer [95]. Even better results could be achieved by a hyaluronic acid bulk modification of PU. Those samples were superior to surface-modified PUs in all dynamic experiments aiming at protein adsorption, platelet adhesion, and EC adhesion and proliferation [96].

The above results show how versatile the field of bioactive surface modification of PU is. Many completely different approaches have been tried to reach the same goal by incorporating cells, anticoagulation agents, or nanoparticles into the PU surface. A summary of the different methods and results is given in Table 10.2.

10.5 Physical surface modification

The general aim of physical surface modification is to improve the hemocompatibility of PU biomaterials by establishing a structured surface and at the same time leave the bulk properties untouched. This ensures that the initial hemocompatibility is not changed or negatively influenced [10,97]. The idea of improving the hemocompatibility

Table 10.2 Chemical surface modifications for bioactive surfaces

Modification	Technique	Variation	Target	Testing conditions	Test medium	Result	
REDV peptide sequence on PU	Multistep covalent binding	–	Cell proliferation	Static cell culture	HUVECS	Good spreading and proper morphology	[77]
Fibroblast seeding on PU	Cell seeding	–	Cell proliferation and response	Static cell culture	Endothelial cells	Confluent and vital cell layer, decrease of inflammatory response	[82]
Au and Pt nanoparticles in PU	Pulsed laser ablation in liquid	wt% of Au resp. Pt	Cell proliferation and platelet adhesion	Dynamic cell culture; static *in vitro*	Endothelial cells forming cells, human PRP	Best cell proliferation on 0.1 wt% Au and <0.25 wt% Pt; additionally no platelet adhesion and activation	[73]
Ti(C, N)-layer on PU	Plasma-activated chemical vapor deposition	Type of PU	Cell proliferation and platelet adhesion	Static cell culture; static *in vitro*	Endothelial cells; human PRP	Confluent cell layer, modified PCU nearly no platelet adhesion	[83]
Au nanoparticles in PU + cell seeding	Spin casting	–	CD31 expression, tissue response	*In vitro*; rabbit *in vivo*	Endothelial cells; rabbit tissue	Best *in vitro* cell growth on PU–Au, *in vivo* more endothelialization	[84]
YIGSR integrin + nitric oxide on PU	Polymer synthesis	–	Platelet adhesion; cell growth	Static, *in vitro*	Human blood; endothelial and smooth muscle cells	Nitric oxide release up to 60 days, platelet-resistant, good endothelial cell proliferation, no smooth muscle cell growth	[85]
Heparin-loaded PU microspheres	Single-step phase separation	–	Heparin release, coagulation times, complement activation	Static, *in vitro*	Rabbit blood plasma	52 % Heparin release over 6 days, aPTT, TT, and PT prolonged, no complement activation (CD62P, CD42)	[89]

Heparin on PU	Dip coating	–	Graft occlusion	*In vivo*	Rabbit	Heparin-coated graft no occlusion and good cell coverage, control only 83% patency	[90]
PEG-modified PU with antithrombin–heparin coating	Multistep modification	Different PEG intermediate layers	ATH efficacy	Static, *in vitro*	Human plasma	Good cell proliferation on ATH–PEG–OH–PU, antihrombin binding superior to fibrinogen	[88]
Heparin-coated and antithrombin-heparin coated PU	Copolymerization and covalent linking	–	Catheter clotting during drawing and release	*Ex vivo*	Rabbit	ATH-catheter no clotting during test duration, heparin-coated failed first	[91]
			Fibrinogen bonding, FXa	Static, *in vitro*	Rabbit plasma	Lower fibrinogen binding on ATH-catheters, high anti-FXa activity	[92]
Argatroban + nitric oxide coating on PU	Coating	–	Platelet aggregation and activation	*Ex vivo*	Rabbit	Reduced thrombus formation, low platelet activation	[94]
Hyaluronic acid on PU	Grafting	–	Platelet adhesion, cell behavior	Static, *in vitro*	Bovine serum and cells, human blood	Decreased platelet adhesion and protein adsorption, viable and round-shape cell layer	[95]
Hyaluronic acid into PU	Bulk modification	Bulk versus surface modification	Platelet response, cell proliferation	Dynamic, *in vitro*	Human PRP, endothelial cells	Hyaluronic acid stable in bulk modified PU, better antiplatelet properties, good cell proliferation	[96]

by means of surface structuring is inspired by nature. The earlier discussed lotus effect is a prominent example for the efficacy of superhydrophobic surfaces [42,46]. On the other hand, natural blood vessels exhibit a microgrooved surface parallel to the main blood stream and thus provide rationale for structuring artificial surfaces that contact blood [98].

In contrast to chemical modification techniques, this approach tends to create (super-)hydrophobic surfaces with a reduced direct contact area for proteins and especially platelets [46]. Many research groups have worked on surface structuring of polymers to improve their hemocompatibility. Therefore, many polymeric materials were structured by different techniques producing various geometries and dimensions and investigated using a variety of test setups and conditions [12,14,99,100]. The results of these investigations vary considerably, but in general come to the conclusion that surface topography does influence the platelet adhesion and activation processes. However, the distinct mechanisms and processes which lead to these results are incompletely understood [101,102]. Furthermore, it is unknown whether the platelets are directly influenced by the surface structure or indirectly by altered protein adsorption [103].

10.5.1 Platelet adhesion on structured surfaces

For structuring polymer surfaces, mostly indirect techniques are used. First, a master template is fabricated by, for example, photolithography, soft lithography, stereo lithography, laser ablation, or acid etching for ordered structures or by sandblasting, abrasion, or plasma spraying for random structures [97,101,104–107]. In a following step, a structured polymer film is molded from these templates by, for example, spin casting, dip coating, or hot embossing [14,99,101]. All techniques can be applied to those PUs that are soluble in solvents such as trichloromethane or dimethylacetamide. The same polymers can also be processed at temperatures around 200 °C due to their thermoplastic properties [12,41]. The resulting structures can be either random with a specific roughness or with a distinct geometry such as grooves, pillars, wells, pits, or pyramids with dimension in the micro- or even nanometer range (see Figure 10.8) [106].

Our group investigated grooved PU samples with variations in the mean groove widths of 1.8 μm, 3.4 μm, and 90 μm [12]. The assumption was that structures in the range of the mean platelet diameter (2 μm–3 μm) will reduce the effective adhesion area. As a consequence, the total amount of adherent platelets and the activation state of those platelets that adhere should be reduced as well. Dynamic testing with porcine whole blood revealed a significantly lowered platelet adhesion and activation on 1.8 μm, and 3.4 μm samples, respectively, compared to the 90 μm sample. It appeared that the mean platelet diameter seems to be an upper threshold for improving the hemocompatibility of medically used PUs [12]. Similar results were achieved by, for example, Chen et al. who used the inspiration of the lotus leaf to manufacture an overlaid double structure with ridges (width = 500 nm, height = 40 nm) and protuberances (diameter = 100 nm, height = 40 nm) on the same surface [98]. Although they used polydimethylsiloxane (PDMS) instead of
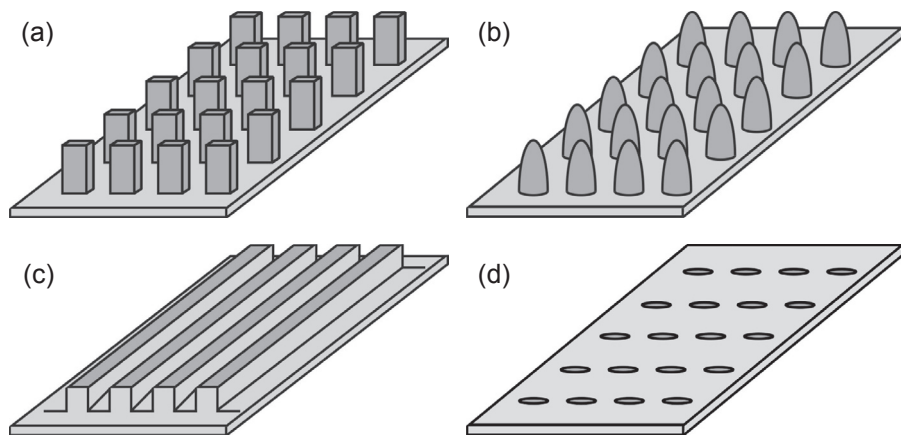
Figure 10.8 Various surface structures: (a) pillars, (b) mastoid, (c) grooves, (d) wells.

PU the results are relevant to PU surfaces as the bulk properties of PU are known to be suitable for biomedical products. The double-structured surfaces resulted in the least amount of activated platelets after dynamic testing. They postulated that an effective structured surface with regard to reduced platelet adhesion should be in the range from 50 nm to 2 μm, which is in agreement with our results regarding the upper threshold. Structures smaller than 50 nm will be considered smooth by platelets and thus will not be effective for improving the hemocompatibility [98]. Milner et al. investigated PU surfaces with nanometer square pillars with diameters and interspacings of 400 nm and 700 nm, respectively. Under different shear rates and compared to flat PU surfaces the structured PU surfaces showed an overall reduced platelet adhesion combined with minimal shape change of the adherent single platelets. Low shear stress smaller than 3.3 dyn/cm² led to actually fewer platelets on the 700 nm samples. Even smaller geometries were investigated by Fan et al. who used structures similar to those of Chen et al., namely protrusions (diameter = 100 nm, height = 10 nm) and interlaced ridges (width of 500 nm, height of 100 nm) on PDMS surfaces. Dynamic experiments with adenosine diphosphate (ADP)-preactivated platelets proved that double-structured surfaces had the least amount of platelet adhesion [97]. Another study of randomly single-structured surfaces in the range of 40 nm–400 nm on PMMA resulted in less platelet adsorption on smaller structures [108]. Comparable results were achieved by dip-coating PU on aligned carbon nanotubes (diameter = 39.7 nm, length = 20 μm). Flat films with a contact angle of 110° had many adherent and activated platelets with pseudopodia on the surface after static PRP testing. In contrast, the structured surfaces with a contact angle of ~160° showed even no adherent platelets (see Figure 10.9) [99]. It appears that a lower threshold of 50 nm is required to suppress platelet adhesion but must be further investigated.

The upper threshold of 2 μm–3 μm was exceeded by several research groups. PU surfaces with fibers of 25 μm base diameter, 100 μm interspacing, and 25 μm, 50 μm, and 100 μm length, respectively, revealed no platelet adhesion in an *ex vivo* ovine shunt
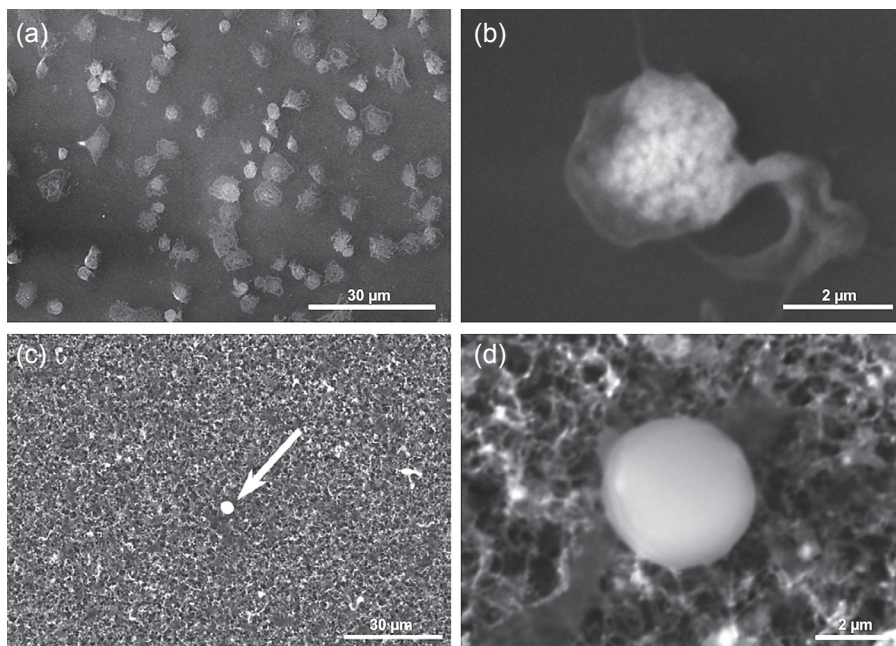
Figure 10.9 Plain (a & b) and structured (c & d) PU after platelet adhesion experiments. Reprinted from Ref. [99], Copyright © 2005, Wiley-VCH Verlag GmbH & Co. KGaA.

model. However, the experiment showed white blood cell adhesion, indicating an activation of the complement system which was inversely related to the wall shear stress [13]. The rabbit heart valve shows a structured surface with cobblestones in the micrometer range combined with small nanometer villus. This structure was partly imitated on PDMS surfaces by introducing a regular mastoid structure with 60 μm in diameter, 30 μm in height, and 40 μm in interspacing. Compared to a smooth PDMS surface with a contact angle of 113°, the structured surface revealed superhydrophobicity with a 163° contact angle. This increase in contact angle led to significantly reduced platelet adhesion in combination with round-shaped platelets without any shape change or pseudopodia formation on contrast to the flat sample (see Figure 10.10). Ye et al. attributed this result to the superhydrophobic properties of the structured surfaces as having a lower surface energy and thereby lower platelet adhesion [49].

To investigate the distinct effect of the interspacing between such structures, pillar geometries with 15 μm in diameter, 5 μm in height with an interspacing varying in 5 μm steps, ranging from 5 μm to 60 μm, were investigated. Those pillars which resulted in the highest contact angle, namely 156° showed the least platelet adhesion. The interspacing was 25 μm, contradictory to the assumption that the effective adhesion area should be beyond the platelet diameter of approximately 3 μm [50]. But at the same time microgrooves with 130 nm depth and several nanometers interspacing were investigated. Although those surfaces had a contact angle of only 120°, the platelet adhesion was lower compared to the best pillar-structured surface [50].
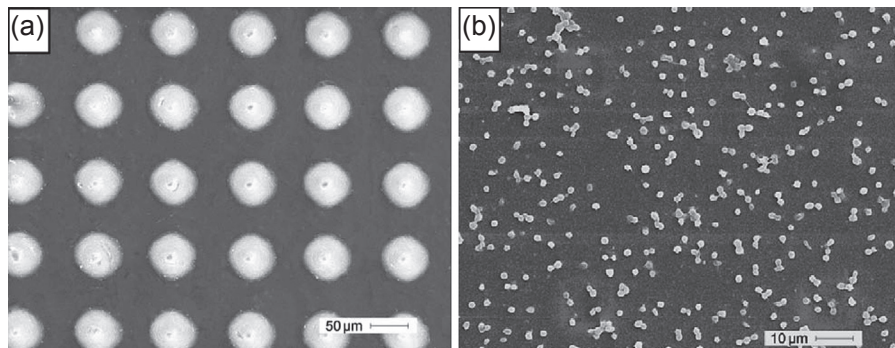
Figure 10.10 Plain (a) and pillar structured (b) PDMS surfaces after platelet adhesion experiments.
Reprinted from Ref. [49], Copyright © 2009 with permission from Elsevier.

These conflicting findings emphasize how diverse the results for improving the hemocompatibility of PU and polymer surfaces in general are. There is no doubt, that surface structuring is a strong tool for making blood-contacting foreign surfaces more hemocompatible, but at the same time it becomes clear that there are still many open questions. The geometry of the most effective structures, their dimensions, and also the kind of testing regarding static or dynamic conditions, the use of PRP or whole blood, etc. require further investigations.

10.5.2 Protein adsorption on structured surfaces

Several groups investigated whether surface structuring influences platelet adhesion directly or indirectly via an influence on protein adsorption. Ten different PUs were preadsorbed either with fibrinogen or with vWF-deficient plasma and then incubated with washed platelets for 90 min under static conditions. The results revealed a high platelet sensitivity for fibrinogen as there was nearly no platelet adhesion on the antifibrinogen surfaces whereas the anti-vWF surfaces showed no change in platelet behavior [100]. Furthermore, no relation between a high contact angle and the amount of adsorbed fibrinogen was found, indicating a direct influence from the surface structure on platelets. Additionally, the amount of adsorbed fibrinogen did not correlate with the amount of adherent platelets, suggesting that, while fibrinogen is the primary platelet adhesion mediator on PU surfaces, the amount is not the determining factor [100]. This assumption is supported by a study taking the conformational change of fibrinogen adsorbed on a foreign surface into account. Incubating self-assembled monolayers of alkanethiols with different concentrations of fibrinogen showed more adsorption with increasing initial concentrations. Inversely, the conformational change in terms of loss of α-helix increased with decreasing concentrations, as the slower adsorption provides more time for an unfolding of the protein. Static platelet adhesion tests showed more adhesion on those surfaces that were preincubated in lower fibrinogen concentrations and thus revealed the importance of protein shape change as indicated by the loss of α-helix. Thus, the amount

of adsorbed fibrinogen is not the determining mediator for platelet adhesion, but its conformational change is [40].

Using this knowledge, studies were performed utilizing structured surfaces that were preadsorbed with fibrinogen and afterward incubated with platelets or whole blood. On PDMS surfaces with regular protrusions of 4 μm diameter, 1 μm height, and 10 μm interspacing most fibrinogen adhesion took place between the protrusions. Compared to flat surfaces the adhesion increased about 46 %, which was inconsistent with the findings from Wu et al. who did not find a correlation between the surface variations and the amount of fibrinogen adsorption [102]. Static experiments with PRP performed on surfaces with and without fibrinogen preadsorption showed that the pattern of platelet adhesion correlated with the prior fibrinogen adhesion, which was highest in the interspace areas. Random platelet adhesion was observed on surfaces without pretreatment (see Figure 10.11). The results were confirmed using a dynamic test setup with whole blood [102]. Contrary to this, Koh et al. performed studies on structured surfaces varying in several dimensions and found a decrease in fibrinogen adsorption for some structures [101]. Poly(lactic-co-glycolic-acid) (PLGA) was structured with round pillars with diameter, height, and interspacings ranging from 40 nm to 15 μm. All surfaces were investigated with regard to static fibrinogen adsorption and static platelet adhesion. The overall degree of platelet adhesion correlated with that of fibrinogen adsorption and differed on various structures [101]. Koh et al. revealed that interspacings smaller than 200 nm led to a significant reduction of platelet adhesion and fibrinogen adsorption. Diameters smaller than the mean platelet diameter of 3 μm contribute to the positive effect, which is in accordance with other studies [12,98]. The authors regarded the absolute height of the structures as less important but the aspect ratio, namely the ratio between height and diameter of the pillars, as very important. According to their studies, the aspect ratio should be between 3 and 5 so that the pillars are flexible, which does not allow the platelets to obtain a tight connection to their top. The result that surface structuring significantly reduces platelet adhesion is supported by the shape change of the platelets on flat surfaces, which did not occur on structured surfaces, especially on those surfaces with 100 nm diameter, 100 nm interspacing, and 800 nm height [101].

The majority of hemocompatibility studies are performed under static conditions, but some groups considered the effect of flow on platelet adhesion in dynamic experiments. As one example, randomly structured PMMA surfaces with feature sizes of 40 nm, 80 nm, and 400 nm and heights of 3 nm, 13 nm, and 50 nm were investigated under flow conditions [108,109]. Experiments with human whole blood showed a preferred adsorption of vWF compared to that of fibrinogen and albumin, which is in conflict with other static studies. It is apparent that different adsorption behaviors of plasma proteins can be observed under different flow conditions. The platelet adhesion was highest on those samples with the most vWF adhesion, namely the larger structures. Experiments were carried out with washed platelets and revealed other results. Platelets preferred the smaller structured surfaces for adhesion, which shows the severe influence of blood cells and plasma proteins on the adhesion behavior of platelets [108].

(a)

(b)
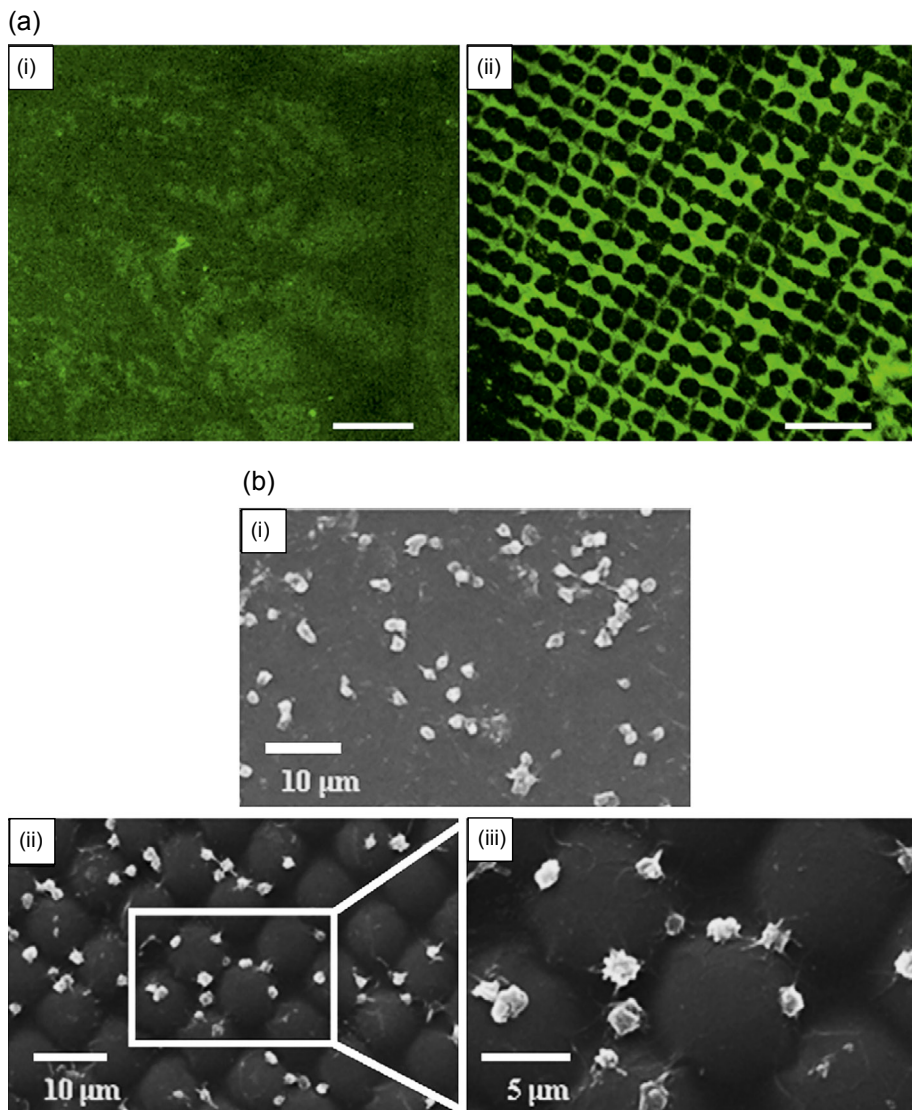
Figure 10.11 (a) Fibrinogen adsorption on plain and structured PDMS; (b) platelet adhesion on plain and structured PDMS.
Reprinted from Ref. [102], Copyright © 2009, with permission from Elsevier.

A summary of all presented physical surface modifications from Sections 10.1 and 10.2 can be found in Table 10.3.

The aforementioned, occasionally contradictory results show how important it is to further investigate the issue of protein adsorption in the context of platelet adhesion on structured surfaces. It is suggested that standardized testing conditions be set up as the diverse studies show how significant the influence of the test conditions are on the results.

Table 10.3 Summary of physical surface modifications

Material	Structure	Dimension	Target	Testing condition	Test medium	Result	
Section 10.1							
PU	Grooves, varying width	Width 1.8 µm, 3.4 µm, 90 µm	Platelet adhesion and activation	Dynamic, *in vitro*	Porcine whole blood	Reduced on groove widths smaller than ~3 µm	[12]
PDMS	Protrusions and ridges	$d=39.7$ nm; 20 µm length	Platelet adhesion	Static, *in vitro*	ADP-activated platelets	Double-structured surfaces most effective	[98]
PU	Pillars, varying interspacing	$d=25$ µm; $i=100$ µm; $l=20$ µm, 50 µm, 100 µm	Platelet adhesion and activation	Dynamic, *ex vivo*	Bovine PRP	At shear stress <3.3 dyn/cm² better for $i=700$ nm	[14]
PDMS	Protrusion and ridges	$d=400$ nm, 700 nm; $i=400$ nm, 700 nm; $h \sim 600$ nm	Platelet adhesion	Dynamic, *in vitro*	ADP-activated platelets	Double-structured surfaces most effective	[97]
PMMA	Random	Protrusions: $h \sim 10$ nm; $d=100$ nm Ridges: $h=100$ nm; $w=500$ nm	Platelet adhesion	Dynamic, *in vitro*	Whole blood, washed platelet	Less platelets on smaller structures (~40 nm)	[109]
PU	Nanotubes	Protrusions: $h \sim 40$ nm; $d=100$ nm Ridges: $h=100$ nm; $w=500$ nm	Platelet adhesion and activation	Dynamic, *in vitro*	Human PRP	Structured surfaces with higher contact angle few platelets, no shape change	[99]
PU	Fibers, varying length	Size: 270 nm–1240 nm; height 3 nm–120 nm	Platelet adhesion	Dynamic, *in vitro*	Ovine whole blood	No platelet adhesion, white cell adhesion instead	[13]

PDMS	Mastoid structure	$d=60\,\mu m$; $h=30\,\mu m$; $I=40\,\mu m$	Platelet adhesion and activation	Static, *in vitro*	Human PRP	Reduced adhesion and activation on superhydrophobic structures	[49]
PDMS	Pillars, varying interspacing	$d=15\,\mu m$; $h=5\,\mu m$; $i=5\,\mu m$–$60\,\mu m$	Platelet adhesion	Static, *in vitro*	Human PRP	Structure with highest contact angle least adhesion	[50]
	Grooves	130 nm deep				Less adhesion than best pillar surface although contact angle lower	
Section 10.2							
PU	Chemically modified	–	Platelet adhesion after fibrinogen and vWF incubation	Static, *in vitro*	Human PRP	Platelet adhesion dependent on fibrinogen adsorption	[100]
Alkanethiols	–	–	Platelet adhesion after fibrinogen incubation	Static, *in vitro*	Human PRP	Platelet adhesion dependent on fibrinogen shape change (loss of α-helix) but not on amount	[40]
PDMS	Protrusion	$d=4\,\mu m$; $h \sim 1\,\mu m$; $i=10\,\mu m$	Platelet adhesion after fibrinogen incubation	Static, *in vitro*	Human PRP	Fibrinogen mostly present on interspacing area, platelet adhesion pattern corresponds to fibrinogen pattern	[102]
PLGA	Round pillars, different dimension	40 nm–15 μm	Fibrinogen and platelet adhesion	Static, *in vitro*	Human fibrinogen, human PRP	Amount of adsorbed fibrinogen similar to platelets Diameter at least <3 μm Height–diameter ratio: 3–5 Interspacings <200 nm	[101]
PMMA	Random	Size: 40 nm–400 nm, height 3 nm–50 nm	Protein adhesion and platelet adhesion	Dynamic, *in vitro*	Whole blood	vWF dominantly adsorbed, highest on larger structures, accordingly most platelet adhesion	[108]
					Washed platelet	Platelets preferred smaller structures for adhesion	

10.6   Conclusion

The need for biomedical devices and thus for hemocompatible foreign materials has grown from the 1990s to 2015 and will further increase in the future [3,98]. Thus, improving the hemocompatibility of materials with initially good properties such as PUs remains a major research focus. A number of different approaches exist, all of which aim at reducing protein adsorption and platelet adhesion and activation on these surfaces. The approach of using chemically modified hydrophilic surfaces is a well-investigated topic with PEG or heparin coatings as typical examples. All these techniques reveal several advantages such as creating protein repellent surfaces with good EC growing properties. At the same time, there are some disadvantages such as cost or unexpected deleterious effects such as activation of the complement system [110]. The newer and therefore not that extensively studied method of physical surface structuring might provide a suitable alternative. Within this approach, the bulk properties of the PU are kept untouched as the topography is changed. This leads to hydrophobic surfaces that are generally liquid repellent and thus reduce protein and platelet adhesion. Up to now, the distinct effects of structure geometry and dimensions such as height, diameter, interspacings, and aspect ratio have not yet been sufficiently investigated. Different research groups who used diverse test setups and testing conditions revealed contradictory results. Nevertheless, this is a promising approach for establishing hemocompatible PU surfaces and is suggested as a focus for future research.

References

[1] Williams DF. The Williams dictionary of biomaterials. Liverpool University Press, Liverpool; 1999.

[2] Ratner BD, Hoffman AS, Schoen FJ, Lemons JE, editors. Biomaterials science: an introduction to materials in medicine. 3rd ed. Academic Press, Waltham; 2013.

[3] Kuetting M, Roggenkamp J, Urban U, Schmitz-Rode T, Steinseifer U. Polyurethane heart valves: past, present and future. Expert Rev Med Devices 2011;8(2):227–33.

[4] Sperling C, Fischer M, Maitz MF, Werner C. Blood coagulation on biomaterials requires the combination of distinct activation processes. Biomaterials 2009;30(27):4447–56.

[5] Ghanbari H, Viatge H, Kidane AG, Burriesci G, Tavakoli M, Seifalian AM. Polymeric heart valves: new materials, emerging hopes. Trends Biotechnol 2009;27(6):359–67.

[6] Feng Y, Zhao H, Behl M, Lendlein A, Guo J, Yang D. Grafting of poly(ethylene glycol) monoacrylates on polycarbonateurethane by UV initiated polymerization for improving hemocompatibility. J Mater Sci Mater Med 2013;24(1):61–70.

[7] Wang H, Feng Y, An B, Zhang W, Sun M, Fang Z, et al. Fabrication of PU/PEGMA crosslinked hybrid scaffolds by in situ UV photopolymerization favoring human endothelial cells growth for vascular tissue engineering. J Mater Sci Mater Med 2012;23(6):1499–510.

[8] Wang H, Feng Y, Fang Z, Yuan W, Khan M. Co-electrospun blends of PU and PEG as potential biocompatible scaffolds for small-diameter vascular tissue engineering. Mater Sci Eng C 2012;32(8):2306–15.

[9] Lamba NM, Woodhouse KA, Cooper SL. Polyurethanes in biomedical applications. CRC press, Boca Raton; 1997.

[10] Hasan J, Crawford RJ, Ivanova EP. Antibacterial surfaces: the quest for a new generation of biomaterials. Trends Biotechnol 2013;31(5):295–304.

[11] Qi P, Maitz MF, Huang N. Surface modification of cardiovascular materials and implants. Surf Coat Technol 2013;233:80–90.

[12] Clauser J, Gester K, Roggenkamp J, Mager I, Maas J, Jansen SV, et al. Micro-structuring of polycarbonate-urethane surfaces in order to reduce platelet activation and adhesion. J Biomater Sci Polym Ed 2014;25(5):504–18.

[13] Fujisawa N, Odell RA, Poole-Warren LA, Bertram CD, Woodard JC, Schindhelm K. Acute cellular interaction with textured surfaces in blood contact. J Biomed Mater Res 2000;52(3):517–27.

[14] Milner KR, Snyder AJ, Siedlecki CA. Sub-micron texturing for reducing platelet adhesion to polyurethane biomaterials. J Biomed Mater Res A 2006;76(3):561–70.

[15] Rose EA, Levin HR, Oz MC, Frazier OH, Macmanus Q, Burton NA, et al. Artificial circulatory support with textured interior surfaces. A counterintuitive approach to minimizing thromboembolism. Circulation 1994;90(5 Pt 2):II87–91.

[16] Frazier O, Gemmato C, Myers TJ, Gregoric ID, Radovancevic B, Loyalka P, et al. Initial clinical experience with the Heartmate II axial-flow left ventricular assist device. Tex Heart Inst J 2007;34(3):275.

[17] Neumann HA. Das Gerinnungssystem. ABW Wissenschaftsverlag GmbH, Berlin; 2007.

[18] Mackman N, Tilley RE, Key NS. Role of the extrinsic pathway of blood coagulation in hemostasis and thrombosis. Arterioscler Thromb Vasc Biol 2007;27(8):1687–93.

[19] Faller A, Schünke M, Schünke G. In: Der Köper des Menschen: Einführung in Bau und Funktion; 15. Georg Thieme Verlag Stuttgart; 2009.

[20] Furie B, Furie BC. Mechanisms of thrombus formation. N Engl J Med 2008;359(9):938–49.

[21] Goeijenbier M, van Wissen M, van de Weg C, Jong E, Gerdes VEA, Meijers JCM, et al. Review: viral infections and mechanisms of thrombosis and bleeding. J Med Virol 2012;84(10):1680–96.

[22] de Mel A, Cousins BG, Seifalian AM. Surface modification of biomaterials: a quest for blood compatibility. Int J Biomater 2012:1–8.

[23] Pschyrembel W, editor. Pschyrembel Klinisches Worterbuch 2012 (German edition). Walter De Gruyter Inc, Berlin; 2011.

[24] Chung I, Lip GYH. Virchow's triad revisited: blood constituents. Pathophysiol Haemost Thromb 2003;33(5–6):449–54.

[25] del Zoppo GJ. Virchow's triad: the vascular basis of cerebral injury. Rev neurological Dis 2008;5(Suppl. 1):S12.

[26] Bagot CN, Arya R. Virchow and his triad: a question of attribution. Br J Haematol 2008;143(2):180–90.

[27] Bluestein D. Research approaches for studying flow-induced thromboembolic complications in blood recirculating devices. Expert Rev Med Devices 2004;1(1):65–80.

[28] Dickson BC. Venous thrombosis: on the history of Virchow's triad. Univ Tor Med J 2004;81(3):166–71.

[29] Lu Q, Hofferbert BV, Koo G, Malinauskas RA. *In vitro* shear stress-induced platelet activation: sensitivity of human and bovine blood. Artif Organs 2013;37(10):894–903.

[30] Makin A, Silverman SH, Lip GYH. Peripheral vascular disease and Virchow's triad for thrombogenesis. QJM 2002;95(4):199–210.

[31] Watson T, Shantsila E, Lip GY. Mechanisms of thrombogenesis in atrial fibrillation: Virchow's triad revisited. Lancet 2009;373(9658):155–66.

[32] Graefe R, Timms D, Böhning F, Schmitz-Rode T, Steinseifer U. Investigation of the influence of volute design on journal bearing bias force using computational fluid dynamics. Artif Organs 2010;34(9):760–5.

[33] Kaufmann T, Linde T, Cuenca-Navalon E, Schmitz C, Hormes M, Schmitz-Rode T, et al. Transient, three-dimensional flow field simulation through a mechanical, trileaflet heart valve prosthesis. ASAIO J 2011;57(4):278–82.

[34] Laumen M, Kaufmann T, Timms D, Schlanstein P, Jansen S, Gregory S, et al. Flow analysis of ventricular assist device inflow and outflow cannula positioning using a naturally shaped ventricle and aortic branch. Artif Organs 2010;34(10):798–806.

[35] Schlanstein PC, Arens J, Borchardt R, Hesselmann F, Jansen SV, Schmitz-Rode T, et al. Oxygenator flow Pattern: PIV of a fiber oxygenator. Int J Artif Organs 2013; 36(8):554.

[36] Sonntag SJ, Kaufmann TA, Büsen MR, Laumen M, Linde T, Schmitz-Rode T, et al. Simulation of a pulsatile total artificial heart: development of a partitioned fluid structure interaction model. J Fluids Struct 2013;38:187–204.

[37] Lip GYH, Blann AD. Does hypertension confer a prothrombotic state? Virchow's triad revisited. Circulation 2000;101(3):218–20.

[38] Braune S, Gros M, Walter M, Zhou S, Dietze S, Rutschow S, et al. Adhesion and activation of platelets from subjects with coronary artery disease and apparently healthy individuals on biomaterials. J Biomed Mater Res Part B Appl Biomater 2015. [online pre-published].

[39] Horbett TA. Chapter 13 Principles underlying the role of adsorbed plasma proteins in blood interactions with foreign materials. Cardiovasc Pathol 1993;2(3):137–48.

[40] Sivaraman B, Latour RA. The relationship between platelet adhesion on surfaces and the structure versus the amount of adsorbed fibrinogen. Biomaterials 2010;31(5):832–9.

[41] Wintermantel E, Ha SW. Medizintechnik: life science engineering (German edition). 5th ed. Springer Verlag, Berlin-Heidelberg; 2009.

[42] Koch K, Barthlott W. Superhydrophobic and superhydrophilic plant surfaces: an inspiration for biomimetic materials. Philosophical transactions of the royal society A: Mathematical. Phys Eng Sci 1893;2009(367):1487–509.

[43] Sepeur S. Nanotechnologie: Grundlagen und Anwendungen. Vincentz Network GmbH & Co KG; 2008.

[44] Yuan L, Yu Q, Li D, Chen H. Surface modification to control protein/surface interactions. Macromol Biosci 2011;11(8):1031–40.

[45] Gao B, Feng Y, Lu J, Zhang L, Zhao M, Shi C, et al. Grafting of phosphorylcholine functional groups on polycarbonate urethane surface for resisting platelet adhesion. Mater Sci Eng C Mater Biol Appl 2013;33(5):2871–8.

[46] Zhao J, Song L, Yin J, Ming W. Anti-bioadhesion on hierarchically structured, superhydrophobic surfaces. Chem Commun 2013;49(80):9191–3.

[47] Ding Y, Leng Y, Huang N, Yang P, Lu X, Ge X, et al. Effects of microtopographic patterns on platelet adhesion and activation on titanium oxide surfaces. J Biomed Mater Res A March 2013;101(3):622–32.

[48] Mao C, Liang C, Luo W, Bao J, Shen J, Houa X, et al. Preparation of lotus-leaf-like polystyrene micro- and nanostructure films and its blood compatibility. J Mater Chem 2009;19:9025–9.

[49] Ye X, Yl S, Zhou M, Li J, Cai L. Research on micro-structure and hemo-compatibility of the artificial heart valve surface. Appl Surf Sci 2009;255(13):6686–90.

[50] Zhou M, Yang J, Ye X, Zheng A, Li G, Yang P, et al. Blood Platelet's behavior on nanostructured superhydrophobic surface. J Nano Res 2008;2:129–36.

[51] Cheng YT, Rodak D, Wong C, Hayden C. Effects of micro-and nano-structures on the self-cleaning behaviour of lotus leaves. Nanotechnology 2006;17(5):1359–62.

[52] Marmur A. The Lotus effect: superhydrophobicity and metastability. Langmuir 2004; 20(9):3517–9.

[53] Blossey R. Self-cleaning surfaces - virtual realities. Nat Mater 2003;2(5):301–6.

[54] Barthlott W, Neinhuis C. Purity of the sacred lotus, or escape from contamination in biological surfaces. Planta 1997;202:1–8.

[55] Marmur A. Wetting on hydrophobic rough surfaces: to be heterogeneous or not to be? Langmuir 2003;19(20):8343–8.

[56] Yoshimitsu Z, Nakajima A, Watanabe T, Hashimoto K. Effects of surface structure on the hydrophobicity and sliding behavior of water droplets. Langmuir 2002;18(15):5818–22.

[57] Wise DL. Biomaterials and bioengineering handbook, vol. 63. New York, NY: Marcel Dekker; 2000.

[58] Yuan W, Feng Y, Wang H, Yang D, An B, Zhang W, et al. Hemocompatible surface of electrospun nanofibrous scaffolds by ATRP modification. Mater Sci Eng C Mater Biol Appl 2013;33(7):3644–51.

[59] Luo Y, Zhang C, Xu F, Chen Y, Fan L, Wei Q. Synthesis and characterization of novel THTPBA/PEG-derived polyurethane scaffolds for tissue engineering. J Mater Sci 2010; 45(7):1866–77.

[60] Chen KY, Kuo JF. Surface characterization and platelet adhesion studies of aliphatic polyurethanes grafted by fluorocarbon oligomers: effect of fluorocarbon chain length and carboxylic acid group. J Mater Sci Mater Med 2002;13(1):37–45.

[61] Tan D, Li Z, Yao X, Xiang C, Tan H, Fu Q. The influence of fluorocarbon chain and phosphorylcholine on the improvement of hemocompatibility: a comparative study in polyurethanes. J Mater Chem B 2014;2(10):1344.

[62] Xie X, Wang R, Li J, Luo L, Wen D, Zhong Y, et al. Fluorocarbon chain end-capped poly(carbonate urethane)s as biomaterials: blood compatibility and chemical stability assessments. J Biomed Mater Res Part B Appl Biomater 2009;89B(1):223–41.

[63] Yin Z, Cheng C, Qin H, Nie C, He C, Zhao C. Hemocompatible polyethersulfone/ polyurethane composite membrane for high-performance antifouling and antithrombotic dialyzer. J Biomed Mater Res Part B Appl Biomater 2014;103(1):97–105.

[64] He C, Wang M, Cai X, Huang X, Li L, Zhu H, et al. Chemically induced graft copolymerization of 2-hydroxyethyl methacrylate onto polyurethane surface for improving blood compatibility. Appl Surf Sci 2011;258(2):755–60.

[65] Butruk-Raszeja B, Trzaskowski M, Ciach T. Cell membrane-mimicking coating for blood-contacting polyurethanes. J Biomater Appl 2014;29(6):801–12.

[66] Huang J, Xu W. Zwitterionic monomer graft copolymerization onto polyurethane surface through a PEG spacer. Appl Surf Sci 2010;256(12):3921–7.

[67] Mikhalovska L, Chorna N, Lazarenko O, Haworth P, Sudre A, Mikhalovsky S. Inorganic coatings for cardiovascular stents: in vitro and in vivo studies. J Biomed Mater Res Part B Appl Biomater 2011;96B(2):333–41.

[68] Sin DC, Kei HL, Miao X. Surface coatings for ventricular assist devices. Exp Rev Med Dev 2009;6:51–60.

[69] Subramanian B, Muraleedharan CV, Ananthakumar R, Jayachandran M. A comparative study of titanium nitride (TiN), titanium oxy nitride (TiON) and titanium aluminum nitride (TiAlN), as surface coatings for bio implants. Surf Coat Technol 2011;205(21–22):5014–20.

[70] Liu H, Zhang D, Shen F, Zhang G, Song S. Hemocompatibility and anti-endothelialization of copper-titanium coating for vena cava filters. Surf Coat Technol 2012;206(16):3501–7.

[71] Riescher S, Wehner D, Schmid T, Zimmermann H, Hartmann B, Schmid C, et al. Titaniumcarboxonitride layer increased biocompatibility of medical polyetherurethanes. J Biomed Mater Res Part B Appl Biomater 2013;102(1):141–8.

[72] Lackner JM, Waldhauser W, Hartmann P, Bruckert F, Weidenhaupt M, Major R, et al. Hemocompatibility of inorganic physical vapor deposition (PVD) coatings on thermoplastic polyurethane polymers. JFB 2012;3(4):283–97.

[73] Hess C, Schwenke A, Wagener P, Franzka S, Sajti CL, Pflaum M, et al. Dose-dependent surface endothelialization and biocompatibility of polyurethane noble metal nanocomposites. J Biomed Mater Res Part A 2013;102(6):1909–20.

[74] Jia RP, Zong AX, He XY, Wei L. Synthesis and blood compatibility of fluorinated polyurethane elastomer. Appl Mech Mater 2014;685:473–6.

[75] Weber N, Wendel HP, Ziemer G. Hemocompatibility of heparin-coated surfaces and the role of selective plasma protein adsorption. Biomaterials 2002;23(2):429–39.

[76] Zietek P, Butruk B, Ciach T. Fabrication of novel material with athrombogenic potential: immobilization of peptides on polyurethane surface. Challenges Mod Technol 2012;3(1):38–41.

[77] Butruk B, Babik P, Marczak B, Ciach T. Surface endothelialization of polyurethanes. Procedia Eng 2013;59:126–32.

[78] Zou L, Cao S, Kang N, Huebert RC, Shah VH. Fibronectin induces endothelial cell migration through beta1 integrin and src-dependent phosphorylation of fibroblast growth factor Receptor-1 at tyrosines 653/654 and 766. J Biol Chem 2012;287(10):7190–202.

[79] Salacinski HJ, Hamilton G, Seifalian AM. Surface functionalization and grafting of heparin and/or RGD by an aqueous-based process to a poly(carbonate-urea)urethane cardiovascular graft for cellular engineering applications. J Biomed Mater Res 2003;66A(3):688–97.

[80] Lin HB, Zhao ZC, Garcia-Echeverria C, Rich DH, Cooper SL. Synthesis of a novel polyurethane co-polymer containing covalently attached RGD peptide. J Biomater Sci Polym Ed 1992;3(3):217–27.

[81] Lin HB, Garcia-Echeverria C, Asakura S, Sun W, Mosher DF, Cooper SL. Endothelial cell adhesion on polyurethanes containing covalently attached RGD-peptides. Biomaterials January 1992;13(13):905–14.

[82] Thierfelder N, Koenig F, Bombien R, Fano C, Reichart B, Wintermantel E, et al. *In vitro* comparison of novel polyurethane aortic valves and homografts after seeding and conditioning. ASAIO J 2013;59(3):309–16.

[83] Lehle K, Li J, Zimmermann H, Hartmann B, Wehner D, Schmid T, et al. *In vitro* endothelialization and platelet adhesion on titaniferous upgraded polyether and polycarbonate polyurethanes. Materials 2014;7(2):623–36.

[84] Hung HS, Yang YC, Lin YC, Lin SZ, Kao WC, Hsieh HH, et al. Regulation of human endothelial progenitor cell maturation by polyurethane nanocomposites. Biomaterials 2014;35(25):6810–21.

[85] Taite LJ, Yang P, Jun HW, West JL. Nitric oxide-releasing polyurethane - PEG copolymer containing the YIGSR peptide promotes endothelialization with decreased platelet adhesion. J Biomed Mater Res Part B Appl Biomater 2007;84B(1):108–16.

[86] Reynolds MM, Frost MC, Meyerhoff ME. Nitric oxide-releasing hydrophobic polymers: preparation, characterization, and potential biomedical applications. Free Radic Biol Med 2004;37(7):926–36.

[87] Frost MC, Reynolds MM, Meyerhoff ME. Polymers incorporating nitric oxide releasing/generating substances for improved biocompatibility of blood-contacting medical devices. Biomaterials 2005;26(14):1685–93.

[88] Sask KN, Berry LR, Chan AKC, Brash JL. Modification of polyurethane surface with an antithrombin-heparin complex for blood contact: influence of molecular weight of polyethylene oxide used as a linker/spacer. Langmuir 2012;28(4):2099–106.

[89] Tong F, Chen X, Chen L, Zhu P, Luan J, Mao C, et al. Preparation, blood compatibility and anticoagulant effect of heparin-loaded polyurethane microspheres. J Mater Chem B 2012;1(4):447–584.

[90] Yan Y, Hong Wang X, Yin D, Zhang R. A new polyurethane/heparin vascular graft for small-caliber vein repair. J Bioact Compatible Polym 2007;22(3):323–41.

[91] Du YJ, Klement P, Berry LR, Tressel P, Chan AKC. *In vivo* rabbit acute model tests of polyurethane catheters coated with a novel antithrombin-heparin covalent complex. Thromb Haemostasis 2005;94(2):366–72.

[92] Du YJ, Brash JL, McClung G, Berry LR, Klement P, Chan AKC. Protein adsorption on polyurethane catheters modified with a novel antithrombin-heparin covalent complex. J Biomed Mater Res 2007;80A(1):216–25.

[93] Haddad S, Zanina N, Othmane A, Mora L. Polyurethane films modified by antithrombin - heparin complex to enhance endothelialization: an original impedimetric analysis. Electrochimica Acta 2011;56(21):7303–11.

[94] Major TC, Brisbois EJ, Jones AM, Zanetti ME, Annich GM, Bartlett RH, et al. The effect of a polyurethane coating incorporating both a thrombin inhibitor and nitric oxide on hemocompatibility in extracorporeal circulation. Biomaterials 2014; 35(26):7271–85.

[95] Chuang TW, Masters KS. Regulation of polyurethane hemocompatibility and endothelialization by tethered hyaluronic acid oligosaccharides. Biomaterials 2009;30(29):5341–51.

[96] Ruiz A, Rathnam KR, Masters KS. Effect of hyaluronic acid incorporation method on the stability and biological properties of polyurethane - hyaluronic acid biomaterials. J Mater Sci Mater Med 2013;25(2):487–98.

[97] Fan H, Chen P, Qi R, Zhai J, Wang J, Chen L, et al. Greatly improved blood compatibility by microscopic multiscale design of surface architectures. Small 2009;5(19):2144–8.

[98] Chen L, Han D, Jiang L. On improving blood compatibility: from bioinspired to synthetic design and fabrication of biointerfacial topography at micro/nano scales. Colloids Surf B 2011;85(1):2–7.

[99] Sun T, Tan H, Han D, Fu Q, Jiang L. No platelet can adhere - largely improved blood compatibility on nanostructured superhydrophobic surfaces. Small 2005;1(10):959–63.

[100] Wu Y, Simonovsky FI, Ratner BD, Horbett TA. The role of adsorbed fibrinogen in platelet adhesion to polyurethane surfaces: a comparison of surface hydrophobicity, protein adsorption, monoclonal antibody binding, and platelet adhesion. J Biomed Mater Res A 2005;74(4):722–38.

[101] Koh LB, Rodriguez I, Venkatraman SS. The effect of topography of polymer surfaces on platelet adhesion. Biomaterials 2010;31(7):1533–45.

[102] Chen H, Song W, Zhou F, Wu Z, Huang H, Zhang J, et al. The effect of surface microtopography of poly(dimethylsiloxane) on protein adsorption, platelet and cell adhesion. Colloids Surf B 2009;71(2):275–81.

[103] Roach P, Eglin D, Rohde K, Perry CC. Modern biomaterials: a review - bulk properties and implications of surface modifications. J Mater Sci Mater Med 2007;18(7):1263–77.

[104] Ross AM, Jiang Z, Bastmeyer M, Lahann J. Physical aspects of cell culture substrates: topography, roughness, and elasticity. Small 2012;8(3):336–55.

[105] Luong-Van E, Rodriguez I, Low HY, Elmouelhi N, Lowenhaupt B, Natarajan S, et al. Review: micro- and nanostructured surface engineering for biomedical applications. J Mater Res 2012;28(02):165–74.

[106] Nikkhah M, Edalat F, Manoucheri S, Khademhosseini A. Engineering microscale topographies to control the cell-substrate interface. Biomaterials 2012;33(21):5230–46.

[107] Hopmann C, Michaeli W, Bobzin EK, Bagcivan N, Theiß S, Hartmann C, et al. Extrusion embossing of hydrophobic films – a study on process characteristics and surface properties. J Plastics Technol 2012;8(3):302–30.

[108] Minelli C, Kikuta A, Tsud N, Ball MD, Yamamoto A. A micro-fluidic study of whole blood behaviour on PMMA topographical nanostructures. J Nanobiotechnol 2008;6:1–11.

[109] Minelli C, Kikuta A, Yamamoto A. Blood interaction with nano-topography. In: International Conference on Nanoscience and Nanotechnology 2006 IEEE; 2006: 263–66.

[110] Szott LM, Horbett TA. Protein interactions with surfaces: cellular responses, complement activation, and newer methods. Curr Opin Chem Biol 2011;15(5):677–82.

Enhancing polyurethane blood compatibility

11

K. Ishihara*, Y. Liu, Y. Inoue
The University of Tokyo, Tokyo, Japan
*Corresponding author: ishihara@mpc.t.u-tokyo.ac.jp

11.1 Introduction

Blood does not coagulate in a living normal blood vessel, with an inside surface covered with endothelial cells. However, when blood encounters a foreign surface, the coagulation mechanisms are immediately activated. Therefore, blood compatibility is the most important property required for biomedical materials, especially blood-contacting devices [1–6]. These materials are used for long periods, in applications such as artificial hearts, vascular prostheses, and cardiovascular stents, and also outside of the body for short periods, in blood purification devices and catheters. These devices must completely prevent activation of the coagulation system leading to thrombus formation. A surface that promotes a pseudointima can be successfully used in a vascular prosthesis provided it has a diameter over 6 mm. The antithrombogenicity is not due to the surface itself, but due to a not well-understood passivation process. However, when these types of vascular prosthesis are applied to arteries with smaller sizes, they are occluded by thrombus. Therefore, it is necessary to develop materials with antithrombogenic surfaces utilizing blood-compatible polymers.

Blood compatibility of a material may be evaluated using *in vitro*, *ex vivo*, and *in vivo* experiments. Such studies involve evaluation of antithrombogenic properties in terms of nonactivation of coagulation and nonadhesion and activation of blood cells when the material is in contact with blood with and without anticoagulant. From the viewpoint of blood coagulation, protein adsorption and platelet adhesion are initial key phenomena of blood coagulation. Thus, there are several reports published evaluating these phenomena (Figure 11.1).

11.2 Structural characteristics of segmented polyurethanes as blood-compatible materials

Segmented polyurethanes (SPUs) are widely used as biomedical materials because of their excellent mechanical properties, stability in the biological environment, and their ease of process [7–11]. The SPU consists of alternating "hard" and "soft" segments. The segments are thermodynamically incompatible and generally, the phases are separated into distinct domains, with a typical domain size in the order of 3–10 nm.

Surface induced thrombus formation

Blood compatibility
- Antithrombogenicity

- Nonadhesion and activation
  of blood cells

- Nonactivation of coagulation and
  complement system

Protein adsorption at materials surface

Figure 11.1 Blood compatibility observed on the surface.

The hard segments contain urethane and/or urea bonds, which are capable of forming hydrogen bonds. In the case of SPUs composed of soft segments of polyether and hard segments of urethane, the extent of phase separation is influenced by the length distributions in both the hard and the soft segments. The variations in segment lengths cause some short, soft segments to be solubilized in the hard domains and short, hard segments to be dissolved in the soft segment matrix. A broad interfacial region between relatively pure hard and soft segment domains characterizes another type of phase mixing. Several strategies for improving the blood compatibility of polyurethanes (PUs), in particular SPUs, have been investigated [12–20]. These are based on the chemical structure of PU. The nature of the hard and soft segments, chain length of the soft segment, and mobility of both segments are key parameters for modification. For example, when polyoxyethylene (PEO) is used as a soft segment, hydrophilicity and mobility may be enhanced. Detailed studies on the morphology and mechanical properties of SPUs have been described [21]. In the development of the blood-compatible SPUs the domain structure is critical. The hydrophilic and hydrophobic heterogenic surfaces of SPUs can reduce a cellular adhesion. Currently, the mechanism is not clear, but it may be due to the state of bound water at the surface [22]. Using the X-ray photoelectron spectroscopy (XPS) on SPUs, Lelah et al. found a linear correlation between the surface concentration of the soft segments and the platelet adhesion [23] (Figure 11.2).

The surface properties of blood-contacting polymers are believed to affect protein adsorption and subsequent events leading to thrombus formation. The chemical nature of SPU surfaces is controversial, with some investigators indicating that the blood-contacting interface consists almost entirely of soft segments, and others claiming that hard segment components are present at the surface [24]. If they are present, hard segment components on an aqueous interface can reside in several environments. In an SPU with a relatively low hard/soft segment ratio, for example, the hard segments can be dissolved in soft segment domains, or the hard segments can be present in distinct domains (Figure 11.3).

The bulk, surface, and blood compatibility properties of a series of SPUs based on PEO (molecular weight (MW) = 1450), poly(tetramethylene oxide) (PTMO) (MW = 1000), and mixed PEO/PTMO soft segments were evaluated [25,26]. Two polymer blends prepared from a PTMO-based and a PEO-based SPU were also
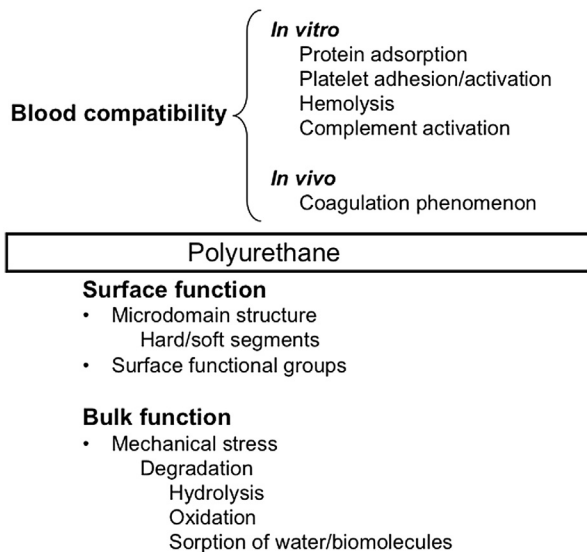
Figure 11.2 Evaluation of blood compatibility and properties of polyurethane.
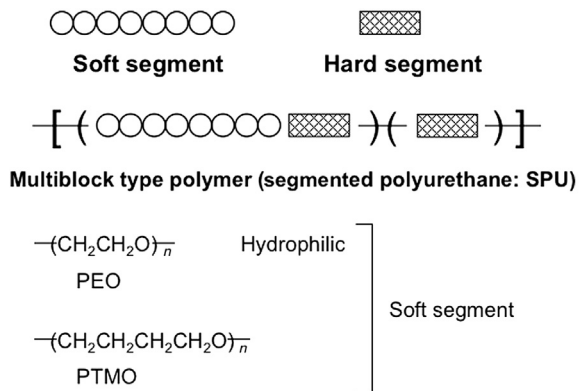
Figure 11.3 Segmented polyurethane as multiblock type polymer.

investigated. Differential scanning calorimetry and dynamic mechanical analysis indicated that the SPUs based on either the PEO or the PTMO soft segments are relatively phase mixed. The degree of phase mixing in the polymers increased with increasing weight fraction of PEO. As expected, the water absorption and hydrophilicity of the polymer increased with increasing PEO soft segment content. In vacuum, XPS shows that the PEO-rich SPUs have a lower concentration of soft segments at the surface, possibly due to the migration of the hydrophilic PEO segments away from the polymer/vacuum interface. Blood-contacting results indicated that the high PEO-containing SPUs were more thrombogenic than the PTMO-based SPUs. In PEO/PTMO-based SPUs, a high surface density of PEO appeared to be required before blood compatibility was significantly decreased.

11.3 Utilizing bioactive molecules for surface modification to prevent thrombus formation

A classic surface treatment used to prevent thrombus formation is heparin immobilization [6,27–29] (Figure 11.4). Heparin is a strong anticoagulant molecule and is used in anticoagulation therapy during hemodialysis and extracorporeal blood circulation. The antithrombogenic activity of immobilized heparin is dependent on its density and mobility. Also, maintaining the biological activity of heparin is essential. A hydrophilic spacer chain between the PU surface and the heparin molecules improves its biological action. As heparin is an anionic polysaccharide, it can be immobilized on a cationic surface via ionic bonding [30]. In addition, covalent bonding may be applied to stabilize the immobilization. There are many review articles that have addressed these types of heparin modifications. For example, heparin was immobilized onto SPU surfaces using hydrophilic PEO spacers of different chain lengths. The use of the PEO hydrophilic spacer reduces protein adsorption and subsequent platelet adhesion on the surface. In addition, the bioactivity of the immobilized heparin to inhibit fibrinogen polymerization is enhanced by the incorporation of these spacers. Immobilized heparin bioactivity is shown to be a function of PEO spacer length [31–33]. The use of hydrophilic PEO spacers has demonstrated that the bioactivity of immobilized heparin is consistently higher than that of immobilized heparin using a hexamethylene (C6) spacer. The heparin-immobilized surfaces demonstrate no spacer chain length effect on platelet adhesion, even though they show less platelet adhesion compared to SPU controls [34]. In *ex vivo* artery–artery shunt experiments performed under low flow and low shear conditions, all heparinized surfaces exhibited significant prolongation of occlusion times compared to SPU controls, indicating an ability of immobilized heparin to inhibit thrombosis in whole blood. Heparin immobilization is effective for preventing clot formation; however, the effects are lessened due to reduced activity of heparin as
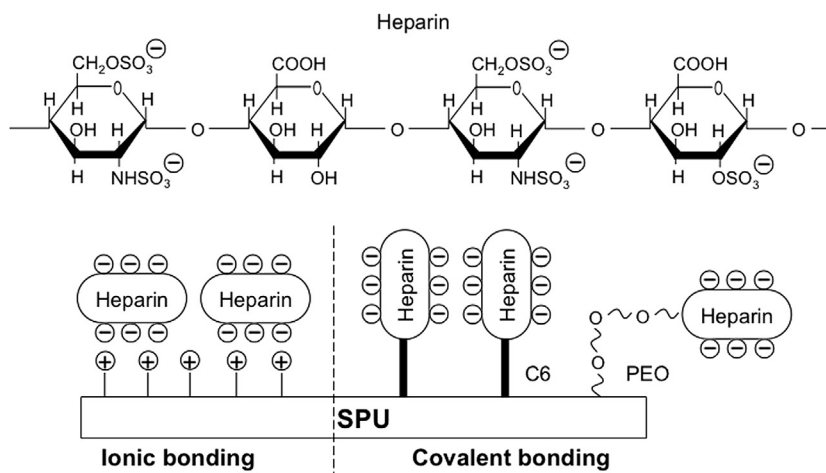
Figure 11.4 Heparin modified surface of segmented polyurethane.

a consequence of protein adsorption on the surface. Thus, heparin-immobilized SPU may be suitable for short-term applications.

Immobilization of the enzyme urokinase has also been utilized [35–37]. Urokinase is used clinically as a thrombolytic agent in the treatment of severe or deep venous thrombosis and occluded intravenous cannulas made with SPUs.

11.4 Modification of PU with functional groups

11.4.1 Noncharged hydrophilic polymers

Surfaces adsorbing a minimal amount of protein are important in many applications such as blood-contacting devices, membrane separators, sensors, and contact lenses. Therefore, much effort has been expended on minimizing or eliminating protein adsorption. To prevent protein adsorption, the utilization of water-soluble polymers such as polyacrylamide, poly(N-vinyl-2-pyrrolidone), and PEO has been considered. In particular, PEO has a low interfacial free energy with water, unique solution properties, molecular conformation in aqueous solution, high surface mobility, and steric stabilization effects [38,39] (Figure 11.5).

Many studies on the synthesis and characterization of PUs modified with PEO and its derivatives have been performed [15,40–45]. The methods used to synthesize PEO surfaces on PU include a coupling reaction, interpenetration, adsorption, and grafting of the PEO chain and its derivatives to the substrate. Generally, the PU surface is activated and a functional group that can react with PEO chains is introduced. Using the terminal hydroxyl group, PEO can react with the carboxyl or isocyanate groups generated on the surface of a PU. Diisocyanate–PEO may potentially react with protein amines to form molecular barriers of adsorbed proteins present on biomaterials, thereby masking adhesive ligands and preventing acute surface thrombosis. To test this notion, polymer and glass substrates were preadsorbed with fibrinogen and treated with diisocyanate–PEO, nonreactive dihydroxyl–PEO, or left untreated. Following perfusion of platelets in whole human blood for 1 min, diisocyanate–PEO-treated
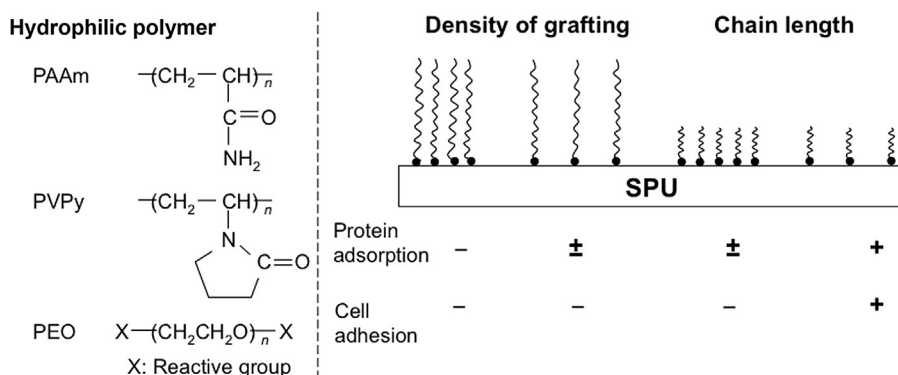
Figure 11.5 Surface modification with hydrophilic polymer on segmented polyurethane. Effects of graft density and chain length on blood compatibility.

surfaces experienced 96% (polyethylene), 97% (polytetrafluoroethylene), and 94% (glass) less platelet deposition than the untreated surfaces [46]. Similar reductions were seen for diisocyanate–PEO versus dihydroxyl–PEO treatment. Similar results were obtained on a PU surface. A marked reduction in platelet adhesion was observed on fibrinogen-adsorbed PU treated with *N*-carboxymethyl succinimidyl ester PEO or diisocyanate–PEO. Relative differences in platelet adhesion on *N*-carboxymethyl succinimidyl ester PEO- and diisocyanate–PEO-modified surfaces were attributed to differences in the reactivity toward fibrinogen and the size of the polymer backbone. Taken together, these findings provide insight and guidance for applying protein-reactive PEGs for the interruption of acute thrombotic deposition.

Grafting of high molecular weight PEO by the action of peroxide and graft polymerization of methoxy group-terminated PEO methacrylate resulted in the formation of surfaces with good water wettability and low platelet adhesion. However, the blood compatibility of the PEO-grafted PU evaluated *in vivo* was the same as that of the unmodified PU. Their surfaces were covered with a thick protein adsorption layer of about 100–200 nm after implantation for 3 weeks, and the tubing occluded within 1 month. The density of PEO chains on the surface and molecular weight of PEO influence protein adsorption resistance [47]. On the other hand, even under biological conditions, PEO chains can exhibit oxidative degradation [48–52]. This induces a reduction in both the density and the chain length of the PEO. Thus, long-term implantation of medical devices made with PEO-modified materials has not been achieved.

11.4.2 Charged groups

11.4.2.1 Cationic groups conjugated with heparin

A significant example of introduction of a charged group into PU is to use cationic amino groups to immobilized heparin (see Figure 11.4). In general, cationic groups play an important role in activation of the coagulation and platelet adhesion [30,32]. However, after immobilization of heparin, the anticoagulant properties improved. If heparin can be attached to a polymer while retaining its antithrombin III activity, an antithrombogenic material can be created. Heparin immobilization can also be carried out by grafting heparin and spacer groups onto a soluble polymer, which can then be coated onto materials or by the direct coupling of heparin using spacer groups onto insoluble materials. The most important detail required for immobilization is increasing the surface concentration of heparin while maintaining biological activity.

11.4.2.2 Anionic sulfonate groups

Cooper et al. modified SPU by grafting propyl sulfonate groups to its backbone. The dynamic contact angle of the resulting sulfonated SPU showed that the propyl sulfonate groups were enriched at the surface [53–55]. A canine *ex vivo* blood-contacting test indicated that the incorporation of propyl sulfonate groups dramatically reduced the number and activation of platelets adherent to the polymer surface. In addition, fibrinogen deposition increased with increasing sulfonate content, despite the low level of platelet activation. Lindon et al. reported that one of the mechanisms of antithrombogenicity appeared on the sulfonated surface [56]. They observed that platelet

adhesion and secretion were independent of the total amount of adsorbed fibrinogen but were directly proportional to the amount of fibrinogen in its native conformation. Santerre et al. also observed high levels of *in vitro* fibrinogen deposition along with the absence of the Vroman effect on a series of PUs based on a sulfonate-containing chain expander; this suggested that the fibrinogen was tightly bound and could not be displaced [57]. Moreover, these sulfonated PUs inhibited the polymerization of fibrinogen to cross-linked fibrin. These findings suggested that the sulfonate groups interact with fibrinogen, subsequently altering its conformation such that its functional domains were not recognizable to platelets, thereby preventing adhesion.

Kim et al. reported an investigation into the negatively charged surface of a PU with a sulfonated PEO graft. They described the importance of the flexible PEO chain on the antithrombogenicity using a "negative cilia concept" [58,59].

11.4.2.3 Zwitterionic groups

Recently, it has been realized that biomaterials that are surface-modified with zwitterionic compounds demonstrate excellent blood compatibility (Figure 11.6). Zwitterionic compounds have both cationic and anionic groups in the same molecules and form a betaine structure. There are three kinds of zwitterionic groups that have been investigated for use in obtaining a blood-compatible surface. Sulfobetaine compounds have a sulfonate anion and trimethyl ammonium cation in the same molecule, similar to heparin. The sulfobetaine group is introduced at the surface of PU and has been evaluated for blood compatibility. Lin et al. reported that sulfobetaine polymers can effectively suppress platelet adhesion and protein adsorption [60–71]. Also, Lowe et al.
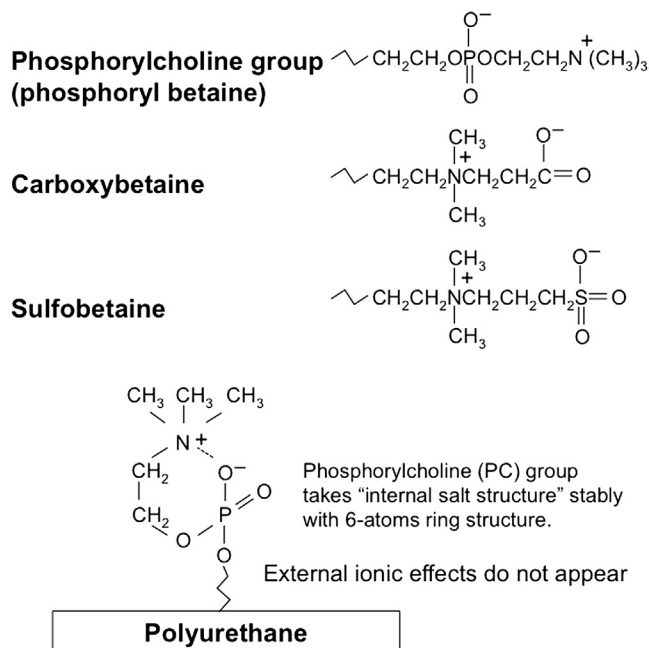
Figure 11.6 Various zwitterionic moieties.

reported that sulfobetaine-based polymer coatings can reduce bacteria, macrophage, and fibroblast adhesion [72,73]. The *N,N*-dimethyl(methacryloyloxyethyl) ammonium propanesulfonate (DMAPS) has been graft-polymerized onto a PU surface in a three-step heterogeneous reaction through the vinyl bonds of acrylic acid (AA) or 2-hydroxyethyl methacrylate (HEMA), which had been immobilized with hexamethylene diisocyanate (HDI). First, PU was activated with isocyanate groups using HDI as a coupling agent. Second, AA or HEMA was introduced through the reaction of AA or HEMA with NCO groups bonded on the PU surface. Last, the DMAPS was graft-polymerized with the vinyl group of AA or HEMA using a polymerization initiator. Ozonization is another good way to introduce active peroxide groups onto an SPU surface. DMAPSs have been grafted onto an ozone-activated SPU surface to improve surface hemocompatibility. The sulfobetain structure accepts ionic species. The possibility for calcification, during exposure to blood for long periods, must be investigated.

The carboxybetaine group has a carboxylate anion group and an ammonium cation group [74,75]. The surface of the PU is treated with a tertiary amino group and then reacted with β-propiolactone. PU surfaces were treated with HDI in toluene in the presence of di-*n*-butyl tin dilaurate as a catalyst. In the second step, the hydroxyl group of *N,N*-dimethylethanolamine (DMEA) or 4-dimethylamino-1-butanol (DMBA) is allowed to react with isocyanate groups bound on the surface. In the final step, carboxybetaines are formed on the surface through the ring-opening reaction between the tertiary amino group of DMEA or DMBA and the β-propiolactone.

Currently, the most important ongoing research is on the phosphorylcholine (PC) group (sometimes described as a phosphobetaine group). Ishihara et al. and other research groups have systematically investigated the preparation of PC group-bearing polymers and demonstrated that these surfaces are antithrombogenic [76–82]. The fundamental concept was inspired by the cell membrane surface, which is mainly constructed of neutral phospholipids with PC groups. The PC group is a zwitterionic group that forms an inner salt between the phosphate anion and the trimethylammonium cation. It is electrically neutral in the pH 2–12 range. Also, the PC groups are not significantly affected by the ions surrounding them. In the following section, surface modification with PC groups is summarized and explained in detail.

11.4.3   PC group-bearing PU

11.4.3.1   Surface reaction on PU substrates

In the field of biomimetic chemistry, phospholipid molecules have been utilized for the preparation of cell membrane–like structures, namely, liposomes and Langmuir–Blodgett membranes. However, a major disadvantage of molecular assemblies of this kind is their inadequate chemical and/or physical stability. Stabilization of the phospholipid assembly is therefore an important topic of focus in the construction of interfaces between living and artificial systems. One approach to addressing this issue is the design of a new type of polymer system with PC groups.

Several studies that involve the introduction of PC groups to a PU surface have been performed. They are summarized in Table 11.1.

Table 11.1 Surface modifications on polyurethanes by introduction of phosphorylcholine (PC) group

Modification	Polyurethane and modified compound	Function evaluation	References
Reaction	Photoreaction on SPU (Pellethane®) with PC compound having phenylazido group chemical reaction on polycarbonate urethane with aldehyde–PC compound	Protein adsorption Platelet adhesion	[83,84] [85,86]
Polymerization	PU with poly(MPC-co-BMA) side chain via macromonomer synthesis	Protein adsorption Cell adhesion	[87]
	PU with poly(MPC-co-MMA) side chain via macromonomer synthesis	Protein adsorption Cell adhesion	[88]
	PU prepared with glyceryl–PC	Cell adhesion	[87,89]
	PEUU prepared with PC–NH$_2$ compound	Platelet adhesion Cell adhesion	[90]
	Surface reaction on PEU with PC group	Platelet adhesion	[91]
	PU prepared with diol–PC via polyaddition	Protein adsorption	[92–94]
	Poly(carbonate urethane) with fluorinated alkyl PC compounds	Platelet adhesion	[95]
	PUU with PC group introducing during polyaddition	Platelet adhesion	[96]
	SI-ATRP of MPC from PU	Protein adsorption Platelet adhesion	[97]
	PU end-capped with PC compound	Platelet adhesion	[98]
	Poly(ester–urethane) with PC group introduced during polyaddition	Platelet adhesion	[99]
Immobilization	PEUU immobilized with MPC polymer	In vivo evaluation as a vascular graft	[100]
Coating	Solution coating with MPC polymer wih urethane methacrylate unit on SPU	Platelet adhesion	[101]
	Solution coating with poly(MPC-co-BMA) on SPU	In vivo evaluation as artificial heart	[102]
	Solution coating with poly(MPC-co-BMA) on SPU (Tecoflex®)	Friction evaluation as catheter	[103]
	Solution coating with poly(MPC-co-BMA) on SPU (Tecoflex®)	Friction evaluation as joint replacement	[104]
Blending	Solution blending of SPU and MPC polymer (random copolymer)	Cell adhesion from whole blood and platelet-rich plasma	[105–109]
	Solution blending of SPU and MPC polymer (random copolymer)	In vivo evaluation as a vascular prosthesis	[110–112]
	Solution blending of SPU and MPC polymer (random copolymer)	Cell adhesion and activation	[113]
	Solution blending of SPU (Pellethane®) and PU with PC group	Platelet adhesion	[114]
Interpenetration	Semi-IPN composed of SPU and cross-linked MPC polymer	Cell adhesion platelet adhesion	[115,116]
Polymer integration	Double polymer layers composed of SPU (Tecoflex®) and well-defined block- and graft-type MPC polymers	Cell adhesion from whole blood Protein adsorption	[117–119]

Simple modification is performed by utilizing reactive compounds with a PC group. The compounds can react with the PU surface and form chemical bonds. When this occurs, the mechanical properties of the base PU should not be affected by the reaction procedure. One of the ideal procedures is the utilization of a photochemical reaction.

Kool et al. prepared PC compounds with a phenylazide group as a photoreactive moiety [83,84]. They synthesized molecules containing a photoinduced reactive 4-azidobenzoyl group at one end of the molecule and a PC group at the other end (Figure 11.7).

On photoinduced activation, a phenylazide splits off nitrogen and a highly reactive intermediate singlet nitrene is formed. The chemistry of nitrenes is complex and not fully understood. The reaction pathways depend on temperature, the presence of ring substituents, and the availability of nucleophiles. Ring expansion of the nitrene leads to a 1,2-didehydroazepine that can react with various nucleophiles. The electron-withdrawing *para*-carboxyl substituent increases the reactivity of the 1,2-didehydroazepine intermediate and as a result it can react not only with amines but also with alcohols. It has been suggested that even NH groups in the urethane bond are nucleophilic enough to react with the didehydroazepine. The density of phenylazide molecules reacted with a poly(ether urethane)-type SPU surface is $25\,nmol/cm^2$ at the outermost PU surface and $7.7\,nmol/cm^2$ within the surface layer of PU. No significant reaction was observed on the PU substrate. After photoreactive treatment with this compound for surface modification of the SPU, there was a dramatic improvement
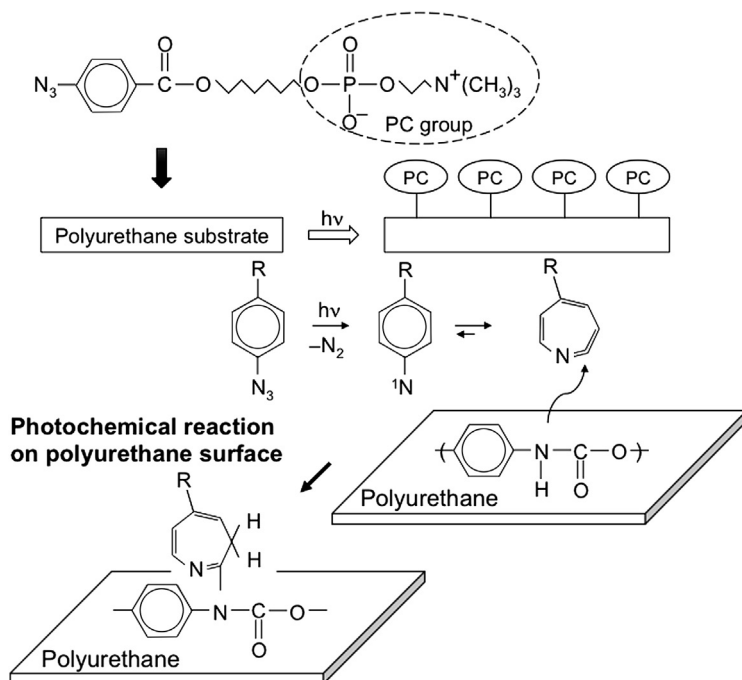
Figure 11.7 Photochemical immobilization of PC group on polyurethane.

in blood compatibility of SPU (Pellethane®). That is, the clotting time of blood in contact with the SPU increased from 8.2 min to a maximum of 22 min following this treatment. Also, the concentration of thrombin generated decreased from 102 nM on the original SPU surface to 56 nM on the modified surface when platelet-rich plasma (PRP) was in contact with these surfaces for 15 min in the presence of Ca^{2+}. Platelet adhesion and activation from PRP on the SPU were significantly reduced. These results show the potential of PU modification using a PC compound for obtaining improved blood compatibility.

Natural phospholipid molecules are glycerol derivatives with one PC group and two fatty acid moieties bound via an ester bond. Thus, glycerol–PC compounds are easily obtained and useful for preparing PUs. Aldehyde groups can be generated from 1,2-diol units by gentle oxidation. Feng et al. described the preparation of PC compounds with aldehyde groups (aldehyde–PC) and the surface reaction of PU with this compound for improving blood compatibility [85,86]. They used poly(carbonate urethane) as a PU substrate. To react at the surface of the PU, primary amino groups were introduced by reaction with additional diisocyanate and tris(aminoethyl)amine. Subsequently the aldehyde–PC reacts. The surface density of the amino group was 1.0 μmol/cm². The reactive efficiency of the amino groups on the surface toward the aldehyde–PC may not be sufficient due to the instability of aldehyde groups in aqueous medium and the bulky structure of the PC group. Thus, amino groups remained, which was confirmed by XPS analysis. However, it was described that platelet adhesion to the original PU was significantly reduced after this surface modification. To improve this, they attempted another process, a Michael addition reaction between the primary amino group and the double bond in the methacrylate group. 2-Methacryloyloxyethyl phosphorylcholine (MPC) is used as a methacrylate compound-bearing PC group (Figure 11.8).

Although MPC has been commercialized since 1999 worldwide, an excellent synthetic route for MPC production was first developed in 1987 and then reported in 1990 by Ishihara et al. [120,121]. The successful obtaining of high purity MPC opened up the field of MPC chemistry for applications in the biomedical and clinical medicine fields. MPC is a monomer used for preparing a polymer using a radical polymerization procedure, and it has been used as a reactive PC compound for introducing other functional groups into molecules [90,93,122]. Using a surface modification procedure MPC that was almost the same as the one used to obtain the aldehyde–PC compound described above, a PC-modified PU was obtained. Improved blood compatibility was confirmed by a platelet adhesion test, hemolysis test, and activated partial thromboplastin time measurement. Every evaluation revealed the positive effect of the PC group on the resistance of thrombus formation.

11.4.3.2   Polyaddition with diol compounds with a PC group

The introduction of a PC group into PU has been conducted during the polymerization process (Figure 11.9). Polyaddition is a common method for preparing PU between diol and isocyanate compounds. Glycerol–PC is an ideal candidate compound for preparing PU by polyaddition. Cooper et al. prepared PU using glycerol–PC as a chain

$$CH_2=\overset{\displaystyle CH_3}{\underset{\displaystyle \underset{\displaystyle OCH_2CH_2O\overset{\displaystyle O^-}{\underset{\displaystyle \underset{\displaystyle O}{\|}}{P}}OCH_2CH_2\overset{+}{N}(CH_3)_3}{\underset{}{C=O}}}{C}}$$

2-Methacryloyloxyethylphosphorylcholine (MPC)
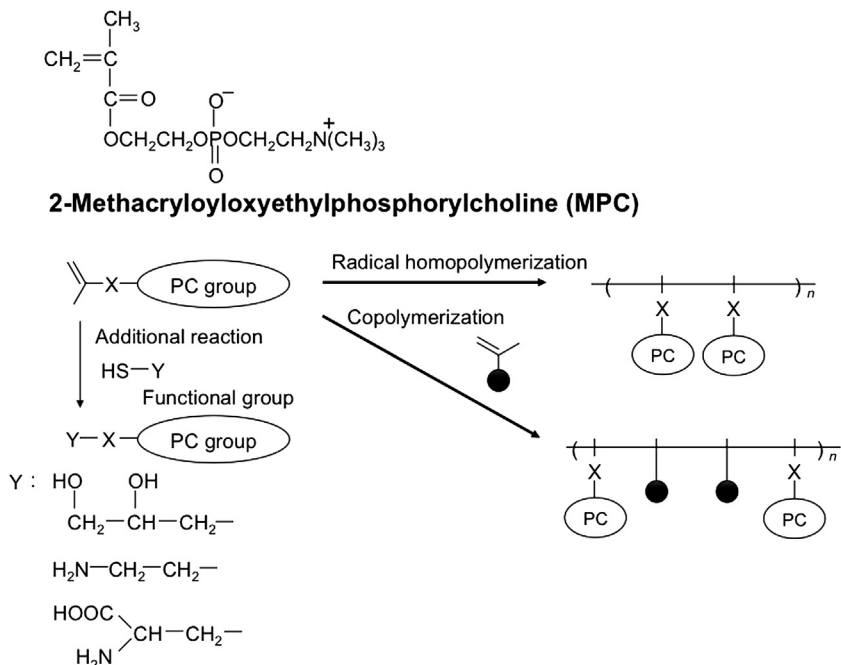
Figure 11.8 2-Methacryloyloxyethyl phosphorylcholine as functional compound.
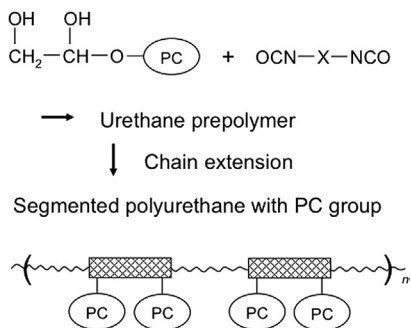
Figure 11.9 Segmented polyurethane with phosphorylcholine group as side chain.

extender [87,88]. By altering the ratio of glycerol–PC to 1,4-butanediol (BD), a series of polymers was obtained composed of different contents of PC groups. The mechanical properties of the PU with the PC group depended on the PC composition. An increase in the PC group composition increases the tensile strength and Young's modulus of the PU. Dynamic contact angle analysis showed that these PUs, especially the ones with a high PC group content, rearranged PC groups to minimize their interfacial tension on contact in an aqueous environment. They did not observe adhesion of neutrophils on the PU with the PC group. Cell spreading was observed on the control PU but not on PU surfaces with PC groups. Finally, they concluded that the incorporation

of the PC group into the PU backbone effectively reduced neutrophil adhesion and thus potentially could result in lower inflammatory and foreign body responses.

Considering the reactivity of the diol compounds with diisocyanate compounds during the polyaddition reaction, primary hydroxyl groups have higher reactivity than secondary hydroxyl groups. In the case of glycerol–PC, both types of hydroxyl groups should react at the same time to obtain higher molecular weight PU. Glycerol–PC, diol compounds with two primary hydroxyl groups and one PC group have been synthesized. Fu et al. synthesized 9-(2-hydroxy-1-hydroxymethyl-1-methyl-ethylcarbamoyl)-nonyl-phosphorylcholine (HDEAPC) and its fluorinated derivative (HFDAPC) [91,95]. Considering the molecular mobility of PC groups when the PU is in contact with aqueous medium, they introduced long alkyl and fluoroalkyl chains as spacers between main polymer chains and PC groups. This molecular design also improves the mechanical properties of PU because hydrophilic PC groups do not disturb the microphase separation of the PU main chain. The adsorption of plasma proteins from the protein solution was evaluated. In the case of conventional poly(carbonate urethane) and poly(ether urethane), several proteins in the range 1.5–4.5 $\mu g/cm^2$ were adsorbed. The amount of protein adsorbed on the PU with PC groups was reduced to about 1.0 $\mu g/cm^2$. This is a small improvement compared to conventional PU; however, the lower values suggest that the PC groups could help improve blood compatibility.

Nagase et al. synthesized diol compounds and 2-[3,5-bis(2-hydroxyethoxy)-benzoyloxy]ethyl phosphorylcholine (BHPC) and polymerized them with methylene diphenyl diisocyanate (MDI) and poly(carbonate diol) [94,99]. A PU chain extension with BD and SPU was obtained. On changing the composition of BHPC from 10 to 50 mol% against poly(carbonate diol), the solubility of PU and the final SPU was altered. Below 30 mol% BHPC, the PU can be dissolved in THF and chloroform. Hence, a high content of PC groups can be incorporated with the PU backbone. The mechanical properties of the PU and SPU are ideal and the polymer films were obtained by a solvent evaporation method using dimethyl sulfoxide (DMSO) solution. Surface blood compatibility was evaluated by investigating the adsorption of the plasma protein, albumin, and fibrinogen, and less adsorption was confirmed compared to poly(ethylene terephthalate) (PET) and the SPU without the PC group. They also prepared polymer thin films from the PU with the BHDC unit. The polymer solution was spin-cast on a water-soluble polymer substrate and the substrate was immersed in water. The water-insoluble PU layer was peeled off the substrate and a thin membrane was obtained. The thickness of the membrane was varied from 35 to 600 nm by changing the polymer concentration. The thin membrane was tough enough to evaluate platelet adhesion on the surface due to the good mechanical properties of the PU. The thin membranes can be used directly or can be bound to other substrates.

Nagase et al. synthesized a diamine monomer containing the PC group to prepare poly(urethane–urea)s containing PC groups [96]. The synthesized poly(urethane–urea)s possessed the high molecular weight required to prepare tough films via solvent casting. A platelet adhesion test showed that the poly(urethane–urea)s exhibited excellent blood compatibility, and adhesion of human platelets to the film surface

was significantly reduced. In addition, stress–strain measurements revealed that the poly(urethane–urea) films exhibited high elastic mechanical properties with Young's modulus increasing with increasing PC content.

As explained above, functional PC compounds can be synthesized from MPC as a starting molecule. Natural PC molecules accept oxidation under normal conditions easily because olefin units are located in the fatty acid moiety. The PC group itself is very hydrophilic and has limited solubility in organic solvent. Therefore, it is hard to use these compounds as starting compounds in organic reactions. MPC is currently produced on an industrial scale with a purity greater than 99%. The methacrylate moiety is the target of the Michael addition reaction along with amino and mercaptan groups (see Figure 11.8). Takami et al. developed a procedure for preparing PC compounds with 1,2-diol groups by a reaction between MPC and α-thioglycerol with a ternary amine as a catalyst [93]. Conversion from an MPC to a diol–PC compound proceeded well and the reaction conversion was above 90% after 5 h. Other functional methacrylates, which possess PEO, fluoroalkyl, or alkyl groups in the side chain, can be converted to the diol compound using the same reaction. PUs were synthesized by a one-pot reaction with the diol–PC compounds and MDI and BD. Protein adsorption was evaluated on these PU surfaces. The amount of albumin adsorbed on conventional PU (Biomate®) and PU without the functional group in the side chain was 3.5 and 1.8 μg/cm^2, respectively. This was decreased by the introduction of hydrophilic functional groups to 1.7 μg/cm^2 for the PEO side chain and 0.15 μg/cm^2 for the PC group in the side chain. Thus, a marked decrease in protein adsorption was observed on the introduction of the PC group.

Wagner et al. reported other reactions between MPC and cysteamine, under photoirradiation to synthesize a primary amino group-modified PC compound [90]. Poly(ester urethane urea) modified with a PC group was synthesized by the reaction of amine–PC compound with the backbone carboxyl groups of a PU synthesized from a soft segment blend of polycaprolactone and dimethylolpropionic acid, a hard segment of 1,4-diisocyanate butane, and a 1,4-butanediamine chain extender. The PC group-modified poly(ester urethane urea) experienced greater degradation than the control samples, that is, poly(ester urethane urea) from a soft segment of polycaprolactone and poly(ester urethane urea), in either a saline or lipase enzyme solution. The PC group-modified poly(ester urethane urea) also exhibited markedly inhibited ovine blood platelet deposition compared with the control PUs. They attempted loading of the bioactive reagent paclitaxel (PTX) in the PC group-modified poly(ester urethane urea). The PU film loaded with PTX did reduce rat smooth muscle cell proliferation. They concluded that the synthesized PC group-modified poly(ester urethane urea) has promising functionality for use as an antithrombogenic, drug-eluting coating on metallic vascular stents and grafts.

Grafting of a poly(MPC) chain on a PU surface by a surface-initiated living radical polymerization technique was reported and the surface platelet adhesion resistance postgrafting was confirmed [97]. Because the procedure for obtaining a blood-compatible PU surface is very complicated, it is not applicable for preparing blood-contacting medical devices.

11.4.3.3 Coating of PU substrates with MPC polymer

Another convenient surface modification of a PU is surface coating with a solution containing a polymer bearing a PC group in the side chain. The MPC polymers are good candidates and those with various methacrylates and styrene derivatives are obtained by conventional radical copolymerization. The MPC polymer is dissolved in a suitable solvent and a substrate for wrapping the MPC polymer layer is immersed into the solution. After removing the polymer substrate, the solvent is evaporated. To control the solubility of the MPC polymer in aqueous media and to obtain films on the substrate by the solvent evaporation procedure, hydrophobic monomer units are necessary. The most typical MPC polymer is poly(MPC-*co-n*-butyl methacrylate (BMA)) (PMB) [121]. Platelet adhesion and activation were completely suppressed on the surface of the PMB when the MPC unit composition was around 30 mol%. These ideal antithrombogenic properties appeared when the PMB was in contact with human whole blood, even in the absence of an anticoagulant. Protein adsorption on the PMB from human plasma determined by radioimmunoassay and immunogold labeling techniques showed that the amount of protein decreased with an increase in MPC moiety and appeared to be absorbed to the surfaces in a uniform and evenly distributed manner. The molecular weight is another important factor to consider when preparing a stable MPC polymer layer on the substrate. Usually, a molecular weight up to 5.0×10^5 Da is favorable. The PMB can be used to treat any kind of substrate including PUs using a simple solvent casting method [102–104]. One example shows the blood-compatible performance of PMB coated on PU *in vivo*. The PMB was coated on a blood pump and implanted into 2- to 3-month-old calves. After 15 days, the surface of the blood pump was observed and there was no visual thrombus formation on the PMB-coated PU. On the other hand, considerable thrombus was formed on the nontreated PU [102]. A PMB-coated PU was also applied as a cannula for an implantable blood pump [121]. The blood pump has been approved by the Japanese National Health Administration and has been implanted into humans since 2005. More than 100 pumps have been implanted at the present time and good blood compatibility has been observed.

Only hydrophobic interactions and van der Waals forces are generated between the BMA units and the substrate. In the case of SPUs, they can be used at the moving or flexible parts of medical devices, that is, the diaphragm portion of a blood pump. Thus, to enhance the molecular interaction forces, methacrylate with a urethane unit in the side chain was copolymerized with the MPC and BMA [101] (Figure 11.10). The monomers are synthesized using an additional reaction between the corresponding alcohol and the 2-isocyanatoethyl methacrylate. One example is 2-methacryloyloxyethyl butylurethane (MEBU). The MPC polymer obtained was characterized and the monomer unit composition for each type of monomer was 36/53/11 (unit mol%) for MPC unit/BMA unit/MEBU units. After the MPC polymers were coated on the SPU, Pellethane®, and TM-3® they were exposed to a water or 40 vol% aqueous ethanol solution for 3 h. XPS results showed improvement in the stability as a result of the introduction of urethane bound to the side chain of the MPC polymer. This was due to hydrogen bonding between the MPC polymer and the SPU. The number of platelets
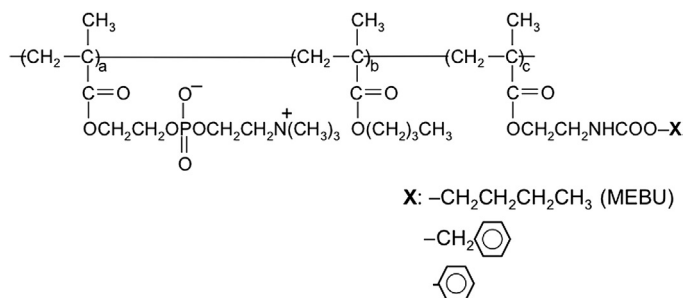
Figure 11.10 Chemical structure of the MPC polymer with various urethane units.

that adhered to the PU was significantly reduced after MPC polymer coating. This process is very useful for modification of PU-based medical devices.

11.5   Blending of a polymer with a PC group to improve blood compatibility

11.5.1   Random-type amphiphilic copolymers

Stable modification of a polymer may be obtained by entanglement of both polymer chains. This constitutes a blending of polymers in solution as a way of preparing a polymer alloy. The first example of a successful improvement in PU thrombogenicity using this technique was reported by Anderson et al. [123,124].

They used amphiphilic methacrylate polymer with a ternary amino group, poly(*N,N*-diisopropylaminoethyl methacrylate (DIPAM)-*co-n*-decyl methacrylate (DMA)) (PDD), composed of 25 unit mol% of DMA in the polymer as a polymeric additive to SPU. The content of the PDD in the SPU was in the range of 1–5 wt%. The surface characteristics of the SPU/PDD polymer alloy were examined by XPS and dynamic contact angle measurements with water. These evaluations revealed that the PDD was located on the surface of the polymer alloy. This induced a more hydrophilic and movable surface compared with untreated SPU. Protein adsorption from human plasma was also reduced on the surface of the SPU/PDD polymer alloy. During the blending process, the solubility of the polymer added to the SPU is important. The solubility parameter of the polymer is one of the factors used to estimate the blending state of both polymers.

MPC polymers were designed and blending was performed with SPUs [105–112] (Figure 11.11). Most of these research groups used random-type MPC polymers such as poly(MPC-*co*-cyclohexyl methacrylate) (PMC) and poly(MPC-*co*-2-ethylhexyl methacrylate) (PMEH) because of their solubility in the solvent and SPU. The solubility parameter of these polymers ranged from 20 to $26 \times 10^{-3} J^{1/2} m^{-3/2}$. The solubility parameter of PMB was above $25 \times 10^{-3} J^{1/2} m^{-3/2}$. The PMB barely dissolved in the solvent for SPU, which contained methylene chloride and tetrahydrofuran, with solubility parameters of 19.8 and $18.6 \times 10^{-3} J^{1/2} m^{-3/2}$, respectively [105]. To improve

Figure 11.11 Polymer alloy composed of MPC polymers and SPU coated on the polyester woven vascular prosthesis. Lower SEM pictures are original polyester prosthesis and that after coating with SPU/PMEH polymer alloy.
Reproduced with permission from Ref. [110].

the solvent system for the MPC polymers, a mixed solvent composed of methylene chloride and ethanol (70/30 v/v) was applied. As the solubility parameter of this mixture was $21.7 \times 10^{-3}\,J^{1/2}\,m^{-3/2}$, it was suitable for mixing with the SPU Tecoflex®. Also, the boiling points of the solvent components methylene chloride and ethanol are 40 and 78 °C, respectively. During the blending process, the migration of both polymer segments and functional groups to the side chain of the MPC polymer is strongly dependent on the concentration of the polymers. The evaporation of the solvents influences the location of the polymers and the functional groups of the polymer alloy. Ethanol is a good solvent for the MPC polymer because ethanol can dissolve the MPC polymer and concentrate at the interface in contact with the support substrate. In this way, the surface density of the MPC polymers becomes enhanced. This was revealed by direct observation of the polymer alloy composed of the MPC polymer and SPU by scanning microscopic observations after staining with osmium tetraoxide [106]. At the air-contacted surface, few MPC polymer domains were observed. In contrast, at the substrate-contact surface, many domains were observed. Since the MPC polymer is responsible for the blood-compatible nature of the polymer alloy, the substrate-contacting surface is ideally used as the blood-contacting surface. This surface enrichment occurs in the SPU/MPC polymer alloy along with maintenance of the original mechanical properties of the SPU.

Although the MPC polymer did not have complete compatibility with the SPU, a phase-separated structure (microdomain structure) was formed with the MPC polymer

located near the surface. The composition of the MPC polymer in the polymer alloy was less than 10 wt%. The mechanical properties of the polymer alloy were equivalent to those of SPU itself. To control the dispersion state of both SPU and MPC polymers in the solution, the effect of ultrasonication on the polymer solution on the microdomain structure of the polymer alloy was examined. Ultrasonication induced better dispersion of the MPC polymer in the SPU matrix. Many small microdomains approximately 0.5 μm in diameter were evenly dispersed on the substrate-contacting surface. The blood compatibility of the polymer alloy composed of SPU and MPC was evaluated by observing protein adsorption from human plasma and platelet adhesion. In comparison with the original SPU surface, both phenomena were reduced significantly by the addition of the MPC polymer. For example, the amount of protein adsorbed on the SPU was $2.8 \pm 0.2 \, \mu g/cm^2$, whereas it was reduced dramatically on the SPU/MPC polymer alloy with PMEH to $0.47 \pm 0.09 \, \mu g/cm^2$ [107].

A small-diameter vascular prosthesis with potential for clinical use was examined using a polyester fiber woven prosthesis coated with MPC polymer (Figure 11.11). When the luminal surface of the vascular prosthesis was coated with only an MPC polymer such as PMB, the polymer was easily washed out into the blood stream soon after implantation or detached by mechanical perturbations during the surgical procedure. The MPC polymer was then blended into the SPU as a polymeric additive. As a coating material, SPU (Tecoflex®) was blended with PMEH. The prosthesis, 2 mm in diameter, was immersed in a solution of the SPU/MPC polymer blend and dried to evaporate the solvent. The SPU/MPC polymer prosthesis was nonwater permeable and could be sewn to a natural vessel using a microsurgical technique. An SPU solution was used instead of the SPU/MPC polymer blend solution to prepare a control prosthesis (SPU prosthesis). The SPU/MPC polymer prosthesis and the SPU prosthesis were introduced as interpositional grafts in rabbit carotid arteries (Figure 11.12). A massive red thrombus became attached to the surface of the SPU prosthesis as early as 90 min after implantation. In the SPU/MPC polymer prosthesis (MPC polymer composition was 7.5 wt%), a clear surface was maintained for 5 days after implantation [110]. A much longer *in vivo* evaluation was also performed. The patency of the SPU/ MPC polymer prosthesis was four out of six at 1 week after implantation and two out

Original SPU (90 min)   **SPU/PMEH polymer alloy (4 weeks)**
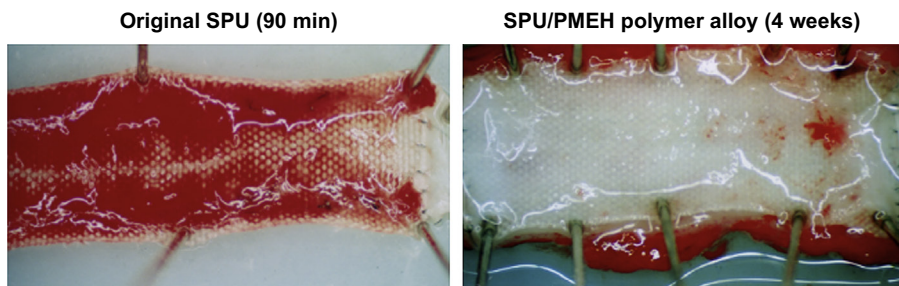
Figure 11.12 *In vivo* evaluation of small-diameter polyester vascular prosthesis coated with SPU and SPU/PMEH polymer alloy.
Reproduced with permission from Ref. [78].

of three at 4 weeks following implantation. An increase in the MPC content increased the patency of the prosthesis, and five out of six were patent for a week after implantation [111], three out of three were patent after 4 weeks, and three out of four were patent after 8 weeks [112].

Other MPC polymers have been blended with SPU. The MPC polymer with urethane bound poly(MPC-*co*-MEBU) (see Figure 11.10) (PMBU) to the side chain was blended by the same procedure described above. Fundamental characterizations regarding the surface and bulk properties were performed [109]. To improve the mechanical properties, a polymer composed of MPC and MEBU units was blended into SPU and fibrous vascular grafts were fabricated [114] (Figure 11.13). To develop a compliant conduit that could serve as a temporary vascular scaffold and facilitate tissue integration *in situ* while avoiding acute thrombosis, an electrospun biodegradable elastomer, poly(ether urethane urea), was employed as a scaffolding material that would be able to match with the native vessel compliance while providing additional
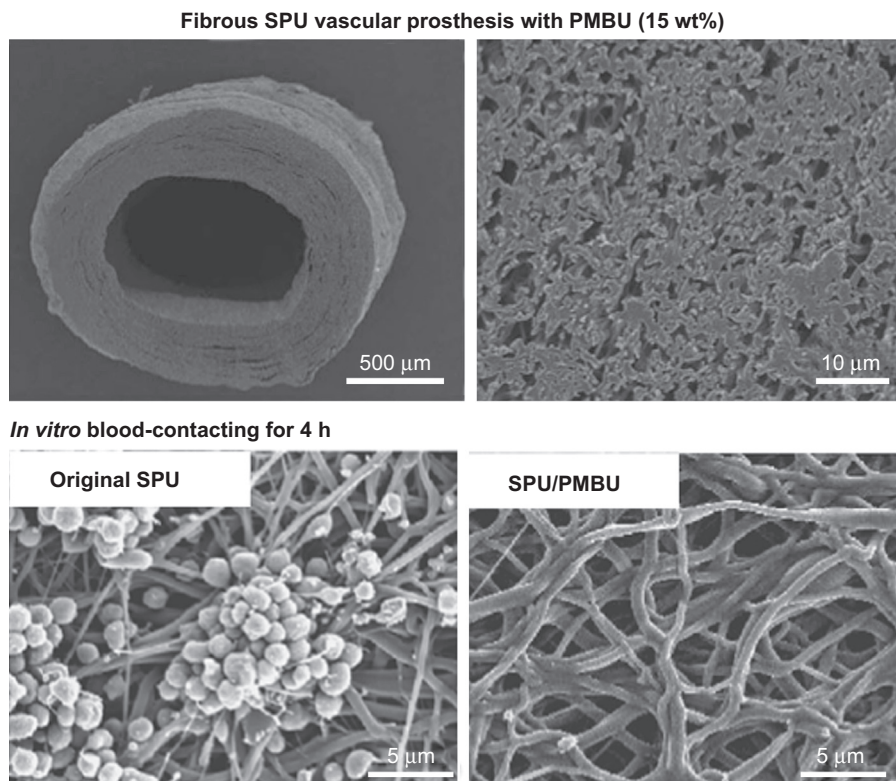
Figure 11.13 Fibrous polyurethane vascular prosthesis. Upper SEM pictures are morphology of the vascular prosthesis prepared with SPU/PMBU polymer alloy by electrospun procedure. Lower SEM pictures are the blood-contacting surface of the vascular prosthesis after 4 h blood circulating.
Reproduced with permission from Ref. [114].

suitable properties for surgical handling. Blends of poly(ether urethane urea) and PMBU with weight fractions of 0–15% were processed. The composite scaffolds were flexible with breaking strains exceeding 300%, tensile strengths of 7–10 MPa, and compliances of 2.9–4.4×10^{-4} mm/Hg. *In vitro* platelet deposition on the scaffold surfaces significantly decreased with increasing PMBU content. For *in vivo* evaluation, electrospun fibrous conduits of 1.3 mm internal diameter were implanted as aortic replacements in a rat model with an evaluation period of 8 weeks. Greater patency for grafts with 15% PMBU blending versus poly(ether urethane urea) without PMBU (67% vs 40%) was observed. A thin neo-intimal layer with endothelial coverage and good anastomotic tissue integration was observed in the poly(ether urethane urea)/PMBU vascular grafts. These results are promising and further evaluation of this technique in larger diameter applications for longer implant periods should be performed.

These observations indicated that MPC polymer in SPU can improve the anti-thrombogenicity of SPU, and the SPU/MPC polymer blend has potential for use in the preparation of small-diameter vascular prostheses.

11.5.2   Well-defined structure polymers as new polymeric additives

As noted above, the PMEH showed good blending with SPUs to produce the SPU/MPC polymer alloys. However, the MPC units of PMEH do not have an affinity for the SPU within the blend and can cause phase separation in the SPU/PMEH alloy. Thus, in the MPC/SPU blend, MPC units did not function as well as desired. The addition of PMEH into the SPU affects the mechanical properties of the SPU because the MPC units of PMEH and disturb hydrogen bonding between hard segments of the SPU. Thus, to improve the blood compatibility of the SPU/PMEH alloy without affecting the bulk properties of the SPU, it is necessary to control the compatibility and phase separation between the SPU and the PMEH. Recent progress in living radical polymerization has brought about a new era of well-defined polymer structures [125–128]. The molecular architecture of the MPC polymer could be modified by hydrophobic EHMA units. It is considered that a block-type copolymer composed of poly(MPC) and poly(EHMA) segments has the potential to make an ideal polymer alloy with SPU. A block-type polymer, poly(MPC-*block*-EHMA) (block-type PMEH), has been obtained by the reversible addition–fragmentation chain transfer (RAFT)-controlled radical polymerization method [117]. The SPU/block-type PMEH polymer alloy membrane was prepared by integration of polymer layers using the alternative solvent evaporation procedure. Indeed orientation of the molecular chains was controlled by use of the amphiphilic block copolymer. Thus, a high concentration of the poly(MPC) segments was achieved at the intended surface by the two-step solvent evaporation method.

Since the solubility of the poly(EHMA) segments is comparable to that of SPU, good mixing between the poly(EHMA) segments and SPU occurs. Additionally, the poly(MPC) segments in the SPU/block-type PMEH membrane orient toward the glass-contacting side because the PC groups in the MPC unit have an affinity for the hydrophilic glass. The orientation of each polymer segment in the block-type PMEH

enhances the hybridization with SPU and allows for maintenance of the mechanical properties. Also, the block-type PMEH layer was stabile on the SPU/block-type PMEH membrane even though the block-type PMEH has an amphiphilic nature.

The amount of fibrinogen adsorbed on the glass-contacting surface of the SPU/block-type PMEH membrane was reduced significantly compared with that of SPU. Also, blood cells did not adhere. The orientation of the poly(MPC) segments in the block-type PMEH allowed for sufficient antiadhesion function. Based on these considerations, it appears that the molecular architecture of the blended polymer provides for biomaterials with suitable mechanical properties and reduced thrombogenicity.

An additional molecular architecture is the graft-type polymer, which possesses a hydrophobic polymer segment as a side chain and a hydrophilic polymer segment in the main chain.

A graft-type PMEH was synthesized by the combination of two kinds of living radical polymerizations, namely RAFT polymerization and atom transfer radical polymerization (ATRP) [118,119] (Figure 11.14). The difference between block-type PMEH and graft-type PMEH is that graft-type PMEH contains many more poly(EHMA) side chains within one copolymer. The blending efficiency of these three kinds of SPU/PMEH can be compared by considering the graft-type PMEH as having an anchor, which sinks deeper into the SPU than random-type PMEH but remains shallower than block-type PMEH.
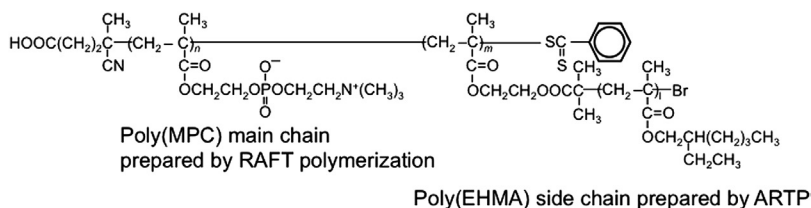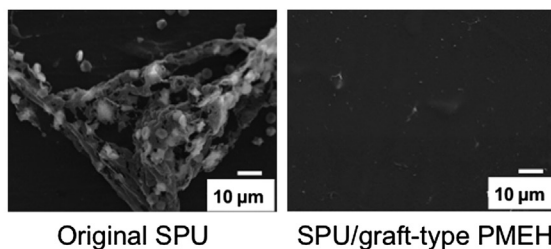
Figure 11.14 Chemical structure of graft-type polymer composed of poly(MPC) main chain and poly(EHMA) side chain prepared by two types of living radical polymerization. Lower SEM pictures show the blood-contacting lumen surface of SPU and SPU/gPMEH tubing after blood was passed for 2 min (scale bar: 10 μm).
Reproduced with permission from Ref. [118].

Liu et al. proposed that SPU membranes be modified by graft-type MPC polymers prepared by a double-solution casting procedure on stainless steel substrates [118]. The graft-type PMEH, which is composed of a poly(MPC) segment as the main chain and poly(EHMA) segments as side chains, shows a higher stability on the SPU membrane after being peeled off from the stainless steel substrate, as well as after immersion in aqueous medium. This stability is caused by the intermiscibility in the domain of the poly(EHMA) segments with the soft segments of the SPU membrane. Each SPU/MPC polymer alloy membrane exhibited a dramatic suppression of protein adsorption from human plasma and endothelial cell adhesion. Albumin, fibrinogen, and γ-globulin adsorbed in a dispersed pattern on the SPU surface. The SPU/graft-type PMEH polymer alloy dramatically suppressed protein adsorption. Compared with block-type PMEH, the molecular architecture suggests that the graft-type PMEH forms a fine and closely knit MPC unit network on the surface to protect against protein adsorption. It was demonstrated that the molecular architecture of the MPC polymer affects the surface characteristics of the modified SPU membranes. Porcine blood without any anticoagulant was passed through the SPU/graft-type PMEH tubing for 2 min for evaluation of initial antithrombogenicity. Red blood cells and platelets adhered to the inner surfaces of the SPU tubing. However, there was minimal adhesion to the SPU/graft-type PMEH tubing. The surface coverage of adherent blood cells including red blood cells and platelets on the blood-contacting surface of the SPU tubing was approximately 28%, and on the SPU/graft-type PMEH tubing it was reduced to less than 1%. Also, some aggregates were observed on the SPU surface. Fewer platelets were observed in each position of the SPU/graft-type PMEH tubing. In the SPU/graft-type PMEH tubing, blood cell adhesion was inhibited even after whole blood was passed through without anticoagulation. These results indicated that the poly(MPC) segments located on the surface of the graft-type PMEH function effectively and obtain antithrombogenicity.

The molecular architecture of the MPC polymers influenced the properties of the SPU/MPC polymer membrane, in particular, the stability of the MPC polymer layer on the SPU surface. The graft-type PMEH had better affinity for the SPU compared to random- and block-type PMEH. The SPU/graft-type PMEH polymer alloy, which has both excellent blood compatibility and mechanical properties, is a potential biomaterial for use in blood-contacting devices.

11.6 Concluding remarks

In this chapter, surface modifications of PU to achieve blood compatibility were summarized. Classical technologies involving conjugation with bioactive molecules such as heparin and urokinase are applied for short-term or single-use medical devices. Although a great deal of research regarding hydrophilic polymer grafting has been performed, no polymer-based or -coated medical devices that can be implanted for the long term have been created. The most attractive modification of the SPU surface is achieved by the bioinspired concept of constructing an artificial cell membrane surface with PC group-incorporated polymers. For example, a PU cannula connected to an implantable blood pump was coated with a phospholipid polymer and has functioned

for more than 9 years in the living body. However, much more stable incorporation of the phospholipid polymers with PU is desired. PUs have suitable mechanical properties and can be stable under biological conditions. Surface modification of the PU blood-contacting surface with other polymers has increased their potential applications in the medical field.

References

[1] Jaganathan SK, Supriyanto E, Murugesan S, Balaji A, Asokan MK. Biomaterials in cardiovascular research: applications and clinical implications. Biomed Res Int 2014;2014:Article ID 459465 (11 p).

[2] Ekdahl KN, Hong J, Hamad OA, Larsson R, Nilsson B. Evaluation of the blood compatibility of materials, cells, and tissues: basic concepts, test models, and practical guidelines. Adv Exp Med Biol 2013;735:257–70.

[3] Sin DC, Kei HL, Miao X. Surface coatings for ventricular assist devices. Expert Rev Med Devices 2009;6(1):51–60.

[4] Sharma CP. Blood-compatible materials: a perspective. J Biomater Appl 2001;15(4): 359–81.

[5] Sefton MV, Gemmell CH, Gorbet MB. What really is blood compatibility? J Biomater Sci Polym Ed 2000;11(11):1165–82.

[6] Kim SW, Jacobs H. Design of nonthrombogenic polymer surfaces for blood-contacting medical devices. Blood Purif 1996;14(5):357–72.

[7] Burke A, Hasirci N. Polyurethanes in biomedical applications. Adv Exp Med Biol 2004;553:83–101.

[8] Xue L, Greisler HP. Biomaterials in the development and future of vascular grafts. J Vasc Surg 2003;37(2):472–80.

[9] Zdrahala RJ, Zdrahala IJ. Biomedical applications of polyurethanes: a review of past promises, present realities, and a vibrant future. J Biomater Appl 1999;14(1):67–90.

[10] Palmaz JC. Review of polymeric graft materials for endovascular applications. J Vasc Interv Radiol 1998;9:7–13.

[11] Stokes K, McVenes R, Anderson JM. Polyurethane elastomer biostability. J Biomater Appl 1995;9(4):321–54.

[12] Guelcher SA, Gallagher KM, Didier JE, Klinedinst DB, Doctor JS, Goldstein AS, et al. Synthesis of biocompatible segmented polyurethanes from aliphatic diisocyanates and diurea diol chain extenders. Acta Biomater 2005;4:471–84.

[13] Chen JH, Wei J, Chang CY, Laiw RF, Lee YD. Studies on segmented polyetherurethane for biomedical application: effects of composition and hard-segment content on biocompatibility. J Biomed Mater Res 1998;41(4):633–48.

[14] Lan PN, Corneillie S, Schacht E, Davies M, Shard A. Synthesis and characterization of segmented polyurethanes based on amphiphilic polyether diols. Biomaterials 1996;17(23):2273–80.

[15] Wesslén B, Kober M, Freij-Larsson C, Ljungh A, Paulsson M. Protein adsorption of poly(ether urethane) surfaces modified by amphiphilic and hydrophilic polymers. Biomaterials 1994;15(4):278–84.

[16] Takahara A, Okkema AZ, Wabers H, Cooper SL. Effect of hydrophilic soft segment side chains on the surface properties and blood compatibility of segmented poly(urethaneureas). J Biomed Mater Res 1991;25(9):1095–118.

[17] Takahara A, Okkema AZ, Cooper SL, Coury AJ. Effect of surface hydrophilicity on ex vivo blood compatibility of segmented polyurethanes. Biomaterials 1991;12(3):324–34.

[18] Takahara A, Coury AJ, Hergenrother RW, Cooper SL. Effect of soft segment chemistry on the biostability of segmented polyurethanes. I. In vitro oxidation. J Biomed Mater Res 1991;25(3):341–56.

[19] Hsu SH, Kao YC, Lin ZC. Enhanced biocompatibility in biostable poly(carbonate)urethane. Macromol Biosci 2004;4(4):464–70.

[20] Hsu SH, Tseng HJ. In vitro biocompatibility of PTMO-based polyurethanes and those containing PDMS blocks. J Biomater Appl 2004;19(2):135–46.

[21] Silver JH, Myers CW, Lim F, Cooper SL. Effect of polyol molecular weight on the physical properties and haemocompatibility of polyurethanes containing polyethylene oxide macroglycols. Biomaterials 1994;15(9):695–704.

[22] Mora M, editor. Water in biomaterials surface science. Wiley-VCH; 2001. ISBN: 978-0-471-49041-8.

[23] Lelah MD, Grasel TG, Pierce JA, Cooper SL. Ex vivo interactions and surface property relationships of polyetherurethanes. J Biomed Mater Res 1986;20(4):433–68.

[24] Horbett T, Brash JL, Norde W, editors. Proteins at interfaces III: state of the art. American Chemical Society; 2012. ISBN13: 9780841227965.

[25] Park JH, Bae YH. Physicochemical properties and in vitro biocompatibility of PEO/PTMO multiblock copolymer/segmented polyurethane blends. J Biomater Sci Polym Ed 2002;13(5):527–42.

[26] Park JH, Cho YW, Kwon IC, Jeong SY, Bae YH. Assessment of PEO/PTMO multiblock copolymer/segmented polyurethane blends as coating materials for urinarycatheters: in vitro bacterial adhesion and encrustation behavior. Biomaterials 2002;23(19):3991–4000.

[27] Eloy R, Belleville J, Rissoan MC, Baguet J. Heparinization of medical grade polyurethanes. J Biomater Appl 1988;2(4):475–519.

[28] Lin SC, Jacobs HA, Kim SW. Heparin immobilization increased through chemical amplification. J Biomed Mater Res 1991;25(6):791–5.

[29] Nojiri C, Park KD, Grainger DW, Jacobs HA, Okano T, Koyanagi H, et al. In vivo nonthrombogenicity of heparin immobilized polymer surfaces. ASAIO Trans 1990;36(3):M168–72.

[30] Barbucci R, Magnani A, Albanese A, Tempesti F. Heparinized polyurethane surface through ionic bonding of heparin. Int J Artif Organs 1991;14(8):499–507.

[31] Sask KN, Berry LR, Chan AK, Brash JL. Polyurethane modified with an antithrombin-heparin complex via polyethylene oxide linker/spacers: influence of PEO molecular weight and PEO-ATH bond on catalytic and direct anticoagulant functions. J Biomed Mater Res A 2012;100(10):2821–8.

[32] Piao AZ, Jacobs HA, Park KD, Kim SW. Heparin immobilization by surface amplification. ASAIO J 1992;38(3):M638–43.

[33] Kim WG, Park KD, Mohammad SF, Kim SW. SPUU-PEO-heparin graft copolymer surfaces. Patency and platelet deposition in canine small diameter arterial grafts. ASAIO Trans 1999;37(3):M148–9.

[34] Park KD, Okano T, Nojiri C, Kim SW. Heparin immobilization onto segmented polyurethane-urea surfaces–effect of hydrophilic spacers. J Biomed Mater Res 1988;22(11):977–92.

[35] Lai ZF, Imamura T, Koike N, Kitamoto Y. Urokinase-immobilization suppresses inflammatory responses to polyurethane tubes implanted in rabbit muscles. J Biomed Mater Res A 2006;76(1):81–5.

[36] Takeda K, Harada A, Kubo M, Inenaga T, Tsuruya K, Mitsuiki K, et al. Successful use of single-lumen, urokinase immobilized femoral catheters as a temporary access for haemodialysis. Nephrol Dial Transplant 1998;13(1):130–3.

[37] Kitamoto Y, Tomita M, Kiyama S, Inoue T, Yabushita Y, Sato T, et al. Antithrombotic mechanisms of urokinase immobilized polyurethane. Thromb Haemost 1991;65(1):73–6.

[38] Leckband D, Sheth S, Halperin A. Grafted poly(ethylene oxide) brushes as nonfouling surface coatings. J Biomater Sci Polym Ed 1999;10(10):1125–47.

[39] Amiji M, Park K. Surface modification of polymeric biomaterials with poly(ethylene oxide), albumin, and heparin for reduced thrombogenicity. J Biomater Sci Polym Ed 1993;4(3):217–34.

[40] Tan J, McClung WG, Brash JL. Nonfouling biomaterials based on polyethylene oxide-containing amphiphilic triblock copolymers as surface modifying additives: protein adsorption on PEO-copolymer/polyurethane blends. J Biomed Mater Res A 2008;85(4):873–80.

[41] Ebert M, Ward B, Anderson J, McVenes R, Stokes K. In vivo biostability of polyether polyurethanes with polyethylene oxide surface-modifying end groups; resistance to biologic oxidation and stress cracking. J Biomed Mater Res A 2005;75(1):175–84.

[42] Chen Z, Ward R, Tian Y, Malizia F, Gracias DH, Shen YR, et al. Interaction of fibrinogen with surfaces of end-group-modified polyurethanes: a surface-specific sum-frequency-generation vibrational spectroscopy study. J Biomed Mater Res 2002;62(2):254–64.

[43] Duan X, Griffith CM, Dubé MA, Sheardown H. Novel dendrimer based polyurethanes for PEO incorporation. J Biomater Sci Polym Ed 2002;13(6):667–89.

[44] Wang DA, Ji J, Gao CY, Yu GH, Feng LX. Surface coating of stearyl poly(ethylene oxide) coupling-polymer on polyurethane guiding catheters with poly(ether urethane) film-building additive for biomedical applications. Biomaterials 2001;22(12):1549–62.

[45] Park JH, Park KD, Bae YH. PDMS-based polyurethanes with MPEG grafts: synthesis, characterization and platelet adhesion study. Biomaterials 1999;20(10):943–53.

[46] Archambault JG, Brash JL. Protein resistant polyurethane surfaces by chemical grafting of PEO: amino-terminated PEO as grafting reagent. Colloids Surf B Biointerfaces 2004;39(1–2):9–16.

[47] Nojiri C, Okano T, Jacobs HA, Park KD, Mohammad SF, Olsen DB, et al. Blood compatibility of PEO grafted polyurethane and HEMA/styrene block copolymer surfaces. J Biomed Mater Res 1990;24(9):1151–71.

[48] Ulbricht J, Jordan R, Luxenhofer R. On the biodegradability of polyethylene glycol, polypeptoids and poly(2-oxazoline)s. Biomaterials 2014;35(17):4848–61.

[49] Browning MB, Cereceres SN, Luong PT, Cosgriff-Hernandez EM. Determination of the in vivo degradation mechanism of PEGDA hydrogels. J Biomed Mater Res A 2014;102(12):4244–51.

[50] Hu T, Li D, Manjula BN, Acharya SA. Autoxidation of the site-specifically PEGylated hemoglobins: role of the PEG chains and the sites of PEGylation in the autoxidation. Biochemistry 2008;47(41):10981–90.

[51] Haseneder R, Fdez-Navamuel B, Härtel G. Degradation of polyethylene glycol by Fenton reaction: a comparative study. Water Sci Technol 2007;55(12):83–7.

[52] Llanos GR, Sefton MV. Does polyethylene oxide possess a low thrombogenicity? J Biomater Sci Polym Ed 1993;4(4):381–400.

[53] Silver JH, Marchant JW, Cooper SL. Effect of polyol type on the physical properties and thrombogenicity of sulfonate-containing polyurethanes. J Biomed Mater Res 1993;27(11):1443–57.

[54] Silver JH, Lewis KB, Ratner BD, Cooper SL. Effect of polyol type on the surface structure of sulfonate-containing polyurethanes. J Biomed Mater Res 1993;27(6):735–45.

[55] Silver JA, Okkema AZ, Hart AP, Cooper SL, Charef S, Labarre D, et al. Anticoagulant effects of sulfonate-containing polyurethanes. Biomaterials 1992;13:339–44.

[56] Lindon JN, McManama G, Kushner L, Merrill EW, Salzman EW. Does the conformation of adsorbed fibrinogen dictate platelet interactions with artificial surfaces? Blood 1986;68(2):355–62.

[57] Santerre JP, ten Hove P, VanderKamp NH, Brash JL. Effect of sulfonation of segmented polyurethanes on the transient adsorption of fibrinogen from plasma: possible correlation with anticoagulant behavior. J Biomed Mater Res 1992;26(1):39–57.

[58] Kim YH, Han DK, Park KD, Kim SH. Enhanced blood compatibility of polymers grafted by sulfonated PEO via a negative cilia concept. Biomaterials 2003;24(13):2213–23.

[59] Kim YH, Han DK, Park KD, Kim SH. Negative cilia model for biocompatibility: sulfonated PEG-grafted polymers and tissues. Macromol Sumpo 1997;118:565–70.

[60] Ye SH, Hong Y, Sakaguchi H, Shankarraman V, Luketich SK, D'Amore A, et al. Nonthrombogenic, biodegradable elastomeric polyurethanes with variable sulfobetaine content. ACS Appl Mater Interfaces 2014;6(24):22796–806.

[61] Wang C, Ma C, Mu C, Lin W. A novel approach for synthesis of zwitterionic polyurethane coating with protein resistance. Langmuir 2014;30(43):12860–7.

[62] Cao J, Yang M, Lu A, Zhai S, Chen Y, Luo X. Polyurethanes containing zwitterionic sulfobetaines and their molecular chain rearrangement in water. J Biomed Mater Res A 2013;101(3):909–18.

[63] Min D, Li Z, Shen J, Lin SC. Research and synthesis of organosilicon nonthrombogenic materials containing sulfobetaine group. Colloids Surf B Biointerfaces 2010;79(2):415–20.

[64] Yuan J, Lin S, Shen J. Enhanced blood compatibility of polyurethane functionalized with sulfobetaine. Colloids Surf B Biointerfaces 2008;66(1):90–5.

[65] Chang Y, Chen S, Yu Q, Zhang Z, Bernards M, Jiang S. Development of biocompatible interpenetrating polymer networks containing a sulfobetaine-based polymer and a segmented polyurethane for protein resistance. Biomacromolecules 2007;8(1):122–7.

[66] Yuan J, Chen L, Jiang X, Shen J, Lin S. Chemical graft polymerization of sulfobetaine monomer on polyurethane surface for reduction in platelet adhesion. Colloids Surf B Biointerfaces 2004;39(1–2):87–94.

[67] Yuan Y, Ai F, Zang X, Zhuang W, Shen J, Lin S. Polyurethane vascular catheter surface grafted with zwitterionic sulfobetaine monomer activated by ozone. Colloids Surf B Biointerfaces 2004;35(1):1–5.

[68] Jiang Y, Rongbing B, Ling T, Jian S, Sicong L. Blood compatibility of polyurethane surface grafted copolymerization with sulfobetaine monomer. Colloids Surf B Biointerfaces 2004;36(1):27–33.

[69] Jiang Y, Qingfeng H, Baolei L, Jian S, Sicong L. Platelet adhesive resistance of polyurethane surface grafted with zwitterions of sulfobetaine. Colloids Surf B Biointerfaces 2004;36(1):19–26.

[70] Yuan J, Zhang J, Zhu J, Shen J, Lin SC, Zhu W, et al. Reduced platelet adhesion on the surface of polyurethane bearing structure of sulfobetaine. J Biomater Appl 2003;18(2):123–35.

[71] Yuan YL, Ai F, Zhang J, Zang XB, Shen J, Lin SC. Grafting sulfobetaine monomer onto the segmented poly(ether-urethane) surface to improve hemocompatibility. J Biomater Sci Polym Ed 2002;13(10):1081–92.

[72] Lowe AB, Vamvakaki M, Wassall MA, Wong L, Billingham NC, Armes SP, et al. Well-defined sulfobetaine-based statistical copolymers as potential antibioadherent coatings. J Biomed Mater Res 2000;52(1):88–94.

[73] Lowe AB, McCormick CL. Synthesis and solution properties of zwitterionic polymers. Chem Rev 2002;102(11):4177–89.

[74] Coneski PN, Wynne JH. Zwitterionic polyurethane hydrogels derived from carboxybetaine-functionalized diols. ACS Appl Mater Interfaces 2012;4(9):4465–9.

[75] Yuan J, Zhang J, Zhou J, Yuan YL, Shen J, Lin SC. Platelet adhesion onto segmented polyurethane surfaces modified by carboxybetaine. J Biomater Sci Polym Ed 2003; 14(12):1339–49.

[76] Nakabayashi N, Ishihara K. Nonthrombogenic polymers – designs and evaluation. Macromol Sympo 1996;101:405–12.

[77] Ishihara K. Novel polymeric materials for obtaining blood compatible surface. Trend Polym Sci 1997;5(12):401–7.

[78] Ishihara K. Bioinspired phospholipid polymer biomaterials for making high performance artificial organs. Sci Technol Adv Mater 2000;1:131–8.

[79] Lewis AL, Lloyd AW. Biomedical applications of biomimetic polymers: the phosphorylcholine-containing polymers. In: Santin M, Phillips G, editors. Biomimetic, bioresponsive, and bioactive materials: an introduction to integrating materials with tissues. John Wiley & Sons; 2012. pp. 95–140. [Chapter 4].

[80] Iwasaki Y, Ishihara K. Phosphorylcholine-containing polymers for biomedical applications. Ann Bioanal Chem 2005;381:534–46.

[81] Iwasaki Y, Ishihara K. Cell membrane-inspired phospholipid polymers for developing medical devices with excellent biointerfaces. Sci Technol Adv Mater 2012;13:064–101 (14p).

[82] Monge S, Canniccioni B, Graillot A, Robin JJ. Phosphorus-containing polymers: a great opportunity for the biomedical field. Biomacromolecules 2011;12(6):1973–82.

[83] van der Heiden AP, Goebbels D, Pijpers AP, Koole LH. A photochemical method for the surface modification of poly(etherurethanes) with phosphorylcholine-containing compounds to improve hemocompatibility. J Biomed Mater Res 1997;37(2):282–90.

[84] van der Heiden AP, Willems GM, Lindhout T, Pijpers AP, Koole LH. Adsorption of proteins onto poly(ether urethane) with a phosphorylcholine moiety and influence of preadsorbed phospholipid. J Biomed Mater Res 1998;40(2):195–203.

[85] Lu J, Feng Y, Gao B, Guo J. Preparation and characterization of phosphorylcholine glycerol grafted polycarbonateurethane films. J Polym Res 2012;19:9959 (5p).

[86] Gao B, Feng Y, Lu J, Zhang L, Zhao M, Shi C, et al. Grafting of phosphorylcholine functional groups on polycarbonate urethane surface for resisting platelet adhesion. Mater Sci Eng C Mater Biol Appl 2013;33(5):2871–8.

[87] Yung LY, Colman RW, Cooper SL. Neutrophil adhesion on polyurethanes preadsorbed with high molecular weight kininogen. Blood 1999;94(8):2716–24.

[88] Yung LY, Cooper SL. Neutrophil adhesion on phosphorylcholine-containing polyurethanes. Biomaterials 1998;19(1–3):31–40.

[89] Ruiz L, Fine E, Vörös J, Makohliso SA, Léonard D, Johnston DS, et al. Phosphorylcholine-containing polyurethanes for the control of protein adsorption and cell attachment via photoimmobilized laminin oligopeptides. J Biomater Sci Polym Ed 1999;10(9):931–55.

[90] Hong Y, Ye SH, Pelinescu AL, Wagner WR. Synthesis, characterization, and paclitaxel release from a biodegradable, elastomeric, poly(ester urethane)urea bearing phosphorylcholine groups for reduced thrombogenicity. Biomacromolecules 2012;13(11):3686–94.

[91] Tan D, Zhang X, Li J, Tan H, Fu Q. Modification of poly(ether urethane) with fluorinated phosphorylcholine polyurethane for improvement of the blood compatibility. J Biomed Mater Res A 2012;100(2):380–7.

[92] Tan H, Ji J, Luo J, Xie X, Zhong Y, Fu Q. Synthesis and properties of novel segmented polyurethanes containing alkyl phosphatidylcholine side groups. Eur Polym J 2005;41:1893–900.

[93] Takami K, Matsuno R, Ishihara K. Synthesis of polyurethanes by polyaddition using diol compounds with methacrylate-derived functional groups. Polymer 2011;52(24):5445–51.

[94] Sakagami Y, Horiguchi K, Narita Y, Sirithep W, Morita K, Nagase Y. Syntheses of a novel diol monomer and polyurethane elastomers containing phosphoripid moietyes. Polym J 2013;45:1159–66.

[95] Tan H, Liu J, Li J, Jiang X, Xie X, Zhong Y, et al. Synthesis and hemocompatibility of biomembrane mimicing poly(carbonate urethane)s containing fluorinated alkyl phosphatidylcholine side groups. Biomacromolecules 2006;7(9):2591–9.

[96] Nagase Y, Nakajima S, Oku M, Iwasaki Y, Ishihara K. Synthesis and properties of segmented poly(urethane-urea)s containing phosphorylcholine moiety in the side chain. Polym J 2008;40(12):1149–52.

[97] Jin Z, Feng W, Zhu S, Sheardown H, Brash JL. Protein-resistant materials via surface-initiated atom transfer radical polymerization of 2-methacryloyloxyethyl phosphorylcholine. J Biomater Sci Polym Ed 2010;21(10):1331–44.

[98] Zhang X, Tan D, Li J, Tan H, Fu Q. Synthesis and hemocompatibity evaluation of segmented polyurethane end-capped with both a fluorine tail and phosphatidylcholine polar head groups. Biofouling 2011;27(8):919–30.

[99] Sirithep W, Morita K, Iwano A, Komachi T, Okamura Y, Nagase Y. Syntheses and properties of elastic copoly(ester-urethane)s containing a phospholipid moiety and the fabrication of nanosheets. J Biomater Sci Polym Ed 2014;25(14–15):1540–57.

[100] Soletti L, Nieponice A, Hong Y, Ye SH, Stankus JJ, Wagner WR, et al. In vivo performance of a phospholipid-coated bioerodable elastomeric graft for small-diameter vascular applications. J Biomed Mater Res A 2011;96(2):436–48.

[101] Ishihara K, Hanyuda H, Nakabayashi N. Synthesis of phospholipid polymers having a urethane bond in the side chain as coating material on segmented polyurethane and their platelet adhesion-resistant properties. Biomaterials 1995;16(11):873–9.

[102] Lee I, Kobayashi K, Sun HY, Takatani S, Zhong LG. Biomembrane mimetic polymer: poly(2-methacryloyloxyethyl phosphorylcholine-co-n-butyl methacrylate) at the interface of polyurethane surfaces. J Biomed Mater Res A 2007;82(2):316–22.

[103] Ho SP, Nakabayashi N, Iwasaki Y, Boland T, LaBerge M. Frictional properties of poly(MPC-co-BMA) phospholipid polymer for catheter applications. Biomaterials 2003;24(28):5121–9.

[104] Foy JR, Williams 3rd PF, Powell GL, Ishihara K, Nakabayashi N, LaBerge M. Effect of phospholipidic boundary lubrication in rigid and compliant hemiarthroplasty models. Proc Inst Mech Eng H 1999;213(1):5–18.

[105] Ishihara K, Tanaka S, Furukawa N, Kurita K, Nakabayashi N. Improved blood compatibility of segmented polyurethanes by polymeric additives having phospholipid polar groups. I. Molecular design of polymeric additives and their functions. J Biomed Mater Res 1996;32(3):391–9.

[106] Ishihara K, Shibata N, Tanaka S, Iwasaki Y, Kurosaki T, Nakabayashi N. Improved blood compatibility of segmented polyurethane by polymeric additives having phospholipid polar group. II. Dispersion state of the polymeric additive and protein adsorption on the surface. J Biomed Mater Res 1996;32(3):401–8.

[107] Ishihara K, Iwasaki Y. Biocompatible elastomers composed of segmented polyurethane and 2-methacryloyloxyethyl phosphorylcholine polymer. Polym Adv Technol 2000;11(8–12):626–38.

[108] Ishihara K, Fujita H, Yoneyama T, Iwasaki Y. Antithrombogenic polymer alloy composed of 2-methacryloyloxyethyl phosphorylcholine polymer and segmented polyurethane. J Biomater Sci Polym Ed 2000;11(11):1183–95.

[109] Ogawa R, Iwasaki Y, Ishihara K. Thermal property and processability of elastomeric polymer alloy composed of segmented polyurethane and phospholipid polymer. J Biomed Mater Res 2002;62(2):214–21.

[110] Yoneyama T, Ishihara K, Nakabayashi N, Ito M, Mishima Y. Short-term in vivo evaluation of small-diameter vascular prosthesis composed of segmented poly(etherurethane)/2-methacryloyloxyethyl phosphorylcholine polymer blend. J Biomed Mater Res Appl Biomater 1998;43(1):15–20.

[111] Yoneyama T, Sugihara K, Ishihara K, Iwasaki Y, Nakabayashi N. The vascular prosthesis without pseudointima prepared by antithrombogenic phospholipid polymer. Biomaterials 2002;23(6):1455–9.

[112] Yoneyama T, Ito M, Sugihara K, Ishihara K, Nakabayashi N. Small diameter vascular prosthesis with a nonthrombogenic phospholipid polymer surface: preliminary study of a new concept for functioning in the absence of pseudo- or neointima formation. Artif Organs 2000;24(1):23–8.

[113] Sawada S, Iwasaki Y, Nakabayashi N, Ishihara K. Stress response of adherent cells on a polymer blend surface composed of a segmented polyurethane and MPC copolymers. J Biomed Mater Res A 2006;79(3):476–84.

[114] Hong Y, Ye SH, Nieponice A, Soletti L, Vorp DA, Wagner WR. A small diameter, fibrous vascular conduit generated from a poly(ester urethane)urea and phospholipid polymer blend. Biomaterials 2009;30(13):2457–67.

[115] Iwasaki Y, Aiba Y, Morimoto N, Nakabayashi N, Ishihara K. Semi-interpenetrating polymer networks composed of biocompatible phospholipid polymer and segmented polyurethane. J Biomed Mater Res 2000;52(4):701–8.

[116] Morimoto N, Iwasaki Y, Nakabayashi N, Ishihara K. Physical properties and blood compatibility of surface-modified segmented polyurethane by semi-interpenetrating polymer networks with a phospholipid polymer. Biomaterials 2002;23(24):4881–7.

[117] Asanuma Y, Inoue Y, Yusa S, Ishihara K. Hybridization of poly(2-methacryloyloxyethyl phosphorylcholine-block-2-ethylhexyl methacrylate) with segmented polyurethane for reducing thrombogenicity. Colloids Surf B Biointerfaces 2013;108:239–45.

[118] Liu Y, Inoue Y, Mahara A, Kakinoki S, Yamaoka T, Ishihara K. Durable modification of segmented polyurethane for elastic blood-contacting devices by graft-type 2-methacryloyloxyethyl phosphorylcholine copolymer. J Biomater Sci Polym Ed 2014;25(14–15):1514–29.

[119] Liu Y, Inoue Y, Sakata S, Kakinoki S, Yamaoka T, Ishihara K. Effects of molecular architecture of phospholipid polymers on surface modification of segmented polyurethanes. J Biomater Sci Polym Ed 2014;25(5):474–86.

[120] Ishihara K, Ueda T, Nakabayashi N. Preparation of phospholipid polymers and properties as hydrogel membranes. Polym J 1990;22:355–60.

[121] Ishihara K, Fukazawa K. 2-methacryloyloxyethyl phosphorylcholine polymer. In: Monge S, David G, editors. Phosphorus-based polymers: from synthesis to applications. (Cambridge, UK): RSC Publishing; 2014. pp. 68–96. [Chapter 5].

[122] Matsuno R, Takami K, Ishihara K. Simple synthesis of a library of zwitterionic surfactants via Michael-type addition of methacrylate and alkane thiol compounds. Langmuir 2010;26(16):13028–32.

[123] Brunstedt MR, Ziats NP, Robertson SP, Hiltner A, Anderson JM, Lodoen GA, et al. Protein adsorption to poly(ether urethane ureas) modified with acrylate and methacrylate polymer and copolymer additives. J Biomed Mater Res 1993;27(3):367–77.

[124] Brunstedt MR, Ziats NP, Schubert M, Hiltner PA, Anderson JM, Lodoen GA, et al. Protein adsorption onto poly(ether urethane ureas) containing methacrol 2138F: a surface-active amphiphilic additive. J Biomed Mater Res 1993;27(2):255–67.

[125] Lobb EJ, Ma I, Billingham NC, Armes SP, Lewis AL. Facile synthesis of well-defined, biocompatible phosphorylcholine-based methacrylate copolymers via atom transfer radical polymerization at 20 °C. J Am Chem Soc 2001;123(32):7913–4.

[126] Yusa S, Fukuda K, Yamamoto T, Ishihara K, Morishima Y. Synthesis of well-defined amphiphilic block copolymers having phospholipid polymer sequences as a novel biocompatible polymer micelle reagent. Biomacromolecules 2005;6(2):663–70.

[127] Inoue Y, Watanabe J, Takai M, Ishihara K. Surface characteristics of block-type copolymer composed of semi-fluorinated and phospholipid segments synthesized by living radical polymerization. J Biomater Sci Polym Ed 2004;15(9):1153–66.

[128] Ahmed M, Bhuchar N, Ishihara K, Narain R. Well-controlled cationic water-soluble phospholipid polymer-DNA nanocomplexes for gene delivery. Bioconjug Chem 2011;22(6):1228–38.

Antimicrobial polyurethanes for intravascular medical devices

12

I. Francolini*, A. Piozzi
Sapienza Univeristy of Rome, Piazzale Aldo Moro, Rome, Italy
*Corresponding author: iolanda.francolini@uniroma1.it

12.1 Introduction

Intravascular devices have become an indispensable part of modern medical care. In past decades, many novel synthetic materials were developed for the manufacturing of temporary or permanent devices including prostheses, bone replacement implants, heart valves, intravascular catheters, urinary catheters, and other devices providing clinicians with useful means for improving health care. Notwithstanding their considerable success, clinical complications are still associated with the use of medical devices, the most common of which is the onset of local and systemic infections (nosocomial infections or hospital-acquired infections, HAIs). When a biomaterial is implanted in the body, a biological response of the organism occurs, causing the covering of the medical device surface with a conditioning film, rich in proteins, polysaccharides, and cells. This covering plays an important role in the early stages of microbial biofilm formation, as it alters the surface properties of the biomaterial, thereby influencing the magnitude and speed of microbial adhesion.

In the United States hospitals, about 2 million people acquire bacterial infections each year. The World Health Organization has reported that the highest prevalence of nosocomial infections occurs in acute surgical and orthopedic wards and in intensive care units (ICU). Among medical devices, catheters are invaluable tools in medical practice. Intravascular catheters are employed in the administration of fluids, medications, and blood products, as well as in the monitoring of hemodynamic status of critically ill patients and in chronic outpatient hemodialysis. Their use is associated with a high risk of development of catheter-related bloodstream infections (CR-BSIs) causing a considerable increase of morbidity and mortality, prolonged hospitalization, and additional medical costs. Risk factors in the development of catheter bacterial colonization and bloodstream infection include patient factors (increased risk associated with malignancy, neutropenia, and shock) and treatment-related factors (increased risk associated with total parenteral nutrition, ICU admission for any reason, and endotracheal intubation). Other risk factors are prolonged catheter indwelling time, lack of asepsis during central venous catheter (CVC) insertion, and frequent manipulation of the catheter.

Since the eradication of these infections with antimicrobial agents is more difficult and often such infections cause the devices to malfunction, leading to their removal, new approaches are needed to prevent bacterial colonization.

The recommended prevention strategies include: (1) educating and training of health care providers who insert and maintain catheters; (2) using full barrier precautions during CVC insertion; (3) using antiseptics for skin; (4) developing antiadhesive biomaterials using physicochemical methods; (5) using antiseptic/antibiotic impregnated short-term CVCs.

The last method of prevention represents one of the most promising strategies developed in recent years since the antimicrobial agent adsorbed on the catheters is released directly at the infection site. Recently, intrinsically antimicrobial polymers have emerged as promising candidates to address biofilm-based medical device-related infections.

Catheter material can play an important role in the prevention of catheter-related infections (CR-Is). Indeed, more infectious complications have been associated with the use of polyvinyl chloride (PVC) or polyethylene catheters compared to catheters made of Teflon or polyurethane (PU).

This chapter will be focused on antimicrobial PUs for intravascular applications. First, a classification of the types of PU intravascular devices and their impact in the medical field will be introduced. Then, a survey of infections associated with intravascular devices in terms of incidence, etiology, and pathogenesis will be presented. Next, management of device-related infections and the role of modified PUs in preventing intravascular device-related infections will be discussed. Finally, the future direction of novel antimicrobial polymers as biomaterials for the development of devices preventing biofilm-based infections will be described.

12.2 PUs in intravascular applications

The medical device industry has witnessed remarkable growth from 1995 to 2015, with a huge differentiation in the types of available products. The medical device industry is estimated at 150 billion US$ worldwide.[1] Medical devices have now become indispensable tools in modern clinical practice. This is also thanks to the enormous advances achieved in biomaterials science from 1985 to 2015. The concept of a biomaterial has changed radically over the years. In the early 1980s, a biomaterial was defined as "a systemically and pharmacologically inert substance designed for implantation within or incorporation with living systems"[2] while in the late 1980s a biomaterial was considered as "a nonviable material used in a medical device, intended to interact with biological systems" (Williams, 1987). Scientists have realized that to be functional, a biomaterial must interact properly, and not be inert, with the surrounding tissues. This has triggered the development of new classes of biomaterials that work with the physiological environment and have specific chemical features, porosity, degradability, and mechanical properties.

The biological response of an organism to a biomaterial depends on the body site of device implantation.

A classification often used to distinguish the different typologies of intracorporeal medical devices is that considering their localization into the vascular system (intravascular devices) or not (extravascular devices). It is clear how these two classes of devices interact very differently with the host. Indeed, intravascular devices are destined to interact with the blood components while extravascular devices interact with the surrounding tissues or interstitial fluids.

Table 12.1 Main intravascular applications of polyurethanes

Intravascular device	Uses
Peripheral venous catheters	Administration of intravenous fluids, medication, or parenteral nutrition; sampling blood
Central venous catheters (tunneled, nontunneled, or totally implanted ports)	Administration of medication or fluids
	Monitoring venous pressure
	Sampling blood
Pulmonary artery catheters	Diagnostic applications
Artificial heart valves	Replacement of dysfunctional heart valves
Vascular grafts	Redirect blood flow in a specific region of the body
Coronary stents	Treatment of coronary arteries suffering from stenosis
Pacemakers	Control abnormal heart rhythms
Left ventricular assist devices	Support heart function and blood flow

Segmented PUs are considered the materials of choice for manufacturing intravascular devices. Blood compatibility of PUs was first claimed by Boretos and Pierce[3] and Lyman et al.[4] in the late 1960s and early 1970s. This property was soon related to the PU unique molecular structure constituted by separated microphases composed of *hard* and *soft* segment domains.[5] Blood response following interaction with a PU was shown to be dependent on hard/soft segment type and concentration.[6,7] The flexibility of the soft segment has also been shown to play a positive role for polymer interaction with the biological system while hard segments with high crystallinity were shown to promote thrombogenicity of the polymer. Therefore, thanks to their fairly good bio- and hemocompatibility and excellent physicomechanical properties,[8] a number of different intravascular devices from catheters to heart valves are currently made with PU (Table 12.1).

The features required for each of these applications can be very different depending on the site of implant, length of implantation, method of application, and function. For this reason, a large variety of biomedical-grade PUs with different compositions have been produced and marketed (Table 12.2). These products differ in terms of elastomeric properties, degradation rate, hydrophilicity, fatigue resistance, resistance to stress cracking, and so on.

Biomer® and Pellethane® are traditional segmented polyether urethanes based on polytetramethylene oxide (PTMO), methylene-bis-phenyldiisocyanate (MDI), and ethylenediamine (ED) or butanediol (BD), respectively. They possess an excellent balance between physicochemical and biological properties together with ease of processing. For many years, they have been employed for fabrication of artificial ventricles or heart valves as well as for other cardiovascular devices. However, their use has been discontinued due to their lack of long-term performance[9] and permeability to water and water vapor.[10] That makes polyether urethanes suitable only for short-term applications such as peripheral or CVCs.

To increase hemocompatibility and biostability, siloxanes have been incorporated into PUs. The ability of siloxane to improve PU blood compatibility has already been

Table 12.2 Examples of biomedical-grade polyurethanes

Trade name	Supplier	Description
Biomer®	Ethicon	Polyether urethane urea (PTMO/MDI/ED)
Pellethane®	Dow Chemical USA	Polyether urethane (PTMO/MDI/BD)
Tecoflex HR™	Thermodics	Aliphatic polyether urethane (PTMO/HMDI/BD)
Vialon	Becton Dickinson polymer	Polyether urethane (PTMO/MDI/BD)
Cardiothane-51™	Kontron Instruments	PDMS-grafted polyether urethane
Rimplast™	Petrarch System Inc.	Silicone–polyurethane interpenetrating network
PurSil® TSPU	DSM Corporate	Silicone-based PU
Corethane®	Corvita Corp	Polycarbonate-based PU
Bionate® PCU	DSM Corporate	Polycarbonate-based PU
ChronoFlex C	AdvanSource Biomaterials	Aromatic polycarbonate-based PU
CarboSil® TSPCU	DSM Corporate	Silicone–polycarbonate–urethane copolymer
ChronoSil®	AdvanSource Biomaterials	Silicone–polycarbonate–urethane copolymer

demonstrated in the early 1990s by Cooper et al. who performed an investigation on the influence of the chemistry of the soft segment on blood interactions.[11] They tested different PUs containing the following soft segments: polyethylene oxide (PEO), PTMO, polybutadiene (PBD), hydrogenated PBD (HPBD), and polydimethylsiloxane (PDMS). Their findings showed that the most hydrophobic PDMS-based segmented PU had the lowest platelet adhesion among the investigated PUs, while the initial rate of platelet adhesion increased with the increase in hydrophilicity of the polyol soft segment. The authors concluded that PU blood compatibility depends on a combination of factors including microphase separation, surface heterogenicity, and surface hydrophilicity.

Cardiothane-51™ is one of the first commercially available polymers coupling PDMS and PUs. It consists of Pellethane® grafted with 10% acetoxy-terminated PDMS. The availability of PDMS on the PU surface depends on the techniques used to prepare the sample. Rimplast™ is a PU/silicone interpenetrating network obtained by mixing reactive silicone pellets with pellets of base PU at high temperature in the extrusor or injection molding. The mechanical and physiological properties of Rimplast™ can be modulated by varying silicone content and cross-link density. PurSil® is a PDMS-based PU in which the silicone is used in the PU synthesis as the soft segment. This polymer is claimed to be thromboresistant and to have excellent mechanical properties compared to conventional silicone elastomers.

Polycarbonate-based PUs were later developed to further extend biostability, to improve PU mechanical properties, and to reduce water permeability. Corethane® and Bionate® PCU are examples of polycarbonate-based PUs and are claimed to possess

enhanced biostability, load-bearing capability, water resistance, and radiation resistance. Therefore, these products are intended for long-term applications such as vascular grafts, artificial heart, and cardiac assist devices.

Finally, CarboSil® and ChronoSil® are thermoplastic polysiloxane/polycarbonate/PU copolymers able to combine the mechanical strength of polycarbonate-based PUs with the biostability and hemocompatibility of siloxane-based PUs. These products are also resistant to environmental stress cracking and therefore suitable for long-term cardiovascular applications.

12.3   Infections associated with intravascular devices

Intravascular devices are essential tools for the management of patients suffering from cardiovascular diseases, cancer, and other diseases. However, their implantation in the body exposes the patient to a substantial risk of infection.

Globally, urinary tract and surgical site infections are the most frequent health-care-associated infections (HAIs) followed by respiratory and BSIs.[12] The highest proportion of BSIs is related to the implant of intravascular devices, especially CVCs, originated by hematogenous spreading. BSIs have the highest impact in terms of associated morbidity and mortality. Indeed, according to Klevens et al.,[13] in 2002 the estimated deaths associated with HAIs in US hospitals were 98,987 (ca. 6% of the total HAIs), of these ca. 30% for BSIs, 13% for urinary tract infections, and 8% for surgical site infections.

12.3.1   Incidence of CVC-related infections

A large number of CVCs are inserted yearly in hospitalized or outpatient settings for a variety of different indications, including administration of drugs, monitoring central venous pressure, total parenteral nutrition, poor peripheral venous access, and cardiac catheterization. According to recent data, the worldwide usage of catheters per years is around 400 million[1] and this number is likely to increase. In the United States, more than 5 million CVCs are implanted each year, with approximately 200,000 cases of BSIs related to their use.[14]

Many different types of venous-access devices are available. Peripherally inserted central venous catheters (PICCs), which can be made of PU or silicone, are inserted into a vein in the arm rather than in the neck or chest. Nontunneled CVCs are short-term catheters, made of PU or silicone as well, inserted into the internal jugular, subclavian, or femoral vein. Tunneled CVCs are long-term catheters implanted surgically under the skin. One end of the catheter remains outside the skin and the exit site is typically located in the chest. Passing the catheter under the skin helps to reduce the infection risk and provides stability. Implantable ports are similar to tunneled catheters but are left completely under the skin. They consist in small devices, made of plastic or titanium, inserted beneath the skin and connected to a catheter allowing vascular access. Under the skin, the port has a septum through which drugs can be injected and blood samples can be withdrawn.

The risk of catheter-associated BSIs (CA-BSIs) has been estimated from 11% to 14% with an attributable mortality that can exceed 25%.[15] That risk has been shown to be dependent on the length of catheterization, the type of venous-access device, and the underlying patient characteristics. Particularly, the incidence of CVC-related infections was found to be higher in CVCs kept in place for more than 7 days.[16] Several studies have tried to compare the incidence of infections in PICCs, CVCs, and ports. Al Raiy et al.[17] followed hospitalized patients who were implanted either a CVC or a PICC. A number of 638 CVCs was placed for 4917 catheter-days versus a total of 622 PICCs for 5703 catheter-days. A similar rate of infection was found for both groups of venous access (rate of 2.4 and 2.3 per 1000 catheter-days for CVCs and PICCs, respectively). However, the median time to infection development was significantly higher in the patients with a PICC, suggesting that this device is a safe choice for prolonged venous access.

Also Chopra et al.,[18] in a systematic review and meta-analysis, compared the risk of BSIs associated with PICCs with that related to CVCs in adults. Pooled meta-analyses of the 20 available studies revealed that PICCs were associated with a lower risk of CA-BSIs than CVCs, but the greatest reduction in CA-BSIs was recorded in outpatients. Therefore, the authors concluded that hospitalized patients may be just as likely to experience CA-BSIs with PICCs and CVCs.

The underlying patient characteristics, especially type of disease and age, significantly influence the rate, morbidity, and mortality of CR-Is. According to the National Nosocomial Infections Surveillance (NNIS) System Report, the rate for CA-BSIs varies from 4.0 per 1000 catheter days in medical–surgical ICUs to 7.0 per 1000 catheter days in burn ICU units.[19] CR-Is remain among the most frequent complications in cancer patients,[20] 33% of whom experiences at least an episode of infection during catheterization.[21] Two risk factors have been identified for early CRIs: young age (<10 years) and difficulties during insertion.[22]

12.3.2 Incidence of infections in patients with permanent pacemakers or implantable cardioverter defibrillators

Cardiac prosthetic devices are routinely employed in modern cardiovascular medicine. Permanent indwelling devices, including permanent pacemakers (PPMs) and implantable cardioverter defibrillators (ICDs), have been shown to improve survival rates and reduce symptoms. More than 3 million PPMs and ca. 180,000 ICDs were functioning in 2000 worldwide.[23] Infection of these cardiac devices is a serious complication occurring either within 1 year after implantation as a surgical site infection or later as a lead endocarditis.[24] The most common signs and symptoms of infection are pocket erythema and local pain while the most common pathogens are coagulase-negative staphylococci and *Staphylococcus aureus*.[23] The estimated rate of infection following implantation of cardiac prosthetic devices in adults is between 1% and 2%[25,26] but increases in young patients (<40 years old) and reaching 5.5% in young patients with congenital heart disease.[27] Data collected from the National Hospital Discharge Survey from 1996 to 2003 evidenced an increase in the infection rate related to implantable antiarrhythmic systems faster than the rate of device implantation.[28] In addition,

in the same period, the risk of infection was found to be greater in ICD than in permanent pacemakers.[28] Use of temporary pacing before implantation, fever within 24 h before implantation, and early reinterventions have also been identified as risk factors by a large prospective study performed in 44 French medical centers.[29] Additional risk factors are pulse generator replacement surgery and dual- or triple-chamber device implantation.

An optimal procedure for management of such infections has yet to be defined. Usually the management consists in antimicrobial therapy combined with complete device removal. However, mortality rates of device-related endocarditis remain as high as 18%.[30,31]

12.3.3   Incidence of left ventricular assist device infections

Left ventricular assist devices (LVADs) have become an effective treatment support for patients with severe heart failure awaiting transplantation. Indeed, there is a significant gap between the population of patients with congestive heart failure and the number of donors, which has been filled by the recent implementation of LVADs. The new generation continuous-flow assist devices have also provided a destination therapy for end-stage heart failure patients who are not candidates for cardiac transplantation.[32] Infection is one of the most prevalent complications of these devices.[33] Infections related to these devices can be broadly divided into driveline infections, pump-pocket infections (PPIs), and LVAD-associated endocarditis.[34] Driveline infections occur along the percutaneously implanted lead connecting the device motor to its external power source. PPIs occur within the recess made in the abdominal cavity to house the device. According to the major trials performed in recent years on LVADs,[35–38] driveline infections occur more frequently than PPIs while the incidence of blood infection ranged from 20% to 44% with the exception of the ADVANCE trial in which blood infection was lower (11.4%).[38]

12.3.4   Incidence of infections related to intra-aortic balloon pump

Intra-aortic balloon pump (IABP) is a mechanical device that increases myocardial oxygen perfusion in critically ill patients with cardiac diseases such as cardiogenic shock (CS), acute myocardial infarction (AMI), and ventricular arrhythmias.[39]

The IABP consists in a polyethylene or PU balloon mounted at the distal tip of a large bore catheter. The catheter is generally inserted into the aorta through the femoral artery in the leg. Outside the catheter is connected to a console that inflates the balloon with helium. The goal of IABP is to support a failing heart by increasing the myocardial oxygen supply and decreasing myocardial oxygen demand. To do so, the balloon inflates in diastole, augmenting coronary perfusion, and deflates in early systole (counterpulsation). The duration of IABP treatment ranges normally from few hours to few days and in some cases can be prolonged for weeks.[40]

Several complications are known to be associated to IABP implantation.[40–42] The main vascular complications are thrombocytopenia, bleeding, systemic embolization, and limb ischemia. IABP may also be associated with mechanical complications, including balloon rupture or inadequate inflation.[39,41]

Vales et al.[43] performed a retrospective cohort study by collecting clinical data from 150 patients admitted to the Beth Israel Medical Center in New York and receiving IABP therapy between 2004 and 2009. The results showed that thrombocytopenia was the most common adverse event, occurring in 50% of the involved patients, followed by fever (36%) and bleeding (27%). Patients who developed fever had higher in-hospital mortality (31% vs 16%) and longer duration of IABP was significantly associated with the development of fever. The duration of IABP treatment has been recognized as a risk factor for development of IABP-related complications also in a recent investigation performed by Valente et al.[44] on 481 patients admitted to the Intensive Care Unit of the Careggi University Hospital in Florence, Italy. In this study complications were observed in ca. 13% of patients, among whom ca. 50% showed major bleeding. Other variables identified as predictors for major IABP-related complications are: (1) age (>70 years); (2) female gender; (3) history of peripheral vascular disease; and (4) diabetes mellitus.[41]

An IABP-associated infection is rare (<1%).[40,42] Local wound infections have been reported to occur in up to 5% of patients and bacteremia in up to 2.2%.[45] Several factors have been implicated in the genesis and rate of IABP-related infections, including improper preparation or contamination of the femoral area during surgical insertions, the clinical settings in which the IABP procedure is carried out,[46] and the duration of IABP treatment.[47]

Even if the infection rate is low, in view of a steadily increasing use of IABPs, the absolute number of IABP-related infections is expected to grow. Therefore, certain clinical and epidemiological issues should not be neglected. Yu et al.[48] recently reported a clinical case concerning a 78-year-old woman with AMI complicated by CS who needed bypass surgery. An IABP was inserted to reduce afterload in view of the bypass surgery. After surgery, IABP was removed and the device was cut in pieces and inoculated in culture media to assess possible bacterial load. The Gram-positive methicillin-susceptible *S. aureus* was found to grow on the IABP. The patient was submitted to antibiotic therapy but her condition deteriorated up to death 3 weeks later. The authors remarked that the possibility of bacteremia is often overlooked in IABP patients with systemic inflammatory response syndrome (SIRS), especially fever.

Crystal et al.[49] evaluated the incidence of bacteremia and sepsis in IABP patients and determined the clinical significance of fever after IABP implantation. Seventy-one patients over a 2-year period (1996–1998) admitted at the Cardiology Department of the Soroka University Medical Center (Israel) were studied. The length of IABP therapy ranged from 3 h to 9 days. Thirty-one patients (52%) developed SIRS during treatment, 90% of whom had fever. Bacteremia and sepsis occurred in 15% and 125 of patients, respectively. Coagulase-negative staphylococci were the most prevalent species in broth cultures. Bacteremia was detected mainly during the first hours after IABP insertion. The authors raised a question as to the need for antibiotic prophylaxis administration before IABP placement.

12.3.5   Incidence of prosthetic vascular graft-related infections

Vascular grafts are used to replace, bypass, or maintain function of damaged, occluded, or diseased blood vessels. They can be obtained through the use of either blood vessels of the patient's own body (autogenous grafts) or synthetic materials (artificial grafts).

The most used materials to manufacture artificial grafts are polyethylene terephthalate (PET, Dacron®), polytetrafluoroethylene (PTFE), and PUs. The first PU vascular graft was a polyester-based PU (Vascugraft®). These prostheses showed good biocompatibility but a poor chemical stability *in vivo*.[50,51] Also polyether-based PUs (Pulse-Tec®) were found to be susceptible to oxidative degradation.[52] On the contrary, a new generation of PU grafts based on poly(carbonate urethanes) (Corvita®) showed superior biostability.[53]

The complication and patency rates of PTFE and PU grafts implanted for hemodialysis vascular access were compared by Kiyama et al.[54] by a long-term follow up of 53 patients who received 58 arteriovenous grafts between 1997 and 2000. Both problem-free (primary) and functional (secondary) patency rates for PU and PTFE grafts were similar at 1 year and 2 years.

An ideal synthetic vascular graft should possess several features: biocompatibility; mechanical strength, and compliance for long-term devices; thromboresistance; availability in various sizes; satisfactory graft healing and ability to withstand infection.

Infection of a vascular graft is a potentially life-threatening complication. The incidence of prosthetic vascular graft infection is between 1% and 6%.[55] The Infection risk was also found to vary with the location of the vascular graft: 1% for abdominal grafts, 2% for aortofemoral grafts, and 6% for infrainguinal grafts.[56–59] The clinical presentation of prosthetic graft infection can vary according to infection location. Infections that involve an extremity, such as the femoral component of an aortic prosthetic graft, tend to present with focal inflammatory changes. In contrast, infections of intracavitary graft locations are more difficult to diagnose since they do not present specific symptoms.[60] To permit a more precise prognostication and treatment, a classification of vascular graft infections has been established by Szilagyi,[61] later modified by Samson.[62] Several risk factors have been identified for vascular graft infections including groin incisions, emergent surgery, diabetes mellitus, chronic renal disease, obesity, and immunocompromised conditions.[56]

Recently, Zetrenne et al.[55] performed a multicenter review to determine the primary mode of therapy and rate of limb salvage for major prosthetic graft infections. The review of records was completed at three hospitals: the Hospital of California–Irvine Medical Center, the Yale New Haven Medical Center, and the Hospital of Saint Raphael. Only extracavitary and distal limb aortofemoral graft infections belonging to groups 3, 4, and 5 of the Samson classification[62] were reviewed. According to the pooled results, 34 out of 45 infected grafts were done in PTFE, 8 in Dacron, and the remaining were composite grafts. The 64% of infections developed early (less than 4 months) and the groin was the most common site of infection (82%). *Staphylococcus epidermidis* was the most common Gram-positive organism cultured (32%), followed by methicillin-resistant *S. aureus* (26%). Gram negatives were also isolated in 16 cases, and of those, only 3 were *Pseudomonas aeruginosa*.

12.4   Pathogenesis of intravascular device–related infections

Microbial colonization of intravascular catheters can follow either an extraluminal route, for which microorganisms arising from skin at the catheter insertion site migrate along the external catheter surfaces up to the catheter tip, or an intraluminal route by inoculation of microorganisms from the catheter hub or contaminated intravenous fluids. Less frequently, microorganisms can be hematogenously seeded from another focus of infection. Most studies suggest that an extraluminal colonization of the catheter is more frequent in short-term catheterization (less than 7 days), whereas an intraluminal colonization predominates with long implantation times.[63]

Important pathogenic factors for catheter contamination are related to: (1) the properties of the material constituting the device, (2) host factors, and (3) the intrinsic virulence factors of the involved microorganisms (ability to form biofilm).[64] In Table 12.3, the factors controlling microbial adhesion to abiotic surfaces are listed.

12.4.1   Physicochemical properties of the catheter surface

There is a great diversity in the available intravascular devices, in terms of both chemical composition of the material constituting the catheter and features of the final product. Some catheter materials have surface irregularities that can provide protection for bacterial cells and promote their attachment. However, the influence of surface roughness on microbial adhesion is still controversial. Some studies show an increase in bacterial adhesion with increasing roughness of the substratum.[65,66] Other authors believe that surface roughness does not significantly affect bacterial adhesion and biofilm formation.[67,68] These controversial results are presumably related to the different bacterial species studied, determined roughness parameters, and methods to detect

Table 12.3 Factors controlling microbial adhesion to abiotic surfaces are listed

Factor	Specific variable
Physical properties of the surface	Porosity
	Roughness
Chemical properties of the surface	Hydrophobicity/hydrophilicity
	Polar groups
	Charged groups
Environmental conditions	Host protein conditioning layer
	Shear rate
	pH and temperature
Pathogen	Gram positive/Gram negative
	Genus/species
	Surface charge
	Ability to form biofilm

microbial adhesion on the surface. In general, it was shown in some *in vitro*[66,69] and *in vivo* studies[70,71] that there exists a threshold average surface roughness (0.2 μm) for bacterial retention, below which surface roughness has no significant effect on microbial adhesion. Above this threshold, an increase in biofilm accumulation was instead observed.[72]

Some polymeric materials are more thrombogenic than others, and this has been shown to favor catheter colonization and infection development.[73] Indeed, in a prospective multicenter study carried on ICU patients requiring internal jugular or subclavian catheterization[74] a relationship between CVC-related thrombosis and infection was found. In fact, the risk of sepsis was 2.62-fold higher in patients with thrombosis. Similarly, van Rooden et al.[75] found a temporal association of CVC-related infection and thrombosis. In addition, the absolute risk of developing a thrombotic event in patients with CVC-associated sepsis (57%) was higher compared to that found in patients with a local CVC-related infection (27%). These findings explain why silicone intravascular catheters are associated with higher risk of infection than PU catheters.[76]

The interaction of microorganisms with a biomaterial may also be described in thermodynamic terms by applying concepts of the Derjaguin, Landau, Verway, and Ocerbeek (DLVO) theory.[77] Indeed, because of their small size, low density, and net negative surface charge, bacteria can be considered as living colloids. Therefore, the interaction forces occurring at the biomaterial surface are electrostatic forces generated by a net charge distribution on both the biomaterial surface and the bacterial wall, van der Waals forces arising from permanent dipoles, and Brownian motion forces. Electrostatic interactions are negligible when neutral polymers are considered while the van der Waals forces are predominant and account for the different extents of microbial adhesion on different substrates. Speranza et al.[78] studied the *Escherichia coli* adhesion on three clinical grade polymers, PVC, polymethyl methacrylate, and polyethylene, having different acidic/basic properties. The extent of bacterial adhesion depended on the presence of acidic or basic sites on the polymer surface. In particular, because of its basic character, *E. coli* had a higher interaction with PVC.

Tegoulia and Cooper[79] studied *S. aureus* adhesion on self-assembled monolayers terminated with methyl, hydroxyl, carboxylic acid, and tri(ethylene oxide) groups. Results showed how bacterial adhesion was lower on the hydrophilic ethylene oxide-bearing and hydroxyl-bearing surfaces. However, preincubation of surfaces with fibrinogen increased microbial adhesion on all surfaces and minimized the effect of the surface properties of the substrate. The authors concluded that even if surfaces rich in ethylene oxide groups can be used to prevent bacterial adhesion under physiological conditions, most of the substrate properties are masked and their effect on adhesion becomes minimal.

12.4.2 Host factors

The adhesiveness of a given microorganism to specific host factors is also important in the pathogenesis of CR-BSIs. The first biological response of the host organism to the presence of a foreign body consists in depositing on the device surfaces host

proteins, mainly albumin, fibronectin, and fibrinogen. These proteins can mediate microbial adhesion. Albumin was shown to have inhibitory effects on bacterial adhesion to polymer, ceramic, and metal surfaces. *S. aureus* adhesion to different types of PUs (positively charged PUs, aminated PUs, negatively charged sulfonated PUs) was also studied.[80] Materials were tested bare, or coated with human fibrinogen, plasma, or albumin. The results showed how the presence of fibrinogen or plasma enhanced the attachment rate constants while albumin inhibited microbial adhesion. Although it has not been clarified, its mechanism of action is presumably reduction of the hydrophobicity of the surface of the polymer substrate.[81]

Fibronectin is one of the main protein components of the extracellular matrix and is known to mediate the phenomena of surface adhesion in eukaryotic cells. This protein plays an important role in infections associated with biomaterials and it has been shown that *S. aureus* has specific receptors for this protein.[82,83] Similarly, fibrinogen promotes adherence of bacteria, especially staphylococci to biomaterials.[84]

12.4.3 Microbial ability to form a biofilm

It is now widely accepted that microbial biofilms play a key role in all types of health-care-associated infections and especially in those related to medical devices. Particularly, biofilm formation on the device surfaces contributes to the severity of these infections. Indeed the development of biofilm is responsible for the chronic nature of related infections, and for the inherent resistance to antibiotic therapy.[85] Raad et al.[86] were among the first investigators who isolated biofilm-producing microorganisms from the intraluminal surface of CVCs, which remained *in situ* for more than 30 days.

Understanding the mechanisms of biofilm formation has been crucial for the design of new biomaterials able to prevent microbial adhesion and biofilm formation on device surfaces. The use of microscopic techniques, including scanning electron microscopy (SEM) and confocal laser scanning microscopy (CLSM), has elucidated the complex morphology assumed by surface-adherent bacteria. Biofilms are now defined as microbial sessile communities, often multispecies, irreversibly attached to a surface, either biotic or abiotic, and embedded in a self-produced matrix consisting of polysaccharides, proteins, and nucleic acid.[87] Biofilms are heterogeneous mushroom-like structures in which microcolonies are glued together by the sticky exopolysaccharide matrix. Water-filled channels are present between the microcolonies to allow nutrients and oxygen to reach the bacteria located in the bottom layers of the biofilm.

Biofilm development is a multistage process. In Figure 12.1 the biofilm formation onto the external surface of a catheter (convex surface) is seen. In Stage 1 (*Reversible adhesion*), planktonic microorganisms approach the surface and adhere to it via van der Waals or electrostatic interactions. In Stage 2 (*Irreversible adhesion*), microorganisms permanently attach to the surface by using cell-adhesion structures (such as pili) or producing specific adesins, resulting in the formation of a monolayer of microcolonies. In Stage 3 (*Early biofilm development*), microorganisms begin to secrete extracellular components with early vertical development. The ability of microorganisms to produce these components is a prerequisite for biofilm formation. Stage 4
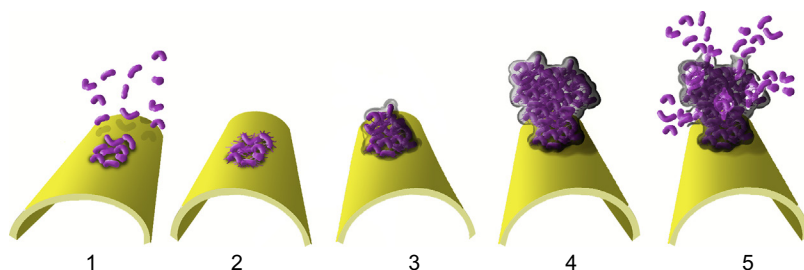
Figure 12.1 Stages of biofilm formation.

(*Biofilm maturation*) concerns the maturation of the typical three-dimensional mushroom-like architecture of biofilms. In Stage 5 (*Cell dispersal*), detachment of bacterial cells or clumps from the biofilm external layer or within the interior of the biofilm by a "swarming" phenomenon occurs resulting in a so-called "seeding dispersal."

Microorganisms growing as biofilms exhibit a resistance to antibiotics higher than their planktonic counterpart. The mechanisms involved in the increased drug resistance of biofilms are many.[85,88,89] The biofilm matrix can act as a barrier delaying the diffusion of antibiotics into the inner layers of biofilm. This phenomenon depends on the type of antibiotic and biofilm. Indeed, fluoroquinolones have been shown to readily penetrate *P. aeruginosa* biofilms,[90] while positively charged aminoglycosides showed a delayed diffusion[91] due to their interaction with the negatively charged *P. aeruginosa* biofilm matrix.

The presence of subpopulations of persister or dormant bacterial cells in a spore-like, nondividing state has been also suggested as a possible mechanism of biofilm resistance.[88,92] Many antibiotics targeting growth-specific factors are poorly effective against slow- or nongrowing cells. For instance, fluoroquinolones are more efficacious on biofilm-growing *P. aeruginosa* with respect to with β-lactams since these latter antibiotics are active only against growing bacterial cells. However, fluoroquinolones work better against planktonic cells compared to biofilm-growing *P. aeruginosa*.[93] Persister cells may therefore survive after antibiotic therapy and may regrow causing chronic infections.

The conjugation frequency seems to be higher in bacteria growing as biofilms than in the planktonic mode,[94] and this contributes to amplification of both naturally occurring and induced antibiotic resistance.

Finally, an important variable that can influence the antibiotic susceptibility of biofilm-growing microorganisms is the age of the biofilm. Particularly, as the biofilm ages its treatment becomes more difficult as demonstrated for *S. epidermidis* biofilms, which were more resistant to cefalotin, clindamycin, erythromycin, vancomycin, and teichoplanin with increased age.[95] Finally, the presence of a mixed microbial population in the biofilm can influence susceptibility to antimicrobial agents. Adam et al.[96] showed by using a catheter disk model system how, in a mixed species biofilm of *Candida albicans* and *S. epidermidis*, *C. albicans* protected the *staphylococcus* against vancomycin and *S. epidermidis* protected the fungus against fluconazole.

12.4.4 Microrganisms involved in intravascular device-related infections

The most commonly reported causative pathogens remain coagulase-negative staphylococci, *S. aureus*, enterococci, and *Candida* spp.[97] Gram-negative bacilli accounted for 19% and 21% of CR-BSIs reported to CDC[98] and the Surveillance and Control of Pathogens of Epidemiological Importance (SCOPE) database, respectively.[97]

The main problem related to CA-BSIs is the antimicrobial resistance of the involved pathogens. Particularly, infections caused by methicillin-resistant *S. aureus* (MRSA) can be life-threatening especially for ICU patients.

According to Klevens et al.,[99] the proportion of MRSA isolated in ICUs in US hospitals increased from 35.9% in 1992 to 64.4% in 2003. However, a decrease in multidrug resistance among MRSA isolates was observed. The incidence of MRSA central line-associated BSIs has decreased in recent years, presumably due to prevention efforts.[100]

An increasing proportion of intravascular device-related infections are being caused by *Candida* spp. and the management of these infections can be challenging. *Candida* infections account for ca. 10% of the whole number of intravascular catheter-associated infections.[101] Usually the management of these infections requires the device removal.

Biofilm-based central line-associated infections are often polymicrobial.[102,103] Particularly, *C. albicans* and *S. aureus* can be found coexisting as polymicrobial biofilms on catheter surfaces.[104]

It is estimated that *S. aureus* is the third most common organism isolated in conjunction with *C. albicans*.[105] It was demonstrated *in vitro* that *S. aureus* can form microcolonies on the surface of *C. albicans* biofilm, serving as scaffolding. In addition, the *S. aureus* resistance to vancomycin was enhanced within the polymicrobial biofilm while the sensitivity of *C. albicans* to amphotericin B was not altered.[105]

12.5 Prevention of intravascular device–related infections

The management of intravascular device–related infections depends on several factors related to the patient, pathogen, and type of infected device. Removal of the device is recommended when signs of severe infection are present or if virulent pathogens, such as *S. aureus* or *P. aeruginosa*, are isolated.[106] However, removing the infected device is not always possible or easy to perform. Therefore, salvage of the device is preferred and the patient is given the antibiotic therapy. Particularly, infections associated with long-term or permanent CVCs are frequently treated with success by systemic antibiotic therapy combined with "antibiotic lock" therapy for 2 weeks.[106]

To reduce the incidence of such infections, specific guidelines providing strategies for prevention are available.[107] Strict adherences to hygienic rules during insertion or implantation of the device are aspects of particular importance. According to these guidelines, despite the use of maximal sterile barrier precaution and skin cleaning with

antiseptic agents, the implantation of antimicrobial-coated CVCs is recommended in patients whose catheter is expected to remain in place >5 days.[107]

Therefore, besides strict hygienic rules during insertion of the device, the development of new materials able to counteract microbial adhesiveness and colonization has become a critical issue in recent years. The two principal approaches to prevent microbial adhesiveness are (1) the development of polymers with antifouling properties, and (2) the development of polymers with antimicrobial properties.[108,109] Such materials either repel microbes (antifouling) or kill bacteria (antimicrobial) present in the surface proximity.

Antifouling polymers are usually obtained by modification of the polymer surface by physicochemical methods leading to unspecific interactions with microorganisms. Since the surface of microbial cells is mainly hydrophobic and negatively charged, chemical modifications generally aim to either (1) increase surface hydrophilicity; (2) introduce negatively charged groups; or (3) decrease surface free energy.[110] Antifouling polymers are interesting since they avoid the use of drugs but their efficacy is strongly dependent on the microbial species. In addition, it is difficult to create a surface with no adhesion also considering that *in vivo* the material surface is rapidly covered by plasma proteins. Therefore, the strategy more pursued for preventing microbial adhesion is the development of antimicrobial polymers. Such polymers can be obtained by (1) surface adsorption of antimicrobial drugs; (2) drug entrapping in the polymer bulk; (3) drug grafting on the device surface; and (4) introduction in the polymer backbone or side-chain functionalities exerting antimicrobial activity (Figure 12.2).
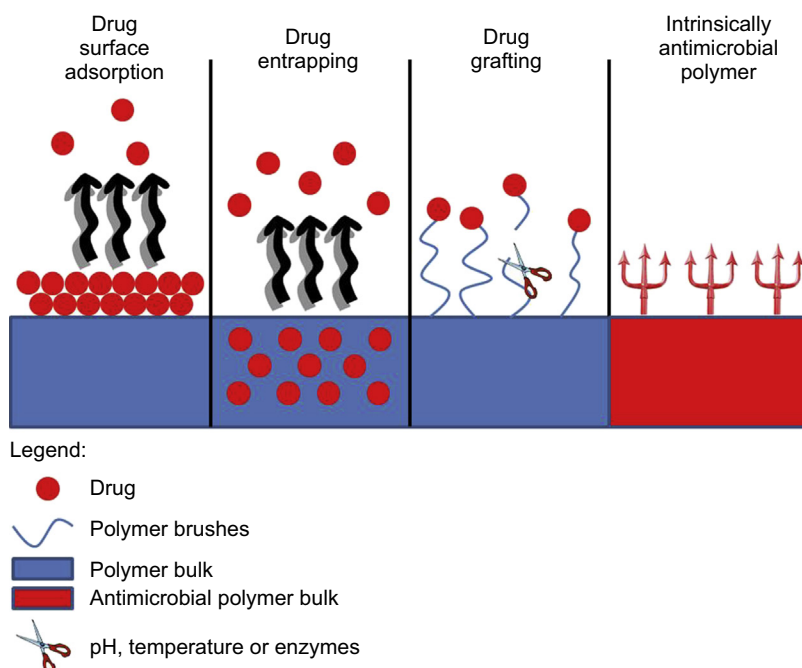
Figure 12.2 Main strategies for developing antimicrobial polymers.

In the first three approaches, the polymer acts as a carrier for the antimicrobial agent that once released can exert its action (antimicrobial agent-releasing polymers). In the first case the antibiotic is adsorbed mainly on the device surface, in the second case the drug is physically entrapped, while in the third case the antibiotic is grafted by labile bonds. In the fourth approach, the whole polymer (the bulk and the surface) is intrinsically antimicrobial and exerts its killing action when microorganisms contact the surface. These polymers are often called biocidal polymers.

In the following sections, antifouling and antimicrobial PUs will be presented in relation to their application for preventing intravascular device-related infections.

12.5.1 Antifouling PUs

The most investigated strategy for developing antifouling PUs involves increasing the hydrophilicity of the polymer surface. On the basis of the empirical criteria recently proposed by Ostuni et al.,[111] antifouling polymers should be hydrophilic, electrically neutral, and possess hydrogen-bond acceptors. To increase the hydrophilicity of segmented PUs, two strategies can be investigated: (1) variation of the PU soft phase,[11,112] and (2) application of hydrophilic coatings.[113,114]

Recently, to obtain antifouling materials, segmented PUs having the same hard domain but a variable soft domain have been synthesized.[112] The soft phase was constituted by polypropylene oxide (PPO), polycaprolactone (PCL), or poly-L-lactide (PLA). PCL- and PLA-containing PUs reduced the adhesion of *S. epidermidis* compared to the PPO-containing PU; this ability is presumably related to their greater hydrophilicity.

Several hydrophilic coatings were applied to PUs to increase surface hydrophilicity, including poly(ethylene glycol) (PEG), hyaluronan, dermatan sulfate, and heparin.

12.5.1.1 PU functionalization with PEG

PEG is widely known for its resistance to protein adsorption, nonimmunogenicity, and antithrombogenicity.[115] It is believed that PEG's antifouling ability is related to hydration and steric effects.[116] Several studies have been focused on PEG grafting onto PUs.[117–122] Particularly, PEG was either introduced in the polymer backbone,[123,124] by Michael addition onto main chain double bonds[125] and click chemistry,[117] or grafted in the polymer side chain by urethane[120] or allophanate linkages.[126]

In general, PEG-modified PUs shower better hemocompatibility properties in comparison with the unmodified PUs with a significant decrease in platelet adsorption.[120,127] Better performances of the PEG-functionalized PUs in terms of bacterial adhesion and infection development were also reported. Corneillie et al.[123] introduced PEG in segmented PUs as a soft segment in different ratios with PPO and PTMO. The PUs having PEG/PPO or PEG/PTMO in 1/1 molar ratio were able to significantly reduce the adhesion of *S. aureus* and *Enterococcus faecalis* with respect to glass, but were not able to reduce the adhesion of *P. aeruginosa.* Park et al.[119] grafted PEG 1000 and 3400 g/mol with different chain end groups (—OH, —NH_2, and SO_3) onto Pellethane® and tested the behavior of these PUs versus the adhesion of *S. epidermidis*

and *E. coli* in three different media, tryptic soy broth (TSB), brain heart infusion, and human plasma. PEG 3400-containing PUs showed better antifouling properties versus *S. epidermidis* compared to PEG 1000-containing PUs. The PEG 1000-modified surfaces did not show any reduction in *S. epidermidis* adhesion in TSB media regardless of the PEG chain end group. On the contrary, in plasma *S. epidermidis* adhesion was reduced especially when SO_3 chain groups were present. As for *E. coli*, a significant reduction in adherent bacteria was found in all media.

Taken together, these studies suggest how the ability of PEG-containing PUs to reduce bacterial adhesion can have variable degree of success depending on PEG molecular weight, bacterial species involved, and environmental factors (culture medium).

12.5.1.2 Heparin coating of PUs

From the early 1990s, a number of strategies have been pursued to improve the hemocompatibility of PUs. The physical adsorption or chemical grafting of heparin to PUs has been shown to be successful in improving PU hemocompatibility.[128–130] Also our group has developed different functionalized PUs able to bind heparin ionically[129] or covalently.[131]

Heparin coatings have also been shown to prevent microbial adhesion and colonization *in vitro* and *in vivo*.[132] This activity is presumably related to heparin's ability to favor albumin adsorption while reducing fibrinogen adsorption, and to its negative net charge repelling negatively charged bacteria.

Heparinization of CVCs and dialysis catheters resulted in a significant reduction of CR-Is, as seen in a randomized-controlled clinical trial of heparin-coated and uncoated nontunneled CVCs inserted in 246 patients[133] and a retrospective comparative analysis of coated and uncoated tunneled dialysis catheters.[134]

12.5.1.3 Heparin-like PUs

As an alternative to heparin coatings, heparin-like polymers, that are polymers able to mimic the biological behavior of heparin, have been developed mainly to reduce thrombotic events associated with intravascular devices. These polymers are characterized by the presence of sulfonate and sulfamate groups in the backbone or side chain. The first heparin-like PU was obtained by the group of Cooper[135] by reaction of propyl sulfonate with the urethane hydrogens of a PTMO-based PU. A reduction of platelet adhesion was found with the increase in the sulfonate group content. Few studies evaluated the efficacy of heparin-like polymers in reducing infection. Recently, PUs were synthesized having sulfonate and sulfamate in the hard segment by employing a carboxylated diol, dihydroxymethylpropionic acid, as chain extender.[136] The resulting carboxylated PU was further amidated with different functional amines and reacted with pyridine—SO_3 or DMF—SO_3 adducts. The —SO_3H-containing polymers, possessing a degree of sulfonation ranging from 30% to 40%, not only had good hemocompatibility but were also able to inhibit *S. epidermidis* adhesion. These features seemed to be related to the polymers phase segregation and content of —SO_3H groups. Other studies confirmed the sulfate

group content in PUs to be a crucial parameter for impart antifouling properties to heparin-like PUs. Indeed, a sulfonated pellethane with a 20% degree of sulfonation failed in reducing *S. aureus* adhesion.[137]

12.5.1.4 Other hydrophilic coatings for PUs

Other hydrophilic coatings have been proposed to reduce bacterial adhesion onto PUs.[138–140] Morra et al. studied *in vitro* the adhesion of *S. epidermidis* onto bare PU catheters and PU catheters coated with hyaluronan. A significant reduction in bacterial adhesion was found by using the soft, hydrated surface of the modified PU.[140] Highly sulfonated hyaluronan as PU coating resulted in the inhibition of *S. epidermidis* adhesion with respect to the unmodified PU.[141]

Xu et al.[142] used hyaluronic acid (HA) as a chain extender during PU synthesis with the aim of developing inherently nonthrombogenic materials. The physical and biological properties of the resulting PUs were modulated by varying the HA content. The results showed a linear increase in hydrophilicity with increase in HA content. Incorporation of HA resulted in negligible platelet adhesion compared to a standard PU. However, HA significantly stiffened the material and a relatively small fraction of the HA was exposed on the material surface. Better hemocompatibility was obtained more recently by the same research group through HA grafting onto the surface of a PU.[143] The grafting reaction consisted in first the incorporation of branched polyethylenimine into the PU backbone, followed by the covalent attachment of HA. Also dermatan sulfate/PU copolymers showed fairly good hemocompatibility and antiadhesive features, making these materials attractive for blood-contacting or nonfouling applications.[144]

Other than HA other polysaccharides were investigated as antifouling macromolecules including dextran,[145] dermatan sulfate,[144] and chitosan.[146,147] In particular, chitosan was shown to possess antibacterial activity against different microorganisms including *S. aureus* and *E. coli*.[148] This polysaccharide has been blended with stearyl poly(ethylene oxide) and used as a surface-modifying additive for PUs. The results indicated that the coated surface could effectively resist clotting. However no tests to evaluate microbial adhesion were done.[149] A chitosan/poly(vinyl alcohol) hydrogel was similarly used as a coating for segmented PUs for application as urethral catheters. The coating provided the catheter with antibacterial properties against *S. aureus*, *P. aeruginosa,* and *E. coli*.[150]

Another hydrophilic polymer studied as antifouling coating is poly-*N*-vinylpyrrolidone (Hydromer®). PU catheters coated with Hydromer® significantly reduced the adhesion of five strains of *S. epidermidis* and one strain of *S. aureus*.[139] More recently, a PVP coating was applied to PU for application as urinary tract biomaterial.[151] While encrustation was less on the PVP-coated PU than on the uncoated PU and silicone catheters, *E. coli* and *E. faecalis* adhesion was similar on the coated and uncoated PUs.

12.5.2 Antimicrobial PUs

As described above, several experimental approaches have been reported in the literature for introducing antimicrobial agents in PUs, including (1) drug entrapping

Table 12.4 Main medicated CVCs present on the market

Type of medicated CVC	Main characteristics	Manufacturer
First-generation chlorhexidine and silver sulfadiazine-coated CVC	Drugs are adsorbed onto the external CVC surface	Vygon Ltd, Ecouen, France Arrow International, Inc., PA, USA
Second-generation chlorhexidine and silver sulfadiazine-coated CVC	Silver sulfadiazine is present on the external CVC surface; chlorhexidine on the intraluminal CVC surface	Arrow International, Inc., PA, USA
Minocycline and rifampin-coated CVC	The antibiotics, present both onto the external and the internal CVC surface, are to the catheter surface through a TDMAC coating	Cook Critical Care, Inc., IN, USA
Miconazole and rifampin-coated CVC	Drugs are adsorbed onto both catheter surfaces	Vygon Ltd, Ecouen, France
Benzalkonium chloride and heparin-coated CVC	Sold under the trade name AMC Thromboshield™, this catheter has the two bioactive agents onto both the internal and the external surfaces	Baxter Healthcare Corporation, Irvine, CA, USA
Silver ion-impregnated CVC	The catheter is based on Agion® silver ion release technology	Multicath Expert, Vygon Ltd, Ecouen, France
Silver, platinum, and carbon-impregnated CVC	This CVC is known as Oligon CVC, where Oligon stands for polyurethane/antimicrobial agent mix. The antimicrobial agents are impregnated in the polymer bulk	Vantex CVC, Edwards Life Science, CA, USA

into the polymer bulk during device manufacturing; (2) drug adsorption or grafting on the device surface after manufacturing; (3) use of intrinsically antimicrobial polymers.

However, the majority of the antimicrobial-treated CVCs available on the market (Table 12.4) are obtained by adsorption of the drug onto the catheter surface, since this method is facile, inexpensive, and potentially applicable for a wide range of drugs. Only in the two types of CVCs treated with silver, the antimicrobial agents are impregnated in the polymer bulk. Often, to improve drug affinity for the device surface, cationic surfactants are used, such as tridodecylmethylammonium chloride (TDMAC) and benzalkonium chloride employed for the adsorption of minocycline/rifampin and heparin, respectively.

12.5.2.1 Antimicrobial-coated PUs

Coating devices with antibiotics or other antimicrobial agents is undoubtedly simple and applicable to all types of drugs. However, limitations of this strategy are insufficient drug loading and the rapid release of the adsorbed drug in the first hours following implantation. Both of these phenomena cause a short-term antimicrobial activity and can contribute to the development of antimicrobial resistance.

The most experimented antimicrobial drugs for intravascular devices are chlorhexidine/silver sulfadiazine (CH/SS) and minocycline–rifampin (MR). From a historical point of view, CVCs coated with one of these two drugs are the first medicated catheters approved for clinical trials.

The first generation of CH/SS-coated CVCs possessed both antimicrobial agents on the external surface. These catheters were extensively studied in the early 1990s[152–154] and the results showed that the infection rate was reduced only for short (approximately 2 weeks) catheterization times.[109,155]

In the early 2000s, the second-generation CH/SS-coated CVCs were marketed. These catheters have both surfaces coated with antimicrobials; silver sulfadiazine is present on the external surface and chlorhexidine on the intraluminal surface. In addition, the concentration of chlorhexidine was three times higher than that present into the first-generation catheters.

Three clinical trials[156–158] were performed to test the efficacy of these second-generation CH/SS-coated catheters. The first multicenter randomized double-blind trial[156] was carried out on 175 ICU patients receiving uncoated CVCs and 188 patients receiving CH/SS-coated CVCs for a mean duration of catheterization of ca. 11 days. A 3.7% incidence of catheter colonization in the treated group compared to the control group (13.1%) was observed. Also a slight reduction of CVC-related BSIs was recorded when using CH/SS-coated CVCs, even if in a context of a low baseline infection rate. Similar results were obtained by Ostendorf et al.[157] in hemato-oncological patients. Rupp et al.[158] showed that CH/SS-coated catheters did not promote antibiotic resistance.

In the early 1990s, the group of Raad and Darouiche showed *in vitro*[159,160] and in rabbit models[161] that minocycline and rifampicin could be adsorbed together onto catheters and had a synergistic and prolonged antimicrobial action.

A clinical trial performed at the end of the 1990s showed the efficacy of M/R-coated catheters in reducing bacterial colonization and CR-Is for short-term catheterization (approximately 7 days).[162] Similarly, in a more recent prospective randomized double-blind controlled multicenter trial in which MR-coated catheters were implanted in ICU patients requiring a triple-lumen CVC for more than 3 days, a low rate of colonization by staphylococci was found.[163] The efficacy of these medicated catheters was confirmed also for long-term (up to a 60 day) implantation.[164] Particularly, the long-term clinical trial was performed on tunneled CVCs inserted in adult patients admitted in seven university-affiliated US hospitals.[164,165] This long-lasting efficacy seems to be associated with a controlled release of the drugs from the catheter surface. Indeed, rifampin and minocycline were still detected on the surfaces of M/R-coated indwelling catheters explanted after at least 2 weeks of implantation but the two antibiotics were not present in the patient serum.[166] This good affinity

for the catheter surfaces was realized by precoating the catheter with the cationic surfactant triiododecylmethylammonium chloride able to interact with anionic drugs. Similar results were obtained by synthesizing differently functionalized PUs.[167–171] Particularly, high antibiotic loading and controlled drug release were obtained by introducing polymer side chain-specific functional groups able to interact with the selected drugs. This approach was similar to the use of TDMAC but in this case the functional groups interacting with the drugs are linked to the polymer main or side chain. In a recent review published in 2013, the efficacies of M/R-coated and CH/SS-coated CVCs were compared *in vivo*.[172] M/R-coated CVCs were able to reduce catheter colonization and CR-BSIs significantly more than CH/SS-coated devices.

Unfortunately, MR-coated intravascular catheters do not possess antimicrobial activity against strains of *P. aeruginosa* causing ca. 5% of CR-BSIs and *Candida* spp. contributing up to 12% of CR-BSIs.[173,174]

To counteract CVC colonization by *Candida* spp., a novel PU incorporated with the antifungal drug miconazole and rifampicin was developed. The activity of this rifampicin/miconazole (RM)-loaded PU was evaluated *in vitro* versus 158 clinical isolates of CR-BSIs.[175] The first clinical trial to assess the efficacy of RM-coated CVCs was performed in two German university hospitals on 223 adult patients.[176] This trial showed a reduction in colonization and related infection when using the RM-coated CVCs with respect to the uncoated ones for a catheterization period of ca. 7 days (5% vs 36%).[176] In addition, a more pronounced reduction of catheter colonization was found in male, overweight, and oncology patients.[177] The efficacy of RM-coated CVCs in reducing the incidence of CR-BSIs for short-term catheterization was confirmed in a more recent study.[178]

To provide protection against *P. aeruginosa*, Raad et al.[179] developed novel antimicrobial-coated PU CVCs based on a combination of chlorhexidine and minocycline–rifampin (CH-MR). CH-MR coating was shown to provide better protection against methicillin-resistant *S. aureus*, *P. aeruginosa*, and *Candida* spp. and a prolonged antimicrobial durability than CH/SS and MR coatings.[180]

To enhance the activity of antibiotics against microbial biofilm, the enzyme Dispersin B was absorbed in combination with cefamandole nafate onto the surface of functionalized PUs.[181] Dispersin B is a β-*N*-acetylglucosaminidase, produced by the Gram-negative *Actinobacillus actinomycetemcomitans*, able to dissolve mature biofilms produced by *S. epidermidis* as well as some other bacterial species.[182] The functionalized PUs absorbed a significant amount of dispersin B, which was able to exert its hydrolytic activity against the exopolysaccharide matrix of staphylococcal strains. In addition, when microbial biofilms were exposed to both dispersin B and CEF, a synergistic activity between these two agents was found.

Silver-treated intravascular catheters have been also developed and tested for their ability to reduce infection rate. A conventional approach to coat devices with silver is the direct deposition of metallic silver onto the device surface by vapor coating, sputter coating, ion beam coating,[21,183] or electrochemical deposition.[184] More recent methods to incorporate silver in polymers consisted in the coordination of silver ions by anionic PUs[185,186] or direct formation of silver nanoparticles onto the surface of PU hemodialysis catheters by photoreduction of a silver salt.[187]

The majority of the clinical trials performed on silver-coated CVCs failed in showing a statistically significant reduction either in catheter colonization or in CR-BSIs.[188–191] In addition, a recent *in vitro* study[192] showed that silver nanoparticle coatings applied to CVCs or the release of silver ions from the catheter may affect blood coagulation. Indeed, following contact of the silver-coated CVCs with plasma, an acceleration of thrombin formation and a stronger platelet activation were found compared to other coatings.

12.5.2.2 Antimicrobial-entrapped PUs

Entrapping antimicrobial agents into the polymeric bulk during device manufacturing permits the loading of significant drug amounts but is limited to thermally stable drugs. Other drawbacks of this strategy are (1) possible drug diffusion limitations from the polymer bulk to the surface[193] and (2) possible degradation of polymer mechanical properties.[194]

The studies available in the literature on this topic are lower in number compared to those concerning drug adsorption and most of the systems described did not reach clinical evaluation. One of the first studies focused on antibiotic entrapping into PUs was performed by Schierholz et al. who loaded ciprofloxacin–HCl salt and lipophilic ciprofloxacin–betaine into PU matrices.[195] A sustained and prolonged release was obtained when the lipophilic ciprofloxacin–betaine was entrapped due to the good affinity of this drug for the polymer. The initial burst release was avoided and a continuous and long-lasting release was obtained.

Usnic acid, a secondary lichen metabolite, possessing antimicrobial activity against a number of planktonic Gram-positive bacteria, including *S. aureus*, *E. faecalis*, and *Enterococcus faecium*, was incorporated into functionalized PUs.[196] The ability of usnic acid–loaded PUs to control biofilm formation by either *S. aureus* or *P. aeruginosa* was assessed under laminar flow conditions by using CLSM. The modified PUs did inhibit biofilm formation by *S. aureus* but not by *P. aeruginosa*. However, the morphology of the *P. aeruginosa* biofilm grown on the usnic acid–loaded PU was altered, possibly indicating a role of usnic acid in interfering with the bacterial signaling pathways.

In a more recent study rifampin was loaded into biodegradable polyester urethanes.[197] The authors suggested the use of this antimicrobial-entrapped polyester urethane as a coating material for intravascular devices. Indeed, a sustained delivery of the antibiotic was obtained and related to a diffusion-dependent release mechanism.

To control the release of the drug entrapped in a polymer matrix, the use of pore-forming agents, such as entrapped PEG or albumin, together with antibiotics has been investigated.[169,198,199] In particular, cefadroxil entrapped in a PU, together with PEG, D-mannitol, or bovine serum albumin as pore formers,[198] was evaluated by measuring the diameter of the inhibition zones. Changing the amount and particle size of the pore formers influenced drug release from the matrix. Particularly, the release rate of cefadroxil increased with increasing loading amount. The best cefadroxil releasing system exhibited antibacterial activity for 5–6 days against *E. coli* and *Bacillus subtilis*.

Similarly, a sustained drug release was obtained by our group entrapping the antibiotics, cefamandole nafate and rifampin, in a PU matrix together with the pore former PEG.[169] Three PEG molecular weights investigated were 2000, 10,000, and 35,000 g/mol. The PEG 10,000–containing PU exhibited a long-lasting antimicrobial activity (up to 23 days) against *S. aureus*. To inhibit fungal biofilm formation on intravascular devices, fluconazole plus pore formers were incorporated into functionalized PU matrices.[199] PEG and albumin were investigated as pore-forming agents. PEG significantly improved the fluconazole release while albumin, having a higher molecular weight, provided a controlled drug release and prolonged antifungal activity versus *C. albicans.*

Polymer nanocomposites were also investigated for their ability to control drug release and provide prolonged antimicrobial activity.[193,200] A nanostructured polymer system consisting of PUs entrapped with either albumin or polyallylamine nanoparticles and adsorbed with cefamandole nafate was developed.[193] Antibiotic release and duration of antimicrobial activity depended on porosity of the nanoparticle/polymer systems as well as on the drug/polymer interaction. Fong et al.[200] developed antibacterial PU–montmorillonite (MMT) nanocomposites using chlorhexidine diacetate (CHX) both as an organic modifier for silicate dispersion and as an antibacterial agent. Antibacterial activity against *S. epidermidis* was significant in materials with higher MMT and containing free CHX, for which 2-log reductions in adherent bacteria were found after 24 h incubation. CHX also modulated the material properties.

Silver was also impregnated into CVCs, and at least two products have been marketed (Table 12.4): silver ion-impregnated CVCs and silver, platinum, and carbon-impregnated CVCs (iontophoretic). The first type of CVC is based on Agion® technology consisting of entrapped silver-containing zeolites in the CVC polymer matrix. Two recent clinical trials addressed the efficacy of this silver ion-impregnated CVC,[201,202] the most recent of which was performed on a significant number of ICU patients (577) requiring a CVC for more than 3 days.[201] Similar rates of colonization for silver-impregnated CVCs and standard uncoated CVCs (14.7% vs 12.1%) were found.[201]

Silver, platinum, and carbon-impregnated CVCs were manufactured using a PU combined with silver, platinum, and a carbon black. Conflicting results were found in clinical trials evaluating the efficacy of this catheter.[203–206] The most recent prospective, randomized, multicenter clinical trial, involving a large number of patients (539), failed to demonstrate the efficacy of this silver CVC in preventing catheter colonization and reducing of CR-BSIs compared to untreated CVCs.[203]

The poor protection of silver in preventing CVC-related infections may be due either to the low susceptibility of staphylococcal species to silver ions[207] or to deactivation of silver by interaction with the host blood proteins.[208]

12.5.2.3   Antimicrobial-grafted PUs

Some studies have investigated the covalent binding of antimicrobial agents, either antiseptic or antibiotic molecules, on the polymer main or side chains. These systems are considered drug-releasing systems since, usually, hydrolysis of the drug/polymer linkage is required to have antimicrobial activity. Hydrolysis may be pH, temperature, or enzyme triggered (Figure 12.2).

Woo et al. covalently linked ciprofloxacin to an aliphatic biodegradable PU based on polycaprolactone diol.[209] This polymer was able to release the drug in the presence of cholesterol esterase up to 30 days while its activity against *P. aeruginosa* lasted for 10 days. In a preliminary cell study, this biodegradable antibiotic polymer did not show any observable effects on cell proliferation or cell membrane structure.[210]

A drug precursor was grafted to PUs and further activated to release the biocide.[211] PUs having soft blocks containing semifluorinated and 5,5-dimethylhydantoin pendant groups were employed as coatings for a conventional PTMO-based PU. Then, the coated PU was activated with hypochlorite to convert the surface amide groups to chloramide. The activated PU was effective against *S. aureus*, *P. aeruginosa*, and *E. coli*.

12.5.2.4   Intrinsically antimicrobial PUs

From 2005 to 2015, the development of intrinsically antimicrobial polymers (biocidal polymers) has emerged as a promising alternative approach for preventing biofilm formation on medical devices. The advantage of this strategy is that the polymer matrix will not release antimicrobial substances but microorganisms will be killed while entering in contact with the surface.

Features that biocidal polymers should possess include[212]: (1) inexpensive synthesis; (2) good chemical stability; (3) tunable water solubility; and (4) not releasing toxic products, especially for applications in the biomedical field or in the food industry.

Among intrinsically antimicrobial polymers, cationic polymers have been extensively studied. Their activity is related to their ability to bind to the negatively charged bacterial cell surface promoting cell wall and/or membrane disruption.[212,213]

Cationic PUs possessing phosphonate or quaternized amine groups were synthesized by Flemming et al.[137] Better activity was shown by the quaternized amine PUs which significantly reduced the number of adherent bacteria compared to control PUs. A reduction in bacterial adhesion was also found on the surface of the zwitterionic phosphonated PU but to a lesser extent.

A series of quaternized PUs were prepared by using different contents of the monomer *N*,*N*-bis(2-hydroxyethyl)isonicotinamide (BIN) during the synthesis of PTMO-based PUs.[214] The pyridine ring in BIN was then quaternized with different alkyl halides obtaining polymers with bactericidal activity against *S. aureus* and bacteriostatic activity against *E. coli*.

PUs having random copolymer 1,3-propylene oxide soft blocks with alkylammonium (C6 or C12 alkylammonium chain lengths) and either trifluoroethoxy or PEGylated side chains were recently prepared as polymer surface modifiers.[215] The coatings were highly effective against *P. aeruginosa* and *E. coli*. The extent of the antimicrobial effectiveness of these polymers was influenced by the alkylammonium chain length.[216]

12.6   Future perspectives

Biostable PUs are considered the materials of choice for the manufacturing of cardiovascular devices that need high flexural endurance, fatigue resistance, and good blood compatibility.

From 1995 to 2015, a deep understanding of the mechanisms involved in biomaterial/tissue interaction gave new direction to scientists working in the biomaterials field. Indeed, to provide better functionality, to last longer, and to meet patient requirements, biomaterials should work in harmony with biology.

A crucial feature required for a successful application of PUs as biomaterials is their ability to prevent microbial colonization. Indeed, any implanted biomaterial is known to have the potential to put the patient at high risk of infection. In case of intravascular devices, the development of device-related infections may result in life-threatening consequences for the patient.

Drug-releasing PUs can be considered the first milestone in the prevention of intravascular device-related infections. Already, their clinical application has contributed to decreasing infection risk, mortality rate, and patient morbidity. However, the use of these drug-releasing polymers has elicited concerns in terms of durability and possible local emergence of resistant microorganisms.

Intrinsically antimicrobial PUs and antifouling PUs represent promising alternatives to the use of drug-releasing PUs. Since these polymers do not release low molecular weight drugs in the surrounding environment, their activity does not exhaust with time, at least in theory, and they do not promote bacterial resistance.[217] However, so far, only a few studies have focused on the development of such new classes of PUs. Beside the development of novel intrinsically antimicrobial/antifouling PU matrices, the application of nano- or microtechnology could contribute in preventing biofilm-based, intravascular device-related infections. Indeed, nano- or microparticles could be used as tools for loading significant amounts of drug, deliver drugs in a controlled fashion, and protect the drug from degradation.[218,219] These system could be entrapped in PUs and be used as antimicrobial coatings for medical devices.

In conclusion, the development of antimicrobial PUs is currently an area of active and ongoing research. The key for their success relies on the tight collaboration of scientists working in the field of macromolecular science, microbiology, and medicine.

References

1. Ratner BD. A paradigm shift: biomaterials that heal. *Polym Int* October 2007;**56**(10):1183–5.
2. Black J. The education of the biomaterialist: report of a survey, 1980–81. *J Biomed Mater Res* March 1982;**16**(2):159–67.
3. Boretos JW, Pierce WS. Segmented polyurethane: a polyether polymer. An initial evaluation for biomedical applications. *J Biomed Mater Res* March 1968;**2**(1):121–30.
4. Lyman DJ, Kwan-Gett C, Zwart HH, et al. The development and implantation of a polyurethane hemispherical artificial heart. *Trans Am Soc Artif Intern Organs* 1971;**17**:456–63.
5. Cooper SL, Tobolsky AV. Properties of linear elastomeric polyurethanes. *J Appl Polym Sci* 1966;**10**:1837–44.
6. Takahara A, Kajiyama T. Effect of polyether components on surface-composition and blood compatibility of segmented polyurethaneureas. *Nippon Kagaku Kaishi* 1985;(6):1293–301.
7. Takahara A, Tashita J, Kajiyama T, et al. Microphase separated structure, surface-composition and blood compatibility of segmented poly(urethaneureas) with various soft segment components. *Polymer* 1985;**26**(7):987–96.

8. Piozzi A, Francolini I. Biomimetic polyurethanes. In: Muñoz-Bonilla A, Cerrada M, Fernández-García M, editors. *Polymeric materials with antimicrobial activity from synthesis to applications*. RSC; 2014. pp. 224–78.

9. Brandwood A, Meijs GF, Gunatillake PA, et al. In vivo evaluation of polyurethanes based on novel macrodiols and MDI. *J Biomater Sci Polym Ed* 1994;**6**(1):41–54.

10. Reid JS, Rosenberg G, Pierce WS. Transmission of water through a biocompatible polyurethane: application to circulatory assist devices. *J Biomed Mater Res* November 1985;**19**(9):1181–202.

11. Takahara A, Okkema AZ, Cooper SL, et al. Effect of surface hydrophilicity on ex vivo blood compatibility of segmented polyurethanes. *Biomaterials* April 1991;**12**(3):324–34.

12. Eggimann P, Pittet D. Infection control in the ICU. *Chest* December 2001;**120**(6):2059–93.

13. Klevens RM, Edwards JR, Richards Jr CL, et al. Estimating health care-associated infections and deaths in U.S. hospitals, 2002. *Public Health Rep* March 2007;**122**(2):160–6.

14. Mermel LA, Farr BM, Sherertz RJ, et al. Guidelines for the management of intravascular catheter-related infections. *Clin Infect Dis* May 2001;**32**(9):1249–72.

15. Lynch AS, Robertson GT. Bacterial and fungal biofilm infections. *Annu Rev Med* 2008;**59**:415–28.

16. Oncu S, Ozsut H, Yildirim A, et al. Central venous catheter related infections: risk factors and the effect of glycopeptide antibiotics. *Ann Clin Microbiol Antimicrob* February 2003;**2**:3.

17. Al Raiy B, Fakih MG, Bryan-Nomides N, et al. Peripherally inserted central venous catheters in the acute care setting: a safe alternative to high-risk short-term central venous catheters. *Am J Infect Control* March 2010;**38**(2):149–53.

18. Chopra V, O'Horo JC, Rogers MA, et al. The risk of bloodstream infection associated with peripherally inserted central catheters compared with central venous catheters in adults: a systematic review and meta-analysis. *Infect Control Hosp Epidemiol* September 2013;**34**(9):908–18.

19. Cardo D, Horan T, Andrus M, et al. National Nosocomial Infections Surveillance (NNIS) System Report, data summary from January 1992 through June 2004, issued October 2004. *Am J Infect Control* December 2004;**32**(8):470–85.

20. van de Wetering MD, van Woensel JB. Prophylactic antibiotics for preventing early central venous catheter Gram positive infections in oncology patients. *Cochrane Database Syst Rev* 2007;(1):CD003295.

21. Groeger JS, Lucas AB, Coit D, et al. A prospective, randomized evaluation of the effect of silver impregnated subcutaneous cuffs for preventing tunneled chronic venous access catheter infections in cancer patients. *Ann Surg* August 1993;**218**(2):206–10.

22. Penel N, Neu JC, Clisant S, et al. Risk factors for early catheter-related infections in cancer patients. *Cancer* October 2007;**110**(7):1586–92.

23. Chua JD, Wilkoff BL, Lee I, et al. Diagnosis and management of infections involving implantable electrophysiologic cardiac devices. *Ann Intern Med* October 2000;**133**(8):604–8.

24. Johansen JB, Jorgensen OD, Moller M, et al. Infection after pacemaker implantation: infection rates and risk factors associated with infection in a population-based cohort study of 46299 consecutive patients. *Eur Heart J* April 2011;**32**(8):991–8.

25. Harcombe AA, Newell SA, Ludman PF, et al. Late complications following permanent pacemaker implantation or elective unit replacement. *Heart* September 1998;**80**(3):240–4.

26. Nery PB, Fernandes R, Nair GM, et al. Device-related infection among patients with pacemakers and implantable defibrillators: incidence, risk factors, and consequences. *J Cardiovasc Electrophysiol* July 2010;**21**(7):786–90.

27. Klug D, Vaksmann G, Jarwe M, et al. Pacemaker lead infection in young patients. *Pacing Clin Electrophysiol* July 2003;**26**(7 Pt 1):1489–93.
28. Voigt A, Shalaby A, Saba S. Rising rates of cardiac rhythm management device infections in the United States: 1996 through 2003. *J Am Coll Cardiol* August 2006;**48**(3):590–1.
29. Klug D, Balde M, Pavin D, et al. Risk factors related to infections of implanted pacemakers and cardioverter-defibrillators: results of a large prospective study. *Circulation* September 2007;**116**(12):1349–55.
30. Arber N, Pras E, Copperman Y, et al. Pacemaker endocarditis. Report of 44 cases and review of the literature. *Med Baltim* November 1994;**73**(6):299–305.
31. Klug D, Lacroix D, Savoye C, et al. Systemic infection related to endocarditis on pacemaker leads: clinical presentation and management. *Circulation* April 1997;**95**(8):2098–107.
32. Rose EA, Gelijns AC, Moskowitz AJ, et al. Long-term use of a left ventricular assist device for end-stage heart failure. *N Engl J Med* November 2001;**345**(20):1435–43.
33. Pereda D, Conte JV. Left ventricular assist device driveline infections. *Cardiol Clin* November 2011;**29**(4):515–27.
34. Maniar S, Kondareddy S, Topkara VK. Left ventricular assist device-related infections: past, present and future. *Expert Rev Med Devices* September 2011;**8**(5):627–34.
35. Pae WE, Connell JM, Adelowo A, et al. Does total implantability reduce infection with the use of a left ventricular assist device? The LionHeart experience in Europe. *J Heart Lung Transplant* March 2007;**26**(3):219–29.
36. Starling RC, Naka Y, Boyle AJ, et al. Results of the post-U.S. Food and Drug Administration-approval study with a continuous flow left ventricular assist device as a bridge to heart transplantation: a prospective study using the INTERMACS (Interagency Registry for Mechanically Assisted Circulatory Support). *J Am Coll Cardiol* May 2011;**57**(19):1890–8.
37. John R, Kamdar F, Liao K, et al. Improved survival and decreasing incidence of adverse events with the HeartMate II left ventricular assist device as bridge-to-transplant therapy. *Ann Thorac Surg* October 2008;**86**(4):1227–34.
38. Aaronson KD, Slaughter MS, Miller LW, et al. Use of an intrapericardial, continuous-flow, centrifugal pump in patients awaiting heart transplantation. *Circulation* June 2012;**125**(25):3191–200.
39. Trost JC, Hillis LD. Intra-aortic balloon counterpulsation. *Am J Cardiol* May 2006;**97**(9):1391–8.
40. Arceo A, Urban P, Dorsaz PA, et al. In-hospital complications of percutaneous intraaortic balloon counterpulsation. *Angiology* September 2003;**54**(5):577–85.
41. Parissis H, Soo A, Al-Alao B. Intra aortic balloon pump: literature review of risk factors related to complications of the intraaortic balloon pump. *J Cardiothorac Surg* November 2011;**6**.
42. Azeem T, Stephens-Lloyd A, Spyt T, et al. Intra-aortic balloon counterpulsation: variations in use and complications. *Int J Cardiol* April 2004;**94**(2–3):255–9.
43. Vales L, Kanei Y, Ephrem G, et al. Intra-aortic balloon pump use and outcomes with current therapies. *J Invasive Cardiol* March 2011;**23**(3):116–9.
44. Valente S, Lazzeri C, Crudeli E, et al. Intraaortic balloon pump: incidence and predictors of complications in the Florence registry. *Clin Cardiol* April 2012;**35**(4):200–4.
45. Baddour LM, Bettmann MA, Bolger AF, et al. Nonvalvular cardiovascular device-related infections. *Circulation* October 2003;**108**(16):2015–31.
46. Kantrowitz A, Wasfie T, Freed PS, et al. Intraaortic balloon pumping 1967 through 1982: analysis of complications in 733 patients. *Am J Cardiol* April 1986;**57**(11):976–83.
47. Macoviak J, Stephenson LW, Edmunds Jr LH, et al. The intraaortic baloon pump: an analysis of five years' experience. *Ann Thorac Surg* May 1980;**29**(5):451–8.

48. Yu F, Yang L, Pan J, et al. Intra-aortic baloon pump infection: a neglected nosocoial infection? *J Hosp Infect* 2011;**77**:91–2.

49. Crystal E, Borer A, Gilad J, et al. Incidence and clinical significance of bacteremia and sepsis among cardiac patients treated with intra-aortic balloon counterpulsation pump. *Am J Cardiol* December 2000;**86**(11):1281–4. A9.

50. Guidoin R, Sigot M, King M, et al. Biocompatibility of the vascugraft: evaluation of a novel polyester urethane vascular substitute by an organotypic culture technique. *Biomaterials* 1992;**13**(5):281–8.

51. Zhang Z, Marois Y, Guidoin RG, et al. Vascugraft polyurethane arterial prosthesis as femoro-popliteal and femoro-peroneal bypasses in humans: pathological, structural and chemical analyses of four excised grafts. *Biomaterials* January 1997;**18**(2):113–24.

52. Santerre JP, Labow RS, Duguay DG, et al. Biodegradation evaluation of polyether and polyester-urethanes with oxidative and hydrolytic enzymes. *J Biomed Mater Res* October 1994;**28**(10):1187–99.

53. Salacinski HJ, Tai NR, Carson RJ, et al. In vitro stability of a novel compliant poly(carbonate-urea)urethane to oxidative and hydrolytic stress. *J Biomed Mater Res* February 2002;**59**(2):207–18.

54. Kiyama H, Imazeki T, Kurihara S, et al. Long-term follow-up of polyurethane vascular grafts for hemoaccess bridge fistulas. *Ann Vasc Surg* September 2003;**17**(5):516–21.

55. Zetrenne E, McIntosh BC, McRae MH, et al. Prosthetic vascular graft infection: a multi-center review of surgical management. *Yale J Biol Med* September 2007;**80**(3):113–21.

56. Oderich GS, Panneton JM. Aortic graft infection – what have we learned during the last decades? *Acta Chir Belg* February 2002;**102**(1):7–13.

57. Valentine RJ. Diagnosis and management of aortic graft infection. *Semin Vasc Surg* December 2001;**14**(4):292–301.

58. Hallett Jr JW, Marshall DM, Petterson TM, et al. Graft-related complications after abdominal aortic aneurysm repair: reassurance from a 36-year population-based experience. *J Vasc Surg* February 1997;**25**(2):277–84.

59. Bandyk DF, Berni GA, Thiele BL, et al. Aortofemoral graft infection due to *Staphylococcus epidermidis*. *Arch Surg* January 1984;**119**(1):102–8.

60. Orton DF, LeVeen RF, Saigh JA, et al. Aortic prosthetic graft infections: radiologic manifestations and implications for management. *Radiographics* July 2000;**20**(4):977–93.

61. Szilagyi DE, Smith RF, Elliott JP, et al. Infection in arterial reconstruction with synthetic grafts. *Ann Surg* September 1972;**176**(3):321–33.

62. Samson RH, Veith FJ, Janko GS, et al. A modified classification and approach to the management of infections involving peripheral arterial prosthetic grafts. *J Vasc Surg* August 1988;**8**(2):147–53.

63. Mermel LA. What is the predominant source of intravascular catheter infections? *Clin Infect Dis* January 2011;**52**(2):211–2.

64. Katsikogianni M, Missirlis YF. Concise review of mechanisms of bacterial adhesion to biomaterials and of techniques used in estimating bacteria-material interactions. *Eur Cell Mater* December 2004;**8**:37–57.

65. Zhao Q, Liu Y, Wang C, et al. Reduction of bacterial adhesion on ion-implanted stainless steel surfaces. *Med Eng Phys* April 2008;**30**(3):341–9.

66. Mei L, Busscher HJ, van der Mei HC, et al. Influence of surface roughness on streptococcal adhesion forces to composite resins. *Dent Mater* August 2011;**27**(8):770–8.

67. Grossner-Schreiber B, Griepentrog M, Haustein I, et al. Plaque formation on surface modified dental implants. An in vitro study. *Clin Oral Implants Res* December 2001;**12**(6):543–51.

68. Hilbert LR, Bagge-Ravn D, Kold J, et al. Influence of surface roughness of stainless steel on microbial adhesion and corrosion resistance. *Int Biodeterior Biodegrad* 2003;**52**(3):175–85.

69. Tang H, Cao T, Liang X, et al. Influence of silicone surface roughness and hydrophobicity on adhesion and colonization of *Staphylococcus epidermidis*. *J Biomed Mater Res A* February 2009;**88**(2):454–63.

70. Quirynen M, Bollen CM, Papaioannou W, et al. The influence of titanium abutment surface roughness on plaque accumulation and gingivitis: short-term observations. *Int J Oral Maxillofac Implants* March 1996;**11**(2):169–78.

71. Bollen CM, Papaioanno W, Van EJ, et al. The influence of abutment surface roughness on plaque accumulation and peri-implant mucositis. *Clin Oral Implants Res* September 1996;**7**(3):201–11.

72. Bollen CM, Lambrechts P, Quirynen M. Comparison of surface roughness of oral hard materials to the threshold surface roughness for bacterial plaque retention: a review of the literature. *Dent Mater* July 1997;**13**(4):258–69.

73. Raad II, Luna M, Khalil SA, et al. The relationship between the thrombotic and infectious complications of central venous catheters. *JAMA* April 1994;**271**(13):1014–6.

74. Timsit JF, Farkas JC, Boyer JM, et al. Central vein catheter-related thrombosis in intensive care patients: incidence, risks factors, and relationship with catheter-related sepsis. *Chest* July 1998;**114**(1):207–13.

75. van Rooden CJ, Schippers EF, Barge RM, et al. Infectious complications of central venous catheters increase the risk of catheter-related thrombosis in hematology patients: a prospective study. *J Clin Oncol* April 2005;**23**(12):2655–60.

76. Mehall JR, Saltzman DA, Jackson RJ, et al. Fibrin sheath enhances central venous catheter infection. *Crit Care Med* April 2002;**30**(4):908–12.

77. Derjaguin B, Landau L. Theory of the stability of strongly charged lyophobic sols and of the adhesion of strongly charged-particles in solutions of electrolytes. *Prog Surf Sci* May 1993;**43**(1–4):30–59.

78. Speranza G, Gottardi G, Pederzolli C, et al. Role of chemical interactions in bacterial adhesion to polymer surfaces. *Biomaterials* May 2004;**25**(11):2029–37.

79. Tegoulia VA, Cooper SL. *Staphylococcus aureus* adhesion to self-assembled monolayers: effect of surface chemistry and fibrinogen presence. *Colloids Surf B Biointerfaces* April 2002;**24**(3–4):217–28.

80. Dickinson RB, Nagel JA, Proctor RA, et al. Quantitative comparison of shear-dependent *Staphylococcus aureus* adhesion to three polyurethane ionomer analogs with distinct surface properties. *J Biomed Mater Res* August 1997;**36**(2):152–62.

81. Fletcher M, Marshall KC. Bubble contact angle method for evaluating substratum interfacial characteristics and its relevance to bacterial attachment. *Appl Environ Microbiol* July 1982;**44**(1):184–92.

82. Vaudaux P, Suzuki R, Waldvogel FA, et al. Foreign body infection: role of fibronectin as a ligand for the adherence of *Staphylococcus aureus*. *J Infect Dis* October 1984;**150**(4):546–53.

83. Vaudaux PE, Waldvogel FA, Morgenthaler JJ, et al. Adsorption of fibronectin onto polymethylmethacrylate and promotion of *Staphylococcus aureus* adherence. *Infect Immun* September 1984;**45**(3):768–74.

84. Vaudaux P, Pittet D, Haeberli A, et al. Fibronectin is more active than fibrin or fibrinogen in promoting *Staphylococcus aureus* adherence to inserted intravascular catheters. *J Infect Dis* March 1993;**167**(3):633–41.

85. Stewart PS, Costerton JW. Antibiotic resistance of bacteria in biofilms. *Lancet* July 2001;**358**(9276):135–8.

 86. Raad I, Costerton W, Sabharwal U, et al. Ultrastructural analysis of indwelling vascular catheters: a quantitative relationship between luminal colonization and duration of placement. *J Infect Dis* August 1993;**168**(2):400–7.

 87. Costerton JW, Lewandowski Z, Caldwell DE, et al. Microbial biofilms. *Annu Rev Microbiol* 1995;**49**:711–45.

 88. Lewis K. Multidrug tolerance of biofilms and persister cells. *Curr Top Microbiol Immunol* 2008;**322**:107–31.

 89. Sun F, Qu F, Ling Y, et al. Biofilm-associated infections: antibiotic resistance and novel therapeutic strategies. *Future Microbiol* July 2013;**8**(7):877–86.

 90. Shigeta M, Tanaka G, Komatsuzawa H, et al. Permeation of antimicrobial agents through *Pseudomonas aeruginosa* biofilms: a simple method. *Chemotherapy* September 1997;**43**(5):340–5.

 91. Kumon H, Tomochika K, Matunaga T, et al. A sandwich cup method for the penetration assay of antimicrobial agents through *Pseudomonas* exopolysaccharides. *Microbiol Immunol* 1994;**38**(8):615–9.

 92. Stewart PS, Franklin MJ. Physiological heterogeneity in biofilms. *Nat Rev Microbiol* March 2008;**6**(3):199–210.

 93. Tanaka G, Shigeta M, Komatsuzawa H, et al. Effect of the growth rate of *Pseudomonas aeruginosa* biofilms on the susceptibility to antimicrobial agents: beta-lactams and fluoroquinolones. *Chemotherapy* January 1999;**45**(1):28–36.

 94. Hausner M, Wuertz S. High rates of conjugation in bacterial biofilms as determined by quantitative in situ analysis. *Appl Environ Microbiol* August 1999;**65**(8):3710–3.

 95. Monzon M, Oteiza C, Leiva J, et al. Biofilm testing of *Staphylococcus epidermidis* clinical isolates: low performance of vancomycin in relation to other antibiotics. *Diagn Microbiol Infect Dis* December 2002;**44**(4):319–24.

 96. Adam B, Baillie GS, Douglas LJ. Mixed species biofilms of *Candida albicans* and *Staphylococcus epidermidis*. *J Med Microbiol* April 2002;**51**(4):344–9.

 97. Wisplinghoff H, Bischoff T, Tallent SM, et al. Nosocomial bloodstream infections in US hospitals: analysis of 24,179 cases from a prospective nationwide surveillance study. *Clin Infect Dis* August 2004;**39**(3):309–17.

 98. Gaynes R, Edwards JR. Overview of nosocomial infections caused by gram-negative bacilli. *Clin Infect Dis* September 2005;**41**(6):848–54.

 99. Klevens RM, Edwards JR, Tenover FC, et al. Changes in the epidemiology of methicillin-resistant *Staphylococcus aureus* in intensive care units in US hospitals, 1992–2003. *Clin Infect Dis* February 2006;**42**(3):389–91.

100. Burton DC, Edwards JR, Horan TC, et al. Methicillin-resistant *Staphylococcus aureus* central line-associated bloodstream infections in US intensive care units, 1997–2007. *JAMA* February 2009;**301**(7):727–36.

101. Kojic EM, Darouiche RO. *Candida* infections of medical devices. *Clin Microbiol Rev* April 2004;**17**(2):255–67.

102. Yousif A, Jamal MA, Raad I. Biofilm-based central line-associated bloodstream infections. *Adv Exp Med Biol* 2015;**830**:157–79.

103. Larsen MK, Thomsen TR, Moser C, et al. Use of cultivation-dependent and -independent techniques to assess contamination of central venous catheters: a pilot study. *BMC Clin Pathol* 2008;**8**:10.

104. Shirtliff ME, Peters BM, Jabra-Rizk MA. Cross-kingdom interactions: *Candida albicans* and bacteria. *FEMS Microbiol Lett* October 2009;**299**(1):1–8.

105. Harriott MM, Noverr MC. *Candida albicans* and *Staphylococcus aureus* form polymicrobial biofilms: effects on antimicrobial resistance. *Antimicrob Agents Chemother* September 2009;**53**(9):3914–22.

106. von EC, Jansen B, Kohnen W, et al. Infections associated with medical devices: pathogenesis, management and prophylaxis. *Drugs* 2005;**65**(2):179–214.
107. O'Grady NP, Alexander M, Burns LA, et al. Guidelines for the prevention of intravascular catheter-related infections. *Am J Infect Control* May 2011;**39**(4 Suppl. 1):S1–34.
108. Francolini I, Donelli G. Prevention and control of biofilm-based medical-device-related infections. *FEMS Immunol Med Microbiol* August 2010;**59**(3):227–38.
109. Donelli G, Francolini I. Efficacy of antiadhesive, antibiotic and antiseptic coatings in preventing catheter-related infections: review. *J Chemother* December 2001;**13**(6):595–606.
110. Chen SF, Li LY, Zhao C, et al. Surface hydration: principles and applications toward low-fouling/nonfouling biomaterials. *Polymer* October 2010;**51**(23):5283–93.
111. Ostuni E, Chapman RG, Holmlin E, et al. A survey of structure-property relationships of surfaces that resist the adsorption of protein. *Langmuir* 2001;**17**:5605–20.
112. Francolini I, Donelli G, Vuotto C, et al. Antifouling polyurethanes to fight device-related staphylococcal infections: synthesis, characterization, and antibiofilm efficacy. *Pathog Dis* April 2014;**70**(3):401–7.
113. Schuler M, Hamilton DW, Kunzler TP, et al. Comparison of the response of cultured osteoblasts and osteoblasts outgrown from rat calvarial bone chips to nonfouling KRSR and FHRRIKA-peptide modified rough titanium surfaces. *J Biomed Mater Res B Appl Biomater* November 2009;**91**(2):517–27.
114. Zoulalian V, Zurcher S, Tosatti S, et al. Self-assembly of poly(ethylene glycol)-poly(alkyl phosphonate) terpolymers on titanium oxide surfaces: synthesis, interface characterization, investigation of nonfouling properties, and long-term stability. *Langmuir* January 2010;**26**(1):74–82.
115. Banerjee I, Pangule RC, Kane RS. Antifouling coatings: recent developments in the design of surfaces that prevent fouling by proteins, bacteria, and marine organisms. *Adv Mater* February 2011;**23**(6):690–718.
116. Chen S, Yu F, Yu Q, et al. Strong resistance of a thin crystalline layer of balanced charged groups to protein adsorption. *Langmuir* September 2006;**22**(19):8186–91.
117. Rana S, Lee SY, Cho JW. Synthesis and characterization of biocompatible poly(ethylene glycol)-functionalized polyurethane using click chemistry. *Polym Bull* 2010;**64**:401–11.
118. Lee JH, Ju YM, Lee WK, et al. Platelet adhesion onto segmented polyurethane surfaces modified by PEO- and sulfonated PEO-containing block copolymer additives. *J Biomed Mater Res* May 1998;**40**(2):314–23.
119. Park KD, Kim YS, Han DK, et al. Bacterial adhesion on PEG modified polyurethane surfaces. *Biomaterials* April 1998;**19**(7–9):851–9.
120. Orban JM, Chapman TM, Wagner WR, et al. Easily grafted polyurethanes with reactive main chain functional groups. Synthesis, characterization, and antithrombogenicity of poly(ethylene glycol)-grafted poly(urethanes). *J Polm Sci A Polm Chem* 1999;**37**(17):3441–8.
121. Tuominen J, Lee JJ, Livingstone M, et al. Synthesis of novel poly(ethylene glycol)-based polyurethanes for drug delivery systems. *J Control Release* January 2005;**101**(1–3):316–7.
122. Chen X, Liu W, Zhao Y, et al. Preparation and characterization of PEG-modified polyurethane pressure-sensitive adhesives for transdermal drug delivery. *Drug Dev Ind Pharm* June 2009;**35**(6):704–11.
123. Corneillie S, Lan PN, Schacht E, et al. Polyethylene glycol-containing polyurethanes for biomedical applications. *Polym Int* 1999;**46**(3):251–9.
124. Rao L, Zhou H, Li T, et al. Polyethylene glycol-containing polyurethane hydrogel coatings for improving the biocompatibility of neural electrodes. *Acta Biomater* July 2012;**8**(6):2233–42.

125. Stern T, Penhasi A, Cohn D. Derivatization of a new poly(ether urethane amide) containing chemically active sites. *Biomaterials* January 1995;**16**(1):17–23.

126. Park JH, Lee KB, Kwon IC, et al. PDMS-based polyurethanes with MPEG grafts: mechanical properties, bacterial repellency, and release behavior of rifampicin. *J Biomater Sci Polym Ed* 2001;**12**(6):629–45.

127. Park KD, Suzuki K, Lee WK, et al. Platelet adhesion and activation on polyethylene glycol modified polyurethane surfaces. Measurement of cytoplasmic calcium. *ASAIO J* September 1996;**42**(5):M876–81.

128. Albanese A, Barbucci R, Belleville J, et al. In vitro biocompatibility evaluation of a heparinizable material (PUPA), based on polyurethane and poly(amido-amine) components. *Biomaterials* January 1994;**15**(2):129–36.

129. Marconi W, Galloppa A, Martinelli A, et al. New polyurethane compositions able to bond high amounts of both albumin and heparin: Part I. *Biomaterials* April 1995;**16**(6):449–56.

130. Kang IK, Kwon OH, Kim MK, et al. In vitro blood compatibility of functional group-grafted and heparin-immobilized polyurethanes prepared by plasma glow discharge. *Biomaterials* August 1997;**18**(16):1099–107.

131. Marconi W, Benvenuti F, Piozzi A. Covalent bonding of heparin to a vinyl copolymer for biomedical applications. *Biomaterials* June 1997;**18**(12):885–90.

132. Appelgren P, Ransjo U, Bindslev L, et al. Surface heparinization of central venous catheters reduces microbial colonization in vitro and in vivo: results from a prospective, randomized trial. *Crit Care Med* September 1996;**24**(9):1482–9.

133. Abdelkefi A, Achour W, Ben OT, et al. Use of heparin-coated central venous lines to prevent catheter-related bloodstream infection. *J Support Oncol* June 2007;**5**(6):273–8.

134. Jain G, Allon M, Saddekni S, et al. Does heparin coating improve patency or reduce infection of tunneled dialysis catheters? *Clin J Am Soc Nephrol* September 2009;**4**(11):1787–90.

135. Grasel TG, Cooper SL. Properties and biological interactions of polyurethane anionomers: effect of sulfonate incorporation. *J Biomed Mater Res* March 1989;**23**(3):311–38.

136. Francolini I, Crisante F, Martinelli A, et al. Synthesis of biomimetic segmented polyurethanes as antifouling biomaterials. *Acta Biomater* February 2012;**8**(2):549–58.

137. Flemming RG, Capelli CC, Cooper SL, et al. Bacterial colonization of functionalized polyurethanes. *Biomaterials* February 2000;**21**(3):273–81.

138. Jansen B, Goodman LP, Ruiten D. Bacterial adherence to hydrophilic polymer-coated polyurethane stents. *Gastrointest Endosc* September 1993;**39**(5):670–3.

139. Bridgett MJ, Davies MC, Denyer SP, et al. In vitro assessment of bacterial adhesion to hydromer-coated cerebrospinal fluid shunts. *Biomaterials* February 1993;**14**(3):184–8.

140. Morra M, Cassinelli C. Non-fouling properties of polysaccharide-coated surfaces. *J Biomater Sci Polym Ed* 1999;**10**(10):1107–24.

141. Magnani A, Barbucci R, Montanaro L, et al. In vitro study of blood-contacting properties and effect on bacterial adhesion on a polymeric surface with immobilized heparin and sulphated hyaluronic acid. *J Biomater Sci Polym Ed* 2000;**11**:801–15.

142. Xu F, Nacker JC, Crone WC, et al. The haemocompatibility of polyurethane-hyaluronic acid copolymers. *Biomaterials* January 2008;**29**(2):150–60.

143. Chuang TW, Masters KS. Regulation of polyurethane hemocompatibility and endothelialization by tethered hyaluronic acid oligosaccharides. *Biomaterials* October 2009;**30**(29):5341–51.

144. Xu FM, Flanagan CE, Ruiz A, et al. Polyurethane/dermatan sulfate copolymers as hemocompatible, non-biofouling materials. *Macromol Biosci* February 2011;**11**(2):257–66.

145. Perrino C, Lee S, Choi SW, et al. A biomimetic alternative to poly(ethylene glycol) as an antifouling coating: resistance to nonspecific protein adsorption of poly(L-lysine)-graft-dextran. *Langmuir* August 2008;**24**(16):8850–6.

146. Sagnella S, Mai-Ngam K. Chitosan based surfactant polymers designed to improve blood compatibility on biomaterials. *Colloids Surf B Biointerfaces* May 2005;**42**(2):147–55.

147. Wang Y, Hong Q, Chen Y, et al. Surface properties of polyurethanes modified by bioactive polysaccharide-based polyelectrolyte multilayers. *Colloids Surf B Biointerfaces* December 2012;**100**:77–83.

148. Zheng L, Zhu J. Study of antimicrobial activity of chitosan with different molecular weights. *Carbohydr Polym* 2003;**54**(4):527–30.

149. Wang DA, Ji J, Sun YH, et al. Blends of stearyl poly(ethylene oxide) coupling-polymer in chitosan as coating materials for polyurethane intravascular catheters. *J Biomed Mater Res* 2001;**58**(4):372–83.

150. Yang SH, Lee YS, Lin FH, et al. Chitosan/poly(vinyl alcohol) blending hydrogel coating improves the surface characteristics of segmented polyurethane urethral catheters. *J Biomed Mater Res B Appl Biomater* November 2007;**83**(2):304–13.

151. Tunney MM, Gorman SP. Evaluation of a poly(vinyl pyrollidone)-coated biomaterial for urological use. *Biomaterials* December 2002;**23**(23):4601–8.

152. Bach A. Clinical studies on the use of antibiotic- and antiseptic-bonded catheters to prevent catheter-related infection. *Zentralbl Bakteriol* December 1995;**283**(2):208–14.

153. Greenfeld JI, Sampath L, Popilskis SJ, et al. Decreased bacterial adherence and biofilm formation on chlorhexidine and silver sulfadiazine-impregnated central venous catheters implanted in swine. *Crit Care Med* May 1995;**23**(5):894–900.

154. Maki DG, Stolz SM, Wheeler S, et al. Prevention of central venous catheter-related bloodstream infection by use of an antiseptic-impregnated catheter. A randomized, controlled trial. *Ann Intern Med* August 1997;**127**(4):257–66.

155. Walder B, Pittet D, Tramer MR. Prevention of bloodstream infections with central venous catheters treated with anti-infective agents depends on catheter type and insertion time: evidence from a meta-analysis. *Infect Control Hosp Epidemiol* December 2002;**23**(12):748–56.

156. Brun-Buisson C, Doyon F, Sollet JP, et al. Prevention of intravascular catheter-related infection with newer chlorhexidine-silver sulfadiazine-coated catheters: a randomized controlled trial. *Intensive Care Med* May 2004;**30**(5):837–43.

157. Ostendorf T, Meinhold A, Harter C, et al. Chlorhexidine and silver-sulfadiazine coated central venous catheters in haematological patients–a double-blind, randomised, prospective, controlled trial. *Support Care Cancer* December 2005;**13**(12):993–1000.

158. Rupp ME, Lisco SJ, Lipsett PA, et al. Effect of a second-generation venous catheter impregnated with chlorhexidine and silver sulfadiazine on central catheter-related infections: a randomized, controlled trial. *Ann Intern Med* October 2005;**143**(8):570–80.

159. Darouiche RO, Raad II, Bodey GP, et al. Antibiotic susceptibility of staphylococcal isolates from patients with vascular catheter-related bacteremia: potential role of the combination of minocycline and rifampin. *Int J Antimicrob Agents* September 1995;**6**(1):31–6.

160. Raad I, Darouiche R, Hachem R, et al. Antibiotics and prevention of microbial colonization of catheters. *Antimicrob Agents Chemother* November 1995;**39**(11):2397–400.

161. Raad I, Darouiche R, Hachem R, et al. The broad-spectrum activity and efficacy of catheters coated with minocycline and rifampin. *J Infect Dis* February 1996;**173**(2):418–24.

162. Darouiche RO, Raad II, Heard SO, et al. A comparison of two antimicrobial-impregnated central venous catheters. Catheter Study Group. *N Engl J Med* January 1999;**340**(1):1–8.

163. Leon C, Ruiz-Santana S, Rello J, et al. Benefits of minocycline and rifampin-impregnated central venous catheters. A prospective, randomized, double-blind, controlled, multicenter trial. *Intensive Care Med* October 2004;**30**(10):1891–9.

164. Darouiche RO, Berger DH, Khardori N, et al. Comparison of antimicrobial impregnation with tunneling of long-term central venous catheters: a randomized controlled trial. *Ann Surg* August 2005;**242**(2):193–200.

165. Gilbert RE, Harden M. Effectiveness of impregnated central venous catheters for catheter related blood stream infection: a systematic review. *Curr Opin Infect Dis* June 2008;**21**(3):235–45.

166. Raad II, Darouiche RO, Hachem R, et al. Antimicrobial durability and rare ultrastructural colonization of indwelling central catheters coated with minocycline and rifampin. *Crit Care Med* February 1998;**26**(2):219–24.

167. Donelli G, Francolini I, Piozzi A, et al. New polymer-antibiotic systems to inhibit bacterial biofilm formation: a suitable approach to prevent central venous catheter-associated infections. *J Chemother* October 2002;**14**(5):501–7.

168. Piozzi A, Francolini I, Occhiaperti L, et al. Polyurethanes loaded with antibiotics: influence of polymer-antibiotic interactions on in vitro activity against *Staphylococcus epidermidis*. *J Chemother* October 2004;**16**(5):446–52.

169. Ruggeri V, Francolini I, Donelli G, et al. Synthesis, characterization, and in vitro activity of antibiotic releasing polyurethanes to prevent bacterial resistance. *J Biomed Mater Res A* May 2007;**81**(2):287–98.

170. Piozzi A, Francolini I, Occhiaperti L, et al. Antimicrobial activity of polyurethanes coated with antibiotics: a new approach to the realization of medical devices exempt from microbial colonization. *Int J Pharm* August 2004;**280**(1–2):173–83.

171. Marconi W, Francolini I, Piozzi A, et al. Antibiotic releasing urethane polymers for prevention of catheter-related infections. *J Bioact Compat Polym* 2001;**16**:393–407.

172. Lai NM, Chaiyakunapruk N, Lai NA, et al. Catheter impregnation, coating or bonding for reducing central venous catheter-related infections in adults. *Cochrane Database Syst Rev* 2013;**6**:CD007878.

173. Raad I, Reitzel R, Jiang Y, et al. Anti-adherence activity and antimicrobial durability of anti-infective-coated catheters against multidrug-resistant bacteria. *J Antimicrob Chemother* October 2008;**62**(4):746–50.

174. Sampath LA, Tambe SM, Modak SM. In vitro and in vivo efficacy of catheters impregnated with antiseptics or antibiotics: evaluation of the risk of bacterial resistance to the antimicrobials in the catheters. *Infect Control Hosp Epidemiol* October 2001;**22**(10):640–6.

175. Schierholz JM, Fleck C, Beuth J, et al. The antimicrobial efficacy of a new central venous catheter with long-term broad-spectrum activity. *J Antimicrob Chemother* July 2000;**46**(1):45–50.

176. Yucel N, Lefering R, Maegele M, et al. Reduced colonization and infection with miconazole-rifampicin modified central venous catheters: a randomized controlled clinical trial. *J Antimicrob Chemother* December 2004;**54**(6):1109–15.

177. Schierholz JM, Nagelschmidt K, Nagelschmidt M, et al. Antimicrobial central venous catheters in oncology: efficacy of a rifampicin-miconazole-releasing catheter. *Anticancer Res* April 2010;**30**(4):1353–8.

178. Lorente L, Lecuona M, Ramos MJ, et al. The use of rifampicin-miconazole-impregnated catheters reduces the incidence of femoral and jugular catheter-related bacteremia. *Clin Infect Dis* November 2008;**47**(9):1171–5.

179. Raad I, Mohamed JA, Reitzel RA, et al. Improved antibiotic-impregnated catheters with extended-spectrum activity against resistant bacteria and fungi. *Antimicrob Agents Chemother* February 2012;**56**(2):935–41.

180. Jamal MA, Rosenblatt JS, Hachem RY, et al. Prevention of biofilm colonization by Gram-negative bacteria on minocycline-rifampin-impregnated catheters sequentially coated with chlorhexidine. *Antimicrob Agents Chemother* February 2014;**58**(2):1179–82.

181. Donelli G, Francolini I, Romoli D, et al. Synergistic activity of dispersin B and cefamandole nafate in inhibition of staphylococcal biofilm growth on polyurethanes. *Antimicrob Agents Chemother* August 2007;**51**(8):2733–40.

182. Kaplan JB, Ragunath C, Velliyagounder K, et al. Enzymatic detachment of *Staphylococcus epidermidis* biofilms. *Antimicrob Agents Chemother* July 2004;**48**(7):2633–6.

183. Dowling DP, Donnelly K, McConnell ML, et al. Deposition of anti-bacterial silver coatings on polymeric substrates. *Thin Solid Films* 2001;**398**:602–6.

184. Gray JE, Norton PR, Alnouno R, et al. Biological efficacy of electroless-deposited silver on plasma activated polyurethane. *Biomaterials* July 2003;**24**(16):2759–65.

185. Francolini I, D'Ilario L, Guaglianone E, et al. Polyurethane anionomers containing metal ions with antimicrobial properties: thermal, mechanical and biological characterization. *Acta Biomater* September 2010;**6**(9):3482–90.

186. Francolini I, Ruggeri V, Martinelli A, et al. Novel metal-polyurethane complexes with enhanced antimicrobial activity. *Macromol Rapid Commun* February 2006;**27**(4):233–7.

187. Paladini F, Pollini M, Talà A, et al. Efficacy of silver treated catheters for haemodialysis in preventing bacterial adhesion. *J Mater Sci Mater Med* 2012;**23**:1983–90.

188. Bach A, Eberhardt H, Frick A, et al. Efficacy of silver-coating central venous catheters in reducing bacterial colonization. *Crit Care Med* March 1999;**27**(3):515–21.

189. Bambauer R, Schiel R, Bambauer C, et al. Surface-treated versus untreated large-bore catheters as vascular access in hemodialysis and apheresis treatments. *Int J Nephrol* 2012;**2012**:956136.

190. Trerotola SO, Johnson MS, Shah H, et al. Tunneled hemodialysis catheters: use of a silver-coated catheter for prevention of infection–a randomized study. *Radiology* May 1998;**207**(2):491–6.

191. Antonelli M, De PG, Ranieri VM, et al. Comparison of triple-lumen central venous catheters impregnated with silver nanoparticles (AgTive(R)) vs conventional catheters in intensive care unit patients. *J Hosp Infect* October 2012;**82**(2):101–7.

192. Stevens KN, Crespo-Biel O, van den Bosch EE, et al. The relationship between the antimicrobial effect of catheter coatings containing silver nanoparticles and the coagulation of contacting blood. *Biomaterials* August 2009;**30**(22):3682–90.

193. Crisante F, Francolini I, Bellusci M, et al. Antibiotic delivery polyurethanes containing albumin and polyallylamine nanoparticles. *Eur J Pharm Sci* March 2009;**36**(4–5):555–64.

194. Jones DS, McGovern JG, Woolfson AD, et al. Physicochemical characterization of hexetidine-impregnated endotracheal tube poly(vinyl chloride) and resistance to adherence of respiratory bacterial pathogens. *Pharm Res* June 2002;**19**(6):818–24.

195. Schierholz JM, Rump A, Pulverer G. New antiinfectious biomaterials. Ciprofloxacin containing polyurethanes as potential drug delivery systems to prevent foreign-body infections. *Arzneimittelforschung* January 1997;**47**(1):70–4.

196. Francolini I, Norris P, Piozzi A, et al. Usnic acid, a natural antimicrobial agent able to inhibit bacterial biofilm formation on polymer surfaces. *Antimicrob Agents Chemother* November 2004;**48**(11):4360–5.

197. Basak P, Adhikari B, Banerjee I, et al. Sustained release of antibiotic from polyurethane coated implant materials. *J Mater Sci Mater Med* December 2009;**20**(Suppl. 1):S213–21.

198. Kim JE, Kim SR, Lee SH, et al. The effect of pore formers on the controlled release of cefadroxil from a polyurethane matrix. *Int J Pharm* May 2000;**201**(1):29–36.

199. Donelli G, Francolini I, Ruggeri V, et al. Pore formers promoted release of an antifungal drug from functionalized polyurethanes to inhibit *Candida* colonization. *J Appl Microbiol* March 2006;**100**(3):615–22.

200. Fong N, Simmons A, Poole-Warren LA. Antibacterial polyurethane nanocomposites using chlorhexidine diacetate as an organic modifier. *Acta Biomater* July 2010;**6**(7): 2554–61.

201. Kalfon P, de VC, Samba D, et al. Comparison of silver-impregnated with standard multi-lumen central venous catheters in critically ill patients. *Crit Care Med* April 2007;**35**(4):1032–9.

202. Stoiser B, Kofler J, Staudinger T, et al. Contamination of central venous catheters in immunocompromised patients: a comparison between two different types of central venous catheters. *J Hosp Infect* March 2002;**50**(3):202–6.

203. Moretti EW, Ofstead CL, Kristy RM, et al. Impact of central venous catheter type and methods on catheter-related colonization and bacteraemia. *J Hosp Infect* October 2005;**61**(2):139–45.

204. Bong JJ, Kite P, Wilco MH, et al. Prevention of catheter related bloodstream infection by silver iontophoretic central venous catheters: a randomised controlled trial. *J Clin Pathol* October 2003;**56**(10):731–5.

205. Corral L, Nolla-Salas M, Ibanez-Nolla J, et al. A prospective, randomized study in critically ill patients using the Oligon Vantex catheter. *J Hosp Infect* November 2003;**55**(3): 212–9.

206. Ranucci M, Isgro G, Giomarelli PP, et al. Impact of oligon central venous catheters on catheter colonization and catheter-related bloodstream infection. *Crit Care Med* January 2003;**31**(1):52–9.

207. Modak C, Fox C. Binding of silver sulfadiazine in the cellular components of *Pseudomonas aeruginosa*. *Biochem Pharm* 1973;**22**(2392):2404.

208. Schierholz JM, Lucas LJ, Rump A, et al. Efficacy of silver-coated medical devices. *J Hosp Infect* December 1998;**40**(4):257–62.

209. Woo GL, Mittelman MW, Santerre JP. Synthesis and characterization of a novel biodegradable antimicrobial polymer. *Biomaterials* June 2000;**21**(12):1235–46.

210. Woo GL, Yang ML, Yin HQ, et al. Biological characterization of a novel biodegradable antimicrobial polymer synthesized with fluoroquinolones. *J Biomed Mater Res* January 2002;**59**(1):35–45.

211. Makal U, Wood L, Ohman DE, et al. Polyurethane biocidal polymeric surface modifiers. *Biomaterials* March 2006;**27**(8):1316–26.

212. Kenawy E, Worley S, Broughton R. The chemistry and application of antimicrobial polymers: a state-of-the-art review. *Biomacromolecules* 2007;**8**(5):1359–84.

213. Palermo E, Lee D, Ramamoorthy A, et al. The role of cationic group structure in membrane binding and disruption by amphiphilic copolymers. *J Phys Chem B* 2011;**115**(2):366–75.

214. Grapski JA, Cooper SL. Synthesis and characterization of non-leaching biocidal polyurethanes. *Biomaterials* August 2001;**22**(16):2239–46.

215. Kurt P, Wood L, Ohman DE, et al. Highly effective contact antimicrobial surfaces via polymer surface modifiers. *Langmuir* April 2007;**23**(9):4719–23.

216. Kurt P, Gamble LJ, Wynne KJ. Surface characterization of biocidal polyurethane modifiers having poly(3,3-substituted)oxetane soft blocks with alkylammonium side chains. *Langmuir* June 2008;**24**(11):5816–24.

217. Mizerska U, Fortuniak W, Chojnowski J, et al. Polysiloxane cationic biocides with imidazolium salt (ImS) groups, synthesis and antibacterial properties. *Eur Polym J* March 2009;**45**(3):779–87.
218. Martinelli A, Bakry A, D'Ilario L, et al. Release behavior and antibiofilm activity of usnic acid-loaded carboxylated poly(ʟ-lactide) microparticles. *Eur J Pharm Biopharm* October 2014;**88**(2):415–23.
219. Taresco V, Francolini I, Padella F, et al. Design and characterization of antimicrobial usnic acid loaded-core/shell magnetic nanoparticles. *Mater Sci Eng C* 2015;**52**:72–81.

Polyurethanes for cardiac applications

13

*M. Boffito, S. Sartori, C. Mattu, G. Ciardelli**
Politecnico di Torino, Torino, Italy
*Corresponding author: gianluca.ciardelli@polito.it

13.1   Introduction: cardiovascular diseases

Cardiovascular diseases (CVDs) remain the biggest cause of deaths worldwide. According to the World Health Organization more than 17 million people died from CVDs in 2008, representing 30% of total deaths worldwide (Mendis et al., 2011). Cardiovascular disease is a general term that describes a disease affecting the heart or the blood vessels. There are four main types of CVD: heart disease (heart attack), cerebrovascular disease (stroke), peripheral arterial disease, and aortic disease (Figure 13.1). Atherosclerosis is responsible for a large proportion of CVDs. Other CVDs such as disorders of the heart muscle (e.g., cardiomyopathy) and of the heart electrical conduction system (e.g., cardiac arrhythmias) and heart valve diseases are less common than heart attacks and strokes.

In atherosclerosis, fatty material and cholesterol are deposited inside the lumen of medium- and large-sized blood vessels (arteries). Eventually, the plaque can rupture, triggering the formation of a blood clot. If the blood clot develops in the brain, it can cause a **stroke**; if it develops in a coronary artery, it can cause a vessel occlusion and consequently a **heart attack**: the supply of nutrients and oxygen to the heart muscle is reduced and the contractile muscle cells (cardiomyocytes) die within the blood-deprived myocardium. The tissue becomes necrotic and cardiac performances are impaired.

Aortic diseases can be classified in aortic enlargement (aneurysms) or tears (dissections) and in either case, the rupture may have fatal results. Aging can lead to atherosclerosis of the aorta with involvement of the aortic valve. This may result in valvular stenosis, regurgitation, aneurysm formation, and acute dissections.

Peripheral vascular diseases (PVDs) are circulation disorders that affect blood vessels outside of the heart and brain. PVD typically strikes the veins and arteries that supply the arms, legs, and organs located below the stomach. These vessels are distant from the heart and they are known as peripheral vessels.

Cardiomyopathies are diseases of an abnormal heart muscle. There are three main types of cardiomyopathy: dilated, hypertrophic, and restrictive. Dilated cardiomyopathy is a condition in which the heart becomes weaker and the chambers get larger. Hypertrophic cardiomyopathy is a condition in which the heart muscle becomes thick. Ischemic cardiomyopathy is caused by a narrowing of the arteries that
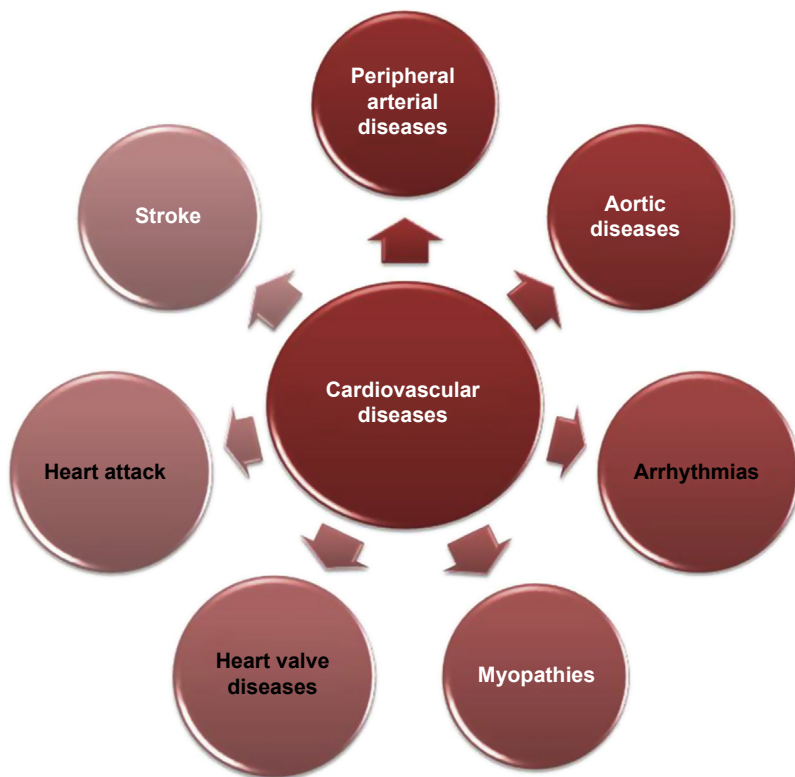
Figure 13.1 Cardiovascular diseases.

supply the heart with blood. Cardiomyopathies make it harder for the heart to pump and deliver blood to the rest of the body. Cardiomyopathy can lead to heart failure.

An **arrhythmia** is a problem with the rate or rhythm of the heartbeat. During an arrhythmia, the heart can beat too fast, too slow, or with an irregular rhythm. A heartbeat that is too fast is called tachycardia. A heartbeat that is too slow is called bradycardia. Most arrhythmias are harmless, but some may be serious or even life threatening. During an arrhythmia the heart may not be able to pump enough blood to the body and this can damage the brain, heart, and other organs. Rhythm disorders are the leading cause of morbidity, impaired quality of life, and mortality in adults with congenital heart disease.

Heart valve disease occurs when a valve does not work properly. In valvular stenosis, the valve leaflets tissues become stiffer, narrowing the valve opening and reducing the blood flow. If the narrowing is mild, the overall functioning of the heart may not be reduced. However, the valve can become so narrow (stenotic) that heart function is reduced, and the rest of the body may receive inadequate blood flow. Another valvular heart disease condition, called valvular regurgitation, occurs when the leaflets do not close completely, letting blood leak backward across the valve.

13.2   Polyurethanes in cardiovascular applications

Successful treatment of cardiovascular diseases is limited in many situations by the lack of autologous tissue; therefore artificial materials may open a new era in the treatment of these pathologies. The artificial tissues should match the mechanical properties of the native ones to avoid the mechanical failure of the construct and provide mechanical support during regeneration. Force-generating contractile tissues, such as cardiac and vascular ones, may undergo significant deformation and show an anisotropic viscoelastic behavior. Their mechanical properties can be mimicked by a handful of materials of synthetic origin, especially elastomers. Among them, polyurethanes (PURs) have been demonstrated to be valid candidates due to their enhanced physical properties: in addition to their elastomer-like character, they show durability, fatigue resistance, compliance, and blood compatibility (Zdrahala and Zdrahala, 1999; Lamba et al., 1998). Furthermore, they are attractive for their ability to undergo bulk and surface modification via tailoring their hydrophilic/hydrophobic balance or by attachment of biologically active species. Polymers modified with extracellular matrix (ECM) components, such as proteins or their fragments (mainly peptides), are indicated as biomimetic materials (biochemical biomimicry). Moreover, some devices or scaffolds can mimic native tissues also with regard to mechanical properties (mechanical biomimicry) and structural-morphological composition (morphological biomimicry). These modifications are designed to mediate and enhance implant integration in the host tissue.

By virtue of their excellent mechanical properties and blood compatibility, PURs have emerged as optimal candidate materials for cardiovascular devices in both tissue substitution and regeneration. This chapter provides a review of their application in this field, starting with commercial PURs that have found practical application in cardiac surgery and mainly in heart valve replacement. Recently, the versatile chemistry and the possibility of modulating mechanical and physical properties and inserting biological cues, in the bulk material or on the surface, have opened the way for the application of novel PUR formulations in cardiac tissue engineering approaches, with promising preclinical results. This chapter also reports the future trends on the application of PURs in the design of innovative drug delivery systems for cardiac disease, a pioneering research field that could lead to advanced therapies and devices. An extensive description of the application of PURs in the vascular field is reported in Chapter 10, 11, 12 and 15.

13.3   Polyurethanes in heart valve replacement

There are three types of prosthetic heart valves:

- bioprosthetic or biological valves, from animal or human sources (e.g., cadaver, porcine, bovine);
- mechanical heart valves (MHVs), which are made entirely of plastics and metallic materials;
- tissue engineered valves, which are realized through a multidisciplinary approach combining principles from biology and engineering.

The main problems related to bioprosthetic heart valves are due to calcification and tissue failure. However, compared to MHVs, these valves offer a physiological flow pattern and require less anticoagulation than mechanical valves.

Mechanical valves are divided into two kinds based on their flow patterns: valves with lateral flow (e.g., the ball in cage valves) and valves with a more central flow (e.g., the tilting disc and bileaflet valves) (Kidane et al., 2009a). MHVs made out of metal are often susceptible to fatigue failure owing to the polycrystalline characteristic of metals. Polymeric materials have shown great potential in this application and have a long history in heart valve replacement. For instance, thermoplastic PUR elastomers have been used since the 1960s, because they possess high tensile strength, excellent resistance to cyclic fatigue, desirable hemodynamic characteristics, and good biocompatibility (Hilbert et al., 1987).

The disadvantage of polymeric heart valves is their susceptibility to biodegradation and mineralization. This has somewhat limited the use of PUR for prosthetic heart valves.

Different types of biostable PURs have been used in heart valve components, including polyether urethanes (PEUs), polyether urethane ureas (PEUUs), polycarbonate urethane (PCUs), polycarbonate urethane ureas (PCUUs), polycarbonate-based materials that contain polyhedral oligomeric silsequioxane nanoparticles (POSS) (Ghanbari et al., 2010; Kidane et al., 2009b), and those that contain polysiloxane soft segments (Bezuidenhout et al., 2015).

PEUs were used since they have excellent hydrolytic stability. In the 1980s two types of trileaflet PUR valves made of Biomer (Ethicon) and Lycra Spandex (DuPont) were developed. The Lycra valves showed low regurgitation *in vitro*, and lasted for one year or more in large animal models, but calcification and thrombosis became evident in growing sheep (Wisman et al., 1982). Calcification was also seen with Biomer valves in juvenile sheep (Hilbert et al., 1987).

Wheatley and colleagues worked with a variety of PURs (Bernacca et al., 1992, 1995, 1996, 1997a,b). The early studies were focused on a PEU (Estane) and a PEUU (Lycra). Durability of more than 300 million cycles at 12 Hz was achieved with Estane valves (Hilbert et al., 1987) and 800 million cycles were completed with Lycra PEUU devices. *In vitro* dynamic testing showed some calcification in the leaflets of these valves and at degradation sites (Hilbert et al., 1987; Bernacca et al., 1992). Static *in vitro* and *in vivo* studies underlined the effect of low molecular mass components in the polymeric materials: lower degrees of calcification were observed after extraction of these components with methanol and chloroform. Hydrodynamic function tests in a simulated mitral position evidenced that the valves had less reverse flow and energy loss than both bioprosthetic and mechanical valves (Mackay et al., 1996) and mean pressure drops similar to those of bioprostheses. *In vivo* tests in a 6 month sheep mitral model showed similar performance for both the PUR and the mechanical valves in terms of hemodynamics, while a porcine valve became compromised with time. However, calcification of the PUR valve was marked and it was generally associated with surface thrombus and degraded areas on the leaflets.

Several studies demonstrated that, despite the hydrolytic stability of polyether soft segments, they are susceptible to oxidative degradation and consequently undergo environmental stress cracking (Christenson et al., 2004a,b).

Subsequently different hydrolytic stable macrodiols were used in PUR synthesis. For instance PCUs were tested and proven to have an increased oxidative stability compared with PEUs (Tang et al., 2001; Salacinski et al., 2002) and the biodegradation was limited to a thinner surface layer (Kidane et al., 2009a). The company ADIAM (which closed the production) developed bi- and trileaflet valves from a PCU for mitral and aortic positions, respectively (Daebritz et al., 2004a; Sachweh and Daebritz, 2006). These valves were subjected to *in vitro* testing, showing that the durability of the mitral valves ranged from 600 to 1000 million cycles, equivalents to 16–26 years (Daebritz et al., 2003), while the aortic trileaflet exhibited improvements from 300 to 600 million cycles (Daebritz et al., 2004b). A comparative study of these valves with two different bioprosthetic valves was conducted in a growing calf mitral model for 20 weeks, showing little regurgitation, mild leaflet thickening, and calcification, and no degeneration has been observed with the PCU valves, while the bioprosthetic ones induced congestive heart failure, due to severe calcification, degeneration, and thrombosis. When the *in vivo* tests were conducted in the aortic position, the synthetic valves had a variable degree of calcification and a mild degeneration and there was little thrombus (Bernacca et al., 1997a).

Poly(dimethyl siloxane) (PDMS) provides good thermal and oxidative stability and was incorporated into a PUR backbone in the presence of polyhexamethylene oxide (PHMO), a compatibilizer that facilitates the incorporation of the nonpolar PDMS macrodiol. Long-term stability was demonstrated for PDMS-based PUR synthesized using 20% PHMO and 80% PDMS (Dabagh et al., 2005; Simmons et al., 2004).

Similarly, our group studied a series of PDMS–poly(tetramethylene oxide) (PTMO)-based PUR formulations, including composites containing a clay as a filler, as new biomaterials for the realization of annuloplastic rings in mitral valve repair (Silvestri et al., 2011). The clays, which were introduced to further improve the mechanical properties, were two commercial organomodified montmorillonites, Cloisite 20A and 30B. These clays were selected because they showed antimicrobial activity in several studies (Nigmatullin et al., 2008). The PURs were synthesized starting from an aliphatic diisocyanate, namely 1,6-diisocyanatohexane (HDI), because of its low cost and the negligible toxicity of its biodegradation products. The mechanical behavior of the prepared formulations makes them suitable for annuloplastic applications since Young's modulus values at 37 °C were in the range required for the realization of these kinds of devices. It could be possible to choose two or more materials characterized by different elastic modulus values and combine them in the manufacturing of ring components. By taking into account creep tests, the best PUR-based formulations turned out to be the PURs containing 60% and 80% PTMO in the soft segment and the composites containing Cloisite 30B as filler.

Seifalian synthesized a novel nanocomposite PUR with a polycarbonate soft segment (PCU) and POSS covalently bound as a pendant cage to the hard segment (Kannan et al., 2007). *In vitro* studies demonstrated that the POSS groups protected the soft segment of the PUR from oxidative and hydrolytic degradation (Kannan et al., 2006). The polymer also demonstrated resistance to degradation by plasma proteins compared to PCU in an *in vitro* enzymatic degradation study. Furthermore, the polymer is nontoxic and possesses greater thromboresistance than polytetrafluoroethylene (PTFE). An *in vivo* study in a sheep model

showed minimal inflammation and capsular formation and no degradation after 36 months of postimplantation compared to a control (Simmons et al., 2004). The POSS–PCU nanocomposite (Figure 13.2) also possesses excellent mechanical strength, good surface properties, and resistance to platelet adhesion. It has also shown a hardness and tear strength comparable to those of Estane, Chronoflex, and Elasteon, and elongation comparable to that of Elasteon, but higher tensile strength than all of these (Kidane et al., 2009b). In an *in vitro* accelerated physiological pulsatile pressure system model study the PCU nanocomposite revealed lower platelet adhesion and higher calcification resistance compared to the respective PCU and glutaraldehyde-fixed bovine pericardium.

13.3.1 Functionalized and biomimetic polyurethanes for the development of advanced heart valves

As previously described, device failure has frequently occurred as a result of both thrombosis and calcification. PUR valve calcification occurs on the blood-contacting surfaces of these devices, and in general results from calcified thrombus (Bezuidenhout et al., 2015). This is caused in part by the lack of an intact endothelium on device surfaces, with resulting thromboembolic activity.

Stachelek et al. (2006) modified a polyether urethane to promote cell adhesion and produce an antitrombogenic surface. Their work was based on the hypothesis that endothelial seeding of a PUR heart valve leaflet with autologous sheep blood outgrowth endothelial cells (BOECs) could be achieved with a cholesterol-modified PUR (PUR-Chol) to promote
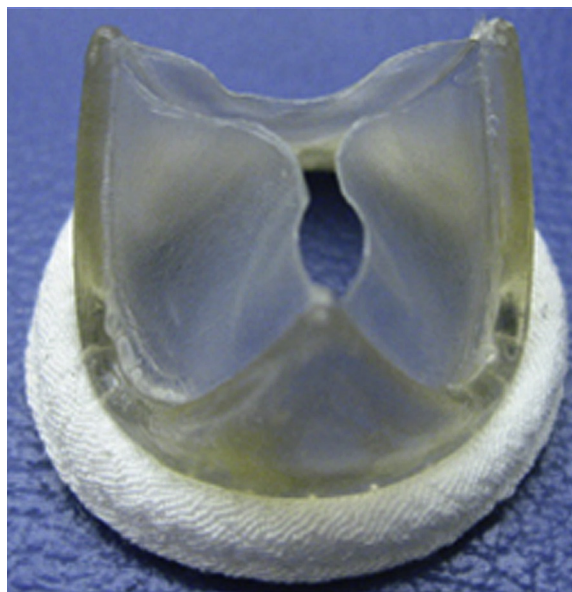
Figure 13.2 A prototype valve fabricated from POSS–PCU nanocomposite with a Dacron suture ring.
Reprinted with permission from Ghanbari et al. (2010). Copyright 2010, Elsevier.

BOEC adhesion, resulting in an intact, shear-resistant endothelium that would promote resistance to thrombosis. The PUR used in these studies was Tecothane TT1074A (Thermedics, Waltham). This PUR was covalently modified with cholesterol (Chol) by means of bromoalkylation. Uniaxial stress–strain experiments revealed no significant differences in elastic behavior in a comparison between unmodified PUR and PUR-Chol. PUR-Chol was markedly different than unmodified PUR in terms of increased surface energy, a relatively smooth surface, and a different surface chemistry. Summing up, the surface modification leads to a more lipophilic surface with increased collagen synthesis. Successful BOEC seeding on a PUR heart valve leaflet was achieved, with significantly greater retention of seeded BOECs than controls, both *in vitro*, under simulated valve shear, and *in vivo*. Calcification was not observed in any of the explants, but the authors underlined that previous investigations have shown that more extended *in vivo* studies are required for investigating PUR-related pathologic calcification mechanisms (Stachelek et al., 2006).

Wong et al. (2010) studied blends of natural and synthetic polymers with the aim of creating biomimetic materials for heart valve leaflets. They examined electrospun gelatin–chitosan PUR, polyglycolide (PGA)/PLA and collagen-coated bovine pericardium. Ovine endothelial cells were seeded onto these materials and exposed to a range of shear stresses for a period of 1–3 h.

Through the exposure time and the shear-stress range tested, the gelatin–chitosan PUR group showed the best results, with a mean cell retention rate of 80%. For all ranges of physiological flow conditions examined, the electrospun gelatin–chitosan PUR demonstrated good biocompatibility and cell retention properties.

Alves et al. (2014) used a commercial preprocessed polyether-based PUR (Elastollan1180A50) to formulate films whose surfaces were modified by grafting 2-hydroxyethyl-methacrylate (HEMA) to increase its hydrophilicity and improve its biological properties. Elastollan was chosen because it does not contain plasticizers; it has good heat resistance, high mechanical flexibility, and the ability to be processed by molding. HEMA was grafted onto the surface of Elastollan by plasma and UV irradiation. X-ray photoelectron spectroscopy (XPS), atomic force microscopy (AFM), and static contact angle measurements suggested that the surfaces were successfully grafted and argon plasma treatment turned out to be more efficient for the grafting of HEMA when compared to the UV method. The plasma-modified surface showed higher HEMA density, which led to a smoother and more hydrophilic surface. Furthermore, argon plasma treatment showed lower values of thrombogenicity in comparison with those of unmodified and UV-modified thermoplastic polyurethanes (TPUs) and enhanced the bactericidal activity of the materials. Human fibroblasts cells were seeded on unmodified and modified films, showing higher viabilities in the presence of modified TPUs during the first 72 h. Based on the overall results the authors concluded that the proposed plasma modification of Elastollan leads to a suitable material for heart valve replacement.

13.3.2 *Future prospective of polyurethane heart valve replacement*

Long-term material calcification has been the major factor that has limited the success of PUR heart valves. To overcome this problem, several efforts have been made to

modify PUR materials by incorporating soft segments, such as polycarbonate and polysiloxane, into the backbone. These changes led to materials with improved long-term biocompatibility and biostability.

Another interesting strategy adopted to improve PUR heart valve performance was the functionalization with bioactive molecules. Encouraging preliminary results were obtained, but more comprehensive studies should be carried out.

More recently scaffold recellularization in a bioreactor before implantation has been described as a strategy for obtaining a fully recolonized living autologous valve. These approaches were tested with polyester scaffolds (Mendelson and Schoen, 2006), showing promising results, but to our knowledge, similar studies were not conducted with PUR. In a work of Aleksieva et al. PUR heart valve prostheses were manufactured by using a PUR spraying technique. In this study endothelial cells and fibroblasts were seeded onto PUR heart valve scaffolds and static cultivation (SC) and dynamic cultivation (DC) were compared. DC intensified formation of cell connecting molecules, and a higher expression of collagen IV, VE-cadherin, and fibronectin was observed, indicating the formation of an ECM, crucial for tissue regeneration. These observations indicate that a combination of PUR modification and dynamic cell culture may lead to devices with superior performance.

However, *in vitro* culture steps, especially using bioreactors, are delicate, require time, and sophisticated devices and methods. Hence, a procedure that avoids cell seeding, allowing direct scaffold implantation, and additionally induces *in vivo* recolonization would be ideal, since it simplifies clinical studies and applications.

13.4 Cardiac tissue engineering/regenerative medicine

Although the heart plays an essential role in living organisms, mammals show a poor natural capacity to repair injured heart tissue. Contractile cells, indeed, do not repopulate the injured area, while fibroblasts gradually replace them (Cohen and Leor, 2004; Holmes et al., 2005; Sun and Weber, 2000). After a myocardial infarction (MI), the proliferative capacity is limited to the noninfarcted area and the border zone (interface area between infarcted and healthy tissue) and, as a consequence, the injured tissue in gradually replaced by a noncontractile scar (Nadal-Ginard et al., 2003; Baig et al., 1998; Krupnick et al., 2004). Therefore, at least one-third of patients who survive an MI develop heart failure (HF) (Cohen and Leor, 2004). The gold standard treatment in case of HF is heart transplantation (Stehlik et al., 2010; Ramakrishna and Pajaro, 2011). Despite the improvements made in heart transplantation surgery, several problems still remain in both the short and the long term and transplanted people are continuously subjected to the risk of developing malignancies and allograft coronary vasculopathy (Ramakrishna and Pajaro, 2011). In addition, only a small percentage of patients can undergo heart transplantation due to the shortage of heart donors. All these issues explain the need for alternative treatments to heart transplantation. Ventricular assist devices and total artificial hearts are gaining more and more interest as temporary assist systems in the management of patients waiting for heart transplantation. However, all traditional therapies aim at restoring blood flow from the heart to the surrounding tissues and organs,

but are unable to make the heart infarcted region again functional. As a consequence, patient's final outcome will gradually worsen due to the progress of the remodeling cascade (Dobaczewski et al., 2010; Frangogiannis, 2008; Holmes et al., 2005; Zamilpa and Lindsey, 2010). In this context, tissue engineering/regenerative medicine (TERM) may represent an efficient alternative to stimulate the regeneration of the infarcted tissue, avoiding remodeling and scar formation (Figure 13.3).

One of the most promising approaches in myocardial TERM involves the design and fabrication of scaffolds to be implanted on the damaged heart tissue in the form of cellularized or cell-free patches. The implantation of cellularized or noncellularized 3D scaffolds provides several advantages over cell injection: (1) patches temporally replace the damaged tissue providing a substrate for cell proliferation and eventually differentiation, and a mechanical support for the reparative process (Leor and Cohen, 2004), (2) cell injection procedures require the injection of a billion of cells, since an MI can damage up to 50 g of tissue (Curtis and Russell, 2009) and about 90% of the injected cells are lost in the blood circulation and 90% of the successfully injected cells dies within a week due to the adverse cardiac microenvironment (Curtis and Russell, 2009; Laflamme and Murry, 2005; Murry et al., 2006). Scaffold-embedded cells show higher survival and secrete more cytokines
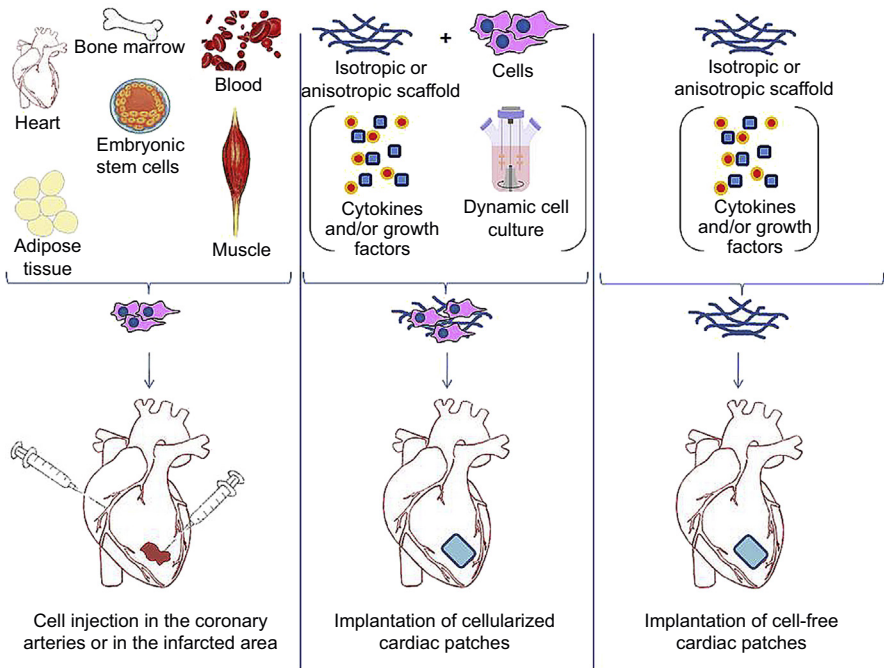
Figure 13.3 Cardiac TERM approaches. Cells from several sources, for example, bone marrow, blood, embryo, cardiac and skeletal muscle tissue, adipose tissue, can be injected in the coronary arteries or directly on the infarcted area, or seeded on scaffolds prior to implantation. Noncellularized cardiac patches can also be implanted. Cytokines and/or growth factors can be incorporated to make the developed scaffolds bioactive.

with respect to injected cells, thus resulting in improved cardiac repair (Shimizu, 2011). This behavior can be related to the scaffold's ability to create a favorable environment for cell homing, proliferation, and differentiation. Several studies have reported the capability of heart patches to alleviate left ventricular (LV) remodeling (LV dilatation reduction) and induce cardiac function improvement (improvement in LV ejection fraction) in both acute and chronic conditions (Fujimoto et al., 2007a; Kelley et al., 1999; Liao et al., 2010). Scaffold constituent materials and design are crucial points for the development of suitable and promising matrices for cardiac TERM application. A suitable patch for cardiac TERM should meet strict prerequisites in terms of physicochemical, mechanical, structural, and surface properties (Silvestri et al., 2013; Boffito et al., 2014).

The scientific literature describes both natural and synthetic polymers for the fabrication of suitable scaffolds for cardiac TERM (Silvestri et al., 2013; Chen et al., 2008a). Synthetic polymers overcome some disadvantages of natural polymers, for example, their poor mechanical properties, fast degradation, and composition variability (Sui et al., 2011), allowing a fine tuning of the degradation kinetics and the mechanical and structural properties of the resulting scaffolds (Sui et al., 2011; Boffito et al., 2014; Silvestri et al., 2013). Among them, polymers belonging to both the polyester and the PUR families have been considered for the design of suitable 3D scaffolds for infarcted cardiac tissue repair (Chen et al., 2008a, 2013; Sartori et al., 2013; McDevitt et al., 2003; Fujimoto et al., 2007a,b; Guan et al., 2002, 2005, 2008; Bursac et al., 2007; McDevitt et al., 2002; Zong et al., 2005; Tay et al., 2010; Stout et al., 2011; Ishii et al., 2005; Shin et al., 2004; Piao et al., 2007; Kenar et al., 2010; Silvestri et al., 2013; Boffito et al., 2014). Among polyesters, those showing elastomeric mechanical properties, that is, poly(glycerol sebacate) and poly(1,8-octanediol-co-citric acid), turned out to be the most promising materials for the intended application (Ravichandran et al., 2013; Chen et al., 2013; Hidalgo-Bastida et al., 2007; Stuckey et al., 2010; Chen et al., 2008b; Rai et al., 2012; Liang et al., 2010; Yang et al., 2004; Guillemette et al., 2010; Engelmayr et al., 2008). These materials unfortunately lack PUR versatility in terms of available building blocks, which results in the possibility of providing the synthesized polymer with tuned physicochemical and mechanical properties, degradation kinetics, and interactions with cells (Silvestri et al., 2013). Several conveniently synthesized biodegradable and biomimetic PURs have been described in the literature, with properties that make them suitable raw materials for the development of innovative cardiac patches (Chen et al., 2013; Sartori et al., 2013; Courtney et al., 2006; Fujimoto et al., 2007a,b; Guan et al., 2002, 2005, 2006, 2007, 2008; Nelson et al., 2011; Stankus et al., 2004, 2006). With the aim of fabricating suitable PUR scaffolds for cardiac TERM application, several conventional (e.g., salt leaching, electrospinning, phase separation) and advanced fabrication techniques (i.e., rapid prototyping) have been explored (Silvestri et al., 2013; Boffito et al., 2014). Indeed PURs show wide versatility in terms of available techniques that can be exploited to process them into porous scaffolds, thanks to their high thermal stability (Chiono et al., 2014) and solubility in a wide spectrum of solvents, for example, tetrahydrofuran, dimethylformamide, dimethylsiloxane, and hexafluoroisopropanol.

13.4.1 Biodegradable and biomimetic polyurethanes and polyurethane-based scaffolds for cardiac tissue engineering/regenerative medicine application

Polyester-based PURs have been widely investigated in the field of cardiac tissue engineering/regenerative medicine due to their biocompatibility (Jawad et al., 2007, 2008; Rechichi et al., 2008; Sartori et al., 2013; Guan et al., 2002, 2005; Guan and Wagner, 2005) and elastomeric mechanical properties (Guan et al., 2002; Sartori et al., 2013). Polycaprolactone (PCL)-based PURs have been thoroughly explored for the design of innovative cardiac patches by the Ciardelli and Wagner groups. Guan et al. successfully synthesized PCL-based elastomeric PURs for cardiac TERM applications containing putrescine or the enzyme target alanine–alanine (AA) peptide sequence as chain extenders, with the final aim of modulating the degradation kinetics of the resulting scaffold (elastase-mediated degradation was more pronounced in AA-sequence containing PUR with respect to the putrescine-based one) (Guan et al., 2008; Fujimoto et al., 2007a,b; Guan et al., 2002, 2007). The latter was used by Guan et al. (2008) to produce random and oriented scaffolds by thermally induced phase separation (TIPS). Oriented scaffolds better supported muscle-derived stem cell growth probably because of their less tortuous structure, which facilitates oxygen and nutrient diffusion and makes cell seeding more efficient. Scaffold subcutaneous implantation in rats demonstrated their cytocompatibility (absence of infections during the postoperative period and at the time of explant) and degradability (a substantial portion of the scaffold was degraded after 8 weeks) and showed their progressive colonization by cells. Fujimoto et al. produced similar scaffolds starting from a PUR synthesized by using putrescine as chain extender (Fujimoto et al., 2007a,b; Guan et al., 2002). *In vitro* cell tests demonstrated cell adhesion, migration, and proliferation inside the scaffolds, while *in vivo* tests carried out using a cell-free scaffold sutured on a rat infarcted myocardium showed a complete integration of the patch in the host tissue, 8 weeks after implantation (Fujimoto et al., 2007a,b; Guan et al., 2002, 2005). In addition, on week 8 after surgery, the patch was largely degraded and the left ventricular wall was thicker than that of untreated animals. Moreover, scaffold-treated animals showed higher capillary density and overexpressed both transcription factors connected to the cardiac phenotype (Nkx2.5 and GATA4) and growth factors related to angiogenesis (vascular endothelial and basic fibroblast growth factors (VEGF and bFGF)) (Fujimoto et al., 2007a,b, 2012). Hashizume et al. (2013a) have recently tested these scaffolds in a porcine model, reporting an attenuation in LV remodeling and functional deterioration, accompanied by increased vascularization, thus confirming the results previously obtained in a rodent ischemic cardiomyopathy model (Fujimoto et al., 2007a,b, 2012). To further stimulate angiogenesis, laser-induced forward-transfer (LIFT) cell printing was implemented on the PUR-based scaffolds, produced by a thermally induced phase separation technique and previously characterized by Guan et al. (2002, 2005). Cellularized scaffolds were produced by printing human vein endothelial cells (HUVECs) and human mesenchymal stem cells (hMSCs) according to a predefined pattern (HUVEC were printed according to an orthogonal grid, while hMSCs were printed as squares between HUVEC lines) (Gaebel

et al., 2011). The cell printing pattern was conveniently designed to mimic native tissue vasculature; as a matter of fact, LIFT-cellularized scaffolds, unlike randomly seeded ones, induced angiogenesis and new blood vessel formation in infarcted rat models. In addition, as a consequence of the improved angiogenesis, a complete functional integration of LIFT-cellularized patches in the host myocardium was observed.

In 2013 and 2014 two works were published that highlighted the significant effects of chain extender selection on PUR physicochemical properties (Sartori et al., 2013; Silvestri et al., 2014). In addition, a correlation between PUR surface organization and biological response was suggested: better myoblast adhesion, proliferation, and organization were observed for PURs showing a less ordered surface structure. Cell tests with C_2C_{12} myoblasts together with PUR mechanical characterization allowed the selection of a PCL-based PUR containing lysine ethyl ester as chain extender for the production of scaffolds for the repair of soft contractile tissues, such as the myocardium. This PUR showed mechanical properties closest to those required for contractile tissue repair (low elastic modulus and high strain at break) and the best results in terms of C_2C_{12} myoblast adhesion and spreading. The selected PCL-based PUR was used for the fabrication of TIPS scaffolds showing long and stretched pores along a preferred direction that make them able to mimic the typical striated myocardial tissue anisotropy (Silvestri et al., 2014). Preliminary cell tests with H9C2 rat heart cells revealed the capability of the proposed substrates to support cell adhesion and proliferation. In addition, TIPS-produced anisotropic scaffolds were characterized by atomic force microscopy, showing the presence of a well-organized structure at the nanoscale (highly oriented fibrils were observed in the direction of the applied cooling gradient during TIPS) (Boffito et al., 2015). In this work it was demonstrated that the application of a cooling gradient during the TIPS procedure allows the fabrication of anisotropic scaffolds at both the micro- (aligned pores) and the nanoscale (aligned fibrils) (Figure 13.4). This two-scale structure is expected to have positive effects on cell alignment, morphology, and cytoskeletal organization.

| Optical microscope | Scanning electron microscopy | Atomic force microscopy |

1000 µm   200 µm   100 µm   0.5 µm
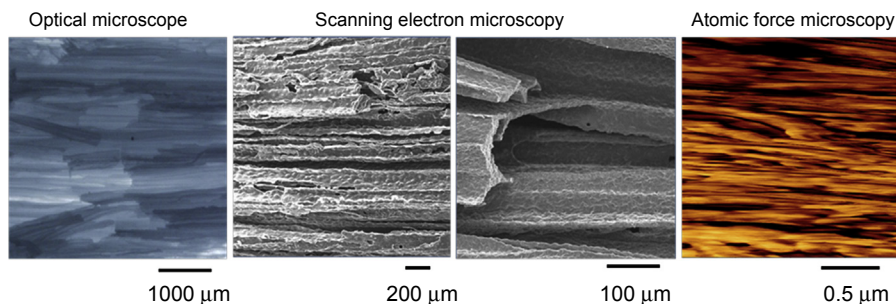
Figure 13.4 Optical, scanning electron and atomic force micrographs of a PUR-based anisotropic scaffold produced through TIPS under application of a thermal cooling gradient. Cooling gradient application allows the fabrication of anisotropic scaffolds at both the micro (aligned pores) and the nanoscale (aligned fibrils).
Adapted with permission from Boffito et al. (2015). Copyright 2015, Wiley Periodicals.

With the final aim of tuning PUR physicochemical properties, the addition of poly-ethylene glycol (PEG) as macrodiol was investigated (Silvestri et al., 2014). The addition of 10% or 20% w/w of PEG to PCL–diol during prepolymer synthesis resulted in the modulation of PUR thermal and mechanical properties (decrease in crystallization, melting temperature, and elastic modulus and increase in the maximum strain and stress with increasing PEG content). PEG introduction in the polymeric chains also has significant effects on PUR degradation kinetics with an increased degradation rate in PCL–PEG-containing PURs with respect to PCL-based PUR, as reported by Skarja and Woodhouse (Skarja and Woodhouse, 1998).

Hashizume et al. (2013b) have recently tried to answer an unresolved question: how long should a cardiac patch remain in place. They compared the efficacy of 3D salt-leached scaffolds produced according to the same protocol using three different PURs, PEUU (PCL-based PUR), PCUU (poly(hexamethylene carbonate) (PHC)-based PUR), and a poly(ester carbonate urethane)urea (PECUU) (PUR based on a blend of PCL and PHC 50/50 molar ratio). Previously, Hong et al. (2010) showed that PHC introduction in the backbone of a PCL-based PUR makes the resulting polymer softer and more distensible, with degradation slower than PCL-based PURs and faster than PHC-based PURs. *In vivo* tests carried out by Hashizume et al. (2013b) showed that a moderately slow degrading cardiac patch, such as that made from PECUU, ameliorates rat functional outcomes (PECUU-treated rats showed greater vascular density and enhanced LV contractility and end diastolic performance).

Electrospun PUR-based matrices have been produced and characterized by several groups (Rockwood et al., 2008; Fromstein et al., 2008; Parrag et al., 2012; Guan et al., 2011). Rockwood et al. electrospun random and aligned fibrous scaffolds starting from a poly(ester urethane) synthesized from PCL–diol, 2,6-diisocyanate methylcaproate, and a chain extender based on 1-phenylalanine (Rockwood et al., 2008). Similar to other studies comparing isotropic and anisotropic scaffolds (Kai et al., 2011a), Rockwood et al. reported an improved cardiac cell adhesion and orientation in aligned fibrous scaffolds. The same PUR was used by Fromstein and colleagues to produce scaffolds by either TIPS or electrospinning (Fromstein et al., 2008). Embryonic stem cell–derived cardiomyocytes showed a different morphology and viability on the two produced substrates probably because of their different thickness (1 mm and 70 μm for TIPS and electrospun matrices, respectively) that strongly influences fluid and nutrient uptake: a better cell spreading and colonization were observed on electrospun matrices with respect to the TIPS scaffolds. Irrespective of the substrate, all cells over-expressed sarcomeric myosin and connexin-43 and spontaneously contracted, proving that scaffold structure has more significant effects on cell morphology than on their functionality. The influence of scaffold architecture on cell behavior was also studied by Parrag et al. (2012) using PUR-based electrospun matrices with aligned or random fibers. Murine embryonic stem cell–derived cardiomyocytes (mESCDCs) cultured on anisotropic matrices showed a higher cell organization (well-organized sarcomeric structures) compared to the randomly oriented fibrous scaffolds. The cells aligned parallel to the fiber direction and expressed end-to-end gap junctions (Figure 13.5).

In 2006, Stankus et al. (2006) proposed an innovative technology for the fabrication of cellularized grafts, by combining polymer electrospinning with concurrent cell
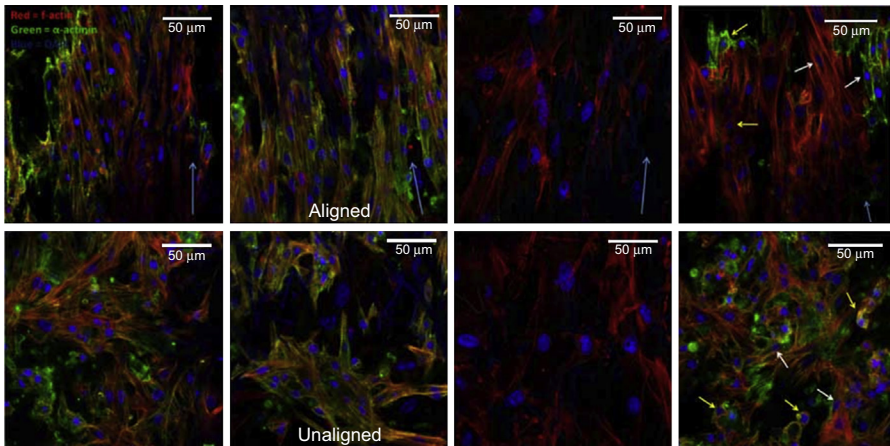
Figure 13.5 Cell organization on electrospun aligned (top) and unaligned (bottom) scaffolds produced starting from a PUR based on PCL–diol, 2,6-diisocyanate methylcaproate, and a chain extender based on 1-phenylalanine, 6 days post-mESCDC seeding. Red, cytoskeleton (F-actin); green, sarcomere (α-actinin); blue, cell nuclei (DAPI); blue arrows indicate fiber orientation. PUR scaffolds showed cells with varying levels of differentiation, but an increase in the number of rod-shaped cells with striated sarcomeric patterns was observed with fiber alignment. Yellow arrows represent round mESCDCs with poorly defined sarcomeric structures, while white arrows represent rod-shaped mESCDCs with well-defined and organized sarcomeres. Scale bars represent 50 μm.

Adapted with permission from Parrag et al. (2012). Copyright 2012, Wiley Periodicals.

electrospray. This setup, first used to produce smooth muscle cell–seeded PUR matrices, has been recently employed to fabricate mesenchymal stem cell (MSC)-embedded scaffolds. The scaffolds were fabricated from a PECUU based on a multiblock copolymer PTMC–PEO–PPO–PEO–PTMC diol (PEO, poly(ethylene oxide); PPO, poly(propylene oxide); PTMC, poly(trimethyl carbonate)), 1,4-butandiisocyanate, and putrescine (Guan et al., 2011). Electrospray did not have negative effects on MSC viability, proliferation, and stemness. In addition, the scaffolds showed anisotropic properties and the encapsulated cells were uniformly distributed within the scaffold wall. Dynamic cell culture was applied to induce cell alignment in the direction of PECUU fibers. Both in the presence and in the absence of mechanical cues, the cultured cells upregulated several cardiac transcription factors (MEF-2C, Nkx2.5, GATA4); however, a more pronounced upregulation was observed in the scaffolds subjected to mechanical stimulation.

Senel-Ayaz et al. (2014) have recently combined electrospinning and textile-manufacturing technologies with the final aim of producing anisotropic cardiac patches. Briefly, knitted conventional textiles made of cotton or polyester yarns were employed as templates to produce electrospun anisotropic matrices made from a commercial PCU (Bionate®) (Figure 13.6). Although the authors selected Bionate®, a biostable PUR, as an example to provide a proof of concept of the feasibility of the method and plan to apply it to degradable PURs, the produced porous matrices showed suitable mechanical properties for cardiac TERM application and were tested,
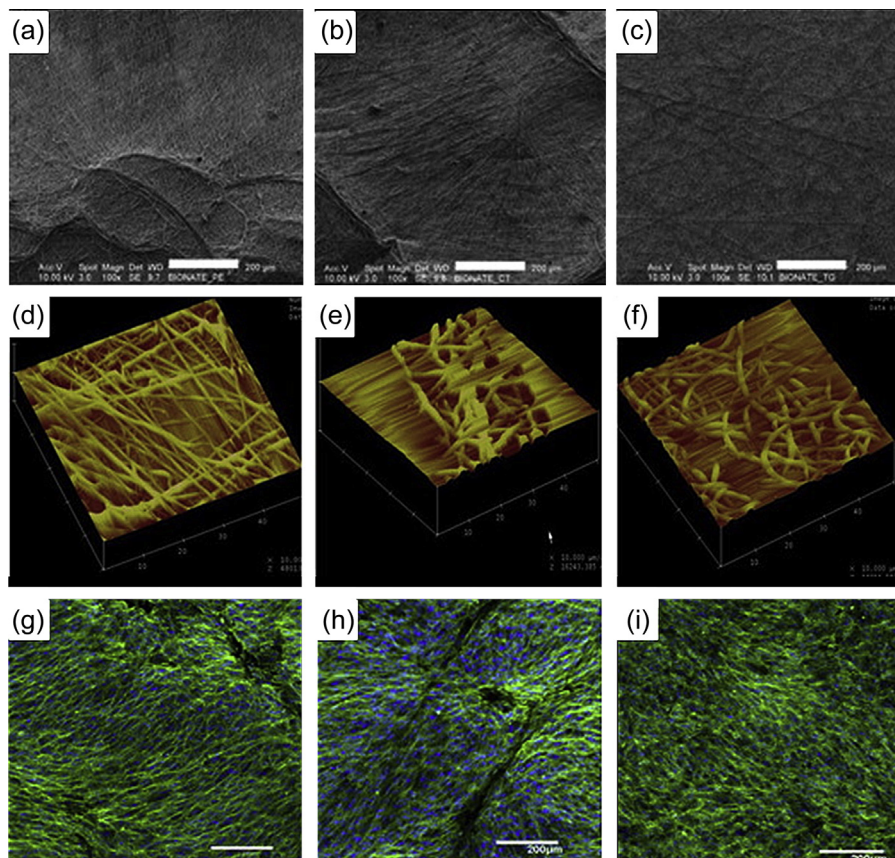
Figure 13.6 Scanning electron micrographs (a–c) and atomic force microscopic (AFM) images (d–f) showing the morphology of Bionate scaffolds electrospun on polyester template (a) and (d), cotton template (b) and (e), or flat aluminum target (c) and (f). Confocal micrographs (g–i) of Bionate scaffolds seeded with H9C2 cardiomyocytes: (g) Bionate scaffolds electrospun on polyester template, (h) Bionate scaffolds electrospun on cotton template, (i) Bionate scaffolds electrospun on flat aluminum target. Scale bar: 200 μm. Size of scanning area in AFM images: 50×50 μm. Adapted with permission from Senel-Ayaz et al. (2014). Copyright 2014, Elsevier.

in vitro, with H9C2 cardiac cells. Scaffold structural and mechanical characterization revealed that the patches were characterized by anisotropic properties at the microscale (no mechanical anisotropy was observed at the macroscale). Nevertheless, cell tests demonstrated that local anisotropy is sufficient to exert significant effects on cardiac cell behavior: cells were able to detect the local anisotropy, rearranged themselves accordingly, and exhibited synchronous spontaneous beating.

Despite the encouraging results obtained by testing *in vitro* and *in vivo* of conventionally produced cardiac patches, there is an increasing interest in scaffold production via rapid prototyping technologies that allow a more precise control over scaffold properties, e.g. scaffold shape and dimensions, pore size, geometry, and

interconnectivity (Silvestri et al., 2013; Boffito et al., 2014). Recently it has been demonstrated that a PCL-based PUR can be melt-processed avoiding PUR thermal degradation during scaffold fabrication (processing temperature was defined by rheological characterization, differential scanning calorimetry, and thermogravimetric analysis) (Chiono et al., 2014). Bilayered scaffolds with a 0°/90° lay-down pattern were successfully produced, with an optimal reproduction of computer-aided design geometry (Figure 13.7). In addition, preliminary cell tests carried out with human cardiac progenitor cells demonstrated that the scaffolds support cell adhesion and spreading; however, further surface functionalization with bioactive peptides/proteins seems to be essential for properly directing cell behavior.

From 2005 to 2015, several research groups have focused their attention on conductive polymers, such as polyaniline and polypyrrole, with the final aim of developing scaffolds showing electrical properties that make them able to direct cell adhesion, migration, proliferation, and differentiation (Li et al., 2006; Pedrotty et al., 2005; Kai et al., 2011b; Fernandes et al., 2010). In 2011, Broda et al. *in situ* polymerized pyrrole within a PUR emulsion mixture to obtain a composite polymer with a PUR-based matrix incorporating an electrically percolating network of polypyrrole (PPy) nanoparticles. As expected, PPy content influenced composite properties in terms of conductivity and mechanical properties (conductivity and stiffness increase, while strain at break decreases with increasing PPy content). In addition, cytotoxicity tests reported the cytocompatibility of the designed composites by supporting C_2C_{12} myoblast proliferation and differentiation with respect to pure PUR samples. Cell-to-cell interactions provided by the composite substrates were also observed. Baheiraei et al. (2014) have recently synthesized a novel biodegradable electroactive PCL/PEG-based PUR containing aniline pentamer moieties. This PUR blended at equal weight ratio with PCL to improve biocompatibility showed a cytocompatibility comparable to that of the positive control (tissue culture plates) and appropriate mechanical properties (elastic modulus of 10 MPa) for the design of scaffolds for cardiac TERM applications. Finally, this innovative PUR showed antioxidant properties that makes it a promising material for the fabrication of scaffolds that aim at healing tissues suffering high oxidative stress, such as infarcted myocardial tissue. Another approach to
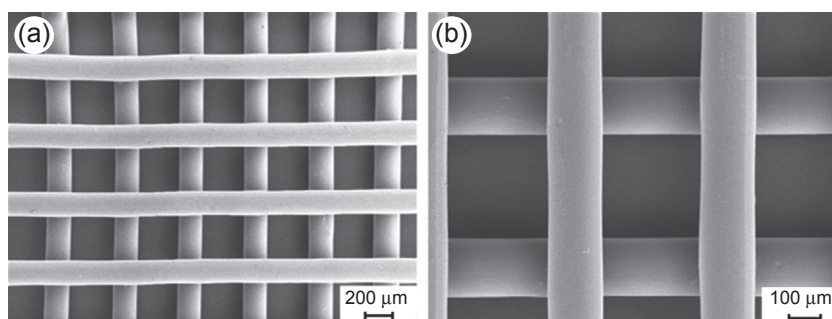
Figure 13.7 (a) Scanning electron micrograph of a PUR scaffold obtained by melt-extrusion additive manufacturing; (b) higher magnification detail of the trabecular arrangement. Reprinted with permission from Chiono et al. (2014). Copyright 2014, The Royal Society.

the design of conductive scaffolds consists in blending a polymer with gold nanowires or carbon nanotubes (CNTs) (Dvir et al., 2011; Stout et al., 2011; Mackle et al., 2011; Crowder et al., 2013; Sirivisoot and Harrison, 2011; Kharaziha et al., 2014). Sirivisoot and Harrison (2011) tested electrospun CNT/PUR scaffolds as supports for muscle cell adhesion, proliferation, and differentiation, reporting an increased myotube formation in electrically stimulated composite scaffolds compared to PUR alone. Crowder et al. (2013) reported that hMSCs cultured on three-dimensional PCL–CNT electrospun substrates tend to assume an elongated spindle shape morphology, associated with overexpression of actin and α-myosin heavy chains, suggesting their early differentiation toward a cardiac phenotype. Similarly, Wickham et al. (2014) reported an enhanced cardiac progenitor cell (CPC) proliferation on thiophene-conjugated CNT/PCL electrospun matrices; however, thiophene-conjugated CNT incorporation had no effects on CPC differentiation. Martinelli et al. (2013) have recently reviewed the effects of CNT incorporation in polymeric scaffolds on cardiomyocyte growth, pointing out their capability for improving cardiac myocyte proliferation, maturation, and electrical coupling.

A very interesting strategy for improving PUR biocompatibility and making them biomimetic consists in blending them with natural polymers (Guan et al., 2006; Chen et al., 2015). Wagner's group produced composite scaffolds starting from a blend of a PCL-based PUR with collagen type I, showing an interconnected porous structure, high strain at break (up to 440%) and tensile strength in the range 0.97–4.11 MPa, and tuned degradation kinetics (they can degrade by both hydrolysis and collagenase degradation) (Guan et al., 2006; Stankus et al., 2004). In addition, collagen incorporation resulted in improved cell behavior (higher cell numbers on scaffolds containing collagen compared to PUR-based ones). Chen and colleagues have recently fabricated aligned and randomly oriented electrospun PUR/ethyl cellulose fibrous matrices with uniform fiber diameters. The scaffolds showed an interconnected structure and suitable mechanical properties (ultrathin scaffolds—thickness of about tens-hundreds of micrometers—are expected to have a Young modulus in the required range and elastomeric mechanical properties) to withstand cyclic stresses and support contractile cardiac tissue (Chen et al., 2015). Soldani and Briganti have recently produced biocompatible composite scaffolds starting from a poly(ether)urethane–polydimethylsiloxane and fibrin (PEtU–PDMS/fibrin) by combining phase separation with material deposition via a spray machine (Briganti et al., 2006; Losi et al., 2010; Soldani et al., 2004; Soldani and Briganti, 2012). These substrates provided a more cell-friendly environment with respect to traditional cell culture plates: human amniotic mesenchymal stromal cells showed higher proliferation and metabolic activity on the newly developed substrates compared to petri dishes (Lisi et al., 2012). Finally, another way to make PUR biomimetic consists in coating them with proteins or peptide sequences (surface functionalization). Guan et al. (2005) covalently bound the adhesion motif arginine–glycine–aspartic acid–serine to plasma-modified biodegradable PUR films and showed an increased endothelial cell adhesion on functionalized samples with respect to control surfaces and tissue culture polystyrene plates. McDevitt et al. (2003) investigated the effects of PUR coating and patterning on cardiomyocyte behavior. They microcontact-printed lines of laminin

on PUR films, demonstrating their capability of guiding cardiomyocyte alignment in highly organized arrays. Siepe et al. (2007) developed myoblast-seeded Artelon porous scaffolds and studied the effects of scaffold coating with different proteins (laminin, fibronectin, and human immunoglobulin) on myoblast behavior. Precoating with laminin showed the most enhanced cell adhesion. Four weeks after implantation on rat infarcted hearts, myoblasts completely colonized the scaffolds and no differentiation was observed. The superiority of laminin coating was also reported by Alperin et al. (2005) who cultured embryonic stem cell–derived cardiomyocytes on PUR films coated with gelatin, laminin, or collagen type IV.

Finally, regarding diisocyanate selection, broad attention has been directed to aliphatic diisocyanates, for example, 1,4-butane diisocyanate (BDI), HDI, and 2,6-diisocyanate methyl caproate (LDI), due to the biocompatibility of their degradation products (as an example, BDI hydrolysis produces putrescine that is commonly present in the body and is essential for cell growth and differentiation (Skarja and Woodhouse, 2000; Cooke et al., 2003)). However, aromatic diisocyanate-based PURs have also been investigated for cardiac TERM applications. Siepe et al. (2007) used the PUR Artelon® (Artimplant, AB, Västra Frölunda, Sweden), a PCL-based PUR synthesized from 1,3-diaminopropane and 4,4′-diphenylmethane diisocyanate, for the fabrication of cellularized patches for cardiac TERM.

13.4.2 Cardiac tissue engineering/regenerative medicine: future trends

Several research groups have recently reported encouraging results from *in vitro* and *in vivo* testing of PUR-based cardiac patches. This success must be ascribed to the great versatility of PURs in terms of their physicochemical, mechanical, and degradation properties. Moreover, they can be easily processed in the form of 3D porous scaffolds to be employed as cardiac patches in the treatment of heart infarcted patients. However, considerable effort is still required to identify the ideal cardiac patch, that is, one which provides mechanical support for the regenerative process, properly directs cell orientation, and degrade as the need for structural support decreases due to new tissue formation. PCL-based PUR scaffolds have been investigated for years and their suitability for cardiac repair has been proven in several animal models. The pioneering work by Hashizume et al. (2013b) has recently resulted in a new generation of cardiac patches with improved performance due to the fine modulation of the mechanical and degradation properties deriving from the introduction of PHC in the PUR backbone. Several studies of scaffold architecture have highlighted the importance of accurately reproducing the characteristic anisotropy of the myocardium. A comparison between random and aligned scaffolds produced with the same PUR and technology has revealed the superiority of the latter in terms of cell viability, organization, and differentiation toward the cardiac phenotype (Guan et al., 2011). In this context, rapid prototyping technologies are gaining increasing interest thanks to the possibility of precisely controlling the properties and architecture of the resulting scaffolds, an issue that is inadequately addressed by conventional scaffold fabrication techniques. Finally, in response to the increasing interest in conductive scaffolds and

with the final aim of overcoming drawbacks related to conductive polymer biostability, PURs have been modified to introduce aniline pentamer moieties in the polymer backbone, thus successfully synthesizing a biodegradable conductive antioxidant PUR (Baheiraei et al., 2014). The results summarized in this chapter prove that PURs may serve as materials for the design of the optimal cardiac patch, one exhibiting structural, functional, and mechanical biomimicry of the native cardiac tissue. Once the ideal cardiac patch has been designed, its *in vitro* and *in vivo* characterization must be properly defined to allow its validation under conditions mimicking its real working environment. Since cardiac patches will be subjected to cyclic stresses after implantation, a mechanical characterization under dynamic conditions mimicking cardiac cycle is also essential to validate them (fatigue tests should be performed on millions of cycles at a proper frequency and strain to mimic myocardium working conditions).

13.5   Polyurethane devices for drug delivery in cardiovascular applications

Due to the high versatility of their chemical structure (which allows the modulation of their physicochemical properties and degradation kinetics by simply varying the building blocks), biodegradable and biostable PURs have been proposed for drug delivery devices (Sartori et al., 2014; Cherng et al., 2013).

In the case of biostable PURs, that is, materials that remain stable under physiological conditions, drug delivery is mainly controlled by drug diffusion from the material structure. In contrast, for biodegradable PURs the release rate of pharmacologically active molecules is mostly governed by the degradation rate of the polymer, which in turn depends on several different parameters (Storey and Hickey, 1994).

Several authors have studied the dependence of the degradation rate on the composition and molecular weight of the macrodiol, the crystallinity of the polymer, and the presence of enzymatically cleavable sequences.

It has been shown that PURs with hydrophilic soft segments are more susceptible to hydrolytic degradation due to facilitated water uptake. Moreover, more crystalline polymers and polymers prepared with higher molecular weight biostable macrodiols have lower degradation rates (Cherng et al., 2013).

PUR-based drug delivery systems have been fabricated in different forms, such as scaffolds, fibers, micro- and nanoparticles, membranes, and foams (Mattu et al., 2013). PURs can be designed to be thermoresponsive and pH-responsive and to carry positive charges or pendant functional groups, which can be exploited to establish physical and/or chemical interactions with several different drugs (Kucinska-Lipka et al., 2015; Sartori et al., 2014).

Hafeman et al. (2010) obtained a PUR network using hexamethylene diisocyanate trimer and a polyester-ether-based macrodiol containing poly(ε-caprolactone), glycolyde, and D,L-lactide. Their system was able to sustain the release of tobramycin over an extended period of time (up to 2 weeks) with a burst release ranging from 45% to 95%, depending on the glycolide content in the macrodiol.

Moura et al. (2011) prepared dexamethasone-loaded PUR matrices and reported a linear release profile, associated with drug diffusion and matrix degradation, in both *in vitro* and *in vivo* experiments.

Recently, we reported the preparation of polyester urethane nanoparticles for the release of the anticancer drug paclitaxel. The study showed the ability of PURs to encapsulate hydrophobic drugs and to extend the release period compared to commercial polyester nanoparticles (Mattu et al., 2012).

Mishra et al. (2014) reported the release of dexamethasone from blood-compatible PURs and PUR–clay nanocomposites. They showed that PUR and PUR nanocomposite films did not induce platelet damage or aggregation in *in vitro* tests, thus displaying excellent blood compatibility. They were able to sustain dexamethasone release for up to 2 weeks depending on the polymer composition. PUR/clay nanocomposites possessed a slower release rate compared to pure PURs and were able to minimize the burst effect in the first hours of release.

Sivak et al. (2008a,b) developed drug-containing PURs, to where the drug was chemically linked to the polymer chains. Two different anticancer drugs, doxorubicin and hydroxyl-camptothecin, were covalently incorporated in the polymer backbone. These authors showed a very slow release of less than 0.1% over a tested period of 70 days, indicating that a stable linkage between the drug and the PUR backbone was established.

All these studies highlight the possibility of using PURs as drug delivery systems with the potential of a modulated release profile obtained by properly tuning material composition. PURs, as discussed in the previous sections of this chapter, also display excellent mechanical and blood compatibility properties, suggesting their use for implanted drug release devices.

Despite the great potential of PURs in both cardiovascular and drug delivery applications, the combination of a PUR-based cardiovascular device that also can release a drug delivery deserved more attention.

In 1988 Robert Levy developed a PUR-based drug release system for the controlled release of lidocaine to normalize the cardiac rhythm (Sintov et al., 1988). They used a commercial poly(ether urethane) (Tecoflex) and traditional casting or compression molding techniques. Lidocaine release was dependent on the technique used to prepare the matrix, that is, films prepared by solvent casting showed faster release with 40% of the loaded drug released in nearly 20 min. Rapid-release matrices were successful in quickly resolving ventricular tachycardia in dogs.

Briganti et al. (2010) developed a PEtU–PDMS/fibroin composite scaffold by a spray, phase-inversion technique. The composite served as a delivery vehicle for pro-angiogenic factors for application in cardiac tissue engineering. They investigated the release of both VEGF and bFGF, at varying fibroin concentrations in the scaffold composition. Their results indicate that mixed PUR/fibroin scaffolds were able to sustain the release of growth factors for 14 days, with about 50% of protein release in the first 4 days. The initial fibroin concentration slightly affected growth factor release. Scaffolds obtained with higher concentration showed a slower release, reaching about 30% and 40% of VEGF and bFGF release, respectively, at day 4. Moreover the composite, drug-loaded scaffolds retained their excellent mechanical and biological properties and did not alter the integrity of the entrapped protein.

Similarly, Guan et al. (2007) developed an elastomeric poly(ester urethane)–urea scaffold by a thermally induced phase separation method for the release of bFGF. The scaffold maintained bFGF bioactivity over a period of 21 days and showed a two-phase protein release pattern, characterized by a fast initial release of about 30% in the first 2 days, followed by a slow release over a period of 4 weeks.

Recently, Han et al. (2013) prepared PUR nanofibers loaded with rapamycin by electrospinning and incorporated them into a vascular graft. Their system was able to sustain the release of rapamycin over a long period of at least 77 days and showed effective local suppression of smooth muscle cell proliferation.

13.5.1 Drug release in cardiovascular applications: conclusions and future trends

Recent studies suggest that PURs may be excellent candidates for the preparation of drug eluting cardiovascular devices, due to the combination of good mechanical and biological properties with the possibility of a wide modulation of the drug release profile according to the therapeutic need. Despite these encouraging results there is still ample space for investigation and optimization of PUR-based drug delivery devices for cardiovascular applications. The excellent properties and versatility of these polymers warrant their further investigation.

13.6 General conclusions

In the last decades, PURs have emerged as promising materials for the replacement of damaged heart tissue or valves, providing an adequate mechanical and structural support and eventually stimulating a reparative process (Silvestri et al., 2013; Boffito et al., 2014; Kütting et al., 2011). PURs are extensively used as blood-contacting biomaterials due to their relatively good blood- and biocompatibility.

The latest advances in polymer science have led to the design of PURs with improved long-term biostability, compared to PEU and PEUU used in the first generation heart valves (Ghanbari et al., 2010; Kidane et al., 2009b; Bezuidenhout et al., 2015). The availability of these materials has rekindled interest in the use of these polymers for such applications.

PURs with appropriate composition, surface properties, degradation kinetics, and biocompatibility have been widely investigated in cardiac tissue regeneration (Silvestri et al., 2013; Boffito et al., 2014). Due to their elastomeric mechanical properties and tunable degradability, PURs, especially polyester-based ones, have been thoroughly studied for the design of cardiac patches (Rockwood et al., 2008; Fromstein et al., 2008; Parrag et al., 2012; Guan et al., 2011; Chiono et al., 2014; Stankus et al., 2006; Boffito et al., 2015; Silvestri et al., 2014; Sartori et al., 2013; Fujimoto et al., 2007a,b, 2012; Guan et al., 2005). In addition, the possibility of conferring biomimetic properties through bulk or surface functionalization has further increased the interest for cardiac TERM and heart valve replacement.

Recently, PURs have been proposed for a combined regenerative and pharmacological treatment in tissue engineering with promising results (Sartori et al., 2014; Cherng et al., 2013). Several authors have shown that pharmacologically active molecules can be either physically entrapped or chemically conjugated to the polymer backbone, allowing a fine modulation of the drug release kinetics (Sintov et al., 1988; Briganti et al., 2010; Guan et al., 2007; Han et al., 2013).

In conclusion, PURs are effective raw materials for the design of successful therapeutic devices for patients suffering heart valve disease or myocardial infarction. However, efforts are still needed to bring PUR-based therapeutic devices to clinical application. More controlled and automated manufacturing processes and detailed and controlled *in vitro* and *in vivo* characterizations are essential to finally gain PUR-based cardiac patches and heart valves approved as medical devices.

References

Alperin, C., Zandstra, P.W., Woodhouse, K.A., 2005. Polyurethane films seeded with embryonic stem cell-derived cardiomyocytes for use in cardiac tissue engineering applications. Biomaterials 26, 7377–7386.

Alves, P., Cardoso, R., Correia, T.R., Antunes, B.P., Correia, I.J., Ferreira, P., 2014. Surface modification of polyurethane films by plasma and ultraviolet light to improve haemocompatibility for artificial heart valves. Colloids and Surfaces B: Biointerfaces 113, 25–32.

Baheiraei, N., Yeganeh, H., Ai, J., Gharibi, R., Azami, M., Faghihi, F., 2014. Synthesis, characterization and antioxidant activity of a novel electroactive and biodegradable polyurethane for cardiac tissue engineering application. Materials Science and Engineering: C 44, 24–37.

Baig, M.K., Mahon, N., Mckenna, W.J., Caforio, A.L.P., Bonow, R.O., Francis, G.S., Gheorghiade, M., 1998. The pathophysiology of advanced heart failure. American Heart Journal 135, S216–S230.

Bernacca, G.M., Mackay, T.G., Wheatley, D.J., 1992. In vitro calcification of bioprosthetic heart valves: report of a novel method and review of the biochemical factors involved. Journal of Heart Valve Disease 1, 115–130.

Bernacca, G.M., Mackay, T.G., Wilkinson, R., Wheatley, D.J., 1995. Calcification and fatigue failure in a polyurethane heart valve. Biomaterials 16, 279–285.

Bernacca, G.M., Mackay, T.G., Wheatley, D.J., 1996. In vitro function and durability of a polyurethane heart valve: material considerations. Journal of Heart Valve Disease 5, 538–542.

Bernacca, G.M., Mackay, T.G., Gulbransen, M.J., Donn, A.W., Wheatley, D.J., 1997a. Polyurethane heart valve durability: effects of leaflet thickness and material. International Journal of Artificial Organs 20, 327–331.

Bernacca, G.M., Mackay, T.G., Wilkinson, R., Wheatley, D.J., 1997b. Polyurethane heart valves: fatigue failure, calcification, and polyurethane structure. Journal of Biomedical Materials Research 34, 371–379.

Bezuidenhout, D., Williams, D.F., Zilla, P., 2015. Polymeric heart valves for surgical implantation, catheter-based technologies and heart assist devices. Biomaterials 36, 6–25.

Boffito, M., Sartori, S., Ciardelli, G., 2014. Polymeric scaffolds for cardiac tissue engineering: requirements and fabrication technologies. Polymer International 63, 2–11.

Boffito, M., Bernardi, E., Sartori, S., Ciardelli, G., Sassi, M.P., 2015. A mechanical characterization of polymer scaffolds and films at the macroscale and nanoscale. Journal of Biomedical Materials Research Part A 103, 162–169.

Briganti, E., Losi, P., Raffi, A., Scoccianti, M., Munao, A., Soldani, G., 2006. Silicone based polyurethane materials: a promising biocompatible elastomeric formulation for cardiovascular applications. Journal of Materials Science: Materials in Medicine 17, 259–266.

Briganti, E., Spiller, D., Mirtelli, C., Kull, S., Counoupas, C., Losi, P., Senesi, S., Di Stefano, R., Soldani, G., 2010. A composite fibrin-based scaffold for controlled delivery of bioactive pro-angiogenetic growth factors. Journal of Control Release 142, 14–21.

Broda, C.R., Lee, J.Y., Sirivisoot, S., Schmidt, C.E., Harrison, B.S., 2011. A chemically polymerized electrically conducting composite of polypyrrole nanoparticles and polyurethane for tissue engineering. Journal of Biomedical Material Research Part A 98, 509–516.

Bursac, N., Loo, Y., Leong, K., Tung, L., 2007. Novel anisotropic engineered cardiac tissues: studies of electrical propagation. Biochemical and Biophysical Research Communications 361, 847–853.

Chen, Q.Z., Harding, S.E., Ali, N.N., Lyon, A.R., Boccaccini, A.R., 2008a. Biomaterials in cardiac tissue engineering: ten years of research survey. Materials Science and Engineering Reports 59, 1–37.

Chen, Q.Z., Bismarck, A., Hansen, U., Junaid, S., Tran, M.Q., Harding, S.E., Ali, N.N., Boccaccini, A.R., 2008b. Characterisation of a soft elastomer poly(glycerol sebacate) designed to match the mechanical properties of myocardial tissue. Biomaterials 29, 47–57.

Chen, Q., Liang, S., Thouas, G.A., 2013. Elastomeric biomaterials for tissue engineering. Progress in Polymer Science 38, 584–671.

Chen, P.H., Liao, H.C., Hsu, S.H., Chen, R.S., Wu, M.C., Yang, Y.F., Wu, C.C., Chen, M.H., Su, W.F., 2015. A novel polyurethane/cellulose fibrous scaffold for cardiac tissue engineering. RSC Advances 5, 6932–6939.

Cherng, J.Y., Hou, T.Y., Shih, M.F., Talsma, H., Hennink, W.E., 2013. Polyurethane-based drug delivery systems. International Journal of Pharmaceutics 450, 145–162.

Chiono, V., Mozetic, P., Boffito, M., Sartori, S., Gioffredi, E., Silvestri, A., Rainer, A., Giannitelli, S.M., Trombetta, M., Nurzynska, D., Di Meglio, F., Castaldo, C., Miraglia, R., Montagnani, S., Ciardelli, G., 2014. Polyurethane-based scaffolds for myocardial tissue engineering. Interface Focus 4 20130045.

Christenson, E.M., Anderson, J.M., Hiltner, A., 2004a. Oxidative mechanisms of poly(carbonate urethane) and poly(ether urethane) biodegradation: in vivo and in vitro correlations. Journal of Biomedical Material Research Part A 70, 245–255.

Christenson, E.M., Dadsetan, M., Wiggins, M., Anderson, J.M., Hiltner, A., 2004b. Poly (carbonate urethane) and poly(ether urethane) biodegradation: in vivo studies. Journal of Biomedical Material Research Part A 69, 407–416.

Cohen, S., Leor, J., 2004. Rebuilding broken hearts. Biologists and engineers working together in the fledgling field of tissue engineering are within reach of one of their greatest goals: constructing a living human heart patch. Scientific American 291, 44–51.

Cooke, M., Leeves, N., White, C., 2003. Time profile of putrescine, cadaverine, indole and skatole in human saliva. Archives of Oral Biology 48, 323–327.

Courtney, T., Sacks, M.S., Stankus, J., Guan, J., Wagner, W.R., 2006. Design and analysis of tissue engineering scaffolds that mimic soft tissue mechanical anisotropy. Biomaterials 27, 3631–3638.

Crowder, S.W., Liang, Y., Rath, R., Park, A.M., Maltais, S., Pintauro, P.N., Hofmeister, W., Lim, C.C., Wang, X., Sung, H.J., 2013. Poly(ε-caprolactone)-carbon nanotube composite scaffolds for enhanced cardiac differentiation of human mesenchymal stem cells. Nanomedicine (London, England) 8. http://dx.doi.org/10.2217/nnm.12.204.

Curtis, M.W., Russell, B., 2009. Cardiac tissue engineering. Journal of Cardiovascular Nursing 24, 87–92.

Dabagh, M., Abdekhodaie, M.J., Khorasani, M.T., 2005. Effects of polydimethylsiloxane grafting on the calcification, physical properties, and biocompatibility of polyurethane in a heart valve. Journal of Applied Polymer Science 98, 758–766.

Daebritz, S.H., Sachweh, J.S., Hermanns, B., Fausten, B., Franke, A., Groetzner, J., Klosterhalfen, B., Messmer, B.J., 2003. Introduction of a flexible polymeric heart valve prosthesis with special design for mitral position. Circulation 108, II-134–II-139.

Daebritz, S.H., Fausten, B., Hermanns, B., Franke, A., Schroeder, J., Groetzner, J., Autschbach, R., Messmer, B.J., Sachweh, J.S., 2004a. New flexible polymeric heart valve prostheses for the mitral and aortic positions. Heart Surgery Forum 7, E525–E532.

Daebritz, S.H., Fausten, B., Hermanns, B., Schroeder, J., Groetzner, J., Autschbach, R., Messmer, B.J., Sachweh, J.S., 2004b. Introduction of a flexible polymeric heart valve prosthesis with special design for aortic position. European Journal of Cardio-Thoracic Surgery 25, 946–952.

Dobaczewski, M., Gonzalez-Quesada, C., Frangogiannis, N.G., 2010. The extracellular matrix as a modulator of the inflammatory and reparative response following myocardial infarction. Journal of Molecular and Cellular Cardiology 48, 504–511.

Dvir, T., Timko, B.P., Brigham, M.D., Naik, S.R., Karajanagi, S.S., Levy, O., Jin, H., Parker, K.K., Langer, R., Kohane, D.S., 2011. Nanowired three-dimensional cardiac patches. Nature Nanotechnology 6, 720–725.

Engelmayr, G.C., Cheng, M., Bettinger, C.J., Borenstein, J.T., Langer, R., Freed, L.E., 2008. Accordion-like honeycombs for tissue engineering of cardiac anisotropy. Nature Materials 7, 1003–1010.

Fernandes, E.G.R., Zucolotto, V., De Queiroz, A.A.A., 2010. Electrospinning of hyperbranched poly-l-lysine/polyaniline nanofibers for application in cardiac tissue engineering. Journal of Macromolecular Science Part A 47, 1203–1207.

Frangogiannis, N.G., 2008. The immune system and cardiac repair. Pharmacological Research 58, 88–111.

Fromstein, J.D., Zandstra, P.W., Alperin, C., Rockwood, D., Rabolt, J.F., Woodhouse, K.A., 2008. Seeding bioreactor-produced embryonic stem cell-derived cardiomyocytes on different porous, degradable, polyurethane scaffolds reveals the effect of scaffold architecture on cell morphology. Tissue Engineering Part A 14, 369–378.

Fujimoto, K.L., Guan, J., Oshima, H., Sakai, T., Wagner, W.R., 2007a. In vivo evaluation of a porous, elastic, biodegradable patch for reconstructive cardiac procedures. Annals of Thoracic Surgery 83, 648–654.

Fujimoto, K.L., Tobita, K., Merryman, W.D., Guan, J., Momoi, N., Stolz, D.B., Sacks, M.S., Keller, B.B., Wagner, W.R., 2007b. An elastic, biodegradable cardiac patch induces contractile smooth muscle and improves cardiac remodeling and function in subacute myocardial infarction. Journal of the American College of Cardiology 49, 2292–2300.

Fujimoto, K.L., Tobita, K., Guan, J., Hashizume, R., Takanari, K., Alfieri, C.M., Yutzey, K.E., Wagner, W.R., 2012. Placement of an elastic biodegradable cardiac patch on a subacute infarcted heart leads to cellularization with early developmental cardiomyocyte characteristics. Journal of Cardiac Failure 18, 585–595.

Gaebel, R., Ma, N., Liu, J., Guan, J., Koch, L., Klopsch, C., Gruene, M., Toelk, A., Wang, W., Mark, P., Wang, F., Chichkov, B., Li, W., Steinhoff, G., 2011. Patterning human stem cells and endothelial cells with laser printing for cardiac regeneration. Biomaterials 32, 9218–9230.

Ghanbari, H., Kidane, A.G., Burriesci, G., Ramesh, B., Darbyshire, A., Seifalian, A.M., 2010. The anti-calcification potential of a silsesquioxane nanocomposite polymer under in vitro conditions: potential material for synthetic leaflet heart valve. Acta Biomaterialia 6, 4249–4260.

Guan, J., Wagner, W.R., 2005. Synthesis, characterization and cytocompatibility of polyurethaneurea elastomers with designed elastase sensitivity. Biomacromolecules 6, 2833–2842.

Guan, J., Sacks, M.S., Beckman, E.J., Wagner, W.R., 2002. Synthesis, characterization, and cytocompatibility of elastomeric, biodegradable poly(ester-urethane)ureas based on poly(caprolactone) and putrescine. Journal of Biomedical Materials Research Part A 61, 493–503.

Guan, J., Fujimoto, K.L., Sacks, M.S., Wagner, W.R., 2005. Preparation and characterization of highly porous, biodegradable polyurethane scaffolds for soft tissue applications. Biomaterials 26, 3961–3971.

Guan, J., Stankus, J.J., Wagner, W.R., 2006. Development of composite porous scaffolds based on collagen and biodegradable poly(ester urethane)urea. Cell Transplantation 15, S17–S27.

Guan, J., Stankus, J.J., Wagner, W.R., 2007. Biodegradable elastomeric scaffolds with basic fibroblast growth factor release. Journal of Controlled Release 120, 70–78.

Guan, J., Fujimoto, K.L., Wagner, W.R., 2008. Elastase-sensitive elastomeric scaffolds with variable anisotropy for soft tissue engineering. Pharmaceutical Research 25, 2400–2412.

Guan, J., Wang, F., Li, Z., Chen, J., Guo, X., Liao, J., Moldovan, N.I., 2011. The stimulation of the cardiac differentiation of mesenchymal stem cells in tissue constructs that mimic myocardium structure and biomechanics. Biomaterials 32, 5568–5580.

Guillemette, M.D., Park, H., Hsiao, J.C., Jain, S.R., Larson, B.L., Langer, R., Freed, L.E., 2010. Combined technologies for microfabricating elastomeric cardiac tissue engineering scaffolds. Macromolecular Bioscience 10, 1330–1337.

Hafeman, A.E., Zienkiewicz, K.J., Carney, E., Litzner, B., Stratton, C., Wenke, J.C., Guelcher, S.A., 2010. Local delivery of tobramycin from injectable biodegradable polyurethane scaffolds. Journal of Biomaterials Science, Polymer Edition 21, 95–112.

Han, J., Farah, S., Domb, A.J., Lelkes, P.I., 2013. Electrospun rapamycin-eluting polyurethane fibers for vascular grafts. Pharmaceutical Research 30, 1735–1748.

Hashizume, R., Fujimoto, K.L., Hong, Y., Guan, J., Toma, C., Tobita, K., Wagner, W.R., 2013a. Biodegradable elastic patch plasty ameliorates left ventricular adverse remodeling after ischemia-reperfusion injury: a preclinical study of a porous polyurethane material in a porcine model. Journal of Thoracic and Cardiovascular Surgery 146, 391–399.

Hashizume, R., Hong, Y., Takanari, K., Fujimoto, K.L., Tobita, K., Wagner, W.R., 2013b. The effect of polymer degradation time on functional outcomes of temporary elastic patch support in ischemic cardiomyopathy. Biomaterials 34, 7353–7363.

Hidalgo-Bastida, L.A., Barry, J.J., Everitt, N.M., Rose, F.R., Buttery, L.D., Hall, I.P., Claycomb, W.C., Shakesheff, K.M., 2007. Cell adhesion and mechanical properties of a flexible scaffold for cardiac tissue engineering. Acta Biomaterialia 3, 457–462.

Hilbert, S.L., Ferrans, V.J., Tomita, Y., Eidbo, E.E., Jones, M., 1987. Evaluation of explanted polyurethane trileaflet cardiac valve prostheses. Journal of Thoracic and Cardiovascular Surgery 94, 419–429.

Holmes, J.W., Borg, T.K., Covell, J.W., 2005. Structure and mechanics of healing myocardial infarcts. Annual Review of Biomedical Engineering 7, 223–253.

Hong, Y., Guan, J., Fujimoto, K.L., Hashizume, R., Pelinescu, A.L., Wagner, W.R., 2010. Tailoring the degradation kinetics of poly(ester-carbonate urethane)urea thermoplastic elastomers for tissue engineering scaffolds. Biomaterials 31, 4249–4258.

Ishii, O., Shin, M., Sueda, T., Vacanti, J.P., 2005. In vitro tissue engineering of a cardiac graft using a degradable scaffold with an extracellular matrix-like topography. Journal of Thoracic and Cardiovascular Surgery 130, 1358–1363.

Jawad, H., Ali, N.N., Lyon, A.R., Chen, Q.Z., Harding, S.E., Boccaccini, A.R., 2007. Myocardial tissue engineering: a review. Journal of Tissue Engineering and Regenerative Medicine 1, 327–342.

Jawad, H., Lyon, A.R., Harding, S.E., Ali, N.N., Boccaccini, A.R., 2008. Myocardial tissue engineering. British Medical Bulletin 87, 31–47.

Kai, D., Prabhakaran, M.P., Jin, G., Ramakrishna, S., 2011a. Guided orientation of cardiomyocytes on electrospun aligned nanofibers for cardiac tissue engineering. Journal of Biomedical Materials Research Part B: Applied Biomaterials 98B, 379–386.

Kai, D., Prabhakaran, M.P., Jin, G., Ramakrishna, S., 2011b. Polypyrrole-contained electrospun conductive nanofibrous membranes for cardiac tissue engineering. Journal of Biomedical Materials Research Part A 99A, 376–385.

Kannan, R.Y., Salacinski, H.J., Odlyha, M., Butler, P.E., Seifalian, A.M., 2006. The degradative resistance of polyhedral oligomeric silsesquioxane nanocore integrated polyurethanes: an in vitro study. Biomaterials 27, 1971–1979.

Kannan, R.Y., Salacinski, H.J., Ghanavi, J.E., Narula, A., Odlyha, M., Peirovi, H., Butler, P.E., Seifalian, A.M., 2007. Silsesquioxane nanocomposites as tissue implants. Plastic and Reconstructive Surgery 119, 1653–1662.

Kelley, S.T., Malekan, R., Gorman, J.H., Jackson, B.M., Gorman, R.C., Suzuki, Y., Plappert, T., Bogen, D.K., Sutton, M.G.S.J., Edmunds, L.H., 1999. Restraining infarct expansion preserves left ventricular geometry and function after acute anteroapical infarction. Circulation 99, 135–142.

Kenar, H., Kose, G., Hasirci, V., 2010. Design of a 3D aligned myocardial tissue construct from biodegradable polyesters. Journal of Materials Science: Materials in Medicine 21, 989–997.

Kharaziha, M., Shin, S.R., Nikkhah, M., Topkaya, S.N., Masoumi, N., Annabi, N., Dokmeci, M.R., Khademhosseini, A., 2014. Tough and flexible CNT–polymeric hybrid scaffolds for engineering cardiac constructs. Biomaterials 35, 7346–7354.

Kidane, A.G., Burriesci, G., Cornejo, P., Dooley, A., Sarkar, S., Bonhoeffer, P., Edirisinghe, M., Seifalian, A.M., 2009a. Current developments and future prospects for heart valve replacement therapy. Journal of Biomedical Materials Research Part B: Applied Biomaterials 88, 290–303.

Kidane, A.G., Burriesci, G., Edirisinghe, M., Ghanbari, H., Bonhoeffer, P., Seifalian, A.M., 2009b. A novel nanocomposite polymer for development of synthetic heart valve leaflets. Acta Biomaterialia 5, 2409–2417.

Krupnick, A.S., Kreisel, D., Riha, M., Balsara, K.R., Rosengard, B.R., 2004. Myocardial tissue engineering and regeneration as a therapeutic alternative to transplantation. Current Topics in Microbiology and Immunology 280, 139–164.

Kucinska-Lipka, J., Gubanska, I., Janik, H., Sienkiewicz, M., 2015. Fabrication of polyurethane and polyurethane based composite fibres by the electrospinning technique for soft tissue engineering of cardiovascular system. Material Science and Engineering: C Materials for Biological Applications 46, 166–176.

Kütting, M., Roggenkamp, J., Urban, U., Schmitz-Rode, T., steinseifer, U., 2011. Polyurethane heart valves: past, present and future. Expert Review of Medical Devices 8, 227–233.

Laflamme, M.A., Murry, C.E., 2005. Regenerating the heart. Nature Biotechnology 23, 845–856.

Lamba, N.M.K., Woodhouse, K.A., Cooper, S.L., 1998. Polyurethanes in Biomedical Applications. CRC Press, USA.

Leor, J., Cohen, S., 2004. Myocardial tissue engineering: creating a muscle patch for a wounded heart. Annals of the New York Academy of Science 1015, 312–319.

Li, M., Guo, Y., Wei, Y., Macdiarmid, A.G., Lelkes, P.I., 2006. Electrospinning polyaniline-contained gelatin nanofibers for tissue engineering applications. Biomaterials 27, 2705–2715.

Liang, S.L., Cook, W.D., Thouas, G.A., Chen, Q.Z., 2010. The mechanical characteristics and in vitro biocompatibility of poly(glycerol sebacate)-Bioglass® elastomeric composites. Biomaterials 31, 8516–8529.

Liao, S.Y., Siu, C.W., Liu, Y., Zhang, Y., Chan, W.S., Wu, E.X., Wu, Y., Nicholls, J.M., Li, R.A., Benser, M.E., Rosenberg, S.P., Park, E., Lau, C.P., Tse, H.F., 2010. Attenuation of left ventricular adverse remodeling with epicardial patching after myocardial infarction. Journal of Cardiac Failure 16, 590–598.

Lisi, A., Briganti, E., Ledda, M., Losi, P., Grimaldi, S., Marchese, R., Soldani, G., 2012. A combined synthetic-fibrin scaffold supports growth and cardiomyogenic commitment of human placental derived stem cells. PLoS One 7, e34284.

Losi, P., Briganti, E., Magera, A., Spiller, D., Ristori, C., Battolla, B., Balderi, M., Kull, S., Balbarini, A., Di Stefano, R., Soldani, G., 2010. Tissue response to poly(ether)urethane-polydimethylsiloxane-fibrin composite scaffolds for controlled delivery of pro-angiogenic growth factors. Biomaterials 31, 5336–5344.

Mackay, T.G., Wheatley, D.J., Bernacca, G.M., Fisher, A.C., Hindle, C.S., 1996. New polyurethane heart valve prosthesis: design, manufacture and evaluation. Biomaterials 17, 1857–1863.

Mackle, J.N., Blond, D.J., Mooney, E., Mcdonnell, C., Blau, W.J., Shaw, G., Barry, F.P., Murphy, J.M., Barron, V., 2011. In vitro characterization of an electroactive carbon-nanotube-based nanofiber scaffold for tissue engineering. Macromolecular Bioscience 11, 1272–1282.

Martinelli, V., Cellot, G., Fabbro, A., Bosi, S., Mestroni, L., Ballerini, L., 2013. Improving cardiac myocytes performance by carbon nanotubes platforms. Frontiers in Physiology 4, 239.

Mattu, C., Boffito, M., Sartori, S., Ranzato, E., Bernardi, E., Sassi, M.P., Di Rienzo, A.M., Ciardelli, G., 2012. Therapeutic nanoparticles from novel multiblock engineered polyesterurethanes. Journal of Nanoparticle Research 14, 1–13.

Mattu, C., Pabari, R.M., Boffito, M., Sartori, S., Ciardelli, G., Ramtoola, Z., 2013. Comparative evaluation of novel biodegradable nanoparticles for the drug targeting to breast cancer cells. European Journal of Pharmaceutics and Biopharmaceutics 85, 463–472.

Mcdevitt, T.C., Angello, J.C., Whitney, M.L., Reinecke, H., Hauschka, S.D., Murry, C.E., Stayton, P.S., 2002. In vitro generation of differentiated cardiac myofibers on micropatterned laminin surfaces. Journal of Biomedical Materials Research 60, 472–479.

Mcdevitt, T.C., Woodhouse, K.A., Hauschka, S.D., Murry, C.E., Stayton, P.S., 2003. Spatially organized layers of cardiomyocytes on biodegradable polyurethane films for myocardial repair. Journal of Biomedical Materials Research, Part A 66A, 586–595.

Mendelson, K., Schoen, F., 2006. Heart valve tissue engineering: concepts, approaches, progress, and challenges. Annals of Biomedical Engineering 34, 1799–1819.

Mendis, S., Puska, P., Norrving, B., 2011. Global Atlas on Cardiovascular Disease Prevention and Control. World Health Organization in Collaboration with the World Heart Federation and the World Stroke Organization, Geneva.

Mishra, A., Singh, S.K., Dash, D., Aswal, V.K., Maiti, B., Misra, M., Maiti, P., 2014. Self-assembled aliphatic chain extended polyurethane nanobiohybrids: emerging hemocompatible biomaterials for sustained drug delivery. Acta Biomaterialia 10, 2133–2146.

Moura, S.A., Lima, L.D., Andrade, S.P., Da Silva-Cunha Jr., A., Orefice, R.L., Ayres, E., Da Silva, G.R., 2011. Local drug delivery system: inhibition of inflammatory angiogenesis in a murine sponge model by dexamethasone-loaded polyurethane implants. Journal of Pharmaceutical Sciences 100, 2886–2895.

Murry, C.E., Reinecke, H., Pabon, L.M., 2006. Regeneration gaps: observations on stem cells and cardiac repair. Journal of the American College of Cardiology 47, 1777–1785.

Nadal-Ginard, B., Kajstura, J., Leri, A., Anversa, P., 2003. Myocyte death, growth, and regeneration in cardiac hypertrophy and failure. Circulation Research 92, 139–150.

Nelson, D.M., Baraniak, P.R., Ma, Z., Guan, J., Mason, N.S., Wagner, W.R., 2011. Controlled release of IGF-1 and HGF from a biodegradable polyurethane scaffold. Pharmaceutical Research 28, 1282–1293.

Nigmatullin, R., Gao, F., Konovalova, V., 2008. Polymer-layered silicate nanocomposites in the design of antimicrobial materials. Journal of Materials Science 43, 5728–5733.

Parrag, I.C., Zandstra, P.W., Woodhouse, K.A., 2012. Fiber alignment and coculture with fibroblasts improves the differentiated phenotype of murine embryonic stem cell-derived cardiomyocytes for cardiac tissue engineering. Biotechnology and Bioengineering 109, 813–822.

Pedrotty, D.M., Koh, J., Davis, B.H., Taylor, D.A., Wolf, P., Niklason, L.E., 2005. Engineering skeletal myoblasts: roles of three-dimensional culture and electrical stimulation. American Journal of Physiology – Heart and Circulatory Physiology 288, H1620–H1626.

Piao, H., Kwon, J.S., Piao, S., Sohn, J.H., Lee, Y.S., Bae, J.W., Hwang, K.K., Kim, D.W., Jeon, O., Kim, B.S., Park, Y.B., Cho, M.C., 2007. Effects of cardiac patches engineered with bone marrow-derived mononuclear cells and PGCL scaffolds in a rat myocardial infarction model. Biomaterials 28, 641–649.

Rai, R., Tallawi, M., Grigore, A., Boccaccini, A.R., 2012. Synthesis, properties and biomedical applications of poly(glycerol sebacate) (PGS): a review. Progress in Polymer Science 37, 1051–1078.

Ramakrishna, H., Pajaro, O., 2011. Heart transplantation in the era of continuous flow ventricular assist devices and the total artificial heart: will new technologies surpass the gold standard? Annals of Cardiac Anaesthesia 14, 174–175.

Ravichandran, R., Venugopal, J.R., Sundarrajan, S., Mukherjee, S., Sridhar, R., Ramakrishna, S., 2013. Expression of cardiac proteins in neonatal cardiomyocytes on PGS/fibrinogen core/shell substrate for cardiac tissue engineering. International Journal of Cardiology 67, 1461–1468.

Rechichi, A., Ciardelli, G., D'acunto, M., Vozzi, G., Giusti, P., 2008. Degradable block polyurethanes from nontoxic building blocks as scaffold materials to support cell growth and proliferation. Journal of Biomedical Materials Research, Part A 84, 847–855.

Rockwood, D.N., Akins Jr., R.E., Parrag, I.C., Woodhouse, K.A., Rabolt, J.F., 2008. Culture on electrospun polyurethane scaffolds decreases atrial natriuretic peptide expression by cardiomyocytes in vitro. Biomaterials 29, 4783–4791.

Sachweh, J.S., Daebritz, S.H., 2006. Novel "biomechanical" polymeric valve prostheses with special design for aortic and mitral position: a future option for pediatric patients? ASAIO Journal 52, 575–580.

Salacinski, H.J., Odlyha, M., Hamilton, G., Seifalian, A.M., 2002. Thermo-mechanical analysis of a compliant poly(carbonate-urea)urethane after exposure to hydrolytic, oxidative, peroxidative and biological solutions. Biomaterials 23, 2231–2240.

Sartori, S., Boffito, M., Serafini, P., Caporale, A., Silvestri, A., Bernardi, E., Sassi, M.P., Boccafoschi, F., Ciardelli, G., 2013. Synthesis and structure-property relationship of polyester-urethanes and their evaluation for the regeneration of contractile tissues. Reactive and Functional Polymers 73, 1366–1376.

Sartori, S., Chiono, V., Tonda-Turo, C., Mattu, C., Gianluca, C., 2014. Biomimetic polyurethanes in nano and regenerative medicine. Journal of Materials Chemistry B 2, 5128–5144.

Senel-Ayaz, H.G., Perets, A., Ayaz, H., Gilroy, K.D., Govindaraj, M., Brookstein, D., Lelkes, P.I., 2014. Textile-templated electrospun anisotropic scaffolds for regenerative cardiac tissue engineering. Biomaterials 35, 8540–8552.

Shimizu, T., 2011. Myocardial tissue engineering. In: Eberli, D. (Ed.), Tissue Engineering for Tissue and Organ Regeneration. InTech.

Shin, M., Ishii, O., Sueda, T., Vacanti, J.P., 2004. Contractile cardiac grafts using a novel nanofibrous mesh. Biomaterials 25, 3717–3723.

Siepe, M., Giraud, M.N., Liljensten, E., Nydegger, U., Menasche, P., Carrel, T., Tevaearai, H.T., 2007. Construction of skeletal myoblast-based polyurethane scaffolds for myocardial repair. Artificial Organs 31, 425–433.

Silvestri, A., Serafini, P.M., Sartori, S., Ferrando, P., Boccafoschi, F., Milione, S., Conzatti, L., Ciardelli, G., 2011. Polyurethane-based biomaterials for shape-adjustable cardiovascular devices. Journal of Applied Polymer Science 122, 3661–3671.

Silvestri, A., Boffito, M., Sartori, S., Ciardelli, G., 2013. Biomimetic materials and scaffolds for myocardial tissue regeneration. Macromolecular Bioscience 13, 984–1019.

Silvestri, A., Sartori, S., Boffito, M., Mattu, C., Di Rienzo, A.M., Boccafoschi, F., Ciardelli, G., 2014. Biomimetic myocardial patches fabricated with poly(varepsilon-caprolactone) and polyethylene glycol-based polyurethanes. Journal of Biomedical Materials Research Part B: Applied Biomaterials 102, 1002–1013.

Simmons, A., Hyvarinen, J., Odell, R.A., Martin, D.J., Gunatillake, P.A., Noble, K.R., Poole-Warren, L.A., 2004. Long-term in vivo biostability of poly(dimethylsiloxane)/poly(hexamethylene oxide) mixed macrodiol-based polyurethane elastomers. Biomaterials 25, 4887–4900.

Sintov, A., Scott, W., Dick, M., Levy, R.J., 1988. Cardiac controlled release for arrhythmia therapy: lidocaine-polyurethane matrix studies. Journal of Controlled Release 8, 157–165.

Sirivisoot, S., Harrison, B.S., 2011. Skeletal myotube formation enhanced by electrospun polyurethane carbon nanotube scaffolds. International Journal of Nanomedicine 6, 2483–2497.

Sivak, W.N., Pollack, I.F., Petoud, S., Zamboni, W.C., Zhang, J., Beckman, E.J., 2008a. Catalyst-dependent drug loading of LDI-glycerol polyurethane foams leads to differing controlled release profiles. Acta Biomaterialia 4, 1263–1274.

Sivak, W.N., Pollack, I.F., Petoud, S., Zamboni, W.C., Zhang, J., Beckman, E.J., 2008b. LDI-glycerol polyurethane implants exhibit controlled release of DB-67 and anti-tumor activity in vitro against malignant gliomas. Acta Biomaterialia 4, 852–862.

Skarja, G.A., Woodhouse, K.A., 1998. Synthesis and characterization of degradable polyurethane elastomers containing and amino acid-based chain extender. Journal of Biomaterials Science, Polymer Edition 9, 271–295.

Skarja, G.A., Woodhouse, K.A., 2000. Structure-property relationships of degradable polyurethane elastomers containing an amino acid-based chain extender. Journal of Applied Polymer Science 75, 1522–1534.

Soldani, G., Briganti, E., 2012. Method for Producing a Device Applicable to Biological Tissues, Particularly a Patch for Treating Damaged Tissues, and Device Obtained by Said Method. US patent application.

Soldani, G., Bernabei, M., Losi, P., Crucean, A., Chiappino, D., Burchielli, S., Bernini, F., 2004. In vitro experiments and in vivo implants to evaluate a new silicone-based polyurethane material for replacement of small vessels. Cardiology in the Young 3, 20–23.

Stachelek, S.J., Alferiev, I., Connolly, J.M., Sacks, M., Hebbel, R.P., Bianco, R., Levy, R.J., 2006. Cholesterol-modified polyurethane valve cusps demonstrate blood outgrowth endothelial cell adhesion post-seeding in vitro and in vivo. Annals of Thoracic Surgery 81, 47–55.

Stankus, J.J., Guan, J., Wagner, W.R., 2004. Fabrication of biodegradable elastomeric scaffolds with sub-micron morphologies. Journal of Biomedical Materials Research Part A 70A, 603–614.

Stankus, J.J., Guan, J., Fujimoto, K., Wagner, W.R., 2006. Microintegrating smooth muscle cells into a biodegradable, elastomeric fiber matrix. Biomaterials 27, 735–744.

Stehlik, J., Edwards, L.B., Kucheryavaya, A.Y., Aurora, P., Christie, J.D., Kirk, R., Dobbels, F., Rahmel, A.O., Hertz, M.I., 2010. The registry of the international society for heart and lung transplantation: twenty-seventh official adult heart transplant report–2010. Journal of Heart and Lung Transplantation 29, 1089–1103.

Storey, R.F., Hickey, T.P., 1994. Degradable polyurethane networks based on D,L-lactide, glycolide, ε-caprolactone, and trimethylene carbonate homopolyester and copolyester triols. Polymer 35, 830–838.

Stout, D.A., Basu, B., Webster, T.J., 2011. Poly(lactic–co-glycolic acid): carbon nanofiber composites for myocardial tissue engineering applications. Acta Biomaterialia 7, 3101–3112.

Stuckey, D.J., Ishii, H., Chen, Q.Z., Boccaccini, A.R., Hansen, U., Carr, C.A., Roether, J.A., Jawad, H., Tyler, D.J., Ali, N.N., Clarke, K., Harding, S.E., 2010. Magnetic resonance imaging evaluation of remodeling by cardiac elastomeric tissue scaffold biomaterials in a rat model of myocardial infarction. Tissue Engineering Part A 16, 3395–3402.

Sui, R., Liao, X., Zhou, X., Tan, Q., 2011. The current status of engineering myocardial tissue. Stem Cell Reviews and Reports 7, 172–180.

Sun, Y., Weber, K.T., 2000. Infarct scar: a dynamic tissue. Cardiovascular Research 46, 250–256.

Tang, Y.W., Labow, R.S., Santerre, J.P., 2001. Enzyme-induced biodegradation of polycarbonate-polyurethanes: dependence on hard-segment chemistry. Journal of Biomedical Materials Research 57, 597–611.

Tay, C.Y., Yu, H., Pal, M., Leong, W.S., Tan, N.S., Ng, K.W., Leong, D.T., Tan, L.P., 2010. Micropatterned matrix directs differentiation of human mesenchymal stem cells towards myocardial lineage. Experimental Cell Research 316, 1159–1168.

Wickham, A.M., Islam, M.M., Mondal, D., Phopase, J., Sadhu, V., Tamas, E., Polisetti, N., Richter-Dahlfors, A., Liedberg, B., Griffith, M., 2014. Polycaprolactone-thiophene-conjugated carbon nanotube meshes as scaffolds for cardiac progenitor cells. Journal of Biomedical Materials Research Part B: Applied Biomaterials 102, 1553–1561.

Wisman, C.B., Pierce, W.S., Donachy, J.H., Pae, W.E., Myers, J.L., Prophet, G.A., 1982. A polyurethane trileaflet cardiac valve prosthesis: in vitro and in vivo studies. Transactions – American Society for Artificial Internal Organs 28, 164–168.

Wong, C., Shital, P., Chen, R., Owida, A., Morsi, Y., 2010. Biomimetic electrospun gelatin–chitosan polyurethane for heart valve leaflets. Journal of Mechanics in Medicine and Biology 10, 563–576.

Yang, J., Webb, A.R., Ameer, G.A., 2004. Novel citric acid-based biodegradable elastomers for tissue engineering. Advanced Materials 16, 511–516.

Zamilpa, R., Lindsey, M.L., 2010. Extracellular matrix turnover and signaling during cardiac remodeling following MI: causes and consequences. Journal of Molecular and Cellular Cardiology 48, 558–563.

Zdrahala, R.J., Zdrahala, I.J., 1999. Biomedical applications of polyurethanes: a review of past promises, present realities, and a vibrant future. Journal of Biomaterials Applications 14, 67–90.

Zong, X., Bien, H., Chung, C.Y., Yin, L., Fang, D., Hsiao, B.S., Chu, B., Entcheva, E., 2005. Electrospun fine-textured scaffolds for heart tissue constructs. Biomaterials 26, 5330–5338.

Nitric oxide-releasing polyurethanes

14

J. Pant[1], M.J. Goudie[1], E.J. Brisbois[2], H. Handa[1,*]
[1]University of Georgia, Athens, GA, USA; [2]University of Michigan Medical Center, Ann Arbor, MI, USA
*Corresponding author: hhanda@uga.edu

14.1   Introduction

As a replacement for natural rubber, Dr Otto Bayer first discovered polyurethane (PU) during World War II. Since then, PUs have been used in biomedical applications due to their excellent stability, mechanical properties, and biocompatibility (Boretos and Pierce, 1968; Lyman et al., 1971). From 1995 to 2015, PUs have gained popularity in several blood-contacting device applications including synthetic conduits, extracorporeal life supports (ECLSs), intravascular stents, *in vivo* sensors, defibrillators, and intravascular catheters. Thrombosis is one of the primary problems associated with blood-contacting devices that can cause life-threatening complications for patients. The blood coagulation cascade is a complex process, where protein adsorption occurs within a few seconds to minutes when blood comes in contact with a foreign surface (Figure 14.1). This is followed by platelet adhesion and activation that finally leads to thrombus formation (Horbett, 1993). Adsorbed plasma proteins, such as fibrinogen, bind to glycoprotein GPIIb/IIIa receptors on activated platelets (Gorbet and Sefton, 2004). The activation of platelets also leads to conformation changes and the excretion of intracellular granulates containing adhesion molecules (P-selectin, coagulation factor V and VII, calcium ions, etc.), leading to additional adhesion and activation of platelets. From 1955 to 2015, much has been learned about blood–surface interactions, and many approaches have been studied to prevent thrombosis with systemic anticoagulation and surface modification. In a clinical setting, many of these devices require the use of anticoagulant therapies (e.g., heparin) to avoid device failure (Gaffney et al., 2010). Unfortunately, the long-term use of systemic anticoagulation can be harmful to the patient, and can result in bleeding, increased thrombosis, and thrombocytopenia (Ahanchi et al., 2007; Menajovsky, 2005; Robinson et al., 1993).

Infection and foreign body response (FBR) are among other significant problems faced by long-term use of medical devices. The mechanism of bacterial adhesion is a very complex process. Bacterial adhesion involves initial reversible physicochemical interactions, followed by time-dependent irreversible molecular and cellular interactions (An and Friedman, 2000). Due to various physical forces, such as Brownian movement, van der Waals forces, and hydrophobic and electrostatic interactions, bacteria move to the implant surface. In the second phase, molecular and cellular interactions become predominant where bacteria attach irreversibly to the surface
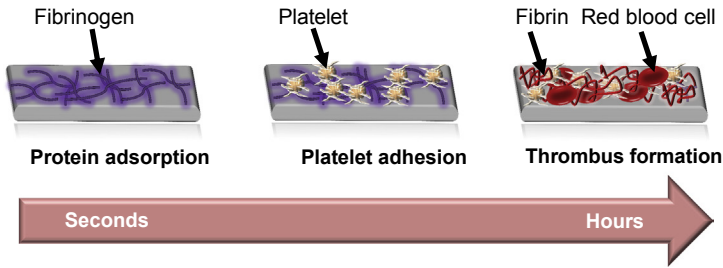
Figure 14.1 Series of steps involved in thrombus formation on an implanted surface. These events include fibrinogen adsorption and platelet adhesion and activation, finally leading to a clot formation.
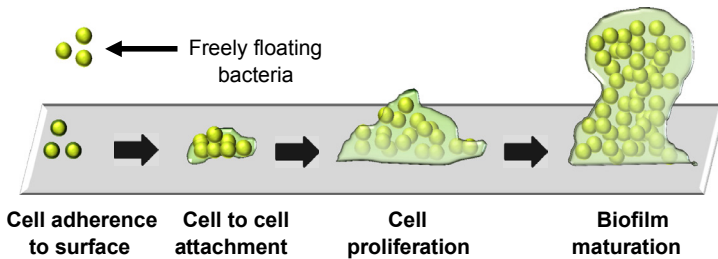
Figure 14.2 Series of events leading to biofilm formation on an implant surface. These events include (a) cell adherence to the implant's surface with the help of a specialized structure on the bacterial cell wall, (b) cell to cell attachment, (c) cell proliferation leading to growth and aggregation, and (d) biofilm maturation and development of resistance against antibacterial agents.

using various bacterial polymeric structures including fimbriae, capsules, and slimes (An and Friedman, 2000). At this time most bacteria multiply and produce extracellular polymeric substances (EPS) to stabilize the biofilm structure. This accumulation of bacterial biomass and EPS on a surface leads to biofilm formation over time (Figure 14.2). In a biofilm, bacteria are protected from adverse environmental conditions, including the application of antiseptics as well as host defense, which makes them difficult to eradicate (Costerton et al., 1995; Hall-Stoodley et al., 2004; Parsek and Singh, 2003; O'Toole et al., 2000; Fux et al., 2005). The presence of fibrinogen and thrombus on the surface also promotes bacterial adhesion (Harris et al., 2004).

14.1.1 Properties of polyurethanes and their compatibility for medical use

PUs are used for a wide range of medical applications including wound dressings, intraaortic balloon pumps, catheters, pace makers, feeding tubes, dialysis bags, sutures, needle hubs, oxygen masks, nonallergic gloves, medical garments, hospital bedding, artificial hearts, and drug delivery systems (Davis and Mitchell, 2008). The versatility of PUs can be attributed to their flexibility, tear resistance, abrasion resistance, biocompatibility, and flexible processing. One important feature that makes

them useful for biomedical applications is that fully reacted PUs are chemically inert (Dernehl, 1966). PUs consist of soft (flexible) and hard segments made of three building blocks: (1) long chain molecule, which acts as backbone, (2) diisocyanate, and (3) chain extender. The backbone provides flexibility to polymer while diisocyanate and the chain extender combined to form the hard segment and act as a cross-link. The hard segment provides high tensile strength and elongation to the PU. PUs are formed by the exothermic reaction between isocyanate (with more than one reactive isocyanate group per molecule) and alcohol (with more than two hydroxyl group per molecule) in the presence of a catalyst. These isocyanates can be either aromatic or aliphatic. Aromatic diisocyanates are preferred if the purpose is to create strong and tough PUs with higher tensile strength and elongation than corresponding PUs prepared with aliphatic isocyanates. Aliphatic PUs with hydrocarbon backbones also form strong polymers, but lack the chemical resistance and properties of their aromatic counterparts. They are mostly used in biodegradable PU formulations with biodegradable hard segments (Jun et al., 2005; Hou et al., 1999). Numerous combinations of the basic building blocks provide an opportunity to use PUs in a variety of biomedical devices. Nonisocyanate-based polyurethanes have been studied for reducing potential toxicity concerns related to isocyanates (Kuo and Schroeder, 1995).

14.1.2 Introduction to nitric oxide

Nitric oxide (NO) is a free radical, water-soluble, ubiquitous gas, which influences various biological functions. It is a cellular signaling molecule naturally secreted by vascular endothelial cells, and is involved in many physiological and pathological processes (Hou et al., 1999). As shown in Figure 14.3, nitric oxide is enzymatically synthesized endogenously from L-arginine by nitric oxide synthase (NOS). There are three NOS synthase isoforms: eNOS (endothelial NOS, generates NO from the endothelial lining of blood vessels), nNOS (neuronal NOS, present in neurons and produces NO that acts as a neurotransmitter), and iNOS (inducible NOS, present in macrophages as a response to bacterial/viral infections) (Knowles and Moncada, 1994; Dicks et al., 1996). The eNOS and nNOS isoforms are calcium dependent and increased NO production occurs when there is an increase in Ca^{2+}. The iNOS isoform is calcium independent and is involved in immune responses, including autoimmune diseases, and is the predominate cause of septic shock (Stuehr, 1999).

Radomski et al. first described NO as a potent vasodilator secreted by the normal endothelium that has the ability to inhibit platelet adhesion and aggregation to the blood vessel wall (Radomski et al., 1987; Radomski and Moncada, 1993a). In 1992, the free radical NO received approbation as "molecule of the year" by the journal *Science* and was the subject of a Nobel Prize. Numerous published reviews have been devoted to a comprehensive discussion of different NO-releasing/generating materials and their many potential biomedical applications (Frost et al., 2005; Seabra et al., 2012; Riccio and Schoenfisch, 2012; Kim et al., 2014; Jen et al., 2012; Halpenny and Mascharak, 2010; Carpenter and Schoenfisch, 2012).
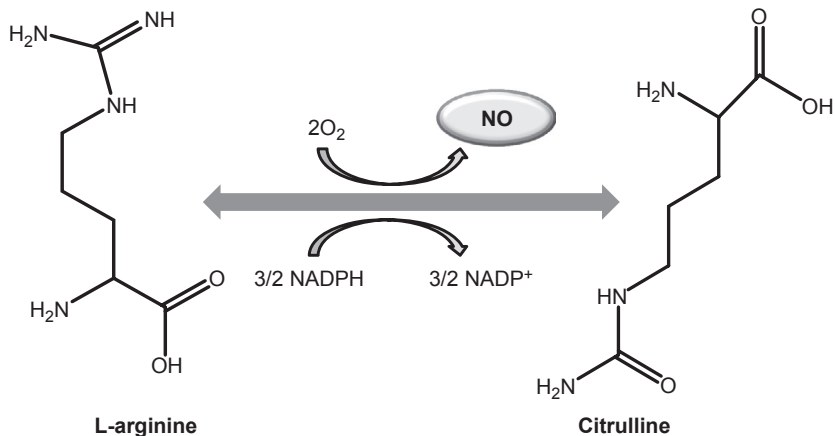
Figure 14.3 Enzymatic (nitric oxide synthase, NOS) conversion of L-arginine to citrulline resulting in nitric oxide (NO) release.

Nitric oxide offers great potential to be utilized in biomedical applications due to its impact on wide ranging biological functions including infection, angiogenesis, inflammation, vasodilation, thrombosis, smooth muscle cell proliferation and migration, wound healing, cardiovascular diseases, nervous system diseases, mammalian cell growth, and tumor formation (Marín and Rodríguez-Martínez, 1997; Vural and Bayazit, 2001; Radomski and Moncada, 1993b; Cai et al., 2005; Chen, 2005; Feldman, 1993; Kuo and Schroeder, 1995). Nitric oxide is known to be a potent inhibitor of platelet activation and adhesion. Healthy endothelial cells exhibit an NO flux of $0.5–4.0 \times 10^{-10}$ mol/cm^2/min (Vaughn et al., 1998). In addition, NO released within the sinus cavities and macrophages functions as a natural antimicrobial agent (Rouby, 2003; Halpenny and Mascharak, 2010). McMullin et al. showed that gaseous NO is bactericidal against several strains of bacteria derived from tracheal aspirates of mechanically ventilated patients in the intensive care unit (McMullin et al., 2005). Therefore, using NO-releasing polymers that can locally deliver NO at or above physiologically relevant levels has the advantage of creating implantable devices that can possess both antithrombotic and antibacterial properties.

Due to the fact that NO is highly reactive under physiological conditions, many molecules with functional groups that can store and release NO have been studied. Among various NO donors, diazeniumdiolates and S-nitrosothiols (RSNOs) have been studied widely (Shin and Schoenfisch, 2006; Hetrick and Schoenfisch, 2006; Handa et al., 2014; Brisbois et al., 2013, 2014, 2015; Reynolds et al., 2006; Major et al., 2010, 2013; Frost and Meyerhoff, 2006; Frost et al., 2005). Diazeniumdiolates are synthetic NO donors that undergo proton or thermally driven mechanisms to release 2 mol of NO per diazeniumdiolate molecule (Figure 14.4) (Batchelor et al., 2003; Mowery et al., 2000; Smith et al., 1996). Both endogenous and synthetic RSNOs have been studied (Figure 14.5). Some of the endogenous RSNOs include S-nitrosoglutathione (GSNO), S-nitrosocysteine (CysNO), and S-nitrosoalbumin. S-nitroso-N-acetylpenicillamine (SNAP) and S-nitroso-N-acetylcysteine are two examples of synthetic RSNOs. These RSNOs can release NO via thermal decomposition, catalysis (using metals ions such
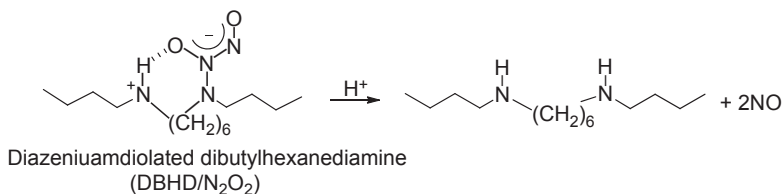
Figure 14.4 Mechanism of NO release from diazeniumdiolated dibutylhexanediamine (DBHD/N$_2$O$_2$).
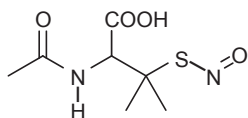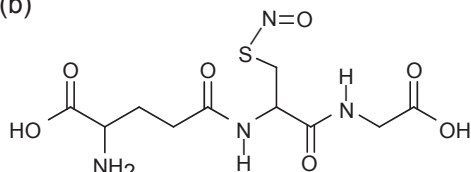
Figure 14.5 Structures of example synthetic (a) and endogenous (b) S-nitrosothiol species.

as Cu$^+$), or by exposure to light (wavelengths of 340 and/or 590 nm), resulting in disulfide species (RSSR) formation (Wood et al., 1996; Frost and Meyerhoff, 2004; Singh et al., 1996; Dicks et al., 1996; Williams, 1999).

The two commonly used approaches to release NO from polymeric surface are: (1) NO-releasing polymers (NORel), where NO donor molecules (e.g., diazeniumdiolates or RSNOs) that can release NO under physiological conditions are incorporated into the polymer; and (2) NO-generating (NOGen) polymers, where catalysts that can react with endogenous RSNOs to generate NO are incorporated into the polymers (Figure 14.6) (Dicks et al., 1996; Holmes and Williams, 2000; Singh et al., 1996; Williams, 1999). Nitric oxide-releasing/generating PUs have been successfully reported for use in many biomedical applications. This chapter discusses in detail some of the biomedical applications of NO-releasing PUs, their advantages and limitations associated with each of the applications.

14.2 Nitric oxide-releasing/generating polyurethanes

PUs offer several applications in blood-contacting devices. Many strategies have been studied to create localized NO release/generation from various PU materials. As discussed above, NORel polymers are prepared by covalently or noncovalently incorporating NO donor molecules into polymer matrices. Diazeniumdiolates have been incorporated into polymers for a variety of potential applications. Taite et al.,
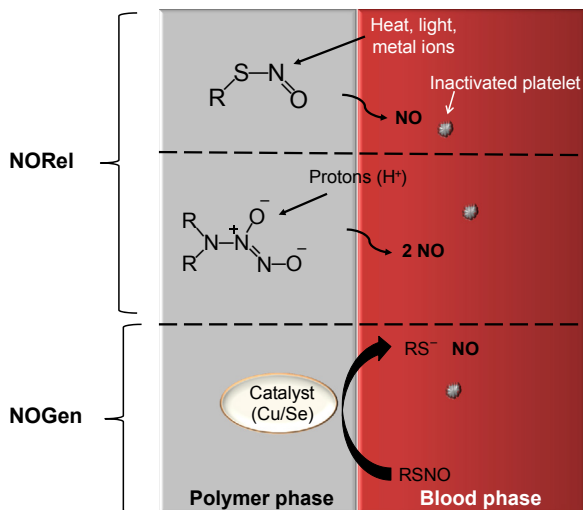
Figure 14.6 Two examples of NO-releasing (NORel) polymers where NO donor molecules (e.g., RSNOs or diazeniumdiolates) can be covalently or noncovalently incorporated into the PU. NO-generating (NOGen) polymers consist of immobilized catalysts that can generate NO from endogenous RSNO species.

incorporated poly(ethylene glycol) and a diazeniumdiolate NO donor into the backbone of PU in addition to incorporating the laminin-derived cell adhesive peptide sequence tyrosine–isoleucine–glycine–serine–arginine (YIGSR) (Taite et al., 2008). Nitric oxide release was sustained over a 2 month period as measured by Griess assay. The NO release and YIGSR sequence worked synergistically, where NO improved thromboresistance and endothelial cell proliferation while YIGSR promoted endothelial cell adhesion and migration.

Reynolds et al. suggested two novel strategies for the synthesis of NO-releasing PU with covalently linked diazeniumdiolated secondary amines (Reynolds et al., 2006). To achieve this, the diazeniumdiolate moiety was covalently attached onto amines within the polymer backbone of Pellethane 2363-80AE. However the NO-releasing polymers resulting from this synthetic strategy required incorporation of countercations to stabilize the diazeniumdiolates. In the second approach, the polymer was derivatized to contain pendant polyamine sites, which act as a linker to covalently bind the diazeniumdiolates. These diazeniumdiolates were found to be stable without additives, likely because the pendant amines are less rigid than the polymer backbone and allow the zwitterionic diazeniumdiolate to form more easily. Covalently bound NO donors have the advantage that the by-products remain covalently bound to the polymer matrix. The results showed an initial NO flux of 14 pmol/cm^2/s when immersed in pH 7.4 buffer at 37 °C for up to 6 days. Other diazeniumdiolate-based NO-releasing implants have proved helpful in decreasing the local chronic inflammation response by 33% and enhancing formation of blood vessels by >77% *in vivo* in adult male Sprague–Dawley rats (Hetrick et al., 2007). In addition, NO release helped in reducing collagen capsule thickness in rat models by >50% around the implant as compared to controls.

Success in using NO donors for preventing thrombosis either by covalently linking NO donors to the polymer or by embedding them within the polymers (NORel polymers) has been reported. However, the utility of NORel PUs can be limited by their sensitivity toward heat, light, and moisture, leading to decreased NO release lifetimes. One of the obstacles in delivering NO from the polymers is rapid leaching of the NO donor species, resulting in nonlocalized NO release. For example, rapid leaching of SNAP from PUs with high water uptake such as Techophilic SP-60D6-and Tecoflex SG80A was observed, while PUs with low water uptake such as CarboSil and Elasteon E2As had minimal leaching (Brisbois et al., 2013). Another concern, especially with diazeniumdiolated-based polymers, is the formation of potentially toxic decomposition products such as *N*-nitrosoamines, which can lead to cancer (Mowery et al., 2000; Annich et al., 2000). Other limitations include issues with sustained NO release and stability of the NO donor, which could limit shelf life or ability to be sterilized.

To address this stability issue, several NO-generating PUs have been studied. These NOGen polymers have the advantage that they could potentially generate NO for long periods, provided that there is a constant source of endogenous RSNOs. One approach has been the use of various covalently linked Cu(II)–cyclen moieties that have been immobilized onto PU backbones (Oh and Meyerhoff, 2003). Hwang et al. covalently linked Cu(II)–cylen moieties to Tecophilic SP-93A-100, which could potentially be applied to various biomedical devices to improve their hemocompatibility by catalytically generating NO from endogenous RSNOs (Hwang and Meyerhoff, 2008). Puiu et al. derivatized two different PUs, Pellethane™ and Tecophilic®, to incorporate NO-generating Cu(II)–cyclen moieties on the backbone of the PU (Puiu et al., 2009). Tecophilic® thermoplastic PUs are aliphatic, polyether-based PUs, which have high water uptakes (up to 150% of the weight of the dry resin). In contrast, Pellethane™ is a high-strength, aromatic thermoplastic PU. A three-step synthetic approach is used to prepare Cu(II)–cyclen–PU material with these polymers. This NOGen polymer was able to produce physiological levels of NO in the presence of RSNOs without the use of an aminated linker. Tecophilic® thermoplastic PU, due to its lower reactivity, had a lower percentage of incorporation of isocyanate (NCO) and therefore fewer cyclen/Cu(II) sites. However, higher water uptake allows for greater NO generation due to better diffusion of the RSNO species to the active Cu(II) sites. Owing to these properties, the newly developed material possesses great potential to be utilized *in vivo* as a coating material for various blood-contacting device applications.

These examples demonstrate the various chemistries that have been used to incorporate NO-releasing/generating materials in medical grade PUs. Below are specific examples of NO-releasing/generating PUs that have been examined for some specific biomedical applications.

14.3   Biomedical applications of nitric oxide-releasing polyurethanes

14.3.1   *Extracorporeal circuits*

Extracorporeal circulation (ECC) is used in a wide variety of hospital procedures including short-term hemodialysis, extracorporeal membrane oxygenation, and other

ECLS devices (Reynolds and Annich, 2011). These procedures involve blood coming in contact with various tubing, pumps, and artificial devices, all of which are foreign surfaces and activate the blood (Bartlett, 2005). While patients are on ECLS devices, preventing fibrin formation as well as platelet and monocyte activation is critical for successful clinical outcomes. The clinical practice during ECLS is administration of systemic anticoagulants, such as heparin, to avoid device failure and has allowed the continued success of ECLS (Gaffney et al., 2010). Bleeding and thrombosis (7–33%) are the most common complications with ECLS circuits (Paden et al., 2013). Systemic administration of anticoagulants, like heparin, has some adverse side effects including hemorrhage, thrombocytopenia, and thrombosis (Robinson et al., 1993). Despite these complications, heparin is still used as the standard in anticoagulation therapy for patients on ECC.

The ideal ECLS procedures would consist of nonthrombogenic surfaces and little to no systemic anticoagulant administration needed. Novel methods to suppress the thrombogenicity of ECLS circuits are still needed. One strategy has included immobilized heparin; however, ECC circuits coated with heparin are still thrombogenic (Ihno et al., 1997; Wendel and Ziemer, 1999; Bartlett, 2005). As discussed in the Section 14.1, the normal endothelial lining continuously releases NO, at a surface flux of $0.5–4 \times 10^{-10}$ mol/cm^2/min, which inhibits platelet activation and prevents intravascular thrombosis (Vaughn et al., 1998). It also has been reported that NO can inhibit the activation of circulating granulocytes (Wright et al., 1989; Niu et al., 1994). Gaseous NO has been applied in the sweep gas of membrane oxygenators and has shown promise in improving their hemocompatibility by preventing platelet activation as well as reducing the inflammatory response associated with ECC (Hayashi et al., 1998; Keh et al., 1999; Mellgren et al., 1996, 1998; Tevaearai et al., 2000). To localize the administration of NO, NO-releasing polymers have been applied to the ECC circuit tubing and tested in a rabbit thrombogenicity model for their hemocompatibility properties. NO-releasing polymers for ECC circuits have been studied by incorporating NO donor species (e.g., diazeniumdiolates, RSNOs) as well as catalysts for *S*-nitrosothiol decomposition (Jen et al., 2012). NO is advantageous for blood-contacting device applications because of its short half-life in blood, due to rapid scavenging by hemoglobin (Hakim et al., 1996), and the localized effect of temporarily inhibiting the activation of platelets that approach the polymer surface.

The rabbit thrombogenicity model provides a simplified ECC circuit arteriovenous (AV) shunt that is useful for investigating the hemocompatibility of novel polymers. The ECC circuit consists of 16-gauge and 14-gauge PU IV angiocatheters (Kendall Monoject Tyco Healthcare Mansfield, MA), two 16 cm in length of 1/4 inch inner diameter (i.d.) Tygon tubing, and an 8 cm length of 3/8 inch i.d. Tygon tubing, which creates a thrombogenicity chamber where thrombus forms due to more disturbed blood flow (Figure 14.7). The inner walls of the ECC circuit are coated with solutions containing the NORel, NOGen, or control polymer. As shown in Figure 14.7, the ECC is pieced together, starting at the left carotid artery side, with the 16-gauge angiocatheter, one 15 cm length 1/4 inch i.d. tubing, the 8 cm length thrombogenicity chamber, the second 15 cm length 1/4 inch i.d.
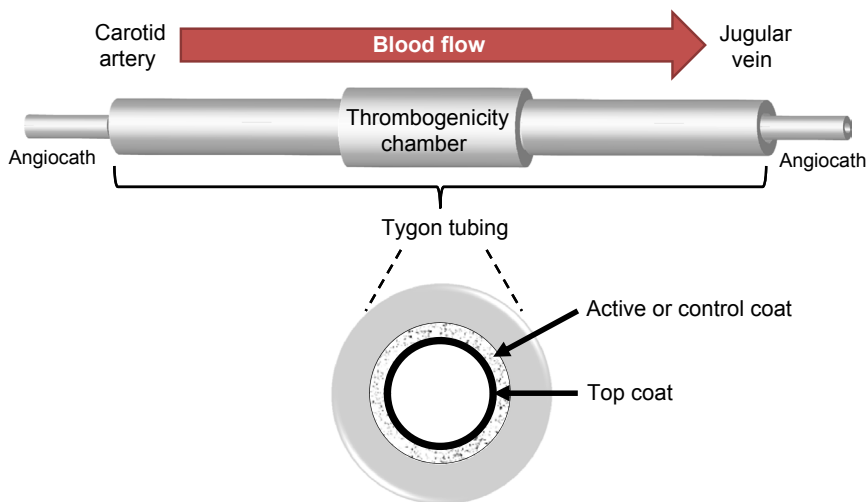
Figure 14.7 Schematic of the assembled extracorporeal circulation (ECC) circuit and cross section showing generic coatings. Inner walls of the Tygon tubing and angiocatheters are coated with an active coat (containing the NORel or NOGen chemistry) or control coat (without NO chemistry), followed by a polymer top coat.

tubing, and finally the 14-gauge angiocatheter. The angiocatheters are interfaced with tubing using two luer-lock PVC connectors. The 3/8 inch i.d. tubing and the 1/4 inch tubing are welded together using Tetrahydrofuran (THF) (Brisbois et al., 2013; Handa et al., 2013, 2014; Major et al., 2010, 2011, 2013, 2014a,b). Briefly, the assembled ECC circuit is positioned on the rabbit as an AV shunt, connecting the left carotid artery and right jugular vein. During the 4 h of blood flow through the ECC circuit the rabbit hemodynamics (blood flow rate, platelet count, plasma fibrinogen levels, and platelet functionality) are monitored and compared to baseline values (prior to ECC placement). After 4 h of blood flow, the 2D representation of the clot that formed in the thrombogenicity chamber is quantitated using NIH ImageJ software.

The intrinsic hemocompatibility of the base polymer (in which the NO chemistry is incorporated) has direct effects on the resulting effectiveness of the NO released from that polymer. Handa et al. conducted a study where four polymers (without any NO release) were coated on the inner walls of the ECC circuit and tested in the rabbit model. The polymers compared in this study were Tecoflex SG80A, Tecophilic SP-60D-60, and Elast-eon E2As PUs, as well as plasticized poly(vinyl chloride) (PVC/DOS). Only one out of five of the E2As coated circuits were occluded prior to the end of the 4 h blood flow, while two to three out of four circuits occluded for the SG80A, SP-60D-60, and PVC/DOS ECC circuits. The Elast-eon E2As polymer exhibited the best hemocompatibility properties in terms of preserving platelets and reducing clot formation. This corresponds with previous reports that E2As has excellent hemocompatibility because it exhibits low levels of blood protein adhesion (Cozzens et al., 2011; Simmons et al., 2008).

Nitric oxide-releasing polymers, containing NO donor diazeniumdiolated dibutyl-hexanediamine (DBHD/N_2O_2) have been tested in the rabbit ECC model (Handa et al., 2013, 2014; Major et al., 2010). Through these studies various modifications have been made to improve the NO release chemistry. Studies have shown that DBHD/N_2O_2 is an excellent donor for incorporation into hydrophobic polymers (Major et al., 2010; Batchelor et al., 2003). DBHD/N_2O_2 releases NO through thermal and proton driven mechanisms (Davies et al., 2001; Zhang et al., 2002). The loss of NO from the DBHD/N_2O_2 results in lipophilic amine species that react with water, thereby increasing the pH within the organic polymer phase, which effectively turns off the NO release before a significant fraction of the NO payload is released (Batchelor et al., 2003). Initially, tetrakis-(p-chlorophenyl) borate was added to the DBHD/N_2O_2 polymers to help maintain a low enough pH to prolong the NO release (Batchelor et al., 2003; Major et al., 2010). However, this borate additive was not effective at completely depleting the NO payload, resulted in a large initial burst of NO, and also was found to be toxic toward endothelial and smooth muscle cells (Wu, 2009). Further studies demonstrate an alternative method of prolonging the NO release from DBHD/N_2O_2 using poly(lactic-co-glycolic acid) (PLGA) additives (Handa et al., 2013). PLGA is a biodegradable and biocompatible polymer that slowly hydrolyzes in the presence of water to produce lactic and glycolic acid species. This continuous acid production promotes the NO release reaction by compensating for the increase in pH from the generation of organoammonium hydroxide (reaction of DBHD amine species with water in the polymer film) resulting from the NO release reaction, thereby providing the acidic environment needed to prolong the NO release. Handa et al. demonstrated that PLGA additives with carboxylic acid end groups create a more acidic environment resulting in an initial burst of NO, while PLGAs with ester end groups that have slower hydrolysis rates were able to prolong the NO release from DBHD/N_2O_2 for up to 2 weeks (Handa et al., 2013, 2014).

Initial ECC studies with DBHD/N_2O_2 were conducted using the PVC/DOS polymer with the borate additive. Skrzypchak et al. coated the inner walls of the ECC circuits with 2–50 wt% DBHD/N_2O_2 doped within the PVC/DOS polymer. The circuits with at least 25 wt% DBHD/N_2O_2 were able to preserve platelet count and reduce fibrinogen consumption, leading to the conclusion that the NORel polymers need an NO flux of at least $\sim 14 \times 10^{-10}$ mol/cm^2/min to be effective (Skrzypchak et al., 2007). ECC circuits coated with PVC/DOS containing 25 wt% DBHD/N_2O_2 and borate (average NO flux $\sim 13 \times 10^{-10}$ mol/cm^2/min) were able to preserve platelets at $79 \pm 7\%$ of baseline (vs $54 \pm 7\%$ for controls) and reduce clot area to 2.8 ± 0.7 pixels/cm^2 (vs 6.7 ± 0.4 pixels/cm^2 for controls) (Major et al., 2010). These circuits were also found to attenuate the activation of monocytes, as measured by CD11b expression, which is a key component of a proinflammatory response. Similar platelet preservation and clot area results were obtained for NORel ECC circuits coated with 25 wt% DBHD/N_2O_2 and 10 wt% 5050DLG7E PLGA additive (in PVC/DOS) with an NO flux of 11×10^{-10} mol/cm^2/min (Handa et al., 2013). Combining the DBHD/N_2O_2 and PLGA chemistry with the E2As PU resulted in a coating with an NO flux of $\sim 6 \times 10^{-10}$ mol/cm^2/min that significantly improved the hemocompatibility of the ECC

circuits over previous studies, preserving platelets at $97 \pm 10\%$ and reducing clot area to $0.9 \pm 0.3\,cm^2$ (vs $58 \pm 3\%$ and $5.2 \pm 0.3\,cm^2$, respectively, for E2As controls) after 4 h of blood flow (Handa et al., 2014). Platelet functionality (as measured by aggregometry) was preserved for the NO-releasing ECC circuits in these studies, indicating that the NO release has a localized effect that temporarily prevents the activation of platelets that approach the surface and allows them to aggregate normally downstream from the circuit (Major et al., 2013). Studies have also suggested that combining nitric oxide-releasing (DBHD/N$_2$O$_2$) coatings with immobilized active anticoagulants, heparin (Zhou and Meyerhoff, 2005) and argatroban (a direct thrombin inhibitor) (Major et al., 2014a), can further improve the hemocompatibility of polymers by preventing both platelet activation and fibrin formation, two key components in the coagulation cascade. These studies demonstrate the importance of combining the NO release chemistry with hemocompatible polymers to effectively reduce thrombus formation during ECC procedures.

NOGen polymers consist of catalysts immobilized within the polymer that can liberate NO from endogenous RSNOs, thus locally generating NO at the blood–polymer interface. Major et al. used polymeric coating composed of a Cu(0) nanoparticle (80 nm)-containing hydrophilic PU (Tecophilic SP-60D-60) combined with the intravenous infusion of SNAP and evaluated this NOGen coating in the 4 h rabbit ECC model (Major et al., 2011). The Cu(0) nanoparticles corrode to generate Cu(II) species, which then can be reduced to Cu(I) by the presence of thiols (RSH) or other reducing equivalents (e.g., ascorbic acid) that exist in the blood. The Cu(I) is the active species that can catalytically generate NO from endogenous RSNO species (e.g., GSNO) (Williams, 1996) as shown in Figure 14.8. This NOGen approach would ideally be able to continually generate NO from the endogenous RSNOs. However, in the study it was found that the endogenous RSNO levels were not sufficient and systemic SNAP infusion (0.1182 mmol/kg/min) was administered to improve the efficacy of the device. Platelet counts were preserved after 4 h blood exposure with NOGen/SNAP compared to the corresponding controls (3.9 ± 0.7 NOGen/SNAP vs 1.8 ± 0.1 control/SNAP or $3.0 \pm 0.2 \times 10^8\,mL^{-1}$ NOGen/saline). The intravenous infusion of SNAP did have the
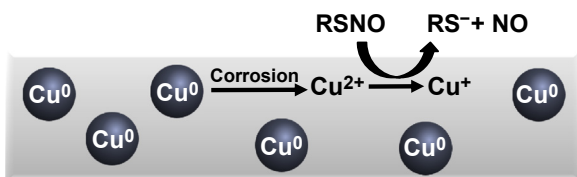
Figure 14.8 Scheme showing the mechanism of localized NO generation from Tecophilic SP-60D-60 coating containing 80 nm Cu(0) nanoparticles. The Cu(0) nanoparticles will corrode in the presence of water to generate Cu(II) ions. The Cu(II) will be reduced to the active species, Cu(I), in the presence of thiolates or other reducing equivalents that exist in the physiological environment (e.g., ascorbic acid). The Cu(I) catalyzes the decomposition of endogenous RSNOs (e.g., GSNO, CysNO) to locally generate NO.

side effect of hypotension; however, the coadministration of intravenous fluids counteracted this effect.

To obviate the need for SNAP infusion, Brisbois et al. studied the effects of noncovalently incorporating SNAP into a variety of PUs to create an NO-releasing polymer (Brisbois et al., 2013). The polymers with low water uptakes (CarboSil, Elast-eon E2As, and silicone rubber) minimized the amounts of SNAP leaching into PBS buffer in comparison to PUs with higher water uptakes (Tecoflex SG80A and Tecophilic SP-60D-60). SNAP incorporated into the E2As polymer (a copolymer with a mixed soft segment of poly(dimethylsiloxane) and poly(hexamethylene oxide) with a methylene diphenyl isocyanate (MDI) hard segment) created an inexpensive coating that could release NO via thermal and photochemical reactions. SNAP was found to be stable within E2As during a shelf life stability study, where only ~18% of the SNAP was lost during 2 months storage at 37 °C. The SNAP/E2As polymer was coated on the inner walls of ECC circuits (average NO flux ~2×10^{-10} mol/cm^2/min) and exposed to 4 h blood flow in the rabbit model. After 4 h, the SNAP/E2As coating preserved the platelet count at 100 ± 7% of baseline, as compared to 60 ± 6% for E2As control circuits. This coating also reduced the amount of thrombus formation as compared to the controls (2.3 ± 0.6 and 3.4 ± 1.1 pixels/cm^2, respectively).

14.3.2 Intravascular glucose sensors

Glucose plays a pivotal role in respiration and other metabolic processes in humans. Disturbed glucose concentration (hyperglycemia or hypoglycemia) may lead to many other metabolic disorders and neuropathic consequences. These medical complications include decrease in insulin sensitivity (diabetes), obesity, delay in wound healing, increased formation of reactive oxygen species, premature ageing, increase risk of Crohn's disease and ulcerative colitism migraines, enhancement in development of Alzheimer's disease, aggravation in premenstrual syndrome, increase in amount of liver fat, development of Parkinson's disease, decrease in amount of growth hormones in the body, ovarian cancer, suppression of immune response, attention deficit disorder in children, and encephalopathy (Sanchez et al., 1973; Cerami et al., 1987; Thomas et al., 1981; Darlington et al., 1986; Ma et al., 2006; Furth and Harding, 1989; Lee and Cerami, 1992; Girardi et al., 1995; Schulze et al., 2005). According to the National Diabetes Statics Report published in 2014 by Center for Disease Control and Prevention, 29.1 million people in the United States are diabetic (9.3% of the United States total population) and only 21.0 million are diagnosed, while 8.1 million (27.8% of the diabetic population) of those having diabetes are undiagnosed (Centers for Disease Control, 2014). The total (direct and indirect) medical cost associated with Diabetes in the United States is estimated to be $245 billion in 2012 (Centers for Disease Control, 2014).

Patients with diabetes need to test their blood glucose levels several times a day using finger pricking and test strip glucometers. Due to wide range of implications of disturbed glucose metabolism and huge medical cost associated with it, continuous glucose monitoring (CGM) becomes critical for proper management

of body sugar, particularly in cases of type I diabetes (Wang, 2008). While conventional methods like finger pricking cannot be used for CGM, the implantable electrochemical-based blood sensors face the issues of incompatibility, frequent calibration (2–4 times/day finger pricking), short implantable lifetime (less than 1 week), and nonreproducible results, which limit their medical utility (Klonoff, 2005a,b; Frost et al., 2013). Even the existing commercial implantable glucose sensors have significant limitations with their accuracy and require frequent calibration (Cheyne and Kerr, 2002; Kubiak et al., 2004). Lack of success in developing implantable glucose sensors can be attributed to the biological response against the indwelling sensor. Surface fouling, scar tissue formation, and bacterial adhesion around the implanted glucose sensor not only reduce the rate of glucose diffusion but also increase the risk of sepsis and leukocyte infiltration (Frost and Meyerhoff, 2002; Wisniewski et al., 2000; Koh et al., 2011a). A cumulative effect of all these detrimental events ultimately leads to an FBR, which can lead to a sheath of leukocytes, macrophages, and collagen formed around the device (Ratner, 2002). This sheath can alter the glucose levels by consuming glucose at an accelerated rate, resulting in false glucose sensor readings (Frost and Meyerhoff, 2006; Wilson and Gifford, 2005; Anderson, 1993; Daley et al., 1990). To fully utilize the potential of implantable glucose sensor for CGM, there is an urgent need to overcome these limitations. Koh et al. suggested that an ideal *in vivo* sensor for continuous and real time measurement should have four attributes: (1) a very small size (<1 mm o.d.) for comfortable placement within a blood vessel or under the skin, (2) provide reliable results, (3) nontoxicity under physiological conditions, and (4) provide long-term analytical signal stability (Koh et al., 2011b).

To date electrochemical detection and enzyme-modified electrodes offer the most successful technologies for measurement of glucose level. One approach for achieving CGM has been the development of needle-type electrochemical sensors for intravascular use. Many of these sensors have been developed using an enzyme layer of glucose oxidase (GOx) that converts glucose to peroxide (H_2O_2), which then is detected by the electrode. Both active strategies (e.g., use of NO release) and passive strategies (e.g., surface modifications) have been employed to enhance *in vivo* biosensor performance (Bota et al., 2010; Ju et al., 2010; Koschwanez et al., 2008; Sanders et al., 2005; Soto et al., 2014; Koh et al., 2011a, 2013). Various strategies including development of a polymeric membrane and doping of the biomaterial with antimicrobial agents have been employed to overcome FBR, surface fouling, and microbial infection of glucose sensors (Lindner et al., 1994; Yoda, 1998; Moussy et al., 1994; Valdes and Moussy, 1999; Hendricks et al., 2000; Rojas et al., 2000; Umar et al., 2013; Koh et al., 2013; Zhang et al., 2013). Many detailed studies have been published on implantable glucose sensors (Meyerhoff et al., 1992, 1993, 1994; Soto et al., 2014; Mortellaro and DeHennis, 2014; Huang et al., 2013; Ballesteros et al., 2014; Balaconis et al., 2015; Koh et al., 2013; Koschwanez and Reichert, 2007). Utilizing NO-releasing PUs is one approach used to improve the biocompatibility of these devices.

PUs can address the surface fouling issue associated with *in vivo* glucose sensors, while NO plays a critical role in mediating inflammatory response in addition to

being antithrombotic and antibacterial. Gifford et al. used DBHD/N_2O_2 with a semi-permeable glucose membrane layer of Tecoflex PU and polydimethylsiloxane. The NO-releasing sensors exhibited excellent *in vitro* and *in vivo* performance with suppressed inflammatory response in a rat model (Gifford et al., 2005). Nichols et al. reported increase in recovery of *in vivo* glucose from NO-releasing microdialysis probes during a 2 week implantation in a rat model (Nichols et al., 2011). Decreased inflammatory cell density and decreased capsule thickness was observed on the probe surface.

Hybrid NO-releasing sol–gel particles developed by Schoenfisch received much attention for their tremendous chemical flexibility, porosity, and mild synthesis conditions (Shin et al., 2004). The NO-releasing sol–gel particles were embedded within a PU matrix and used to coat the glucose biosensors. Sol–gels containing aminosilanes were coated on platinum electrodes and exposed to high pressure NO to convert accessible amine groups to diazeniumdiolate groups. The NO release was controlled by varying the amount of diazeniumdiolate-modified sol–gel particles in PU. This combination has advantages for coating the sensor as it combines the controlled release of NO with the versatility of sol–gel chemistry. Another advantage of this biosensor was that it improved the NO donor sensitivity as well as provided microencapsulation to the GOx enzyme within the sol–gel. This model with an NO-releasing xerogel fabricated glucose biosensors proved successful in terms of reducing bacterial adhesion but with compromised detection sensitivity due to significantly limited glucose diffusion. To address this, Oh et al. used an NO-releasing xerogel microarray on top of PU sensor membranes but again a reduced sensitivity was observed for NO-releasing micropatterned sensors compared to the corresponding controls (Oh et al., 2005). A significant reduction in FBR and improvement in analytical performance of implantable biosensors can be achieved using NO, but there is still room for improvement of the NO release chemistry for efficient analytical performance.

Koh et al. demonstrated the impact of the NO release vehicle and its release kinetics on the performance of a glucose sensor by using two NO donor classes (*N*-diazeniumdiolates and RSNOs) in combination with different PUs (Tecoplast TP-470-000, Tecophilic HP-93A-100) (Koh et al., 2011b). Glucose sensor membranes were prepared using PUs doped with NO-releasing silica particles and then used as the outermost coating of a GOx enzyme-based glucose sensor. Such membranes are also known to have adequate selectivity over known interferents (Heller and Feldman, 2008; Wilson and Gifford, 2005). NO-releasing silica particles were prepared via cocondensation of various aminosilanes or mercaptosilane with tetraethoxysilane or tetramethoxysilane followed by diazeniumdiolation of amine-containing particles under high pressure of NO. The NO-releasing silica particles were dispersed in PUs with different water uptakes (Tecoplast TP-470-000, Tecophilic HP-93A-100) and PU topcoats were used to further control the release of NO. Using NO donor-modified silica nanoparticles the sensors were able to achieve NO fluxes in the range of 5 pmol/cm^2/s–2.5 nmol/cm^2/s for up to 14 days. The result demonstrated that the use of NO donor-modified silica nanoparticles resulted in decreased glucose sensitivity by ~57% as compared to the

control. However, this reduction in glucose sensitivity was independent of NO release from the membrane, and was not enough to change GOx activity. In addition, H_2O_2 permeability through the silica particle-doped films was also reduced by ~58%, likely to the greater thickness of the particle-doped films as compared to the control (14 vs 2 μm thick).

In an another study, the Meyerhoff group developed NO-releasing needle-type glucose sensors with Nafion, 1,3-diaminobenzene, and resorcinol layers to prevent interference from other electroactive species present in blood (e.g., acetaminophen, ascorbic acid, etc.) (Yan et al., 2011). The sensors were prepared with an NO-releasing layer containing lipophilic diazeniumdiolate species (DBHD/N_2O_2) embedded within a layer of PLGA. A top coat of PurSil (copolymer of PU and siloxane) was used to prevent leaching of the NO donor compound, as well as limit the diffusion of glucose to the enzyme layer. These sensors could release NO for more than 7 days above the physiological levels. The sensors were tested *in vivo* for glucose monitoring in an 8 h rabbit model. The reduction of thrombus formation due to the NO release improved the accuracy of the continuous glucose measurement in blood.

Electrospun fibers have been used as glucose sensor membranes due to their mechanical strength and high surface to volume ratio (Teo and Ramakrishna, 2006). Wang et al. suggested that the coating of PU electrospun fibers on sensor surfaces can be done to modify microsensors having porous membranes (Wang et al., 2013). Gifford et al. used a rodent model and suggested that NO fluxes >0.83 pmol/cm^2/s from needle-type glucose biosensors are required to obtain satisfactory reduction in inflammation and improvement in measured glucose accuracy (Gifford et al., 2005). The Schoenfisch group developed NO-releasing thin porous PU membrane-coated needle-type implantable glucose sensors using Tecophilic HP-93A-100, Tecoflex SG-80A, and Tecoplast TP-470 (Koh et al., 2013). The 1,2-epoxy-9-decene-functionalized poly(amidoamine) dendrimers were converted to diazeniumdiolates under high pressure of NO for 3 days in the presence of sodium methoxide. Electrospinning was used to make NO-releasing dendrimer-doped PU fibers to fabricate a porous mat for sensor membranes. The porous NO-releasing PU membranes may reduce the FBR without affecting the sensor performance.

To summarize, the results suggest that sustained release of NO from implanted PU-based sensors can improve glucose sensing by mitigating the FBR, clot formation, and surface biofouling. It is evident that for successful implementation of *in vivo* glucose sensors, further research in sustaining the release of NO more than a few weeks is needed. More chronic animal studies need to be performed where the effects of longer term NO release on the FBR and overall quality of sensing need to be studied.

14.3.3   Wound healing

A wound can technically be defined as a disturbance in the steady state equilibrium between the outermost skin layer (epidermis) and the inner layer (dermis).

The definition of wound includes a wide range of damages to the skin, which can be as simple as a small cut (heals in 2–3 days) or can be as severe as chronic wounds, such as malignant and diabetic foot ulcers, which can take more than 3 months to heal. There are more than one million annual burn injuries reported in the United States and these result in 3500 deaths per year (Horan and Mallonee, 2003; Runyan et al., 2005). A delay in wound healing not only adds to the suffering of affected individuals but also substantially increases the overall medical cost (Fife et al., 2012). Approximately, over $25 billion is spent every year in the United States alone for treatment and caring of chronic wounds (Brem et al., 2007). In fact, the cases of chronic wounds in the United States are as prevalent as cases of heart failure (prevalence rate 2%) (Sen et al., 2009; Berry et al., 2001). Thus, proper wound management can facilitate faster healing and thus reducing the cost of overall treatment.

Chronic wounds are often complicated by bacterial infections, leading to scar tissue formation, and delaying the overall wound healing process. The resistance developed against antibiotics used during such infection also demands alternative approaches for wound management (Stadelmann et al., 1998). A report from the American Diabetes Association suggested that 25% of the diabetic population is likely to face wound healing issues in their lifetime (American Diabetes Association, 2014). Foot ulcers are examples of chronic wounds that, in many cases, may lead to the amputation of a lower limb (Driver et al., 2010). In general, the natural healing of wounds occurs in a complex manner aimed at repairing the dermis of skin or other effected organ tissue and typically involves four phases namely homeostasis, inflammation, proliferation, and remodeling, which overlap in time and do not occur in series (Figure 14.9) (Simon, 2014). Homeostasis involves clot formation and collagen interaction with blood, which stimulates platelets to release
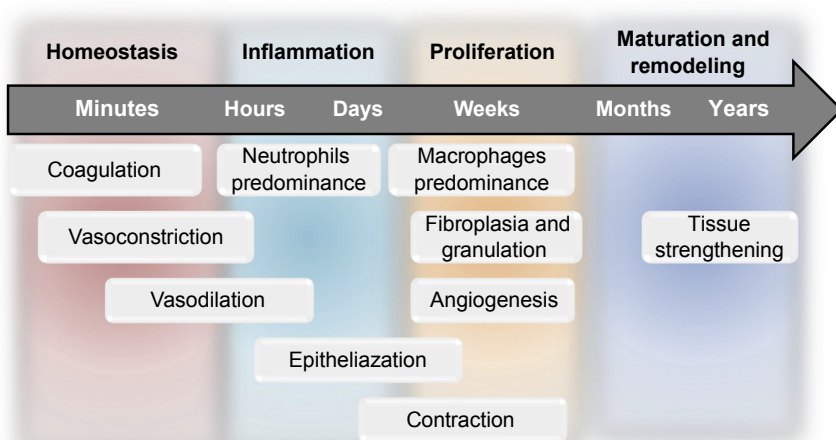
Figure 14.9 Major events that occur during the four phases of wound healing: (a) homeostasis; (b) inflammation; (c) proliferation; and (d) maturation and tissue remodeling.

inflammatory factors (Gabriel et al., 2009). The inflammatory phase involves various events aimed toward preventing microbial infection at the injured site. The onset of the proliferative phase overlaps with the inflammatory phase and is marked by fibroblasts entering the wound site (Falanga, 2004). In addition to active involvement during the inflammatory phase, macrophages also play a crucial role in the proliferative phase (in addition to the inflammatory phase) by contributing to regeneration (Ovchinnikov, 2008; Newton et al., 2004) and formation of extracellular matrix leading to angiogenesis, granular tissue formation, and fibroblast formation (Stashak et al., 2004). The final phase of wound healing is maturation and tissue remodeling, which begins when there is an equilibrium between collagen production and degradation (Greenhalgh, 1998). Depending on the nature of the wound (acute or chronic), the maturation phase may take several days, weeks, or even years (Schultz et al., 2005; Mercandetti and Cohen, 2008). In the case of chronic wounds, the total time taken during wound healing is often unpredictable due to inappropriate progression of the healing process (Midwood et al., 2004; Desmouliere et al., 2005). The complication underlying the wound healing mechanism demands a strategy that can aid the endogenous wound healing mechanism and enhance the overall process. In this regard, the use of smart biomaterials, such as NO-releasing PUs, can improve the chronic wound healing process, prevent associated complexity, and reduce the overall medical cost.

Modern wound dressings include the use of hydrogels, hydrocolloids, hydrofibers, dextranomers, alginates, and PU foam (PUF) (Rusak and Rybak, 2012). Winter et al. first popularized the concept of enhancement of wound healing in a moist environment in the 1960s (Winter, 1962). Hydrophilic PUFs can maintain a moist environment, enhance water vapor permeability, increase adsorption of blood, and prevent the wound bed from drying out, thus enhancing the overall healing process. In 1979, Salisbury et al. reported that PUF accelerates epithelialization of wounds (Salisbury et al., 1979). Ruff et al. used PU dressing-assisted epidermal suturing in a rat model, which prevented wound infection by acting as a barrier to microbes, water, and irritants, and thus helped in minimizing postoperation care (Ruff et al., 2008). Yoo et al. used PUF for wound healing without any significant side effects (Yoo and Kim, 2008).

In multiple studies, NO has been associated with wound healing, thus acting as a central player in the process (Witte and Barbul, 2002; Han et al., 2012; Blecher et al., 2012; Schäffer et al., 1996; Stechmiller et al., 2005). Furthermore, all three NOS enzymes are reported to be associated with the wound healing process (Bulgrin et al., 1995; Frank et al., 1998; Boissel et al., 2003; Luo et al., 2004). The presence of stable derivatives of NO, nitrite and nitrate, in the wound site hints that NO is crucial for collagen synthesis and deposition at the site of injury, ultimately providing mechanical strength to the tissues (Schäffer et al., 1996; Smith and Dunphy, 1991; Schäffer et al., 1997a,b). A marked decrease in collagen deposition and strength has been reported using inhibitors of NOS, indicating the importance of NO in wound healing (Schäffer et al., 1996; Bulgrin et al., 1995). Collagen deposition and fibroblast migration can be accelerated by NO-releasing nanoparticles, thus resulting in faster wound healing in mice (Han et al., 2012).

Chronic burn wounds often lead to sepsis that can be lethal (Macherla et al., 2012). In fact, among all burn victims the microbial infection rate is approximately 30–63% (Holzheimer and Dralle, 2002). Studies have shown that NO possesses antimicrobial activity (Jones et al., 2010; De Groote and Fang, 1995; McMullin et al., 2005; Weller, 2009; de la Fuente-Núñez et al., 2013; Martinez et al., 2009). There are several examples in the literature demonstrating that NO-releasing materials can decrease infection in wound sites. Macherla et al. developed stable NO-releasing nanoparticles (NO-np) and demonstrated its antifungal activity against *Candida albicans in vivo* using a murine burn model (Macherla et al., 2012). To achieve this, nitrite containing hydrogel/glass composite was synthesized using glucose, chitosan, polyethylene glycol, tetramethyl orthosilicate, and sodium nitrite. Nitric oxide was produced by reducing nitrite with thermally generated electrons from glucose within the matrix. In another report, Weller presented NO-containing nanoparticles as antimicrobial and an enhancer of wound healing (Weller, 2009; Martinez et al., 2009). These NO-np were also effective against wound infections caused by *Acinetobacter baumannii*, which is also major cause of nosocomical pneumonia (Mihu et al., 2010). Martinez et al. also showed that nitrite-containing hydrogel/glass used for sustained release of NO-np can be used to accelerate wound healing in mice by reducing the burden of methicillin resistant *Staphylococcus aureus* (MRSA) at cutaneous wound sites. Furthermore, it also resulted in decreased inflammation and collagen degradation caused by MRSA (Martinez et al., 2009). Amadeu et al. showed that GSNO-containing hydrogels when applied topically to a rat cutaneous wound model affected granulation and accelerated wound closure and tissue reepithelialization (Amadeu et al., 2007). Seabra et al. showed that topical application of GSNO donors might promote the local vasodilation in both diabetic and healthy rats (Seabra et al., 2007). A new NO delivery approach has been used in the form of NO-releasing bandages, in which electrospun acrylonitrile-based terpolymers fibers were loaded with diazeniumdiolate functional groups in the polymer backbone (Lowe et al., 2015). These wound dressings were shown to upregulate gene expression associated with NO exposure (JunB, cFOS, enOS, and VEGF) within 30h of application in an excision wound in mice. These results suggested that these bandages accelerate wound healing through NO-induced angiogenesis.

Brisbois et al. used DBHD/N_2O_2-doped PU-based wound patches for preventing bacterial growth in a mouse burn wound model (Brisbois et al., 2014). The NO-releasing patches were optimized using two different PUs with different water uptakes, Tecoflex SG-80A (6.2 ± 0.7 wt%) and Tecophilic SP-60D-20 (22.5 ± 1.1 wt%), for their effects on the NO release from the DBHD/N_2O_2 chemistry. Varying amounts of DBHD/N_2O_2 and PLGA additives were used in this study. PLGA hydrolyzes to form lactic acid and glycolic acid, which results in the acidic pH needed to sustain NO release from DBHD/N_2O_2-doped polymers. The lower water uptake of the Tecoflex SG-80A slows the hydrolysis of the PLGA, resulting in shorter durations of NO release. A mouse model was used to observe the effects of the NO-releasing patches on scald burn wounds that were inoculated with antibiotic-resistant *A. baumannii*. The NO-releasing SG-80A patches were able to significantly reduce the *A. baumannii* wound infection (4 log reduction) after 24h of application (compared to controls). Furthermore, there was a significant reduction in the expression level of transforming growth factor-β, which is responsible for immunosuppression (Varedi et al., 2001) and scar formation (Tredget et al., 1998).

14.3.4   Catheters

A catheter is a thin, flexible tube (typically extruded) of medical grade polymers that have a number of applications in medicine today. Some common materials used for catheters today include silicone, latex, Teflon, and PU. Catheters that are inserted into the body can enable physicians to treat different diseases, or to perform surgical functions in cardiovascular, urological, gastrointestinal, neurovascular, and ophthalmic applications. However, the primary functions of catheters are the removal or supply of fluids and/or to allow access for surgical equipment. Catheters may have multiple lumens (1–4) in a single device, leading to less tissue trauma from catheter insertion sites. These lumens can be used for delivery of other fluids, enable easy access for blood sampling, or control accessories on the catheters such as balloons, which are used to hold catheters in place. The size of catheters, measured using the French (Fr) scale, can vary depending on the application and patient size, where French is three times the outer diameter of the catheter in millimeters.

Indwelling catheters pose as a major risk factor for infections, and are among the most common hospital-acquired infections (Eggimann et al., 2004). It is estimated that up to 150 million intravascular devices are inserted annually in the United States alone, leading to 200,000–400,000 nosocomial blood stream infections each year (Eggimann et al., 2004). There are multiple factors that contribute to the risk of infection, including the method and duration of catheterization, quality of catheter care, and host susceptibility (Platt et al., 1982; Stamm, 1991). The colonization of bacteria can cause infection through a number of pathways; the two most common are colonization at the insertion site by microorganisms that move through the transcutaneous part of the dermal tunnel surrounding the catheter, and colonization in the internal surface and intraluminal surface (Figure 14.10) (Eggimann et al., 2004; O'Grady et al., 2011; Gamer et al., 1988). Bacteria adhering to the catheter surface can form biofilms over time. Biofilms are formed when the bacteria embed themselves within a polysaccharide matrix that protects them from antibiotic administration. To address this problem, antibiotic-coated catheters have been designed, but run a high risk of developing antibiotic-resistant strains of bacteria (Ha and Cho, 2006; Johnson et al., 2006; Parker et al., 2009; Tambyah, 2004). Silver has also been shown to have antibacterial properties and has been incorporated in vascular catheters (Geis, 1999; Boswald et al., 1995; Münstedt, 1999; Guggenbichler, 1999). An even more life-threatening event can occur in vascular catheters when thrombus formed on the catheter is dislodged (van Rooden et al., 2005). This loss clot can form an embolism in the lungs, brain, etc., which causes further medical complications for the patients and may result in patient death. Currently, heparin lock solutions are injected to combat thrombus formation; however, this increases the risk of systematic anticoagulation and heparin allergic responses (Shah and Shah, 2008).

Nitric oxide has been shown to prevent bacterial infection, as well as thrombus formation (Langford et al., 1994; Radomski et al., 1992; Salas et al., 1994). These attributes have the potential to improve the efficacy of catheter devices. Many combinations of polymer chemistries and delivery methods of NO have been investigated (Parker et al., 2009; Tambyah, 2004; van Rooden et al., 2005; Regev-Shoshani et al., 2010; Kishikawa et al., 2013; Ren et al., 2014; Schoenfisch et al., 2000; Harnek et al., 2011).
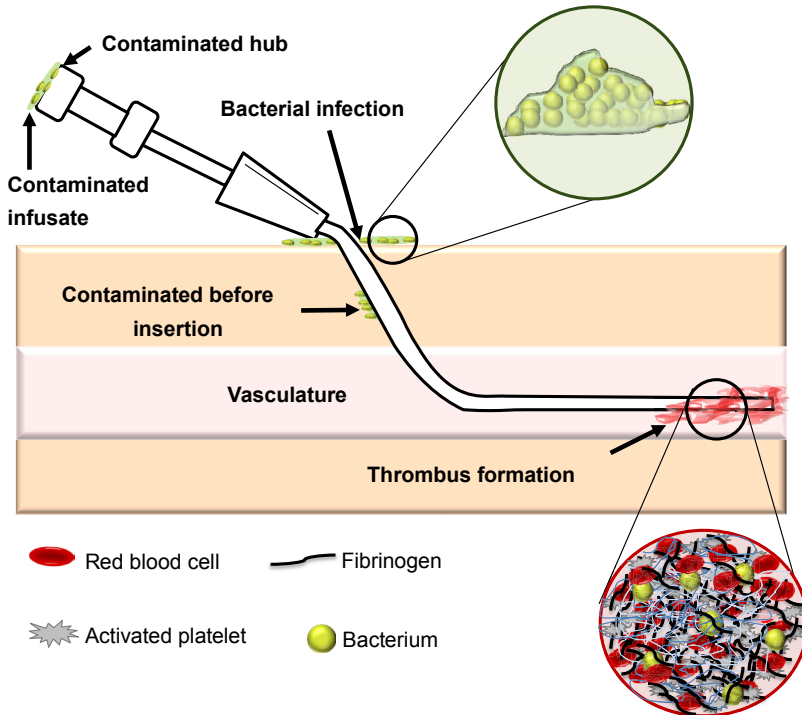
Figure 14.10 Scheme depicting some methods by which catheter-related infections can occur in patients.

Brisbois et al. incorporated SNAP into Elast-eon E2As, a copolymer of poly(dimethylsiloxane), poly(hexamethylene oxide), and MDI (Brisbois et al., 2015). The SNAP and control catheters were prepared by dip coating polymer solutions on stainless steel mandrels. The SNAP-doped E2As catheters had a trilayer configuration, with base and top E2As coats and a 10 wt% SNAP-containing middle active layer (Figure 14.11). These SNAP/E2As catheters were able to withstand the EO sterilization process, retaining $88.8 \pm 0.7\%$ of the original SNAP. The NO lost during sterilization can be attributed to the elevated temperature and exposure to humidity used in the EO sterilization procedure. The SNAP/E2As catheters were able to continually release NO at physiological levels (greater than 0.5×10^{-10} mol/cm^2/min) for up to 20 days. The catheters exhibited a higher NO flux on the first day of soaking due to the initial water uptake of the polymer and slight leaching of SNAP that is on the surface. Even though NO release from the catheters reaches the lower end of endothelial NO release, it continues to reduce intravascular thrombosis and bacterial adhesion. The SNAP and control catheters were implanted in the jugular veins of sheep for 7 days. The SNAP/E2As catheters had significantly less thrombus formation than controls (1.56 ± 0.34 and 5.06 ± 0.64 cm^2, respectively) as well as a 90% reduction in adherence of living bacteria to the surface as compared to control E2As catheters.
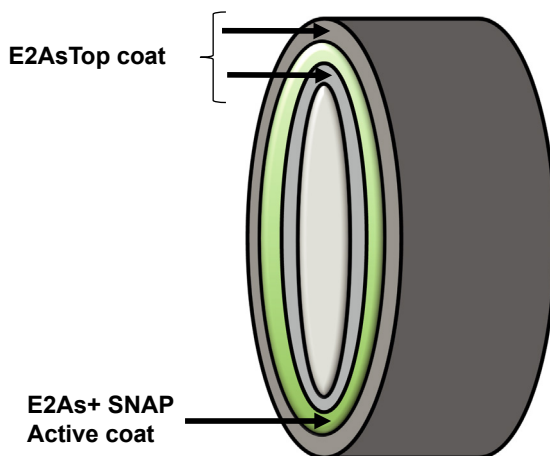
Figure 14.11 Cross section of SNAP-based NO-releasing catheter.

Another approach for improving the hemocompatibility of catheters is the use of NOGen polymers as a coating. A novel strategy where a layer by layer (LbL) deposition method is used to immobilize catalytic organoselenium species was described (Cha and Meyerhoff, 2007; Yang et al., 2008). Organoselenium species have been studied as mimics of glutathione peroxidase, and are selective for decomposing RSNO species (Cha and Meyerhoff, 2007). This LbL method has been used to demonstrate the antithrombic effect of NO generation from immobilized organoselenium species deposited on PU catheters (Yang et al., 2008). This multilayer approach showed the potential to generate NO from endogenous NO precursor, GSNO. The results demonstrated that the LbL coating possessed catalytic activity even after prolonged contact with blood, demonstrating that catalytic sites do not leach. The results suggested that there were no toxic effects in the preliminary tests done on mice for systemic toxicity following ISO 10993-11 and ISO 10993-12 procedures (Yang et al., 2008). Cai et al. demonstrated a similar LbL catalytic coating using another selenium catalyst, carboxyl-ebselen, that was coated on PU catheters (Cai et al., 2011). This coating could also generate physiological levels of NO from RSNOs without catalyst leaching, and also had significant anti-bacterial effect toward *Escherichia coli*.

14.4 Conclusion

To improve the clinical applications of implantable devices, issues associated with their biocompatibility must be addressed. Over the years, there has been a significant advancement in the medical device industry. In this regards, PUs have emerged as a promising synthetic polymer with many potential applications in biomedical science due to their stability, flexibility, tear resistance, abrasion resistance, biocompatibility, hemocompatibility, and flexible processing. However, all blood-contacting devices face the problem of thrombosis and microbial infection. It has been demonstrated that

NO-releasing PUs can improve hemocompatibility by reducing platelet activation and infection. In this chapter we discussed some of the applications of NO-releasing PUs that have been studied, including intravascular glucose sensors, extracorporeal circuits, electrospun fibers, wound healing patches, and catheters. The NO-releasing PUs are helpful in reducing the FBR, thrombosis, and microbial infection associated with biomedical devices. However, clinical applications of NO-releasing PUs have been limited by the potential loss of NO during storage and sterilization. Further addressing issues related to leaching of NO donors, NO shelf life, and sustaining the release of NO will help improve the potential for clinical applications of these materials and greatly improve patient outcomes.

References

Ahanchi, S.S., Tsihlis, N.D., Kibbe, M.R., 2007. The role of nitric oxide in the pathophysiology of intimal hyperplasia. Journal of Vascular Surgery 45, A64–A73.

Amadeu, T.P., Seabra, A.B., de Oliveira, M.G., Costa, A.M., 2007. *S*-nitrosoglutathione-containing hydrogel accelerates rat cutaneous wound repair. Journal of the European Academy of Dermatology and Venereology 21, 629–637.

American Diabetes Association, 2014. National Diabetes Statistics Report.

An, Y., Friedman, R., 2000. Handbook of Bacterial Adhesion: Principles, Methods, and Applications. Humana Press Inc, pp. 1–28 (Chapter 1).

Anderson, J.M., 1993. Mechanisms of inflammation and infection with implanted devices. Cardiovascular Pathology 2, 33–41.

Annich, G.M., Meinhardt, J.P., Mowery, K.A., Ashton, B.A., Merz, S.I., Hirschl, R.B., Meyerhoff, M.E., Bartlett, R.H., 2000. Reduced platelet activation and thrombosis in extracorporeal circuits coated with nitric oxide release polymers. Critical Care Medicine 28, 915–920.

Balaconis, M.K., Luo, Y., Clark, H.A., 2015. Glucose-sensitive nanofiber scaffolds with an improved sensing design for physiological conditions. Analyst 140, 716–723.

Ballesteros, D., Martínez, Ó., Gómez-Casero, R.B., Parra, C.M., Matamala, B.L., Estébanez, B., Chana, M., 2014. Continuous tissue glucose monitoring correlates with measurement of intermittent capillary glucose in patients with distributive shock. Medicina Intensiva (14), 00213–00217.

Bartlett, R.H., 2005. Extracorporeal life support: history and new directions. Seminars in Perinatology, 2–7.

Batchelor, M.M., Reoma, S.L., Fleser, P.S., Nuthakki, V.K., Callahan, R.E., Shanley, C.J., Politis, J.K., Elmore, J., Merz, S.I., Meyerhoff, M.E., 2003. More lipophilic dialkyldiamine-based diazeniumdiolates: synthesis, characterization, and application in preparing thromboresistant nitric oxide release polymeric coatings. Journal of Medicinal Chemistry 46, 5153–5161.

Berry, C., Murdoch, D.R., McMurray, J.J., 2001. Economics of chronic heart failure. European Journal of Heart Failure 3, 283–291.

Blecher, K., Martinez, L.R., Tuckman-Vernon, C., Nacharaju, P., Schairer, D., Chouake, J., Friedman, J.M., Alfieri, A., Guha, C., Nosanchuk, J.D., 2012. Nitric oxide-releasing nanoparticles accelerate wound healing in NOD-SCID mice. Nanomedicine: Nanotechnology, Biology and Medicine 8, 1364–1371.

Boissel, J.-P., Ohly, D., Bros, M., Gödtel-Armbrust, U., Förstermann, U., Frank, S., 2003. The neuronal nitric oxide synthase is upregulated in mouse skin repair and in response to epidermal growth factor in human HaCaT keratinocytes. Journal of Investigative Dermatology 123, 132–139.

Boretos, J.W., Pierce, W.S., 1968. Segmented polyurethane: a polyether polymer. An initial evalution for biomedical applications. Journal of Biomedical Materials Research 2, 121–130.

Boswald, M., Girisch, M., Greil, J., Spies, T., Stehr, K., Krall, T., Guggenbichler, J.-P., 1995. Antimicrobial activity and biocompatibility of polyurethane and silicone catheters containing low concentrations of silver: a new perspective in prevention of polymer-associated foreign-body-infections. Zentralblatt für Bakteriologie 283, 187–200.

Bota, P., Collie, A., Puolakkainen, P., Vernon, R.B., Sage, E.H., Ratner, B.D., Stayton, P.S., 2010. Biomaterial topography alters healing in vivo and monocyte/macrophage activation in vitro. Journal of Biomedical Materials Research Part A 95, 649–657.

Brem, H., Stojadinovic, O., Diegelmann, R.F., Entero, H., Lee, B., Pastar, I., Golinko, M., Rosenberg, H., Tomic-Canic, M., 2007. Molecular markers in patients with chronic wounds to guide surgical debridement. Molecular Medicine 13, 30.

Brisbois, E.J., Handa, H., Major, T.C., Bartlett, R.H., Meyerhoff, M.E., 2013. Long-term nitric oxide release and elevated temperature stability with *S*-nitroso-*N*-acetylpenicillamine (SNAP)-doped Elast-eon E2As polymer. Biomaterials 34, 6957–6966.

Brisbois, E.J., Bayliss, J., Wu, J., Major, T.C., Xi, C., Wang, S.C., Bartlett, R.H., Handa, H., Meyerhoff, M.E., 2014. Optimized polymeric film-based nitric oxide delivery inhibits bacterial growth in a mouse burn wound model. Acta Biomaterialia 10, 4136–4142.

Brisbois, E.J., Davis, R.P., Jones, A.M., Major, T.C., Bartlett, R.H., Meyerhoff, M.E., Handa, H., 2015. Reduction in thrombosis and bacterial adhesion with 7 day implantation of *S*-nitroso-*N*-acetylpenicillamine (SNAP)-doped Elast-eon E2As catheters in sheep. Journal of Materials Chemistry B 3 (8), 1639–1645.

Bulgrin, J., Shabani, M., Chakravarthy, D., Smith, D., 1995. Nitric oxide synthesis is suppressed in steroid-impaired and diabetic wounds. Wounds 7, 48–57.

Cai, T.B., Wang, P.G., Holder, A.A., 2005. NO and NO donors. In: Pg, W., Tb, C., Taniguchi, N. (Eds.), Nitric Oxide Donors for Pharmaceutical and Biological Applications. Wiley VCH, Weinheim.

Cai, W., Wu, J., Xi, C., Ashe III, A.J., Meyerhoff, M.E., 2011. Carboxyl-ebselen-based layer-by-layer films as potential antithrombotic and antimicrobial coatings. Biomaterials 32, 7774–7784.

Carpenter, A.W., Schoenfisch, M.H., 2012. Nitric oxide release: part II. Therapeutic applications. Chemical Society Reviews 41, 3742–3752.

Centers for Disease Control, 2014. National Diabetes Statistics Report: Estimates of Diabetes and its Burden in the United States, 2014. US Department of Health and Human Services, Atlanta, GA.

Cerami, A., Vlassara, H., Brownlee, M., 1987. Glucose and Aging. WH Freeman.

Cha, W., Meyerhoff, M.E., 2007. Catalytic generation of nitric oxide from *S*-nitrosothiols using immobilized organoselenium species. Biomaterials 28, 19–27.

Chen, A.F., 2005. Nitric oxide: a newly discovered function on wound healing. Acta Pharmacologica Sinica 26, 259–264.

Cheyne, E., Kerr, D., 2002. Making 'sense' of diabetes: using a continuous glucose sensor in clinical practice. Diabetes/Metabolism Research and Reviews 18, S43–S48.

Costerton, J.W., Lewandowski, Z., Caldwell, D.E., Korber, D.R., Lappin-Scott, H.M., 1995. Microbial biofilms. Annual Reviews in Microbiology 49, 711–745.

Cozzens, D., Luk, A., Ojha, U., Ruths, M., Faust, R., 2011. Surface characterization and protein interactions of segmented polyisobutylene-based thermoplastic polyurethanes. Langmuir 27, 14160–14168.

Daley, J., Shearer, J., Mastrofrancesco, B., Caldwell, M., 1990. Glucose metabolism in injured tissue: a longitudinal study. Surgery 107, 187–192.

Darlington, L., Ramsey, N., Mansfield, J., 1986. Placebo-controlled, blind study of dietary manipulation therapy in rheumatoid arthritis. The Lancet 327, 236–238.

Davies, K.M., Wink, D.A., Saavedra, J.E., Keefer, L.K., 2001. Chemistry of the diazeniumdiolates. 2. Kinetics and mechanism of dissociation to nitric oxide in aqueous solution. Journal of the American Chemical Society 123, 5473–5481.

Davis, F.J., Mitchell, G.R., 2008. Polyurethane based materials with applications in medical devices. In: Bio-Materials and Prototyping Applications in Medicine. Springer, US, pp. 27–48.

Dernehl, C.U., 1966. Health hazards associated with polyurethane foams. Journal of Occupational and Environmental Medicine 8, 59–62.

Desmouliere, A., Chaponnier, C., Gabbiani, G., 2005. Tissue repair, contraction, and the myofibroblast. Wound Repair and Regeneration 13, 7–12.

Dicks, A., Swift, H., Williams, D., Butler, A., Alsadoni, H., Cox, B., 1996. Identification of Cu$^+$ as the effective reagent in nitric oxide formation from *S*-nitrosothiols (RSNO). Journal of the Chemical Society, Perkin Transactions 2, 481–487.

Driver, V.R., Fabbi, M., Lavery, L.A., Gibbons, G., 2010. The costs of diabetic foot: the economic case for the limb salvage team. Journal of Vascular Surgery 52, 17S–22S.

Eggimann, P., Sax, H., Pittet, D., 2004. Catheter-related infections. Microbes and Infection 6, 1033–1042.

Falanga, V., 2004. The chronic wound: impaired healing and solutions in the context of wound bed preparation. Blood Cells, Molecules, and Diseases 32, 88–94.

Feldman, P.L., 1993. The surprising life of nitric oxide. Chemical and Engineering News 71, 26–38.

Fife, C.E., Carter, M.J., Walker, D., Thomson, B., 2012. Wound care outcomes and associated cost among patients treated in US outpatient wound centers: data from the US Wound Registry. Wounds 24, 10–17.

Frank, S., Madlener, M., Pfeilschifter, J., Werner, S., 1998. Induction of inducible nitric oxide synthase and its corresponding tetrahydrobiopterin-cofactor-synthesizing enzyme GTP-cyclohydrolase I during cutaneous wound repair. Journal of Investigative Dermatology 111, 1058–1064.

Frost, M.C., Meyerhoff, M.E., 2002. Implantable chemical sensors for real-time clinical monitoring: progress and challenges. Current Opinion in Chemical Biology 6, 633–641.

Frost, M.C., Meyerhoff, M.E., 2004. Controlled photoinitiated release of nitric oxide from polymer films containing *S*-nitroso-*N*-acetyl-DL-penicillamine derivatized fumed silica filler. Journal of the American Chemical Society 126, 1348–1349.

Frost, M., Meyerhoff, M.E., 2006. In vivo chemical sensors: tackling biocompatibility. Analytical Chemistry 78, 7370–7377.

Frost, M.C., Reynolds, M.M., Meyerhoff, M.E., 2005. Polymers incorporating nitric oxide releasing/generating substances for improved biocompatibility of blood-contacting medical devices. Biomaterials 26, 1685–1693.

Frost, M.C., Wolf, A.K., Meyerhoff, M.E., 2013. In vivo sensors for continuous monitoring of blood gases, glucose, and lactate: biocompatibility challenges and potential solutions. Detection Challenges in Clinical Diagnostics 2, 129.

Furth, A., Harding, J., 1989. Why Sugar Is Bad for You? New Scientist, United Kingdom.

Fux, C., Costerton, J., Stewart, P., Stoodley, P., 2005. Survival strategies of infectious biofilms. Trends in Microbiology 13, 34–40.

Gabriel, A., Mussman, J., Rosenberg, L., de la Torre, J., 2009. Wound Healing and Growth Factors. University School of Medicine, pp. 1–11.

Gaffney, A.M., Wildhirt, S.M., Griffin, M.J., Annich, G.M., Radomski, M.W., 2010. Extracorporeal life support. BMJ 341, 982–986.

Gamer, J., Jarvis, W., Emori, T., Horan, T., Hughes, J., 1988. CDC definitions for nosocomial infections. American Journal of Infection Control 16, 128–140.

Geis, D.-B.C., 1999. Reduced rates of catheter-associated infection by use of a new silver-impregnated central venous catheter. Infection 27, S56–S60.

Gifford, R., Batchelor, M.M., Lee, Y., Gokulrangan, G., Meyerhoff, M.E., Wilson, G.S., 2005. Mediation of in vivo glucose sensor inflammatory response via nitric oxide release. Journal of Biomedical Materials Research Part A 75, 755–766.

Girardi, N.L., Shaywitz, S.E., Shaywitz, B.A., Marchione, K., Fleischman, S.J., Jones, T.W., Tamborlane, W.V., 1995. Blunted catecholamine responses after glucose ingestion in children with attention deficit disorder. Pediatric Research 38, 539–542.

Gorbet, M.B., Sefton, M.V., 2004. Biomaterial-associated thrombosis: roles of coagulation factors, complement, platelets and leukocytes. Biomaterials 25, 5681–5703.

Greenhalgh, D.G., 1998. The role of apoptosis in wound healing. The International Journal of Biochemistry & Cell Biology 30, 1019–1030.

de Groote, M.A., Fang, F.C., 1995. NO inhibitions: antimicrobial properties of nitric oxide. Clinical Infectious Diseases 21, S162–S165.

Guggenbichler, J.-P., 1999. The Erlanger silver catheter: in vitro results for antimicrobial activity. Infection 27, S24–S29.

Ha, U., Cho, Y.-H., 2006. Catheter-associated urinary tract infections: new aspects of novel urinary catheters. International Journal of Antimicrobial Agents 28, 485–490.

Hakim, T.S., Sugimori, K., Camporesi, E.M., Anderson, G., 1996. Half-life of nitric oxide in aqueous solutions with and without haemoglobin. Physiological Measurement 17, 267–277.

Hall-Stoodley, L., Costerton, J.W., Stoodley, P., 2004. Bacterial biofilms: from the natural environment to infectious diseases. Nature Reviews Microbiology 2, 95–108.

Halpenny, G.M., Mascharak, P.K., 2010. Emerging antimicrobial applications of nitric oxide (NO) and NO-releasing materials. Anti-Infective Agents in Medicinal Chemistry (Formerly Current Medicinal Chemistry-Anti-Infective Agents) 9, 187–197.

Han, G., Nguyen, L.N., Macherla, C., Chi, Y., Friedman, J.M., Nosanchuk, J.D., Martinez, L.R., 2012. Nitric oxide–releasing nanoparticles accelerate wound healing by promoting fibroblast migration and collagen deposition. The American Journal of Pathology 180, 1465–1473.

Handa, H., Brisbois, E.J., Major, T.C., Refahiyat, L., Amoako, K.A., Annich, G.M., Bartlett, R.H., Meyerhoff, M.E., 2013. In vitro and in vivo study of sustained nitric oxide release coating using diazeniumdiolate-doped poly(vinyl chloride) matrix with poly(lactide-*co*-glycolide) additive. Journal of Materials Chemistry B 1, 3578–3587.

Handa, H., Major, T.C., Brisbois, E.J., Amoako, K.A., Meyerhoff, M.E., Bartlett, R.H., 2014. Hemocompatibility comparison of biomedical grade polymers using rabbit thrombogenicity model for preparing nonthrombogenic nitric oxide releasing surfaces. Journal of Materials Chemistry B 2, 1059–1067.

Harnek, J., Zoucas, E., de Sá, V.P., Ekblad, E., Arner, A., Stenram, U., 2011. Intimal hyperplasia in balloon dilated coronary arteries is reduced by local delivery of the NO donor, SIN-1 via a cGMP-dependent pathway. BMC Cardiovascular Disorders 11, 30.

Harris, L., Tosatti, S., Wieland, M., Textor, M., Richards, R., 2004. *Staphylococcus aureus* adhesion to titanium oxide surfaces coated with non-functionalized and peptide-functionalized poly(L-lysine)-grafted-poly(ethylene glycol) copolymers. Biomaterials 25, 4135–4148.

Hayashi, Y., Sawa, Y., Nishimura, M., Chang, J.-C., Amemiya, A., Kagisaki, K., Taketani, S., Yamaguchi, T., Hirata, N., Ohtake, S., 1998. Nitric oxide gas infusion to the oxygenator enhances the biocompatibility of heparin coated extracorporeal bypass circuits. ASAIO 44, M456–M461.

Heller, A., Feldman, B., 2008. Electrochemical glucose sensors and their applications in diabetes management. Chemical Reviews 108, 2482–2505.

Hendricks, S.K., Kwok, C., Shen, M., Horbett, T.A., Ratner, B.D., Bryers, J.D., 2000. Plasma-deposited membranes for controlled release of antibiotic to prevent bacterial adhesion and biofilm formation. Journal of Biomedical Materials Research 50, 160–170.

Hetrick, E.M., Schoenfisch, M.H., 2006. Reducing implant-related infections: active release strategies. Chemical Society Reviews 35, 780–789.

Hetrick, E.M., Prichard, H.L., Klitzman, B., Schoenfisch, M.H., 2007. Reduced foreign body response at nitric oxide-releasing subcutaneous implants. Biomaterials 28, 4571–4580.

Holmes, A.J., Williams, D.L.H., 2000. Reaction of ascorbic acid with *S*-nitrosothiols: clear evidence for two distinct reaction pathways. Journal of the Chemical Society, Perkin Transactions 2, 1639–1644.

Holzheimer, R., Dralle, H., 2002. Management of mycoses in surgical patients–review of the literature. European Journal of Medical Research 7, 200–226.

Horan, J.M., Mallonee, S., 2003. Injury surveillance. Epidemiologic Reviews 25, 24–42.

Horbett, T.A., 1993. Principles underlying the role of adsorbed plasma proteins in blood interactions with foreign materials. Cardiovascular Pathology 2, 137–148.

Hou, Y., Janczuk, A., Wang, P., 1999. Current trends in the development of nitric oxide donors. Current Pharmaceutical Design 5, 417–442.

Huang, X., Li, S., Davis, E., Leduc, C., Ravussin, Y., Cai, H., Song, B., Li, D., Accili, D., Leibel, R., 2013. A MEMS differential viscometric sensor for affinity glucose detection in continuous glucose monitoring. Journal of Micromechanics and Microengineering 23, 055020.

Hwang, S., Meyerhoff, M.E., 2008. Polyurethane with tethered copper (II)–cyclen complex: preparation, characterization and catalytic generation of nitric oxide from *S*-nitrosothiols. Biomaterials 29, 2443–2452.

Ihno, T., Nakagawa, T., Furukawa, H., Shimizu, K., Egi, K., Maemura, T., Motomiya, T., 1997. Various problems during long-term percutaneous cardiopulmonary support. Artificial Organs 21, 766–771.

Jen, M.C., Serrano, M.C., van lith, R., Ameer, G.A., 2012. Polymer-based nitric oxide therapies: recent insights for biomedical applications. Advanced Functional Materials 22, 239–260.

Johnson, J.R., Kuskowski, M.A., Wilt, T.J., 2006. Systematic review: antimicrobial urinary catheters to prevent catheter-associated urinary tract infection in hospitalized patients. Annals of Internal Medicine 144, 116–126.

Jones, M.L., Ganopolsky, J.G., Labbé, A., Wahl, C., Prakash, S., 2010. Antimicrobial properties of nitric oxide and its application in antimicrobial formulations and medical devices. Applied Microbiology and Biotechnology 88, 401–407.

Ju, Y.M., Yu, B., West, L., Moussy, Y., Moussy, F., 2010. A novel porous collagen scaffold around an implantable biosensor for improving biocompatibility. II. Long-term in vitro/in vivo sensitivity characteristics of sensors with NDGA- or GA-crosslinked collagen scaffolds. Journal of Biomedical Materials Research Part A 92, 650–658.

Jun, H.-W., Taite, L.J., West, J.L., 2005. Nitric oxide-producing polyurethanes. Biomacromolecules 6, 838–844.

Keh, D., Gerlach, M., Kurer, I., Spielmann, S., Kerner, T., Busch, T., Hansen, R., Falke, K., Gerlach, H., 1999. Nitric oxide diffusion across membrane lungs protects platelets during simulated extracorporeal circulation. European Journal of Clinical Investigation 29, 344–350.

Kim, J., Saravanakumar, G., Choi, H.W., Park, D., Kim, W.J., 2014. A platform for nitric oxide delivery. Journal of Materials Chemistry B 2, 341–356.

Kishikawa, H., Ebberyd, A., Römling, U., Brauner, A., Lüthje, P., Lundberg, J.O., Weitzberg, E., 2013. Control of pathogen growth and biofilm formation using a urinary catheter that releases antimicrobial nitrogen oxides. Free Radical Biology and Medicine 65, 1257–1264.

Klonoff, D.C., 2005a. Continuous glucose monitoring roadmap for 21st century diabetes therapy. Diabetes Care 28, 1231–1239.

Klonoff, D.C., 2005b. A review of continuous glucose monitoring technology. Diabetes Technology & Therapeutics 7, 770–775.

Knowles, R.G., Moncada, S., 1994. Nitric oxide synthases in mammals. Biochemical Journal 298, 249.

Koh, A., Nichols, S.P., Schoenfisch, M.H., 2011a. Glucose sensor membranes for mitigating the foreign body response. Journal of Diabetes Science and Technology 5, 1052–1059.

Koh, A., Riccio, D.A., Sun, B., Carpenter, A.W., Nichols, S.P., Schoenfisch, M.H., 2011b. Fabrication of nitric oxide-releasing polyurethane glucose sensor membranes. Biosensors and Bioelectronics 28, 17–24.

Koh, A., Lu, Y., Schoenfisch, M.H., 2013. Fabrication of nitric oxide-releasing porous polyurethane membranes-coated needle-type implantable glucose biosensors. Analytical Chemistry 85, 10488–10494.

Koschwanez, H.E., Reichert, W.M., 2007. In vitro, in vivo and post explantation testing of glucose-detecting biosensors: current methods and recommendations. Biomaterials 28, 3687–3703.

Koschwanez, H., Yap, F., Klitzman, B., Reichert, W., 2008. In vitro and in vivo characterization of porous poly-L-lactic acid coatings for subcutaneously implanted glucose sensors. Journal of Biomedical Materials Research Part A 87, 792–807.

Kubiak, T., Hermanns, N., Schreckling, H., Kulzer, B., Haak, T., 2004. Assessment of hypoglycaemia awareness using continuous glucose monitoring. Diabetic Medicine 21, 487–490.

Kuo, P.C., Schroeder, R.A., 1995. The emerging multifaceted roles of nitric oxide. Annals of Surgery 221, 220.

de La Fuente-Núñez, C., Reffuveille, F., Fairfull-Smith, K.E., Hancock, R.E., 2013. Effect of nitroxides on swarming motility and biofilm formation, multicellular behaviors in *Pseudomonas aeruginosa*. Antimicrobial Agents and Chemotherapy 57, 4877–4881.

Langford, E., Brown, A., de belder, A., Smith, R., Martin, J., Wainwright, R., Thomas, M., Radomski, M., Moncada, S., 1994. Inhibition of platelet activity by *S*-nitrosoglutathione during coronary angioplasty. The Lancet 344, 1458–1460.

Lee, A.T., Cerami, A., 1992. Role of glycation in aging. Annals of the New York Academy of Sciences 663, 63–70.

Lindner, E., Cosofret, V., Ufer, S., Buck, R., Kao, W., Neuman, M., Anderson, J., 1994. Ion-selective membranes with low plasticizer content: electroanalytical characterization and biocompatibility studies. Journal of Biomedical Materials Research 28, 591–601.

Lowe, A., Bills, J., Verma, R., Lavery, L., Davis, K., Balkus, K., 2015. Electrospun nitric oxide releasing bandage with enhanced wound healing. Acta Biomaterialia 13, 121–130.

Luo, J.-D., Wang, Y.-Y., Fu, W.-L., Wu, J., Chen, A.F., 2004. Gene therapy of endothelial nitric oxide synthase and manganese superoxide dismutase restores delayed wound healing in type 1 diabetic mice. Circulation 110, 2484–2493.

Lyman, D.J., Kwan-Gett, C., Zwart, H.H., Bland, A., Eastwood, N., Kawai, J., Kolff, W., 1971. The development and implantation of a polyurethane hemispherical artificial heart. ASAIO 17, 456–463.

Ma, Y., Li, Y., Chiriboga, D.E., Olendzki, B.C., Hebert, J.R., Li, W., Leung, K., Hafner, A.R., Ockene, I.S., 2006. Association between carbohydrate intake and serum lipids. Journal of the American College of Nutrition 25, 155–163.

Macherla, C., Sanchez, D.A., Ahmadi, M.S., Vellozzi, E.M., Friedman, A.J., Nosanchuk, J.D., Martinez, L.R., 2012. Nitric oxide releasing nanoparticles for treatment of *Candida albicans* burn infections. Frontiers in Microbiology 3.

Major, T.C., Brant, D.O., Reynolds, M.M., Bartlett, R.H., Meyerhoff, M.E., Handa, H., Annich, G.M., 2010. The attenuation of platelet and monocyte activation in a rabbit model of extracorporeal circulation by a nitric oxide releasing polymer. Biomaterials 31, 2736–2745.

Major, T.C., Brant, D.O., Burney, C.P., Amoako, K.A., Annich, G.M., Meyerhoff, M.E., Handa, H., Bartlett, R.H., 2011. The hemocompatibility of a nitric oxide generating polymer that catalyzes *S*-nitrosothiol decomposition in an extracorporeal circulation model. Biomaterials 32, 5957–5969.

Major, T.C., Handa, H., Brisbois, E.J., Reynolds, M.M., Annich, G.M., Meyerhoff, M.E., Bartlett, R.H., 2013. The mediation of platelet quiescence by NO-releasing polymers via cGMP-induced serine 239 phosphorylation of vasodilator-stimulated phosphoprotein. Biomaterials 34, 8086–8096.

Major, T.C., Brisbois, E.J., Jones, A.M., Zanetti, M.E., Annich, G.M., Bartlett, R.H., Handa, H., 2014a. The effect of a polyurethane coating incorporating both a thrombin inhibitor and nitric oxide on hemocompatibility in extracorporeal circulation. Biomaterials 35, 7271–7285.

Major, T.C., Handa, H., Annich, G.M., Bartlett, R.H., 2014b. Development and hemocompatibility testing of nitric oxide releasing polymers using a rabbit model of thrombogenicity. Journal of Biomaterials Applications 29, 479–501.

Marín, J., Rodríguez-Martínez, M.A., 1997. Role of vascular nitric oxide in physiological and pathological conditions. Pharmacology & Therapeutics 75, 111–134.

Martinez, L.R., Han, G., Chacko, M., Mihu, M.R., Jacobson, M., Gialanella, P., Friedman, A.J., Nosanchuk, J.D., Friedman, J.M., 2009. Antimicrobial and healing efficacy of sustained release nitric oxide nanoparticles against *Staphylococcus aureus* skin infection. Journal of Investigative Dermatology 129, 2463–2469.

Mcmullin, B.B., Chittock, D.R., Roscoe, D.L., Garcha, H., Wang, L., Miller, C.C., 2005. The antimicrobial effect of nitric oxide on the bacteria that cause nosocomial pneumonia in mechanically ventilated patients in the intensive care unit. Respiratory Care 50, 1451–1456.

Mellgren, K., Friberg, L.G., Mellgren, G., Hedner, T., Wennmalm, Å., Wadenvik, H., 1996. Nitric oxide in the oxygenator sweep gas reduces platelet activation during experimental perfusion. The Annals of Thoracic Surgery 61, 1194–1198.

Mellgren, M., Lundin, M., Wennmalm, M., Wadenvik, M., 1998. Effect of nitric oxide gas on platelets during open heart operations. The Annals of Thoracic Surgery 65, 1335–1341.

Menajovsky, L.B., 2005. Heparin-induced thrombocytopenia: clinical manifestations and management strategies. The American Journal of Medicine 118, 21–30.

Mercandetti, M., Cohen, A.J., 2008. Wound Healing: Healing and Repair. eMedicine WebMD, http://emedicine.medscape.com/article/1298129-overview#showall.

Meyerhoff, C., Bischof, F., Sternberg, F., Zier, H., Pfeiffer, E., 1992. On line continuous monitoring of subcutaneous tissue glucose in men by combining portable glucosensor with microdialysis. Diabetologia 35, 1087–1092.

Meyerhoff, C., Bischof, F., Mennel, F., Sternberg, F., Pfeiffer, E., 1993. Use of the microdialysis technique in the monitoring of subcutaneous tissue glucose concentration. The International Journal of Artificial Organs 16, 268–275.

Meyerhoff, C., Mennel, F., Bischof, F., Sternberg, F., Pfeiffer, E., 1994. Combination of microdialysis and glucose sensor for continuous on line measurement of the subcutaneous glucose concentration: theory and practical application. Hormone and Metabolic Research 26, 538–543.

Midwood, K.S., Williams, L.V., Schwarzbauer, J.E., 2004. Tissue repair and the dynamics of the extracellular matrix. The International Journal of Biochemistry & Cell Biology 36, 1031–1037.

Mihu, M.R., Sandkovsky, U., Han, G., Friedman, J.M., Nosanchuk, J.D., Martinez, L.R., 2010. The use of nitric oxide releasing nanoparticles as a treatment against *Acinetobacter baumannii* in wound infections. Virulence 1, 62–67.

Mortellaro, M., Dehennis, A., 2014. Performance characterization of an abiotic and fluorescent-based continuous glucose monitoring system in patients with type 1 diabetes. Biosensors and Bioelectronics 61, 227–231.

Moussy, F., Harrison, D., Rajotte, R., 1994. A miniaturized Nafion-based glucose sensor: in vitro and in vivo evaluation in dogs. The International Journal of Artificial Organs 17, 88–94.

Mowery, K.A., Schoenfisch, M.H., Saavedra, J.E., Keefer, L.K., Meyerhoff, M.E., 2000. Preparation and characterization of hydrophobic polymeric films that are thromboresistant via nitric oxide release. Biomaterials 21, 9–21.

Münstedt, H., 1999. Determination of the silver ion release from polyurethanes enriched with silver. Infection 27, S46–S48.

Newton, P., Watson, J., Wolowacz, R., Wood, E., 2004. Macrophages restrain contraction of an in vitro wound healing model. Inflammation 28, 207–214.

Nichols, S.P., Le, N.N., Klitzman, B., Schoenfisch, M.H., 2011. Increased in vivo glucose recovery via nitric oxide release. Analytical Chemistry 83, 1180–1184.

Niu, X., Smith, C.W., Kubes, P., 1994. Intracellular oxidative stress induced by nitric oxide synthesis inhibition increases endothelial cell adhesion to neutrophils. Circulation Research 74, 1133–1140.

O'grady, N.P., Alexander, M., Burns, L.A., Dellinger, E.P., Garland, J., Heard, S.O., Lipsett, P.A., Masur, H., Mermel, L.A., Pearson, M.L., 2011. Guidelines for the prevention of intravascular catheter-related infections. American Journal of Infection Control 39, S1–S34.

Oh, B.K., Meyerhoff, M.E., 2003. Spontaneous catalytic generation of nitric oxide from *S*-nitrosothiols at the surface of polymer films doped with lipophilic copper(II) complex. Journal of the American Chemical Society 125, 9552–9553.

Oh, B.K., Robbins, M.E., Nablo, B.J., Schoenfisch, M.H., 2005. Miniaturized glucose biosensor modified with a nitric oxide-releasing xerogel microarray. Biosensors and Bioelectronics 21, 749–757.

O'toole, G., Kaplan, H.B., Kolter, R., 2000. Biofilm formation as microbial development. Annual Reviews in Microbiology 54, 49–79.

Ovchinnikov, D.A., 2008. Macrophages in the embryo and beyond: much more than just giant phagocytes. Genesis 46, 447–462.

Paden, M.L., Conrad, S.A., Rycus, P.T., Thiagarajan, R.R., 2013. Extracorporeal life support organization registry report 2012. ASAIO Journal 59, 202–210.

Parker, D., Callan, L., Harwood, J., Thompson, D.L., Wilde, M., Gray, M., 2009. Nursing interventions to reduce the risk of catheter-associated urinary tract infection. Part 1: catheter selection. Journal of Wound Ostomy & Continence Nursing 36, 23–34.

Parsek, M.R., Singh, P.K., 2003. Bacterial biofilms: an emerging link to disease pathogenesis. Annual Reviews in Microbiology 57, 677–701.

Platt, R., Polk, B.F., Murdock, B., Rosner, B., 1982. Mortality associated with nosocomial urinary-tract infection. New England Journal of Medicine 307, 637–642.

Puiu, S.C., Zhou, Z., White, C.C., Neubauer, L.J., Zhang, Z., Lange, L.E., Mansfield, J.A., Meyerhoff, M.E., Reynolds, M.M., 2009. Metal ion-mediated nitric oxide generation from polyurethanes via covalently linked copper(II)-cyclen moieties. Journal of Biomedical Materials Research Part B: Applied Biomaterials 91, 203–212.

Radomski, M.W., Moncada, S., 1993a. The Biological and Pharmacological Role of Nitric Oxide in Platelet Function. Mechanisms of Platelet Activation and Control. Springer, US, pp. 251–264.

Radomski, M.W., Moncada, S., 1993b. Regulation of vascular homeostasis by nitric oxide. Thrombosis and Haemostasis 70, 36–41.

Radomski, M.W., Palmer, R.M., Moncada, S., 1987. The role of nitric oxide and cGMP in platelet adhesion to vascular endothelium. Biochemical and Biophysical Research Communications 148, 1482–1489.

Radomski, M.W., Rees, D.D., Dutra, A., Moncada, S., 1992. S-nitroso-glutathione inhibits platelet activation in vitro and in vivo. British Journal of Pharmacology 107, 745–749.

Ratner, B.D., 2002. Reducing capsular thickness and enhancing angiogenesis around implant drug release systems. Journal of Controlled Release 78, 211–218.

Regev-Shoshani, G., Ko, M., Miller, C., Av-Gay, Y., 2010. Slow release of nitric oxide from charged catheters and its effect on biofilm formation by *Escherichia coli*. Antimicrobial Agents and Chemotherapy 54, 273–279.

Ren, H., Colletta, A., Koley, D., Wu, J., Xi, C., Major, T.C., Bartlett, R.H., Meyerhoff, M.E., 2014. Thromboresistant/anti-biofilm catheters via electrochemically modulated nitric oxide release. Bioelectrochemistry 104, 10–16.

Reynolds, M.M., Annich, G.M., 2011. The artificial endothelium. Organogenesis 7, 42–49.

Reynolds, M.M., Hrabie, J.A., Oh, B.K., Politis, J.K., Citro, M.L., Keefer, L.K., Meyerhoff, M.E., 2006. Nitric oxide releasing polyurethanes with covalently linked diazeniumdiolated secondary amines. Biomacromolecules 7, 987–994.

Riccio, D.A., Schoenfisch, M.H., 2012. Nitric oxide release: part I. Macromolecular scaffolds. Chemical Society Reviews 41, 3731–3741.

Robinson, T., Kickler, T.S., Walker, L.K., Ness, P., Bell, W., 1993. Effect of extracorporeal membrane oxygenation on platelets in newborns. Critical Care Medicine 21, 1029–1034.

Rojas, I.A., Slunt, J.B., Grainger, D.W., 2000. Polyurethane coatings release bioactive antibodies to reduce bacterial adhesion. Journal of Controlled Release 63, 175–189.

van Rooden, C.J., Schippers, E.F., Barge, R.M., Rosendaal, F.R., Guiot, H.F., van der Meer, F.J., Meinders, A.E., Huisman, M.V., 2005. Infectious complications of central venous catheters increase the risk of catheter-related thrombosis in hematology patients: a prospective study. Journal of Clinical Oncology 23, 2655–2660.

Rouby, J.J., 2003. The nose, nitric oxide, and paranasal sinuses: the outpost of pulmonary anti-infectious defenses? American Journal of Respiratory and Critical Care Medicine 168, 265–266.

Ruff, C.A., Vujevich, J.J., Goldberg, L.H., 2008. Polyurethane dressing assisted epidermal suturing minimizes postoperative wound care. Journal of Drugs in Dermatology 7, 675–677.

Runyan, C.W., Casteel, C., Perkis, D., Black, C., Marshall, S.W., Johnson, R.M., Coyne-Beasley, T., Waller, A.E., Viswanathan, S., 2005. Unintentional injuries in the home in the United States: part I: mortality. American Journal of Preventive Medicine 28, 73–79.

Rusak, A., Rybak, Z., 2012. New directions of research related to chronic wound healing. Polimery w Medycynie 43, 199–204.

Salas, E., Moro, M., Askew, S., Hodson, H., Butler, A., Radomski, M., Moncada, S., 1994. Comparative pharmacology of analogues of S-nitroso-N-acetyl-DL-penicillamine on human platelets. British Journal of Pharmacology 112, 1071–1076.

Salisbury, R.E., Bevin, A.G., Dingeldein, G.P., Grisham, J., 1979. A clinical and laboratory evaluation of a polyurethane foam: a new donor site dressing. Archives of Surgery 114, 1188–1192.

Sanchez, A., Reeser, J., Lau, H., Yahiku, P., Willard, R., Mcmillan, P., Cho, S., Magie, A., Register, U., 1973. Role of sugars in human neutrophilic phagocytosis. The American Journal of Clinical Nutrition 26, 1180–1184.

Sanders, J.E., Lamont, S.E., Karchin, A., Golledge, S.L., Ratner, B.D., 2005. Fibro-porous meshes made from polyurethane micro-fibers: effects of surface charge on tissue response. Biomaterials 26, 813–818.

Schäffer, M.R., Tantry, U., Gross, S.S., Wasserkrug, H.L., Barbul, A., 1996. Nitric oxide regulates wound healing. Journal of Surgical Research 63, 237–240.

Schäffer, M., Tantry, U., Ahrendt, G.M., Wasserkrug, H.L., Barbul, A., 1997a. Acute protein-calorie malnutrition impairs wound healing: a possible role of decreased wound nitric oxide synthesis. Journal of the American College of Surgeons 184, 37–43.

Schäffer, M.R., Tantry, U., Efron, P.A., Ahrendt, G.M., Thornton, F.J., Barbul, A., 1997b. Diabetes-impaired healing and reduced wound nitric oxide synthesis: a possible pathophysiologic correlation. Surgery 121, 513–519.

Schoenfisch, M.H., Mowery, K.A., Rader, M.V., Baliga, N., Wahr, J.A., Meyerhoff, M.E., 2000. Improving the thromboresistivity of chemical sensors via nitric oxide release: fabrication and in vivo evaluation of NO-releasing oxygen-sensing catheters. Analytical Chemistry 72, 1119–1126.

Schultz, G.S., Ladwig, G., Wysocki, A., 2005. Extracellular Matrix: Review of Its Roles in Acute and Chronic Wounds. World Wide Wounds.

Schulze, M.B., Hoffmann, K., Manson, J.E., Willett, W.C., Meigs, J.B., Weikert, C., Heidemann, C., Colditz, G.A., Hu, F.B., 2005. Dietary pattern, inflammation, and incidence of type 2 diabetes in women. The American Journal of Clinical Nutrition 82, 675–684.

Seabra, A., Pankotai, E., Fehér, M., Somlai, A., Kiss, L., Biro, L., Szabo, C., Kollai, M., de Oliveira, M., Lacza, Z., 2007. S-nitrosoglutathione-containing hydrogel increases dermal blood flow in streptozotocin-induced diabetic rats. British Journal of Dermatology 156, 814–818.

Seabra, A.B., Marcato, P.D., de Paula, L.B., Durán, N., 2012. New strategy for controlled release of nitric oxide. Journal of Nano Research 20, 61–67 Trans Tech Publ.

Sen, C.K., Gordillo, G.M., Roy, S., Kirsner, R., Lambert, L., Hunt, T.K., Gottrup, F., Gurtner, G.C., Longaker, M.T., 2009. Human skin wounds: a major and snowballing threat to public health and the economy. Wound Repair and Regeneration 17, 763–771.

Shah, P.S., Shah, V.S., 2008. Continuous Heparin Infusion to Prevent Thrombosis and Catheter Occlusion in Neonates with Peripherally Placed Percutaneous Central Venous Catheters. The Cochrane Library.

Shin, J.H., Schoenfisch, M.H., 2006. Improving the biocompatibility of in vivo sensors via nitric oxide release. Analyst 131, 609–615.

Shin, J.H., Marxer, S.M., Schoenfisch, M.H., 2004. Nitric oxide-releasing sol-gel particle/polyurethane glucose biosensors. Analytical Chemistry 76, 4543–4549.

Simmons, A., Padsalgikar, A.D., Ferris, L.M., Poole-Warren, L.A., 2008. Biostability and biological performance of a PDMS-based polyurethane for controlled drug release. Biomaterials 29, 2987–2995.

Simon, P.E., 2014. Skin Wound Healing (Online) Medscape. Available from: http://emedicine.medscape.com/article/884594-overview.

Singh, R.J., Hogg, N., Joseph, J., Kalyanaraman, B., 1996. Mechanism of nitric oxide release from S-nitrosothiols. Journal of Biological Chemistry 271, 18596–18603.

Skrzypchak, A.M., Lafayette, N.G., Bartlett, R.H., Zhou, Z., Frost, M.C., Meyerhoff, M.E., Reynolds, M.M., Annich, G.M., 2007. Effect of varying nitric oxide release to prevent platelet consumption and preserve platelet function in an in vivo model of extracorporeal circulation. Perfusion 22, 193–200.

Smith, D.J., Dunphy, M., 1991. The influence of wound healing of urinary nitrate levels in rats. Wounds 3, 50–58.

Smith, D.J., Chakravarthy, D., Pulfer, S., Simmons, M.L., Hrabie, J.A., Citro, M.L., Saavedra, J.E., Davies, K.M., Hutsell, T.C., Mooradian, D.L., 1996. Nitric oxide-releasing polymers containing the [N(O)NO]⁻group. Journal of Medicinal Chemistry 39, 1148–1156.

Soto, R.J., Privett, B.J., Schoenfisch, M.H., 2014. In vivo analytical performance of nitric oxide-releasing glucose biosensors. Analytical Chemistry 86, 7141–7149.

Stadelmann, W.K., Digenis, A.G., Tobin, G.R., 1998. Physiology and healing dynamics of chronic cutaneous wounds. The American Journal of Surgery 176, 26S–38S.

Stamm, W.E., 1991. Catheter-associated urinary tract infections: epidemiology, pathogenesis, and prevention. The American Journal of Medicine 91, S65–S71.

Stashak, T.S., Farstvedt, E., Othic, A., 2004. Update on wound dressings: indications and best use. Clinical Techniques in Equine Practice 3, 148–163.

Stechmiller, J.K., Childress, B., Cowan, L., 2005. Arginine supplementation and wound healing. Nutrition in Clinical Practice 20, 52–61.

Stuehr, D.J., 1999. Mammalian nitric oxide synthases. Biochimica et Biophysica Acta (BBA)-Bioenergetics 1411, 217–230.

Taite, L.J., Yang, P., Jun, H.W., West, J.L., 2008. Nitric oxide-releasing polyurethane–PEG copolymer containing the YIGSR peptide promotes endothelialization with decreased platelet adhesion. Journal of Biomedical Materials Research Part B: Applied Biomaterials 84, 108–116.

Tambyah, P.A., 2004. Catheter-associated urinary tract infections: diagnosis and prophylaxis. International Journal of Antimicrobial Agents 24, 44–48.

Teo, W., Ramakrishna, S., 2006. A review on electrospinning design and nanofibre assemblies. Nanotechnology 17, R89.

Tevaearai, H.T., Mueller, X.M., Tepic, S., Cotting, J., Boone, Y., Montavon, P., von Segesser, L.K., 2000. Nitric oxide added to the sweep gas infusion reduces local clotting formation in adult blood oxygenators. ASAIO Journal 46, 719–722.

Thomas, B.J., Jarrett, R., Keen, H., Ruskin, H., 1981. Relation of habitual diet to fasting plasma insulin concentration and the insulin response to oral glucose. Human Nutrition. Clinical Nutrition 36, 49–56.

Tredget, E.E., Shankowsky, H.A., Pannu, R., Nedelec, B., Iwashina, T., Ghahary, A., Taerum, T.V., Scott, P.G., 1998. Transforming growth factor-[beta] in thermally injured patients with hypertrophic scars: effects of interferon [alpha]-2b. Plastic and Reconstructive Surgery 102, 1317–1328.

Umar, A., Chauhan, M., Chauhan, S., Kumar, R., Sharma, P., Tomar, K.J., Wahab, R., Al-Hajry, A., Singh, D., 2013. Applications of ZnO nanoflowers as antimicrobial agents for *Escherichia coli* and enzyme-free glucose sensor. Journal of Biomedical Nanotechnology 9, 1794–1802.

Valdes, T., Moussy, F., 1999. A ferric chloride pre-treatment to prevent calcification of Nafion membrane used for implantable biosensors. Biosensors and Bioelectronics 14, 579–585.

Varedi, M., Jeschke, M.G., Englander, E.W., Herndon, D.N., Barrow, R.E., 2001. Serum TGF-beta in thermally injured rats. Shock 16, 380–382.

Vaughn, M.W., Kuo, L., Liao, J.C., 1998. Estimation of nitric oxide production and reaction rates in tissue by use of a mathematical model. American Journal of Physiology-Heart and Circulatory Physiology 274, H2163–H2176.

Vural, K., Bayazit, M., 2001. Nitric oxide: implications for vascular and endovascular surgery. European Journal of Vascular and Endovascular Surgery 22, 285–293.

Wang, N., Burugapalli, K., Song, W., Halls, J., Moussy, F., Ray, A., Zheng, Y., 2013. Electro-spun fibro-porous polyurethane coatings for implantable glucose biosensors. Biomaterials 34, 888–901.

Wang, J., 2008. Electrochemical glucose biosensors. Chemical Reviews 108, 814–825.

Weller, R.B., 2009. Nitric oxide–containing nanoparticles as an antimicrobial agent and enhancer of wound healing. Journal of Investigative Dermatology 129, 2335–2337.

Wendel, H.P., Ziemer, G., 1999. Coating-techniques to improve the hemocompatibility of artificial devices used for extracorporeal circulation. European Journal of Cardio-Thoracic Surgery 16, 342–350.

Williams, D.L.H., 1996. The Mechanism of Nitric Oxide Formation from *S*-nitrosothiols (Thionitrites). Chemical Communications, pp. 1085–1091.

Williams, D.L.H., 1999. The chemistry of *S*-nitrosothiols. Accounts of Chemical Research 32, 869–876.

Wilson, G.S., Gifford, R., 2005. Biosensors for real-time in vivo measurements. Biosensors and Bioelectronics 20, 2388–2403.

Winter, G.D., 1962. Formation of the scab and the rate of epithelization of superficial wounds in the skin of the young domestic pig. Nature 193, 293–294.

Wisniewski, N., Moussy, F., Reichert, W., 2000. Characterization of implantable biosensor membrane biofouling. Fresenius' Journal of Analytical Chemistry 366, 611–621.

Witte, M.B., Barbul, A., 2002. Role of nitric oxide in wound repair. The American Journal of Surgery 183, 406–412.

Wood, P.D., Mutus, B., Redmond, R.W., 1996. The mechanism of photochemical release of nitric oxide from *S*-nitrosoglutathione. Photochemistry and Photobiology 64, 518–524.

Wright, C.D., Mu, A., Busse, R., Osswald, H., 1989. Generation of nitric oxide by human neutrophils. Biochemical and Biophysical Research Communications 160, 813–819.

Wu, B., 2009. Development of Hemocompatible Polymeric Materials for Blood-Contacting Medical Devices. University of Michigan.

Yan, Q., Major, T.C., Bartlett, R.H., Meyerhoff, M.E., 2011. Intravascular glucose/lactate sensors prepared with nitric oxide releasing poly(lactide-*co*-glycolide)-based coatings for enhanced biocompatibility. Biosensors and Bioelectronics 26, 4276–4282.

Yang, J., Welby, J.L., Meyerhoff, M.E., 2008. Generic nitric oxide (NO) generating surface by immobilizing organoselenium species via layer-by-layer assembly. Langmuir 24, 10265–10272.

Yoda, R., 1998. Elastomers for biomedical applications. Journal of Biomaterials Science, Polymer Edition 9, 561–626.

Yoo, H.J., Kim, H.D., 2008. Synthesis and properties of waterborne polyurethane hydrogels for wound healing dressings. Journal of Biomedical Materials Research Part B: Applied Biomaterials 85, 326–333.

Zhang, H., Annich, G.M., Miskulin, J., Osterholzer, K., Merz, S.I., Bartlett, R.H., Meyerhoff, M.E., 2002. Nitric oxide releasing silicone rubbers with improved blood compatibility: preparation, characterization, and in vivo evaluation. Biomaterials 23, 1485–1494.

Zhang, L., Cao, Z., Bai, T., Carr, L., Ella-Menye, J.-R., Irvin, C., Ratner, B.D., Jiang, S., 2013. Zwitterionic hydrogels implanted in mice resist the foreign-body reaction. Nature Biotechnology 31, 553–556.

Zhou, Z., Meyerhoff, M.E., 2005. Preparation and characterization of polymeric coatings with combined nitric oxide release and immobilized active heparin. Biomaterials 26, 6506–6517.

Mechanical behavior of polyurethane-based small-diameter vascular grafts

15

*F. Montini-Ballarin, G.A. Abraham, P.C. Caracciolo**
Research Institute for Materials Science and Technology, INTEMA (UNMdP-CONICET), Mar del Plata, Argentina
*Corresponding author: pcaracciolo@fi.mdp.edu.ar

15.1   Vascular tissues: structure, diseases, and current treatments

Vascular tissues comprise arteries, capillaries, and veins. Due to the risk and impact of vascular diseases in arteries, efforts have been focused on replacement and regeneration strategies. Arteries present a complex structure as they are composed of three layers, intima, media, and adventitia, each with a different composition and function. Additionally, artery composition changes depending on its location.

The intima is the innermost layer and it is composed mainly of endothelial cells (ECs). This layer controls the molecular transfer inside the wall, provides antithrombogenicity, and is involved in homeostasis maintenance, muscular tone, and immunogenic and inflammatory regulation.

The media is the artery's middle layer, composed of mainly smooth muscle cells (SMCs) in a circumferential arrangement, alternating with elastin sheets and, to a lesser extent, collagen fibers. SMCs become contractile in maturity and are responsible for regulating vessel size. Elastin provides high compliance since it is responsible for high arterial deformation capacity at low pressures.

The adventitia is the artery's outer layer, composed of collagen fibers and fibroblasts. Collagen is disposed in a circumferential orientation as corrugated fibers that stretch and act at higher pressures, protecting and strengthening the vessel [1,2].

Cardiovascular diseases are the main cause of death worldwide. Every year 17 million lives are lost due to these diseases, which represent 29% of global deaths [3].

In some forms of heart disease, bypass surgery is the chosen treatment when stenosis and thrombosis are severe. Bypass consists of diverting the blood flow from the blocked zone to irrigate the rest of the cardiac tissue. Grafts from autologous arteries and veins from a human or animal donor are used for this procedure. Autologous grafts are today the gold-standard structure to use for bypass. The major saphenous vein and the internal thoracic artery (also known as internal mammary artery) are the grafts that have shown the best results over the years. However, in some situations, these vessels are not available and others are used instead, such as the radial artery, the right gastro-omental artery, the inferior epigastric artery, the small saphenous vein, and veins from upper extremities [4].

Table 15.1 Mechanical performance of natural vessels and classical vascular grafts

Natural vessels/vascular graft	Mechanical performance	References
Coronary artery	$\sigma = 0.5–2$, $\varepsilon = 40–100$, $E_\theta = 1–2$, $E_z = 4–6$, $P_b = 2000$, $C = 3.39 \pm 6.03$[a]	[7,8]
Saphenous vein	$\sigma = 1.5–4$, $\varepsilon = 40–100$, $E_\theta = 43$, $E_z = 130$, $P_b = 1250 \pm 500$, $C = 1.77 \pm 1.20$[a], $SS = 1.81 \pm 0.02$	[7,9–11]
Internal thoracic artery	$\sigma = 1.5–4$, $\varepsilon = 40–100$, $E_\theta = 2.5–7.5$, $E_z = 12–16$, $P_b = 2031–4225$, $C = 5.22$[a], $SS = 1.4 \pm 0.01$	[7,10,12]
Dacron® (PET)	$\sigma = 170–180$, $E = 14,000$	[5]
Goretex® (ePTFE)	$\sigma = 14$, $E = 500$, $C = 0.1$	[5,12]

σ, tensile strength (MPa); ε, strain at break (%); E, Young's modulus (MPa); C, compliance (%/100 mm Hg); P_b, burst pressure (mm Hg); SS, suture strength (N).
[a]Value calculated by the authors from data reported in [13].

Although autologous grafts have good performance, 15% of patients who suffer from vascular disease need alternative grafts due to the unavailability of the grafts aforementioned. Synthetic grafts are an alternative in these situations. However, those used as bypass grafts are stiff and biostable. Tubular structures of poly(ethylene terephthalate) (PET) or Dacron® were introduced in 1957. Dacron® has high crystallinity, high elastic modulus, and tensile strength (Table 15.1). These grafts are successfully used in aorta bypasses and as large-diameter peripheral grafts. Expanded poly(tetrafluoroethylene) (ePTFE) grafts, known by their commercial name Goretex®, also present high crystallinity and high stiffness, although both values are lower than those in Dacron® grafts. Goretex® is used with excellent results in lower-extremity grafts of internal diameters between 7 and 9 mm. Both grafts fail in bypass applications at small diameters (<6 mm), mainly due to their poor blood compatibility, high stiffness, and compliance mismatch at the anastomotic area. Today, major effort is focused on developing small-diameter vascular grafts [5,6].

From 1985 to 2015, little has changed regarding synthetic vascular grafts and obtaining a small-diameter vascular graft with biomimetic behavior still poses a great challenge. The development of a conduit for bypass surgery that is available off-the-shelf without prolonged *in vitro* culture time but with proper mechanical and biological properties is at the center of current research in vascular tissue engineering.

15.2 The importance of a biomimetic mechanical response

The layered hierarchical structure of natural arteries confers on them a singular mechanical behavior [2]. The viscoelasticity of the arterial wall together with blood viscosity gives the arterial system a damping characteristic. This helps to avoid a
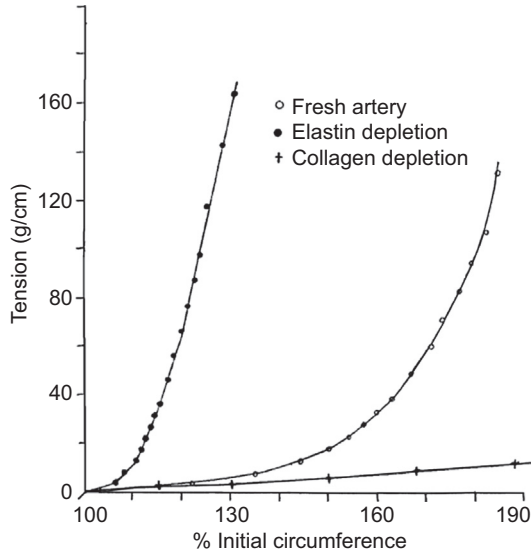
Figure 15.1 Elastic diagram of a fresh human external iliac artery, one depleted of collagen (formic acid digestion), and another of elastin (trypsin).
Adapted from Ref. [17].

resonance effect in the energy propagation from the heart to the vascular periphery, as would occur if the circulatory system were perfectly elastic [14,15].

Arteries are subject to pulsatile internal pressure. The properties of the arterial wall depend on the mechanical role of each of its passive (elastin and collagen fibers) and active (SMCs) components. These components determine the vessel's elastic, viscous, and inertial properties, though the inertial component is negligible [16]. Consequently, it is possible to identify the contribution of each component to the total elastic response. Collagen and elastin fibers' Young's moduli are extremely different, and contribute individually to arterial elasticity. Changes in elasticity are also observed due to the activation of SMCs and the recruitment of collagen fibers, which support arterial wall stresses [14,15,17–20]. Elastin is the main contributor to the damping function of the circulatory system. Collagen fibers are disposed in such a way that they act to protect the vessel from large deformation rupture by limiting its circumferential expansion [19–22]. When arteries are subject to lower pressures, high compliance and low stiffness are observed. This effect is attributed mainly to elastin fibers. As pressure increases, collagen fibers are aligned and oriented, reducing artery compliance. Finally, at higher pressures the artery's mechanical response is predominantly due to collagen, since it provides high artery stiffness. This nonlineal behavior is known as a "J" curve (Figure 15.1) [16,17,23].

The mechanical behavior and, as a consequence, mechanical properties of its materials are key factors in vascular tissue engineering graft design. The vascular environment is subject to cyclic pressure imposed by the heart [24], which also influences the behavior of tissues and cells. The implantation of grafts or prostheses interrupts

the local hemodynamic and the arterial wall stress distribution at the anastomosis, causing mechanical restrictions in the receptor artery during the cardiac cycle [25]. Currently, clinically approved vascular grafts exhibit a high failure probability *in vivo* due, in most cases, to a mechanical mismatch with the native artery [24]. This mismatch causes intimal hyperplasia and a reduction in patency rate [26]. In addition, the compliance mismatch between the natural artery and the vascular graft leads to failure after long periods of implantation, in particular for small-diameter conduits [23]. The mechanical characterization of vascular grafts plays a crucial role in their design and development. The properties of importance are failure strength, mechanical compliance, and suture-retention strength, with all of these compared to physiologic values [27]. In particular, characterization of blood vessel and/or vascular graft simultaneous pressure and diameter are important in vascular graft design. Knowing the vascular graft diameter response to internal pressure waves provides important baseline information [16,19,28]. Thus, valuable biomechanical properties can be obtained *in vitro*, in which hemodynamic conditions close to those observed physiologically can be reproduced [29,30].

15.3   Characterization of mechanical behavior

15.3.1   Uniaxial tensile tests

Uniaxial tensile tests are most commonly performed on vascular grafts to study their elastic properties. In particular, the elastic modulus, tensile strength, and elongation at break are the properties used to characterize the grafts. Most existing synthetic grafts fail when utilized as small-diameter vascular grafts due to their high stiffness and lack of compliance at the anastomosis. Therefore, the elastic modulus value should be similar to the natural artery being replaced. This response should be measured *in vitro*, in a physiological environment at 37 °C. Since water acts as a plasticizer to many polymers [31,32], it is important to measure the elastic properties in the hydrated state. Some researchers have characterized the graft properties by presoaking the sample before testing [33–35]. However, the use of a physiologic chamber with controlled temperature is a more appropriate test environment [7,36]. Taking into account the anisotropic nature of natural arteries, it is also important to test the graft in both axial and circumferential directions.

15.3.2   Pressure–diameter tests

Arteries are subject to a pulsatile continuous internal pressure, requiring that both static and dynamic responses be evaluated. Even though uniaxial tensile tests provide important information of the graft stiffness and strength, it is very important to characterize the mechanical response when grafts are subject to cyclic deformation. Internal pressure–diameter measurements make it possible to characterize the graft's stiffness and compliance in a biomimetic way. Different approaches have been used to characterize the diameter change when applying an internal pressure. In most cases, a continuous inner pressure is applied and the change in the graft diameter is measured

with an optical or laser micrometer [35,37–40]. The utilization of a pulsatile pump, which acts as an artificial heart mimicking the blood pulse at 37 °C, results in a more biomimetic response as recommended by the standard testing guide for cardiovascular implants and tubular–vascular prostheses [41]. The measurement of the change in the graft diameter can be performed with different optical or laser micrometers. However, these devices require an open view of the graft that prevents its use *in vivo*. Sonomicrometry determines instantaneous external vessel diameter by means of measuring the flight time of an ultrasound burst between a pair of small transducers. These transducers are fixed diametrically opposed on a vessel's external wall. Since its first implementation in 1956 by Rushmer et al. [42], this procedure has been improved and refined, becoming a gold standard for *in vivo* physiological research.

Stiffness and compliance of the grafts are evaluated through different moduli (Petterson modulus (E_P) or pressure–deformation modulus ($E_{P\varepsilon}$), incremental elastic modulus (E_{INC}), pressure–diameter modulus (E_{PD})) and distensibility measurements (compliance (%C), stiffness (β), distensibility (D)) [43–45] (Eqns (15.1–15.6)).

$$E_P = d_D \cdot \frac{P_S - P_D}{d_S - d_D} \tag{15.1}$$

$$E_{INC} = 0.75 \cdot \frac{dP}{dR} \cdot \frac{R_m^2}{h} \tag{15.2}$$

$$E_{PD} = \frac{dp}{dd} \tag{15.3}$$

$$\% C = \frac{\frac{R_S - R_D}{R_D}}{P_S - P_D} \cdot 10^4 \tag{15.4}$$

$$\beta = \ln\left(\frac{P_S}{P_D}\right) \cdot \frac{d_D}{d_S - d_D} \tag{15.5}$$

$$D = \frac{CSA_S - CSA_D}{CSA_D \cdot (P_S - P_D)} \tag{15.6}$$

where P is the intraluminal pressure; d and R are the diameter and radius at P; P_S and P_D are the internal pressure at systole and diastole; d_S and d_D, R_S and R_D are the internal diameters and radios, respectively, at P_S and P_D; R_m is the mean external radius; h is the grafts thickness; and CSA_S and CSA_D are the cross-sectional areas at systole and diastole.

15.3.3 Suture retention and burst pressure tests

Apart from stiffness determination, other mechanical characterizations are required to qualify vascular grafts, including suture-retention strength and burst pressure testing. The suture-retention strength test aims at determining the force necessary to pull a

suture from the prosthesis or cause the wall of the prosthesis to fail. A universal testing machine is normally used: the vascular graft is clamped at one end, and at the other extremity the suture is inserted 2 mm from the end through one wall of the prosthesis to form a half loop [41].

The burst pressure test characterizes the maximum internal pressure, the vascular graft resists before failure. The burst test is carried out in the hydrated state using a setup similar to that of the pressure–diameter test that allows the system to achieve pressures higher than the physiological range (>2000 mm Hg).

15.3.4   Other mechanical tests

The previous tests are used to fully characterize the mechanical behavior of the vascular grafts and determine their potential to succeed *in vivo*. However, other tests have been used to provide complementary or equivalent properties using simpler methods. Among these, the ring test has been extensively used [46]. This test requires a ring sample that is gripped by two pins that are gradually separated until the ring specimen fails. The load-application conditions do not resemble the physiological situation; however, a significantly smaller specimen is required, which is a major advantage. To estimate the burst pressure from this test, Laplace's law has been applied to the results. The combination of Laplace's law with the ring's test data using the final internal diameter as the geometry parameter results in a good estimation of the vascular graft's burst pressure, failure strain, and stiffness.

15.4   Polyurethanes for vascular tissue engineering

Natural polymers such as collagen, elastin, and fibrin make up much of the body's native extracellular matrix (ECM), and they were explored as platforms for tissue engineered constructs [34,47–49]. Polysaccharides such as chitosan, starch, alginate, and dextran were also studied for these purposes. Simultaneously, silk fibroin was widely explored for vascular applications due to its higher mechanical properties in comparison to other natural polymers, such as fibrin [48]. The utilization of natural polymers to create tissue-engineered scaffolds has yielded promising results, both *in vitro* and *in vivo*, due in part to the enhanced bioactivity provided by materials normally found within the human body [50]. However, their mechanical response is usually below the required values; therefore, synthetic polymers have been explored to achieve the desired properties.

Classical synthetic polyesters such as poly(ε-caprolactone) (PCL), poly(L-lactic acid) (PLLA), poly(glycolic acid) (PGA), and their copolymers can provide the necessary strength for structural stability, and their scaffolds have been explored for the regeneration of blood vessel substitutes [51–53]. However, they are relatively stiff, nonelastomeric materials and not ideally suited for engineering of soft flexible tissues such as vascular grafts.

The development of soft-tissue engineering needs bioresorbable materials exhibiting elastomeric properties. Elastomeric polyurethane (PU) vascular grafts can withstand the action of stress and load and undergo an elastic recovery with little or no hysteresis. In recent years, biocompatible and biodegradable segmented polyurethanes (SPUs) have been studied for applications in the tissue engineering field,

such as cardiovascular tissue engineering, musculoskeletal applications (anterior cruciate ligament, knee joint meniscus, SMC constructs for contractile muscle), and nerve regeneration. Their highly variable chemistry allows the preparation of biocompatible materials with controlled physicochemical, mechanical, and biodegradation properties that can be achieved by selecting the appropriate monomers and manipulating hard and soft segment contents. Biodegradation into nontoxic components can be promoted by the use of aliphatic diisocyanates. Bioresorbable polyester soft segments are commonly used to provide hydrolytically labile linkages, whereas chain extenders containing easily hydrolyzable bonds increase the SPU degradation rate [54].

Surprisingly, bioresorbable SPUs and segmented poly(urethane urea)s (SPUUs) have been infrequently used for the fabrication of vascular grafts. Our group reported the preparation, characterization, and properties of novel electrospun elastomeric polyurethane scaffolds based on bioresorbable SPUs and SPUUs, synthesized from PCL, hexamethylene diisocyanate (HDI), and novel chain extenders containing urea groups or an aromatic amino acid derivative with ester groups [55]. These polymers were chosen for their unique composition and mechanical properties, as well as for their promising *in vitro* biological properties [56,57]. It was shown that the degradation rate depends on the chemical structure of the chain extenders, as well as on the morphology and crystallinity of the materials [58].

Aliphatic polyesters, copolyesters, and natural macromolecules (mainly collagen, elastin, fibrin, chitosan, and hyaluronic acid (HA)), as well as their blends, have also been used to prepare polymeric-based vascular grafts with tuned mechanical properties. Couet et al. reported a comprehensive overview of materials that have been explored as scaffolds for vascular tissue engineering [59]. The analysis of the mechanical behavior of non-PU-based vascular grafts is beyond the scope of this chapter.

15.4.1 Biodegradable and biostable polyurethane-based vascular grafts

As noted before, mechanical mismatch, added to an inadequate biological response, constitutes the main cause for failure of small-diameter synthetic vascular grafts. These result in unsatisfactory arterial prostheses for diameters smaller than 6 mm [60,61] mainly due to their thrombogenicity, lack of support for EC attachment and proliferation, and lack of radial compliance. Due to the stringent nature of these requirements (i.e., the inhibition of platelet adhesion frequently leads also to EC adhesion inhibition), the creation of a small-diameter vascular graft satisfying both biological and mechanical requirements has been unsuccessful. Initially, as commercial PUs were mostly aromatic segmented poly(ether urethane)s (SPEUs), these were the first and most extensive PUs explored as small-diameter vascular grafts. SPEUs commercialized under different trade names as well as many others synthesized for research purposes, which contain poly(tetramethylene oxide) (PTMO) as soft segment, 4,4′-methylene diphenyl diisocyanate (MDI), and 1,4-butanediol (BDO) as chain extender, were employed in several studies. This was due to their appropriate mechanical properties, durability, and improved blood response. Table 15.2 summarizes the mechanical performance of some selected biostable PU vascular grafts.

Table 15.2 **Some selected biostable polyurethane scaffolds and their mechanical characteristics**

Scaffold	Fabrication technique	Mechanical performance	References
PTMO:MDI:BDO	Electrospinning	$E=1.1$, $\varepsilon=400$, $\sigma=4.9$, SS$=4.0$, $C=6$	[62]
PTMO:MDI:BDO	Electrospinning	Study of the effect of the processing parameters on the mechanical properties	[63]
Cardiomat 610	Electrospinning	$E_z=0.64$, $E_\theta=0.46$, $C=3.4$ (150 rpm); $E_z=0.54$, $E_\theta=0.53$, $C=2.6$ (3400 rpm)	[64]
Cardiomat 610	Electrospinning	$E=0.59$, $E=2.43$ (DMF/THF 0/100 and 30/70)	[65]
Tecothane	Spin casting/ electrospinning	$E=2.0$, $\varepsilon=300$	[66]
Pellethane® 2363 80A	Electrospinning	Mean $E_z=10.3$, $E_\theta=26.4$, $\varepsilon_z=413$, $\varepsilon_\theta=216$	[67]
Pellethane® 2363 80A	Electrospinning/ UV cross-linking	$P_b>550$, $C=6.2$	[68]
Pellethane® 2363 80A	Electrospinning	$\sigma=20.2/20.6$, $C=4.1/3.9$, SS$=2.8$ (53% porosity mesh); $\sigma=16.3/15.4$, $C=7.2/4.9$, SS$=2.1$ (80% porosity mesh) (before/ after 6 month implantation, respectively)	[69]
Estane® 5714	Electrospinning/ spray phase inversion	T-peel$=\sim27$	[71]
Texin® Rx85A, graphene oxide (GO)	Electrospinning	SS$=\sim2.5$, $P_b=\sim31000$ (0.5% GO/Texin®)	[74]
PTMO: MDI:BDO— hyaluronic acid (HA)	Flat electrospinning	$E=\sim6/\sim7/\sim8$, (0% HA, 0.33% 4.7 kDa HA, 0.33% 9.7 kDa HA)	[76]
Selectophore™	Electrospinning	$E=5.85$, $\sigma=5.77$, $\varepsilon=294.5$	[77]
Biomer®	Dip-coating/salt leaching	$C=0.7$–27.2 (depending on polymer/NaCl ratio)	[79]
Biomer®	Dip-coating/salt leaching	$C=10.3$, 6.8, and 3.6 (before implantation, at implant, and after 6 weeks of implantation, respectively)	[80]
Biomer®	Electrospinning	Stiffer than PTMO:MDI:BDO, with similar compliance behavior	[84]

Biomer®	Electrospinning	Study of the effect of dimensions on mechanical properties	[85]
BioSpan®, Rapa-mycin (RM)	Electrospinning	$E=4.44$–3.48 (RM 20% w/w)	[86]
PIB–PTMO (80:20): MDI:BDO	Flat electrospinning	$E=0.87$, $\sigma=1.63$, $\varepsilon=282$; $E=4.53$, $\sigma=4.70$, $\varepsilon=129$; $E=7.83$, $\sigma=6.53$, $\varepsilon=105$ (21, 35, 40% HS content, respectively)	[87]
Polycarbon-ate:MDI:EDA, oligomeric silsesquioxane (POSS)	Extrusion/phase inversion	$C=5.4$, SS$=2.5$–4.5	[40]
Chronoflex® 80A	Electrospinning	$C=2.4$, $P_b=1680$	[90]
Carbothane® PC3575A	Electrospinning	$C=3.8$, $P_b=1330$	[90]
Carbothane® PC3575A	Electrospinning/ fibers fused by heat	$C=6.0$, $P_b=2260$	[90]

σ, tensile strength (MPa); ε, strain at break (%); E, Young's modulus (MPa); C, compliance (%/100 mm Hg); P_b, burst pressure (mm Hg); SS, suture strength (N); subscript θ, circumferential; subscript Z, tangential; T-peel, peel attachment strength (g/mm^2).

Annis et al. employed a biostable SPEU based on this formulation (Imperial Chemical Industries) to produce 10 mm vascular grafts displaying promising mechanical properties by a process of electrospinning [62]. The grafts were characterized by uni-axial tensile tests in the circumferential direction. Their stress–strain curve was very different from that of solid SPEU. Compliance could be controlled by varying the thickness of the graft wall. Distention values and suture-retention strengths compa-rable to those of natural arteries were obtained. The grafts were also tested *in vivo*, where creep and aneurism formation were not observed. The grafts remained flexible after 9 months of implantation. In a later work, How and Clarke studied the effect of the modification of the electrospinning parameters on the mechanical properties of grafts obtained from the same material [63] to obtain compliance values similar to those of carotid and femoral arteries. The average longitudinal Young's modulus (E_z) decreased and the average circumferential Young's modulus (E_θ) increased by increas-ing mandrel rotation speed. These parameters seemed to be independent of traverse speed. Increasing the solution concentration decreased E_θ, but there was no definite trend for E_z. It was found that this anisotropy was dependent on the rotational speed of the mandrel. Thus, to achieve the same degree of anisotropy smaller diameter grafts should be processed at higher rotational speeds.

Matsuda et al. explored solvent effects and rotational speed on the mechani-cal properties of electrospun grafts obtained from another SPEU based on PTMO, MDI, and BDO commercialized under the trade name of Cardiomat 610 (Zeon Kasei

Co., Ltd, Tokyo, Japan) [64]. An increase in the *N,N*-dimethylformamide (DMF)/tetrahydrofuran (THF) ratio led to fiber fusion and a decrease in fiber diameter, leading to lower compliance values. An increase in rotational speed led to stiffer, less compliant tubes. Another study confirmed that an increase in the DMF/THF ratio significantly increased fiber bonding and elastic modulus [65].

Uttayarat et al. prepared a vascular graft through a combination of spin casting and electrospinning of Tecothane [66], another aromatic SPEU (Thermedics Inc., Woburn, MA, USA). The hybrid graft was composed of an inner layer with aligned microgrooves and an outer electrospun layer with random microfibers. The microgrooves promoted alignment of a cultured EC monolayer. The average E_z was similar to those of the native aorta, but no compliance or burst pressure values were determined.

Grasl et al. prepared electrospun vascular grafts from Pellethane® 2363-80A (Dow Chemical Company, Midland, MI, USA), another SPEU based on PTMO, MDI, and BDO. Fiber orientation produced due to the use of a rotating mandrel led to a circumferential ultimate tensile strength (σ_θ) about 2.6 times higher than the longitudinal strength (σ_z) [67]. The graft showed *in vitro* extensive attachment of ECs providing potential antithrombotic behavior. Theron et al. modified Pellethane® with pentenoyl groups, which was electrospun into tubular grafts cross linked with UV radiation during and after electrospinning [68]. The cross-linked grafts displayed a significant improvement in degradation resistance *in vitro* as well as in their viscoelastic properties, with a decreased hysteresis and creep, which should assist in preventing aneurismal dilation. Bergmeister et al. prepared Pellethane® small-diameter vascular grafts with similar fiber diameters and different pore sizes [69] to study the effect of porosity on cellular growth and migration. It was observed that grafts with higher porosity exhibited higher cell populations after implantation; while compliance, ultimate tensile strength, and suture-retention strength values remained higher compared to native blood vessels for grafts before and after 6 months of implantation in rats.

Soldani et al. employed Estane® 5714 (Lubrizol Advanced Materials, Cleveland, OH, USA), another SPEU synthesized from PTMO, MDI, and BDO [70], dusted with calcium stearate, to obtain bilayered vascular grafts [71]. The inner layer was prepared by electrospinning to support EC attachment while a highly porous outer layer was obtained using a spray, phase-inversion method [70]. Adhesion strength between both layers was determined by using a T-peel test. The graft contained a homogeneous microporous layer firmly attached to the electrospun layer, though optimization of mechanical properties was not pursued.

Although Pellethane® and other SPEUs synthesized from the same components were chosen in several studies to fabricate cardiovascular implants (involving, in most cases, highly porous structures with acceptable biomechanical response), this formulation has been proven to biodegrade *in vivo* in long-term applications [72]. For this reason, the use of Pellethane® has been restricted to short implantation periods. Moreover, it has been suggested that MDI-based PUs release carcinogenic and mutagenic aromatic diamines on degradation [73].

Jing et al. employed Texin® Rx85A (Bayer Material Science, Inc.), a medical grade biostable MDI-based SPEU, loaded with graphene oxide (GO) in the preparation of electrospun vascular grafts [74]. GO provides large numbers of hydrophilic groups

with a cytotoxicity that seems to be dependent on concentration. A low content of GO may stimulate cell adhesion and proliferation, while higher concentrations can cause oxidative stress and loss of cell viability [75]. Grafts were prepared with a maximum of 2% GO/SPEU, and surfaces were treated with oxygen plasma to improve the hydrophilicity of the scaffold. The GO-loaded matrices exhibited higher Young's modulus and ultimate tensile strength values than pure SPEU matrices. A 0.5% GO tubular graft was chosen because it promoted the highest human umbilical vein EC (HUVEC) adhesion and proliferation, displayed higher suture-retention strength than human mammary arteries and human saphenous veins, and had a higher burst pressure than carotid arteries and saphenous veins. However, compliance data were not provided. Nevertheless, the manufacturer does not recommend Texin® for applications involving contact with blood or other body fluids for periods greater than 30 days. In addition, the effect of plasma treatment on surface degradation was not explored.

Ruiz et al. obtained flat electrospun meshes from an SPEU series from PTMO, MDI, and BDO with different HA contents and molecular weights [76]. The incorporation of HA in the SPEU structure resulted in a small increase in Young's modulus, which was independent of HA molecular weight. Both ultimate tensile strength and Young's modulus of all SPEU–HA materials provided a much better approximation to native vessels than commercial graft materials (Dacron® and Goretex®). Moreover, these materials were shown to reduce protein adsorption, platelet and bacterial adhesion, and fibroblast and macrophage proliferation. In addition, SPEUs containing HA supported the growth of ECs with a better performance found using lower molecular weight HA. Although these HA-modified SPEUs appear to be promising for vascular graft applications, their biostability may be reduced due to the increase in hydrophilicity caused by the presence of HA.

He et al. prepared electrospun tubular grafts from Selectophore™ (Sigma–Aldrich, St. Louis, MO, USA), also commercialized under the name of Tecoflex™, a cycloaliphatic SPEU synthesized from PTMO, 4,4′-methylene dicyclohexyl diisocyanate (HMDI) and BDO [77]. Higher fiber diameters and lower porosity values were obtained from higher solution concentrations, while adjusting the rotation speed led to circumferentially oriented fibers. Moreover, ECs exhibited higher adhesion and displayed higher proliferation rates when compared to PTFE surfaces. Though this material was described as biostable, thromboresistant, and nontoxic, it was reported to display more severe cracking than Pellethane® under accelerated *in vitro* experimental conditions [78].

Segmented poly(ether urethane urea)s (SPEUUs) have been explored as alternatives to SPEUs to improve the mechanical properties of vascular grafts. Thus, Biomer®, a biostable SPEUU obtained from PTMO, MDI, and a mixture of ethylenediamine (EDA) and 1,3-diaminocyclohexane as chain extender (Ethicon Inc., NJ, USA), was employed in a number of studies as a biomaterial to obtain porous tubular grafts. Nose et al. employed a dip-coating technique and solutions with different Biomer®/NaCl ratios and obtained tubular structures with a higher inner porosity [79]. The effect of gelatin coating and cross-linking with glutaraldehyde was also studied. These grafts provided a wide range of compliance values at constant wall thickness by varying the Biomer®/NaCl ratio. *In vivo* testing revealed that graft patency is dependent on

compliance. After 1 year of implantation in dogs, a thickening of both intimal and medial layers was observed, increasing graft rigidity. In addition, degradation of the SPEUU occurred as early as 6 weeks after implantation, and a decrease in molecular weight was observed [80]. This process, together with calcification, led to a significant decrease in compliance. Degradation, as for the case of Pellethane®, was attributed to the scission of molecular chains due to oxidative degradation of the polyether soft segment [81–83]. Annis et al. obtained electrospun tubes [84] and observed that the grafts were stiffer than others previously obtained from PTMO:MDI:BDO [63], but compliance was not significantly affected by strain or temperature. The compliance–wall-thickness correlation was similar for both SPEU and SPEUU polymer materials. In a series of grafts with constant wall thickness, they became more compliant by increasing the diameter. Moreover, grafts with a constant diameter became stiffer with an increase in wall thickness [85].

BioSpan® (DSM, Biomedical, Berkeley, CA, USA), is another biostable medical grade MDI-based SPEUU that has been explored for vascular graft applications. Han et al. developed electrospun BioSpan®–Rapamycin (RM) bilayered grafts to suppress local SMC proliferation [86]. This was due to the fact that restenosis remains one of the major failure modes after implantation. As expected, Young's modulus increased with higher RM content and lower fiber diameters; thus, they were able to obtain values comparable to those of natural arteries. The grafts also exhibited higher failure strain than rabbit aortae.

Several formulations have also been explored to improve *in vivo* stability, together with acceptable mechanical properties. In this way, Cozzens et al. obtained a series of SPEU employing hydroxypropyl telechelic polyisobutylene (PIB) and PTMO (80:20) as soft segments, and MDI and BDO, with different hard segment ratios [87]. The PIB-based SPEU displayed superior oxidative stability than PTMO-based SPEU [88]. As expected, Young's modulus and ultimate tensile strength increased and elongation at break decreased with higher hard segment content. These materials were electrospun as flat meshes and displayed higher mechanical properties than native vessels, suggesting that they are promising materials for the production of biostable vascular grafts. In this way, compliance and burst pressure should be measured, and all properties should be studied as a function of implantation time.

A novel segmented poly(carbonate urethane urea) (SPCUU) obtained from polycarbonate diol, MDI, and EDA with a 2% load of polyhedral oligomeric silsesquioxane (POSS), SPCUU–POSS, was used to produce vascular grafts [89]. The grafts produced by an extrusion, phase inversion method were mechanically characterized *in vitro* and *in vivo* [40]. Most grafts' compliance measured *in vitro* presented a value of approximately 5%/100 mm Hg for all pressure ranges studied. However, grafts with lower thickness showed an increase in compliance with pressure. This behavior is the opposite of that observed in natural arteries. *In vivo*, compliance was only measured at physiologic pressures: the value was $5.4 \pm 1.6\%$/100 mm Hg and was not significantly altered after 9 months of implantation in sheep. Natural sheep arteries studied showed similar compliance values. The patency rate was found to be 64% and the grafts were free of intimal hyperplasia, aneurysm, and calcification, indicating promising properties for these tubular structures.

Nezarati et al. evaluated the mechanical behavior of vascular grafts obtained from Chronoflex® 80A (Chronoflex, Advan-Source Biomaterials) and Carbothane® PC3575A (Carbothane, Lubrizol), two poly(carbonate urethane)s (SPCUs) containing MDI and HMDI, respectively [90]. The Carbothane® had a lower initial Young's modulus due to its aliphatic hard segments, and an increased compliance, and was selected for fabrication into an electrospun vascular graft. The Carbothane® was chosen to explore modifications in fiber tortuosity and fiber fusion. Both the reduction in fiber tortuosity and the generation of fiber partial fusion mediated by solvent led to higher compliance values but also to lower burst pressures. Moreover, fiber fusion generated by heat treatment led to vascular grafts with both compliance and burst pressure exceeding saphenous vein's autografts.

Approaches to develop vascular grafts from bioresorbable PUs are ongoing, and while many laboratory studies have been performed there are hardly any bioresorbable PUs available in the market. Table 15.3 summarizes the mechanical performance of some selected bioresorbable PU vascular grafts.

Krynauw et al. obtained electrospun small-diameter tubular scaffolds from DegraPol® D30, a bioresorbable segmented poly(ester urethane) (SPEsU) that consists of poly[3-(R-hydroxybutyrate)-co-(ε-caprolactone)]–diol (hard segment) and poly(ε-caprolactone-co-glycolide)–diol (soft segment). The mechanical properties of these grafts were lower than those of native tissues [91].

Our group has obtained electrospun small-diameter tubular scaffolds from previously synthesized SPEsU (PHD), employing PCL, HDI, and an amino acid-derived chain extender (DED, desaminotyrosine diester) [57]. The mechanical properties of this electrospun SPEsU were measured under physiological conditions and are listed in Table 15.3.

The aliphatic diisocyanates used in most bioresorbable PUs result in a less reinforcing hard segment phase than aromatic-based PUs, leading to lower mechanical properties. The use of aromatic or diamine chain extenders can strengthen hard segment interactions due to π-bond stacking or an increase in hydrogen bonding, respectively, providing a better mechanical response. For this reason, the use of segmented poly(ester urethane urea)s (SPEsUUs), with higher degrees of microphase separation, has been explored as candidates for vascular graft scaffolds.

Han et al. synthesized a SPEsUU from PCL, L-lysine ethyl ester diisocyanate (LDI), and L-lysine ethyl ester (LEE) as chain extender [92]. The mechanical properties of the electrospun tubular scaffolds increased with solution concentration, as the fiber diameter was progressively increased. The values of suture-retention strength were higher than those of native blood vessels, whereas the burst pressure strength was slightly lower. No compliance data were reported. The scaffolds displayed no cytotoxicity against L-929 mouse fibroblasts or HUVECs, and in vitro cell attachment proved to be successful.

Wagner et al. employed a previously synthesized SPEsUU [93] from PCL, 1,4-butanediisocyanate (BDI), and putrescine as chain extender, obtaining a vascular graft through thermally induced phase separation (TIPS) [94]. The scaffold incorporated muscle-derived stem cells in vitro using a rotational vacuum seeding device, allowing a rapid and uniform cell distribution, while maintaining cell viability without

Table 15.3 **Some selected biodegradable polyurethane scaffolds and their mechanical characteristics**

Scaffold	Fabrication technique	Mechanical performance	References
DegraPol® D30	Electrospinning	$E=1.14$, $\sigma=0.52$, $\varepsilon=176.8$; $E=0.43$, $\sigma=0.033$, $\varepsilon=24.6$ (0 and 34 degree days, respectively)	[91]
PCL: HDI:DED (PHD)	Electrospinning	$E=0.56$, $C=2.46$	Montini-Ballarin, work unpublished
PCL:LDI:LEE	Electrospinning	$\sigma=2.82$, $P_b=540$, SS$=2.48$ $\sigma=7.07$, $P_b=1290$, SS$=8.38$ (8% and 15%, respectively)	[92]
PCL:BDI: putrescine	TIPS	$\sigma=2.6$, $\varepsilon=150$, $P_b=2130$, SS$=1.3$	[94]
PCL:BDI: putrescine	Internal layer: TIPS/external layer: electrospinning	$E=1.4$, $\sigma=8.3$, $\varepsilon=520$, $P_b=2300$, $C=4.6$, SS$=3.4$	[11]
PCL:BDI: putrescine— MPC	Electrospinning/ MPC plasma-mediated modification	σ and ε: higher prior to implantation, and in the order of native rat aorta after implantation. C: lower than native tissue, except for 4 weeks after implantation.	[101]
PCL:BDI: putrescine— sulfobetaine (SB)	Electrospinning	$E=4.7$, $\sigma=9.5$, $\varepsilon=278$, $C=7.2$; $E=2.5$, $\sigma=7.9$, $\varepsilon=301$, $C=4.0$; $E=3.5$, $\sigma=4.8$, $\varepsilon=163$, $C=5.3$ (for 0, 50% and 75% SB content, respectively)	[104]

σ, tensile strength (MPa); ε, strain at break (%); E, Young's modulus (MPa); C, compliance (%/100 mm Hg); P_b, burst pressure (mm Hg); SS, suture strength (N).

losing cell phenotype. Burst pressure and suture retention were slightly lower than those of native arteries, while compliance was not measured. The group also fabricated this material into small-diameter bilayered scaffolds, with an internal layer prepared by TIPS, and an external electrospun layer (ES-TIPS) [11]. The ES-TIPS scaffold had good layer integration and showed no delamination. The stress–strain curve for TIPS-obtained scaffolds displayed an almost linear behavior, whereas the one for electrospun scaffolds showed a nonlinear trend, closer to that of native tissues. Scaffolds were mechanically anisotropic, showing a circumferential Young's modulus and an ultimate tensile strength comparable to those of native vessels, and intermediate between grafts formed by TIPS and ES grafts. The circumferential ultimate strain was higher for the ES-TIPS grafts when compared to the TIPS grafts, the ES grafts,

or that of native vessels. The burst pressure and the compliance were on the order of the saphenous vein. Cell seeding showed a bulk integration of cells and, overall, this approach appeared very promising for tissue engineered vascular grafts.

Several approaches have been explored to reduce the thrombogenicity of polymers for applications that require blood contact, such as modification of hydrophilicity [95,96], heparinization [97,98], and incorporation of zwitterions [99,100]. Bioresorbable SPUs have incorporated phosphorylcholine by surface modification and copolymer blending for vascular applications, displaying good thrombogenicity both *in vitro* and *in vivo* [37]. Wagner et al. also explored surface modification to improve PU blood compatibility. An electrospun vascular scaffold obtained from the previously discussed SPEsUU [93] was coated with an MPC (2-methacryloyloxyethyl phosphorylcholine)-based copolymer after surface activation by an ammonia plasma [101]. The coated samples exhibited compliance values in the order of native rat aortas after 4 weeks of implantation but then decreased during the following 8 weeks. Ultimate tensile strength and strain were on the order of native rat aorta after an implantation period of 12 weeks. Further studies, such as burst pressure tests, should be performed to demonstrate the potential use of the grafts as vascular substitutes.

Surface modification can be a possible solution for improving biocompatibility and blood response, but its effect may be influenced by degradation. Polyurethanes can be designed to incorporate active compounds in their formulation, so that the biological response can be maintained during degradation. Surfaces incorporating sulfobetaine (SB, a zwitterionic molecule) have displayed a reduction in platelet and protein adsorption [102,103]. Wagner et al. employed SB in the synthesis of a series of biodegradable SPEsUU, obtained from PCL:SB different ratios, BDI, and putrescine [104]. The electrospun SPEsUU with 50% SB content showed mechanical properties similar to those of the control SPEsUU (with no SB) under wet conditions. Compliance results were similar to those of saphenous veins, and the burst pressure was not measured. The materials also showed decreased enzymatic degradation, and a markedly reduced thrombogenicity *in vitro*.

15.4.2 *Polyurethane blend vascular grafts*

Beyond the biocompatibility presented by medical grade and novel synthesized bioresorbable PUs, they lack the bioactivity of natural biopolymers such as collagen and elastin. In response to this challenge, many authors have blended PUs with natural polymers to improve the biocompatibility and bioactivity of vascular grafts. Table 15.4 summarizes the mechanical performance of some selected vascular grafts based on PU blends.

Matsuda's group employed Cardiomat 610 to develop a microporous SPEU-based artificial graft by a computer-aided excimer laser ablation technique. The vascular grafts were coated with photoreactive gelatin on the outer and luminal surfaces as an artificial ECM for the enhancement of tissue ingrowth [105,106]. The graft's compliant nature was studied by the stiffness parameter (β) in a pressure–diameter apparatus. The stiffness of the most compliant graft was close to that of a human coronary artery. The graft's patency rate was 100% after 24 months implantation in male

Table 15.4 Some selected polyurethane-based scaffolds and characteristics

Scaffold	Fabrication technique	Mechanical performance	References
Cardiomat 610, photoreactive gelatin	Computer-aided excimer laser (KrF) ablation technique	$\beta = 37.7$	[105,106]
Cardiomat 610, photoreactive gelatin	Coaxial computer-aided excimer laser (KrF) ablation technique	$\beta_{\text{preimplanted}} = 9.2$, $\beta_{\text{12-months}} = 19.6$	[23,107]
Selectophore™, PCL, gelatin type B	Coaxial electrospinning	$E_{\text{0week}} = 93.36$, $\varepsilon_{\text{0week}} = 36$, $\sigma_{\text{0week}} = 1.67$ $E_{\text{4week}} = 40.43$, $\varepsilon_{\text{4week}} = 130$, $\sigma_{\text{4week}} = 1.29$	[108]
Selectophore™, elastin, collagen	Blend electrospinning	$E_{\text{col}} = 57.32$, $\varepsilon_{\text{col}} = 173.35$ $E_{\text{elas}} = 20.24$, $\sigma_{\text{elas}} = 7.86$, $\varepsilon_{\text{elas}} = 112.28$ $E_{\text{col-elas}} = 42.32$	[109]
Tecoflex® EG-80A, gelatin	Coelectrospinning	$\sigma_{\text{wet}} = 2.55$, $\varepsilon_{\text{wet}} = 330$, $E_{\text{wet}} = 0.5$	[31]
Tecoflex® EG-80A, collagen	Core–shell electrospinning	$\sigma = 3.9$, $\varepsilon = 145.6$	[110]
Tecoflex® EG-80A, collagen, chitosan	Blend electrospinning	$\sigma_{\text{ran}} = 9.38$, $\varepsilon_{\text{ran}} = 9.87$, $\sigma_{\text{all}} = 14.93$, $\varepsilon_{\text{all}} = 58.92$	[111]
PCL:BDI:putrescine, collagen	Blend electrospinning	$\sigma = 2–13$, $\varepsilon = 160–280$	[112]
PCL:BDI:putrescine, phospholipid polymer (PMBU)	Blend electrospinning	$C = 2.9–4.4$, $\sigma = 7–10$, $E = 5–10$, $\varepsilon = 301–342$	[37]
PCL:HDI:1,3-propanediol bis(4-aminobenzoate), fibrin hydrogel	Electrospinning bonded by hydrogel	$SS = 1.16$, $E_z = 0.48$, $\sigma = 0.32$	[113]
Pellethane®, polyester/spandex	Phase separation, yarn knitting	$C = 1.5–2.5$	[38,39]
Chronoflex® AL 80A, PEG	Blend electrospinning	$\sigma = 7$, $E = 2$, $\varepsilon = 250$	[32]
Chronoflex® AL 80A, PEGMA	Blend electrospinning	$\sigma = 5.98–12.04$, $\varepsilon = 285–234$	[114]
Tecothane TT1074A, PGA mesh	Electrospinning	$E_{\text{low-}\varepsilon} = 0.5$, $E_{\text{high-}\varepsilon} = 36.09$, $P_b = 3095$	[115]
Selectophore™, PCL	Electrospinning	$\sigma_z = 69.95$, $\varepsilon_z = 255$, $\sigma_\theta = 42.5$, $\varepsilon_\theta = 175$	[116]

σ, tensile strength (MPa); ε, strain at break (%); E, Young's modulus (MPa); C, compliance (%/100 mm Hg); P_b, burst pressure (mm Hg); SS, suture strength (N); β, stiffness parameter; subscripts: θ, circumferential; Z, tangential; col, collagen; elas, elastin; ran, random; all, alligned.

Sprague–Dawley rats, with no observation of stenotic or occluded grafts. To obtain a more compliant vascular graft that mimics the J-shaped mechanical response of natural arteries, Matsuda's group used these microporous SPEU-based artificial grafts to design a coaxial double layer compliant vascular graft [23,107]. The device consisted of two concentric layers separated by a slight distance from each other. The inner layer presented a mechanical response similar to that of natural arteries at lower pressures, while the behavior of both layers was similar to the response of natural arteries at high pressures. The distance between the layers was fixed to match the deformation level at which collagen fibers start to act. A study of the stiffness and J-shaped response change on *in vivo* implantation time was performed. Regenerated neoarterial wall and tissue adhesion to the inner tube caused an increase in the graft's stiffness and impaired the J curve with time. At 12 months after implantation a revert-back J curve was observed, associated with the deterioration of the SPEU. While these coaxial vascular grafts showed an unsatisfactory mechanical response at long implantation times, the design is promising for the utilization of other materials and processing technologies.

Gluck et al. produced a coaxial nanofibrous scaffold for vascular tissue engineering [108]. A coaxial electrospinning technique was used to obtain fibers with SPEU Selectophore™ in their core and blended PCL/gelatin in their sheath. The modulus, the tensile strength, and the strain of the coaxial scaffolds dropped after 1 week under culture-like conditions. The properties remained steady thereafter over the following 3 weeks. The inclusion of the SPEU inside the nanofibers adds the necessary elasticity for the mechanical response. Additionally, the SPEU improved the structural and mechanical integrity for long-term studies both *in vitro* and *in vivo*. Wong et al. studied the mechanical properties and cellular interactions of aligned nanofibrous Selectophore™ scaffolds blended with elastin and collagen [109]. The addition of collagen to the SPEU resulted in a stiffer scaffold, with increased Young's modulus and smaller failure strain. On the other hand, the addition of elastin to Selectophore™ resulted in a more compliant scaffold, with lower Young's modulus and a reduction in the peak stress and strain. The combination collagen/elastin/SPEU resulted in a scaffold with mechanical properties that were a combination of the individual proteins. The combination of elastin, which produced a viscoelastic material that could be useful for vascular grafts, and collagen, which provided biological signals that increased cell proliferation of SMC, resulted in a promising material for cardiovascular applications. Both these scaffolds were produced in a flat configuration; therefore only a uniaxial tensile test was used and a partial mechanical characterization of the scaffolds was performed.

Detta et al. employed Tecoflex® EG-80A to develop a composite SPEU/gelatin vascular graft by coelectrospinning [31]. The vascular grafts were characterized by tensile tests in both the circumferential and the longitudinal directions. No anisotropy on the mechanical properties was observed; however, the grafts presented adequate strength, low elastic modulus, and good extensibility. Gelatin fibers increased the rigidity of the composite mesh, providing appropriate mechanical properties combined with good cytocompatibility. The ultimate tensile strength and strain to failure were higher than those of native human coronary arteries, while elastic modulus was comparable to that of coronary arteries. Mo's group also used Tecoflex® EG-80A and

blended it with collagen and chitosan. They developed a coaxial scaffold with collagen as the sheath and the SPEU as the core [110]. The tensile properties of the scaffold were measured and it was possible to adjust the mechanical behavior of the scaffold by changing the SPEU concentration in the coaxial system. In a second study, Huang et al. added chitosan to the SPEU/collagen hybrid scaffold [111]. Random and aligned nanofibrous scaffolds based on collagen/chitosan/SPEU blends were electrospun to mimic the native extracellular matrix. Collagen and chitosan were selected to resemble the native ECM while the SPEU was added to improve mechanical properties of the scaffold. However, the mechanical properties obtained were not comparable to those of natural arteries. The incorporation of Tecoflex® improved the elasticity of the scaffolds, yet the elongation at break was low.

These studies focused on the biological characterization since the purpose of blending was to improve their bioactivity. Incomplete mechanical characterization was carried out, with some promising results and others out of the range of the properties of natural arteries. These studies also used biostable SPEU combined with bioresorbable biopolymers and in some cases the increase in graft stiffness after implantation was observed due to the lack of remodeling capability. A few studies have been made using biodegradable PUs blended with natural polymers.

Wagner et al. employed a biodegradable SPEsUU synthesized from PCL, BDI, and putrescine [93] which was blended with collagen and a phospholipid polymer to produce bioactive electrospun vascular grafts [37,112]. The incorporation of collagen resulted in a significant decrease in tensile strength, as well as reductions in initial and 100% elastic modulus. The SPEsUU was also blended with a nonthrombogenic bioinspired phospholipid poly-(methacryloyloxyethyl phosphorylcholine-co-methacryloyloxyethyl butyl urethane), PMBU. A more complete mechanical study was performed, with tensile tests and dynamic compliance measurements. The blend did not significantly modify the tensile strength, breaking strain, initial modulus, or 100% modulus and compliance. The mechanical property values were amenable to vascular applications with compliance values comparable with those of natural arteries.

McMahon et al. fabricated a multicomponent scaffold formed by SPEsUU electrospun mesh layers (intended to mimic the role of arterial collagen fibers) bonded together by a fibrin hydrogel matrix (designed to mimic the role of arterial elastic fibers) [113]. The biodegradable SPEsUU was synthesized from PCL, HDI, and 1,3-propanediol bis(4-aminobenzoate) as chain extender. The fibrin hydrogels were chosen due to their low stiffness, ideal for mimicking the initial toe region of the J curve at low internal pressure. The hybrid vascular grafts were characterized by circumferential mechanical tests on ring segments, suture-retention strength, and dynamic culture in a bioreactor, after which circumferential strains were estimated. The mechanical contribution of each component to the whole graft response was studied. The electrospun SPEsUU presented a more rigid J curve, similar to the contribution of collagen in natural arteries. The J curve of poly(ethylene glycol) (PEG)–fibrin hydrogel was much lower and resembled the elastin response in natural arteries. These hybrid vascular grafts displayed J-shaped stress–strain curves, with the region of upturning occurring at similar strains as for native human coronary

artery. Thus, the vascular graft retained the high tensile strength and suture-retention strength of the electrospun mesh but displayed a J-shaped mechanical response similar to that of the native coronary artery.

Besides the overall good mechanical behavior of PU-based vascular grafts, occasionally, the ultimate properties of the porous PU grafts are not adequate. Therefore, even though these grafts copy elastin's behavior at lower pressures, the reinforcing function of collagen fibers at higher pressures is missing. To obtain a more biomimetic mechanical response some authors have blended PUs with other synthetic polymers or used reinforcements.

Yang et al. produced a porous PU (Chemical Industry Co. Ltd, Yantai, China) vascular graft with a weft-knitted texture yarn of polyester/spandex blend as reinforcement [38]. To obtain the reinforced PU vascular grafts, glass mandrels of different diameter (from 4 to 8 mm) were coated with weft-knitted tubular fabrics. The mandrels were then immersed in a PU solution, and then placed in a coagulating bath to form porous vascular grafts. The graft's mechanical response was examined in a ring test and the circumferential tensile strength was characterized. The reinforced vascular graft circumferential strength was improved if compared to the control PU porous grafts; elasticity, however, was reduced but not significantly. The composite vascular grafts combined PU's good elasticity with the strength of weft-knitted fabrics. No other mechanical tests, such as suture-retention strength, dynamic pressure–diameter cycling, or burst pressure, were performed. Moreover, the measured circumferential properties were not presented in standard units, which makes it difficult to compare with the mechanical behavior of natural arteries. Furthermore, both the PU and the reinforcement used were biostable. This group continued studying these reinforced porous vascular grafts [39]. In a second work Pellethane® 2363-80AE was used and the compliance of the grafts was also characterized. Different polyester/spandex reinforcement ratios and wall thicknesses were studied. The more compliant vascular graft presented a compliance of 2.5%/100 mm Hg. The results showed that the compliance value increased by reducing wall thickness.

Wang et al. employed Chronoflex® AL 80A to develop a nanofibrous SPCU/PEG vascular graft by electrospinning [32]. The grafts were characterized biologically and mechanically; the latter was performed with a tensile test. The authors selected PEG to improve the hydrophilicity and nonthrombogenicity properties of the graft, but an increase in the tensile strength and elastic modulus was observed when incorporating PEG. The SPCU/PEG hybrid scaffolds response in wet conditions was elastic and the tensile properties were close to those of human and pig arteries. This work lacks a more complete mechanical characterization; however, a complete biological study was carried out. Good results regarding platelet adhesion, hemolysis rate, and cell attachment and proliferation were found for the scaffolds containing 20 and 30 wt% PEG content. In a second study, Wang et al. also produced a hybrid SPCU electrospun vascular graft, but this time it was blended with poly(ethylene glycol methacrylate) (PEGMA) [114]. The scaffold was photopolymerized and cross linked simultaneously during the electrospinning process. The authors used the blend to improve the biological properties of the vascular grafts; however, they also hypothesized that combining the SPCU with the cross-linking network

of PEGMA would give rise to improved mechanical properties. The mechanical characterization consisted of tensile testing. The cross-linked SPCU/PEGMA hybrid scaffolds presented appropriate mechanical properties combined with good cytocompatibility. Nevertheless, a more complete mechanical characterization needs to be carried out.

Rapoport et al. developed a modified electrospinning technique to obtain a vascular graft that mimics the J-shaped mechanical response of natural arteries [115]. The authors fabricated an expanding mandrel, which helps to obtain a reinforced graft with the undulated collagen fibers. Tecothane TT1074A was first electrospun over the mandrel at its smaller diameter. Later, the mandrel was expanded to a larger diameter and a reinforcing PGA woven tube was added to the PU layer. Finally, the mandrel was taken back to its original size, forcing the PGA layer to form corrugations. The mechanical biomimetic J-shaped response was studied by a quasi-static ring test. In addition, the burst pressure was analyzed. The vascular grafts presented a low stiffness $(0.5 \pm 0.17\,\text{MPa})$ at small strains, with the modulus increasing to $36.09 \pm 6.72\,\text{MPa}$. Burst pressure was $3095 \pm 1016\,\text{mm Hg}$, which was due to the failure of the reinforcing mesh and not the SPEU inner layer. The work presented a novel technique for obtaining a J-shaped mechanical response and a mechanism for adjusting the graft properties.

Guo et al. developed an electrospun blended vascular graft [116] from Selectophore™ and PCL. PCL was selected to substantially enhance the strength of the SPEU fibers due to its semicrystallinity. The authors emphasized the importance of a complete mechanical characterization of the vascular grafts to study their biomimetic behavior. They performed tensile tests in the graft circumferential and longitudinal direction, as well as cyclic tensile tests. The vascular grafts presented good anisotropic mechanical properties, appropriate porosity, cycling stability, and cytocompatibility, which make them a promising replacement for small-diameter blood scaffolds. However, the graft's strength is higher than the strength observed for natural arteries, and some other tests like pressure–diameter cycling and burst pressure were not performed.

All these studies show the improvement in PU mechanical response when a stiffer material is blended or a reinforcement is added to the vascular graft. However, they all employed biostable PUs that lack the ability to remodel and biodegrade, which should facilitate natural tissue regeneration. Our group has worked with a bioresorbable SPEsUU (PHD) with an elastomeric mechanical response similar to that of elastin fibers, blended with PLLA, a stiffer and bioresorbable polymer that has a mechanical behavior similar to that of collagen fibers [117]. A bilayered electrospun vascular graft was developed with two different blend ratios in each layer to mimic the elastin/collagen ratio present in natural coronary arteries. A complete mechanical characterization was performed, including uniaxial tensile tests in the circumferential and longitudinal directions of the graft, suture-retention tests, and burst pressure assays performed in a physiologic chamber at 37 °C and dynamic pressure–diameter tests in a bioreactor (Montini-Ballarin, work unpublished). The bilayered vascular grafts presented a J-shaped response and a mechanical behavior similar to that of natural blood vessels, such as coronary arteries, radial and internal mammary arteries and saphenous vein.

15.5 Future trends and perspectives

Recently, bioactive PU tubular scaffolds have been developed. Strategies such as the incorporation of single or multiple growth factors, with different delivery profiles, surface modification of the graft lumen with antithrombogenic molecules like heparin, and even the synthesis and utilization of novel nonthrombogenic polymers have been employed. In some studies, the influence of these modifications on mechanical properties was also examined, along with the graft's biological properties [33,104,118].

Besides advances in the synthesis and processing of biodegradable PUs conducted in recent years, their utilization in small-diameter vascular grafts is still very sparse. In addition, there are few studies where a complete characterization of the mechanical behavior under physiological conditions was performed.

There is a dilemma about which PU type is more appropriate for long-term implantation of vascular grafts. The use of biostable SPEUs has shown oxidative degradation and also an increase in graft stiffness after implantation due to the load supported by the polymer and new host tissue as well. However, the use of biodegradable PUs may also have a weakness. If the tissue that replaces the degrading graft does not have the biomechanical properties to support the internal load, the development of weak spots after implantation and subsequently aneurism formation can occur. The synchronization between the degradation rate and the time to regenerate new vascular tissue with adequate mechanical behavior is crucial for the graft's success when biodegradable polymers are used. Therefore, it is important to evaluate the vascular graft's mechanical behavior over implantation time. Very few works have performed such studies with biostable PUs [107] and even less with biodegradable PUs [101].

The development of an off-the-shelf small-diameter vascular graft for bypass surgery with proper mechanical properties and biologic response is still an ongoing issue of current research in the field of vascular tissue engineering.

References

[1] Bouten CVC, Dankers PYW, Driessen-Mol A, Pedron S, Brizard AMA, Baaijens FPT. Substrates for cardiovascular tissue engineering. Adv Drug Deliv Rev 2011;63:221–41.

[2] Rhodin JAG. Architecture of the vessel wall in comprehensive physiology. Supplement 7: Handbook of physiology, the cardiovascular system, vascular smooth muscle. 2014. p. 1–31. First published in print 1980. http://dx.doi.org/10.1002/cphy.cp020201.

[3] Seifu DG, Purnama A, Mequanint K, Mantovani D. Small-diameter vascular tissue engineering. Nat Rev Cardiol Adv 2013. http://dx.doi.org/10.1038/nrcardio.2013.77. (online publication).

[4] Canver CC. Conduit options in coronary artery bypass surgery. Chest 1995;108:1150–5.

[5] Kannan RY, Salacinski HJ, Butler PE, Hamilton G, Seifalian AM. Current status of prosthetic bypass grafts: a review. J Biomed Mater Res B Appl Biomaterials 2005;74B:570–81.

[6] Ravi S, Chaikof EL. Biomaterials for vascular tissue engineering. Regen Med 2010;5:107–20.

[7] Claes E, Atienza JM, Guinea GV, Rojo FJ, Bernal JM, Revuelta JM, et al. Mechanical properties of human coronary arteries. Conf Proc IEEE Eng Med Biol Soc 2010;2010:3792–5.

[8] L'Hereux N, Dusserre N, Konig G, Victor B, Keire P, Wight TN, et al. Human tissue engineered blood vessels for adult arterial revascularization. Nat Med 2006;12:361–5.

[9] Donovan DL, Schmidt SP, Townshend SP, Njus GO, Sharp WV. Material and structural characterization of human saphenous vein. J Vasc Surg 1990;12:531–7.

[10] Konig G, McAllister TN, Dusserre N, Garrido SA, Iyican C, Marini A, et al. Mechanical properties of completely autologous human tissue engineered blood vessels compared to human saphenous vein and mammary artery. Biomaterials 2009;30:1542–50.

[11] Soletti L, Hong Y, Guan J, Stankus JJ, El-Kurdi MS, Wagner WR, et al. A bilayered elastomeric scaffold for tissue engineering of small diameter vascular grafts. Acta Biomater 2010;6:110–22.

[12] Yin A, Zhang K, McClure MJ, Huang C, Wu J, Fang J, et al. Electrospinning collagen/chitosan/poly(L-lactic acid-co-ε-caprolactone) to form a vascular graft: mechanical and biological characterization. J Biomed Mater Res A 2013;101A:1292–301.

[13] Claes E. Estudio mecánico de las arterias coronarias humanas y sus sustitutos vasculares, tesis doctoral, Escuela técnica superior de ingenieros de caminos, canales y puertos. Universidad Politécnica de Madrid; 2010.

[14] O'Rourke MF. Arterial function in health and disease. Edinburgh: Churchill Livingstone; 1982. p. 153–69.

[15] Shadwick RE. Mechanical design in arteries. J Exp Biol 1999;202:3305–13.

[16] Armentano RL, Barra JG, Levenson J, Simon A, Pichel RH. Arterial wall mechanics in conscious dogs: assessment of viscous, inertial, and elastic moduli to characterize aortic wall behavior. Circ Res 1995;76:468–78.

[17] Roach MR, Burton AC. The reason for the shape of the distensibility curves of arteries. Can J Physiol Pharmacol 1957;35:681–890.

[18] Armentano RL, Levenson J, Barra JG, Fischer EI, Breitbart GJ, Pichel RH, et al. Assessment of elastin and collagen contribution to aortic elasticity in conscious dogs. Am J Physiol 1991;260:H1870–7.

[19] Barra JG, Armentano RL, Levenson J, Fischer EI, Pichel RH, Simon A. Assessment of smooth muscle contribution to descending thoracic aortic elastic mechanics in conscious dogs. Circ Res 1993;73:1040–50.

[20] Fung YC. Biomechanics: mechanical properties of living tissues. 2nd ed. Heidelberg: Springer; 1993.

[21] Bergel DH. The static elastic properties of the arterial wall. J Physiol 1961;156:445–57.

[22] Bergel DH. The dynamic elastic properties of the arterial wall. J Physiol 1961;156:458–69.

[23] Sonoda H, Takamizawa K, Nakayama Y, Yasui H, Matsuda T. Small-diameter compliant arterial graft prosthesis: design concept of coaxial double tubular graft and its fabrication. J Biomed Mater Res 2001;55:266–76.

[24] Lee H, Kim SH, Jung YM, Chung JH, Kim SH, Kim SH. Novel measurement of pressure inside a compliant vascular scaffold of PLCL. J Tissue Eng Regen Med 2010;7:298–308.

[25] Rachev A, Felden L, Ku DN. Design and fabrication of a mechanically matched vascular graft. J Biomech Eng 2011;133:091004–8.

[26] Abbott W, Megerman J, Hasson J, L'Italien G, Warnock D. Effect of compliance mismatch on vascular graft patency. J Vasc Surg 1987;5:376–82.

[27] Nerem RM. Role of mechanics in vascular tissue engineering. Biorheology 2003;40:281–7.

[28] Gamero LG, Armentano RL, Barra JG, Simon A, Levenson J. Identification of arterial wall dynamics in conscious dogs. Exp Physiol 2001;86:519–28.

[29] Brum J, Bia D, Benech N, Balay G, Armentano RL, Negreira C. Setup of a cardiovascular simulator: application to the evaluation of the dynamical behavior of atheroma plaques in human arteries. Phys Procedia 2010;3:1095–101.

[30] Suárez-Bagnasco D, Armentano RL, Balay G, Cymberknop LJ, Brum J, Bia D, et al. Measurement system for an in- vitro characterization of the biomechanics and hemodynamics of arterial bifurcations. J Phys Conf Ser 2013;421:012018–26.

[31] Detta N, Errico C, Dinucci D, Puppi D, Clarke DA, Reilly GC, et al. Novel electrospun polyurethane/gelatin composite meshes for vascular grafts. J Mater Sci Mater Med 2010;21:1761–9.

[32] Wang H, Feng Y, Fang Z, Yuan W, Khan M. Co-electrospun blends of PU and PEG as potential biocompatible scaffolds for small-diameter vascular tissue engineering. Mater Sci Eng C 2012;32:2306–15.

[33] Han F, Jia X, Dai D, Yang X, Zhao J, Zhao Y, et al. Performance of a multilayered small-diameter vascular scaffold dual-loaded with VEGF and PDGF. Biomaterials 2013;34:7302–13.

[34] Marelli B, Achilli M, Alessandrino A, Freddi G, Tanzi MC, Farè S, et al. Collagen reinforced electrospun silk fibroin tubular construct as small calibre vascular graft. Macromol Biosci 2012;12:1566–74.

[35] McClure MJ, Simpson DG, Bowlin GL. Tri-layered vascular grafts composed of polycaprolactone, elastin, collagen, and silk: optimization of graft properties. J Mech Behav Biomed Mater 2012;10:48–61.

[36] Salvucci FP, Bia D, Armentano RL, Barra JG, Craiem D, Zócalo Y, et al. Association between mechanics and structure in arteries and veins: theoretical approach to vascular graft confection. Conf Proc IEEE Eng Med Biol Soc 2009;2009:4258–61.

[37] Hong Y, Ye S-H, Nieponice A, Soletti L, Vorp DA, Wagner WR. A small diameter, fibrous vascular conduit generated from a poly(ester urethane)urea and phospholipid polymer blend. Biomaterials 2009;30:2457–67.

[38] Yang H, Xu W, Ouyang C, Zhou F, Cui W, Yi C. Circumferential compliance of small diameter polyurethane vascular grafts reinforced with elastic tubular fabric. Fibres Text East Eur 2009;17(6(77)):89–92.

[39] Yang H, Zhu G, Zhang Z, Wang Z, Fang J, Xu W. Influence of weft-knitted tubular fabric on radial mechanical property of coaxial three-layer small-diameter vascular graft. J Biomed Mater Res B 2012;100B:342–9.

[40] Ahmed M, Hamilton G, Seifalian AM. The performance of a small-calibre graft for vascular reconstructions in a senescent sheep model. Biomaterials 2014;35:9033–40.

[41] ANSI/AAMI/ISO 7198:1998/2001/(R). Cardiovascular implants-tubular vascular prostheses. 2010.

[42] Rushmer RF, Franklin DL, Ellis RM. Left ventricular dimensions recorded by sonocardiometry. Circ Res 1956;4:684–8.

[43] O'Rourke MF, Staessen JA, Vlachopoulos C, Duprez D, Plante GE. Clinical applications of arterial stiffness: definitions and reference values. Am J Hypertens 2002;15:426–44.

[44] Peterson LH, Jensen RE, Parnell J. Mechanical properties of arteries in vivo. Circ Res 1960;8:622–39.

[45] Gosling RG, Budge MM. Terminology for describing the elastic behavior of arteries. Hypertension 2003;41:1180–2.

[46] Laterreur V, Ruel J, Auger FA, Vallières K, Tremblay C, Lacroix D, et al. Comparison of the direct burst pressure and the ring tensile test methods for mechanical characterization of tissue-engineered vascular substitutes. J Mech Behav Biomed Mater 2014;34:253–63.

[47] McKenna KA, Hinds MT, Sarao RC, Wu PC, Maslen CL, Glanville RW, et al. Mechanical property characterization of electrospun recombinant human tropoelastin for vascular graft biomaterials. Acta Biomater 2012;8:225–33.

[48] Yao L, Liu J, Andreadis ST. Composite fibrin scaffolds increase mechanical strength and preserve contractility of tissue engineered blood vessels. Pharm Res 2008;25:1212–21.

[49] Syedain ZH, Meier LA, Bjork JW, Lee A, Tranquillo RT. Implantable arterial grafts from human fibroblasts and fibrin using a multi-graft pulsed flow-stretch bioreactor with noninvasive strength monitoring. Biomaterials 2011;32:714–22.

[50] Sell SA, Wolfe PS, Garg K, McCool JM, Rodriguez IA, Bowlin GL. The use of natural polymers in tissue engineering: a focus on electrospun extracellular matrix analogues. Polymers 2010;2:522–53.

[51] Inoguchi H, Kwon IK, Inoue E, Takamizawa K, Maehara Y, Matsuda T. Mechanical responses of a compliant electrospun poly(ʟ-lactide-co-ε-caprolactone) small-diameter vascular graft. Biomaterials 2006;27:1470–8.

[52] Crapo PM, Wang Y. Physiologic compliance in engineered small-diameter arterial constructs based on an elastomeric substrate. Biomaterials 2010;31:1626–35.

[53] Dargaville BL, Vaquette C, Rasoul F, Cooper-White JJ, Campbell JH, Whittaker AK. Electrospinning and crosslinking of low-molecular-weight poly(trimethylene carbonate-co-ʟ-lactide) as an elastomeric scaffold for vascular engineering. Acta Biomater 2013;9:6885–97.

[54] Moore T. Design and synthesis of biodegradable thermoplastic polyurethanes for tissue engineering. (Australia): Swinburne University of Technology; 2005. [Ph.D. thesis].

[55] Caracciolo PC, Thomas V, Vohra YK, Buffa F, Abraham GA. Electrospinning of novel biodegradable poly(ester urethane)s and poly(ester urethane urea)s for soft tissue-engineering applications. J Mater Sci Mater Med 2009;20:2129–37.

[56] Caracciolo PC, de Queiroz AAA, Higa OZ, Buffa F, Abraham GA. Segmented poly(ester-urethane urea)s from novel urea–diol chain extenders: synthesis, characterization and in vitro biological properties. Acta Biomater 2008;4:976–88.

[57] Caracciolo PC, Buffa F, Abraham GA. Effect of the hard segment chemistry and structure on the thermal and mechanical properties of novel biomedical segmented poly(ester-urethanes). J Mater Sci Mater Med 2009;20:145–55.

[58] Caracciolo PC, Buffa F, Thomas V, Vohra YK, Abraham GA. Biodegradable polyurethanes: comparative study of electrospun scaffolds and films. J Appl Polym Sci 2011;121:3292–9.

[59] Couet F, Rajan N, Mantovani D. Macromolecular biomaterials for scaffold-based vascular tissue engineering. Macromol Biosci 2007;7:701–18.

[60] Sauvage LR, Berger KE, Mansfield PB, Wood SJ, Smith JC, Overton JB. Future directions in the development of arterial prostheses for small and medium caliber arteries. Surg Clin North Am 1974;54:213–28.

[61] Lindenauer SM, Weber TR, Miller TA, Ramsburgh SR, Salles CA, Kahn SP, et al. The use of velour as a vascular prosthesis. Biomed Eng 1976;11:301–6.

[62] Annis D, Bornat A, Edwards RO, Higham A, Loveday B, Wilson J. An elastomeric vascular prosthesis. Trans Am Soc Artif Intern Organs 1978;24:209–14.

[63] How TV, Clarke RM. The elastic properties of a polyurethane arterial prosthesis. J Biomech 1984;17:597–608.

[64] Matsuda T, Ihara M, Inoguchi H, Kwon IK, Takamizawa K, Kidoaki S. Mechano-active scaffold design of small-diameter artificial graft made of electrospun segmented polyurethane fabrics. J Biomed Mater Res A 2005;73A:125–31.

[65] Kidoaki S, Kwon IK, Matsuda T. Structural features and mechanical properties of in situ–bonded meshes of segmented polyurethane electrospun from mixed solvents. J Biomed Mater Res B Appl Biomater 2006;76B:219–29.

[66] Uttayarat P, Perets A, Li M, Pimton P, Stachelek SJ, Alferiev I, et al. Micropatterning of three-dimensional electrospun polyurethane vascular grafts. Acta Biomater 2010;6:4229–37.

[67] Grasl C, Bergmeister H, Stoiber M, Schima H, Weigel G. Electrospun polyurethane vascular grafts: in vitro mechanical behavior and endothelial adhesion molecule expression. J Biomed Mater Res A 2010;93A:716–23.

[68] Theron JP, Knoetze JH, Sanderson RD, Hunter R, Mequanint K, Franz T, et al. Modification, crosslinking and reactive electrospinning of a thermoplastic medical polyurethane for vascular graft applications. Acta Biomater 2010;6:2434–47.

[69] Bergmeister H, Schreiber C, Grasl C, Walter I, Plasenzotti R, Stoiber M, et al. Healing characteristics of electrospun polyurethane grafts with various porosities. Acta Biomater 2013;9:6032–40.

[70] Soldani G, Losi P, Bernabei M, Burchielli S, Chiappino D, Kull S, et al. Long term performance of small-diameter vascular grafts made of a poly(ether)urethane-polydimethylsiloxane semi-interpenetrating polymeric network. Biomaterials 2010;31:2592–605.

[71] Kayal TA, Maniglio D, Bonani W, Losi P, Migliaresi C, Soldani G. A combined method for bilayered vascular graft fabrication. J Mater Sci Mater Med 2015;26:96–100.

[72] Christenson EM, Dadsetan M, Wiggins M, Anderson JM, Hiltner A. Poly(carbonate urethane) and poly(ether urethane) biodegradation: in vivo studies. J Biomed Mater Res A 2004;69A:407–16.

[73] Heijkants RGJC, Van Calck RV, Van Tienen TG, De Groot JH, Buma P, Pennings AJ, et al. Uncatalyzed synthesis, thermal and mechanical properties of polyurethanes based on poly(ε-caprolactone) and 1,4-butane diisocyanate with uniform hard segment. Biomaterials 2005;26:4219–28.

[74] Jing X, Mi H-Y, Salick MR, Cordie TM, Penga X-F, Turng L-S. Electrospinning thermoplastic polyurethane/graphene oxide scaffolds for small diameter vascular graft applications. Mater Sci Eng C Mater Biol Appl 2015;49:40–50.

[75] Chang YL, Yang ST, Liu JH, Dong E, Wang YW, Cao AN, et al. In vitro toxicity evaluation of graphene oxide on A549 cells. Toxicol Lett 2011;200:201–10.

[76] Ruiz A, Flanagan CE, Masters KS. Differential support of cell adhesion and growth by copolymers of polyurethane with hyaluronic acid. J Biomed Mater Res A 2013;101A:2870–82.

[77] He W, Hu Z, Xu A, Liu R, Yin H, Wang J, et al. The preparation and performance of a new polyurethane vascular prosthesis. Cell Biochem Biophys 2013;66:855–66.

[78] Stokes KB. Polyether polyurethanes: biostable or not? J Biomater Appl 1988;3: 228–59.

[79] Murabayashi S, Kambic H, Harasaki H, Morimoto T, Yozu R, Nose Y. Fabrication and long-term implantation of semi-compliant small vascular prosthesis. Trans Am Soc Artif Intern Organs 1985;31:50–4.

[80] Uchida N, Kambic H, Emoto H, Chen J-F, Hsu S-H, Murabayshi S, et al. Compliance effects on small diameter polykethane graft patency. J Biomed Mater Res 1993;27:1269–79.

[81] Stokes KB, Coury AJ, Urbanski P. Autooxidative degradation of implanted polyether polyurethane devices. J Biomater Appl 1987;1:411–8.

[82] Coury AJ, Stokes KB, Cahalan PT, Slaikeu PC. Biostability considerations for implantable polyurethanes. Life Support Syst 1987;5:25–39.

[83] Takahara A, Coury AJ, Hergenrother RW, Cooper SL. Effect of soft segment chemistry on the biostability of segmented polyurethanes. I. In vitro oxidation. J Biomed Mater Res 1991;25:341–56.

[84] How TV, Annis D. Viscoelastic behavior of polyurethane vascular prostheses. J Biomed Mater Res 1987;21:1093–108.

[85] How TV. Elastic deformation of a tapered vascular prosthesis. J Mater Sci Mater Med 1991;2:94–100.

[86] Han J, Farah S, Domb AJ, Lelkes PI. Electrospun rapamycin-eluting polyurethane fibers for vascular grafts. Pharm Res 2013;30:1735–48.

[87] Cozzens D, Wei X, Faust R. Electrospinning of biostable polyisobutylene-based thermoplastic polyurethanes. J Polym Sci B Polym Phys 2013;51:452–9.

[88] Stansby G, Berwanger C, Shukla N, Schmitz-Rixen T, Hamilton G. Endothelial seeding of compliant polyurethane vascular graft material. Br J Surg 1994;81:1286–9.

[89] Ahmed M, Ghanbari H, Cousins BG, Hamilton G, Seifalian AM. Small calibre polyhedral oligomeric silsesquioxane nanocomposite cardiovascular grafts: influence of porosity on the structure, haemocompatibility and mechanical properties. Acta Biomater 2011;7:3857–67.

[90] Nezarati RM, Eifert MB, Dempsey DK, Cosgriff-Hernandez E. Electrospun vascular grafts with improved compliance matching to native vessels. J Biomed Mater Res B Appl Biomater 2015;103B:313–23.

[91] Krynauw H, Bruchmüller L, Bezuidenhout D, Zilla P, Franz T. Degradation-induced changes of mechanical properties of an electro-spun polyester-urethane scaffold for soft tissue regeneration. J Biomed Mater Res B Appl Biomater 2011;99B:359–68.

[92] Han J, Cao R-W, Chen B, Ye L, Zhang A-Y, Zhang J, et al. Electrospinning and biocompatibility evaluation of biodegradable polyurethanes based on L-lysine diisocyanate and L-lysine chain extender. J Biomed Mater Res A 2011;96A:705–14.

[93] Guan J, Sacks MS, Beckman EJ, Wagner WR. Synthesis, characterization, and cytocompatibility of elastomeric, biodegradable poly(ester-urethane)ureas based on poly(caprolactone) and putrescine. J Biomed Mater Res 2002;61:493–503.

[94] Nieponice A, Soletti L, Guan J, Deasy BM, Huard J, Wagner WR, et al. Development of a tissue-engineered vascular graft combining a biodegradable scaffold, muscle-derived stem cells and a rotational vacuum seeding technique. Biomaterials 2008;29:825–33.

[95] Sun T, Tan H, Han D, Fu Q, Jiang L. No platelet can adhere-largely improved blood compatibility on nanostructured superhydrophobic surfaces. Small 2005;1:959–63.

[96] Xiang T, Yue WW, Wang R, Liang S, Sun SD, Zhao CS. Surface hydrophilic modification of polyethersulfone membranes by surface-initiated ATRP with enhanced blood compatibility. Colloids Surf B Biointerfaces 2013;110:15–21.

[97] Wang LR, Qin H, Nie SQ, Sun SD, Ran F, Zhao CS. Direct synthesis of heparin-like poly(ether sulfone) polymer and its blood compatibility. Acta Biomater 2013;9:8851–63.

[98] Pan CJ, Hou YH, Zhang BB, Dong YX, Ding HY. Blood compatibility and interaction with endothelial cells of titanium modified by sequential immobilization of poly(ethylene glycol) and heparin. J Mater Chem 2014;2:892–902.

[99] Sin MC, Chen SH, Chang Y. Hemocompatibility of zwitterionic interfaces and membranes. Polym J 2014;46:436–43.

[100] Sin MC, Sun YM, Chang Y. Zwitterionic-based stainless steel with well-defined polysulfobetaine brushes for general bioadhesive control. ACS Appl Mater Interfaces 2014;6:861–73.

[101] Soletti L, Nieponice A, Hong Y, Ye S-H, Stankus JJ, Wagner WR, et al. In vivo performance of a phospholipid-coated bioerodable elastomeric graft for small-diameter vascular applications. J Biomed Mater Res A 2011;96A:436–48.

[102] Zhang Z, Zhang M, Chen S, Horbett TA, Ratner BD, Jiang S. Blood compatibility of surfaces with superlow protein adsorption. Biomaterials 2008;29:4285–91.

[103] Kuo WH, Wang MJ, Chien HW, Wei TC, Lee C, Tsai WB. Surface modification with poly(sulfobetaine methacrylateco-acrylic acid) to reduce fibrinogen adsorption, platelet adhesion, and plasma coagulation. Biomacromolecules 2011;12:4348–56.

[104] Ye S-H, Hong Y, Sakaguchi H, Shankarraman V, Luketich SK, D'Amore A, et al. Nonthrombogenic, biodegradable elastomeric polyurethanes with variable sulfobetaine content. ACS Appl Mater Interfaces 2014;6:22796–806.

[105] Doi K, Matsuda T. Significance of porosity and compliance of microporous, polyurethane-based microarterial vessel on neoarterial wall regeneration. J Biomed Mater Res 1997;37:573–84.

[106] Doi K, Nakayama Y, Matsuda T. Novel compliant and tissue-permeable microporous polyurethane vascular prosthesis fabricated using an excimer laser ablation technique. J Biomed Mater Res 1996;31:27–33.

[107] Sonoda H, Takamizawa K, Nakayama Y, Yasui H, Matsuda T. Coaxial double-tubular compliant arterial graft prosthesis: time-dependent morphogenesis and compliance changes after implantation. J Biomed Mater Res A 2003;65A:170–81.

[108] Gluck JM, Rahgozar P, Ingle NP, Rofail F, Petrosian A, Cline MG, et al. Hybrid coaxial electrospun nanofibrous scaffolds with limited immunological response created for tissue engineering. J Biomed Mater Res B Appl Biomater 2011;99B:180–90.

[109] Wong CS, Liu X, Xu Z, Lin T, Wang X. Elastin and collagen enhances electrospun aligned polyurethane as scaffolds for vascular graft. J Mater Sci Mater Med 2013;24:1865–74.

[110] Chen R, Huang C, Ke Q, He C, Wang H, Mo X. Preparation and characterization of coaxial electrospun thermoplastic polyurethane/collagen compound nanofibers for tissue engineering applications. Colloids Surf B Biointerfaces 2010;79:315–25.

[111] Huang C, Chen R, Ke Q, Morsi Y, Zhang K, Mo X. Electrospun collagen–chitosan–TPU nanofibrous scaffolds for tissue engineered tubular grafts. Colloids Surf B Biointerfaces 2011;82:307–15.

[112] Stankus JJ, Guan J, Wagner WR. Fabrication of biodegradable elastomeric scaffolds with sub-micron morphologies. J Biomed Mater Res A 2004;70A:603–14.

[113] McMahon RE, Qu X, Jimenez-Vergara AC, Bashur CA, Guelcher SA, Goldstein AS, et al. Hydrogel–electrospun mesh composites for coronary artery bypass grafts. Tissue Eng C 2011;17:451–61.

[114] Wang H, Feng Y, An B, Zhang W, Sun M, Fang Z, et al. Fabrication of PU/PEGMA cross-linked hybrid scaffolds by in situ UV photopolymerization favoring human endothelial cells growth for vascular tissue engineering. J Mater Sci Mater Med 2012;23:1499–510.

[115] Rapoport HS, Fish J, Basu J, Campbell J, Genheimer C, Payne R, et al. Construction of a tubular scaffold that mimics J-shaped stress/strain mechanics using an innovative electrospinning technique. Tissue Eng C 2012;18:567–74.

[116] Guo F, Wang N, Wang L, Hou L, Ma L, Liu J, et al. An electrospun strong PCL/PU composite vascular graft with mechanical anisotropy and cyclic stability. J Mater Chem A 2015;3:4782–7.

[117] Montini-Ballarin F, Caracciolo PC, Blotta E, Ballarin VL, Abraham GA. Optimization of poly(L-lactic acid)/segmented polyurethane electrospinning process for the production of bilayered small-diameter nanofibrous tubular structures. Mater Sci Eng C 2014;42:489–99.

[118] Lu G, Cui SJ, Geng X, Ye L, Chen B, Feng ZG, et al. Design and preparation of polyurethane-collagen/heparin-conjugated polycaprolactone double-layer bionic small-diameter vascular graft and its preliminary animal tests. Chin Med J (Engl) 2013;126:1310–6.

Polyurethanes for bone tissue engineering

16

S. Fernando[1], M. McEnery[2], S.A. Guelcher[2,3,*]

[1]School of Medicine, Vanderbilt University Medical Center, Nashville, TN, USA;
[2]Department of Biomedical Engineering, Vanderbilt University, Nashville, TN, USA;
[3]Department of Chemical and Biomolecular Engineering, Vanderbilt University, Nashville, TN, USA
*Corresponding author: scott.guelcher@vanderbilt.edu

16.1   Introduction

Bone grafting is required for treatment of open fractures larger than critical size that will not heal without a scaffold to support bone ingrowth [1]. While autograft bone has long been considered the gold standard, it is limited in availability, and harvesting of autograft is a source of donor site morbidity. Synthetic bone grafts are relatively simple to manufacture, broadly available, and generally lower cost. Ceramics, such as bioactive glasses [2], calcium phosphate granules [3], and injectable calcium phosphate cements [4], have been used extensively for bone grafting due to their similarities in chemical composition to the mineral components in bone. Polyurethanes have also been investigated as synthetic bone grafts. This family of materials offers the advantages of injectability and settability, tunable mechanical properties, controlled degradation to noncytotoxic breakdown products, and local diffusion-controlled release of biologics [5]. Polyurethane bone grafts can be formed as implantable gas-blown porous scaffolds [6,7], injectable composites with ceramic particles [8,9], or as drug delivery systems [10,11].

This chapter will review polyurethane-derived bone grafts used in orthopedic applications, such as bone void fillers, bone cements, and osteoinductive scaffolds. First, the term "polyurethane" is defined and polyurethane chemistry specific to bone grafts is reviewed. An overview of osteoconductive polyurethane bone cements and bone void fillers is presented, including a review of their handling properties, mechanical properties, degradation rates, and preclinical studies. Finally, the incorporation of biologics to enhance osteoinductivity or provide antimicrobial activity is reviewed to illustrate the potential of polyurethane-derived grafts for bone regeneration.

16.2   Chemistry of polyurethane bone grafts

The chemistry of polyurethane scaffolds for tissue regeneration has been reviewed [5,12]. In this section, polyurethane chemistry relevant to bone scaffolds will be presented.

16.2.1   Raw materials

16.2.1.1   Polyisocyanates

Polyisocyanates are characterized by multiple —N═C═O functionality and react with polyalcohols (polyols), polyamines, or water to form urethane or urea linkages. Their chemistry has been extensively reviewed [13,14]. The reactions with polyols and polyamines are known as the gelling reaction, since the two liquid components react to form a solid cross-linked polymer. The water (blowing) reaction is important for the synthesis of polyurethane foams, where the carbon dioxide gas functions as a biocompatible blowing agent. While carboxylic acids, ureas, urethanes, and amides also react with isocyanates, these reactions are generally much slower and not as important for the synthesis of polyurethane bone grafts. Polyurethane bone grafts are most frequently synthesized from either lysine- or hexamethylene diamine-derived polyisocyanates due to toxicity concerns associated with aromatic polyisocyanates.

16.2.1.2   Polyols

Polyols are multifunctional alcohols with a polyether, polyester, or polycarbonate backbone. They are typically viscous liquids with molecular weights ranging from 200 to 5000 g/mol. The polyol component of the polyurethane significantly affects the degradation rate of the final cured polyurethane. Typically, the rate of hydrolytic degradation of polyols observes the order polycarbonate < polyether < polyester.

16.2.2   Prepolymers

Prepolymers are frequently used in injectable two-component systems to improve handling properties or reduce toxicity. Isocyanate-terminated prepolymers are prepared by reacting an excess of a polyisocyanate with a polyol at 60–90 °C in the presence of a urethane catalyst, such as dibutyltin dilaurate. By varying the molar ratio of polyisocyanate:polyol, prepolymers with targeted NCO content and average molecular weight can be prepared. The NCO content of prepolymers typically ranges from 5 to 25 wt%, while less viscous quasiprepolymers typically have NCO content exceeding 25% [14].

16.2.3   Reactive liquid molding

Two-component polyurethanes can be fabricated by reactive liquid molding, a process in which a polyisocyanate or prepolymer is mixed with a polyol and either injected or cast into a mold. The reactive liquid mixture cures after injection to form a solid scaffold. Water can be included as a blowing agent to generate carbon dioxide gas and consequently form pores [15,16]. To enhance the osteoconductivity and mechanical properties of the scaffolds, allograft bone [8,17,18], bioactive glass [19,74], or ceramic [9] particles can be added to the reactive polyurethane liquid. Segmented polyurethane elastomers, cross-linked cast elastomers, porous cross-linked foams, and cross-linked polyurethane/ceramic composites can be processed by reactive liquid molding. If the

extent of chemical cross-linking is sufficiently high (functionality > 2), then the material is an insoluble thermoset. Triols and hexols, as well as low molecular weight triol and triamine cross-linkers, are commonly used to prepare chemically cross-linked polyurethanes [13].

16.3 Bone grafting

When discussing materials used for bone grafting for regeneration, it is important to first describe the categories of materials that are generally used for bone tissue regeneration. These categories are briefly reviewed below.

16.3.1 Types of bone grafts

16.3.1.1 Bone void fillers

Bone void fillers (BVFs) are used to promote more reproducible healing of metaphyseal bone defects. BVFs are designed to fill a large bone void and provide an osteoconductive scaffold for new bone formation, thereby preventing failure of fixation, supporting alignment of bone articulating surfaces, and preventing formation of fibrous tissue (scarring) [20]. In contrast to bone cements, BVFs do not require bonelike strength, and therefore are used in non-load-bearing metaphyseal bone defects. Materials used for BVFs include bone, allograft bone (including demineralized bone matrix), ceramics, and synthetic polymers. Polyurethanes are well suited as BVFs due to their favorable handling properties (injectability and settability), their ability to foam *in situ*, and their potential for augmentation with mineralized particles to enhance the osteoconductivity of the graft.

16.3.1.2 Bone cements

Bone cements are used for metaphyseal bone defects where the mechanical forces that the graft will be subjected to require bone-like strength. Bone cements have been commonly used in the placement of artificial joints and repair of cortical bone. Calcium phosphate cements have been reported to be superior to autograft for reconstruction of weight-bearing tibial plateau fractures [21]. Nonresorbable poly(methymethacrylate) (PMMA) cements are also frequently used to stabilize vertebral fractures by vertebroplasty [22]. Due to their favorable handling properties, tunable degradation, and ability to reinforce with ceramics, polyurethanes have been investigated as weight-bearing bone cements [9, 23–25, 74].

16.3.1.3 Osteoinductive bone grafts

A number of orthopedic procedures, including tibial fractures of the mid-diaphysis [26], spine fusion [27], and alveolar ridge augmentation [28], require an osteoinductive agent to ensure predictable and reliable healing. Osteoinductive bone grafts are augmented with biologics, such as recombinant human bone morphogenetic

protein-2 (rhBMP-2) [29,30], that recruit local osteoprogenitor cells and promote their differentiation to osteoblasts. A number of carriers for rhBMP-2 have been investigated, including ceramics [31] and an absorbable collagen sponge [32]. However, these carriers typically result in a bolus release of the drug within the first several days. Polyurethanes offer advantageous handling properties and diffusion-controlled release, since the powdered drug can be mixed with the reactive liquid polyurethane immediately prior to grafting.

16.3.2   Graft requirements

A suitable biomaterial for bone grafts must be osteoconductive to promote cell proliferation and neotissue formation [33]. Most polymers, including polyurethanes, are moderately osteoconductive, and thus incorporation of a ceramic component to form a composite has been investigated to enhance bone ingrowth. Degradation rate and breakdown products must also be considered in biomaterial design. The rate and mechanism of degradation should ideally be tailored so that the rate of degradation matches that of cellular infiltration and new tissue generation [34]. Premature degradation may lead to the formation of scar tissue, while a material that persists too long at the defect site will hinder cells from fully infiltrating the scaffold, preventing complete remodeling [35]. The polymer and its degradation products should not cause cytotoxic effects that may lead to inflammation at the implantation site, which could complicate and delay regeneration [34].

The requirements for mechanical properties depend on the grafting site. While BVFs are used only to fill a bone defect with no need for mechanical support, bone cements require properties similar to those of the tissue being replaced [36,37]. Young's modulus of trabecular bone ranges from 50 to 300 MPa and the compressive strength from 5 to 10 MPa, while cortical bone has a modulus of 10–20 GPa with compressive strengths of 130–220 MPa [38] (Table 16.1). Materials lacking mechanical stability fail to support the surrounding tissue, while too high strength can lead to stress shielding and initiate resorption around the defect or injury [39]. Scaffold strength and stiffness also play a role in progenitor cell differentiation [40,41]. Biomaterials with mechanical properties close to bone are more likely to influence these cells to differentiate to bone-generating osteoblasts [42]. Polymer/ceramic composites offer the potential advantage of increased toughness by mixing a brittle ceramic with a ductile polymer [43]. Reactive two-component polyurethanes facilitate interfacial bonding between the ceramic and the polymer components [44,74], which further enhances mechanical properties.

Handling properties are also an important component of graft design. Injectable compositions allow for filling of irregular defects using minimally invasive surgical techniques. The initial dynamic viscosity must be sufficiently low to enable injection, and the graft must cure *in situ* within 5–10 min [45]. Implantable grafts are suitable for use in many applications where a preformed material can be scaled to the appropriate size and implanted in the defect. Implantable polyurethane bone grafts can be fabricated by casting, foaming, electrospinning, and other methods (Figure 16.1).

Table 16.1 **Mechanical properties of cortical and trabecular bone**

	Modulus				Strength			
	Compressive	Tensile	Shear	Flexural	Compressive	Tensile	Shear	Flexural
Cortical/ compact bone	4–25 GPa[b,c]	17–20 GPa[a,b]	3 GPa[b]	3 GPa[a]	130–220 MPa[a,b]	80–150 MPa[a,b,d]	53–76 MPa[b,d]	150–240 MPa[c]
Trabecular/ cancellous bone	50–400 MPa[b]	50–100 MPa[a]		50–100 MPa[a]	5–10 MPa[a] (Mugli, Anseth)	5–10 MPa[a]		

[a]Muggli [108].
[b]Karageorgiou [109].
[c]Gibson [110].
[d]Cowin [111].
Adapted from Muggli et al. [107].
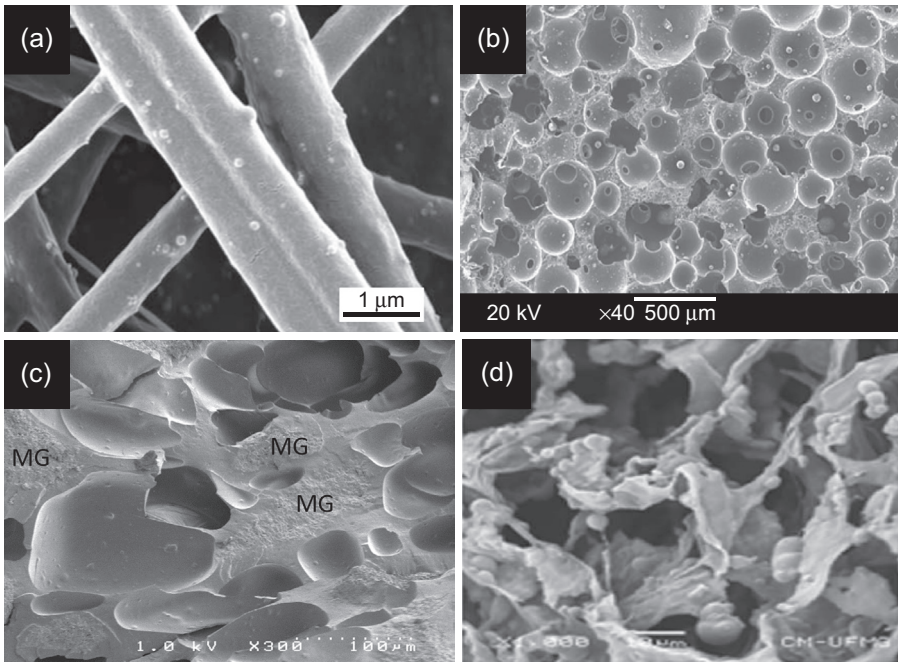
Figure 16.1 Polyurethane composites of nano-HA (a) and (b), commercially available MasterGraft™ (MG) (c), and bioglass fabricated via electrospinning (a), foaming (b) and (d), and *in situ* reactive liquid molding (c).
(a) Mi et al. [59,64]; (b) Liu et al. [63]; (c) Guelcher (unpublished); (d) Rocha de Oliveira et al. [73].

16.4 Osteoconductive bone grafts

In early experiments, degradable polyurethane scaffolds derived from lysine polyiso-cyanates and hexamethylene diisocyanate (HDI) were shown to support attachment, proliferation, and differentiation of osteoblasts. To enhance the modest osteoconduc-tivity of polyurethane scaffolds, recent studies have investigated addition of a ceramic component. Both polyurethane scaffolds and polyurethane/ceramic composites have been shown to support new bone formation in a number of preclinical studies.

16.4.1 *Polyurethane scaffolds*

Scaffolds synthesized from HDI-derived segmented polyurethane elastomers have been reported to support bone healing in an ovine iliac crest defect model [46,47]. Chain extenders comprising 1,4-butanediol, 2-amino-1-butanol, 2-mercaptoethyl ether, and isosorbide diol [48–50] were investigated, as well as poly(ethylene oxide) (PEO), poly(ethylene-*b*-propylene-*b*-ethylene oxide) (PEO–PPO–PEO) block copoly-mers, and poly(caprolactone) macrodiols. Using a salt leaching/phase inversion tech-nique, porous scaffolds with up to 90% porosity were fabricated from the HDI-derived

segmented polyurethane elastomers. *In vitro* calcification of the scaffolds increases with increasing hydrophilicity of the macrodiol [49]. When implanted in ovine iliac crest defects for 6 months, the scaffolds supported formation of new bone with a calcium-to-phosphorus ratio comparable to that of healthy cancellous bone [47].

Foams and cast elastomers exhibiting mechanical properties ranging from elastomeric to rigid have been prepared from lysine-derived polyisocyanates for injectable applications such as bone void fillers and cements [6,23,51–53]. These materials utilize liquid short-chain polyols, such as polyesters synthesized by ring-opening polymerization of lactide, glycolide, and/or caprolactone monomers, and NCO-terminated prepolymers that are liquids above room temperature. Bone cements with compressive strengths exceeding 60 MPa have been synthesized from lysine diisocyanate (LDI)-pentaerthyritol prepolymers and glycolic acid–pentaerthyritol polyols [23]. Similar cements have also been prepared from lysine triisocyanate (LTI)–PCL prepolymers and glycolide–caprolactone–lactide–glycerol polyols [53]. In other studies, flexible porous foams (>90% porosity) were synthesized from LDI or LTI and polyester triols [6,16]. All these materials supported the attachment, proliferation, and differentiation of viable osteoblasts.

16.4.2   Composites

16.4.2.1   Calcium phosphates

Polymers are commonly augmented with calcium phosphates to enhance their osteoconductivity, considering their similar chemical composition to that of bone. Although calcium phosphates have been shown to be osteoconductive and integrate with bone, they are generally very brittle due to their ceramic nature [4]. Blending calcium phosphates with a ductile polymer has been proposed as an approach for improving the strength of the material [54], although a recent review has reported that for many polymer/ceramic composites osteoconductivity increases but strength does not [43].

Hydroxyapatite

Hydroxyapatite (HA) is a calcium phosphate mineral with the chemical formula $Ca_{10}(PO_4)_6(OH)_2$. HA-like compounds compose approximately 65% of bone, making it an appealing option for a synthetic bone composite [55]. The addition of up to 30 wt% HA to a polycaprolactone-based polyurethane scaffold has been shown to increase degradation rates both *in vitro* and *in vivo* when the particles are only physically combined with the polymer [56]. HA/polyurethane composites are generally used for implantable scaffolds rather than injectable grafts, since it is difficult to maintain appropriate viscosities for injectability with high HA content. A recent study capitalized on the bone-integrative properties of HA to create a degradable bone adhesive that cures *in situ* for fracture fixation [57]. A moisture-reactive methylene diphenyl diisocyanate monomer was reacted with a caprolactone-based polyol to generate a porous foam subsequently combined with 1% HA and brushed onto the bone surface. The scaffold achieved an elastic modulus comparable to the lower end of cancellous bone stiffness, and the strength was increased with the addition of HA as expected for

a polymer/ceramic composite [54]. Electrospun HA/polyurethane composites have also been used to make fibrous, porous bone scaffolds (Figure 16.2) [58–61]. There are discrepancies in the literature in determining the effects of HA on the mechanical properties of electrospun composites. One study reported an increase in tensile properties, Young's modulus, and yield strength of the meshes with the incorporation of HA, while another observed an opposite effect [59,61]. These differences could be attributed to the polyurethane used or the properties of the HA particles; however, both used micro- and nano-HA and based the conclusion on HA in general. Incorporating HA in electrospun polyurethane scaffolds has the ability to increase collagen production and has been shown to initiate apatite precipitation, both markers of osteogenesis [60,61]. HA has also been incorporated into scaffolds fabricated from more conventional methods such as salt leaching, solvent casting, and phase separation [62–65]. The 20–40 wt% HA composites have been reported to increase *in vitro* protein adsorption and promote mineralization (Figure 16.3) [62,65], and composites made by a thermally induced phase-separation technique have stronger compressive properties with both nano- and micro-HA than polyurethane alone [64].

Beta-tricalcium phosphate

Beta-tricalcium phosphate (β-TCP) is a highly porous ceramic with chemical and physical structures that mimic bone [66,67]. While it is osteoconductive and porous, the compressive mechanical properties of β-TCP are considerably lower than those of HA [66–69] and it degrades more rapidly than HA [70]. β-TCP has been incorporated in both injectable and implantable polyurethane composites to capitalize on its osteoconductive properties and overcome weaker mechanical strength [39]. Addition of as little as 10 wt% β-TCP increased the modulus and strength of the composites, and the composites approach the strength of cancellous bone with incorporation of 70 wt%
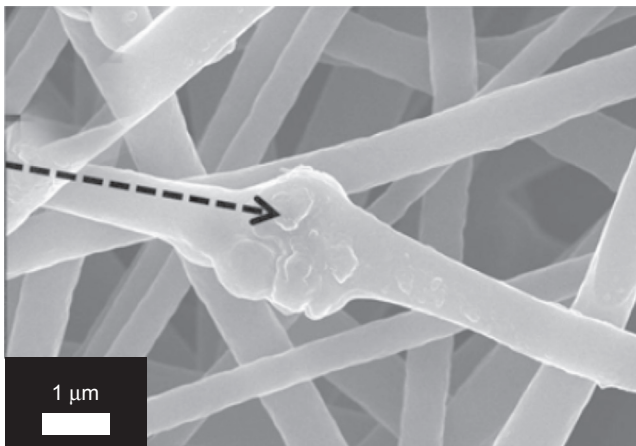
Figure 16.2 SEM image of polyurethane/hydroxyapatite nanofiber composite formed by electrospinning showing a larger particle protruding from the polymer fiber. Sheikh et al. [60].

β-TCP [23,69]. Furthermore, β-TCP/polyurethane composites showed enhanced osteoblast attachment and proliferation compared to polyurethanes alone [23,71].

Bioactive glass

Bioactive glasses are synthetic, silicone oxide ceramics with a structure of the form Na_2—CaO—SiO_2—P_2O_5. Of particular interest in bone tissue engineering is the 45S5 composition (with respective mole percentages of 24.4, 26.9, 46.1, and 2.6), later named Bioglass®, which has been shown to form a very strong chemical bond with bone by stimulating growth of a hydroxycarbonate apatite layer on the surface [2].
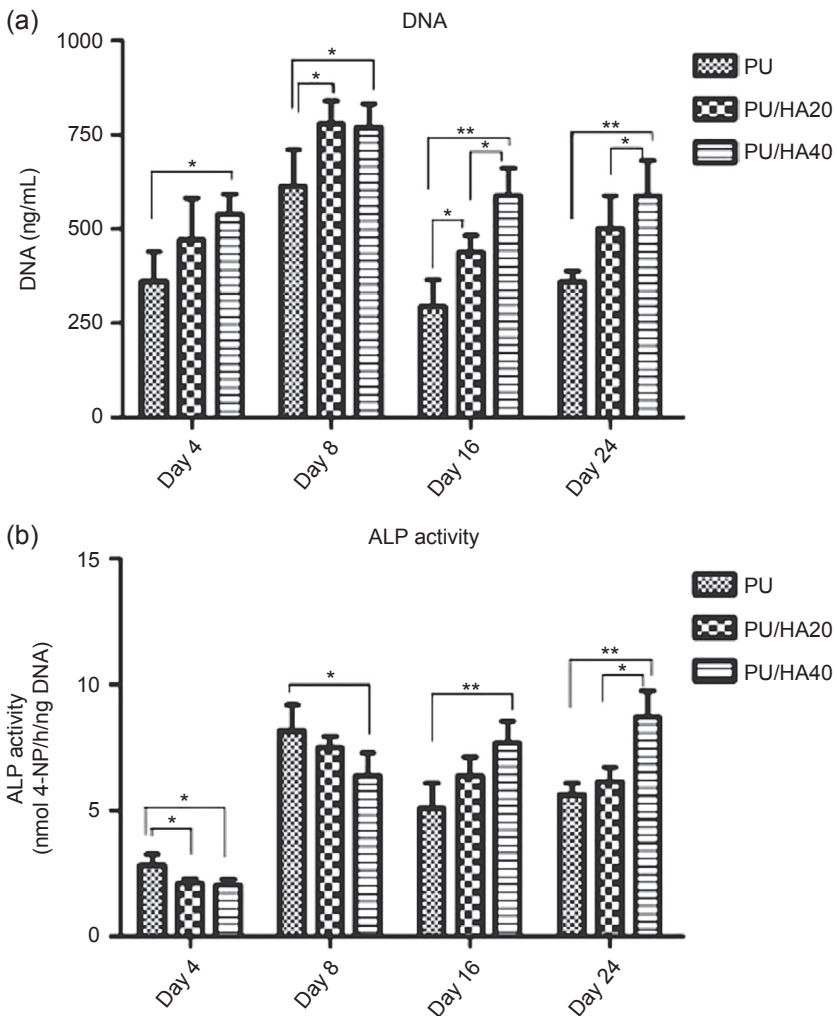
Figure 16.3 DNA and ALP activity of polyurethane/hydroxyapatite (PU/HA) composites of 20 and 40 wt% HA over 24 days.
Yang et al. [65].

For example, polyurethane scaffolds coated with 45S5 bioactive glass showed good polymer–glass bonding and formation of a layer of carbonate-containing apatite after 7 days immersion in simulated body fluid compared to >21 days for uncoated polyurethane [72]. Histology provides *in vivo* evidence of new bone growth from a polyurethane/45S5 bioactive glass composite 16 weeks postimplantation (Figure 16.4). Bioactive glasses generally lack the porosity of calcium phosphates, lending superior mechanical properties to their composites. Ryszkowska et al. showed an increase in storage modulus of a polyurethane/bioactive glass composite with increasing Bioglass® content up to 20 wt%. This increase in mechanical properties was accompanied by an increase in degradation rates compared to the polyurethane alone probably due to the presence of silanol groups of the glass on the polymer surface [19]. The incorporation of strong bioactive glass nanoparticles has been described to act as a reinforcement mechanism for the composites and improves compressive modulus up to 25 wt% glass [73]. Bioactive glasses can be functionalized for better polymer integration to further improve composite properties. For example, surface polymerization of poly(ε-caprolactone) on the surface of 45S5 bioactive glass particles prior to blending with a reactive LTI-derived polyurethane resulted in a two- to five fold increase in torsional and compressive properties [74]. These low-porosity composites supported cellular infiltration and new bone formation at 8 weeks when injected into rat femoral condyle defects.

16.4.2.2 Allograft bone

Allograft bone has been very extensively investigated as a commercial bone graft material. One of the first studies on the development of an injectable lysine-derived polyurethane bone graft investigated an LDI-based carrier for demineralized bone matrix [18]. An LDI–poly(p-dioxanone-co-glycolate) prepolymer was mixed with demineralized bone matrix to form a reactive putty. Implantation of the putty in an intramuscular site did not elicit an adverse inflammatory response. Several more recent studies have
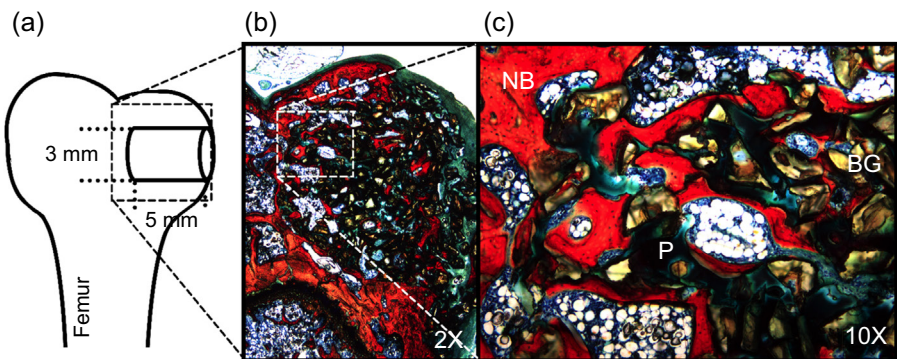
Figure 16.4 Histology of new bone growth from a polyurethane/45S5 bioglass composite after 16 weeks *in vivo* in a rat femoral condyle plug defect (P, polymer; NB, new mineralized bone; BG, 45S5 bioglass).
Harmata et al. [74].

investigated mineralized allograft bone particles as an osteoconductive matrix blended with polyurethanes [8,17,24,25,75]. Remodeling of the allograft particles proceeds from the outside surface to the interior of the graft by creeping substitution [76,77], and therefore the rate of remodeling increases with allograft loading. Remodeling is fastest for particles ranging in size from 150 to 500 μm, and slowest for particles <100 μm [17,76]. Several studies have investigated allograft/polyurethane composites as weight-bearing bone grafts [17,24,25]. The biodegradable polyurethane was synthesized from a polyester triol and lysine-derived polyisocyanates. By varying the molecular weight of the polyol and manipulating the surface chemistry of the allograft particles via surface demineralization, compressive modulus and strength values of 3–6 GPa and 107–172 MPa were achieved, respectively. When implanted in bilateral femoral condyle plug defects in New Zealand white rabbits, the composites exhibited resorption of the allograft and polymer components, extensive cellular infiltration deep into the interior of the implant, and bone healing at 6 and 12 weeks. At volume fractions approaching or exceeding the random close-packing limit, the allograft particles presented a nearly continuous osteoconductive pathway for cells into the interior of the implant. Injectable allograft/polyurethane composites have also been reported [8,17,75]. By varying the water concentration, porosities ranging from 30 to 70% were achieved. The injectable void fillers exhibited an initial dynamic viscosity of 220 Pa s at clinically relevant shear rates (40 s^{-1}), working times from 3 to 8 min, and setting times from 10 to 20 min, which are comparable to the properties of calcium phosphate bone cements [75]. When injected into femoral plug defects in rats or rabbits, the composites supported extensive cellular infiltration, allograft resorption, collagen deposition, and new bone formation. While allograft/polyurethane composites have shown considerable potential for bone regeneration, it is important to consider that the rate of new bone formation must be balanced with polymer degradation. One study examined this question using settable weight-bearing polyurethane/allograft composites in a rabbit femoral condyle defect model [24]. The grafts induced progressive healing *in vivo*, as evidenced by an increase in new bone formation and a decrease in residual allograft and polymer from 6 to 12 weeks. However, the mismatch between the rates of oxidative and hydrolytic polyurethane degradation, osteoclast-mediated allograft resorption, and new bone formation resulted in incomplete healing in the interior of the composite. Augmentation of the grafts with rhBMP-2 increased the rate of new bone formation to better match the rates of allograft and polyurethane resorption, which resulted in more extensive healing at later time points in all regions of the graft.

16.4.2.3 New frontiers

Emerging work on new polyurethane scaffolds aims to enhance osteoconductivity and mechanical properties using novel methods and additives. Ionic liquids have been proposed to add antibacterial properties to polyurethanes while improving mechanical properties and increasing hydrophilicity. 1-butyl-3-methylimidazolium hexafluorophosphate ionic liquid blended with a thermoplastic polyurethane improved the electrospun fiber morphology and nonwoven mats exhibited 99.9% antibacterial efficiency against *Escherichia coli* and *Staphylococcus aureus* [78].

This new knowledge could be applied to the design of rigid polyurethanes for bone scaffolds with antibacterial properties.

Sunflower oil-based, hyperbranched polyurethane nanocomposites with functionalized multiwalled carbon nanotubes have been shown to increase tensile strength nearly twofold and toughness by about 50%. Early *in vitro* studies highlight the potential for these composites to improve osteolytic activity to accelerate bone growth in bone tissue engineering applications [79].

16.5   Biologically active bone grafts

Osteoinductive bone grafts are required for healing bone defects that do not heal by ingrowth of new bone alone. rhBMP-2 is FDA-approved for fractures of the tibial mid-diaphysis, lumber spine fusion, and ridge augmentation/sinus lift procedures. However, the collagen carrier for rhBMP-2 promotes a fast release of the drug [80], is not injectable, and is not compression resistant [31]. Considering their advantages of diffusion-controlled drug release, injectability and settability, and tunable mechanical properties, polyurethanes have been investigated as carriers for rhBMP-2.

16.5.1   *Local delivery of recombinant human bone morphogenetic protein-2*

Early work on osteoinductive polyurethane bone grafts utilized ascorbic acid chain extenders, which were subsequently released over time as the polymer degraded [15,81]. These biomaterials supported sustained release of ascorbic acid for up to 30 days, which stimulated osteoblast differentiation *in vitro*. rhBMP-2 is a growth factor that plays a robust role in osteogenesis and the formation of new bone. Local delivery of rhBMP-2 is achieved commercially using a collagen sponge delivery system; however, there are concerns regarding pharmacokinetic mismatch with the osseous wound healing cascade and immunogenicity [82]. The pharmacokinetics of delivery of rhBMP-2 from polyurethane scaffolds has been investigated as an alternative to the collagen carrier. The release of rhBMP-2 from polyurethane scaffolds is biphasic, characterized by a burst followed by a sustained release for up to 21 days [10,82,83]. In these studies, the rhBMP-2 powder was added to the reactive liquid polyurethane mixture, resulting in encapsulation of the drug within the wall of the cured scaffold. Human mesenchymal stem cells treated with rhBMP-2-releasing scaffolds showed earlier osteogenic differentiation and mineralization compared to cells treated with exogenous rhBMP-2 [82]. Substitution of the polyester triol with PEG increased the release kinetics of rhBMP-2 from polyurethane, likely due to the more hydrophilic nature of the polyurethanes incorporating PEG, resulting in increased swelling [83]. rhBMP-2 has been incorporated into biodegradable poly (lactic-*co*-glycolic acid) (PLGA) microspheres with both fast and slow release kinetics and has demonstrated superior release characteristics to a collagen sponge loaded with rhBMP-2 control [10]. With this in mind, further attempts to slow rhBMP-2 release kinetics include encapsulation of rhBMP-2 in 1.3 or 114 μm PLGA microspheres that are then incorporated in a polyurethane scaffold (Figure 16.5) [10,83]. Small (1.4 μm)
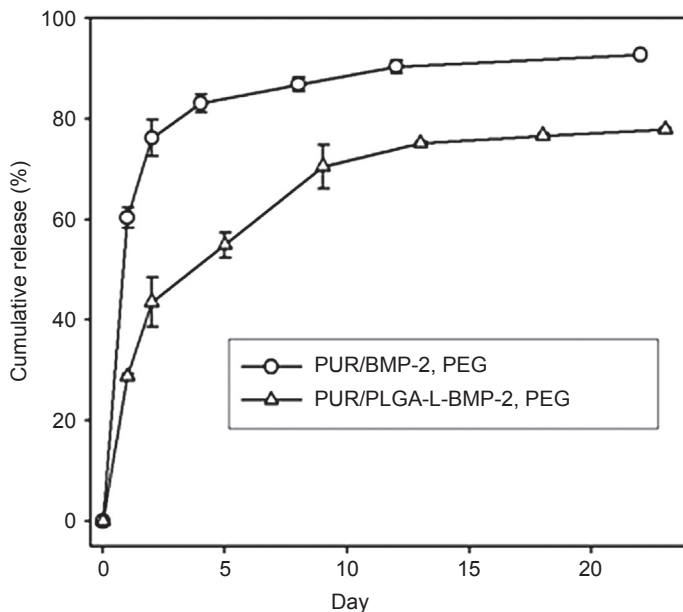
Figure 16.5 *In vitro* cumulative release of rhBMP-2 from polyurethane (PUR)/PEG scaffolds comparing release profiles with and without PLGA encapsulation of the biologic. Li et al. [83].

microspheres were completely embedded in the 10–100 μm scaffold walls, resulting in negligible burst release of rhBMP-2. In contrast, large (114 μm) microspheres were only partially embedded in the scaffold walls, resulting in a negligible reduction in the burst release compared to encapsulation of the drug in the polyurethane alone. In a rat femoral critical-size defect model, minimal new bone formation was observed for the polyurethane scaffolds with small microspheres as well as the collagen scaffold, which supported only a burst release of rhBMP-2. Consequently, a burst followed by a sustained release of rhBMP-2 has been proposed as the optimal release kinetics for new bone formation [10,79]. The burst release of rhBMP-2 promotes recruitment of osteoprogenitor cells, while the sustained release promotes osteoblastic differentiation.

16.5.2 Local delivery of antimicrobials

16.5.2.1 Antibiotics

The threat of infectious disease is omnipresent in the surgical setting and presents the possibility for compromise of healing open fractures or osteomyelitis [84]. Local delivery of antimicrobials from polyurethane scaffolds has been explored as a strategy for prevention of infection [11,85,86]. Tobramycin is an aminoglycoside antibiotic that primarily has activity against Gram-negative microorganisms, but notably has activity against *S. aureus*, which is the microorganism most frequently implicated as a cause of osteomyelitis [87,88]. Furthermore, local delivery of tobramycin from implanted

PMMA cement beads has been a clinically utilized therapy for treating infected fractures [89]. A significant limitation of PMMA beads is that they must be removed prior to the placement of bone graft. Therefore, utilization of a biodegradable polyurethane scaffold with drug-eluting properties would prove advantageous in decreasing the amount of necessary surgical procedures. Use of injectable polyurethane incorporating tobramycin encapsulated in PLGA microspheres has demonstrated both space-maintaining mechanical properties (compressive moduli of 15–115 kPa) and sustained release of the antibiotic for up to 2 weeks [90]. The release kinetics for the polyurethane scaffolds were comparable to those of drug releasing PMMA and calcium sulfate bone cements, and exceeded the minimum inhibitory concentration (MIC, 4–8 μg/mL) and minimum bactericidal concentration (MBC, 16 μg/mL) for tobramycin against *S. aureus* [91]. The addition of PEG to the two-component polyurethane increased the tobramycin release kinetics due to the increased hydrophilicity of the polymer [90].

Vancomycin is another antibiotic that may prove to have clinical utility in preventing infection when delivered locally from a polyurethane scaffold. Vancomycin is a glycopeptide antibiotic that has efficacy against most Gram-positive organisms including *S. aureus*. Vancomycin is unique in that it has been utilized in combatting resistant strains of microorganisms, including methicillin resistant *S. aureus* (MRSA), which can be the cause of significant morbidity and mortality. Vancomycin has low release efficiency when delivered from PMMA beads or spacers [92–94], and is further limited by the inability to achieve sustained release [95,96]. Hydrophobic vancomycin free base incorporated in polyurethane scaffolds demonstrated more than 80% release over the course of 8 weeks (Figure 16.6) [11]. This study further demonstrated that vancomycin free base had lower
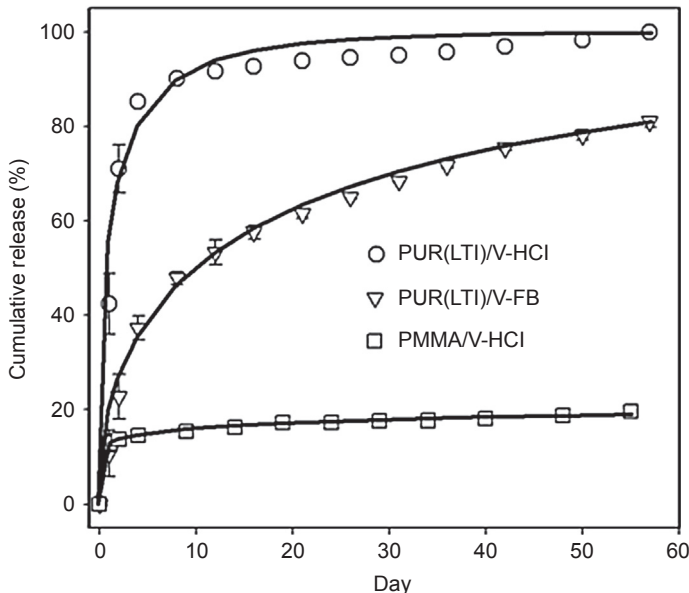
Figure 16.6 *In vitro* release of vancomycin from polyurethane (PUR) scaffolds. Li et al. [11].

solubility in the polyurethane scaffold compared to the more hydrophilic hydrochloride form, which accounted for the more sustained release kinetics. When implanted in a rat femoral segmental defect, polyurethane scaffolds augmented with vancomycin free base performed comparable to the clinical control of PMMA loaded with vancomycin when assessed for bacterial colony forming units found within the soft tissue [11].

Of additional consideration are dual-purpose bone grafts that contain both an osteoinductive drug and an antibiotic [97]. The antibiotic protects the graft from infection, thereby facilitating the bone regeneration through the osteoinductive agent, which also promotes vascularization of the bone graft critical for protecting the newly formed bone from further infection. A recent study investigated the effects of dual delivery of rhBMP-2 and vancomycin from a porous biodegradable polyurethane scaffold implanted in a contaminated rat segmented femoral defect [86]. The combination of drugs in the graft did not affect the individual release profiles, with each drug maintaining its previously demonstrated release kinetics. In the infected rat femoral segmental defect model, the dual-purpose graft demonstrated superior bone regeneration to the collagen sponge with rhBMP-2 (clinical control) as assessed by μCT and histomorphometry [86].

16.5.2.2 Antibiofilm agents

The role of biofilms, which are bacteria attached to a substratum of extracellular polymeric substance, in perpetrating bacterial persistence following administration of antibiotics has been increasingly recognized [87]. *S. aureus* has demonstrated the ability to synthesize biofilms that allow for high bacterial tolerance of antimicrobials due to limited antimicrobial penetrance and persistent cells within the biofilm. Thus, use of agents that hinder biofilm formation and aid in dispersal is an area of active research [98–100]. Recent studies have assessed the efficacy of D-isomer amino acids (D-AAs) for hindering biofilm formation as well as their effect on osteogenesis and new bone formation *in vitro* and *in vivo* [101,102]. A composite comprising Master-Graft™ ceramic Mini Granules and an LTI-derived polyurethane was loaded with D-AAs and evaluated *in vitro* and *in vivo*. The study found that a 1:1:1 mixture of D-Met:D-Pro:D-Phe inhibited *S. aureus* biofilms at concentrations ≥13.5 mM, but osteogenesis and osteoclastogenesis were inhibited at ≥27 mM [102]. *In vivo*, while biofilm was inhibited at D-AA concentrations <50 mM [101], new bone formation was not inhibited at concentrations of at least 200 mM [102]. Taken together, these studies highlight local delivery of antimicrobials such as antibiotics and biofilm dispersal agents from polyurethane bone grafts as an effective strategy for preventing infection while promoting new bone formation and healing.

16.5.3 New frontiers

The highly tunable characteristics of polyurethanes have enabled the study of drug delivery from scaffolds for the purposes of tissue regeneration. Further investigations have explored the delivery of biologics, including siRNA for the purposes of gene silencing. One mechanism for delivering siRNA from polyurethane scaffolds has been

to use pH-responsive, endosomolytic micellular nanoparticles [103]. siRNA micelles achieved 50% silencing of GAPDH in NIH3T3 mouse fibroblasts, thereby demonstrating the potential for this approach in introducing siRNA for gene silencing. Maintaining adequate colloidal stability of the siRNA nanoparticles in the reactive liquid polyurethane was shown to be critical for achieving good knockdown. A follow-up study further demonstrated that siRNA delivery from nanoparticles blocked degradation of proangiogenic transcription factors and achieved an increase in vascular volume of 300% and an increase in the mean vascular thickness of 137% [104].

Similarly, cell-based therapies have emerged as a new promising approach for tissue regeneration. As injectable cell delivery carriers, lysine-derived polyurethanes offer many advantages including curing without cytotoxic catalysts or UV radiation [75,105], supporting cell attachment without cell adhesion peptides [53], tunable biodegradability [106], and adjustable mechanical properties ranging from soft tissue to bone. In consideration of these properties, injectable polyurethane scaffolds augmented with cells encapsulated in degradable oxidized alginate beads have been optimized for cell survivability [107]. The generation of CO_2 and heat by the polymerization controlled cell survival prior to gelation, while permeability of the polyurethane scaffolds influenced cell survival following gelation. Cells survived for up to 7 days and enhanced new matrix deposition and angiogenesis *in vivo*.

References

[1] Hollinger JO, Kleinschmidt J. The critical size defect as an experimental model to test bone repair materials. J Craniofac Surg 1990;1:60–8.

[2] Jones JR. Review of bioactive glass: from Hench to hybrids. Acta Biomater 2013;9(1):4457–86.

[3] Jarcho M. Calcium phosphate ceramics as hard tissue prosthetics. Clin Orthop Rel Res 1981;157:259–77.

[4] Bohner M. Design of ceramic-based cements and putties for bone graft substitution. Eur Cell Mater 2010;20:1–12.

[5] Guelcher SA. Biodegradable polyurethanes: synthesis and applications in regenerative medicine. Tissue Eng B Rev 2008;14(1):3–17.

[6] Guelcher S, et al. Synthesis, in vitro degradation, and mechanical properties of two-component poly(ester urethane)urea scaffolds: effects of water and polyol composition. Tissue Eng 2007;13(9):2321–33.

[7] Gorna K, Gogolewski S. Preparation, degradation, and calcification of biodegradable polyurethane foams for bone graft substitutes. J Biomed Mater Res A 2003;67: 813–27.

[8] Dumas JE, et al. Synthesis and characterization of an injectable allograft bone/polymer composite bone void filler with tunable mechanical properties. Tissue Eng Part A 2010;16(8):2505–18.

[9] Adhikari R, et al. Biodegradable injectable polyurethanes: synthesis and evaluation for orthopaedic applications. Biomaterials 2008;29(28):3762–70.

[10] Brown KV, et al. Improving bone formation in a rat femur segmental defect by controlling bone morphogenetic protein-2 release. Tissue Eng Part A 2011;17(13–14): 1735–46.

[11] Li B, et al. Sustained release of vancomycin from polyurethane scaffolds inhibits infection of bone wounds in a rat femoral segmental defect model. J Control Release 2010;145(3):221–30.

[12] Santerre JP, et al. Understanding the biodegradation of polyurethanes: from classical implants to tissue engineering materials. Biomaterials 2005;26:7457–70.

[13] Oertel G. Polyurethane handbook. 2nd ed. (Berlin): Hanser Gardner Publications; 1994.

[14] Szycher M. Szycher's handbook of polyurethanes. Boca Raton: CRC Press; 1999.

[15] Zhang J, et al. A biodegradable polyurethane-ascorbic acid scaffold for bone tissue engineering. J Biomed Mater Res A 2003;67:389–400.

[16] Guelcher SA, et al. Synthesis and in vitro biocompatibility of injectable polyurethane foam scaffolds. Tissue Eng 2006;12(5):1247–59.

[17] Prieto EM, et al. Effects of particle size and porosity on in vivo remodeling of settable allograft bone/polymer composites. J Biomed Mater Res B Appl Biomater 2015; 103(8):1641–51.

[18] Bennett S, et al. Initial biocompatibility studies of a novel degradable polymeric bone substitute that hardens in situ. Bone 1996;19(Suppl. 1):101S–7S.

[19] Ryszkowska JL, et al. Biodegradable polyurethane composite scaffolds containing Bioglass® for bone tissue engineering. Compos Sci Technol 2010;70(13):1894–908.

[20] Tay BK, Patel VV, Bradford DS. Calcium sulfate- and calcium phosphate-based bone substitutes. Mimicry of the mineral phase of bone. Orthop Clin North Am 1999;30(4):615–23.

[21] Russell TA, Leighton RK. Comparison of autogenous bone graft and endothermic calcium phosphate cement for defect augmentation in tibial plateau fractures. A multicenter, prospective, randomized study. J Bone Joint Surg Am 2008;90(10):2057–61.

[22] Verlaan JJ, Oner FC, Dhert WJ. Anterior spinal column augmentation with injectable bone cements. Biomaterials 2006;27(3):290–301.

[23] Bonzani IC, et al. Synthesis of two-component injectable polyurethanes for bone tissue engineering. Biomaterials 2007;28:423–33.

[24] Dumas JE, et al. Balancing the rates of new bone formation and polymer degradation enhances healing of weight-bearing allograft/polyurethane composites in rabbit femoral defects. Tissue Eng A 2014;20(1–2):115–29.

[25] Dumas JE, et al. Synthesis of allograft bone/polymer composites and evaluation of remodeling in a rabbit femoral condyle model. Acta Biomater 2010;6:2394–406.

[26] Swiontkowski MF, et al. Recombinant human bone morphogenetic protein-2 in open tibial fractures. A subgroup analysis of data combined from two prospective randomized studies. J Bone Joint Surg Am 2006;88(6):1258–65.

[27] Glassman SD, et al. Initial fusion rates with recombinant human bone morphogenetic protein-2/compression resistant matrix and a hydroxyapatite and tricalcium phosphate/ collagen carrier in posterolateral spinal fusion. Spine (Phila Pa 1976) 2005;30(15):1694–8.

[28] McKay WF, Peckham SM, Badura JM. A comprehensive clinical review of recombinant human bone morphogenetic protein-2 (INFUSE Bone Graft). Int Orthop 2007;31(6):729–34.

[29] Haidar ZS, Hamdy RC, Tabrizian M. Delivery of recombinant bone morphogenetic proteins for bone regeneration and repair. Part B: delivery systems for BMPs in orthopaedic and craniofacial tissue engineering. Biotechnol Lett 2009;31(12):1825–35.

[30] Urist MR. Bone morphogenetic protein: the molecularization of the skeletal system. J Bone Min Res 1997;12(3):343–6.

[31] Herford AS, et al. Recombinant human bone morphogenetic protein 2 combined with an osteoconductive bulking agent for mandibular continuity defects in nonhuman primates. J Oral Maxillofac Surg 2012;70(3):703–16.

[32] Bessa PC, Casal M, Reis RL. Bone morphogenetic proteins in tissue engineering: the road from laboratory to clinic, part II (BMP delivery). J Tissue Eng Regen Med 2008;2(2–3):81–96.

[33] LeGeros RZ. Properties of osteoconductive biomaterials: calcium phosphates. Clin Orthop Relat Res 2002;395:81–98.

[34] Langer R. Biodegradable polymer scaffolds for tissue engineering. Nat Biotechnol 1994;12:689–93.

[35] Lorden ER, et al. Mitigation of hypertrophic scar contraction via an elastomeric biodegradable scaffold. Biomaterials 2015;43:61–70.

[36] Hollinger J, Chaudhari A. Bone regeneration materials for the mandibular and craniofacial complex. Cells Mater 1992;2(2):143–51.

[37] Hutmacher DW. Scaffolds in tissue engineering bone and cartilage. Biomaterials 2000;21(24):2529–43.

[38] Smith KE, et al. The dependence of MG63 osteoblast responses to (meth)acrylate-based networks on chemical structure and stiffness. Biomaterials 2010;31(24):6131–41.

[39] Khan Y, et al. Tissue engineering of bone: material and matrix considerations. J Bone Joint Surg Am 2008;90:36–42.

[40] Dawson E, et al. Biomaterials for stem cell differentiation. Adv Drug Deliv Rev 2008;60(2):215–28.

[41] Engler AJ, et al. Matrix elasticity directs stem cell lineage specification. Cell 2006;126(4):677–89.

[42] Guo R, et al. Fabrication of 3D scaffolds with precisely controlled substrate modulus and pore size by templated-fused deposition modeling to direct osteogenic differentiation. Adv Healthc Mater 2015;4(12):1826–32.

[43] Wagoner Johnson AJ, Herschler BA. A review of the mechanical behavior of CaP and CaP/polymer composites for applications in bone replacement and repair. Acta Biomater 2011;7(1):16–30.

[44] Dumas JE, et al. Synthesis, characterization, and remodeling of weight-bearing allograft bone/polyurethane composites in the rabbit. Acta Biomater 2010;6(7):2394–406.

[45] Dumas JE, et al. Injectable reactive biocomposites for bone healing in critical-size rabbit calvarial defects. Biomed Mater 2012;7(2):024112.

[46] Gogolewski S, Gorna K, Turner AS. Regeneration of bicortical defects in the iliac crest of estrogen-deficient sheep, using new biodegradable polyurethane bone graft substitutes. J Biomed Mater Res A 2006;77:802–10.

[47] Gogolewski S, Gorna K. Biodegradable polyurethane cancellous bone graft substitutes in the treatment of iliac crest defects. J Biomed Mater Res A 2007;80:94–101.

[48] Gorna K, Gogolewski S. In vitro degradation of novel medical biodegradable aliphatic polyurethanes based on e-caprolactone and Pluronics with various hydrophilicities. Polym Degrad Stab 2002;75:113–22.

[49] Gorna K, Gogolewski S. Biodegradable polyurethanes for implants. II. In vitro degradation and calcification of materials from poly(epsilon-caprolactone)-poly(ethylene oxide) diols and various chain extenders. J Biomed Mater Res 2002;60(4):592–606.

[50] Gorna K, Gogolewski S. Biodegradable porous polyurethane scaffolds for tissue repair and regeneration. J Biomed Mater Res A 2006;79:128–38.

[51] Gunatillake PA, Mayadunne R, Adhikari R. Recent developments in biodegradable synthetic polymers. Biotechnol Annu Rev 2006;12:301–47.

[52] Adhikari R, Gunatillake PA. Biodegradable polyurethane/urea compositions. (Australia): Commonwealth Scientific and Industrial Research Organization; 2004.

[53] Guelcher SA, Srinivasan A, Dumas JE, et al. Synthesis, mechanical properties, biocompatibility, and biodegradation of polyurethane networks from lysine polyisocyanates. Biomaterials 2008;29(12):1762–75.

[54] Rezwan K, et al. Biodegradable and bioactive porous polymer/inorganic composite scaffolds for bone tissue engineering. Biomaterials 2006;27(18):3413–31.

[55] Buckwalter J, et al. Bone biology. J Bone Joint Surg Am 1995;77(8):1256–75.

[56] Fu S-Z, et al. In vitro and in vivo degradation behavior of n-HA/PCL-Pluronic-PCL polyurethane composites. J Biomed Mater Res A 2014;102(2):479–86.

[57] Schreader KJ, et al. A polyurethane-based nanocomposite biocompatible bone adhesive. J Appl Polym Sci 2013;127(6):4974–82.

[58] Khan A, et al. Preparation and characterization of a novel bioactive restorative composite based on covalently coupled polyurethane–nanohydroxyapatite fibres. Acta Biomater 2008;4(5):1275–87.

[59] Mi HY, et al. Thermoplastic polyurethane/hydroxyapatite electrospun scaffolds for bone tissue engineering: effects of polymer properties and particle size. J Biomed Mater Res B Appl Biomater 2014;102(7):1434–44.

[60] Sheikh FA, et al. A simple approach for syntheis, characterization and bioactivity of bovine bones to fabricate the polyurethane nanofiber containing hydroxyapatite nanoparticle. Express Polym Lett 2012;6(1):41–53.

[61] Tetteh G, et al. Electrospun polyurethane/hydroxyapatite bioactive scaffolds for bone tissue engineering: the role of solvent and hydroxyapatite particles. J Mech Behav Biomed Mater 2014;39:95–110.

[62] Laschke MW, et al. In vitro and in vivo evaluation of a novel nanosize hydroxyapatite particles/poly(ester-urethane) composite scaffold for bone tissue engineering. Acta Biomater 2010;6(6):2020–7.

[63] Liu H, et al. Hydroxyapatite/polyurethane scaffold incorporated with drug-loaded ethyl cellulose microspheres for bone regeneration. J Biomed Mater Res B Appl Biomater 2010;95(1):36–46.

[64] Mi H-Y, et al. Morphology, mechanical properties, and mineralization of rigid thermoplastic polyurethane/hydroxyapatite scaffolds for bone tissue applications: effects of fabrication approaches and hydroxyapatite size. J Mater Sci 2014;49(5):2324–37.

[65] Yang W, et al. Biological evaluation of porous aliphatic polyurethane/hydroxyapatite composite scaffolds for bone tissue engineering. J Biomed Mater Res A 2014;103(7): 2251–9.

[66] Gaasbeek RDA, et al. Mechanism of bone incorporation of β-TCP bone substitute in open wedge tibial osteotomy in patients. Biomaterials 2005;26(33):6713–9.

[67] Giannoudis PV, Dinopoulos H, Tsiridis E. Bone substitutes: an update. Injury 2005;36(3):S20–7.

[68] Sammarco VJ, Chang L. Modern issues in bone graft substitutes and advances in bone tissue technology. Foot Ankle Clin 2002;7(1):19–41.

[69] Yoshii T, et al. Synthesis, characterization of calcium phosphates/polyurethane composites for weight-bearing implants. J Biomed Mater Res B Appl Biomater 2012; 100(1):32–40.

[70] Oonishi H, et al. Comparative bone formation in several kinds of bioceramic granules. Bioceramics 1995;8:137–44.

[71] Hutmacher D, et al. Matrix and carrier materials for bone growth factors: state of the art and future perspectives. In: Biological matrices and tissue reconstruction. Springer, London; 1998. p. 197–206.

[72] Bil M, et al. Bioactivity of polyurethane-based scaffolds coated with Bioglass. Biomed Mater 2007;2(2):93–101.

[73] de Oliveira AAR, et al. Development of biodegradable polyurethane and bioactive glass nanoparticles scaffolds for bone tissue engineering applications. J Biomed Mater Res B Appl Biomater 2012;100(5):1387–96.

[74] Harmata AJ, et al. Investigating the effects of surface-initiated polymerization of ε-caprolactone to bioactive glass particles on the mechanical properties of settable polymer/ceramic composites. J Mater Res 2014;29(20):2398–407.

[75] Page JM, et al. Biocompatibility and chemical reaction kinetics of injectable, settable polyurethane/allograft bone biocomposites. Acta Biomater 2012;8:4405–16.

[76] Malinin TI, Carpenter EM, Temple HT. Particulate bone allograft incorporation in regeneration of osseous defects; importance of particle sizes. Open Orthop J 2007;1:19–24.

[77] Eagan MJ, McAllister DR. Biology of allograft incorporation. Clin Sports Med 2009;28:203–14.

[78] Chenyang X, et al. Novel multifunctional nanofibers based on thermoplastic polyurethane and ionic liquid: towards antibacterial, anti-electrostatic and hydrophilic nonwovens by electrospinning. Nanotechnology 2015;26(10):105704.

[79] Das B, et al. Nanocomposites of bio-based hyperbranched polyurethane/funtionalized MWCNT as non-immunogenic, osteoconductive, biodegradable and biocompatible scaffolds in bone tissue engineering. J Mater Chem B 2013;1(33):4115–26.

[80] Boerckel JD, et al. Effects of protein dose and delivery system on BMP-mediated bone regeneration. Biomaterials 2011;32(22):5241–51.

[81] Zhang J, et al. Three-dimensional biocompatible ascorbic acid-containing scaffold for bone tissue engineering. Tissue Eng 2003;9(6):1143–57.

[82] Kim J, Hollinger JO. Recombinant human bone morphogenetic protein-2 released from polyurethane-based scaffolds promotes early osteogenic differentiation of human mesenchymal stem cells. Biomed Mater 2012;7(4):045008.

[83] Li B, et al. The effects of rhBMP-2 released from biodegradable polyurethane/microsphere composite scaffolds on new bone formation in rat femora. Biomaterials 2009;30(35):6768–79.

[84] Bosse MJ, et al. An analysis of outcomes of reconstruction or amputation after leg-threatening injuries. N Engl J Med 2002;347(24):1924–31.

[85] Hafeman AE, et al. Local delivery of tobramycin from injectable biodegradable polyurethane scaffolds. J Biomater Sci Polym Ed 2010;21(1):95–112.

[86] Guelcher SA, et al. Dual-purpose bone grafts improve healing and reduce infection. J Orthop Trauma 2011;25(8):477–82.

[87] Brady RA, et al. Osteomyelitis and the role of biofilms in chronic infection. FEMS Immunol Med Microbiol 2008;52(1):13–22.

[88] Carek PJ, Dickerson LM, Sack JL. Diagnosis and management of osteomyelitis. Am Fam Physician 2001;63(12):2413–20.

[89] Hedstrom SA, et al. Antibiotic containing bone cement beads in the treatment of deep muscle and skeletal infections. Acta Orthop Scand 1980;51(6):863–9.

[90] Hafeman AE, et al. Local delivery of tobramycin from injectable biodegradable polyurethane scaffolds. J Biomater Sci Polym 2010;21(1):95–112.

[91] Ambrose CG, et al. Effective treatment of osteomyelitis with biodegradable microspheres in a rabbit model. Clin Orthop Relat Res 2004;(421):293–9.

[92] Nelson CL, et al. In vitro elution characteristics of commercially and noncommercially prepared antibiotic PMMA beads. Clin Orthop Relat Res 1992;(284):303–9.

[93] Mader JT, Calhoun J, Cobos J. In vitro evaluation of antibiotic diffusion from antibiotic-impregnated biodegradable beads and polymethylmethacrylate beads. Antimicrob Agents Chemother 1997;41(2):415–8.

[94] Adams K, et al. In vitro and in vivo evaluation of antibiotic diffusion from antibiotic-impregnated polymethylmethacrylate beads. Clin Orthop Relat Res 1992;(278):244–52.

[95] Adams CS, et al. Controlled release of vancomycin from thin sol-gel films on implant surfaces successfully controls osteomyelitis. J Orthop Res 2009;27(6):701–9.

[96] Ruiz JC, et al. Polypropylene grafted with smart polymers (PNIPAAm/PAAc) for loading and controlled release of vancomycin. Eur J Pharm Biopharm 2008;70(2):467–77.

[97] Wenke JC, Guelcher SA. Dual delivery of an antibiotic and a growth factor addresses both the microbiological and biological challenges of contaminated bone fractures. Expert Opin Drug Deliv 2011;8(12):1555–69.

[98] Hochbaum AI, et al. Inhibitory effects of D-amino acids on *Staphylococcus aureus* biofilm development. J Bacteriol 2011;193(20):5616–22.

[99] Jennings JA, Courtney HS, Haggard WO. Cis-2-decenoic acid inhibits *S. aureus* growth and biofilm in vitro: a pilot study. Clin Orthop Relat Res 2012;470(10):2663–70.

[100] Folsom JP, Baker B, Stewart PS. In vitro efficacy of bismuth thiols against biofilms formed by bacteria isolated from human chronic wounds. J Appl Microbiol 2011;111(4):989–96.

[101] Sanchez CJ, et al. Effects of local delivery of D-amino acids from biofilm-dispersive scaffolds on infection in contaminated rat segmental defects. Biomaterials 2015; 34(30):7533–43.

[102] Harmata AJ, et al. D-amino acid inhibits biofilm but not new bone formation in an ovine model. Clin Orthop Relat Res 2015;473(12):3951–61.

[103] Nelson CE, et al. Sustained local delivery of siRNA from an injectable scaffold. Biomaterials 2012;33(4):1154–61.

[104] Nelson CE, et al. Tunable delivery of siRNA from a biodegradable scaffold to promote angiogenesis in vivo. Adv Mater 2014;26(4):607–14, 506.

[105] Nguyen KT, West JL. Photopolymerizable hydrogels for tissue engineering applications. Biomaterials 2002;23(22):4307–14.

[106] Hafeman AE, et al. Characterization of the degradation mechanisms of lysine-derived aliphatic poly(ester urethane) scaffolds. Biomaterials 2011;32(2):419–29.

[107] Guo R, et al. A transient cell-shielding method for viable MSC delivery within hydrophobic scaffolds polymerized in situ. Biomaterials 2015;54:21–33.

[108] Muggli DS, Burkoth AK, Anseth KS. Crosslinked polyanhydrides for use in orthopedic applications: degradation behavior and mechanics. J Biomed Mater Res 1999;46(2):271–8.

[109] Karageorgiou V, Kaplan D. Porosity of 3D biomaterial scaffolds and osteogenesis. Biomaterials 2005;26(27):5474–91.

[110] Gibson LJ. The mechanical behaviour of cancellous bone. J Biomech 1985;18(5):317–28.

[111] Cowin, S.C., Bone mechanics. 1989: CRC.

Antimicrobial nanostructured polyurethane scaffolds

17

S. Chung[1], T.J. Webster[1,2]*
[1]Northeastern University, Boston, MA, USA; [2]Center of Excellence for Advanced Materials Research, King Abdulaziz University, Jeddah, Saudi Arabia
*Corresponding author: th.webster@neu.edu

17.1 Introduction

Polyurethanes (PUs) have been used as a biomaterial for many years due to their excellent mechanical properties, biocompatibility, and adaptability (Coury et al., 1988). For example, traditional medical applications of PUs involve catheters, transdermal patches, transient cardiovascular devices, and intraaortic balloon pumps, among others (Chen et al., 2013).

In recent years, PUs have been used increasingly as tissue engineering scaffolds (Jia et al., 2013; Keck et al., 2013; Mi et al., 2014; Tsai et al., 2015). Because of the uniquely segmented structure of PUs, many diverse materials that are suitable to a number of tissue engineering applications may be obtained. Due to the increase in antibiotic-resistant microbes, the need for scaffolds with antibacterial properties has become paramount to reduce the dosage of oral antibiotics needed to prevent infection. This chapter discusses common techniques for constructing these scaffolds, strategies to impart antibacterial properties, and copolymer blends used to construct these scaffolds.

17.2 Techniques for constructing polyurethanes scaffolds

There are many techniques that may be used for constructing PU scaffolds. For the purposes of this chapter, only the most commonly used techniques will be briefly discussed. These techniques are solvent casting/particle leaching (SC/PL), thermally induced phase separation (TIPS), melt molding, gas foaming, emulsion freeze drying, electrospinning, and hydrogels (Table 17.1). Examples of the latest research on these fabrication methods will be discussed below.

17.2.1 Solvent casting/particle leaching

Solvent casting is likely the most basic technique for creating a polymer scaffold (Janik and Marzec, 2015). First, the PU is dissolved in a solvent such as dimethylformamide (DMF) and tetrahydrofuran (THF) and then casted onto a mold to produce a scaffold. Then, when the solvent evaporates, which may be accomplished by

Table 17.1 **Summary of common tissue engineering scaffolds for polyurethanes fabrication**

Fabrication technique	Advantages	Disadvantages	Pore sizes (μm)	Porosity (%)	Applications	References
Solvent casting: particle leaching	Does not require specialized equipment	Optimization needed for high porosity without loss of mechanical properties Particles difficult to leach May leave residual solvent	100–400	>70	Soft tissue engineering: coronary arteries, bone	Farè et al. (2007), Laschke et al. (2010), Rogers et al. (2013), Ryszkowska et al. (2010), and Sin et al. (2010)
Thermally induced phase separation	Good control of pore size and structure	Difficult to obtain pore size >200 μm	36–203	>80	Cardiovascular, bone	Guan et al. (2005), Mi et al. (2014), and Saad et al. (1996)
Melt molding	Easy scale up No solvents	Nonporous layer on the surface Residual porogens in the scaffold Requires high operating temperatures	30–450	64–88	HA, bone	Haugen et al. (2004) and Shokrolahi et al. (2011)
Electrospinning	Fiber morphology and geometry easily controlled Drug loading widely investigated	Small pore sizes Small thickness	0.007–1.5	15–99	Vascular, bone, neural, tendon/ligament, wound dressing	Demir et al. (2002), Sheikh et al. (2009), and Sill and Recum (2008)

Hydrogel	Does not require specialized equipment Easily customizable based on monomer and cross-linking agent concentration	Low mechanical properties Shrinkage when dried	>10	15–99	Wound dressing, optical, cartilage, bone, smooth muscle	Butcher et al. (2014) and Drury and Mooney (2003)
Gas foaming	No solvent	Difficult to control pore size	50–2000	>75	Bone	Gorna and Gogolewski (2006), Kim et al. (2012), and Parks and Beckman (1996)
Emulsion freeze drying	Requires less solvent Does not require the drying and leaching of porogen	Emulsions may be unstable and may require the addition of surfactants	10–300	>80		Hsu et al. (2014) and Jiang et al. (2010)

air-drying, vacuum-drying, or freeze-drying methods, the polymer remains, forming a 3D structure in the shape of the mold. This process may be combined with particle leaching to produce a porous structure. The addition of solid particles, usually salts, to the polymer solution will result in a suspension with solid particles dispersed throughout the solution after solvent evaporation. Immersion in water will then remove the salts, resulting in a porous structure.

The major advantage of this technique lies in its simplicity, because this technique does not require access to any specialized equipment. However, there are a number of drawbacks to this technique. Optimization is needed to obtain a material with high porosity without significant loss of mechanical properties. In addition, particles may be difficult to leach out from a thick material. Finally, contact with residual organic solvents, such as DMF and THF, may induce toxicity to cells and to other biological molecules.

17.2.2   Thermally induced phase separation

Similar to SC/PL, TIPS requires the use of solvent to dissolve the PU (Janik and Marzec, 2015). Liquid–liquid separation may be achieved by reducing the temperature to below the solvent's freezing point, forming two phases, a polymer-rich phase, which solidifies, and a polymer-poor phase, which crystallizes. The crystals can then be removed to generate a highly porous structure. The main advantage to this technique is the ability to control the pore size and structure by varying preparation conditions (Martínez-Pérez et al., 2011). The shape of the pore may be controlled through a modified TIPS method called the directional thermally induced phase separation (dTIPS). Phase separation is carried out by maintaining a uniaxial temperature gradient through insulation of side walls of the polymer mold, which also increases thermal conductivity throughout the solution. dTIPS allows for the formation of an array of parallel microtubules and microchannels as well as an array of straight parallel channels with side tubular branches (Ma and Zhang, 2001; Mandoli et al., 2010). In contrast, classical TIPS does not have uniaxial temperature gradients, and thus the pore structures are generated randomly. Various morphologies of the scaffold may be obtained by adjusting TIPS parameters such as polymer composition, solvent ratios, and polymer concentration (de Lima and Felisberti, 2009; Luo et al., 2008).

The main disadvantage to the TIPS technique is that it is difficult to obtain pore sizes above 200 μm and to control the micro- and macrostructure of the scaffold (Thomson et al., 2000). Recent efforts have combined TIPS with PL to better control pore structures either by leaching out the solid particles or by using a polymer-poor phase (Gorna and Gogolewski, 2006; Heijkants et al., 2008; Podporska-Carroll et al., 2014).

17.2.3   Melt molding

Melt molding shares many similarities with TIPS and SC/PL. The starting materials include polymeric compounds with porogens, particles used to make pores, which are then placed inside a mold. In contrast with TIPS, the polymer used is solid, granulated,

or powdered and forms a scaffold to the shape of the mold after heating above the polymer's glass transition temperature (T_g) at an elevated pressure (Thomson et al., 1995). Using the same PL techniques from SC/PL, the porogen is leached out, forming a porous PU scaffold.

Melt molding is very advantageous for industrial applications and scale-up. Among different processes for creating porous scaffolds, melt molding is the most convenient and rapidly produces structures with varying shapes and sizes (Hou et al., 2003). Additionally, melt molding does not require organic solvents to create scaffolds (Haugen et al., 2004), further easing the production processes for scaffolds fabricated by melt molding.

Melt molding has a number of limitations and disadvantages. Melt molding creates nonporous layers on the surface and likely leaves behind porogen compounds in the scaffold, due to the difficulty in leaching out the particles. The fabrication process requires high operating temperatures (Leong et al., 2003).

17.2.4 Electrospinning

Electrospinning is a common approach for fabricating PU scaffolds. The process of electrospinning usually involves the use of a polymer solution in a solvent; a high voltage is applied to the solution, causing the polymer solution to become charged and stretching the liquid into what is known as the Taylor cone. Eventually, the induced electrostatic repulsion reaches a critical limit and overcomes the surface tension of the liquid, and the polymer solution then travels toward a charged collector; and as the solvent evaporates, the dried polymers deposit onto the collector in a randomly oriented fashion, although the use of rotating collectors may align fibers in specific geometries (Teo and Ramakrishna, 2006). Groups have also utilized melt electrospinning, a process where a polymer melt is electrospun by cooling the electrified jet causing it to solidify, forming, solvent-free fibrous scaffolds (Karchin et al., 2011). Thermoplastic PUs (TPUs) have also been electrospun in recent years (Mi et al., 2013). For the purposes of this chapter, neither melt electrospinning of PUs nor electrospinning of TPUs will be discussed as research into these areas is still fundamental and has not been utilized for antimicrobial applications.

There are a number of advantages to using electrospinning over other methods, many of which are due to the ease of control over the physical morphology as compared to other fabrication techniques. A wide range of PUs have been electrospun (Demir et al., 2002; Khil et al., 2003; Puppi et al., 2010; Unnithan et al., 2014). By adjusting the solution concentration, fibers from 7 nm to 1.5 μm may be obtained (Demir et al., 2002). Complex fiber structures, for example: core–shell, fiber assembly, multilayers, fiber orientation, and scaffold shaping, may all be manipulated by adjusting collector and setup of needles (Puppi et al., 2014). Drug loading using electrospun constructs has also been widely investigated for applications such as antibiotics, anticancer agents, and peptides (Aguilar et al., 2015; Hong et al., 2008; Rockwood et al., 2008; Sheikh et al., 2009). Common drawbacks to the electrospinning technique include small pore size, ~1–5 μm, which prevents cell penetration, and the small thickness of nanofiber scaffolds.

17.2.5   Hydrogels

Hydrogels are one of the most common tissue engineering scaffolds. In its most basic form, a hydrogel consists of a solution of hydrophilic polymer, suspended in water, that forms a gel on cross-linking. Cross-linking may be induced by a radical initiator, usually photo- or heat activated, which cross-links linear or branched polymers. As with electrospinning, there are many polymers and polymer blends that have been made into hydrogels (Li et al., 2015; Lin and Li, 2014; Sun et al., 2014).

Hydrogels possess a number of processing advantages. Fabrication of a hydrogel does not require any specialized equipment as the application of heat is enough to initiate cross-linking. Polymers are suspended in water instead of a solvent, and porosity is easily controlled by polymer concentration to cross-linking agent concentration. Because of the ease of fabrication and functionalization, hydrogels have been used in a wide variety of tissue engineering applications (Butcher et al., 2014). However, hydrogels have low mechanical properties and cannot be used for any load-bearing applications. In addition, the loss of water will cause shrinkage in the gel, although the amount of shrinking may be alleviated with increased cross-linking and higher polymer concentration.

17.2.6   Gas foaming

Gas foams of PUs are formed either by releasing the gas of the gas foaming agent to the reaction mixture (Huang and Miao, 2007) or by introducing gas to the melted polymer (Di Maio et al., 2005). PU foam is fabricated when water is added to the reaction mixture, reacting with the isocyanate group to form a carbamic acid derivative, which is then transformed into CO_2 after decarboxylation (Janik and Marzec, 2015). Although gas foaming is a commonly used industry process, it has been less commonly used for scaffold fabrication due to the difficulty in controlling the size and interconnectivity of pores, and large pores may be formed inside the polymer structure during the foaming process. Gas foaming has the advantage of not requiring organic solvents.

17.2.7   Emulsion freeze drying

Scaffolds formed by emulsion freeze drying start with the mixing of two immiscible phases with the polymer suspended in a solvent in the continuous phase and the water in the dispersed phase. The emulsion is then homogenized and frozen quickly, for example, in liquid nitrogen; pressure is then dropped, allowing the frozen water molecules to sublimate into a gas phase and then subsequently be removed by vacuum. The pore sizes and interconnectivity may be controlled by altering processing parameters, such as volume, concentration and viscosity of the polymer solution, amount of dispersed phase, ratio of volume in the continuous and dispersed phase, and cooling rate. Specifically, macro- (12–18 μm) and micro- (1.5–7 μm) pores may be formed. The micropores are formed by the removal of the solvent while the macropores are formed by the coalescing of the micropores during the homogenization step and, thus, are partially interconnected by the micropores (Grinberg et al., 2010).

Processing parameters greatly affect the structure of the scaffolds created using this technique. The volume of water is directly correlated to the average pore size (Whang et al., 1995) while the polymer concentration in the continuous phase is inversely proportional to the porosity and the pore sizes. As the polymer concentration increases, the dispersed phase is subjected to higher shear forces, reducing the size of the water domains (Place et al., 2009). Constant cooling rate freezing leads to uniform porous structures while rapid quenching leads to non uniform nucleation and growth of ice crystals due to heterogeneity caused by variable heat transfer throughout the system.

Emulsion freeze drying requires less solvent and does not require the time-consuming processes of drying and leaching of porogen. The main disadvantage of the emulsion freeze-drying technique is that the emulsions may be unstable and may require the addition of surfactants (Whang et al., 1995). The use of waterborne polyurethane (WBPU) may be used to form surfactant-free scaffolds (Jiang et al., 2010). The initial synthesis of WBPUs may be more complicated than PUs, but subsequent fabrication of scaffolds is easier.

17.3   Strategies to impart antibacterial activity to polyurethanes

Although PUs have many good mechanical and biocompatibility properties, PU scaffolds do not inherently possess antimicrobial activity. To impart antibacterial properties, additional functional groups are needed to impart antibacterial activity. There are a few strategies that have been commonly employed: tethering of an antimicrobial moiety directly to the monomer structure, loading PUs with antimicrobial agent, using a copolymer that has inherent antimicrobial properties, or creating a nanofeatured surface that retains the surface chemistry while altering surface energy and other physical features.

17.3.1   Antimicrobial moieties

This section will discuss chemical changes affected on the PU monomer or surface to impart antibacterial properties.

17.3.1.1   Bacteria surface contact killing

Effective bacteria surface killing is ideal for biomedical applications. If bacteria can be killed without the release of antimicrobial drug compounds, the growth of antibiotic-resistant bacteria may be alleviated, as antibiotic-resistant bacteria are becoming increasingly resistant to higher doses of conventionally approved antibiotics (Frieden, 2013). By far, the most commonly used chemistry for surface contact killing is the quaternary ammonium compounds (QACs), positively charged cations with the structure NR_4^+, with R being either an alkyl or aryl group. The addition of quaternary ammonium salts to PUs by reaction of hydroxyl hydroxytelechelic

polybutadienes covalently bound with quaternary ammonium salts with an aliphatic triisocyanate has shown at least a 6 log bacterial load reduction, 5 log reduction in yeast, and 1 log reduction in mold (Nurdin et al., 1993). The mechanism has been proposed to involve cell wall disruption by the polycations (Chen et al., 2000; Ishitsuka et al., 2006; Kuroda and DeGrado, 2005; Tew et al., 2002). In designing the QACs, the length of the alkyl chain and the amount of QAs loaded both affect bacterial killing. As the length of the alkyl chain increases and the amount of QACs grafted onto PUs increases, the contact killing effect of the QACs increases (Grapski and Cooper, 2001). In addition, the QAC surface concentration must be optimized, as at high concentrations QACs are lethal to mammalian cells as well, although concentrations that inhibited bacteria are sublethal to mammalian epithelial cells as tested on MDCK II cells (Inácio et al., 2013).

Although biocidal properties are beneficial, incorporation of the release mechanism to release dead bacteria from the surface will help reduce fouling on the scaffold. Taking advantage of the biocidal effects of QACs, Liang et al. (2006) also incorporated *N*-halamines to release chloride or hypochloride.

Table 17.2 lists chemical and physical surface modifications used to impart antibacterial properties on PU (Kugel et al., 2011).

Table 17.2 Surface treatment for imparting antibacterial properties to polyurethanes

Treatment method	References
Tetramethylene glycol-4,4′-diphenylmethane diisocyanate prepolymers extended with diethylenetriamine, reacted with epichlorohydrin and quaternized	Wang and Lin (1998)
Methylenediphenylamine diisocyanate reacted with polytetramethylene oxide and chain extended with 1,4 butanediol (sulfonated, phosphonated, zwitterionic, quaternary)	Flemming et al. (2000)
Quaternized *N,N*-bis(2-hydroxyethyl)isonicotinamide as a chain extender in poly(tetramethylene oxide)-based PU block copolymers	Grapski and Cooper (2001)
N,N-bis(Hydroxyethyl)*N,N*-dimethyl quaternary ammonium methane sulfonate–diisocyanate prepolymers extended with water or diamine	Bechara and Baranowski (2001)
Poly[3-(5,5-dimethylhydantoinylpropyl)siloxane-*co*-3-dimethyldodecylammoniumpropylsiloxane chloride] was formed by the reaction of poly(3-chloropropylsiloxane) and hydantoin salt	Liang et al. (2006)
Diisocyanate–polyol prepolymer reacted with hydroxyethyl acrylate, polymerized by free radical polymerization with *N,N*-dimethylaminoethyl acrylate hexadecyl ammonium chloride	Sengupta et al. (2008)
Nitric acid-treated PU to create nanofeatures on surface	Yao et al. (2014)

17.3.1.2 Polymer scaffold modifiers and surface modifications

The QAC modifications described in the previous section are bulk phase modifications to the polymer itself. Efforts have been undertaken to concentrate the contact killing moieties, such as QACs, to the surface of the polymer by using polymer scaffold modifiers (PSMs) (Kurt et al., 2007; Makal et al., 2006; Waschinski et al., 2008). These modifications are driven by low solubility and/or low surface energy (Luzinov et al., 2004). Kurt et al. (2007) used a hard-block/soft-block strategy, with the bulk PU as the hard block and the antibiotic-loaded PSM as the soft block. Alkylammonium polyoxetane telechelics (Figure 17.1) react with the hard block PU formed by the reaction of 4,4′-(methylene bis(p-cyclohexyl isocyanate) and 1,4-butanediol.

Alternatively, Makal et al. (2006) and Waschinski et al. (2008) adopted a different strategy. They used a type of PSM that contained fluoroalkyl groups adjacent to biocidal moieties; these fluoropolymer segments migrated through the bulk PU and chaperoned the chloroamide or quaternary ammonium to the surface. Another method for concentrating QACs to the surface is the use of amphiphilic compounds (Harney et al., 2009); by using hydrophobic *n*-alkyl groups and hydrophilic oxyethlene chains of varying length (Figure 17.2), Harney et al. (2009) were able to mimic the ability of the fluoropolymer segments to chaperone QACs while synthesizing a nonpolymer additive that delivered an impressive 7 log reduction to both Gram-positive *Staphylococcus aureus* and Gram-negative *Escherichia coli*.

Although changing the chemistry of the surface undoubtedly has a drastic improvement in antibacterial properties, the downstream approval process becomes more cumbersome with each chemical modification. An alternative approach is to change only the physical features of the surface by etching with acid and studying the resultant
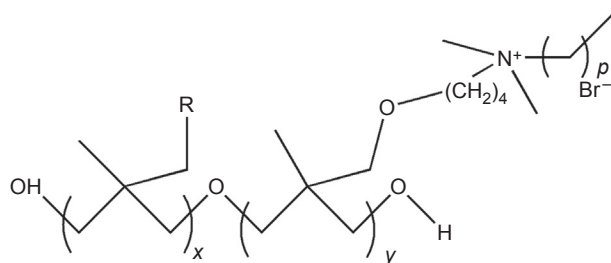
Figure 17.1 Cotelechelics, $R = CF_3CH_2O$—$(3FO_x)$, $CH_3O(CH_2CH_2O)_2$—(ME_2O_x) and $p = 5$ (C6) or 11 (C12); x's are 0.86 and 0.89 and y's are 0.11 and 0.14 (Kurt et al., 2007).
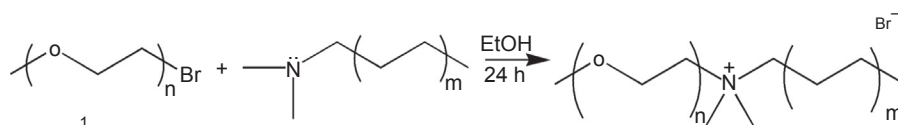
Figure 17.2 Reaction of oxyethylene bromides (a) with tertiary amines (b) in ethanol to afford the desired ammonium bromide compounds (Harney et al., 2009).

(a)   (b)
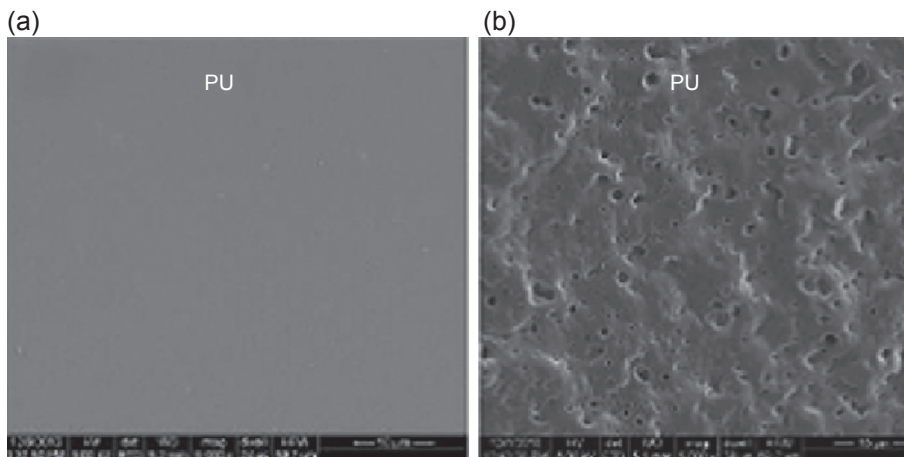
Figure 17.3 (a) Untreated PU, (b) nitric acid-treated PU with significantly more nanofeatures on the surface (Yao et al., 2014).

nanometer roughness change (Yao et al., 2014). By treating with nitric acid, HNO_3, nanoscale roughness and hydrophobicity increased, which led to at least fivefold decrease in colony forming units from *Staphylococcus epidermidis*, *E. coli*, and *Proteus mirabilis* (Figure 17.3). In addition, treated surfaces showed a 15% increase in adsorption of fibronectin. Researchers have shown that increased protein adsorption has improved cellular adhesion and tissue growth (Khang et al., 2007; Webster et al., 2000; Woo et al., 2003). Furthermore, there is a linear relationship among nanoroughness, surface energy, and protein adsorption (Puckett et al., 2010). Generally, as surface roughness increases, proliferation of bacterial cells decreases while proliferation of mammalian cells increases.

17.3.1.3   Antibiotic delivery

In addition to grafting bactericidal moieties to either the monomer backbone or the surface, PU scaffolds may also be used to deliver drugs. As noted earlier, PU scaffolds have been widely investigated for the delivery of molecules, ranging from anticancer drugs, antibiotics, to peptides. For the purposes of this chapter, the mechanisms to drug delivery will only be discussed briefly to highlight common drugs used to impart antibacterial properties.

As with other tissue engineering polymers, the use of silver has been widely investigated for imparting antimicrobial activity to PUs (Filip et al., 2014; Jain and Pradeep, 2005; Sheikh et al., 2009). Other nanoparticle carriers include iron oxide (Das et al., 2014), zinc oxide (Kantheti et al., 2014), copper oxide (Amna et al., 2014), selenium (Tran and Webster, 2013), and gold (Sawant et al., 2013). Although many groups are investigating decorating carbon nanotubes (CNTs) onto PU scaffolds for other applications, some have studied CNTs for antibacterial applications (Das et al., 2014; Yadav et al., 2012). FDA-approved antibiotics such as rifampicin, gentamicin,

ciprofloxacin (Basak and Adhikari, 2012), tetracycline (Grinberg et al., 2010), and vancomycin (Li et al., 2010) have all been delivered using PU scaffolds. Delivery of antimicrobial peptides (AMPs) has been an emerging area of research as researchers realize the antimicrobial potential of AMPs (Wang et al., 2015). Due to the versatility of PUs, most commonly investigated antimicrobial chemistries have been investigated for delivery in a PU system. Long-term toxicity of many of these chemistries is unknown, especially regarding nanoparticles, and more research will be needed to fully elucidate their long-term effects.

17.3.2   Polyurethanes blends

Many groups have blended PU with other polymers that possess inherent antibacterial properties to synergize the beneficial mechanical properties of PU with the antibacterial properties of other polymers. In particular, zein and chitosan have been used most frequently (Kara et al., 2014; Unnithan et al., 2014). Both zein, a plant protein, and chitosan, derived from chitin, are natural polymers. Both are also cationic, which is thought to disrupt bacterial cell wall interactions (Chen et al., 2000; Ishitsuka et al., 2006; Kuroda and DeGrado, 2005; Tew et al., 2002) as well as having poor mechanical properties, making both polymers good candidates for copolymer blends with PUs.

Compared to common synthetic polymers used to blend with PU, zein has better biocompatibility and good biodegradability (Unnithan et al., 2014). In addition, zein possesses good mechanical properties: toughness, flexibility, compressibility, and glossiness. Most importantly, zein has inherent antimicrobial properties (Shukla and Cheryan, 2001). Unnithan et al. (2014) found that an electrospun copolymer of PU–cellulose acetate–zein possessed enhanced platelet activation, clotting ability, and bactericidal activity. In addition, a copolymer of zein and PU possessed excellent tensile properties and flexibility as well as good mammalian cell viability when tested with L929, mouse fibroblast cells (Du et al., 2013).

Chitosan is a linear, cationic (1–4)-2-amino-2-deoxy-β-D-glucan produced from chitin through partial deacetylation. Chitosan has good antibacterial properties (Liu et al., 2000) and good cytocompatibility (Shalumon et al., 2009). PU films modified with different concentrations of chitosan demonstrated good bactericidal activity, at least 4 log, against both *Pseudomonas aeruginosa* and *S. aureus* (Kara et al., 2014). Furthermore, the films were shown to moderately inhibit bacterial adhesion as well. Interestingly, although Kara et al. (2014) did not test for mammalian cell viability with their constructs, other groups have tested for mammalian cells lines such as fibroblasts and MG63, osteoblast-like cells, and found comparable cell viability and function (Lv et al., 2013; Zhang and Zhang, 2002).

17.4   Conclusions and future directions

PUs are a versatile biomaterial that has been utilized for many tissue engineering applications due to their excellent mechanical properties, biocompatibility, and adaptability. Despite these excellent properties, PUs do not inherently possess

antibacterial properties. With the growing threat of increased antibiotic-resistant bacteria, there is great demand for antibacterial PU scaffolds. Current strategies focus on four main strategies for imparting antibacterial properties and can be described as follows: grafting of antimicrobial moieties to the PU, delivering antibiotics with the PU, nanostructuring PU surfaces, and blending polymers with antibacterial polymers with PU.

Grafting of antimicrobial moieties, such as QACs, has been studied for many years, and there are many variations of this technique. There are newer, emerging chemistries, but by and large, the field is still working on QAC chemistry. In the future, new chemistries are needed to address the growing plethora of bacteria. In addition, combinatorial mechanism systems will become more important; for example, scaffolds that can combine the bactericidal properties of QACs with release and/or bacterial static mechanisms would be much more effective. In addition, nanofeatured surfaces have shown inherent antibacterial properties in the absence of antibiotic chemistries while promoting mammalian cell functions necessary for tissue engineering applications; future studies that synergize the physical and chemical effects would greatly contribute to the field.

PUs have been studied as drug delivering vehicles for many existing antibiotic molecules. Many of these molecules have been in use clinically for many years and suffer from increasing bacterial resistance. Newer chemistries, such as AMPs, would help address the growing antibiotic resistance. Combinatorial approaches utilizing existing antibiotics have shown tremendous efficacy against antibiotic-resistant infections, and delivering these combination therapies may provide significant improvement in addressing microbial infection in the future (Geilich et al., 2014).

Finally, current research in PU blends is focused on developing antimicrobial PUs using zein and chitosan polymers, both cationic natural polymers with good antibacterial properties but poor mechanical properties for tissue engineering applications. PU blends have shown a synergistic effect of maintaining good mechanical properties while improving antibacterial properties. A better understanding of blend chemistry and morphology would help in making improved materials for the other modifications described in this chapter.

References

Aguilar, L.E., Unnithan, A.R., Amarjargal, A., Tiwari, A.P., Hong, S.T., Park, C.H., Kim, C.S., 2015. Electrospun polyurethane/Eudragit® L100-55 composite mats for the pH dependent release of paclitaxel on duodenal stent cover application. International Journal of Pharmaceutics 478, 1–8. http://dx.doi.org/10.1016/j.ijpharm.2014.10.057.

Amna, T., Hassan, M.S., Yang, J., Khil, M.S., Song, K.D., Oh, J.D., Hwang, I., 2014. Virgin olive oil blended polyurethane micro/nanofibers ornamented with copper oxide nanocrystals for biomedical applications. International Journal of Nanomedicine 9, 891–898. http://dx.doi.org/10.2147/IJN.S54113.

Basak, P., Adhikari, B., 2012. Effect of the solubility of antibiotics on their release from degradable polyurethane. Materials Science and Engineering: C 32, 2316–2322. http://dx.doi.org/10.1016/j.msec.2012.07.002.

Bechara, I., Baranowski, T.R., 2001. Polyetherurethane Copolymer. US6221954 B1.

Butcher, A.L., Offeddu, G.S., Oyen, M.L., 2014. Nanofibrous hydrogel composites as mechanically robust tissue engineering scaffolds. Trends in Biotechnology 32, 564–570. http://dx.doi.org/10.1016/j.tibtech.2014.09.001.

Chen, C.Z., Beck-Tan, N.C., Dhurjati, P., van Dyk, T.K., LaRossa, R.A., Cooper, S.L., 2000. Quaternary ammonium functionalized poly(propylene imine) dendrimers as effective antimicrobials: structure-activity studies. Biomacromolecules 1, 473–480. http://dx.doi.org/10.1021/bm0055495.

Chen, Q., Liang, S., Thouas, G.A., 2013. Elastomeric biomaterials for tissue engineering. Progress in Polymer Science 38, 584–671. http://dx.doi.org/10.1016/j.progpolymsci.2012.05.003.

Coury, A.J., Slaikeu, P.C., Cahalan, P.T., Stokes, K.B., Hobot, C.M., 1988. Factors and interactions affecting the performance of polyurethane elastomers in medical devices. Journal of Biomaterials Applications 3, 130–179.

Das, B., Chattopadhyay, P., Upadhyay, A., Gupta, K., Mandal, M., Karak, N., 2014. Biophysico-chemical interfacial attributes of Fe_3O_4 decorated MWCNT nanohybrid/bio-based hyperbranched polyurethane nanocomposite: an antibacterial wound healing material with controlled drug release potential. New Journal of Chemistry 38, 4300. http://dx.doi.org/10.1039/C4NJ00732H.

De Lima, J.A., Felisberti, M.I., 2009. Porous polymer structures obtained via the TIPS process from EVOH/PMMA/DMF solutions. Journal of Membrane Science 344, 237–243. http://dx.doi.org/10.1016/j.memsci.2009.08.008.

Demir, M.M., Yilgor, I., Yilgor, E., Erman, B., 2002. Electrospinning of polyurethane fibers. Polymer (Guildford) 43, 3303–3309. http://dx.doi.org/10.1016/S0032-3861(02)00136-2.

Di Maio, E., Mensitieri, G., Iannace, S., Nicolais, L., Li, W., Flumerfelt, R.W., 2005. Structure optimization of polycaprolactone foams by using mixtures of CO_2 and N_2 as blowing agents. Polymer Engineering and Science 45, 432–441. http://dx.doi.org/10.1002/pen.20289.

Drury, J.L., Mooney, D.J., 2003. Hydrogels for tissue engineering: scaffold design variables and applications. Biomaterials 24, 4337–4351. http://dx.doi.org/10.1016/S0142-9612(03)00340-5.

Du, X., Li, Y., Liu, X., Wang, X., Huselstein, C., Zhao, Y., Chang, P.R., Chen, Y., 2013. Fabrication and evaluation of physical properties and cytotoxicity of zein-based polyurethanes. Journal of Materials Science: Materials in Medicine 25, 823–833. http://dx.doi.org/10.1007/s10856-013-5117-9.

Farè, S., De Nardo, L., Cicco, S.D., Jovenitti, M., Tanzi, M.C., 2007. Different processing methods to obtain porous structure in shape memory polymers. Materials Science Forum 539–543, 663–668. http://dx.doi.org/10.4028/www.scientific.net/MSF.539-543.663.

Filip, D., Macocinschi, D., Paslaru, E., Munteanu, B.S., Dumitriu, R.P., Lungu, M., Vasile, C., 2014. Polyurethane biocompatible silver bionanocomposites for biomedical applications. Journal of Nanoparticle Research 16. http://dx.doi.org/10.1007/s11051-014-2710-x.

Flemming, R.G., Capelli, C.C., Cooper, S.L., Proctor, R.A., 2000. Bacterial colonization of functionalized polyurethanes. Biomaterials 21, 273–281. http://dx.doi.org/10.1016/S0142-9612(99)00176-3.

Frieden, T., 2013. Antibiotic Resistance Threats. CDC, pp. 22–50. doi:CS239559-B.

Geilich, B.M., Singleton, G.L., van de Ven, A.L., Sridhar, S., Webster, T.J., 2014. Silver nanoparticle-embedded polymersome nanocarriers for the treatment of antibiotic-resistant infections. In: Northeast Bioengineering Conference (NEBEC), 2014 40th Annual. IEEE, pp. 1–2.

Gorna, K., Gogolewski, S., 2006. Biodegradable porous polyurethane scaffolds for tissue repair and regeneration. Journal of Biomedical Materials Research – Part A 79, 128–138.

Grapski, J.A., Cooper, S.L., 2001. Synthesis and characterization of non-leaching biocidal poly-urethanes. Biomaterials 22, 2239–2246. http://dx.doi.org/10.1016/S0142-9612(00)00412-9.

Grinberg, O., Binderman, I., Bahar, H., Zilberman, M., 2010. Highly porous bioresorbable scaf-folds with controlled release of bioactive agents for tissue-regeneration applications. Acta Biomaterialia 6, 1278–1287. http://dx.doi.org/10.1016/j.actbio.2009.10.047.

Guan, J., Fujimoto, K.L., Sacks, M.S., Wagner, W.R., 2005. Preparation and characterization of highly porous, biodegradable polyurethane scaffolds for soft tissue applications. Biomate-rials 26, 3961–3971. http://dx.doi.org/10.1016/j.biomaterials.2004.10.018.

Harney, M.B., Pant, R.R., Fulmer, P.A., Wynne, J.H., 2009. Surface self-concentrating amphi-philic quaternary ammonium biocides as coating additives. ACS Applied Materials and Interfaces 1, 39–41. http://dx.doi.org/10.1021/am800046r.

Haugen, H., Ried, V., Brunner, M., Will, J., Wintermantel, E., 2004. Water as foaming agent for open cell polyurethane structures. Journal of Materials Science: Materials in Medicine 15, 343–346. http://dx.doi.org/10.1023/B: JMSM.0000021099.33619.ac.

Heijkants, R.G.J.C., Van Calck, R.V., Van Tienen, T.G., De Groot, J.H., Pennings, A.J., Buma, P., Veth, R.P.H., Schouten, A.J., 2008. Polyurethane scaffold formation via a combination of salt leaching and thermally induced phase separation. Journal of Biomedical Materials Research – Part A 87, 921–932. http://dx.doi.org/10.1002/jbm.a.31829.

Hong, Y., Fujimoto, K., Hashizume, R., Guan, J., Stankus, J.J., Tobita, K., Wagner, W.R., 2008. Generating elastic, biodegradable polyurethane/poly(lactide-co-glycolide) fibrous sheets with controlled antibiotic release via two-stream electrospinning. Biomacromolecules 9, 1200–1207. http://dx.doi.org/10.1021/bm701201w.

Hou, Q., Grijpma, D.W., Feijen, J., 2003. Porous polymeric structures for tissue engineering prepared by a coagulation, compression moulding and salt leaching technique. Biomateri-als 24, 1937–1947. http://dx.doi.org/10.1016/S0142-9612(02)00562-8.

Hsu, S., Hung, K.-C., Lin, Y.-Y., Su, C.-H., Yeh, H.-Y., Jeng, U.-S., Lu, C.-Y., Dai, S.A., Fu, W.-E., Lin, J.-C., 2014. Water-based synthesis and processing of novel biodegradable elas-tomers for medical applications. Journal of Materials Chemistry B 2, 5083–5092. http://dx.doi.org/10.1039/c4tb00572d.

Huang, X., Miao, X., 2007. Novel porous hydroxyapatite prepared by combining H_2O_2 foaming with PU sponge and modified with PLGA and bioactive glass. Journal of Biomaterials Applications 21, 351–374.

Inácio, A.S., Costa, G.N., Domingues, N.S., Santos, M.S., Moreno, A.J.M., Vaz, W.L.C., Vieiraa, O.V., 2013. Mitochondrial dysfunction is the focus of quaternary ammonium surfactant toxicity to mammalian epithelial cells. Antimicrobial Agents and Chemotherapy 57, 2631–2639. http://dx.doi.org/10.1128/AAC.02437-12.

Ishitsuka, Y., Arnt, L., Majewski, J., Frey, S., Ratajczek, M., Kjaer, K., Tew, G.N., Lee, K.Y.C., 2006. Amphiphilic poly(phenyleneethynylene)s can mimic antimicrobial peptide mem-brane disordering effect by membrane insertion. Peptides 85, 231–236. http://dx.doi.org/10.1016/.j.bbamem.r006.08.001.13124.

Jain, P., Pradeep, T., 2005. Potential of silver nanoparticle-coated polyurethane foam as an antibacterial water filter. Biotechnology and Bioengineering 90, 59–63. http://dx.doi.org/10.1002/bit.20368.

Janik, H., Marzec, M., 2015. A review : fabrication of porous polyurethane scaffolds. Materials Science and Engineering C: Materials for Biological Applications 48, 586–591.

Jia, L., Prabhakaran, M.P., Qin, X., Kai, D., Ramakrishna, S., 2013. Biocompatibility evalua-tion of protein-incorporated electrospun polyurethane-based scaffolds with smooth muscle cells for vascular tissue engineering. Journal of Materials Science 48, 5113–5124. http://dx.doi.org/10.1007/s10853-013-7359-9.

Jiang, X., Yu, F., Wang, Z., Li, J., Tan, H., Ding, M., Fu, Q., 2010. Fabrication and charac-terization of waterborne biodegradable polyurethanes 3-dimensional porous scaffolds for vascular tissue engineering. Journal of Biomaterials Science: Polymer Edition 21, 1637–1652.

Kantheti, S., Narayan, R., Division, F.M., 2014. Pyrene anchored ZnO nanoparticles through click reaction for the development of antimicrobial and fluorescent polyurethane nano-composite. Polymer International 64, 267–274. http://dx.doi.org/10.1002/pi.4785.

Kara, F., Aksoy, E.A., Yuksekdag, Z., Hasirci, N., Aksoy, S., 2014. Synthesis and surface mod-ification of polyurethanes with chitosan for antibacterial properties. Carbohydrate Poly-mers 112, 39–47. http://dx.doi.org/10.1016/j.carbpol.2014.05.019.

Karchin, A., Simonovsky, F.I., Ratner, B.D., Sanders, J.E., 2011. Melt electrospinning of biodegradable polyurethane scaffolds. Acta Biomaterialia 7, 3277–3284. http://dx.doi.org/10.1016/j.actbio.2011.05.017.

Keck, M., Kober, J., Hacker, S., Laube, T., Walter, T., Kasper, C., Hatlapatka, T., Grönninger, E., Schnabelrauch, M., Wyrwa, R., 2013. LOP12: adipose-derived stem cells and electrospun modified polyurethane scaffolds as a new approach in adipose tissue engineering. Plastic and Reconstructive Surgery 132, 501.

Khang, D., Kim, S.Y., Liu-Snyder, P., Palmore, G.T.R., Durbin, S.M., Webster, T.J., 2007. Enhanced fibronectin adsorption on carbon nanotube/poly(carbonate) urethane: independent role of surface nano-roughness and associated surface energy. Biomaterials 28, 4756–4768. http://dx.doi.org/10.1016/j.biomaterials.2007.07.018.

Khil, M.-S., Cha, D.-I., Kim, H.-Y., Kim, I.-S., Bhattarai, N., 2003. Electrospun nanofibrous polyurethane membrane as wound dressing. Journal of Biomedical Materials Research Part B: Applied Biomaterials 67, 675–679. http://dx.doi.org/10.1002/jbm.b.10058.

Kim, H.J., Park, I.K., Kim, J.H., Cho, C.S., Kim, M.S., 2012. Gas foaming fabrication of porous biphasic calcium phosphate for bone regeneration. Tissue Engineering and Regenerative Medicine 9, 63–68. http://dx.doi.org/10.1007/s13770-012-0022-8.

Kugel, A., Stafslien, S., Chisholm, B.J., 2011. Antimicrobial coatings produced by "tethering" biocides to the coating matrix: a comprehensive review. Progress in Organic Coatings 72, 222–252. http://dx.doi.org/10.1016/j.porgcoat.2011.07.004.

Kuroda, K., DeGrado, W.F., 2005. Amphiphilic polymethacrylate derivatives as antimicro-bial agents. Journal of the American Chemical Society 127, 4128–4129. http://dx.doi.org/10.1021/ja044205+.

Kurt, P., Wood, L., Ohman, D.E., Wynne, K.J., 2007. Highly effective contact antimicrobial sur-faces via polymer surface modifiers. Langmuir 23, 4719–4723. http://dx.doi.org/10.1021/la063718m.

Laschke, M.W., Strohe, A., Menger, M.D., Alini, M., Eglin, D., 2010. In vitro and in vivo evalu-ation of a novel nanosize hydroxyapatite particles/poly(ester-urethane) composite scaffold for bone tissue engineering. Acta Biomaterialia 6, 2020–2027. http://dx.doi.org/10.1016/j.actbio.2009.12.004.

Leong, K.F., Cheah, C.M., Chua, C.K., 2003. Solid freeform fabrication of three-dimensional scaffolds for engineering replacement tissues and organs. Biomaterials 24, 2363–2378. http://dx.doi.org/10.1016/S0142-9612(03)00030-9.

Li, B., Brown, K.V., Wenke, J.C., Guelcher, S.A., 2010. Sustained release of vancomycin from polyurethane scaffolds inhibits infection of bone wounds in a rat femoral segmen-tal defect model. Journal of Controlled Release 145, 221–230. http://dx.doi.org/10.1016/j.jconrel.2010.04.002.

Li, L., Ying, X., Liu, J., Li, X., Zhang, W., 2015. Molecularly imprinted polyurethane grafted calcium alginate hydrogel with specific recognition for proteins. Materials Letters 143, 248–251. http://dx.doi.org/10.1016/j.matlet.2014.12.108.

Liang, J., Chen, Y., Barnes, K., Wu, R., Worley, S.D., Huang, T.S., 2006. N-halamine/quat silox-
ane copolymers for use in biocidal coatings. Biomaterials 27, 2495–2501. http://dx.doi.
org/10.1016/j.biomaterials.2005.11.020.

Lin, Y., Li, G., 2014. An intermolecular quadruple hydrogen-bonding strategy to fabricate
self-healing and highly deformable polyurethane hydrogels. Journal of Materials Chemis-
try B 2, 6878–6885. http://dx.doi.org/10.1039/C4TB00862F.

Liu, X.F., Guan, Y.L., Yang, D.Z., Li, Z., Yao, K.D., 2000. Antibacterial action of chitosan and
carboxymethylated chitosan. Journal of Applied Polymer Science 79, 1324–1335.

Luo, B., Li, Z., Zhang, J., Wang, X., 2008. Formation of anisotropic microporous isotactic
polypropylene (iPP) membrane via thermally induced phase separation. Desalination 233,
19–31. http://dx.doi.org/10.1016/j.desal.2007.09.023.

Luzinov, I., Minko, S., Tsukruk, V.V., 2004. Adaptive and responsive surfaces through
controlled reorganization of interfacial polymer layers. Progress in Polymer Science 29,
635–698. http://dx.doi.org/10.1016/j.progpolymsci.2004.03.001.

Lv, W., Luo, J., Deng, Y., Sun, Y., 2013. Biomaterials immobilized with chitosan for recharge-
able antimicrobial drug delivery. Journal of Biomedical Materials Research – Part A 101,
447–455. http://dx.doi.org/10.1002/jbm.a.34350.

Ma, P.X., Zhang, R., 2001. Microtubular architecture of biodegradable polymer scaffolds.
Journal of Biomedical Materials Research 56, 469–477. http://dx.doi.org/10.1002/
1097-4636(20010915)56:4<469::AID-JBM1118>3.0.CO;2-H.

Makal, U., Wood, L., Ohman, D.E., Wynne, K.J., 2006. Polyurethane biocidal polymeric
surface modifiers. Biomaterials 27, 1316–1326. http://dx.doi.org/10.1016/j.biomaterials.
2005.08.038.

Mandoli, C., Mecheri, B., Forte, G., Pagliari, F., Pagliari, S., Carotenuto, F., Fiaccavento, R.,
Rinaldi, A., Di Nardo, P., Licoccia, S., Traversa, E., 2010. Thick soft tissue reconstruction
on highly perfusive biodegradable scaffolds. Macromolecular Bioscience 10, 127–138.
http://dx.doi.org/10.1002/mabi.200900323.

Martínez-Pérez, C.A., Olivas-Armendariz, I., Castro-carmona, J.S., García-Casillas, P.E., 2011.
Scaffolds for tissue engineering via thermally induced phase separation. Advanced Regen-
erative Medicine 275–294.

Mi, H.-Y., Jing, X., Jacques, B.R., Turng, L.-S., Peng, X.-F., 2013. Characterization and proper-
ties of electrospun thermoplastic polyurethane blend fibers: effect of solution rheological
properties on fiber formation. Journal of Materials Research 28, 2339–2350. http://dx.doi.
org/10.1557/jmr.2013.115.

Mi, H.-Y., Palumbo, S., Jing, X., Turng, L.-S., Li, W.-J., Peng, X.-F., 2014. Thermoplastic poly-
urethane/hydroxyapatite electrospun scaffolds for bone tissue engineering: effects of poly-
mer properties and particle size. Journal of Biomedical Materials Research Part B: Applied
Biomaterials 1–11. http://dx.doi.org/10.1002/jbm.b.33122.

Mi, H.Y., Jing, X., Salick, M.R., Cordie, T.M., Peng, X.F., Turng, L.S., 2014. Morphology,
mechanical properties, and mineralization of rigid thermoplastic polyurethane/hydroxyap-
atite scaffolds for bone tissue applications: effects of fabrication approaches and hydroxy-
apatite size. Journal of Materials Science 49, 2324–2337. http://dx.doi.org/10.1007/
s10853-013-7931-3.

Nurdin, N., Helary, G., Sauvet, G., 1993. Biocidal polymers active by contact. II. Biological
evaluation of polyurethane coatings with pendant quaternary ammonium salts. Journal of
Applied Polymer Science 50, 663–670. http://dx.doi.org/10.1002/app.1993.070500411.

Parks, K.L., Beckman, E.J., 1996. Generation of microcellular polyurethane foams via polym-
erization in carbon dioxide. II: foam formation and characterization. Polymer Engineering
and Science 36, 2417–2431.

Place, E.S., George, J.H., Williams, C.K., Stevens, M.M., 2009. Synthetic polymer scaffolds for tissue engineering. Chemical Society Reviews 38, 1139–1151. http://dx.doi.org/10.1039/b811392k.

Podporska-Carroll, J., Ip, J.W.Y., Gogolewski, S., 2014. Biodegradable poly(ester urethane) urea scaffolds for tissue engineering: interaction with osteoblast-like MG-63 cells. Acta Biomaterialia 10, 2781–2791. http://dx.doi.org/10.1016/j.actbio.2014.02.016.

Puckett, S.D., Taylor, E., Raimondo, T., Webster, T.J., 2010. The relationship between the nanostructure of titanium surfaces and bacterial attachment. Biomaterials 31, 706–713. http://dx.doi.org/10.1016/j.biomaterials.2009.09.081.

Puppi, D., Detta, N., Piras, A.M., Chiellini, F., Clarke, D.A., Reilly, G.C., Chiellini, E., 2010. Development of electrospun three-arm star poly(e-caprolactone) meshes for tissue engineering applications. Macromolecular Bioscience 10, 887–897. http://dx.doi.org/10.1002/mabi.200900422.

Puppi, D., Zhang, X., Yang, L., Chiellini, F., Sun, X., Chiellini, E., 2014. Nano/microfibrous polymeric constructs loaded with bioactive agents and designed for tissue engineering applications: a review. Journal of Biomedical Materials Research Part B: Applied Biomaterials 1562–1579. http://dx.doi.org/10.1002/jbm.b.33144.

Rockwood, D.N., Akins, R.E., Parrag, I.C., Woodhouse, K.A., Rabolt, J.F., 2008. Culture on electrospun polyurethane scaffolds decreases atrial natriuretic peptide expression by cardiomyocytes in vitro. Biomaterials 29, 4783–4791. http://dx.doi.org/10.1016/j.biomaterials.2008.08.034.

Rogers, L., Said, S.S., Mequanint, K., 2013. The effects of fabrication strategies on 3D scaffold morphology, porosity, and vascular smooth muscle cell response. Journal of Biomaterials and Tissue Engineering 3, 300–311.

Ryszkowska, J.L., Auguścik, M., Sheikh, A., Boccaccini, A.R., 2010. Biodegradable polyurethane composite scaffolds containing Bioglass® for bone tissue engineering. Composites Science and Technology 70, 1894–1908. http://dx.doi.org/10.1016/j.compscitech.2010.05.011.

Saad, B., Matter, S., Ciardelli, G., Uhlschmid, G.K., Welti, M., Neuenschwander, P., Suter, U.W., 1996. Interactions of osteoblasts and macrophages with biodegradable and highly porous polyesterurethane foam and its degradation products. Journal of Biomedical Materials Research 32, 355–366. http://dx.doi.org/10.1002/(SICI)1097-4636(199611)32:3<355::AID-JBM8>3.0.CO;2-R.

Sawant, S.N., Selvaraj, V., Prabhawathi, V., Doble, M., 2013. Antibiofilm properties of silver and gold incorporated PU, PCLm, PC and PMMA nanocomposites under two shear conditions. PLoS One 8, 1–9. http://dx.doi.org/10.1371/journal.pone.0063311.

Sengupta, A., Jacobs, J.L., Scholz, M.T., Tautvydas, K.J., 2008. Biocidal Polyurethane Compositions and Methods of Use. US7459167 B1.

Shalumon, K.T., Binulal, N.S., Selvamurugan, N., Nair, S.V., Menon, D., Furuike, T., Tamura, H., Jayakumar, R., 2009. Electrospinning of carboxymethyl chitin/poly(vinyl alcohol) nanofibrous scaffolds for tissue engineering applications. Carbohydrate Polymers 77, 863–869. http://dx.doi.org/10.1016/j.carbpol.2009.03.009.

Sheikh, F.A., Barakat, N.A.M., Kanjwal, M.A., Chaudhari, A.A., Jung, I.-H., Lee, J.H., Kim, H.Y., 2009. Electrospun antimicrobial polyurethane nanofibers containing silver nanoparticles for biotechnological applications. Macromolecular Research 17, 688–696. http://dx.doi.org/10.1007/BF03218929.

Shokrolahi, F., Mirzadeh, H., Yeganeh, H., Daliri, M., 2011. Fabrication of poly(urethane urea)-based scaffolds for bone tissue engineering by a combined strategy of using compression moulding and particulate leaching methods. Iranian Polymer Journal 20, 645–658.

Shukla, R., Cheryan, M., 2001. Zein: the industrial protein from corn. Industrial Crops and Products 13, 171–192. http://dx.doi.org/10.1016/S0926-6690(00)00064-9.

Sill, T.J., von Recum, H.A., 2008. Electrospinning: applications in drug delivery and tissue engineering. Biomaterials 29, 1989–2006.

Sin, D., Miao, X., Liu, G., Wei, F., Chadwick, G., Yan, C., Friis, T., 2010. Polyurethane (PU) scaffolds prepared by solvent casting/particulate leaching (SCPL) combined with centrifugation. Materials Science and Engineering: C 30, 78–85. http://dx.doi.org/10.1016/j.msec.2009.09.002.

Sun, P., Wang, J., Yao, X., Peng, Y., Tu, X., Du, P., Zheng, Z., Wang, X., 2014. Facile preparation of mussel-inspired polyurethane hydrogel and its rapid curing behavior. ACS Applied Materials and Interfaces 6, 12495–12504. http://dx.doi.org/10.1021/am502106e.

Teo, W.E., Ramakrishna, S., 2006. A review on electrospinning design and nanofibre assemblies. Nanotechnology 17, R89–R106. http://dx.doi.org/10.1088/0957-4484/17/14/R01.

Tew, G.N., Liu, D., Chen, B., Doerksen, R.J., Kaplan, J., Carroll, P.J., Klein, M.L., DeGrado, W.F., 2002. De novo design of biomimetic antimicrobial polymers. Proceedings of the National Academy of Sciences of the United States of America 99, 5110–5114. http://dx.doi.org/10.1073/pnas.082046199.

Thomson, R.C., Wake, M.C., Yaszemski, M.J., Mikos, A.G., 1995. Biodegradable polymer scaffolds to regenerate organs. Advances in Polymer Science 122, 247–277.

Thomson, R.C., Shung, A.K., Yaszemski, M.J., Mikos, A.G., 2000. Principles of Tissue Engineering. Elsevier. http://dx.doi.org/10.1016/B978-012436630-5/50025-8.

Tran, P.A., Webster, T.J., 2013. Antimicrobial selenium nanoparticle coatings on polymeric medical devices. Nanotechnology 24, 155101.

Tsai, M.-C., Hung, K.-C., Hung, S.-C., Hsu, S., 2015. Evaluation of biodegradable elastic scaffolds made of anionic polyurethane for cartilage tissue engineering. Colloids and Surfaces B: Biointerfaces 125, 34–44. http://dx.doi.org/10.1016/j.colsurfb.2014.11.003.

Unnithan, A.R., Gnanasekaran, G., Sathishkumar, Y., Lee, Y.S., Kim, C.S., 2014. Electrospun antibacterial polyurethane-cellulose acetate-zein composite mats for wound dressing. Carbohydrate Polymers 102, 884–892. http://dx.doi.org/10.1016/j.carbpol.2013.10.070.

Wang, H.-H., Lin, M.-S., 1998. Biocidal polyurethane and its antibacterial properties. Journal of Polymer Research 5 (3). http://dx.doi.org/10.1007/s10965-006-0054-7.

Wang, J., Liu, Q., Tian, Y., Jian, Z., Li, H., Wang, K., 2015. Biodegradable hydrophilic polyurethane PEGU25 loading antimicrobial peptide Bmap-28: a sustained-release membrane able to inhibit bacterial biofilm formation in vitro. Scientific Reports 5, 8634. http://dx.doi.org/10.1038/srep08634.

Waschinski, C.J., Zimmermann, J., Salz, U., Hutzier, R., Sadowski, G., Tiller, J.C., 2008. Design of contact-active antimicrobial acrylate-based materials using biocidal macromers. Advanced Materials 20, 104–108. http://dx.doi.org/10.1002/adma.200701095.

Webster, T.J., Ergun, C., Doremus, R.H., Siegel, R.W., Bizios, R., 2000. Specific proteins mediate enhanced osteoblast adhesion on nanophase ceramics. Journal of Biomedical Materials Research 51, 475–483. http://dx.doi.org/10.1002/1097-4636(20000905)51:3<475::AID-JBM23>3.0.CO;2–9.

Whang, K., Thomas, C.H., Healy, K.E., Nuber, G., 1995. A novel method to fabricate bioabsorbable scaffolds. Polymer (Guildford) 36, 837–842. http://dx.doi.org/10.1016/0032-3861(95)93115-3.

Woo, K.M., Chen, V.J., Ma, P.X., 2003. Nano-fibrous scaffolding architecture selectively enhances protein adsorption contributing to cell attachment. Journal of Biomedical Materials Research Part A 67, 531–537. http://dx.doi.org/10.1002/jbm.a.10098.

Yadav, S.K., Mahapatra, S.S., Cho, J.W., 2012. Synthesis of mechanically robust antimicrobial nanocomposites by click coupling of hyperbranched polyurethane and carbon nanotubes. Polymer (Guildford) 53, 2023–2031. http://dx.doi.org/10.1016/j.polymer.2012.03.010.

Yao, C., Webster, T.J., Hedrick, M., 2014. Decreased bacteria density on nanostructured polyurethane. Journal of Biomedical Materials Research Part A 102, 1823–1828. http://dx.doi.org/10.1002/jbm.a.34856.

Zhang, Y., Zhang, M., 2002. Three-dimensional macroporous calcium phosphate bioceramics with nested chitosan sponges for load-bearing bone implants. Journal of Biomedical Materials Research 61, 1–8. http://dx.doi.org/10.1002/jbm.10176.

Interaction of cells with polyurethane scaffolds

18

*Y. Xu, J. Guan**
The Ohio State University, Columbus, OH, USA
*Corresponding author: guan.21@osu.edu

18.1   Introduction

Polyurethane (PU) scaffolds are attractive for tissue regeneration owing to their excellent mechanical properties, ease of processing, and good biocompatibility. PU scaffolds have been used to engineer tissues such as bone, blood vessel, heart muscle, heart valve, skeletal muscle, skin, and cartilage.[1–10] These scaffolds are essentially biodegradable. The biodegradability can be introduced into PUs by using degradable polymers as soft and/or hard segments, such as polycaprolactone (PCL),[11,12] poly-L-lactide (PLA),[13] polyglycolic acid (PGA),[13] and their copolymers. PUs can be fabricated into fibers,[14–17] foams,[18–21] nanostructures,[13,22] and multilayers[23,24] for various tissue engineering applications. When using PU scaffolds and cells to engineer tissues, cell fate is in part controlled by biochemical and biophysical properties of the scaffolds. The focus of this chapter is to review how these different properties affect cell adhesion, migration, proliferation, and differentiation.

18.2   Interaction of cells with fibrous polyurethane scaffolds

One of the widely used PU scaffolds is fibrous networks. The PU fibers mimic the fibrous morphology of extracellular matrix in tissues. Electrospinning is a commonly used approach to fabricate fibrous PU scaffolds. The typical fibers are continuous and long with diameters ranging from micrometers to nanometers. Scaffold mechanical properties, fiber diameter, and fiber orientation can be tuned by fabrication parameters such as PU chemistry, concentration and flow rate of PU solution, and rotation speed of the collection mandrel. In fibrous PU scaffolds, the mechanical properties including single fiber modulus and global scaffold modulus, fiber orientation, fiber diameter, and fiber composition control cell adhesion, migration, proliferation, and differentiation (Table 18.1).

18.2.1   Cell fate controlled by scaffold mechanical properties

Matrix mechanical properties especially stiffness are known to affect stem cell fate.[32–38] Engler et al. found that mesenchymal stem cells (MSCs) differentiated into different

Table 18.1 **Summary of recent works using fibrous scaffolds to control cell fates**

Cellular activity	Main results	References	Properties
Cell proliferation and differentiation	Anisotropic mechanical properties were obtained and remarkable cardiac differentiation of seeded MSCs was observed with increased 3D cell alignment along the fibers (with external stretching applied).	Guan et al.[7]	Mechanical/morphology
Cell proliferation and differentiation	Cell-seeded fibrous scaffold was fabricated via electrospinning/electrospraying method, and scaffold mechanical and structural properties were controlled by polymer solution pumping speed and polyurethane/hydrogel ratio. CDC cardiac differentiation was successfully achieved in scaffolds with high fiber volume fraction and small scaffold modulus at small strains.	Xu et al.[8]	Mechanical/morphology/composition
Cell retention and proliferation	The polyurethane–ethyl cellulose electrospun scaffold promoted proliferation of cardiac myoblast H9C2 cells.	Chen et al.[6]	Morphology
Cell attachment and proliferation	hESC attachment and proliferation were increased on randomly oriented plasma-modified (hydrogen, argon, and oxygen) polyurethane fibers, while contact-guided cell migration was observed on aligned ones.	Zanden et al.[54]	Morphology/composition
Cell growth	When seeded on electrospun fibrous collagen-blended or elastin/collagen-blended polyurethane scaffolds, the growth of smooth muscle cells (SMCs) increased by 283% and 224%, respectively.	Wong et al.[1]	Composition
Cell proliferation and differentiation	Electric conductivity was introduced by electrospinning carbon nanotubes with polyurethane. Myotube formation and myoblast differentiation were significantly increased with electrical stimulation applied on the scaffolds.	Sirivisoot et al.[26]	Composition
Cell migration and proliferation	Fibrous scaffolds consisted of nanotubes and polyurethanes were fabricated by electrospinning. The scaffolds promoted endothelial cell proliferation and migration along the aligned fibers.	Han et al.[17]	Morphology/composition

Cell proliferation	Four different kinds of proteins (collagen, gelatin, fibrinogen, and bovine serum) were incorporated with polyurethane to produce fibrous scaffolds. Higher bladder SMC proliferation and alignment along fibers were observed.	Jia et al.[27]	Composition/morphology
Cell attachment	Thermoplastic polyurethane (TPU)/graphene oxide (GO) scaffolds were fabricated via electrospinning. Higher fibroblast proliferation and endothelial cell attachment were observed on scaffolds with 0.5 wt% GO loading. In addition, oxygen plasma treatment also enhanced endothelial cell viability and adhesion significantly.	Jing et al.[3]	Composition
Cell viability, adhesion and proliferation	Fibrous structures of multiwalled carbon nanotubes and polyurethane composites with average fiber diameters of 300–500 nm were fabricated via electrospinning. These MWNT-incorporated scaffolds exhibited high enhancement on cell adhesion, proliferation, migration, and aggregation.	Meng et al.[28]	Composition
Cell proliferation and differentiation	TPU and hydroxyapatite were blended and fabricated into fibrous scaffolds via electrospinning. MSCs on the hard scaffolds actively proliferated and migrated, while those on soft scaffolds exhibited osteogenic differentiation.	Mi et al.[29]	Mechanical
Cell proliferation and differentiation	Successful propagation and neuronal differentiation from hESCs were found when cocultured with electrospun polyurethane-based scaffolds.	Carlberg et al.[16]	Morphology
	Polyurethane–hydroxyapatite (PU–HA) scaffolds were fabricated via electrospinning, and fiber morphology can be controlled by using different solvents and sizes of HA particles. The produced scaffolds were biocompatible.	Tetteh et al.[30]	Morphology
Cell alignment	Bovine annulus fibrous cells were seeded onto strained electrospun polyurethane scaffolds, and they exhibited higher alignment than those seeded on relaxed scaffolds. Cells on relaxed scaffolds showed higher proliferation and differentiation capability (higher gene expression of collagen type I and TGF β-1).	Turner et al.[31]	Morphology
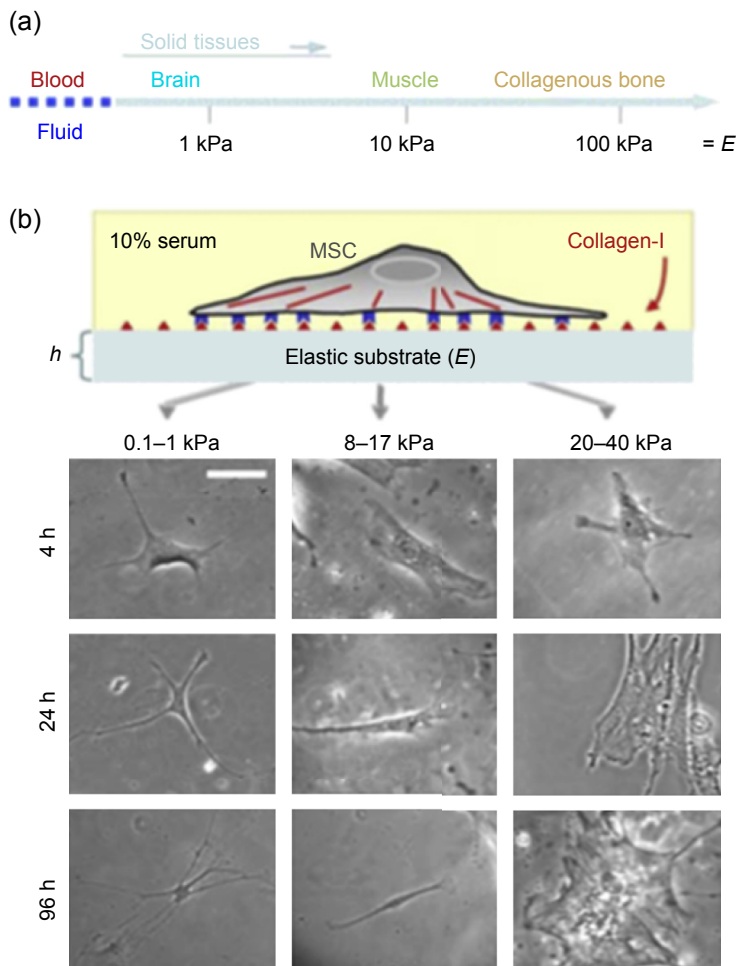
Figure 18.1 (a) Matrix elasticity and (b) differentiation of naïve MSCs on 2D substrate.

lineages when seeded on polyacrylamides with different stiffnesses.[33] On soft poly-acrylamide where the stiffness ($E = 0.1–1\,kPa$) mimics that of the brain tissue, MSCs underwent neurogenic differentiation (Figure 18.1). When the stiffness of polyacrylamide was increased to match those of the muscle ($E = 8–17\,kPa$) and bone ($E = 25–40\,kPa$) tissues, MSCs underwent myogenic and osteogenic differentiation, respectively.

For fibrous PU scaffolds, the mechanical environment is much more complex than 2D polyacrylamide since the scaffolds are porous, fibers are distributed within the constructs, and cells are attached to single fibers. As a result, the stiffness character-istics for both single fibers and scaffolds may have an impact on stem cell differentia-tion. We recently studied the effects of PU scaffold stiffness at small and large strains (before and after alignment of fibers, respectively) and single fiber stiffness on cardiac differentiation of cardiosphere-derived cells (CDCs).[8] The single fiber stiffness was

modulated by blending a stiff PU with a soft hydrogel based on poly(*N*-isopropylacrylamide) copolymer. The PU was synthesized using PCL as soft segment, and hexamethylene diisocyanate and butanediamine as hard segment. Poly(*N*-isopropylacrylamide) copolymer was synthesized from *N*-isopropylacrylamide, acrylic acid, and degradable hydroxyethyl methacrylate-oligohydroxybutyrate. It is a soft hydrogel at 37 °C. A novel electrospraying/electrospinning method was used to distribute CDCs homogeneously in the fibrous constructs. Scaffold macrostiffness at small and large strains and single fiber stiffness were tuned by the pumping speed of PU/hydrogel solution and ratio of PU/hydrogel (Table 18.2 and Figure 18.2). A significantly higher cardiac differentiation at both gene and protein levels was achieved at a comparatively smaller scaffold stiffness at small strain ($E \sim 48$ kPa) regardless of the single fiber stiffness and scaffold stiffness at large strain.

18.2.2 Cell fate control by scaffold morphologies

Scaffold morphological characteristics play a critical role in cell fate. For fibrous PU scaffolds, fiber diameter, and orientation may affect cell spreading, proliferation, and differentiation due to the fact that cells grown on them exhibit a higher aspect ratio and smaller projection than those grown on flat surfaces.[7,14,16,31,39] When fabricating scaffolds to engineer highly aligned tissues such as myocardium and skeletal muscles, the highly aligned fibers allow the cells to align along the fibers by inducing cell actin cytoskeleton and cell–matrix focal adhesions on the fiber surface, thus developing native-like tissue morphology. Parrag et al. studied the differentiation of embryonic stem cells (ESCs) on the surfaces of aligned electrospun PU fibers.[40] The ESCs demonstrated a rod-shaped morphology and an organized sarcomeric structure with a cross-striated pattern perpendicular to the major cell axis. In contrast, a mixed cell shape and less organized sarcomere were found on random fibers. After differentiation into cardiomyocytes using differentiation medium, the cells developed end-to-end gap junctions on aligned scaffolds but not on random scaffolds. This demonstrates that aligned scaffolds induced a higher degree of cardiac maturation. Similar phenomena were found for other cell types including MSCs,[7,41] CDCs,[8] myoblasts,[26] and neurons.[16]

Cell alignment on aligned scaffolds can be further increased by stretching the scaffolds during tissue culture. In a previous work,[7] it was demonstrated that applying static strain to the fibrous PU scaffolds increases MSC alignment. The degree of alignment was increased with strain (Figure 18.3). Interestingly, the MSCs showed cardiac differentiation when the cells have a high anisotropic index. This work is significant as it suggests that a combination of scaffold structural properties and mechanical training can direct stem cell differentiation without using cell differentiation medium.

Fiber diameter determines the area in which the fiber and cell interact. Larger fiber diameters provide greater surface area for cells to attach. Cardwell et al. found that fiber diameter also affects cell proliferation and differentiation.[42] When seeding C3H10T1/2 stem cells on random and aligned scaffolds with small (<1 μm), medium (1–2 μm), and large (>2 μm) fibers, the cells proliferated faster initially on scaffolds with small fibers, and the proliferation slowed down after further culture regardless of fiber alignment. In addition, the cells seeded on larger fibers exhibited higher

Table 18.2 A summary of process and response parameters of the tissue constructs[8]

Scaffold	Process parameters		Geometric and mechanical parameters					Functional response
	P^a	H^b	$m_L{}^c$	$A_0{}^d$	$V_f{}^e$	$M_0{}^f$	$M_L{}^g$	GP^h
(A)	7.5	90	2.0 ± 0.4	4.5 ± 0.6	8.5 ± 1.3	0.48 ± 0.11	1.7 ± 0.3	87 ± 4
(B)	4.5	90	3.5 ± 0.2	6.1 ± 0.7	3.2 ± 0.5	0.60 ± 0.05	1.2 ± 0.1	12 ± 1
(C)	4.5	70	9.0 ± 0.8	6.0 ± 0.2	4.2 ± 0.9	2.2 ± 0.3	3.9 ± 0.5	0.03 ± 0.00
(D)	4.5	50	26.0 ± 0.3	5.9 ± 0.4	3.1 ± 0.6	4.6 ± 0.4	8.1 ± 1.0	0.01 ± 0.00

[a]P, polymer solution pumping speed (mL/h).
[b]H, hydrogel content in fibers (wt%).
[c]m_L, fiber modulus at large strain (10^2 kPa).
[d]A_0, fiber alignment at small strain at $v=0.3$ (10^{-1}).
[e]V_f, fiber volume fraction, experimental (10^{-3}).
[f]M_0, scaffold modulus at small strain (10^2 kPa).
[g]M_L, scaffold modulus at large strain (10^2 kPa).
[h]GP, gene and protein expressions; gene and protein expressions were normalized first based on the results of real time RT–PCR and immunohistology, respectively, and then multiplied to give the GP value listed here.
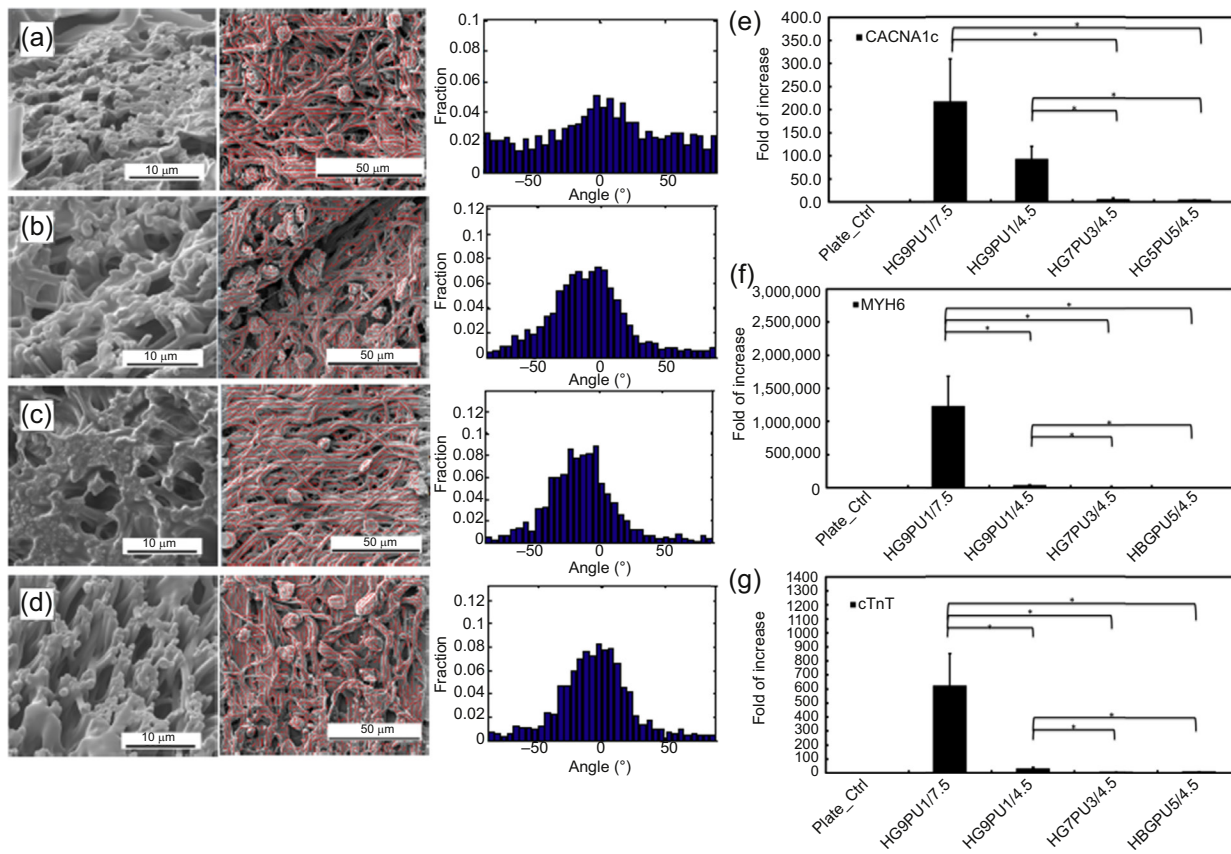
Figure 18.2 Controlled stem cell cardiac differentiation via mechanical and structural properties of polyurethane/hydrogel scaffolds.
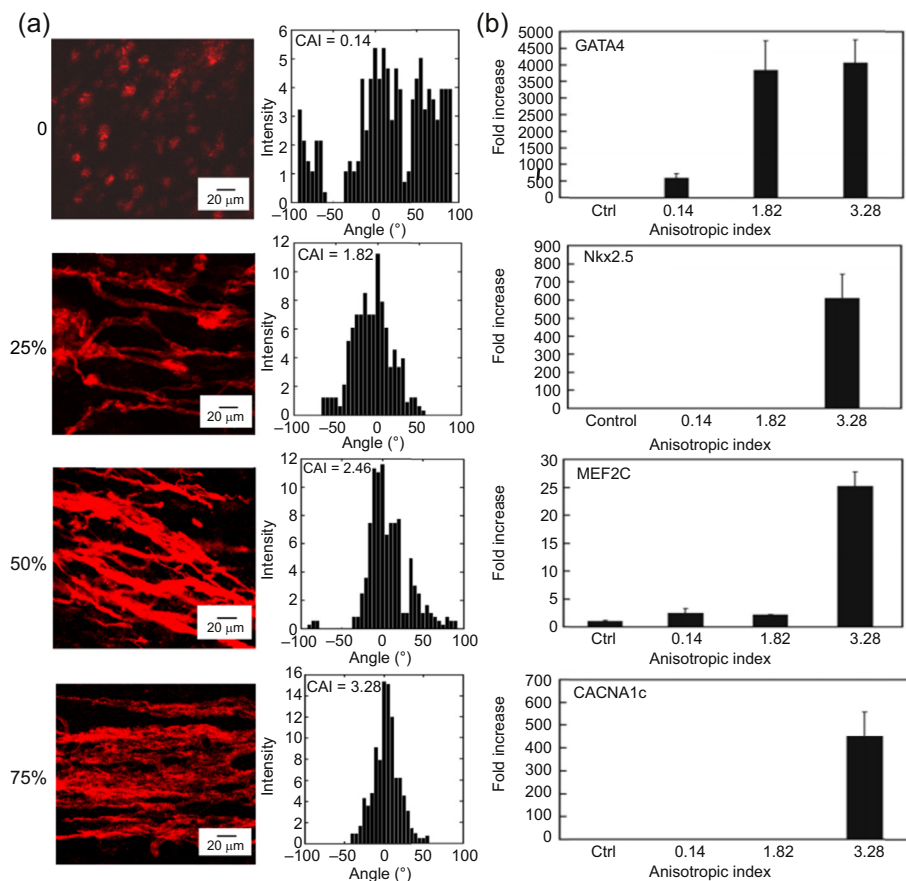
Figure 18.3 MSC alignment in tissue constructs stretched at different strains (a) and their cardiac differentiation (b).

levels of expression of tendon/ligament transcription factor scleraxis than those on medium-sized fibers.

Besides fiber alignment and diameter, fiber volume fraction also showed an impact on cell differentiation. In a previous study,[8] fibrous PU scaffolds were fabricated with different fiber volume fractions (or different fiber spacing) by controlling the flow rate during the electrospinning process. The scaffolds with a higher fiber volume fraction significantly improved cell differentiation at both the gene and the protein levels.

18.2.3 Control of cell fate by polyurethane scaffold composition

PU scaffolds usually have a relatively inert surface. Modification is often necessary for enhanced cell attachment. This can be achieved by immobilization of functional groups

Table 18.3 **Summary of functionalization of polyurethane-based scaffolds related to material properties**

Method	Functionalization
Incorporation and immobilization of biomolecules and conductive material into scaffolds	• Collagen[1,27] • Heparin[14,43–45] • Fibrin[27] • Elastin[1] • Graphene oxide[3] • Carbon nanotubes[17,26,28] • RGD peptide[19,46–49] • Cellulose[6] • Gelatin[27,50] • Other proteins[9,46,51–53]
Chemical and plasma modification to introduce functional groups	• Functional groups[3,14,44,54,55]

and biomolecules on the surface and encapsulation of biomolecules in the scaffolds. Table 18.3 summarizes the functionalization methods that have been applied to PU scaffolds.

18.2.3.1 Modification of scaffold surface to control cell fate

Scaffold chemical properties are of great importance in controlling stem cell fate such as attachment, proliferation, and differentiation. In order to improve cell attachment on PUs, various surface modification methods including ion beam irradiation,[56,57] protein immobilization,[44,46] and plasma treatment[54,58] have been used. This is especially crucial for fibrous scaffolds since the cells within fiber networks usually experience much smaller surface areas for focal adhesions than those on solid surfaces. Ion beam irradiation and plasma treatment introduce functional groups such as hydroxyl ($-OH$), carbonyl ($C=O$), carboxyl ($-COOH$), and amine (NH_2) on the surface. These groups have been shown to improve cell–matrix interaction.[59] Zanden et al. treated electrospun PU fibers with oxygen, hydrogen, and argon plasma. The fibrous PU scaffolds obtained had a large number of carboxyl and carbonyl groups on the surfaces.[54] When human embryonic stem cells (hESCs) were seeded on the randomly aligned fibers, all of the plasma-treated scaffolds dramatically improved ESC expansion, with a sevenfold increase for argon treatment, a fivefold increase for hydrogen treatment, and a fourfold increase for oxygen treatment. Another application of these functional groups is to covalently bond molecules including collagen and heparin[44] onto the PU scaffold surfaces to enhance cell attachment.

18.2.3.2 Incorporation of biomolecules and carbon nanotubes to control cell fate

For tissue engineering applications, the fibrous PU scaffolds can also serve as a delivery vehicle of various biomolecules and drugs. The biomolecules and drugs can be incorporated into the scaffold during the electrospinning process. This method

provides a quick and simple way to deliver biomolecules and drugs. Jia et al. blended a PU solution with four different types of naturally derived proteins, (collagen, gelatin, fibrinogen, and bovine serum album), and successfully fabricated composite fibrous scaffolds via electrospinning.[27] The MSCs seeded on the scaffolds surface were metabolically active. Cells on PU/collagen fibers demonstrated the highest proliferation capacity after 12 days of culture *in vitro* compared to scaffolds blended with other proteins. In another study, Beachley et al. blended PU with amine-terminated poly(propylene glycol)-block-poly(ethylene glycol) and immobilized heparin to the electrospun scaffolds.[14] When culturing endothelial cells on the modified scaffolds, the cells formed a complete monolayer on the scaffold surface without apparent separation between cells.

Single-walled or multiwalled carbon nanotubes (MWNTs) were also blended with PU to fabricate fibers for regenerating tissues such as skin, skeletal muscle, and nerves.[18,27,29] Carbon nanotubes have attracted intense interest in biomedical field due to their excellent electrical conductivity, mechanical strength, and binding capacity with various biomolecules. Meng et al. fabricated fibrous PU networks incorporated with MWNTs by electrospinning. The scaffolds were used to culture fibroblasts.[28] Among the four groups of substrates that had been studied (smooth film of PU, smooth film of MWNT/PU, nanofibrous PU scaffold, and nanofibrous MWNT-incorporated PU scaffold), the nanofibrous MWNT/PU scaffold demonstrated the highest ability to support fibroblast adhesion, proliferation, and protein secretion. The total amount of proteins released from cells seeded on nanofibrous MWNT/PU scaffolds was the highest among all of the tested groups, which was almost two times of those secreted by cells on smooth PU films. In addition, these cells secreted more collagenase that may degrade the collagen between cells and scaffolds, thus encouraging cells to migrate and aggregate. In another work, Sirivisoot et al. took advantage of the electrical conductivity of carbon nanotubes to enhance skeletal myotube formation.[26] Single-walled or MWNTs were blended with PU to fabricate scaffolds with electrical conductivity. The use of nanotubes significantly increased the number and length of myotubes.

18.3   Interaction of stem cells with microporous polyurethane scaffolds

Microporous PU scaffolds are another type of scaffold used for tissue regeneration. In order for the cells to migrate, communicate, and proliferate within the scaffolds, uniformly distributed and interconnected pores are necessary. Various techniques have been used to fabricate porous PU scaffolds, including solvent casting/particle leaching (SC/PL),[60] thermally induced phase separation (TIPS),[61] emulsion freeze drying,[62] gas foaming,[63] and melt molding.[64] Table 18.4 summarizes PU scaffolds fabricated by these techniques. The scaffolds have porosity and pore size suitable for tissue regeneration. Generally, scaffolds for tissue regeneration should have high porosity (>90%) and suitable pore size. The high porosity provides the high pore area for cell and tissue ingrowth as well as adequate transport of nutrients and metabolic waste. The pore size should be greater than cell size to support cell infiltration.

Table 18.4 **Summary of approaches for porous polyurethane scaffolds fabrication**

Approach	PU system	Solvent	PU concentration (wt%)	Porosity (%)	Pore size (μm)
SC/PL	Zytar®Z1A1 (thermoplastic polyether urethane)[60]	DMF/THF	15	83–92	~250
	Biostable PUR[43]	NMP	20	–	147±2
	Tecoflex 80A[19]	DMAC	25	79±2	30–300
	PCL/HMDI/isosorbide diol[65]	DMF	–	90	200±16
TIPS	PCL–PEG/BDI/putrescine[61]	DMSO	10	94	76–387
	PDLLA/PCL/BDO/BDI[66]	–	5	95	20±6
	PCL/BDI/BDO[61]	DMSO	10	>80	36–203
TIPS/PL	PCL/BDI/BDO[67]	DMSO/water	35	80	–
	Poly(ethylene adipate) diol/IPDI/ hexamethylene diamine[68]	–	–	87	50–400
Freeze drying	PCL–PEG/IPDI/BDO/L-lysine[62]	Water	16	–	10–172
	PCL–PEBA–PLA/IPDI[69]	–	5	97	–
Freeze drying/PL	Polyurethane estane 5701-F1[70]	Dioxane/water	–	72–87	–
Melt molding	Texin (thermoplastic polyether urethane)[64]	–	–	64	30–450
	PCL–PEG/HDI/benzoic acid[71]	–	–	88	153±70
Melt molding/PL	TPU, Elastollan 1185A[72]	Water	–	20–67	42–210
Gas foaming	HA/IPDI/BDO[73]	–	–	78–81	300–1000
	PEG–PPG/TDI[63]	–	–	85	300–800

18.3.1 Cell fate controlled by pore shape

Pore shape plays an important role in cellular behaviors, especially when engineering tissues with anisotropic characteristics. Musculoskeletal tissues and meniscus, for example, have well-defined anisotropic properties resulting from the anisotropic organization of the extracellular matrix and cells. To mimic the natural structures of these tissues, de Mulder et al. fabricated anisotropic porous PU scaffolds with channels (channel diameter of $20 \pm 6.0\,\mu m$, and anisotropic degree of 0.39).[66] The scaffolds were fabricated by TIPS method. As shown in Figure 18.4, the anisotropic scaffolds exhibited channels mostly in one direction and the walls of the channels had a ladder-like morphology. In contrast, the isotropic scaffolds (pore diameter of $35 \pm 14.7\,\mu m$, and anisotropic degree of 0.18) had randomly distributed pores. After 24 weeks of postimplantation, both scaffold types were completely filled with tissue. Collagen fibers were randomly oriented in the isotropic scaffolds, similar to those of the avascular zone of the meniscus. The collagen fibers in the anisotropic scaffolds aligned along the channels, closely resembling those in the vascularized zone of the meniscus. It is expected that combing scaffolds with isotropic and anisotropic structures has a great potential in creating both anisotropic and isotropic structures in meniscus.

18.3.2 Cell fate controlled by scaffold surface composition

The surface of the microporous PU scaffolds can be modified to control cell fate. Similar approaches as those used for fibrous PU scaffolds can be employed.[45,74] For example, to induce endothelial cell migration into scaffolds for accelerated vascularization, heparin was bound to the scaffold surface.[44] An aminolysis step was first used to introduce amine groups on the surface, and then the cross-linking of heparin
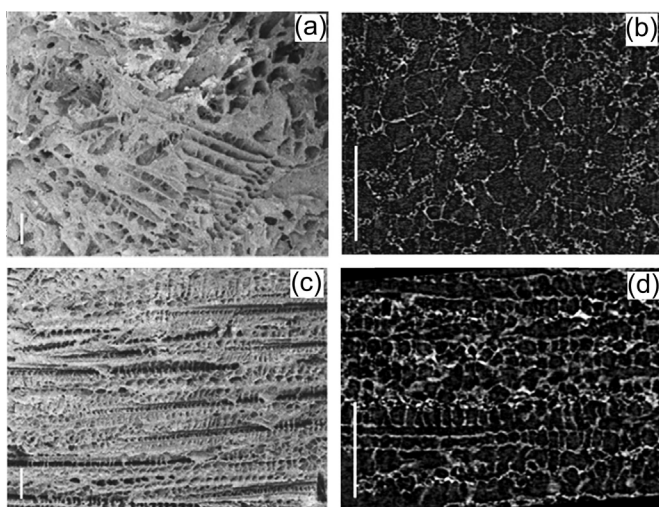
Figure 18.4 SEM and nano-CT images of isotropic and anisotropic scaffolds in a sagittal plane. (a) and (b) Isotropic scaffold shows randomly distributed pores. (c) and (d) Anisotropic scaffold has channels within it, and the walls of the channels have a ladder-like appearance.

with amine groups immobilized heparin on the surface. This heparinization process was able to introduce a uniform layer of heparin on the scaffold surfaces without any sign of pore obliteration or pore size change.[43] After 28 days of implantation using a rat subcutaneous model, the heparin-modified porous PU scaffold showed a significant increase in vascularization. Capillary density and vascularization total area were increased by 62% and 56%, respectively.

To improve cell adhesion and infiltration in the PU scaffolds, RGD, a peptide that is well recognized as possessing cell adhesive properties, was immobilized on the scaffold surface using bioactive fluorinated surface modifiers.[4] After 3 days of culture, the RGD-modified PU scaffolds demonstrated significantly deeper cell infiltration (cell infiltrated >300 μm into the scaffold) than the nonmodified scaffolds. After 2 weeks of culture, cells were distributed throughout the full thickness of the scaffolds (5 mm of total thickness) and more cells were found at all depths in the scaffolds.

18.4   Interaction of cells with other types of polyurethane scaffolds

18.4.1   Polyurethane nanostructures

Creating nanostructures on PU scaffold surfaces is attractive for tissue regeneration. The nanostructures possess high surface energy, which promotes protein adsorption on the scaffold leading to improved cell adhesion. In addition, nanostructures on a PU scaffold mimic the topography of various tissues.[13] Motivated by the nanostructured topography of native bladder tissue, Thapa et al. developed nanoscale surface features in PU by a chemical etching method using HNO_3 solution.[75] When seeding bladder SMCs on the etched PU surface, cell attachment and proliferation were significantly increased. A similar cellular response was found for vascular cells and chondrocytes.[76,77] Yao et al. tested nanostructured polyurethane/poly(lactic-co-glycolic acid) (PU/PLGA) scaffolds *in vivo*.[13] The scaffolds had a porosity of 87.6% and pore sizes of 150–250 μm. The HNO_3-etched scaffolds exhibited submicrometer to nanoscale features. After functionalization with IKVAV and YIGSR peptides, these scaffolds were implanted *in vivo* for bladder augmentation in a partial cystoplasty model. After 11 months of implantation, the bladder tissue was fully formed within the scaffolds. In addition, both smooth muscle and urothelial cell layers were formed on the scaffolds with nanostructures.

18.4.2   Polyurethane multilayer scaffolds

Multilayered PU scaffolds have been developed to engineer tissues with complex structures. Choi et al., for example, developed multilayered tracheal prostheses for ingrowth of new vessels and connective tissues (Figure 18.5).[24] The prostheses had PU film as the outer layer and a highly porous PU scaffold as the inner layer. The nonporous outer PU layer was designed to prevent adhesion with the surrounding tissues. The outer layer can also reinforce the porous PU layer. The surface of the generated bilayered scaffolds was then coated with poly(ethylene glycol) to prevent granulation formation as well as to promote epithelialization from normal mucosa. When implanted *in vivo*
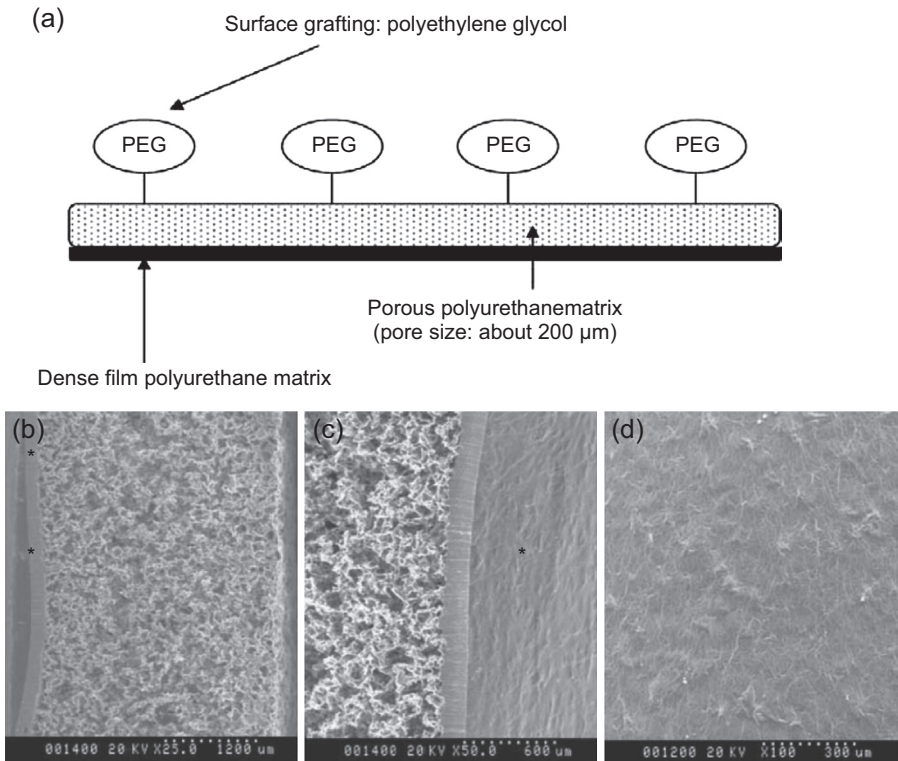
Figure 18.5 (a) Scheme of structure of the bilayer scaffold. (b) Cross section of the scaffold. (c) The three-dimensional angle section view. (d) Surface of the nonporous PU film.

using a beagle dog model, fibrous tissue was found to grow into the inner layer and pseudostratified columnar ciliated mucosa was formed on the scaffold surface.

Multilayered PU scaffolds have also been used for the delivery of biomolecules. Reyes et al. encapsulated bone morphogenetic protein-2 (BMP-2) and transforming growth factor-beta1 (TGF-β1) into a bilayered scaffold.[9] One layer consisted of a porous PLGA, and the other layer was porous PU loaded with growth factor-containing PLGA microspheres. The growth factor demonstrated a zero-order release kinetics *in vivo*. 12 weeks after implantation in a rabbit model, cell chondrogenic differentiation was observed.

18.5   Current challenges to understanding the effect of polyurethane scaffold properties on cell fate

As discussed in the above sections, biodegradable PU scaffolds have been attractive for tissue regeneration. Various scaffold fabrication techniques and surface modification approaches have been developed to tailor scaffold properties for

better control of cell–matrix interactions and tissue growth. However, challenges remain for using PU scaffolds to control cell fate. First, various scaffold properties, such as the surface chemistry, pore structural, and mechanical properties, affect cell fate. These properties are dependent on each other to some extent. Therefore, a change in a single property may simultaneously alter other properties. It remains challenging to decouple the effects from different properties. For an electrospun fibrous scaffold, its global stiffness can be modulated by properties including single fiber stiffness, fiber orientation, fiber volume fraction, and fiber composition. Thus, global stiffness and one or more other properties simultaneously affect cellular behaviors. We have previously fabricated fibrous scaffolds based on PUs and hydrogels (Figure 18.2).[8] The electrospun scaffold mechanical and structural properties were controlled by the feed speed of polymer solution and the ratio of PU/hydrogel. Varying the feed speed changed not only fiber alignment and volume fraction but also scaffold modulus at small and large strains. All these properties affect cell fate. Similarly, the change in PU/hydrogel ratio resulted in different single fiber stiffness and global scaffold stiffness.

Surface modification of PU scaffolds may also change scaffold properties. When modifying PU scaffolds with hydrogen, oxygen, or argon plasma, different functional groups such as carboxyl and carbonyl groups can be introduced on the surfaces.[54] However, the modification also changes fiber surface texture and roughness. Argon plasma-treated scaffolds demonstrated a grainy structure with an average grain diameter of around 25 μm, while a hydrogen plasma treatment resulted in a smooth surface, and an oxygen plasma treatment introduced a surface with randomly elongated granular structures. Both surface functional groups and topography affect cell fate. To better understand how different scaffold properties affect cell fate, development of new approaches that independently change PU properties is necessary.

Second, the mechanisms of how different scaffold properties influence cell fate are not well understood. Matrix stiffness, for example, has been widely used to induce stem cell differentiation by the initiation of mechanotransduction cascades in cells. However, the exact underlying mechanisms have not been well established. Some studies found that matrix stiffness regulated integrin binding and adhesion ligand reorganization, resulting in stem cell differentiation.[38,78,79] Other studies demonstrated that cell-generated traction forces triggered signaling pathways that lead to cell differentiation. However, why and how different signaling pathways are associated with scaffold property-mediacted cell differentiation are still not well understood.

18.6 Future perspectives

We hypothesize that tailoring PU chemistry and developing new fabrication techniques will address current challenges in using PU scaffolds to regulate cell fate and tissue regeneration. It is possible that selectively tailoring of PU soft and hard segment chemistry will allow PUs to have different chemical compositions but similar mechanical and physicochemical properties. It is also possible that control of PU molecular

weight while using the same chemistry will impart PUs with different mechanical properties but with the same chemical composition. Fabrication of these PUs using the same technique is expected to achieve scaffolds with decoupled properties. For the same PU, developing fabrication techniques capable of finely controlling fabrication parameters might also generate scaffolds with decoupled properties. These well-defined scaffolds can provide an effective approach to help in the study of mechanisms of scaffold property-mediated cell fate decisions.

Finally, when implanting cell-seeded PU scaffolds for tissue regeneration, a potential challenge is that cells in the scaffold may experience significant death in the poorly vascularized tissue environment. Efforts are needed to quickly relieve the ischemic conditions and induce rapid angiogenesis after implantation to promote long-term cell survival.

References

[1] Wong CS, Liu X, Xu ZG, Lin T, Wang XG. Elastin and collagen enhances electrospun aligned polyurethane as scaffolds for vascular graft. *J Mater Sci Mater Med* 2013;**24**:1865–74.

[2] Wang WS, Wang C. Polyurethane for biomedical applications: a review of recent developments. Design and Manufacture of Medical Devices, *Woodhead Publ Rev Mech* 2012:115–51.

[3] Jing X, Mi HY, Salick MR, Cordie TM, Peng XF, Turng LS. Electrospinning thermoplastic polyurethane/graphene oxide scaffolds for small diameter vascular graft applications. *Mater Sci Eng C Mater Biol Appl* 2015;**49**:40–50.

[4] Adolph EJ, Pollins AC, Cardwell NL, Davidson JM, Guelcher SA, Nanney LB. Biodegradable lysine-derived polyurethane scaffolds promote healing in a porcine full-thickness excisional wound model. *J Biomater Sci Polym Ed* 2014;**25**:1973–85.

[5] Boffito M, Sartori S, Ciardelli G. Biomimetic polyurethanes scaffolds for cardiac tissue engineering. *J Tissue Eng Regen Med* 2014;**8**:34–5.

[6] Chen PH, Liao HC, Hsu SH, Chen RS, Wu MC, Yang YF, et al. A novel polyurethane/cellulose fibrous scaffold for cardiac tissue engineering. *RSC Adv* 2015;**5**:6932–9.

[7] Guan JJ, Wang F, Li ZQ, Chen J, Guo XL, Liao J, et al. The stimulation of the cardiac differentiation of mesenchymal stem cells in tissue constructs that mimic myocardium structure and biomechanics. *Biomaterials* 2011;**32**:5568–80.

[8] Xu Y, Patnaik S, Guo X, Li Z, Lo W, Butler R, et al. Cardiac differentiation of cardiosphere-derived cells in scaffolds mimicking morphology of the cardiac extracellular matrix. *Acta Biomater* 2014;**10**:3449–62.

[9] Reyes R, Delgado A, Solis R, Sanchez E, Hernandez A, San Roman J, et al. Cartilage repair by local delivery of transforming growth factor- beta 1 or bone morphogenetic protein-2 from a novel, segmented polyurethane/polylactic-*co*-glycolic bilayered scaffold. *J Biomed Mater Res A* 2014;**102**:1110–20.

[10] Long C, Gang W. Biomimetic multilayer polyurethane porous scaffold for cartilage tissue engineering. *Rare Met Mater Eng* 2014;**43**:1–4.

[11] Ciardelli G, Sartori S, Silvestri A, Serafini P, Caporale A, Boccafoschi F. Multiblock polyurethanes in biomedical applications: fine tuning of degradation and biomimetic properties. *AIP Conf Proc* 2010;**1255**:16–8.

[12] Niu YQ, Chen KVC, He T, Yu WY, Huang SW, Xu KT. Scaffolds from block polyurethanes based on poly(epsilon-caprolactone) (PCL) and poly(ethylene glycol) (PEG) for peripheral nerve regeneration. *Biomaterials* 2014;**35**:4266–77.

[13] Yao C, Hedrick M, Pareek G, Renzulli J, Haleblian G, Webster TJ. Nanostructured polyurethane-poly-lactic-*co*-glycolic acid scaffolds increase bladder tissue regeneration: an in vivo study. *Int J Nanomed* 2013;**8**:3285–96.

[14] Beachley V, Serpe A, Hepfer RG, Wen XJ. Surface functionalization of electrospun polyurethane scaffolds using blended polymer solutions. *J Biomater Tissue Eng* 2013;**3**:472–8.

[15] Caracciolo PC, Buffa F, Thomas V, Vohra YK, Abraham GA. Biodegradable polyurethanes: comparative study of electrospun scaffolds and films. *J Appl Polym Sci* 2011;**121**:3292–9.

[16] Carlberg B, Axell MZ, Nannmark U, Liu J, Kuhn HG. Electrospun polyurethane scaffolds for proliferation and neuronal differentiation of human embryonic stem cells. *Biomed Mater* 2009;**4**.

[17] Han ZZ, Kong H, Meng J, Wang CY, Xie SS, Xu HY. Electrospun aligned nanofibrous scaffold of carbon nanotubes-polyurethane composite for endothelial cells. *J Nanosci Nanotechnol* 2009;**9**:1400–2.

[18] Baino F, Verne E, Vitale-Brovarone C. Feasibility, tailoring and properties of polyurethane/bioactive glass composite scaffolds for tissue engineering. *J Mater Sci Mater Med* 2009;**20**:2189–95.

[19] Blit PH, Shen YH, Ernsting MJ, Woodhouse KA, Santerre JP. Bioactivation of porous polyurethane scaffolds using fluorinated RGD surface modifiers. *J Biomed Mater Res A* 2010;**94**:1226–35.

[20] Ramrattan NN, Heijkants RGJC, van Tienen TG, Schouten AJ, Veth RPH, Buma P. Assessment of tissue ingrowth rates in polyurethane scaffolds for tissue engineering. *Tissue Eng* 2005;**11**:1212–23.

[21] Zawadzak E, Bil M, Ryszkowska J, Nazhat SN, Cho J, Bretcanu O, et al. Polyurethane foams electrophoretically coated with carbon nanotubes for tissue engineering scaffolds. *Biomed Mater* 2009;**4**.

[22] Das B, Chattopadhyay P, Mishra D, Maiti TK, Maji S, Narayan R, et al. Nanocomposites of bio-based hyperbranched polyurethane/funtionalized MWCNT as non-immunogenic, osteoconductive, biodegradable and biocompatible scaffolds in bone tissue engineering. *J Mater Chem B* 2013;**1**:4115–26.

[23] Shin JW, Lee YJ, Heo SJ, Park SA, Kim SH, Kim YJ, et al. Manufacturing of multi-layered nanofibrous structures composed of polyurethane and poly(ethylene oxide) as potential blood vessel scaffolds. *J Biomater Sci Polym Ed* 2009;**20**:757–71.

[24] Choi HS, Suh H, Lee JH, Park SN, Shin SH, Kim YH, et al. A polyethylene glycol grafted bi-layered polyurethane scaffold: preliminary study of a new candidate prosthesis for repair of a partial tracheal defect. *Eur Arch Otorhinolaryngol* 2008;**265**:809–16.

[25] Chen H, Truckenmuller R, van Blitterswijk C, Moroni L. Fabrication of nanofibrous scaffolds for tissue engineering applications. Nanomaterials in Tissue Engineering: Fabrication and Applications, *Woodh Publ Ser Biomater* 2013:158.

[26] Sirivisoot S, Harrison BS. Skeletal myotube formation enhanced by electrospun polyurethane carbon nanotube scaffolds. *Int J Nanomed* 2011;**6**:2483–97.

[27] Jia L, Prabhakaran MP, Qin XH, Kai D, Ramakrishna S. Biocompatibility evaluation of protein-incorporated electrospun polyurethane-based scaffolds with smooth muscle cells for vascular tissue engineering. *J Mater Sci* 2013;**48**:5113–24.

[28] Meng J, Kong H, Han ZZ, Wang CY, Zhu GJ, Xie SS, et al. Enhancement of nanofibrous scaffold of multiwalled carbon nanotubes/polyurethane composite to the fibroblasts growth and biosynthesis. *J Biomed Mater Res A* 2009;**88**:105–16.

[29] Mi HY, Palumbo S, Jing X, Turng LS, Li WJ, Peng XF. Thermoplastic polyurethane/hydroxyapatite electrospun scaffolds for bone tissue engineering: effects of polymer properties and particle size. *J Biomed Mater Res B* 2014;**102**:1434–44.

[30] Tetteh G, Khan AS, Delaine-Smith RM, Reilly GC, Rehman IU. Electrospun polyurethane/ hydroxyapatite bioactive scaffolds for bone tissue engineering: the role of solvent and hydroxyapatite particles. *J Mech Behav Biomed Mater* 2014;**39**:95–110.

[31] Turner KG, Ahmed N, Santerre JP, Kandel RA. Modulation of annulus fibrosus cell alignment and function on oriented nanofibrous polyurethane scaffolds under tension. *Spine J* 2014;**14**:424–34.

[32] Reilly GC, Engler AJ. Intrinsic extracellular matrix properties regulate stem cell differentiation. *J Biomechanics* 2010;**43**:55–62.

[33] Engler AJ, Sen S, Sweeney HL, Discher DE. Matrix elasticity directs stem cell lineage specification. *Cell* 2006;**126**:677–89.

[34] Discher DE, Sweeney L, Sen S, Engler A. Matrix elasticity directs stem cell lineage specification. *Biophys J* 2007;32a.

[35] Gilchrist CL, Darling EM, Chen J, Setton LA. Extracellular matrix ligand and stiffness modulate immature nucleus pulposus cell–cell interactions. *PLoS One* 2011;**6**:e27170.

[36] Li ZQ, Guo XL, Palmer AF, Das H, Guan JJ. High-efficiency matrix modulus-induced cardiac differentiation of human mesenchymal stem cells inside a thermosensitive hydrogel. *Acta Biomater* 2012;**8**:3586–95.

[37] Li ZQ, Guo XL, Guan JJ. A thermosensitive hydrogel capable of releasing bFGF for enhanced differentiation of mesenchymal stem cell into cardiomyocyte-like cells under ischemic conditions. *Biomacromolecules* 2012;**13**:1956–64.

[38] Huebsch N, Arany PR, Mao AS, Shvartsman D, Ali OA, Bencherif SA, et al. Harnessing traction-mediated manipulation of the cell/matrix interface to control stem-cell fate. *Nat Mater* 2010;**9**:518–26.

[39] Amoroso NJ, D'Amore A, Hong Y, Wagner WR, Sacks MS. Elastomeric electrospun polyurethane scaffolds: the interrelationship between fabrication conditions, fiber topology, and mechanical properties. *Adv Mater* 2011;**23**:106–11.

[40] Parrag IC, Zandstra PW, Woodhouse KA. Fiber alignment and coculture with fibroblasts improves the differentiated phenotype of murine embryonic stem cell-derived cardiomyocytes for cardiac tissue engineering. *Biotechnol Bioeng* 2012;**109**:813–22.

[41] Bashur CA, Dahlgren LA, Goldstein AS. Effect of fiber diameter and orientation on fibroblast morphology and proliferation on electrospun poly(D,L-lactic-*co*-glycolic acid) meshes. *Biomaterials* 2006;**27**:5681–8.

[42] Cardwell RD, Dahlgren LA, Goldstein AS. Electrospun fibre diameter, not alignment, affects mesenchymal stem cell differentiation into the tendon/ligament lineage. *J Tissue Eng Regen Med* 2014;**8**:937–45.

[43] Bezuidenhout D, Davies N, Black M, Schmidt C, Oosthuysen A, Zilla P. Covalent surface heparinization potentiates porous polyurethane scaffold vascularization. *J Biomater Appl* 2010;**24**:401–18.

[44] de Mulder ELW, Hannink G, Koens MJW, Lowik DWPM, Verdonschot N, Buma P. Characterization of polyurethane scaffold surface functionalization with diamines and heparin. *J Biomed Mater Res A* 2013;**101**:919–22.

[45] Schmidt C, Bezuidenhout D, Higham L, Zilla P, Davies NH. Induced chronic hypoxia negates the pro-angiogenic effect of surface immobilized heparin in a polyurethane porous scaffold. *J Biomed Mater Res A* 2011;**98**:621–8.

[46] Wang DA, Ji J, Sun YH, Shen JC, Feng LX, Elisseeff JH. In situ immobilization of proteins and RGD peptide on polyurethane surfaces via poly(ethylene oxide) coupling polymers for human endothelial cell growth. *Biomacromolecules* 2002;**3**:1286–95.

[47] Choi WS, Bae JW, Lim HR, Joung YK, Park JC, Kwon IK, et al. RGD peptide-immobilized electrospun matrix of polyurethane for enhanced endothelial cell affinity. *Biomed Mater* 2008;**3**:044104.

[48] Jiang X, Wang KJ, Ding MM, Li JH, Tan H, Wang ZG, et al. Quantitative grafting of peptide onto the nontoxic biodegradable waterborne polyurethanes to fabricate peptide modified scaffold for soft tissue engineering. *J Mater Sci Mater Med* 2011;**22**:819–27.

[49] Kidane AG, Punshon G, Salacinski HJ, Ramesh B, Dooley A, Olbrich M, et al. Incorporation of a lauric acid-conjugated GRGDS peptide directly into the matrix of a poly(carbonate-urea)urethane polymer for use in cardiovascular bypass graft applications. *J Biomed Mater Res Part A* 2006;**79**:606–17.

[50] Kucinska-Lipka J, Gubanska I, Janik H. Gelatin-modified polyurethanes for soft tissue scaffold. *Sci World J* 2013;**2013**:450132.

[51] Chiono V, Sirianni P, Boffito M, Silvestri A, Sartori S, Gioffredi E, et al. Polyurethane scaffolds coated with biomimetic proteins for myocardial regeneration. *J Tissue Eng Regen Med* 2014;**8**:385–6.

[52] Kim J, Hollinger JO. Recombinant human bone morphogenetic protein-2 released from polyurethane-based scaffolds promotes early osteogenic differentiation of human mesenchymal stem cells. *Biomed Mater* 2012;**7**.

[53] Pra D, Chiarini A. Silk fibroin-coated three-dimensional polyurethane scaffolds for tissue engineering: interactions with normal human fibroblasts (vol 9, pg 1113, 2003). *Tissue Eng A* 2013;**19**:316.

[54] Zanden C, Erkenstam NH, Padel T, Wittgenstein J, Liu J, Kuhn HG. Stem cell responses to plasma surface modified electrospun polyurethane scaffolds. *Nanomed Nanotechnol* 2014;**10**:949–58.

[55] Lopez-Perez PM, da Silva RMP, Sousa RA, Pashkuleva I, Reis RL. Plasma-induced polymerization as a tool for surface functionalization of polymer scaffolds for bone tissue engineering: an in vitro study. *Acta Biomater* 2010;**6**:3704–12.

[56] Hearon K, Smith SE, Maher CA, Wilson TS, Maitland DJ. The effect of free radical inhibitor on the sensitized radiation crosslinking and thermal processing stabilization of polyurethane shape memory polymers. *Radiat Phys Chem* 2013;**83**:111–21.

[57] Pignataro B, Conte E, Scandurra A, Marletta G. Improved cell adhesion to ion beam-irradiated polymer surfaces. *Biomaterials* 1997;**18**:1461–70.

[58] Zhang S, Mao T, Chen F. Influence of platelet-rich plasma on ectopic bone formation of bone marrow stromal cells in porous coral. *Int J Oral Maxillofac Surg* 2011;**40**:961–5.

[59] Arima Y, Iwata H. Effects of surface functional groups on protein adsorption and subsequent cell adhesion using self-assembled monolayers. *J Mater Chem* 2007;**17**: 4079–87.

[60] Sin D, Miao XG, Liu G, Wei F, Chadwick G, Yan C, et al. Polyurethane (PU) scaffolds prepared by solvent casting/particulate leaching (SCPL) combined with centrifugation. *Mat Sci Eng C* 2010;**30**:78–85.

[61] Guan J, Fujimoto KL, Sacks MS, Wagner WR. Preparation and characterization of highly porous, biodegradable polyurethane scaffolds for soft tissue applications. *Biomaterials* 2005;**26**:3961–71.

[62] Jiang X, Yu F, Wang Z, Li J, Tan H, Ding M, et al. Fabrication and characterization of waterborne biodegradable polyurethanes 3-dimensional porous scaffolds for vascular tissue engineering. *J Biomater Sci Polym Ed* 2010;**21**:1637–52.

[63] Kim HJ, Park IK, Kim JH, Cho CS, Kim MS. Gas foaming fabrication of porous biphasic calcium phosphate for bone regeneration. *Tissue Eng Regen Med* 2012;**9**:63–8.

[64] Haugen H, Ried V, Brunner M, Will J, Wintermantel E. Water as foaming agent for open cell polyurethane structures. *J Mater Sci Mater Med* 2004;**15**:343–6.

[65] Laschke MW, Strohe A, Menger MD, Alini M, Eglin D. In vitro and in vivo evaluation of a novel nanosize hydroxyapatite particles/poly(ester-urethane) composite scaffold for bone tissue engineering. *Acta Biomater* 2010;**6**:2020–7.

[66] de Mulder ELW, Hannink G, Verdonschot N, Buma P. Effect of polyurethane scaffold architecture on ingrowth speed and collagen orientation in a subcutaneous rat pocket model. *Biomed Mater* 2013;**8**.

[67] Heijkants RGJC, van Calck RV, van Tienen TG, de Groot JH, Pennings AJ, Buma P, et al. Polyurethane scaffold formation via a combination of salt leaching and thermally induced phase separation. *J Biomed Mater Res A* 2008;**87**:921–32.

[68] Podporska-Carroll J, Ip JWY, Gogolewski S. Biodegradable poly(ester urethane) urea scaffolds for tissue engineering: interaction with osteoblast-like MG-63 cells. *Acta Biomater* 2014;**10**:2781–91.

[69] Hsu SH, Hung KC, Lin YY, Su CH, Yeh HY, Jeng US, et al. Water-based synthesis and processing of novel biodegradable elastomers for medical applications. *J Mater Chem B* 2014;**2**:5083–92.

[70] Heijkants RGJC, Van Tienen TG, De Groot JH, Pennings AJ, Buma P, Veth RPH, et al. Preparation of a polyurethane scaffold for tissue engineering made by a combination of salt leaching and freeze-drying of dioxane. *J Mater Sci* 2006;**41**:2423–8.

[71] Shokrolahi F, Mirzadeh H, Yeganeh H, Daliri M. Fabrication of poly(urethane urea)-based scaffolds for bone tissue engineering by a combined strategy of using compression moulding and particulate leaching methods. *Iran Polym J* 2011;**20**:645–58.

[72] Mi HY, Jing X, Salick MR, Turng LS, Peng XF. Fabrication of thermoplastic polyurethane tissue engineering scaffold by combining microcellular injection molding and particle leaching. *J Mater Res* 2014;**29**:911–22.

[73] Yang W, Both SK, Zuo Y, Birgani ZT, Habibovic P, Li Y, et al. Biological evaluation of porous aliphatic polyurethane/hydroxyapatite composite scaffolds for bone tissue engineering. *J Biomed Mater Res A* 2014;**103**.

[74] Blit PH, Shen YH, Ernsting MJ, Woodhouse KA, Santerre JP. Bioactivation of porous polyurethane scaffolds using fluorinated RGD surface modifiers. *J Biomed Mater Res A* 2010;**94**:1226–35.

[75] Thapa A, Miller DC, Webster TJ, Haberstroh KM. Nano-structured polymers enhance bladder smooth muscle cell function. *Biomaterials* 2003;**24**:2915–26.

[76] Miller DC, Thapa A, Haberstroh KM, Webster TJ. Enhanced functions of vascular and bladder cells on poly-lactic-*co*-glycolic acid polymers with nanostructured surfaces. *IEEE Trans Nanobiosci* 2002;**1**:61–6.

[77] Kay S, Thapa A, Haberstroh KM, Webster TJ. Nanostructured polymer/nanophase ceramic composites enhance osteoblast and chondrocyte adhesion. *Tissue Eng* 2002;**8**:753–61.

[78] Friedland JC, Lee MH, Boettiger D. Mechanically activated integrin switch controls alpha(5)beta(1) function. *Science* 2009;**323**:642–4.

[79] Martino MM, Mochizuki M, Rothenfluh DA, Rempel SA, Hubbell JA, Barker TH. Controlling integrin specificity and stem cell differentiation in 2D and 3D environments through regulation of fibronectin domain stability. *Biomaterials* 2009;**30**:1089–97.

Electrospun fibrous polyurethane scaffolds in tissue engineering

19

*Y. Hong**

University of Texas at Arlington, Arlington, TX, USA; Joint Biomedical Engineering Program, University of Texas Southwestern Medical Center, Dallas, TX, USA
*Corresponding author: yihong@uta.edu

19.1   Introduction

Electrospinning of nano/submicrometer fiber fabrication is an old technique for material processing, but it is still new to tissue engineering [1]. In 1897, Rayleigh observed the electrospinning phenomenon for the first time. In 1934, Dr Formhals was the first to patent the electrospinning technique, where cellulose acetate was electrospun into filaments [2]. In recent years, electrospinning has seen improvements in apparatus design and applications, utilizing polymers suitable for biomedical applications. As a result, electrospinning has gained increasing attention in the field of biomedical engineering, due to the development of tissue engineering to repair and regenerate tissues/organs [3–5]. Classic tissue engineering is the use of a biodegradable three-dimensional scaffold combined with human cells and biological signals to form a cellularized construct to regenerate a native tissue. Because of the 3D nanofibrous structure of human tissue extracellular matrix (ECM), a scaffold with mimetic ECM structure is assigned to be an advantageous application. Electrospinning is a simple, effective technique used to process biodegradable polymers into nano/submicrometer scale fibers and has been widely utilized for tissue engineering scaffold fabrication. Various biodegradable polymers including natural polymers, synthetic polymers, and their combinations have been electrospun into fibrous scaffolds [6,7]. Biodegradable thermoplastic polyurethane having robust mechanical properties and good biocompatibility is an excellent material candidate for tissue engineering use [8], and has been processed into nanofibrous scaffolds using electrospinning (Figure 19.1). In this chapter, we will introduce the electrospinning technique, describe some of the processing parameters, and discuss applications of electrospun polyurethane fibrous scaffolds.

19.2   Electrospinning technique and apparatus

Electrospinning utilizes an electrostatic force to draw fine fibers (micro-, submicrometer), and nanoscales from a polymer solution. The basic and classic electrospinning apparatus is very simple and consists of a high voltage supply, a syringe pump, a syringe loaded with polymer solution with a metal tip, and a conductive collector (Figure 19.2).

The high voltage supply can provide up to tens of kV positive voltage, which is charged to the metallic tip of the syringe. The syringe pump accurately controls the infusion rate of the polymer solution. The conductive collector is made of metal (e.g., steel or aluminum), which is grounded, and is used for fiber deposition. The tip can be either perpendicularly located on the top of the collector (Figure 19.2(a)) or horizontally placed at the side of the collector (Figure 19.2(b)). After switching on the voltage and syringe pump, polymer fibers are produced immediately and deposit on the collector. When the electrospinning is complete, the fibrous scaffold can be removed from the collector.

To improve the electrospinning technique and electrospun scaffolds, the electrospinning device can be modified. For example, to increase fiber collection, an extra high voltage supply can be used to connect to the collector to provide a negative charge. This can
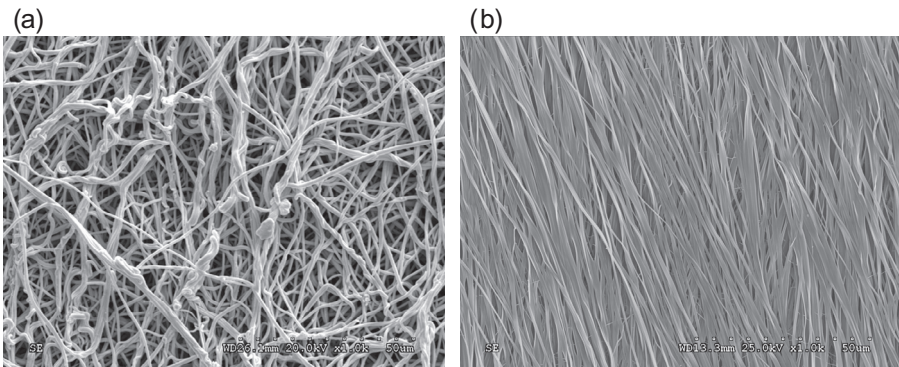
Figure 19.1 (a) Random and (b) aligned electrospun fibers of biodegradable polyurethane.
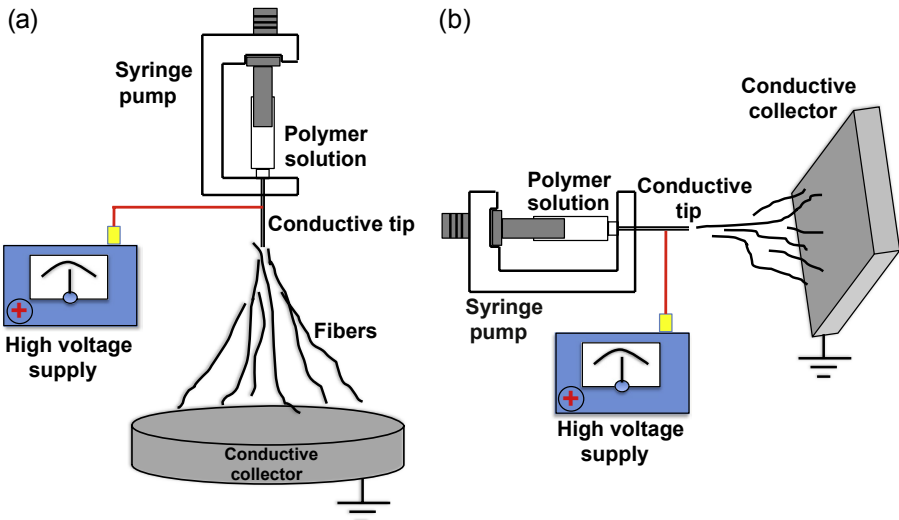
Figure 19.2 The classic electrospinning setup in a perpendicular direction (a) and a horizontal direction (b).

prevent fiber loss because the fibers with the positive charges easily deposit onto a negatively charged surface [9]. Multiple spinnerets are often used to shorten the electrospinning time to rapidly produce a large-sized sample [10,11]. The collector can also be located on an *x–y* axial rastering device with a rotation motor to achieve more uniform samples.

19.3 Factors that affect the electrospinning process

The fiber diameter of an electrospun scaffold is closely related to the scaffold properties and the biological response. It is influenced by the properties of the polymer solution and the parameters of the electrospinning process (Figure 19.3). Although the electrospinning device setup is simple, it is important that these parameters be comprehensively considered to achieve an optimal scaffold. The major parameters affecting the fiber diameter and the sample morphology are described as below.

Figure 19.3 A list of electrospinning factors including properties of the polymer solution and parameters of the electrospinning process.

19.3.1 Polymer properties

The chemical structure and molecular weight of the polymer significantly affects the fiber formation. The polymers must be soluble in the organic solvent, and thus cross-linked polymers and some linear polymers with high crystallinity (e.g., PTFE) cannot be electrospun. However, for tissue engineering applications, most of the biodegradable polymers are polyester, polyamide, and polyurethane based, which are feasible for electrospinning. Most importantly, the molecular weight of the polymer affects the rheological and electrical properties of the polymer solution, including viscosity, surface tension, conductivity, and dielectric strength [12]. The fiber diameter generally increases with increasing polymer molecular weight. If the molecular weight is too low, no continuous fiber is obtained, and microbeads form. Fiber formation is dependent on the interactions of the polymer chains, such as physical entanglements. Low molecular weight results in a small number of polymer chain entanglements in the solution, which makes it hard for the polymer chains to form a fiber.

19.3.2   Polymer concentration

Altering polymer concentration is an effective way to tune the fiber diameter. The polymer concentration is associated with solution viscosity, which increases with the increase of the polymer concentration and then leads to a larger fiber diameter. However, if the concentration is too low, continuous polymer fibers cannot be achieved, and polymer beads are obtained. When the concentration is too high, the polymer solution becomes very viscous and fibers are obtained along with many drops. Highly viscous solutions have difficultly flowing through the syringe tip, resulting in droplet formation. Thus, an appropriate polymer concentration is very important to the electrospinning process.

19.3.3   Solvent

The solvent for polymer solution in electrospinning generally should be highly volatile. The solvent should quickly evaporate during electrospinning to solidify the polymer fiber surface. The common solvents for electrospinning include 1,1,1,6,6,6-hexafluoroisopropanol (HFIP), trifluoroacetic acid (TFA), dichloromethane (DCM), formic acid, dimethyl formamide (DMF), tetrahydrofuran (THF), etc. For biodegradable polyurethanes, HFIP and DMF are two common solvents for electrospinning use. There are little data comparing the polymer fiber morphologies spun from different solvents. The conductivity of the solvent affects electrospinning with increased conductivity reducing the fiber diameter. Polymer solution with very low conductivity may form drops during the electrospinning. Thus, in the latter case, salt may be added into the polymer solution to improve the conductivity, facilitating electrospinning [13,14].

19.3.4   Voltage

Altering the voltage is another convenient way to manipulate fiber morphology; however, it is not very effective. Drops form at a relatively low voltage. At a higher voltage polymer fibers can form. Increased voltage increases the electrostatic force and can reduce the fiber diameter. However when the voltage is too high, the electrospinning process becomes unstable. Thus, an optimized voltage is critical for stable electrospinning. The voltage usually is set at around 10–40 kV.

19.3.5   Distance between the tip and the collector

The distance between the tip and the collector is a factor easily neglected. The distance is related to the solvent evaporation and the electrostatic force. Thus, with the increasing distance, the solvent can evaporate completely and the fiber diameter becomes smaller.

However, if the distance is too great, this causes failure of the fiber formation. If the distance is too short, the solvent may not be completely evaporated, resulting in a larger fiber diameter. Reducing the distance also can increase fiber fusion and adherence to the collector surface [15].

19.3.6 Infusion rate

The infusion rate of the polymer solution is very important in the electrospinning proce-dure, and can be adjusted using a syringe pump. Generally, increasing the infusion rate increases the fiber diameter. However, if the infusion rate is too slow, it takes a long time for sample fabrication, and it may induce a temporary break in the electrospin-ning process. Polymer drops can form when the infusion rate is too high because the fiber production rate cannot catch up with the infusion rate. The ideal situation is that a stable Taylor cone forms during electrospinning, and the fiber formation rate is equal to the infusion rate, resulting in a stable and fast electrospinning process.

19.3.7 Tip diameter

The tip diameter is closely related to the formation of a stable Taylor cone, but it does not have an obvious relationship to the fiber diameter. In general, the tip inner diame-ter is smaller than 2 mm. The typical size of the syringe needle is 16G to 23G.

19.3.8 Collector

The fiber collector is crucial for the macroscopic shape and microscopic morphology of the electrospun scaffold. The fiber collector shape and whether it is moving have no effect on fiber diameter, but it has a significant effect on fiber direction and pattern, as well as scaffold shape. The collector is made of a conductive metal, which allows it to be connected to the ground or a negative charge. For random fibrous scaffolds, a metallic disk or a rectangular sheet can be used for fiber collection and fibrous sheet formation (Figure 19.4(a)). A metal mandrel as a collector can achieve tubular fibrous scaffolds (Figure 19.4(c)). For anisotropic aligned fibrous scaffolds, a rotating disk/cylinder (Figure 19.4(b)) or a set of two parallel blade-like collectors (Figure 19.4(d)) is required [16]. The disk diameter and its rotation speed determine the degree of fiber alignment. At a low speed, the fiber direction is random, independent of the disk diam-eter. At a high speed (above 1 m/s), highly aligned fibers can be achieved. However, if
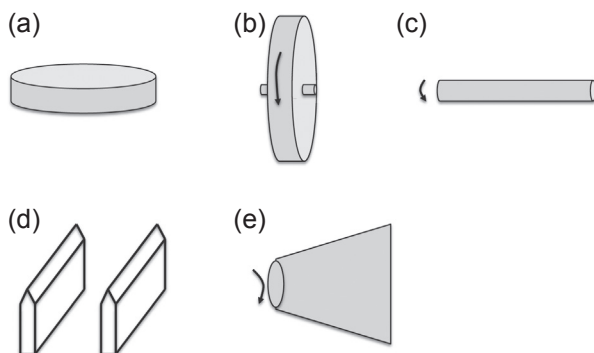
Figure 19.4 Schematics of metallic collectors. (a) Plate, (b) rotating disk, (c) rotating mandrel, (d) two blades, (e) rotating cone.

the disk diameter is too small, it is difficult to achieve aligned fibers. For two parallel blade-like collectors, the electrostatic force distribution allows highly aligned fibers to deposit between the blades (Figure 19.4(d)). The fiber alignment decreases with the increasing sample thickness for the two-blade collector since the electronic field is affected by the fiber deposition. Compared to two-blade collectors, the rotating disk method produces a sample with a lower level of fiber alignment, but the sample alignment degree is not thickness dependent.

Various collectors have been designed for fabricating fibrous materials for different applications besides the above-noted common collectors (Figures 19.4(a–d)). For example, a cone collector was used to obtain a fibrous sheet with regionally different fiber alignment to mimic heart valve fiber structure. The fiber alignment gradient is due to the different linear speed at different diameters [17] (Figure 19.4(e)). Using a metallic patterned collector one can obtain a fibrous pattern sheet for cell behavior research [18,19], Thus, rationally designing unique collectors is an effective way to fabricate novel fibrous scaffolds for tissue engineering use.

Besides the above-noted parameters, there exist some other factors affecting electrospinning, such as the surrounding environment (e.g., humidity [20]). However, all these parameters interact and cannot be individually considered to achieve a perfect fibrous scaffold. All parameters must be comprehensively studied and optimized for electrospinning control.

19.4   Methods to enhance cellular infiltration of electrospun scaffolds

Tissue engineering requires that cells extensively infiltrate into the scaffold for new tissue formation. However, because of superfine fiber diameters, the electrospun polymer scaffolds are very dense with a pore size of ~1 μm, while the cell size is around 7 μm in general. Hence, the cells cannot infiltrate into the scaffolds, and it is also difficult to achieve good transport into the scaffold. Improving cell infiltration of the electrospun scaffold is critical for tissue engineering. A variety of approaches have been developed for this purpose. Three mechanisms for enhancing cell infiltration include (1) accelerate scaffold degradation to provide more space for cell growth; (2) reduce electrospun fiber intersections to loosen the scaffold structure to allow more cell infiltration; and (3) directly load cells into the electrospun scaffold. Some specific methods are described below.

19.4.1   Coelectrospinning

Coelectrospinning is described as blending two or more polymers for electrospinning. To accelerate the degradation, some relatively quickly degradable materials are combined with the major polymer in a single solution to achieve a composite scaffold. The material introduction can increase the scaffold degradation rate, which may allow more cell infiltration, and it also can render some extra functionality to

the scaffold. Biodegradable polyurethane was blended with porcine dermal extra-cellular matrix powder in HFIP and then electrospun into a fibrous patch [21]. The ECM material can leach out of the fiber patch and also quickly degrade. The patch was implanted into the rat full-thickness abdominal wall defect model and exhibited better cell infiltration than for the polyurethane alone. However, the cellular infiltration only occurred at the patch peripheries, and poor cell infiltration was observed at the center of the scaffold.

19.4.2   Unique collector design

Unique fiber collector designs have been attempted to loosen the electrospun scaffold to improve cell infiltration. The principle of the collector design is to reduce the fiber intersections. For example, a half-ball collector containing pillars was designed to achieve cotton ball-like fibrous scaffolds by changing the fiber deposition space (Figure 19.5(a)) [22]. An ethanol bath was used as a collector to obtain low-density electrospun polycaprolactone scaffolds (Figure 19.5(b)) [23]. The ethanol quickly stabilizes the polymer fiber surface to reduce the intersections between fibers.
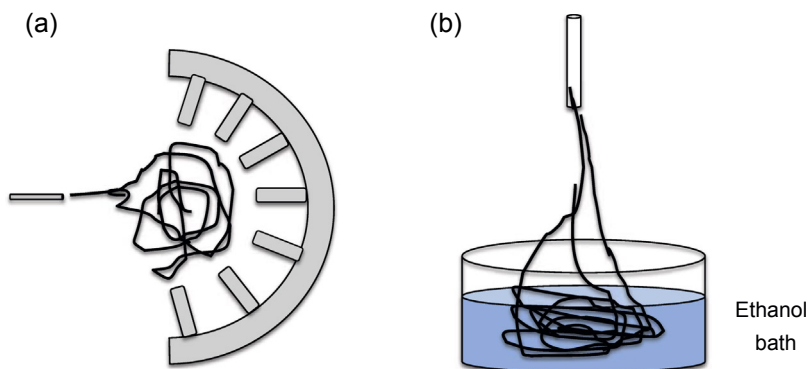
Figure 19.5 (a) A half-ball collector and (b) an ethanol bath collector.

19.4.3   Porogen method

Porogen leaching is a popular method for preparing porous scaffolds. This method can also be used for improving the structure of the electrospun scaffold. The porogen and the electrospun fibers can be simultaneously deposited on the collector, and then the porogen is removed, which can build macropores inside the electrospun scaffold. These large pores can allow for cell infiltration. This concept has been demonstrated by simultaneously depositing polycaprolactone polymer fiber and sodium chloride particles through a specifically designed coaxial needle [24]. The inner tube held the polymer solution, while the outer annular region held the salt particles. After the salt particles were removed by water immersion, the electrospun scaffold showed a delaminated layer structure, which allowed for cell infiltration into the scaffold. Salt particles can also be codeposited with

electrospun fibers using a sieve along with a vibrating orbital shaker [25]. The particles were uniformly dispersed in a hyaluronic acid/collagen fibrous scaffold. After salt leaching, the scaffold contained large pores with cubic shapes, which allowed chondrocyte growth and proliferation inside the scaffold.

19.4.4 Sacrificed fiber method

The sacrificed fiber method combines two kinds of fibers into a scaffold and then removes one of the fibers, which reduces the fiber intersections and loosens the scaffold (Figure 19.6). Poly(ethylene glycol) has been usually used for the sacrificed fibers because it is water soluble and easily removed by immersing the scaffold in water. For this purpose, the electrospinning device requires two spinnerets. One spinneret is for a polymer solution to produce the targeted polymer fibers, and the other one is for the polymer solution to produce the sacrificial fibers. The two spinnerets can be placed parallel or perpendicularly with two kinds of fibers depositing on a collector. For example, two different fibers of slow-degradable polycaprolactone and water-soluble, sacrificial poly(ethylene oxide) (PEO) were combined into a composite [26]. The PEO fibers were selectively removed using water to increase the pore size of the electrospun scaffold, which facilitated cell infiltration and enhanced matrix distribution.
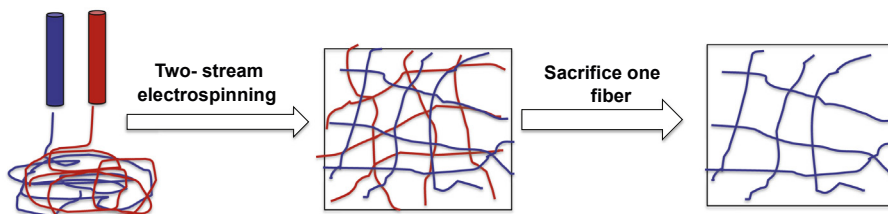
Figure 19.6 Schematic procedure of the sacrificed fiber method.

19.4.5 Concurrent electrospray/electrospin method

The concurrent electrospray/electrospin method is an effective method for loosening the fibrous scaffold, allowing extensive cell infiltration. At least two spinnerets are required. One spinneret is used to produce the electrospun polymer fibers, while the other spinneret is used to electrospray a flowable liquid, such as PBS, cell culture medium, or even pregel solution (Figure 19.7) [27–29]. These droplets produced by electrospray and the electrospun fibers concurrently deposit on a collector. The droplets can accelerate the polymer fiber surface solidification and prevent direct overlap of fibers to reduce the fiber intersections, and their volume can also occupy the space inside the scaffold, which can loosen the electrospun scaffolds. Electrospun poly(ester urethane) urea and electrosprayed cell culture medium concurrently deposited on a rotating cylinder collector were used to achieve a looser fibrous scaffold, called a "wet-electrospun" scaffold [27], Furthermore, the pregel solution from enzymatically digested dermal extracellular matrix was electrosprayed, concurrently depositing with

the electrospun PEUU fibers [28]. After the pregel solution was gelled at 37 °C, a hydrogel/electrospun fiber composite scaffold was obtained. The above two scaffolds exhibited extensive cell infiltration after 4 weeks of implantation in a rat full-thickness abdominal wall defect model, while the conventional polymer scaffolds showed very poor cell infiltration.

19.4.6 Cell microintegration method

The cell microintegration method is a direct way to cellularize an electrospun scaffold. The electrosprayed cell suspension and the polymer fibers concurrently deposit on a collector (Figure 19.7). It is notable that the cells can survive after high voltage treatment during electrospray. The solvent residual does not obviously induce severe cell death. Vascular smooth muscle cells, cardiac progenitor cells, and mesenchymal stem cells have been electrosprayed concurrently with electrospinning biodegradable polyurethane, which resulted in cell/fiber microintegrated constructs [30–33]. The cells inside the fibrous scaffold survived and proliferated, and the stem cells differentiated into the expected primary cells.

These above methods are feasible and effective for changing the architecture of the dense fibrous scaffolds for improved cell infiltration. However, the scaffold loosening inevitably induces a decrease of the mechanical strength of scaffolds. It can also result in the accelerated degradation of the submicrometer fibrous scaffold as the fluid and the cells can rapidly penetrate into the scaffold. Thus, one must consider these changes of material properties prior to applying a loosened scaffold for tissue engineering.
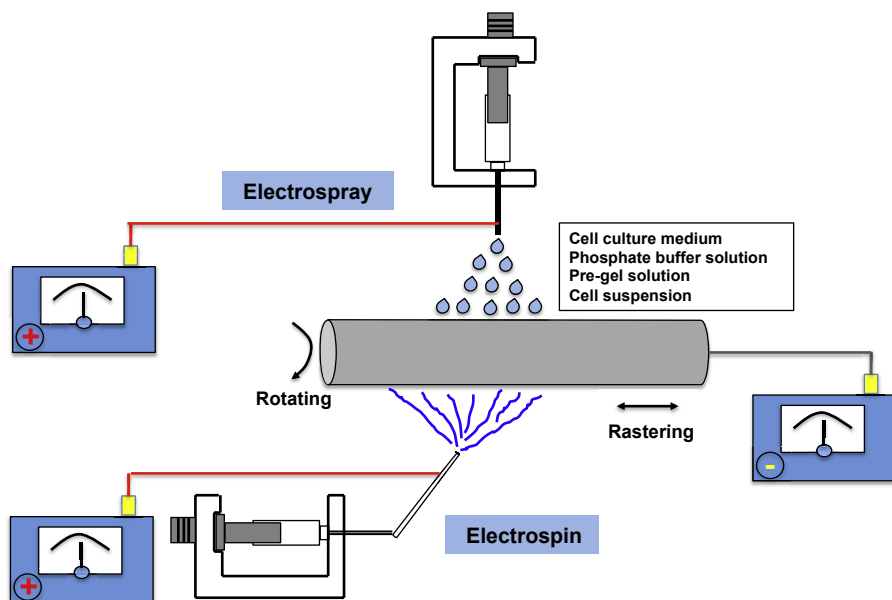
Figure 19.7 Schematic classic setup of electrospray/electrospin method and cell microintegration method.

19.5   Electrospun polyurethane scaffolds in tissue engineering applications

Tissue engineering is the use of a biodegradable scaffold combined with cells and signal molecules to regenerate a native tissue. As a promising candidate, the electrospun polyurethane scaffold has been applied for a variety of tissue repair and regeneration applications. The biodegradable PU scaffold has robust mechanical properties with good elasticity and surgical handling, and it also exhibits good biocompatibility. Other materials and bioactive molecules can also be combined with electrospun polyurethane scaffolds to improve their biofunctionality. The polyurethane scaffolds have been used for tissue engineering blood vessels, myocardia, heart valves, and abdominal walls, as well as skeletal muscle [34], bone [35], and neural tissue [36] (Figure 19.8).
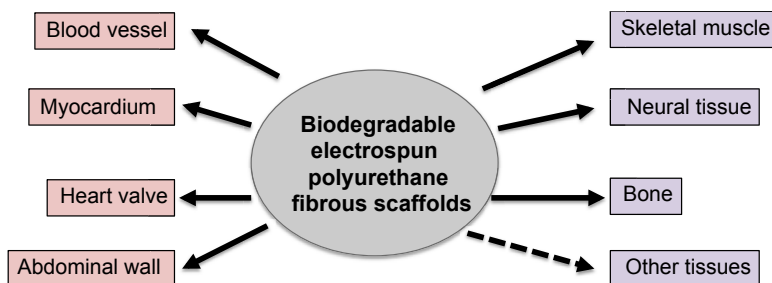
Figure 19.8 Tissue engineering applications of biodegradable electrospun polyurethane scaffolds.

19.5.1   Blood vessel tissue engineering

Autologous vascular transplantation is the gold standard for treating coronary and peripheral vascular diseases. However, the resource for healthy autologous vasculatures is limited in terms of the age and health status of the patient. Thus, the tissue engineering approach for regenerating a native blood vessel has been proposed. Biodegradable polyurethane has been processed into tubular scaffolds by electrospinning, which was applied for blood vessel regeneration, because it has robust mechanical properties with good elasticity and biocompatibility. Two main barriers to blood vessel tissue engineering are material thrombosis (blood compatibility) and hyperplasia (smooth muscle cell overproliferation), which induce restenosis and failure of the implant. Hence, prior to the use of polyurethane scaffolds for blood vessel replacement, their hemocompatibility must be improved. Additionally, it is thought that the mechanical mismatch with the scaffold and the native blood vessel is a main reason to induce hyperplasia; thus, polyurethane scaffolds are required to mechanically match with the native blood vessel.

A biodegradable poly(ester urethane)urea (PEUU) was blended with a phospholipid polymer of poly(methacryloyloxyethyl phosphorylcholine-co-methacryloyloxyethyl butyl urethane) (PMBU) (molar ratio=70/30), in HFIP solvent, and then coelectrospun

into a small diameter conduit (inner diameter, i.d. = 1.2 mm) as a biodegradable vascular graft [37]. The PEUU provided the mechanical support, while PMBU contributed to improve blood compatibility; PMBU addition significantly reduced ovine blood platelet deposition. The generated conduits have compliances comparable to those of the human artery. The 8 week in vivo implantation in a rat aorta model showed that the PMBU addition significantly increased the patency (75%) compared to PEUU alone (25%). A thin layer of neointimal including a layer of von Willebrand factor (vWF)-positive endothelial cell-like cells and a layer of alpha-smooth muscle actin-positive smooth muscle cell-like cells was observed by immunohistological staining. In a related strategy, the nonthrombogenic polymer can be grafted on the luminal surface of an electrospun biodegradable PEUU conduit [38]. This method can provide a blood-compatible surface without adverse effects on the PU conduit properties. The phospholipid polymer (poly(methacryloyloxyethyl phosphorylcholine-co-acrylic acid), PMA, molar ratio = 70/30) was grafted onto the lumen of an electrospun PEUU conduit [38]. The PMA coating significantly reduced the ovine blood platelet deposition. After 8 weeks of implantation into a rat aorta model (end to end implantation), the phospholipid polymer-coated PEUU conduit had a higher patency of 92% than that of PEUU conduit alone (40%). A continuous endothelial cell layer formed on the luminal surface. At 12 weeks, the coated PEUU conduit had mechanical properties including compliance, stiffness, and tensile strength comparable to those of native aorta.

Biodegradable electrospun PU scaffolds can also be combined with drug release to improve blood compatibility. The biodegradable PU was mixed with dipyridamole (DPA) in HFIP, and then electrospun into a drug-eluting small diameter conduit (i.d. = 1.2 mm) [39]. The DPA introduction increased the initial modulus of the PU scaffold because the DPA had strong hydrogen bonding with the polyurethane. This scaffold showed DPA released up to 90 days. The DPA-loaded scaffold showed improved blood compatibility in terms of lower red cell hemolysis and platelet deposition compared to the scaffold without DPA. The DPA-eluting scaffold also supported endothelial cell growth, while inhibiting smooth muscle cell proliferation. Although the above scaffolds are promising as biodegradable vascular grafts for in vivo tissue engineered blood vessels, the dense fibrous structure limits the cell infiltration into the scaffold.

A bilayer scaffold including an outer layer of an electrospun PEUU scaffold and an inner layer of porous PEUU scaffold was developed to address the cellularization issue [15]. The electrospun layer provided the mechanical support, while the porous scaffold layer supplied space for cell loading and infiltration. Prior to implantation, the cells including primary cells or stem cells were uniformly seeded into the porous layer using a customized vacuum device [15,40–42]. Rat vascular smooth muscle cells were seeded into the bilayer conduit and cultured in vitro for 2 days, and then this cellularized scaffold was implanted into the rat aorta model [42]. After 8 weeks, the patency of the cellularized scaffolds increased by 75% compared to 38% of the acellular scaffold. The failed scaffolds were blocked due to the intimal hyperplasia. The patent scaffolds contained a neointimal layer consisting of multiple layers of the immature contractile smooth muscle

cells and a monolayer of endothelial cells. Muscle-derived stem cells and human pericytes were also seeded into this bilayer scaffold and then implanted into the rat aorta model. Both cellularized scaffolds showed markedly improved patency after 8 weeks of implantation compared to the acellular scaffolds [40,41]. It is notable that the human pericyte-seeded scaffolds showed 100% patency without dilation [41]. Good tissue remodeling and the existence of collagen and elastin were observed for the patent pericyte-seeded scaffolds. The multiple layers of smooth muscle cells and a monolayer of endothelial cells were detected on the lumen. Although, it was observed that the smooth muscle cells were not fully contractile, these cellularized bilayer scaffolds showed great promise for tissue engineered vascular grafts, and a long-term animal study is expected.

In addition, direct cellularization for electrospun tubular scaffolds can be accomplished by a cell-microintegration technique. Rat vascular smooth muscle cells were simultaneously electrosprayed while electrospinning PEUU fibers onto a rotating mandrel to form a cell-infused tubular scaffold [30]. The cells survived and proliferated inside the scaffold. Biomechanical testing of the cellularized scaffold showed that it had similar mechanical properties to those of human coronary arteries and saphenous veins. In a recent study, mesenchymal stem cells also were combined with electrospun poly(ester carbonate) urethane fibers using a microintegration method to form a vascular graft [32]. This graft also showed similar mechanical properties with the native blood vessel. Unfortunately, no animal implant result is available at present.

19.5.2 Cardiac tissue engineering

In the area of cardiac tissue engineering, electrospun polyurethane scaffolds have not yet been implanted into animals. However, some reports showed promising in vitro results. Neonatal rat cardiomyocytes were seeded on either random or aligned fibrous biodegradable PU sheets [43]. The aligned fibrous scaffold yielded highly oriented cardiomyocytes. The cells on the aligned scaffold showed a low steady state level of atrial natriuretic protein, and the continuous release of the protein implied that the cell phenotype turned into a more mature status. Furthermore, murine embryonic stem cell-derived cardiomyocytes were seeded on the aligned or random fibrous polyurethane scaffolds along with the mouse embryonic fibroblasts [44]. Compared to the random scaffold, the aligned scaffold resulted in increased anisotropy of rod-shaped cells and promoted sarcomere organization. Coculturing with the mouse fibroblasts further improved the sarcomere organization. In addition, mouse cardiosphere-derived cells were microintegrated with electrospun fibers of a blend of biodegradable polyurethane and a biodegradable thermosensitive hydrogel through a concurrent electrospray/electrospin method [31]. Blending the softer hydrogel and the stiffer polyurethane modulated the global modulus, single fiber modulus, fiber density, and alignment of the construct by altering fabrication parameters. It was found that the construct with low moduli (50–60 kPa) significantly promoted the cardiosphere-derived cell differentiation into mature cardiomyocytes in vitro after a 1 week culture.

19.5.3 Heart valve tissue engineering

A low flexural stiffness is one of the most important features in the design of a biodegradable scaffold for heart valve tissue engineering. Altering the electrospinning parameters can modulate the microstructure and mechanical properties of the biodegradable polyurethane fibrous scaffold. Increasing rastering rates can significantly decrease the fiber intersections, which reduces the bending modulus [45,46]. For a wet-electrospun biodegradable polyurethane scaffold, the fiber intersections associated with the stiffness reduced with increasing the raster speed from 0.3 to 30 cm/s [45]. A cell microintegrated scaffold prepared by combining rat smooth muscle cells and biodegradable polyurethane fibers at a slow rastering rate (3 cm/s) exhibited mechanical anisotropy similar to that of the native porcine pulmonary valve [45]. Furthermore, adding a secondary fiber method can tune the material bending stiffness. When the polyurethane fibers were combined with polycaprolactone (PCL) electrospun fibers, the fiber intersections and tensile modulus increased with the increase of PCL weight ratio [46]. When the PEO fibers were sacrificed from a combined scaffold of the polyurethane and PEO fibers, the fiber intersections and bending modulus of the formed polyurethane fibrous scaffolds were significantly reduced [46]. Recently, by depositing electrospun fibers on a rotating conical mandrel, a curvilinear biodegradable polyurethane fibrous scaffold was prepared [17]. The formed scaffold had a curvilinear fiber structure similar to that of the native pulmonary valve leaflet. Under quasistatic loading, the scaffolds with the curvilinear fiber microstructures had reduced strain concentrations compared to the scaffolds fabricated using a conventional cylindrical mandrel.

19.5.4 Abdominal wall reconstruction

An appropriate biodegradable patch is assigned to treat abdominal wall trauma and hernia through tissue regeneration. An electrospun biodegradable polyurethane scaffold having high elasticity, biocompatibility, and robust mechanical strength meets these needs. However, once again cell infiltration is a major concern due to the dense fibrous structure of the electrospun scaffolds. A wet-electrospun scaffold was fabricated by simultaneously electrospinning PEUU fibers and electrospraying cell culture medium [27]. After 8 weeks of implantation into a rat full-thickness abdominal wall defect model, extensive cellular infiltration was observed for the wet-electrospun PEUU scaffold, while no cellular penetration was seen for the conventional electrospun PEUU scaffold. Biaxial testing exhibited anisotropic tissue remodeling. To further improve the bioactivity of electrospun abdominal wall scaffold, dermal extracellular matrix (ECM) powder was blended with the PEUU, and then electrospun into a scaffold sheet [21]. After an 8 week implantation, it was shown that more positive alpha-smooth muscle actin staining was found surrounding PEUU/ECM hybrid scaffolds compared to the PEUU scaffold alone. However, extensive cell penetration was not found. Through concurrently electrospraying dermal ECM pregel solution and electrospinning the PEUU, a dermal ECM hydrogel/ PEUU fibers hybrid scaffold was fabricated [28]. After a 4 week implantation into the rat abdominal wall model, the PEUU fibers/dermal ECM hydrogel hybrid scaffolds

exhibited extensive cell infiltration with good tissue integration. The tissue remodeling was significantly improved. To further reinforce the dermal ECM hydrogel/PEUU fibers hybrid scaffold, a sandwich scaffold consisting of two fiber-rich layers (top and bottom) of wet-electrospun PEUU scaffolds and one fiber-poor layer (middle) of the hydrogel/ fiber hybrid scaffold was developed using a concurrent electrospray/electrospin method [29]. The three layers were achieved through sequentially electrospraying phosphate buffer solution (PBS), pregel solution and PBS. This sandwich scaffold had significantly greater mechanical strength than the control of the hydrogel/fiber hybrid scaffolds without the two fiber-rich layers. In the rat full-thickness abdominal wall defect model, the control failed at 8 weeks of implantation because of the implant thinning. The sandwich sample showed similar thickness with the native rat abdominal wall at 8 weeks and 12 week, and its explant had increased M2-type macrophages and better tissue remodeling with mimetic structure and mechanical anisotropy comparable to those of the native abdominal wall.

19.6   Summary and future trends

Currently, scaffolds with mimetic structures and mechanical properties of the target native tissue are desired for tissue engineering. Biodegradable polyurethanes, which are mimetic with soft tissue mechanical behavior, have robust mechanical properties with high elasticity and flexibility. The electrospinning technique can process the polymer into nanoscale fibers, which can simulate the extracellular matrix microstructure of the tissue. Thus their combination has high potential for achieving an expected tissue engineering scaffold. In the next step, new biodegradable polyurethanes with additional property optimizations and biofunctionalities are desired. Reducing the initial modulus, increasing the mechanical strength, and combining bioactivity and biofunctions will be major areas of focus in new polymer development. Next, it will be necessary to develop new techniques to facilitate cell infiltration into the electrospun scaffold. Current approaches to the cell infiltration are still complex with limitations. A simple and effective way to achieve a bimodal pore structure would be a significant advantage. Finally, further in vivo testing of novel scaffold constructs is desired. The current biodegradable polyurethane fibrous scaffolds are known to be biocompatible and able to support primary cell growth and stem cell differentiation. The in vivo study, especially for specific tissue replacement, will confirm the feasibility of using polyurethane scaffolds for these applications. In summary, combining biodegradable polyurethanes and electrospinning can achieve promising fibrous scaffolds for tissue engineering applications. By altering the properties of the polymer solution and electrospinning parameters, the characteristics of fibrous scaffolds can be modulated to simulate native tissue. Furthermore, through design evolution of the electrospinning process, it is feasible to address the major challenge of cell penetration into the electrospun scaffolds. Polyurethane fibrous scaffolds are proposed for the regeneration of a variety of tissues, especially soft tissues. Such scaffolds with attractive structural, mechanical, and biodegradable properties have the potential to advance tissue engineering into clinical applications.

Acknowledgments

References

[1] Bhardwaj N, Kundu SC. Electrospinning: a fascinating fiber fabrication technique. Biotechnol Adv 2010;28:325–47.

[2] Formhals A. Apparatus for producing artificial filaments from material such as cellulose acetate. US Patent No 1975504. 1934.

[3] Zhong S, Zhang Y, Lim CT. Fabrication of large pores in electrospun nanofibrous scaffolds for cellular infiltration: a review. Tissue Eng Part B Rev 2012;18:77–87.

[4] Aravindan V, Sundaramurthy J, Suresh Kumar P, Lee YS, Ramakrishna S, Madhavi S. Electrospun nanofibers: a prospective electro-active material for constructing high performance Li-ion batteries. Chem Commun 2015;51:2225–34.

[5] Barnes CP, Sell SA, Boland ED, Simpson DG, Bowlin GL. Nanofiber technology: designing the next generation of tissue engineering scaffolds. Adv Drug Deliv Rev 2007;59:1413–33.

[6] Ingavle GC, Leach JK. Advancements in electrospinning of polymeric nanofibrous scaffolds for tissue engineering. Tissue Eng Part B Rev 2014;20:277–93.

[7] Kai D, Jin G, Prabhakaran MP, Ramakrishna S. Electrospun synthetic and natural nanofibers for regenerative medicine and stem cells. Biotechnol J 2013;8:59–72.

[8] Guelcher SA. Biodegradable polyurethanes: synthesis and applications in regenerative medicine. Tissue Eng Part B Rev 2008;14:3–17.

[9] Hong Y, Fujimoto K, Hashizume R, Guan J, Stankus JJ, Tobita K, et al. Generating elastic, biodegradable polyurethane/poly(lactide-co-glycolide) fibrous sheets with controlled antibiotic release via two-stream electrospinning. Biomacromolecules 2008;9:1200–7.

[10] Tomaszewski W, Szadkowski M. Investigation of electrospinning with the use of a multi-jet electrospinning head. Fibers Text East Eur 2005;13:22–6.

[11] Theron SA, Yarin AL, Zussman E, Kroll E. Multiple jets in electrospinning: experiment and modeling. Polymer 2005;46:2889–99.

[12] Haghi KA, Akbari M. Trends in electrospinning of natural fibers. Phys Status Solidi 2007;204:1830–4.

[13] Zong XH, Kim K, Fang D, Ran SF, Hsiao BS, Chu B. Structure and process relationship of electrospun bioabsorbable nanofiber membranes. Polymer 2002;43:4403–12.

[14] Sui X, Wiesel E, Wagner HD. Enhanced mechanical properties of electrospun nano-fibers through NaCl mediation. J Nanosci Nanotechnol 2011;11:7931–6.

[15] Soletti L, Hong Y, Guan J, Stankus JJ, El-Kurdi MS, Wagner WR, et al. A bilayered elastomeric scaffold for tissue engineering of small diameter vascular grafts. Acta Biomater 2010;6:110–22.

[16] Xie J, Li X, Lipner J, Manning CN, Schwartz AG, Thomopoulos S, et al. "Aligned-to-random" nanofiber scaffolds for mimicking the structure of the tendon-to-bone insertion site. Nanoscale 2010;2:923–6.

[17] Hobson CM, Amoroso NJ, Amini R, Ungchusri E, Hong Y, D'Amore A, et al. Fabrication of elastomeric scaffolds with curvilinear fibrous structures for heart valve leaflet engineering. J Biomed Mater Res Part A 2015;103(9):3101–6.

[18] Song W, An D, Kao DI, Lu YC, Dai G, Chen S, et al. Nanofibrous microposts and microwells of controlled shapes and their hybridization with hydrogels for cell encapsulation. ACS Appl Mater Interfaces 2014;6:7038–44.

[19] Zhang DM, Chang J. Patterning of electrospun fibers using electroconductive templates. Adv Mater 2007;19:3664–7.

[20] Nezarati RM, Eifert MB, Cosgriff-Hernandez E. Effects of humidity and solution viscosity on electrospun fiber morphology. Tissue Eng Part C Methods 2013;19:810–9.

[21] Hong Y, Takanari K, Amoroso NJ, Hashizume R, Brennan-Pierce EP, Freund JM, et al. An elastomeric patch electrospun from a blended solution of dermal extracellular matrix and biodegradable polyurethane for rat abdominal wall repair. Tissue Eng Part C Methods 2012;18:122–32.

[22] Blakeney BA, Tambralli A, Anderson JM, Andukuri A, Lim DJ, Dean DR, et al. Cell infiltration and growth in a low density, uncompressed three-dimensional electrospun nanofibrous scaffold. Biomaterials 2011;32:1583–90.

[23] Yang W, Yang F, Wang Y, Both SK, Jansen JA. In vivo bone generation via the endochondral pathway on three-dimensional electrospun fibers. Acta Biomater 2013;9:4505–12.

[24] Nam J, Huang Y, Agarwal S, Lannutti J. Improved cellular infiltration in electrospun fiber via engineered porosity. Tissue Eng 2007;13:2249–57.

[25] Kim TG, Chung HJ, Park TG. Macroporous and nanofibrous hyaluronic acid/collagen hybrid scaffold fabricated by concurrent electrospinning and deposition/leaching of salt particles. Acta Biomater 2008;4:1611–9.

[26] Baker BM, Shah RP, Silverstein AM, Esterhai JL, Burdick JA, Mauck RL. Sacrificial nanofibrous composites provide instruction without impediment and enable functional tissue formation. Proc Natl Acad Sci USA 2012;109:14176–81.

[27] Hashizume R, Fujimoto KL, Hong Y, Amoroso NJ, Tobita K, Miki T, et al. Morphological and mechanical characteristics of the reconstructed rat abdominal wall following use of a wet electrospun biodegradable polyurethane elastomer scaffold. Biomaterials 2010;31:3253–65.

[28] Hong Y, Huber A, Takanari K, Amoroso NJ, Hashizume R, Badylak SF, et al. Mechanical properties and in vivo behavior of a biodegradable synthetic polymer microfiber-extracellular matrix hydrogel biohybrid scaffold. Biomaterials 2011;32:3387–94.

[29] Takanari K, Hong Y, Hashizume R, Huber A, Amoroso NJ, D'Amore A, et al. Abdominal wall reconstruction by a regionally distinct biocomposite of extracellular matrix digest and a biodegradable elastomer. J Tissue Eng Regen Med 2013. http://dx.doi.org/10.1002/term.1834.

[30] Stankus JJ, Soletti L, Fujimoto K, Hong Y, Vorp DA, Wagner WR. Fabrication of cell microintegrated blood vessel constructs through electrohydrodynamic atomization. Biomaterials 2007;28:2738–46.

[31] Xu Y, Patnaik S, Guo X, Li Z, Lo W, Butler R, et al. Cardiac differentiation of cardiosphere-derived cells in scaffolds mimicking morphology of the cardiac extracellular matrix. Acta Biomater 2014;10:3449–62.

[32] Wang F, Li Z, Guan J. Fabrication of mesenchymal stem cells-integrated vascular constructs mimicking multiple properties of the native blood vessels. J Biomater Sci Polym Ed 2013;24:769–83.

[33] Stankus JJ, Guan J, Fujimoto K, Wagner WR. Microintegrating smooth muscle cells into a biodegradable, elastomeric fiber matrix. Biomaterials 2006;27:735–44.

[34] Riboldi SA, Sadr N, Pigini L, Neuenschwander P, Simonet M, Mognol P, et al. Skeletal myogenesis on highly oriented microfibrous polyesterurethane scaffolds. J Biomed Mater Res Part A 2008;84:1094–101.

[35] Mi HY, Palumbo S, Jing X, Turng LS, Li WJ, Peng XF. Thermoplastic polyurethane/hydroxyapatite electrospun scaffolds for bone tissue engineering: effects of polymer properties and particle size. J Biomed Mater Res Part B Appl Biomater 2014;102:1434–44.

[36] Puschmann TB, de Pablo Y, Zanden C, Liu J, Pekny M. A novel method for three-dimensional culture of central nervous system neurons. Tissue Eng Part C Methods 2014;20:485–92.

[37] Hong Y, Ye SH, Nieponice A, Soletti L, Vorp DA, Wagner WR. A small diameter, fibrous vascular conduit generated from a poly(ester urethane)urea and phospholipid polymer blend. Biomaterials 2009;30:2457–67.

[38] Soletti L, Nieponice A, Hong Y, Ye SH, Stankus JJ, Wagner WR, et al. In vivo performance of a phospholipid-coated bioerodable elastomeric graft for small-diameter vascular applications. J Biomed Mater Res Part A 2011;96:436–48.

[39] Punnakitikashem P, Truong D, Menon JU, Nguyen KT, Hong Y. Electrospun biodegradable elastic polyurethane scaffolds with dipyridamole release for small diameter vascular grafts. Acta Biomater 2014;10:4618–28.

[40] Nieponice A, Soletti L, Guan J, Hong Y, Gharaibeh B, Maul TM, et al. In vivo assessment of a tissue-engineered vascular graft combining a biodegradable elastomeric scaffold and muscle-derived stem cells in a rat model. Tissue Eng Part A 2010;16:1215–23.

[41] He W, Nieponice A, Soletti L, Hong Y, Gharaibeh B, Crisan M, et al. Pericyte-based human tissue engineered vascular grafts. Biomaterials 2010;31:8235–44.

[42] He W, Nieponice A, Hong Y, Wagner WR, Vorp DA. Rapid engineered small diameter vascular grafts from smooth muscle cells. Cardiovasc Eng Technol 2011;2:149–59.

[43] Rockwood DN, Akins Jr RE, Parrag IC, Woodhouse KA, Rabolt JF. Culture on electrospun polyurethane scaffolds decreases atrial natriuretic peptide expression by cardiomyocytes in vitro. Biomaterials 2008;29:4783–91.

[44] Parrag IC, Zandstra PW, Woodhouse KA. Fiber alignment and coculture with fibroblasts improves the differentiated phenotype of murine embryonic stem cell-derived cardiomyocytes for cardiac tissue engineering. Biotechnol Bioeng 2012;109:813–22.

[45] Amoroso NJ, D'Amore A, Hong Y, Wagner WR, Sacks MS. Elastomeric electrospun polyurethane scaffolds: the interrelationship between fabrication conditions, fiber topology, and mechanical properties. Adv Mater 2011;23:106–11.

[46] Amoroso NJ, D'Amore A, Hong Y, Rivera CP, Sacks MS, Wagner WR. Microstructural manipulation of electrospun scaffolds for specific bending stiffness for heart valve tissue engineering. Acta Biomater 2012;8:4268–77.

Embolic applications of shape memory polyurethane scaffolds

20

T.L. Landsman[1], A.C. Weems[1], S.M. Hasan[1], R.S. Thompson[1],
T.S. Wilson[2], D.J. Maitland[1,]*

[1]Department of Biomedical Engineering, Texas A&M University, College Station, TX,
USA; [2]Physical and Life Sciences Directorate, Lawrence Livermore National Laboratory,
Livermore, CA, USA

*Corresponding author: djmaitland@tamu.edu

20.1 Introduction

Researchers in the medical industry have been drawn to the advantages of shape memory materials, such as nitinol, since 1971 (Funakubo, 1987). Until the 1990s, commercially available shape memory materials used in the medical industry were limited to nickel–titanium, copper, and iron-alloy systems (Huang et al., 2010). In 1985 Drs Robert Ward and Judy Riffle of Thoratec Laboratories Corporation, Pleasanton, California, filed a patent titled "Method for making an article with shape-memory properties and some of the thus obtained articles," which is one of the first descriptions of what is considered a shape memory polymer (SMP) today. In 1990 Dr Hayashi of Mitsubishi Heavy Industry, Japan, published his findings on one of the first commercial thermoplastic SMPs (Hayashi, 1990). SMPs offer several advantages over traditional shape memory alloys (SMAs). For instance, SMPs can recover up to 400% plastic strain versus only 7–8% for SMAs, they typically cost approximately 10% of the cost of SMAs, SMPs can be fabricated with densities less than $1.25\,\text{g/cm}^3$, they can be tuned to have a wide range of transition temperatures for numerous applications, and they have demonstrated biocompatibility in various applications (Sokolowski et al., 2007). Since the introduction of SMPs into the marketplace, they have continued to garner significant interest as highly advantageous materials for use in the medical industry.

SMPs are capable of switching between a primary and a secondary shape on the input of an external stimulus, such as heat or UV light (Zhang et al., 2014; Tseng et al., 2013). These materials can be synthesized in their primary shape and programmed into an elongated or compact secondary shape via mechanical programming. The SMP maintains this secondary shape due to the switching segments that undergo thermal transitions during programming while the permanent shape is maintained by the net points of the polymer (Tseng et al., 2013; Zhang et al., 2014). Net points are physical or chemical cross-links that provide the shape memory effect (SME) for the polymer.

SMPs can be fabricated using a variety of polymer systems, including poly(ε-caprolactones), acrylates, polynorbornenes, cross-linked polyethylenes, poly(ether ketones), and polyurethanes (Defize et al., 2011; Hearon et al., 2011; Khonakdar et al., 2007;

Sakurai and Takahashi, 1989; Wu et al., 2014; Yakacki et al., 2007). From 2005 to 2015, polyurethane SMPs have garnered significant interest for use in implantable medical devices. This is primarily because they are easily manufactured in large quantities using conventional polymer fabrication techniques, their mechanical properties and transition temperatures are easily tuned to match specific applications, and they have demonstrated extensive biocompatibility (Cabanlit et al., 2007; Lendlein and Kelch, 2002; Metcalfe et al., 2003; Sokolowski et al., 2007). These characteristics of polyurethanes have resulted in their implementation into the design and fabrication of numerous medical devices, such as thrombectomy devices, cardiovascular stents, self-tightening sutures, and kidney dialysis adapters (Lendlein and Langer, 2002; Ortega et al., 2007; Small et al., 2005; Wache et al., 2003). However, perhaps the most intriguing technologies with the potential to compete with current FDA-approved devices are polyurethane SMP foams used in embolization procedures. The goal of embolization, current treatment methods, and how SMP foams can propel these procedures into a new realm of innovation will be discussed throughout this chapter.

20.1.1 Scaffold fabrication techniques

Numerous fabrication techniques can be used to create porous SMP scaffolds. Each method varies in complexity and results in varying scaffold morphologies, as demonstrated in Figure 20.1.

The best-suited technique for fabricating a given scaffold depends on the intended application, the polymers being used in the fabrication, and the conditions under which the polymer solutions are cured and maintained. Some of these fabrication techniques
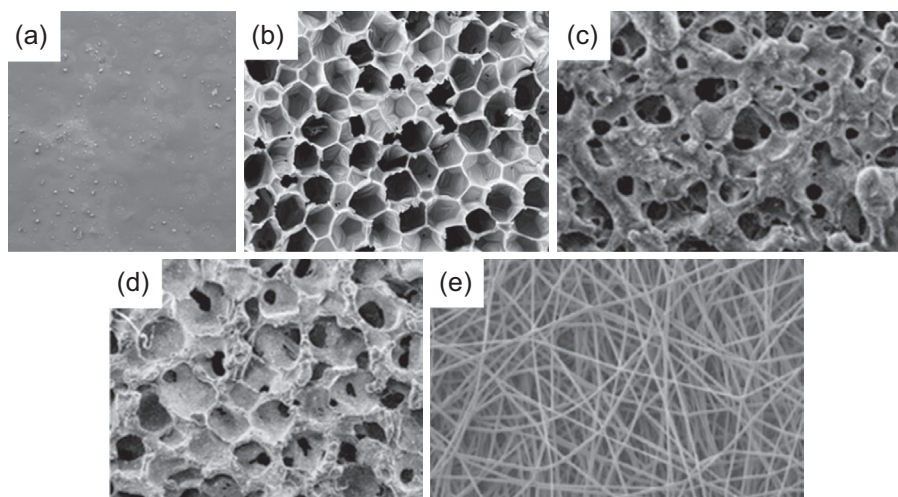
Figure 20.1 SEM image of polymer scaffolds synthesized via (a) solvent casting (Boateng et al., 2009), (b) gas blowing, (c) emulsion templating (Janik and Marzec, 2015), (d) particle leaching (Janik and Marzec, 2015), and (e) electrospinning (Tseng et al., 2013). Reproduced with permission from Elsevier.

include gas blowing, emulsion templating, particle leaching, and electrospinning. Although these are not the only methods that can be used to create a porous polyurethane scaffold, they are the most widely utilized techniques in industry and academia. Each of these techniques will be described in detail in the following sections.

20.1.1.1 Polymer film fabrication

Each foaming technique begins with the preparation of a neat polymer solution. Neat polymer films can be developed by physical treatments such as annealing, elongating the polymer, or by solution casting (Okuno et al., 1993). Physical elongation of the polymer results in a change in the molecular structure of the polymer, while solution casting allows for the structure to develop at the same time as the membrane formation throughout the scaffold (Okuno et al., 1993).

Neat polymer fabrication using solvent casting involves thin film formation by dissolving the polymer in an appropriate solvent, casting the polymer/solvent solution onto a solid substrate or mold, and then evaporating out the solvent. This process can result in a uniform, flat surface as shown in Figure 20.1(a) (Okuno et al., 1993). However, solvent selection is an important parameter for controlling film morphology. Ohuno et al. synthesized poly(vinyl chloride) (PVC) films using different solvents and studied the effects of solvent blends on polymer morphology. Tetrahydrofuran (THF) is a good solvent for PVC; however, when water is added the solvent quality decreases, resulting in a decrease in the size of the polymer chains in solution (Okuno et al., 1993). Additionally, the crystallinity of the polymer may be disrupted with the use of poor or mixed solvents.

Neat polymers have been used extensively for drug delivery applications and as biomaterials that promote cell adhesion. In fact, some of the earliest polymer scaffolds were simply films that promoted cell adhesion and growth (Ito et al., 1991). Aljawish et al. synthesized surface-modified chitosan films and studied the degree of protein adsorption and cell adhesion onto the substrate. Heterogeneous surface morphology of the films improved protein adsorption and subsequently resulted in favorable cell attachment and spreading (Aljawish et al., 2014). Film thickness also played a role in increasing cell viability. It was discovered that thicker films resulted in better cell viability (Aljawish et al., 2014).

20.1.1.2 Gas blowing

Gas blowing has been a popular synthesis technique used for commercial manufacturing of polyurethane foams for years; however, its use in the biomedical engineering field has grown over the last few years (Janik and Marzec, 2015). Gas foaming allows nucleation and growth of gas bubbles that are dispersed within a polymer solution for the development of pores, as shown in Figure 20.1(b) (Ji et al., 2012). There are two ways to generate bubbles during gas blowing: chemical blowing and physical blowing. Chemical blowing requires a reaction between blowing agents for the generation of gas bubbles, while physical blowing agents can be mixed into the polymer to generate a gas–polymer mixture through vaporization. Gas bubbles nucleate, grow, and coalesce within the mixture resulting in pore development. Carbon dioxide (CO_2) is a widely used blowing agent because of its moderate critical point, nonflammability, and lack of toxicity (Ji et al., 2012; Spaans et al., 2000). CO_2 foaming occurs in two

Gas blowing

A side material: polyols,   ✚   B side material:
water, surfactants, catalysts   polyisocyanates

Mixing with
high speed
mixer

Reactive foam mixture

Transfer to
mold

Polymer foam
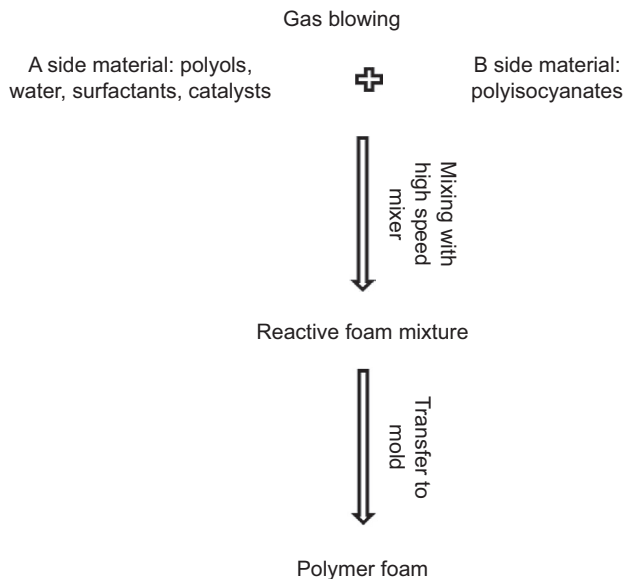
Figure 20.2 Schematic of the steps involved in fabricating porous gas blown scaffolds.

stages: the pressurization stage and the depressurization stage. A gas-saturated polymer phase must be generated followed by pore nucleation, growth, and coalescence. As the foam rises, the gas bubbles trapped in the foam mixture coalesce and the pores grow larger. The processes used in gas blowing are summarized in Figure 20.2.

Stabilization of the porous structure can be achieved by chemical cross-linking of the polymer system during foaming, by phase separation, or by cooling it below its glass transition temperature (Frerich, 2015). For polyurethane foams, chain extension with water is effectively used to develop polyurethane ureas (Spaans et al., 2000). During the foaming step, water is reacted with isocyanate monomers to generate carbon dioxide, resulting in a porous material. Pore structure and interconnectivity can be controlled by varying foaming agent and its concentration in the polymer–gas mixture (Dement'ev et al., 1991; Spaans et al., 2000). A significant advantage of gas blowing is the lack of organic solvents used in the fabrication, which reduces scaffold toxicity for *in vivo* applications (Janik and Marzec, 2015). However, controlling pore sizes and connectivity can be very difficult when using this technique (Janik and Marzec, 2015).

Gas blown polyurethane foams have a wide range of biomedical applications as tissue repair scaffolds. Spaans et al. developed biodegradable, biocompatible polyurethane scaffolds for replacement and repair of the meniscus. The group utilized a 50/50 blend of poly(ε-caprolactone) and poly(L-lactide) for a soft segment, while 1,4-butane diisocyanate constituted the hard segment (Spaans et al., 2000). The scaffold was synthesized using a combination of CO_2 gas blowing and chain extension using adipic acid. CO_2 use resulted in interconnected macropores in the final scaffold while chain extension created smaller, homogeneous pores with interconnectivity (Spaans et al., 2000).

Emulsion templating

Internal phase:
oil/water

External phase:
polymer solution

Surfactant
and catalyst
addition

Mixing

Cured polymer scaffold with
internal phase

Removal of
internal
phase

Porous polymer scaffold
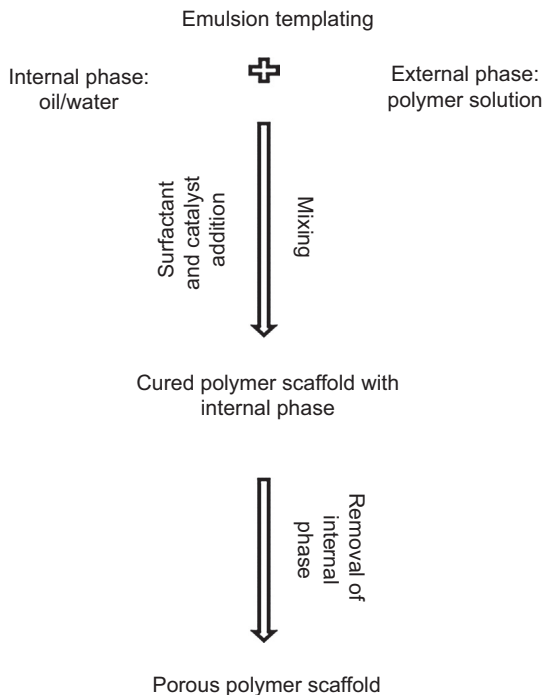
Figure 20.3 Schematic of the emulsion templating process.

20.1.1.3 Emulsion templating

Emulsion templating is a popular scaffold fabrication technique that was first utilized in the 1960s (Kimmins and Cameron, 2011). A diagram showing the steps involved in this fabrication technique is shown in Figure 20.3. This technique involves the use of two liquid phases, the external and the internal phase (Silverstein, 2014a). The external phase, also called the nondroplet phase, forms the solid polymeric scaffold while the internal phase, or the droplet phase, consists of oil or water droplets (Silverstein, 2014b). Simply put, the emulsion of oil in an aqueous/polymer phase allows for the development of a polymer shell around the oil droplets, resulting in a porous scaffold with controlled pore sizes (Figure 20.1(c)). Additional components such as surfactants and catalysts are added to stabilize the pores and speed up the reaction kinetics for scaffold synthesis (Sarvi et al., 2012; Silverstein, 2014a). High internal phase emulsions (HIPEs) are a widely used type of emulsion templating for polymer scaffolds (Silverstein, 2014a). For this type of emulsion, the droplet phase consists of 70% of the volume of the emulsion and the resulting scaffold has small, interconnected pores (Silverstein, 2014a). A polymerized HIPE is often called a polyHIPE. To differentiate pore characterization from gas blowing techniques, the spherical cavities generated from the emulsion droplets are called voids (Cameron, 2005). The voids normally have interconnected holes which are referred to as windows. Synthesis of a polyHIPE consists of mixing reactive monomers, catalysts, and surfactant while slowly adding the droplet phase (Cameron, 2005). Mixing is required to break up the

formation of larger droplets due to phase separation. Once the nondroplet phase has cured, the resulting polyHIPE is washed and dried to remove the droplet phase (Cameron, 2005).

Void size can be controlled by altering the concentration and viscosity of the external phase and the volume of the internal phase (Kimmins and Cameron, 2011). Surfactant concentration also plays a major role in altering the polyHIPE morphology (Kimmins and Cameron, 2011). Yao et al. studied the effects of a triblock surfactant concentration on polyHIPE morphology. The void structure became more homogeneous and interconnected when surfactant concentration was increased from 2% to 7% (v/v) (Yao et al., 2009). Increasing surfactant concentration allows thinning of the polymer films separating adjacent emulsion droplets, allowing for windows to develop in the void structure as the polymer cures (Cameron, 2005). However, one disadvantage of polyHIPEs is the large amount of droplet phase that is required during synthesis (Kimmins and Cameron, 2011). If the droplet phase is organic, further postfabrication cleaning of the scaffold is required to ensure removal of all organic solvents that might cause cell toxicity.

Emulsion freeze drying is another form of emulsion templating that utilizes droplet formation from mixing two immiscible phases as well (Janik and Marzec, 2015). However, with emulsion freeze drying the droplet phase is normally water and the emulsion can be frozen quickly once homogeneous voids have been achieved (Janik and Marzec, 2015). The scaffold is then freeze-dried to remove the aqueous phase, leaving behind a porous polymer structure. One of the main advantages of this technique is the lack of organic solvents and minimizing the time-consuming drying processes associated with polyHIPEs (Janik and Marzec, 2015).

20.1.1.4 Particle leaching

Particle leaching involves dispersing solid particles into a polymer solution (El-Kady et al., 2012). First, a polymer solution is synthesized at 5–20% concentration in an organic solvent (Hariraksapitak et al., 2008). Then the particles are added to the polymer solution before the solvent is evaporated via air drying, vacuum drying, or freeze drying to embed the solid particles within the polymer matrix (Yoon et al., 2003). After drying, the polymer/solid composite is immersed in water to dissolve the solid particles, leaving behind a porous polymer scaffold (Figure 20.1(d)). This process is summarized in Figure 20.4. Most particle leaching techniques utilize salts; however, sugar, ammonium chloride, sucrose, starch, paraffin, and gelatin particles have also been reported in the literature (Janik and Marzec, 2015). Microspheres are preferred for salt leaching because they result in regular pore geometry that enhances the mechanical properties of the scaffold and improves fluid exchange and nutrient supply to cells (Janik and Marzec, 2015).

Scaffold porosity can be controlled by varying the particle concentration, while pore sizes depend on the size of the particles added to the polymer solution (De Nardo et al., 2012; Janik and Marzec, 2015). If the particle concentration is insufficient, isolated pores will be generated as the polymer surrounds each particle. Hariraksapitak et al. reported an increase in porosity with higher concentrations of particles (25× to 40×) due to the generation of more voids. However, pore sizes remained in the range of 200–400 μm as a result of the particle size utilized during scaffold synthesis, which indicates that particle size and shape are directly related to the pore size and geometry

Particle leaching

Polymer solution ✚ Salt particles

Mixing

Salt dispersed in polymer solution

Solvent evaporation

Polymer scaffold with salt particles ✚ Water

Salt leaching

Porous polymer scaffold
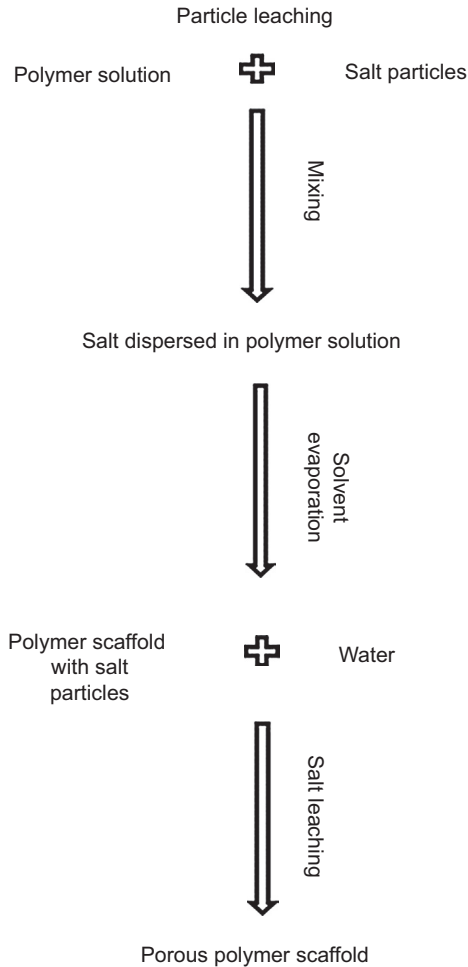
Figure 20.4 Summary of the processes used in creating porous scaffolds by means of particle leaching.

of the scaffold (Hariraksapitak et al., 2008). Increased particle loading can result in void formation within the scaffold, due to close packing, which will ultimately decrease the overall mechanical properties of the scaffold (Janik and Marzec, 2015). Hariraksapitak et al. evaluated compressive and tensile properties for scaffolds with varying porosity. It was reported that higher porosity scaffolds experienced a decrease in both compressive and tensile strength (Hariraksapitak et al., 2008).

An advantage of using particle leaching is the ease of fabrication since no specialized equipment is required for scaffold synthesis. However, the difficulty associated with selecting particle type and size is a disadvantage, because attaining high porosity while maintaining adequate mechanical strength is a challenge. The ability to control and tune the porosity and interconnectivity of a scaffold is especially important for

optimizing cell ingrowth and diffusion (Heijkants et al., 2006). Another disadvantage of this technique is that it yields thin materials due to difficulties in leaching salt from large volumes. Organic solvents provide a means of removing salt, although residual solvent may affect cell growth and adhesion.

20.1.1.5   Electrospinning

Electrospinning is a unique scaffold fabrication technique that yields a porous, three-dimensional scaffold that mimics the extracellular matrix (Figure 20.1(e)) (Rogina, 2014). This process involves the use of a high voltage power supply applied to the polymer solution to induce jet formation (Rogina, 2014). The basic setup consists of a syringe with a feed pump, high voltage power supply to provide an electrical field, and grounded fiber collector, which is normally a metal plate or a rotating mandrel (Figure 20.5) (Sell and Bowlin, 2008). The electrical field generates a charged polymer jet which deforms uniaxially from the needle tip to the grounded collector (Jiang et al., 2014). During this process, the solvent evaporates, leaving behind dried polymer fibers that form the fibrous scaffold.

Electrospun scaffolds are continuous fibrous scaffolds that result from a polymer melt or solution and have fiber diameters ranging from micro to nanoscale (Rogina, 2014). Electrospinning can be utilized for a wide range of polymers and composite materials, making it a versatile, cost-effective technique for developing biomedical scaffolds with controlled production and easy scale-up (Rogina, 2014). This technique was first used in the 1990s to develop polymer nanofibers and is currently popular for developing tissue engineering and drug delivery scaffolds (Sell and Bowlin, 2008). A diagram of a typical electrospinning setup is shown in Figure 20.5.

Polymer properties, such as viscosity, surface tension, and conductivity, play an important role in controlling the size, density, and morphology of the electrospun fibers (Rogina, 2014). Solution viscosity is dependent on the polymer molecular weight and degree of entanglements/cross-linking (Jiang et al., 2014). This affects
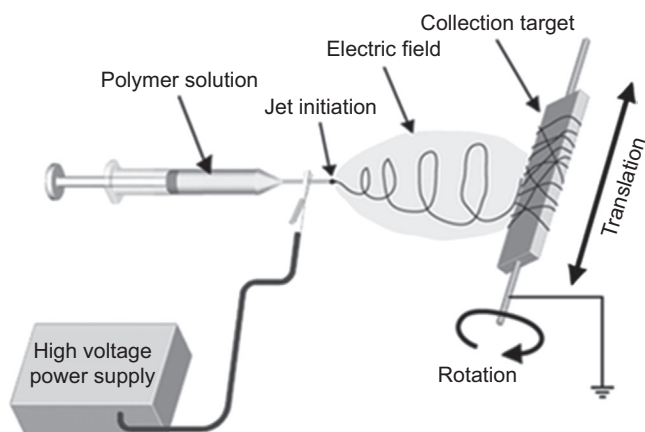
Figure 20.5   Common electrospinning setup used in academia (Sell and Bowlin, 2008). Reprinted with permission from Royal Society of Chemistry.

the development of fibers versus droplets during jet formation, and the subsequent final scaffold could potentially have a combination of both. Lower viscosity solutions generally result in droplet formation while higher viscosity solutions may result in poor jet formation and an increase in fiber diameter (Jiang et al., 2014). Surface tension of the solution is directly related to the nature of the solvent. A lower surface tension solution may allow the utilization of lower electric fields for fiber formation (Rogina, 2014). However, this may change the solution viscosity and result in droplet formation in the scaffold. Conductivity of the solution is affected by the nature of the solvent and by the incorporation of inorganic salts (Rogina, 2014). Addition of salts, such as sodium chloride, will increase solution conductivity, which in turn increases its mobility under the electric field (Rogina, 2014). This provides greater elongations and thinner diameters of the resulting fibers. Fine-tuning the various parameters of the polymer solution can result in controlled fiber diameters of less than 300 nm for optimal cell infiltration and growth (Jing et al., 2015).

20.2 Embolization and occlusion

20.2.1 Goal of embolization

In some circumstances blood flow through specific vascular pathways can cause potentially life-threatening complications. In these instances physicians rely on embolization devices to block blood flow to the region. Embolization is a technique in which a physician places a material within a cavity or blood vessel with the intent of completely occluding that region or diverting blood flow from that region. Oftentimes, endovascular embolization supplants highly invasive surgeries used to treat the same morbidity. This is primarily due to reduced treatment costs, recovery time, and patient discomfort, as well as improved clinical outcomes (Carradice et al., 2011; Molyneux et al., 2002). This type of treatment is used for a wide variety of morbidities, such as arteriovenous malformations (AVM), aneurysms, venous insufficiency, and patent foramen ovale (PFO) (Bendok et al., 2003; Knerr et al., 2014; Min et al., 2012; Qureshi et al., 1996; Rodriguez et al., 2014). However, researchers and physicians continue to discover novel indications for endovascular embolization as catheterization technology evolves.

20.2.2 Current treatment methods

Although a number of different methodologies exist to exclude vessels from undesired blood flow, such as endovenous ablation, surgical ligation, and sclerotherapy, the following sections describe FDA-approved interventional embolic devices that are most similar to SMP foam scaffolds.

20.2.2.1 Coiling

Embolic coiling involves the placement of a fine coil in a vascular defect to generate and maintain a clot. Initially coils were composed of steel guidewires tipped with cotton or wool strands that were navigated to the desired location through a catheter

under fluoroscopy. This is still the standard procedure used today, but the design of the coils has experienced some changes (Gianturco et al., 1975). The first modern coils were composed of a bare platinum coil and were developed as a method of retaining a clot that was formed by electrothrombosis, a process by which a positive charge is applied to a lead within the aneurysm that attracts negatively charged components of the blood, namely platelets, and forms a clot. Conveniently this same electric current could be used to detach the coil through electrolysis, making a very effective and simple delivery method (Guglielmi et al., 1991). Though some alternative detachment methods have been used, most of the variation in embolic coils comes from technologies developed to increase the volume filling and surface area properties of the devices through the addition of hydrogels or fibers, as shown below in Figure 20.6 (Chuang et al., 1981; Kallmes and Fujiwara, 2002; Miller and Mineau, 1983).

Many coils still use a pushable design that allows them to be delivered using standard guidewires or custom pusher wires. The relative ease of use and low cost of these coils have made them the most popular type of coil in interventional radiology. Detachable coils are still the preferred method where precise positioning is critical for optimal filling, or when coil migration during the procedure is of serious concern. These coils are also typically used when a tortuous pathway may lead to an inability
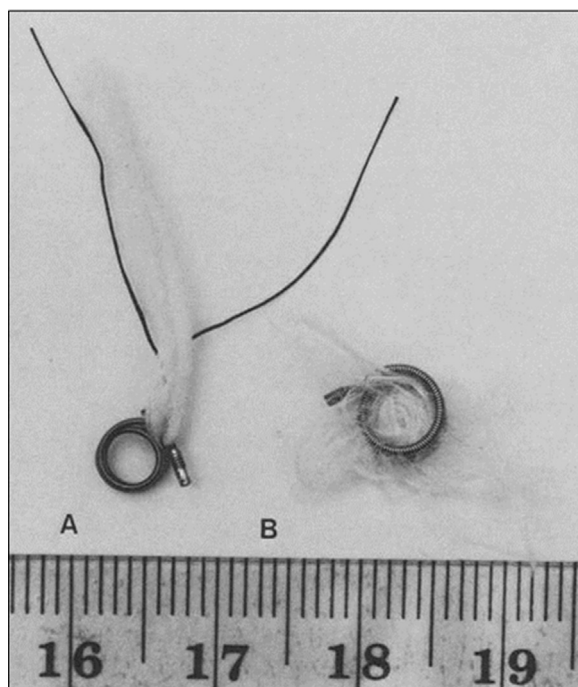
Figure 20.6 (a) Original fibered coils with Dacron fibers attached at the proximal and distal ends of the coil, and (b) the newer style of fibered coils with Dacron fibers attached throughout the length of the coil (Miller and Mineau, 1983).
Reprinted with permission from Springer.

to advance the coil through the entirety of the catheter, which is the case in interventional procedures performed to treat intracranial aneurysms (Park et al., 2015; Vaidya et al., 2008). Endovascular coiling is the most widely used embolization method but it still has a number of complications. Coils can protrude or fully migrate into the parent vessel and potentially cause a thromboembolism, and the procedure itself is dangerous and can lead to aneurysm rupture (Bilbao et al., 2006). Approximately 20% of aneurysms, particularly those with an internal diameter larger than 25 mm or a neck diameter larger than 4 mm, will experience rebleeding due to coil compaction or device migration (Currie et al., 2011). Coiling is typically not well suited for clotting in high flow areas or in areas where the coils could easily migrate (Chuang et al., 1981; Currie et al., 2011; Lubarsky et al., 2009).

20.2.2.2 Gelfoam® plug

Gelfoam®, a gelatin foam available in sheet or powder form that can be formed into a variety of shapes by an interventionalist, is often used off-label to completely occlude specific vessels, although it is not indicated specifically for intravascular embolization (Patel et al., 2005). The foam can also be cut into fine segments and mixed with a diluted contrast agent to create a slurry that is injected into the target site, as shown in Figure 20.7.

   The device functions as a physical barrier to prevent blood flow through the vessel, but due to the gelatinous and bioabsorbable nature of the foam on saturation, it does not provide a scaffold for clot formation and connective tissue ingrowth (Speakman, 1964). Gelfoam® treatments can lead to downstream embolization due to the nature of the particles and may have a connection with infections, potentially caused by air bubbles trapped in the materials during the mixing process used to prepare the foam.
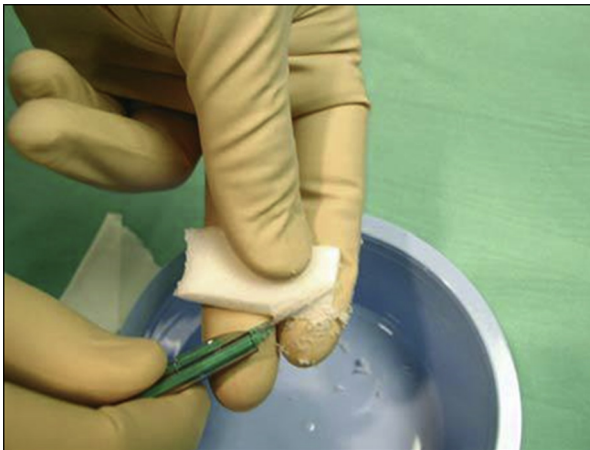
Figure 20.7 A Gelfoam® pledget is shaved with a blade at a 45° angle, allowing the shavings to mix with a contrast agent to produce a slurry that is then injected to the target site (Golzarian, 2006).
Reprinted with permission from Springer.
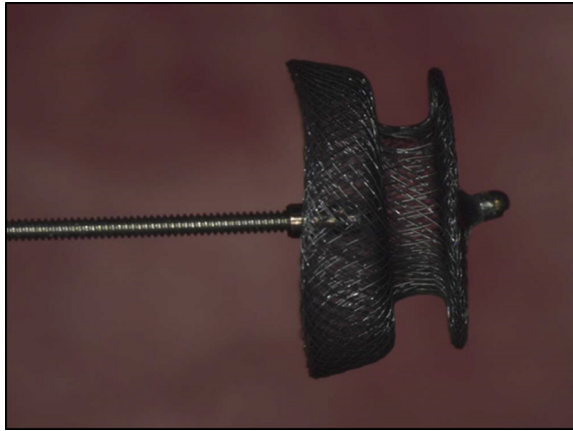
Figure 20.8 Image of an Amplatz® canine duct occluder (ACDO), which shows the fine nitinol wire mesh used as an embolic device to completely occlude patent ductus arteriosus (PDA) in dogs.

There are also issues with frequent recanalization of treated vessels because the gel is resorbable, and as such, the gel may be fully resorbed before stable fibrosis occurs. Gelfoam® use is often combined with embolic coils so that the gel creates the initial occlusion and the coils are implanted to retain the clot at the treatment region after the body begins resorbing the gelatin (Lubarsky et al., 2009; Vaidya et al., 2008).

20.2.2.3   Nitinol mesh

Nitinol mesh devices, the most notable of which is the Amplatzer Vascular Plug, are a family of endovascular embolization devices that take advantage of nitinol's highly elastic nature to create multiple fine-meshed discs and ovoids that instantly expand on exiting the catheter. One such device is shown below in Figure 20.8. The goal of these devices is to provide a sufficiently fine mesh to create flow stagnation and recirculation zones in the device to activate thrombus formation. They have a cost advantage over embolic coils because only one device is used to occlude the target region. However, nitinol mesh devices typically do not create a stable thrombus as rapidly as coils (Tuite et al., 2007; Vaidya et al., 2008). Newer nitinol mesh devices seek to combine the flexible, self-expanding nature of nitinol with thrombogenic, biocompatible materials like PTFE. One such device is the micro vascular plug system manufactured by Reverse Medical®. This device combines a stent-like structure of nitinol completely covered with PTFE (Pellerin et al., 2014). The inclusion of PTFE seeks to reduce the time to occlusion by forcing the blood flow through the significantly smaller pore sizes of the PTFE cover rather than the nitinol cage.

20.2.2.4   Polyvinyl alcohol foam

Polyvinyl alcohol (PVA) foams can have plastic memory capabilities similar to those of polyurethanes (Tadavarthy et al., 1975). Currently PVA is mostly used as a foam in
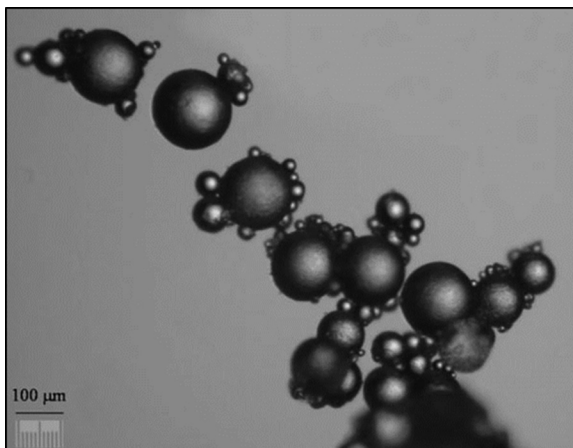
Figure 20.9 Optical microscopy image of unexpanded poly(vinyl acetate)/poly(vinyl alcohol) particles used for embolization in 20 wt% heptane (Peixoto et al., 2009).
Reprinted with permission from John Wiley and Sons.

a method similar to that of Gelfoam®; it is typically packaged as particles produced from a foam sheet and sorted by size. Typical PVA particles are shown in Figure 20.9. PVA foam treatments consist of injecting hundreds to thousands of these particles into the treatment region where they adhere to the vessel wall and produce an inflammatory response resulting in fibrosis. The major issue faced with these PVA treatments is that they can aggregate in the catheter or clot downstream vessels and there have been reports of the foam migrating from the treatment region and causing a pulmonary embolism (Thompson et al., 1993; Vaidya et al., 2008; Whiting et al., 1992; Derauf et al., 1987).

20.2.3   Indications for embolization

20.2.3.1   Ateriovenous malformations

Vascular malformations, often described as a bag of worms, can occur throughout the body but are most prevalent in the central nervous system. There are many types of vascular malformations, but on their most basic level they are an abnormal connection between an artery and a vein that bypasses or "shunts" a capillary bed (Stapf et al., 2001). The differentiation in the cellular composition of AVMs varies from distinguishable arterial and venous portions to hyalinized thick and thin-walled portions with no discernable features specific to arteries or veins (McCormick, 1966). Though they are not neoplasms since they possess a nervous parenchyma between the vessels of the malformation, the endothelial cells of the AVM do express higher than normal levels of growth factors and growth factor receptors (Jabbour et al., 2009; Noran, 1945). These malformations are typically angiographically occult, meaning that the whole vessel system does not always appear on an angiogram. A typical arteriogram of an AVM is shown below in Figure 20.10.

Figure 20.10 Selective vesicle arteriogram showing two right internal iliac arteries feeding an AVM and early drainage to the right internal iliac vein. The nidus of the AVM (black arrow), dilation of the draining vein (black arrowhead), and early drainage of iliac vein (thin black arrow) are shown (Koganemaru et al., 2012).
Reprinted with permission from Springer.

This is because the radio-opaque dye used in angiography will follow the straighter, faster paths through the system rather than the more circuitous routes that make up the majority of the malformation. Bruits, unusual sounds in the vasculature caused by turbulence, can sometimes be detected in the presence of these malformations (Lanzino et al., 1994).

Although these formations are often asymptomatic, they may cause central nervous symptoms such as seizures and ischemia, among other conditions. Localized effects such as hearing and vision loss have also occurred (Lasjaunias et al., 1986). Treatment for complications associated with AVMs is focused on treating the symptoms of the morbidity. Embolization and resection are used in cases where the physical presence of the AVM poses a concern, such as the structure contacting nerves or, in the presence of endothelium weakening or calcification, a potential for rupture. Treatment typically
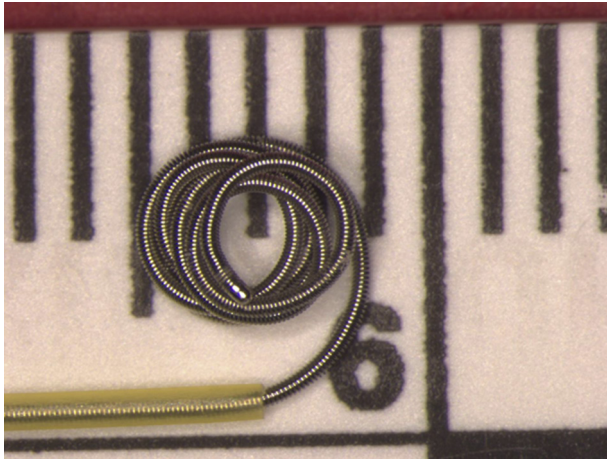
Figure 20.11 Image of a GDC® Ultrasoft detachable coil currently sold by Stryker Corporation. Each line on the scale in the background corresponds to 1 mm.

involves both embolization and resection, sometimes called skeletonization. Embolization is typically done preoperatively to lessen the risk of rupture during the resection procedure and is not usually used as a standalone treatment (Gupta and Periakaruppan, 2009; Ogilvy et al., 2001).

20.2.3.2   Aneurysms

In its simplest form an aneurysm is a dilation of a vessel, typically an artery, at a threshold diameter of about 1.5 times larger than the normal vessel. Abdominal aortic aneurysms (AAA) occur in 5–6% of men and 1–2% of women over the age of 65. The annual mortality rate associated with AAA rupture is approximately 13,000 deaths per year, but this is often thought to be an underestimation (Brown et al., 2003; Kent, 2014; Norman and Powell, 2010). Intracranial aneurysms are the second most common aneurysm, occurring in 3% of the adult population (Morita, 2014), followed by peripheral aneurysms (Lawrence et al., 1995). Like vascular malformations, aneurysms are often asymptomatic but can present with ischemia or other symptoms stemming from increased pressure on the CNS. The most serious complications associated with aneurysms occur when they rupture. Loss of integrity in an intracranial aneurysm can lead to subarachnoid hemorrhage, which has a 30 day mortality rate of 45%, which is mild compared to the 90% mortality rate of a ruptured abdominal aortic aneurysm (Assar and Zarins, 2009; Bederson et al., 2000; Walker et al., 2010). Treatment is indicated for intracranial aneurysms of any size if they are symptomatic, but oftentimes no intervention is recommended for aneurysms smaller than 10 mm due to a limited likelihood of rupture. The age of the patient is also a significant consideration in determining whether intervention is needed and whether the patient can withstand the trauma associated with surgical intervention.

Currently embolic coils, such as those shown in Figure 20.11, are the standard treatment for virtually all aneurysms with the exception of AAAs (Bederson et al., 2000).

Intervention is indicated for abdominal aortic aneurysms if it becomes symptomatic, once the diameter of the aneurysm has reached 5.5 cm, is 250% larger than the patient's normal aortic diameter, or has a growth rate of greater than 1 cm per year. The predominant treatment for an AAA involves the placement of a branched graft spanning a length longer than the dilated portion of the aorta. Occasionally embolic devices are placed in the lumen between the vessel wall and the graft to prevent endoleak, a continued flow of blood into the aneurysm sac rather than through the graft that can potentially lead to aneurysm rupture (Walker et al., 2010).

20.2.3.3 Venous insufficiency

When venous valves are weakened and allow regurgitation of blood, there is an abrupt increase in venous pressure (Alguire and Mathes, 1997; Beebe-Dimmer et al., 2005; Hjelmstedt, 1968). The increased pressure and resulting venous hypertension are the primary cause of chronic venous insufficiency (CVI) (Belcaro et al., 1989; Browse, 1986; Browse and Burnand, 1982; Hjelmstedt, 1968). The continued prevalence of hypertension leads to dilation of the incompetent veins, resulting in varicose veins like those shown in Figure 20.12, the most common manifestation of CVI (Alguire and Mathes, 1997; Bhutia et al., 2008; McLafferty et al., 2007). If left untreated, CVI can cause dramatic cosmetic changes in skin, lower limb pain, edema, deep vein thrombosis, and ulcers (Adhikari et al., 2000; McLafferty et al., 2007; Robertson et al., 2008; Schoonover et al., 2009; Tran and Meissner, 2002; Van Den Bos and

Figure 20.12 Pretreatment image of a patient with varicose veins as a result of CVI (Kapoor et al., 2010).
Reprinted with permission from Springer.

de Maeseneer, 2012). Approximately 400,000–500,000 Americans with CVI have or will develop venous ulcers, typically referred to as venous stasis ulcers (Callam et al., 1985; Coon et al., 1973; Dalen et al., 1986). Venous ulcers account for the majority of annual health care costs associated with CVI, which are more than 1 billion dollars in the United States and over 650 million dollars in the United Kingdom (Nicolaides et al., 2000). The potential consequences of not treating CVI in a timely manner have prompted physicians to adopt multiple treatment modalities.

The current gold standard for treating CVI is endovenous ablation (EVA) (Van Den Bos and de Maeseneer, 2012). EVA makes use of a radiofrequency generator or laser energy to denude the endothelium of the target vessel and cause fibrous obliteration of the vessel lumen (Bhutia et al., 2008; Van Den Bos and de Maeseneer, 2012). Another common technique used to treat CVI is sclerotherapy, in which a liquid or foam detergent is injected into the vessel that chemically damages the endothelium and subsequently causes fibrosis (Deatrick et al., 2010). Both sclerotherapy and EVA have demonstrated usefulness in treating CVI; however, each treatment comes with its own drawbacks. More than 20% of patients receiving sclerotherapy have to undergo retreatment for recurrent varicose veins, which is greater than the retreatment rate of conventional surgical ligation and stripping procedures (Darvall et al., 2011; Negus, 1993). In EVA procedures, multiple injections of local anesthesia are required, followed by injections of tumescent anesthesia. The anesthesia helps prevent pain caused by the laser heating, compresses the vein to make fibrous obliteration of the lumen easier, and also acts as a heat sink around the treatment vessel to minimize thermal damage to surrounding tissue (Min et al., 2003). The number of shots required for this form of treatment results in significant patient pain and discomfort, which is reported in 100% of cases (Van Den Bos and de Maeseneer, 2012). Although the equipment used in endovenous ablation and the substances used in sclerotherapy continue to evolve, these issues still persist.

20.2.3.4 Patent foramen ovale

In utero, there are ostia that allow a patent connection between the left and right atria, which allows oxygenated blood from the maternal circulation to enter the left atrium of the fetus. This connection is known as the foramen ovale, and on the baby taking its first breath, the increased pressure in the left side of the heart permanently fuses the septum primum and septum secundum over the foramen ovale in 80% of cases. In the other 20% of cases, the septa do not completely occlude the foramen ovale, resulting in a condition known as a patent foramen ovale (PFO), which is demonstrated in Figure 20.13 (Kumar et al., 2013). PFOs frequently go undiagnosed for a number of years since patients typically show no clinical symptoms. However, if steps are not taken to occlude the PFO, paradoxical embolisms may occur where emboli from the peripheral veins enter the arterial circulation through the PFO shunt—a well-known cause of cryptogenic stroke (Kasper et al., 1992; Kerut et al., 2001). Studies have also shown that PFOs may be to blame for a large percentage of patients who experience migraines. In one study of 162 patients, 35% of individuals diagnosed with a PFO concurrently experienced frequent migraines (Reisman et al., 2005).
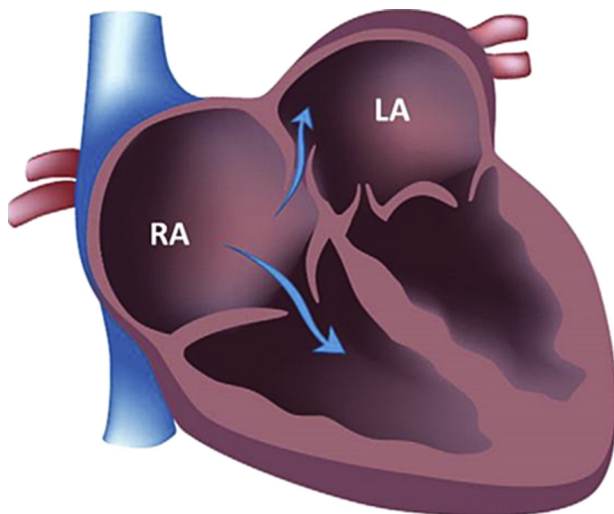
Figure 20.13 Demonstration of the right to left shunt between the atria within the heart caused by a PFO, which can lead to paradoxical emboli and cryptogenic stroke (Leong et al., 2013). Reprinted with permission from Elsevier.

To eliminate the risks associated with a PFO, physicians used to attempt surgical closure of the PFO, but this technique is virtually never used in current practice (Leong et al., 2013; Strunk et al., 1987). Instead, PFOs are now treated using a transcatheter approach in which an embolic device is placed between the atria to prevent blood flow from the right atrium directly into the left atrium (Knerr et al., 2014). This procedure has become known as the simplest procedure in interventional cardiology, primarily due to the low incidence of surgical complications and the effectiveness of current devices (Meier, 2010). Reisman et al. have demonstrated that PFO occlusion results in complete resolution of migraine symptoms in 56% of patients 1 year posttreatment, and patients reported having 80% fewer migraine episodes per month (Reisman et al., 2005). With regard to recurrent neurological events (RNE), such as cryptogenic stroke and transient ischemic attacks from paradoxical thromboembolisms, transcatheter embolization of the PFO resulted in an 84% reduction in RNE compared to medical treatment with only pharmaceuticals (Agarwal et al., 2012). The benefits of PFO closure have illuminated the necessity for percutaneous stable occlusion of PFOs, especially in elderly patients who are more susceptible to peripheral thromboembolisms.

One of the most widely used and successful devices for percutaneous PFO closure is the Amplatzer PFO Occluder (St. Jude Medical Inc., St. Paul, MN), which is a device consisting of two nitinol discs that contain a polypropylene mesh (Meier, 2009). These types of devices have demonstrated complication rates of less than 5% and procedural success in 100% of cases (Taaffe et al., 2008). However, only 65% of the patients showed complete occlusion of the foramen ovale at 30 day follow-up. New generations of PFO closure devices could benefit from tissue scaffold technologies to allow rapid healing and tissue integration to achieve complete occlusion of PFOs at

earlier time points. Another likely trend in future PFO devices is the use of biodegradable materials, which would allow treatment of younger patients since no permanent metallic structure would remain in the heart during its growth and development. The potential to treat patients earlier on would provide preventative measures that would dramatically decrease the likelihood of cryptogenic stroke and transient ischemic attacks as a result of a PFO.

20.3 Why shape memory polymer scaffolds?

20.3.1 Biocompatibility

Immediately on implantation and exposure of a material to the host, biocompatibility is primarily dependent on the material, as the cell–polymer and polymer–protein interactions are the dominant causes of host response; after the material begins to degrade, biocompatibility becomes a function of the bulk material. Implant size, geometry, surface chemistry, roughness, surface energy, porosity, composition, sterility, and chemical composition are major factors in determining overall biocompatibility (Pavithra and Doble, 2008). While many advances have been made to improve thromboresistance or to reduce inflammatory responses of implantable materials, there still exists a great need for understanding how and why the body responds to certain stimuli more intensely compared with others (Ratner, 2007). Without dealing with a specified definition of biocompatibility, several materials are presented that have been proven to be biocompatible.

Polyhedral oligomeric silsesquioxane (POSS) core and poly(D,L-lactide) (PLA) were fabricated into PLA-grafted nanocomposites with shape memory capabilities and implanted into rats. The degradation rate was directly proportional to the length of the PLA segments. These materials exhibited mild inflammatory response on implantation, and a secondary acute response with degradation. At 1 year follow-up, the inflammatory response was resolved and no pathologic abnormalities were found in any organs. The results indicate that these materials have promise as scaffolds for tissue repair and medical devices (Filion et al., 2011). The use of POSS has also been proposed for nanocomposite films on metallic stents for prevention of late stage thrombosis (Bakhshi et al., 2011).

SMP foams evaluated by Sokolowski using the Mitsubishi thermoplastic SMP composition have showed no cell lysis, cytotoxicity, or mutagenicity. They also showed good neointimal formation over the aneurysm neck when implanted as a potential aneurysm filling device, and explanted devices showed favorable ingrowth of cells (Sokolowski, 2005). In a similar study, polyurethane SMPs developed by Wilson et al. have demonstrated biocompatibility, with little variation seen between the thermoplastic and the thermoset compositions. Thermoplastic SMPs showed higher cytokine production compared with thermosets, but both compositions showed no contact activation, thrombin, or plasmin generation (Cabanlit et al., 2007; Wilson et al., 2007). SMP foams based on this composition have also shown excellent biocompatibility when tested using porcine models. These foams

demonstrate very low inflammation response compared with FDA-approved silk and polypropylene sutures after 4 weeks. The foams also have organized collagen throughout the entire volume of the foam, and the inflammatory response was substantially reduced compared with the suture materials (Rodriguez et al., 2014; Singhal et al., 2012).

20.3.2 Thrombus formation

The mechanism of thrombus formation and the effects of polymer surfaces are briefly discussed here (Chen et al., 2008; Furie and Furie, 2008; Gorbet and Sefton, 2004; Ratner, 2007). Endothelial cells generally produce three thromboregulators: nitric oxide, prostacyclin, and ectonucleotides CD39. These products prevent thrombus formation until they are disrupted. When the endothelium is disrupted, tissue factors and collagen that are exposed to blood flow begin initiating thrombus formation. This occurs due to the accumulation of activated platelets, a result of the exposed collagen, and the generation of thrombin, which simultaneously activates platelets and converts fibrinogen into a fibrin mesh. A number of other factors interact to allow for platelet adhesion to the injury site, with certain environmental or chemical conditions providing opportunities for either the collagen or the tissue factors dominating the pathway to cause thrombogenesis. Due to these redundancies in the pathway to clotting, this can provide difficulties in preventing clot formation. This also provides a beginning explanation for why prevention of thrombus formation on materials surface is so difficult, even with specialized coatings (Furie and Furie, 2008). When a foreign surface comes into contact with blood, factor XII is converted into factor XIIa, which is a part of the intrinsic clotting system. Eventually, this results in factor X being cleaved into factor Xa, which will in turn cleave prothrombin into thrombin. Thrombin activates the monomer fibrinogen, which polymerizes into fibrin. Fibrin as a polymer is not completely stable until factor XIIIa is present to stabilize it. Additionally, as the clot is forming the matrix will be supported by platelets and fragments attaching to the polymer. The control mechanisms for clot formation include control of local flow, surface-mediated controlled release of catalyst, release of thrombus inhibitors (antithrombin III, tissue factor pathway inhibitor, etc.), and degrading coagulation factor release (fibrinolytic enzyme plasmin, which can degrade fibrinogen and fibrin, as well as inactivate cofactors V and VIII). In this way, blood flow normally does not cause significant clotting to occur until the tissue is damaged, but once damage is detected, clotting can rapidly occur. Due to this, the presence of certain material surfaces can cause continual clotting and result in eventual failure of the device. By altering the surface chemistry or present local chemical factors near the material, these failures can be mitigated. Several research trends attempting this are presented as well (Ratner, 2004; Esmon, 2009).

At the end of healing, fibrosis or fibrous encapsulation is the ideal response for an embolic device. The process begins with injury to the tissue and implantation of the material. Thrombi, or blood clots, begin to form immediately based on the processes previously described, over the course of minutes to hours. This is enhanced by changes in blood flow patterns, permeability of blood vessels, and composition

of the fluid flowing through the area of interest. The thrombus matrix is composed primarily of fibrin, activated platelets, inflammatory cells, and endothelial cells. Platelets in the matrix release a series of factors that contribute to the recruitment of fibroblasts; monocytes and lymphocytes also assist in recruiting fibroblasts. The fibrin in the clot, which has fibronectin bound to it, is cross-linked by factor XII, and other adhesive factors provide a means for cell adhesion and proliferation into the clot. During acute inflammation primarily neutrophils are recruited to the site of device implantation, which will see the initiation of phagocytosis, recruitment and attachment of cells to the foreign material, and the release of degradation-inducing chemicals near the implant surface. This is followed by chronic inflammation, which involves the recruitment of monocytes, lymphocytes, and plasma cells; the other path is the formation of granulation tissue, which begins to occur within days after implantation with the recruitment and proliferation of fibroblasts into the target site. Granulation tissue contains vascular buds, which is recruited by the fibrin present in the thrombus. Collagen and proteoglycans begin to organize in the clot matrix due to the fibroblasts. As granulation tissue progresses, collagen becomes the dominant tissue type present and begins to contract. Based on the chemical structure of the material and the protein adhesion to the material on implantation, the foreign body response will occur to varying degrees. The number of macrophages present at the site will depend on these factors, as well as the irritation that the material causes. Macrophage fusion into foreign body giant cells, along with remaining clot, will result in encapsulation of the material. The ideal final healing stage for embolic devices is fibrous encapsulation or full reintegration; passive surfaces will have very little or no encapsulation and so will be fully reintegrated into the host. Porous media are an excellent choice for resolutions that do not involve encapsulation, as the porous structure provides a matrix that allows for cellular infiltration and connective tissue proliferation throughout the entire device (Anderson, 2001; Dvorak et al., 1987).

Polyurethanes are a preferred material for blood contacting applications due to superior hemo- and biocompatibility, which are due to the surface properties, chemical structure, interfacial free energy, balance of hydrophobicity with hydrophilicity, and basic surface topography. All of these factors can be tailored in other polymer compositions using a variety of techniques to improve overall compatibility or to tailor the *in vivo* response to the material. In SMP foams, the scaffold morphology and porosity create areas of low blood shear rates and recirculation zones, which are necessary for rapid clotting. Figure 20.14 shows SMP foam threaded over nitinol and platinum coil devices that were delivered endovascularly to a porcine sidewall aneurysm. The explant of the devices showed organized, stable thrombus throughout the entire volume of treatment devices, which completely occluded the aneurysm. These porous media structures provide an effective means of creating flow stasis, but then provide a structural entity to allow rapid cellular infiltration and swift reintegration of the tissue/material matrix with the surrounding tissue (Anderson, 2001). Even with the time required to achieve complete healing at the implantation site, faster stabilization of the clot will create superior clinical outcomes and shorter times until the patient is ambulatory without the risk of thromboembolism.
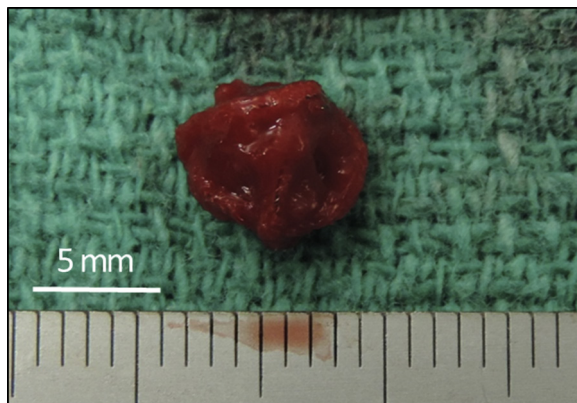
Figure 20.14 Explanted SMP foam-over-coil devices that were delivered using a transcatheter approach to occlude a carotid porcine sidewall aneurysm. Explant occurred less than 2 h after treatment began. Visible throughout the volume of devices is stable thrombus formation. Image provided courtesy of Anthony J. Boyle.

20.3.3 Recanalization

One of the most concerning complications associated with vascular embolization is recanalization. Recanalization is the reestablishment of blood flow into a formerly occluded region (Hall et al., 1989). This phenomenon destabilizes the occluded region and may lead to significant rebleeding at the treatment site. As a common metric used in describing the efficacy of embolization techniques, recanalization is the primary reason for retreatment procedures. Recanalization rates as high as 34.3% have been recorded for endovascular aneurysm coiling (Cho et al., 2012). This statistic highlights the need to continue improving embolization technologies to reduce the prevalence of recanalization.

Experiments have shown that the size of the vascular anomaly being occluded, as well as the total volumetric filling of the embolic device, plays a critical role in the likelihood of recanalization (Pierot et al., 2008). Recanalization is thought to initiate in the first weeks after treatment. On observing fibrin matrix replacement with a collagen matrix, recanalization can no longer occur out to 3 months (Kroon et al., 2002; Raymond et al., 2004). However, until collagen replacement of the fibrin matrix, the potential for angiogenesis and the generation of microvessels that may cause recanalization exists. Some researchers have demonstrated the ability to prevent angiogenesis by using radiofrequency energy to completely denude the endothelium of the implantation site (Raymond et al., 2004). Although this method proved effective in preventing recanalization, concerns of thromboembolism, long-term efficacy, and overall clinical safety have prevented widespread adoption of this technique.

In preliminary animal studies that sought to treat surgically induced carotid sidewall aneurysms in a porcine model, polyurethane SMP scaffolds proved to be highly advantageous materials to create long-term, stable occlusion without recanalization (Rodriguez et al., 2014). The histology performed in this study 90 days postimplantation
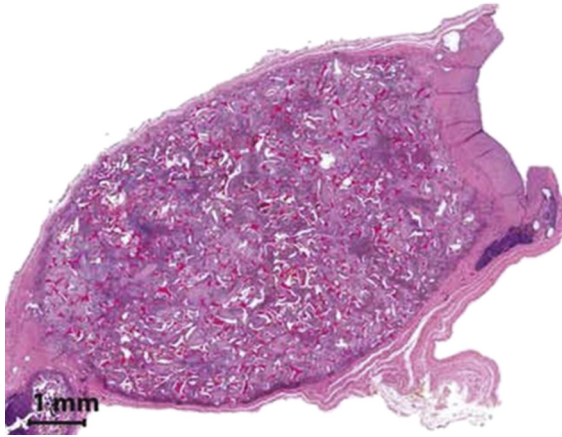
Figure 20.15 H&E stain of a porcine carotid sidewall aneurysm filled with a polyurethane SMP foam 90 days postimplantation demonstrating complete endothelialization across the aneurysm neck and 75% connective tissue within the aneurysm sac (Rodriguez et al., 2014). Reprinted with permission from John Wiley and Sons.

demonstrated a mature endothelial layer completely isolating the aneurysm from the parent vessel, and dense connective tissue deposition throughout the entire volume of the device, as shown in Figure 20.15.

The organized collagen shown throughout the entire volume of the SMP scaffold and the neointimal layer across the aneurysm neck both support the notion that vascular anomalies treated with this material are highly unlikely to require retreatment as a result of recanalization.

20.3.4 Endovascular treatments

SMP technology allows devices to be delivered through small catheters and then expand to fill large volumes. Non-SMP foams experience excessive friction when navigated through the catheter, whereas SMP foams can counteract this with the shape memory effect. It has been reported that when technologies like Gelfoam® are delivered via catheter, it is possible that smaller particles of Gelfoam® embolize and flow downstream creating a thromboembolism (Vaidya et al., 2008). This creates a potential problem for the physician since Gelfoam® is typically cut into numerous pieces before being delivered through a catheter. This methodology prompts the user to cut large enough sections to prevent embolizing downstream of the treatment region on ejecting the Gelfoam® from the catheter, but not large enough to cause excessive friction inside the catheter to prevent advancement to the desired location.

A common problem with expandable implants that are delivered through catheters is failure to deliver the device if it expands too quickly and can no longer be advanced. Because of this complication, a working time must be defined. Working time is the amount of time from device introduction into the catheter to the time at which the device can no longer be retracted or advanced within the catheter (Nambiar et al., 2008;

Guo et al., 2011). The first generation of HydroCoil® implants (MicroVention, Inc., Tustin, CA) was limited to a 5 min working time, which proved to be an insufficient amount of time to place the implant at the desired location within the neurovasculature (Guo et al., 2011). Newer generations of hydrogel-containing coils, such as HydroSoft® (MicroVention, Inc., Tustin, CA), have at least 30 min of working time. As expandable implants, working time must also be considered when designing an SMP scaffold device that will be delivered via catheter. With a 100× volume expansion ratio, SMP foams can exert substantial frictional force on the inner lumen of the catheter if the working time is exceeded. This can lead to an inability to advance the device to the treatment region or improper placement of the device at the target region.

Despite the necessity to adhere to a defined working time when using SMP devices, they offer the enormous advantage of being able to crimp to a diameter of less than 1 mm, be delivered using a minimally invasive catheterization technique, and expand to a final diameter of 10 mm. To put this advantage in terms of surface area, a 1-cm-long SMP scaffold with a 10 mm diameter provides approximately 14,000 mm^2 of surface area. A 1 cm length of a typical large bare metal coil used for peripheral occlusion provides approximately 40 mm^2 of surface area. Both devices can be delivered through a typical 5 French catheter, but the SMP foam device expands on deployment to provide three orders of magnitude greater surface area than the bare metal coil. It is well known that increased surface area of a procoagulant material results in increased activation of the clotting cascade, which means that an increase in surface area likely results in reduced time to occlusion for these embolic materials (Margolis, 1957). However, a direct comparison of acute time to occlusion has not yet been performed between embolic coils and SMP foams.

20.4 The future of shape memory polymer scaffolds

20.4.1 Tissue engineering applications

The shape memory behavior of an SMP makes it a very desirable material for use in biomedical applications. Thermally activated SMPs can be programmed and stored in a small secondary shape, and on introduction to the body and water plasticization, recover their large original shape (Beilvert et al., 2014). This property of SMPs can be harnessed for minimally invasive surgery and tissue engineering scaffolds (Beilvert et al., 2014). However, cell compatibility of an SMP biomaterial needs to be extensively understood to determine its feasibility as a short-term or long-term implant and the impact of its SME on cells.

Studying the inflammatory response and biocompatibility of an SMP scaffold was conducted by Filion et al. This group developed SMPs with POSS nanoparticle cores as the net points and PLA with varying chain lengths as the switching segment (Filion et al., 2011). SMP degradation and the *in vivo* inflammatory response were directly related. Longer PLA segments resulted in a more densely packed polymer chain structure that was less prone to hydrolysis (Filion et al., 2011). This delayed degradation onset resulted in a late acute inflammatory response, which allowed for tunable

degradation profiles that could be useful for numerous tissue engineering applications (Filion et al., 2011).

While biocompatibility studies are critical for using SMP as a biomaterial, cell adhesion and proliferation on the material also need to be understood. Davis et al. developed a thermoresponsive 2D cell culture system using the commercially available SMP Norland Optical Adhesive 63 (NOA-63, Norland Products, Cranbury, NJ, USA). This adhesive is a polyurethane that is end-linked with a thiol-based cross-linker using UV click chemistry (Davis et al., 2011). The group observed changes in cell behavior as a result of surface shape memory. The substrates were synthesized in a flat topography but shape set so that the secondary shape contained grooves. Mouse embryonic fibroblasts were then seeded onto the grooved substrates. The cells became aligned in the grooved topography but scattered into random alignment after the substrate was actuated such that the topography returned to its flat, primary shape. Nevertheless, the cells maintained 95% viability and no detachment from the substrate was observed (Davis et al., 2011). This work demonstrated the use of SMPs to control cell activity and their potential use as tissue engineering scaffolds.

Similarly, Neuss et al. studied different cellular interactions with oligo(ε-caprolactone) dimethacrylate. The group utilized mouse fibroblasts, human mesenchymal stem cells, human omentum majus cells, and rat omentum majus cells for this study (Neuss et al., 2009). Overall, the cells maintained good viability and attachment over a time period of 3 weeks, supporting the SMP's suitability for medical applications (Neuss et al., 2009). However, the thermal input and the shear forces necessary for shape change resulted in subconfluent and apoptotic regions (Neuss et al., 2009). These studies serve as a platform for the development and utility of SMP scaffolds for tissue engineering applications due to their biocompatibility and cell attachment/proliferation. Further investigations may explore whether the shape changing ability of SMPs can drive stem cells down specific lineages or express specific phenotypes. However, optimization of these materials needs to be conducted such that the transition temperature is close to physiological temperature, therefore minimizing adverse effects from overheating the surrounding tissue.

20.4.2 Controlled pharmaceutical release

One area where SMPs have a new frontier for innovation is in the design and fabrication of controlled release platforms for pharmaceuticals. Drug-eluting stents have shown reduced rates of restenosis in patients, generally through a polymer-coated stainless steel stent; the drug of choice is sirolimus or paclitaxel, which can limit migration of smooth muscle cells to reduce neointimal hyperplasia. Several good reviews of drug-eluting stents cover topics in greater detail (Sousa et al., 2003; Brieger and Topol, 1997; Mani et al., 2007). A brief overview of notable studies is presented here. A study by M.C. Chen demonstrated the viability of an SMP stent made from chitosan and epoxy with a heparin coating and sirolimus elution. The surface coating reduced the platelet adhesion to the stent while providing a diffusion barrier for drug elution that allowed for a sustained release profile for the sirolimus. Significant

reduction in neointimal formation was seen when implanted in rabbits compared with noneluting stents (Chen et al., 2009).

Another SMP system from star caprolactone cross-linked with hexamethylene diisocyanate that eluted theophylline was synthesized in the same pot as the drug, with up to 20% wt of the drug included in the polymers. This method was used to achieve sustained release for approximately 1 month without bolus release of the drug when tested in an *in vitro* setup. However, this method of drug loading altered the mechanical and shape memory properties of the material; 20% loading demonstrated decreasing elongation to break below 100% and sufficient rigidity to inhibit shape memory. At approximately 10% loading, there were no significant mechanical changes reported, and the shape fixity and recovery were approximately 99%. Loading of the drug into the polymer did not seem to alter the pore size of the material, as the release profiles were similar for 10% and 20% drug loading (Nagahama et al., 2009). Salicylic acid and adipic acid were also used to produce a bioabsorbable polymer, with sirolimus included as a drug for elution. This stent demonstrated a reduction in angiographic stenosis compared with stents without the sirolimus (Jabara et al., 2008). It has been suggested the polymers used for drug elution stents may cause inflammation in proportion to the mass of the polymer present. It has been shown that the use of drug-eluting stents lengthen time to resolution of conditions, as fibrin thrombus is often found at time points greater than those seen in untreated arteries during restenosis therapies. Another avenue for the use of drug elution is in cellular migration and proliferation. Gene suppression therapy has had some success in this regard, using rapamycin and paclitaxel, drugs which can act on a number of cellular targets as well as interrupt cell cycle progression (Schwartz et al., 2004).

The shape memory behavior of SMPs opens new doors for designing controlled release platforms in the pharmaceutical industry. The ability to actuate these polymers via light, heat, or magnetic energy offers the opportunity to implant an SMP containing a pharmaceutical reservoir and actuate the device using noninvasive means. On actuation, miniature SMP doors, latches, apertures, or pores could be opened without requiring the physician to break the patient's skin. This technique could be used to administer multiple boluses of a drug while minimizing patient pain and potentially providing more targeted, local delivery of the drug. The actuation rate of SMPs is also highly tunable. This means that an SMP device loaded with a pharmaceutical agent could be delivered using a minimally invasive endovascular approach, and designed so that it only actuates and releases the pharmaceutical after a given duration of time when the device reaches a specific location in the vasculature. The potential for combining controlled release theories and SMP technology is virtually limitless, and this specialty is likely to be a very active area of research in the future.

20.4.3 Degradable shape memory polymer scaffolds

SMPs, like other polymers, can be biostable or degradable. A substantial amount of the work done on degradable SMP scaffolds has been performed by Langer or Lendlein, and is too great to be covered sufficiently here (Ullm et al., 2014; Nochel et al., 2014; Schmidt et al., 2014; Friess et al., 2014; Lendlein et al., 2014; Yang et al., 2013;

Nochel et al., 2013; Wischke et al., 2013; Feng et al., 2013; Wang et al., 2013; Kolewe et al., 2013; Mizrahi et al., 2013; Heller et al., 2013; Neal et al., 2013; Pereira et al., 2013; Mizrahi et al., 2012; Tekin et al., 2011; Dvir et al., 2011; Cheng et al., 2011). A small selection of their work, as well as that of several other significant findings as they relate to cardiovascular applications, is presented. The Langer group developed a series of poly(polyol sebacate) SMPs, with tailorable transition temperatures between 7 and 40 °C. *In vitro* degradation and compatibility of these materials showed similar behavior to poly(lactide-*co*-glycolic acid). These materials would be ideal for a variety of medical devices, including surgical sutures to tighten at body temperature, cardiovascular stents to expand on arrival at the implant site, or other devices that require a transition at body temperature (Bruggeman et al., 2008).

A very exciting application of biodegradable polymers is in the field of cardiovascular devices. Guglielmi detachable coils (GDCs) have been the interventional device of choice for intracranial aneurysm filling, but there are problems with healing and recanalization when using these devices. Murayama et al. developed a biodegradable polymer poly(glycolic-L-lactic acid) over a GDC coil and compared this device with standard GDCs in experimentally created aneurysms in porcine models. Despite having a lower packing density in the aneurysm sac after the implantation procedure, the biodegradable GDC hybrids demonstrated complete occlusion of the aneurysm, whereas standard GDCs did not. There was a distinct separation between the parent vessel and the hybrid coil-packed mass using angiography at 3 months, which was not visible when using standard GDCs, indicating improved healing response with the hybrids. Additionally, the hybrid-filled aneurysms were smaller and softer, similar to tissue, 3 months after the implantation. After 3 months, GDC-filled aneurysms were a hard, solid mass distinctly dissimilar from surrounding tissue. Finally, mildly organized connective tissue was present 2 weeks postimplantation, as well as only a mild immune response for hybrid coils. Standard GDCs showed the same immune response, but no connective tissue organization (Murayama et al., 2001).

Copolymers of lactide, glycolide, and caprolactone have been synthesized in block copolymer compositions that demonstrated shape memory while also possessing degradability. These materials showed rapid degradation rates in temperature-controlled PBS, with total mechanical property loss within 2 months based on molecular weight of the lactide and glycolide–caprolactone segments. For tissue scaffolds, this is ideal as the loss of mechanical properties could be tailored to allow for material degradation as connective tissue infiltrates the material (Min et al., 2005).

Hyperbranched PCL as a soft segment and hard segment of poly((*R*)-3-hydroxy-butyrate-*co*-(*R*)-3-hydroxyvalerate) were compared with linear PCL-based SMPs. These polymers were poly(ester urethanes), using aromatic diisocyanates, showed good biocompatibility, and allowed for cellular attachment and growth on the surface. The use of these materials in stents was examined, showing quick recovery from the secondary shape to the original shape at body temperature, indicating good promise for these materials in stent applications (Xue et al., 2010). Other compositions and composite materials have also shown a variety of degradation profiles, thermomechanical properties, and biocompatibilities (Xue et al., 2010). Adding a degradation functionality to SMPs provides a means of developing minimally invasive tissue scaffolds

and medical devices that do not require a second medical procedure for removal. As the presented works indicate, a wide variety of chemical compositions and properties can be obtained for SMPs, including the mechanism and rate of degradation. For cardiovascular applications, materials can be produced that have tunable mechanical and thermal properties with selective coagulation and degradation times while promoting cellular ingrowth and proliferation. With SMPs, the promises made by tissue engineering, to provide methods for the body to heal and repair itself with minimal interference from external sources, are becoming realized. As this field progresses, healing responses and clinical outcomes for patients will begin to improve.

References

Alguire, P.C., Mathes, B.M., 1997. Chronic venous insufficiency and venous ulceration. Journal of General Internal Medicine 12, 374–383.

Adhikari, A., Criqui, M.H., Wooll, V., Denenberg, J.O., Fronek, A., Langer, R.D., Klauber, M., 2000. The epidemiology of chronic venous diseases. Phlebology 15, 2–18.

Anderson, J.M., 2001. Biological responses to materials. Annual Review of Materials Research 31, 81–110.

Assar, A.N., Zarins, C.K., 2009. Ruptured abdominal aortic aneurysm: a surgical emergency with many clinical presentations. Postgraduate Medical Journal 85, 268–273.

Agarwal, S., Bajaj, N.S., Kumbhani, D.J., Tuzcu, E.M., Kapadia, S.R., 2012. Meta-analysis of transcatheter closure versus medical therapy for patent foramen ovale in prevention of recurrent neurological events after presumed paradoxical embolism. Journal of the American College of Cardiology 5, 777–789.

Aljawish, A., Muniglia, L., Jasniewski, J., Klouj, A., Scher, J., Chevalot, I., 2014. Adhesion and growth of HUVEC endothelial cells on films of enzymatically functionalized chitosan with phenolic compounds. Process Biochemistry 49, 863–871.

Browse, N.L., Burnand, K.G., 1982. The cause of venous ulceration. Lancet 2, 243–245.

Browse, N.L., 1986. The etiology of venous ulceration. World Journal of Surgery 10, 938–943.

Belcaro, G., Grigg, M., Rulo, A., Nicolaides, A., 1989. Blood flow in the perimalleolar skin in relation to posture in patients with venous hypertension. Annals of Vascular Surgery 3, 5–7.

Brieger, D., Topol, E., 1997. Local drug delivery systems and prevention of restenosis. Cardiovascular Research 35, 405–413.

Bederson, J.B., Awad, I.A., Wiebers, D.O., Piepgras, D., Haley, E.C., Brott, T., Hademenos, G., Chyatte, D., Rosenwasser, R., Caroselli, C., 2000. Recommendations for the management of patients with unruptured intracranial aneurysms – a statement for healthcare professionals from the Stroke Council of the American Heart Association. Circulation 102, 2300–2308.

Bendok, B.R., Levy, E.I., Hanel, R.A., Qureshi, A.I., Guterman, L.R., Hopkins, N.L., 2003. Brain AVM embolization. Operative Techniques in Neurosurgery 2, 64–74.

Brown, P.M., Zelt, D.T., Sobolev, B., 2003. The risk of rupture in untreated aneurysms: the impact of size, gender, and expansion rate. Journal of Vascular Surgery 37, 280–283.

Beebe-Dimmer, J.L., Pfeifer, J.R., Engle, J.S., Schottenfeld, D., 2005. The epidemiology of chronic venous insufficiency and varicose veins. Annals of Epidemiology 15, 175–184.

Bilbao, J.I., Martinez-Cuesta, A., Urtasun, F., Cosin, O., 2006. Complications of embolization. Seminars in Interventional Radiology 23, 126–142.

Bhutia, S.G., Balakrishnan, A., Lees, T., 2008. Varicose veins. Journal of Perioperative Practice 18, 346–353.

Bruggeman, J.P., de Bruin, B.J., Bettinger, C.J., Langer, R., 2008. Biodegradable poly(polyol sebacate) polymers. Biomaterials 29, 4726–4735.

Boateng, J.S., Matthews, K.H., Auffret, A.D., Humphrey, M.J., Stevens, H.N., Eccleston, G.M., 2009. In vitro drug release studies of polymeric freeze-dried wafers and solvent-cast films using paracetamol as a model soluble drug. International Journal of Pharmaceutics 378, 66–72.

Bakhshi, R., Darbyshire, A., Evans, J.E., You, Z., Lu, J., Seifalian, A.M., 2011. Polymeric coating of surface modified nitinol stent with POSS-nanocomposite polymer. Colloids and Surfaces B: Biointerfaces 86, 93–105.

Beilvert, A., Chaubet, F., Chaunier, L., Guilois, S., Pavon-Djavid, G., Letourneur, D., Meddahi-Pelle, A., Lourdin, D., 2014. Shape-memory starch for resorbable biomedical devices. Carbohydrate Polymers 99, 242–248.

Coon, W.W., Willis 3rd, P.W., Keller, J.B., 1973. Venous thromboembolism and other venous disease in the Tecumseh community health study. Circulation 48, 839–846.

Chuang, V.P., Wallace, S., Gianturco, C., Soo, C.S., 1981. Complications of coil embolization: prevention and management. American Journal of Roentgenology 137, 809–813.

Callam, M.J., Ruckley, C.V., Harper, D.R., Dale, J.J., 1985. Chronic ulceration of the leg: extent of the problem and provision of care. British Medical Journal (Clinical Research Edition) 290, 1855–1856.

Cameron, N.R., 2005. High internal phase emulsion templating as a route to well-defined porous polymers. Polymer 46, 1439–1449.

Cabanlit, M., Maitland, D., Wilson, T., Simon, S., Wun, T., Gershwin, M.E., Van de Water, J., 2007. Polyurethane shape-memory polymers demonstrate functional biocompatibility in vitro. Macromolecular Bioscience 7, 48–55.

Chen, H., Yuan, L., Song, W., Wu, Z.K., Li, D., 2008. Biocompatible polymer materials: role of protein-surface interactions. Progress in Polymer Science 33, 1059–1087.

Chen, M.C., Chang, Y., Liu, C.T., Lai, W.Y., Peng, S.F., Hung, Y.W., Tsai, H.W., Sung, H.W., 2009. The characteristics and in vivo suppression of neointimal formation with sirolimus-eluting polymeric stents. Biomaterials 30, 79–88.

Carradice, D., Mekako, A.I., Mazari, F.A.K., Samuel, N., Hatfield, J., Chetter, I.C., 2011. Clinical and technical outcomes from a randomized clinical trial of endovenous laser ablation compared with conventional surgery for great saphenous varicose veins. British Journal of Surgery 98, 1117–1123.

Cheng, H., Hill, P.S., Siegwart, D.J., Vacanti, N., Lytton-Jean, A.K.R., Cho, S.W., Ye, A., Langer, R., Anderson, D.G., 2011. A novel family of biodegradable poly(ester amide) elastomers. Advanced Materials 23, H95–H100.

Currie, S., Mankad, K., Goddard, A., 2011. Endovascular treatment of intracranial aneurysms: review of current practice. Postgraduate Medical Journal 87, 41–50.

Cho, Y.D., Lee, J.Y., Seo, J.H., Lee, S.J., Kang, H.S., Kim, J.E., Son, Y.J., Jung, K.H., Kwon, O.K., Han, M.H., 2012. Does stent implantation improve the result of repeat embolization in recanalized aneurysms? Neurosurgery 71, 253–259.

Dalen, J.E., Paraskos, J.A., Ockene, I.S., Alpert, J.S., Hirsh, J., 1986. Venous thromboembolism. Scope of the problem. Chest 89, 370S–373S.

Derauf, B.J., Hunter, D.W., Sirr, S.A., Cardella, J.F., Castaneda-Zuniga, W., Amplatz, K., 1987. Peripheral embolization of diffuse hepatic arteriovenous malformations in a patient with hereditary hemorrhagic telangiectasia. Cardiovascular and Interventional Radiology 10, 80–83.

Dvorak, H.F., Harvey, V.S., Estrella, P., Brown, L.F., Mcdonagh, J., Dvorak, A.M., 1987. Fibrin containing gels induce angiogenesis – implications for tumor stroma generation and wound-healing. Laboratory Investigation 57, 673–686.

Dement'ev, A.G., Khlystalova, T.K., Demina, A.I., Zinger, P.A., 1991. Structural-physical properties of foam polyurethanes with various foaming agents. Polymer Science U.S.S.R. 33, 2125–2134.

Deatrick, K.B., Wakefield, T.W., Henke, P.K., 2010. Chronic venous insufficiency: current management of varicose vein disease. The American Journal of Surgery 76, 125–132.

Darvall, K.A., Bate, G.R., Adam, D.J., Silverman, S.H., Bradbury, A.W., 2011. Duplex ultrasound outcomes following ultrasound-guided foam sclerotherapy of symptomatic recurrent great saphenous varicose veins. European Journal of Vascular and Endovascular Surgery 42, 107–114.

Davis, K.A., Burke, K.A., Mather, P.T., Henderson, J.H., 2011. Dynamic cell behavior on shape memory polymer substrates. Biomaterials 32, 2285–2293.

Defize, T., Riva, R., Raquez, J.M., Dubois, P., Jerome, C., Alexandre, M., 2011. Thermoreversibly crosslinked poly(ε-caprolactone) as recyclable shape-memory polymer network. Macromolecular Rapid Communications 32, 1264–1269.

Dvir, T., Timko, B.P., Brigham, M.D., Naik, S.R., Karajanagi, S.S., Levy, O., Jin, H.W., Parker, K.K., Langer, R., Kohane, D.S., 2011. Nanowired three-dimensional cardiac patches. Nature Nanotechnology 6, 720–725.

Van Den Bos, R.R., de Maeseneer, M.M.G., 2012. Endovenous thermal ablation for varicose veins: strengths and weaknesses. Phlebolymphology 19, 163–169.

Esmon, C.T., 2009. Basic mechanisms and pathogenesis of venous thrombosis. Blood Reviews 23, 225–229.

El-Kady, A.M., Rizk, R.A., Abd El-Hady, B.M., Shafaa, M.W., Ahmed, M.M., 2012. Characterization, and antibacterial properties of novel silver releasing nanocomposite scaffolds fabricated by the gas foaming/salt-leaching technique. Journal of Genetic Engineering and Biotechnology 10, 229–238.

Funakubo, H., 1987. Shape Memory Alloys. Gordon and Breach Science Publishers, New York.

Furie, B., Furie, B.C., 2008. Mechanisms of disease: mechanisms of thrombus formation. New England Journal of Medicine 359, 938–949.

Filion, T.M., Xu, J., Prasad, M.L., Song, J., 2011. In vivo tissue responses to thermal-responsive shape memory polymer nanocomposites. Biomaterials 32, 985–991.

Feng, Y.K., Zhao, H.Y., Behl, M., Lendlein, A., Guo, J.T., Yang, D.Z., 2013. Grafting of poly(ethylene glycol) monoacrylates on polycarbonateurethane by UV initiated polymerization for improving hemocompatibility. Journal of Materials Science-Materials in Medicine 24, 61–70.

Friess, F., Nochel, U., Lendlein, A., Wischke, C., 2014. Polymer micronetworks with shape-memory as future platform to explore shape-dependent biological effects. Advanced Healthcare Materials 3, 1986–1990.

Frerich, S.C., 2015. Biopolymer foaming with supercritical CO_2-thermodynamics, foaming behaviour and mechanical characteristics. Journal of Supercritical Fluids 96, 349–358.

Gianturco, C., Anderson, J.H., Wallace, S., 1975. Mechanical devices for arterial occlusion. The American Journal of Roentgenology, Radium Therapy, and Nuclear Medicine 124, 428–435.

Guglielmi, G., Vinuela, F., Sepetka, I., Macellari, V., 1991. Electrothrombosis of saccular aneurysms via endovascular approach. Part 1: electrochemical basis, technique, and experimental results. Journal of Neurosurgery 75, 1–7.

Gorbet, M.B., Sefton, M.V., 2004. Biomaterial-associated thrombosis: roles of coagulation factors, complement, platelets and leukocytes. Biomaterials 25, 5681–5703.

Golzarian, J., 2006. Embolization Tools. Springer, New York.

Gupta, A., Periakaruppan, A., 2009. Intracranial dural arteriovenous fistulas: a review. Indian Journal of Radiology and Imaging 19, 43–48.

Guo, X.B., Fan, Y.M., Zhang, J.N., 2011. HydroSoft coil versus HydroCoil for endovascular aneurysm occlusion study: a single center experience. European Journal of Radiology 79, E42–E46.

Hjelmstedt, A., 1968. Pressure decrease in the dorsal pedal veins on walking in persons with and without thrombosis. A study of a fracture series. Acta Chirurgica Scandinavica 134, 531–539.

Hall, W.A., Oldfield, E.H., Doppman, J.L., 1989. Recanalization of spinal arteriovenous malformations following embolization. Journal of Neurosurgery 70, 714–720.

Hayashi, S., 1990. Technical Report on Shape Memory Polymers. Nagoya Research and Development Center: Mitsubishi Heavy Industries, Inc., Japan.

Heijkants, R.G.J.C., Van Tienen, T.G., de Groot, J.H., Pennings, A.J., Buma, P., Veth, R.P.H., Schouten, A.J., 2006. Preparation of a polyurethane scaffold for tissue engineering made by a combination of salt leaching and freeze-drying of dioxane. Journal of Materials Science 41, 2423–2428.

Hariraksapitak, P., Suwantong, O., Pavasant, P., Supaphol, P., 2008. Effectual drug-releasing porous scaffolds from 1,6-diisocyanatohexane-extended poly(1,4-butylene succinate) for bone tissue regeneration. Polymer 49, 2678–2685.

Huang, W.M., Ding, Z., Wang, C.C., Wei, J., Zhao, Y., Purnawali, H., 2010. Shape memory materials. Materials Today 13, 54–61.

Hearon, K., Gall, K., Ware, T., Maitland, D.J., Bearinger, J.P., Wilson, T.S., 2011. Post-polymerization crosslinked polyurethane shape-memory polymers. Journal of Applied Polymer Science 121, 144–153.

Heller, D.A., Levi, Y., Pelet, J.M., Doloff, J.C., Wallas, J., Pratt, G.W., Jiang, S., Sahay, G., Schroeder, A., Schroeder, J.E., Chyan, Y., Zurenko, C., Querbes, W., Manzano, M., Kohane, D.S., Langer, R., Anderson, D.G., 2013. Modular 'click-in-emulsion' bone-targeted nanogels. Advanced Materials 25, 1449–1454.

Ito, Y., Liu, S.Q., Imanishi, Y., 1991. Enhancement of cell growth on growth factor-immobilized polymer film. Biomaterials 12, 449–453.

Jabara, R., Chronos, N., Robinson, K., 2008. Novel bioabsorbable salicylate-based polymer as a drug-eluting stent coating. Catheterization and Cardiovascular Interventions 72, 186–194.

Jabbour, M.N., Elder, J.B., Samuelson, C.G., Khashabi, S., Hofman, F.M., Giannotta, S.L., Liu, C.Y., 2009. Aberrant angiogenic characteristics of human brain arteriovenous malformation endothelial cells. Neurosurgery 64, 139–146.

Ji, C.D., Annabi, N., Hosseinkhani, M., Sivaloganathan, S., Dehghani, F., 2012. Fabrication of poly-(DL)-lactide/polyethylene glycol scaffolds using the gas foaming technique. Acta Biomaterialia 8, 570–578.

Jiang, T., Carbone, E.J., Lo, K.W.H., Laurencin, C.T., 2014. Electrospinning of polymer nanofibers for tissue regeneration. Progress in Polymer Science. http://dx.doi.org/10.1016/j.progpolymsci.2014.12.001.

Janik, H., Marzec, M., 2015. A review: fabrication of porous polyurethane scaffolds. Materials Science and Engineering C 48, 586–591.

Jing, X., Mi, H.Y., Peng, J., Peng, X.F., Turng, L.S., 2015. Electrospun aligned poly(propylene carbonate) microfibers with chitosan nanofibers as tissue engineering scaffolds. Carbohydrate Polymers 117, 941–949.

Kasper, W., Geibel, A., Tiede, N., Just, H., 1992. Patent foramen ovale in patients with haemo-dynamically significant pulmonary embolism. Lancet 340, 561–564.

Kerut, E.K., Norfleet, W.T., Plotnick, G.D., Giles, T.D., 2001. Patent foramen ovale: a review of associated conditions and the impact of physiological size. Journal of the American College of Cardiology 38, 613–623.

Kallmes, D.F., Fujiwara, N.H., 2002. New expandable hydrogel-platinum coil hybrid device for aneurysm embolization. American Journal of Neuroradiology 23, 1580–1588.

Kroon, M.E., Van Schie, M.L., Van Der Vecht, B., Van Hinsbergh, V.W., Koolwijk, P., 2002. Collagen type 1 retards tube formation by human microvascular endothelial cells in a fibrin matrix. Angiogenesis 5, 257–265.

Khonakdar, H.A., Jafari, S.H., Rasouli, S., Morshedian, J., Abedini, H., 2007. Investigation and modeling of temperature dependence recovery behavior of shape-memory crosslinked polyethylene. Macromolecular Theory and Simulations 16, 43–52.

Kapoor, A., Kapoor, A., Mahajan, G., 2010. Endovenous ablation of saphenofemoral insufficiency: analysis of 100 patients using RF closure fast technique. Indian Journal of Surgery 72, 458–462.

Kimmins, S.D., Cameron, N.R., 2011. Functional porous polymers by emulsion templating: recent advances. Advanced Functional Materials 21, 211–225.

Koganemaru, M., Abe, T., Iwamoto, R., Suenaga, M., Matsuoka, K., Hayabuchi, N., 2012. Pelvic arteriovenous malformation treated by superselective transcatheter venous and arterial embolization. Japanese Journal of Radiology 30, 526–529.

Kolewe, M.E., Park, H., Gray, C., Ye, X.F., Langer, R., Freed, L.E., 2013. 3D structural patterns in scalable, elastomeric scaffolds guide engineered tissue architecture. Advanced Materials 25, 4459–4465.

Kumar, V., Abbas, A.K., Aster, J.C., Robbins, S.L., 2013. Robbins Basic Pathology. Elsevier/Saunders, Philadelphia, PA.

Kent, K.C., 2014. Abdominal aortic aneurysms. The New England Journal of Medicine 371, 2101–2108.

Knerr, M., Bertog, S., Vaskelyte, L., Hofmann, I., Sievert, H., 2014. Results of percutaneous closure of patent foramen ovale with the GORE® septal occluder. Catheterization and Cardiovascular Interventions 83, 1144–1151.

Lasjaunias, P., Chiu, M., Terbrugge, K., Tolia, A., Hurth, M., Bernstein, M., 1986. Neurological manifestations of intracranial dural arteriovenous-malformations. Journal of Neurosurgery 64, 724–730.

Lanzino, G., Jensen, M.E., Kongable, G.L., Kassell, N.F., 1994. Angiographic characteristics of dural arteriovenous-malformations that present with intracranial hemorrhage. Acta Neurochirurgica 129, 140–145.

Lawrence, P.F., Lorenzorivero, S., Lyon, J.L., 1995. The incidence of iliac, femoral, and popliteal artery aneurysms in hospitalized-patients. Journal of Vascular Surgery 22, 409–416.

Lendlein, A., Kelch, S., 2002. Shape-memory polymers. Angewandte Chemie-International Edition 41, 2034–2057.

Lendlein, A., Langer, R., 2002. Biodegradable, elastic shape-memory polymers for potential biomedical applications. Science 296, 1673–1676.

Lubarsky, M., Ray, C.E., Funaki, B., 2009. Embolization agents-which one should be used when? Part 1: large-vessel embolization. Seminars in Interventional Radiology 26, 352–357.

Leong, M.C., Uebing, A., Gatzoulis, M.A., 2013. Percutaneous patent foramen ovale occlusion: current evidence and evolving clinical practice. International Journal of Cardiology 169, 238–243.

Lendlein, A., Neffe, A.T., Jerome, C., 2014. Advanced functional polymers for medicine. Advanced Healthcare Materials 3, 1939–1940.

Margolis, J., 1957. Initiation of blood coagulation by glass and related surfaces. Journal of Physiology-London 137, 95–109.

Mccormick, W.F., 1966. The pathology of vascular ("arteriovenous") malformations. Journal of Neurosurgery 24, 807–816.

Miller, F.J., Mineau, D.E., 1983. Transcatheter arterial embolization – major complications and their prevention. Cardiovascular and Interventional Radiology 6, 141–149.

Murayama, Y., Vinuela, F., Tateshima, S., Song, J.K., Gonzalez, N.R., Wallace, M.P., 2001. Bioabsorbable polymeric material coils for embolization of intracranial aneurysms: a preliminary experimental study. Journal of Neurosurgery 94, 454–463.

Molyneux, A., Kerr, R., Stratton, I., Sandercock, P., Clarke, M., Shrimpton, J., Holman, R., Grp, I.C., 2002. International Subarachnoid Aneurysm Trial (ISAT) of neurosurgical clipping versus endovascular coiling in 2143 patients with ruptured intracranial aneurysms: a randomised trial. Lancet 360, 1267–1274.

Metcalfe, A., Desfaits, A.C., Salazkin, I., Yahia, L., Sokolowski, W.M., Raymond, J., 2003. Cold hibernated elastic memory foams for endovascular interventions. Biomaterials 24, 491–497.

Min, R.J., Khilnani, N., Zimmet, S.E., 2003. Endovenous laser treatment of saphenous vein reflux: long-term results. Journal of Vascular and Interventional Radiology 14, 991–996.

Min, C.C., Cui, W.J., Bei, J.Z., Wang, S.G., 2005. Biodegradable shape-memory polymer-poly-lactideco-poly(glycolide-*co*-caprolactone) multiblock copolymer. Polymers for Advanced Technologies 16, 608–615.

Mani, G., Feldman, M.D., Patel, D., Agrawal, C.M., 2007. Coronary stents: a materials perspective. Biomaterials 28, 1689–1710.

Mclafferty, R.B., Lohr, J.M., Caprini, J.A., Passman, M.A., Padberg, F.T., Rooke, T.W., Bush, R.L., Zakaria, A.A., Flinn, W.R., Eklof, B.G., Dalsing, M.C., Markwell, S.J., Wakefield, T.W., 2007. Results of the national pilot screening program for venous disease by the American Venous Forum. Journal of Vascular Surgery 45, 142–148.

Meier, B., 2009. Stroke and migraine: a cardiologist's headache. Heart 95, 595–602.

Meier, B., 2010. Current Best Practice in Interventional Cardiology. Wiley-Blackwell, Chichester, UK; Hoboken, NJ.

Min, R.J., Almeida, J.I., Mclean, D.J., Madsen, M., Raabe, R., 2012. Novel vein closure procedure using a proprietary cyanoacrylate adhesive: 30-day swine model results. Phlebology 27, 398–403.

Mizrahi, B., Stefanescu, C.F., Yang, C., Lawlor, M.W., Ko, D., Langer, R., Kohane, D.S., 2012. Elasticity and safety of alkoxyethyl cyanoacrylate tissue adhesives (vol 7, pg 3150, 2011). Acta Biomaterialia 8, 458.

Mizrahi, B., Shankarappa, S.A., Hickey, J.M., Dohlman, J.C., Timko, B.P., Whitehead, K.A., Lee, J.J., Langer, R., Anderson, D.G., Kohane, D.S., 2013. A stiff injectable biodegradable elastomer. Advanced Functional Materials 23, 1527–1533.

Morita, A., 2014. Current perspectives on the unruptured cerebral aneurysms: origin, natural course, and management. Journal of Nippon Medical School 81, 194–202.

Noran, H.H., 1945. Intracranial vascular tumors and malformations. Archives of Pathology 39, 393–416.

Negus, D., 1993. Recurrent varicose veins: a national problem. British Journal of Surgery 80, 823–824.

Nicolaides, A.N., Cardiovascular Disease Educational and Research Trust, European Society of Vascular Surgery, The International Angiology Scientific Activity Congress Organization, International Union of Angiology, Union Internationale de Phlebologie at the Abbaye des Vaux de Cernay, 2000. Investigation of chronic venous insufficiency: a consensus statement (France, March 5–9, 1997). Circulation 102, E126–E163.

Nambiar, A.P., Bozlar, U., Angle, J.F., Jensen, M.E., Hagspiel, K.D., 2008. Initial clinical experience with biopolymer-coated detachable coils (hydrofoil) in peripheral embolization procedures. Journal of Vascular and Interventional Radiology 19, 995–1001.

Nagahama, K., Ueda, Y., Ouchi, T., Ohya, Y., 2009. Biodegradable shape-memory polymers exhibiting sharp thermal transitions and controlled drug release. Biomacromolecules 10, 1789–1794.

Neuss, S., Blomenkamp, I., Stainforth, R., Boltersdorf, D., Jansen, M., Butz, N., Perez-Bouza, A., Knuchel, R., 2009. The use of a shape-memory poly(is an element of-caprolactone)dimethacrylate network as a tissue engineering scaffold. Biomaterials 30, 1697–1705.

Norman, P.E., Powell, J.T., 2010. Site specificity of aneurysmal disease. Circulation 121, 560–568.

de Nardo, L., Bertoldi, S., Cigada, A., Tanzi, M.C., Haugen, H.J., Fare, S., 2012. Preparation and characterization of shape memory polymer scaffolds via solvent casting/particulate leaching. Journal of Applied Biomaterials & Functional Materials 10, 119–126.

Neal, R.A., Jean, A., Park, H., Wu, P.B., Hsiao, J., Engelmayr, G.C., Langer, R., Freed, L.E., 2013. Three-dimensional elastomeric scaffolds designed with cardiac-mimetic structural and mechanical features. Tissue Engineering Part A 19, 793–807.

Nochel, U., Reddy, C.S., Uttamchand, N.K., Kratz, K., Behl, M., Lendlein, A., 2013. Shape-memory properties of hydrogels having a poly(epsilon-caprolactone) crosslinker and switching segment in an aqueous environment. European Polymer Journal 49, 2457–2466.

Nochel, U., Kumar, U.N., Wang, K., Kratz, K., Behl, M., Lendlein, A., 2014. Triple-shape effect with adjustable switching temperatures in crosslinked poly[ethylene-*co*-(vinyl acetate)]. Macromolecular Chemistry and Physics 215, 2446–2456.

Okuno, H., Renzo, K., Uragami, T., 1993. Influence of casting solution additive, degree of polymerization, and polymer concentration on poly(vinyl chloride) membrane-properties and performance. Journal of Membrane Science 83, 199–209.

Ogilvy, C.S., Stieg, P.E., Awad, I., Brown, R.D., Kondziolka, D., Rosenwasser, R., Young, W.L., Hademenos, G., 2001. Recommendations for the management of intracranial arteriovenous malformations – a statement for healthcare professionals from a special writing group of the stroke council, American Stroke Association. Stroke 32, 1458–1471.

Ortega, J.M., Small, W., Wilson, T.S., Benett, W.J., Loge, J.M., Maitland, D.J., 2007. A shape memory polymer dialysis needle adapter for the reduction of hemodynamic stress within arteriovenous grafts. IEEE Transactions on Biomedical Engineering 54, 1722–1724.

Park, S., Lee, S.J., Lee, M., Lee, M.S., Kim, G.M., Kim, M.D., Won, J.Y., Lee, D.Y., 2015. Prospective randomized trial comparing pushable coils and detachable coil during percutaneous implantation of port-catheter system for hepatic artery infusion chemotherapy. Abdominal Imaging 40, 595–600.

Patel, A.A., Solomon, J.A., Soulen, M.C., 2005. Pharmaceuticals for intra-arterial therapy. Seminars in Interventional Radiology 22, 130–138.

Pavithra, D., Doble, M., 2008. Biofilm formation, bacterial adhesion and host response on polymeric implants – issues and prevention. Biomedical Materials 3, 1–13.

Pierot, L., Leclerc, X., Bonafe, A., Bracard, S., Registry, F.M., 2008. Endovascular treatment of intracranial aneurysms with matrix detachable coils: midterm anatomic follow-up from a prospective multicenter registry. American Journal of Neuroradiology 29, 57–61.

Peixoto, L.S., Melo, P.A., Nele, M., Pinto, J.C., 2009. Expanded core/shell poly(vinyl acetate)/ poly(vinyl alcohol) particles for embolization. Macromolecular Materials and Engineering 294, 463–471.

Pereira, M.J.N., Ouyang, B., Sundback, C.A., Lang, N., Friehs, I., Mureli, S., Pomerantseva, I., Mcfadden, J., Mochel, M.C., Mwizerwa, O., Del Nido, P., Sarkar, D., Masiakos, P.T., Langer, R., Ferreira, L.S., Karp, J.M., 2013. A highly tunable biocompatible and multifunctional biodegradable elastomer. Advanced Materials 25, 1209–1215.

Pellerin, O., Maleux, G., Dean, C., Pernot, S., Golzarian, J., Sapoval, M., 2014. Microvascular plug: a new embolic material for hepatic arterial skeletonization. Cardiovascular and Interventional Radiology 37, 1597–1601.

Qureshi, S.A., Reidy, J.F., Binalwi, M., Lim, M.K., Wong, J., Tay, J., Baker, E.J., Tynan, M., 1996. Use of interlocking detachable coils in embolization of coronary arteriovenous fistulas. American Journal of Cardiology 78, 110–113.

Ratner, B.D., 2004. Biomaterials Science: An Introduction to Materials in Medicine. Elsevier Academic Press, Amsterdam; Boston.

Raymond, J., Guilbert, F., Metcalfe, A., Gevry, G., Salazkin, I., Robledo, O., 2004. Role of the endothelial lining in recurrences after coil embolization: prevention of recanalization by endothelial denudation. Stroke 35, 1471–1475.

Reisman, M., Christofferson, R.D., Jesurum, J., Olsen, J.V., Spencer, M.P., Krabill, K.A., Diehl, L., Aurora, S., Gray, W.A., 2005. Migraine headache relief after transcatheter closure of patent foramen ovale. Journal of the American College of Cardiology 45, 493–495.

Ratner, B.D., 2007. The catastrophe revisited: blood compatibility in the 21st century. Biomaterials 28, 5144–5147.

Robertson, L., Evans, C., Fowkes, F.G., 2008. Epidemiology of chronic venous disease. Phlebology 23, 103–111.

Rodriguez, J.N., Clubb, F.J., Wilson, T.S., Miller, M.W., Fossum, T.W., Hartman, J., Tuzun, E., Singhal, P., Maitland, D.J., 2014. In vivo response to an implanted shape memory polyurethane foam in a porcine aneurysm model. Journal of Biomedical Materials Research Part A 102, 1231–1242.

Rogina, A., 2014. Electrospinning process: versatile preparation method for biodegradable and natural polymers and biocomposite systems applied in tissue engineering and drug delivery. Applied Surface Science 296, 221–230.

Speakman, T.J., 1964. Internal occlusion of a carotid-cavernous fistula. Journal of Neurosurgery 21, 303–305.

Strunk, B.L., Cheitlin, M.D., Stulbarg, M.S., Schiller, N.B., 1987. Right-to-left interatrial shunting through a patent foramen ovale despite normal intracardiac pressures. American Journal of Cardiology 60, 413–415.

Sakurai, K., Takahashi, T., 1989. Strain-induced crystallization in polynorbornene. Journal of Applied Polymer Science 38, 1191–1194.

Spaans, C.J., Belgraver, V.W., Rienstra, O., de Groot, J.H., Veth, R.P.H., Pennings, A.J., 2000. Solvent-free fabrication of micro-porous polyurethane amide and polyurethane-urea scaffolds for repair and replacement of the knee-joint meniscus. Biomaterials 21, 2453–2460.

Stapf, C., Mohr, J.P., Pile-Spellman, J., Solomon, R.A., Sacco, R.L., Connolly Jr., E.S., 2001. Epidemiology and natural history of arteriovenous malformations. Neurosurgical Focus 11, 1–5.

Sousa, J.E., Serruys, P.W., Costa, M.A., 2003. New frontiers in cardiology – drug-eluting stents: part I. Circulation 107, 2274–2279.

Schwartz, R.S., Chronos, N.A., Virmani, R., 2004. Preclinical restenosis models and drug-eluting stents – still important, still much to learn. Journal of the American College of Cardiology 44, 1373–1385.

Small, W., Wilson, T.S., Benett, W.J., Loge, J.M., Maitland, D.J., 2005. Laser-activated shape memory polymer intravascular thrombectomy device. Optics Express 13, 8204–8213.

Sokolowski, W., 2005. Potential bio-medical and commercial applications of cold hibernated elastic memory (CHEM) self-deployable foam structures. Smart Materials III 5648, 397–405.

Sokolowski, W., Metcalfe, A., Hayashi, S., Yahia, L., Raymond, J., 2007. Medical applications of shape memory polymers. Biomedical Materials 2, S23–S27.

Sell, S.A., Bowlin, G.L., 2008. Creating small diameter bioresorbable vascular grafts through electrospinning. Journal of Materials Chemistry 18, 260–263.

Schoonover, J.P., King, J.T., Gray, C., Campbell, K., Sherman, C., 2009. 3 alternatives to standard varicose vein treatment. Journal of Family Practice 58, 522–526.

Sarvi, M.N., Stevens, G.W., Gee, M.L., O'connor, A.J., 2012. The co-micelle/emulsion templating route to tailor nano-engineered hierarchically porous macrospheres. Microporous and Mesoporous Materials 149, 101–105.

Singhal, P., Rodriguez, J.N., Small, W., Eagleston, S., de Water, J.V., Maitland, D.J., Wilson, T.S., 2012. Ultra low density and highly crosslinked biocompatible shape memory polyurethane foams. Journal of Polymer Science Part B-Polymer Physics 50, 724–737.

Schmidt, C., Behl, M., Lendlein, A., Beuermann, S., 2014. Synthesis of high molecular weight polyglycolide in supercritical carbon dioxide. RSC Advances 4, 35099–35105.

Silverstein, M.S., 2014a. Emulsion-templated porous polymers: a retrospective perspective. Polymer 55, 304–320.

Silverstein, M.S., 2014b. PolyHIPEs: recent advances in emulsion-templated porous polymers. Progress in Polymer Science 39, 199–234.

Tadavarthy, S.M., Moller, J.H., Amplatz, K., 1975. Polyvinyl alcohol (Ivalon)–a new embolic material. The American Journal of Roentgenology, Radium Therapy, and Nuclear Medicine 125, 609–616.

Thompson, N.P., Scheuer, P.J., Dick, R., Hamilton, G., Burroughs, A.K., 1993. Intraperitoneal ivalon mimicking peritoneal malignancy after plugged percutaneous liver biopsy. Gut 34, 1635.

Tran, N.T., Meissner, M.H., 2002. The epidemiology, pathophysiology, and natural history of chronic venous disease. Seminars in Vascular Surgery 15, 5–12.

Tuite, D.J., Kessel, D.O., Nicholson, A.A., Patel, J.V., Mcpherson, S.J., Shaw, D.R., 2007. Initial clinical experience using the amplatzer vascular plug. Cardiovascular and Interventional Radiology 30, 650–654.

Taaffe, M., Fischer, E., Baranowski, A., Majunke, N., Heinisch, C., Leetz, M., Hein, R., Bayard, Y., Buscheck, F., Reschke, M., Hoffmann, I., Wunderlich, N., Wilson, N., Sievert, H., 2008. Comparison of three patent foramen ovale closure devices in a randomized trial (Amplatzer versus CardioSEAL-STARflex versus Helex occluder). American Journal of Cardiology 101, 1353–1358.

Tekin, H., Sanchez, J.G., Tsinman, T., Langer, R., Khademhosseini, A., 2011. Thermoresponsive platforms for tissue engineering and regenerative medicine. AIChE Journal 57, 3249–3258.

Tseng, L.F., Mather, P.T., Henderson, J.H., 2013. Shape-memory-actuated change in scaffold fiber alignment directs stem cell morphology. Acta Biomaterialia 9, 8790–8801.

Ullm, S., Kruger, A., Tondera, C., Gebauer, T.P., Neffe, A.T., Lendlein, A., Jung, F., Pietzsch, J., 2014. Biocompatibility and inflammatory response in vitro and in vivo to gelatin-based biomaterials with tailorable elastic properties. Biomaterials 35, 9755–9766.

Vaidya, S., Tozer, K.R., Chen, J., 2008. An overview of embolic agents. Seminars in Interventional Radiology 25, 204–215.

Whiting Jr., J.H., Morton, K.A., Datz, F.L., Patch, G.G., Miller Jr., F.J., 1992. Embolization of hepatic arteriovenous malformations using radiolabeled and nonradiolabeled polyvinyl alcohol sponge in a patient with hereditary hemorrhagic telangiectasia: case report. Journal of Nuclear Medicine 33, 260–262.

Wache, H.M., Tartakowska, D.J., Hentrich, A., Wagner, M.H., 2003. Development of a polymer stent with shape memory effect as a drug delivery system. Journal of Materials Science-Materials in Medicine 14, 109–112.

Wilson, T.S., Bearinger, J.P., Herberg, J.L., Marion, J.E., Wright, W.J., Evans, C.L., Maitland, D.J., 2007. Shape memory polymers based on uniform aliphatic urethane networks. Journal of Applied Polymer Science 106, 540–551.

Walker, T.G., Kalva, S.P., Yeddula, K., Wicky, S., Kundu, S., Drescher, P., D'othee, B.J., Rose, S.C., Cardella, J.F., 2010. Clinical practice guidelines for endovascular abdominal aortic aneurysm repair: written by the Standards of Practice Committee for the Society of Interventional Radiology and endorsed by the Cardiovascular and Interventional Radiological Society of Europe and the Canadian Interventional Radiology Association. Journal of Vascular and Interventional Radiology 21, 1632–1655.

Wang, J., Boutin, K.G., Abdulhadi, O., Personnat, L.D., Shazly, T., Langer, R., Channick, C.L., Borenstein, J.T., 2013. Fully biodegradable airway stents using amino alcohol-based poly(ester amide) elastomers. Advanced Healthcare Materials 2, 1329–1336.

Wischke, C., Schneider, C., Neffe, A.T., Lendlein, A., 2013. Polyalkylcyanoacrylates as in situ formed diffusion barriers inmultimaterial drug carriers. Journal of Controlled Release 169, 321–328.

Wu, X.L., Huang, W.M., Ding, Z., Tan, H.X., Yang, W.G., Sun, K.Y., 2014. Characterization of the thermoresponsive shape-memory effect in poly(ether ether ketone) (PEEK). Journal of Applied Polymer Science 131. http://dx.doi.org/10.1002/app.39844.

Xue, L.A., Dai, S.Y., Li, Z., 2010. Biodegradable shape-memory block co-polymers for fast self-expandable stents. Biomaterials 31, 8132–8140.

Yoon, J.J., Kim, J.H., Park, T.G., 2003. Dexamethasone-releasing biodegradable polymer scaffolds fabricated by a gas-foaming/salt-leaching method. Biomaterials 24, 2323–2329.

Yakacki, C.M., Shandas, R., Lanning, C., Rech, B., Eckstein, A., Gall, K., 2007. Unconstrained recovery characterization of shape-memory polymer networks for cardiovascular applications. Biomaterials 28, 2255–2263.

Yao, C.H., Qi, L., Jia, H.Y., Xin, P.Y., Yang, G.L., Chen, Y., 2009. A novel glycidyl methacrylate-based monolith with sub-micron skeletons and well-defined macropores. Journal of Materials Chemistry 19, 767–772.

Yang, J., Lv, J., Behl, M., Lendlein, A., Yang, D., Zhang, L., Shi, C., Guo, J., Feng, Y., 2013. Functionalization of polycarbonate surfaces by grafting PEG and zwitterionic polymers with a multicomb structure. Macromolecular Bioscience 13, 1681–1688.

Zhang, D.W., George, O.J., Petersen, K.M., Jimenez-Vergara, A.C., Hahn, M.S., Grunlan, M.A., 2014. A bioactive "self-fitting" shape memory polymer scaffold with potential to treat cranio-maxillo facial bone defects. Acta Biomaterialia 10, 4597–4605.

Scaffolds of biodegradable block polyurethanes for nerve regeneration

21

K.T. Xu[1,], Y.Q. Niu[1], Y.H. Zhu[1], X.Y. Liu[1], C. Liu[2]*
[1]Department of Materials Science and Engineering, Jinan University, Guangzhou, China;
[2]Aleo BME, Inc., Innovation Boulevard, State College, PA, USA
*Corresponding author: kaitianxu@yahoo.com

21.1 Introduction

Large-gap peripheral nerve defect is a very common clinical trauma and often leads to permanent disability of feeling and movement function in affected patients [1–3]. Transplantation of autologous nerve graft has typically been used for the repair of injured peripheral nerves as a first line therapy. However, there are many disadvantages with this method including mismatch between the defect nerve and the graft nerve diameter, a second surgical step for the extraction of donor nerves, a shortage in the supply of donor grafts, donor site morbidity, inadequate return of function, and aberrant regeneration [4–6]. Due to host immunogenic rejection of the donor graft, the method of using allografts has had little success in clinical practice [3,7]. Morbidity of harvesting donor grafts hinders development of the muscle and vein grafts during repair of severed peripheral nerves [3,8,9]. Furthermore, none of these surgical approaches has resulted in axonal connections. To overcome these problems, an alternative approach would be to use a biodegradable nerve repair scaffold serving to both promote nerve regeneration and provide a pathway for nerve outgrowth.

In the 1990s, Schakenraad, Robinson, and colleagues performed systematic research on nerve regeneration using scaffolds based on biodegradable copolymers of DL-lactide and ε-caprolactone [10,11]. Based on this work, the first and only commercialized artificial nerve repair scaffold was prepared from the biodegradable copolymers of DL-lactide and ε-caprolactone [P(DLLA–ε-CL)] and is now used clinically under the trade name Neurolac® [12].

Biodegradable polyurethanes (PUs), however, have been recently explored as novel biomaterials due to their excellent mechanical and processing properties and good biocompatibility [13–16]. To further augment these properties, we have successfully formulated a class of PU biomaterials called alternating block PUs (PU-*alt*), which possess well-controlled and determined chemical structures as well as regular microstructures [17]. The regular structures endow the polymers with special properties, such as excellent biocompatibility and shape-forming ability, providing the capability

for sophisticated applications [13,18,19]. A number of PU-*alt* were synthesized by incorporating various biodegradable blocks such as polycaprolactone (PCL) [18], poly(lactic acid) (PLA) [20], and poly(hydroxyalkanoates) [17,21,22] into the backbone of the PUs. Results showed that all of these PU-*alt* have much better biocompatibility than their random block PU counterparts as well as traditional biodegradable biomaterials such as PLA and PCL.

Even though much effort has been spent in applying PUs for different biomedical purposes, there is a scarcity of research on nerve regeneration based on PUs as scaffold materials. The first attempt using PUs in preparation of a double-layered nerve conduit appeared in 1990 by Pennings and colleagues, in which a mixture of biodegradable PU and poly(L-lactide) served as the outer microporous layer of the double-layered conduit [23]. Although this dual-component PU-based nerve conduit demonstrated high performance in nerve regeneration across an 8 mm gap, the conduit failed to degrade completely and was marred by cytotoxic degradation products. This led to the emergence of another nerve-guided conduit composed of semicrystalline poly-L-lactide and poly-ε-caprolactone (50/50), which showed much improved nerve regeneration through the conduit [5]. However, remnants of the biomaterial lingered around the regenerating nerve up to 2 years postimplantation. A comprehensive review on nerve repair using biodegradable artificial nerve guides was addressed by Johnson and Soucacos in 2008 [24]. Furthermore, a systematic review on animal models used to study nerve regeneration was reported by Windebank and colleagues in 2012, in which PU and PU/PLA were briefly noted for nerve scaffolds [25].

Yang recently described a systematic investigation on the application of crosslinked urethane-doped biodegradable polyester (CUPE) scaffolds for nerve regeneration [26]. Porous, elastic, and biomimetic CUPE scaffolds consisting of parallel and longitudinally oriented microchannels with a nonporous outer sheath were designed and fabricated to guide the outgrowth of nerve fibers and to prevent the ingrowth of fibrous tissue into the nerve gap. By using a simple and cost-effective sodium chloride particulate leaching technique in combination with microengineering approaches, biomimetic multichanneled porous CUPE nerve guides with various channel numbers were fabricated and displayed an ultimate peak stress of 1.38 ± 0.22 MPa with a corresponding elongation at break of $123 \pm 42\%$, which were comparable to those of native nerve tissue. The CUPE nerve guides were also evaluated *in vivo* for the repair of a 1 cm rat sciatic nerve defect. Although histological evaluations revealed collapse of the inner structure from CUPE nerve guides, they still displayed fiber populations and densities comparable to those of nerve autograft controls after 8 weeks of implantation.

Our recent investigations revealed that PCL and poly(ethylene glycol) (PEG)-based alternating block PUs (PUCL-*alt*-PEG) possess better cytocompatibility with fibroblast L929 and neural rat glial cells than the traditional random block counterpart PUCL-*ran*-PEG [18]. In Sprague–Dawley (SD) rat animal models of nerve repair, scaffolds based on PUCL-*ran*-PEG showed superior nerve repair results compared to PCL and silicon tubes, though they were still inferior to autografts [14]. We found that scaffolds from PUCL-*alt*-PEG polymer displayed comparable or better nerve repair than autografts by analysis of sciatic function index (SFI), histological assessment including hematoxylin/eosin (HE) staining, immunohistochemistry, ammonia silver staining, and

Masson's trichrome staining, as well as TEM observation. In this chapter, a systematic investigation and comparison of nerve repair is made using scaffolds made from PUCL-*alt*-PEG, PUCL-*ran*-PEG, autograft, PCL, silicone tube, and negative control in an SD rat model.

21.2 Experimental procedures

21.2.1 Materials

PCL (M_w 100,000 Da; Guanghuaweiye, Guangdong, China), poly(ethylene glycol) (PEG, Sigma–Aldrich), 1,6-hexamethylene diisocyanate (HDI, Alfa-Aesar), and stannous octanoate (Alfa-Aesar) were used as received. Toluene-*p*-sulfonic acid, chloroform, 1,4-butanediol, 1,2-dichloroethane, dichloromethane, petroleum ether, ethylene glycol, and methanol were AR grade, purchased from Guanghua Co. Ltd (Guangdong, China) and used as received. PCL–diol prepolymer was prepared via acid-catalyzed alcoholysis as reported under procedures [22].

21.2.2 Preparation of poly(ethylene glycol)–diisocyanate prepolymer

Diisocyanate-terminated PEG was prepared according to a modified protocol [18]. First, 0.8 g PEG ($M_n = 400$, 2×10^{-3} mol) was dissolved in 10 mL 1,2-dichlorethane in a 50 mL two-necked flask at 100 °C. Next, any trace of water in the system was removed through azeotropic distillation until roughly 4 mL of 1,2-dichloroethane was left in the flask. The remaining 4 mL of solution, along with two drops of stannous octanoate ($\sim 5 \times 10^{-3}$ g), was transferred into a 5 mL syringe. This solution was added dropwise into a 100 mL four-necked flask inside of which 0.75 g HDI (4.4×10^{-3} mol) and 10 mL 1,2-dichloroethane were placed in advance. The reaction was carried out at 50 °C for 5 h under nitrogen gas, followed by complete removal of the solvent and excessive HDI under vacuum. Remaining PEG–diisocyanate was kept in the flask for further use.

21.2.3 Preparation of polycaprolactone and poly(ethylene glycol)-based alternating block polyurethanes

The amount of 0.002 mol PCL–diol was dissolved in 30 mL 1,2-dichloroethane. The moisture was removed by azeotropic distillation. The remaining solution of about 15 mL was transferred into a 25 mL injector and was dropped slowly into the flask of PEG–diisocyanate prepared from the previous step, in the presence of 20 mL 1,2-dichloroethenae. After a 48 h reaction at 75 °C, the product was cooled to room temperature and allowed to precipitate in a mixture of petroleum ether and methanol (20/1, v/v%). Next, the precipitate was redissolved in 40 mL 1,2-dichloroethane and filtrated to remove any insoluble substances. To remove stannous octanoate residues and any possible remaining oligomers, the filtrate was precipitated again in a mixture
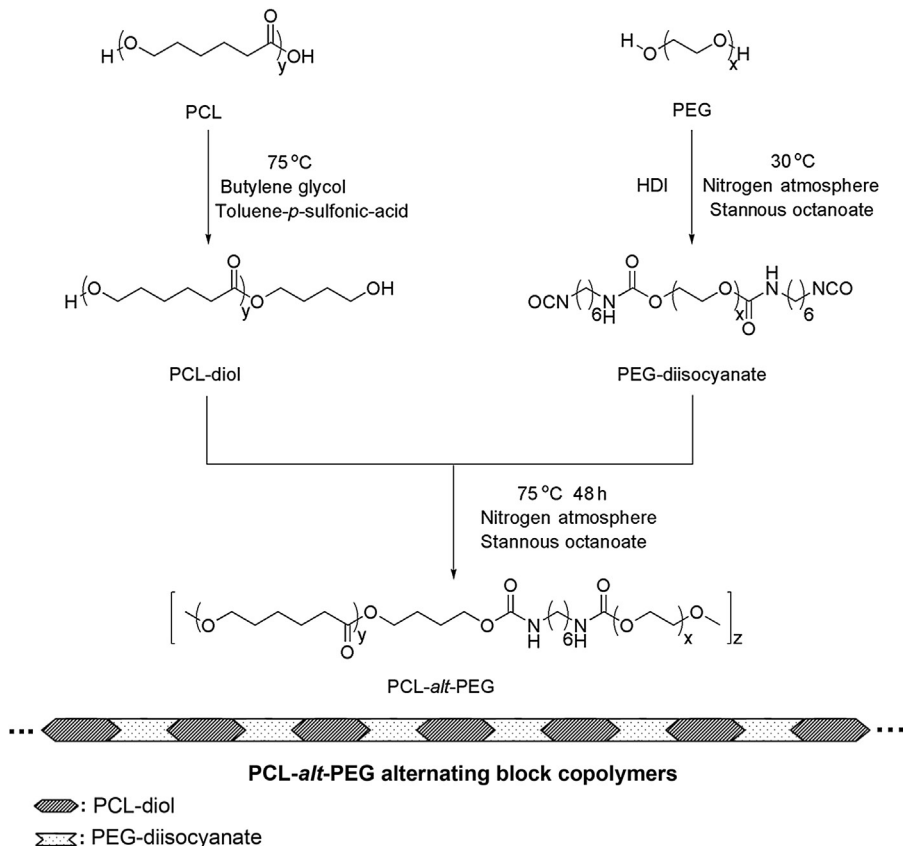
Figure 21.1 Synthesis of alternating block polyurethane PUCL-*alt*-PEG.

of petroleum ester and methanol. The product was collected and dried under vacuum to a constant weight at 40 °C. The average yield was 80%. The synthetic procedure is described in Figure 21.1. PUCL-*ran*-PEG was synthesized from PCL–diol and PEG using HDI as a coupling reagent [18].

21.2.4 Characterization

The chemical structure and composition of the PUs were determined by ^{1}H NMR spectra using a Bruker AV 400 NMR spectrometer (Bruker, Switzerland). The NMR spectrum was obtained at room temperature in CDCl$_3$ (20 mg/mL) with tetramethyl-silane (TMS) as an internal standard. Tensile mechanical properties were tested on strip-shaped films (thickness 0.1–0.2 mm, width 10 mm) on a universal testing machine (CMT 4204 Sans, Shenzhen, China) at a pulling rate of 50 mm/min. At least five sample determinations were conducted to obtain the average values. Scanning electron micros-copy (SEM, JSM-6360 LA, Nikon, Japan) was used for film surface observations. Film

samples were mounted on aluminum stumps coated with gold in a sputtering device (JFC-1600, Japan) for 1.5 min at 10 mA. Other characterizations of the above prepared PUCL-*alt*-PEG and PUCL-*ran*-PEG were described elsewhere [18].

21.2.5 Hemocompatibility

Rabbit blood was drawn from a live rabbit and mixed with a 3.8% sodium citrate solution (ratio: 9/1, v/v%), which was then centrifuged at 1500 rpm for 15 min at 4 °C to obtain platelet-rich plasma (PRP). Material films on a glass dish were sterilized with 75% ethanol, washed three times with phosphate buffer solution (PBS), and equilibrated in PBS for 1 h. Then 1 mL PRP was placed on testing films at 37 °C for 1 h after removing the PBS solution. After 1 h incubation, the films were dipped in a 2.5% glutaraldehyde buffer solution overnight. Finally, the films were dehydrated in an ethanol-gradient series (30%, 50%, 70%, 80%, 90%, 95%, and 100%) for 15 min each, sequentially, and were dried under vacuum. The morphologies of the platelets adhered onto the film surfaces were observed by SEM.

21.2.6 Preparation of nerve regeneration scaffolds

A porous PU or PCL nerve repair scaffold was prepared using a dipping–leaching method [14,27]. Representatively, 1 g of PUCL-*alt*-PEG was dissolved in 10 mL *N,N*-dimethyl formamide (DMF) at 60 °C for 1 h. Then 2 g of NaCl particles (5–10 μm), as porogen for scaffold fabrication, was added into the solution and thoroughly mixed. A stainless steel wire with an outer diameter of 1.28 mm was used as a mold. The mold was immersed in the above salt suspension for 15 s and then taken out for evaporation for another 50 s. The above dip coating and drying cycles were repeated five times. The resulting polymer/salt coatings were subject to air drying for 2 days and vacuum drying for 2 days, followed by salt leaching in deionized water, freeze drying, and demolding to obtain a porous nerve repair scaffold.

21.2.7 Morphology and porosity of the nerve repair scaffold

The microstructure of the scaffolds was characterized under SEM (Model JSM-6360LA, JEOL, Japan) at an accelerating voltage of 10 kV. Before observation, specimens were coated with platinum using a sputter coater (JFC-1600, Japan) under argon gas. The average pore sizes of the scaffolds were measured using an image analysis program (i-solution, IMT, Korea) from SEM photographs. The porosities of scaffolds were measured using a specific gravity bottle (Hubbard, Hanil, Korea) based on Archimedes' principle [28]. Briefly, the porosity of scaffolds was determined as

$$\text{Porosity}\,(\,\%\,) = \frac{(W_2 - W_3 - W_s)\,/\rho_e}{(W_1 - W_3)\,/\rho_e} \times 100\,\%$$

where W_1 is the specific gravity bottle weight filled with ethanol, W_2 the specific gravity bottle weight including ethanol and scaffold, W_3 the specific gravity bottle weight

with the ethanol-saturated scaffolds from W_2 removed, W_s the scaffold weight, ρ_e the density of ethanol; thus $(W_1 - W_3)/\rho_e$ is the total volume of a scaffold including pores and $(W_2 - W_3 - W_s)/\rho_e$ is the pore volume of the scaffold.

The mechanical properties of a nerve repair scaffold were tested with a universal testing machine (CMT 4204 Sans, Shenzhen, China). Samples were immersed in deionized water for 2 h and then tested in a wet state. Tensile strength was studied by applying a force parallel to the axis of a conduit at a speed of 50 mm/min.

21.2.8   In vitro *degradation of the nerve repair scaffold*

To determine the *in vitro* biodegradation rate of both PUCL-*alt*-PEG and PUCL-*ran*-PEG scaffolds, 48 samples of the PU scaffolds were cut into cylinders 1.5 mm in diameter and approximately 10 mm in length, weighing about 110 mg each. All samples were immersed in 5 mL of 0.1 M sterile PBS at pH 7.4. The PBS solution was not refreshed in the entire 16 weeks period. All vials were lidded and kept in a shaking incubator at $37 \pm 0.5\,°C$ (30 strokes per min). The pH value of suspension liquor was measured every 2 weeks for 16 weeks using a pH PB-10 m. Three samples were prepared for each scaffold, and the average pH value was reported. Four vials were taken out every 2 weeks to discharge the PBS solution. Scaffolds and the fragments were rinsed with distilled water and dried to a constant weight in vacuum for molecular weight and weight loss ratio measurements. Weight loss ratio was calculated according to the equation

$$\text{Weight loss ratio} = \frac{W_0 - W_1}{W_0} \times 100\,\%$$

where W_0 and W_1 are weights of the sample before and after the hydrolytic degradation, respectively. The reported weight loss ratio is the average of the four samples.

21.2.9   In vitro *cell culture*

Material films and scaffolds, which were sterilized by UV lamp for 24 h and then washed by sterilized PBS, were placed into a 12-well polystyrene (PS) dish (Corning, USA). Rat glial cells (Shantou University, China) were used as model cells to estimate the nerve cell compatibility of the films and scaffolds [18]. PCL films and scaffolds were used as a comparison. A cell suspension in DMEM medium (Hyclone) supplemented with 10% FBS (Hyclone), 100 U/mL penicillin (Sigma), and 100 U/mL streptomycin (Sigma) was seeded onto the film and scaffold-coated dishes (cell density, 1×10^4 cells/specimen). The cell-seeded films and scaffolds were maintained at $37\,°C$ for 8 h in an incubator with a 5% CO_2 humidified atmosphere for cell adhesion. The films and scaffolds were then transferred to a new 12-well PS dish. Next, cultivation was conducted for 24, 48, and 72 h in that order. CCK-8 assay was used for cell viability while SEM was used for cell morphology observation. For viability assays, the culture medium was removed and the culture was washed with PBS twice.

Approximately 450 μL serum-free DMEM and 50 μL CCK-8 solution were added to each sample, followed by incubation at 37 °C for 3 h to form water-soluble formazan. The supernatant was transferred into a 96-well plate, and the optical density (OD) at 450 and 630 nm was determined using a microplate reader (Multiskan MK3, Thermo Labsystems, Finland), with six parallel experiments of each sample used to assess cell viability. The adhered cells on films and scaffolds were fixed with 2.5% glutaraldehyde (Alfa-Aesar) at 4 °C for 12 h. After thorough washing with PBS, cells adhered on films and scaffolds were dehydrated in an ethanol-graded series (50%, 60%, 70%, 80%, 90%, and 100%) for 15 min each and allowed to dry via lyophilization to be used for SEM observations.

21.2.10 Animal and surgical procedures

Eighty adult SD rats weighing 200–250 g were used to evaluate nerve repair. Animals were divided into five groups, each with 15 rats. The nerve regeneration capabilities of hydrophilic PUCL-*alt*-PEG and PUCL-*ran*-PEG scaffolds were compared with those of autograft nerve, PCL with similar dimensions (inner diameter, about 1.28 mm; wall thickness about 0.4 mm), nonporous silicone tube (inner diameter 1.5 mm; wall thickness 0.4 mm), and an untreated group (negative control). Defects of 12 mm in sciatic nerves created by surgical removal of the nerve tissue were repaired with the nerve conduits. A schematic illustration of the nerve repair microsurgery is depicted in Figure 21.2. Animals were anesthetized with 50 mg/kg body weight pentobarbital sodium [3,4,14]. Sciatic nerve on right side was exposed, and a 12 mm segment of nerve was removed from the mid-thigh level. A 14 mm scaffold or the removed nerve itself was interposed between the proximal and the distal stumps with 8-0 absorbable PLGA at each junction. Following implantation, muscle incision was closed using a 5-0 chromic gut suture and the skin was closed with 2-0 silk suture. Each rat received one implant, which was removed at various time intervals. Postoperatively, each animal was housed in a single cage with
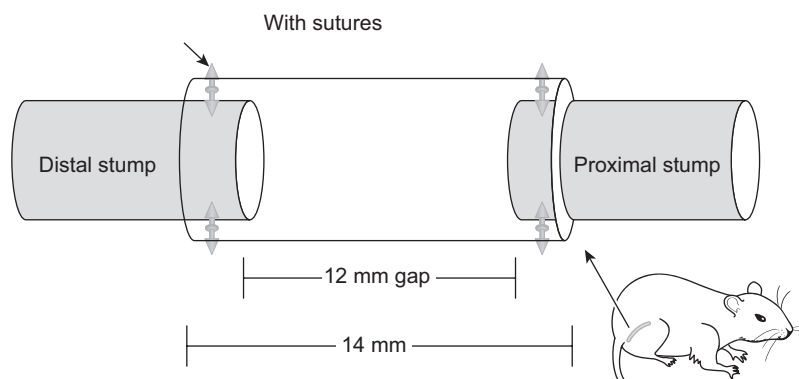
Figure 21.2 Schematic illustration of nerve repair microsurgery.

free access to food and water. The animals were intensively examined for signs of autotomy and contracture. At each time interval, SFI and electrophysiological and histomorphometric analyses were performed to evaluate the efficiency of nerve repair. All animal experiments were conducted according to the ISO100993-2:1992 animal welfare requirements.

21.2.11   Functional assessment of nerve regeneration

Walking track analysis was carried out to evaluate the functional recovery following sciatic nerve injury repair after 2, 4, 8, 10, 14, and 20 weeks. All rats were first allowed conditioning trials on an 8×42 cm walking track. The hind feet of rats were dipped in black ink. The rat was permitted to walk down the track, leaving its hind footprints on a white paper. From the footprints, the following measurements were obtained: (1) distance from the heel to the third toe, the print length (PL); (2) distance from the first to the fifth toe, the toe spread (TS); and (3) distance from the second to the fourth toe, the intermediary toe spread (ITS).

Three measurements were taken from the right operated foot (OPL, OTS, OITS) as well as the contralateral nonoperated foot (NPL, NTS, NITS). SFI can be calculated by the formula proposed by Bain et al. [29]:

$$SFI = -38.3 * PLF + 109.5 * TSF + 13.3 * ITF - 8.8$$

where PLF = (OPL − NPL)/NPL; TSF = (OTS − NTS)/NTS; ITF = (OITS − NITS)/NITS. Before implantation, the SFI for preoperative index value is given at time point 0 (our actual SFI = −7.51 before implantation; number of rates for each evaluation group for SFI is 20). An SFI of 0 is normal. An SFI of −100 indicates total impairment. To obtain statistically significant data, several prints were measured for each rat. Sometimes several walks were required to obtain clear print marks.

21.2.12   Electrophysiological analysis

To evaluate motor reinnervation, electrophysiological recordings of the compound muscle action potential (CMAP) were performed on the experimental animals after 4, 9, or 14 weeks postconduit implantation. On anesthetization, a bipolar stimulation hook electrode was placed directly around the sciatic nerve ~20 mm upstream of the graft site. A needle-type differential recording electrode was inserted into the anterior tibialis muscle with the reference side placed approximately in the middle of the stimulating electrode and the recording electrode. The ground electrode was positioned at the tail. Nerves were stimulated by a 0.2 ms pulse for every 10 s, with stimulating intensity adjusted to invoke supramaximal compound action potentials. The reference-subtracted signals were sampled at 20 kHz and filtered at 3 kHz before sending them to an A/D converter (PCIe-6251, National Instruments, TX, USA), which were analyzed on a personal computer by a LabView-based homemade program. Latency (time lag between the stimulus artifact and the minimum of the first negative deflection) and the conduction velocity were calculated accordingly.

21.2.13   Histological assessment

Implanted nerve repair scaffolds were harvested immediately after recording CMAPs. The nerve grafts were immediately fixed in a cold buffered 4% paraformaldehyde solution for 24 h. Nerve grafts were then washed in distilled water and sciatic nerve sections were taken from middle portions of the regenerated nerves. After fixation, tissues in each group were embedded with olefin, cut to 4 μm thickness, and then stained with HE staining. Remaining tissues in each group were cut to 10 μm thickness for immunohistochemistry analysis. After soaking in 1 M PBS for 10 min, antigen retrieval was performed on the nerve sections by incubating in sodium citrate solution for 8 min at P100 microwave temperature, blocking in a 10% normal goat serum for 60 min at room temperature, and incubating with rabbit anti-NF200 polyclonal antibody (N4142, Sigma, St. Louis, MO, USA) at 4 °C for 18 h, followed by reaction with fluorescein isothiocyanate-labeled secondary antibody goat anti-rabbit IgG (BA1105, Boster, Wuhan, China) for 30 min at room temperature. The stained sections were observed under a fluorescent microscope (EX465-495, Nikon, Japan).

To observe more detailed axons and myelin sheath regeneration inside the scaffolds, nerve grafts were embedded with Epon 812 epoxy resin, and the mid and distal portions of the specimens were cut into ultrathin sections (50 nm thick) and then viewed and photographed with a Hitachi H7500 transmission electron microscope (TEM; Tokyo, Japan). The thickness of myelin sheath and diameters of myelinated axons were quantified from TEM images using the Image J software. For each specimen, a total of 100–120 random axons were analyzed.

Nerve longitudinal sections of 5 μm thickness for each group were employed for ammoniacal silver staining to evaluate neurofibril regeneration at the 14th week postoperatively [30]. The longitudinal sections were embedded with 20% silver nitrate solutions at 37 °C for 30 min in a dark environment and rinsed with 10% formaldehyde to obtain a yellow color, followed by rinsing with silver ammoniacal nitrate for 40 s and 10% formaldehyde for 2 min [31,32] to prepare sections for light microscopy (TE2000-U, Nikon, Japan).

Gastrocnemius muscles from the operated limbs of rats in each group were harvested from the mid-belly. Muscle samples were fixed in 4% paraformaldehyde buffered solution for 24 h, embedded by olefin, and then cut into thin sections of 5 μm. The sections were stained by Masson's Trichrome (D026, Jiancheng Biotech, Nanjing, China) and then observed under a light microscope (TE2000-U, Nikon, Japan) [33]. Microstructures of the nerve repair scaffolds during *in vivo* biodegradation were characterized under SEM (Model JSM-6360LA, JEOL, Japan) at an accelerating voltage of 15 kV.

21.3   Results and discussion

In the sample abbreviation PUC20-*a*-E4 or PUC10-*r*-E4, U represents block PU; *a*, alternating; *r*, random; C20 and E4, PCL–diol ($M_n = 2000$), and PEG ($M_n = 400$), respectively. The structures of PUCL-*alt*-PEG and PUCL-*ran*-PEG were confirmed

Table 21.1 **Mechanical properties of polycaprolactone and poly(ethylene glycol)-based block polyurethanes**

Sample	σ_t (MPa)[a]	σ_s (MPa)[b]	E (MPa)[c]	ε (%)[d]
PUC20-*a*-E4	7.9	3.3	45.2	1352.5
PUC20-*a*-E10	5.9	2.2	30.9	750.9
PUC20-*r*-E4	7.0	3.0	43.9	545.7
PUC20-*r*-E10	4.5	2.4	41.5	552.4

Sample abbreviation PUC20-*a*-E4 or PUC10-*r*-E4 represents U, block polyurethane; *a*, alternating; *r*, random; C20 and E4, PCL–diol (M_n=2000) and PEG (M_n=400), respectively; same for text.
[a]σ_t, tensile strength.
[b]σ_s, yield strength.
[c]*E*, Young's modulus.
[d]ε, elongation at break.

in our previous investigation [18]. The higher crystallinity of PUCL-*alt*-PEG was demonstrated, which confirmed the theory that PU-*alt* possess a more regular microstructure than their random block counterparts [18].

21.3.1 Mechanical properties

Mechanical properties of the PU samples, including tensile strength (σ_t), yield strength (σ_s), Young's modulus (E), and elongation at break (ε) are listed in Table 21.1. Among these samples, PUs with higher PCL content, higher degree of crystallinity, and urethane linkage such as in PUC20-*a*-E4 and PUC20-*r*-E4 correlate to higher strength, modulus, and elongation at break. The high elongation at break and relatively low modulus values provide evidence that the PUs are soft thermoplastic elastomers. It was noted that PU-*alt* displayed higher tensile strength and elongation than random block PUs (Table 21.1), which may be due to their higher crystallinity, higher molecular weight, and lower block polydispersity. The alternating block arrangements leads to better phase separation in the PUs. Furthermore, the higher degree of crystallinity from stiff and immobile urethane-based hard segment domains serves as more effective physical cross-links between the flexible soft PEG segment domains. This would therefore enhance the elastic mechanical properties.

21.3.2 Surface properties

Static contact angle and surface energy results are summarized in Table 21.2. It can be seen that due to the inclusion of the PEG segment in the backbone, the PU products exhibit lower contact angles and hence are more hydrophilic than the PCL. With an increase of PEG content, the surfaces of PUs become more hydrophilic. However, by varying the length of PCL and PEG segments, it was found that PUC10-*a*-E4 with a PEG content of 23.0% has a lower contact angle and hence is more hydrophilic than PUC20-*a*-E10 with a PEG content of 30.0%.

Table 21.2 Contact angle and surface energy of polycaprolactone and poly(ethylene glycol)-based block polyurethanes

Sample	W_{PEG}	θ_{H_2O} (°)	$\theta_{CH_2I_2}$ (°)	Dispersive component (r_s^d)	Polar component (r_s^p)	Surface energy $(r_s = r_s^d + r_s^p)$
PLA	–	84.3±0.7	35.4±1.2	35.1±0.5	7.4±1.0	42.5±0.6
PCL	–	89.1±1.3	37.5±0.9	36.0±1.2	5.3±0.7	41.3±0.8
PUC10-*a*-E4	23.0	67.2±2.5	23.0±0.9	35.9±1.6	14.7±1.3	50.6±1.5
PUC20-*a*-E4	14.6	83.9±1.8	47.8±2.0	28.7±1.7	9.0±2.0	37.6±2.1
PUC20-*a*-E10	30.0	74.6±2.5	56.1±1.4	23.0±2.0	15.3±2.1	38.3±1.9
PUC10-*r*-E4	23.0	69.3±1.5	21.7±1.8	36.5±1.6	13.8±1.5	50.3±1.9
PUC20-*r*-E4	14.6	88.3±1.7	47.0±2.5	30.4±2.1	6.7±2.0	37.1±2.5
PUC20-*r*-E10	30.0	77.8±1.1	55.4±3.1	23.8±3.2	13.4±2.8	37.2±3.0

W_{PEG}, weight percentage of PEG in sample.

This phenomenon was also observed in the random block PUs. The lower contact angle in the case of PU-*alt* indicated a more hydrophilic surface and higher surface energy than the random series of PUs (Table 21.2). A possible mechanism may be that alternating structures enhance phase separation and allow more PEG to be located on the surface [21,34].

The surface morphology of the obtained PU films prepared by solution casting was investigated by SEM. Typical SEM photos of both types of PUs are given in Figure 21.3. The alternating block PU PUC10-*a*-E4 was shown to display a more regular and rougher surface than its random counterpart PUC10-*r*-E4 (Figure 21.3) [18] due to higher crystallinity from the alternating block series resulting in a more regular architecture as discussed above. This discrepancy has significant biomedical implications, as biocompatibility may be improved with higher surface roughness providing a favorable environment for adhesion and growth of certain cells such as fibroblast and neural cells.

21.3.3 Platelet adhesion

As shown in Figure 21.4, platelets adhered onto PCL and PLA films show an abundance of extended pseudopods, indicating that all of the platelets are activated and blood coagulation should be easily induced. In contrast, on the synthesized PU film surface, there were fewer adherent platelets with no obvious pseudopods, suggesting a weak attachment or even only a physical precipitation of platelets onto the surfaces. Therefore, the hemocompatibility is expected to be greatly improved. In particular, the alternating block PU PUCL-*alt*-PEG revealed even less platelet adhesion on the surface than their random counterpart PUCL-*ran*-PEG. This suggests that PUCL-*alt*-PEG possesses much better hemocompatibility than other biodegradable polymers, including its random block counterpart PUCL-*ran*-PEG.
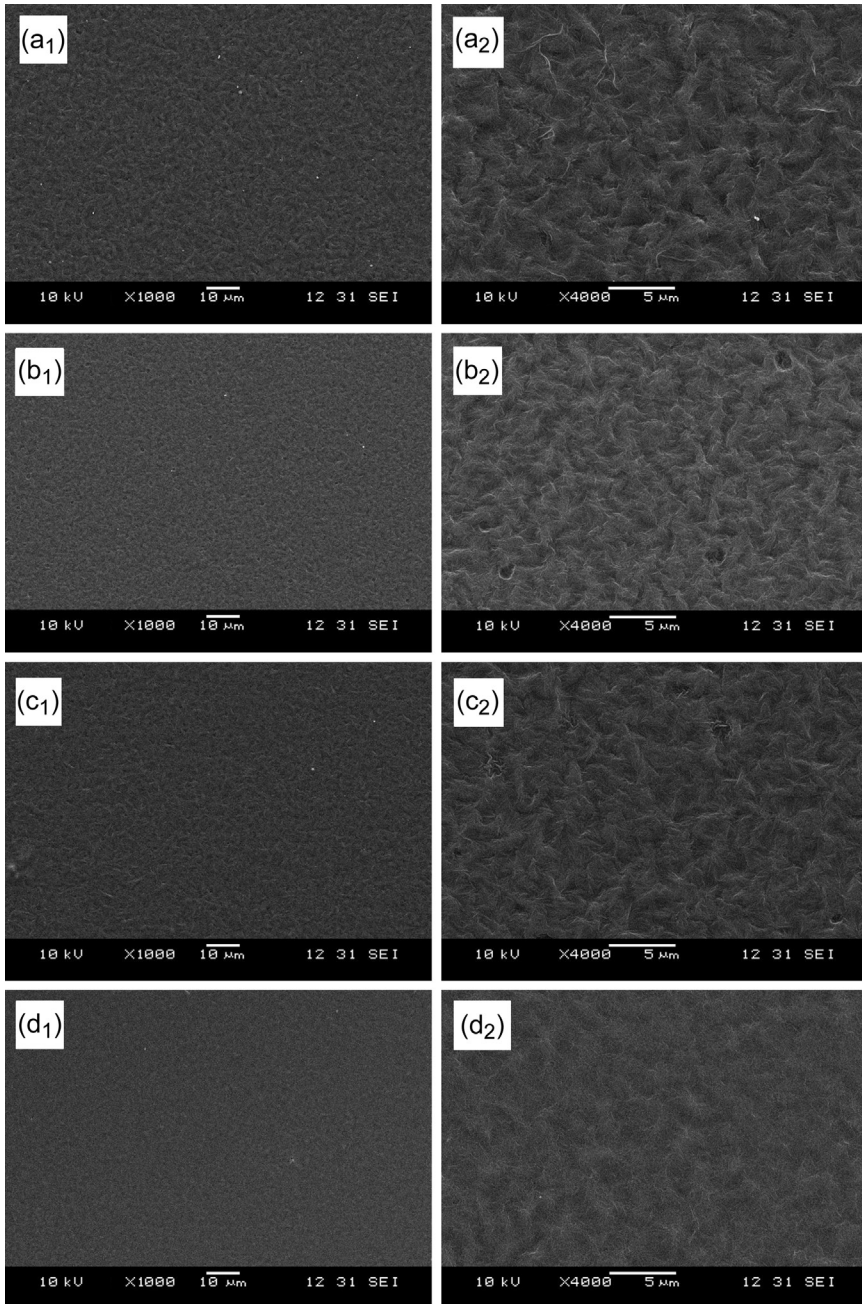
Figure 21.3 SEM images of PCL and PEG-based block polyurethane films (×1000, left) and ×4000, right): (a₁–a₂) PUC10-*a*-E4; (b₁–b₂) PUC20-*a*-E10; (c₁–c₂) PUC10-*r*-E4; (d₁–d₂) PUC20-*r*-E10.
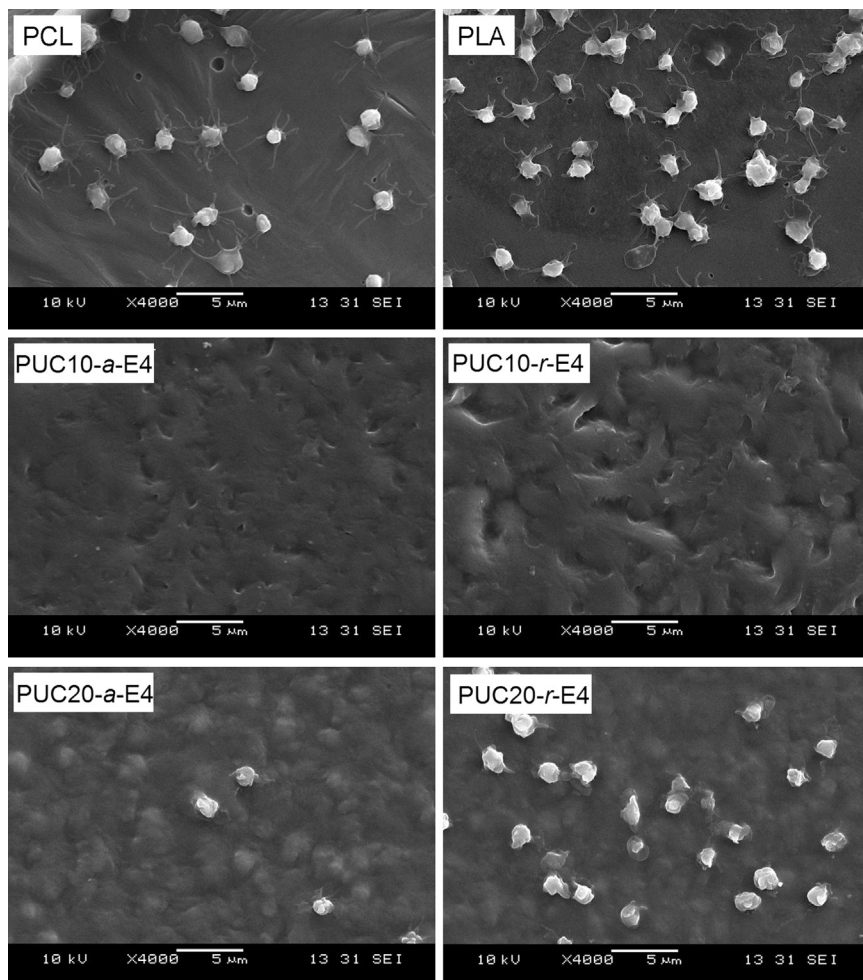
Figure 21.4 SEM images of platelet adhesion on tested films (×4000).

21.3.4 Preparation and characterizations of polyurethane nerve repair scaffolds

Autograft-based nerve transplantation is the first line of therapy for injured peripheral nerve repair in human clinical applications. However, limited graft availability and permanent loss of the donor site as well as the possibility of a mismatch between the defective nerve and the graft nerve diameter encourage investigations toward a safe and easily accessible artificial nerve scaffold to repair nerve gaps [2,3,6]. Our studies revealed here have reached preclinical animal testing trials, a necessary step before moving onto hospital patients. A vast number of tissue-engineering conduits of diverse materials have been explored to reconstruct the injured nerves [25], but

very few scaffolds have reached patients with limited clinical applications [1,35]. The major challenge in peripheral nerve tissue engineering is the determination of optimum materials for nerve regeneration. Biodegradable (co)polymers such as PCL have been widely used in nerve tissue engineering [10,11,36]. However, the hydrophobicity and poor mechanical properties of PCL limit its applications in medicine. The research presented here shows that block PUs based on PCL and PEG reduce the crystallization of PCL and improve their hydrophilicity. The alternating block PU based on PCL and PEG demonstrates excellent mechanical properties, facile processing, and compatibility for blood, cell, and tissue, suggesting that PUCL-*alt*-PEG is a suitable material for medical applications such as artificial nerve scaffolds (Figure 21.5).

In the beginning, chloroform was used for the scaffold preparation. However, due to its rapid volatility, scaffolds could not be properly obtained. Through trial and error, DMF was found to be a good solvent for the preparation of scaffolds. The PU nerve repair scaffolds show internal diameters of 1.28 mm with a wall thickness of approximately 260 μm. The external diameter was found to range from 1.78 to 1.8 mm (Figure 21.5(a)). SEM shows a well-distributed porous structure of PU scaffolds with pore sizes from 1 to 10 μm (Figure 21.5(b)). Porosity of the scaffolds was about 88−92% with pore interconnectivity. Proper mechanical properties are necessary for nerve repair scaffolds since they should remain intact during the suture process and during the long *in vivo* implant period after surgery. *In vitro* mechanical tests indicated that the PU nerve repair scaffolds possess suitable mechanical properties, including max loads of 4.98 ± 0.35 N and max stresses of 6.37 ± 0.5 MPa under wet conditions.

Generally, cells need pores to be large enough to allow them to migrate and to allow effective nutrient supply and metabolic waste removal, which is essential for cell growth. The inner diameter of the scaffolds is 1.28 mm, while the sciatic nerve diameter of the SD rat is 1.25 mm. Our goal is to design PUCL-*alt*-PEG nerve repair scaffolds that closely mimic native tissue microenvironments and provide a 3D mechanical framework for nerve cell attachment, proliferation, and nerve regeneration. Closer examination of the scaffold surface at higher magnification revealed that the web-like interconnected porous structures of PUCL-*alt*-PEG scaffolds should facilitate glial

(a)   (b)
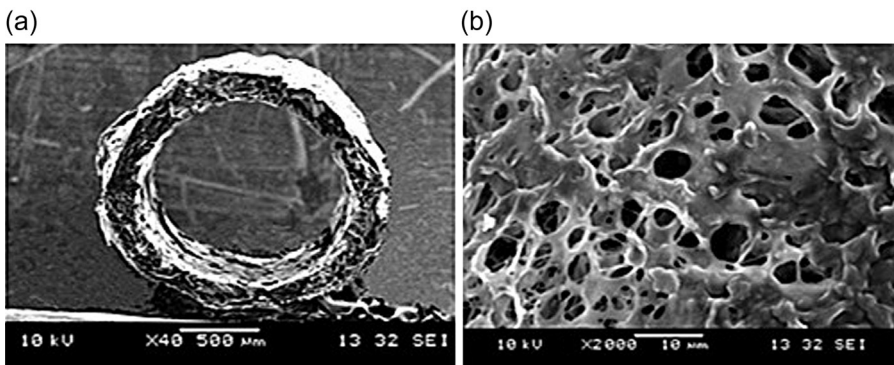
Figure 21.5 SEM images of polyurethane nerve-guided scaffold with controlled microporosity: (a) cross section morphology; (b) wall microstructure.

cell attachment and cellular communication, as well as cell division (Figure 21.5(b)). These results indicate that the PUCL-*alt*-PEG scaffold is a biocompatible and nerve conductive substrate that can provide structural cues for the cells to take up the proper shape and morphology and stimulate and guide axonal growth in the animal models [14,30]. Improved cytocompatibility of the alternating block PU scaffolds may be due to its improved hydrophilicity, flexibility of PEG chain, and surface array patterned microstructures stemming from its regular chemical structures. The improved hydrophilicity can also endow scaffold surfaces with superior initial cell attachment [18,37]. Because the cell membrane is a phospholipid bilayer, appropriate hydrophilic surfaces can be more conductive to initial cell attachments, while slightly hydrophobic surfaces would be suitable for growth and proliferation of some cell lines such as L929 [37].

21.3.5 In vitro *degradation of polyurethane scaffolds*

PCL is FDA-approved biodegradable polymer that is used as matrices for nerve tissue-engineering applications [38–40]. However, such biodegradable polyesters suffer from significant pH value changes that can cause inflammation in local tissue. To elucidate the degradation profiles of the PU scaffolds *in vitro*, change in pH value, weight loss ratio, ^{1}H NMR spectrum, and change of molecular weight during degradation *in vitro* were studied (Figures 21.6 and 21.7). Regarding the pH value change for PU scaffolds, degradation of the PU nerve-guided scaffolds studied over a 16 week period *in vitro* (Figure 21.6(a)) showed no significant pH value change (Figure 21.6(a)), even with a 17.5–24% weight loss during the 16 week *in vitro* degradation study (Figure 21.6(a)). Particularly, the PUCL-*alt*-PEG displayed a much smaller pH value change, even less than their random block PU counterparts PUCL-*ran*-PEG. It is interesting to note that a significant, sharp drop of pH value was observed between 12 and 14 weeks for PUCL-*ran*-PEG. The block PUs have a rapid swelling rate in first 72 h due to the hydrophilic PEG component that allows for enhanced hydrolytic degradation of the scaffolds.

The small changes in the pH values of degraded PU nerve-guided scaffolds may be due to the urethane chemical structure, which simultaneously generates acidic
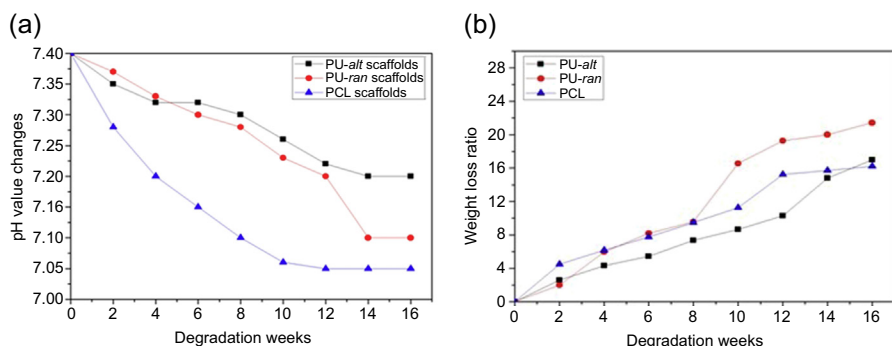
Figure 21.6 Degradation of polyurethane and PCL scaffolds *in vitro*: (a) pH value change; (b) weight loss ratio.

carboxylic groups and basic amine groups during degradation, unlike aliphatic polyesters such as PCL and PLA that generate only acidic carboxylic groups during degradation, resulting in significant reduction of pH. This small change in pH value of the PU scaffolds should reduce the inflammatory risk compared to PCL and PLA. In particular, PUCL-*alt*-PEG showed the lowest change in pH value during a 16 week degradation period from 7.40 to 7.23, compared with pH values of PUCL-*ran*-PEG from 7.40 to 7.08 and of PCL from 7.40 to 7.05 (Figure 21.6(a)). Furthermore, the relatively slow original weight loss of 17.5% of the PUCL-*alt*-PEG nerve-guided scaffold, determined from the *in vitro* 16 weeks degradation study, prevents premature scaffold collapse (Figure 21.6(b)). ¹H NMR analysis indicated that the degradation of block PU occurs from a break in the PCL–diol and urethane linkage —OOCNH—, resulting in PEG fragments that subsequently dissolve in PBS (Figure 21.7(a)).

Weight loss of the PU scaffolds proceeded much more quickly than that of PCL scaffolds from the 8th week (Figure 21.6(b)). Such results are in agreement with those revealed by ¹H NMR spectra (Figure 21.7(a)). Examination of the ¹H NMR spectra of PUCL-*alt*-PEG copolymer [18] revealed that proton signals of the urethane group —OOCNH— at $\delta = 4.94$ ppm and $\delta = 4.75$ ppm, where the former is connected to the PEG segment and the latter is connected to PCL, have disappeared after 16 weeks of degradation *in vitro*. The ¹H NMR spectrum showed that the degradation profile of PUCL-*alt*-PEG PUs resulted from the splitting of the urethane group —OOCNH— into small molecules (Figure 21.7(a)). Gel permeation chromatography (GPC) shows that almost all of the sample degraded into lower molecular weight components supporting the ¹H NMR data (Figure 21.7(b)).

21.3.6   In vitro *cell interactions*

The rat glial cell is a crucial cell in the nervous system, which not only connects and supports nerve components but also provides growth factors and distributes nutrients throughout the nervous system [41]. Thus these cells were selected to study *in vitro* cell interactions with nerve repair scaffolds. The cells were seeded onto
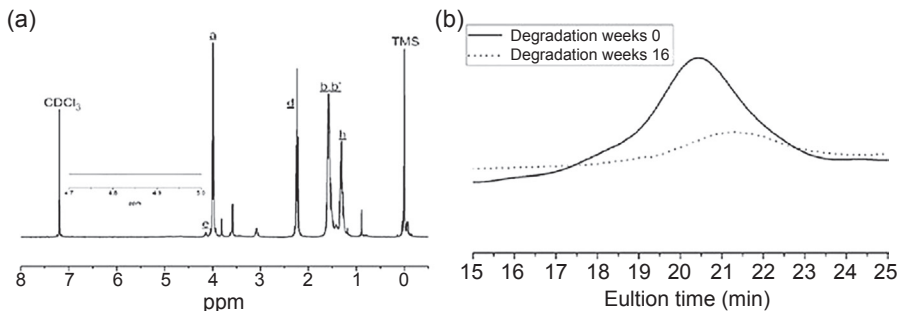
Figure 21.7 Degradation of PUCL-*alt*-PEG scaffolds at 16 weeks *in vitro*: (a) ¹H NMR spectrum; (b) GPC profiles before and after degradation.

films and scaffolds of PUCL-*alt*-PEG, PUCL-*ran*-PCL, and PCL with a cell density of 1.0×10^4 cells per well on a 12-well dish to examine the nerve cell compatibility. The cells were cultured on the films and scaffolds for 24, 48, and 72 h and the viable cell numbers in each specimen were estimated by a CCK-8 assay method. Results showed that the cell number increased significantly on PUCL-*alt*-PEG films and scaffolds, as PUCL-*alt*-PEG films and scaffolds give much higher optical values than PCL films and scaffolds, and also 20−30% higher than that of the PUCL-*ran*-PEG film and scaffold on 24 h incubation. As the water contact angles of both PUs are somewhat similar (Table 21.2), it is postulated that the surface roughness allows a higher growth rate during 24–72 h incubations on PUCL-*alt*-PEG films and scaffolds (Figure 21.8). Additionally, rat glial cells of PUCL-*alt*-PEG demonstrated a well-spread morphology bridging the pore, aligning themselves according to the shape and pattern of the scaffold, while most cells in the PCL scaffold were dead (Figure 21.8(a)).

Both PU materials display moderately hydrophilic surfaces, as alternating block PU PUCL-*alt*-PEG (sample PUC20-*a*-E4) and random block PU PUCL-*ran*-PEG (PUC20-*r*-E4) exhibited water contact angles of 88.9° and 88.3°, respectively. PUC20-*a*-E4 and PUC20-*r*-E4 films displayed the highest OD values among their own series on 72 h cell incubation, respectively [18], suggesting that the water contact angle of 88° may provide ideal wettability for glial cell growth. The greater optical density value of PUCL-*alt*-PEG on 24 h incubation on both film and scaffold suggests that initial cell attachment is more favorable on the surface of alternating PUs, most likely due to advantageous surface topography compared to that of PUCL-*ran*-PEG [42]. Measurements at later time points showed a remarkable increase in mitochondrial activity of glial cells on the PUCL-*alt*-PEG surface, demonstrating that cell attachment, proliferation, and extensive migration takes
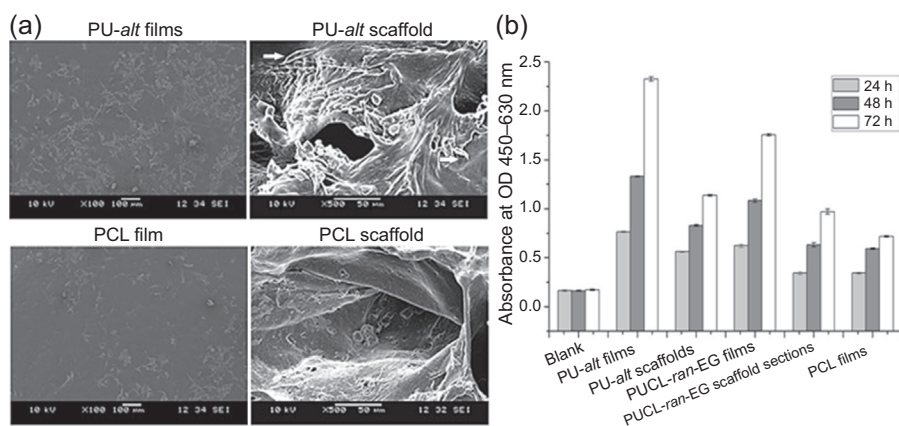
Figure 21.8 SEM images and CCK-8 assay: (a) glial cell adhesion and proliferation on films and scaffolds of PUCL-*alt*-PEG and PCL cultured at 48 h; white arrow, three-dimensional cell growth in PUCL-*alt*-PEG scaffold; (b) CCK-8 assays of glial cell viability on PUCL-*alt*-PEG, PUCL-*ran*-PEG and PCL-based films and scaffolds.

place on the PUCL-*alt*-PEG surface. PUCL-*ran*-PEG, however, gives lower CCK-8 values and displays anomalous cell morphology, indicating lower attachment and proliferation of glial cells (Figure 21.8). Cell morphologies further confirm that PUCL-*alt*-PEG surfaces support attachment, growth, and proliferation of glial cells with better original spread star-shaped morphology than the random block counterpart PUCL-*ran*-PEG.

The viability of glial cells cultured on random block PU PUCL-*ran*-PEG was compared with that of alternating block PU PUCL-*alt*-PEG (Figure 21.8(b)). It was clear that PUCL-*alt*-PEG provided much better cytocompatibility for neural glial cells than traditional random block PU. SEM images and CCK-8 assays confirmed that PUCL-*alt*-PEG possessed excellent cell compatibility with respect to the nerve cell line (Figure 21.8). Figure 21.9 provides a morphological comparison of glial cells on both alternating and random PU films. After 72 h incubation, glial cells spread well and exhibited their original star-shaped morphology on the alternating series PUCL-*alt*-PEG. However, on the random series PUCL-*ran*-PEG, the cells tended to be fibroid and some lacked the star-shaped morphology.

From the above discussion, it can be concluded that alternating block PU PUCL-*alt*-PEG displays the highest cell viability of rat glial cells. This suggests that alternating block PU (such as sample PUC20-*a*-E4) would be an ideal class of PUs with
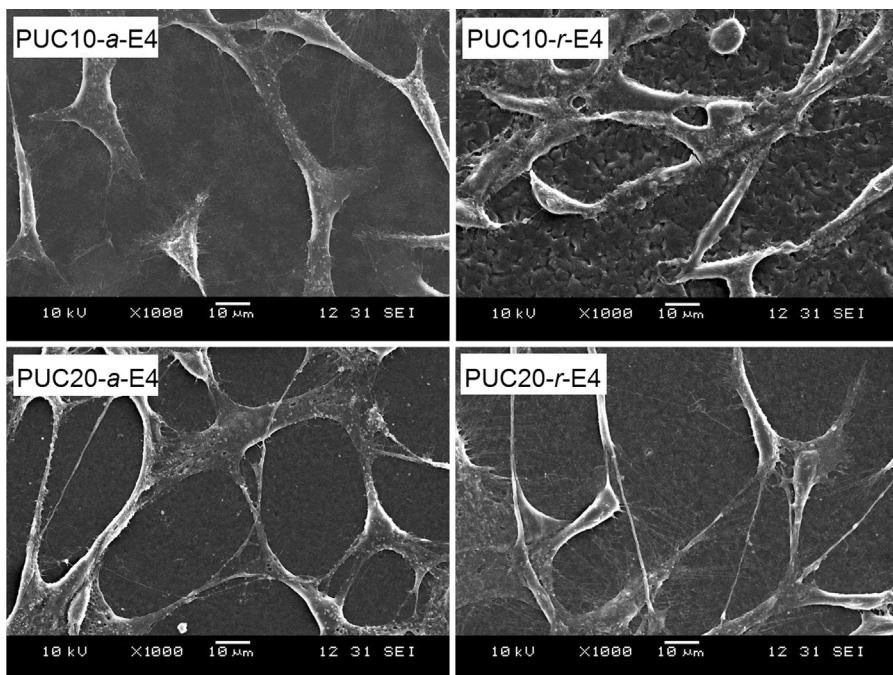
Figure 21.9 Morphology of glial cell proliferation on PCL and PEG-based block polyurethane films at 3 days culture (×1000).

optimum composition and proper surface properties for cell compatibility. In terms of optimal material composition, similar conclusions were made in previous research on fibroblast L929 cells and rat aortic smooth muscle cells [43].

21.3.7 Functional behavior training and electrophysiological assays for nerve repair

The SD rat (sciatic nerve defect) model was used to evaluate the peripheral nerve regeneration capabilities of the six prepared groups, that is, PUCL-*alt*-PEG, autograft, PUCL-*ran*-PEG scaffold, PCL scaffold, silicone tube, and negative control. To determine the functional characteristics of our scaffolds, PU and PCL nerve guides of 1.28 mm in diameter were determined to be strong enough to maintain an intact structure throughout the surgical implantation process. During the experiments, all rats remained in good health and did not show any wound-related complications except for the silicone tube and negative control groups. At predetermined periods (2, 4, 8, 10, and 14 weeks postoperatively), the nerve regeneration behavior was observed by walking track analysis. SFI values of different groups are compared in Figure 21.10(a). In our study, an SFI value of −24% recovery was observed in the PUCL-*alt*-PEG group after 14 weeks postimplantation, which was higher than the −28% recovery SFI value of the autograft group (Figure 21.10(a)) and much better than the −35% recovery SFI value of PUCL-*ran*-PEG, and also the SFI values of PCL, silicone tube, and negative control groups. The silicone and negative control groups gave quite poor results and the negative group showed no signs of nerve repair. The footprints of animals implanted with PUCL-*alt*-PEG scaffolds at 4, 8, and 14 weeks postoperatively are also displayed in Figure 21.10(b). It can be seen that at 2 and 8 weeks, the footprint images were quite narrow and abnormal. The motor function was not at all recovered at this time. At the 14th week mark, the footprint images returned to normal, indicating that the nerve motor function recovered significantly.

CMAP evaluation can offer an important parameter for studying the conducting function of a peripheral nerve. To determine whether or not the functional reinnervation occurred through the scaffolds, electrophysiological analysis was performed. The electrophysiological signals of CMAP from different groups, that is, PUCL-*alt*-PEG, PUCL-*ran*-PEG, autograft, PCL scaffolds, silicone tube, and negative control, are compared in Figure 21.11. It is noted that the PUCL-*alt*-PEG group gave the best signal (Figure 21.11(a)), much better than PUCL-*ran*-PEG and other groups, and importantly, better than the autograft (Figure 21.11(c)).

The signals of CMAPs and the corresponding action potentials of PUCL-*alt*-PEG, PUCL-*ran*-PEG, autograft, PCL scaffolds, silicone tube, and negative control after 4, 8, and 14 weeks implantation were also compared with the signals of the rats' normal sides (Figure 21.12). The action potentials were clearly noticeable in PUCL-*alt*-PEG, PUCL-*ran*-PEG, autograft, and PCL scaffold groups after 4 weeks, indicating rapid functional recovery of the injured nerves. The potentials became more intense after 9 and 14 weeks, indicating notable nerve repair. It was impressive that the PUCL-*alt*-PEG group displayed stronger signals than the autograft group.
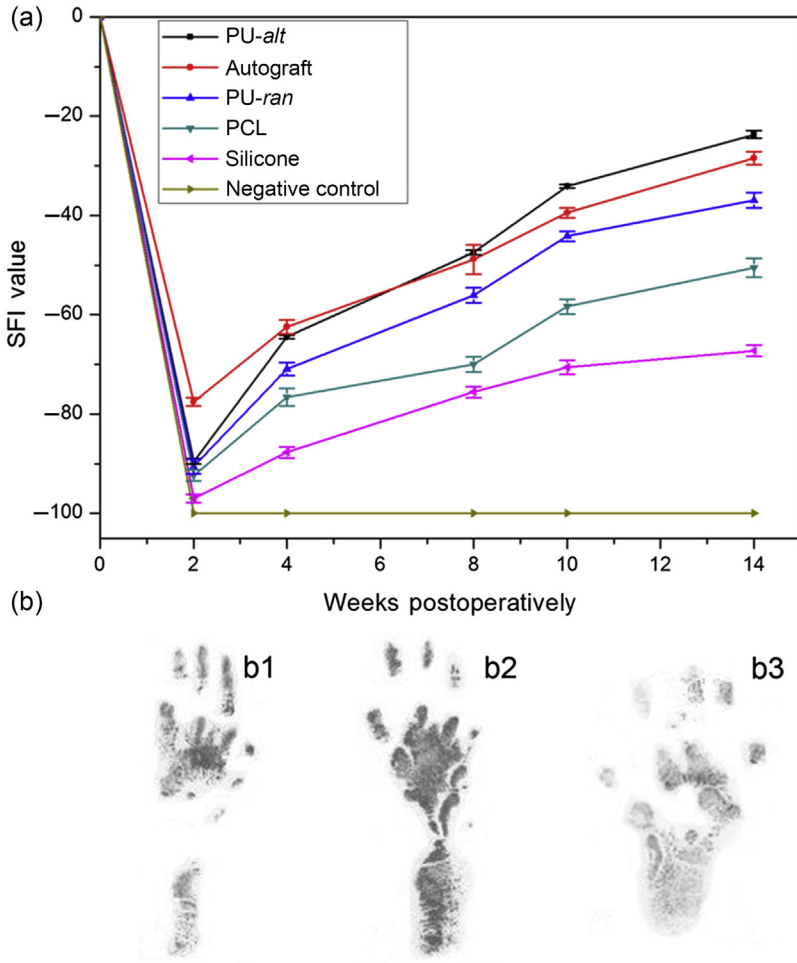
Figure 21.10 Walking track analysis, (a) sciatic function index (SFI) values of rats at 2, 4, 8, 10, and 14 weeks after implantation, $n=3$; *$P<0.05$; (b) footprints at 4 (b1), 8 (b2), and 14 (b3) weeks postoperatively.

This demonstrates that scaffolds of novel PU-*alt* (PUCL-*alt*-PEG) show comparable or better nerve repair results than the autograft, which is considered a "gold standard" in medical implantation [24].

21.3.8 Histological assessment

Throughout the nerve regeneration process, structures of PU and PCL nerve-guided scaffolds remained stable (Figure 21.13(b) and (e)). This is an important factor for axon growth. After 9 weeks, the PUCL-*ran*-PEG nerve-guided scaffolds were degraded duly and the boundaries between nerve and scaffold were barely
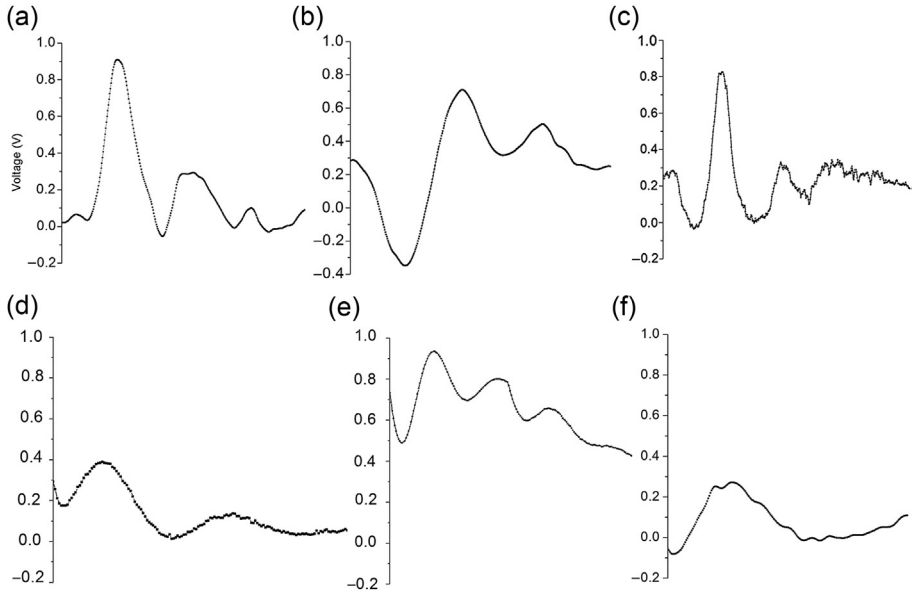
Figure 21.11 Electrophysiological signals of CMAP examinations carried out at 14 weeks after implantation at the injured side in each group: (a) PUCL-*alt*-PEG, (b) PUCL-*ran*-PEG, (c) autograft, (d) PCL, (e) silicone tube, and (f) negative control. $n=4$; $*P<0.05$.
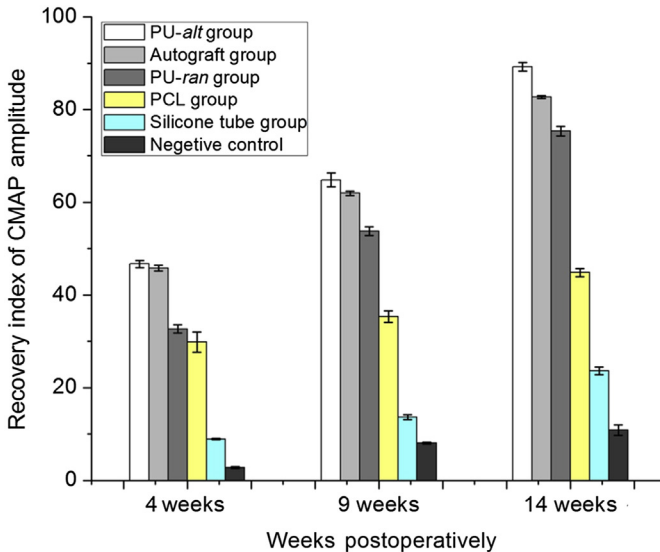
Figure 21.12 CMAP signals were compared with the animal's contralateral control and expressed as the CMAP ratio, $n=4$; $*P<0.05$.

distinguishable (Figure 21.13(b)). The regenerative nerve tissues could be clearly observed as the PUCL-*ran*-PEG nerve-guided scaffold degraded completely at 20 weeks postoperatively (Figure 21.13(c)). Notably, the regenerated nerve from the proximal and distal nerve endings grew into the middle of the scaffold, as the structures of PUCL-*alt*-PEG nerve repair scaffolds were stably maintained, while no inflammatory signs or adverse tissue reactions were seen at the implantation site (Figure 21.14(a) and (b)). On the other hand, PCL and silicon tubes showed very slow or nonexistent degradation (Figure 21.13(e) and (f)). After the PU scaffolds were dissected carefully under high magnification microsurgery at the 9th week
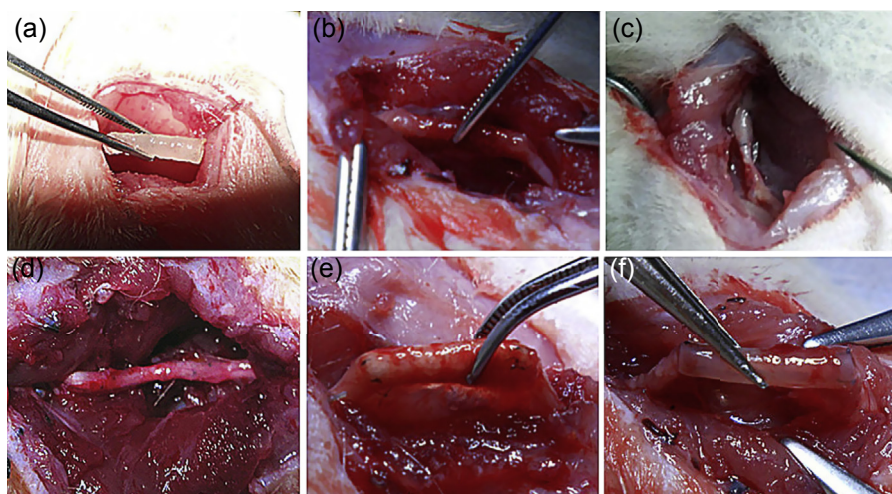
Figure 21.13 PUCL-*ran*-PEG nerve scaffolds prior to and after the implantation: (a) the sciatic nerve was transected and bridged by a PU nerve-guided scaffold; (b) PUCL-*ran*-PEG implanted in rat after 9 weeks was surrounded with abundant capillaries; (c) PUCL-*ran*-PEG degraded almost completely at 20 weeks implantation; (d) autologous nerve-guided defected nerve in rat after 9 weeks; (e) PCL implant in rat after 9 weeks was surrounded by a layer of fibrous connective tissue; (f) silicone tube implant in rat after 9 weeks.

Figure 21.14 Scaffold degradation and regenerated nerves of PUCL-*alt*-PEG scaffolds: (a) implanted in rat at 9 weeks postoperatively (surrounded with abundant capillaries); (b) a regenerated nerve after taking off the scaffolds; (c) scaffolds degraded completely at 32 weeks implantation with a mature regenerated nerve.

postoperatively, a regenerated nerve was observed. The mature regenerated nerve tissues could be clearly observed as the PUCL-*alt*-PEG scaffolds degraded completely at 32 weeks postimplantation (Figure 21.14(c)). No inflammatory signs or adverse tissue reactions were observed. The growth rate of the nerve matched very well with the degradation rate of the scaffold (Figure 21.14(c)).

21.3.9 *Immunofluorescent staining and scaffold* in vivo *degradation*

HE staining was employed to assess the morphology of regenerated nerves at the mid section at the 9th week postoperatively (Figure 21.15(a–e)). It was observed that the neurofilaments grew rapidly along the entire space of PUCL-*alt*-PEG, PUCL-*ran*-PEG scaffolds, and autografts (Figure 21.15(a–c)). The neurofilaments distributed regularly in these groups. On the contrary, PCL scaffold and silicone tube showed less neurofilament growth (Figure 21.15(d) and (e)). To observe axonal growth, Neurofilament-200 (NF-200) used as a protein marker of axons. The anti-NF200 cross section immunochemical stainings at mid sections of regenerated axons are shown in Figure 21.15(f–j). PUCL-*ran*-PEG nerve-guided scaffolds were found to have axons with larger diameters compared with those of PCL groups, and much larger than those of silicone tube groups (Figure 21.15(g), (i), and (j)). The PUCL-*alt*-PEG scaffold group was found to have larger axon diameters compared with the autograft group (Figure 21.15(f) and (h)).

To observe in more detail the axon and myelin sheath regeneration inside the scaffolds, TEM was used to examine cross sections of regenerated axons and myelin sheath (Figure 21.16). At 14 weeks postoperatively, most myelinated nerves have matured in PUCL-*alt*-PEG, PUCL-*ran*-PEG scaffolds, and autograft groups (Figure 21.16(a–c)), while PCL and silicone tube groups had very thin myelinated nerves in both middle and distal sites. The negative control did not generate any nerve at all (not shown).

As regenerated nerves matured, both the diameters of myelinated nerves and the thickness of myelin sheath ranked from high to low accordingly: PUCL-*alt*-PEG, autograft, PUCL-*ran*-PEG, PCL, and silicone tube (Figure 21.17). The diameter
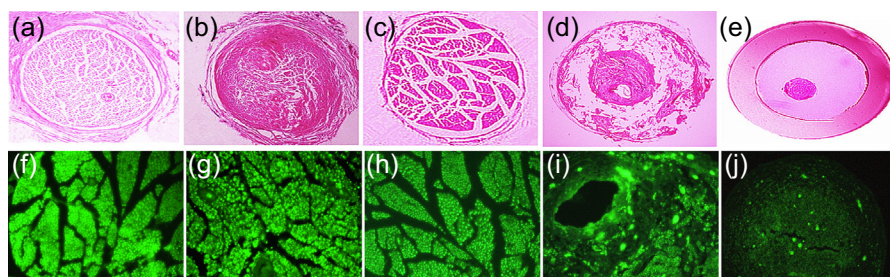
Figure 21.15 Cross section of the mid section of regenerated nerve at 9 weeks postoperatively: (a, f) PUCL-*alt*-PEG; (b, g) PUCL-*ran*-PEG scaffolds; (c, h) autograft; (d, i) PCL scaffold; (e, j) silicone tube. (a–e) HE staining, ×4; (f–j) antineurofilament staining, ×20.
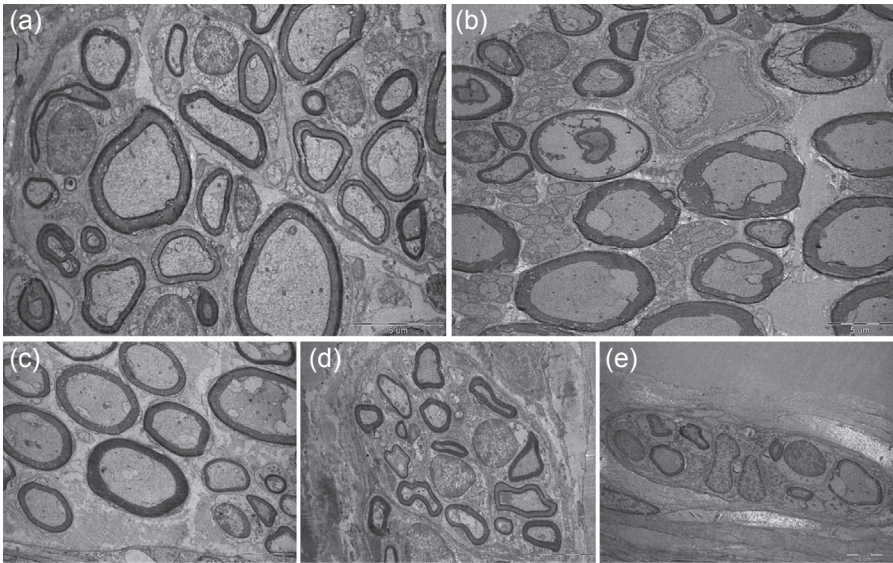
Figure 21.16 TEM images of ultrathin sections showing myelinated axons at the middle portion at 14 weeks postoperatively. Images (a) PUCL-*alt*-PEG; (b) PUCL-*ran*-PEG scaffolds; (c) autograft; (d) PCL scaffold; (e) silicone tube.
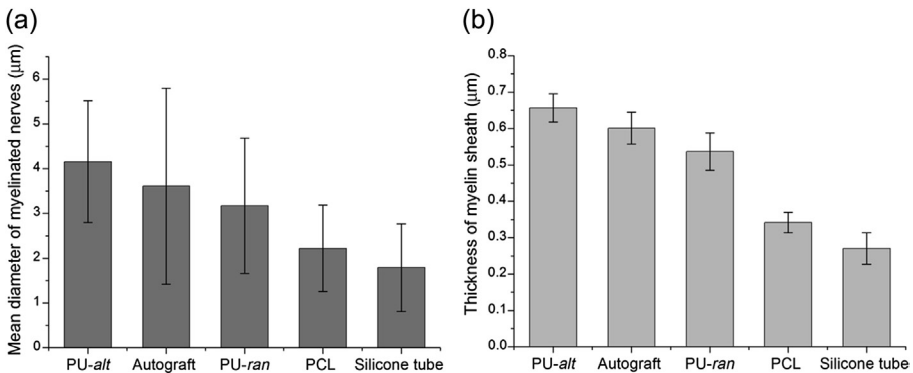
Figure 21.17 Statistical analysis of diameters of myelinated nerves (a) and myelin sheath thickness (b) for each group: $n=6$, *$P<0.05$.

of the myelinated nerves and the thickness of myelin sheath in the PUCL-*ran*-PEG group were almost 1.5 times than that of the silicone tube group and close to that of the autograft group. The average diameter and thickness of myelin sheath at the mid-portion of myelinated nerves in the PUCL-*alt*-PEG scaffold group were larger than those of the autograft group. These results revealed that biodegradable block PUs, especially PU-*alt*, are potentially suitable biomaterials for peripheral nerve regeneration [18].
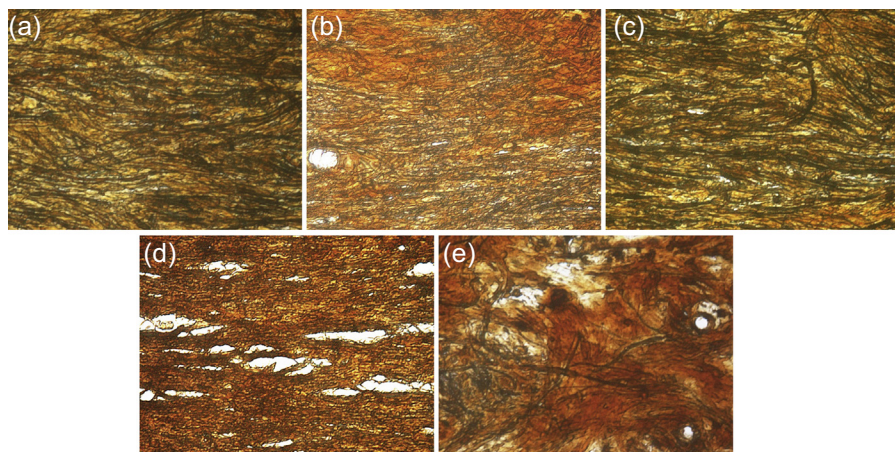
Figure 21.18 Ammonia silver staining of the longitudinal section of mid section of nerves at 14 weeks postimplantation: (a) PUCL-*alt*-PEG; (b) PUCL-*ran*-PEG; (c) autograft; (d) PCL; (e) silicone.

Ammonia silver staining, which was used to show regenerated nerve fibers and axons, demonstrated that axon myelin was nearly completely regenerated in PUCL-*alt*-PEG, PUCL-*ran*-PEG scaffold, and autograft groups with a bit of irregularity in their arrangements (Figure 21.18(a–c)). The axon myelin is almost completely regenerated and regularly spread throughout the PUCL-*ran*-PEG nerve-guided scaffold compared with the autograft group at 14 weeks postoperatively (Figure 21.18(b) and (c)). However, axon myelin showed little regeneration as well as a lack of regular arrangements in the PCL and silicone tube groups (Figure 21.18(d) and (e)). The axon myelins regenerated completely and spread regularly throughout the PUCL-*alt*-PEG scaffold group (Figure 21.18(a)). In the autograft group, axon myelins generally regenerated well but showed a slight irregularity in their arrangement (Figure 21.18(b)). Nerve regeneration in PUCL-*alt*-PEG scaffolds looked better than that of the autograft. The reasons may be in part due to the porous structures and high permeability of the PUCL-*alt*-PEG scaffolds, as the amphiphilic PU nerve-guided scaffolds can readily allow nutrient and metabolites to permeate through the scaffold.

To evaluate the atrophy of rat gastrocnemius muscles resulting from dysfunction of the sciatic nerves, gastrocnemius muscles of rats in the six groups were stained with Masson's trichrome staining since gradual functional recovery of the sciatic nerves is accompanied by reduction of atrophy [6,27]. Prominent reduction in muscle mass was obvious in rats with disrupted sciatic nerves that were implanted with silicone tubes, showing serious muscle atrophy (Figure 21.19(d)). In contrast, muscle atrophy was insignificant in rats implanted with PU nerve-guided scaffolds and autograft (Figure 21.19(a–c)). The average diameters of the muscle fibers in PU scaffolds and autograft were all larger than those of the fibers in PCL scaffold, silicone tube, and negative control groups (Figure 21.20). The PUCL-*alt*-PEG scaffold group had the highest average diameter of the muscle fiber, slightly larger than that of the autograft.
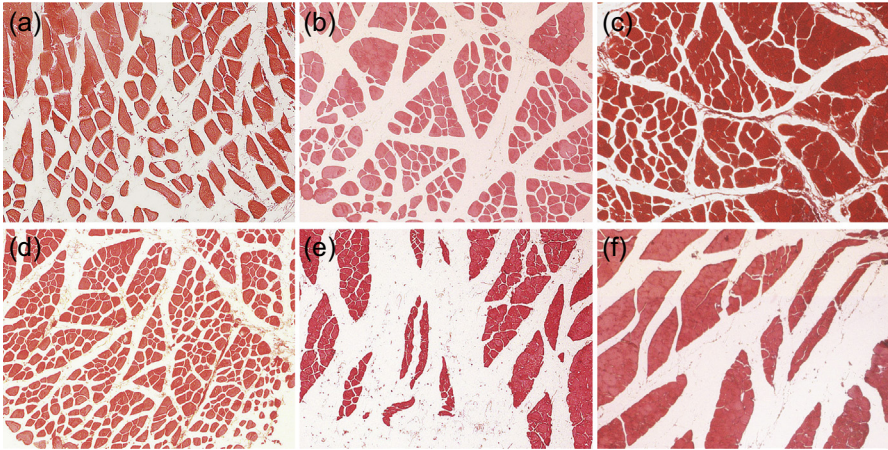
Figure 21.19 Masson's trichrome staining of gastrocnemius muscle cross section at 14 weeks implantation. (a) PUCL-*alt*-PEG; (b) PUCL-*ran*-PEG; (c) autograft; (d) PCL; (e) silicone tube; (f) negative control groups, $n=4$; *$P<0.05$; scale bar$=60\,\mu$m.
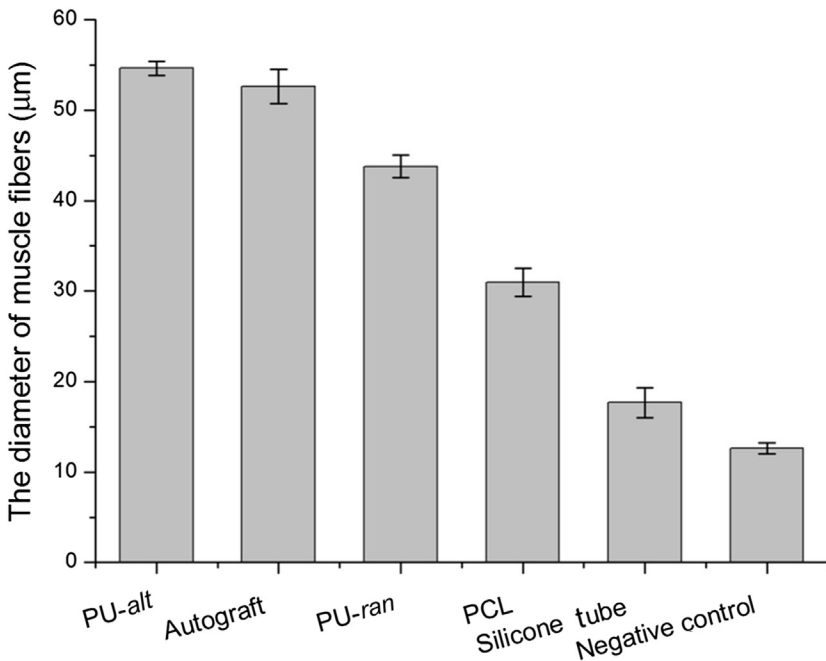
Figure 21.20 The average diameters of rat gastrocnemius muscle fibers in different groups, $n=4$, *$P<0.05$.

Results of the histological assessment along with that of SFI and CMAP analysis confirm that PUCL-*alt*-PEG nerve-guided scaffolds are most suitable for applications in nerve regeneration. Nerve defects were successfully bridged in PUCL-*alt*-PEG groups from the 8th week postoperatively. The walking track and electrophysiological
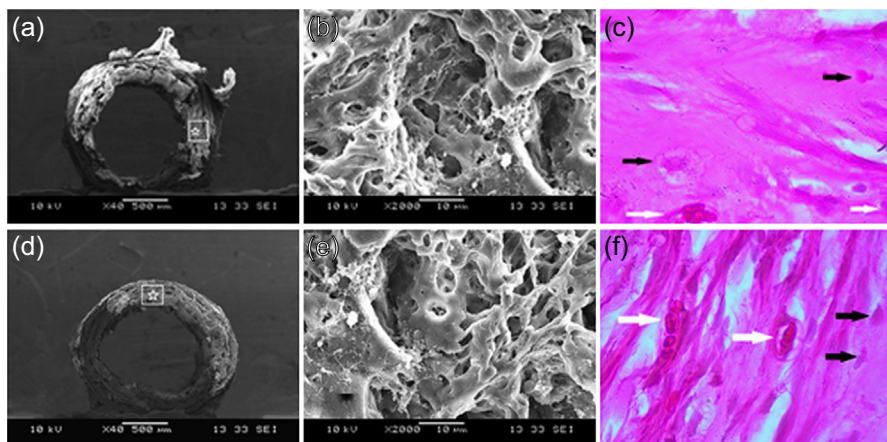
Figure 21.21 Surface morphology of polyurethane scaffolds *in vivo* degradation at 9 weeks implantation *in vivo*, upper row: (a) a PUCL-*alt*-PEG scaffold at low magnification; (b) higher magnification ×2000 of dotted box from panel A star; (c) HE staining ×100 from dotted box from panel A; lower row: (d) PUCL-*ran*-PEG scaffold at low magnification; (e) higher magnification ×2000 of dotted box from panel D star; (f) HE staining ×100 from dotted box from panel D. Black arrow, blood vessels; white arrow, connective tissues.

evaluations showed quick nerve functional recovery (Figures 21.9–21.12), further proving tissue compatibility of the PUCL-*alt*-PEG scaffolds. According to the HE staining results, the quicker nerve regeneration of PUCL-*alt*-PEG scaffold compared to that of nonporous silicone tube and negative control may be explained by vascular ingrowth into the scaffold through its column-shape porous structure (Figure 21.21). Although the PUCL-*ran*-PEG nerve-guided scaffold demonstrates good nerve repair, it is inferior to PUCL-*alt*-PEG scaffold and autograft groups in terms of nerve repair capability.

From the HE staining, TEM observation of ultrathin sections, ammonia silver staining, Masson's trichrome staining, and statistical analysis of the diameter and thickness measurements of the myelinated nerves and myelin sheath (immunohistochemistry analysis), all results support the conclusion that the PUCL-*alt*-PEG nerve-guided scaffold provides the best nerve function repair capability among all the groups (Figures 21.15–21.20). Possible explanations for the optimal nerve function repair capability of the PUCL-*alt*-PEG nerve-guided scaffold include the well-controlled chemical structure of the alternating block PU, which results in a regular microstructure that displays a more regular and rougher surface than its random counterpart (Figure 21.3). Combined with appropriate hydrophilicity, these factors facilitate cell attachment and provide biochemical and topographic cues to enhance nerve regeneration. Another reason may be that PUCL-*alt*-PEG allows for the mildest pH value change during implantation resulting in less inflammation, enhancing nerve generation and growth.

In vivo degradation of PUCL-*alt*-PEG and PUCL-*ran*-PEG scaffolds after 9 weeks is shown in Figure 21.21, which demonstrates significant degradation and tissue compatibility of the PUCL-*alt*-PEG nerve repair scaffolds. According to the *in vivo* studies, degradation of the scaffolds at the 9th week was accompanied by invasion

of blood vessels and connective tissue (Figure 21.21(c) and (f)), indicating that the PU scaffolds can provide structural features adaptable to the physiological environment, and possess adequate strength and elasticity to allow regular motion of muscles around the conduit without resulting in scaffold collapse during degradation (Figure 21.21(a) and (d)). Sciatic nerve cells, showing well-spread and flattened morphology, aligned themselves following the physical shape of the nerve-guided scaffold, further demonstrating that PU nerve scaffolds, being cytocompatible nerve conductive substrates, provide structural cues for the cells to take up the desired morphology (Figure 21.6(a)). Blood vessels infiltrated into the PU scaffold walls through the column-shaped micro-sized pores of the outer surface as shown in Figure 21.21(c) and (f). The satisfactory nerve regeneration through PU scaffolds may be due to its porous structure and high permeability.

Combined with its suitable mechanical properties, impressive nerve regeneration ability, and cytocompatibility, biodegradable PUCL-*alt*-PEG nerve repair scaffolds show potential in clinical applications for peripheral nerve repair.

21.4   Conclusions

Nerve repair scaffolds based on a novel, alternating block PU PUCL-*alt*-PEG show proper mechanical strength and biodegradability. An *in vivo* SD rat sciatic nerve damage model revealed that the nerve repair scaffolds achieved satisfactory nerve regeneration associated with excellent neurogenesis, and functional rehabilitation of neurons after 32 weeks postimplantation. The amphiphilic PUCL-*alt*-PEG scaffolds exhibited comparable or slightly better nerve regeneration than autografts, which are widely used clinically. These results indicate that PUCL-*alt*-PEG nerve repair scaffolds have potential applications in large nerve gap repair and possibly even in central nervous system regeneration.

Acknowledgments

References

[1] Daly WT, Knight AM, Wang H, de Boer R, Giusti G, Dadsetan M, et al. Comparison and characterization of multiple biomaterial conduits for peripheral nerve repair. Biomaterials 2013;34:8630–9.

[2] Scott JB, Afshari M, Kotek R, Saul JM. The promotion of axon extension *in vitro* using polymer-templated fibrin scaffolds. Biomaterials 2011;32:4830–9.

[3] Pabari A, Yang SY, Seifalian AM, Mosahebi A. Modern surgical management of peripheral nerve gap. J Plast Reconstr Aesthet Surg 2010;63:1941–8.

 [4] Chew SY, Mi R, Hoke A, Leong KW. Aligned protein-polymer composite fibers enhance nerve regeneration: a potential tissue-engineering platform. Adv Funct Mater 2007;17:1288–96.

 [5] Meek MF, Varejao AS, Geuna S. Muscle grafts and alternatives for nerve repair. J Oral Maxillofac Surg 2002;60:1095–6.

 [6] Tang S, Zhu JX, Xu YB, Jiang MH, Quan DP. The effects of gradients of nerve growth factor immobilized PCLA scaffolds on neurite outgrowth *in vitro* and peripheral nerve regeneration in rats. Biomaterials 2013;34:7086–96.

 [7] Zhan XD, Gao MY, Jiang YW, Zhang WW, Wong WM, Yuan QJ, et al. Nanofiber scaffolds facilitate functional regeneration of peripheral nerve injury. Nanomedicine 2012;9:305–15.

 [8] Whitlock EL, Tuffaha SH, Luciano JP, Yan Y, Hunter DA, Magill CK, et al. Processed allografts and type I collagen conduits for repair of peripheral nerve gaps. Muscle Nerve 2009;39:787–99.

 [9] Angius D, Wang H, Robert JS, Yearim GC, Michael JY, Anthony JW. A systematic review of animal models used to study nerve regeneration in tissue-engineered scaffolds. Biomaterials 2012;33:8034–9.

[10] Den Dunnen WFA, Van der Lei B, Schakenraad JM, Stokeroos I, Blaauw E, Bartel H, et al. Poly(DL-lactide-e-caprolactone) nerve guides perform better than autologous nerve grafts. Microsurgery 1996;17:348–57.

[11] Meek MF, Den Dunnen WFA, Schakenraad JM, Robinon PH. Long-term evaluation of functional nerve recovery after reconstruction with a thin-walled biodegradable Poly(DL-lactide-e-caprolactone) nerve quide, using walking track analysis and electrostimulation tests. Microsurgery 1999;19:247–53.

[12] Luis AL, Rodrigus JM, Lobato JV, Lopes MA, Amado S, Veloso AP, et al. Evaluation of two biodegradable nerve guides for the reconstruction of the rat sciatic nerve. Biomed Mater Eng 2007;17:39–52.

[13] Santerre JP, Woodhouse K, Laroche G, Labow RS. Understanding the biodegradation of polyurethanes: from classical implants to tissue engineering materials. Biomaterials 2005;26:7457–70.

[14] Niu YQ, Chen KC, He T, Yu WY, Huang SW, Xu KT. Scaffolds from block polyurethanes based on poly(ε-caprolactone) (PCL) and poly(ethylene glycol) (PEG) for peripheral nerve regeneration. Biomaterials 2014;35:4266–77.

[15] Loh XJ, Sng KBC, Li J. Synthesis and water-swelling of thermoresponsive poly(ester urethane)s containing poly(ε-caprolactone)poly(ethylene glycol) and poly(propylene glycol). Biomaterials 2008;29:3185–94.

[16] Yang LX, Wei JZ, Yan L, Huang YB, Jing XB. Synthesis of OH group-containing, biodegradable polyurethane and protein fixation on its surface. Biomacromolecules 2011;12:2032–8.

[17] Pan JY, Li GY, Chen ZF, Chen XY, Zhu WF, Xu KT. Alternative block polyurethanes based on poly(3-hydroxybutyrate-*co*-4-hydroxybutyrate) and poly (ethylene glycol). Biomaterials 2009;30:2975–84.

[18] Li GY, Li D, Niu YQ, Chen KC, Xu KT. Alternating block polyurethanes based on PCL and PEG as potential nerve regeneration materials. J Biomed Mater Res A 2014;102:685–97.

[19] Niu YQ, Li LJ, Chen KC, Chen FR, Liu XY, Ye JF, et al. Scaffolds from alternating block polyurethanes of PCL and PEG with stimulation and guidance of nerve growth and better nerve repair than autograft. J Biomed Mater Res Part A 2015;103(7):2355–64. http://dx.doi.org/10.1002/jbm.a.35372.

[20] Mei TZ, Zhu YH, Ma TC, He T, Li LJ, Wei CJ, et al. Synthesis, characterization and biocompatibility of alternating block polyurethanes based on PLA and PEG. J Biomed Mater Res A 2014;102:3243–54.

[21] Li GY, Liu YH, Li DD, Zhang LL, Xu KT. A comparative study on structure-property elucidation of P3/4HB and PEG based block polyurethanes. J Biomed Mater Res A 2012;100:2319–29.

[22] Li GY, Li P, Qiu HD, Li DD, Xu KT. Synthesis, characterizations and biocompatibility of alternating block polyurethanes based on P3/4HB and PPG-PEG-PPG. J Biomed Mater Res A 2011;98:88–9.

[23] Hoppen HJ, Leenslag J, Pennings AJ, Van der Lei B, Robinson PH. Two-ply biodegradable nerve guide: basic aspects of design, construction and biological performance. Biomaterials 1990;11(4):286–90.

[24] Johnson EO, Soucacos PN. Nerve repair: experimental and clinical evaluation of biodegradable artificial nerve guides. Injury 2008;39S:S30–6.

[25] Angius D, Wang H, Spinner RT, Gutierrez-Cotto Y, Yaszemski MJ, Windebank AJ. A systematic review on animal models used to study nerve regeneration in tissue-engineering scaffolds. Biomaterials 2012;33:8034–9.

[26] Tran RT, Choy WM, Cao H, Qattan I, Chiao JC, Ip WY, et al. Fabrication and characterization of biomimetic multichanneled crosslinked-urethane doped polyester nerve guides. J Biomed Mater Res A 2014;102:2793–804.

[27] Bian YZ, Wang Y, Aibaidoula G, Chen GQ, Wu Q. Evaluation of Poly(3-hydroxybutyrate-*co*-3-hydroxyhexanoate) conduits for peripheral nerve regeneration. Biomaterials 2009;30:217–25.

[28] Oh SH, Park IK, Kim JM, Lee JH. *In vitro* and *in vivo* characteristics of PCL scaffolds with pore size gradient fabricated by a centrifugation method. Biomaterials 2007;28:1664–71.

[29] Bain JR, Mackinnon SE, Hunter DA. Functional evaluation of complete sciatic, peroneal, and posterior tibial nerve lesions in the rat. Plast Reconstr Surg 1989;83:129–38.

[30] Quigley AF, Razal JM, Thompson BC, Moulton SE, Kita M, Kennedy EL, et al. A conducting-polymer platform with biodegradable fibers for stimulation and guidance of axonal growth. Adv Mater 2009;21:4393–7.

[31] Arriagada PV, Growdon JH, Hedley-Whyte ET, Hyman BT. Neurofibrillary tangles but not senile plaques parallel duration and severity of Alzheimer's disease. Neurology 1992;42:631–9.

[32] Arriagada PV, Marzloff K, Hyman BT. Distribution of Alzheimer-type pathologic changes in nondemented elderly individuals matches the pattern in Alzheimer's disease. Neurology 1992;42:1681–8.

[33] Yang Y, Ding F, Wu J, Hu W, Liu J, Gu X. Development and evaluation of silk fibroin-based nerve grafts used for peripheral nerve regeneration. Biomaterials 2007;28:5526–35.

[34] Chen ZF, Cheng ST, Xu KT. Block Poly(ester-urethane)s based on poly(3-hydroxybutyrate-co-4-hydroxybutyrate) and poly(3-hydroxyhexanoate-co-3-hydroxyoctonoate). Biomaterials 2009;30(12):2219–30.

[35] Oh HH, Ko YG, Kawazoe N, Chen GP. Preparation of porous collagen scaffolds with micropatterned structures. Adv Mater 2012;24:4311–6.

[36] Zhang HF, Cooper AI. Aligned porous structures by directional freezing. Adv Mater 2007;19:1529–33.

[37] Ou WF, Qiu HD, Chen ZF, Xu KT. Biodegradable block poly(ester-urethane)s based on poly(3-hydroxybutyrate-co-4-hydroxybutyrate) copolymers. Biomaterials 2011;32:3178–88.

[38] Mobarakeh LG, Prabhakaran MP, Moeshed M, Nasr-Esfahani MH, Ramakrishna S. Bio-functionalized PCL nanofibrous scaffolds for nerve tissue engineering. Mater Sci Eng C 2010;30:1129–36.

[39] Schnell E, Klinkhammer K, Balzer S, Brook G, Klee D, Dalton P, et al. Guidance of glial cell migration and axonal growth on electrospun nanofibers of poly(ε-caprolactone) and a collagen/poly(ε-caprolactone) blend. Biomaterials 2007;28:3012–25.

[40] Rodríguez FJ, Gómez N, Perego G, Navarro X. Highly permeable polylactide–caprolactone nerve guides enhance peripheral nerve regeneration through long gaps. Biomaterials 1999;20:1489–500.

[41] Aarum J, Sandberg K, Haeberilein SLB, Persson MAA. Migration and differentiation of neural precursor cells can be directed by microglia. PNAS 2003;100:15983–8.

[42] Kaiser JP, Reinmann A, Bruinink A. The effect of topographic characteristics on cell migration velocity. Biomaterials 2006;27:5230–41.

[43] Qiu HD, Li DD, Chen X, Fan KY, Chen KC, Xu KT. Synthesis, characterizations and biocompatibility of block poly(ester-urethane)s based on biodegradable poly(3-hydroxybutyrate-co-4-hydroxybutyrate) (P3/4HB) and poly(ε-caprolactone) (PCL). J Biomed Mater Res A 2013;101A(1):75–86.

The use of biodegradable polyurethane in the development of dermal scaffolds

22

J.E. Greenwood[1,], M.J.D. Wagstaff[2]*
[1]Skin Engineering Laboratory, Hanson Institute, Adelaide, South Australia; Royal Adelaide Hospital, Adelaide, South Australia; [2]Royal Adelaide Hospital, Adelaide, South Australia
*Corresponding author: john.greenwood@sa.gov.au

22.1 Introduction

The issues posed to the burn surgeon in the Emergency Room by patients who have suffered extensive and deep burn injuries are manifold. Modern burn management techniques involve immediate (or very early) excision of all deep burns and this, together with advances in intensive care medicine, means that the initial injury is usually survived. What follows is the tricky bit!

22.2 Why are dermal substitutes necessary?

Cutaneous burn injuries can, very basically, be divided into two groups. There are those that, with optimal support and good wound management, are superficial enough to heal spontaneously and quickly and with an excellent functional and cosmetic result. Then there are those that are sufficiently deep to undergo prolonged healing by secondary intention (granulation tissue formation and wound contraction), often complicated by recurrent episodes of wound infection, resulting in "pathological" scarring that reduces, impairs, or abolishes function, is hypertrophic, dysesthetic, and often symptomatic (causing itching and pain). It is this second group that contains those burns described clinically as "deep dermal" and "full thickness."

Physiologically, and from an evolutionary standpoint, the open wound where the full thickness (or near full thickness) of the skin has been lost is a major problem for the organism as a whole, and the body has two main mechanisms for dealing with it. The first is the generation of a vascular tissue composed of blood vessels and loose collagen from the wound bed (granulation tissue) to create a layer across which keratinocytes can migrate. The second is the differentiation of a group of fibroblasts within that tissue into myofibroblasts that have the capacity to contract, pulling on collagen strands as they do so, resulting in wound contraction. The outcome is a smaller wound (thus a shorter distance across which epithelialization has to occur) full of vascular supportive tissue that will allow such migration to succeed. If the desired outcome is

wound closure at any cost (to make an injured animal less likely to be a prey victim the next time a predator arrives), then this strategy is effective. However, in humans and our societal situation, if the healed wound crosses a major joint reducing or abolishing movement, it may prevent or reduce our capacity to work and earn. If on the face, it can cause eye-threatening ectropion, oral dysfunction, and such severe dysesthesia to result in social withdrawal, depressive illness, and suicide. For this reason, even "small" deep burn wounds in the developed world are not allowed to heal spontaneously. Extensive deep burn injuries carry another danger. The retention of large volumes of burn eschar (burn-killed tissue) has been intensively investigated. The release of lipid–protein complexes from the eschar as it degrades can result in severe toxicity with effects on the immune system (one reason why death by Gram-positive, and later Gram-negative, sepsis was a common outcome in large burns) and on general organ function (leading to multiorgan failure and death). It must be removed, but unless the wound can be closed quickly and definitively, it will heal spontaneously by undergoing the same processes described above, namely granulation tissue formation and contraction.

While narrow wounds left after linear burn excision might be closed directly by pulling the edges together and suturing, and some other small wounds might be closed by the use of local tissue flaps or full-thickness skin grafts, the split-skin graft is the mainstay of extensive wound closure. The split-skin graft has been in clinical use since the third quarter of the nineteenth century. Its survival as a technique for over 140 years indicates that it is highly effective in closing large wounds. The characteristics and properties that make it successful can be summed up quite succinctly. It is "self" (autologous) and as such elicits no host versus graft reaction to result in its rejection. It has an inosculatory capacity for rapid take because its harvest transects thousands of blood vessels supplying the papillary dermis and thus (by diffusion) the epidermis. New vessel growth (angiogenesis) from the wound bed is stimulated by growth factors (VEGF, etc.) from these vessels, directing the new growth toward them. This results in "anastomosis" of new vessel to existing graft vessels and a blood supply far earlier than would be guaranteed by neovascularization (new vessels invading a tissue or material where vessels do not already exist) alone. It contains some dermal supporting elements, a basement membrane, and an intact epidermis, thus signaling early after application that the wound is "closed" and that inflammation can abate. It is fiscally "free"—the surgeon does not have to pay for the repair (but the patient does). Finally, the donor site heals spontaneously, apparently allowing a deep wound to be closed without physiological cost.

Although it remains the workhorse of the burn surgeon, the split-skin graft has multiple limitations. These have been largely overlooked because of the advantages that the skin graft confers and because no alternative(s) existed. As burn surface area increases, available donor site decreases. Eventually the point is reached when, even with maximal (reasonable) mechanical expansion, sufficient skin cannot be harvested to cover all debrided burn wounds and still achieve an acceptable functional result and cosmetic appearance. The number of reharvests from a donor area is finite because each harvest (no matter how thin) includes a variable thickness of dermis, which will not be replaced when donor site reepithelialization occurs. The surgeon must gauge

correctly when a further reharvest will result in a donor wound which will not heal spontaneously and promptly. In certain populations (e.g. the elderly), the dermis is thinner and donor sites frequently struggle to heal, causing pain with recurrent breakdowns and repeated infections. How frequently these limited reharvests can occur is dependent on robust reepithelialization, itself a factor of the thickness of the harvested graft as well as the thickness of the remaining dermis at the site. It is seldom, if ever, that reharvesting can be contemplated within 10 days. With the patient already susceptible to infection due to loss of mechanical restriction to pathogen ingress and general immune compromise, the donor site extends the area of skin loss and inflicts further physiological insult and nutritional demand. The pain generated by the donor site often far exceeds that caused by the burn and creates more patient complaint. It can be sufficiently severe to delay mobilization and therapy; in the elderly, the pain of the donor site alone can "keep them in bed," which can result in a range of deleterious sequelae (such as pneumonia). The use of the split-skin graft does not replace "like with like." Skin grafts are thin (generally between 8 and 14 thousandths of an inch) and, when used to replace deep or full-thickness skin loss, cannot confer the same degree of robustness to mechanical, thermal, or chemical insult, such that future injury requires less insult. Nor does providing a reduced thickness of elastic dermis often allow complete restitution of the supple envelope that uninjured skin provides to facilitate joint mobility and range. Without underlying dermal support the edge of the excised burn, where skin graft meets normal skin, is often depressed and very obvious. Because the skin graft contains dermis, a donor site scar (however good) is always created since the dermis is not capable of regaining its preinjury architecture.

Some of these issues can be solved, or at least have their urgency delayed, by the use of a biodegradable temporizing dermal matrix (BTM), which physiologically, but temporarily, closes the debrided burn wound, integrates, and provides "dermal" structure in anticipation of later (delayed) application of split-skin graft, cultured epithelial cells, or (eventually) cultured composite skin (CCS). This strategy has been fulfilled successfully by animal-sourced collagen templates (such as Integra® dermal regeneration template) for many years and has allowed reduction of graft contraction and improvement in functional and cosmetic outcomes after split-skin grafting, where burn debridement has extended deeply into fat, fascia, or muscle.[1,2] In particular, a marked cosmetic improvement is observed when widely meshed graft is applied over the integrated matrix (compared to the unsightly, wide "chicken-skin" appearance otherwise achieved by applying widely meshed graft on fat). Although a split-skin graft donor site is needed to effect permanent closure, this can be acquired serially, buying time for surgeon and patient.

Collagen-based dermal matrices are underused globally, mainly because of their prohibitive cost.[3] Their biological composition and delayed neovascularization make them easy targets for infection.[2,4] These factors make the argument for inexpensive synthetic alternatives. Additionally, the need for the split-skin graft could be abolished altogether if a composite cultured skin could be created using a synthetic biodegradable matrix as a scaffold. Since it takes approximately 3 to 4 weeks to create such a composite cultured skin,[5] with autologous cellular material creating both a dermis and an epidermis *in vitro*, the debrided wound needs to be stabilized to limit contraction and infection.

A successful skin graft replacement strategy for extensive wound healing must thus have two component parts: (1) a material capable of performing the "dermal integration/temporary physiological closure" action for up to 4 weeks, and (2) an autologous composite cultured skin that can be applied over the integrated first material when its culture is complete to afford permanent wound closure.

22.3   Skin structure and function

The skin is the heaviest organ of the human body, making up about 16% of the dry weight. It appears to represent a single organ when viewed macroscopically, but there are two components, each completely different from the other and arising from different embryological germ lines (epidermis from ectoderm, dermis from mesoderm). The epidermis is cellular. When lost, it can be regenerated by cellular proliferation, differentiation, and migration without the formation of scar. The dermis is molecular, consisting mainly of collagen and elastin, supported by glycosaminoglycan ground substance. When damaged or lost, it can only be repaired by the rapid and "haphazard" deposition of new collagen, which subsequently undergoes remodeling to result in what we call a scar. Whenever an injury involves the dermis, a scar is inevitable, and the more deeply the dermis is injured, the more significant the scar will be in terms of its effect on function and appearance.

Of the thickness of skin, the epidermis contributes about 5% and the dermis, 95%. Each has its own contributions to function also. The superficially positioned epidermis creates a complex keratin/lipid barrier, which restricts water movement both out of and into the body through its large surface area (important on such a watery planet when our internal enzyme systems, which control life and all of its processes, can only function within rigidly controlled ranges of temperature and pH). It also contains cellular components (Langerhans cells) capable of stimulating an immune response against the pathogenic organisms that live as commensals on the skin and the presence of foreign bodies. Other epidermal residents protect the DNA of exposed epidermal cells from the ionizing action of ultraviolet radiation from the sun (melanocytes). By virtue of its molecular structure, the dermis, which is the key to skin suppleness and mobility (allowing movement, respiration, and accommodating specialized conditions such as pregnancy), contains the nerve endings that make the skin such an essential protective sensory envelope and the blood vessels that allow us to maintain mammalian temperature. Other functions, like the skin's contribution to our appearance, seem less important (until they are deranged by injury or disease).

22.4   The ideal dermal substitute

The ideal dermal substitute obviously needs to integrate into the wound in which it has been implanted, by allowing the invasion into it of fibroblasts, other cells, and angiogenetic vascular buds/vessels from the wound bed. Once established, the fibroblasts need to be stable enough to lay down autologous collagen.

However, to fulfill this task, it requires several other fundamental properties to function as a "dermis."[6] Without intrinsic blood vessels, dermal substitutes have no innate immunological function. The composition of the substitute must therefore be able to resist infection. Secondly, it must be able to survive, persist, and reconstitute a neo-dermal structure even if the wound bed environment is not ideal (be able to withstand wound hypoxia). Global market economies vary widely, so the material must be simple and thus cost-efficient to produce, otherwise the end-user is unlikely to be able to afford the product, and those using alternatives will be less likely to consider change. If the production method is simple, the upscaling production to allow wide availability and "surge production" for mass casualty incidents will be easily possible (another desirable attribute). The substitute must be easy to transport and store (without complex packaging, refrigeration, etc.), and its handling by surgeons should be simple in terms of preparing for use, shaping, cutting to size, fixation, and subsequent monitoring and, once integrated, its preparation for definitive closure. As a neodermis, it must be flexible and possibly mildly elastic, able to resist shear force and offering long-term wound stability (not eroding through the surface of the developing scar and extruding). It should not be recognized as "foreign" by the recipient's immune system, but be tolerated.

22.4.1   Biodegradable polyurethane suitability as a dermal substitute

The high cost, low production, and vulnerability to infection of both biological-based dermal matrices and composite cultured skins have created interest in synthetic polymer technology. These fiscal and supply arguments are not the only impetus for this exploration, as synthetic polymers have the added advantage of "customized" design to enable properties such as molecular elution or fluid absorption to effect better wound healing.

Biodegradable polyurethanes are of great interest for medical applications because of their variable mechanical properties, biocompatibility, and structural versatility. They are currently used in bone and cartilage applications, as well as in nerve regeneration.

The desirability of a dermal matrix composed of a synthetic material was recognized early, but the available materials of the time were not ideal. Despite the potential of Poly-Gycolic Acid (PGA)/Poly-Lactic Acid (PLA)-based scaffolds for wound repair, the generation of acidic degradation products was postulated to interfere with, rather than enhance, the wound healing response by stimulating local inflammation in tissues and initiating enzyme hydrolysis. Biodegradable polyurethanes were identified for their orthopedic potential in the 1980s[7] and in 2008, Huss and colleagues reported on their attempts to modify a commercially available polyurethane matrix, developed for orthopedic indications, for use as a dermal matrix.[8] Despite encouraging in-growth of fibroblasts into the material implanted into cutaneous wounds, and the production of procollagen by those fibroblasts, excessive inflammatory responses were observed in every subject and the material degradation profile was not ideal for the dermal indication (50% loss of mass over 6 years!)

It was clear that this family of polymers had potential but required considerable modification. A great deal of work followed. Guelcher and colleagues began characterizing biodegradable polyurethane foams in 2006,[9] examined their *in vitro* biocompatibility,[10] and demonstrated that the chemistry could be designed to allow the elution of important, prohealing factors.[11] They have subsequently been pivotal in explaining many of the hydrolytic and enzyme-induced reactions, which characterize the degradation products of biodegradable polyurethanes.[12] Their demonstration of the attenuated and transient inflammatory response combined with controlled degradation to noncytotoxic breakdown products has been fundamental in our understanding of our clinical observations while using these materials in the development of dermal matrices and other skin wound products *in vitro* and *in vivo* in animals and humans.

NovoSorb™ represents a family of novel polyurethanes. A subclass of this family is biodegradable, designed and constructed to degrade by hydrolysis to naturally occurring and biologically tolerated products. The NovoSorb™ technology was invented in 2000 by scientists working for the Molecular Science division of the Commonwealth Scientific and Industrial Research Organisation (CSIRO) based in Melbourne, Australia. In 2004, PolyNovo Biomaterials Pty Ltd was formed to develop and commercialize NovoSorb™ and its IP portfolio. PolyNovo owns the IP portfolio. NovoSorb™ foam biocompatibility has been tested as per the ISO 10993 standard and under good laboratory practice conditions.

22.4.1.1   NovoSorb™ biodegradable temporizing matrix

The BTM has been designed to overcome most of the issues encountered during the use of dermal matrices of biological origin. The advantages of using synthetic polymers, such as the NovoSorb™ biodegradable polyurethane, as a dermal scaffold are low antigenicity and that they can be manufactured to display specific degradation profiles and desired mechanical properties. They can be constructed to degrade by hydrolysis to naturally occurring and biologically tolerated products, be enriched with instructional molecules such as growth factors, and be designed to elute antimicrobial and analgesic agents to improve wound healing. Their chemistry is (relatively) simple and uses inexpensive raw materials, allowing rapid mass production, wide availability, and process upscalability. This ensures cost-effective production and facilitates lower pricing and thus more widespread use.

The BTM is a totally synthetic bilayer, dermal replacement scaffold for use in major burn injury using open-cell foam. The dermal component is a 2 mm-thick foam, which biodegrades predominantly by hydrolysis. A nonbiodegradable polyurethane film (seal) is bonded to the upper surface and functions as a pseudo-epidermis. The bonded seal pseudo-epidermis prevents evaporative water loss (thus minimizing wound contraction) and, after integration, is peeled away to expose the vascularized foam for skin grafting. The primary aims of this dermal substitute are (1) to temporize extensive, surgically debrided wounds while waiting for skin graft donor site recovery for delayed split-skin grafting, (2) to allow integration of vascular tissue into the foam dermal component to create a neodermis, (3) to sustain split-skin grafting once integrated, and (4) to reduce wound contraction during the remodeling phase.

Following several years of development and optimization (described below), the bonding of the 50 μm-thick polyurethane seal to the matrix prevents early delamination. The seal resists fragmentation and restricts tissue in-growth to the foam matrix only. The integrated, sealed BTM is reliably and consistently well vascularized, flush with the wound edge, soft and pliable, and clinically as thick as the surrounding skin. The seal delaminates easily by gentle teasing and separates with a "Velcro™-like" action, leaving vascularized tissue below. During delamination, the superficial surface of the polymer separates below the level of the bond, allowing the exposed polymer on the superficial surface of the neodermis to retract back into the tissue. This ensures that all of the seal and the bond are removed during delamination, leaving a partially refreshed wound bed, requiring minimal abrasion to refresh the surface.

The NovoSorb™ biodegradable polyurethane has been designed to maintain physical strength and structure until 3 months postapplication. After this time point, progressive hydrolysis of the material results in matrix degradation and absorption.

BTM is solely constructed from polymeric components using commercially available chemicals and using processing techniques that are common in general industry. Thanks to these features, BTM can be produced in large quantities for relatively low cost, making the device highly suitable for global, not just "First World," use. The maximum size of the device is limited only by commercially available equipment and would be sufficiently large to cover the entire back of a patient, limiting the number of "seams" required. In terms of storage, BTM is terminally sterilized by gamma irradiation; it is dry-packed and can be stored at ambient temperature. The BTM has a minimum 3 year shelf life.

The BTM has been demonstrated in humans to resist spontaneous delamination up to 49 days postapplication (although the bonding method is expected to maintain the seal lamina for longer).

22.4.1.2 Cultured composite skin

In current practice, deep burns extending to >50% TBSA are excised in the initial operation, but are then serially "grafted" or "closed" over many weeks. This is due to a number of reasons including burn site, patient stability, surgeon desire to minimize early iatrogenic physiological insult, etc. The prime reason, however, is a paucity of skin graft donor site. This "delay" in time to closure provides the opportunity to serially cultivate CCSs, ensuring that 100% TBSA coverage can be achieved if necessary.

The CCS takes 21–28 days to produce and can be applied from its time of readiness. Since its cellular components are produced from a small sample of unburned skin from the individual, the rate of production of sufficient CCS for complete coverage depends on the size of the biopsy of unburned tissue that can be harvested.

A 20 × 20 cm biopsy harvested from unburned skin can create coverage of the entire TBSA of a human in 21–28 days, depending on the structural maturity required.

Once the CCS is applied, robust epithelialization has been observed as early as 7 days later. Extrapolating from this, an extensive deep burn victim (e.g., 80% TBSA) could be in the acute care hospital for as little as 5–6 weeks using the outlined two-stage

strategy, beginning physiotherapy as soon as the BTM is immovably adhered (at approximately 14 days) up to the CCS application (21–28 days), recommencing after CCS take at 31–38 days until discharge.

22.5 Development history of NovoSorb™ biodegradable temporizing dermal matrix for major burn injury

The introduction of a product designed for implantation into humans requires a comprehensive development program, structured to address issues of potential toxicity, safety, and efficacy *in vitro*, followed by preclinical *in vivo* testing in appropriate animal models. Only after safety and efficacy are established, can human trials be considered. Since the employment of the NovoSorb™ biodegradable polyurethane platform was entirely novel in both material and concept, we followed this strategy. All trial proposals were submitted to, and approved by, the relevant Animal or Human Research Ethics Committee.

22.5.1 In vitro *degradation rates and evaluation of toxicity of the biodegradable polyurethane matrix*

From the outset it was necessary that any biodegradable polyurethane intended for use as a dermal substitute would need to be nontoxic to cells (noncytotoxic) and support the growth of fibroblasts (and their production of collagen) and keratinocytes.[13] Ultimately, in the wound, the matrix would need to sustain blood vessel in-growth to supply the overlying skin-grafted epidermis with nutrients, oxygen, immune cells, and factors, and transport out the toxic by-products of cellular respiration. Therefore, microvascular endothelial cells (MVECs) would also need to thrive in the presence of BTM.

The structure of NovoSorb™ gives it the inherent capacity to completely biodegrade by hydrolysis over variable time periods, dependent on the strategic chemical placement of the degradable chain extenders in the urethane structure. Therefore, 70 NovoSorb™ variants were initially synthesized, three of which were chosen as potential BTM prototypes (BTM-1, -2, and -3). At this time, we could not predict how long each of these would take to biodegrade *in vivo*.

Two initial forms of each of these polymers were created. The first were 60- to 100-μm-diameter cured polymer fibrils of 10 cm length wound around two parallel rods spaced 1 cm in a "figure of eight" conformation and tied in the center to form bundles.

Secondly flat, nonporous films of the three polymers were created by curing them between two glass plates. From these films, 1-cm-diameter discs were cut and placed into tissue culture plates.

To test *in vitro* degradation rates, bundles were incubated in suitable media in individual glass vials. At various time points the degradation rate of each prototype was assessed by molecular mass (M_n) measurement through gel permeation chromatography. Qualitative observations on physical shape such as fiber breaks or changes in

the bundle shape were also recorded. BTM-1 degraded most rapidly, losing more than 50% of its molecular mass after 7 days, becoming soft and fragile by 3 weeks; BTM-2 lost 50% of its molecular mass around 90 days and approximately 90% by 6 months. BTM-3 had only lost approximately 30% of its molecular mass by the end of 6 months.

BTM-2 appeared therefore to possess the degradation profile *in vitro* that, if replicated *in vivo*, would be most appropriate for a scaffold sustaining dermal repair, which can maintain its cellular integrity until split-skin grafts have taken and then biodegrade as the scar matures.

With regard to cytotoxicity *in vitro*, BTM fibers from all three prototypes were cultured in suitable media with human fibroblasts, keratinocytes, and MVECs, which, in comparison to control cultures in the absence of polymer and also cultures in the presence of commercially available polypropylene or poliglecaprone sutures, exerted minimal cytotoxic effects to all three cell types, allowing comparable rates of cell population growth. BTM-1 fibers were noted to become fragile after 3–4 days; however, BTM-2 and BTM-3 fibers remained firm and intact.

Culture of the cell types on the nonporous discs demonstrated a comparable rate of dermal fibroblast growth on BTM-2 and BTM-3, but not on BTM-1 where a failure to replicate was noted. Keratinocytes exhibited limited growth and MVECs were scattered and spindle shaped, unlike their more rounded counterparts in the negative control cultures.

22.5.2 *Early* in vivo *implantation*

BTM bundles were implanted under the skin of rats for 24 weeks. Commercially available polypropylene and poliglecaprone sutures were also implanted for comparison. None of the rats exhibited behavioral changes, gaining weight and thriving alongside controls. Blood tests at all time points revealed no abnormalities and, at necropsy, no organ damage was identified. Implanted NovoSorb™ caused no apparent adverse systemic effect and no adverse local reactions were observed in any of the rats. BTM-1 was undetectable at 3 weeks, with BTM-2 becoming more difficult to discern macroscopically by 12 and 24 weeks. BTM-3 was located at weeks 3 and 6, in most rats at week 12, and in one rat at week 24.

BTM-2 possessed the appropriate degradation rates combined with a minimal cytotoxicity profile *in vitro* and exhibited comparable degradation rates with no local or systemic adverse reactions *in vivo*. A third formulation of a 6-layered 0.65 mm-thick spun-weaved mat of BTM-2 fibers was then created for further assessment of cytotoxicity and ability to sustain human fibroblast, keratinocyte, and MVEC growth *in vitro*, and implantation as a dermal matrix in surgically created cutaneous wounds in sheep *in vivo*. *In vitro*, fibroblast population growth continued along the time period over 30 days, migrating along the fibers and filling the smaller interstices of the mat. Staining for collagen confirmed production by the fibroblasts. MVECs grew along fibers over 7 days, surrounding them and forming blood vessel-like structures. Limited keratinocyte growth was observed when cultured in BTM-2; however, when seeded on a fibroblast/BTM-2 composite culture, a keratinocyte monolayer was generated illustrating the potential for an epithelialized CCS substitute.

Four full-thickness wounds were created surgically in each of six sheep. Two were implanted with the BTM-2 spun mats secured with sutures. Integra® dermal regeneration template was implanted in another. The fourth was left to heal without reconstruction, by "secondary intention," that is, migration of fibroblasts, deposition of collagen and angiogenesis (new growth of blood vessels) from the wound bed, myofibroblast differentiation, and induction of wound contraction with keratinocyte migration from the wound edges. All wounds had healed by epithelialization by Day 29. Over this period, both the BTM and the Integra®-implanted wounds contracted to a similar degree to each other, but to a lesser extent than the control wounds.

Histological examination of the BTM specimens at necropsy confirmed the presence of epithelioid macrophages (scavenger immune cells) and multinucleate giant cells exhibiting a granulomatous "foreign-body" reaction around the dermal BTM fibers; however, most of the fibers were in the subcutis. The dermis was composed principally of reparative collagenous connective tissue with capillary blood vessels. Some fibers had migrated to be found superficial to the epithelium, suggesting expulsion. A basement membrane was established between the epithelium and the fibrotic dermal tissue. Like Integra®, BTM-2 had resisted wound contraction and allowed controlled development of dermal granulation tissue. It was unclear at this stage whether the BTM had integrated to create a dermal-like structure and biodegraded, or had formed a base onto which a dermal "scar" could form with overlying epithelium. However, it did provide evidence that BTM-2 implanted *in vivo* supported *functional* cellular proliferation, that is, fibroblast proliferation *with* collagen production, keratinocyte proliferation *with* epithelium and basement membrane formation, and angiogenesis.

22.5.2.1 Change in implant structure and preclinical in vivo *animal model*

The spun mat was not ideal, given its thin and dense structure and its tendency for fiber expulsion *in vivo*. To create a 2 mm-thick implant, for example, would require a weave of considerable amounts of polymer material (40 layers), which would be time-consuming and expensive to manufacture and upscale and would produce a dense product that would generate large amounts of degradation by-products. An alternative scaffold design was sought for NovoSorb™ BTM-2 (hereinafter referred to as simply NovoSorb™).[14] An open-cell foam was manufactured. This allowed for more control of pore size (cell size) and was less dense (requiring less polymer/volume and degrading into smaller volume of breakdown products), thus less costly and safer in theory.

The porcine model used to test this foam became the standard animal model for all subsequent preclinical testing. Under general anesthetic, four 8 × 8 cm full-thickness wounds were excised from the backs of pigs. To compare the degree of contraction and integration of the spun mat against the new 1 mm-thick NovoSorb™ foam, they were implanted into such wounds. All foam and spun mat matrices integrated. The foam matrices were found to be more robust and permitted less wound contraction than the spun mats from Day 12 onward.

Histology confirmed that the mat allowed wound bed proliferation to extend through it, to create a dense scar tissue layer superficially. Within the foam cells, however,

proliferation took the form of loose irregular collagen deposition with few fibroblasts. The mat showed no evidence of degradation at 3 months whereas the foam had appreciably started to degrade, with no polymer visible by 5 and 6 months. It was postulated that polymer hydrolysis had been facilitated by the large surface area afforded by the cell walls and lower density of the foam, compared with the mat.

22.5.2.2 In vivo *use of NovoSorb™ foam in an animal model with immediate or delayed skin graft*

Wounds were either implanted with skin graft alone, with the 1 mm-thick NovoSorb™ foam with immediate skin graft applied, or foam alone with delayed skin graft applied at 11, 14, or 18 days postsurgery (depending on appearance of integration).[14]

Immediate skin graft took completely over 1 mm-thick foam NovoSorb™ in three of six animals; 40% surface area take in two of six; and complete failure in one pig. This complete failure may have been artifact due to technical problems using a mechanical dermatome to harvest skin graft when a manual skin graft knife was used for the others, harvesting grafts of far better quality.

Of the BTMs skin grafted at Day 11 (four subjects), delayed skin grafts took completely in two pigs, and failed completely in one. Although one other graft failed, enough viable keratinocytes had "seeded" the integrated foam to then proliferate to reepithelialization.

Graft take of 60% was observed on the BTM skin grafted at Day 11 postimplantation and that grafted at Day 18 took completely.

Macroscopically, the immediate and delayed grafts onto polymer were notably flush with the surrounding wound edges. They were thick and supple and robust, resembling normal skin more than the depressed appearance of the skin graft to wound alone group.

On histological analysis, both the delayed and the immediate graft over polymer groups developed well-vascularized subepidermal scar tissue 0.6–1 mm thick over 4–5 weeks (allowing 17 days post-delayed skin grafting before analysis). Similar to the early results, foreign-body reaction was seen with giant cells, eosinophils, and scant lymphocytes. The control area (immediate graft on wound) created a subepidermal scar layer 0.6 mm thick. The tissue within the polymer did not have the dense, linear, fibroblast-rich scar tissue appearance but remained loose, irregular, fibroblast-poor, and edematous.

Mean wound area assessment of the treatment groups showed that immediate skin graft alone contracted less (7.12% surface area contraction) than both the immediate and the delayed graft over polymer treatment groups (21.63% and 37.57%, respectively). Examination of the curve over time suggests that for the delayed group, wound contraction appreciably stopped on application of the skin graft.

22.5.2.3 In vivo *preclinical model trial against a collagen matrix*

To address this issue of wound contraction, a 30-μm-thick biodegradable, microporous polyurethane membrane was bonded to the superficial surface of a new 2 mm-thick foam matrix. This was intended to "seal" the foam, acting as a barrier to the development of linear collagen fibers on the surface before application of the skin graft, which

might have contributed to the contraction seen in the above studies, prior to delayed skin graft application.[15] This bilayer structure is hereafter referred to as "sealed BTM." The original unsealed foam is referred to as unsealed BTM.

Four wounds were created on each of six pigs as above. The four treatment arms were Integra® dermal regeneration template, sealed BTM, unsealed BTM, and secondary intention. The study period was 28 days.

Wounds receiving the collagen matrix, in five of the six pigs, demonstrated that the silicone epidermis lifted prematurely or required partial excision due to the presence of a yellow, subsilicone collection by Day 14. In four of the pigs, complete spontaneous removal (delamination) of any remaining seal had occurred between Day 7 and Day 14, in the other two by Day 21. The underlying matrix was lost to apparent infection in one pig. Following delamination marked wound contraction continued to Day 28, whether the matrix had been lost or not. The wound surface areas contracted by a mean of 55.6%.

No infection was noted in the matrix of the sealed BTM treatment arm. Although some of the sealed BTMs sheared from the wound at an early stage, they were stapled back into position and integrated over 7 days. Over time the seal fragmented and was completely lost in five of six wounds, and the remainder was easily removed (delaminated) at Day 28. Despite this loss of the seal, however, the sealed BTM wounds underwent the least wound contraction over 28 days of the four treatment arms (mean contraction of 23.4%, significantly less than the collagen matrix group, $P < 0.0001$).

The unsealed BTM and secondary intention treatment arms granulated and contracted without any clinical evidence of infection, consistent with previous observations. The unsealed BTM wounds contracted by a mean of 44.6% surface area at 28 days (significantly less than the collagen matrix treatment arm, $P = 0.01$), and the secondary intention wounds contracted by a mean of 59.0% surface area.

The three treatment groups had similar histological characteristics, scar layer above the implant with a granulomatous reaction with multinucleate giant cells and epithelioid macrophages. Granulation tissue was seen to penetrate the gaps in the sealing membrane of the BTM polymer, with a thin superficial scar under the remaining membrane.

This reduction in the thickness of the scar under the seal might have contributed to the reduction in wound contraction compared to the other treatment arms in the trial. The presence of a seal seems to reduce contraction, either by acting as a physical barrier to overlying scar formation or by preventing evaporative water loss, thereby physiologically closing the wound and reducing the stimulus for scar formation.

22.6 Proof of concept of cultured composite skin on biodegradable temporizing dermal matrix

The overall strategy for retiring the skin graft requires the stable and reproducible culture of recreated epithelium and neodermis *in vitro* by serially seeding a 1 mm-thick layer of NovoSorb™ with autologous fibroblasts (into the matrix) and keratinocytes (on its superficial surface). Once created, the CCS was implanted onto an integrated, delaminated BTM in the wound. Proof of this concept could herald an entirely new

approach to large wounds such as those seen following debridement of severe burns. This was tested in the described pig model.[16]

Autologous keratinocytes and fibroblasts were extracted from a split-skin graft from the pig. These were cultured *in vitro*. The 1 mm unsealed matrices were soaked in plasma before the addition of thrombin with the fibroblasts to create a gel in the matrix, thereby preventing the cells from falling through the foam to waste. These composite gels were cultured and keratinocytes added to the surface again in a thrombin solution. The composite skin was then cultured until application to integrated BTMs in wounds on the same animal at 28 days postwound creation/BTM implantation/Split Skin Graft (SSG) harvest (Figure 22.1(a–c)).

Sealed, 2 mm-thick BTMs were applied with delamination scheduled for 28 days; however, spontaneous delamination and fragmentation were noted in several sites. Only two sites maintained a seal that could be delaminated by Day 28. The wounds contracted to 50% their original size. CCS was applied to delaminated BTMs to test
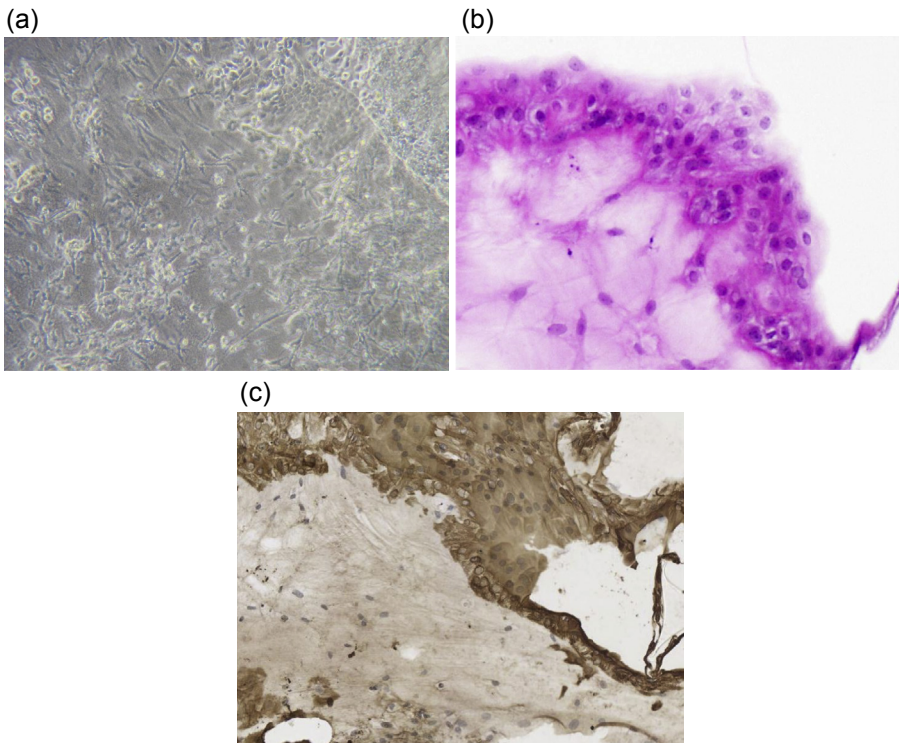
Figure 22.1 (a) Light micrograph demonstrating fibroblast and collagen filling of a matrix pore. Coseeded keratinocytes can be seen in the upper right corner. (b) Hematoxylin and eosin-stained section of composite cultured skin development. The final result is a bilayered skin inside each polymer foam pore. (c) The same section as in (b), stained with anti-bovine keratin antibodies, to confirm that the keratinocytes and fibroblasts had adopted layers within the polymer pores.

for proof of concept and also applied to wounds without BTM present. Split-skin graft was applied directly to the other integrated BTM wounds and subsequently took.

By Day 7 postapplication, it appeared that the CCS had not taken in four wounds; however, on removal there appeared to be a small amount of residual foam on the surface, apparently from adherence of the deeper component of the CCS. The other two wounds had taken, showing vascularization and integration by Day 10 with further consolidation through to Day 14. Histological analysis confirmed the presence of a well-defined epithelium with a thick keratinized layer and a basement membrane. There were areas where the 1 mm-thick CCS had not integrated and may have been shed, seeding cells onto the integrated, delaminated BTM, thus acting as a delivery vehicle. Areas of partial integration were also seen.

CCS was also applied to wounds without previously implanted BTM. This also confirmed the above findings that the 1 mm CCS can act as a cell delivery vehicle to seed the wound with keratinocytes and develop an epithelium, and it can take as a composite implant with a neoepithelium within the foam.

This successfully proved the concept of the CCS strategy. The next focus, however, was to optimize the seal to avoid fragmentation, thereby reducing scar tissue formation on the surface to prevent wound contraction.

22.6.1   Optimizing the seal

Ten variants of BTM seals were tested in a total of 44 pig wounds.[5] The seals had thicknesses ranging from 50 to 150 μm, some perforated, some nonperforated. A commercially available seal was tested, and seal-to-matrix bonding methods were also evaluated.

The 50- and 100-μm-thick seals were easy to apply, compared to the stiffer 150 μm seal. The commercial seal (Tegaderm™; 3M Health Care, St. Paul, MN) was tested and bonded by two different techniques. These spontaneously delaminated by Day 7 and were abandoned.

Analysis of all the seal data suggested that neither the thickness of the seal nor the presence of perforation appeared to influence wound contraction; however, the type of bond consistently affected whether early delamination occurred followed by unacceptable degrees of wound contraction. In other words, if the seal remains intact, and bonded to the matrix without spontaneous delamination, then wound contraction is minimized.

The resultant optimized BTM with the new seal-to-matrix bonding method and a nonbiodegradable 50 μm seal was then tested with application of CCS. During the culture/BTM integration phase all the seals remained intact with no signs of spontaneous delamination until surgical removal at Day 21 with a mean wound surface area of 95.5% of original size (Figure 22.2). By Day 21, in the CCS in culture, the majority of the keratinocytes were present in the deeper levels of the 1 mm matrix. Following application of the CCS onto the integrated, delaminated BTM, CCS take onto the BTM was variable. By Day 10 postapplication, most of the CCS foam was sitting in a hyperkeratotic layer external to a well-developed epidermis with an underlying basement membrane (Figure 22.3). By Day 35 postapplication, some CCS had become
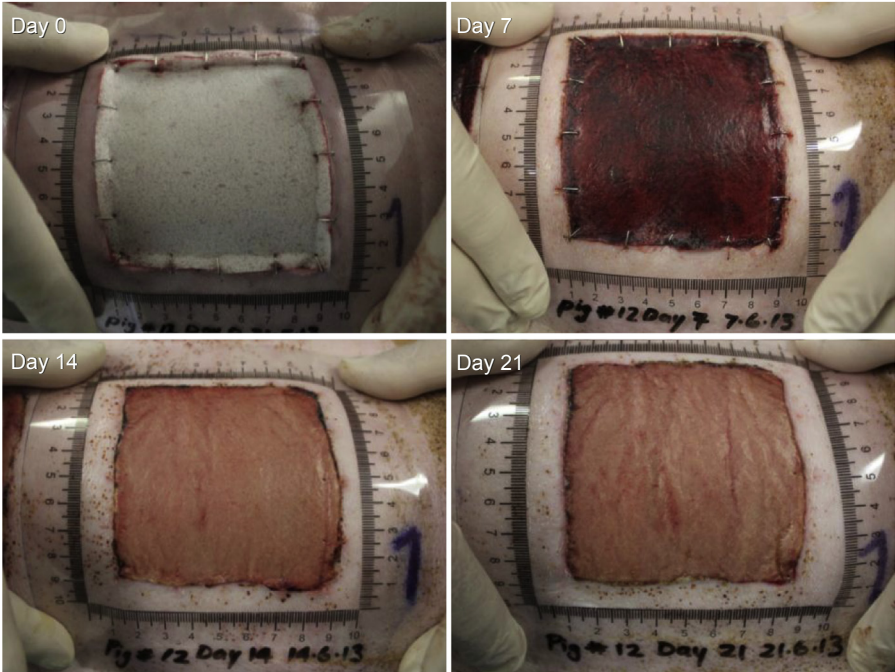
Figure 22.2 Serial progression of integration of the optimized BTM from application at Day 0 to Day 21 postsurgery.
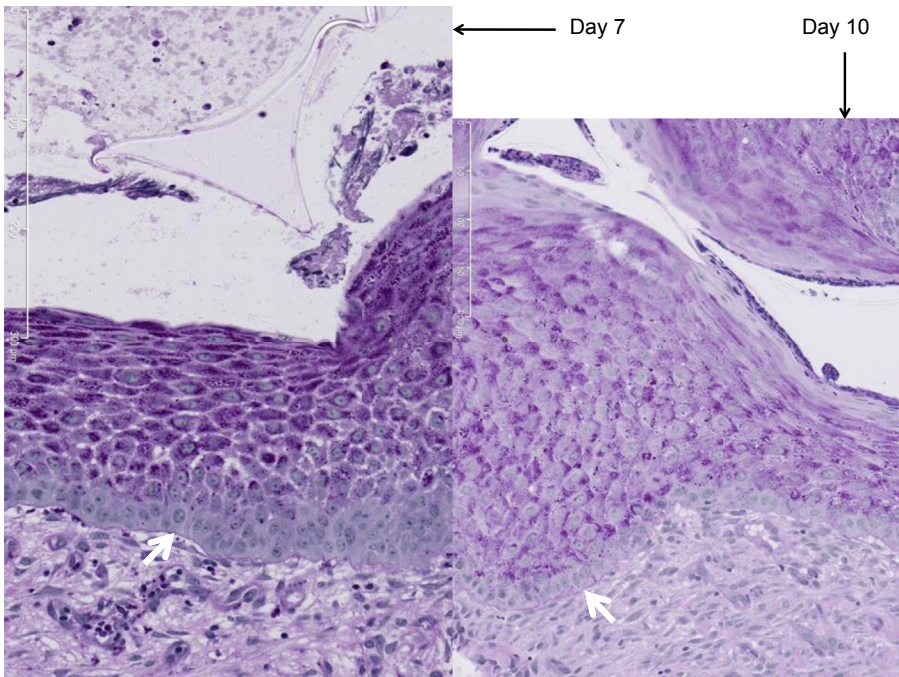
Figure 22.3 Close-ups of the CCS dermo-epidermal junction with periodic acid Schiff (PAS) staining. A basement membrane can be seen as a continuous purple line at both Day 7 and Day 10 (white arrows).
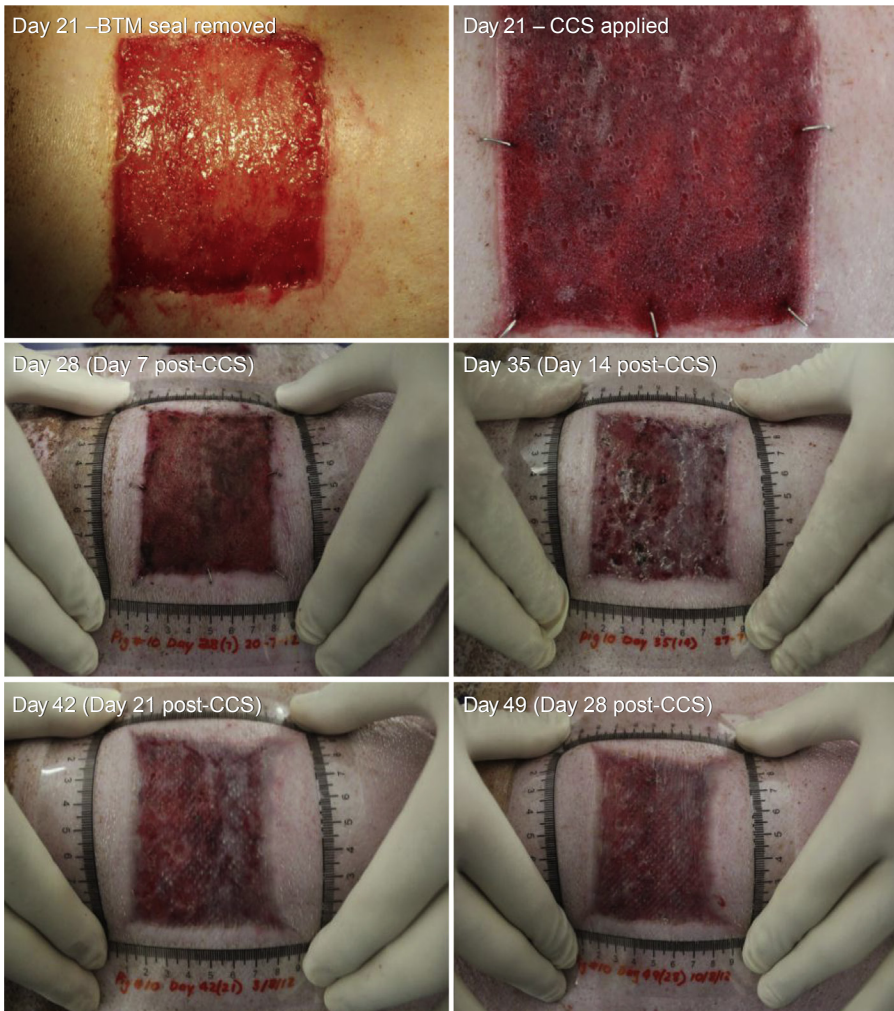
Figure 22.4 Removal of polyurethane seal from the integrated BTM at Day 21 of Figure 22.2, application and fixation of the polyurethane-based CCS, and the development of a stratified squamous epithelium (up to Day 49 postwounding) resulting in wound healing.

incorporated, but the majority had been "shed" leaving a robust underlying epidermis (Figure 22.4). These clinical findings were confirmed on histology, and support the concept of the CCS acting as a cell-delivery vehicle resulting in a stable epidermis (Figure 22.5). Wound surface area was 81% of original size by Day 52 and the new skin was thick and flush with the surrounding edge.

Control wounds that had healed by secondary intention showed epithelialization from the wound margins, differing in nature from the CCS epithelialization, which occurred in islands throughout the surface of the wound, and coalesced to form a
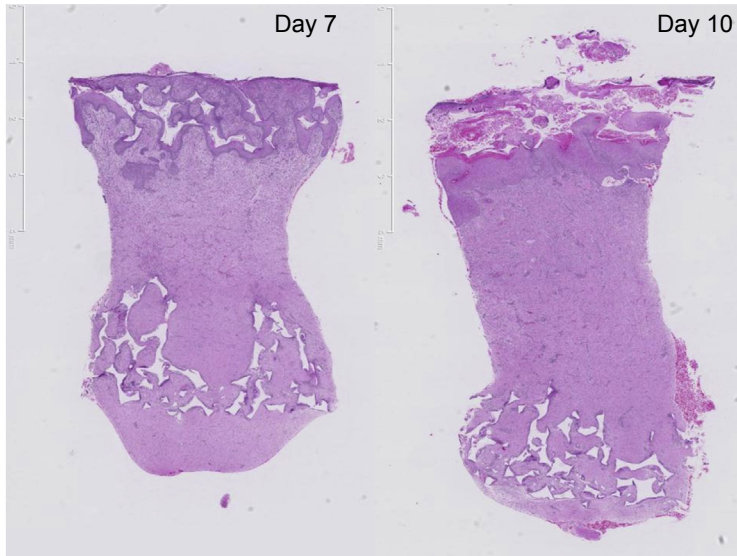
Figure 22.5 Hematoxylin and eosin-stained punch biopsies of the wound with CCS applied at Day 7 and Day 10. The integrated BTM can be seen toward the lower pole of the core biopsy. At Day 7, the CCS has visibly deposited its cellular component to create a stratified squamous epithelium. By Day 10, the CCS polymer is extruded, leaving a healed wound deep to it.

stable epithelium. Secondary intention wound surface area at Day 52 was 36% of the size at wound creation.

Wounds healing by secondary intention contract. In pigs, this is to 36% of original size by Day 52. The compound effect of this unopposed contraction over large surface areas can, at best, lead to reduced joint movement and surgery to release these joints and at worst can be profoundly debilitating and result in amputation of distal parts. Therefore the importance of early skin grafting has always been to prevent such poor outcomes. The absence of available donor sites, as in very large burns, means that multiple harvests from the same areas may be required to reconstruct. This imposes a time period during which these donor sites need to reepithelialize prior to reharvest.

The above studies demonstrate that temporizing such wounds using the sealed BTM is able to reduce contraction rates and that the polymer is noncytotoxic and can support fibroblast, keratinocyte, and blood vessel proliferation to create functional tissue. Optimizing the seal and bond had further reduced wound contracture rates.

Historically, using cultured or sprayed-on epithelial autograft to create stable robust epithelium on large wounds has been expensive and unpredictable in its outcome. The lack of dermal support results in friable, unstable cover that shears readily and allows wound contraction. By culturing autologous skin *in vitro*, the CCS can reduce the morbidity of extensive skin graft harvest and create a stable wound reconstruction with minimal contraction in extensive wounds. The work described above demonstrates proof of concept that CCS can be cultured *in vitro* and can be applied to integrated, delaminated BTM, and can take and/or deliver cells to the wound to result

in a robust, thick, and flush composite wound reconstruction. Although it was not the investigators' concept for the CCS to perform as a cell delivery method (as opposed to solely a composite layer that takes on the BTM), the discovery that it functions as both to provide the desired outcome is serendipitous.

22.7   Human trials

22.7.1   Short-term implantation

As described above, NovoSorb™ had been tested for local and systemic tolerance for up to 6 months in rats and up to 5 months in pigs and complied with a range of independent safety tests (ISO 10993) in rats to 6 months. We felt it prudent to proceed to human implantation by exposing human wounds to the polymer for a short-term period, removing it before it biodegraded.[17] This would enable us to assess any local adverse reactions, tissue hypersensitivity, or systemic reactions, such as anaphylaxis, reserving the ability to remove the dressing before it had become integrated.

Pressure (or decubitus) ulcers afflict many patients with spinal injuries, congenital spinal malformations and paraplegia, the elderly, or those who are chronically unwell, immobile, and/or have poor nutritional status. Common pressure areas that tend to ulcerate include the skin over the sacrum (the bony area you lie on), the ischial tuberosities (the bony prominences you "sit on" at the top of the thighs), and the backs of the heels. Prolonged pressure, combined with shear stress, moisture, and contamination from bladder or bowel incontinence, and poor healing reserve, all contribute to their formation and progression to create deep wounds, through fat to the bony prominence itself. With all reversible factors addressed (e.g., nutrition, pressure relieving mattresses and cushions, regular turning to allow blood flow to pressure areas) the surgical mainstay of management is debridement of the necrotic tissue in the ulcer. This converts a chronic ulcer into an acute wound.

Negative pressure wound therapy (NPWT) dressings can then be applied. These commonly consist of a nonbiodegradable open-cell polyurethane foam, cut to size to fit snugly in the wound cavity, which is covered in an airtight occlusive dressing and connected via tubing to a vacuum pump draining to a waste canister. This dressing seals the wound from surrounding contaminants; the vacuum transmitted through the foam to the wound interface draws out tissue fluid and therefore reduces edema and inflammation, increases blood supply and granulation to the area, and reduces bacterial load. There is also a shrinking force applied to the wound cavity, which reduces the volume over weeks and months, with regular dressing changes (every 2 or 3 days) to subsequently smaller foam pieces. In some cases, NPWT can be used until the wound fills in with granulation tissue and shrinks to a point where epithelialization can occur to heal by secondary intention. Therefore since 1995, NPWT has revolutionized pressure ulcer management. The marginal invasion of granulation tissue into the pores of the foam at the wound interface can cause problems however. When the dressing is removed this tearing of granulation tissue can cause bleeding and fragments of the foam can become retained and become a nidus for infection.

The use of 3-cm-thick blocks of NovoSorb™ foam (NovoPore™) as an NPWT foam interface for pressure ulcers, changed every 2–3 days for 8 weeks, seemed a suitable model that might benefit the patient. The aim was to assess whether the NovoSorb™ would be tolerated by patients in the short term, and whether being an open-cell foam it would effectively function as an NPWT foam. A randomized control trial of NovoPore™ against the market leading foam (Granufoam™, Kinetic Concepts Inc., San Antonio, TX) was performed, using their Vacuum Assisted Closure dressings and device for both treatment arms. Twenty pressure ulcers in 16 patients were recruited (10 ulcers per treatment arm). Each ulcer had surgical debridement and cavity measurements taken prior to allocation to either foam in theater. Following application of the foam and device, the patient had the foam dressed in the community by a dedicated trial nurse every 2–3 days with measurements and photographs taken at dressing changes for a total of 8 weeks or until complete healing, whichever came first. Following this period of data accrual, patients were continued with NPWT using Granufoam™, converted to "conventional" dressings, or reconstructed using flap surgery, depending on indication and patient choice. Qualitative data on handling and dressing changes were collected. Quantitative data consisted of wound measurement.

No systemic or local reaction was noted in either the NovoPore™ or the Granufoam™ cohorts. NovoPore was initially reported as being more difficult to shape than Granufoam™; however, this became easier with increasing familiarity. Dressing changes were more traumatic with Granufoam™ than NovoPore™. Eighty percent of Granufoam™ changes in ischial wounds were described as "difficult" and were accompanied with bleeding and fragmentation. All of the NovoPore™ changes were classed as "easy," with no episodes of bleeding or trauma on removal. Granufoam™ fragmented on withdrawal on 21/69 dressing change episodes, whereas NovoPore™ fragmented in 14/72 changes. One retained fragment of NovoPore™ was easily washed out of the wound with saline whereas four retained fragments of Granufoam™ needed sharp excision, three of which led to infection in the following few days. Wounds dressed with NovoPore™ reduced in size to a similar degree to wounds dressed with Granufoam™, suggesting equivalence in efficacy to transmit the benefits of NPWT.

This trial supported the early biocompatibility of the NovoSorb™ polyurethane, and its efficacy as an NPWT interface, in the NovoPore™ form. Larger numbers would need to be recruited to assess whether our findings of atraumatic dressing changes without bleeding, or the need for sharp excision of fragments, or infective complications extrapolate to wider use.

22.7.2 Long-term implantation of biodegradable temporizing dermal matrix with delayed split-skin grafting

With short-term biocompatibility confirmed, a trial of long-term implantation in small, controlled wounds was designed. Complex cancer excisions result in deep defects requiring reconstruction using autologous free tissue transfer (free flap reconstruction). The tissue to be transferred is chosen for its composition to meet a reconstructive purpose and commonly is harvested from one of three places: the distal forearm on the palmar side (forearm flap—skin, fat, and fascia), the outside of the lower leg

(fibula flap—skin, fat, fascia, and fibula bone), or the outside of the thigh (anterolateral thigh flap—skin, fat, and fascia). Typical defects requiring reconstruction after excision of cancer include the tongue (forearm flap), the jawbone and floor of mouth (fibula flap), and the cheekbone (anterolateral thigh flap). This tissue is shaped and inset into the defect and the blood vessels anastomosed to local vessels using microvascular surgical techniques to contribute a blood supply to the flap in its new position.

Once transferred the flap leaves behind a deep, complex donor site with muscles and tendons in its base, but small and controlled enough to safely test the first human long-term implantation, without removal of the sealed BTM and assuming complete biodegradation.[18] Ten patients were recruited and their donor sites implanted with sealed BTM (three anterolateral thigh flaps, three fibula flaps, four forearm flaps). Delamination and split-skin graft over integrated BTM were performed at a second operation following integration as judged by appearance. Photographs were taken at implantation and at every dressing change along with wound surface area measurements. After 1 year postimplantation, a physiotherapist objectively scored the scars.

Several discoveries were made in the course of this study. No local or systemic adverse reactions were noted attributable to the BTM. The BTM successfully integrated into the large majority of areas and sustained enduring split-skin graft take (Figure 22.6). Matured skin graft over the year's study period and onward has been stable, robust, and flush with the surrounding skin, with high patient satisfaction and no detriment to distal hand/foot function or sensibility. Integration in these complex wounds takes between 3 and 6 weeks depending on the general health of the patient, their capacity to heal, and whether there is underlying tendon (which takes longer).

In some patients, however, the nonperforated seal prevented exudate fluid collections from escaping, which collected under the seal, and within the matrix and caused small areas of delamination and failure of integration. These collections could become secondarily infected at 2–3 weeks postimplantation, indicating partial seal removal to allow drainage (Figure 22.7). No systemic infection was noted, and the infections (in three patients) did not require extensive excision of the matrix. They were treated with topical antimicrobial dressings and ultimately skin-grafted with flush, robust results as above (Figure 22.8). Wound contraction varied depending on donor site, with the greatest contraction seen in forearm wounds with considerably more in those that had been delaminated prematurely (42% of original size). This was to be expected given our preclinical findings. Wound contraction stabilized between 80 and 100 days postimplantation.

Technically, removal of the seal was piecemeal, and thus slow, in all cases and such a lengthy process is inadvisable and undesirable in major burn reconstruction. Fenestration (perforation) of the seal was indicated. This would allow fluid egress out through the implant and prevent subseal collections. Reformulation of the seal and bond, to prevent piecemeal fragmentation on removal, was also indicated before continuing human use.

A new seal structure and bond were developed and a new BTM was trialed in the pig model as described before further human application. In pigs, delamination at Day 28 occurred reliably in one piece, removing a fine layer of underlying matrix.[5]

Figure 22.6 The BTM applied into an ulnar forearm free flap donor site and allowed to integrate. Delamination occurred at Day 36 and split-skin graft was applied. Complete graft take occurred with an excellent result at Day 301.

Histological analysis of a punch biopsy prior to delamination revealed seal/matrix adherence with no significant development of a scar layer between the seal and the polymer matrix. Wound size at Day 28 was 82% of original size, the least wound contraction observed thus far in trials of BTM in pig wounds.

A second cohort of 10 fibular (2) and forearm (8) free flap patients was recruited, under the Therapeutic Goods and Administration status as approved prescribers of an unapproved product. The seal of this new, optimized BTM was hand fenestrated with a scalpel prior to implantation inset at the time of free flap harvest as before.[19] One

Figure 22.7 Seal prevented fluid escape in one patient causing infection in the foam by Day 14. With strips of seal removed and the wound treated with antimicrobial dressings, the infection subsided and the material integrated. Residual seal removed at Day 35, graft applied, and successful take.

Figure 22.8 The infection did not impact on the long-term result.

patient suffered a catastrophic vascular complication of his head/neck surgery and did not survive to delamination. In the other nine, delamination occurred in one piece in a single action. All skin grafts took without loss or complication and no subseal collections were noted (Figures 22.9 and 22.10).

Figure 22.9 Patient 5 from the subsequent free flap cohort. Initial wound and long-term result.

Figure 22.10 Patient 9 from the subsequent free flap cohort. Initial wound and long-term result.

All of the other patients currently have mature, flush, robust wound reconstructions. The fibular flap donor site repairs demonstrated "expansion" of wound area within a few days of BTM implantation, which subsequently reversed. By 1 year postimplantation, the wound areas were almost the same as when the wounds were created (Patient 1: Day 0, 59.4 cm², Day 367, 60.8 cm²; Patient 3: Day 0, 28.1 cm², Day 391, 29.1 cm²). The radial forearm flap reconstructions demonstrated negligible contraction in wound surface area during the 4–5 week integration phase, while

the BTM seal was *in situ* (mean wound area as a percentage of original = 99.01%). Delamination and grafting resulted in a mean scar area 70.66% of the original wound when persisting for ≥1 year. Therapist scoring revealed scar results that were much closer to normal skin than those in the pilot trial. The positive effects of fenestration in the previous study led to this step now being included in the manufacturing process. BTM is now offered as a therapeutic option in free flap donor site reconstruction.

22.8   The first use of biodegradable temporizing dermal matrix in moderate to severe burn repair

Long-term implantation in smaller wounds has not demonstrated local or systemic, immediate or long-term adverse reactions. A five patient prospective pilot study in major burns was thus designed. Inclusion criteria included adults between 18 and 70 years of age presenting with 20–50% TBSA full-thickness burns, which may be on the background of a larger TBSA superficial burns.

Once physiologically stable, debrided burn wounds were implanted with the optimized, perforated, sealed BTM using staples and overdressed with antimicrobial materials.

Twice weekly dressing changes were performed, while awaiting donor site reepithelialization for further SSG harvest. During this time the BTM integrated, becoming vascularized and populated with fibroblasts. Once integrated, it was delaminated, refreshed by dermabrasion, meshed SSG was applied and dressed. Dressings were changed with graft check at 4 days, and then twice weekly to healing.

Photographic records were taken at every intervention. Punch biopsy specimens of representative areas were taken at intervals for histological analysis. Formal scar assessment was performed at 1 year by a physiotherapist.

Three of five patients have been recruited and treated at the time of writing.

Patient 1: A 48-year-old male with 73% TBSA burns, 37% full thickness (Figure 22.11). Day 2, the posterior trunk had SSG applied while BTM was implanted to the dorsum of both hands, bilateral circumferential forearms and arms, posterior right thigh, and posterior left calf (22% TBSA, Figure 22.12). On Day 5, feces had leaked onto a 5 × 2 cm superior edge of the BTM on the posterior right thigh, which was excised to prevent infection. All of the remaining BTM integrated (Figure 22.13). BTM SSG application was staged to allow donor site recovery—the left upper limb at Day 37 postimplantation, the right upper limb and calf at Day 44, and right thigh at Day 48. The patient is currently in day care rehabilitation. Figures 22.14 and 22.15 illustrate the histological process of integration, with fibrous tissue arising on the surface of the fat deep to the BTM and subsequently integrating into it.

His most recent assessment was at Day 369 (12 months postinjury, Figure 22.16).

Figures 22.17 and 22.18 demonstrate the degradation process. By 6 months, the foam walls are rounded but the thickness has not altered from application (2 mm). By 9 months, the BTM is thinned and much of the volume has been degraded. At 12 months, only microscopic remnants, undergoing phagocytosis by giant cells,

Figure 22.11 Presentation pictures of the first significant burn patient to receive BTM.

Figure 22.12 Both upper limbs and dorsal hands were treated.

Figure 22.13 Complete integration by Day 33.
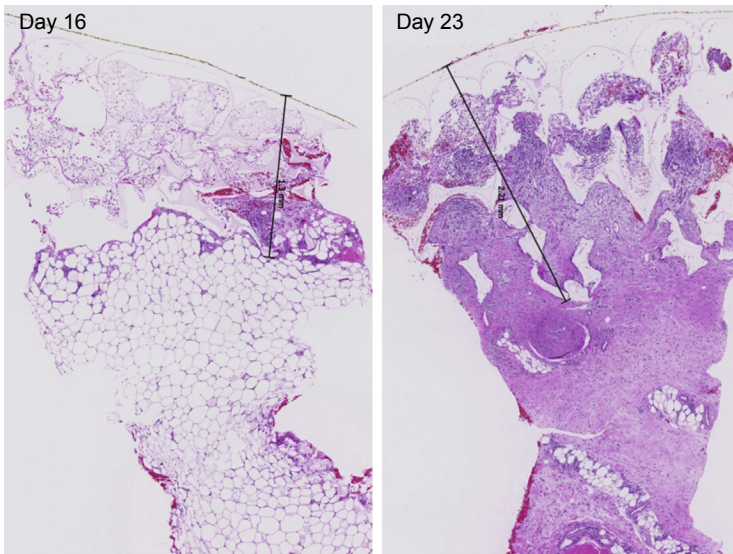
Figure 22.14 Histological progress of integration (Day 16 and Day 23).

remain. At 18 months there is no evidence of residual polymer. In the first burn patient, an injury characterized by a more aggressive inflammatory response, microscopic polymer remnants were visible histologically at 9 months, accompanied by giant cells, some of which contained clear vacuoles, presumably containing ingested polymer. By 12 months, residues were fewer and smaller.
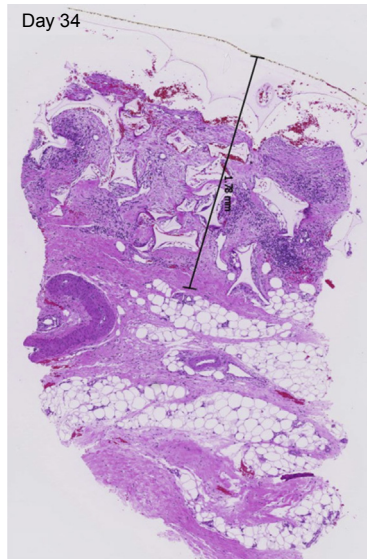
Figure 22.15 Histological progress of integration (Day 34). The polyurethane matrix is filled with tissue.

Figure 22.16 Four days after grafting (left) and 271 days later (right).

Patient 2: A 33-year-old male with 39% TBSA full-thickness burns. His posterior trunk was skin-grafted, as were the hands (he subsequently lost all 10 digits), face, neck, chest, shoulders, and scalp. BTM was applied to bilateral circumferential forearms and arms (16% TBSA, Figure 22.19). His BTM sustained 100% graft take (applied Day 31 postimplantation) and was stable at Day 103 when he was discharged to a rehabilitation center.
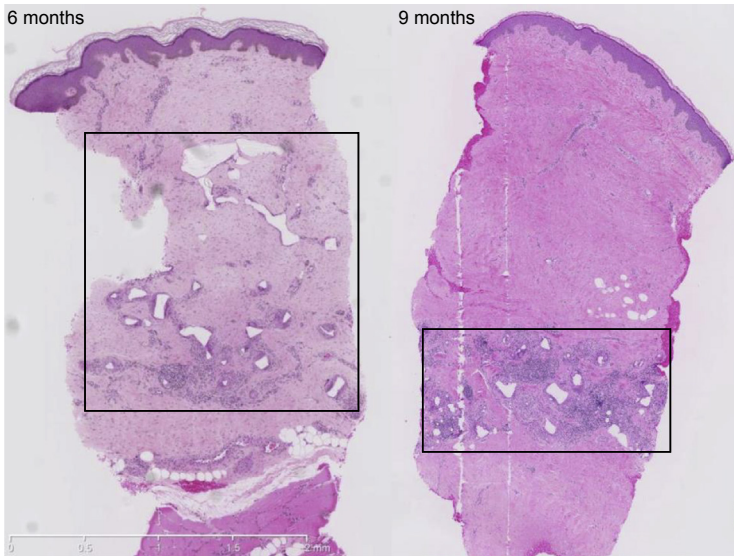
Figure 22.17 Histological progression of polyurethane degradation *in vivo*; 6 and 9 months.
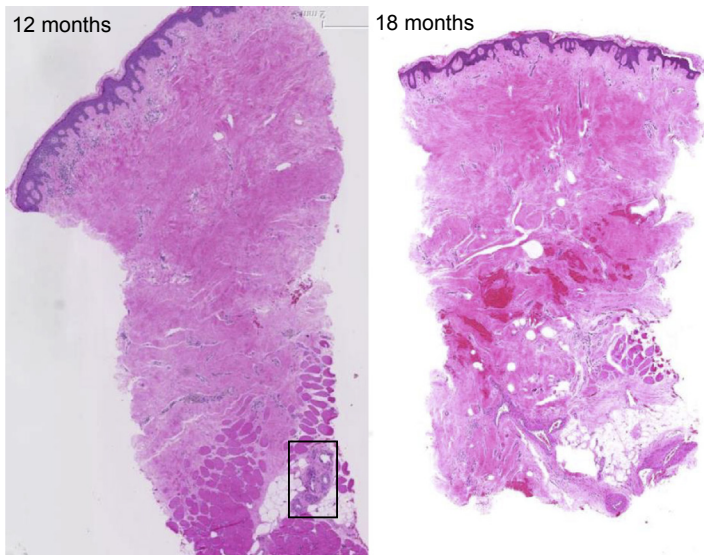
Figure 22.18 Histological progression of polyurethane degradation *in vivo*; 12 and 18 months.

Patient 3: A 47-year-old male with 58% TBSA burns (49% full thickness). His abdomen, chest, and posterior trunk were grafted except for a 2% patch on the chest where BTM was applied. The upper limbs and lower limbs received BTM (21%, Figure 22.20). He lost areas of graft on the chest, abdomen, and back and failed to integrate the patch of BTM on the chest. The arm BTM was skin-grafted on Day 35 postimplantation with 100% take. The legs were grafted on Day 39 with reepithelialized donor skin.

Figure 22.19 Series of Patient 2's right upper limb.

Figure 22.20 Series of Patient 3's right upper limb.

Figure 22.21 Controls—Patients 1 and 2; skin grafts applied directly onto the fat of the back (without underlying BTM).

Figure 22.22 Control—Patient 3; skin grafts applied directly onto the fat of the back (without underlying BTM).

A <1% TBSA SSG failed to take on the legs. His grafts were stable and maturing on review at the time of writing (Day 170).

The BTM was straightforward to apply and delaminate. BTM integrates and sustains stable SSG survival and maturation in patients with severe burns with episodes of concomitant inhalation injury and systemic sepsis. The cosmetic appearances at this early stage are superior to skin grafting alone (Figures 22.21 and 22.22). No adverse outcomes uniquely attributable to the BTM were noted. We await completion of recruitment and formal scar scoring at 1 year in the whole cohort.

22.9 Conclusions

The biodegradable polyurethane has been demonstrated to be a capable and versatile material for the production of skin products for major burn victims. As a synthetic, sealed bilayer dermal temporizing matrix, it is already in regular human use in surgical wounds and is the subject of a five patient pilot human burn trial. As the scaffold for CCS production, the foam is nontoxic to cells, allows attachment, collagen deposition and keratinocyte take *in vitro*, and attachment and take over both in BTM and in fresh wounds *in vivo*.

References

1. Heimbach D, Luterman A, Burke J, Cram A, Herndon D, Hunt J, et al. Artificial dermis for major burns. A multicentre randomized clinical trial. *Ann Surg* 1988;**208**(3):313–20.
2. Heimbach DM, Warden GD, Luterman A, Jordan MH, Ozobia N, Ryan CM, et al. Multicenter postapproval clinical trial of Integra dermal regeneration template for burn treatment. *J Burn Care Rehabil* 2003;**24**(1):42–8.
3. Nguyen DQ, Potokar TS, Price P. An objective long-term evaluation of Integra (a dermal skin substitute) and split thickness skin grafts, in acute burns and reconstructive surgery. *Burns* 2010;**36**:23–8.
4. Peck MD, Kessler M, Meyer AA, Bonham Morris PA. A trial of the effectiveness of artificial dermis in the treatment of patients with burns greater than 45% total body surface area. *J Trauma* 2002;**52**:971–8.
5. Dearman BL, Li A, Greenwood JE. Optimisation of a polyurethane dermal matrix and experience with a polymer-based cultured composite skin. *J Burn Care Res* 2014;**35**(5):437–48.
6. Shores JT, Gabriel A, Gupta S. Skin substitutes and alternatives: a review. *Adv Skin Wound Care* September 2007;**20**(9):509–11.
7. Bruin P, Veenstra GJ, Nijenhuis AJ, Pennings AJ. Design and synthesis of biodegradable poly(ester-urethane) elastomer networks composed of non-toxic building blocks. *Makromol Chem Rapid Commun* 1988;**9**:589–94.
8. Huss FRM, Nyman E, Gustafson C-J, Gisselfält K, Liljensten E, Kratz G. Characterization of a new degradable polymer scaffold for regeneration of the dermis. In vitro and in vivo human studies. *Organogenesis* July–September 2008;**4**(3):195–200.
9. Guelcher SA, Patel V, Gallagher K, Connolly S, Didier JE, Doctor J, et al. Synthesis and biocompatibility of polyurethane foam scaffolds from lysine diisocyanate and polyester polyols. *Tissue Eng* 2006;**12**(5):1247–59.

10. Guelcher SA, Gallagher KM, Srinivasan A, McBride SB, Didier JE, Doctor JS, et al. Synthesis, in vitro biocompatibility and biodegradation, and mechanical properties of two-component polyurethane scaffolds: effects of water and polyol composition. *Tissue Eng* 2007;**13**(9):2321–33.

11. Hafeman AE, Li B, Yoshii T, Zienkiewicz K, Davidson JM, Guelcher SA. Injectable biodegradable polyurethane scaffolds with release of platelet-derived growth factor for tissue repair and regeneration. *Pharm Res* October 2008;**25**(10):2387–99.

12. Hafeman AE, Zienkiewicz KJ, Zachman AL, Sung H-J, Nanney LB, Davidson JM, et al. Characterization of the degradation mechanisms of lysine-derived aliphatic poly(ester urethane) scaffolds. *Biomaterials* January 2011;**32**(2):419–29.

13. Li A, Dearman BL, Crompton KE, Moore TG, Greenwood JE. Evaluation of a novel biodegradable polymer for the generation of a dermal matrix. *J Burn Care Res* July–August 2009;**30**(4):717–28.

14. Greenwood JE, Dearman BL. Split-skin graft application over an integrating, biodegradable temporising polymer matrix: immediate and delayed. *J Burn Care Res* January–February 2012;**33**(1):7–19.

15. Greenwood JE, Dearman BL. Comparison of a sealed, polymer foam biodegradable temporising matrix against Integra™ dermal regeneration template in a porcine wound model. *J Burn Care Res* January–February 2012;**33**(1):163–73.

16. Dearman BL, Stefani K, Li A, Greenwood JE. "Take" of a polymer-based autologous cultured composite "skin" on an integrated temporising dermal matrix: proof of concept. *J Burn Care Res* January–February 2013;**34**(1):151–60.

17. Wagstaff MJD, Driver S, Coghlan P, Greenwood JE. A randomised, controlled trial of negative pressure wound therapy via a biodegradable polyurethane foam in the management of decubitus ulceration. *Wound Repair Regen* 2014;**22**:205–11.

18. Wagstaff MJD, Schmitt BJ, Coghlan P, Finkemeyer JP, Caplash Y, Greenwood JE. A biodegradable polyurethane dermal matrix in reconstruction of free flap donor sites: a pilot study. *ePlasty* 2015;**15**:102–18.

19. Wagstaff MJD, Schmitt BJ, Caplash Y, Greenwood JE. Free flap donor site reconstruction: a prospective case series using an optimised polyurethane biodegradable temporising matrix (BTM). *ePlasty* 2015;**15**:231–48.

Index